Cover

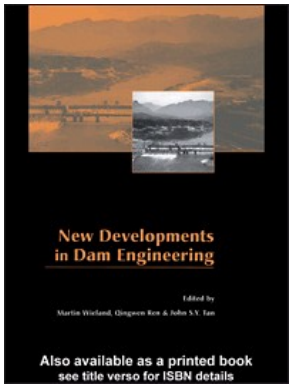
New Developments
in Dam Engineering
Edited by
Martin Wieland, Qingwen Ren & John S.Y. Tan
Also available as a printed book
see title verso for ISBN details

NEW DEVELOPMENTS IN DAM ENGINEERING

This page intentionally left blank.

PROCEEDINGS OF THE 4th INTERNATIONAL CONFERENCE ON DAM ENGINEERING, 18–20 OCTOBER 2004, NANJING, CHINA

New Developments in Dam Engineering

Edited by

Martin Wieland
Electrowatt-Ekono AG, Zurich, Switzerland

Qingwen Ren
Hohai University, Nanjing, China

John S.Y.Tan
CI-Premier Organization, Singapore

A.A.BALKEMA PUBLISHERS LEIDEN/LONDON/NEW YORK/PHILADELPHIA/SINGAPORE

Published by: A.A.Balkema Publishers, a member of Taylor & Francis Group plc
www.balkema.nl and www.tandf.co.uk
This edition published in the Taylor & Francis e-Library, 2006.

To purchase your own copy of this or any of Taylor & Francis or Routledge's collection of thousands of eBooks please go to www.eBookstore.tandf.co.uk.

ISBN 0-203-02067-7 Master e-book ISBN

ISBN 04 1536 240 7 (Print Edition)

Table of Contents

This page intentionally left blank.

New Developments in Dam Engineering—Wieland, Ren & Tan (eds),

Foreword

The development of water resources is a key element in the socio-economic development of many regions in Asia. Very often water availability and rainfall are unequally distributed both in space and time. Dams play a vital role in this respect as there are hardly any viable alternatives for storing water. To satisfy the ever increasing demand for power, irrigation and drinking water and for protection of man, property and environment from catastrophic floods and for regulating the flow of rivers, dams will continue to be the prime infrastructure. Dams have contributed to the development of civilization for over 2000 years. Today, the situation is such that in the "West" where most of the water resources have been developed, the safety of the existing dams and measures for extending their economical life are of prime concern. In developing countries the focus is on the construction of new dams. Small dams are being built and have been built in large numbers. Although this is not directly the subject of this conference it is important that the small dams are properly designed, constructed and maintained. China has some 85,000 dams and reservoirs. Most of them are small dams. Worldwide there are some 45,000 large dams listed by ICOLD, which have a height of over 15m. Most of them are embankment dams and are used for irrigation, water supply, and flood control.

The Asian countries, where most of dam construction is currently taking place are China, India, Iran and Turkey.

The 4th International Conference on Dam Engineering is focusing on dam safety as this is still the number one aspect of dam projects. Economical, financial, environmental, social, political etc. aspects are very important but they are subsidiary to dam safety. The previous International Conferences on Dam Engineering were held in Johore Bahru, Malaysia (1993), Kuala Lumpur, Malaysia (1995), and Singapore (2002) and have covered the following subjects with emphasis on projects in Asia:

- state-of-the-art in the design of small and large dams
- embankment dams including concrete faced rockfill dams (CFRD)
- concrete dams including roller compacted concrete dams (RCC)
- seismic aspects of dam design
- dam safety evaluation
- construction materials for dams
- dam foundation and seepage
- dam monitoring
- dam heightening and rehabilitation of existing dams
- hydraulic aspects of dam design
- environmental aspects and reservoir sedimentation

The large number of papers from the Chinese dam engineers and scientists provide an excellent overview on several aspects of the design and construction of the major dam projects in China. These proceedings are therefore a very useful reference especially for those interested in the development in China.

Qingwen Ren
Martin Wieland

This page intentionally left blank.

New Developments in Dam Engineering—Wieland, Ren & Tan (eds),
© 2004 Taylor& Francis Group, London, ISBN 04 1536 240 7

Preface

The Proceeding contain the papers to be presented at the 4th International Conference on DAM ENGINEERING to be held in Nanjing China during October 18–20, 2004.

The first International Conference on Dam Engineering was held in January 1993 in Johor Bahru, Malaysia. 23 papers (170 pages) with keynote papers by I.B.Donald, Australia and D.G.Fredlund, Canada were included in the proceedings. The second International Conference, held in August 1995 in Kuala Lumpur, Malaysia contained 73 papers (in 555 pages bearing ISBN Ref. 981-00-6274-5) with keynote papers by I.Anderson, Canada; A.Chrzanowski, Canada; R.Fell, Australia and R.Zwahlen, Switzerland. The third international Conference held on 20–22 March 2002 in Singapore discussed and published some 45 papers from 18 countries, with keynote papers by Martin Wieland. (The Proceedings contained 350 pages bearing an ISBN reference)

The theme of the 4th International Conference on DAM ENGINEERING is "new developments in Dam Engineering". It is pleasing to note that the papers included in the Proceeding cover State-of-the art and Hydropower Development, New Type Dam, New Material and New Technology, Dam and Environment besides traditional areas, such as Concrete Dam, Embankment Dam, Methods of Analysis and Design of Dams, Seepage and Dam Foundation, Seismic Analysis, Design and Safety, Stability of Dam and Slope, Dam Safety Monitoring and Instrumentation, Dam Maintenance, Rehabilitation and Heightening and, etc. I believe that the papers will be beneficial to the developing countries.

The two significant aspects related to the papers included in the proceedings are:

- Some of the papers are academic writings by men of thought who have carried out design and construction.
- A number of papers have been written by graduate students and young researchers. This indeed should be heartening to the senior academics and researchers involved in the field of dam engineering for many years.

The Proceedings contain 9 keynote papers, a number of invited papers and papers selected from a vast number of contributions submitted, after review of the abstracts. The final papers included in the Proceeding have been peer reviewed rigorously and revised as necessary by the authors. We acknowledge the help of Dr. Wieland Martin and Prof. Qingwen Ren in maintaining the high standard of the assessment of papers and the co-operation of the authors in complying with the requirements of the editors and the reviewers.

Hong-dao Jiang

This page intentionally left blank.

New Developments in Dam Engineering—Wieland, Ren & Tan (eds),
© 2004 Taylor & Francis Group, London, ISBN 04 1536 240 7

Conference organizations

Conference organizing organizations

Hohai University
No 1, Xikang Road
Nanjing 210098
Jiangsu, China
Tel: 86–025–8378–7781
Fax: 86–025–83786951
E-mail: qingwenren@yeah.net
Web: http://www.hhu.edu.cn

China Society for Hydraulic Engineering
No 2, Lane 2 Baiguang Road
Beijing 100053
China
Tel: 86–010–6320–3076
Fax:: 86–010–63202154
E-mail: Zhuerming@MWR.gov.cn

China Society for Hydropower Engineering
5 Sanlihe Dong Road, Xicheng District
Beijing 100045
China
Tel: 86–010–66061676
Fax: 86–010–66016082
E-mail: dabing-zhou@sp.com.cn

Conference Secretariat
CI-Premier Conference Organization
150 Orchard Road, #07–14
Orchard Plaza
Singapore 238841
Tel: 065–6733–2922
Fax: 065–6235–3530
E-Mail: cipremie@singnet.com.sg
Web: www.cipremier.com

Conference supporting organizations

- National Natural Science Foundation-NSFC
- Jiangsu Association for Science and Technology
- China Yangtze Three Gorges Project Development Corporation
- China Hydropower Engineering Consulting Group Co. (CHEC)
- Water Resources & Hydropower Planning & Design General Institute
- Chengdu Hydroelectric Investigation and Design Inst. of CHEC
- Kunming Hydroelectric Investigation and Design Inst. of CHEC
- Zhongnan Hydroelectric Investigation and Design Inst. of CHEC
- Reconnaissance, Planning, Design & Research Institute, YRCC, MWR
- Yellow River Institute of Hydraulic Research, YRCC, MWR
- Changjiang Inst. of Survey, Planning, Design & Research MWR
- Guizhou Wujiang Hydropower Development Ltd
- Yunnan Lancang River Hydropower Development Ltd
- Three Gorges University
- Qinghua University
- Nanjing Hydraulic Research Institute
- Chinese National Committee on Large Dams

Members of conference committee chairmen

- Prof. Jiang HongDao,
  Hohai University, China
- Prof. LuYouMei,
  China YangTze Three Gorges Project Development Corporation and Chairman,
  CHINCOLD, China.
- Dr. Baba, Kyohei,
  ICOLD Vice-President, Japan

Members of conference advisory committee

- Prof Pan JiaZheng, Vice-President, Chinese Academy of Engineering, China
- Mr. Zhu ErMing, Vice-Chairman, CHINCOLD, China
- Mr. Zhou DaBin, Vice-Chairman, CHINCOLD, China
- Dr. Wieland, Martin, Electrowatt-Ekono AG, Switzerland
- Prof. Liang, Robert, Y., University of Akron, USA
- Mr. Hoeg, Kaare, former ICOLD President, Norway
- Prof. Lee, C.F., The University of Hong Kong, Hong Kong
- Dr. Yoshio, Ohne, former Chairman, JapanCOLD, Japan
- Dr. Sakamoto, Tadahiko, Public Works Research Institute, Japan
- Prof. Noppadol, Phienwej, Asian Institute of Technology, Thailand
- Mr. Yogendra, Prasad, Nat'l Hydroelectric Power Corporation, India
- Prof. Broms, Bengt, B., Past-President, ISSMGE, Sweden

Members of academic committee

- Chairman: Prof. Wu ZhongRu, Academician of Chinese Academy of Engineering, China
- Vice Chairman: Prof. Chen Houqun, Academician of Chinese Academy of Engineering, China
- Vice Chairman: Prof. Ren Qingwen, Hohai University.

Members

- Prof. Lin Gao, Academician of Chinese Academy of Sciences, China
- Prof. Zhang Chuhan, Academician of Chinese Academy of Sciences, China
- Prof. Zheng Shouren, Academician of Chinese Academy of Engineering, China
- Mr. Ma Hongqi, Academician of Chinese Academy of Engineering, China
- Mr. Zhang Chaoran, Academician of Chinese Academy of Engineering, China
- Mr Wang Balie, Chief Engineer, China Hydropower Engineering Consulting Group Co., China
- Mr Wang Yisen, Chief Engineer, Water Resources, Hydropower Planning and Design General Institute
- Mr Hu Bin, Chief Engineer, Chengdu Hydroelectric Investigation & Design Institute of CHEC
- Mr Feng Shulong, Chief Engineer, Zhongnan Hydroelectric Investigation & Design Institute of CHEC
- Mr Fu Shuhong, Chief Engineer, Kunming Hydroelectric Investigation & Design Institute of CHEC

- Dr Brenner, Peter, Applied Geosciences. Switzerland
- Prof Tanaka, Tadatsugu, The University of Tokyo, Japan
- Prof Hasegawa,Takashi, Kinki University, Japan
- Prof Nistor, Georghe, Technical University "Gh. Asachi" of Iasi, Romania
- Mr Ahmed El-Tayeb Ahmed, Universiti Teknologi Malaysia
- Dr Oosthuizen, Chris, Dept of Water Affairs and Forestry, South Africa
- Dr Reza Rakhshandehroo, G, Shiraz University, Iran
- Dr Proca, Gabriela, E., Technical University "Gh. Asachi" of Iasi, Romania

Members of organizing committee

Chairman: Prof Yang Yixin, Vice President, Hohai University

Members

- Li Wanhong, Chief, Div. of Hydraulic Enggrg, NSFC
- Cao Guangjin, Vice President, China Yangtze Three Gorges Project Development Corporation
- Li Jugen, Director, China Hydropower Engineering Consulting Group Co.
- Shen Fengsheng, Director, Water Resources and Hydropower Planning & Design General Institute, MWR
- Zheng Shengan, Director, Chengdu Hydroelectric Investigation and Design Institute of CHEC
- Huang Guangming, Deputy Director, Kunming Hydroelectric Investigation and Design Institute of CHEC
- Li Linglong, Director, Zhnngnan Hydroelectric Investigation and Design Institute of CHEC
- Zong Zhijian, Deputy Director, Reconnaissance, Planning, Design and Research Institute, YRCC, MWR
- Gao Hang, Director, Yellow River Institute of Hydraulic Research Institute, YRRC, MWR
- Niu Xinqiang, Director, Changjiang Institute of Survey, Planning, Design and Research, MWR
- Jin Zehua, General Manager, Guizhou Wujiang Hydropower Development Company Ltd
- Kou Wei, General Manager, Yunnan Lancang River Hydropower Development Ltd
- Liu Defu, President, Three Gorges University
- Zhou Zhifang, Head, College of Civil Engineering, Hohai University
- Yan Zhongming, Dean, College of Hydropower Engineering, Hohai University
- Yukio Aoyagi, CRIEPI, Abiko Research Laboratory, Japan

Conference Secretaries

- Er Tan S.Y.John, CI-Premier Organization, Singapore
- Prof Ren Qingwen, Hohai University, China
- Prof Zhao Jian, Hohai University, China
- Prof Du ChengBin, Hohai University, China

Conference Secretariat Members

- Mdm Wu Xuan, Hohai University, China
- Ms Gan, Jospehine, CI-Premier Conference Organization
- Ms Teo, Lian Peng, Conference Logistics and Services
- Dr Lok Tat Seng, Nanyang Technological University, Singapore
- Ir Khor Chong Liang, BES Perunding Sdn Bhd, Malaysia

This page intentionally left blank.

New Developments in Dam Engineering—Wieland, Ren & Tan (eds),
© 2004 Taylor & Francis Group, London, ISBN 04 1536 240 7

History of the conference

The International Conference on Dam Engineering series was initiated in 1992 following the inspiration from Dr Wieland, then working at the Asian Institute of Technology in Bangkok, Thailand, and undertaken by CI-Premier Conference Organisation, a professional group of international conference organisers.

First International Conference held in January 1993 in Johor Bahru, Malaysia. 23 papers (170 pages) with keynote papers by I B Donald, Australia and D.G.Fredlund, Canada.

Second International Conference, held in August 1995 in Kuala Lumpur, Malaysia 73 papers (in 555 pages) with keynote papers by I.Anderson, Canada; A.Chrzanowski, Canada; R.Fell, Australia and R.Zwahlen, Switzerland. The Conference was sponsored by the Malaysian Water Association with support from the Candadian Dam Safety Assocaiton.

Third international Conference held on 20–22 March 2002 in Singapore 45 papers (in 350 pages) with keynote papers by Martin Wieland.

Fourth International Conference to be held on 18–20 October 2004 in Nanjing, China Some 150 papers (in 1150 pages). Organised by Hohai University, China Society for Hydraulic Engineering and China Society for Hydropower Engineering.

Proceedings of all the above conferences are available

For the 1st, 2nd and 3rd Conferences, please contact:
CI-Premier Pte Ltd
150 Orchard Road #07–14, Orchard Plaza, Singapore 238841
Fax: 065–62353530/Email: cipremie@singnet.com.sg

For the 4th Conference, please contact:
A.A. Balkema Publishers
Taylor & Francis The Netherlands
P.O. Box 447, 2300 AK Leiden
Schipholweg 107C, XC Leiden
The Netherlands
Fax: +31 (0)71 523 4571 Email: germaine.seijger@tandf.co.uk

This page intentionally left blank.

Keynote papers

This page intentionally left blank.

New Developments in Dam Engineering—Wieland, Ren & Tan (eds),
© 2004 Taylor & Francis Group, London, ISBN 04 1536 240 7

Limit states assessment for earthquake resistance of gravity dams based on crack propagation analysis

Yukio Aoyagi
Civil Engineering Laboratory, Central Research Institute of Electric Power Industry, Japan

Hideyuki Horii
Engineering Graduate School, University of Tokyo

Masayuki Kashiwayanagi
Engineering Department, Electric Power Development Company Ltd.

Yoshihisa Uchida
Construction Engineering Center, Tokyo Electric Power Company Ltd.

ABSTRACT: Ultimate States of a gravity dam were appraised by the extension of major cracks caused by seismic responses due to postulated earthquakes. A finite element dynamic analysis was carried out assuming smeared cracks and incorporating a tension-softening diagram for concrete. A new methodology was proposed to assess ultimate seismic performance of a gravity dam based on the relationship between the input earthquake acceleration and the residual ligament length of uncracked portion.

1 INTRODUCTION

In recent years the need to design public infrastructures based on limit states concept against devastating earthquakes has been increasing in view of the serious damages caused by the Great Kobe Earthquake in Japan (1995), Cojarie Earthquake in Turkey (1999), Chi-Chi Earthquake in Taiwan (1999) and others. The fundamental seismic design of concrete gravity dams has hitherto been based on equivalent static earthquake intensity, assuming the dam as a rigid body. Dynamic behavior has also been taken into account, but mostly limited to static properties.

In Japan and other earthquake prone countries very few damages caused by earthquakes have been reported so far, albeit moderate cracks were detected in the dam body of Koyna Dam (India) and Manjil Dam (Iran). During Chi-Chi Earthquake the right bank side of Shigang Dam was severely destroyed due to the direct effect of a fault dislocation. However, in view of the past experience, when we limit the damages attributable to the effect of near field earthquake motions, appearance and subsequent extension of cracks in a gravity dam may be justified as a measure for the evaluation of structural limit states.

Cracking characteristics of mass concrete have been studied both experimentally [1],[2] and analytically [3], but most of them are of static nature. The authors, meanwhile, conducted a wedge penetration test on concrete blocks made with simulated mass concrete with a maximum size of aggregate up to 150mm. Dynamic stress-strain constitutive equations were derived from the test results [4] and applied to the analysis.

A dynamic finite element analysis was performed on a concrete gravity dam incorporating the above tensile softening constitutive diagram. The computer program used was DINA, which was

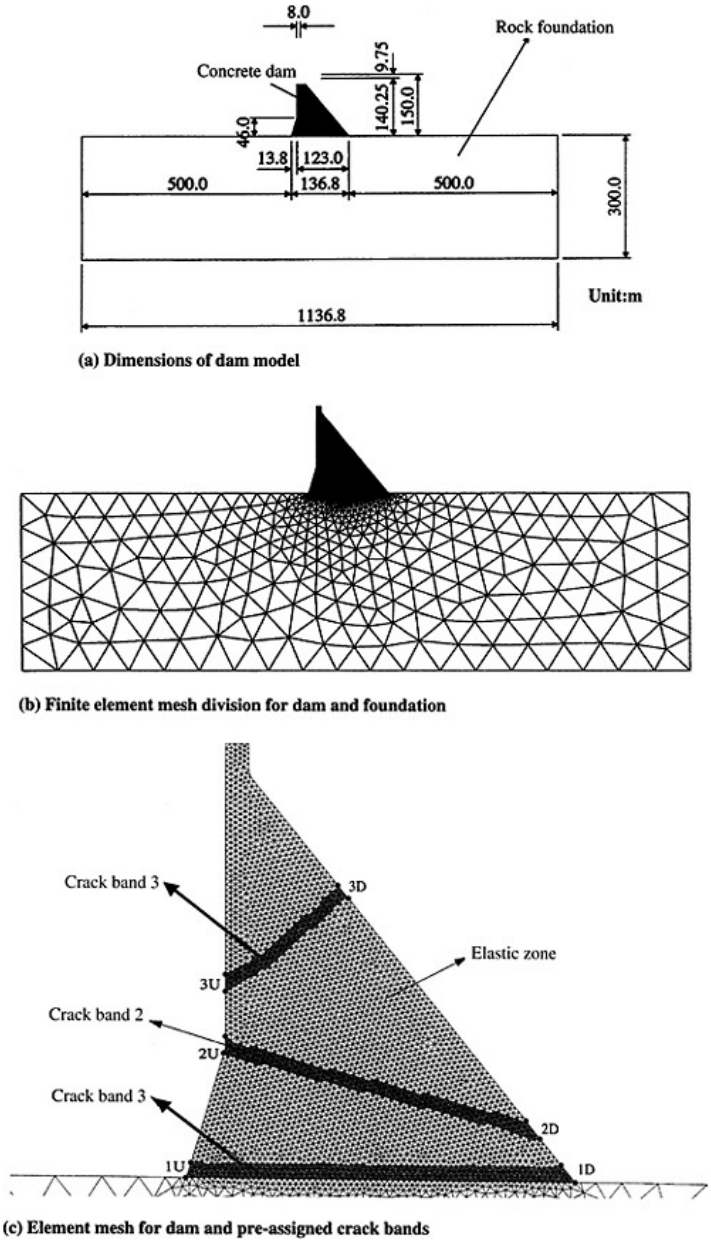

Figure 1. Dam model for analysis.

developed by TNO Co. Ltd. of Holland. In the analysis smeared crack was assumed and the cracking zones were designated in advance of the analysis. A new measure of safety assessment was proposed to specify the level of structural integrity against failure in terms of extension of cracks into the dam body. A parametric study was conducted varying the level of input earthquake accelerations. The proposed method is intended for a part of streamlined seismic design of concrete gravity dams in consideration of limit states.

2 CRACK DEVELOPMENT ANALYSIS

2.1 *Analytical model*

A real sized concrete gravity dam was selected as the analytical model. Configuration and mesh division of the dam are illustrated with the area of rock foundation in Fig. 1(a, b). Finer meshes were employed in the dam body to match the non-linear mechanical behavior to be investigated, while the rock foundation portion was divided into coarser meshes assuming linear elastic properties. The numbers of meshes and nodes were 6,944 and 3,521, respectively. These predetermined bands of cracking area, in which width of three elements (2–3m) was allotted, were specified beforehand referring to the preliminary analysis as depicted in Fig. 1(c). Tensile softening constitutive laws were applied only to these bands. The other portions of dam body and rock foundation were assumed to be linear elastic.

Mechanical properties of concrete were determined based on the static as well as dynamic wedge penetration splitting tests and are listed in Table 1(a). As for rock foundation average values were used for the whole area (Table 1(b)).

2.2 *Tension stiffening model of concrete [4]*

To identify the tensile softening constitutive law to be employed in the dynamic analysis of the dam model, an experimental work was specifically planned and conducted using mass concrete with the maximum size of aggregate of 150mm. Wedge penetration test illustrated in Fig. 2 was performed.

Table 1. Material constants used for analysis.

	Item	Symbol	Unit	Value
(a) Concrete	Static Young's modulus	E_{cs}	MPa	2.1×10^4
	Dynamic Young's modulus	E_{cd}	MPa	2.3×10^4
	Static Poisson's ratio	ν_{cs}	—	0.19
	Dynamic Poisson's ratio	ν_{cd}	—	0.19
	Static compressive strength	f_{ct}	MPa	21.1
	Static tensile strength	f_{ts}	MPa	1.87
	Dynamic softening stress	f_{td}	MPa	1.22
	Stress at the breaking point of bi-linear softening diagram	f_{1d}	MPa	0.35
	Crack opening at the breaking point	W_{1d}	mm	0.298
	Ultimate crack opening	w_{cd}	mm	1.200
	Dynamic fracture energy	G_{Fd}	N	365
	Reduction rate of shear stiffness due to cracking	β	—	0.005
	Unit volumetric mass	ρ_c	kg/m^3	2,400
	Damping factor	h_c	%	7.0
(b) Rock foundation (linear elastic)	Static Young's modulus	E_{rs}	MPa	1.0×10^4
	Dynamic Young's modulus	E_{rd}	MPa	1.0×10^4
	Static Poisson's ration	ν_{rs}	—	0.25
	Dynamic Poisson's ratio	ν_{rd}	—	0.25
	Unit volume mass	ρ_r	kg/m^3	2,500
	Damping factor	h_c	%	7.0

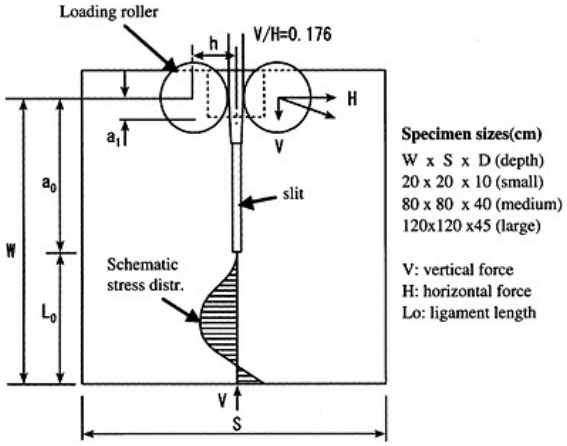

Figure 2. Specimen for wedge penetration test.

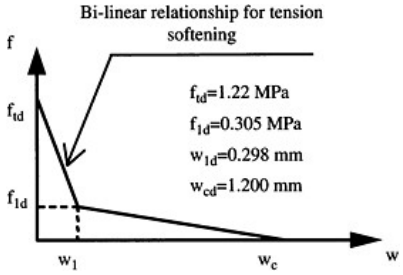

Figure 3. Constitutive diagram for tension softening.

The parameters varied in the experiment were crack opening rates (0.1−12,600mm/min), maximum sizes of aggregates (20, 80 and 150mm), compressive strength of concrete (18 and 30MPa) and dimensions of the specimens. Important findings obtained in the experiment were as follows;

1) A tendency was found that the fracture energy was not dependent on the sizes of the specimens, but rather increased almost proportionally with the maximum sizes of aggregates.
2) Fracture energy was highly affected by the crack extension rate. Maximum increment of fracture energy by about 70% was observed in the dynamic situation than in the static one.
3) A simple bi-linear type tension-softening diagram in Fig. 3 was identified as feasible to express the dynamic characteristics of the dam concrete tested.

Numerical fitting of the experimental data for the purpose of analysis is described below.

$$f_{ts} = 1.55 \times \left(\frac{f_{cd} - 8}{10} \right)^{2/3} \qquad f_{td} = 0.4 V_c^{0.052} \times f_{ts}$$

$$G_{Fs} = (0.79 d_{max} + 80) \left(\frac{f_{cd}}{10} \right)^{10} \qquad f_{1d} = 0.25 f_{td}$$

$$\frac{G_{Fd}}{G_{Fs}} = V_c^{0.034} \qquad w_{cd} = 4 \times \frac{G_{Fd}}{G_{Fs}} \times \frac{1}{f_{td}}$$

$$w_{1d} = 2 \times \frac{G_{Fd}}{1000} \times \frac{1}{f_{td}} - 0.25 w_{cd}$$

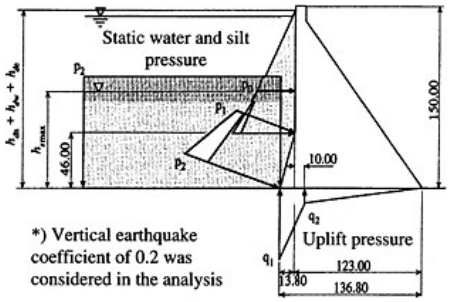

Figure 4. Static loads applied to the dam model.

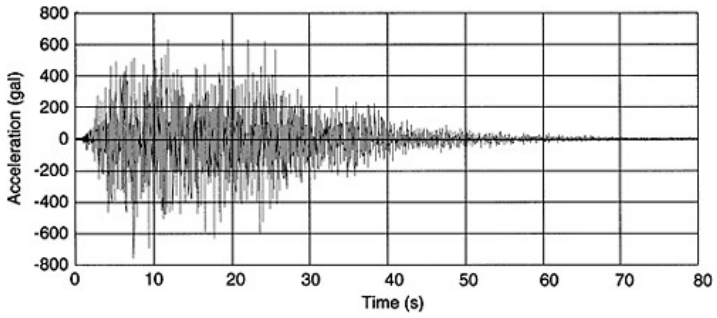

Figure 5. Input earthquake wave applied to the bottom of the model.

The symbols that are not defined in Table 1 are;

G_{Fs}; static fracture energy, d_{max}; maximum size of aggregate (150mm), V_c; crack propagation ratio (assumed as 103,000).

2.3 *Loads and boundary conditions*

Initial conditions for dynamic analysis due to earthquake loading were calculated by static analysis applying normal operating loads other than that of earthquake.

The loads considered in the static analysis (Fig. 4) were water pressure, drifted silt pressure and dead loads of dam body as well as rock foundation together with vertical static effect of earthquake, which was estimated with the upward static earthquake intensity factor of 0.2 G.

In dynamic analysis the maximum conceivable earthquake to be expected on the dam foundation, which was obtained from Osaki spectrum given as magnitude of M=8.0 and hypo-central distance of Δ=25km, was assumed and artificially generated. The maximum acceleration of the input earthquake was 574 gal. For the purpose of analysis the input waves were translated to the basement of the model (Fig. 5) and the maximum input accelerations were modified according to the analytical cases.

As for dynamic water pressure acting on the upstream face of the dam, an additional mass was attached calculated by Westergaad's formula. To simulate the infinite half-space of boundary conditions, viscous dampers were installed to the sides and the bottom of the rock foundation as illustrated in Fig. 6.

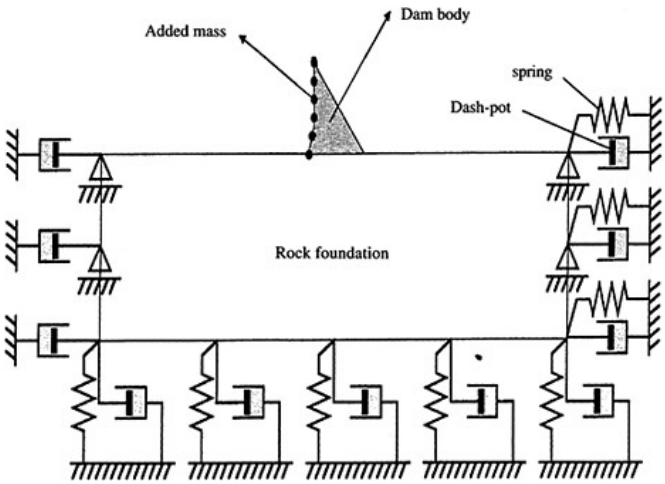

Figure 6. Boundary conditions for dynamic analysis.

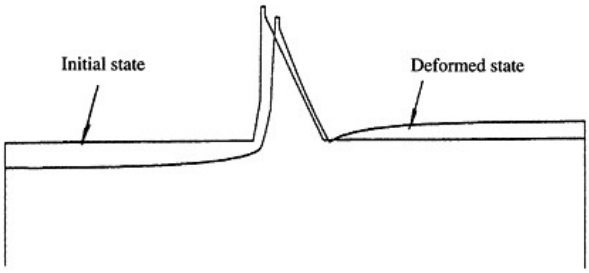

Figure 7. Deformation mode due to static loads.

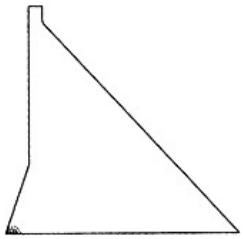

Figure 8. Crack distribution calculated by static analysis.

2.4 *Results of static analysis*

Combination of static loading and static equivalent upward earthquake inertia force caused tensile stresses at the heel of the dam, which led to appearance of cracks in the elements there. Figure 7 depicts the deformational mode and Fig. 8 shows the area of cracking. These cracks, however, were found marginal not to affect the safety of the dam. Starting from the initial conditions, subsequent dynamic analyses were performed.

2.5 *Results of dynamic analyses*

To identify the limit states of concrete gravity dams, parametric analyses were conducted increasing the acceleration amplitude of input earthquake waves. The parameters employed in the analyses are summarized in Table 2. Case 0 corresponds to linear analysis, in which the input acceleration amplitude of the original waves was specified as 753 gal. The objective of this case was to confirm the basic dynamic response behavior of the coupled dam-rock foundation system. Case 1 was a

Table 2. Cases of analyses and conditions.

Case no.	Concrete properties	Maximum input acceleration
Case 0	Linear elastic	753 gal*
Case 1	Tension softening**	753 gal
Case 2	ditto	1,000 gal
Case 3	ditto	1,500 gal

* The maximum acceleration at the bottom of the dam.
** For compression linear elastic.

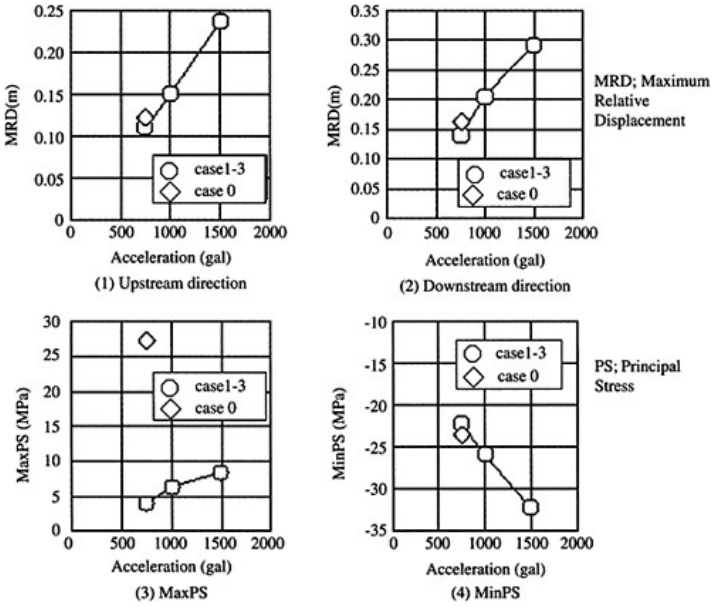

Figure 9. Response values obtained by dynamic analysis.

non-linear analysis with the same wave as case 0. In the non-linear cases of 2 and 3 the acceleration amplitudes were increased to 1.5 and 2 times as high as that of case 0, respectively.

2.5.1 *Dynamic responses*

Relative displacements, maximum and minimum principal stresses are depicted in Fig. 9 corresponding to the cases of analysis. The relative displacement was defined as the difference between the top and the bottom of the dam. For the non-linear cases of 1 to 3, horizontal displacements in the up-and-downstream directions increased almost proportionally with the increment of input acceleration. A slightly larger displacement was obtained in linear analysis than in non-linear cases. The maximum principal (tensile) stresses, which occurred in the adjacent elements to the

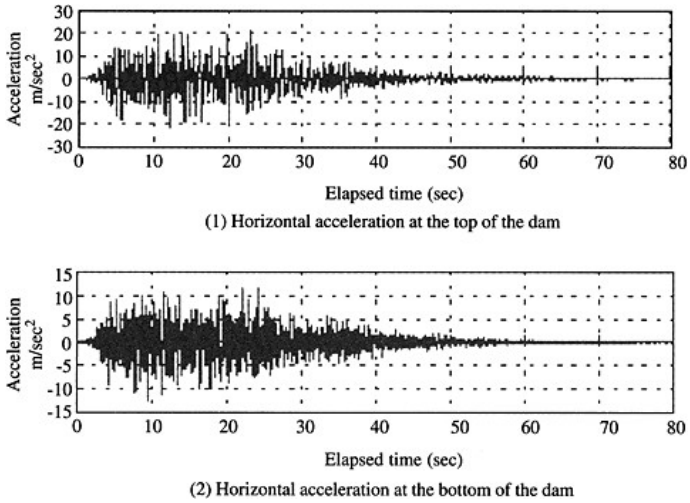

Figure 10. Response accelerations of dam obtained in case 2.

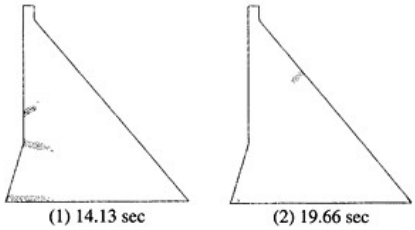

Figure 11. Extension of cracks in case 2.

localized cracking zones, caused the stresses exceeding that of softening initiation in the cases of 1 to 3. In case 3 the stress ratio was as high as 7.

But in the linear analysis of case 0 the maximum tensile stress calculated was several times as high as that of case 3. Since the analysis did not take into account the non-linearity in the compression zones, the minimum principal stress (compressive) surpassed the assumed compressive strength of 21.0 MPa in case 1. In case 3 the calculated maximum stress reached as high as 32.3 MPa. To maintain the consistency of the analysis it is necessary to incorporate the effect of non-linearity also in the compression zones.

As an example of the response acceleration waves the responses at the bottom and top of the dam are presented in Fig. 10 in case 3. Almost fivefold amplification is seen at the top with respect to the bottom. Linear analysis of case 0 showed a tendency to increase slightly the amplification compared to the cases of non-linear analyses. The analytical results, however, did not reveal that the effect of non-linearity played a decisive role on dynamic responses.

2.5.2 *Appearance and extension of cracks*

In the cases of 1 to 3, tensile cracks appeared in the dam body and extended with the increment of input acceleration. For instance the patterns of cracks are sketched in Fig. 11 for case 2. In the preset crack zones of 1 and 2, cracks extended from the upstream face, but in the crack zone of 3,

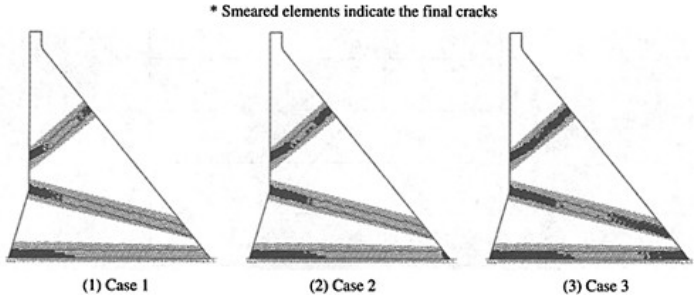

Figure 12. Final crack propagation after the main earthquake waves.

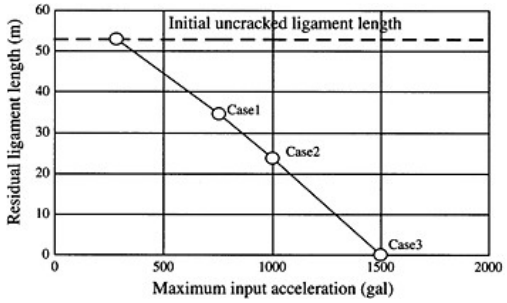

Figure 13. Relationship between maximum input acceleration.

cracks grew both from up-and-downstream sides. Fig. 12 illustrates the states of residual cracks after the main motions of earthquake were over. While in cases 1 and 2 cracks terminated within the dam body leaving some uncracked portions, in case 3 cracks penetrated through the dam body, which led to the ultimate state. The cracks from both sides got connected at the time point of 19.68 sec. When the ultimate state was reached, analysis could not be continued due to divergence of solution.

Based on the analytical results in Fig. 12. the residual uncracked ligament lengths were computed and plotted in Fig. 13 with regard to the maximum input accelerations of a_{max}. The corresponding acceleration for initial cracking was calculated by linear analysis using tensile strength of concrete and was determined as a_{max}=284 gal. The maximum acceleration in case 3 was defined as a_{max}=1500 gal in consideration of the fact that main earthquake waves had already passed.

3 A NEW SEISMIC SAFETY ASSESSMENT OF GRAVITY DAMS BASED ON LIMIT STATES

In the forgoing section a finite element dynamic analysis revealed that a through crack occurred in the upper portion of the dam at about twice the maximum input acceleration corresponding to the postulated design earthquake. This stage may be judged as the ultimate state of a dam. An explicit correlation was found between the input accelerations and the residual ligament lengths. The relationship also infers that the conventionally designed concrete gravity dams retain an ample safety allowance against strong earthquakes. Therefore, a seismic safety margin in terms of

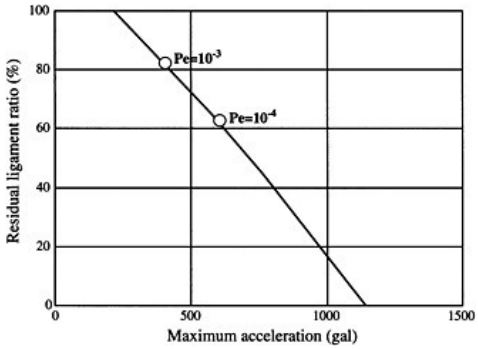

Figure 14. Relationship between maximum input acceleration at free surface of base stratum and residual ligament ratio.

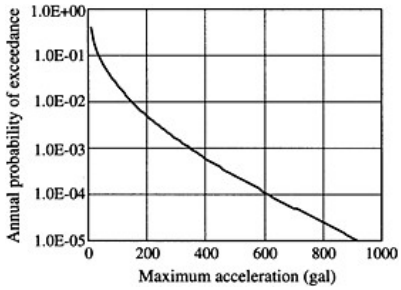

Figure 15. Relationship between the maximum acceleration at free surface of the base stratum and the annual probability of exceedance.

limit states seems to be quantified by the relationship between the input earthquake accelerations and the residual ligament lengths. The practical procedures are described below.

For this purpose it is convenient to convert Fig. 13 to Fig. 14. In Fig. 14 the residual ligament length ratio is defined as the ratio of residual ligament length to the original intact length without cracking. The maximum acceleration of a_{max} is given as that at the free surface of the base stratum.

3.1 *Safety assessment in consideration of earthquake risks*

Referring to the information on historical data of earthquakes and the pertinent active faults the relationship between the maximum acceleration on the free surface of the base stratum and the per annum probability of occurrence can be established for a specific site [5]. Figure 15 depicts an example for a dam site in Japan. If the probabilities of occurrence are assumed as $Pe=10^{-3}$ and $Pe=10^{-4}$, then the maximum accelerations are determined as a_{maxg}=340gal and a_{maxg}=664 gal, respectively. Fitting these acceleration values to Fig. 14, the ligament residual ratios are obtained as 82% and 62%, respectively. Therefore, a figure similar to Fig. 14 will give a quantitative evaluation of seismic resistance of a dam against failure when the required annual probability of exceedance is assigned as a part of seismic design. This idea is also considered useful in selecting a dam site.

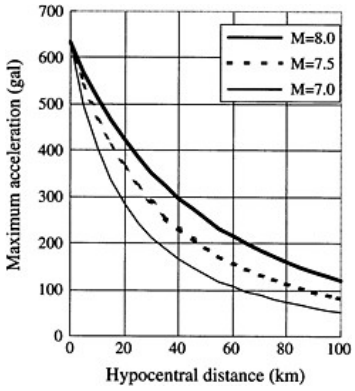

Figure 16. Relationship between the maximum acceleration at free surface of the the base stratum and annual probability of exceedance.

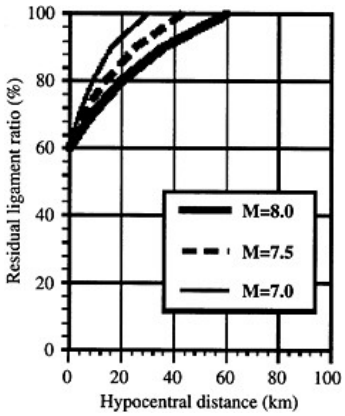

Figure 17. Relationship between hypocentral distance and residual ligment ratio.

3.2 *Seismic evaluation for a specific earthquake*

On the other hand if we could assume the location of epicenter and magnitude M, then the maximum acceleration on the free engineering foundation would be defined in terms of hypo-central distance Δ from such formula as proposed by Fukushima and Tanaka [6]. As an illustration the relationships are shown for the cases of magnitudes M=7.0, 7.5 and 8.0 in Fig. 16. Using these relationships together with that of Fig. 14, the ligament residual ratios are derived with regard to hypo-central distance Δ as shown in Fig. 17. The particular dam investigated in this case study seems to possess enough safety margin against strong earthquakes in view of the fact that the minimum ligament residual ratio is as high as 60%. From the foregoing discussions the proposed seismic assessment method deems effective to quantitatively evaluate the seismic performance of existing dams when the epicenters and magnitudes are identified.

4 SUPPLEMENTARY ANALYSIS OF CRACK PROPAGATION WITHOUT ARRANGING DESIGNATED CRACK BANDS [7]

4.1 *Assumption of analysis*

When all the elements in the dam body were equally equipped with tension stiffening law without arranging crack bands, cracks scattered in wide range, which did not reflect the actual situation of gravity dams subjected to severe earthquakes as were witnessed in Koyna Dam. The analytical distress was probably attributed to the way Raleigh damping was assumed. In the previous analysis Raleigh damping was not adjusted according to stiffness reduction and structural property changes due to cracking. Therefore, we introduced a damping parameter, which was related to the response strains consisting of crack strains and elastic strains. The parameter was defined as 0.05 in compliance with the damping coefFicient of 7% applied in the previous analysis.

4.2 *Computer program*

Computer programming was compiled in the framework of MATHEMATICA, which is a unified numerical processing system capable of dealing a wide range of formulation in a single computer environment. To reduce the volume of computation the FEM analysis was confined only to dam body. The same earthquake wave employed in the previous analysis was used, but the input motion

was directly applied at the bottom of the dam. The maximum acceleration at the bottom was defined as 1,000 gal taking into account the magnification factor of 1.7 ($1.7\,(573 \times 1.7 \fallingdotseq 1{,}000\,\mathrm{gal})$). The numbers of elements and nodes were 1,262 and 1,362 as depicted in Fig. 18. The other analytical parameters including the material properties were assumed in the same way as the previous analysis except that all the elements were equally treated as having tension stiffening characteristics without arranging crack bands.

4.3 *Analytical results and discussions*

Calculation could not be continued until the end of the input wave that had a duration of 80 sec, but up to 8 sec during which time major influential waves were included. Input accelerations at the bottom and response acceleration as well as displacement at the dam top are shown in Fig. 19 for the case of high reservoir water level. Crack patterns at the time points of 4.40, 7.02 and 8.00 sec are sketched in Fig. 20. These time points correspond to the appearance of crack (A), branching of crack A and appearance of crack B, respectively

The first crack (C) appeared along the bottom of the dam immediately after the application of earthquake and extended downstream. The crack, however, was discontinuous and inclined downward (Fig. 21(a)). Therefore, this category of cracks does not seem fatal for dam stability unless the weak layers happen to overlap with the cracks.

The second crack (A), which occurred on the downstream slope at 4.4 sec, displaced the dam top in 2.5cm toward upstream side. However, since displacement responses and input earthquake

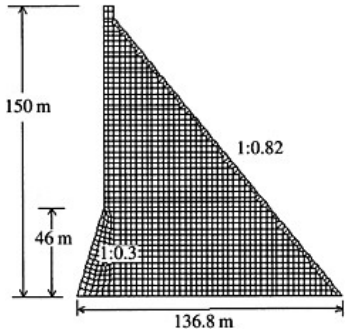

Figure 18. Mesh division of analytical model without pre-arranged crack bands.

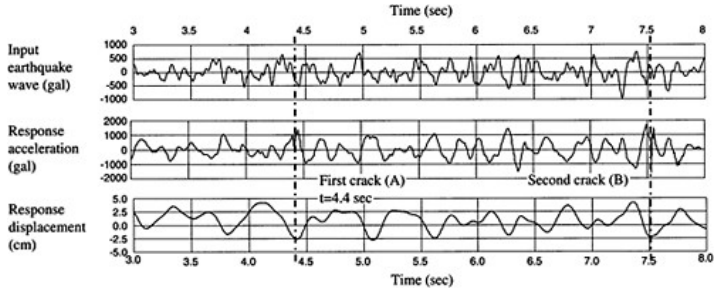

Figure 19. Time dependent response at the top of dam.

accelerations were out of phase, this crack is considered to have appeared as a result of cumulative effect of input earthquake wave which contained the maximum acceleration of 600 gal until that time. The extension of the crack at the time of occurrence 4.4sec was about 1/3 of the total ligament length, but enlarged to half of the ligament at 7.02 sec. At 8.00 sec the crack (A) branched causing an additional crack together with a new crack in the upper portion of the downstream side.

When the reservoir was empty, a crack appeared with an acute downward angle pointing to the upstream side (Fig. 22).

The positions of cracking coincided qualitatively with the crack bands designated in the previous analysis, but the process of crack propagation was found more complex, which could not be reproduced by simply arranging crack bands. Having said that, designation of crack bands looks still effective in evaluating the seismic safety margin in terms of relative comparisons of similar types of gravity dams.

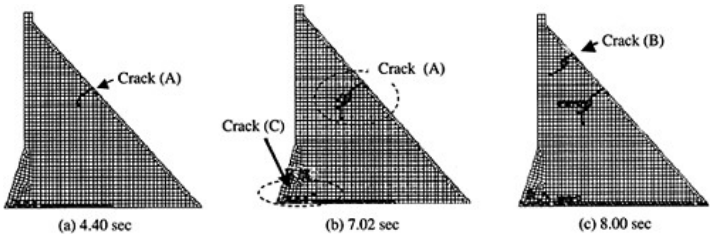

Figure 20. Analytical results of crack propagation in the dam body (high water level).

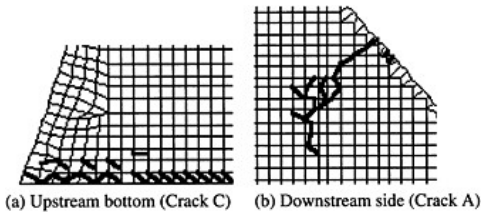

Figure 21. Crack patterns at 7.02 sec (high water level).

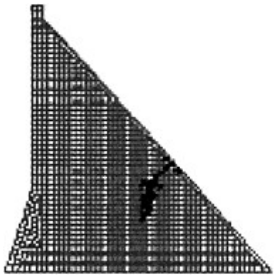

Figure 22. Crack propagation at 3.78 sec with empty reservoir.

5 CONCLUSIONS

A finite element dynamic analysis was applied to a hypothetical concrete gravity dam to investigate the structural limit states in regard to appearance and extension of cracks with increasing input earthquake accelerations. For the non-linear analysis of cracking behavior a tension softening constitutive diagram was derived from the wedge penetration tests on mass concrete specifically conducted for this analysis. The findings are summarized as follows:

1) A new idea was proposed to quantify the structural safety margin in the framework of seismic limit state design of gravity dams. The assessment method consists in the relationships

between the maximum accelerations of input design earthquake waves and the residual (uncracked) ligament ratios.

2) The analysis revealed that a real scale gravity dam, which was modeled after the properties of an existing dam, exhibited a high seismic safety performance. This in turn confirmed an ample earthquake resistance of the gravity dam designed by the conventional procedures based on the static earthquake intensity factors.
3) Two example cases of application of the proposed safety assessment method were described. One was related to selection of dam site and the other dealt with earthquake resistance evaluation of existing dams.
4) A supplemental analysis, in which all the FEM elements in the dam body were incorporated with non-linear tension softening law as well as adjustment for damping, reproduced cracking behavior of a gravity dam more realistically than the previous analysis with crack bands. The problem was that a great deal of time was required for computation.

Since in this paper only an example of the analytical results was presented, there may be some problems when we try to generalize it. The idea itself, however, may be applicable to limit state design and assessment of gravity dams.

Two major problems still remain to be solved; Firstly, the pre-assigned localization of cracking bands should better be replaced by a model without such limitations. Secondly, in this analysis only the maximum acceleration was taken unto account in the assessment of seismic safety, but such important parameters as phase properties and velocity of input earthquake waves are also to be incorporated in the analysis in the future.

ACKNOWLEDGEMENT

This paper presents a part of the results of the research entrusted by Agency of Natural Resources and Energy affiliated with the Ministry of Economy, Trade and Industry Adhoc committee “Rationalization of Seismic Design of Dams” was organized in Japan Electric Power Civil Engineering Association from 1996 through 2000.

The authors appreciate the valuable instruction and advice given by the committee members. We are deeply indebted to late Prof. Hiroyuki Watanbe of Saitama University, who kindly guided us in the research as the chairperson of the Committee.

REFERENCES

[1] Bruhwiler, E., Wittman, F.H., Rokugo, K., *Influence of rate of loading on fracture energy and strain softening of concrete,* Trans. of 9th SMiRT, Vol. H, pp. 25–33, 1987

[2] Saouma, V.E., Broz, J.J., Bruhwiler, E., Boggs, H.L., *Effect of aggregate and specimen size on fracture properties of dam concrete,* Journal of Materials in Civil Engineering, ASCE, Vol. 3, No. 3, pp. 204–218, 1991

[3] El-Aidi, B., Hall, J.F., *Non-linear earthquake response of concrete gravity dam, Part 1: Modelling & Part 2: Behavior,* Earthquake Engineering and Structural Dynamics, Vol. 18, No. 6, pp. 837–865, 1989

[4] Horii, H., Uchida, Y., Kashiwayanagi, M., Kimata, H., Okada, T., *Investigation on tension softening characteristics for the purpose of evaluating ultimate capacity of concrete dams* (in Japanese), Electric Power Civil Engineering, No. 286, pp. 113–119, 2000

[5] Ishikawa, Y., Okumura, T., Kameda, H., *Seismic hazard from frequency—high impact fault activities using probabilistic scenario earthquakes,* Proceedings of 7th International Conference on Structural Safety and Reliability, pp. 1519–1524, 1997

[6] Fukushima, Y., Tanaka, T., *A new attenuation relation for peak horizontal acceleration of strong earthquake ground motion in Japan,* Shimizu Technical Research Bulletin, No. 10, pp. 1–11, 1991

[7] Kashiwayanagi, M., Asaga, H., Horii, H., *Seismic safety evaluation of concrete gravity dams in consideration of material non-linearity* (in Japanese). Electric Power Civil Engineering, No. 308, pp. 80–84, 2003

New Developments in Dam Engineering—Wieland, Ren & Tan (eds),

Continuous compaction control (CCC) for fill dams and roller compacted concrete dams

H.Brandl & D.Adam
Technical University of Vienna, Austria

ABSTRACT: Continuous Compaction Control (CCC) of soil and other granular material is primarily obtained by a roller-integrated method. The motion behavior of the dynamically excited roller drum depends on soil stiffness. Consequently, dynamic compaction values are calculated from measured drum accelerations. Thus, compaction success and increase of soil stiffness can be checked already during the compaction process, leading to an optimised compaction, hence to an increased quality of fill dams.

In a comprehensive research project over 12 years several rollers were equipped with different kind of exciters: Vibratory rollers, oscillatory rollers and rollers with a continuous transition between these two main types. The motion behavior of the rollers with differently adjusted exciter units was investigated theoretically. Furthermore, numerous large-scale in-situ tests were carried out to investigate the effect of combined rollers on cohesive and non-cohesive soil or granular material. Each roller was equipped with adequate CCC-systems and additional transducers. Static and dynamic deformations, pressures and accelerations in two directions were measured in different depths. A measuring depth of CCC up to 2.5m could be found.

CCC provides not only continuous compaction control but also a continuous optimisation and documentation of the entire compaction. All data are available already during compaction thus reducing construction time and cost. The method can be used for soil and rock fills, for recycling materials, for roller compacted concrete and asphalt. Finally, CCC provides reliable data for reliability and safety assessment of the crown zone of old fill dams.

1 INTRODUCTION

The paper summarizes the results of comprehensive research work conducted at the Technical University of Vienna for about two decades. Theory, model tests and site experience lead to sophisticated CCC systems and roller types which have proved suitable on numerous construction sites.

Compaction of soils and fill materials is generally carried out by means of 4 to 25 ton rollers running several passes per layer. Due to the usual heterogeneity of subsoil and compacted material, it is obvious that the compacting procedure provides locally a more or less non-uniform density and bearing capacity of the compacted material. But non-uniformity may cause differential settlements and even cracks in an embankment dam.

So far, compaction control has been carried out mainly by means of punctual test methods with the purpose to check the density or stiffness of the compacted layer. Conventional test methods, like the sand equivalent, the water balloon method, or the Troxler nuclear gauge test to determine the density, and the load plate test for checking soil stiffness, are punctual methods. The uniformity cannot be approved, and weak points can hardly be detected by such spot tests. Moreover, the measuring depth range is only about 20 to 50 cm. Last but not least, all spot test methods are relatively expensive and time consuming. Finally, conventional testing frequently delays construction

work because construction activities must not be carried out in the vicinity of a spot test as ground vibrations might affect the test results.

Therefore these conventional methods of compaction control are not sufficient any more for high quality projects: The increasing demands on engineered structures and fills require as much as possible continuous compaction control and optimisation already during the compaction procedure. The innovative roller-integrated CCC-technique represents a distinctive improvement because all control data are already available during the compaction process and over the roller compacted area.

To a certain extent, continuous compaction control can be also achieved by the spectral analysis surface wave method (SASW) or continuous surface wave technique (CSW). Both compaction control methods are non-intrusive and applicable for soils and other granular materials of all types. But, contrary to the roller-integrated CCC-technique, CSW requires separate external testing equipment that has to be placed on a level ground surface, namely an electromagnetic vibrator to generate surface waves and a row of geophones to detect this waves. Consequently, a really continuous compaction optimisation (i.e. already during rolling) is not possible, and the continuous compaction control may need extensive calibration. However, a significant advantage of the CWS technique is its deep-reaching capacity which makes a post-control of entire soil structures possible.

Due to the superiority of the roller-integrated continuous compaction control, this paper refers exclusively on that method, which is inherently meant by the abbreviation CCC.

2 OPTIMISED COMPACTION CONSIDERING SOIL-ROLLER INTERACTION

Theoretical investigations, field experiments and site measurements have disclosed that there is an intensive interaction between the soil or other granular material (fill layers) and the compaction equipment. Measuring this interaction provides an excellent tool for three important goals of compaction:

- *Compaction optimisation*
  Refers to quality of compaction, to the required compaction energy and time, and to the required geotechnical parameters of the compacted material. Overcompaction and re-loosening of layers should be just as much avoided as heterogeneous compaction degrees. Therefore, a main goal of cooperation between geotechnical and mechanical engineering has been the development of "intelligent" compaction equipment which itself reacts to locally varying soil/granular material properties by automatically changing its relevant machine parameters. Rollers with automatically regulating compaction systems (vibratory/ oscillatory) are already a significant step in this direction which raises compaction from a mere routine craft to a scientifically based high-tech process.
- *Compaction documentation*
  The CCC technology involves an automatic registration of all data in such a way that the results cannot be manipulated. These data collection is essential not only for site acceptance but also for quality control and long-term risk assessment. Furthermore, such information is very helpful for a potential rehabilitation of old dams and dam heightening.
- *Compaction control*
  Should be widely performed already during the compaction procedure. A calibration of the control data based on the reaction between ground and compaction equipment is essential. Control tests after compaction should be increasingly reduced to conventional spot checking, whereas continuous compaction control (compaction equipment-integrated) should be promoted.

The innovative technique represents a distinctive improvement because control data are already available during the compaction process and all over the roller compacted area. Vibratory roller compaction takes place by means of a vibrating drum which is excited by a rotating mass. The oscillation of the roller drum changes depending on the soil response. This fact is used by CCC in

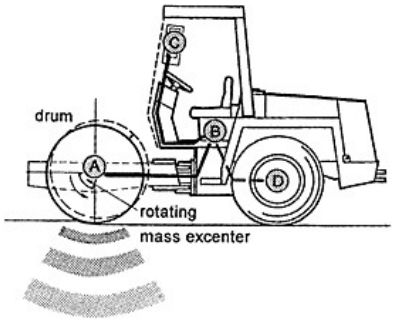

Figure 1. Principle of roller-integrated continuous compaction control (CCC).

order to determine the stiffness of the ground. Accordingly, the drum of the vibratory roller is used as a measuring tool (Figure 1): Its motion behavior is recorded (A), analysed in a processor unit (B) where a dynamic compaction value is calculated, and visualised on a dial or on a display unit (C) where data can also be stored. Furthermore, an auxiliary sensor is necessary to determine the location of the roller (D). By means of GPS (Global Positioning System) the position of the roller can be located up to an accuracy of 5cm.

The dynamic compaction values have to be calibrated on the basis of conventional tests, e.g. compaction degree (D_{Pr}) or density ρ, or deformation modulus E_v. The main advantages of this control method are the following:

- Continuous control of the entire area;
- Results are already available during the compaction process, hence no hindering or delay of the construction work;
- Optimisation of the compaction work, including prevention of local over-compaction (which causes surface-near re-loosening of the layer);
- Full and permanent documentation of the entire area.

CCC possesses the essential advantage that the measuring equipment can be easily mounted on vibratory or oscillatory rollers (smooth rollers or sheep foot rollers). Experience has shown that the roller operators, site supervisors, etc. have very quickly familiarised themselves with this control method. Low quality rollers which provide only low compaction quality can be eliminated, and the documented data cannot be manipulated. CCC has proved suitable on many construction sites, and has therefore become obligatory for several years already in Austria: (mainly for federal roads and highways, but also for railways and clay liners of waste deposits, and for embankment dams).

Furthermore, the measuring depth of roller-integrated continuous compaction control is significantly larger than in the case of conventional methods: While density measurements commonly reach only a depth of 0.1 to 0.3m and standard load plate tests about 0.5 to 0.6m, CCC reaches to a depth of about 2.0m (and even more).

High quality compaction provides numerous advantages for fill dams (embankment dams):

- Increase in safety;
- Improvement of serviceability;
- Increase in life-time;
- Reduction of costs and maintenance;
- Reduction of construction time (especially in the case of roller-integrated continuous compaction control).

3 APPLIED THEORY OF CONTINUOUS COMPACTION CONTROL

The main components of the interaction system of CCC are the roller, the soil/fill layer to be compacted, and the recording system. The rollers may be vibratory or oscillatory ones, or Vario rollers with varying roller parameters. The following sub-chapters focus on vibratory rollers because these compaction equipment is dominating in practice.

3.1 *Vibratory roller*

Vibratory rollers are the mainly used rollers world-wide. They can be employed universally for a wide range of soil types and granular material. The drum of a vibratory roller is excited by a rotating excenter mass which is shafted on the drum axis (Figure 2). The rotating mass sets the drum in a circular translatoric motion, i.e. the direction of the resulting force is corresponding with the excenter position. Compaction is achieved mainly by transmitted compression waves in combination with the effective static drum load. Consequently, the maximum resulting compaction force is supposed to be almost vertical and in fact it is only a little inclined.

The vibratory roller is used both for compaction and as a measuring tool. Significant parameters are the total weight, the excitation frequency and the theoretical amplitude of the drum. Modern rollers are usually equipped with two frequencies and two amplitudes, so called “small amplitude” and “large amplitude”. During compaction and continuous compaction control the operation speed of the roller ranges between 2 and 6 km/h. All these parameters influence both progress of compaction work and CCC data. Comprehensive computer simulations and largescale field tests have disclosed that the drum of a vibratory roller operates in different conditions of motion depending on roller and soil parameters. These so called operating conditions influence the dynamic compaction values distinctively, and consequently, they have to be considered in relation to CCC-data. Five significant operating conditions were determined, they are specified in Table 1. Generally, soil stiffness influences the condition of drum operating, but roller parameters also contribute.

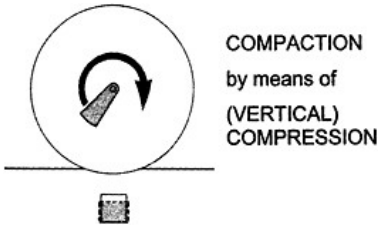

Figure 2. Excitation of a vibratory roller drum and dynamic compaction effect (compression).

Table 1. Operation modes of a vibratory roller drum.

Behavior of motion	Interaction drum-soil	Cycle*	Operating condition	Application of CCC	Soil stiffness
Periodic	Contact	1	Continuous contact	Yes	Low ↓ High
	Partial loss	1	Partial uplift	Yes	
	of contact	2(4)	Double jump	Yes	
		[2(4)]	Rocking motion	No	
Chaotic		–	Chaotic motion	No	

* Specified as a multiple of excitation cycle $T=2\pi/\omega_0$.

Continuous contact only occurs if the soil stiffness is very low, i.e. in the case of uncompacted or soft clayey layers. Partial uplift and double jump (Figure 3) are the most frequent operating conditions. The difference between these two operating conditions consists of the number of excitation cycles; consequently, the motion behavior of the drum repeats itself. When the soil stiffness increases further the motion of the drum axis is no more vertical, the drum starts rocking. Very high soil stiffness in combination with disadvantageous roller parameters can cause chaotic motion of the drum. In the case of rocking and chaotic drum motion the roller is not manoeuvrable any more. No proper compaction is possible then.

3.2 *Soil and other granular material*

Soil represents the second component of the interaction system roller-soil; its properties are determined by CCC. The field of CCC was originally limited to non-cohesive soils but has been widened for cohesive soils, stabilized soils and other granular media. The compaction of recycling material, waste products and of special concrete (RCC) can also be controlled by this method.

3.3 *Recording systems*

Two recording systems of CCC have been established in Europe:

- Compactometer of the Swedish company Geodynamik
- Terrameter of the American-German company Bomag

Both systems consist of a sensor containing one or two accelerometers attached to the bearing of the vibratory roller drum, a processor unit and a display to visualize the measured values. The

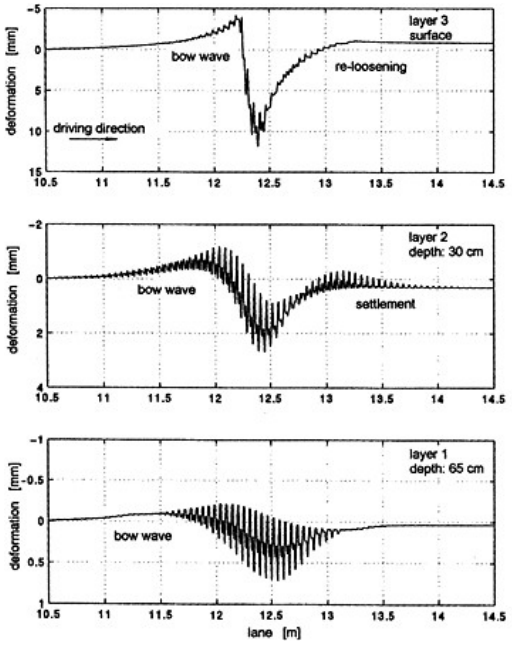

Figure 3. Soil deformation in three depths according to the impact of a vibratory roller drum operating in the condition “double jump”.

sensor continuously records the acceleration of the drum. The time history of the acceleration signal is analyzed in the processor unit in order to determine dynamic compaction values with regard to specified roller parameters. The dynamic compaction values are designated as CMV and OMEGA.

The Compactometer Value (CMV) is calculated by dividing the amplitude of the first harmonic of the acceleration signal by the amplitude of the exciting frequency Former empirical investigations have revealed that the amount of the first harmonic increases with increasing soil stiffness. Moreover, an auxiliary value was created in order to take into consideration the operation conditions of the drum. The Resonant Meter Value (RMV) is calculated by dividing the amplitude of the half frequency of the acceleration signal by the amplitude of the exciting frequency:

$$CMV \sim \frac{\hat{a}(2\omega_0)}{\hat{a}(\omega_0)}, \quad RMV \sim \frac{\hat{a}(0{,}5\omega_0)}{\hat{a}(\omega_0)} \qquad (1), (2)$$

If RMV is different from zero the operation mode of the drum is that of double jump.

The CCC-technique based on the Terrameter calculates the energy absorbed by the soil. The acceleration of the drum $\vec{F}_E$ the energy W_{eff} is calculated as follows:

$$OMEGA \sim W_{eff} = \oint_{2T} \left[-(m_D + m_E)\ddot{\vec{z}}_1 + \vec{F}_{stat} + \vec{F}_E \right] \dot{\vec{z}}_1 dt \qquad (3)$$

The integration is performed by two cycles of excitation in order to take the operating condition of double jump into account.

The operating conditions continuous contact, partial uplift and double jump with a one-degree-of-freedom interaction system can be described theoretically. The operating conditions as rocking motion and chaotic motion require a complicated multi-degree-of-freedom system. Dynamic compaction values are presented as a function of the dynamic shear modulus in Figure 4. An increasing shear modulus causes a change of drum operating. The operating condition influences the dynamic

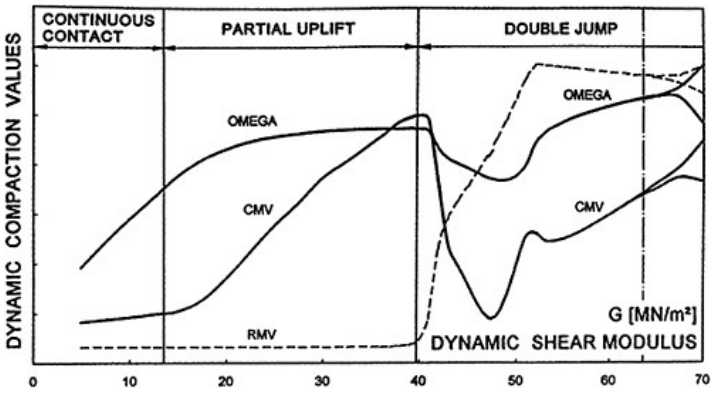

Figure 4. Dynamic compaction values OMEGA, CMV, RMV versus dynamic shear modulus.

compaction values significantly. Therefore, the particular operating condition has to be recorded in practice in order to correctly interpret the dynamic compaction values.

4 DYNAMIC INTERACTION BETWEEN VIBRATORY ROLLER AND SOIL: COMPUTER SIMULATIONS

The behavior of vibratory rollers is investigated by computer simulations in order to determine the motion behavior of the roller-soil-interaction. The substructure method is used. In a first step, soil and roller are treated separately, in a second step these two systems are combined by means of compatibility requirements. The elastic part of the soil is described by a physical cone representing the homogeneous elastic halfspace. The plastic contact zone is described separately for non-cohesive soils.

Interaction vibratory roller—non-cohesive soil

The model is described taking into account the elastic behavior of soil in the far field, elastic plastic properties of the contact zone and the most important roller parameters influencing the system.

As a first approximation, unlayered soil may be idealized as a homogeneous, linearly elastic halfspace with a mass density ρ. Neglecting material damping, the stress-strain relationship is described by two independent elastic constants. In soil dynamics it is useful to specify the shear modulus G and the *Poisson's* ratio ν. The conventional solution of the elastic halfspace is sophisticated and specified by the propagation velocities c_s of shear waves, c_p of dilatational waves and c_R of *Rayleigh* waves representing surface waves. The three-dimensional elastic half space can be physically idealized by a truncated semi-infinite elastic cone with its own apex height ζ_0 (Figure 5).

The part of the halfspace located outside the cone was found to be of no relevance and therefore is disregarded. Already *Wolf* [8] has shown that the one-dimensional translational cone represents the vertically loaded halfspace with sufficient accuracy. The dynamic force-displacement relationship of the elastic cone can be written in unified form:

$$F_0 = K\, z_0 + C\, \dot{z}_0 \tag{4}$$

with the spring coefficient K and the dashpot term C for a rectangular load area:

$$K = G b_0 \frac{1}{1-\nu}\left[3{,}1\left(\frac{a_0}{b_0}\right)^{0{,}75} + 1{,}6\right], \quad C = 4\sqrt{2\rho\, G \frac{1-\nu}{1-2\nu}\, a_0 b_0} \tag{5),(6)}$$

K and C depend on the elastic parameters of the soil and on the dimensions of the rectangular area. Consequently, they are not constant because the width $2b_0$ of the contact area changes with penetration of the smooth cylindrical drum into the soil.

Non-cohesive not saturated soils exhibit a *Poisson's* ratio of 0.25 to 0.35. This coincides with the limit of validity of the predescribed formulation which is limited to compressible soil ($\nu \leq 1/3$). The effective dynamic shear modulus G influences the elastic properties of non-cohesive soil mostly. The determination of G is difficult because its quantity depends strongly on the amplitude of the shear strains. Large shear strains occur in the contact zone between drum and soil. This fact causes plastic deformations and even effects of soil liquefaction. These distinctive elastic plastic effects are responsible for soil compaction. In the contact zone the elastic theory is no more sufficient to describe the behavior of the soil correctly.

A plastic zone is embedded within the contact area of the elastic soil. In accordance to *St. Venant*'s principle, the dimensions of the elastic contact area correspond to the dimensions of the surface load area ($a=a_0$, $b=b_0$, $A=A_0$) and consequently, equilibrium provides equal contact and elastic forces ($F=F_0$). The total elastic plastic deformation z_1 consists of the fictive elastic displacement z_0 and the plastic deformation z^p (Figure 6).

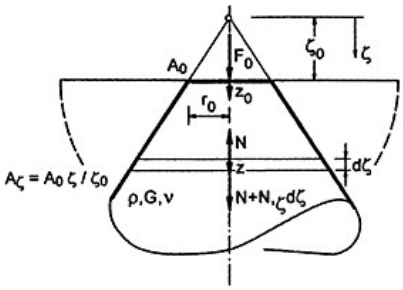

Figure 5. Translational cone for vertical motion.

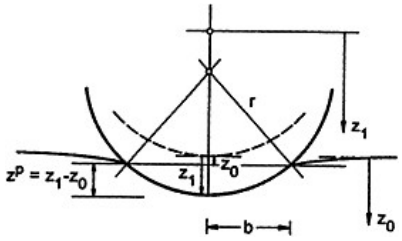

Figure 6. Elastic-plastic deformations of soil during compaction.

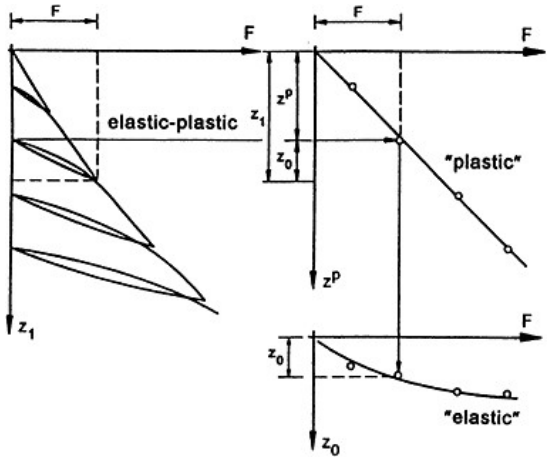

Figure 7. Elastic and plastic portion of soil deformation.

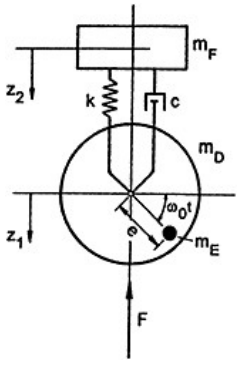

Figure 8. Two-degree-of freedom (2DOF) system describes a vibratory roller.

Plastic deformations are small in relation to the radius of the drum. Due to this fact the cylindrically curved drum can be approximated sufficiently by a parabolic cylinder. Thus, plastic deformation is related to the square of the contact width of the drum. Moreover, a constitutive relation between contact force and plastic deformation has to be determined. The soil drum interaction is considered to be a modified form of bearing capacity problem. The bearing capacity N_B is calculated multiplying the bearing pressure σ_B by the contact area A. During loading plastic deformation are caused at each time, thus bearing capacity is equal to the applied contact force $(F=N_B)$, whereby a constant plastic parameter k^p is introduced:

$$F=k^p z^p=k^p(z_1-z_0) \tag{7}$$

The plastic constitutive equilibrium is built up paradoxically like a linear elastic constitutive relation. This fact is justified considering the geometry of the cylindrically curved drum. The plastic constitutive relation is only valid for loading. During unloading, only elastic effects occur in the soil. Model tests were performed to verify the elastic-plastic behavior of unbound soil loaded by a cylindrically curved drum. The elastic and plastic portion of soil deformation was determined punctually (Figure 7). This procedure represents an approximation but it yields excellent results.

The plastic deformations are linear according to the theory of shear failure, whereas the elastic deformations are non-linear. This behavior corresponds to the spring coefficient K representing the elastic soil stiffness obtained theoretically in equation (11).

In a next step the modeling of the vibratory roller is specified. The consideration of the vertical component provides sufficiently accurate results relating to the effects of CCC. This assumption was confirmed by numerous large-scale field tests.

A vibratory roller can be described by a two-degrees-of-freedom system (Figure 8). The motion of the roller is assumed to be defined by displacements of the drum and the part of the roller frame influencing the drum. The roller drum is connected to the frame with low-damped spring elements. They are designed in such a way that the amplitude of the frame displacement is small compared with the displacement amplitude of the drum. Moreover, the resonance frequencies of the frame are adjusted so that they do not correspond to a multiple of an integer number of the excitation frequency. Consequently, the motion of the frame can be neglected; static forces of the frame are transmitted only to the drum and furthermore into the soil.

Thus the roller is simplified to a one-degree-of-freedom (SDOF) system described as follows:

$$(m_D + m_E)\ddot{z}_1 = (m_F + m_D + m_E)g + m_E e\omega_0^2 \sin\omega_0 t - F \tag{8}$$

The interaction between the drum and the soil is determined by combining the components of soil (equations (4) and (7)) and roller (equation (8)) and by means of the compatibility requirements. Taking into account that tensions cannot be transferred between drum and soil, loss of contact must be possible in the model. Moreover, the soil-drum system passes varying phases during operation. Three different states are possible:

- Loading causes elastic-plastic deformations of soil. This state is defined by contact ($F>0$) and by an increasing soil contact force ($\Delta F>0$). Combining the equations (4), (7) and (8) provides:

$$(m_D + m_E)\varepsilon\frac{C}{k^p}\dddot{z}_1 + (m_D + m_E)\ddot{z}_1 + \varepsilon\ C\ \dot{z}_1 + \varepsilon\ K\ z_1 = p + \dot{p}\ \varepsilon\frac{C}{k^p} - \varepsilon\ K\ z_1^e \tag{9}$$

where

$$p = (m_F + m_D + m_E)g + m_E e\omega_0^2 \sin\omega_0 t \tag{10}$$

denotes the static and excitation force and z_1^e is introduced. A factor of importance is the so called plasticity parameter ε specified as:

$$\varepsilon = \frac{k^p}{K + k^p} \tag{11}$$

The plasticity parameter may assume values between 0 and 1. Ideal elastic behavior is obtained by the upper limit $\varepsilon=1$ since $k^p \to \infty$. No soil resistance may be expected if the lower limit $\varepsilon=0$ takes place because $k^p=0$. Virtually, it may be assumed that the drum is in air.

- Unloading causes only elastic deformations. This state is defined by contact ($F>0$) and by a decreasing soil contact force ($\Delta F\leq 0$). As mentioned before, perfectly elastic behavior is described by equation (9) with $\varepsilon=0$. Equation (9) is simplified and reformulated as:

$$(m_D + m_E)\ddot{z}_1 + C\ \dot{z}_1 + K\ z_1 = p \tag{12}$$

- The so called air phase is characterized by loss of contact ($F=0$) between drum and soil. This state may occur if the excitation of the drum is high or the soil is not too soft. Drum and soil

move independently of each other. Motion behavior of the drum is also described by equation (9) with ε=0, unloaded soil follows equation (4):

$$(m_D + m_E)\ddot{z}_1 = p\,, \quad C\,\dot{z}_0 + K\,z_0 = 0 \tag{13), (14}$$

Equation (9) is valid universally, nevertheless initial conditions must be set at the beginning of each phase because ε changes. The initial conditions are defined by final data of displacements and their derivations of the preceding phase.

5 DYNAMIC INTERACTION BETWEEN ROLLER AND SOIL: LARGE-SCALE FIELD TESTS

Comprehensive large-scale field tests were performed in order to investigate the motion behavior of the drum on layered soil. Specifically, the accelerations of drum and roller frame, and the location of the rotating mass were measured. Influence functions of three-axial accelerations, soil pressure and both dynamical deformations and static settlements in three different depths of soil were determined. For that purpose, acceleration cells, earth pressure cells, and inductive displacement transducers were designed and constructed. By means of the dynamic excitation a measurement frequency of 1200 Hz was necessary in order to achieve reliable results. The recording units of roller and soil had to be separated. A radio remote control unit was developed in order to start the measurement simultaneously and control the correspondence of data. Furthermore, the vibratory roller (Bomag BW 213 D) was equipped with the systems of Compactometer and Terrameter.

Progress of vertical drum accelerations taking into account the contribution of gravity (1) and the excitation acceleration (2) is shown in Figure 9. Reformulation of equation (8) results in:

$$\underbrace{\ddot{z}_1 - (1 + \frac{m_F}{m_D + m_E})g}_{1} \underbrace{- \frac{m_E}{m_D + m_E} e\omega_0^2 \sin\omega_0 t}_{2} = -\frac{F}{m_D + m_E} \tag{15}$$

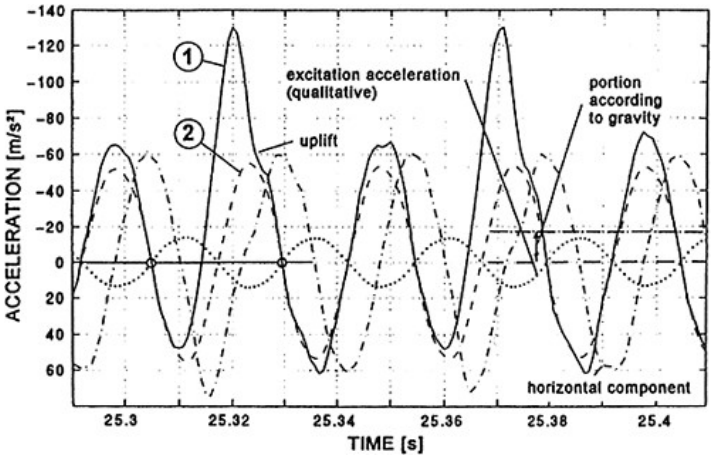

Figure 9. Motion of roller drum.

It is obvious that the drum is in air as soon as the right side of equation (15) becomes zero because the contact force disappears. Thus, contact phase and air phase can be made out easily in Figure 9. Furthermore, the operating condition of double jump can be seen because the acceleration signals of the drum repeat themselves every second cycle.

Acceleration signals are analyzed in frequency domain in order to calculate CMV and in time domain. Velocity and displacement of the drum are calculated from the measured accelerations. Soil reaction force and energy absorbed by the soil are computed taking into consideration roller parameters. The area inside the self-contained curve of the force displacement relationship represents the energy absorbed by the soil which is related to OMEGA.

Figure 10 shows an example of comparative CMV and OMEGA values over a lane of 20m. CMV and OMEGA correspond excellently if taking into account a linear transformation between these values. However, this conformity is valid only for values within the particular operation mode. If the values are not transformed a discrepancy is unavoidable which pretends different results of the control systems (Figure 4) that actually don't exist.

6 OSCILLATORY AND VARIO ROLLERS

6.1 *Oscillatory roller*

The drum of an oscillatory roller oscillates torsionally. The torsional motion is caused by two opposite rotating excenter masses, which shafts are arranged excentrically to the axis of the drum. Thus, soil is loaded horizontally in addition to the vertical static dead load of the drum and the contributing roller frame. These cyclic and dynamic horizontal forces result in additional soil shear deformation; dynamic compaction is achieved mainly by transmitted shear waves (Figure 11).

Investigations have revealed that oscillatory rollers operate in two conditions depending on roller and soil parameters. If the force exceeds the friction force (incl. the adhesion) between drum and soil the drum starts slipping. While slipping the compaction effect is reduced, however, the surface is "sealed" by the slip motion [5]. Consequently, oscillatory rollers are mainly employed for asphalt compaction and cohesive material. Furthermore, oscillatory rollers are used in the vicinity of sensitive structures, because the emitted vibrations are significantly lower than those of vibratory rollers.

6.2 *Vario roller*

The Vario roller is a development of the Bomag company. In a Vario roller two counter-rotating exciter masses, which are concentrically shafted on the axis of the drum, cause a directed vibration.

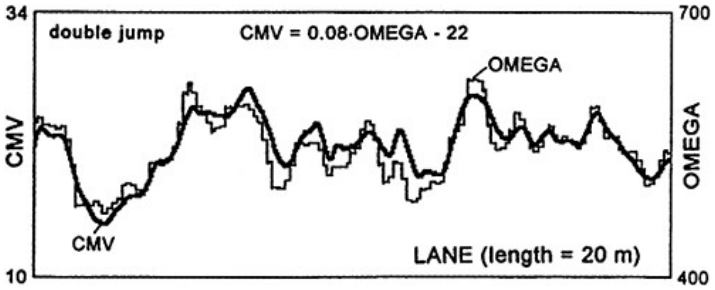

Figure 10. Excellent correlation between dynamic compaction values CMV and OMEGA.

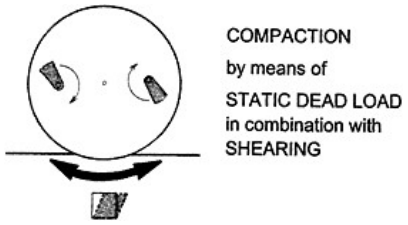

Figure 11. Excitation of an oscillatory roller drum and dynamic compaction effect (shearing).

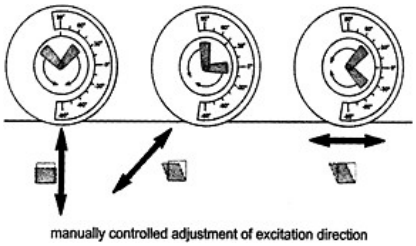

Figure 12. Adjustable excitation direction of a Vario roller drum and specific compaction effect.

The direction of excitation can be adjusted by turning the complete exciter unit in order to optimise the compaction effect for the respective soil type (Figure 12). If the exciter direction is (almost) vertical or inclined, the compaction effect of a Vario roller can be compared with that of a vibratory roller. However, if the exciter direction is horizontal, the Vario roller compacts soil like an oscillatory roller, although the motion behavior of the drum is different. The shear deformation of soil is caused by a horizontally translatoric motion, whereas the drum of an oscillatory roller is working torsionally. Thus, a Vario roller can be used both for dynamic compression compaction (like a vibratory roller), for dynamic shear compaction (like an oscillatory roller), and a combination of these two possibilities, depending only on the adjustable force direction (Figure 13). Consequently, Vario rollers can be employed universally for each soil type, the respective optimum direction can be found by basic investigations on a test field on site.

6.3 *Vario control roller*

Based on the findings relating to the ways of operating of different dynamic rollers, the Bomag company developed the first automatically controlled so called Vario Control roller. In this roller type the direction of excitation (vibrations can be directed infinitely from the vertical to the horizontal direction) is controlled automatically by using defined control criteria, which allow an optimised compaction process and, consequently, a highly uniform compaction (Figure 14). The control criteria are explained in the following [5]:

- *Operating criterion*
  If the drum passes to the operating condition double jump, the excitation direction is immediately changed, so that the operating condition partial uplift is kept.
- *Force criterion*
  If the specified maximum compaction force is reached, the excitation direction is changed by the automatic control system, so that the applied force does not exceed the maximum force.

Two accelerometers, which are mounted on the bearing of the drum, record the dynamic motion behavior continuously. Soil contact force, energy delivered to soil, displacements, etc. are calculated in a processor unit taking into consideration the roller parameters like masses, exciter force and frequency, etc. The data are transmitted to an integrated control system, where the setting of the parameters is managed automatically.

Following significant benefits of Vario control rollers have been revealed by practical application:

- Uniform compaction by continuous adjustment of force direction
- Optimised compaction combined with less roller passes
- Prevention of over-compaction and re-loosenings
- Improved compaction both in deeper layers and on surface
- Reduction of lateral vibrations in the vicinity of sensitive structures.

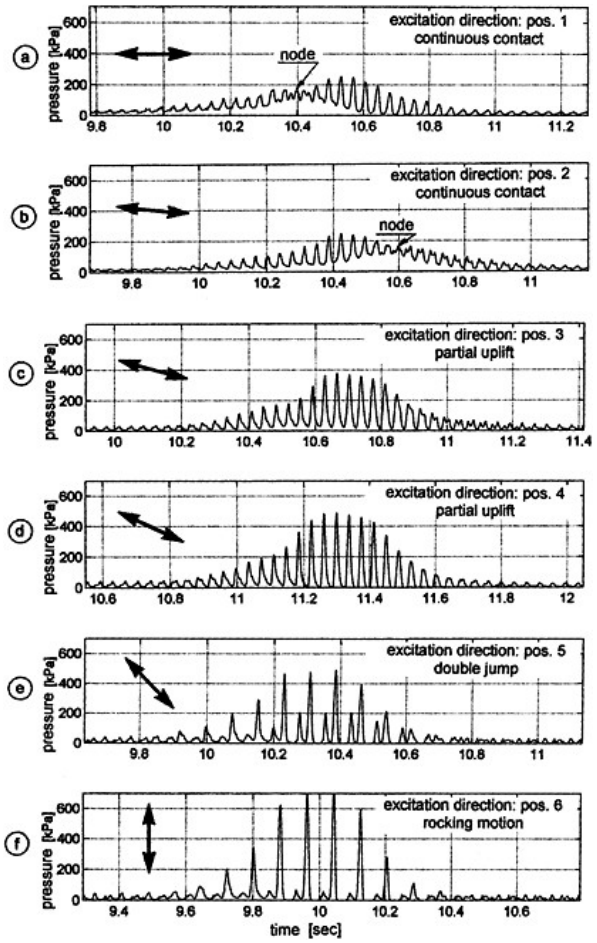

Figure 13. Soil pressure and operating condition depending on the exciter direction of a Vario drum.

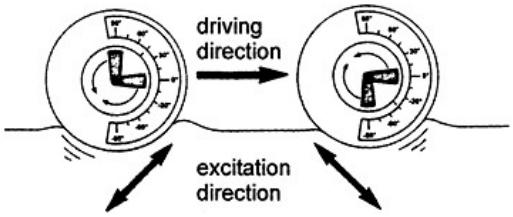

Figure 14. Direction of inclination for optimum compaction taking into account the driving direction.

Vario Control rollers are, therefore, especially suitable for zoned fill dams. The soil characteristics of such dams vary significantly for cohesive core, transition zone fill, outer zone fill, and shoulder fill material.

7 CCC AND STATISTICAL CRITERIA

Quality assurance and the results of risk analyses are strongly influenced by the method of statistical quality control. Figure 15 shows various selection procedures of spot checking:

Selection by an assumed grid (1) is the simplest method but does not provide a statistically comparable interpretation for zones with higher or lower quality. Random selection (2) makes a reduction of the test number possible without lowering the quality of result. Selection by subjective criteria (3) ("appearance") is a rather strict method ("weak point checking"), but the results and the quality of similar test fields cannot be compared. Subjective selection of the control points can be improved by using objective auxiliary criteria (4) (e.g. proof rolling). This leads to a further reduction of the standard deviation, as indicated in Figure 15.

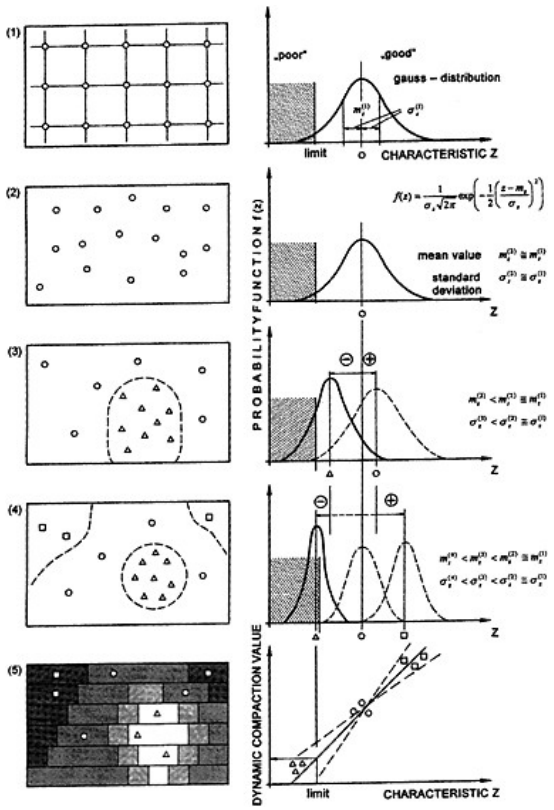

Figure 15. Statistical quality control. Different selection procedures of spot checking. (1) grid, (2) random selection, (3) subjective selection, (4) subjective selection using auxiliary criteria, (5) selection and correlation to continuous methods.

Conventional spot checking only provides punctual results, whereas continuous control represents a significant improvement. Figure 15(5) illustrates this for roller-integrated continuous compaction control (CCC). This technique also involves new statistical criteria because the uniformity of the compacted layer as well as the increase in compaction degree during subsequent roller passes are recorded. Mean value, max. and min. value, standard deviation, and increase of the compaction values represent relevant parameters. Moreover, the "minimum quantile" can be used as soon as sufficient experience with CCC is gained.

Hitherto used statistical parameters do not allow the assessment of the distribution of control data within a section: The plots indicated in Figure 16 have the same mean value, max. and min. value, and standard deviation. Nevertheless, they exhibit different qualities. Figure 16(1) shows only a limited weak zone which can easily be improved, whereas the area of Figure 16(2) requires comprehensive measures to achieve a sufficient and homogeneous quality.

To statistically judge the distribution of control values within a defined area, the statistical methods of "variography" and "Kriging" can be used. These methodologies were originally developed in order to interpret geophysical data and seem to be a useful tool to improve the quality assurance of compacted layers, hence of roads, highways, railways, airfields, embankments, earthand rockfill-dams and other soil structures, and of roller-compacted concrete dams.

The dynamic compaction values are relative values having a clear physical background. If the data shall be compared with common conventional values like the deformation modulus of the static load plate test or the soil density calibrations have to be performed. There are several possibilities to select the spots where conventional tests can be carried out. Best correlation can be achieved if the spots are selected by means of CCC-results. Spots with high, intermediate, and low dynamic compaction values indicate a wide range of soil properties. Nevertheless, different operating conditions have to be taken into account; otherwise completely irrelevant regression lines are determined (Figure 17).

Furthermore, the different capacity of measuring depth of CCC and the conventional test methods must be considered. Generally, the measuring depth of CCC (depending on the total roller weight) is significantly larger than the compaction depth and the measuring depth of common spot tests. Thus, soft soils in deeper layers can be detected with CCC which is not possible with conventional tests.

Figure 18 shows a typical CCC-result as an example involving several control data which have proved in practice. The information provided is used to set up the following control criteria:

- Minimum value in order to locate weak spots and areas.
- Maximum value in order to locate areas with highest soil stiffness.
- Mean value in order to assess the general condition of the checked area.
- Standard deviation in order to assess the uniformity of the checked area.
- Increase of the dynamic compaction value in order to point out the further compactability.
- Decrease of the dynamic compaction values as indication for loosening and/or grain crushing.

The use of CCC for acceptance testing requires contractual limits for minimum, maximum and mean values. These can be set up by conducting correlation tests. Extensive investigations and

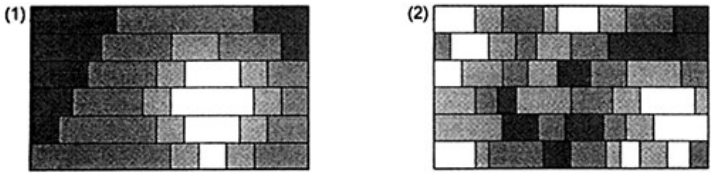

Figure 16. Control plots of compacted zones with the same statistical characteristics. Schematic. The strips indicate the roller lanes (tracks), controlled with CCC. Statistical evaluation can be improved with "variography" or "Kriging".

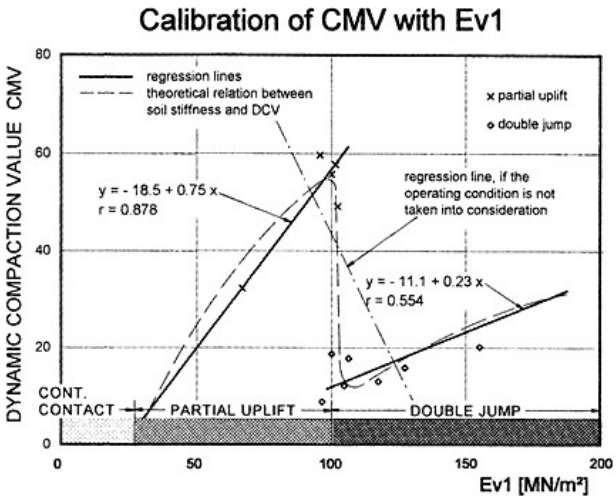

Figure 17. Correlation between modulus E_{v1} (from first loading of static load plate test) and dynamic compaction value CMV taking into account operating conditions.

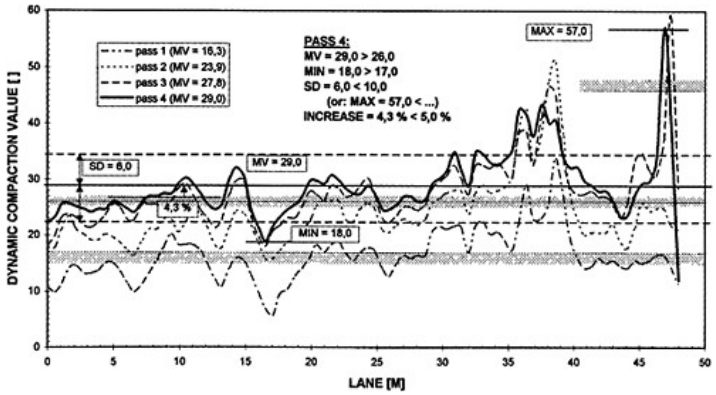

Figure 18. Progress of CCC-data and CCC-criteria: MV—mean value, MIN—minimum value, MAX—maximum value, SD—standard deviation, INCREASE—increase between two roller passes.

practical site experience have revealed that the standard deviation should not be >20% (related to the mean value), the increase of dynamic compaction values between two passes <5%.

8 QUALITY CONTROL OF OLD DAM CRESTS

Overflow and wave overtopping belong to the most critical failure modes of fill dams. Hence, the crown zone is the most critical part, and a long-term deterioration may reduce essentially dam

stability. This happens mainly in flood protection dams along rivers. Repeated high floods near to the most probable events weaken the earth structure and eventually may cause local dam failure or even collapse of a flood defence system. During the catastrophic floods in central Europe in summer/autumn 2002 this could be observed on numerous sites. Consequently, risk assessment of existing dams which potentially were close to failure has been unavoidable regarding public safety etc. This has referred also to several emergency fills that were executed as rapid barriers during the flood, whereby their quality was of minor importance.

The quality of such fill dams can be checked by geophysical methods, soundings, boreholes/ piezometers and roller integrated continuous compaction control (CCC). CCC provided the most reliable data for the top zone (to a depth of about 2.5m). Figures 19, 20 show some results of dam sections which failed during the first flood maximum and were quickly refilled then before the second flood maximum arrived one week later. The weak points of the dam crest have not been visible in the field but were clearly documented by CCC. Furthermore, Figure 20 illustrates the post-compaction effect generated during the roller passes. The weakest point in Figure 20 could not be improved by compaction, because it was obviously situated in greater depth.

In order to achieve a sophisticated interpretation of the measurements correlations between the different test series were developed, whereby the different measuring depth of CCC, load plate tests, soundings and density measurements had to be considered. Otherwise, the correlations were rather uncertain and hardly useful for practical purposes. Furthermore, local anomalies (from a geotechnical point of view) were statistically eliminated. The Figures 21, 22 show two correlations as examples. The conclusion drawn from several dam sections is to rely rather on CCC compaction values for the crest zone, and on soundings and geophysical investigations for deep dam zones. But CCC is not appropriate if the dam crown is covered by a concrete pavement or a rather thick asphalt layer—unless this cover is removed for dam heightening (whereby a plane control surface has to be created).

Roller-integrated continuous compaction control is, therefore, very suitable for fill upgrading and heightening old fill dams. This refers not only to the crown zone but also to additional slope fills. Furthermore, high and uniform compaction of the top zone reduces the "siphoning" in fill dams. This phenomenon was already described by *Terzaghi* as the flow around the compacted core of a dam due to flow in the unsaturated zone, if the elevation above free water level ΔH is smaller than the height of capillary rise of the more permeable fill material (h_c)—Figure 23a. A similar siphon effect takes place in homogeneous earth dams, as shown in Figure 23b: The water percolates through the dam not only below the theoretical line of full saturation but also within the zone of capillary. In both cases the loss of water due to the siphon effect can be rather important, depending on the relationship between suction and water content, and between degree of saturation and coefficient of hydraulic conductivity of a soil. The latter can be significantly reduced by intensive compaction based on roller-integrated continuous compaction control.

9 CCC FOR ROLLER-COMPACTED CONCRETE DAMS

Roller-compacted concrete dams (RCC dams) are constructed in layers compacted with conventional rollers. Interruption of work has to be minimised to facilitate bonding of the layers. Consequently, RCC dams should be constructed continuously (24 hours per day) to avoid joints. Otherwise the connected surfaces require mortar which means more cost associated with it. A roller-compacted concrete dam is less expensive than a conventional concrete dam, and it can be built in one-third to half the time of that. Furthermore, it requires smaller volume than an earth-or rock-fill dam, and it is inherently safer against inner erosion, overtopping, and seismic ground motion.

The concrete of RCC dams is a drier mix than conventional; the non-flowable mix is stiff enough to be compacted by vibratory rollers. The amount of cement can be reduced by adding fly ash, and the strength of the compacted dam increases with age. A RCC dam needs neither forms nor

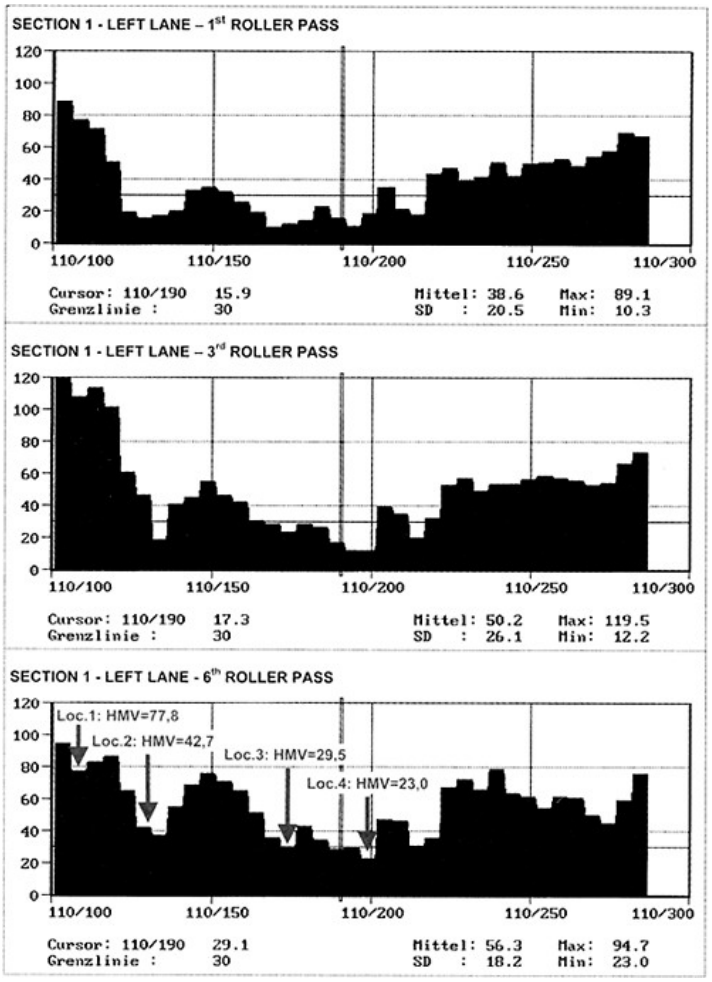

Figure 19. Results of roller integrated continuous compaction control (CCC) in Section 1 of a flood protection dam that failed and was refilled in an emergency action during the catastrophic flood in 2002 in Austria. Heterogeneous quality, weak points and somewhat improving compaction degree after six roller passes clearly visible. Grenzlinie=border line; Mittel=mean value.

finishing, nor does it contain dowels or steel reinforcement. Gate structures and intakes should be located outside the dam mass. Galleries, adits, and other internal openings should be minimized.

The thickness of the placement layers depends on the compaction equipment and concrete properties, typically ranging from 0.2 to 0.6m. A dam consisting of roller-compacted concrete

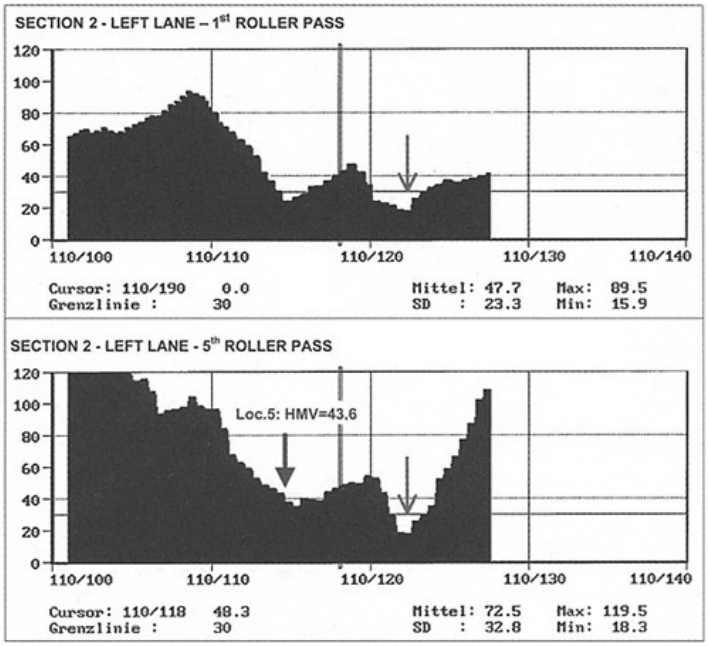

Figure 20. Like Fig. 19, but for Section 2 and different electronic resolving of measured data.

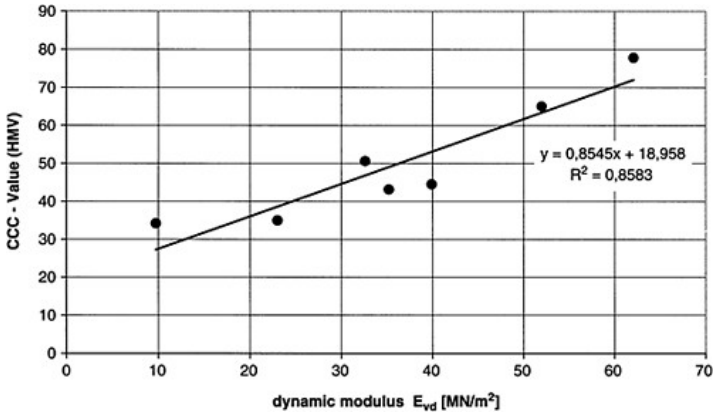

Figure 21. Dynamic compaction value (HMV) versus dynamic modulus *(E_{vd})* from dynamic load plate tests (light falling weight device) on the crown of a refilled dam (to Fig. 19, 20).

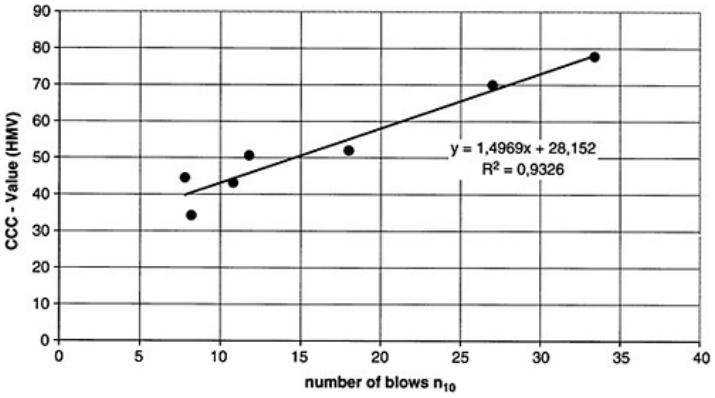

Figure 22. Dynamic compaction value (HMV) versus mean value of blows with heavy sounding (n_{10}) over a depth of 0 to 2.5m. To Fig. 19, 20 (refilled dam).

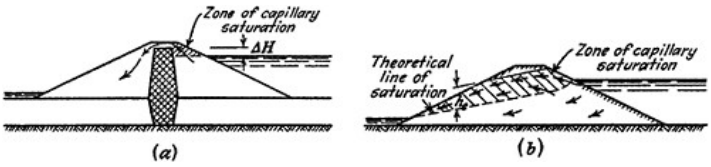

Figure 23. Capillary flow of water out of a reservoir through soil located above a watertight core (a), and (b) the theoretical line of saturation in a homogeneous earth dam [7]. ΔH=elevation above free water level; h_c=height of capillary rise.

which was properly proportioned, mixed, placed and compacted should be as impermeable as conventional concrete dams. Experience has shown that roller-integrated continuous compaction control (involving continuous compaction optimisation) provides highest quality and reduces the construction time compared to conventional spot checking. Moreover, correlations between hydraulic conductivity and dynamic compaction value (Figure 24) allow a first assessment of watertightness. Additionally, the joints between the concrete lifts and interface with structural elements should be treated most carefully because they are the major pathways for potential seepage through the RCC dam.

Roller-integrated continuous compaction control (CCC) can be applied to roller-compacted concrete dams in the same way like to earth- or rock-fill dams (embankment dams). There is no difference in technology, equipment or interpretation system. CCC has also proved suitable for fly ash and several other recycling products or waste material that is used for embankments, liners etc. [3].

CCC should be calibrated on the site using conventional tests and the dynamic load plate test. A test field is recommended for great projects; this may be helpful also for optimising the mix design, the compaction procedure (including roller parameters) and the lift heights. Furthermore, site-specific correlations between conventional compaction degree (e.g. referring to Proctor values, load plate moduli), strength properties (compressive, tensile) and dynamic compaction values (from CCC) should be developed. Before that, the strength properties and compactibility of

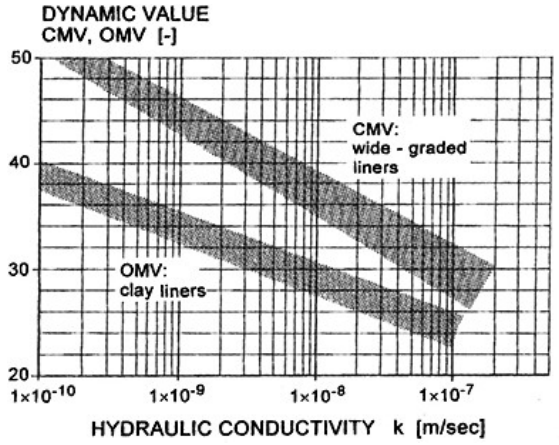

Figure 24. In-situ permeability control of low permeable soil for the core and transition zone of a fill dam (silty clay to wide-graded silty sandy gravel) by means of roller-integrated continuous compaction control. Examples of correlations between the dynamic compaction values CMV or OMV, and the hydraulic conductivity coefficient k.

the concrete should be investigated on preliminary mixes in the laboratory. The compactibility of the RCC granular skeleton should be maximised by optimising the proportions of the various size grading categories (gravel, sand, cement, mineral admixtures). Otherwise densification of the material remains incomplete—which can be registered in-situ by CCC.

CCC is the only method that checks continuously intensity and uniformity of roller-compacted concrete already during compaction. Uniformity cannot be checked by spot or random testing but is essential for the tensile strength capacity of the dam. In earthquake zones tensile stress is the most critical design variable of RCC dams. Potential failures are triggered by weak points or small zone which were not detected by conventional control during construction. Consequently, roller-integrated continuous compaction control provides an essential increase in dam reliability and safety.

10 CCC FOR SLOPED FILL SURFACES AND ASPHALT LAYERS

CCC is also possible on sloped fill surfaces, hence to optimise and control the peripheral zones of an earth or rock fill dam. The maximum allowable slope angle depends on the roller type. If the limit for self-propelled rollers is exceeded, pulling by a machinery on the dam crest is required. This makes the operation of CCC possible up to a slope angle of about β=2:3. The practical limit is set when the roller starts slipping to such an extent that measurement and interpretation provide questionable data.

The possibility to use the CCC-technology also for slopes widens its application for slope-parallel surface sealings of dams, e.g. clay liners or asphalt covers. In such cases oscillating compaction provides better results than a vibrating one. This requires a special roller type, whereby the Vario roller has proved especially successful. This innovative roller changes automatically the roller parameters during the compaction procedure, depending on the registered interaction between fill material and roller. Hence it adapts frequency, amplitude, compaction speed, and magnitude and inlination of the dynamic force to the locally measured data. This means that such rollers can continually and in an infinetely variable manner change from vibration to oscillation and vice versa (Figure 8).

11 COMPACTION CONTROL UNDER CONFINED CONDITIONS—DYNAMIC LOAD PLATE TESTING

11.1 *General*

Structural elements which have to be constructed within a fill dam (monitoring gallery, outlet etc.) make intensive compaction and its control locally more difficult. Confined conditions require small compaction equipment and small device for compaction control. CCC is not possible then and—in many cases—neither conventional load plate testing. Density measurements can be conducted but don't provide information on the stress-deformation behavior of the fill. Long-term research and experience have disclosed that the dynamic load plate test (Light Falling Weight Device Test) provides most reliable results if properly conducted with an appropriate test device. This prerequisite should be emphasized because there exist numerous devices and test interpretation methods which are rather unsuitable.

The dynamic load plate test in the form of the Light Falling Weight Device (LFWD) was developed as a testing device to determine the dynamic deformation modulus of soils and other granular materials. There exist good correlations between the dynamic E_{vd} and the CCC values because both control methods are based on dynamic soil response. Therefore, the dynamic load plate test is very suitable for compaction control under confined conditions.

The components of the Light Falling Weight Device are illustrated in Figure 25. An impact-like loading is applied to the soil via a circular steel plate, which is assumed to be inelastic. The loading device necessary for this purpose consists of a falling weight. After being released the falling weight slides down along a guide rod and hits a spring-damper-element (made of steel or a synthetic material). The loading device rests on a centring ball in the centre of the loading plate. Thus, solely compression forces can be transferred onto the loading plate. A sensor is installed in the centre of the loading plate and connected to an electronic measuring device. Hence, the plate motions can be determined during the test execution.

The evaluation procedure is based on a very simple principle. After the test execution the measured accelerations or velocities are integrated twice or once, respectively, thus providing the

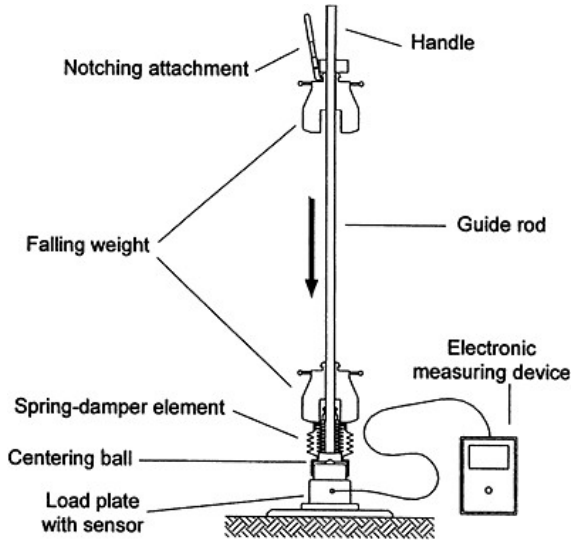

Figure 25. Components of the Light Falling Weight Device (LFWD).

(maximum) plate deflection. All other parameters required for the determination of the dynamic deformation modulus are assumed to be constant. This approximation has shown to be reasonable. The tuning of the device parameters and the characteristic values of the subsoil to be expected result in the approximation to be valid.

11.2 *Testing standards and evaluation of dynamic load plate tests*

Essential part of the technical testing standard are specifications regarding the calibration of the device. The device has to be calibrated before shipment, after repairs and at least once a year by a certified institution: The loading device (maximum impact force) is calibrated by adjusting the falling height. Devices equipped with disc springs (made of steel) can also be calibrated by adjusting the prestressing of the spring-element. The deflection measuring device has to be calibrated for the measuring range of the deflection amplitudes stated in the table below using the already calibrated loading device. Furthermore, the deflection measuring device has to be checked with a simplified procedure by the user within regular time intervals. Table 2 summarizes the most important data of tried and tested, highly proven device parameters.

The plate has to be placed in a level position on the ground and frictionally connected to it (full contact). Sometimes, a thin layer of sand has to be applied below the loading plate in order to level out the testing surface. Three preloading impacts have to be carried out to obtain full contact between the loading plate and the ground. Subsequently, three measuring impacts have to be carried out analogously. The plate motions are recorded by means of the electronic measuring device during the execution of these measuring impacts. The average value of the three maximum vertical plate deflections (indicated with "settlement *s*" in the German testing standard) is used to determine the dynamic deformation modulus E_{vd}. Two simplifying assumptions are made when evaluating the test.

The dynamic load plate test is evaluated on the basis of the equation for the static load plate test, which is based on the theory of the elastic halfspace under static load (Figure 26):

$$E_v = 1.5\, r \frac{\Delta\sigma}{\Delta z} \tag{16}$$

Velocity-dependent terms and forces of inertia are not taken into account when evaluating the test due to this simplified consideration.

Table 2. Standardised test execution and evaluation of the dynamic load plate test.

Load plate made of steel, steel quality at least St 52–3 (tolerances for device dimensions 1%)	
Diameter	300mm
Plate thickness	20mm or
	17mm with 15mm reinforcing plate Ø 150mm
Mass	15 kg±0.25 kg (incl. deflection measuring device, handles)
Roughness	max. 6.3 µm
Deflection measuring device	
Frequency range	8–100 Hz (measuring error max. 2%, temperature from 0°C to 40°C)
Deflection amplitude	0.2–1.0mm measuring accuracy at least ±0.02mm
	1.0–2.0mm measuring accuracy at least ±%
Loading device	
Mass falling weight	10 kg±0.1 kg
Total mass guide rod	5 kg±0.25 kg (incl. spring-damper-element)
Maximum impact force	7.07 kN (tolerance 1%, temperature from 0°C to 40°C)
Impact duration	18 ms±2 ms

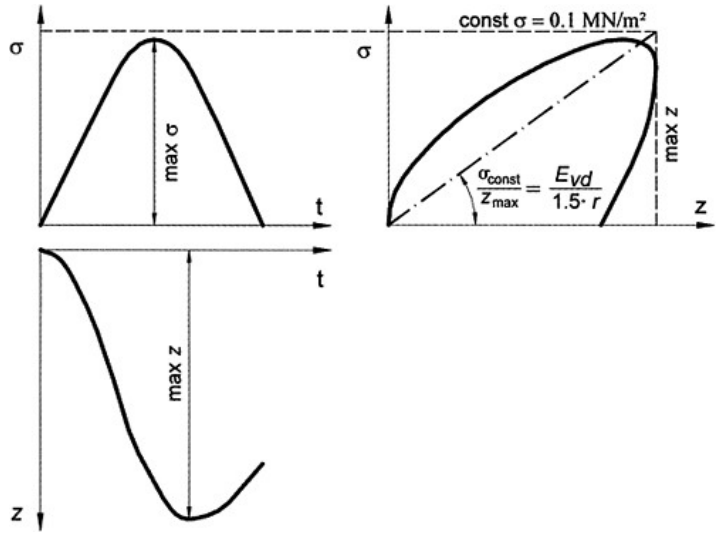

Figure 26. Soil stress, deflection and force-displacement-relation for the dynamic load plate test with the Light Falling Weight Device (LFWD).

Moreover, the maximum average soil stress δ occurring during the test execution is hypothetically assumed to be constant (0.1 MN/m^2). Thus, equation (16) degenerates to following expression for the dynamic deformation modulus for a load plate with a diameter of 300mm:

$$E_{vd}[MN/m^2] = \frac{22.5}{z_{max}[mm]} \tag{17}$$

Therefore, the measured maximum deflection z_{max} is sufficient to determine the dynamic deformation modulus E_{vd} obtained by the test with the Light Falling Weight Device.

11.3 *Theoretical basis*

The motion behavior of the LFWD interacting with the subsoil is a complex process. This process results from the interaction of the testing device with a priori non-linear characteristics with the non-linear, halfinfinite and in general plastically deformable subsoil. The load-deformation-relation of the subsoil under dynamic impact-like loading has to be determined. Studies with different non-linear soil models performed by the authors in order to take different elastic-plastic soil characteristics into account showed that viscous-elastic soil modelling is sufficiently accurate for the scientifically oriented evaluation of the test with the LFWD as well as for the simulation of the test and parametric studies. The same is valid for the LFWD; linear modelling provides sufficiently accurate results.

The mechanical model for the interaction system LFWD—subsoil used for the theoretical studies and the evaluation of the measurements is illustrated in Figure 27. The falling mass m is

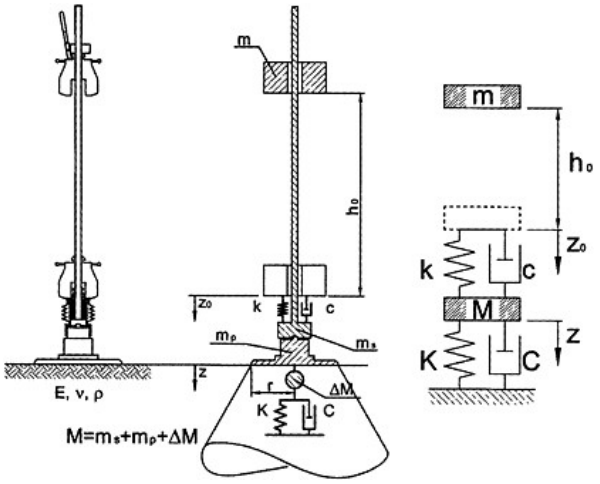

Figure 27. Modelling of the interaction system LFWD—subsoil (cone model). Mechanical modelling by a 2DOF-oscillator.

dropped from the height h_0 onto the spring-damper-element of the loading device. The loading device is modelled as a *Kelvin-Voigt*-body with a spring stiffness k and a velocity-proportional damping coefficient c; m_s indicates the mass of the guide rod. The circular plate with the radius r and the mass m_p rests on the ground modelled by a viscous-elastic cone. The stiffness of the cone is indicated by the spring stiffness K; geometric damping due to wave irradiation into the subsoil is indicated as coefficient C. Both parameters K and C depend on the geometry of the loading area (radius of the loading plate r) and the elastic characteristics of the ground. The modulus of elasticity is defined as dynamic compression modulus E_{dyn}; ν indicates *Poisson's* ratio, while ρ indicates the (wet) density of the subsoil. The derivation results in a resonant soil mass ΔM for cohesive soils.

11.4 *Recommendations for proper LFWD testing*

Uniform and properly working measuring equipment is essential for a successful application of the LFWD. Attention has to be focused on exact specifications of the deflection measuring device (frequency range, filter characteristics, temperature, etc.) and the calibration. The soil stress is assumed to be constant for the evaluation, although it is dependent on the soil stiffness. However, the influence of this theoretical idealisation is small, especially if stiff layers are tested. The dynamic deformation modulus is determined by assuming a constant ground contact stress of 0.1 MN/m^2. Because of this simplified assumption the spring-damper-elements of the loading device have to have constant characteristics within a temperature range from 0°C to 40°C. Disc springs made of steel meet this requirement, while the characteristics of synthetic elements (rubber springs) change for even slight temperature differences (Figure 28): The maximum impact force and the momentum generated by the loading device are plotted in Figure 28 for different spring-damper-elements. Tests were performed at different temperatures, but with constant bedding conditions. The devices equipped with rubber springs show variable impact characteristics in dependence on the temperature, whereas the device equipped with disc springs made of steel is practically independent from the temperature. The measuring depth of the LFWD is approximately 60 cm, i.e. twice the plate diameter.

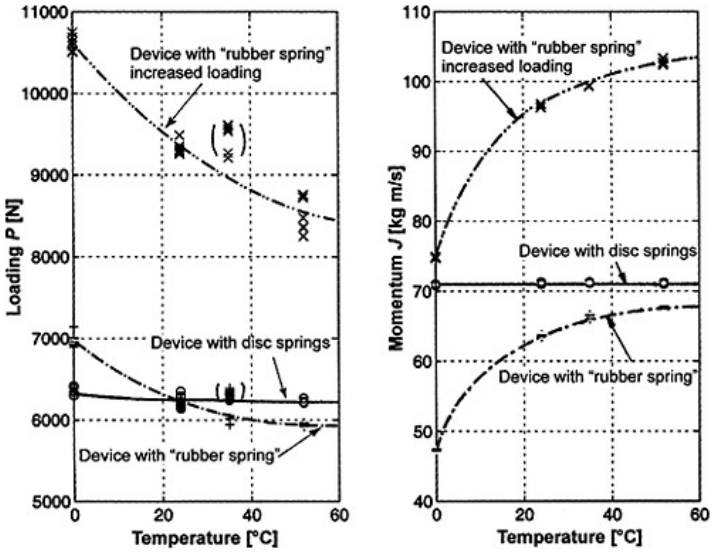

Figure 28. Influence of temperature on maximum impact force and momentum of different loading devices under constant bedding.

12 CONCLUSIONS

Roller-integrated continuous compaction control (CCC) is an innovative method to continuously optimise, control and document the compaction of each fill layer of an embankment dam already during the compaction procedure. Consequently, this method has numerous advantages over conventional tests based on spot checking with random, grid or subjective selection of controlled points. CCC is based on comprehensive theoretical investigations, field tests and site experience. The elastic part of soil and other granular material could be described by a physical cone model representing the half space which resulted in a spring-dashpot system. Systematic comparisons with other test methods provided best correlations with the dynamic load plate test (light falling weight device). Eventually, after site-specific calibration, the dynamic compaction values from CCC can be used directly as quality control.

To sum up, roller-integrated continuous compaction control represents a significant improvement for high-levelled quality management systems. Compaction control is integrated in the compaction process and data are provided over the entire compacted area and for each fill layer. Because of the outstanding advantages of CCC, this technology should be used for the compaction of earth- and rockfill-dams as much as possible.

REFERENCES

[1] Adam, D.: *Roller-integmted continuous compaction control of soils by means of vibratory rollers.* (in German). Doctor's Thesis. Technical University of Vienna, 1996.

[2] Brandl, H., Adam, D.: *Sophisticated continuous compaction control of soils and granular materials.* Proceedings of the 14th Int. Conference on Soil Mechanics and Foundation Engineering. Hamburg, A.A.Balkema, Rotterdam, 1997 (p. 31–36).

[3] Brandl, H., Adam, D.: *Basics andApplication of the Dynamic LoadPlate Test in Form of the Light Falling Weight Device.* A.W.Skempton Memorial Conference. Proceedings of Imperial College, London, 2004.
[4] Brandl, H.: *Risk analyses, quality assurance and regulations in landfill engineering and environmental protection.* Keynote paper at 3rd International Congress on Environmental Geotechnics. ISSMGE, Lisbon. A.A.Balkema, Rotterdam, 1998 (p. 1299–1328).
[5] Kopf, F.: *Roller-integrated continuous compaction control of soils by means of different dynamic rollers.* (in German). Doctor's Thesis. Technical University of Vienna, 1999.
[6] Pouliot, N. et.al.: *Prediction of the compactness of roller-compacted concrete using a granular packing model.* Bulletin des Laboratoires des Ponts et Chaussees, No. 2333. Paris, 2001 (p. 23–36).
[7] Terzaghi, K.: *Theoretical Soil Mechanics.* Wiley Publications, New York, 1943.
[8] Wolf, J.P.: *Foundation Analysis Using Simple Physical Models.* Prentice Hall, Inc. Englewood Cliffs, N.J., 1994.

This page intentionally left blank.

New Developments in Dam Engineering—Wieland, Ren & Tan (eds),
© 2004 Taylor & Francis Group, London, ISBN 04 1536 240 7

Some recent innovative techniques in the design and construction of high dams in China

Guanfu Chen, Jianping Zhou & Baile Wang
China Hydropower Engineering Consulting Group Co., Beijing, P.R. China

ABSTRACT: Based on the characteristics of Chinese high dams built, being built and to be built in the early 21st century, authors introduced new theories, new technologies applied in designing and constructing high dams, analyzed some key technological issues, including project layout, dam type selection, dam structure and zoning, high performance dam materials, seismic design and measures, flood discharge and energy dissipation with high water head and large discharge flow and treatment to complex dam foundation, discuss the new challenges in constructing high dams currently, bring forward some suggestions, expecting to provide valuable suggestions for high dams construction.

1 INTRODUCTION

Chinese hydropower resources are most abundant in the world, the exploitable hydropower potential are 378 GW with an annual electricity output of 1920 TWh, which substitutes for 70 million tons of standard coal every year. At the beginning of 21st century, Chinese government begins to actualize "West Development" strategy, construct "Electric Power Transportation from West to East" project. Till the end of 2003, Chinese hydropower installed capacity sums to 92,170MW, which are 24 percents of national total installed capacity. Apparently, hydropower has been the important component of Chinese energy supply. To meet the needs of national economy increasingly growth and people's life continuously improvement, according to the national electric power planning, hydropower installed capacity will reaches 270,000MW in 2020, accordingly exploitation ratio is up to 68%. Otherwise, with the deep reformation of Chinese electric power system, the situation with many investors for electric power exploitation has been formed, more and more national and private capital are invested in hydropower exploitation. Therefore, in the view of national electric power demands, national industry policies, or means of investing and financing for hydropower exploitation, Chinese hydropower construction meets the best developing opportunity, especially the southwestern regions, with most abundant hydropower resources, meets the new climax of exploiting hydropower. By all appearances, as the important structure of hydropower projects, dam construction will also develop quickly.

As shown in Table 1, a lot of high dams were or are being built in the hydropower step exploitation of great rivers, a complete set of technology specifications, from planning, reconnaissance, test, design, construction, observation and operation management, has been set up. According to the latest statistic, among the dams built and being built in China, 84 dams are more than 100m high. In which, 45 dams are concrete dam, 39 dams are rockfill dam, respectively accounts for 54 percents and 46 percents. The completed Ertan double-curvature arch dam is 240m high, Xiaowan double-curvature arch dam is 292m high both are the highest dams in China. The dam types, which are built most and developed most quickly, are still concrete double-curvature arch dam, compacted rockfill dam and rolled compacted concrete (RCC) gravity dam. Compared with the dam constructions in the world, it is obvious that Chinese high dam constructions are currently standing for the advanced technology level and the dam type development trend.

Table 1. Some high dams of China (Maximal dam height H ≥150m).

Dam name	Location	Status	Height (m)	Storage capacity ($\times10^8m^3$)	Installed capacity (MW)	Dam type	Dam volume ($\times10^4m^3$)
Ertan	Yalongjiang	Completed	240	57.9	3300	DCAD	414
Longyangxia	Yellow river	Completed	178	247	1280	GAD	157
Tianshengqiao I	Hongshuihe	Completed	178	90	1080	CFRD	1800
Dongfeng	Wujiang	Completed	173	8.63	510	DCAD	48
Lijiaxia	Yellow river	Completed	165	16.5	2000	DCAD	124
Wujiangdu	Wujiang	Completed	165	21.4	630	GAD	193.2
Dongjiang	Leishui	Completed	157	81.2	600	DCAD	96
Xiaolangdi	Yellow river	Completed	154	126.5	1800	CWRD	4900
Geheyan	Qingjiang	Completed	151	34	1200	GAD	237
Baishan	Songhuajiang	Completed	149.5	68.12	1500	GAD	163
Xiaowan	Langcangjiang	UC	292	150.4	4200	DCAD	746.96
Shuibuya	Qingjiang	UC	233	45.8	1600	CFRD	1563.74
Goupitan	Wujiang	UC	232.5	64.51	3000	DCAD	346
Longtan	Hongshuihe	UC	216.5	272.7	6300	RCCGD	685
Hongjiadu	Wujiang	UC	191	45.9	540	CFRD	1007
Pubugou	Daduhe	UC	186	50.63	3300	CWRD	2274
Sanbanxi	Qingshuijiang	UC	185.5	42.5	1000	CFRD	994
Three Gorges	Changjiang	UC	181	392.5	18200	GD	2793.5
Tankeng	Xiaoxi	UC	161	35.3	600	CFRD	1000
Zipingpu	Minjiang	UC	159	11.12	720	CWRD	1167
Jilintai I	Kashihe	UC	152	136	460	CFRD	936

Remark: DCAD-Double Curvature Arch Dam; GAD-Gravity Arch Dam; CFRD-Concrete Facing Rockfill Dam; CWRD-Core Wall Rockfill Dam; RCCGD-RCC Gravity Dam; GD-Gravity Dam; UC-Under Construction.

Table 2. Some high dams to be built in China (H≥200 m).

Dam name	Location	Height (m)	Storage capacity ($\times10^8m^3$)	Installed capacity (MW)	Dam type	Dam volume ($\times10^4m^3$)
Jinping I	Yalongjiang	305	77.6	3600	DCAD	435.59
Xiluodu	Jinshajiang	278	126.7	12600	DCAD	703.8
Nuozadu	Lancangjiang	261.5	237	5850	CWRD	3360.64
Laxiwa	Yellow river	254	10.56	3720	DCAD	253
Shuangjiangkou	Daduhe	332	35.36	2000	CWRD	4975
Baihetan	Jinshajiang	277	179.24	12000	DCAD	
Lianghekou	Yalongjiang	270	120.31	3000	CWRD	
Miaojiaba	Bailongjiang	263	43	1040	CWRD	4250
Hutiaoxia	Jinshajiang	216	183.45	2800	DCAD	316.89
Songta	Nujiang	307	63.12	4200	DCAD	1115.9
Maji	Nujiang	300	46.96	4200	DCAD	949.5
Changheba	Dduhe	238	9.85	2200	CWRD	2855.17
Xia'erga	Dduhe	223	28	540	CWRD	1777
Dagangshan	Dduhe	216	7.75	2300	DCAD	367.15

Presently, in Jinshajiang, Yalongjiang, Daduhe, Lancangjiang, Yellow river, Wujiang, Qingjiang and some other mid-scale rivers, hydropower step exploitation started up already or further deepen; prophase tasks of hydropower exploitation for Nujiang is developing roundly. See Table 2, a lot of high dams are to be built in above rivers, many dams are more than 200m high, some are

beyond 300m high. The high dam projects whose feasibility researches already completed are Xiluodu, Nuozhadu, Jinping I, Guandi (168m high gravity dam), dams whose feasibility researches under developing are Xiangjiaba (161m high gravity dam), Shuangjiang Kou, Baihetan, etc. These dam constructions will be confronted with more complex and more difficult technology issues. These issues mainly include project layout, selection of dam type and structure analysis, dam zoning and high performance dam materials, aseismic design and engineering measures, flood discharge and energy dissipation with large flow ratio and high water head, complex foundation treatment, and researches on reconnaissance, test, calculation, construction, instrumentation, and technology standards related to the above issues.

The solving of the above key technology issues and the construction of the above high dams will indicate that the dam technology of China keep ahead fully all over the world. The exploitation of hydropower will bring greater benefits to development of national economy, improvement of people's life and society prosperity.

2 SOME NEW TECHNOLOGIES APPLIED IN HIGH DAMS CONSTRUCTION

2.1 *Project layout*

High dam projects usually are uppermost or controlling reservoir in the river, which have the comprehensive benefits to electric power generation, flood control, runoff regulation and sediment control. Types of high dams mainly are concrete double-curvature arch dam, compacted rockfill dam and concrete gravity dam. Due to the deep narrow canyon at the dam site, project layout should be close and appropriate for reliable operation and economical construction.

2.1.1 *Project layout of high gravity dam*

Under appropriate geological and topographical conditions, Structure safety evaluation of gravity dam is perspicuous, construction quality is more easily ensured. Top and bottom orifices for flood discharge, bottom orifice for river division are convenient to be placed in gravity dam; many types of waterpower plants are neatly suitable for gravity dam projects. Consequently, gravity dam is still one of important dam types. Generally, some characteristics of high gravity dams layout are list as following.

(1) Gravity dam is more safe to control flood, orifice for flood discharge, sediment flushing, empting reservoir neatly placed in dam, structure type is simple and easy to solve such problems as energy dissipation and protection.
(2) With the development of such criterions as flood design standard, stability against sliding, dam foundation uplift pressure, dam and waterpower plant behind dam loading jointly, the dam cross section and foundation treatment are more rational and economical.
(3) Scale increasing of orifices for discharging flood placed on dam top and development of energy dissipation type and structure model, facilitate the innovation and development for high gravity dam layout in gorges with narrow river valley
(4) Large capacity hydraulic turbine generator units are widely adopted for high gravity dam hydropower stations, which can shorten the intake front width and the penstock length, then optimize project layout.

2.1.2 *Project layout of high arch dam*

Due to powerful overload capacity, sound earthquake resistance behavior, large flood releasing from dam, handsome and economical, concrete arch dam becomes one of preferred dam types for high dam hydropower stations, especially built in narrow canyons with good geological conditions. For many high arch dam projects, some layout characteristics can be summarized as following.

(1) For high arch dams built in narrow canyons with large flood flow rate and installed capacity, in general, powerhouse is placed in the underground, orifices in the dam and bank spillway tunnels work jointly for flood discharge, e.g., Xiaowan, Xiluodu and Jinping I hydropower stations.

(2) Development of safety design criterions and methods for design, analysis and test, make arch dam preponderant in high dam projects. Development of such criterions as high arch dam strength, abutment stability, aseismic design, overall safety evaluation and engineering experiences provide a advantageous basis for the design and construction of many 250m~300m high arch dams to be built in the early 21st century, such as Xiaowan, Laxiwa, Xilduodu, Jinping I.
(3) Layout of flood discharge facilities has made great progress. Top and central orifices in the dam, assisted by bank spillway tunnels, work jointly to release flood, cushion pool is placed in riverbed beyond the dam as ski-jump energy dissipater, that becomes an universal layout.
(4) Development of high arch dam structure type promotes the innovation of arch dam layout. e.g., concrete gravity frusta is adopted for abutment with poor geological and topographical conditions.

2.1.3 *Project layout of rockfill dam*

With the advantages of use and design by local materials, good adaptability to dam foundation, highly mechanized and rapid construction and low cost, rockfill dams, including CFRD and CWRD, are being developed quickly and will be still widely used in dam constructions. For many high rockfill dams, some layout characteristics can be summed up as following.

(1) High rockfill dam accompanied with great excavation is the prominent feature in project layout, for the sake of general balance between earth rock excavation and dam filling, reducing project cost, shortening construction period, increasing economic benefits.
(2) Development of dam zoning and dam materials design, can better harmonize the deformation between concrete facing and rockfill, or between impervious core wall and dam shell, that provide good basis for high rockfill dam construction.
(3) Flood is mainly discharged by crest spillway, secondarily by spillway tunnels.
(4) Attach importance to construction organization design such construction equipments matching and construction field and road planning, ensure safety flood control during construction and generate power in advance, that becomes important segment of high rockfill dam layout.

2.2 *Dam type selection and dam structure analysis*

2.2.1 *Selection of dam type*

Not only topography and physiognomy, canyon shape, depth and structure of riverbed overburden layer, engineering behavior of foundation rock, geological formation, project layout, flood discharge of the dam site should be considered for dam type choice, also should comprehensively compare the reserves, engineering behavior, transportation distance and machining processes of local materials with the quality and transportation distance of concrete raw materials such as cement and fly ash, then select dam type, which is reasonable at cost, feasible in technology, convenient for construction. After selecting the dam type, test and numerical evaluation on hydraulics, sediment and structure should be conducted for dam and foundation system, then determine the reliable, effective and economical treatment measures, optimize the layout and dam cross section.

2.2.2 *Dam structure analysis*

Numerical method such as Material Mechanics method and Finite Element Method (FEM), Structural and geomechanical model test method and engineering analogy method can be used to analyze the stresses and deformation of dam and foundation. For the first time, *Design Specification for Concrete Gravity Dams* and *Design Specification for ConcreteArch Dams* use FEM as one of basic methods for evaluating dam strength safety and established the corresponding stress control criterions. In addition, China has conducted a lot of structure and geomechanical model test researches, and made great progress in model simulation ratio, test materials, loading method, collection and analysis of test data, and further understand the working mechanism, limit bearing capacity, process and pattern of stability loss and damage of high dams.

2.3 *Dam zoning and high performance dam materials*

2.3.1 *Dam zoning*

In order to ensure dam safety and construct projects economically, dam zoning and materials should be designed by stress and deformation distribution caused by loads acting on the dam. For rockfill dam, in order to reduce the asymmetric and total deformation of dam during construction and operation, the designing should comprehensively consider dam materials behavior, material zoning, filling standard and construction zoning, high strength rock used in high stress area. For concrete dam, high grade concrete is used in high stress area of the dam, vice versa, then zone the dam concrete strength grade and material grade to make full of materials bearing capacity.

2.3.2 *High performance dam materials*

With the development of dam scales, requirements to dam material performances such as workability, mechanical and thermodynamic behavior and durability is higher and higher. In order to save cement, decrease hydration heat and improve the durability of concrete, extenders such as fly ash are widely mixed in conventional concrete and RCC, many researches have been developed on mix proportion, workability, mechanical behavior and durability, and many valuable experiences have been obtained. In addition, composite induced water reducing is successfully developed to excite the early activity of fly ash, which provides an approach for improving the early strength of highly fly ash mixed concrete. As for conventional concrete, maximal mix ratio of fly ash to cementitious materials usually is below 30 percents for arch dam and 55 percents for gravity dam; for RCC, the ratio is generally below 60 percents for grade III fly ash and 70 percents for grade II.

In order to provide high performance concrete with good abrasion and cavitation resistance for new high dams and repairing built projects, silica concrete, silica steel fiber High Performance Concrete (HPC), special aggregate HPC and vacuum operation HPC have been developed and applied, a lot of researches and tests have been conducted on mix proportion, workability, mechanical behavior, flexible behavior and construction processes, and they have been adopted in many large scale hydropower stations. Mix ratio of silica to cementitious materials usually is from 10 to 30 percents.

2.4 *Earthquake resistance design and measures*

China is situated between the two large active seismic belts in the world and is a country of high seismicity. Even now, many high dams were and will still be built in strong earthquake regions, and that high dam and large reservoir usually induce certain intensity earthquakes. Therefore, aseismic design and measures are very important for high dams in strong earthquake areas.

After selecting dam site, according to the dynamical parameters decided by *seismic zoning map in China (2001 version),* regional formations around the dam site and earthquake geological conditions, earthquake fatalness evaluation should be conducted, then earthquake dynamical parameters, responding to the engineering rank of certain projects, should be selected for seismic design of high dam. *Specifications for seismic design of hydraulic structures* has made two spans for concrete dams, the first one is from pseudo static method to dynamical method considering concrete dam-foundation-reservior interaction, another is from definite method to primary seismic reliability design. Pseudo static method is still adopted for rockfill dam, but modify the earthquake acceleration distribution map according to the relationship between the acceleration on the dam top and the earthquake intensity. In addition, for the complex system of dam, sometimes, dynamical model test or field vibration test are indispensable to modifying the numerical model, verifying the results and improving the earthquake resistant measures.

Xiaowan arch dam is 292m high, crest length of dam top is 819m. The canyon of dam site is wide V shape. Design value of peak ground acceleration is 0.308 g. A lot of numerical analysis and model tests were conducted on seismic design and measures, and great progresses have been made. The researches include 3-D nonlinear dynamical FEM analysis of the dam-foundation-reservior coupling system, considering the effects of transverse contraction joint opening under earthquake, infinite foundation radiation damp, asymmetric input of earthquake loads, test researches on joint behavior under earthquake, seismic stability analysis of abutment with consideration of dynamical coupling between abutment rock and dam, damage mechanism of arch dam under beyond design probability earthquakes. Numerical evaluation and test researches on the effects of earthquake resistant measures have been lucubrated, such as placing damper between transverse joint, reinforced arch beam and prestress anchor cables on dam top, placing steel bar across transverse joints. After comprehensive comparison, the first measure is to be adopted for Xiaowan arch dam.

2.5 *Flood discharge and energy dissipation*

The selection and design of discharge facilities for high dams are mainly determined by dam type, topographical and geological conditions on dam site, discharge flow, requirements of construction and operation, scouring resistant ability on river bed and the layout of whole project. Due to the hydrological, topographical and geological condition of Chinese rivers, flood discharge and energy dissipation facilities of high dam projects mostly have the characteristics of high water head, large discharge flow, huge discharged power and complex geological and topographical conditions. After constructing many projects, new technologies such as large orifices in the dam; dispersible flood discharge and divisional energy dissipation; energy dissipation means such as ski-jump, hydraulic jump, bucket type and flaring pier; many kinds of slotted flip bucket, special-shaped convergent bucket, slit-type bucket, flaring pier and a set of energy dissipation technologies, flows colliding through top and central dam orifices combined with water cushion pool energy dissipation all are successfully applied in many high dam projects. Behavior of some discharge facilities being and to be built in China, whose dam is more than 150 m high, discharge flow is more than 6000 m^3/s, are list in Table 3, where *w* stands for width, *h* for height, *n* for number. Obviously, Chinese technologies on flood discharge and energy dissipation with high water head and large discharge flow reached the advanced level in the world.

Pointing out specially, the energy dissipation type of flow nappe collision combining with water cushion pool is a new type developed to discharge large flow rate through high dam, especially high arch dams built in narrow deep canyons, e.g., Ertan, Xiaowan, Goupitan, Xiluodu and Jinping I high arch dam hydropower stations.

Table 3. Behavior of some discharge facilities in China.

			Flood discharge structures (dimension unit: m)				
Dam name	Dam height (m)	Flow rate (m^3/s)	Top orifice *n*-*w*×*h*	Middle orifice *n*-*w*×*h*	Bottom orifice *n*-*w*×*h*	Spillway *n*-*w*×*h*	Spillway tunnel *n*-*w*×*h*
Three Gorges	181	102500	22–8×17	2–8×11	23–7×9		
Longtan	216	35500	7–15×20		2–5×8		
Goupitan	225	29100	6–12×16	7–7×6	2–4×6		
Xiaowan	292	20701	5–11×15	6–6×7			1–11×12
Shuibuya	232	15243			2–4×5	5–14×21.5	
Pubugou	186	9780				3–12×16	1–9×9
Hongjiadu	182.3	6996					1–12×7.5 12×7.5
Xiluodu	273	50153	7–12.5×13.5		8–6×6.7		5–14×12
Xiangjiaba	161	48660	12–11.2×24	10–7×9			
Nuozadu	261.5	37532				8–15×20	2–5×8.5
Jinping I	305	13854	4–11.5×10		5–5×6		1–14×12
Laxiwa	254	6000	2–13×9		2		

2.6 *Treatment to complex dam foundation*

2.6.1 *Treatment to high rockfill dam foundation*

The main requirements for high rockfill dam foundation treatment are, controlling seepage to reduce seepage gradient and avoid harmful seepage deformation such as piping; ensuring static and dynamical stability of dam and foundation to avoid too large deformation and asymmetric deformation; constructing project at low cost under the precondition of dam safety.

Treatments to deep overburden layer of high rockfill dam usually include seepage control treatment, reinforced treatment to increase its bearing capacity and prevent sand soil from liquefaction by earthquake. Seepage control treatments mainly include concrete impervious wall or high-pressure revolving-spraying grouting curtain. Overburden layer in Xiaolangdi slope core wall rockfill dam foundation is about 82m deep. A set of concrete impervious wall with width of 1.2m is placed below the slope core of main dam. Overburden layer of Pubugou core wall rockfill dam foundation is about 75m deep. Two sets of 1.4 wide concrete impervious walls with neat span of 12m are to be placed below core wall. When deformation modulus and allowable bearing capacity of overburden layer are low, consolidation grouting should be wanted. When sand lens lies in the overburden layer and possibly are liquefied by earthquakes, earthquake resistant measures such as compressed by weight blocks and sand lens replacement should be adopted.

2.6.2 *Treatment to complex foundation of high gravity dam*

Anti-sliding stability of gravity dam along the interface between dam and foundation, superficial or deep sliding planes in the foundation is one of basic ensuring for safe operation of gravity dam projects. Many results and engineering experiences have been achieved on such aspects as numerical evaluation, test researches and treatment measures, such as large cutoff trench, shear concrete cavern plug, shear pile and prestress anchor cable, concrete replacement and consolidation grouting are adopted to enhance the shear capacity and improve the deformation behavior of dam foundation.

2.6.3 *Treatment to fragmentized rock of high arch dam abutment*

Stability against sliding, deformation stability and seepage stability of abutment are the basic assurance for safe operation of arch dam project. Jinping I arch dam to be built in China is 305m high, there are geological imperfections such as deep tensile fissures, relaxed rock strip, low wave-speed rock belts, two large faults and lamprophyre dyke in left bank, which are very disadvantageous to anti-sliding stability, deformation stability, seepage stability and slope stability of left abutment. In order to increase the stiffness and seepage stability of arch abutment, enhance the symmetry of dam stress and deformation, comprehensive treatment measures such as concrete cushion block, replacement by concrete grid, high pressure consolidation grouting through deep hole, drainage cavity or hole and seepage control curtain are adopted.

2.7 *Reinforced treatment to high rock slope*

During constructing high dams, when bank slopes are steep, the excavation of ship lock, dam foundation, arch abutment groove and water intake usually form high slope. Different from slopes in highway, railway and mine projects, slopes in hydropower projects are usually influenced greatly by hydrological and geological factors. Such effects as reservoir storage, water-level descent, fog and rain induced by flood discharge, stream abrasion and earthquake induced by reservoir all are inducements that cause deformation and slippage of slopes.

As for reinforcement of high rock slopes, besides conventional shotcrete and anchorage support, prestress anchor cables are widely used to reinforce rock slopes, and many researches have been conducted on prestress anchorage structure, anchorage system, internal and external anchorage type, drag equipments, bore crafts, grouting materials and antisepsis for anchorage cable and anchorage bar. The magnitude of prestress anchor cable and anchor bar reaches 500 kN~10,000 kN, the cable length reaches 20m~80m.

3 NEW CHALLENGES FACING HIGH DAM CONSTRUCTIONS

3.1 *Project layout*

High dam projects such as Xiaowan, Goupitan, Laxiwa, Xiluodu and Jinping I will bring forth new and more complex key technological issues, such as establishing design criterion suitable for 300m high dams; Flood discharge and energy dissipation; Huge underground hydropower plant; construction layout technologies.

3.2 *Dam structure and zoning*

For structural analysis, matching system between analysis method, action and safety evaluation criterion should be further developed, using the last analysis method and researching results, and paying more attention to verify the method and check the results with the help of test results and observation data. As far as dam zoning is concerned, according to working mechanism and stress and deformation distribution of dam, different dam materials and construction parameters should be selected for corresponding dam area, make full of the bearing capacity of materials, then construct the projects at possible low cost under the precondition of safe operation.

3.3 *High performance dam materials*

Farther researches are wanted for high performance dam materials with the increasing of dam scale, e.g., reducing the early shrinkage and improving the workability of silica abrasion and cavitation pitting resistant concrete; developing high strength and low hydration heat concrete for high stress area of high concrete dam; developing core wall material with excellent performances in compression resistance, seepage control, anti-cracking, abrasion resistance and shear strength for high CWRD, developing water-stop materials for peripheral joints of high CFRD, especially for those high dams built in strong earthquake regions.

3.4 *Flood discharge and energy dissipation*

With the increasing of water head and flood discharge power, complex geological condition in energy dissipation area, design of high dam flood discharge and energy dissipation will at least be confronted with such key technological issues as questions related to high speed stream, safe dissipation of huge energy and Problems related to complex geological conditions.

3.5 *Treatment to high dam foundation*

In order to build high rockfill dam on the deep overburden layers, researches such as stress and displacement distribution of impervious wall, wall materials with excellent performance in high strength, low elastic modulus, flexibility to large deformation should be conducted further.

3.6 *Reinforced treatment to high rock slope*

During analyzing the stability for given high slope, farther researches are still wanted for geometric boundary of potential sliding planes, mechanical parameters of landslide and sliding planes, safety evaluation methods and criterions for anti-sliding stability. In addition, the relationship between rock mass, strength of weak structure planes, action of landslide or slope and water presently are far from perfect. Design safety criterion, treatment measures, drainage design and instrumentation requirements for slopes in hydropower projects are different from the slopes in highway, railway and mining projects. Therefore, it is very indispensable to constitute slope design specification for hydropower slopes.

4 CONCLUSIONS

Based on hydropower projects with high dam and huge reservoir built and to be built in China, authors summarized new theories, new technologies applied in project layout, selection of dam types, dam structure analysis and zoning, high performance dam materials, earthquake resistant design and measures, flood discharge and energy dissipation with large flow ratio and high water head, complex foundation treatment, reinforced treatment to high rock slope; forecast and introduce some key technological issues of high dam projects, for the sake of providing valuable suggestions and information for high dam design and researches at home and abroad.

REFERENCES

Jiazheng Pan, Jing He, 2000. *Large dams in China-A fifty years review,* China Waterpower Press.
Xu Baili, 1999. *Dam Construction of China,* in Dam and Safety, No. 1.
Design Specification for Concrete Gravity Dams, 2000. Industry standard of P.R. China, DL 5108–1999. China Electric Power Press.
Design Specification for ConcreteArch Dams, 2003. Industry standard of P.R. China, SL 282–2003. China Waterpower Press.
Specificationsfor Seismic Design of Hydraulic Structures, 2000. Industry standard of P.R. China, DL 5073–2000. China Electric Power Press.

This page intentionally left blank.

New Developments in Dam Engineering—Wieland, Ren & Tan (eds),
© 2004 Taylor & Francis Group, London, ISBN 04 1536 240 7

Design and study on the layout of the Three Gorges Project of the Yangtze river

Niu Xin-qiang & Wang Xiao-mao
Changjiang Institute of Survey, Planning, Design & Research, CWRC, China

ABSTRACT: Being the key project for harnessing the Yangtze river and developing its water resources, Three Gorges Project (TGP) is mainly aimed to control flood in its downstream, especially in Jingjiang reach, and to supply electric power to mid China, east China and east Sichuan province, as well as to improve conditions of navigable waterway between Yichang and Chongqing. During many past years spent in designing and researching on the arrangement of TGP, a lot of essential technologies were obtained. This paper gives emphasis on design and research into the arrangement of dam site, power house and navigation structures, as well as study on river closure, diversion and navigation during the construction period, and sedimentation, etc.

1 INTRODUCTION

According to the comprehensive benefits of Yangtze river, the Three Gorges Project is the backbone project for the regulation and development of the Yangtze. The first development task is to control the flood of the Yangtze river. Due to very close to the Jingjiang reach, the most dangerous reach of Yangtze in flood season, TGP could control 95% flood amount of Jingjiang reach, or about 2/3 that of reach before Wuhan. Because of the flood control capacity of 22.15 billion m^3 in TGP's reservoir, the fatal disasters are avoided on two sides of Jingjiang reach and the flood control criterion of Jingjiang reach increase from one in 10 years at present to one in 100 years. The second task is water power generation. TGP's installed capacity is 18200 MW, and it supplies power to the central and east China as well as Chongqing. Meanwhile, lying in central China, TGP is in the distance of less than 1000 km far from national power load centers. This contributes to realize a national power network and improve quality and benefit of power. The third task is to improve navigation in Yangtze. When TGP is accomplished, 570~650 km long water way will be improved by back-water, and in TGP's reservoir, rapids are submerged, water gets deeper, water slope gets gently, the 10000t fleet can sail directly from Chongqing to Yichang.

According to those tasks above, the following main issues of TGP's arrangement have been studied and solved: the discharge capacity and safeguard of spillway when reservoir stores flood to meet downstream flood control request, power station running safely and efficiently, navigation facilities and construction navigation, sediment and floatage.

2 DAM SITE SELECTION

Since 1950s, 15 dam sites have been studied. Two sites, named Nanjinguan and Sandouping, were chose to be further studied. Those two sites are compared with each other in topography, geology, structure arrangement, construction condition, BOQ, construction time limit and cost, and finally, Sandouping site was selected.

3 LAYOUT OF PROJECT AND STRUCTURES

3.1 *Project criterion*

TGP lies in Sandouping town Yichang county Hubei province in the midstream of Xilin valley. It is 40km downstream from Gezhouba Project. It controls watershed area of 1 million km^2. Its reservoir has a storage of 39.3 billion m^3. Its total installed capacity is 18200 MW. TGP is a grade 1 project, and the design criterion of dam, power house, ship lock and lift are all class 1. The flood control criterions are one in 1000 years in design and one in 10000 years in verification, the corresponding discharges are 98800m^3/s and 124300m^3/s respectively. The normal water level of reservoir is 175m (156m initially), and its flood control level is 145m (135m initially). The navigation criterions are: 50 thousand tons annual goods transportation for single line, 3.9 million person-time annual passengers transportation for double line. Upstream design water levels are: 135m in cofferdam generation period, 135m~156m in early stage, 145m~175m in late stage. Downstream design water levels are from 63.0m to 73.8m. Maximum fleet grade in planning is 12 thousand tons. Maximum discharge is: 45,000m^3/s for double line 10-thousand-ton fleet, 56700m^3/s for single line 3000t fleet.

3.2 *Study on layout of spillways*

The discharge arrangement schemes should meet flood control firstly. According to request of flood control in Jingjiang reach, TGP reservoir compensated regulate with downstream reaches in order that: water level of Shashi is kept less than 44.5m, the corresponding discharge in Zhicheng hydrologic station is 56700 m^3/s and no flood diversion is need in Jingjiang when in less than 100 years flood, but in 1000 years flood, the water level should be below 45.0m, the corresponding discharge is 80000m^3/s and flood diversion is need. Secondly, it should meet reservoir schedule planning. According to TGP reservoir flood control capacity, the spillway are demanded to pass 56700m^3/s at flood control level of 145m, and to pass 70000m^3/s at corresponding level of 100a flood.

In order to meet those flood control request, the water level in reservoir should fall down below 145m (135m in initial period) to prepare to store water. Therefore, bottom outlets should be concerned. If 1000a designed flood or 10000a verification flood comes and it discharges only through bottom outlets, the anterior border of discharge would be very wide and power house on its two sides would move to rocks which caused investment increasing. So, some crest outlets are needed.

Due to large amount of discharge, the spillway focuses on main riverbed in favor of dissipation and navigation. Three discharge courses are studied: (1) riverbed discharge course. The bottom outlets and crest outlets are all in middle of river. (2) tunnels in right riverside rocks discharge course. There are two tunnels (Φ18m) excavated in right riverside rocks instead of part of bottom outlets. (3) overflow spillway house discharge course. There is an overflow spillway house beside dam instead of part of crest outlets.

The anterior border of discharge dam is shortened and excavation of powerhouse is reduced because of tunnels instead of part of bottom outlets, but the excavation of tunnels is too large and tunnels disturb the construction fields on right riverside. The overflow spillway house discharge course has the same advantages to that of tunnels, but it would delay the construction time limit because it need a temporary low-lying diversion gap on the spillway during third construction period. Therefore, the riverbed discharge course is selected. In this course, three structure layouts are studied as below:

(1) Alternative layout. There is a bottom outlet in center of each dam segment and a crest outlet right on each joint of dam segments. Flood passes through bottom outlet when water level is low and crest outlets join to discharge when flood surpasses 1000a. Two currencies do not disturb each other because they are divided by a frusta on dam. And because of deepwater cushion, dissipation conditions are verified well by experiment on hydraulic model. In this layout,

the anterior border of discharge dam is short and its BOQ is small, and the power houses on two sides may set close to riverbed, thus may reduces rock excavation on two sides as possible.

(2) Separate layout. Bottom outlets and crest outlets are separately set in dam segments. This layout simplifies the dam structure by setting only one outlet in each segment. Meantime it causes anterior border prolonged and BOQ increased.

(3) Overlaying layout. There are two outlets overlapping at different elevations in the center of each segment. The bottom outlet is lower than that of above layouts. The anterior border is shorter than that in alternative layout but BOQ is reduced hardly. The bottom outlets, used as diversion ways, are in favor of river closure. When two lays of outlets work together, the discharge in some width is double as that in above layouts and the dissipation gets more difficult.

Comprehensively concerned with shortening anterior border, layout of powerhouse in left riverside, BOQ and downstream hydraulics, the alternative layout is selected.

Concerned with flood control and regulation of downstream and flood preventing in project, the capacity of spillway should meet flood control and regulation in reservoir with necessary surplus to keep TGP safe. When the reservoir water level is below 150m, the sediment outlets can also used as spillway.

Concerned with desilting and project protection, in order to keep effective capacity of reservoir, drop silting elevation before dams (especially before power house), shorten the time for water level falling down, the elevation of bottom outlet should be lower as possible, at least lower than that of intakes of power house. Also, it might be lower for river closure and sealing diversion bottom outlets during third construction period. However, dissipation would be harder for the currency is too low because of the lower elevation of outlet when one-in-100-year flood passes and downstream water level is very high. According to concerns above and hydraulic experiments on bottom outlets with elevation of 85m and 90m, the elevation of bottom outlet is adopted to be 90m. The bottom outlet section is 7m in width and 9m in height by the limit of gate and its hoist capacity. It stands the water head of 85m, and the pressure of wheel on emergency gate is over 4000 kN/m, also the total thrusting force of working arc gate is over 60000 kN.

Being selected the elevation of outlets and calculated by flood regulation, 23 bottom outlets and 22 crest outlets are required.

3.3 *Study on layout of powerhouse*

Dam site, layout of hydroproject and behaviors of powerhouse should be comprehensively concerned when the type of powerhouse is selected. Being selected Sandouping site, layout of spill-way and stage diversion, three types of powerhouse are studied as below:

(1) Dam-back type. According to layout of project in Sandouping site, the gravity dam with 483m wide spillway dam segment in middle of river is adopted. It is suit for dam-back type power-house because of the expansive topography and long dam axis. There are 26 sets of installation units in TGP, each of 700 MW, totaling 18200 MW in installed capacity, and each of 38.3m, totaling 1231.4m in length. The powerhouse should be located on two sides of spill-way in order to supply power to electric power system on each side. In order to reduce excavation amounts, 14 units are installed in left powerhouse and 12 units in right.

(2) Overflow spillway power house on right riverside. In this layout, the width of spillway is shortened from 483m to 391m and excavation of civil work are reduced slightly. But the layout of machine and electricity equipments is too complex and they cost too much to be accepted.

(3) Tri-team type. In order to generate more power in construction period, the third team of six units is planned to installed in underground powerhouse in right riverside rocks. Compared with dam-back type, by the limit of spillway construction, it is 11 years, the same as that of dam-back type, for the first unit to be put in production, but they can be installed ahead of schedule and produce 46.5 billion kWh additionally in 17 years construction period. However, it will cost 1.1 billion RMB more, and layout, running and construction of powerhouse are more complex than above type. So it is not better than dam-back type.

Finally, the dam-back type powerhouse is adopted with six units obligated in underground powerhouse in right riverside and their intakes can be constructed ahead.

3.4 *Study on navigation structure*

The permanent navigation structure, consisting of ship lock and ship lift, is an important component of TGR It is required to reach the capacity of 50 billion ton annually and pass by 10000 t fleet. The study on navigation structure is going with dam site selection, reservoir water level section, construction scheme all along. Having been studied many issues such as navigation course, structure type, construction navigation, hydraulic and sediment, designers strengthen to convince of main issues of navigation structure in TGP gradually. As the dam site is selected and construction scheme is determined, the permanent navigation structure is determined to locate in a wide zone on right side of river convex bend, where it has no affection on spillway and powerhouse.

Two layout schemes of ship lock which are continues five-step ship pock and disperse three-step ship lock are mainly compared as following:

(1) Hydraulic structure. The chamber wall of five-step ship lock is thin lining structure basically, and that of three-step ship lock is thin lining structure in one step and gravity structure in other two steps, so the civil amounts of the former is less than that of the latter. The time for filling and draining is 12 min for five-step ship lock and 16 min for three-step ship lock. There are swells in middle canal of three-step ship lock. And there is no evident difference of silting and sediment in approach channel between two schemes.
(2) Construction time limit and cost. The amounts of temporary civil work, construction traffic, occupation of three-step ship lock are all larger than that of five-step ship lock, therefore it costs more than five-step ship lock. And it may delay one year for water power generation.
(3) Running condition. Fleet goes through the five-step ship lock in single direction for shorter interval, and it is efficiently centralized controlled. But fleet goes through the three-step ship lock for longer interval and it is dispersedly managed.
(4) Capacity. The capacity of five-step ship lock is slightly larger than that of three-step ship lock.

So, the continues five-step ship lock scheme is prior to the disperse three-step ship lock.

The vertical ship lift, cooperating with ship lock, is mainly used as an express for passenger ships and other special ships. The water level conditions of vertical ship lift are the same to that of ship lock.

The ship lift lies in left riverside and it is about 1 km far from ship lock. It consists of upper lock head, lower lock head, coffer, approach channel sharing with ship lock, guide walls, breasting dolphins.

Concerned that 3000t-grade passenger ships and freighters, sailing between Shanghai and Chongqinq, climb over TGP, the effective size of the coffer of vertical ship lift should be 120m×18m×3.5m, the same as NO. 3 ship lock in Gezhouba.

4 STUDY ON INFLUENCE CAUSED BY CONSTRUCTION DIVERSION AND CONSTRUCTION NAVIGATION

In wide open riverbed of Sandouping site, there stands a island, called Zhongbaodao, dividing the river into two branches. The left branch, the main riverbed, is 700~900m wide and the right branch is about 300m wide. Thus supplies good conditions for stage diversion. Due to the main waterway in China, it is very important for Yangtze river to keep navigable during TGP construction. Therefore the scheme of stage diversion must meet construction navigation.

4.1 *Construction navigation*

In first stage, the right branch is enlarged as diversion canal that is navigable. At the end of the second stage, reservoir water level rises to 135m and ship lock begins to run. So, construction navigation issue is to solve the navigation for six years from the end of first stage, when river is closed,

to reservoir filling, before ship lock runs. Two construction navigation schemes, navigable canal scheme and unnavigable canal scheme, are studied as following:

(1) Navigable canal scheme. It is divided into three stages. The canal is widened from 250m~300m to 350m and there is no structure in canal during the second construction stage, so the canal is navigable when discharge is below 20000m^3/s. Additionally, a temporary ship lock built on left riverside is supplement to navigation in flood season.
(2) Unnavigable canal scheme. It is divided into two stages. The canal is only used for diversion. The construction navigation is solved by the temporary ship lock on left riverside.

Both of two schemes above have concerned that the ship lift begins to run in the last two years of TGP construction.

Compared with two schemes on reliability of navigation, especially on reducing BOQ in initial stage, shortening time limit and generating ahead of schedule, the navigable canal scheme is selected.

4.2 *Influence on layout of TGP caused by construction diversion*

Firstly, the site of longitudinal cofferdam should be selected properly as the layout of TGP influenced by three-stage diversion. Secondly, the issues of equipments and hydraulic in three-stage diversion, river closure and flood discharge should be solved.

As Gezhouba project was built, the water level is raised higher than its natural water level, and the longitudinal concrete cofferdam should be constructed under the protection of earth rockfill cofferdam built in first stage. In order to reduce excavation of canal and be in favor of building earth rockfill cofferdam, the concrete cofferdam is located in the right side of Zhongbaodao island. Thus, the layout of the spillway is restricted from using the deep riverbed, but it is convenient to plus units in left powerhouse and reduce excavation of side slopes. During the third diversion stage, the left powerhouse has been put in production with the water level of 135m. As well as bottom outlets in spillway dam segments, a quantity of temporary diversion bottom outlets installed with gates are required to control discharge in order to control generation water level and supplement insufficient discharge in bottom outlets, so that can meet the flood discharge and river closure in the third diversion stage. Concerned that the anterior border of spillway is not suitable to be widened and that of left powerhouse can't shortened, the diversion bottom outlets are set in spillway dam segments. Due to the lower elevation demanded by river closure in third stage, they can be set on the joints of segments with the same quantity to crest outlets.

5 SEDIMENT AND FLOTAGE

TGP reservoir has large inflow with low sediment concentration. Most of water and sediment coming in to reservoir are centralized in flood seasons. One of the most important task of the reservoir is flood control. In flood season, from June to September, the reservoir contains the water level at the flood control level of 145m. That is very favorable to decrease silting and contain effective volume. The reservoir runs by the means of "impounding the clear and discharging the turbid", the water level would be drawn down to flood control level of 145m in flood season, and it would be raise up to normal level of 175m at the end of flood season. The researches indicate that equilibrium of deposition would be approximately reached in 100 years ignoring the upstream reservoir's influence. At that time, the reservoir may contain 86% flood control volume and 92% regulation volume.

As TGP runs, the sediment issues mainly including silting in approach channels of navigation structure and effect on navigation hydraulic and intakes of powerhouse should be solved by desilting means.

(1) Navigation desilting. Ship lock is far from river and ship lift is in river. Lot's of experiments show that a long breasting wall is needed on the right side of approach channel to ensure the

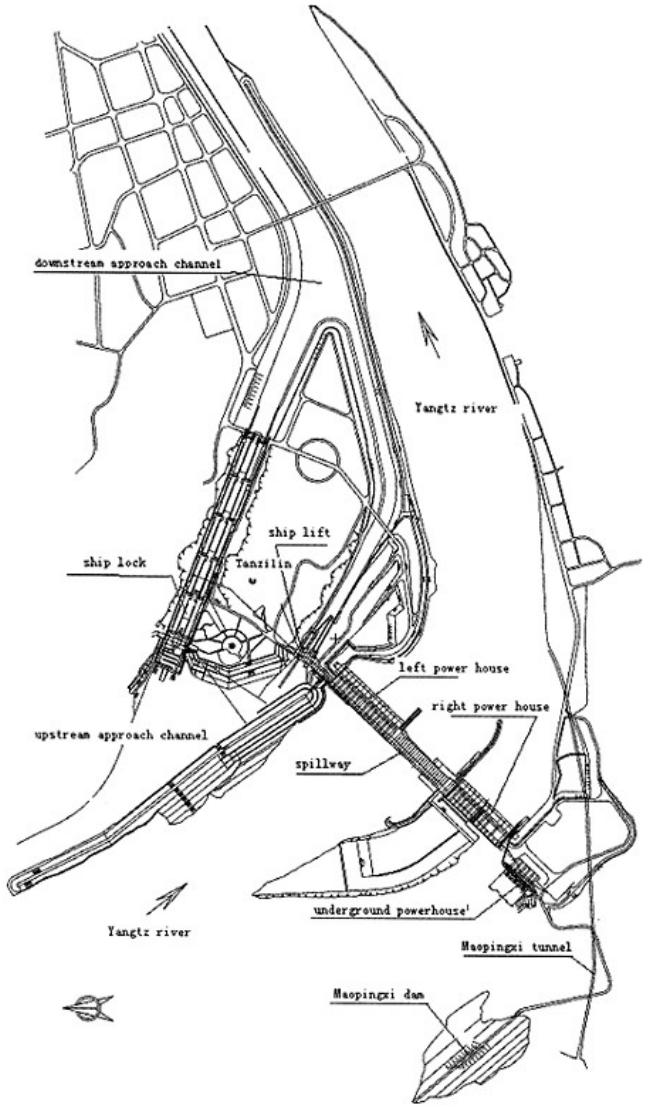

Figure 1. Layout of Three Gorges Project.

hydraulic condition of entrance of ship lock and upstream approach channel of ship lift when navigation level is 145m. They also show that large amount of deposition would occurred in 90th year, which could be desilted by two scouring sluices set in temporary ship lock segment and two scouring tunnels excavated in the rocks between ship lock and dam.

(2) Power house desilting. There are two effects on powerhouse caused by sediment. One is deposition before intakes, the other is sand coming into turbines and abrasing them. Due to bottom outlets in spillway segment are 18m far below the intakes, the deposition before dam would become a large hopper which is low in center and high on its side. Thus would decrease the amount of sand coming into turbines. The sediment experiments indicate that the deposition 30m far from intakes would be slightly higher than the bottom elevation of intakes in the 90th year, the grain size of sand and sediment concentration would rise from the 50th year on. So, scouring outlets in powerhouse segments should be concerned to solve sediment issue after deposition equilibrium. The layout of scouring outlets is studied as two means: dispersion and collection. Experiments show that the collection means of layout of scouring outlets is necessary for intakes to keep sand out and it also could control the deposition below the elevation of 100m efficiently.

Adventures in Gezhouba project show that there would be lot's of flotages deposited before dam to effect power output in flood season. So, in TGP, there are two flotage outlets each on left powerhouse and right powerhouse efficiently outletting the flotages. Meanwhile, the flotage outlets used as flood discharge outlets so that the anterior border of spillway is shortened. However, this is not a thorough means to solve flotage issue for the flotages pollute the ecology environment of Yangtze river. They should be treated in collection.

6 LAYOUT OF TGP

The layout of TGP, shown in Fig. 1, is described as following: spillway dam segments locate in the middle of riverbed, with left power house dam segments, right power house dam segments and non-overflow dam segments on their sides. The powerhouse stands behind the dam, and navigation structure lies in left riverside. An underground powerhouse is obligated in right riverside rocks.

7 CONCLUSION

Having been planned, designed and researched for almost half a century and absorbed successful adventures abroad, many difficult issues have been successfully resolved in studying and researching on TGP layout such as large discharge, huge capacity of unit, complex navigation structure, etc. And the additional units to be installed in future and disadvantages of navigation caused by deposition are all concerned in the layout. Therefore, the layout may ensure TGP running efficiently for a long time.

This page intentionally left blank.

Development of theory and methods on high dam structural analysis*

Qingwen Ren
Hohai University, China

New Developments in Dam Engineering—Wieland, Ren & Tan (eds),

ABSTRACT: The recent development of theory and methods on high dam analysis is presented. The increment of dam height raises the stress level of whole dam. Certain regions of dam and/or the weak structural planes may be failure. The shortcomings of the traditional methods of dam analysis are exposed gradually. Some advanced theories and methods of dam failure analysis, e.g. the indirect method based on nonlinear stability theory, are shown in this paper. The difference between them, the advantages and drawbacks are summarized. The strength and sliding resistance of dam-foundation system not have to be checked separately in failure analysis, the failure process will be shown and the global safety degree of system be obtained. In order to study high dam better to ensure its safety, the theory and method of failure analysis have to be improved further. Some problems that must be solved are presented in this paper.

1 INTRODUCTION

According to the rough estimation[1], over 24,000 dams have been built in China by the end of 2000 and nearly 70 dams are higher than 100m. Estimation in 1999 indicates that the height of 23 dams under construction exceed 100m. With the growth of national economy, more and more high dams are required for the development of hydropower resources in the west. In the completed dams Ertan arch dam and Tianshengqiao CFR dam are 240m and 178m high respectively. In the dams under construction Three Gorges concrete gravity dam, Xiaowan arch dam, Longtan RCC gravity dam and Shuibuya CFR dam are 18m, 292m, 216m and 233m high respectively. In the dams to be built, Jinping first-grade arch dam and Xiluodu arch dam are 305m and 273m high respectively. These huge projects work in complex geological condition and adverse environment, and some of them are built in high earthquake intensity region, So the current codes and standards can not be applicable to them. To ensure the safety of dams, numerical analysis plays an important role even than model test and becomes the predominant method in the study of dam safety.

2 THE DEVELOPMENT OF HIGH DAM

Dam is the main structure in hydropower complex and its function is retaining water and forming reservoir on the upstream of the dam. With the development of economy, the expanded scope of the exploitation of water resources and the advancement of science and technology, dams are built higher and higher. According to the recently estimation, nearly 30 dams that exceed 200m have been built in the world. Among them there are 18 arch dams with the 271.5m high Inguri arch dam in Russia being highest, 4 gravity dams with the 285m high Grande Dixence dam in Swiss being highest and 7 rockfill dams with the 261m high Chicoasen dam in Mexico being highest.

* Sponsored by NSFC (50379005).

Table 1. The high dams building and to be built in China (height over 200m).

Project name	Location	Type	Height (m)	Installation (MW)	Reservoir capacity (10^8m^3)
Xiluodu	Jinsha River, Sichuan, Yunnan	Arch dam	273	12000	115.7
Baihetan	Jinsha River, Sichuan, Yunnan	Arch dam	277	12000	191.5
Hutiaoxia	Jinsha River, Yunnan	Arch dam	278	4200	378.8
Jinping (first-stage)	Yalong river, Sichuan	Arch dam	305	3000	100.0
Shuibuya	Qing river, Hubei	CFRD	233	1500	47.4
Longtan	Hongshui river, Guangxi	RCC gravity dam	216	4200	272.7
Xiaowan	Lancang river, Yunnan	Arch dam	292	4200	151.3
Ruzadu	Lancang river, Yunnan	embankment	258	5000	230.4
Laxiwa	Yellow river, Qinghai	Arch dam	254	3720	10.6
Goupitan	Wu river, Guizhou	Arch dam	225	2000	56.9
Miaoja Dam	Bailong river, Gansu	embankment	263	1000	43.0

In China, only Ertan arch dam exceeds 200m, and the Three Gorges under construction is only 181m. But at the end of 20 century and beginning of 21 century, dams building and to be built higher than 200 m is more than 10 (Table 1). These projects play a very important role in the development of national economy. The scope and difficulty of these dams far exceed the ones built in the world. Owing to the high stress level in the dam body and foundation caused by high dam and the large volume of reservoir, a series of problems on the design and construction of dams will be presented to ensure sufficient degree of safety. To solve them, advanced computational mechanics theory and method are needed, which will provide extensive research space for researchers and promote the further development in this field.

3 THE MAIN CONTENT OF HIGH DAM STRUCTURAL ANALYSIS

Dam and foundation consists a bearing system to sustain the water in the reservoir and other loads. To ensure the safety of dam construction and operation, the stress and strain, strength and sliding resistance of the system under the action of environmental factors should be studied through structural analysis, and probable failure and the corresponding safety degree be predicted. The main content of the structural analysis of high dam consists of:

- The stress and strain analysis of high dam.
- The stability of high dam and its foundation.
- The safety degree assessment and criterion control of high dam.
- The failure theory and analysis method of high dam.

4 THE MAIN FEATURE OF MECHANICS ANALYSIS OF HIGH DAM

The advancement of computational mechanics is closely related to the development of social production and the improvement of computer technology. The characteristic of the computational

mechanics theory and method should be thoroughly understood for its better application to solve technology problems concerning the design and construction of high dam.

(1) High dam, especially arch dam, is a complicated and huge structure, and the computation scale of its analysis is very large. To better simulate the interaction between arch dam and foundation, the foundation area is 1~2 times the height of the dam on both sides of river, 2~4 times along river and not less than 1 time downwards to the base. The calculation scope is wide, and large quantities of thin elements are used for simulation of structural planes in the foundation. For example, in the analysis of Xiaowan arch dam the numbers of elements and nodes are both proximately 100,000, so the computation amount is immense, especially the nonlinear analysis. Thus high performance computers and efficient solving method of system of equations are both required.
(2) There are many kinds of coupling in the analysis. Interaction exists between the dam body and foundation, and between the body and water under the earthquake. Furthermore, the seepage in the foundation and the temperature variation caused by heat of hydration of concrete also have an effect on the stress in dam. So the interaction among the dam body, foundation and water should be studied, and so does that among stress, seepage and temperature field.
(3) Nonlinearity is obvious. Certain areas such as the heel of the dam and the weak structural planes are easily in the yielding state because concrete, rock and soil are typical nonlinear materials and the stress level in the dam body and foundation is very high. When the yielding domain is further expanded, the dam is potentially failure. The rheologic characteristic of the material in the embankment has an effect on the calculation result. According to the analysis of the Shuibuya CFRD, if take the rheology of the rockfill and soil into account, the settlement is increased by 20~30% than that in no consideration of rheology. So nonlinear analysis is unavoidable to high dam.
(4) Most dams are built in deep gorges where traffic is not convenient, topography and geology are complicated and the environment is very adverse, so many undetermined factors exists, such as flood, seepage, the randomness of the physical and mechanical parameters of rock and soil and the ignorance of the geological structure.
(5) The consequence of dam accident is severe, so high level of safety and reliability is required.
(6) The characteristics of dam body and foundation, such as the long construction cycle, the complicated load, the dynamic variation of the structural shape, the material characteristics and the load process, determine the problems in failure analysis of dam, which need further discussion.

5 THE STATE OF ART AND DEVELOPMENT OF THE ANALYTICAL METHOD OF HIGH DAM

5.1 *The analysis of stress and strain*

The available methods of stress analysis of dam in the current codes are based on strength of materials and structural mechanics.

The formula calculating the normal stress on the upper stream and down stream faces of the gravity dam is typical one based on strength of materials:

$$\sigma_y = \frac{\sum W}{T} \pm \frac{6\sum M}{T^2} \tag{1}$$

where the plus and minus are used to calculate the stress on the upper and down stream faces respectively; T is the length of calculating cross-section along the direction from upper to down stream; W and M are the normal force and moment on the calculating cross-section respectively.

The stresses in arch dam are generally calculated by arch-cantilever method based on the structural mechanics. The load distribution and the inner forces in the dam are calculated according to

the displacement coordination on the cross point of the arch and cantilever. The effect of the elasticity of foundation on the stress in the body is roughly considered by use of Vogt coefficient.

The new code[2] on the gravity dam published in 2000 still adopt strength of materials method as the main stress analysis method, and the revising code on the arch dam also gives priority to arch-cantilever method. But these methods cannot be used in the deformation analysis of dam and foundation, and not consider the interaction between the dam and foundation. So these codes are not suitable obviously for high dams. Thus the new code on gravity dam explicitly points out that the FEM should be appropriately used to the calculation of the stress in the dam in addition to strength of materials method, and the verification by structural model and geological mechanics model test should be done when necessary. The revising code on the arch dam requires that arch dams, which are higher than 100m or in complex condition (such as big orifice in the dam, complex geological condition), should be analyzed by use of FEM in addition to arch-cantilever method, and test verification by structural model should be done when necessary

FEM can well simulate the geometry of structure, physical behaviors and loading process in construction, and present the stress distribution and deformation in the dam and foundation. Hence FEM is more and more wildly used in the analysis of high dam. The current main difficulty in the linear elastic finite element analysis is the selection of computational parameters and dependence of the results on the mesh. In the elastoplastic finite element analysis, the result is dependent more closely on the mesh. Furthermore, the constitutive relation of the material, the yielding criterion, the convergence criterion of the nonlinear iteration also have an great effect on the results. The equivalent stress method developed by Fu et al.[3] can weaken the dependence of the result on the mesh, so it is adopted by the revising code on the arch dam.

FEM is essentially a continuous deformation analysis method. To simulate discontinuous planes in the dam and rock such as transverse joints, base surfaces, contact faces between different materials, faults, cracks, fissuring etc., special elements should be added. But excessive discontinuous planes result in large amounts of computation and low accuracy Discontinuous deformation analysis is developing rapidly in recent years, such as Discrete Element Method[4–5], Block Element Method [6],

DDA[7], Numerical Manifold Method[8], FLAC[9] etc. which have been used in the stress and strain analysis of the dam and foundation[10–11].

5.2 *Sliding resistance analysis*

The current codes in China require to adopt Rigid Body Limit Equilibrium Method (RBLEM) to analyze the sliding resistance of the gravity dam along concrete layer faces, base surfaces and weak structural planes in the foundation rock, and that of abutment of arch dam and slope of rockfill dam. For high dams or dams with complicated topography and geology, in addition to RBLEM, FEM and geological mechanics model test are used when necessary.

RBLEM has some advantages such as clear physical definition, simple calculation. And there is the acceptable value given by codes for comparison when using this method. So it is easy to be applied by engineers. But owing to its only consideration of equilibrium condition, the deformation of dam and foundation can't be calculated. Moreover, the method requires the known sliding surface in advance, and only when sliding surface is plane or arc surface, the physical definition of the method is rational.

For high dams and complex foundation with weak structural surfaces, the deformation of dam body and foundation can't be ignored. Excessive deformation will result in the stress deterioration and even failure. So in recent years, Deformable Body Method[12] for stability analysis has great development, in which sliding resistance is studied according to the displacements and stresses obtained by numerical analysis. At the present time, the principle research paths are:

(1) The analysis by direct use of displacements and stresses

- Whether the displacement maximum or rate exceeds the acceptable value;
- Whether the displacement rate decreases continuously according to the shape of displacementtime curve;

• Whether the failure scope is excessive;

All these are qualitative analysis, and the difficulty is the determination of acceptable values.

(2) The calculation of safety factor of sliding resistance according to limit equilibrium formula

• The point safety factor k is calculated by Eqn (2), and the constant value line of it is plotted. Whether the scope of the constant value line for $k \leq 1$ is excessive;

$$k = \frac{f\sigma_n + c}{\tau_t} \tag{2}$$

• Direct Method-the displacements and stresses are calculated under normal conditions (normal loads and normal parameters), and the safety factor of sliding resistance is calculated by limit equilibrium formula directly.

$$K = \frac{fN + cA}{P} \tag{3}$$

The point safety factor only indicates the sliding resistance of the dam-foundation system qualitatively. Strictly speaking, it has directional property, or directions reflected by k of the points on the same constant value line are different. Therefore it is hard to find out the global safety degree of dam. Direct Method can get the global safety Factor of dam, but as RBLEM, the failure surfaces should be known in advance and it is only applicable to simple questions whose failure surfaces are plane or arc face. In a word, when a part of the dam body or rock mass tends to slide along the sliding surfaces, the direct method can be used.

(3) The safety degree of dam-foundation system is determined by use of nonlinear stability theory of elastic system

Since dam-foundation system is a three-dimensional body that the sizes in three directions fall into the same quantity grade, the traditional flexure stability theory is not applicable. The sliding failure of the dam-foundation system generally means the shear failure along a certain surface, which traditionally belongs to strength failure. In fact the formula (2) and (3) reflect the concept of strength failure. But according to the nonlinear stability theory of elastic system, 'state' change of the system means stability failure. Therefore it can be studied from the point of view of 'stability'. This is a 'general stability'. It belongs to extreme point stability failure[12] according to the deformation feature of failure, as shown in Figure 1. The limit equilibrium state corresponding to the extreme point is a critical state of stability. It can be studied by nonlinear stability theory.

The failure of the rock mass of dam foundation has also studied from viewpoint of nonlinear evolution in which dam and rock mass are treated as a dissipation system with time development behavior. The process, which is from the microscopic damage to the formation of sliding surfaces and to failure of the whole body, is a self-organizing one, and can be studied by use of nonlinear theory such as dissipative structure theory, synergism theory and nonlinear dynamic stability theory (including mutation theory and divarication theory)[13,14]

The practical stability analysis formulae based on the above theories are not found. However, From the physical meaning, a limit state method called Indirect Method [15] can be used in analyses,

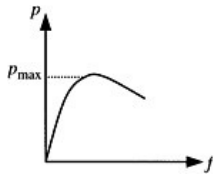

Figure 1. The destabilizing of extreme points.

in which the stability safety degree of the system is regarded as the difference between the limit equilibrium state and the normal state. The current frequent methods are Overload Method and Strength Reserve Method. The strongpoint of Indirect Method is that the failure surface is obtained by searching automatically in the analysis, and need not be given in advance. Thus this method can be used to solve complex problems. But direct method should simulate the failure process of a system, and needs a lot of nonlinear interactive analysis, the computing quantity of which is tremendous. Moreover, it needs the criterion characterizing the limit equilibrium state. The practical stability criterion deduced from the nonlinear stability theory is unavailable. Convergence criterion and mutation criterion proposed by Ren[12] has been used in the stability analysis of high dams such as Three Gorge, Xiaowan, Xiluodu and Baihetan etc.

5.3 *Check of safety degree and control criterions*

The check of dam safety degree according to the current codes in China is done in terms of strength and sliding resistance separately. Since the both have their own control criterion of safety degree, it is difficult to denote the global safety degree of dam. The old code gives the allowable stress in dam body and foundation and the allowable safety factor against sliding, and requires that the maximum stress in the dam body obtained by using strength of materials method and the safety factor against sliding got by using RBLEM should not exceed the allowable value. This is a single safety factor design method. For example, the old design code[16] of arch dams require the tensile stress should not exceed 1.2MPa for the basic load combination, and not exceed 1.5MPa for the special load combination. The requirement for the sliding resistance of rock mass at dam abutment is that the allowable safety factor against sliding under the basic load combination is 3.5 if the dam is a first-level structure and calculated by the shear friction formula (3).

The new code[2,17] adopts the limit sate design method based on the probability statistics theory, and measures the safety of structures with reliability indexes. When the structure is in the limit state, the whole structure or the part of that is deemed not to satisfy the function requirements given by design. The limit states are divided into that of bearing capacity and that of regular service. The criterion of the former is the maximum bearing capacity and the deformation inadequate to further load, and that of the latter is the limited value of certain function of regular service and durability. As the old codes, the new codes ask design to consider three conditions: permanent, temporary and accidental, and two kinds of acting effect combination. All types of requiring to make structure analysis is shown in Table 2.

In the new code, the single safety factor design method is replaced by 5 partial factors: importance coefficient of structure γ_0, design state coefficient Ψ, load action partial coefficients γ_G and γ_Q, material performance partial factor γ_m and structure coefficient γ_d. For example, for the bearing capacity limit state and the basic combination, the limit state equation is:

$$\gamma_0\psi S(\gamma_G G_K, \gamma_Q Q_K, a_K) \le \frac{1}{\gamma_{d1}} R(\frac{f_K}{\gamma_m}, a_K) \tag{4}$$

Table 2. The type of structure analysis.

		Design state		
Limit state	Action effect combination	Permanent	Temporary	Accidental
Limit state of	Basic combination	Yes	Yes	Yes
bearing capacity	Accidental combination	Yes	Yes	Yes
Limit state of	Short-term combination	Yes	Yes	No
regular service	Long-term combination	Yes	No	No

In theory the method can give more scientific assessment of safety degree of dam. But large amounts of samples and statistics data, which is necessary for determination of the partial factors, are unavailable. Especially because of few dam failure, it is difficult to determine the structure coefficient and material partial coefficient by use of finite sample statistics. At present they are mainly obtained by means of the transfer of the single safety factor in the old codes. Hence the calculation results according to the new and old codes are sometimes quite different, which results in the difficulty of adopting new codes.

Generally, the resistance function of the structure R is calculated by strength of materials and structural mechanics for limit state equation of strength of dam, and by rigid body limit equilibrium equation for limit state equation of sliding. For high dams, especially dam foundation with complex geological conditions, the new codes suggest that the check of strength and sliding resistance should be done by use of FEM at the same time. Due to the dependence of the result of FEM on mesh and lack of verification of practice, it should be further discussed that if the partial coefficients are determined according to the code. To decrease the difficulty of strength check induced by stress concentration, the safety is generally assured by restricting the area of tensile stress. Take the limit state of regular service of gravity dams as an example, if uplift pressure is taken into account, the width of the tensile stress area on the dam base surface in upstream side should less than 7% the width of the base surface or the distance between the dam heel and the center line of the curtain.

The above methods of safety assessment of dam are static and local ones, which do not give the probable failure process of dam and foundation and the global safety degree of dam concerned by engineers. In fact, the local material failure and the sliding failure of a little part of dam foundation do not necessarily result in dam failure which should be determined by the study of failure process. Therefore, in recent years the research of failure mechanism and analysis methods is more and more paid attention to especially for high dams.

5.4 *The failure analysis and the safety degree of dam*

For high dams, loads are heavy and then the stress level is high. Concrete, rock and soil are typical of nonlinear materials, and under high stress, they tend to crack or be in the plastic yielding state. The stress redistribution will change the elastic stress field. Moreover people attach more importance to the high dam safety. Therefore, the failure mechanism, evolution and analysis method of the dam-foundation system should be studied. The failure analysis can show the failure process of dam and combine the strength and sliding resistance, which avoids different control criterions used in safety check of the both.

To understand the failure process of high dam and foundation under determined loads and boundary conditions, the material nonlinear FEM is usually used. Considering the rheology, elasticplastic and elastic-fragile behavior of concrete, rock and soil, and using corresponding constitutive relations, the size and distribution of the failure scope can be shown. The research is done from the viewpoint of strength. The failure analysis is also engaged from the viewpoint of damage and fracture, which the failure is deemed as the results of continuous accumulation of initial damage, the formation of cracks and further expansion. So it can be studied by means of damage mechanics and fracture mechanics[18,19] 'state'.

Based on nonlinear stability theory, it is feasible that the failure analysis and the safety degree of high dam-foundation system are studied from the viewpoint of general stability. According to the stability theory of motion for dynamic system[20], the change of any object is a kind of motion in which there is the stability. Therefore, the failure of the system resulted from the high stress of dam body or excessive deformation of foundation can be hold as the stability failure. The characteristic of the failure is that the system is arriving at the limit equilibrium state which means the system to deviate from the original equilibrium state and never return back if there is a little disturbance. In other words, the system state is transforming from the static to movable. Owing to the extreme point on its stress deformation curve, it is the stability failure with extreme point. But an analysis method of stability based on this theory, which can be used to complicated system, is not

found. In present the above Indirect Method can be used alternatively to study the failure process of high dam and foundation to a certain extent.

For high dam normal working under the design running conditions, if the Indirect Method is used to study the failure process and the global safety degree of the dam, Overload Method and Strength Reserve Method are usually adopted. It is to make the dam-foundation system reach the limit equilibrium state closing to structural failure by continuously changing the water pressure acting on the or the upper stream face of dam, or the strength of material, and the global safety degree of the system is the multiple of the variation of the water pressure or strength of material. The former is the overload safety degree, and the latter is the safety degree of strength reserve. Whether the system has arrived at the limit equilibrium state is determined by the convergence criterion and mutation criterion. Figure 2 shows the yielding failure of 11# cross section of Xiangjiaba dam when the shear strength of dam foundation rock is decreased by 1.8 times. It can be seen that the yielding regions has become so wide that the deep slide may occur. And Figure 3 shows the dam displacement increases suddenly. Hence the safety degree of strength reserve of 11# cross section of the gravity dam is assumed as 1.8.

Indirect Method, convergence and mutation failure criterions are not strictly derived from non-linear stability theory, so the determination of the arriving of limit equilibrium state is random. Furthermore, it is difficult to determine the allowable value of safety degree, which needs further study.

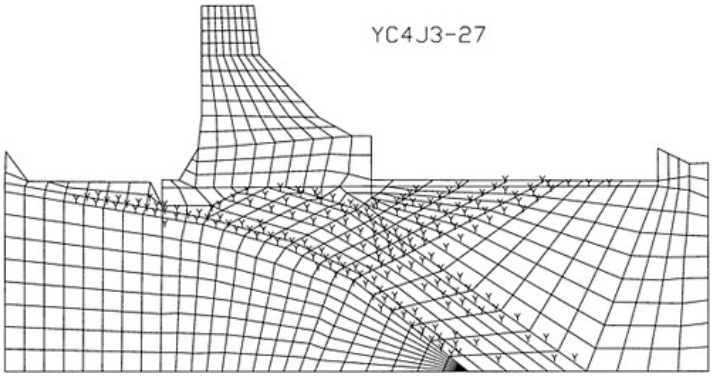

Figure 2. The failure of rock on the 11# cross section of Xiangjia gravity dam (Y-yielding, C-cracking), K=1.8.

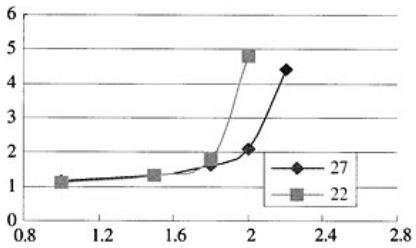

Figure 3. The top horizontal displacement and strength margin K on 11# cross section.

6 THE PROSPECT OF FAILURE ANALYSIS AND ASSESSMENT OF SAFETY DEGREE OF HIGH DAM

In order to make correct failure analysis of high dam and scientific assessment of its safety degree, some problems should be solved:

(1) Failure types and mechanism of high dam-foundation system

Ren and Qian point out the possible failure of high arch dams in the research of failure along base surfaces[21]:

- The dam body failure itself;
- The dam body flexure;
- The sliding of high dams along base surface;
- The sliding of dam abutment rock mass;
- The excessive compression deformation of dam abutment rock mass.

But the numerical analysis and model test[22] show that the final results of the above are the deterioration of stress in dam and foundation, which leads to complete failure of the system, so all of them can be concluded as general stability failure.

(2) Theories and methods of failure analysis

After understanding the failure mechanism of high dam-foundation system, the failure analysis method and failure criterions Based on scientific theory should be found.

(3) Further improvement of numerical models and methods

High dam-foundation system has complex geometry, physical behaviors and environment conditions, and its failure is highly nonlinear phenomenon and should be studied by nonlinear numerical analysis.

Concrete, rock and soil are all typical nonlinear materials. The more actual constitutive relation and physical and mechanical parameters of materials are the important factors to obtain the correct results. In recent years, back analysis is more and more widely adopted, which identifies the parameters and even modifies the constitutive relation according to the measured data.

While materials and structures are approaching failure the increase in deformation is obvious, which is the problem of large deformation. The geometry nonlinearity should be taken into account especially when the failure of dam-foundation system is studied by use of nonlinear stability theory. Therefore failure analysis is a double nonlinear problem.

The dependence of numerical results on mesh should be decreased and the efficiency of solving nonlinear system of equations should be increased.

(4) Assessment of safety degree

Firstly, the safety degree should be defined scientifically. Safety degree is closely related with failure, so it reflects the distance between the critical state closed to failure and the normal design state. To define the safety degree scientifically, the physical index characterizing correctly the distance should be found. Furthermore, the determination of the critical state is also very important to the analysis of safety degree of system.

In order to consider the effects of loads and material parameters on safety degree of damfoundation system, the reliability analysis based on probability theory and mathematical statistics has appeared in the design codes of dam[2,17,23]. But in the safety degree assessment of the system, there are something that cannot be defined and assessed determinately, such as the classification of rock, the values of the allowable safety factor or partial coefficient. Obviously the determination of them are concerned with personal factors and thus has subjectivity and fuzzification. Randomness and fuzziness are two main kinds of indeterminacy, which should be considered in the analysis of dam safety. The main mathematic tool to study fuzziness is fuzzy mathematics which has been used in the optimum design of hydraulic structures, the failure of wall rock of underground cavity and slope, and the effect of reinforcement measures[24] etc. The fuzzy synthesis assessment based on fuzzy mathematics has played an important role in the safety decision[25]. However it is seldom used to safety analysis of high dam. Feng presented his achievements about fuzzy stochastic reliability and fuzzy synthesis assessment for the sliding resistance of abutment rock mass of arch dam in his master's dissertation[26]

Some intelligence method, such as artificial neural network, cluster analysis and fractal theory, have been used in failure analysis of rock mass[27,28] due to their high efficiency of dealing with nonlinear problems. The application to failure analysis and safety degree assessment of high dam should be further studied.

It is worth paying attention that the occurrence of dam failure is not abrupt progressive, which means it experiences a process of good condition, normal working with local damage, serious damage to need repair and complete failure. Therefore, the assessment of safety degree of dams should be gradation.

7 CONCLUSION

With the increase in dam height, the stress level is universally raised especially in high dam under complex geological conditions and severe environment. So safety of dam are more and more concerned. It is of great importance for the safety of high dam to obtain a more rational and correct method of failure analysis and safety degree assessment.

As far as stress analysis of dam is concerned. The methods in the current codes are mainly based on strength of materials and structural mechanics. For high dams, loads become heavy and the stress level in dam and foundation is high. Some parts of dam, weak structural planes of rock and soil tend to be in the yielding state. To simulate complicated geometry shape, boundary conditions and loading processes under construction, numerical analysis methods should be adopted. At present linear elastic and elastic-plastic FEM have been widely used in the stress analysis of high dam-foundation system. Besides further improving the analysis method of continuous deformation, the discontinuous deformation analysis is the direction of development in the future.

With regard to the sliding resistance of dam and foundation, RBLEM still predominates in the current codes. For high dams, the Deformable Body Method of stability analysis based on numerical results has been developed because the stability failure mainly induces by excessive deformation and high stresses. So far the Indirect Method based on nonlinear stability theory is a fairly good one for the stability analysis of complicated system. But it is not derived strictly from non-linear stability theory; so there are many problems to solve.

For the check of dam safety degree, taking the randomness of loads and materials parameters into account, the current codes adopt the limit state design methods based on probability statistics theory instead of the single safety factor method by introducing 5 partial coefficients and measuring the safety by reliability indexes. However, the analysis of dam safety degree is done separately from strength and sliding, and can not obtain the global safety degree and the failure process of dam. Moreover, the local failure of materials do not certainly result in dam failure. Therefore in this paper, failure analysis method is suggested and problems related to correct failure analysis and reasonable safety degree assessment are presented.

REFERENCES

1. 潘家诤，何璟，中国大坝 50 年，北京，中国水利水电出版社，2000, 2000
2. 北京，中国电力出版社, 2000
3. 付作新，钱向东，有限单元法在拱坝设计中的应用[J]，河海大学学报, 1991, 19(2):8–15.
4. Hart, R., Cimdali, P.A. & Lemos, J. Formulations of Three-Dimensional Distinct Element Model, Part II, Mechanical Calculation of ASystem Composed of Many Polyhedral Blocks. Int. J. Rock Mech. Min. Sci. Geomech.Abstn, 1988, 25(3):117–125
5. Zhang Chuhan, O.Pekau, Jin Feng and Wang Guanglun, Application of Distincl Eiement Method in Dynamic Analysis of High Rock Slopes and Blocky Structures. Soil Dynamics and Earthquake Eng., 1997, 16(7):385–394
6. 任青文，余天堂，块体单元法的理论和计算模型，工程力学, 1999, 16(1):67–77
7. Shi. G.H. & Goodman, R.E. Two Dimensional discontinuous Analysis. Int. J. Numer. Anal. Methods Geomech., 1985, 9(7):541–556

8. 石根华，数值流形方法与非连续变形分析，北京：清华大学出版社，1997
9. 黄润秋，许强，显式拉格朗日差分分析在岩石边坡工程中的应用，岩石力学与工程学报, 1995, 14(4):346–354
10. Zhang Guo-xin, Jin Feng, Wang Guang-lun, Seismic Failure Simutation of Gravity Dam by Manifold Based Singular Boundary Element Method, Engineering Mechanics, 2001, Vol. 18(4):18–27.
11. Ruan Mao-tian, Li Yong, Lin Gao, The Discontinuous Deformation Mechanics Model and Its Application in Static Analysis of Ccmcrete Gravity Datn with Vertical Joints, Journal of Hydraulic Engineering, 2001, (4):40–46.
12. 任青文，岩体破坏分析方法的研究进展，岩石力学与工程学报, 2001, 20(supp.2):1303–1309.
13. 黄润秋，许强，开挖过程的非线性理论分析，工程地质学报, 1999, 7(1):9–14
14. 郭火元，突变理论及其在大坝稳定分析中的应用，大坝观测与土工测试, 1993, 17(1):10–13
15. 号坝段稳定性的数值分析和试验研究，中国工程科学, 1999, 1(3):41–45
16. 混凝土拱坝设计规范 1985
17. 中国电力出版社, 1994
18. 杨友卿，岩石强度的损伤力学分析，岩石力学与工程学报, 1999, 18(1):23–27
19. 朱维申，张强勇，节理岩体脆弹性断裂损伤模型及其工程应用，岩石力学与工程学报, 1999, 18(3): 245–249
20. 《力学词典》编辑部，力学词典，北京：中国大百科全书出版社, 1990: 551–552
21. 任青文，钱向东等，高拱坝严建基面抗滑稳定性的分析方法研究，水利学报, 2002, (2):1–7
22. 任青文，钱向东等，高拱坝严建基面的破坏和安全度研究，水力发电, 2002, (12):10–13
23. 中国电力出版社, 1997
24. 中国电力出版社, 1999, 18(6):704–708
25. 夏元友，朱瑞赓. 岩质边坡稳定性多人多层次模糊综合评价系统研究，工程地质学报, 1999, 7(1):46–53
26. 房勇，拱坝坝肩岩体稳定的模糊分析方法，硕士学位论文，河海大学, 2004
27. 卢才金，胡厚田等，改进的 BP 网络在岩质边坡稳定性评判中的应用，岩石力学和工程学报, 1999, 18(3):303–307.
28. Lee Y.H., et al, The Fractal dimension as a measure of the roughness of rock discontinuity profiles, Int. J. Rock Mech Min Sci & Geomech Abstr, 1990, 27(4):453–464.

This page intentionally left blank.

New Developments in Dam Engineering—Wieland, Ren & Tan (eds),
© 2004 Taylor & Francis Group, London, ISBN 04 1536 240 7

Dynamic and pseudo-static failure analyses of embankment dams

T.Tanaka & D.Harada
University of Tokyo, Japan

S.Masukawa
National Research Institute of Agricultural Engineering

H.Mori
Institute of Civil Engineering of Tokyo Metropolitan Government

ABSTRACT: The elasto-plastic soil model is applied to dynamic response analysis of embankment dam. The results of finite element analysis are compared with those from the physical experiments. The seismic slope stability by pseudo-static elasto-plastic finite element analysis was also estimated. When using finite element analysis, the dynamic relaxation method combined with the generalized return-mapping algorithm was applied to the integration algorithms of the elastoplastic constitutive model. The homogenous slope, using the critical horizontal seismic coefficient and maximum shear strain distribution obtained by finite element analysis, exhibited agreement with the result of sliding surface method. Further the three-dimensional finite element analyses were applied to the model experiments with dry sand.

1 INTRODUCTION

The dynamic response method combined with the generalized return-mapping algorithm is applied to the integration algorithms of elasto-plastic constitutive relations including the effect of the shear band. The constitutive model is based on the assumption that the area under the strain softening regime can be regarded as a material parameter. In order to guarantee a mesh-objective consumption of energy, the strain softening modulus is made a function of element size. This kind of shear banding model can incorporate a characteristics length of shear band in the material modeling based on physical experimental observations of strain localization with a finite size. The elasto-perfectly plastic model with residual strength and peak strength is also applied. We will also attempt to estimate the seismic slope stability by comparing the findings of conventional sliding surface analysis with the findings of pseudo-static elasto-plastic finite element analysis. When using finite element analysis, the dynamic relaxation method (Tanaka and Kawamoto, 1988) combined with the generalized return mapping algorithm is applied to the integration algorithms of the elasto-plastic constitutive model. Finally the three dimensional finite element analysis is applied to the pseudo-static seismic stability problem of slope with dry sand.

2 EXPLICIT DYNAMIC RESPONSE ANALYSIS

Solution to systems of nonlinear equations involving the governing non-linear equation is obtained as

$$P - P^{init} = F \quad \text{and} \quad P = \sum_{N} \int_{vol} B^{T} \sigma dv \tag{1}$$

where P is the internal force vector, P^{init} is the nodal forces due to initial stresses, F is the external force vector, B^T is the strain-displacement transformation matrix, N is the number of elements in Finite Element discretization, σ is the stresses at Gauss points in each element, and vol is the volume of each element. The solution to the above governing equation can be obtained by achieving the steady state response of the following dynamic equation of motion;

$$M_D a + C_v + P - P^{init} = F \tag{2}$$

where M_D is the diagonalized mass matrix, C is the damping matrix, which is a vector for critically damped dynamic relaxation, v is the velocity vector, and a is the acceleration vector.

Then, applying the central difference method to Eq.(2) and replacing the damping by the following relation;

$$\boldsymbol{C = \alpha M_D} \tag{3}$$

the following relaxation equation can be derived;

$$q_{n+1} = \frac{1}{1 + 0.5\alpha\Delta t}\left[\frac{\Delta t^2}{M_D}(F - P + P^{init})^t + 2q_n - (1 - 0.5\Delta t)q_{n-1}\right] \tag{4}$$

Here, q_n is the displacement vector at time n, Δt the time increment and α is the damping ratio which is the most critical value to be determined.

As dynamic response computation is based on an explicit integration scheme, it suffers from the stability problem. The condition for stable analysis can be expressed as;

$$\Delta t \le \beta \frac{l}{V_c} \tag{5}$$

where Δt is time required to pass the deformation wave from one node to adjacent node, β is the stability factor (β<1.0), and l is the minimum distance between the adjacent nodal point for an element and V_c is the compression wave velocity of the medium.

3 MATERIAL MODEL FOR SHEAR BAND

A simplified and generalized version of mesh size-dependent softening modulus method (Pietruszczak and Mroz, 1981) is used in this study. A material model for a real granular material (i.e., Toyoura sand) with a high angle of internal friction was used with the features of nonlinear prepeak, pressure-sensitivity of the deformation and strength characteristics of sand, non-associated flow characteristics, post-peak strain softening, and strain-localization into a shear band with a specific width (Tanaka and Kawamoto, 1989; Siddiquee, 1999). The material model will be briefly described in this section.

The yield function *(f)* and the plastic potential function *(Φ)* are given by;

$$f = \alpha I_1 + \frac{\bar{\sigma}}{g(\theta_L)} = 0 \tag{6}$$

$$\Phi = \alpha' I_1 + \bar{\sigma} = 0 \tag{7}$$

where

$$\alpha = \frac{2\sin\phi}{\sqrt{3}(3 - \sin\phi)} \tag{8}$$

$$\alpha' = \frac{2\sin\psi}{\sqrt{3}(3-\sin\psi)} \tag{9}$$

where I_1 is the first invariant (positive in tension) of deviatoric stresses and $\bar{\sigma}$ the second invariant of deviatoric stress. With the Mohr-Coulomb model, $g(\theta_L)$ takes the following form;

$$g(\theta_L) = \frac{3-\sin\phi}{2\sqrt{3}\cos\theta_L - 2\sin\theta_L\sin\phi} \tag{10}$$

ϕ is the mobilized friction angle and θ_L is the Lode angle. The frictional hardening-softening functions expressed as follows were used;

$$\alpha(\kappa) = \left(\frac{2\sqrt{\kappa\ \varepsilon_f}}{\kappa+\varepsilon_f}\right)^m \alpha_p \quad (\kappa \le \varepsilon_f) : \text{hardening-regime} \tag{11}$$

$$\alpha(\kappa) = \alpha_r + (\alpha_p - \alpha_r)\exp\left\{-\left(\frac{\kappa-\varepsilon_f}{\varepsilon_r}\right)^2\right\} \quad (\kappa \ge \varepsilon_f) : \text{softening-regime} \tag{12}$$

where m, ε_f and ε_r are the material constants and α_p and α_r are the values of α at the peak and residual states.

The residual friction angle (ϕ_r) and Poisson's ratio (ν) were chosen based on the data from the test of air-dried dense Toyoura sand. The elastic moduli are estimated using the following equations.

$$G = 900\frac{(2.17-e)^2}{1+e}\left(\frac{p}{p_a}\right)^{0.4} p_a \quad (p_a = 98kPa) \tag{13}$$

$$K = \frac{2(1+\nu)}{3(1-2\nu)}G \tag{14}$$

The peak friction angle (ϕ_P) was estimated from the following empirical relations based on the plane strain compression test on dense Toyoura sand.

$$\phi_p(\text{deg}) = \left\{59.47(1.5-e) - 10(1-e)\log\left\{\frac{\sigma_3}{(\sigma_3)_0}\right\}\right\} g_R(\delta) \tag{15}$$

$$(\sigma_3)_0 = 4(1-Ze)p_a \quad (p_a = 98kPa) \tag{16}$$

The peak friction angle is a function of confining pressure, initial void ratio e and angle δ of the direction of σ_1 relative to the horizontal bedding plane. The dilatancy angle (Ψ) was estimated from Rowe's stress-dilatancy relation.

The introduction of shear banding in the numerical analysis was achieved by introducing a strain localization parameter s in the following additive decomposition of total strain increment as follows;

$$d\varepsilon_{ij} = d\varepsilon_{ij}^e + s\,d\varepsilon_{ij}^p \quad , \quad s = F_b / F_e \tag{17}$$

where F_b is the area of a single shear band in each element; and F_e is the area of the element.

4 DYNAMIC PROGRESSIVE FAILURE OF EMBANKMENT DAMS (Tanaka, Harada and Masukawa, 2004)

The model dams were subjected to simulated earthquake by means of a three-dimensional shaking table apparatus at the National Research Institute of Agricultural Engineering. The shaking table consisted of a 5.67m–3.57m rigid steel slab. Steel walls 1.3m high were provided to support the ends of the model. The model dams were two-dimensional with a plane strain condition. Models were constructed on the table using the Toyoura sand with water content 5%. The sand with predetermined weight was thrown on the shaking table every 5 cm, and compacted so that the relative density might become 50% using the vibrator. In order to measure the response acceleration by simulated earthquake, the accelerometer was embedded in the predetermined layer on the central section A. The simulated earthquake was both horizontal and vertical. The size of a model dam was 255 cm wide, 80 cm high, 277 cm long, and the slope was 1:1.5 (Fig. 1).

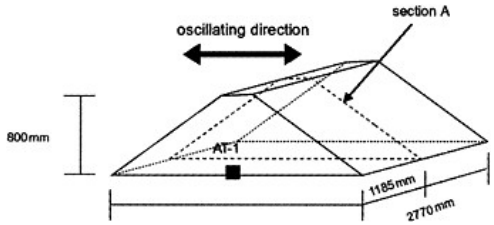

Figure 1. Outline of model dam.

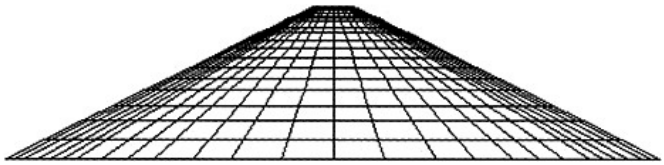

Figure 2. Finite element mesh.

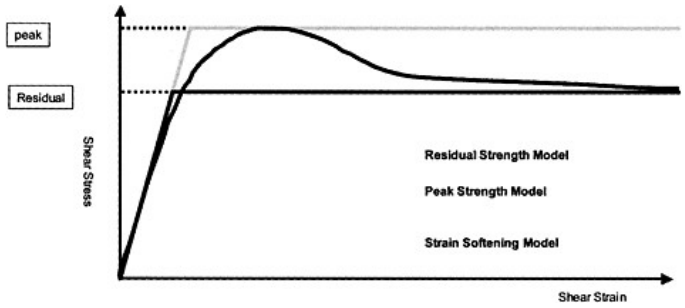

Figure 3. Stress-strain relations used for dynamic analysis.

In finite element analysis, elasto-perfectly plastic constitutive model and the strain hardeningsoftening model with shear band were used (Fig. 3). The linear iso-parametric element with onepoint integration was adopted as the finite element with hour-glass control. Material constants for the constitutive model are shown Table 1.

The input acceleration for computation was measured one at the bottom of model dams. Figure 4 shows the observed horizontal acceleration and Fig. 5 shows the vertical acceleration. The finite element mesh used for the analysis is shown in Fig. 2.

The horizontal accelerations of the model dam from an experiment and an analysis are shown in Fig. 6–7 (at center) and in Fig. 8–9 (at crest). The vertical accelerations at crest are shown in Fig. 10–11. The computed accelerations are obtained using elasto-perfectly plastic model with residual strength. The vertical displacements of the model dam at crest from an experiment and analyses are shown in Fig. 12–15. The computed displacements by elasto-perfectly plastic constitutive model with residual and peak strength exhibited agreement with observed one.

The sectional view of a model dam near the central section after test is shown in Fig. 16. The deformed shape after dynamic experiments is not symmetric, because the direction of combined input motion is tilted. The slip bands were circularly generated on upstream slope and tension cracks were observed on both upstream and downstream slopes. The maximum shear strain contour computed using elasto-perfectly plastic model with residual strength is shown in Fig. 17.

Table 1. Material constants.

ρ_t	Wet density	13.92kN/m^2
ϕ_r	Residual internal friction angle	33°
D_r	Relative density	50%
v	Poisson's ratio	0.2
c	Apparent cohesion	0.98 kN/m^2

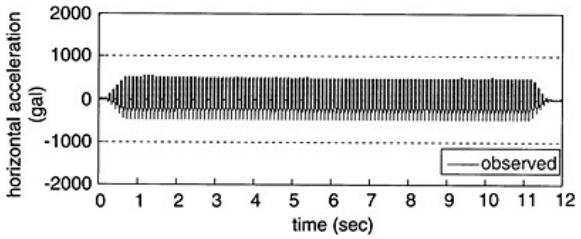

Figure 4. Horizontal acceleration observed at base.

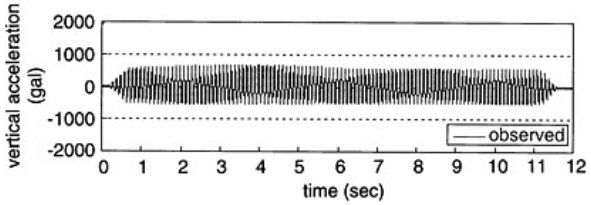

Figure 5. Vertical acceleration observed at base.

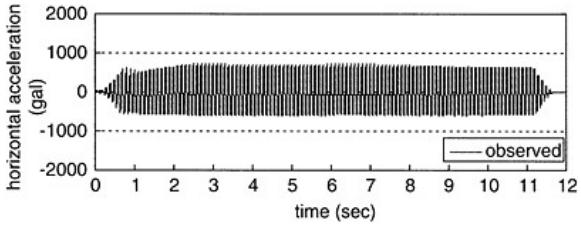

Figure 6. Horizontal acceleration observed at center.

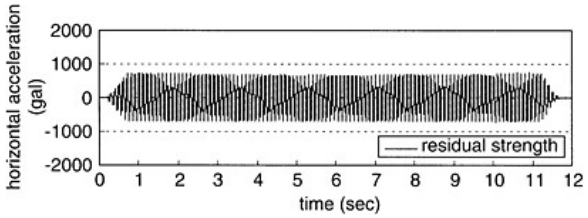

Figure 7. Horizontal acceleration computed at center using residual strength.

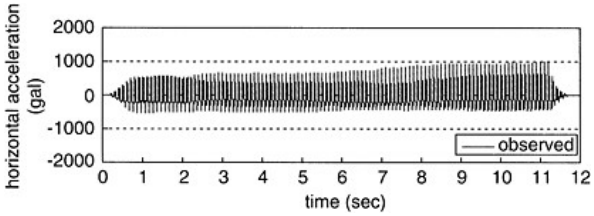

Figure 8. Horizontal acceleration observed at crest.

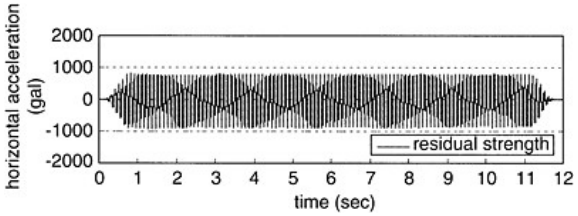

Figure 9. Horizontal acceleration computed at crest using residual strength.

Similar result is obtained for elasto-perfectly plastic model with peak strength (Fig. 18). When using strain-softening constitutive model, good results were not necessarily obtained contrary to the case that the only horizontal accelerations were applied (Tanaka, Saito, Kohgo and Harada, 2002). In these experiments, extremely severe vertical acceleration induced prevailed tension in

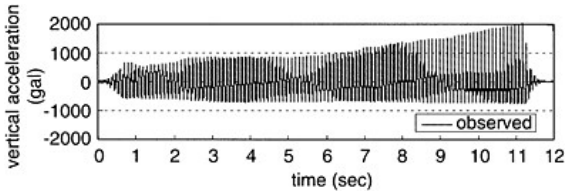

Figure 10. Vertical acceleration observed at crest.

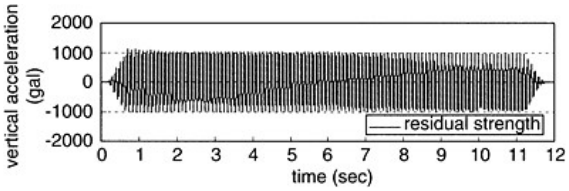

Figure 11. Vertical acceleration computed at crest using residual strength.

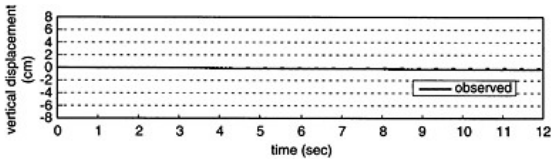

Figure 12. Vertical displacement observed at crest.

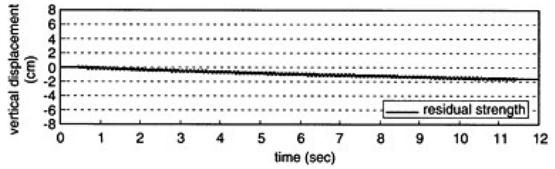

Figure 13. Vertical displacement computed at crest using residual strength.

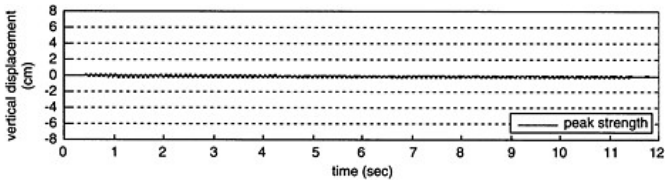

Figure 14. Vertical displacement computed at crest using peak strength.

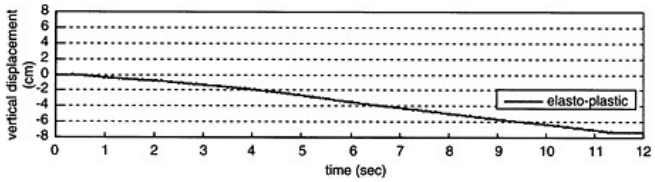

Figure 15. Vertical displacement computed at crest using strain-softening model.

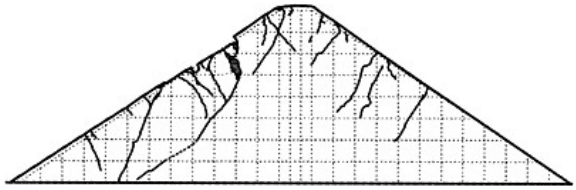

Figure 16. Sectional view of model dam after dynamic test.

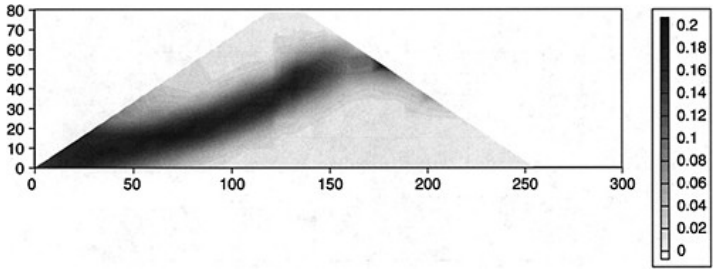

Figure 17. Computed maximum shear strain contour (residual strength).

Figure 18. Computed maximum shear strain contour (peak strength).

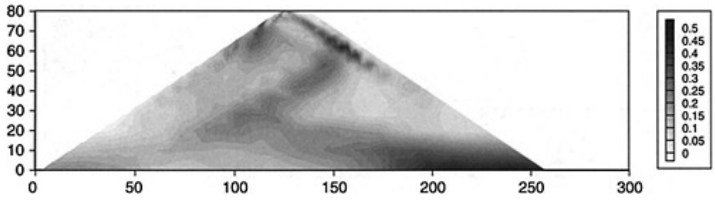

Figure 19. Computed maximum shear strain contour (strain softening).

embankment, so the simple elasto-perfectly plastic constitutive model give superior result to refined strain softening model.

5 PSEUDO-STATIC ELASTO-PLASTIC FINITE ELEMENT ANALYSIS (Mori, Tanaka and Kusano, 2002)

An accurate prediction of the limit load of soil structures is a key facet for problems related to soil mechanics. In this analysis, the dynamic relaxation method combined with the generalized return mapping algorithm (Ortiz and Simo, 1986; Okajima, Tanaka and Mori, 2001) was applied to the integration algorithms of elasto-perfectly plastic constitutive model. These solutions are in a steady state solution of the transient dynamic problem. A constitutive model based on the yield function of Mohr-Coulomb type and the plastic potential function of Drucker-Prager type is employed.

With four types of homogenous slopes from different ground conditions, we assessed the validity of the circular sliding surface method as depicted in Fig. 20. Figure 21 illustrates the finite element mesh of slope. Firstly, the self-weight analysis was performed to obtain the initial stress of slope. Secondly, the equivalent horizontal accelerations corresponding to the seismic coefficient were applied. When applying the horizontal seismic coefficient, the vertical displacement of node No. 104 began to show up as a critical horizontal coefficient *(Kh)*. Figure 22 shows the results by the finite element analyses and the circular sliding surface method by using the Fellenius and Bishop simplified method. A uniform material was assumed for four types of slopes: the elastic modulus (E=40000 kN/m^2) and Poisson's ratio (v=0.4). Type-1 consisted of frictional soil without cohesion, the slip surface by circular sliding surface method appeared at a very shallow depth, so the method was considered difficult in applying to sandy ground. Type-4 consisted of some different layers, although *Kh* obtained by finite element analysis coincided with that by circular sliding surface method, the distribution of maximum shear strain indicated non-circular failure surface. Type-2 consisted of C soil andType-3 consisted of φ-C soil, the concentrated zone of maximum shear strain by finite element analyses coincided with failure surface by circular sliding surface method and *Kh* obtained by both analyses closely correlated. On the other hand the slip surface procedures used in the Bishop method closely correlated to the findings in the finite element analysis rather than those of the Fellenius method.

The pseudo-static model test under centrifuge acceleration 50g was carried out. The soil for this test was a mixture of Toyoura sand and kaolin. Figure 23 shows the finite element mesh for simulating the centrifuge static tilting model test. The material parameters for analysis decided from results of CD-test were unit weight=16kN/m^3, E=40000 kN/m^2, v=0.333, φ=32.4° and C=6.0 kN/m^2. Figure 24 showed the concentrated zone of maximum shear strain at around critical horizontal seismic coefficient *Kh*. When *Kh* was just 0.18, the maximum shear strain was

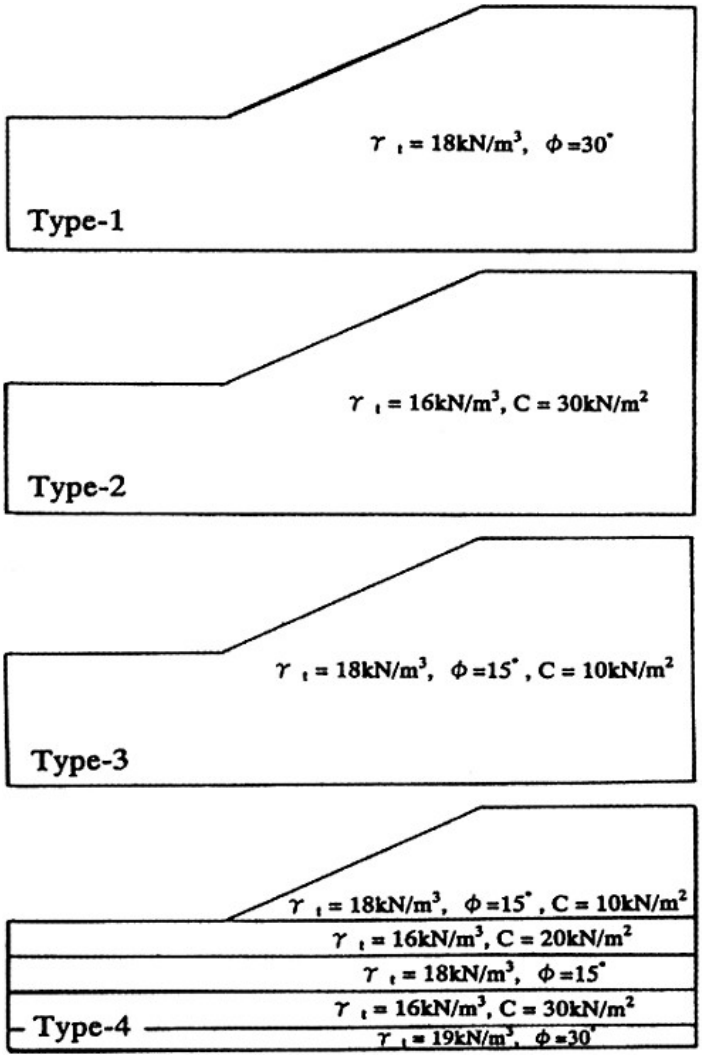

Figure 20. Four type homogenous slopes.

concentrated on the localized zone and the deformation was salient. The collapsing *Kh* by the analysis coincided with those of centrifuge experiment.

A model experiment with normal gravity was carried out using a tilting apparatus of a slope prepared by dry sand without cohesion. The elasto-plastic constitutive soil model including the

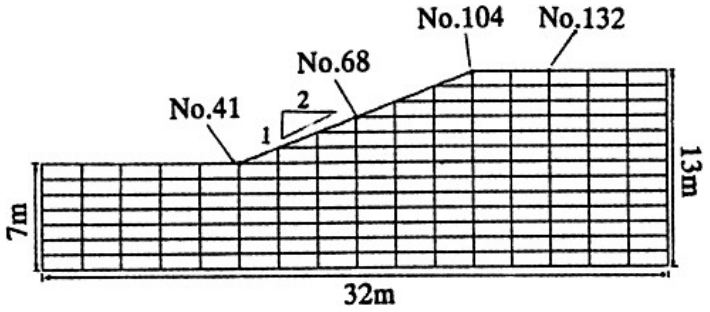

Figure 21. Finite element mesh for slope.

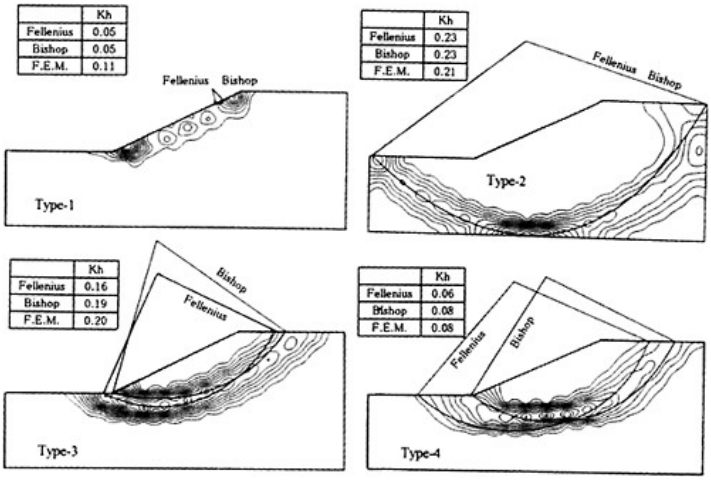

Figure 22. Finite element and circular sliding analyses of slopes.

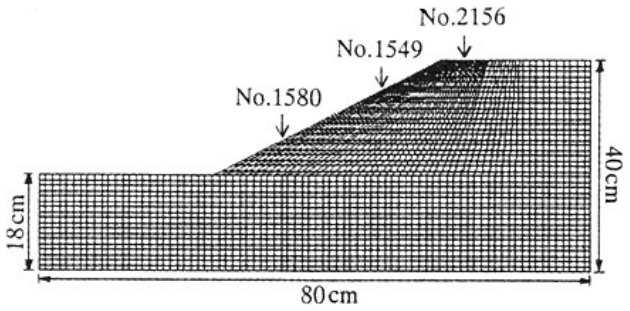

Figure 23. Finite element mesh for centrifuge static tilting model test.

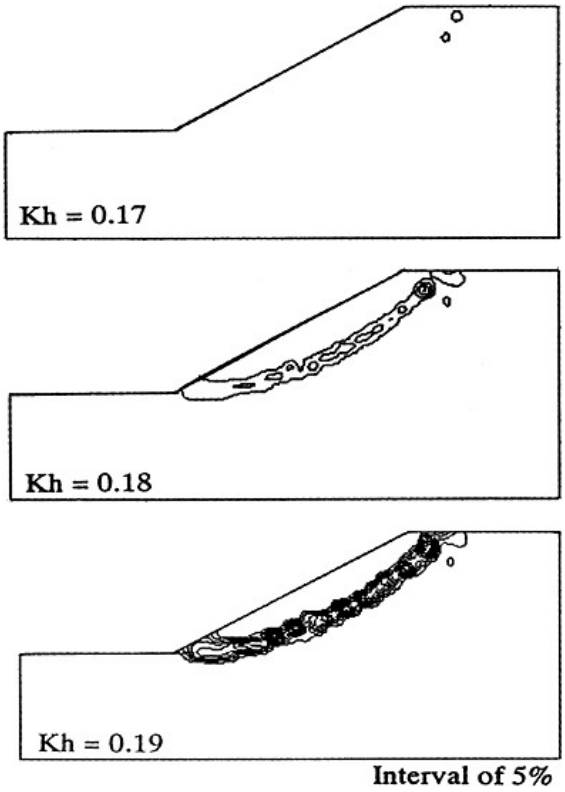

Figure 24. Maximum shear strains by finite element analyses.

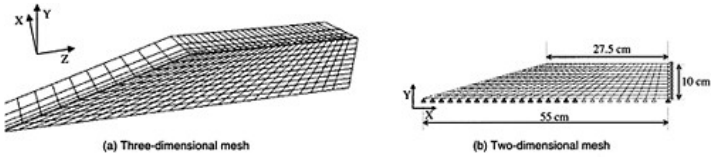

Figure 25. Finite element mesh for slope with dry sand.

effect of shear band is applied to the analyses. Two- and three-dimensional finite element analyses were performed. The three-dimensional analysis was used to estimate the influence of friction by the side glass wall. Figure 25 shows the two- and three-dimensional finite element mesh. This side of three-dimensional mesh is glass side wall with friction and the other side is symmetry surface with no friction. Figure 26 shows the computed deformation of slope and Fig. 27 shows the contours of maximum shear strain. Figure 28 shows relation between relative density and failure

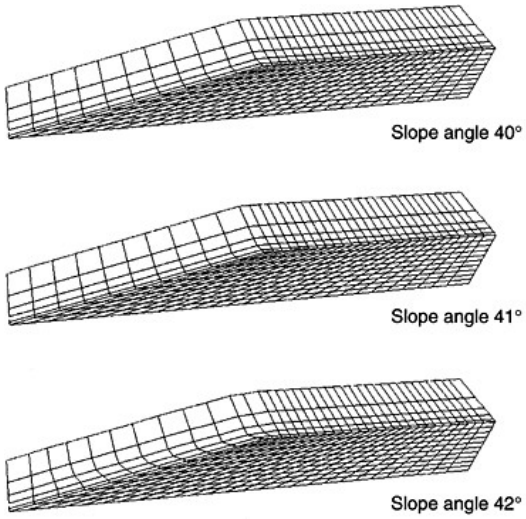

Figure 26. Deformation of slope by three-dimensional finite element analysis (Dr. 90%).

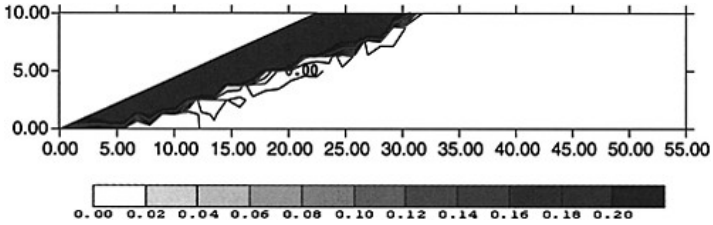

Figure 27. Contours of maximum shear strain (slope angle 43°).

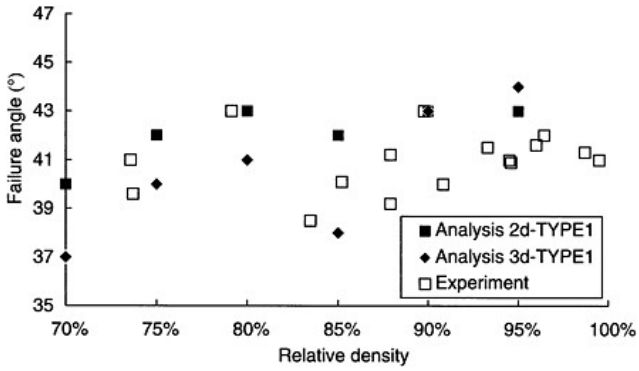

Figure 28. Comparison of two- and three-dimensional finite element analysis.

angle of slopes and illustrates that the failure of dry slope computed by finite element analysis coincided with the experiments. In the case of dry sand slope, straight surface sliding develops and sliding surface is very shallow, so the friction of the side glass wall influences little.

6 CONCLUSION

A mesh size-dependent softening modulus method is used in this study. A material model for a real granular material with a high angle of internal friction was used with the features of non-linear pre-peak, pressure-sensitivity of the deformation and strength characteristics of sand, non-associated flow characteristics, post-peak strain softening, and strain-localization into a shear band with a specific width. The analyses showed almost same acceleration as for a model experiment. Simple elasto-perfectly plastic constitutive model gave zones of concentrated maximum shear strain similar to the observed shear band and cracks.

In case of a homogenous slope, the critical horizontal seismic coefficient and maximum shear strain obtained by finite element analysis exhibited positive correlation with the result of circular slip calculation. The critical horizontal seismic coefficient obtained by the centrifuge test correlated with the circular sliding surface method by Fellenius simplified method. Also, the observed failure surface by experiment was shallower than the calculated circular slip surface.

A model experiment with normal gravity was carried out using a tilting apparatus of a slope prepared by dry sand without cohesion. The elasto-plastic constitutive soil model including the effect of shear band was applied to the analysis of model experiments. The failure of dry slope computed by finite element analysis coincided with the experiments.

REFERENCES

Mori H., Tanaka, T. and Kusano, K. (2002), Pseudo-Static Elasto-Plastic Finite Element and Circular Sliding Surface Analysis for Stability of Slope on Soft Ground. Proc. Int. Conf. On Coastal Geotechnical Engineering in Practice, Atyrau, Kazakhstan, 199–204

Ortiz, M. and Simo J.C. (1986), An Analysis of a New Class of Integration Algorithms for Elasto-Plastic Constitutive Relations. Int. J. Numer. Meth. Engng., 23, 353–366.

Okajima, K., Tanaka, T. and Mori, H. (2001), Elasto-Plastic Finite Element Collapse Analysis of Retaining Wall by Excavation, Computational Mechanics New Frontiers for the New Millennium, Vol. 1, 439–444

Pietruszczak, ST. and Mroz, Z. (1981), Finite Element Analysis of Deformation of Strain Softening Materials, Int. J. Numer. Meth. Engng., 17, 327–334.

Siddiquee, M.S.A., Tanaka, T., Tatsuoka, E, Tani, K. and Morimoto, T. (1999), Numerical Simulation of Bearing Capacity Characteristics of Strip Footing on Sand, Soils and Foundations, Vol. 39, No. 4, 93–109.

Tanaka, T. and Kawamoto, O. (1988), Three Dimensional Finite Element Collapse Analysis for Foundations and Slopes Using Dynamic Relaxation, Proc. Numerical Methods in Geomechanics, Insbruch, 1213–1218.

Tanaka, T. and Kawamoto, O. (1989), Plastic Collapse Analysis of Strain Softening Materials, Proc. Numer. Models in Geomech. (NUMOGIII), 667–674

Tanaka, T., Saito, Y., Kohgo, Y. and Harada, D. (2002), Dynamic Progressive Failure of Earth Dams by FEM and Model Experiments, 3rd Int. Conf. on Dam Engng., Singapore, 323–330.

Tanaka, T., Harada, D. and Masukawa, S. (2004), Dynamic Progressive Failure of Embankment Dams, ASCE, 17th Engineering Mechanics Conf. Newark.

New Developments in Dam Engineering—Wieland, Ren & Tan (eds),
© 2004 Taylor & Francis Group, London, ISBN 04 1536 240 7

Summarization of Xiluodu concrete arch dam design

Wang Renkun
Chengdu Hydroelectric investigation & design institute of SPC, Sichuan Chengdu, P.R China

ABSTRACT: On the basis of the national design code, successful design experiences of large dams and the latest technology home and abroad, Xiluodu Arch Dam design has adopted normal design methods, modern numerical methods with virtual reality technology and geomechanic model test method etc., in cooperation with projects comparative analysis, to study the feasibility of the dam basement, dam shape, dam stress and intensity, anti-slide stability and overall stability, seismic design, concrete temperature control, foundation treatment etc., consequently, a feasible, safe and economical arch dam has been designed. This paper mainly introduces the principle considerations, analysis methods and conclusions of Xiluodu Arch Dam design.

1 INTRODUCTION

Xiluodu Arch Dam is 278m high. The valley in dam site takes on a narrow symmetric "U" shape, where the bed rock is composed of fresh basalt with massive structure and high strength, except for some sheared bands between or in the strata. The basic seismic intensity in dam site is 8 degree. As the height and complexity of the dam exceed the applicable scope of the national arch dam design code, based on the basis of the national design code, successful design experiences of large dams and the latest technology home and abroad, Xiluodu Arch Dam design has utilized normal design methods, modern numerical methods with virtual reality technology and geomechanic model test method etc., in cooperation with projects comparative analysis, to study the feasibility of the dam basement, dam shape, dam stress and intensity, anti-slide stability and overall stability, seismic design, concrete temperature control, foundation treatment etc., consequently, a feasible, safe and economical arch dam has been designed.

2 DESIGN STANDARD OF DAM STRESS AND DAM STABILITY

2.1 *Design standard of dam stress*

In accordance with the code of concrete arch dam design and the code of hydroelectric structure seismic design, and based upon the recent successful experiences of high arch dam designs in china, with reference to the design stress standards of high dam home and broad, the design standard of dam stress of Xiluodu Arch Dam, corresponding to the trial-load method, is put forward, as shown in Table 1 and Table 2.

2.2 *Design standard of dam anti-slide stability*

The limit equilibrium method is utilized as main method in dam stability evaluation, correspondingly, the friction coefficient and shear-friction coefficient is adopted to evaluate the dam anti-slide stability.

Table 1. Arch dam stress standard.

Allowable stress load combination	Compressh (MPa)	Tensile (MPa)		Safety coefficients of concrete compressive strength
		Upstream	Downstream	
Usual loads	9.0	1.2	1.5	4.0
Unusual loads (no earthquake)	10.0	1.5	1.5	3.5

Table 2. Arch dam stress standard under special loads condition (earthquake).

Concrete design strength (MPa)	Allowable compressive stress (MPa)	Allowable tensile stress (MPa)
25	12.9	2.4
30	15.4	2.9
36	17.9	3.3

Note: The concrete design strength is defined as: the limit compressive strength under standard procedure, 20cm cubic specimen, 180d age, with assurance factor of 85% differential coefficients Cv≤0.15.

Table 3. The characteristics of Xiluodu arch dam.

Item	Value	Item	Value
Height (m)	278.0	Thickness to height ratio	0.248
Crest thickness (m)	14.0	Arch length to dam height ratio	2.512
Bottom thickness (m)	69.0	Upstream overhang	0.217
Maximum thickness at dam abutment	75.70(El.360m)	Concrete volume (10^4m^3)	665.60
Center angle of crest arch (°)	93.54	Excavation volume of dam foundation (10^4m^3)	526.00
Maximum center angle (°)	96.21 (El.480 m)	Flexibility of unit height	10.68
The length of the center line of crest arch (m)	698.07	Arch length of upstream crest arch. (m)	710.55

The design standard of dam stability is: 3.5 of shear-friction coefficient and 1.3 of friction coefficient, as well as 1.2 of shear-friction coefficient under seismic condition, according to the code of hydroelectric structure seismic design.

3 DAM BASEMENT AND DAM SHAPE

Due to the dam height and tremendous water pressure, the dam basement will be mainly composed of the fresh and the lower section of the moderately weathered rock at middle and low elevation, while partly of the upper section of the moderately weathered rock at high elevation. The dam basement in river bed is at El.332.00m, while the crest is at El. 610m.

The following factors have been taken into consideration in dam shape design.

1. The valley in dam site takes on a narrow symmetric “U” shape, and the dam foundation is of good geologic condition, therefore, a number of the parabolic dam shapes and 3- center-arc dam shapes are compared to ensure a suitable dam shape to meet all the requirements.
2. Because of the high seismic intensity in dam site and several discharge orifices in dam body, the dam is design to be moderately thick to ensure sufficient rigidness for dam overall stability.

3. The dam shape is considerable flat to make the direction of arch forces at higher angles to river flow.
4. Only longitudinal construction joints are designed and overhang ratio is less than 0.3.

In corporation with the results of "ninth five-year" state key research program, based on a large numbers of dam type studies, dam shape optimization and refinements, a parabolic double conventure dam, which is well adaptive to variations dam foundation, is designed, as shown in Table 3.

4 DAM STRESS ANALYSIS

The trial-load method is principally utilized to study the dam stress, in cooperation with the finite element method (FEM) and geomechanic model test to confirm the rationality of dam intensity design. As indicated by lots of computations under different load combinations, including different construction stage and different parameters of foundation rock, the dam stress is well distributed and the magnitude is quite similar to that of Ertan Arch Dam (also designed by this institute). As a result, the dam can meet the standard and fit for variation of foundation rock. The crest spill-ways and middle outlets will do no harm to the dam overall stability, except for the corner stress concentration, which can be treated by the local concrete reinforcement. The design dam strength is controlled by $R_{180}360$.

5 DAM ABUTMENT STABILITY ANALYSIS

The limit equilibrium method as the main method in dam stability evaluation, as well as the 3D rigid spring elements method and nonlinear FEM, have been adopted to evaluate the dam stability.

The possible sliding blocks of huge slide block, ladder shape slide block and small slide block, which are composed of the unfavorable joint sets or the sheared bands between or in the strata, have been studied, considering the variation of the seepage pressure, rock parameters and attitudes of discontinuities and joints. The controlling bottom planes are sheared bands between stratum 4 and stratum 5 (E1.380m on left bank, E1.410m on right bank). As indicated, the shear—friction coefficient of all the blocks, whose bottom slide planes are shear-bands, is greater than 3.5, while the friction coefficient is greater than 1.3, considering the seepage pressure of 50% discount. Because the dam thrust forces decrease with elevation, the upper slide blocks have larger safety coefficients. As confirmed by the 3D rigid spring elements method and nonlinear FEM, the dam abutment has sufficient safety margin.

6 OVERALL STABILITY

3D nonlinear FEM and geomechanic model test have been adopted to study dam working state and overload ability, taking the unfavorable geologic conditions into consideration. As a result, the dam is in elastic state under normal load condition, while the distributions of stress and deformation are in accordance with that of general high arch dams. The computed cracking length is less than 1/8 of dam thickness at bottom elevation, which is less than that of Ertan and Xiaowan hydroelectric project. The overload capability is 8.0 times normal water pressure.

The geomechanic model test indicate that the cracking starts at dam heel under the water load of $1.2P_0$~$1.5P_0$. Cracks spread all the upstream and downstream dam face under the water load of $4.0P_0$~$5.0P_0$. The dam is of high overall stability.

7 DAM SEISMIC DESIGN

Since the basic seismic intensity in dam site is 8 degree, the design seismic horizontal acceleration is 0.321 g, while vertical one is 65% of the horizontal, corresponding to design seismic intensity

of exceeding probability of 0.02 within the basic period of 100 year. Because the dam is 278m high and has exceeded the code of hydroelectric structure seismic design, special research has been conducted.

The seismic design is based on the static analysis, while checked for dynamic conditions. If the dam cannot meet the requirement of the code, then shall be revised or some adequate seismic measure shall be adopted. The seismic design begin with the trial and load method corresponding to the design code, as well as FEM dynamic analysis and dam abutment 3D limit equilibrium method analysis. As the computation proved, dam stress and dam stability basically meet the requirement of stress standard and anti-slide stability, except for excessive tensile stress in a small area less than 5% of the total dam face.

Consequently, the 3D nonlinear FEM analysis and 3D dynamic model tests have been implemented, as well as the projects analogy analysis, to evaluate the overall dam anti-seismic ability. The 3D nonlinear FEM analysis has considered the following factors: the input mechanism of seismic wave (sensitivity analysis of differential of phase and amplitude), emission damping of foundation, transverse joint cracking and the material nonlinear properties. The dynamic model test has firstly considered dam foundation and damping boundary, besides the water pressure and transverse joints. The numerical and physical researches both have proved that the dam has good overall bearing capacity, except that there are small crack areas near the high arch ends. Under normal water level and low water level, the resultant stress of dam static and dynamic stresses are within the dam dynamic strength, the computed maximum crack of the transverse joint is less 10mm. According to project comparison, the dynamic stress and crack of the transverse is small than that of Xiaowan project, mainly due to the narrow shape of the cannon. The dam concrete zoning is implemented according to the resultant stress of static and dynamic stress, consequently, the concrete of $R_{180d}300$ has been adopted in middle part of the upper arch, where the dynamic tensile force is big, while the concrete of $R_{180d}350$ has been used in the high stress area close to the dam abutment. According to the researches above, no anti-seismic steel bar is required and the transverse joints will open 10mm, and will not destroy the anti-seepage facilities. In general, the dam can meet all the requirement of seismic design.

8 DAM FOUNDATION TREATMENT

Foundation rock is mainly composed of fresh basalt of $P_2\beta^3$~$P_2\beta^{12}$, some lower section of moderately weathered basalt locally in river bed and high elevation abutment, and the sheared bands at the proportion 3% of total foundation rock. The bed rock is integrate and of massive structure and high strength. The treatment mainly aims at the sheared bands and the lower section of moderately weathered rock. The concrete replacement and consolidation grouting will adopted to improve the rock integrity, comprehensive deformation modulus and homogeneity. According to the field test results, these measures work better to the sheared bands and jointed rock mass, well to the general foundation rock within the depth of 20~25m, and well to contact grouting in steep dam segments. The sheared bands, the main seepage channels in dam site, is vital to dam abutment stability. The foundation anti-seepage treatment design follows the rule of "cutoff the first and drainage the second, both are need". The anti-seepage curtain in foundation and drainage system in abutment is laid out respectively, according to the foundation seepage profile and requirements of different location. The pumping test proved that the sheared bands are improved by the curtain grouting.

9 DAM CONCRETE AND TEMPERATURE CONTROL

It is vital for Xiluodu Arch Dam, which is 278m high and of volume of 6.66 million m^3, to avoid the concrete cracking. The solution lies in the concrete design, temperature controls and maintenance during construction. On the basis of dam stress standard, dam concrete placement span and reservoir storage time, the standard strength of dam concrete is designed to be 36 MPa of maximum

compressive strength at the age of 180d and the assurance probability of 85%. According to dam stress and the outlets layout, the dam concrete is zoned to A, B and C region, corresponding to the strength of 36 MPa, 30 MPa and 25 MPa. 30 transverse joints are designed to divide the dam to 31 segments. Concrete will be constructed once without longitudinal joints with the maximum casting area is 1800m^2. As proved by test aggregates of basalt, limestone and artificial, the compound of coarse basalt aggregate and fine limestone aggregates will insure good concrete properties. On the basis of complete investigation of climate data in dam site, as is proved by the temperature boundary condition and temperature field study that, the joint closure temperature of 3° lower than the stable temperature is necessary, reasonable and reliable. The final joint closure temperature is designed to be 12°~16°. 3D FEM concrete creeping analysis has studied the thermal difference between dam and foundation, the thermal lift difference between, surface thermal difference, thermal stress around the outlets and thermal stress in steep dam segments, consequently. The concrete placement lift is design to be 1.5 m thick in constrained region and 3.0m thick in unconstrained region, while the thermal difference standard is $\Delta T \leq 15°$ in constrained region and $\Delta T \leq 20°$ in unconstrained region. The concrete placing temperature is 10°~14°, and the lift span is 5d~14d. Some parameters are determined for the first stage pipe line water cooling, the second stage pipe line water cooling, concrete surface maintenance. All these measures result in the anti-cracking coefficient bigger than 1.8 ($Kf \geq 1.8$) and convenience for the fast construction.

This page intentionally left blank.

New Developments in Dam Engineering—Wieland, Ren & Tan (eds),
© 2004 Taylor& Francis Group, London, ISBN 04 1536 240 7

Dam safety aspects of reservoir-triggered seismicity

Martin Wieland
Chairman, ICOLD Committee on Seismic Aspects of Dam Design, Electrowatt-Ekono Ltd., Zurich, Switzerland

ABSTRACT: Reservoir-triggered seismicity is a phenomenon, which has been observed in several large storage dam projects all over the world.

If a large dam has been designed according to the current state-of-practice (ICOLD, 1989), which requires that the dam can safely withstand the ground motions caused by the maximum credible earthquake (MCE), it can also withstand the effects of the largest reservoir-triggered earthquake, as the maximum reservoir-triggered earthquake cannot be stronger than the MCE. Thus, reservoir-triggered seismicity is not a direct safety problem for a well designed dam or the people who could be at risk in the case of a dam failure. However, reservoir-triggered seismicity may still be a problem for the buildings and structures in the vicinity of the dam, because they have often a much lower earthquake resistance than the dam.

In the great majority of reservoir-triggered events, the magnitudes are small and of no dam safety concern. Up to now, the maximum magnitude of reservoir-triggered earthquakes is 6.3. As the correlation between the filling of the reservoir and the occurrence of a damaging earthquake in the reservoir region is extremely weak, severe doubts remain if some of the largest observed earthquakes are actually reservoir-triggered seismicity events.

The paper focuses on the various aspects of reservoir-triggered seismicity.

1 INTRODUCTION

The first well documented case of reservoir-triggered seismicity was observed in the 1930s at Lake Mead, which was created by the 220m high Hoover arch dam. By the end of the 1960s, strong earthquakes, which are suspected of being reservoir-triggered, have occurred in the reservoirs formed by the Koyna gravity dam (India), Hsinfengkiang buttress dam (China), Kremasta embankment dam (Greece), and Kariba arch dam (Zambia), so that the general interest for this phenomenon has sharply increased. The maximum magnitudes of the seismic events observed in these reservoirs were in the range of 6.0 to 6.3. As reservoir-triggered earthquakes tend to have shallow focus, the ground motion at the dam sites of Koyna (1967) and Hsinfengkiang dams (1962) was very severe and caused structural damage to both dams. These two approximately 100m high concrete dams were subsequently repaired and strengthened and are still in operation. The microseismic activity in the reservoir region of Koyna and Hsinfengkiang dams is still very high. For example, in the Koyna dam region nearly 100 earthquakes with magnitude M>4 and about 10 events with M>5 have occurred since 1967 (Fig. 1). The ground motions caused by these earthquakes are of no serious concern for the safety of the strengthened dams.

From the very beginning, the reservoir-triggered seismicity was controversial and the problem remained as a target of sustained interest and studies, mainly because of its environmental impact and risk considerations. At the same time, the number of dam projects with reservoir-triggered seismicity was increasing in line with the growth of the overall number of dams and the improvement in the seismic monitoring systems.

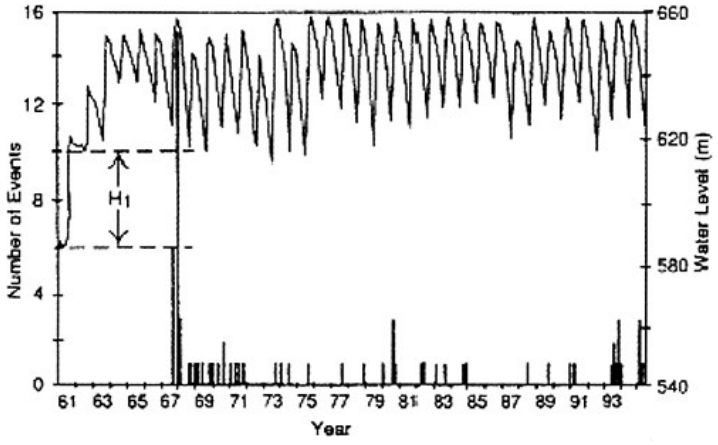

Figure 1. Reservoir water levels at Koyna from 1961 to 1995 and M>4.0 events. Three periods of M>5.0 activity occurred in 1967, 1973 and 1980 (Talwani, 2000).

The features outlined above make the reservoir-triggered seismicity a concept of permanent interest for the design and monitoring of dams.

The relatively strong seismic events described above, which are mainly observed at large storage dams with a height of over approximately 100m and which tend to decrease with time, have been referred to as reservoir-induced seismicity in the past. In 1999 ICOLD has accepted the use of reservoir-triggered seismicity as the most adequate expression as it best reflects the nature of this type of seismic events. Accordingly, the phenomena that were called reservoir induced seismicity in the past are called reservoir-triggered seismicity today.

2 EFFECTS ON DAM SAFETY

Today it is generally accepted that significant reservoir-triggered earthquakes can only occur in regions with high tectonic stresses in the earth crust, i.e. the causative fault that can produce the earthquake is already in near failure conditions, so that added gravity stresses and pore pressure propagation due to reservoir impounding, can trigger the seismic energy release. This means that triggering due to impounding cannot change the underlying tectonic processes and the long-term seismic hazard at the dam site, if the seismic potential at a dam site is correctly assessed.

The basic requirements for reservoir-triggered seismic activity are:

- the existence of active faults, or
- the existence of faults near failure limit.

A large dam, which has been designed against earthquakes according to the current state of practice requiring that the dam can safely withstand the ground motions caused by the maximum credible earthquake (MCE), can also withstand the effects of the largest reservoir-triggered However, the short-term seismic risk could very well be increased for buildings and appurtenant structures, which have not been designed for the MCE.

Table 1. List of large dam projects with reservoir-triggered seismicity (USCOLD, 1997).

Reservoir	Country	Depth (m)	Volume (million m^3)	Magnitude or intensity of the event	No
Akosombo	Ghana	109	148,000	MMI V	1
Almendra	Spain	185	2,649	3.2	1
Aswan	Egypt	90	160,000	5.2	3
Benmore	New Zealand	96	2,040	5.0	3
Blowering/Taibingo	Australia	142	2,559	3.5	3
Camarillas	Spain	43	37	4.1	3
Canelles	Spain	132	678	4.7	1
Capivara	Brazil	60	10,500	4.4	1
Cenajo	Spain	97	472	4.2	4
Danjianangkou	China	97	16,000	4.7	4
El Grado	Spain	85	400	MMI IV	1
Eucumbene	Australia	106	4,761	5.0	3
Furnas	Brazil	111	22,950	MMI V	4
Grandval	France	78	292	MMI V	1
Hoover	USA	191	36,703	5.0	3
Jocassee	USA	107	1,431	3.8	3
Kariba	Zambia	122	160,368	6.25	2
Kastraki	Greece	91	100	4.6	2
Khoa Laem	Thailand	80	7,000	4.5	2
Koyna	India	100	2,780	6.3	3
Kremasta	Greece	120	4,750	6.3	3, 5
Kurobe	Japan	180	199	4.9	1
Manicouagan 3	Canada	96	10,423	4.1	2
Marathon	Greece	60	41	5.75	4
Monteynard	France	125	275	MMI VII	4
Mossyrock	USA	124	1,957	4.3	4
Nurek	Tajikistan	285	11,000	4.5	2
Oroville	USA	204	4,400	5.7	2 o
Paraibuna/Paraitinga	Brazil	102	4,740	3.2	4
Piastra	Italy	84	13	MMI V	4
Preve Di Cadore	Italy	98	69	MMI V	4
Porto Columbia/ Voltagrande	Brazil	50	3,760	5.1	4
Pukaki	New Zealand	108	10,500	4.6	4
Shenwo	China	75	790	4.8	4
Swift	USA	116	932	5.0	4
Srinagarind	Thailand	133	17,745	5.9	3
Vouglans	France	112	605	4.4	4
Hsingfengkiang	China	105	13,896	6.0	3
Zhelin	China	62	7,170	3.2	4

The following types of earthquakes are used for the seismic design of dams and structures:

(i) Dam body, dam abutments and safety relevant hydromechanical components (spillway gates, bottom outlet, etc.), (current ICOLD requirements):

- **Operating Basis Earthquake (OBE):** average return period of ca. 145 years (50% probability of exceedence in 100 years); no structural damage is accepted, the dam shall remain operable after the OBE.
- **Maximum Credible Earthquake (MCE) and Maximum Design Earthquake (MDE):** average return period of ca. 10,000 years for a country of low to moderate seismicity like Thailand (Note: The MCE is a deterministic event, but in practice, due to the problems involved in the estimate of the corresponding ground motion, the MCE is usually defined statistically with a

typical return period of 10,000 years for countries of low to moderate seismicity.). The stability of the dam must be ensured and no uncontrolled release of water from the reservoir shall take place, however, structural damage is accepted. In the case of significant damage, the reservoir has to be lowered after the MCE. Earthquakes exceeding the OBE may cause structural damage but should not jeopardize the safety of the people living in the downstream region of the dam and their property. A 'walkdown' of the dam will show what emergency actions have to be taken. Reservoir-triggered earthquakes exceeding the OBE are possible and may cause structural damage in a dam, but such earthquake ground motions are less severe than those of the MCE, which a well designed dam must be able to safely withstand.

(ii) Buildings and other structures (non safety relevant appurtenant structures, bridges etc.)

- **Design Basis Earthquake (DBE):** average return period of 475 years (10% probability of exceedence in 50 years) is specified in most earthquake codes and regulations for buildings. For certain types of structures an importance factor is specified in several codes, ranging from 1.0 to 1.5. An importance factor exceeding 1.0 has the same consequence as an elongation of the return period of the DBE. Under the effect of the DBE buildings may experience substantial structural (and especially non-structural) damage but life safety must be ensured, i.e. the buildings or the load bearing walls and columns shall not collapse.

As a conclusion we can state that a dam designed according to the current state of practice published by ICOLD should be able to safely withstand any reservoir-triggered earthquake.

As the magnitudes of reservoir-triggered earthquakes is decreasing with time, it is rather unlikely that such an event will jeopardize the safety of an existing dam, which has not been designed according to the current state of practice. However, it is strongly recommended that the earthquake safety of dams, which have a record of reservoir-triggered seismicity be re-assessed especially when they have been designed against earthquakes using design criteria and methods of analysis, which are considered as outdated or even obsolete today, such as the pseudostatic seismic design method based on a seismic coefficient of 0.1 or so.

3 EFFECTS ON BUILDINGS AND INFRASTRUCTURE IN RESERVOIR REGION

Relatively strong reservoir-triggered earthquakes may cause damage and loss of lives in communities in the dam and reservoir region. During the 1967 Koyna earthquake in India (magnitude 6.3), which is considered as a reservoir-triggered earthquake, about 100 people were killed in villages in the dam region. The destroyed buildings were not designed for earthquakes as the region of the dam was considered as an area of low seismicity at the time the dam was constructed.

A reservoir-triggered earthquake with a magnitude of 6.3 (observed maximum magnitude for reservoir-triggered earthquake) can cause peak ground accelerations, which in the extreme case may approach those caused by the MCE. However, the duration of strong ground shaking of reservoirtriggered earthquakes is usually much smaller than that of the MCE. It has to be kept in mind that the duration of strong ground shaking is responsible for a major part of the earthquake damage and not the peak ground acceleration, especially when there is a single, high-frequency peak of the ground acceleration. Nevertheless, reservoir-triggered earthquakes can still cause considerable damage to buildings and structures in the dam region, which have not been designed for earthquake actions. However, the same—or even more severe—damage and loss of lives can be caused in the same region by a natural earthquake (i.e. an earthquake, which would occur if no dam were built).

The main difference between a reservoir-triggered earthquake and a natural earthquake is that the reservoir-triggered earthquake has a relatively high likelihood of occurring within the first few years after impounding of the reservoir or when the reservoir level has reached its maximum elevation. These earthquakes have often a shallow focus and their epicentres are relatively close to the dam sites or the reservoir. In the case of a major natural earthquake the date and place of occurrence cannot be predicted accurately. Thus the short-term seismic hazard for moderate earthquakes (say within 5 years after completion of a dam project) may be considerably higher than the corresponding long-term seismic hazard covering a period of say 500 to 1000 years in zones of low to moderate seismicity.

If buildings are damaged and people killed by a strong earthquake, which has occurred within the first years of completion of a dam, the question remains, if this earthquake has been triggered by the reservoir or if this event would have occurred naturally when no dam would have been built. It is rather straightforward to associate microseismic activity in the reservoir if the seismicity has been monitored in the reservoir region prior to the dam construction and filling of the reservoir. However, in the case of strong earthquakes with a relatively long return period the correlation between the filling of the reservoir and the occurrence of a strong earthquake becomes extremely weak. The uncertainties will be of the same order as those in the prediction of natural earthquakes especially when no long-term microseismic observations were carried out prior to the filling of the reservoir.

This is also the reason why dam owners object to the classification of strong earthquakes in the reservoir region of large storage dams as being triggered by the reservoir. As a matter of fact, if there would be a clear correlation between the occurrence of a damaging earthquake and the filling of the reservoir, then the affected population may claim compensation from the dam owner. The author is not aware of any reports where compensation was claimed and received from dam owners. However, A.Bozovic, the former Chairman of the ICOLD Committee on Seismic Aspects of Dam Design, has mentioned in a private communication that he remembered a small but significant precedent. 'During the peaking period of reservoir-triggered seismicity around Mratinje storage (M=4.8) in 1978 (220m high arch dam) a claim was made for a damaged house, and was not accepted. But in 1994 a similar (nearly total) emptying and subsequent quick filling of the storage caused similar phenomena (M=3.8) damaging again the same house. By court order, compensation was paid by the owner as monitoring results were considered clear and convincing.'

However, for settling any reservoir-triggered earthquake claims it has to be considered that:

- comprehensive monitoring of reservoir-triggered seismicity before and after dam construction is required in order to dispel any doubts about what is actually happening; and
- the maximum reservoir-triggered magnitude is less than 6.3, which represents the worldwide reached ceiling of reservoir-triggered earthquakes and that it is very unlikely to actually trigger the MCE.

As large dam construction has peaked off in many countries, it is unlikely that the new dam projects, which will experience reservoir-triggered seismicity, is growing substantially in the coming years. The dams where reservoir-triggered seismicity was observed and is still taking place are not considered as a major risk as the seismicity and the maximum magnitudes of the shocks tend to decrease with time. However, it is strongly recommended to monitor continuously the ongoing seismicity in the reservoir region where reservoir-triggered seismicity has been observed in the past and to install monitoring systems in the reservoir region of future dams where reservoir-triggered seismicity is expected.

4 OTHER EFFECTS

Reservoir-triggered seismicity is often taken up as a safety issue by pressure groups opposing new dams. It is obvious that reservoir-triggered seismicity is an undesirable phenomenon for all parties involved in or affected by a large dam project.

As pointed out in the previous sections, reservoir-triggered seismicity is not a safety problem for a well designed dam or the people who could be at risk in the case of a dam failure but it is a problem because (i) the buildings and structures built in the dam region have usually a much lower earthquake resistance than the dam, and (ii) mass movements in to the reservoir, triggered by local earthquakes, can cause waves that my lead to overtopping of a dam if the freeboard is not sufficiently large. Thus, in very rare cases an earthquake, which occurs shortly after impounding of the reservoir, can cause damage and loss of lives in the vicinity of the dam.

Moreover, if unexpected extraordinary seismic events occur suddenly more frequently, people living below a dam may start to question its seismic safety. To dispel such safety concerns may not be that straightforward, because acceptance of scientific and technical arguments is often still limited among the people living in the dam area.

Microseismic activity can also cause disturbing noise. This creates safety concerns and promotes irrational and superstitious beliefs especially when such noise is persisting.

Reservoir-triggered microseismic activity is directly linked to the filling and operation of the reservoir during the first years after completion. After the major shock, the seismic activity is usually decreasing.

Continuous monitoring of the seismic activity in the reservoir region before, during and after dam construction is probably one of the best ways to respond to psychological concerns of any parties involved in a dam project. Monitoring is very effective if the seismic activity is moderate to low. In this case the sudden appearance of seismic activity during the filling and the first years of operation of a dam can be clearly identified. However, in the case of high seismic activity, earthquake swarms may have occurred already prior to the filling of the reservoir and may appear again after the start of operation of the reservoir. In such cases, the identification of reservoir-triggered seismicity may be rather difficult and would need long-term monitoring with a sophisticated monitoring system.

An aspect that could also be mentioned in this context refers to displacements on faults or shears crossing the dam, triggered by reservoir filling. Filling of the Katse reservoir in Lesotho triggered notable displacements on shears that normally would not have been considered “active faults”.

5 CONCLUSIONS

In the seismic safety assessment of dams it is not necessary to treat the reservoir-triggered seismicity as a separate issue as the ground motion, caused by the maximum credible earthquake (MCE) that is used for the safety evaluation of a dam according to the current state of practice, is more severe than that of the largest reservoir-triggered earthquake.

The maximum observed magnitude for reservoir-triggered earthquakes is about 6.3. However it has to be pointed out that it is almost impossible to prove that the occurrence of a strong earthquake has been caused or influenced by the reservoir as the focal depth is usually several kilometres.

Reservoir-triggered earthquakes may cause mass movements (landslides, rockfalls, avalanches, debris flows etc.) into the reservoir, resulting in water waves that could cause overtopping of a dam. An adequate freeboard has to be provided during the period of increased mass movement hazard.

The seismic safety of dams, where reservoir-triggered seismicity has taken place or is being observed, has to be re-assessed based on the current state of practice.

Buildings and structures in the reservoir region are normally designed for seismic forces, which are considerably less than those of the MCE, thus a major reservoir-triggered earthquake may cause damage and loss of lives in these communities.

Reservoir-triggered microseismic activity, which can be felt or heard, creates safety concerns in the population, which have to be taken up seriously by the dam owners.

Monitoring of the seismic activity prior, during and after construction of a dam is highly recommended for large storage dams and dams located in tectonically stressed regions.

REFERENCES

ICOLD Draft Bulletin (2003): Reservoir-triggered seismicity, state of knowledge, Committee on Seismic Aspects of Dam Design, ICOLD, Paris
ICOLD Bulletin 72 (1989): Selecting Seismic Parameters for Large Dams, Guidelines, Committee on Seismic Aspects of Dam Design, ICOLD, Paris
ICOLD Bulletin 112 (1998): Neotectonics and dams, Committee on Seismic Aspects of Dam Design, ICOLD, Paris
ICOLD Bulletin 120 (2001): Design features of dams to effectively resist seismic ground motion, Committee on Seismic Aspects of Dam Design, ICOLD, Paris
Talwani P. (2000): Seismogenic properties of the crust inferred from recent studies of reservoir-induced seismicity—Application to Koyna, Current Science, Vol. 79, No. 9, 10 Nov. 2000
USCOLD (1997): Reservoir-triggered seismicity, USSD

New Developments in Dam Engineering—Wieland, Ren & Tan (eds),
© 2004 Taylor& Francis Group, London, ISBN 04 1536 240 7

Benefits of strong motion instrumentation of large dams

Martin Wieland
Chairman, ICOLD Committee on Seismic Aspects of Dam Design, Electrowatt-Ekono Ltd., Zurich, Switzerland

ABSTRACT: Substantial progress has been achieved in the last couple of years in the development of instruments for recording strong earthquake ground motions, and because of their benefits, improved reliability and relatively low cost, these instruments are gaining importance in the safety monitoring and safety management of large dams. It is proposed that major dams with large damage potential, dams located in areas of high seismicity, and dams showing abnormal behaviour be equipped with strong motion instruments. Moreover, by increasing the reading frequency of deformation measurements, earthquake-generated oscillations of penduli can be recorded, and sudden changes in seepage flow before and after an earthquake could be detected etc.

1 STRONG GROUND SHAKING AT DAM SITES AND SEISMIC INSTRUMENTATION

During the last three decades major progress has been made in the understanding of earthquake action on concrete and embankment dams. The progress was mainly due to the development of computer programs for the dynamic analysis of dams. However, it is still not possible to reliably predict the behaviour of dams during very strong ground shaking due to the difficulty in modelling the inelastic behaviour of dams, the insufficient information on the spatial variation of ground motion and other factors.

During the Bhuj earthquake of January 26, 2001 in Gujarat Province in India, about 245 earth dams were damaged and need repair and/or strengthening (Figure 1). Because the reservoir levels were extremely low during the time of the earthquake, no water was released from the reservoirs of the severely damaged dams.

None of the dams damaged by the Bhuj earthquake was instrumented with strong motion instruments. Therefore, it is not known what level of ground shaking has caused the observed damage. This would be essential information to judge the vulnerability of the many irrigation dams to strong ground shaking all over the world. A back analysis would also be based on numerous analysis assumptions and, therefore, a reliable estimate of the peak ground acceleration and the other characteristics of the ground motion at the sites of the damaged dams would be extremely difficult. At this time it is assumed that the Peak Ground Acceleration (PGA) was of the order of 0.5g at the severely damaged dams. One could easily imagine that there would be serious safety concerns, if the PGA would have been less than half of that as the return period of an event that could produce such shaking levels would be quite short and thus the risk of dam failure may increase substantially.

Also during the devastating earthquakes, which hit Turkey and Taiwan in 1999, very few earthquake records of dams that experienced strong ground shaking are available. It was reported that at the 181m high Techi arch dam, where below the crest spillway a PGA of 0.87g was recorded, power failure of some strong motion instruments at the dam site made them useless. Also the critically damaged Shih-Kang dam (Figure 2) was not instrumented, despite the fact that Taiwan has

Figure 1. Earth dams damaged by the January 26, 2001 Bhuj earthquake, Gujarat, India (courtesy Prof. S.K.Jain).

Figure 2. Shih-Kang weir in Taiwan, destroyed by fault movement during the September 21, 1999 Chi-Chi earthquake (courtesy Dr. R.Charlwood).

one of the densest and most sophisticated strong motion networks. In a nearby town a PGA of 0.57g was recorded.

In 1994, during the Northridge earthquake near Los Angeles some of the important records obtained from the well-instrumented Pacoima arch dam, where peak acceleration values exceeding 2g were recorded at the dam crest, could not be used as some of the older strong motion instruments could not accommodate that high accelerations. Therefore, it was not possible to perform a reliable back analysis, which would be needed, for example, to determine the damping of the dam during very strong ground shaking. This is still a key problem in many seismic analyses of concrete dams that has not yet been resolved satisfactorily.

Also the 106m high Sefid Rud buttress dam (Figure 3) in the Northwest of Iran, which was severely damaged during the 1990 Manjil earthquake and which is one of the most important reference cases for dam engineers, had no properly functioning seismic instruments. It was reported that at the time of the earthquake, the epicenter of this magnitude 7.5 earthquake was located within less than one kilometer of the dam site, the seismograph was being repaired in Tehran.

These examples show that there is a real need for the strong motion instrumentation of large dams. The following dam safety aspects have to be considered in the future:

- Appropriate site-specific instruments shall be in place to monitor a dam, both for ongoing behaviour and safety of the dam, and for identifying changes in its performance after an earthquake or other unusual events; and

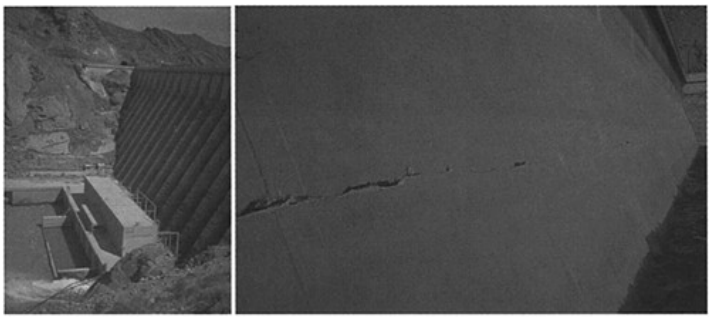

Figure 3. Sefid Rud buttress dam in Iran, damaged by the June 21, 1990 Manjil earthquake (left: dam with powerhouse; right: horizontal crack at upstream face of dam.

- Back-analysis of dams that were subjected to strong earthquake shaking would help provide calibration of analytical methods used in dam design and to develop new analysis tools.

Over the last decades it has also turned out that for dam safety considerations, the earthquake action has developed from an almost negligible action into the most important one. This fact has been true in the nuclear industry for quite some time. The majority of the older dams were built using methods of seismic analysis and seismic design criteria, which, today, are considered as obsolete or outdated. Therefore, in many cases, it is not known if an old dam complies with the current seismic safety guidelines. Today, according to current ICOLD guidelines, the dam safety must be guaranteed for the worst earthquake, i.e. the so-called maximum credible earthquake. This is an event, which up to now only very few of the over 40,000 existing large dams have experienced and as discussed above very few records exist for such events.

The dynamic behaviour of dams under severe motion is not known satisfactorily, therefore, data from strong motion instruments will eventually form the basis for a more reliable seismic safety assessment of the existing and future dams. Experimental investigations, which would be an alternative, would generally be too costly for most dams.

Therefore, in view of the ever-increasing safety concerns and rapidly increasing risks of large dam projects, low-cost seismic instrumentation is the future state-of-the-practice in dam safety monitoring.

Following the 1995 Kobe earthquake in Japan, it was decided to place strong motion instruments in all of the 413 dams under the jurisdiction of the Ministry of Land, Infrastructure and Transport. 1152 strong motion instruments are currently installed in these dams. 236 seismic stations at 50 dam sites are directly connected to a common monitoring centre. A significant number of acceleration records exist from this network, but no records of dam damaging ground motions are available yet.

A significant number of dams has been instrumented in the USA, Iran, Italy, China and other countries, so it is only a question of time until records of very strong ground shaking at dam sites will become available.

2 OVERVIEW ON DAM INSTRUMENTATION

The conventional monitoring instruments installed in large dams are well suited for the control of the long-term and quasi-static behaviour of a dam. Accordingly, the frequency of most static readings is

of the order of one measurement per week or month. However, processes such as cracking in concrete dams and actions like earthquakes cannot be recorded satisfactorily by these instruments.

The main dynamic actions are those caused by strong earthquakes in the vicinity of a dam, i.e. vibrations in the dam body causing cracks and settlements, faulting in the dam foundation and water waves in the reservoir. Other short-duration phenomena are impulsive waves caused by mass movements and avalanches into the reservoir, wind-induced water waves, terrorist attacks and military actions, and dynamic loads caused by faulty operation of hydro- and electro-mechanical equipments as well as accidents during repair and maintenance works. In addition, it is necessary to monitor fracture processes in concrete dams (formation and propagation of cracks in concrete dams), progressive failure of slopes in embankment dams, which may be triggered by sudden changes in the water level in the reservoir, effects due to very low temperatures, reservoirtriggered seismic phenomena, etc.

As some of these processes and actions may jeopardize the safety of a dam, it is important to monitor the response of the dam caused by such unpredictable phenomena.

Today, the strong motion accelerometers available on the market are highly reliable, are able to record both small amplitude vibrations as well as motions caused by strong earthquakes or even explosions. Moreover, during the last decade the cost of digital sensors and recorders have dropped and at the same time the performance of these instruments and the data analysis features built in these systems have improved dramatically.

Similar to other types of monitoring systems, strong motion instruments do not improve the structural safety of an existing dam. But dam monitoring forms a key element in the overall safety concept of a dam, which comprises the following:

(i) Structural safety (capability of a dam to resist water load, earthquake forces and other types of forces and actions);
(ii) Dam safety monitoring (evaluation of dam behaviour and safety based on visual and instrumentally recorded data);
(iii) Safe operation (safe operation of reservoir on the basis of reliable rule curves and well-trained staff); and
(iv) Emergency management (timely warning of the population in the case of an accident and preparation of evacuation plans, etc.).

Records of strong motion instruments could actually be used to contribute to all four of the above safety elements of a large dam project. But dam safety monitoring is the most obvious application for accelerometers. However, these state-of-the-art instruments can easily be used to issue an alarm, if critical acceleration or spectrum intensity values etc. are exceeded.

Therefore, strong motion instruments installed within the dam are important components of an alarm and rapid response system and allow:

(i) the timely warning of the population living in the downstream valley (water alarm),
(ii) to operate safety devices such as valves in penstocks, and
(iii) to shut down the turbines and generators etc.

Despite the fact that it may take some time to safely close valves and to shut down turbines without causing large dynamic effects in the pressure system, the consequences of earthquake damage to these devices would be greatly reduced.

Therefore, today, strong motion instruments and a rapid alarm system should belong to the standard instruments for the safety monitoring of large dams. To complement the standard static instruments with dynamic strong motion instruments allows the comprehensive monitoring of a dam under the whole spectrum of actions affecting the safety of a dam. In view of the large damage potential of most large dams, it is in the interest of the dam owners, the dam safety agencies and in particular of the people affected by a possible dam incident to reduce the earthquake risk of a dam as far as possible.

As the prediction of the time, location and magnitude of strong earthquakes, which may affect the safety of a dam, will not be possible in the foreseeable future, the aspect of pre-warning of the population living downstream of a dam is an important issue.

In addition, today's strong motion instruments have a large dynamic range, i.e. they can be used for recording small and high amplitude vibrations ranging from a few micro g's to over ten g (acceleration due to gravity, $g=9.81 m/s^2$). The records of continuous monitoring of small amplitude vibrations of a dam caused by ground motions, wind, water waves in the reservoir, operation of equipment in the dam etc. can be used for the health monitoring of the dam and for the calibration of numerical dam models. Real time health monitoring on the basis of monitoring changes in the fundamental frequencies of the dam, can easily be implemented in these instruments.

Moreover, the data collected from strong motion instruments can be used

(i) to check and to improve the seismic design criteria of the dam, and
(ii) to locate micro-earthquakes in the vicinity of the dam.

Because of these unique features and advantages, it is highly recommended to install strong motion instruments in all large dams, which are already equipped with pendulums for deflection measurement. Three instruments would be the absolute minimum for a large dam as it has to be assumed based on the past experience that one or the other instrument may not be working properly at the time of a strong earthquake due to maintenance problems as experienced in the past.

The number of large dams equipped with strong motion devices is steadily increasing. Because of the long return period of strong earthquakes in many parts of the world, the owners lack proper justification for this additional investment, which may be of the order of USD 50,000 for a minimum set up. The annual operation and maintenance costs including the costs for routine data interpretation should not exceed 20% of the initial investment.

We hope that this paper provides sufficient arguments for the dam owners and dam safety agencies to recommend and also to justify the installation of strong motion instruments in large dams.

Any new dam with a large damage potential should have at least a few strong motion instruments and the monitoring systems of the existing dams should eventually be upgraded as well (Figure 4).

Moreover, the damage caused to a considerable number of irrigation dams during the 2001 Bhuj earthquake in India has shown that there is also a need for strong motion instrumentation of smaller dams, which are vulnerable to strong ground shaking.

Finally, we should also keep in mind that by increasing the reading frequency of deformation measurements, earthquake-generated oscillations of penduli can be recorded, and sudden changes in seepage flow before and after an earthquake could be detected etc. The automated monitoring of pendulum motions, seepage flow and other quantities should no longer be any major concern, as this is technically and economically feasible today.

3 TECHNICAL ASPECTS OF STRONG MOTION INSTRUMENTS

The development in the field of electronics and sensor technology is proceeding very rapidly. Automatic recording of measured data and applications of data communication techniques are widely used. Strong motion instruments have gained a lot from this recent development.

The earthquake motions to be recorded and which are of greatest interest from the dam engineering point of view are ground accelerations with frequencies up to 20Hz. For traditional dam monitoring instruments relatively long measuring intervals of say one to four weeks are sufficient under normal operation. Some parameters like water level in the reservoir and ambient temperatures are measured continuously. Due to this fact man-operated measuring is widely used in the field of dam monitoring.

In the meanwhile the technology of strong motion instruments was developing to a stable level and thousands of instruments have been installed and are operating world-wide. The resolution capability has improved over the last ten years by a factor of 4000, allowing now the accurate measurement of very small ground movements. The measuring range is actually only limited by the noise level of the sensor. Since the sensor noise level is far below the natural ground acceleration at the measuring site, therefore, with a sensor fixed to a dam the eigenfrequencies of the structure can be calculated easily based on power spectra of the recorded accelerations. Due to the high dynamic

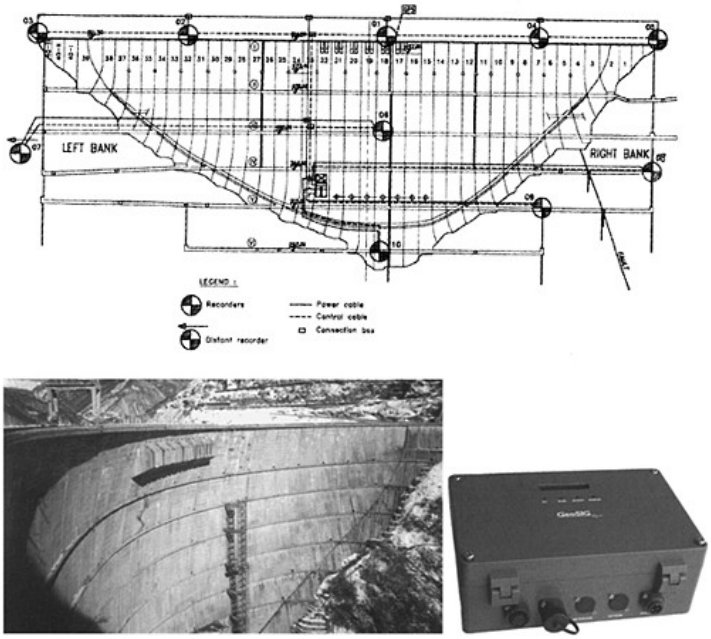

Figure 4. Layout of strong motion instruments in the 272m high Enguri arch dam in Georgia and picture of a strong motion instrument.

range of modern strong motion instruments and due to the fact that all the recordings are in digital form, the following goals can be reached:

(i) Alerting in the case that a pre-defined peak acceleration is exceeded and the event is identified by a suitable software to be of seismic source.
(ii) Recording of all the events exceeding a pre-defined peak acceleration with appropriate pre-and post-event time series. Based on the recorded acceleration time histories the velocity and displacement time histories can be calculated.
(iii) Continuous recording of the complete time series during a period of several days before having them deleted or overwritten. This allows the analysis of the history of an event.

The continuous recording may also be used for 'health monitoring' by continuously checking any short-term or long-term changes in the dominant eigenfrequencies of the dam.

4 CONCLUSIONS

Modern strong motion instruments, having been ignored for some time, have been developed with the latest sensor and communications technologies. In the meanwhile very user friendly and

versatile instruments are available. These instruments can contribute significantly to the safety monitoring of dams. Therefore, strong motion instruments are expected to become useful additions to the standard instrumentation of dams.

Moreover, the recorded data will be retrievable from centralised recording units through the Internet, thus instantaneous data access can easily be provided for all parties involved in the dam safety evaluation process.

REFERENCES

ICOLD (1989): Selecting Seismic Parameters for Large Dams, Guidelines, Bulletin 72, Committee on Seismic Aspects of Dam Design, ICOLD, Paris

ICOLD (1999): Seismic Observation of Dams, Bulletin 113, Committee on Seismic Aspects of Dam Design, ICOLD, Paris

Ikeuchi K., Tanida H., Inagaki K., Sasaki T. & Uesaka T. (2003): Strong Motion Measurement and Seismograph Network of Dams in Japan, Report R.38, Q.83, Proc. 21st ICOLD Congress, Montreal, Canada

This page intentionally left blank.

Technical papers

This page intentionally left blank.

Foundation treatment of hydroelectric projects in Thailand

Chanin Areepitak
Hydro Power Construction Department, Electricity Generating Authority of Thailand, Thailand

New Developments in Dam Engineering—Wieland, Ren & Tan (eds),

ABSTRACT: The Electricity Generating Authority of Thailand (EGAT) has constructed many large hydroelectric projects, both conventional and pump storage types during the last 3 decades i.e. Srinagarind dam and Vajiralongkorn dam (1974–1985) in the western part of Thailand, Bang Lang dam and Rajjaprabha dam (1976–1987) in the south, Lower Mae Ping dam of Bhumibol dam and "Underground Powerhouse" Lam Ta Khong Pump Storage (1995–2004) in the central part of Thailand and "Run off the River" Pak Mun dam (1990–1995) in the northeastern part of Thailand. Up till now, all of them have been operated successfully and well functioning of the dams are still obtained. The country's social and economic development have got continuous benefit from them. Well design and execution of foundation treatment in different geological condition have been some of the crucial factors for those successful dams. All those dams were constructed in different foundation types e.g. hard rock of sandstone, calsilicate and quartzite, highly weathered calcareous sandstone, karstic limestone with numerous of solution joints and cavities, crushed rock and clayey gouge in fault zones, siltstone/mudstone with slaking property, susceptible to water of claystone, alluvial sand and gravel etc. This paper will present and discuss some methods which used in foundation treatment, are conventional surface treatment, drilling and grouting, flushing and grouting, a secant pile concrete cut off wall, dynamic compaction, vibrofloation etc. in different foundation characteristic of the dams.

1 INTRODUCTION

Development of natural water resource has long been conducted in Thailand and it mostly served for irrigation and flood control. It was not until the Bhumibol dam which belong to Irrigation Department was launched in the 1950s, that the hydro potential has been harnessed for electricity generation as well as many other benefits such as irrigation, flood control, recreation, fishery etc.

The Electricity Generating Authority of Thailand (EGAT)'s main mission is to provide an adequate and reliable power supply to meet the satisfaction of its customer. The country's installed generating capacity is 23,800MW, consisting of 15,000MW (63%) from EGAT's own power plant and 8,800MW (37%) from private power sources. In Thailand, EGAT has totally 23 hydro power plants as shown in Figure 1 which provide the combined installed capacity of 3,300MW (more than 2,200MW has been developed since 1974) and yield an average annual 7,000GWh of energy to the country's grid system. Of the total 23 hydro power developments, 16 of them are large multipurpose dams while the others are implemented particularly to electrify remote rural area. EGAT's hydro powerplants account for 30% of the system's installed capacity and they have provide enormous benefits to the country up till now.

2 GEOLOGY AND FOUNDATION TREATMENT

2.1 *Srinagarind dam*

The construction of Srinagarind dam, on the western part of Thailand, was carried out on the Quae Yai river from 1974 to 1980. It is Thailand's largest rockfill dam with impervious clay core.

Figure 1. Location map.

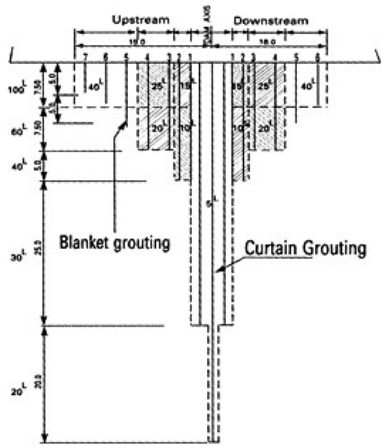

Figure 2. Lugeon and grouting pattern.

The dam is 140m high, 610m long at dam crest and its volume is 12MCM. It comprises 5 units of generator which total installed capacity are 720MW. The foundation rocks at river bed and on the right abutment consisted of the alternation between hard calcareous sandstone, hard limestone and soft sheared shale. In general, the rocks are strongly weathered, especially at the violent folding area, around 8m deep from the original river bed. The bedding plane is clear and showing folding structure and its strike is N 40–80W and dip of 10–40NE. Many joint systems which attitude are N 40–50W/60–70NE, are found. The forming of solution opening and cavities along the joints and faults are common and often encountered. Two big caves were found at the upstream and downstream side of the abutment. Small fault, due to folding, having clay seams are remarkable in the zone of about 10m and cracky in general. On the left abutment, the rocks are mainly quartzite in the upper part and calcareous sandstone in the lower part which characteristics are hard in fresh or slightly weathered but where folding is severe, crushing and weathering are prominent and as a whole they have become brittle. Intercalated shale has changed into clay in the most case. At the lower portion of the abutment, the 15m deep of high permeable, strongly weathered and sheared rock was found.

Regarding foundation treatment work in Champa, S. (1978) [1], traditional surface treatment, trench cutoff, drilling and grouting in the core contact area are mainly employed to obtain 5 lugeon cut off for the dam. The foundation excavation had to be generally executed 15m deep from the original ground and at the lower portion of the left abutment, 20 to 30m deep of cutoff trench had to be carried out for the removal of the worse rock condition to favourable rock foundation and then the concrete wall was placed. Dental treatment, backfill grouting, 10 to 20cm thick of shotcrete, slush grout and concreting have been elaborately applied for fault/sheared zones, clay seams, solution cracks, joints, caves and total used of concrete and shotcrete in the core contact portion were 12,900cu m. There are totally 6 grouting galleries which have been provided in the riverbed under the core contact, in the lower portion of the right abutment and in the left abutment, 4 horizontal galleries (50m vertically spacing) including inclined shaft were designed for the execution of grouting in the weak zones. In the middle level of the left abutment, an additional horizontal grouting gallery was driven at 13.50m upstream from dam axis.

The patterns of blanket grouting in Figure 2 which were divided into 5 zones of different Lugeon (10 to 40) values and the Lugeon values in each zones are adopted from the values of 95% excess probability as the target for foundation improvement. In the riverbed portion, there are 13 rows at

Table 1. Grout mix proportion (by weight).

	Cement	Water	Bentonite	Sodium silicate	Soil
Pure cement	1	10, 5, 3, 2, 1, 0.8	–	–	–
Bentonite cement	1	10, 5, 3, 2, 1, 0.8	2%	–	–
Silicate cement 1	2kg	74 litres	–	18.2kg	–
Silicate cement 2	27.7kg	83.2 litres	0.55kg	11.1kg	–
Soil cement 1	10.9kg	83.9litres	–	1.0litre	31.1kg
Soil cement 2	4.72kg	9.2 litres	–	0.43 litre	13.5kg

3m spacing to cover the upstream and downstream zone of 19m and 16m respectively from the dam axis. The vertical hole spacing was also 3m and the depth varied from 5m at the outermost to 20m at the innermost row. These pattern are gradually changed depending on site and rock conditions. Low pressure up to 10 bars were applied through 56mm drill holes by packer and stage methods for grouting and pure cement slurry was mainly used for injection starting with the lean mix (water to cement=10) to thickest mix(water to cement=0.8 with sand). Soil cement grouting was sometimes used through additional holes in the zone of high Lugeon but low grout take. Additional hoes were necessary carried out at 1.5m spacing in the highly sheared and fault zones on the left abutment and in some cavernous spots and sometimes higher pressure and more penetrable grout material were elaborately applied to overcome these difficulties. The total quantities of drilling for blanket grouting are 36,500m and 1500 tons of cement were used to achieve the target.

The curtain grouting was planned to form 7.5m wide in the upper 45m deep where the rock foundation is highly fractured and cavernous with clay infilled. Below 45 m deep the rock condition is more favourable, the width of the curtain of 1.5m was expected. The typical pattern mostly comprised 3 rows at 3m spacing upstream and downstream from the dam axis. The 45m deep of vertical grout holes for U/S and D/S rows, 65m deep for the center row were designed. The pattern including number of rows, hole depth, and its direction was always modified depending on the rock conditions and the space available especially in the fault and sheared zones. Split spacing method and 5m stage length of packer grouting were mainly employed to achieve 5 Lugeon target. The Tube-a-Manchette method were firstly applied to areas of chemically altered calcareous sandstone but because of time consumption and very high pressure in operation, it was totally replaced by 105mm "down-the-hole" percussion drilling. The rotary drill was applied for the center row while the down-the-hole percussion drill was allowed to used for the outer rows. High pressure grouting of 0.7 to 1.0 bar/m but not exceed 30 bars, is carefully applied. There are 4 grout mixes as shown in Table 1 applied indifferent purposes i.e. the pure cement grout for the outer row, the soil cement grout for the middle row, cement bentonite for finishing grout, silicate cement grout for area of high Lugeon but low grout take and additional holes. Before grouting operation, the pressure water test was always performed to determine Lugeon of each stage and the grout mix was then injected with the appropriate pressure starting from thin to thicker mix until refusal.

The result of grout take and Lugeon values were analyzed and checked and for grout curtain, if the permeability at 95% of excess probability was still higher than 5 lugeon at any spot, the additional holes had to be carried out. In the highly crushed and fault zones as well as cavernous zones the quaternary and quinary holes and rows had to be provided and carried out with more penetrable grout of soil cement and sodium silicate cement grout and the results after additional grouting were conformed and met with the requirement. The total quantities of drilling for curtain grouting was 86,053m and the average grout take was 35kg of cement per meter length and the cost incurred for foundation treatment was 12.30 million US dollars which was 13.02% of the total civil work and it was 40% higher than the original estimate. After the reservoir impounding, the result of 42 piezometers, 24 observation holes, 10 weirs installed in the dam body, foundation and galleries presently show no abnormality and the total amount of leakage into grouting galleries and access galleries of the left abutment is very small (300 l/min.) as mentioned in EGAT (1982) [2]. Up till now, no heavily leakage has been reported.

Table 2. Methods of karstic foundation treatment.

	Dam cut-off	Right abutment cut-off
Overlapping piled diaphragm wall	760mm pile/15,500sq m/ 55m deep/17,800cu m of concrete	300mm pile/450sqm/15m deep/3,800m of drilling
Drilling and high pressure grouting	Maximum 180m deep/ 179,000m/14,000 tons	Maximum 250m deep/377,000m/ 60,300 tons of cement
Flushing and low pressure grouting	Maximum 25m deep/4,000sq m	–
Closely spaced (33cm) 165mm drill holes	–	14,500sq m/11m deep/43,500m
Cavity backfilling, mined cut-off wall	280sq m/70cu m concrete	68,000cu m of concrete

2.2 *Vajiralongkorn dam*

The dam was constructed from 1979 to 1985 on the Quae Noi river, Kanchanaburi province about 280km northwest of Bangkok. It is a 92m high concrete faced rockfill dam and 1,019m long. Its volume is 8.1MCM. The power plant houses three sets of 100MW Francis turbines and generators which supply the average annual energy of 760GWh to the country's power system.

The dam foundation is located mainly on karstic limestone which contain various solution features such as solution joints, chimneys, cavities, big caves etc. with infilled material and the solution features appear to be 50m below the river bed. On the right abutment of the dam is located in limestone massif which contain 3% to 4% of solution cavities. The presence of deep pocket of highly weathered calcareous sandstone is also found in the foundation during construction. On the whole, the foundation rocks comprise interbedding between argillaceous limestone shale and calcareous sandstone/siltstone. The right abutment is formed by a rugged limestone massif and there are 9 distinct faults found within the dam site and the prominent one exposed on the right abutment and separate two mentioned rock group. Areepitak, C. (1983) [3] mentioned that karst characteristics which was investigated by mapping, core drilling, bore hole T.V. camera., caliper log etc., were simply classified for treatment into major karst (>20cm to 10m), minor karst (5 to 20cm) and open fissure (<5mm). Karst's attitude conforming with bedding and major joints are mainly along the north-south to east-west direction and karsts are developed predominantly steeply dipping joints or have a tendency to develop vertically and they are generally developed with the fluctuation of groundwater level and flow direction. The karsts may be either continuous or isolated cavities and degree of them are reduced in the deeper part. It was found that the microfractured limestone at the cliff face fault on the right abutment containing zone of small and large rock elements of fault origin, solution cavities and partially to fully clayfilled seams and it was considered that erosion potential of the microfractured limestone could not be reduced by grouting, therefore a continuous vertical concrete wall by mining was provided for the cut off.

Karstic rock treatment methods, as reported by EGAT (1985) [4], are to treat the solution cavities and fissures simultaneously by sealing, filling, flushing, replacing, reinforcing, encapsuation of infilled cavities with grout or concrete. The cut off for the dam was executed along its plinth and 6 galleries, 3.5km long in each galleries, on the right abutment. The methods of foundation treatment are shown in Table 2.

Regarding to the plinth foundation, high pressure grouting was elaborately performed by using conventional split spacing and packer grouting technique after major karst treatment had been finished. The grout curtain comprise 3 rows with 1.5m spacing and the outer row being half the depth of the center row. The upstream and downstream rows were grouted first, followed by the center row.

Additional holes were provided locally to consolidate the foundation upstream and downstream of the plinth, particularly to fill cavities and seams which had been flushed out by the action of the superdrill during construction. The stage length adopted for grouting was 10m, with an allowable maximum of 20m and downstage grouting was adopted in areas of extensive karst especially for

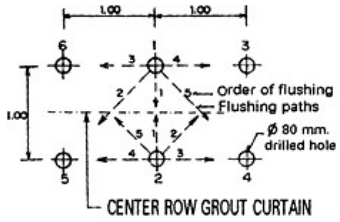

Figure 3. Flushing cell.

the outer rows and for primary holes in the center row. Upstage method was always applied in the next sequence of holes where the foundation was mostly consolidated. Grouting pressure up to a maximum of 30 bars (0.5 to 1.2bar/m) were used with grout mixes being progressively thickened from water to cement by weight 2 to 1 to 0.7 to 1 with 3% by volume of sodium silicate and 2% by weight of bentonite. In the decalcified sandstone area, it is found possible to make conventional grouting more effective in the upper karstic zone by first removing silty infilled material using high pressure flushing with air and water. The 80mm percussion holes were drilled and flushed with 2 to 3 bars of pressure in cell of six (3 holes in 2 rows, spacing 1m) as shown in Figure 3, in 5m stage downstaging to a depth of 25m until substantially clear water (outflow material not exceed 6gm in 1,000cc) was ejected from the other holes and then the holes were backfill grouted by 1 to 5 bars of injection pressure.

Grouting in 6 galleries, 14m equally spaced in a vertical plane, in the right abutment was carried out to provide a watertight curtain between row and below the galleries and to consolidate the rock around and thus prevent leakage into galleries. Radial and intergallery grouting was executed by using 5 to 15 bars (1 bar/m) of injection pressure and grout mix was the same as for curtain grouting. The single row of grout curtain was mostly performed below galleries apart from a 3 rows section under the portion close to the dam. Primary holes were generally drilled at 12m center to minimize grout interconnections. Conventional split spacing method was used until 5 Lugeon target was achieved. The maximum depth of grout holes was reached at 250m comparing to the design depth of 50m and at this depth 75% of primary holes had very high grout take with some take as high as 7.62 ton/m. It then became necessary to accept the principle of a "floating curtain" instead of "anchor curtain" with the possibility of some minor leakage under the bottom especially for the curtain below 150m. Grouting pressure was designed up to a maximum pressure of 30 bars (0.7 to 1.2bars/m) to overcome karstic features. A base mix of 0.7 water to 1 cement by weight plus 2% bentonite and thickened by adding 2 to 3% of sodium silicate to limit grout travel and control setting. In the deep holes >180m. Downstage method in 20m stage was adopted for below 180m. The top 180m was then grouted upstage. Mechanic packer was crucial used throughout rather than pneumatic packer, but it was not possible to set below 170m due to limiting of coupling thread's strength.

Assessment of curtain grouting effectiveness had been based on grout absorption and a statistic analysis of the curtain grouting under the dam and in the right abutment galleries showed diminishing grout take with each successive stage of closure. Grouting criteria were met in all but a few isolated instance in the deepest part of the curtain. Seepage measurement was designed by installing seepage detection holes, seepage weirs, observation holes and the result of them show effective cut off was satisfactory obtained by showing a favourable pressure difference across the cut off and low seepage. At present, the total seepage is in the order of 0.2cu m/sec.

2.3 *Lam Ta Khong Pumped Storage powerplant: Upper Pond*

The Lam Ta Khong Pumped Storage powerplant was constructed from 1997 to 2004, is located about 200km northeast of Bangkok and the existing lower reservoir of the Lam Ta Khong dam

connected to a new upper reservoir named Upper Pond situated on a plateau some 350m above, by a system of shaft and tunnels through an 4,100sq m underground powerhouse which contain four numbers of 250MW reversible Francis type generating/pumping units. The Upper Pond is a rectangular pond with a surface area of 0.34sq km and a volume of 9.9MCM, bounded by rockfill dam and lined with an 350mm thick of asphaltic concrete covered with 3mm thick HPDE sheet. The dam has a maximum height of 50m and 2.2km of crest length. The dam's volume is 5.4MCM. The bed rocks at the Upper Pond site consisted of interbedded of sandstone, claystone and alternation of sandstone and siltstone. The attitude of bedding trend west to northwest and gently dips north to northwest with 5 degree and no distinct folding. Sandstone is massive, hard and slightly jointed. On the other hand, claystone is soft and susceptible to water and can deform or become soft plastic clay if saturation occur while medium hard siltstone is susceptible to change in moisture and then become deteriorate and slaking.

To improve foundation bearing capacity, avoid and reduce substantial settlement, foundation preparation and surface treatment performed after excavation by conventional drilling and blasting were mostly completed. Due to characteristic of rock, EGAT (1996) [5] commented that gently dip of their bedding and method of excavation, unavoidably results in step of sandstone in bottom and cut slope was found including some open cracks, some loose blocks. In areas of s iltstone and claystone, some slaking and deterioration occur when they were uncovered and/ or exposed to the atmosphere and where groundwater outflow, claystone became soft. To avoid possible significant differential surface deflection of the impervious facing, the excavated material of sandstone was left in place at the benches of the cut slope with only rocks projecting beyond design line being removed. At the bottom of the pond, all excavated material, loose rock, debris etc. were substantial removed to sound rock and all open cracks or joints and any holes were replaced or filled by grout and concrete. EGAT (1997) [6] stated that all steps of sandstone were improved by trimming and concreting to become smooth and gentle slope foundation. The total amount of concrete used was 2,500cu m. According to EPDC (2002) [7], the drainage system as presented in Figure 4 which is composed of 2.0m wide and 1.50m deep of excavated drainage trenches and 150mm drainage pipes is neatly designed and provided in network at the bottom of the pond and the peripheral area to collect groundwater and water leakage from the impervious layer and drain out through the drainage tunnel, therefore the impervious face could be secured from damage. After finished foundation treatment, the performing of the facing process commenced. The total seepage detected is 20 litres/min after filling the pond to maximum water level.

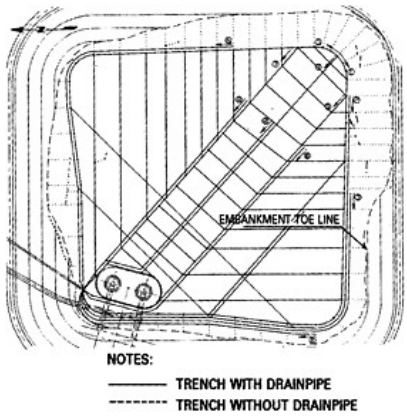

Figure 4. Drainage system.

2.4 *The Lower Mae Ping dam; after bay dam*

The Lower Mae Ping dam was constructed at 5km downstream of the Bhumibol dam along the Mae Ping river and located around 400km north of Bangkok to ensure that the reversible pump/ turbine generator of unit 8 can supply adequate power production as required. The dam consists of a 10 gate concrete spillway and earthfill with impervious core dam. The overall length of dam is 335m and 12m high. The dam foundation comprises 20m thick of high permeable alluvial sand (8% finer than 0.074mm) and gravel deposit on bedrock of quartzite and mica schist. Subsurface investigations were performed prior to and during construction to determine appropriate methods of foundation treatment. Investigation techniques comprised geological mapping, core drilling, standard penetration test, cone penetration test kunzel stab, permeability test and open trenching.

To increase foundation bearing capacity and stability, the dynamic compaction and vibrofloatation were selected. The dynamic compaction method in Jivanond, T. and Khongtip, P. (1994) [8], was executed in 5×5m pattern by dropping maximum weight of 15 tons from maximum height of 24m giving a maximum potential energy of 360 ton-m per drop and carried out in 4 passes and 6 to 25 times of dropping per passes as shown in Table 3. The results of dynamic compaction by considering the test data from cone resistance greater than 14MPa show that only 30% of cone resistance greater than 14MPa was obtained upto 8m deep from the surface so vibrofloatation was additionally performed for the deeper part. The layout of vibrofloatation as mentioned in Sucharitkul, K. and Khongtip, P. (1995) [9], were equilateral triangular spacing of 2.5m measured between treatment points or 5sq m per hole and vibrofloatation method was adopted in the depth between 8 to 13m from the ground surface and sinking rate of 300mm vibrator probe (weight 1600kg with 2 holes for water jet) was 0.5 to 3.0m/min for non prebore and 0.5 to 3.6m/min for prebore and rate of vibration was 0.6 to 2.0m/min. After having finished, standard penetration test was conducted and the result show that dense sand foundation was satisfactory obtained. The study of both compaction methods found that the depth less than 10m, working rate of dynamic compaction was 2 times faster than vibrofloatation method, which were 120sq m (1,130cu m) per day for vibrofloatation and 250sq m (1,900cu m) per day for dynamic compaction method while vibrofloatation was suitable to be adopted in deeper area.

The performance criteria at permanent cut off wall beneath the dam structure and spillway activate the permeability and settlement. As reported by Sucharitkul, K., Bumrungpaisarn, O. and Khongtip, P. (1995) [10], the 3,200sq m cut off wall in the form of secant pile wall were constructed as alternating series of interlocking 1,200mm diameter unreinforced piles with thus arrangement the minimum wall thickness was 79cm. Prior to start the construction of secant pile wall, guide wall was installed parallel to the wall axis and primary holes were drilled along the guide wall using the hydraulically operated Bauers BG rig to a design depth using double wall casing to pass through alluvial sand and cut in the rock formation about 1.0m. The secondary piles were commenced when the primary holes had been already placed with plastic concrete for 24 hours. The mix of the plastic concrete comprised 25% of cement, 5% of bentonite and 5% of flyash and the property of this mix conform and meet with the requirement. The modulus of elasticity of the cut off wall was

Table 3. Dynamic compaction method.

Area	Depth (m)	Grid (m)	Pass 1	Pass 2	Pass 3	Pass 4	Ironing
Zone A	8–12	5×5	15 tons	15 tons	15 tons	15 tons	9 tons
7,500sq m		2×2 for ironing	24m	24m	12m	12m	5m
			25 times	25 times	15 times	15 times	1 time
Zone B	4–8	5×5	15 tons	15 tons	15 tons	15 tons	9 tons
3,400sq m		2×2 for ironing	12m	12m	12m	12m	5m
			15 times	15 times	15 times	15 times	1 time
Zone C	0–4	2.5×2.5	15 tons	15 tons	15 tons	15 tons	9 tons
2,100sq m		2×2 for ironing	6m	6m	6m	15m	5m
			6 times	6 times	6 times	6 times	1 time

Table 4. Summary of foundation treatment of hydro-electric dam in Thailand (1974–2004).

Dam	Srinagarind	[12] Bang Lang	Vajiralong Korn	[13] Rajjaprabha (ChiewLarn)	[14] Pak Mun	Lower Mae Ping	Lam Ta Khong
Dam type	rockfill	rockfill	CFRD	rockfill	concrete	earthfill	rockfill
– height	140m	85m	92m	94m	17m	12m	50m
– volume	12MCM	2.86MCM	8.1MCM	6.51MCM	50,000m^3	0.28MCM	5.4MCM
Consultants	Electric Power Develop. Co. Ltd.	Sverdrup & Parcel and Associates	Snowey Mountains Engineer. Corp.	Electro-consult	Sogreah & Team	Klohn-Crippen & Team	Electric Power Develop. Co. Ltd.
Geology	heavily sheared fractured sandstone limestone	sandstone shale schist with sheared & fractured	karstic-limestone with fault zone	greywacke/ black shale sandstone	sandstone/ shale	Alluvial sand/ gravel	sandstone claystone
Curtain grouting;							
– lugeon	5	10	5	5	7	–	–
– grout row	3	2	1–3	2	single	–	–
– grout dept	65m	55m	250m	75m	35m	–	–
– spacing	3m	3m	1.5m	3m	3m	–	–
– pressure	0.7–1bar/m	0.3bar/m	0.5–1.2bar/m	0.3–0.7bar/m	1bar/m	–	–
– grout mix (w/c)	see Table 1	5 to 1	0.7+2% bentonite 3% sodium silicate	0.8+2% bentonite/ sand/sodium silicate	1.5+4% bentonite/ sand/ sodium silicate	–	–
– grout take	35kg/m	18.5kg/m	133kg/m	33kg/m	190kg/m	–	–
Concrete	12,900m^3	–	74,032m^3	6,988m^3	3,830m^3	–	2,500m^3
Secant pill wall	–	–	15,950m^2	–	–	3,200m^2	–
Compaction	–	–	–	–	–		–
– dynamic	–	–	–	–	–	5×5m grid	
– vibrofloat.	–	–	–	–		5m^2/hole	–

[]=Reference's number.

designed to be approximately the same as or less than the modulus of surrounding compacted foundation material which was 40MPa. The permeability of the wall was established at less than 5×10^{-8}m/sec or flow through the cut off less than 1×10^{-6}cum/sec/sqm under the operating head difference of 9.5m and 1.1×10^{-6}cum/sec/sq m under the maximum head difference of 11m. The wall could be capable of accepting differential settlements of the overlying structures of 100mm vertical displacement over 20m horizontal alignment without detrimental effect to its function and its effectiveness in terms of its permeability and no long term reduction in permeability occurred due to internal erosion, piping under the maximum water head of 11m. After having finished with totaling of 357 piles, 25 core holes were drilled in the cut off wall to check its permeability and quality of plastic concrete. The result of permeability test conform with the requirement which was less than 5×10^{-8}m/sec and its compressive strength and elastic modulus of the wall were 0.26 to 0.46MPa and 27 to 35MPa respectively. The homogeneity of the piles were also obtained. Regarding the internal erosion-resistant of the cut-off material, pin hole test was carried out and non dispersive plastic concrete was clearly shown.

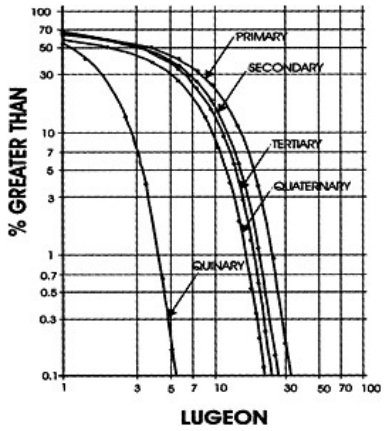

Figure 5.

3. CONCLUSIONS

3.1 Summary of various foundation treatment methods in different geological conditions of dam is presented in Table 4. In Thailand, the design of foundation treatment for the dam is usually based on the results of geological & geophysical surveys, permeability test, groundwater table study and grouting test is sometimes performed. Foundation preparation including surface treatment is usually executed before grouting work to reduce grout leakage to the surface and prevent foundation from uplift. Regarding grouting method, application of high pressure is prefer to low pressure and cement based grout with 2 to 3% by weight of bentonite is normally used in either fractured hard rock or highly sheared rock. Concrete cut off wall which is more relialble than grouting, employed in soil foundation, high extensive karst and ungroutable fault zone. Statistical & probability method is elaborately applied in analysis of grouting results during and after execution as shown in Figure 5 for an example.

3.2 The grouting methods employed with penetrable cement-bentonite and sodium silicate cement mixtures by the application of high pressure are more effective in the highly sheared and fractured zone of calcareous sandstone, shale, quartzite and limestone in Srinagarind dam, however, at the zone of poor geological condition; strongly weathered and highly sheared rock, near the ground surface in the lower part of the left abutment, a deep cut off trench was additionally provided.

3.3 In high degree of karstification, karst characteristic including infilled material and ground-water should thoroughly studied to select proper methods for treatment. As stated by Areepitak, C. (1983) [3], the experience from Vajiralongkorn dam show that the combination methods as primary and secondary treatment for karstic rock would be essential tool for the completion of a successful project at an exceptionally difficult site. After having analysis of such as the grout absorption characteristics, grouting records of adjacent stages, drilling reports, core inspection, water pressure test, groundwater observation etc., EGAT (1985) [11] concluded that regarding the overall results, the work were carried out both extremely thoroughly and most effectively as evidenced by the very low total seepage and absence of serious leakage since impounding.

REFERENCES

[1] Champa, S. (1978), *Foundation Treatment and Grouting Work for Srinagarind Dam,* Srinagarind Hydro-Electric Project, Electricity Generating Authority of Thailand, September 1978.

[2] Electricity Generating Authority of Thailand (1982), *Report on Inspection of Srinagarind(Ban Chao Nen),* Report No. 13, Hydro-Electric Project, International Board of Consultants, Hydro Electric Construction Department, December 1982, pp. 3, 6.
[3] Areepitak, C. (1983), *Karstic Rock Treatment on Khao Laem Dam Foundation and Abutments with the Purpose of Positive Watertight Cut Off Construction,* Thesis No.GT-82–22, Asian Institute of Technology, Thailand, April 1983.
[4] Electricity Generating Authority of Thailand (1985), *Completion Report,* Khao Laem Multipurpose Project, Hydro Electric Construction Department, August 1985.
[5] Electricity Generating Authority of Thailand (1996), *Report No. 4 of the International Board of Experts,* Lam Ta Khong Pumped Storage Project, October 1996.
[6] Electricity Generating Authority of Thailand (1997), *Report No. 6 of the International Board of Experts,* Lam Ta Khong Pumped Storage Project, November 1997.
[7] Electric Power Development Corporation-EPDC (2002), *Final Report of Remedial Works for Damages on Asphalt Concrete Surfacing,* Lam Ta Khong Pumped Storage Project, February 2002.
[8] Jivanond, T. and Khongtip, P. (1994), *Technical Report on Dynamic Compaction Stage 1 at Lower Mae Ping Dam,* Bhumibol Hydro Power Plant Unit 8, Hydro Power Construction Department, Electricity Generating Authority of Thailand, August 1994. (in Thai)
[9] Sucharitkul, K. and Khongtip, P. (1995), *Technical Report on Vibrofloatation at Lower Mae Ping Dam,* Bhumibol Hydro Power Plant Unit 8, Hydro Power Construction Department, Electricity Generating Authority of Thailand, September 1995. (inThai)
[10] Sucharitkul, K., Bumrungpaisarn, O. and Khongtip, P. (1995), *Technical Report on Permanent Cut-Off Wall,* Bhumibol Hydro Power Plant Unit 8, Hydro Power Construction Department, Electricity Generating Authority of Thailand, December 1985. (inThai)
[11] Electricity Generating Authority of Thailand (1985), *Report No. 16 of the International Board of Consultants,* Khao Laem Project, January 1985. (in Thai)
[12] Areepitak, C. (1980), *Report on Engineering Geology and Foundation Treatment,* Pattani Multipurpose Project, Bang Lang Storage Dam, Hydro Electric Construction Department, Electricity Generating Authority of Thailand, November 1980.
[13] Areepitak, C. (1987), *Technical Report on Geology and Foundation Work for Chiew Larn Project,* Hydro Power Construction Department, Electricity Generating Authority of Thailand, August 1987.
[14] Electricity Generating Authority of Thailand (1993), *Completion Report on Geology/Foundation Treatment,* Geology & Foundation Treatment Section, Civil Construction Project Division, Pak Mun Project.

New Developments in Dam Engineering—Wieland, Ren & Tan (eds),
© 2004 Taylor & Francis Group, London, ISBN 04 1536 240 7

Computation of optimal top width of gravity dam

S.L.Atmapoojya, S.K.Mahajan & A.N.Dabhade
Department of Civil Engineering, Kavikuluguru Institute of Technology and Science, Ramtek. District, Nagpur (MS), India

ABSTRACT: When a solid gravity dam is to be designed for an irrigation project, initially its elementary profile (triangular Section) is decided then, it is modified to suit the practical conditions. These conditions are

(i) A suitable free board is provided to prevent overflow, and
(ii) A suitable top width is provided for inspection and conveyance purposes.

Due to such provisions the weight of the dam is to be increased at the top portion, which creates instability of the section in reservoir empty condition and tension may be develop at the toe. Hence it becomes necessary to increase weight in the upstream and a batter is provided on the upstream side. In reservoir full condition, the resultant of all the forces remains in the middle third portion and the section becomes quite safe, hence to provide economy, the material from downstream may be removed.

The addition of the quantity of material on the upstream and deduction of quantity of material from the downstream are the function of the top width of section. The net cross sectional area of the dam is determined at a particular value of top width. The top width for which the net cross sectional area of the dam is minimum, is known as the optimal top width. The top width is taken as the function of the height of the dam.

The paper deals with the preparation of a simplified computerized method to evaluate the value of the optimal top width of the dam. The result obtained are almost similar to as obtained by Creager (1916).The computerized methodology may provide the help for computation of the optimal top width for a wide range of height of a gravity dam.

1 INTRODUCTION

The procedure of the design of a solid gravity dam involves the determination of theoretical profile initially and then the modification from practical point of view.

The basic modifications required in the theoretical profile are:-

1. The sufficient freeboard is provided to avoid over flow from the dam. The requirement of free board is decided from the wave action created at the water surface. The minimum free board should be provided as 0.9m as specified by Indian standards.
2. The sufficient top width is provided which is required for the provision of road above the dam for inspection purposes.

Due to above provisions, extra material is required at the top of the dam, which results in shifting of resultant towards the heel in reservoir empty condition and chances of development of tension at the toe. To avoid this tension, base width of the dam is increased at the upstream side and upstream batter is provided. Hence material is increased on the upstream side of the dam.

In reservoir full condition, the resultant remains in middle third portion due to provision of top width and the section remains quite safe, hence the material from the downstream side may be removed to bring resultant in the outer middle third point.

The material required in modification of theoretical profile consists of the material required at the top plus the material required at the upstream bottom minus material removed from downstream side.

The net material required is a function of top width. Hence a particular top width is to be decided for which the net material required is the minimum. This top width is known as the optimal top width.

Creager[1] had proposed that the economical top width of gravity dam can be adopted as 14% of height of the dam. He had not considered earthquake forces. He [2] also suggested, if earthquake forces are considered then the obtained top width is much more which cannot be provided in the dam.

The paper deals with the determination of the optimal top width by a proposed Computer program in which the top width is taken as a function of water depth and systematic checking of the section is done. The net required material is calculated for the dam section in which no tension is developed any where in the dam section. The proposed methodology can be used very conveniently to determine the safe and economical dam section corresponding to the optimal top width.

2 APPROACH OF DESIGN

The elementary or theoretical profile is determined and then it is modified for the practical consideration. The bottom width is extended in upstream side such that tension should not develop at the toe in reservoir empty condition.

The bottom width is reduced in the downstream side to save the construction material and precaution is taken that the tension should not develop at the heel in reservoir full condition.

The procedure of design is based on trial and error approach. First the top width is assumed as percentage of the height of dam. For this top width, the extension of bottom width at upstream side is determined for no tension at the toe in reservoir empty condition.

Similarly the reduction in the bottom width is determined at the downstream side for no tension at the heel in reservoir full condition. The top width *(a)* is assumed as percentage of the water depth *(h)*. For the selected top width, the bottom width of upstream batter *(x)* is assumed as a fraction of top width (α/x_1) and reduction in bottom width *(y)* in the down stream is also assumed as a fraction of top width (α/y_1). By changing values of x_1 and y_1, the values of width x and y are determined such that the dam section is safe for reservoir empty as well as for reservoir full conditions.

For various values of top width, the final profile of the dam section is obtained. The top width, corresponding to the minimum cross section of profile will be the optimal top width section.

A computer program is developed in Visual Basic language for the design of dam corresponding to the optimal top width.

3 METHODOLOGY

3.1 *Derivation of elementary profile*

The height of dam=H in meter

The height of water surface=h in meter.

The base width of the profile from no tension criteria is given by

$$b = \frac{h}{\sqrt{S-1}} \tag{i}$$

where S=specific gravity of dam material.

3.2 *Derivation of practical profile*

Let top width provided=a in meter

Free board=f in meter

The depth up to which vertical upstream face is provided=h_1 in meter.

This is given by

$$h_1 = 2.1a\sqrt{S-1} \quad \text{(ii)}$$

The height of upstream batter from the base=h_2 in meter

The width of upstream batter=$x=\alpha/x_1$

The height of downstream sloping face from the base=h_3

The base width reduced in the downstream=$y=\alpha/y_1$

3.3 *Calculation of moments*

With reference to Figure 1, forces acting, lever arm from the toe and moments about toe are tabulated in Table 1.

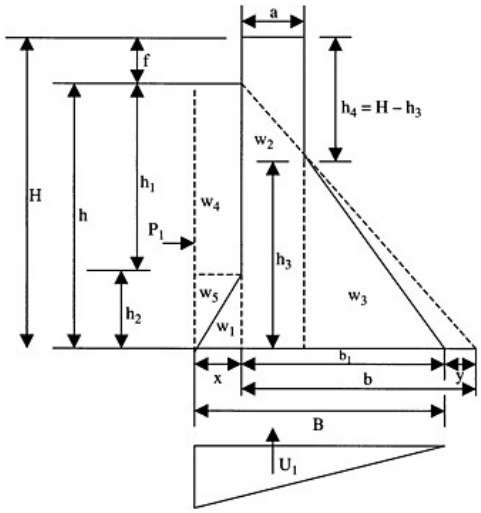

Figure 1.

Table 1.

S.N.	Forces	Expression	Nature	Lever arm	Moment
1	Weight of dam				
	(w_1)	0.5 h_2 Sw	Vertical (d)	$B+x/3$	M_1
	(w_2)	a H Sw	Vertical (d)	(b_1−a)+0.5a	M_2
	(w_3)	0.5(b_1−a) h_3Sw	Vertical (d)	(2/3)(b_1−a)	M_3
2	Weight of water supported by				
	upstream face (w_4)	×h_1w	Vertical (d)	b_1+0.5x	M_4
	(w_5)	0.5×h_2 w	Vertical (d)	b_1+x(2/3)	M_5
3	Hydrostatic pressure				
	(P_1)	0.5 w h^2	Horizontal	h/3	M_6
4	Uplift pressure				
	(U_1)	0.5 w h B	Vertical (u)	(2/3) B	M_7

In the above Table: S=specific gravity of dam material, w=specific weight of water in N/m^3, M_1, M_2,= moments of corresponding forces about the toe, vertical (d)=vertical downward forces, vertical (u)= vertical upward forces.

3.4 *Computation of eccentricity*

3.4.1 *Reservoir empty condition*

$$\bar{X} = \frac{w1 + w2 + w3}{M1 + M2 + M3} \quad \text{(iii)}$$

$$e_d = \bar{X} - \frac{B}{2} \quad \text{(iv)}$$

For no tension at toe - $e_d \leq \frac{B}{6}$ (v)

3.4.2 *Reservoir full condition*

$$\bar{X} = \frac{w1 + w2 + w3 + w4 + w5 - U1}{M1 + M2 + M3 + M4 + M5 - M6 - M7} \quad \text{(vi)}$$

$$e_f = \frac{B}{2} - \bar{X} \quad \text{(vii)}$$

For no tension at heel - $e_f \leq \frac{B}{6}$ (viii)

4 THE PROGRAM

This program is developed by utilizing the power of latest standard of *Visual Basic (VB6)*[3] and works in *MS-Windows* environment. The program is able to interact with the screen, keyboard, mouse and printer in graphical environment, which is supported by *VB6* language and it has the required graphical interface needed for today's computers. Numerous forms, menus, buttons and functions are developed to facilitate graphical and text output with menu-driven navigation. The program generates cross section of the dam showing the dam shape details graphically on the screen. The program also generates the upstream water pressure, uplift water pressure diagrams graphically on the screen which is easy to understand by the user.

Output is generated through the *reports* and result can be export to various destinations like Disk file, application, Lotus Database, Microsoft Mail in number of formats like *character separated values, Data interchange format (DIF), Excel, HTML, DHTML, LOTUS, ODBC, Record Style, Rich text Format, Text, word for windows document*.

5 FUNCTIONING OF THE PROGRAM

For design purpose, the height of water surface, freeboard, specific gravity of dam material and range of assumed top width in terms of percentage of height of water are to be fed as input on input screen as shown in Figure 2. After getting input data, the top width is assumed as percentage of the height of dam given by the user. For this top width, the extension of bottom at upstream side is determined for no tension at the toe in reservoir empty condition. Similarly the reduction in the bottom width is determined at the downstream side for no tension at the heel in reservoir full condition.

For various values of top width, the final profile of the dam section is obtained. The top width, corresponding to the minimum cross section of profile is selected which is the optimal top width section. By clicking the *"Compute Optimal Section"* button, the design details for the optimal top

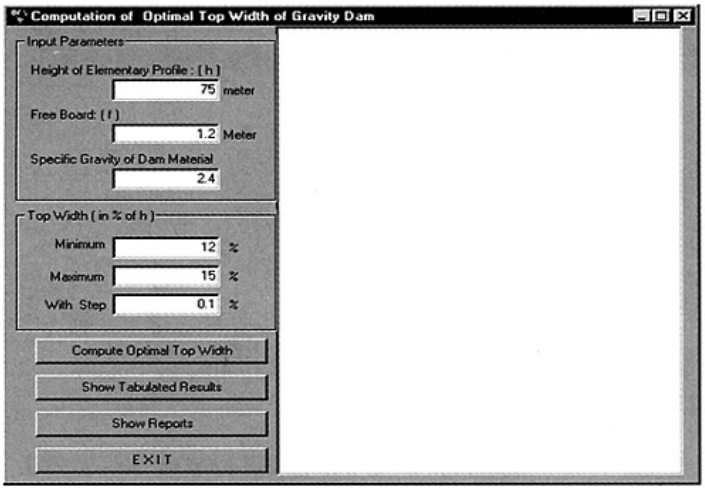

Figure 2. Input data screen.

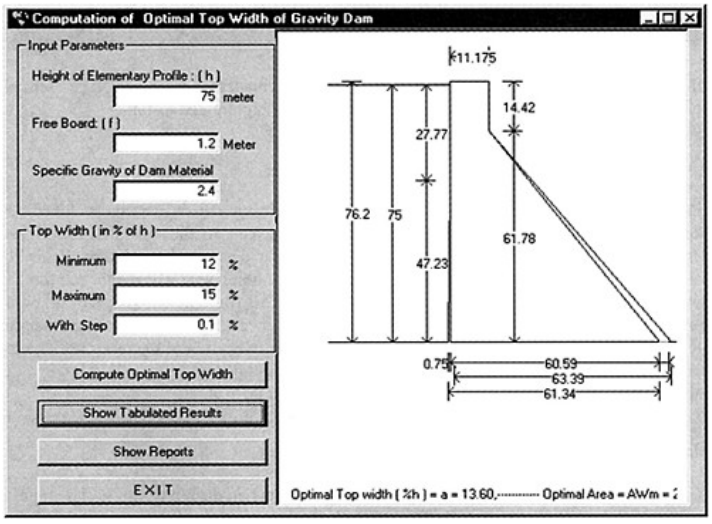

Figure 3. Output data screen.

width section are displayed on screen in text mode as well as in the form of drawing. By clicking the *"Show tabulated Results",* the design details for various values of top width, height of dam can also be displayed on the screen with drawing of dam cross sections, corresponding to the optimal top width, which is shown in Figure 3.

Table 2.

Comparative Results

% h	Top Width l	x1	y1	ed	ef	B/6	AWmin	x
12.00	9.000	10.800	3.000	10.183	10.202	10.203	2361.122	
12.10	9.075	11.100	3.000	10.186	10.196	10.197	2360.853	
12.20	9.150	11.300	3.000	10.186	10.189	10.191	2360.802	
12.30	9.225	11.400	3.000	10.185	10.180	10.187	2360.953	
12.40	9.300	10.700	2.950	10.158	10.182	10.184	2361.000	
12.50	9.375	11.000	2.950	10.161	10.177	10.177	2360.729	
12.60	9.450	11.200	2.950	10.161	10.169	10.171	2360.685	
12.70	9.525	11.500	2.950	10.164	10.163	10.164	2360.473	
12.80	9.600	11.500	2.950	10.160	10.152	10.161	2360.835	
12.90	9.675	10.800	2.900	10.132	10.156	10.158	2360.798	
13.00	9.750	11.100	2.900	10.135	10.150	10.150	2360.551	
13.10	9.825	11.300	2.900	10.136	10.143	10.145	2360.532	
13.20	9.900	11.500	2.900	10.136	10.135	10.139	2360.531	
13.30	9.975	11.600	2.900	10.134	10.125	10.134	2360.733	
13.40	10.050	10.800	2.850	10.102	10.130	10.132	2360.817	
13.50	10.125	11.100	2.850	10.105	10.124	10.124	2360.584	
13.60	10.200	11.400	2.850	10.108	10.117	10.117	2360.388	
13.70	10.275	11.600	2.850	10.108	10.109	10.111	2360.413	
13.80	10.350	11.700	2.850	10.106	10.100	10.107	2360.641	
13.90	10.425	10.700	2.800	10.068	10.104	10.106	2361.062	
14.00	10.500	11.000	2.800	10.071	10.097	10.099	2360.834	

Effect of top width on the design of the dam section is represented in Table 2. The optimal top width corresponding to minimum cross section of the dam is highlighted in Table.

6 INPUT/OUTPUT FOR THE PROGRAM

The input data is given through screen mode and a user-friendly interface has been developed for this purpose. Once the input is entered, the software processes the data. As the software is developed on the *MS-Windows* platform, the user has to give all numeric input data in text boxes through keyboard.

Using this program, the user can get the design details including details of shape, and forces acting on the dam section in graphic as well as in the form of text file. The hard copy of graphic can be taken directly or through any *MS-Windows* based image processing software through the printer. The text output is generated in the form of reports during the execution of the program. The report consists of details of all input made during execution and final design.

The hard copy of the report can be taken directly through the printer.

7 DESIGN EXAMPLE

The practical utility of the developed program has been shown in design example. The input data and text output are given in *Appendix-I* the typical graphical output of the program is shown in Figure 3 and Table 2.

8 CONCLUSIONS

The design of gravity dam corresponding to the optimal top width can be carried out for any required height of the dam; however the design is based on single zone approach. The obtained

design is the most economical and the safest in which no tension is developed any where in the dam section.

The visual Basic language available on MS-Windows platform has been exploited to develop an interactive, user friendly and menu driven software for computation of optimal top width of gravity dam. The developed software offers a strong graphic support in the form of dam cross section sketches.

REFERENCES

[1] Creager W.P. (1916) "The economical top width of non overflow dams", *ASCE, vol. 80,* 1916, pp 723.
[2] Creager W.P., Justin J.D. and Hinds J. *Engineering for Dams, vol-II* John Wiler & Sons Inc. London. pp 306–312.
[3] Tetroutsos, Evangelos *Mastering Visual Basic 6,* BPB Publication, New Delhi, 1997.

APPENDIX I

Input data

1.	Height of Water surface	h=75m
2.	FreeBoard	f=1.2m
3.	Specific Gravity of dam Material	S=2.4
4.	Specific weight of water	w=9810N/m^3

Output data

1.	Optimal Top Width a=13.60% of	h=10.20m
2.	Extended width of upstream batter	x=0.895m
3.	Reduced width on downstream side	y=3.579m
4.	Total base width	B=60.702m
5.	Eccentricity of the resultant	
	(a) In reservoir empty condition	ed=10.108m from center of base width
	(b) In reservoir full condition	ef=10.117m from center of base width

Hence the resultant is lying in the middle third portion.

6.	The minimum cross sectional area of the dam section	aw=2360.388m^2

This page intentionally left blank.

New Developments in Dam Engineering—Wieland, Ren & Tan (eds),
© 2004 Taylor & Francis Group, London, ISBN 04 1536 240 7

Planning and operation of dams

Recep Bakiş & Mehmet Bilgin
Anadolu University, Turkey

ABSTRACT: The water discharged from a dam during operation must not cause floods downstream. Especially, if there is a large subcatchment area downstream and if surface runoff water due to rainfall cannot to be controlled, there is a considerable risk of flood downstream. Under these circumstances, the additive water coming from the reservoir will cause an increase in the flood damages. In this paper, the flood risks of rainfall water discharge from the subcatchment area, which is located in the downstream area of a dam and not completely controlled have been investigated. For this purpose, the decision matrix achieved from the rainfall of subcatchment, which lies between the Porsuk dam and Eskişehir city, was examined by taking the Porsuk sub-catchment as a basis.

1 INTRODUCTION AND LOCATION OF PORSUK CATCHMENT AREA

If discharge of any river flows observed through a definite time period, i.e. Q=f(t), local needs, regional needs, national needs or international needs with wider perspective are determined in a definite period or if Q_i=f(t) function is determined, after comparison of these two functions, themselves or their derivatives are made in planning and feasibility works phase, reservoir found suitable will be constructed and water needs will be tried to be supplied from here [1,2].

In this paper, decision matrix obtained from downstream rainfall matrixes will affect decision-making mechanisms in dam operation works examined for Porsuk basin. Porsuk catchment area which will be examined drainage area of Porsuk river is about 11188km^2 until it joins with Sakarya river. Catchment's area of Porsuk River is a very big area which containing Kiitahya, Eskişehir and many small settlement centers. The total rainfall water of Porsuk River basin gives its waters to the Sakarya River. General layout plan of Porsuk catchment area is given in Figure 1. The water of catchment area up to the point A is controlled by PORSUK Dam. Also, flood detention dams and small volume ponds have been constructed on tributaries of Porsuk River. Average yearly rainfall height of Porsuk catchment area is about 450mm [4] and average yearly rainfall height of Eskişehir region is about 371,3mm [5,6]. The total water potential of Porsuk catchment area is about 480×10^6m^3 [4]. Total rainfall water is approximately 5000×10^6m^3 and average representative yearly runoff coefficient is about C=0.10.

B is a point that given in Figure 1 is the total part of the Porsuk catchment area, which extends from the beginning until the entrance of Eskişehir. There isn't any water structures i.e. dam or any structure, to control the water of subcatchment area, which is between A–B points on the main collector of Porsuk River. However, there are flood traps on the side branch of the river and Dodurga dam on Sarisu creek. The water coming from the big portion of the subcatchment area between A–B points discharges without any control into the Porsuk River.

By assuming that no water is coming from Porsuk catchment's area up to point "A", flood hydrographs that can come from uncontrolled subcatchment area due storm water between points "A–B" are given in Figure 2. These hydrographs given in figure 2 are with various return periods has been prepared by DSI for point "B" in entry of Eskişehir [5,4]. According to the improvement

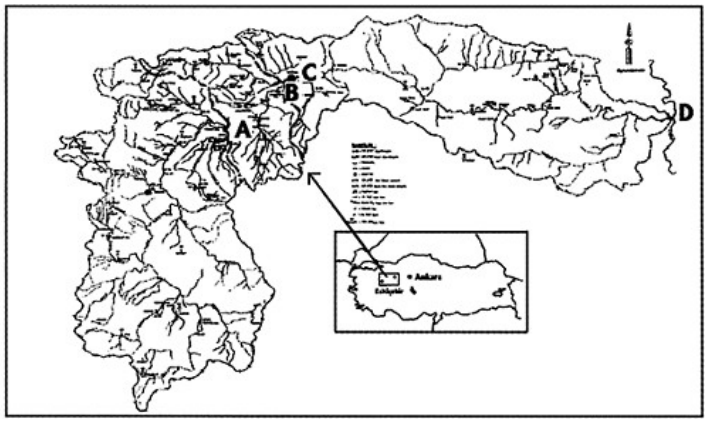

Figure 1. General layout plan of Porsuk catchment's area [4].

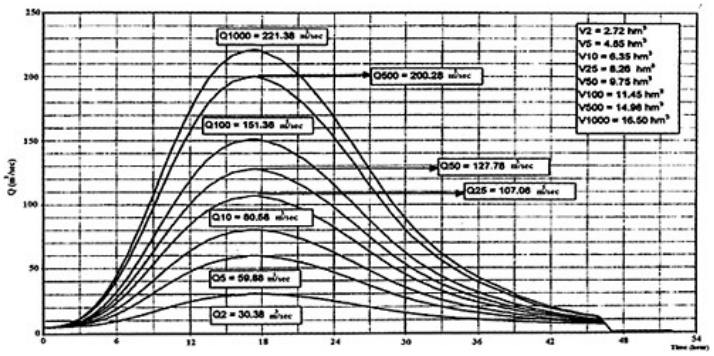

Figure 2. Flood hydrographs of A–B subcatchment areas for various return periods (The water of these hydrographs is uncontrolled coming from A to point B, and it states the condition that no water is coming from point A).

of Porsuk river and cross section of its bed around Eskişehir, performed by DSI, project flow around Eskişehir (in cross-sections of around point C given in Figure 1) has been taken as Q_p=45,1m^3/sn and cross-section arrangement has been performed [5].

In this case, since cross-sections of Porsuk river after passing of Eskişehir is generally not sufficient, even if no water is given from Porsuk dam according to the examination of results of DSI flood hydrographs, several years return period floodwaters will certainly flood into the agricultural areas and will damage them partly.

If water is given into downstream additionally from Porsuk Dam during rainfall and if this water is considered as a base current under flood hydrograph, it will be a component that will increase the flood damages. Therefore, when there is rain on uncontrolled area during dam operation works, no water should be released from dam as far as possible except critical conditions. Decision making matrix explained below is developed in order to be helpful for a dam operation works.

2 INVESTIGATION OF RUN OFF WATER IN DOWNSTREAM AREA OF PORSUK DAM

In this study, rainfall on this subcatchment area will be represented by Eskişehir Meteorology Station with no 17706. The values of monthly total rain data belonging to measuring station with no 17706 are given in Table 1. This table named rain matrix belonging to Eskişehir Meteorology Station.

Rows (i=1, 2,…, 17) of rain matrix are on a yearly basis given in Table 1 and they show the monthly rain values (in mm). Sum of 12 months is shown at the end of rows with Σ_i marking, and it expresses ith the total rain of the year.

Statistics such as monthly average rain height belonging to that year ($\bar{y}_i$), standard deviation of rain (sd_i), variation coefficient (cov_i), skewness coefficient (as_i) and correlation coefficient ($r_{i,\,i+1}$) are shown in next rows in the same table, respectively.

Distribution parameters calculated in Table 1 will be calculated for each year (i=1,…, 17) with the formulas given below [7,8].

a. Average value of monthly rain is the most meaningful parameter of the distribution and is calculated by equation (1).

$$\bar{y}_i = \frac{1}{n}\sum_{j=1}^{n=12} y_{i,j} \tag{1}$$

where $y_{i,j}$ is the observed monthly rain heights, $\bar{y}_i$, ith is the average of monthly rain height of the year.

b. Standard deviations of monthly rain are the parameters used to express the extend of distribution, if the value of standard deviations is bigger, that means random variable is more widely distributed around average and it is calculated by equation (2).

$$sd_i = \sqrt{\frac{\sum_{j=1}^{n=12} (y_{i,j} - \bar{y}_i)^2}{n-1}} \tag{2}$$

where $y_{i,j}$ is the observed monthly rain heights $\bar{y}_i$, ith is the average of monthly rain height of the year and sd_i shows the standard deviation which belong to the ith the year.

c. Variation coefficient (cov_i) is obtained by dividing standard deviation by average value of the monthly rain. It has no dimension and it is expressed with equation (3).

$$cov_i = \frac{sd_i}{\bar{y}_i} \tag{3}$$

d. Skiwness coefficient is an important parameter in determining the skewness of random variables and it is calculated by equation (4).

$$as_i = \frac{\sum_{j=1}^{n=12} (y_{i,j} - \bar{y}_i)^3}{\left[(n-1)(n-2)/n\right] sd_i^3} \tag{4}$$

where $y_{i,j}$ is the observed monthly rain heights, n=12 is the total sum of examples, $\bar{y}_i$, ith is the average of monthly rain height of the years, sd_i, is the standard deviation belonging to the ith year, and as_i is ith skewness coefficient of the year.

Table 1. Monthly rain belonging to Eskişehir measuring Station with no 17706 (in mm) and statistics of monthly rain within years.

Years		Jan. j=1	Feb. j=2	Marc j=3	April j=4	May j=5	June j=6	July j=7	August j=8	Sept. j=9	Oct. j=10	Nov. j=11	Dec. j=12	Monthly mean Σ_i	$\bar{y}_i$	sd_i	cov_i	as_i	$\Gamma_{i,i+1}$
1973	i=1	11,8	39,4	20,6	59,6	29,4	78,3	64,2	17,8	1,6	42,8	45,5	62,2	473,2	39,433	23,771	0,603	0,009	0,101
1974	i=2	13,5	49,2	45,3	50,5	70,8	29,1	0,6	19,5	10,6	27,2	30,1	37,2	383,6	31,967	19,829	0,620	0,330	0,738
1975	i=3	49,3	28,9	41,0	29,0	126,9	32,6	0,2	15,2	1,6	7,5	4,3	42,4	414,9	34,575	33,467	0,968	2,000	0,822
1976	i=4	43,3	24,6	27,2	33,2	87,4	47,3	10,6	3,5	3,8	37,3	17,5	62,4	398,1	33,175	24,719	0,745	0,871	0,211
1977	i=5	32,7	18,0	30,3	61,3	16,8	35,2	7,0	39,7	16,3	38,9	29,8	56,3	382,3	31,858	16,160	0,507	0,408	0,388
1991	i=6	15,2	40,8	23,1	71,3	50,8	26,0	34,0	25,8	11,7	64,5	31,3	35,7	430,2	35,850	18,389	0,513	0,781	0,238
1992	i=7	2,8	5,9	33,9	30,3	14,9	78,8	12,0	11,1	0,0	47,1	38,4	33,7	308,9	25,742	22,735	0,883	1,099	0,010
1993	i=8	22,6	34,7	31,6	12,9	68,8	17,7	0,3	16,7	2,7	1,7	62,8	30,2	302,7	25,225	22,230	0,881	0,935	0,680
1994	i=9	56,3	33,9	19,3	26,5	36,8	6,9	1,8	3,0	3,4	21,4	63,0	25,5	297,8	24,817	20,240	0,816	0,671	0,402
1995	i=10	49,9	7,1	53,5	35,6	32,1	11,1	2,7	3,7	24,6	66,0	29,9	19,9	336,1	28,008	20,631	0,737	0,463	0,359
1996	i=11	25,4	25,5	28,3	30,5	43,3	22,5	22,6	6,3	32,3	37,1	6,1	44,9	324,8	27,067	12,210	0,451	−0,433	0,558
1997	i=12	41,0	10,0	8,0	50,1	40,5	23,9	8,0	23,7	5,2	50,4	17,6	82,8	361,2	30,100	23,458	0,779	0,993	0,275
1998	i=13	28,8	18,8	19,7	53,3	129,7	68,6	6,9	0,0	22,2	33,5	47,2	30,1	458,8	38,233	34,634	0,906	1,815	−0,316
1999	i=14	40,5	78,8	55,5	40,8	0,7	22,4	11,4	11,5	19,6	9,6	25,7	21,1	337,6	28,133	22,245	0,791	1,160	0,223
2000	i=15	28,6	18,7	42,1	125,1	33,1	8,7	15,3	14,7	10,9	27,7	4,7	30,5	360,1	30,008	31,972	1,065	2,739	0,269
2001	i=16	7,0	14,6	23,7	66,8	37,5	0,0	23,9	15,2	6,3	0,2	95,7	108,0	398,9	33,242	37,046	1,115	1,233	0,440
2002	i=17	22,2	9,4	24,1	57,4	44,3	11,3	35,1	6,6	44,5	24,1	25,9	38,6	343,5	28,625	15,701	0,549	0,267	0,060
Σ_i		490,9	458,3	527,2	834,2	863,8	520,4	256,6	234,0	217,3	537,0	575,5	761,5						
$\bar{y}_i$		28,876	26,959	31,012	49,071	50,812	30,612	15,094	13,765	12,782	31,588	33,853	44,794						
SD_j		15,980	18,455	12,821	25,445	35,998	24,296	16,790	10,032	12,417	19,755	23,789	23,290						
COV_j		0,553	0,685	0,413	0,519	0,708	0,794	1,112	0,729	0,971	0,625	0,703	0,520						
AS_j		0,085	1,403	0,460	1,603	1,145	1,033	1,778	0,960	1,258	0,047	1,093	1,524						
$R_{j,j+1}$		**−0,274**	**0,062**	**0,371**	**−0,018**	**−0,197**	**0,196**	**0,273**	**0,094**	**−0,261**	**0,128**	**−0,346**	**0,316**						

Note: Data of the rain from 1978 to 1990 cannot be obtained from gauging station.

e. Correlation coefficient is an important parameter measuring the degree of linear dependence between two random variables and it is calculated by equation (5).

$$r_{i,i+1} = \frac{\sum_{j=1}^{n=12}(y_{i,j} - \bar{y}_i)(y_{i+1,j} - \bar{y}_{i+1})}{\sqrt{\left[\sum_{j=1}^{n}(y_{i,j} - \bar{y}_i)^2\right]\left[\sum_{j=1}^{n}(y_{i+1,j} - \bar{y}_{i+1})^2\right]}} \quad (5)$$

where $y_{i,j}$, $y_{i+1,j}$, ith and (i+1)th years are the observed monthly rain heights, n=12 is the total sum of examples; $\bar{y}_{i+1}$, ith and (i+1)th are the average of monthly rain height of the years; $r_{i,\,i+1}$, ith and (i+1)th are the correlation coefficient between years. When it is i=17 here, concerned values of the first year are taken for (i+1) value.

When statistical parameters calculated in Table 1 are examined, standard deviation values (sd_i) for in any ith year are being big. Therefore, when standard deviation is getting bigger, distribution of these values around average is getting bigger. Depending on this, calculated variation coefficient (cov_i) is taking big values. Variation coefficient (cov_i) is sometimes bigger than 1. In this case, values smaller than ($\bar{x}_i - sd_i$) values are being negative. Since observed ones here are monthly rain, negative values will have no physical meaning. According to Table 1, skiwness coefficient is generally being (+). According to this, Skiwness expresses the distribution leaning to right. It is seen that correlation coefficient ($r_{i,\,i+1}$) expressing the relation of monthly rain between years with each others is generally very weak and also sometimes reverse weak dependent (−) (Table 1).

Columns of rain matrix show the monthly rain heights belonging to same month in various years (i=1,…, 17 years) in Table 1. Column number shows the months (j=1,…, 12) of a year (for example: j=1 shows January, j=5 shows May, etc.). Total rain belonging to that month are shown the end of columns with Σ_i symbol. Statistics such as average monthly rain ($\bar{y}_j$), standard deviation of rain (SD_i), variation coefficient (COV_i), Skiwness coefficient (AS_i) and correlation coefficient ($R_{j,j+1}$) are shown in next rows in Table 2.

Table 2. Decision matrix, (d, n, w) and (D, N, W) condition of rain within one year and within one month as to years.

		Months											
Years		Jan. j=1	Feb. j=2	Mar. j=3	Apr. j=4	May j=5	Jun. j=6	Jul. j=7	Aug. j=8	Sep. j=9	Oct. j=10	Nov. j=11	Dec. j=12
1973	i=1	d-D	n-W	d-D	w-N	n-W	w-W	w-W	d-N	d-D	n-W	n-N	w-W
1974	i=2	d-D	n-W	n-W	n-N	w-W	n-N	d-D	n-W	d-N	n-N	n-N	n-N
1975	i=3	n-W	n-N	n-W	n-D	w-W	n-N	d-D	d-N	d-D	d-D	n-D	n-N
1976	i=4	n-W	n-N	n-N	n-D	w-W	w-W	d-N	d-D	d-D	n-N	d-D	w-W
1977	i=5	n-N	d-N	n-N	w-N	d-D	n-N	d-N	n-W	d-N	n-N	n-N	w-N
1991	i=6	d-D	n-W	d-D	w-W	w-N	d-N	n-W	d-W	d-N	w-W	n-N	n-N
1992	i=7	d-D	d-D	n-N	n-D	n-D	w-W	d-N	d-N	d-D	w-W	w-N	n-N
1993	i=8	n-N	n-N	n-N	d-D	w-N	n-D	d-D	n-N	d-D	d-D	w-W	n-D
1994	i=9	w-W	n-N	n-D	n-D	w-N	d-D	d-D	d-D	d-D	n-D	w-W	n-D
1995	i=10	w-W	d-D	w-W	n-D	n-D	d-D	d-D	d-D	n-W	w-W	n-N	n-D
1996	i=11	n-N	n-N	n-N	n-D	w-N	n-N	n-N	d-D	n-W	w-N	d-D	w-N
1997	i=12	n-W	d-D	d-D	w-N	n-N	n-N	d-N	n-W	d-D	w-W	d-D	w-W
1998	i=13	n-N	d-N	d-D	n-N	w-W	w-W	d-N	d-D	n-W	n-N	n-W	n-D
1999	i=14	w-W	w-W	w-W	w-N	d-D	n-N	d-N	d-N	n-W	d-D	n-N	n-D
2000	i=15	n-N	n-N	n-W	w-W	n-D	d-D	n-N	n-N	d-N	n-N	d-D	n-D
2001	i=16	d-D	d-D	n-D	w-W	n-N	d-D	n-W	n-N	d-D	d-D	w-W	w-W
2002	i=17	n-N	d-D	n-D	w-N	w-N	d-D	n-W	d-D	w-W	n-N	n-N	w-N

The distribution parameters in Table 2 are calculated similarly;

a. Average value of the monthly rain heights is calculated by equation (6).

$$\bar{Y}_j = \frac{1}{N}\sum_{i=1}^{N=17} y_{i,j} \tag{6}$$

b. Standard deviation of the monthly rain heights is calculated by equation (7).

$$SD_j = \sqrt{\frac{\sum_{i=1}^{N=17}(y_{i,j} - \bar{Y}_j)^2}{N-1}} \tag{7}$$

c. Variation coefficient is calculated by equation (8).

$$COV_j = \frac{SD_j}{\bar{Y}_j} \tag{8}$$

d. Skiwness coefficient is calculated by equation (9).

$$AS_j = \frac{\sum_{i=1}^{N=17}(y_{i,j} - \bar{Y}_j)^3}{\frac{[(N-1)(N-2)/N]}{SD_j^3}} \tag{9}$$

e. Correlation coefficient is calculated by equation (10).

$$R_{j,j+1} = \frac{\sum_{i=1}^{N=17}(y_{i,j} - \bar{Y}_j)(y_{i,j+1} - \bar{Y}_{j+1})}{\sqrt{\left[\sum_{i=1}^{N=17}(y_{i,j} - \bar{Y}_j)^2\right]\left[\sum_{i=1}^{N}(y_{i,j+1} - \bar{Y}_{j+1})^2\right]}} \tag{10}$$

Since example numbers are not sufficient in finding both the statistics of monthly rain belonging to months within year and the statistics of monthly rain belonging to years, statistics should be used cautiously.

When statistics in Table 1 are examined, it is seen that monthly standard deviation (SD_j) values are taking very big values, consequently, that variation coefficient (COV_j) is getting bigger as depending on this. As it is understood from these statistical parameters, monthly rain is not heaped around average; on the contrary, they spread on wide area. Skiwness coefficient has generally become (+). According to this, Skiwness shows the distribution leaning to right. It can be told that correlation coefficient ($R_{i,\,i+1}$) expressing the relation of monthly rain between months with each others is generally very weak and also sometimes reverse weak dependent (−) (Table 1).

In order to convert the rain matrix into auxiliary matrix in making decision in Porsuk Dam operation works, if average monthly rain belonging to a definite year in row are shown with $\bar{y}_i + sd_i/2$) as normal rain and lets show it with letter (n). If rain fits to normal distribution, which is known that the total area of normal distribution in statistics is equal to 1, 38,3% of observed rain will fall on this area,

which is accepted as normal rain that dropped on this area. Similarly, lets show rain heights bigger than ($\bar{y}_i - sd_i/2$) show with letter (d). Here, it should be understood that those months of that year shown with letter (d) that are dry months and 30,85% of the observed rain will fall onto this area.

If process is made on columns again, $\bar{Y}_j - SD_j/2$) are shown with capital letter D, rainfall heights can be obtained from rain matrix; (d, n, w) matrix and (D, N, W) matrix.

If matrixes with letters are formed by these letters shown in same matrix, Table 2 is obtained. This matrix is named shortly as decision matrix with the idea of that it will be helpful for making decision in dam operation works. Table 3 has been prepared with the aim of using matrix given in Table 2 easily. This table is arranged according to the monthly rain which is less, normal and more; namely, it has been arranged according to probability of being Dry, Normal and Wet position and of which possibilities of rain belonging to that month are less, normal and more are given average as percentage. Probabilities of rain for being Dry, Normal and Wet are given in Table 4 by taking these average as percentages. So, decision-making matrix is converted into decision-making row. If data of Table 4 is sequenced from big to small according to Dry (D) percentages, it will have been sequenced according to Dry months probabilities. This sequence is given in Table 5.

At the beginning months of Table 5, flood risk will be relatively low since the water is released from dam at the desired amount and due to rain condition in downstream. In the last months of Table 6, flood risk will increase due to rain condition of the water released from reservoir in downstream area. If data of Table 4 is sequenced from big to small according to the wet months (W) percentages, it will have been sequenced according to wet condition probabilities. Also, this sequence is given in Table 6.

At the first months of Table 6, releasing water from dam will increase the flood risk because of the rain conditions in downstream. In another expression, actual examples that will prove the sequences of Table 5 are the flood which are observed in Eskişehir and its surrounding in 2000. Nearly, $30m^3/sn$ flow has been released from Porsuk Dam in April 2002 that this discharges cause flood and this flood dad grown due to rain in Porsuk Dam downstream has caused important agricultural damages on Eskişehir downstream, around Point C (Fig. 1). That year, because sown agricultural area stayed under torrent waters for a long period, it was not possible to sow these area again within same year. Although no water had been released from dam, the flood occurred again in December 2001 and the waters only coming from subcatchment area of dam downstream had become and reached as approximately around the total quantity of waters in 2002. The areas damaged by this flood were sowed again since there was a time for agricultural activities within same year, so agricultural damages have been reduced relatively. The biggest flood risk will occur in the months of May, April, December and October, respectively. Then the flood risk reduces in alter months.

3 CONCLUSION

After construction of a dam, operation work of the dam should be arranged so as to ensure optimum benefit. During dam operation, waters released into downstream should not cause flood damages. Furthermore, as subcatchment area expands in downstream, it should be kept in mind that surface flow waters coming from here could cause the floods. Reevaluation of water to be given from dam in any month according to probability of rain being less (dry), normal (normal) and more (wet) on downstream, and releasing water into downstream according to that will be beneficial with regard to flood risk.

Table 3. Percents (%) and averages (as %) of rain conditions for each month.

Months	Rainfall position		Number of observed rain in 17 years	Percentage of appearance in 17 years (%)	Rainfall position	Number of appearance in 17 years	Percentage of appearance in 17 years (%)	Mean (%)
January	Dry	D	5	30	d	5	30	30
	Normal	N	6	35	n	9	53	44
	Wet	W	6	35	w	3	17	26
	Total		17	100		17	100	100
February	Dry	D	5	30	d	7	41	35
	Normal	N	8	47	n	9	53	50
	Wet	W	4	23	w	1	6	15
	Total		17	100		17	100	100
March	Dry	D	7	41	d	4	23	32
	Normal	N	5	30	n	11	65	47
	Wet	W	5	30	w	2	12	21
	Total		17	~100		17	100	100
April	Dry	D	7	41	d	1	6	24
	Normal	N	7	41	n	8	47	44
	Wet	W	3	17	w	8	47	32
	Total		17	~100		17	100	100
May	Dry	D	6	35	d	2	11	23
	Normal	N	7	41	n	6	35	38
	Wet	W	4	24	d	9	53	39
	Total		17	100		17	100	100
June	Dry	D	6	35	d	6	35	35
	Normal	N	7	41	n	7	41	41
	Wet	W	4	24	w	4	24	24
	Total		17	100		17	100	100
July	Dry	D	5	29	d	11	65	47
	Normal	N	8	47	n	5	29	38
	Wet	W	4	24	w	1	6	15
	Total		17	100		17	100	100
August	Dry	D	6	35	d	11	65	50
	Normal	N	7	41	n	6	35	38
	Wet	W	4	24	w	0	0	12
	Total		17	100		17	100	100
September	Dry	D	8	47	d	12	70	58
	Normal	N	4	24	n	4	24	24
	Wet	W	5	29	w	1	6	18
	Total		17	100		17	100	100
October	Dry	D	5	29	d	4	24	27
	Normal	N	7	41	n	8	47	44
	Wet	W	5	29	w	5	29	29
	Total		17	~100		17	100	100
November	Dry	D	5	29	d	4	23	26
	Normal	N	8	47	n	9	53	50
	Wet	W	4	24	w	4	23	24
	Total		17	100		17	~100	100
December	Dry	D	6	35	d	0	0	18
	Normal	N	7	41	n	10	59	50
	Wet	W	4	24	w	7	41	32
	Total		17	100		17	100	100

Table 4. Conversion of decision-making matrix into decision-making row matrix.

	Months											
Positionof rainfall	Jan. (%)	Feb. (%)	Mar. (%)	Apr. (%)	May (%)	Jun. (%)	Jul. (%)	Aug. (%)	Sept. (%)	Oct. (%)	Nov. (%)	Dec. (%)
Dry	30	35	32	24	23	35	47	50	58	27	26	18
Normal	44	50	47	44	38	41	38	38	24	44	50	50
Wet	26	15	21	32	39	24	15	12	18	29	24	32

Table 5. Months sequenced according to the condition of Dry months probabilities.

	Months											
Position of rainfall	Sept. (%)	August (%)	July (%)	June (%)	Feb. (%)	Mar. (%)	Jan. (%)	Oct. (%)	Nov. (%)	Apr. (%)	May (%)	Dec. (%)
Dry	58	50	47	35	35	32	30	27	26	24	23	18
Normal	24	38	38	41	50	47	44	44	50	44	38	50
Wet	18	12	15	24	15	21	26	29	24	32	39	32

Table 6. Months sequenced according to the condition of Wet months probabilities.

	Months											
Position of rainfall	May (%)	Apr. (%)	Dec. (%)	Oct. (%)	Jan. (%)	Nov. (%)	June (%)	March (%)	Sept. (%)	July (%)	Feb. (%)	August (%)
Dry	23	24	18	27	30	26	35	32	58	47	35	50
Normal	38	44	50	44	44	50	41	47	24	38	50	38
Wet	39	32	32	29	26	24	24	21	18	15	15	12

Table 5 expresses the flood risks in Eskişehir and its surrounding large area. By looking at this row matrix (Table 4), the probability of rain occurred in months for being Dry (less), Normal (normal) and Wet (much) can be understood. According to these probabilities, it can be decided on releasing water from dam into downstream as much as possible or holding water. According to probability bigness (see Table 6), since it is seen that May (39%), April (32%) and December (32%) will be wet (much), i.e. rainy, it is seen that water should not be given into downstream from Porsuk Dam as much as possible. On the other hand, according to probability bigness again, September (58%), August (50%) and July (47%) will be Dry, namely releasing water from dam into downstream in the first months of Table 6 will not create a risk for flood danger.

In the event that if there are fairly large subcatchment areas in dam downstream, the risks of flood caused by the rain in downstream should be reduced. Therefore, the months in which the probabilities of wet periods belonging to subcatchment areas of dam are too much water should not be released from dam into downstream. As a result, giving water as little as possible in this wet period should be considered as a criteria in dam operation works.

REFERENCES

[1] Smakhtin, V.U., 2001. Low flow hydrology: a review. Journal of Hydrology 240, pp 147–186.
[2] Bilgin, M., 1979. Calculation of Reservoir Volume, Publications of State Academy-Faculty of Engineering and Architecture, Eskişehir-Turkey (in Turkish).

[3] Bingöl, M.T., 2003. The Determination of Water Required to Find Active Volume of Reservoir of Dams and Its Application in Bursa dams. Anadolu University, Institute of Science, Civil Engineering Department, pp 80, (Master Thesis) Eskişehir, Turkey (in Turkish).
[4] DSI, 2001. The Project of Water Management Plan of Porsuk Basin. Final Report, Volume 2/3, "Operating Works", Turkey's Ministry of Energy and Natural Resources, General Directorate of State Hydraulic Works (DSI), III. Regional Directorate of DSI, Prepared by the company of SU/YAPI, Turkey (in Turkish).
[5] Harvey, A.M., 1996. Channel Capacity and Adjustment of Streams to Hydrologic Regime. Journal of Hydrology, Volume 8, Issue 1, pp 82–98.
[6] Tombul, M. and Gerek, A.C., 2003. Flood Protection and Potential Flood Damage Estimates in the Porsuk River in Eskişehir, Turkey. River symposium 2003, Sixth International River Management Symposium, 2–5 September 2003, Carlton Crest Hotel Brisbane, Queensland, Australia.
[7] Bilgin, M., 2003. Expert Report of Eskişehir Court. Court File No.: 2002/1622, Technical Analysis of Center Çatma Farm's agricultural fields damaged by the flood of Porsuk River on the date of 18.04.2002, Expert report prepared for the Court, Eskişehir, Turkey (in Turkish).
[8] DMI, 2003. Turkish State Meteorological Service. (http://wwww.Meteor.gov.tr)
[9] MAFA, 1994. Frequency Analysis of Maximum Discharges of Turkey's River Basins. Turkey's Ministry of Public Works and Settlement, General Directorate of State Hydraulic Works (DSI), Turkey.
[10] Bayazit, M., 1981. Statistical Methods in Hydrology. Istanbul Technical University, Turkey (in Turkish).
[11] Bayazit, M., ve Oğuz, B., 1985. Statistic for Engineers. Istanbul Technical University, Turkey (in Turkish).
[12] Plate, E.J., 2002. Flood risk and flood management, Journal of Hydrology 267, pp 2–11.
[13] Andrade, M.G., Fragoso, M.D. and Carneiro, A.F.M., 2001. A stochastic approach to the flood control problem, Applied Mathematical Modeling 25, 499–511.

New Developments in Dam Engineering—Wieland, Ren & Tan (eds),

Constitutive modeling of the influence of pressure, density and moisture content on the mechanical behavior of rockfill materials

Erich Bauer
Institute of General Mechanics, Graz University of Technology, Graz, Austria

Yueming Zhu
College of Water Conservancy and Hydroelectric Engineering, Institute of Hydraulic Structural Engineering, Hohai University, Nanjing, People's Republic of China

ABSTRACT: In this paper the essential mechanical behavior of rockfill dam materials is modeled using a hypoplastic continuum approach. The concept of hypoplasticity is based on rational mechanics and differs from the classical elasto-plastic concept in that no decomposition of the deformation into elastic and plastic parts is needed. Critical states are included in the model for large shearing. With respect to a pressure dependent relative density the model can capture the essential mechanical properties of initially loose and dense granular materials within a single set of constants. While the calibration and application of hypoplastic models is already extensively investigated for fine-grained materials like sand and powders, the present application to rockfill materials is a first attempt to describe coarse-grained materials with a low and decreasing grain hardness. Particular attention is paid to modeling the influence of the pre-compaction and moisture content of the material on the incremental stiffness. The numerical simulation of oedometric compression tests and biaxial compression tests shows that the model captures the essential features of rockfill materials under both dry and moist conditions.

1 INTRODUCTION

For the prediction of settlements of rockfill dams during construction and flooding a suitable constitutive model is necessary which takes into account the essential mechanical properties of the dam material. In particular the mechanical behavior of rockfill materials is mainly determined by the grain hardness, the grain shape, the grain size distribution, the packing density, the orientation of contact planes, the stress state and the loading history. Stiffness and shear strength are influenced by the pressure level, the packing density and the deformation path and are therefore no material constants [1]. Depending on the state of weathering of the material the abrasion and breakage resistance of particles can be different for dry or water-saturated states. Under higher stress levels the disintegration of grains can be accelerated under water and leads to a reduction of the resistance against compaction and shearing [2,3]. Thus, a significant part of settlements occurring after the first flooding of a dam can be related to the reaction of the rockfill material with water.

The focus of the present paper is on modeling the mechanical behavior of broken rock materials using a hypoplastic continuum approach. In hypoplasticity the evolution equation for the stress tensor is formulated with a single isotropic tensor-valued function depending on the current state quantities and the total rate of deformation. In order to model inelastic material properties the rate of deformation tensor is incorporated in the constitutive equation in a certain non-linear formulation. With a pressure dependent density factor the influence of pressure and density on the incremental

stiffness and the peak friction angle can be modeled for an initially loose or dense state using a single set of constants [4–6]. Limit states or so-called critical states are included in the constitutive equation for a simultaneous vanishing of the stress rate and volume strain rate. Originally hypoplastic material models were developed and calibrated for dry and cohesionless granular materials like sand [e.g. 4–7]. Concerning the application to rockfill materials the modeling of the following two aspects are discussed in the present paper: the influence of a pre-compaction of the material and the disintegration of the material as a result of a reaction of the stressed material with water. In order to model such properties an extension of the constitutive equation by Gudehus [5] and Bauer [6] is proposed, where the stiffness factor and the so-called granular hardness is related to a pre-compaction pressure and the moisture content, respectively.

2 THE HYPOPLASTIC CONSTITUTIVE MODEL

2.1 *Inelastic material properties*

In hypoplasticity inelastic material properties are modeled with a constitutive equation of the rate type where the objective stress rate $\mathbf{B}\sqrt{\mathbf{D}:\mathbf{D}}$, which is non-linear in **D,** i.e.

$$\mathring{\mathbf{T}} = \mathcal{A} : \mathbf{D} + \mathbf{B}\sqrt{\mathbf{D}:\mathbf{D}}. \tag{1}$$

Herein $\mathcal{A}$ and **B** have been proposed in the literature. A comprehensive historical review can be found for instance in Wu and Kolymbas [8], Bauer and Herle [9].

2.2 *Pressure and density dependent properties*

Under the same pressure a cohesionless granular material can show different packing densities of the grain assenbly so that the void ratio can range between a maximum void ratio e_i and a minimum void ratio e_d. The limit void ratios e_i and e_d are pressure dependent and they decrease with an increase of the mean pressure p=−**I**:**T**/3 as sketched out in Figure (1.a). In order to model the influence of the density and pressure on the mechanical behavior the set of state variables of the constitutive equation (1) was extended with the current void ratio e. In the following the constitutive model by Gudehus [5] and Bauer [6] for a dry and cohesionless granular material is considered, where the current void ratio e was related to the pressure dependent limit void ratios and embedded in the scalar factors f_s and f_d, i.e.

$$\mathring{\mathbf{T}} = f_s(e,p)\left[\mathcal{L}(\hat{\mathbf{T}}) : \mathbf{D} + f_d(e,p)\mathbf{N}(\hat{\mathbf{T}})\sqrt{\mathbf{D}:\mathbf{D}}\right], \tag{2}$$

with:

$$\mathcal{L}(\hat{\mathbf{T}}) = \hat{a}^2 I + \hat{\mathbf{T}}\otimes\hat{\mathbf{T}}, \tag{3}$$

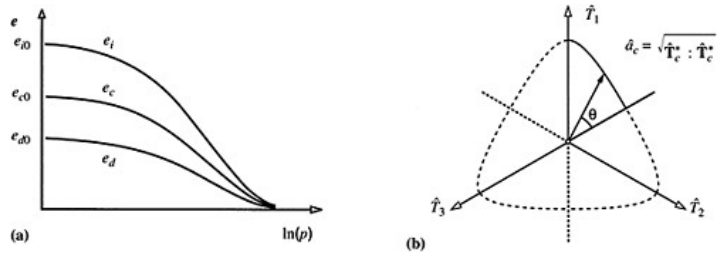

Figure 1. (a) Decrease of the maximum void ratio e_i, the critical void ratio e_c and the minimum void ratio e_d with increasing mean pressure p, (b) contour of the stress limit condition in the π-plane.

and

$$\mathbf{N}(\hat{\mathbf{T}}) = \hat{a}(\hat{\mathbf{T}} + \hat{\mathbf{T}}^*) . \tag{4}$$

Herein the tensors $\hat{\mathbf{T}}^*$ and the critical friction angle φ:

$$\hat{a} = \frac{\sin\varphi}{3-\sin\varphi}\left[\sqrt{\frac{(8/3) - 3(\hat{\mathbf{T}}^* : \hat{\mathbf{T}}^*) + \sqrt{3/2}(\hat{\mathbf{T}}^* : \hat{\mathbf{T}}^*)^{3/2}\cos(3\theta)}{1 + \sqrt{3/2}(\hat{\mathbf{T}}^* : \hat{\mathbf{T}}^*)^{1/2}\cos(3\theta)}} - \sqrt{\hat{\mathbf{T}}^* : \hat{\mathbf{T}}^*}\right] . \tag{5}$$

Herein the Lode-angle θ is defined as:

$$\cos(3\theta) = -\sqrt{6}\frac{\mathbf{I} : \hat{\mathbf{T}}^{*3}}{[\mathbf{I} : \hat{\mathbf{T}}^{*2}]^{3/2}} .$$

For limit states or so-called critical states ($\mathbf{T}_c$, e_c), which are defined for a simultaneously vanishing of the stress rate, $\mathring{\hat{\mathbf{T}}} = \mathbf{0}$, and the volume strain rate, $\mathbf{I}:\mathbf{D}=0$, factor $\hat{a}$ is equal to the Euclidean norm of the normalized stress deviator, i.e.

$$\hat{a}(\hat{\mathbf{T}}_c^*) = \hat{a}_c = \sqrt{\hat{\mathbf{T}}_c^* : \hat{\mathbf{T}}_c^*} . \tag{6}$$

In particular for limit states relation $\hat{a}$ in (5) represents the stress limit condition given by Matsuoka and Nakai [10] as shown in Figure (1.b). It can be proved that for monotonic shearing the limit stress states given by relation (6) will asymptotically be reached independent of the initial void ratio and stress state [11]. The influence of the mean pressure p and the current void ratio e on the response of the constitutive equation (2) is taken into account by the density factor f_d, i.e.

$$f_d = \left(\frac{e - e_d}{e_c - e_d}\right)^{\alpha} , \tag{7}$$

and the stiffiness factor f_s, i.e.

$$f_s = \left(\frac{e_i}{e}\right)^{\beta} \frac{1+e_i}{e_i} \frac{h_s}{n h_i (\hat{\mathbf{T}} : \hat{\mathbf{T}})} \left(\frac{3p}{h_s}\right)^{1-n} , \tag{8}$$

with:

$$h_i = \frac{8\sin^2\varphi}{(3-\sin\varphi)^2} + 1 - \frac{2\sqrt{2}\sin\varphi}{3-\sin\varphi}\left(\frac{e_{io}-e_{do}}{e_{co}-e_{do}}\right)^{\alpha}.$$

Herein $\alpha<0.5$ and $\beta>1$ are constitutive constants. Inparticular factor f_d models the dilatancy behavior and the maximum stress ratio while factor f_s models the influence of the stress and density on the incremental stiffness. In relations (7) and (8) the maximum void ratio e_i, the minimum void ratio e_d and the critical void ratio e_c are pressure dependent according to

$$\frac{e_i}{e_{io}} = \frac{e_d}{e_{do}} = \frac{e_c}{e_{co}} = \exp\left[-\left(\frac{3p}{h_s}\right)^n\right], \qquad (9)$$

where e_{io}, e_{do} and e_{co} are the corresponding values for $p\approx 0$ (Fig. 1.b). In relation (9) the so-called granular hardness h_s scales the mean pressure p while the dimensionless exponent n reflects the degradation of the limit void ratios and the critical void ratio with increasing pressure. With the factor f_d the dependence of the peak friction angle and the dilatancy behavior on the density and pressure are included in the present model as sketched out in Figure (2) for shearings starting from different initial void ratios. For $e_1<e_c$ Eq.(7) yields $f_d<1$ while for $e_2>e_c$ a value of $f_d>1$ is obtained. The peak friction angle (Fig. 2.a) is higher for a lower void ratio because the influence of the part f_d *(e, p)* $\mathbf{N}(\hat{\mathbf{T}})\sqrt{\mathbf{D}:\mathbf{D}}$ of the constitutive equation (2) decreases if $f_d<1$. After the peak strain softening can be observed as a consequence of dilatancy and with advanced monotonic shearing the density factor tends towards $f_d=1$ (Fig. 2.c). For $e_2>e_c$ the material shows contractancy

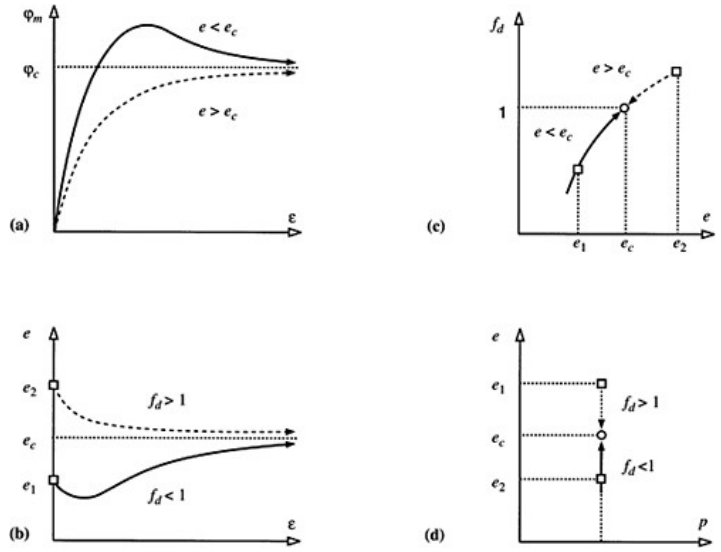

Figure 2. Homogeneous monotonic shearing under constant mean pressure for different initial void ratios e_1 and e_2: (a) mobilized friction angle ϕ_m versus shear strain ε, (b) void ratio e versus shear strain ε, (c) void ratio *e v*ersus density factor f_d. (d) void ratio e versus mean pressur*e* p.

up to the critical state (Fig. 2.b) and for $e=e_c$ the value of the density factor again becomes $f_d=1$ (Fig. 2.c). Consequently, in a critical state the value of the density factor is independent of the initial void ratio and the pressure level. This means that for unlimited monotonic shearing a stationary state can be reached asymptotically both for an initially dense and for an initially loose state.

For the evolution of the current void ratio e the assumption is made that the volume change of the solid material can be neglected. To this end, the rate of the void ratio can be directly derived from the mass balance, which yields:

$$\dot{e} = (1+e)\mathbf{I} : \mathbf{D} . \tag{10}$$

The hypoplastic constitutive equation (2) for dry and cohesionless granular materials includes 8 constants which can be determined from simple index and element tests [6,12]. In particular h_s and n are determined by the compression behavior, φ and e_{c0} are related to the critical state in triaxial compression, α and β depend on the peak friction angle, and e_{i0} and e_{d0} are the limit void ratios. Since the current void ratio e is related to the limit void ratios by the pressure dependent functions f_s and f_d, the constitutive constants are not restricted to a certain initial density. As long as the mechanical behavior does not change substantially due to grain abrasion and grain crushing the parameters of the hypoplastic model remain constant for one granular material and the mechanical behavior of an initially dense or loose state can be described using a single set of constants. However, these assumption is restricted to a certain range of pressures where a disintegration of the material under load and water can be excluded.

Figure (3) shows the results obtained for numerical simulations of homogeneous bixial compression tests under a constant lateral stress and various initial void ratios. The calculations were carried out with the following set of constants: $\varphi = 35°$, h_s=14MPa, n=0.21, e_{io}=0.92, e_{co}=0.78, e_{do}=0.4, α=0.25 and β=1.0. As can be seen the stress strain behavior (Fig. 3.a) and the evolution of the void ratio (Fig. 3.b) is strongly influenced by the initial density. For an initially dense state the stiffness at the beginning of loading and the maximum stress ratio is higher than for an initially loose state. In particular a pronounced stress peak and dilatancy can only be observed for initial dense states. With advanced deformation the stress ratio tends towards a stationary value which is independent of the initial density.

2.3 *Modeling a pre-compaction*

The influence of a static or dynamic pre-compaction of rockfill materials on the incremental stiffness is modeled in a simplified manner based on the assumption that the grain arrangement as a

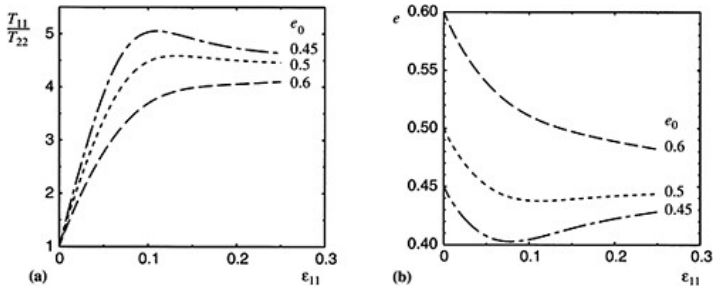

Figure 3. Biaxial compression under a constant lateral stress of T_{22}=−0.1MPa and different initial void ratios e_0: (a) stress ratio T_{11}/T_{22} versus strain ε_{11}, (b) void ratio e versus strain ε_{11}.

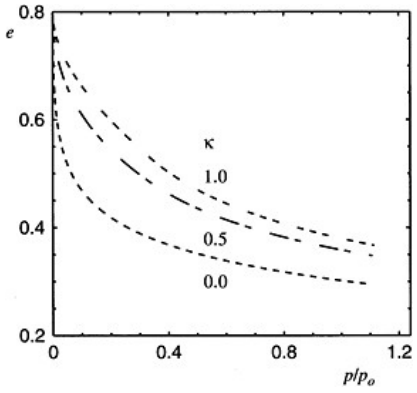

Figure 4. Influence of κ on the compressibility under oedometric condition.

result of the pre-compaction history can be expressed in the form of a virtual consolidation pressure. To this end the set of state variables of the constitutive equation is extended with a pre-compression pressure p_o, i.e.

$$\mathring{\mathbf{T}} = \mathring{\mathbf{T}}(e, p_o, \mathbf{T}, \mathbf{D}). \tag{11}$$

In order to incorporate p_o in the hypoplastic constitutive equation the stiffness factor f_s in Eq. (2) is replaced by the modified factor f_s^*:

$$f_s^* = f_s f_c \tag{12}$$

with:

$$f_c = 1 + \kappa \ln\left(\frac{p_o}{p}\right). \tag{13}$$

Herein k≥0 is a constitutive constant and p is the current mean pressure. For stress states exceeding the initial pre-compaction pressure, the quantity p_o in Eq.(13) must be updated, so that $|P_o| \geq |P|$ always holds. For states with $p_o = p$ the quantity $f_c = 1$ and the mechanical response of the original constitutive equation (2) is obtained. It can be noted that for $f_c > 1$ a higher incremental stiffness for unloading and reloading is modeled. In Figure (4) the influence of κ is demonstrated for an oedometric compression starting from an initial void ratio of $e_o = 0.8$. As can be seen the incremental stiffness is higher for a higher value of κ. The calibration of κ and p_o can be carried out by comparing the compression curve of a virgin loading with the compression curve of the pre-compacted material.

2.4 *Degradation of the granular hardness*

It is worth noting that the so-called granular hardness h_s introduced in compression relation (9) is related to the grain assembly in the sense of a continuum description and does not mean the hardness of an individual grain. In particular h_s is the pressure where the compression curve in a half logarithmic representation shows the point of inflection. Experimental investigations show that the quantity h_s reflects the pressure level where grain crushing under compression becomes dominant. In order to model the influence of disintegration of a stressed rockfill by a reaction with water a

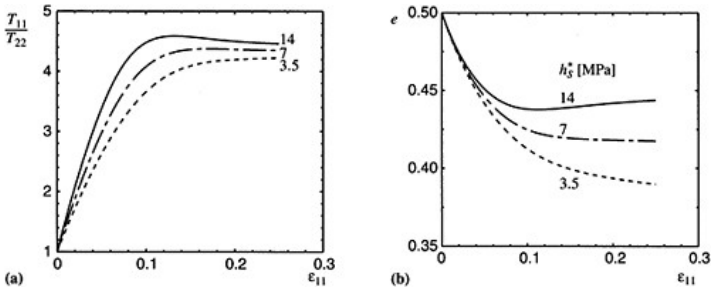

Figure 5. Influence of the granular hardness h_s^* on biaxial compression under a constant lateral stress of T_{22}=−0.1MPa and an initial void ratio of e_o=0.5. (a) stress ratio T_{11}/T_{22} versus strain ε_{11}, (b) void ratio e versus strain ε_{11}.

degradation of the granular hardness is assumed. To this end the moisture content w is included in the constitutive equation (2) as an additional state variable, i.e.

$$\mathring{\mathbf{T}} = \mathring{\mathbf{T}}(e, p_o, w, \mathbf{T}, \mathbf{D}). \tag{14}$$

The constant h_s in (8) and (9) is replaced by the quantity h_s^*, i.e.

$$h_s^* = h_{so}\,\psi(w). \tag{15}$$

Herein h_{so} is the value of the granular hardness obtained for the dry material under compression and $\psi(w)$ can be obtained by comparing the compression behavior for the dry material with the water saturated material using the compression relation (9) for the maximum void ratio e_i. It is obvious that with a degradation of the granular hardness the pressure dependent minimum void ratio e_d and the critical void ratio e_c also decrease.

The influence of h_s^* (Fig. 6).

3 CONCLUSIONS

A hypoplastic continuum model is presented to describe the essential properties of rockfill materials. The constitutive equation for the evolution of the stress is based on non-linear tensor-valued functions depending on the current void ratio, stress, consolidation stress, moisture content and rate of deformation. As the hypoplastic concept does not need to distinguish between elastic and plastic deformation the calibration of the constitutive constants is rather easy. The numerical

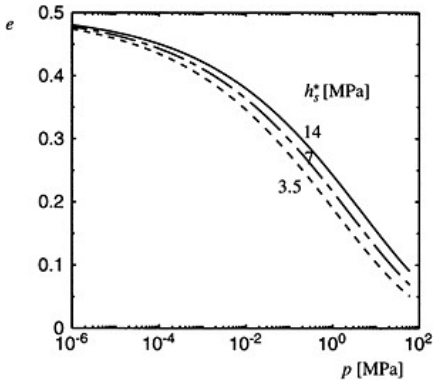

Figure 6. Influence of the granular hardness h_s^* on the compressibility under oedometric condition.

results of oedometric compression tests and biaxial compression test show that the model appears to capture the influence of pressure, density, pre-compaction and a degradation of the granular hardness depending on the moisture content.

ACKNOWLEDGEMENTS

Support from the Ministry for Science an Technology in China and the Federal Ministry of Education, Science and Culture in Austria for the bilateral scientific-technological co-operation between Hohai University in Nanjing and Graz University of Technology is greatly acknowledged.

REFERENCES

[1] Charles, J.A. and Watts, K.S. (1980): The influence of confining pressure on the shear strength of compacted rockfill. Geotechnique, Vol. 30, 4, 353–367.
[2] Nobari, E.S. and Duncan, J.M., (1972): Efiect of reservoir filling on stress and movements in earth and rockfill dams. U.S.Army Engineers Waterways Experiment Station.
[3] Kast, K., Blinde, A. and Brauns, J. (1985): Verdichtungs-, Verformungs- und Sattigungsverhalten von Schttungen in Abhangigkeit von der geologischen Gesteinsentfestigung. Ingenieurgeologische Probleme im Grenzbereich zwischen Locker- und Festgesteinen, Springer- Verlag, Berlin Heidelberg.
[4] Wu, W., Bauer, E. and Kolymbas, D. (1996): Hypoplastic constitutive model with critical state for granular materials. Mechanics of Materials, No. 23, 45–69.
[5] Gudehus, G. (1996): A comprehensive constitutive equation for granular materials. Soils and Foundations, 36, No. 1, 1–12.
[6] Bauer, E. (1996): Calibration of a comprehensive hypoplastic model for granular materials. soil and Foundations, 36(1), 13–26.
[7] Kolymbas, D. (1991): An outline of hypoplasticity. Arch. of Appl. Mechanics, 3, 143–151.
[8] Wu, W. and Kolymbas, D. (2000): Hypoplasticity then and now. Constitutive Modelling of Granular Materials, Kolymbas (ed), Springer press, 57–105.
[9] Bauer, E. and Herle, I. (2000): Stationary states in hypoplasticity. Constitutive Modelling of Granular Materials, Kolymbas (ed), Springer-Verlag, 167–192.
[10] Matsuoka, H. and Nakai, T. (1977): Stress-strain relationship of soil based on the 'SMP'. Proc. of Speciality Session 9, IX Int. Conf. Soil Mech. Found. Eng., Tokyo, 153–162.
[11] Bauer, E. (2000): Conditions for embedding Casagrande's critical states into hypoplasticity. Mechanics of Cohesive-Frictional Materials, 5, 125–148.
[12] Herle, I. and Gudehus, G. (1999): Determination of parameters of a hypoplastic constitutive model from properties of grain assemblies. Mech. of Cohesive-Fric. Mater., 4, 461–486.

New Developments in Dam Engineering—Wieland, Ren & Tan (eds),
© 2004 Taylor & Francis Group, London, ISBN 04 1536 240 7

Application of fiber optical sensing technology to the Three Gorges Project*

Cai Desuo
Three Gorges University, China

Dai Huichao
China Yangtze Three Gorges Project Development Corporation, China

He Xinji, Cai Shunde & Zhang Cunji
Three Gorges University, China

ABSTRACT: Based on the Three Gorges Project over the Yangtze River, China, researches were carried out on the fiber optical sensing technology for temperature and crack monitoring. The research results showed that at the elevation of 140.56m, 3 days after the pouring of the concrete the temperature inside the block on the upstream face and the temperature at the central point reached the peak values of 34.75°C and 26.85°C respectively while the temperature on the downstream face reached its peak value of 30.4°C, 5 days after pouring. The temperature tended to go down and to be steady 22–28 days later. According to the monitoring results, the surface crack, created on the upstream face of No. 16 monolith of the spillway dam section, was tending to close (under pressure) at a slow and smooth rate and tended to be steady. The dealing with the crack was successful.

1 BASIC PRINCIPLE OF THE DISTRIBUTED FIBER OPTICAL SENSING TECHNOLOGY

When a beam of pulse light is emitted to an optical fiber, the pulse light will travel at a little smaller velocity than in vacuum. At the same time it also gives off diffused light, some of which will return through the optical fiber to the incident point from where the impulse light emitted[1,2]. The time difference T between incident light and reflected light can be measured and thus the distance X from the scattering point to the incident point can be obtained through the following formula:

$$X = C\frac{T}{2} \tag{1}$$

where: C=light velocity in optical fiber=Co/n; Co=light velocity in vacuum; n=refraction index of optical fiber

Of the reflected light to the incident point, there is a scattering light known as Raman, which can be separated again into a Stokes and an Anti-Stokes-part. The intensity of the latter is finally

* Program (No. 59879002) funded by National Natural Science Foundation of China; Key program (SPJK007–09) of the State Power Corporation of China.

depending on the temperature while the temperature has nothing to do with the former. The relation of Anti-Stokes and Stokes to temperature can be formulated as follows:

$$\frac{las}{ls} = ae^{\frac{hcv}{kt}} \tag{2}$$

where: las=Anti-Stokes; Ls=Stokes; a=temperature correlation coefficient; h=Planck's constant (J.s); c=light velocity in vacuum (m/s); v=Raman translatory energy (m-l); k=Boltzmann's constant (J/k); t=absolute temperature

The temperature value can be calculated through formula (2) and the measurement of Anti-Stokes to Stokes ratio:

$$t = \frac{hcv}{k\left[\ln\alpha - \ln\left(\frac{las}{ls}\right)\right]} \tag{3}$$

Since the aim of temperature measurement with the fiber optical sensing system is to directly measure the Anti-Stokes-to-Stokes ratio of Raman reflecting light, which has nothing to do with absolute value, the light losses caused by aging of optical fiber and its increasing along path can be eliminated and the accuracy of measurement can also be guaranteed all the time.

2 TEMPERATURE FIELD MONITORING OF CONCRETE STRUCTURE IN NO. 14 MONOLITH ON THE LEFT BANK

The scale of the Three Gorges Project is so huge and its influence is so great that it tops the first of this kind of project in the world[3]. Its concrete placement totals 28 million m^3 with maximum monthly placement of over 0.5 million m^3. Furthermore, since the concreting block is so tremendous in size and so complex in structure, it is a rather hard task to control temperature and avoid cracking. Academician Mr. Zhu Baifang also pointed out that according to the experience available at home and abroad it is possible but not easy to prevent harmful crack in mass concrete structure and it needs to be meticulous in design and construction.

2.1 *Fiber optical sensing cable and its network*

No. 14 monolith of left bank is the last mass block to be concreted in the second stage of the Three Gorges Project. The block, whose locality used to be the tower belt, has a dimension of 32m×20m with the elevation of 140.56m and the minimum lift thickness of 1.5m. According to the aim of field test the designs for sensing network, concrete grade and aggregate gradation are shown in Fig. 1, where Point 77, 80, 90 etc are measurement node and snake-shaped cooling pipes are furnished within the block. The stainless steel armored fiber optical cable with diameter of 3mm and a single core of 50 μm is used to not only ensure that the detected results are purely temperature values of concrete but also prevent the cable from being damaged by the coarse work of placement. Fig. 2 shows the site of cable installation. Installation and concrete placement were carried out simultaneously for three days and two nights. The sensing cable of 81.1m of length was embedded in the dam body. According to the general rule of dissipation of hydration heat of concrete, as soon as the pouring was finished temperature measurement were started three times a day at three time intervals when the ambient temperature was relative low (at 8:30a.m.), relative high (at 14:30p.m.) or dropped (at 22:30p.m.). For simplification we singled out the result for analysis at ambient temperature 14.30°C.

2.2 *Intermediate results and analysis*

2.2.1 Embedding finished on April 2, fiber optical sensing monitoring followed (Fig. 3). In order to understand the dissipation of hydration heat of the concrete within the block, measurement were

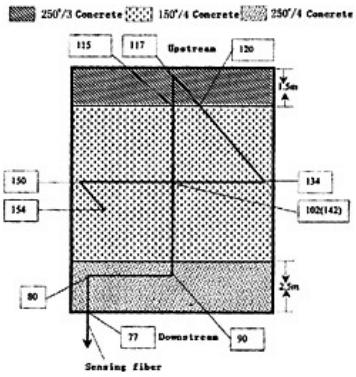

Figure 1. Installation of sensing network.

Figure 2. Installation site of sensing cable.

Figure 3. Field measurement.

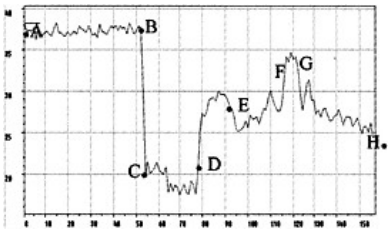

Figure 4. Temperature curve.

performed three times a day within a week under different ambient temperature. Three days after the concrete pouring, the temperature of upstream face at sensing Point 115 with the network locality of 118.975m reached the peak value of 34.75°C. The curve of temperature distribution measured by fiber optical sensing network at that time is shown in Fig. 4, where: AB is the internal fiber of the sensing system, BC is the external rear section, CD is the stainless steel armored optical cable for transmitting from the joint box to the inlet of the block, D is the inlet point from where the following optical cable works for both sensing and transmitting so as to measure the temperature values of 80 sensing points at any time. In order to verify the accuracy of fiber optical temperature measurement, the regular thermometer was used to measure section AB, BC and CD with an error of only 0.1°C. As shown in Fig.4, section FG (Point 115–117) got the highest temperature during the dissipation of hydration heat mainly because from Point 113, no cooling pipes were furnished with inside the block, and Point 117 was the farthest to the cooling pipes with a distance of 1.5m to the upstream face. Four days later peak value started to drop and came to 24°C–25°C steadily after April 30.

2.2.2 The second highest temperature zone is on the downstream face within the block (Section DE, Point 80–90).The temperature reached peak value of 30.4°C with the network locality of 87.451m the fifth day after the pouring and its temperature curve is shown in Fig. 5. There was no cooling pipe in this zone, either, which was only 1m to the nearest cooling pipe. The concrete grade is 250 in these two high temperature sections and 150 in others. That is another main reason why these two sections reached high temperature. Section DE is 4-grade aggregate gradation while 3-grade in Section FG, which is one more reason causing Section FG to get high temperature. Six days later, peak value started to go down and came to 23°C–25°C steadily after April 22.

The temperature curves of Point 117 on the upstream face, Point 90 on the downstream face and Point 102 at the center of the sensing network were plotted in Fig. 6. It can be clearly visible that the temperature curve of Point 117, the highest temperature zone, forms the envelope curve while Point 90 in the medium, which is the second high temperature locality, but the temperature at both points drop down quickly at nearly the same rate. The temperature curve of Point 102 is at the bottom with low value, but drops down very slowly. The temperature curve of hydration heat of concrete within the dam block is a bias normal curve, which conforms to the conventional theory of temperature calculation and thermo conduction.

3 BACKGROUND KNOWLEDGE OF FIBER OPTICAL SENSING SYSTEM FOR CRACK MONITORING

The Three Gorge Dam is equipped with 23 monoliths of the spillway dam section with 21m of transverse joint interval. Each monolith is furnished with deep outlets in the middle (dimension of 7m×9m with the bottom elevation of the intake 90m), diversion bottom outlets across the transverse joints (dimension of 6×12m, bottom elevation 56m) and surface bays with a maximum discharge capacity of 120600m^3/s. Surrounding of the diversion bottom outlet is the 400 abrasion resistance concrete with thickness of 1m. Its side and top were concreted with the corresponding dam blocks simultaneously, while its floor slab (known as crossing joint) was directly placed after the grouting of transverse joint between two adjacent blocks. In the floor slab there are longitudinal and transverse reinforcement net connecting to the dam.

At the end of October 2000, a 13m high (elevation 47–60m) 60–80cm deep and 0.2mm wide vertical crack was found on the upstream face of No. 16 monolith of the spillway dam section (Fig.7). The occurrence of cracking is characteristic by the following time and locality:

Locality: The average elevation of the crack was just at the floor slab (elevation 55–56m) and on the symmetry plane of block between two adjacent bottom outlets. The floor slabs at both sides of blocks where cracking occurred had been placed, while floor slabs where crack was never found, had not been placed.

Time: After the mass concrete except the floor was placed, no crack occurred from the first winter of 1999 to January–April of 2000 when grouting of longitudinal and transverse joints were completed. It was not until March–October 2000 when floor slabs were placed that cracking occurred.

These cracks were highly seriously taken into account by various departments. Academician, Mr. Pan Jiazeng suggested “making a mountain out of a molehill”, gathering information, figuring out the causes of cracking and carrying out special subject researches. China Three Gorges Project Corporation (CTGC) called on designers, supervision and contractors to discuss this issue several times. After analyzing the locality and time of cracking, experts in various fields agreed that cracking was mainly caused by three factors, namely, variation of annual temperature, sudden

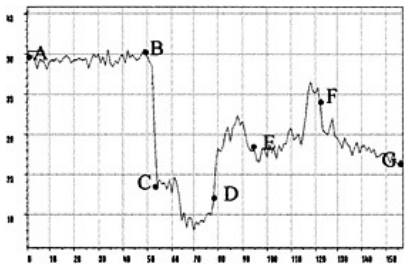

Figure 5. Temperature curve.

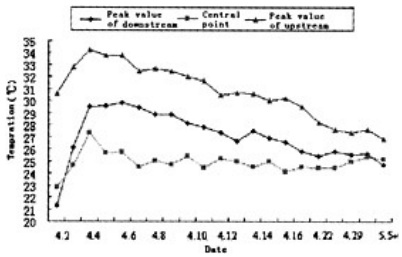

Figure 6. Envelope curve of temperature variations.

drop of temperature and the restraining function led to by grouting of floor slabs and transverse joints, but the pouring course of mass concrete gave little influence on the cracking.

On a whole, the causes leading to regular cracking on the upstream face of the spillway dam section are various. It is caused by comprehensive factors. A great deal of further analysis has to be carried out because some present analysis is still initiative. Meanwhile, trace monitoring of crack should be implemented. An optical fiber crack meter manufactured by a Canadian company ROCKTEST was used for vertical crack monitoring on the upstream face of No. 16 monolith.

4 PRINCIPLE AND EMBEDDING TECHNOLOGY OF FIBER OPTICAL CRACK METER OF ROCKTEST

4.1 *Principle*

Interferometer developed in recent years with white light as its source has been gradually taken into account by experts for its absolute measurement and has been widely used in architectural construction, biomedical science, petroleum industry, environment, electric energy, intelligent structure and noise engineering etc. ROCKTEST fiber optical crack meter's main part is an interferometer (TFFI) fixed to a sliding axle (Fig. 8). TFFI can be regarded as a Fabri-Paro cavity pocket with space distribution. Its length changes along the transverse direction. The end of an optical fiber is fixed to a place very close to the surface of the TFFI which can localize by moving back and from along the transverse direction. It can be seen from the Fig.8 that the end of the optical fiber is equal to a typical Fabric-Paro cavity length formed by TFFI wherever TFFI goes[4,5]. In other words, wherever the TFFI goes, a corresponding part of the fiber always creates a typical cavity length similar to the Fabri-Paro sensor. If this design is connected to a white light fiber optical signal regulator, a fiber optical crack meter for absolute measurement can be created.

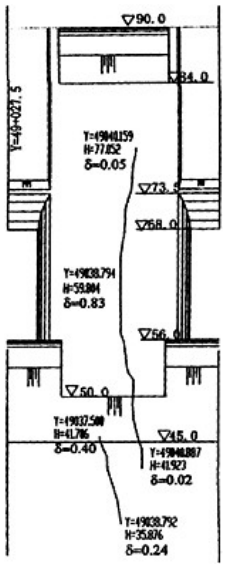

Figure 7. Vertical crack.

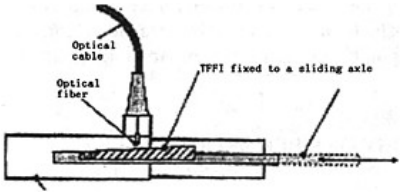

Figure 8. Principle of fiber optical crack meter.

Figure 9. Fiber optical crack meter after installation.

4.2 *Embedding technology*

On the vertical crack of upstream face of No.16 monolith of the spillway dam section, two ROCK-TEST crack meters were embedded at the elevation of 53m (No. 2 meter) and 69.5m (No. 1 meter) respectively. At the same time, two conventional displacement sensors were installed by the Test Center of Gezhouba Group Company for verifying each other at the same elevation with the same layout of optical cables. Installation was started as soon as the crack was strictly treated. As shown in Fig. 9, the conventional displacement sensor is on the upper and the fiber optical crack meter below, which is much smaller than the upper one in size.

4.3 *Monitoring material and analysis*

Monitoring was started from April 30, 2002. The changing tendency of crack is plotted in Fig. 10 with the data measured by No. 1 crack meter and in Fig. 11 by No. 2. On a whole, the vertical crack on the upstream face of No. 16 monolith is tending to be closed (under pressure), which is of benefits to the project. From the Fig. 10 it can be seen that as soon as the installation of No. 1 fiber optical crack meter was completed, the crack there starts being closed smoothly at a slow speed. On July 14, the maximum closure value was 0.064mm (pressure). Similarly, it can be visible from the Fig. 11 that when installation of No. 2 fiber optical crack meter was completed, the crack remains unchanged for a week. With the water level rising up in the spillway dam section the crack steadily tends to be closed. After that, because No. 2 was working under water, the closure value of displacement measured by it is evidently larger than that of No. 1 and reached the maximum of 0.1mm at the end of July.

In order to examine the reliability and accuracy of the data measured by the fiber optical crack meter, the data got in May, June and July was compared with those measured by the conventional displacement sensor taken from Gezhouba Group Company's Test Center (Table 1). The changing tendency of crack seems consistent and both values are also close to each other. However, the effective digits of the former are three decimal places while the latter only two. As shown in Table 1 the measurement is reliable and the treatment of vertical crack on the upstream face of No. 16 monolith of the spillway dam section is successful and the crack tends to be in a steadily closed condition.

5 CONCLUSION

5.1 The distributed fiber optical sensing system can be used for real-time temperature field measurement of the normal mass concrete in construction and operation. The system is easy to install and works quickly and accurately with a very strong anti-interference performance. It is the innovation of conventional monitoring equipment, theory and methods of temperature measurement to dams.

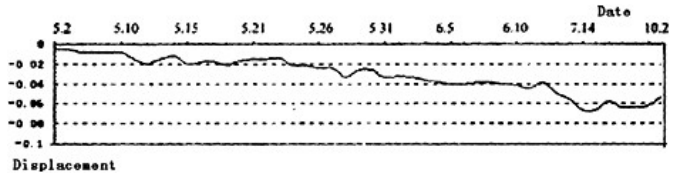

Figure 10. Changing tendency of crack shown by No. 1 fiber optical crack meter.

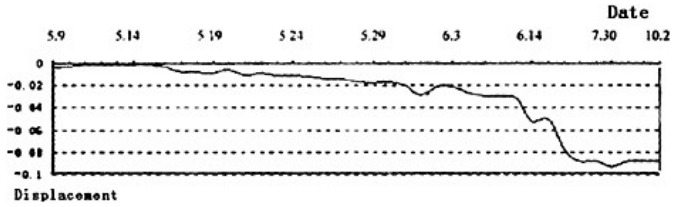

Figure 11. Changing tendency of crack shown by No. 2 fiber optical crack.

Table 1. Data comparison between the fiber optical crack meter and the conventional displacement sensor.

	Elevation of No.1 meter		Elevation of No.2 meter	
Period	69.5m (optical fiber)	70m (regular)	53m (optical fiber)	57m(regular)
May	−0.001~−0.02	−0.04~−0.05	−0.005~−0.033	−0.01~−0.04
June	−0.−21~−0.052	−0.05~−0.08	−0.032~−0.044	−0.01~+0.02
July	−0.078~−0.093	−0.06~−0.09	−0.049~−0.067	−0.02~+0.00

5.2 The fiber optical sensing network basically covers the pouring block with a dimension of 32m×20m and the influence on real temperature field by cooling pipes, concrete grade and aggregate gradation can be clearly reflected in the curves. Test results show that snake-shaped cooling pipes play an evident role in enforcing cooling; the bigger grade of concrete, the higher temperature caused by hydration heat of concrete; and the bigger aggregate gradation the less influence on the temperature.

5.3 During the development of hydration heat the peak temperature of 34.75°C occurred at Point 117 on the upstream face, which is in the allowable requirement. After 28 days the temperature gradually went down and came to be steady at 24°C–25°C.

5.4 The connection between fiber optical crack meter and white light fiber optical signal regulator forms the fiber optical crack sensing system for absolute measurement, which can be easily connected and measured. The fiber optical crack meter, installed vertically to the crack on the upstream face of No. 16 monolith of the spillway dam section of TGP, is compact and 100% trouble-free for installation and application.

5.5 The monitoring of the vertical crack on the upstream face of No. 16 monolith of the spillway dam section of TGP shows that the crack tended to be closed (under pressure) at a slow speed and to be steady gradually, which indicated that the treatment of the vertical crack there was successful.

REFERENCES

[1] Gusmeroli V, Martinelli M and Barberis A, Thermal expansion measurements of a concrete structure by embedded fiber-optic an effective example of simultaneous strail-temperature detection, Second

European Conference on Smart Structures and Materials, Glagow, Scotland, 12–14, October, 1994d, SPIE, 1994D:220–223.
[2] Aufleger M, Strobl Th and Dornstadter J, Fibre Optic Temperature Measurements for Dam Monitoring, International Conference on Health Monitoring of Civil Infrastructure Systems, 24–26, October, 1994, Chongqing University Press, 121–128.
[3] Cai Desuo, Applications of the Optical Fiber Sensing Technology in Dam Engineering, China Water Power Press, 2002, 12, 129–168.
[4] Rossi P and Lemaou F, New method for detecting cracks in concrete using fiber optics. Materials and Structures, Research and Testing (RILEM), 1989, 22(132):437–442.
[5] Abdunur C, Monitoring of bridges subject to transversal cracks, Proc. 2th European Conf. On Smart structures and Materials, Glasgow, Scotland, 1994:156–159.

New Developments in Dam Engineering—Wieland, Ren & Tan (eds),
© 2004 Taylor & Francis Group, London, ISBN 04 1536 240 7

Fiber optic deflection measurement of high concrete-faced rockfill dam*

Cai Desuo, Ding Tao & Cai Shunde
Three Gorges University, China

Wei Yan & Li Rong
Shanghai Optical Fiber Center of China Aerospace Science & Industry Corporation, China

ABSTRACT: This paper studies the performance of DSP in digital logic circuit and digital processing of fiber optic gyro (FOG) signals. The noise model of gyro signal has been built by analyzing the noise caused by the optical path and electric circuit of FOG. The test results measured by FOG system totally conform to the deflection of plywood model and are close to the deflection of large-scale model of concrete-faced dam. According to the extensive experiments with these two models, the principle, the method and the technology of FOG have been proved feasible and reliable for the deflection measurement of concrete-faced rockfill dams and this approach can satisfy the demand for high accuracy in engineering.

1 DIGITAL FOG CLOSED-LOOP DETECTING SYSTEM

The closed-loop detecting proposal with digital phase stepped wave can obtain wide detecting dynamic range and better scale factor linearity if A/D (analog digital converter) and D/A (digital analog converter) with proper bit size are adopted[1,2]. Its function consists of two parts: one realizes the null-closed-loop control of FOG and the other is to process angular velocity signals output by the first accumulator of closed-loop control system to realize the improvement of signal accuracy. The functional scheme of the closed-loop control system is shown in Fig. 1.

To establish above-mentioned system circuit, an operational amplifier OP-37 is used to make up a preamplifier circuit, AD7821 and AD7535 are used to build up A/D and D/A converted circuit, and an operational amplifier AD744 to form a driving circuit of LiNbO3 phase modulator, in addition to some digital logic devices. Besides, software and hardware for collecting and processing the first accumulator output signals (rotational angular velocity signals) have been designed.

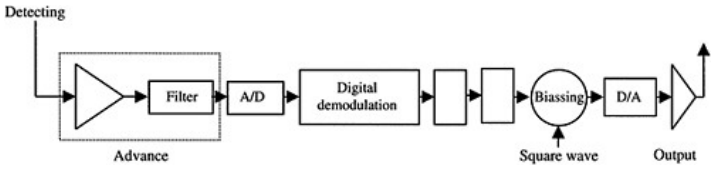

Figure 1. Functional scheme of the closed-loop control system.

* Key program of the State Education Ministry of China.

A joint test showed that the digital closed-loop control system was of very good tracing, detecting and processing performance. Experiments reveal that when the rotational angular velocity of gyro varies within the designed requirement, the system is always able to be in an extremely sound detecting condition with zero error so as to ensure the scale factor linearity. Furthermore, the first accumulator output signals (rotational angular velocity signals) can be input into the working point according to the output range of AD converter and thus the scale factor linearity can be further calibrated by processing the digital signal. Compared with others this design can obtain better scale factor linearity.

2 MEASUREMENT PRINCIPLE

2.1 *Principle*

FOG is a Sagnac fiber optical interferometer, as shown in Fig. 2. The light emitted by a laser or other suitable light sources is divided by 3dB coupler into half and half beams which are continuously coupled into two ends of a multi-turn fiber coil where the output light is sent through the coupler to the detector. Given R is the radius of the coil. When the FOG is still to the relative inertia space, two light waves traveling in opposite direction in the fiber coil propagate in the same optical path. As a result, the optical path difference is equal to zero but interference light is in maximum. When the FOG turns at rotation rate Ω to the relative inertia space, the light traveling in the same direction as the turning of FOG reaches earlier to the detector than the one in the opposite direction, which leads to a optical path difference. It can be converted to phase difference ϕ_S (Sagnac phase-shift).

$$\Phi_S = \frac{8\pi AN\Omega}{\lambda c} \tag{1}$$

where:

C=light velocity

A=area of fiber coil coverage

N=number of coil turn

λ=wave length of laser

As a result, rotation rate Ω can be calculated by detecting ϕ according to the optical interfering principle[3].

Output voltage can be achieved finally at the preamplifier when the turning of FOG creates Sagnac phase-shift ΔΦs.

$$I = K \cdot I_0\{1 + \cos[\Delta\Phi_m \sin(2\pi f_m t) + \phi_s]\} \tag{2}$$

where:

Io=SLD output light power

$\Delta\phi_m$=PZT modulating degree

f_m=PZT modulating frequency

ϕ_S=Sagnac phase-shift

K=attenuation coefficient

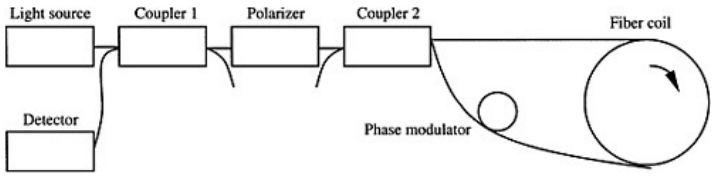

Figure 2. Illustration of FOG principle.

It can be seen from the extension of above-mentioned formula by Fourier that the signal output is a multiple harmonic signal and the first-order Bessel function filtered signal which contains turning message can be obtained through a demodulation circuit. For the low-dynamic FOG, the fundamental phase sensitive detection value of the electric signal output can be directly input as a rotating signal into the following system (Fig. 3).

The theory of FOG for dam measurement is as follows: The concrete face deflection changes due to relative loose structure of the rockfill dam body when the reservoir stores water. The deflection creates a turning component on the moving FOG when the FOG translates at a uniform velocity on the dam surface (the rotating direction of gyro is parallel to the dam surface but vertical to the movement). The amount of turning component is directly proportional to the translational velocity of FOG and the deflection. Therefore, the development of deflection can be measured out by means of a mathematic model if the FOG translates at a uniform velocity and thus the deflection can be calculated. More parallel measurements can be carried out focusing on the parts of the dam where stress concentrates so as to monitor the deflection development of the whole dam.

2.2 *Assumption*

2.2.1 FOG moves at the uniform velocity V which is related to the relative amount of deformation measured.

2.2.2 Every bit of moving track can be assumed as a bit arc in the motion track and the motion track is these arcs' integrate.

2.2.3 FOG is a small dynamic system. Therefore, FOG creates a small turning angle $\Delta\phi$ within time Δt when moving from A to B.

$$\theta_B=\theta_A-\Delta\Phi_{AB},\ \Delta\Phi_{AB}=\Omega_{AB}(t)\times\Delta t \tag{3}$$

where: Ω AB is the rotational angular velocity of FOG. The angle measured by FOG at any time t (horizontal direction is based as criterion) is shown below.

$$\theta_i=\theta_o+\sum_{j=1}^{n}\Omega_{AB}\times\Delta t_j \tag{4}$$

In the physical formula of calculation the two-dimensional velocity components are shown below:

$$\begin{aligned} V_x(t)&=V\cos\theta_0\\ V_y(t)&=V\sin\theta_0 \end{aligned} \tag{5}$$

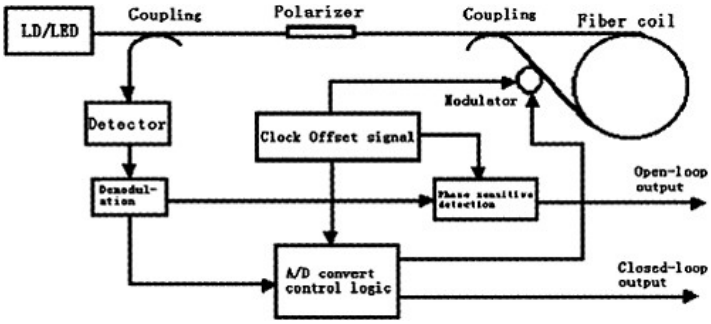

Figure 3. Principle of FOG signal processing.

And the two-dimensional track curves of dam surface are shown below:

$$X(t)=\sum V_x(t)\bullet \Delta t$$
$$Y(t)=\sum V_y(t)\bullet \Delta t \quad (6)$$

By means of computer a simulation deformation curve can be plotted through X(t) and Y(t) in formula (6). FOG measurement system consists of FOG, power, processing circuit of gyro, A/D converted data acquisition card. The light signals output by FOG is converted into electric signal and then processed by circuit where signals are filtered and detected. In the end, they are converted by A/D converter and sent to a computer for analysis through serial interface RS-232 and then a deformation curve of the dam is plotted.

3 EXPERIMENT RESEARCHES

3.1 *Test equipment*

Test equipment mainly consists of #501 FOG, small-sized signal processing circuit, A/D data acquisition card and serial interface transmission circuit. The technical measures of FOG are: random walk 20°/*h;* bias drifting 5°/h; stability of scaling factor ≤1%; angular velocity ≥+/−60°/s; operating temperature 0~+50°C. The measurement also needs portable computer for data acquisition and processing, deflection curve plotting and data save; and directional power composed of a set of AC-DC and three sets of DC-DC; and a digital multi-meter FLUKE45 for measuring the direct-current voltage and output signals.

Measurement vehicle is reformed from a toy trolley for carrying FOG and signal processor (Fig. 4). It can move on the simulation curved surface and simulate sensitively the deflection development of the curved surface.

Traction device, composed of pulley, traction line and speed regulator, is used to pull the measurement vehicle at a uniform speed on the curved surface.

3.2 *Measurement results*

3.2.1 Plywood model experiment in Shanghai

Plywood, head block, gravity clip plate, and tape etc. are used for simulating the deflection of concrete-faced dam.

(1) Simulation test of unimodal deflection

Table 1 is the test results of unimodal deflection and Fig. 5 is the illustration of results in three times.

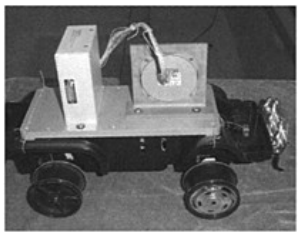

Figure 4. Measurement vehicle.

(2) Simulation test of bimodal deflection

Fig. 6 is the plywood model of bimodal deflection, Table 2 is the test results of bimodal deflection and Fig. 7 is the illustration of results in three times.

(3) Simulation test of tri-modal deflection

Table 3 is the test results of tri-modal deflection and Fig. 8 is the illustration of results in three times.

3.2.2 Large-scaled model experiment of concrete-faced rockfill dam in the Three Gorges University

Fig. 9 is the large-scaled model of concrete-faced rockfill dam and Fig. 10 is the curves of three tests.

Table 1. Test results of unimodal deflection. (Unit: cm)

Unimodal factual height	Test data 1	Test data 2	Test data 3	Error
10.00	10.04	9.98	9.87	0.13
12.00	11.85	11.93	11.81	0.19
16.00	15.83	15.93	15.88	0.17

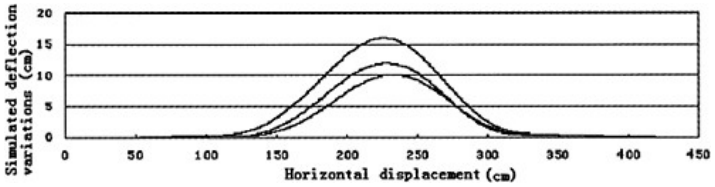

Figure 5. Illustration of unimodal deflection test in three times.

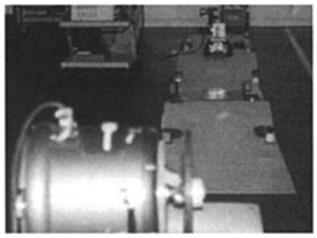

Figure 6. Plywood model of bimodal deflection.

Table 2. Test results of bimodal deflection. (Unit: cm)

Bimodal factual height	Test data 1	Test data 2	Test data 3	Error
12.00	11.93	11.85	11.87	0.15
10.00	9.87	10.04	9.90	0.13

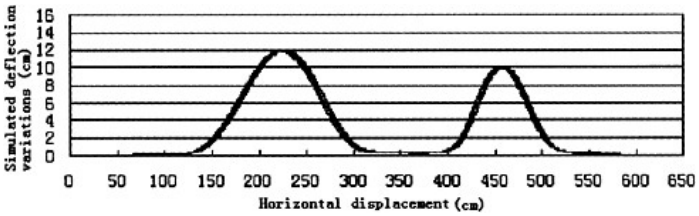

Figure 7. Illustration of bimodal deflection test in three times.

Table 3. Test results of tri-modal deflection. (Unit: cm)

Tri-modal factual height	Test data 1	Test data 2	Test data 3	Error
1.00	0.94	0.89	0.96	0.11
2.50	2.45	2.41	2.47	0.09
3.00	3.02	2.88	2.91	0.12

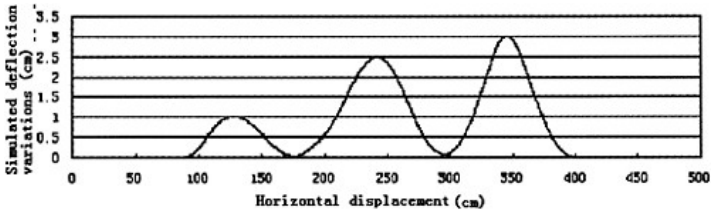

Figure 8. Illustration of tri-modal deflection test in three times.

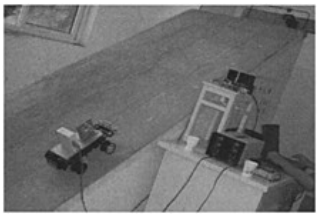

Figure 9. Model of the concrete-faced dam.

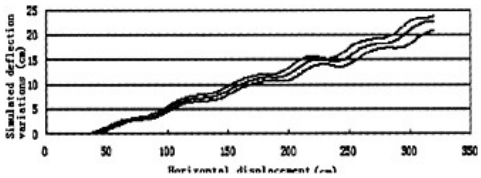

Figure 10. Curves for three tests.

4 CONCLUSION

4.1 This paper describes an up-to-date FOG closed-loop detecting and control system with digital phase ramp feedback technology which can satisfy the demand for high sensitivity and large dynamic range required by gyro signal measurement and is incomparably superior to other proposals in zero drift, linearity of scale factors and the like.

4.2 Based on the theoretic model and large quantity of experiments, the results measured by FOG system totally conform to the deflection of plywood model in Shanghai. In the large-scale model test of concrete-faced dam in Three Gorges University, the changing tendency of deflection is good though the measurement accuracy is little low due to traction by hand.

4.3 The principle and technical proposal for deflection measurement of high concrete-faced rockfill dam by using FOG has been proven to be feasible according to the tests in Shanghai and Yichang. The key problem for further consideration is the designing scheme for practical engineering.

REFERENCES:

[1] L.K.Strandjord, and G.A.Sanders, Resonator Fiber Optic Gyro Employing a Polarization-Resonator. SPIE Proceeding, Vol. 1585, 1991:163–172.
[2] R.Adar, Y.Shani, C.H.Henry, R.C.Kistler, G.E.Blonder, and N.A.Olsson, Measurement of Very Low-Loss Silica on Silicon Waveguides With a Ring Resonator., Applied Physics Letters, Vol.58, 1991:444–445.
[3] Cai Desuo, Applications of the Optical Fiber Sensing Technology in Dam Engineering, China Water Power Press, 2002, 12, 169–186.

This page intentionally left blank.

New Developments in Dam Engineering—Wieland, Ren & Tan (eds),
© 2004 Taylor & Francis Group, London, ISBN 04 1536 240 7

Concrete construction technology in Phase II dam of Three Gorges Project

Cao Guangjing
Peng Gang, Project Construction Department, CTGPC, China

ABSTRACT: Concrete construction is one of the most important and most challenging projects in the Three Gorges Project (hereinafter called TGP) Construction since it features mammoth amount, high intensity, complex structure, and strict requirement in the Phase II dam and powerhouse construction. The paper is intended to analyze difficulties of the quality control of concrete construction, to systematically present the concrete construction scheme and temperature control measures to prevent concrete cracks, and to brief concrete construction progress and quality control effect.

1 BRIEF OF THE PROJECT

1.1 *Project scope*

The Phase II dam and powerhouse work is one of the most important and most challenging projects in the TGP Construction. It mainly includes the spillway dam, the left-bank dam intake section, the left-bank non-overflow section (12#~18#), and the left-bank powerhouse. The total length along the dam axis is approximately 1304.5m, and the total amount of concrete placement is about 12,380,000m^3. The dam is of concrete gravity type with maximum height of 181m, and maximum bottom width of 126.5m. The construction period on the critical path is 44 months.

1.2 *Critical schedule arrangement*

The general critical schedule of the Phase II dam and powerhouse work is arranged as follows:

1. In mid June 1998 the first cut-off wall of the cofferdam is completed, and restrictive dewatering of the foundation pit begin;
2. In mid September the dewatering of the foundation pit is completed;
3. In the first quarter of 1999, all-around concrete placement begin;
4. In May 2002 the upstream foundation pit is filled with water, in July 2002 the downstream foundation pit is filled with water, and in October 2002 every section of the concrete dam is placed to elevation 185m;
5. In June 2003 the diversion bottom outlets are closed to impound the reservoir;
6. The first batch of four units is commissioned in 2003.

2 DIFFICULTIES FOR CONCRETE QUALITY CONTROL

The following major difficulties of the quality control of the concrete construction are determined by the natural environment of the dam area, the structure of the dam and the critical schedule arrangement.

(1) Concrete placement on the restrained area of the foundation amid high temperature of the summer. Due to the huge quantity of excavation works and tight schedule, especially the huge work quantity of clearing foundation interface as well as some interface areas lagging behind, and furthermore the concrete placement methods to be gradually finalized and optimized, concrete placement on a large number of strong restriction area of the foundation is postponed to high temperature season of summer. This leads to strict requirement on temperature control to prevent concrete cracks. It shall be guaranteed that comprehensive measures are taken in every step of concrete making and placing to keep the maximum concrete temperature of the dam within design requirement.

(2) Three tiers of discharge outlets (i.e. diversion bottom outlets, discharge deep outlets, and surface outlets) are arranged at the spillway dam, as a result, more grades of concrete are used around outlets, and therefore the construction requirement is high with more difficulties. Around outlets is high grade anti-impact and anti-abrasion concrete strengthened with layers of steel bars to take forces on it. Furthermore, as a major difficulty in the construction, high speed water jet requires the levelness of concrete surface, which is guaranteed by the quality of form, the compactness of concrete, and temperature control to prevent cracks.

(3) It's difficult to carry out intense concrete construction with high quality. The total amount of concrete placement of the Phase II dam and powerhouse work is about 12,380,000m^3. Limited by timing of the preceding works such as dewatering the Phase II foundation pit and excavating for the foundation interface, and timing of the succeeding works such as filling the foundation pit and Phase III river close-off, the construction period is fixed with high intensity of concrete construction. The Period between 1999 and 2001 is the peak years for concrete construction, and the maximum yearly record is 3.86 million m^3 in 2000; the maximum monthly record is 0.44 million m^3, Concrete placement intensity of above 0.35 million m^3 per month lasted for about one year.

3 CONCRETE CONSTRUCTION SCHEME

Reasonable construction scheme is the fundamental guarantee for construction schedule and concrete quality. So after years of thorough and all-around verification and comparison on various construction schemes, the designer and the owner finally decided to select the construction scheme with Rotec tower belt-conveyers as main equipment and swing-tower cable cranes and high-rise gantry crane (tower crane) as auxiliary equipment, in accordance with the characteristics of the Phase II dam and powerhouse work.

3.1 *Layout of main construction equipment*

Major construction equipment comprises six Rotec tower cranes, four belt-conveyers, two swing-tower cable cranes, and nine large gantry cranes. In addition, some middle/small sized equipment is furnished by the contractors.

3.1.1 *Tower belt-cranes*

They are arranged at the spillway dam and dam intake 7□14# in the foundation fit, where it is of critical importance, since the foundation surface is low, and the volume of the dam is big, and construction period is short. Therefore six Tower Belt-Conveyers, laid-out at spillway dam 1#, 7#, 14#, 21# and dam intake 8#, 12#, cover all the above-mentioned scope to give full play to the tower belt-conveyers for high intense concrete placement. They help to place concrete to El. 155~160m of the Dam with concrete quantity of 7.40 million m^3, or 60 percent of the total.

3.1.2 *Cable cranes*

Two swing-tower cable cranes are set up to span the whole dam with coverage of 15m to the upstream of the dam axis and 65m to the downstream. They help, within this zone, to erect metal

structures, to transfer placement equipment and materials and to provide aerial assistance in case of tower belt-conveyer failure.

Parameters of the cable crane: span 1416m, lifting capacity 25t, joint capacity of two cranes 46t$_o$.

3.1.3 *Trestles and gantry cranes*

Three Construction Trestles are laid out as follows: trestle at El. 45m in the downstream of spillway dam, trestle at El. 120m on the downstream face of the dam (60.5m from the dam axis), trestle at El. 82m between the powerhouse dam and the powerhouse. In addition, construction platform at certain elevation is established between the upstream of the dam and downstream of the powerhouse. Nine large gantry cranes are arranged at the above mentioned trestles and platform to erect metal structure and embedded parts of the units, to place concrete, and to prepare placement surface.

3.2 *Layout of concrete mixing system*

Four concrete mixing systems are arranged, in seven batching plants with corresponding cooling systems to guarantee concrete temperature at the exit to be 7°C. Batching plants are setup as close as possible to the dam, to abridge the distance of the conveyance belts, and therefore guarantee the concrete quality and curb the temperature rise during the concrete conveyance. As for the match between the batching plant and the conveyance lines, any batching plant is capable to feed every conveyance belt for mutual support. The configuration and capacity for every mixing system is shown in Table 1 below.

3.3 *Arrangement of concrete conveyance line*

(1) The configuration of one crane and one belt. The tower crane and the corresponding batching are connected with special conveyance line to ensure intense and continuous concrete supply.
(2) The conveyance line is supported with means of one column and two belts to reduce the work quantity and to simplify the field layout.
(3) The conveyance line is smoothly and simply arranged to reduce the joints of the belt conveyer.
(4) The routing of the conveyance line is optimized to reduce interference to the dam structure and concrete placement.

3.4 *Accessory equipment for concrete placement*

(1) Vibration equipment shall match with the tower belt conveyer in respect of the placement capacity. Two 4–8 head vibrators are furnished for every placement, and manual vibration is provided as supplementary.

Table 1. Configuration of concrete mixing system.

Name	El. 79 system	El. 90 system	El. 120 system	El. 82 system
System location	Right downstream corner of the foundation pit	Left upstream corner of the foundation pit	Left downstream of non-overflow 12#	Left downstream corner of the foundation pit
Placement location	Dam	Dam	Dam	Powerhouse
Configuration of batching plant	2 plant each 4×4.5m^3	1 plant 4×6m^3 1 plant 4×3m^3	2 plant each 4×3m^3	1 plant 4×3m^3 240
Capability of normal temp. concrete m^3/h	2×320	360+240	2×240	
Capability of low temp. concrete m^3/h	2×250	250+180	2×180	180
Cooling capacity MW	27.912	18.608	15.119	8.723

Note: The manufacture capability is shown as nameplate value.

(2) A certain number of small placement cranes shall be furnished to lift forms, steel re-bars, and prefabricated parts so that the tower crane is freed to concentrate on concrete placement.

4 CONCRETE QUALITY CONTROL MEASURES

4.1 *Quality control measures for concrete placement with tower belt-conveyer*

(1) Technology to prevent aggregate separation during Gradation IV concrete placement by the tower belt-conveyer. Field practice and field tests show that proper engineering measures help to guarantee quality in

- that Gradation II concrete or Gradation III concrete rich in mortar (20~40cm thick), in place of the traditional technology of spreading mortar, helps to strengthen the adherence of the interface between the existing layer and fresh layer; and
- that limiting the content of extra large stone of Gradation IV concrete under 20~25% (while the normal content is 30%), and strict control on the diameter of extra large stone, helps to prevent aggregate separation; and
- that controlling the height of the nose pipe in the range of 90~150cm, and moving at appropriate time, help to effect even distribution. But in the following locations the gradation shall be reduced: concrete under horizontal steel re-bar network, concrete around pre fabricated gallery.

(2) Technology to prevent temperature rise of the pre-cooled concrete by the tower belt-conveyer. According to the survey in the summer of 1999, rate of temperature rise for the pre-cooled concrete of 7°C is 1°C /150m, and total temperature rise is 4~6°C, exceeding 2°C the design requirement. In light of this, the following measures are taken:

- to further improve and optimize the temperature control facilities of the conveyance line. Although a cover is furnished at the top, the sides are not protected against temperature rise. So rubber skirt boards are arranged to prevent convection of the pre-cooled concrete.
- to stabilize the manufacture capacity of the batching plant and vibration capability on the placement, so that the concrete on the belt forms continuous and coherent flow.
- to control the timing for concrete placement and avoid placing concrete during the high temperature period between 10am and 5pm.
- to lower concrete temperature at the exit of the batching plant. In August and September 1999, the air temperature is high in the day time. And we changed the concrete temperate from 14°C to 7°C to ensure the concrete quality with a rise on the costs. In the summer of 2000, the dam grew out of the restrained foundation area, and 14°C concrete fulfills the requirement. But if taking the temperature rise on the concrete conveyance line into consideration, we may continue adopt the 7°C concrete measure to address the problem.

(3) Certain blind areas for concrete placement exist around tower column and under belt conveyer. Measures such as placement leveling, machine distribution relay, and lowering the gradation help to ensure the concrete quality.

(4) By studying the important coordination and control of the tower belt-conveyer and its conveyance line which features long line, multiple steps, continuous operation, we can avoid quality problems arising from improper operation. We worked out methods for effective management on the coordination and communication of the intermediate steps, the control on exit arc gate, and the sequence of concrete placement. So that effective and efficient operation on concrete placement, its conclusion, concrete gradation and grade change can be carried out.

4.2 *Temperature control and anti-cracking measures for concrete*

In purpose of protecting dam concrete from creating thorough cracking and surface cracking, the concrete temperature should meet the standards of temperature control set on the temperature difference in dam concrete foundation, between inner and outer parts of the concrete and between upper and lower layers of concrete etc. During the actual construction practice, the temperature

control was conducted in line with the designed allowable maximum temperature of the dam body in full consideration of the previously mentioned temperature differences and temperature for a steady dam been. As a typical temperature control standard, the designed allowable maximum temperature in Block No. 3 of the spillway dam section from June to September should meet the following requirements: temperature in the restrained zone of the foundation shall be maintained between 31°C and 32°C and the outside of the restrained zone of the foundation between 36°C and 37°C.

Main temperature control and anti-cracking measures to be adopted are as below.

(1) Thermal Source Control

– To optimize the raw materials as well as the mix proportion in order to decrease the hydration heat of the cement. Adding high quality and efficiency water reducer and fly-ash? helps to limit the water consumption for concrete gradation IV to 90 kg/m^3 so that the consumption of the cementitious materials could be reduced.
– To pre-cool the concrete by procedure of "Twice wind-cooling and ice mixed" in order to control the temperature of concrete at outlet of batching plant at 7°C and 14°C. Meanwhile temperature rise both during conveying and at placing points should be controlled so as to meet the designed temperature requirement of concrete placing.

(2) Appropriate Control on Lift Thickness and Interval Period

– To limit the lift thickness between 1.5m–2.0m and to adjust by taking the part, outside temperature and progress schedule into account so as to bettering the heat dissipation of the top surface.
– To proceed uniformly with reasonable interval. Generally interval could be 5–10 days. The interval should be strictly managed when outside temperature changes markedly.
– To avoid placing in thin lifts and at long interval within the restrained zone of the foundation. Cracking usually created when coldness impacts the placement in thin lifts and at interval of long period should be avoided as much as possible. However, when inevitable cracking occurred in such case due to some special restrains from construction procedures and methods etc., anti-cracking measures such as placing reinforcing steel bar should be actively taken.

(3) Cooling by Water Circulation

– Circulation of water at early stage of concrete placement is to reduce maximum temperature of concrete with 10–15d circulation of water flow of 6°C–8°C and not less than 18L/min.
– Circulation of water in middle stage, with a flow of 20~25 L/min, shall be carried out to decrease temperature difference between outside and inside the concrete with river water. It will last for 1.5–2.5 months from September until the temperature of concrete monolith reaches 20°C~22°C.
– Circulation of water in final stage is to lower the temperature of the dam body at 14°C~18°C for joint grouting.

(4) Curing with Flow Water

Timely and continuous curing of newly placed concrete is of great importance to the normal growth of the concrete strength and avoidance of surface contraction cracking, and of great help of heat dissipation and temperature lowering of the concrete as well.

– Circulation of water shall start after 12 hours upon completion of concrete placement of any pour, and continuous curing shall be carried out at least throughout the design service life of the concrete.
– Water flow shall especially be taken for the curing of the upstream and downstream face of the dam and powerhouse as well as exposed side area of concrete in order to maintaining continuous humid condition.

(5) Surface protection

Protection of concrete surface is an important measure to prevent concrete from cracking. Since the exposed area of the dam and powerhouse is very huge and sudden temperature drop occurs frequently in the dam region, protection of concrete surface is considered particularly

important, especially for concrete placed in restrained zone of the foundation, upstream face of the dam and other important structures.

– As to permanent exposed surface, concrete placed during October through April next year shall be provided with permanent heat insulation layer immediately after form removal, while concrete poured during May–September shall be provided with permanent heat insulation layer at the beginning of October.
– All diversion bottom outlets and other openings shall be blocked at the beginning of autumn (from end of September) in each year.
– For concrete placed, within the age of 28 days when daily temperature decreases more than 6°C within 2–3 days, its surface shall be protected.
– As for concrete poured in season of low temperature or period of sudden temperature drop, form removal will be delayed or surface protection shall be carried out immediately after form removal.

4.3 *Construction measures for anti-abrasion concrete around outlet of spillway*

Anti-abrasion concrete with grade of $R_{28}400^{\#}D_{250}S_{10}$, $R_{28}450^{\#}D_{250}S_{10}$ will be adopted for the construction of 1–2m around the outlets of Spillway. Requirements on the surface planeness as well as the longitudinal and traverse gradients have been strictly specified in the design code. High requirements on the temperature control has also been specified that the maximum allowable temperature of concrete shall be maintained between 25°C to 27°C in cold seasons and 39°C to 40°C in hot seasons.

The following measures had been incorporated during the construction.

(1) To adopt specialized form

Adoption of large-scale high-strength DOIKA form sticked with Finland faceboard outside effectively avoids problems of staggering and overflow on the concrete surface caused by form deformation and grout-leakage. Meanwhile, wooden faceboard which is characterized in water-absorbing is effective in reducing the air bubble in the surface of concrete. As to the bottom slab concrete, bridge-type smoother combined with manual smoothing will work to ensure the flow surface quality of the concrete.

(2) High efficiency water reducer

Tests indicate that the Italian X404 retarding high efficiency water reducer makes remarkable results in decreasing the consumption of cementitious materials of high grades concrete. The cementitious materials in $R_{28}450^{\#}$ concrete which is blended with X404 amounts to 377kg/m^3,40kg (36kg of which is cement and 4kg fly-ash) less than that blended with naphthalenic water reducer, resulting in a decrease of 4–5°C, less collapse and a rise of strength and limit tensility.

(3) Intense cooling by water circulation in early stage

Besides the measure of setting a layer of cooling pipes on the closing placing points, more could be conducted as the following:

– To add one more layer of cooling pipe along the horizontal layer of reinforcing steel bar in the anti-abrasion concrete;
– To carry out upright water circulation in early stage, namely to bind the polythene plastic pipes over the reinforcing steel bars around the concrete of the outlets exits so as to reduce the hydration heat.

5 CONCRETE CONSTRUCTION PROGRESS AND QUALITY CONTROL

5.1 *Project progress*

11.38 million m^3 of concrete has been poured from the onset of concrete placement at the Phase II Powerhouse and dam intake at the beginning of 1998 to the July of 2002, with annual peak intensity

Table 2. Concrete placement by tower belt cranes (Unit: 10,000m^3).

Items	1998	1999	2000	2001	2002	Total
Pours by tower-belt cranes from No. 1 to No. 6	0.59	146.71	183.31	177.56	11.45	519.62
Pours for dam	41.19	312.52	352.00	238.83	58.84	1003.38
Portion by tower belt cranes (%)	1.43	46.94	52.08	74.35	19.50	51.79
Pours for dam & powerhouse	54.27	364.79	385.58	263.43	69.47	1137.54
Pours for TGP	91.88	455.38	542.85	402.88	109.74	1602.73

Remarks: concrete placement in 2002 is counted until 25 July.

of 3.85 million m^3 in 2000 and monthly peak load of 441,000m^3 in December of 1999. 5.19 millionm^3 of concrete has been poured by 6 sets of tower belt cranes, accounting for 51.79% of the total volume of 100.3 million m^3 for the dam (Table 2), which demonstrates primary effects of tower-belt cranes in concrete placement.

Thanks to the progress of dam concrete construction and installation of metal structure and Mechanical and Electrical equipment, the scheduled dam rise to its crest level, watering the construction pit and initial reservoir impoundment have been achieved on time and 6 sets of generating units with unit capacity of 700MW each have been put online in 2003.

The Phase II powerhouse and dam intake have been put into service after the acceptance surveillance conducted by the Three Gorges Construction Committee of the State Council. It is worthwhile noting that a great number of core-sampling, forced water testing and in-hole video have been performed at critical parts of the dam to check the compactness of the concrete with the density of 10m per 10 thousand m^3 concrete. The results show that despite few surface cracks that have been treated carefully and would cause no negative impact on the dam, the overall compactness of the dam is very good, demonstrating that the comprehensive measures for temperature control is highly effective.

This page intentionally left blank.

New Developments in Dam Engineering—Wieland, Ren & Tan (eds),

Analysis of seepage through dam foundation with closed system of grouting curtain, drainage and pumping measures

Chai Junrui
Three Gorges University, China

Li Shouyi
Xi'an University of Technology, China

ABSTRACT: The closed system of grouting curtain, drainage and pumping measures should be designed and built where the downstream water level is high. The combined theoretical and numerical method is utilized to analyze the seepage field and its factors in the dam foundation with the close system. It can be shown that, (1) seepage flows from the upstream to the downstream, also flows mainly from the upstream and the downstream to the pimping well in dam foundation; (2) the grouting curtain controls the seepage discharge; and (3) the good service condition of the drainage and pumping system can decrease largely the hydrostatic seepage pressure (or the uplift pressure).

1 INTRODUCTION

The dam is the barraging structure to block river water, so its permeability is the issue during research, design, construction and service of a dam. If severe leakage occurs in dam foundation or abutments, the design water level of the reservoir would not be reached and the dam would fail to service its functions. Furthermore, the dam stability and safety relevant to seepage or leakage is more important. Hence, researchers and engineers of dam engineering pay more and more attentions at seepage problems because of the characteristic of the dam. Nevertheless, due to the complexity of the seepage mechanism of rock and soil media, variable troubles resulted from seepage problems have occurred in the foundations or banks of some dam projects over the world[1]. It could be shown from the facts that the inherent nature of lasting variation of seepage through rock and soil media often troubles or even endangers the dam construction. It can be also summarized that 90% of all slope failures in dam area and one third of all dam failures are resulted from seepage problems. The failure of Malpasset arch dam in France in 1959 and the big landslide in Vajont arch dam area in Italy in 1963 are the typical examples of failures resulted from seepage problems[2]. So, anti-seepage and drainage measures are very important to early all dams in dam body, dam foundation and abutments. At present, the principle of "blocking at upstream part, draining at downstream part" is applied to the design of anti-seepage and drainage measures of dams[3]. The anti-seepage measures such as anti-seepage concrete plates, curtain groutings, anti-seepage walls and blankets are often designed at the upstream part, the drainage measures such as drain pipes, drain holes, drain tunnels and pumping wells are often designed at the downstream part. When the downstream water level is high at some dam blocks, the close system of anti-seepage and drainage measures (see Fig. 1) should be designed, which is also applied in some dam blocks at Three Gorges Project[4].

The present research[5–7] involves little information about the close system of anti-seepage and drainage measures of dams. The purpose of this paper is to systematically analyze the seepage field with the close system of anti-seepage and drainage measures of dams by means of both the theoretical and numerical methods to serve the design of dam engineering.

2 THEORETICAL SOLUTION TO THE SEEPAGE FIELD

Figure 1 is the sketch of close system of anti-seepage and drainage measures in dam foundation. Suppose that both the upstream curtain and downstream curtain with the mean hydraulic conductivity of K_g are complete ones which reach the impermeable stratus. The mean depth and hydraulic conductivity of the permeable stratus of dam foundation are T and K, respectively. For simplicity and safety, it is assumed that the drain holes at H, I, J and K are the assistant drain measures and the pumping well at D is the main drain measures where the water table is always below the dam foundation plane, hence the hydraulic head at D is taken as 0. In order to obtain the distribution of seepage pressure along the dam foundation plane, we can apply the one-dimensional flow continuity principle combined with Darcy's law to get the following equations[8].

$$H_B = \frac{nt_1 + b_1}{a_1 + nt_1 + b_1} H_1 \; ; \qquad H_C = \frac{b_1}{a_1 + nt_1 + b_1} H_1 \tag{1}$$

$$H_F = \frac{nt_2 + b_2}{a_2 + nt_2 + b_2} H_2 \; ; \qquad H_E = \frac{b_2}{a_2 + nt_2 + b_2} H_2 \tag{2}$$

$$Q = nK_g T \left(\frac{H_1}{a_1 + nt_1 + b_1} + \frac{H_2}{a_2 + nt_2 + b_2} \right) \tag{3}$$

$$P = \frac{\gamma H_1}{2} \cdot \frac{t_1^2 + 2a_1 t_1 + \beta L_1^2}{t_1 + \beta L_1} + \frac{\gamma H_2}{2} \cdot \frac{t_2^2 + 2a_2 t_2 + \beta L_2^2}{t_2 + \beta L_2} \tag{4}$$

where H_B, H_C, H_E and H_F are the hydraulic heads at B, C, E and F, respectively; $n=K/K_g$; Q is the approximate total seepage discharge within the whole permeable stratus along 1m long of dam axis; P is the resultant of seepage pressure along the dam foundation along 1m long of dam axis; γ is the gravity density of water; $\beta=(n-1)^{-1}$; $L_1=a_1+t_1+b_1$; $L_2=a_2+t_2+b_2$; other symbols are illustrated in Figure 1.

From equations (1) and (2), the distribution of seepage pressure along the dam foundation[9] can be shown in Figure 2.

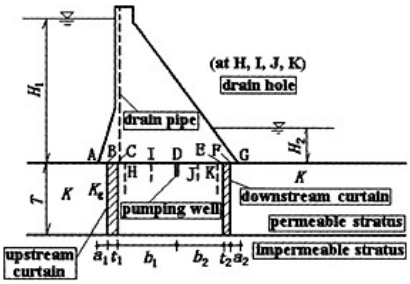

Figure 1. Close system of anti-seepage and drainage measures.

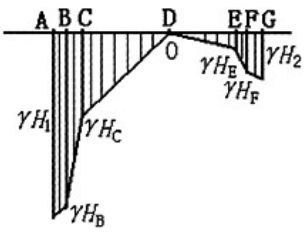

Figure 2. Theoretical distribution of hydrostatic seepage pressure on dam foundation plane.

It can be shown that the total seepage discharge Q mainly depends on the mean hydraulic conductivity K_g of the curtain grouting zone; the good service condition of the pumping measures makes important effects on decreasing the seepage pressure on the dam foundation; and the curtain grouting also makes effects on decreasing the seepage pressure.

3 FINITE ELEMENT NUMERICAL SOLUTION TO THE SEEPAGE FIELD

To overcome the limitation of the simplified assumption of the theoretical solution, we performed the finite element numerical analysis of the seepage field in dam foundation with the closed system of grouting curtain, drainage and pumping measures. Figure 3 shows the computation area (240m×60m) and the finite element meshing model. H_1=100m, H_2=30m. The permeability parameters are K=10^{-7}m/s, K_g=10^{-8}m/s. The boundary co^{nditions} of the seepage field are the given heads $H|_{MA}$=100m, $H|_{GN}$=30m, $H|_{D,\,H,\,I,\,J,\,K}$=0; the given discharges $q|_{Mp,\,PQ,,\,NQ}$=0.

By means of the finite element numerical analysisc[10], we can get the distribution of seepage pressure on the dam foundation plane shown as Figure 4 and the contour of hydraulic head in the seepage field shown as Figure 5.

4 COMPARISON OF FEM TO THEORETICAL METHOD

For the example shown in Figure 3, Table 1 is the comparison of analysis results of FEM to the above theoretical method.

It can be shown from the comparison that the maximum relative difference between the numerical method and the theoretical method is below 10%. From the viewpoint of the resultant of seepage pressure and the total seepage discharge, the theoretical method is more conventional. It can be also illustrated from Figure 5 that the hydraulic gradient within the upstream curtain zone is very sharp, and besides the seepage direction from upstream to downstream water also seeps from upstream and downstream to the middle pumping well, which agree with the theoretical method.

5 CONCLUSIONS AND DISCUSSIONS

(1) In dam foundation with the closed system of grouting curtain, drainage and pumping measures, besides the main seepage direction from upstream to downstream, water also seeps from upstream and downstream to the middle pumping well. But the hydraulic gradient within the upstream curtain zone is very sharp, so the upstream part is the key part of anti-seepage measures. Relatively, the downstream curtain and drainage could be simplified.

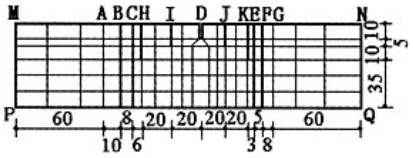

Figure 3. FEM mesh for seepage field (unit: m).

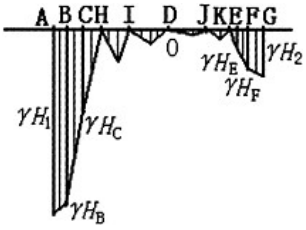

Figure 4. Distribution of hydrostatic seepage pressure on dam foundation plane by FEM.

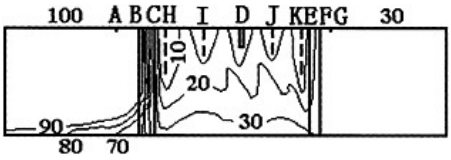

Figure 5. Contour map of hydraulic head within seepage field by FEM (unit: m).

Table 1. Comparison of results of FEM to theoretical method.

Method	Hydraulic head (m)									Resultant of seepage Pressure(10^4KN)	Total seepage discharge ($10^{-6}m^3/s$)
	H_B	H_c	H_H	H_I	H_D	H_J	H_K	H_E	H_F		
FEM	90.9	37.1	0	0	0	0	0	14.0	26.8	2.56	5.88
Theoretical method	92.6	33.8	29.4	14.7	0	5.9	11.9	12.8	27.6	2.80	6.19
Difference (%)	1.87	8.89	–	–	0	–	–	8.57	2.99	9.38	5.27

(2) Both the grouting curtain and the draining and pumping system make effects on decreasing the seepage pressure on dam foundation plane. Only if the relative hydraulic conductivity of the curtain zone is very small (or n is very big), the pressure-decreasing effect of curtain would be obvious. The good service condition of the draining and pumping measures makes obvious effects on decreasing the seepage pressure on the dam foundation plane.
(3) The total seepage discharge through the dam foundation mainly depends on the mean hydraulic conductivity of the curtain grouting zone.
(4) It can be shown from the comparison of analysis results of FEM to the theoretical method that the simplified theoretical method is more conventional, but meets the engineering demand and is more applicable to engineering practice.
(5) If the geological formation of dam foundation is complex and the faults and fractures are intersecting, it is necessary to apply the fracture network seepage model combined with FEM to analyze the seepage field.
(6) Further studies should be carried out to analyze the effects of the closed system of grouting curtain, drainage and pumping measures on the stresses at the dam heel and the stability along dam foundation plane.

ACKNOWLEDGEMENTS

The financial support from the Project 10202015 sponsored by National Natural Science Foundation of China (NSFC), the Project 106–220331 sponsored by the Scientific Research Foundation (SRF) for the Returned Overseas Chinese Scholars (ROCS) by State Education Ministry (SEM), the Research Project 03JK098 sponsored by Shaanxi Provincial Education Department (SNED), the "Chutian Scholar" Project 8096 and the Scientific Innovation Group Project 200402 sponsored by China Three Gorges University (CTGU) and the Scientific Innovation Project 106–210303, 220275 sponsored by Xi'an University of Technology (XAUT) is gratefully acknowledged.

REFERENCES

[1] Zhu Yueming. Review on research on seepage analysis and seepage control measures for dams. *Hohai Scientiflc Progress.* 1993. (4):109–116.

[2] Wu Yanqing, Zhang Zhuoyuan. *Introduction to Rock Mass Hydraulics.* Chengdu: Southwest Jiaotong University Press. 1995.
[3] Qi Qinghe. *Hydraulic Structures.* Beijing: Hydropower Press. 1997.
[4] Yangtze Water Resources Commission. *Research on Dam and Power Plant of Three Gorges Project.* Wuhan: Hubei Science and Technology Press. 1997.
[5] Chai Junrui, Wu Yanqing. Seepage through layers in roller compacted concrete dam and its effects on stresses of the dam. *Journal of Hydropower Energy.* 2001. 19 (1): 55–58.
[6] Chai Junrui. On water loads applied on the concrete dam. *Journal of Hydropower Energy.* 2000. 18(2): 18–20.
[7] Chai Junrui. Analysis of non-Darcy's seepage through dam foundation. *Journal of Hydropower Energy.* 2001. 19(4). 1–3.
[8] Chai Junrui. On the optimal thickness of curtain groutings in dam foundation. *Journal of Applied Science and Engineering Science.* 1999.7(2): 198–203.
[9] Chai Junrui, Han Qunzhu, Kou Xiaozhong. Research on seepage pressure on the foundation plane of dams and gates. *Shaanxi Water Power.* 1996. 12(4): 47–51.
[10] Li Shouyi, Chen Yaolong, Chai Junrui. On seepage body force in roller compacted concrete dam. *Journal of Applied Science and Engineering Science.* 1996. 4(4): 395–402.

This page intentionally left blank.

New Developments in Dam Engineering—Wieland, Ren & Tan (eds),
© 2004 Taylor & Francis Group, London, ISBN 04 1536 240 7

Hydropower of Thailand—a perspective

C.C.Chang
Parsons Brinckerhoff Quade & Douglas, Inc., New York, U.S.A.

ABSTRACT: As a developing country, Thailand has been under a tremendous pressure to harness its natural resources to meet the ever-growing demand for power that began in the late 1950's. Sverdrup & Parcel had the great privilege of assisting Thailand in its very first hydropower plant at Bhumibol Dam with its initial phase of construction completed in late 1950's as the Construction Managers. In the mid1980's, Svdrdrup completed yet another multipurpose project at Bang Lang Dam as the designer and Construction Managers in southern Thailand. During these years the mix of the installed power plants has undergone a significant change. In the last fifteen years, the installed capacity has again shown a significant shift to a more affordable energy source. This paper will give a brief history of the power generation—as witnessed by Sverdrup & Parcel's involvement in the Bhumibol and Bang Lang (Pattani) projects—and discuss the direction it appears to be heading in the future. Although the prime subject is hydropower, the mention of other forms of power is inevitable. In perspective a brief description of Southeast Asian regional cooperation in shearing power and management will be discussed. Also, a brief discussion will be made with regard to search for the renewable energy sources. In all cases the opinions and conclusions provided are those of the author alone.

1 THE ELECTRICITY GENERATING AUTHORITY OF THAILAND

The Electricity Generation Authority of Thailand (EGAT) is a state-owned enterprise under the Prime Minister's Office, which is responsible for producing electricity. At the top line of command is the Board of Directors, appointed by the Government. The Board of Directors generates and enforces policies and exercises general control over the operation of EGAT. The chief executive officer is the Governor who is appointed by the Board with consent from the Government. The organization structure is comprised of various divisions under the control of each division's directors or managers. EGAT was established in 1969 to nationalize and consolidate the functions and responsibilities of the three power utilities, namely the Yanhee Electricity Authority, the Lignite Authority, and the Northeast Electricity Authority. The key policy of EGAT throughout the past 29 years has been to provide adequate, reliable and economical electricity to meet the demands of the country. Therefore, EGAT's activities[1] encompass the development, construction and operation of dams, reservoirs, power plants, transmission systems and substations; the production of lignite and its by-products; and the formulation of policies concerning the production and sales of electricity, lignite and lignite by-products. However, the EGAT Act of 1992 further authorized it to engage in businesses that support its power generating activities. The Act permits

[1] The responsibilities of power distribution are shared by Metropolitan Electricity Authority (MEA) for Bangkok region and Provincial Electricity Authority (PEA) for the rest of the country.

EGAT to establish private limited companies or public limited companies, and to collaborate with other local or international entities in business concerning or in continuity with its activities, or to hold interest in any company.

In 1969, EGAT began its operation with a small installed capacity. During the first 29 years, however, it has greatly expanded the power generation and transmission system to meet the power demand that grew by 12% per year on average. At the end of fiscal year 1997, the total system capacity was 16,980MW. Of this, 14,687MW belonged to EGAT's system and the remaining 2,293MW were provided through purchases. However, the development of any power project always has negative impacts on the environments. For this reason, every power development will have to be subject to a thorough examination in order to minimize such impacts to meet the environmental as well as social responsibilities. In the meantime, organizational restructuring has been adopted to improve efficiency and to create an autonomous business-like operation in order to increase its competitive edge. In 1997, EGAT was the first and only power utility in Asean[2] to be awarded the ISO 9002 standard certification for its quality installation of hydroelectric power plants. By 2002, all of its major power plants have achieved the ISO 14001 standard for environmental management.

2 BHUMIBOL DAM DESCRIPTION

The Bhumibol Dam of the Yanhee Project is the first multipurpose dam and the highest dam in Thailand. This is also the first hydro project Sverdrup & Parcel was involved in. The Bhumibol Dam was constructed across the Ping River at Khao Kaew, Sam Nagao District, Tak Province, approximately 480km north of Bangkok. It has provided Thailand great benefits in the intervening years, such as electrical generation, irrigation, flood control and recreation. The project covers the construction of a dam, later named "Bhumibol" by the royal permission of the King of Thailand, and a power plant designed with eight generating units of 70MW each. The Yanhee project was approved on Mary 30, 1951, and hence the design began in 1952, followed by the construction itself. Three years after the Foundation Stone Laying Ceremony on June 24, 1961, the dam and the two initial hydropower generating units were completed.

The dam is a concrete arch-gravity structure (see Photos 1 and 2), 154m in height, with the crest elevation at 261m (MSL). The reservoir maximum water level is 260m (MSL). The storage capacity is 13,462MCM. The spillway consists of two tunnels; each with two radial gates. The maximum discharge capacity is 6,000CMS. The lower reservoir for Hydro Unit 8 has a storage capacity of 4.92MCM. The reservoir is equipped with an open channel chute spillway, having a crest elevation at 140.25m (MSL) with ten radial gates and a maximum discharge capacity of 3,842CMS.

2.1 *Augmentation of Bhumibol hydro units*

The provisions for adding six generating units were in place when the initial project was completed. Sverdrup & Parcel was involved in designing and construction of the Bhumibol dam for the Yanhee Electricity Authority, which was absorbed into the EGAT in 1969. In February 1966, four generating units of 70MW capacity were installed and were brought on-line between 1968 and 1969. In keeping with the increasing demand, Hydro Unit 7 with an installed capacity of 115MW was completed in 1979 and officially placed in operation in 1982. Still another, Hydro Unit 8, a reversible pumped turbine, with an installed capacity of 171MW was finally brought online in 1998 after EGAT constructed the Lower Mae Ping Concrete Barrage downstream of the Bhumibol

[2] Association of South East Asia Nations (Brunei Darussalam, Indonesia, Malaysia, the Philippines, Singapore and Thailand).

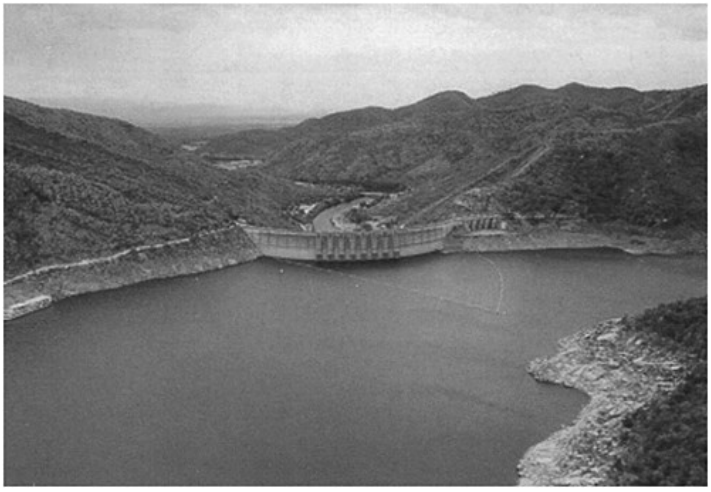

Photo 1. Bhumibol Dam upstream view.

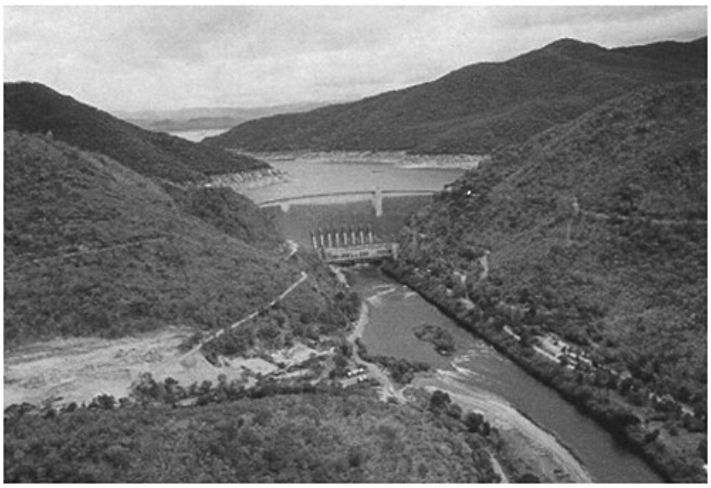

Photo 2. Bhumibol Dam downstream view.

Dam. In the meantime, EGAT renovated the first two hydro units and increased their generating capacity to 75.3MW each. Thus, a total ultimate capacity of 720MW was reached. Bhumibol Hydro Power Plant won the Prime Minister's Award 1997 for the Best Industrial Plant (Modern Safety Management Category).

Table 1. Investment costs (Million Baht).

Installation	Foreign exchange	Local currency	Total
Dam & Units 1–2	1,335	941	2,276
Units 3–4	101	48	149
Units 5–6	–	81	81
Unit 7	318	92	410
Unit 8	N/A	N/A	N/A
Total	1,754	1,162	2,916
(%)	(60)	(40)	(100)

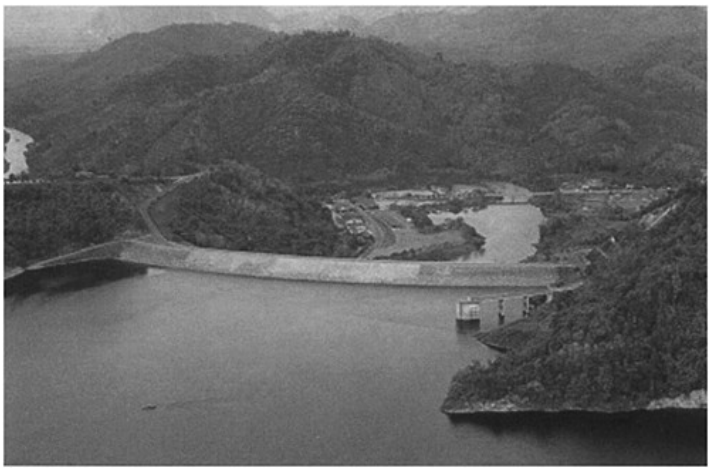

Photo 3. Bang Lang Dam upstream view.

2.2 *Investment on Bhumibol Dam*

The total investment cost of Bhumibol Dam and the Hydro Power Plant was 2,916 Million Baht, which is categorized in Table 1.

3 BANG LANG DAM (a.k.a. PATTANI DAM) AND ITS HYDRO POWER PLANT

The Bang Lang Dam is the first multipurpose dam in the southern region of Thailand, located in the Bang Lang Sata District, Yala Province, bordering Malaysia to the south, approximately 800km south of Bangkok. The dam and the power plant were constructed under the Pattani Project, since its location was right on the Pattani River. Sverdrup & Parcel was retained by the EGAT for the design of the project in early 1970's. The project construction began in 1977 and completed in November 1981. The project consisted of the following: construction of a rockfill dam, construction of a power plant with three generating units including power transmission and the resettlement of inhabitants living in the reservoir area. Since the completion of the project, Thailand has received numerous benefits, such as power, irrigation, flood mitigation, fishery and recreation.

The Bang Lang Dam (see Photos 3 and 4) is a rockfill dam with impervious center core is 85m high with the crest elevation at 120m (MSL). The maximum flood water level is at 117.5m

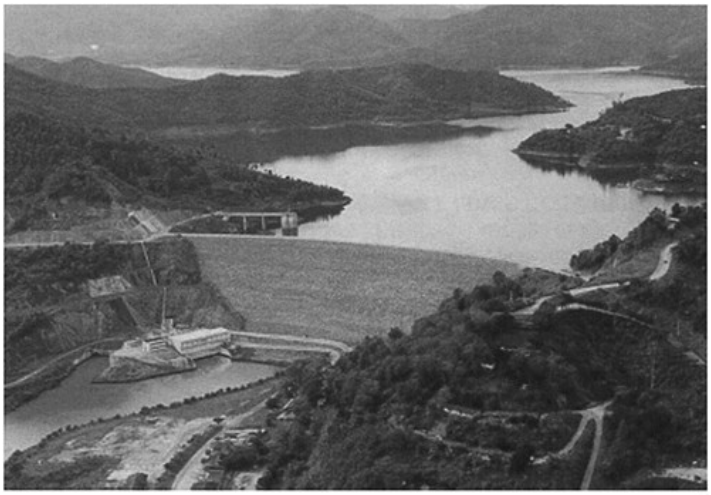

Photo 4. Bang Lang Dam downstream view.

(MSL). The effective storage at normal high water is 1,143.8MCM. The power plant is a reinforced concrete building, which houses three hydro generating units each with an installed capacity of 24MW.

A mini hydro project was implemented at Ban Santi, comprising the construction of a concrete weir and the installation of a 1.275MW generating unit. The project was completed with the power plant on-line in November 1982, yielding an annual energy of 6GWh. The total annual power generation of the Pattani Project includes both hydro installations is 200GWh.

3.1 *Investment of Bang Lang (Pattani) Dam*

The project expenditure was $133.13 Million where $86.52 Million (65%) was local currency and $46.61 Million (35%) in foreign currency. Of the $46.61 Million, the World Bank financed $34.39 Million.

4 ENVIRONMENTAL RESPONSIBILITY

The year 2002 marked the 10th anniversary of the United Nations Conference on Environment and Development, or the Earth Summit, which was held in Rio de Janeiro in 1992. At the Conference, the international community subscribed to the definition of sustainable development resulting from the World Commission on Environment and Development in Stockholm in 1972. The common theme of sustainable development, which combines the economic, social and environmental dimensions of development has been widely recognized and integrated into EGAT's social and economic development strategic plans: (1) Improve the efficient use of natural energy resources, (2) Foster and maximize electricity generation from renewable and alternative energy, (3) Adopt advanced, cleaner and more efficient fossil fuel technologies for new power plants and improve efficiency of existing power facilities to reduce primary fuel consumption and greenhouse gas emissions, (4) Implement demand side management to promote energy efficiency and conservation, and (5) Develop power generation sources that are appropriate to local social and

economic conditions and promote participation and effective involvement of local communities and organizations and other relevant stakeholders in business decision-making processes and practices to achieve mutual benefits and sustainable development.

In addition EGAT also focuses on instilling permanent public awareness of energy efficiency and energy conservation. To that end, in "green" learning room program will be further expanded to cover 145 additional schools across the country by the year 2006.

5 DEMAND SIDE MANAGEMENT

Aside from electricity generation and transmission, EGAT is embracing the demand side management, or DSM, in planning power development. Therefore, it does not rely solely on the supply-side management. The demand-side option has also been taken into account so as to ensure the efficient use of energy resources. The reason for this consideration is due to the fact that the available energy resources can be depleted and their ultimate utilization sometimes can cause environmental concerns, such as carbon dioxide emission. In addition, the investment in new power projects is an expensive proposition especially for Thailand because it will depend mostly on foreign loans. At EGAT, DSM is considered to be a new source of electricity supply, which has a potential to greatly reduce electricity consumption by enhancing the end-users' awareness in energy efficiency and energy conservation. EGAT was entrusted by the Thai Government to be responsible for DSM in cooperation with other energy-related agencies.

Implementation since 1992, EGAT's DSM programs have proven a real achievement in potential peak load reductions and energy savings. It was estimated that the cumulative peak demand reductions of 735.7MW, energy savings of 4,163.8GWh and emissions reductions of 3.08 million tons of carbon dioxide have been achieved. Despite the high investment cost the project has proven to be worthwhile, considering the economic and socio-environmental benefits. To ensure the sustained success of its DSM efforts, EGAT has formulated a master plan for the second phase DSM program for 2002–2006. This plan sets further targets of 632MW of peak load reductions and 2,508GKh of energy savings to be achieved through its DSM program for residential, commercial and industrial sectors. According to the program monitoring and evaluations, both initiated in prior years and existing ones, these goals have already been attained ahead of the schedule in 2002, e.g., the accumulative peak demand reductions of 735.70MW, energy savings of 4,163.80GWh and emissions reductions of 3.08 million tons of carbon dioxide.

6 SOCIAL RESPONSIBILITY

Social responsibility is an integral part of EGAT's operations. It is committed to conducting business in a responsible way that respects ethical values, people, communities and the environment. In March 2002, EGAT issued its People Policy reaffirming its resolve to the public and society; it strives to develop and nurture collaborative relationships, which are built on mutual understanding and respect with the local communities and society. In order to encourage public participation in its project development, EGAT has created partnerships with public and private agencies, communities and all groups or civil society in a wide variety of social development activities with a view to enhancing the quality of life of the Thai people.

7 EGAT'S HISTORIC INSTALLED POWER PLANT CAPACITY

Apart from its own capacity, EGAT also purchases electricity from other power producers, Independent Power Producers (IPPs), Small Power Producers (SPPs), and power utilities of Lao PDR and Malaysia. A mini hydro power plant of the Department of Energy Development and Promotion (DEDP) is also connected to EGAT power system.

Table 2. Installed capacity[3] (MW).

Plant type	Fiscal year 1962	1970	1980	1997	2000	2002
Hydro	–	451.2	1,269.2	2,873.67	2,879.97	2,886.27
Thermal	135.0	327.5	1,777.5	6,517.50	7,962.50	6,255.00
Combined cycle*	–	–	–	4,392.60	5,534.60	5,074.60
Gas turbine	–	150.0	165.0	886.00	656.00	778.00
Diesel	43.4	41.0	34.6	16.60	6.00	6.00
Alternate (Wind, Solar and Geothermal)	–	–	–	0.53	0.53	0.53
IPP	–	–	–	2,056.00	3,456.00	6,346.00
SPP	–	–	–	224.00	1,433.40	1,768.40
Khiridham Hydro**	–	–	–	12.70	–	–
Neighboring power sources	–	–	–	–	340.00	640.00
Grand total	178.4	969.7	3,246.30	16,979.60	22,269.00	23,754.80

* Unlike a conventional gas turbine power plant, hot exhaust gas from the combustion turbine is used to raise steam in heat recovery steam generators without added fuel. Steam is then fed to drive the steam turbine generator to produce electricity.
** Construction being delayed.

The above Table 2 gives a picture of the plant composition over the last 35 years.

8 HYDROPOWER FROM NEIGHBORING COUNTRIES

As recent as in May 1998, EGAT opened a high-voltage power station in Sakon Nakhon to receive electricity from the Thuen Hinboun Hydropower Project in Laos. Thuen Hinboun is the first of ten Laotian power generation projects under development to export electricity to Thailand. The Yunnan Province of China has 22,240MW of hydropower potential. EGAT will purchase the power of 1,500MW from the Jinghong Project located in Yunnan Province, China. Myanmar hydropower resources are also considerable, particularly in the Salween River basin adjacent to Thailand's border—eight projects totaling 6,400MW capacity have been identified. The power exchange with Malaysia presently at 80 to 100MW levels via the interconnection system comprises 115/132kV-circuit line. Cambodia and Vietnam also have significant hydropower resources, which can be jointly developed for export to Thailand.

9 FUTURE ELECTRICITY SUPPLY OPTIONS

Thailand has the following 13 sources for supplying electricity: hydropower, domestic natural gas, imported natural gas, import LNG, oil, imported orimulsion, domestic lignite, imported coal, new renewable energies, imported electricity, demand side management[4], nuclear power, purchase of electricity from the Independent Power Producers (IPP). Thailand has a total exploitable hydropower potential of about 7000MW, which can produce about 18,5000GWh of energy annually. Besides, there is additional potential from pumped storage schemes of about 6,000MW. Up to March 1996, only 3,874MW (28%) of the total potential had been harnessed—a total installed

[3] Personal communication with Uthai Songtis, EGAT.

[4] Generally the power saved from the Demand Side Management would not be considered to be a new power source.

capacity of 2,874MW has been in operation. Of this capacity, 531MW belongs to pumped storage installations. And, 1,000MW of pumped storage capacity is under construction. The remaining potential is environmentally difficult to exploit. Therefore, any further development of hydropower sources will be limited to a few of the most economically and environmentally sound projects. Pumped storage projects will be the most competitive option to peak gas turbine in the future.

EGAT has continually pursued the development of renewable energy as well as new energy technology. It has also maintained close collaborations with local and foreign agencies in several research and development programs to develop alternative energy sources, which are environmentally friendly, in order to reduce and substitute for fossil fuels used in power generation. Here are two examples: (1) A 534MW power station comprising a 42KW from photovoltaic power stations including one PV and two grid-connected PV hybrid stations in Chiang Mai, Sa Kaeo and Phuket provinces, 300KW from Fang geothermal power plant in Chiang Mai, and 192KW from wind turbines in Phuket province; (2) A 20MW rice husk fuelled power plants in Pichit, Nakhon Pathom, Nakhon Sawan and Singburi Provinces.

10 REGIONAL SHARING OF POWER

The history of the development of a South East Asian power grid can be traced back to a 1966 agreement between Laos and Thailand. Other milestones include the signing of power exchange agreement between Thailand and Malaysia, Malaysia and Singapore in 1978, and the establishment of ASEAN Task Force in 1981 involving heads of all ASEAN power utilities and authorities.

In 1992, the six countries in the Great Mekong-Subregion (GMS) which include Cambodia, the People's Republic of China, Lao People's Democratic Republic, Myanmar, Thailand, and Vietnam began deliberating ways of coordinating infrastructure investment, and various social and economic activities to strengthen their competitive position and growth prospects. One of the major activities was the conduct of studies in energy sector. With the exception of Thailand, Vietnam and Yunnan Province of China the degree of electrification in the GMS is generally low. Even with this obstacle many projects are considered to be meaningful, and perhaps the quickest and lowest cost options to electrify remote areas located closed to the power grid of neighboring countries. Many examples exist in Lao PDR, importing power from Thailand at mostly the 22kV voltage level. A project interconnecting to Vietnam also exists. More possibilities for interconnection exist, and several projects are planned to import power into Lao PDR from Thailand, Yunnan and Vietnam, and to import power to Cambodia from Laos and possibly to or from Vietnam. The ASEAN grid and the Asean-Indochina grid, if accomplished, will be a breakthrough in the regional cooperation for the betterment of the electric supply industry. But the geographical setting and financial problems will remain the major hindrance to the success of the projects.

11 PRIVATIZATION

In the recent past, EGAT has undergone numerous organizational changes for its privatization scheme endorsed by the Government. The enactment of EGAT Act of 1992 has liberated EGAT to become a business entity. The first subsidiary was then established and registered in the Stock Exchange of Thailand (SET). After being approved as "Good State Enterprise" in 1994, EGAT was allowed greater autonomy in its operation and management. In 1996, EGAT requested that the Government change its status from being wholly privatized to one that could set up subsidiary companies, which will eventually be privatized, and registered on the SET. Their shares will be sold to public when the privatization is eventually completed.

Since the financial crisis began in July 1997, the neighboring countries have had every reason to send in their support. The International Monetary Fund (IMF) by far is the most influential—not only does it provide the necessary funds on a timely manner, it also demands that the Government do certain things in order to ensure the success of the bailout package. For example, one of the requirements is to privatize the major state-owned enterprises (SOEs) in order to reduce Government's burden of subsidies as well as loan guarantees. EGAT is one of the major SOE's considered to be privatized. Since EGAT was already being re-organized for this purpose, IMF's mandate only accelerates the privatization process. Although there was initial resistance from the EGAT workers, the privatization plan is expected to succeed.

12 REPERCUSSIONS FROM THE ECONOMIC DOWNTURN AT THE END OF THE 20TH CENTURY

The country's economic downtown in 1997 had strong and widespread repercussions in most economic sectors, particularly industries, business and services. In response to the changing situations in power demand, EGAT's power development plan was revised to avoid an excessively high system reserve margin and over-investment in the power industry. Those projects which are affected by this decision are as follows: (1) the installation of 3 thermal units—delayed to 2004/2005, (2) Khiridham pumped storage project—put off until 2006, (3) a new round of power purchase from IPP—delayed until 1999, (4) power purchase from Laos hydropower is postponed to 2006.

As the economy continues to recover, in fiscal year 2000 alone, following power plants have been installed: (1) Ratchaburi thermal plant, two units, 735MW each; (2) Two 230MW gas turbine units of Ratchaburi combined cycle Block 1; (3) Lan Krabu's 14MW gas turbine power plant, and (4) Bhumibol hydro Unit 5 upgraded from 70MW to 76.3MW each.

13 CONCLUSION

Hydropower has played an important role in Thailand and will continue to do so in Thailand. There are alternative sources of energy, which have been effectively brought into the distribution system. However, the primary source of energy will continue to be hydropower and natural gas for many years to come. Hydropower being a renewable energy source has a definitive advantage over other primary or alternative sources of energy. Additional hydropower could be extracted from the existing hydropower by upgrading the turbine/generator facilities; Bhumibol is an example. Mini hydro and pumped storage projects will be encouraged, as the hydropower could be further explored when the environmental and social impacts are carefully considered. The enormous power demand of Thailand will require import from neighboring countries. The import energy has been primarily fueled by natural gas, which was recently found in the region. The potential and momentum of hydropower development in the neighboring countries cannot be ignored. There are plenty of water resources in these neighboring countries as well as in China for hydropower development. Though Thailand does not share borders with China, China's immense hydropower based energy could someday be imported across the international borders via Laos. Since these countries also recognize the importance of preserving nature and enhancing the ecosystem, hydropower becomes a natural source of electricity generation. Like other power source development, the hydro projects considered the direct, indirect, tangible and intangible benefits when they were being considered. For example, the added benefit of water supply from the Sirikit and Bhumibol multi-purpose projects cannot be provided by the other power sources. Given the slim possibility of developing large water resources projects, the pumped storage hydro projects will go on unabated as a champion of providing the peaking power, which is the necessary ingredient in providing the reliable power supply. The neighboring countries, e.g., Malaysia, Laos, Myanmar, Vietnam, Cambodia and China will continue to develop hydropower and become the sources for import to Thailand, although these countries may face the similar constraints in developing water resources in the near future. In addition, the dialogs among the Asean energy ministers will continue to keep the strategic long-term energy projects moving despite a year of the most recent economic turmoil.

The hydro projects have been financed with 40 per cent foreign funds and 60 per cent local currencies. When the privatization process is completed the future power plants will have to be totally financed by private funds, like every other private industry. The new power projects will eventually be undertaken by IPP and SPP, and EGAT will purchase this new power from them. But, EGAT still has the sole responsibility to transmit the power to the local distribution centers.

ACKNOWLEDGEMENTS

The author would like to thank M.L.Chanaphun Kridakom, former Assistant Governor—Hydro Plant for his encouragement in writing this paper, and to Uthai Songtis, Director of System Control and Operation Division, for providing the plant capacity for the power plants. Special thanks are due to Dusdee Sungkhasuwan, Director of Srinagarind Plant (former Director of Bhumibol Plant), for sharing with us, in particular, the power plant upgrade of the Bhumibol Dam, and to two other EGAT personnel—Obhas Chanpayom, former General Manager Construction, and Kittivatana Sucharitpongse, former Project Manager of the Bang Lang (Pattani) Dam—for their kind assistance in preparing this paper. The author also wishes to acknowledge his former colleagues at Sverdrup & Parcel for their arduous work on these projects.

REFERENCES

[1] Koomchoak Biyaem, “Thailand electricity Review,” March 1997.
[2] Annual Report, Electricity Generating Authority of Thailand, March 1997.
[3] Koomchoak Biyaem, “ASEAN Power Grid Development and Business Opportunities,” May 1998.
[4] EGAT Annual Reports 2000, 2001, 2002.

New Developments in Dam Engineering—Wieland, Ren & Tan (eds),
© 2004 Taylor & Francis Group, London, ISBN 04 1536 240 7

Three-dimensional viscoelastic finite element analysis of large underground powerhouse

Guorong Chen
Engineering Mechanics Department, Hohai University, Nanjing, China

Rongmei Jiang
Longtan Hydroelectric Project Co. Ltd., Changsha, China

Xuming Zhang & Shuping Huang
Engineering Mechanics Department, Hohai University, Nanjing, China

ABSTRACT: A three-dimensional viscoelastic finite element analysis is conducted on **Longtan** underground caves, adopting the Kelvin and 3-parameter viscoelasticity model with tandem spring components. The calculation results demonstrate: the surrounding rock of **Longtan** underground caves has distinct rheological properties; the rheological displacement accounts for a comparatively high proportion of the total shift, about 46%; the rheological stabilization time is about 240 days; during the early stage of excavation, the rheological deformation, which constitutes 45% of the total displacement in the initial 30 days and 75% in the preliminary 70 days, is quite obvious; the displacement increases slowly afterwards and tends to become steady in the main 240 days later. This proves that it is appropriate to conduct support between 30 to 50 days after completing excavation to enable the surrounding rock and the support body to bear 50% of the rheological displacement respectively, thus giving full play to the rock's inherent stability and making the support body be optimized and reliable. It is suggested that support should be conducted about 40 days after excavation, which provides scientific basis for support design.

1 INTRODUCTION

Longtan hydroelectric project is one of the ten symbolic projects and one of the strategic projects of "transmitting electricity from west to east" of the country's Western Development. The development and construction of the project will play an important role in satisfying the increasing demand for electricity in Guangdong and Guangxi, optimizing the supply source and electric power structures in south China, reducing the flood threat to the Red River's lower reaches and West River's banks, promoting the overall economic and social development of the minority nationalities in Guangxi and Guizhou.

Longtan hydroelectric project is located in Tian'er county at the Red River's lower reaches, 15 kilometers from Tian'er county town. The drainage area above the dam site is 98,500 square kilometers, accounting for 71% of the river's drainage area. The total installed capacity is 35–40% of the possible exploitation capacity of the Red River, only next to the huge Three-gorge hydroelectric project on the Yangtze River. The planned total installed capacity of Longtan hydroelectric project is 5.4 million kilowatts. With nine hydroelectric 0.6-million-kilowatt generating sets, the annual generated energy is 18.7 billion kilowatt hours. The normal water storage level of corresponding reservoirs is 400 meters. The total storage capacity is 27.3 billion cubic meters and the flood control storage is 7 billion cubic meters. The underground electric power generation powerhouse of Longtan project is the largest in the world (388.5 meters long, 28.5 meters wide and 74.5 meters high).

2 VISCOELASTICITY MODEL AND COMPUTING PRINCIPLE OF ROCK MASS

2.1 *Mechanics analysis model*

The mechanics model is the basis of computational analysis. A lot of engineering practice demonstrates that rock mass and concrete material has distinct rheological properties under sustained stress. There are basically two viscoelasticity models describing rock mass rheological properties: the Kelvin and the Maxwell models. An inversion analysis is conducted on Longtan underground caves surrounding rock rheological model, using the displacement observation data in four time slots of Longtan exploratory cave's six measured sections and the displacement observation material of Longtan underground powerhouse model cave. First a general expression is set up of rock mass rheological model; then an error fitting analysis is done, comparing the predicted result of the model with the measured value of cave displacement, to establish the target function of the error fitting. The inversion analysis shows the cave surrounding rock fits the three-parameter standard linear rheological model. Moreover, it can be seen from the measured displacement process curve that Longtan rock mass has distinct rheological properties and the deformation finally tends to become steady (see Figure 1). This paper adopts the Kelvin and the spring component series three-parameter viscoelasticity models based on the fact that the deformation properties are close to the three-parameter viscoelasticity model (see Figure 2). This model, a stable one, has complete rheological properties and is able to reflect instantaneous elasticity, creep and relaxation.

The rheological parameters are obtained from the three-parameter model, employing the test model cave's measured data and the rheological model's identification principle and method.

E0=9.49E+3 (MPa), E1=8.228E+3 (MPa), η=8.786E+5(MPa·d)

2.2 *Basic theory of viscoelastic rock mass*

Viscoelastic material's total strain is the addition of elastic strain and viscous strain; it can be shown as

$\varepsilon=\varepsilon^{e}+\varepsilon^{v}$

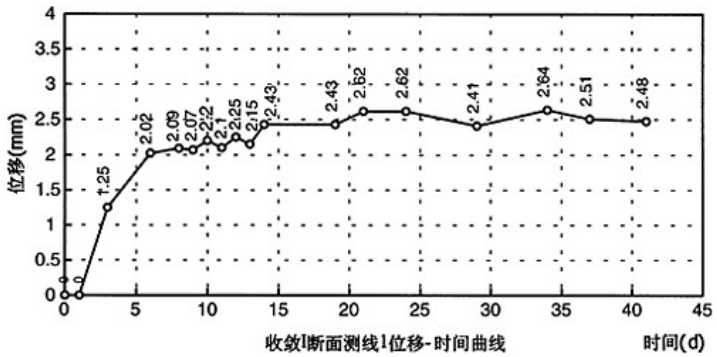

Figure 1. Measured displacement process curve of Longtan rock mass test model cave.

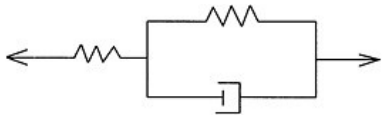

Figure 2. Viscoelasticity model.

Viscous strain ε^v is defined by the Kelvin model. The stress-strain relation is

$$\dot{\varepsilon}^v + \frac{E_1}{\eta}\varepsilon^v = \frac{1}{\eta}\sigma$$

When stress is a constant, the integral result of the above equation is:

$$\varepsilon^v = \frac{\sigma}{E_1}(1 - e^{-\frac{E_1}{\eta}t})$$

When stress changes with time, divide the process into several time slots and suppose stress increment is a constant in every time slot. Given that at τ moment the received stress increment $\Delta\sigma=\Delta\sigma(\tau)$, the total strain after duration $t-\tau$ is:

$\Delta\varepsilon=\Delta\varepsilon^e+\Delta\varepsilon^v$

$\Delta\varepsilon^e$ is instantaneous elasticity strain.

$$\Delta\varepsilon^e = \frac{\Delta\sigma}{E}$$

$\Delta\varepsilon^v$ is viscous strain:

$$\Delta\varepsilon^v = \Delta\sigma\frac{1}{E_1}(1 - e^{-\frac{E_1}{\eta}(t-\tau)}) = \Delta\sigma c(t,\tau)$$

C (t, τ) in form is equal to concrete material's creep degree, that is, the viscous strain under unit stress.

$$c(t,\tau) = \frac{1}{E_1}(1 - e^{-\frac{E_1}{\eta}(t-\tau)})$$

Under continuous changing stress, the process can be divided into several time slots. At t moment the creep strain is the superimposition of the creep strain caused by the stress increment in each time slot.

In Δt_n time slot, the strain increment caused by the stress is:

$$\Delta\varepsilon_n^v = \varepsilon^v(t_n) - \varepsilon^v(t_{n-1}) = \int_{t_{n-1}}^{t_n} c(t,\tau)\frac{d\sigma}{d\tau}d\tau$$
$$\approx c(t,t_n)\Delta\sigma_n$$

The recursion formula is obtained after derivation.

$$\begin{aligned}\Delta\varepsilon_n^v &= \omega_n\left(1 - e^{-\gamma\Delta t_n}\right)\\ \omega_{n+1} &= \omega_n e^{-\gamma\Delta t_n} + \Delta\sigma_n\phi\\ \omega_1 &= \Delta\sigma_0\phi\end{aligned} \qquad (1)$$

In the formula, $\phi = 1/E1$, γ=E1/η.

2.3 *Finite element alignment of viscoelastic rock mass*

With the incremental method, obtained is the structure equilibrium equation in any time interval Δt of a certain phase:

$$[K]\{\Delta\delta\}=\{\Delta R^{w}\}+\{\Delta R^{v}\} \tag{2}$$

$\{\Delta\delta\}$ is the displacement increment; $\{\Delta R^{w}\}$ is the equivalent nodal load caused by external force; $\{\Delta R^{v}\}$ is the equivalent contact load caused by viscous deformation. They are the superimposition of each unit:

$$\{\Delta R^{w}\}=\sum\{\Delta R^{w}\}^{e}$$
$$\{\Delta R^{v}\}=\sum\{\Delta R^{v}\}^{e}$$

$\{\Delta R^{w}\}^{e}$ is the equivalent nodal load caused by unit external force. $\{\Delta R^{v}\}^{e}$ is the equivalent nodal load caused by unit viscous deformation.

$$\{\Delta R^{w}\}^{e}=\iiint[N]^{T}\{\Delta P\}dv+\iint[N]^{T}\{\Delta\bar{P}\}ds$$

$$\{\Delta R^{v}\}^{e}=\iiint[B]^{T}[D]\{\Delta\varepsilon^{v}\}dv$$

$\{\Delta P\}$ and $\{\Delta\bar{P}\}$ are the unit physical capacity and the unit surface force respectively. $\{\Delta\varepsilon^{v}\}$ is the unit viscous strain increment.

3 COMPUTATIONAL RESULT AND ANALYSIS

In order to study the deformation regularity during construction phase, considering the effects of construction and support procedures on deformation, three computational plans are worked out. (1) One-off excavation is called plan 1; (2) sequence seven-level excavation from top to bottom is called plan 2; (3) general seven-level excavation on reality is called plan 3. Plan 2 is better through computational comparison and analysis of the surrounding rock's deformation and stress state in construction process.

In finite-element computation model, take the eight-node entity isoparametric element as the principal thing; fault uses contact surface element; the rock mass elements excavated are discarded and will not take part in computation. A few 6-node pentahetron transition elements are also used. The whole computational region is subdivided into 44,982 elements, 46,612 nodes altogether. Time interval is 400 days.

3.1 *Surrounding rock deformation analysis*

In order to know surrounding rock flowing deformation pattern, analyze one-off excavation surrounding rock deformation properties first. Figure 4 is the displacement process curve of main factory III section vault.

The displacement process curve shows that surrounding rock's displacement with time is quite obvious, having distinct rheological properties, including instantaneous elastic deformation, accelerated and stable rheological deformation. In addition, rheological displacement accounts for a fairly large proportion of the total shift. Its instantaneous elastic displacement is 1.77cm; the final stable displacement, 3.28cm. The difference between the two, 1.51cm, is the flowing displacement, constituting 46% of the total. The other control points' deformation properties and regularity are basically the same and will not be repeated here. The value of flowing displacement changes with time as shown in Table 1.

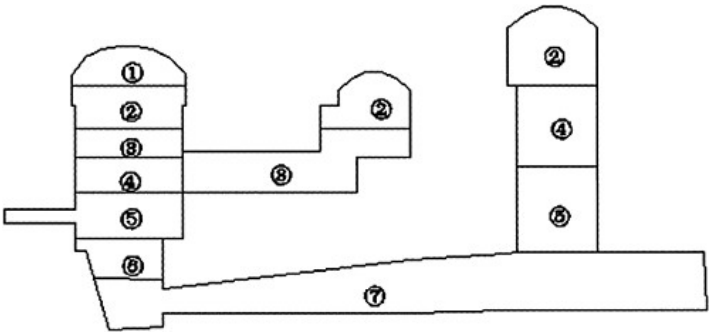

Figure 3. Sketch map of sequence excavation (plan 2).

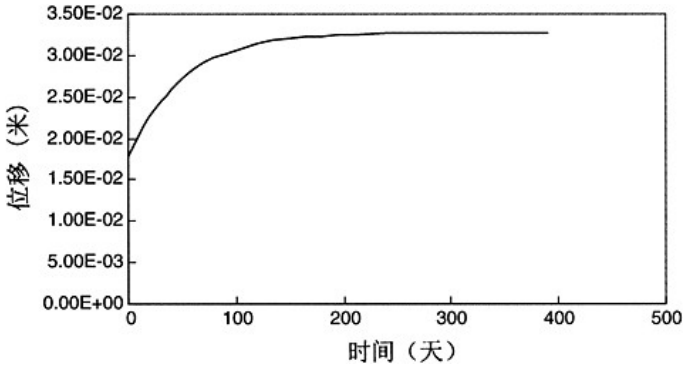

Figure 4. One-off excavation, main factory III section vault displacement process curve.

Table 1. Main factory III section vault's rheological displacement change with time.

Time (day)		0	10	20	30	50	70	90	120	150
Rheological displacement (cm)		0	0.27	0.49	0.68	0.95	1.14	1.26	1.37	1.43
Proportion of total displacement	(1.51) (%)	0	18	32	45	63	75	83	91	95
Time (day)		180	210	240	270	300	330	360	390	∞
Rheological displacement (cm)		1.47	1.49	1.50	1.50	1.50	1.51	1.51	1.51	1.51
Proportion of total displacement	(1.51) (%)	97	99	99	99	99	100	100	100	

It can be seen from the above Table that the final stable rheological shift is 1.51cm; the rheological stabilization time is 240 days or so. Rheological deformation is obvious in the early stage of excavation: it is 0.68cm in the preliminary 30 days, accounting for 45% of the total shift, and 1.14cm in 70 days, constituting 75%. Rheological displacement increases slowly afterwards and tends to become steady in the main after 240 days. This proves it appropriate to conduct support between 30 to 50 days to enable the surrounding rock and the support body to bear 50% of the rheological displacement respectively, thus giving full play to the rock's auto stability and making the

Table 2. Vault displacement comparison of different plans (unit: cm)

		Section III		Section V	
Location	Plan	Rheological displacement	Total displacement	Rheological displacement	Total displacement
Main powerhouse	Plan 1	1.51	3.28	1.91	4.21
	Plan 2	1.24	3.01	1.65	3.95
	Plan 3	1.28	3.05	1.71	4.01
Main transformer room	Plan 1	1.57	3.51	1.94	4.42
	Plan 2	1.20	3.14	1.51	3.99
	Plan 3	1.26	3.20	1.63	4.11
Pressure regulating well	Plan 1	1.54	3.38	2.03	4.47
	Plan 2	1.30	3.14	1.70	4.14
	Plan 3	1.35	3.19	1.84	4.28

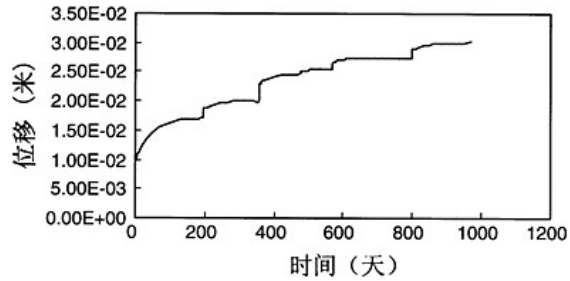

Figure 5. Sequence excavation (plan 2), main factory III section vault displacement process curve.

support body optimized and reliable. Therefore, 40 days is adopted for support time in the following step excavation computation. In other words, support is conducted 40 days after excavation.

3.2 *Plan 2 construction deformation analysis*

Table 2 gives surrounding rock's deformation result and comparison of various construction plans.

The Table shows that the excavation method has certain impact on rheological displacement. Plan 2 (sequence excavation) has the smallest displacement. Main factory vault is 1.65cm. Plan 1 (one-off excavation) has the biggest flowing shift. Main factory vault is 1.91cm. Displacement in plan 3 is 1.71cm, between the other two values. Plan 1's displacement is 16% larger than that of plan 2 and plan 3's displacement is 4% larger than that of plan 2. It shows through comparisons that plan 2's excavation method produces the smallest flowing displacement and is a better scheme.

Figure 5 is plan 2's deformation process curve. The total shift is 3.01, in which rheological shift is 1.24, accounting for 41%.

The computation result shows: the main powerhouse upstream sidewall's displacement is larger than that of the downstream walls, because the excavation of the bus-bar cave and the main transformer room weakens main factory lower massif's rigidity and causes release power resulting in main powerhouse massif's downward deformation, offsetting some of the displacement caused by main powerhouse's release power; the main transformer room's sidewalls' displacement both directs the downstream, deforming as a whole directing the downstream, because the excavation of the pressure regulating well weakens the rigidity of the main transformer room's lower massif

Table 3. Plan 2, each section vault's displacement after second excavation (unit: cm).

Location	Section III			Section V		
	Instantaneous displacement	Rheological displacement	Total displacement	Instantaneous displacement	Rheological displacement	Total displacement
Main powerhouse	1.12	0.89	2.01	1.46	1.15	2.61
Main transformer room	1.03	0.51	1.54	1.17	0.71	1.88
Pressure regulating well	1.44	1.02	2.46	1.60	1.15	2.75

and causes the release power resulting in the main transformer room's lower massif's downward deformation; the displacement of the pressure regulating well's upper wall is larger than that of the downstream wall. Seen from the displacement process curve, surrounding rock's displacement has distinct rhoelogical properties. Various excavation procedures result in different deformation processes. And the final displacement values are distinct.

3.3 *Surrounding rock deformation situation after second level excavation*

The Table 3 shows that the surrounding rock displacement is not very big after the second level excavation. V section's displacement is larger than that of section III. The main factory vault displacement of section V is 2.61cm. The main transformer vault's displacement is 1.88cm. The pressure regulating well vault's shift is 2.75cm. Given that support increases rheological parameters, the displacement of each cave vault are only 2.43cm, 1.78cm and 2.57cm respectively. The corresponding rhoelogical displacement are 0.97cm, 0.61cm and 0.97cm, all under 1cm, which conform to the measured values. In effect mostly rheological shift can be monitored.

3.4 *Surrounding rock stress*

The stress of various cave surrounding rock is mainly compressive stress. Pulling stress occurs chiefly in only a few places of main factory upper sidewall and the bottom of pressure regulating well's lower sidewall, and the value is small. The toroidal compressive stress of the various cave vaults is relatively high. It is also quite clear that stress concentrates at the rendezvous of the main factory's upper sidewall and the bottom, the arch foot of the upper and the lower streams, and the cave's excavated concave angle. Step excavation distinctly reduces the stress concentration phenomenon in local area. Similarly, stress state is better in plan 2. The stress is relatively high around the V section cave. The stress is −22.66Mpa at the arch foot of the pressure regulating well's upper streams and −20.84Mpa at that of the lower streams. The stress is −18.89Mpa at the pressure regulating well vault. The maximum compressive stress is −25.7Mpa, occurring at the upper sidewall of pressure regulating well's upper streams, but only in local area. The stress of both the main powerhouse and the main transformer room is not above −20Mpa.

4 CONCLUSION

(1) The computational results show that the caves' deformation and the stress' distribution accord with mechanics theory. The level of the surrounding rock's stress is not high. The cave's surrounding rock's stress is mainly compressive stress. The tensile stress occurs at the main powerhouse's upstream sidewalls and separate places of the bottom of the pressure regulating well's downstream sidewalls, but the value is small. Step excavation obviously reduces the stress concentration phenomena in local areas. By comparison, the state of deformation and of stress are quite good in plan 2 (sequence excavation from top to bottom). The stress is relatively high around the section V cave. The stress at the pressure regulating well's upstream arch foot

is −22.66Mpa as to the section V (HL0+258.25). It is −20.84Mpa at the downstream. The stress is −18.89Mpa at the pressure regulating well's vault. The maximum stress is −25.7Mpa, occurring at the upper sidewall of the pressure regulating well, but only in local areas. The stress of the main factory and main transformer room are not over 20Mpa.

(2) The surrounding rock has distinct rheological properties and the flowing shift accounts for a large proportion of the total displacement, about 46%. The flowing deformation stabilization time is 240 days or so. During the early stage of excavation, the rheological deformation, which constitutes 45% of the total displacement in the first 30 days and 75% in the preliminary 70 days, is quite obvious; the displacement increases slowly afterwards and tends to become steady in the main 240 days later. This proves it appropriate to conduct support between 30 to 50 days after completing excavation to enable the surrounding rock and the support body to bear 50% of the rheological displacement respectively, thus giving full play to the rock's auto stability and making the support body optimized and reliable. It is suggested that support should be conducted about 40 days after excavation.

(3) After the second level excavation, the displacement is not large around the cave. At the section V, the total shift of the main factory's vault is 2.61cm, 1.88cm of the main transformer room's vault and 2.75cm of the room pressure regulating well's vault. Given the parameter addition caused by support, the total shifts of the rooms' vault are only 2.43cm, 1.78cm and 2.57cm respectively, and corresponding rhoelogical deformation are 0.97cm, 0.61cm and 0.97cm respectively, all under 1cm, which meet the measured values.

REFERENCES

Longtan Plant Area Rock Mass Mechanics Parameter Study Intennediate Result, National Electric Power Company Zhongnan Survey Research Institute, August, 2002.

Zhu Bofang, *Principle and Practice of Infinite Unit Method,* Water Conservancy and Electric Power press, 1998.

Chen Guorong, "Three-dimensional Rock Mass Viscoelasticity Parameter Inverse Analysis", Hohai University Journal, No. 6, 1996.

New Developments in Dam Engineering—Wieland, Ren & Tan (eds),

A combined anchor bar-rock element model and its application to the construction of underground powerhouse

Guorong Chen & Xuming Zhang
Hohai University, P.R. China

Rongmei Jiang
Longtan Hydroelectric Project Co. Ltd., Changsha, China

Shuping Huang
Hohai University, P.R. China

ABSTRACT: The Kelvin model and the 3-parameter viscoelasticity model with tandem spring components are adopted in applying the 3-dimensional viscoelastic finite element method to the analysis of Longtan underground powerhouse. A combined rock element with anchor bar is proposed with which the construction of finite element mesh becomes very easy and the actual arrangement of anchor bars can be modeled accurately because the anchor bar elements or prestressed anchor bar elements do not connect the element nodes necessarily. The computational results show that rheologic displacement is confined by the support obviously and the descent of the rheologic displacement is about 16%. When the second layer is excavated 4 anchor bars, which are located at the left side of the top arch in the sidewall of the main powerhouse, are overstressed and the maximum value of stress is equal to or greater than 350MPa. When the last excavation is completed there exists some anchor bars in every chamber, which are overstressed and most of them are in the left abutment and sidewall. It is suggested that proper increase of anchor bars is needed for a good many of anchor bars are overstressed.

1 INTRODUCTION

Longtan water conservancy project is located in Tianer county. The dam site is situated in downstream of Red River, 15km from the town of Tianer county. Basin area from the upstream to the dam site is about 98500km^2 which accounts for about 71% of the total basin area of Red River. The proportion of total installation of generating capacity of Longtan project is about 40% of the capacity of Red River. It is a very large scale water conservancy project which is only smaller than the Three Gorges Project in Yangtze River (Changjiang River). The total installation of generating capacity 5.40MW, with an average annual output of 18.7TW · h. The normal water height is 400m. The total storage capacity of the reservoir is 273 million m^3 and the flood control storage capacity is 70 million m^3. The underground powerhouse of Longtan project is the largest one all over the world with length 388.5m, width 28.5m and height 74.5m. The procedure of construction and the determination of parameters of support play a key roll in construction.

A combined anchor bar-rock element is implemented to model the support of the anchor bars to the surrounding rock. With this element it is allowed to position the anchor bar arbitrarily in rock element so that the arrangement of anchor bars can be simulated accurately.

2 COMBINED ANCHOR BAR-ROCK ELEMENT AND MODELING OF CHAMBER SUPPORT

2.1 *Combined anchor bar-rock element*

The combined anchor bar-rock element is proposed to simulate the arrangement of anchor bars accurately. The element allows anchor bar to be positioned arbitrarily in rock element and integrates two materials, reinforcement and rock, into a single element. The stiffness matrix of the combined element is determined by assembling the rock and steel element, i.e.

$$[k] = [k_y] + [k_g]$$

where $[k]$ is the element stiffness matrix of rock element with anchor bar while $[k_y]$ is rock element stiffness matrix and $[k_g]$ is element stiffness matrix of anchor bar.

A anchor bar element, the numbers of its nodes are *i* and *j,* is combined with a rock element, as shown in Figure 1. The local coordinate system (x', y', z') is established along the longitudinal direction of anchor bar x'. The transformation matrix from local to global coordinate system (x, y, z) is

$$[T] = \begin{bmatrix} \alpha_{1'1} & \alpha_{1'2} & \alpha_{1'3} \\ \alpha_{2'1} & \alpha_{2'2} & \alpha_{2'3} \\ \alpha_{3'1} & \alpha_{3'2} & \alpha_{3'3} \end{bmatrix}$$

where $\alpha_{i'j} = \cos(x'_i, x_j)$

The strain matrix in global coordinate system is

$$[g] = \begin{bmatrix} \frac{\partial u}{\partial x} & \frac{\partial v}{\partial x} & \frac{\partial w}{\partial x} \\ \frac{\partial u}{\partial y} & \frac{\partial v}{\partial y} & \frac{\partial w}{\partial y} \\ \frac{\partial u}{\partial z} & \frac{\partial v}{\partial z} & \frac{\partial w}{\partial z} \end{bmatrix} = \begin{bmatrix} \frac{\partial N_1}{\partial x} & \Lambda & \frac{\partial N_8}{\partial x} \\ \frac{\partial N_1}{\partial y} & \Lambda & \frac{\partial N_8}{\partial y} \\ \frac{\partial N_1}{\partial z} & \Lambda & \frac{\partial N_8}{\partial z} \end{bmatrix} \begin{bmatrix} u_1 & v_1 & w_1 \\ \mathrm{M} & \mathrm{M} & \mathrm{M} \\ u_8 & v_8 & w_8 \end{bmatrix}$$

$$[g'] = \begin{bmatrix} \frac{\partial u'}{\partial x'} & \frac{\partial v'}{\partial x'} & \frac{\partial w'}{\partial x'} \\ \frac{\partial u'}{\partial y'} & \frac{\partial v'}{\partial y'} & \frac{\partial w'}{\partial y'} \\ \frac{\partial u'}{\partial z'} & \frac{\partial v'}{\partial z'} & \frac{\partial w'}{\partial z'} \end{bmatrix} = [T][g][T]^{\mathrm{T}}$$

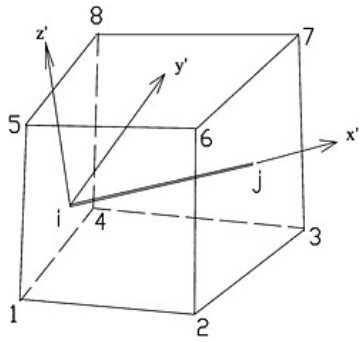

Figure 1. Combined anchor bar-rock element.

The axial strain of anchor bar element is

$$\varepsilon = \begin{bmatrix} l & m & n \end{bmatrix} \begin{bmatrix} l\frac{\partial}{\partial x} & m\frac{\partial}{\partial x} & n\frac{\partial}{\partial x} \\ l\frac{\partial}{\partial y} & m\frac{\partial}{\partial y} & n\frac{\partial}{\partial y} \\ l\frac{\partial}{\partial z} & m\frac{\partial}{\partial z} & n\frac{\partial}{\partial z} \end{bmatrix} \begin{Bmatrix} u \\ v \\ w \end{Bmatrix}$$

$$= \begin{bmatrix} l & m & n \end{bmatrix} \begin{bmatrix} l\frac{\partial N_1}{\partial x} & m\frac{\partial N_1}{\partial x} & n\frac{\partial N_1}{\partial x} & \Lambda & \Lambda \\ l\frac{\partial N_1}{\partial y} & m\frac{\partial N_1}{\partial y} & n\frac{\partial N_1}{\partial y} & \Lambda & \Lambda \\ l\frac{\partial N_1}{\partial z} & m\frac{\partial N_1}{\partial z} & n\frac{\partial N_1}{\partial z} & \Lambda & \Lambda \end{bmatrix} \{\delta\}^e$$

$$= [B]\{\delta\}^e$$

Matrix *[B]* is

$$[B] = \left[\left(l^2\frac{\partial N_1}{\partial x} + lm\frac{\partial N_1}{\partial y} + \ln\frac{\partial N_1}{\partial z}\right) \left(ml\frac{\partial N_1}{\partial x} + m^2\frac{\partial N_1}{\partial y} + mn\frac{\partial N_1}{\partial z}\right) \left(nl\frac{\partial N_1}{\partial x} + nm\frac{\partial N_1}{\partial y} + n^2\frac{\partial N_1}{\partial z}\right) \ \Lambda \right]$$

where *l, m, n* are direction cosines, i.e. the elements in first line of matrix *[T]*. Thus, the additional stiffness matrix of anchor bar element is

$$[k_g] = \int_{-1}^{1} [B]^T AE[B]hd\xi'$$

where

$$h = \sqrt{\left(\frac{\partial x}{\partial \xi'}\right)^2 + \left(\frac{\partial y}{\partial \xi'}\right)^2 + \left(\frac{\partial z}{\partial \xi'}\right)^2}$$

and A, E are area and modulus of elasticity respectively. ξ' is the local coordinate along the longitudinal direction of anchor bar.

2.2 *Design parameters of support and computational model*

The supports of Longtan underground powerhouse are sprayed concrete, anchor bars (including prestressed anchor bars) and anchor lines. The diameters of three types of anchor bars are Φ25, Φ28, Φ32. The length of anchor bars varies from 4500mm to 9500mm.The space length takes 1500×1500mm and 3000×300mm.The diameter of prestressed anchor bars is only Φ32,The length of prestressed anchor bars are 8000mm and 9500mm. The space length takes 1500×1500mm and 3000×3000mm. The prestress are 150KN and 200KN.There are four types of prestressed anchor lines. They are: (2000KN, 20m, 4500×6000mm), (1200KN, L=32m, 3000×3000mm), (1200KN, L=20m, 4500×4500mm), (1200KN, L=20m, 4500× 6000mm), (prestress, length, space length).

Employing combined anchor bar-rock element, anchor bars can be positioned arbitrarily in rock element. So when considering anchor bars there is no restriction in construction FE mesh and the

Figure 2. The arrangement of anchor bars.

arrangement of anchor bars can be simulated accurately. However, the total number of anchor bars is very great. In computational model, the space length is doubled to reduce the total number to a half by enlarging the areas of anchor bars. The arrangement of anchor bars is shown in Figure 2.

The stiffness of anchor bars (including prestressed anchor bars) and prestressed anchor lines are considered. The prestress is simulated by a pair of concentrated forces between sides of two neighboring elements and the prestressing losses of anchor bar elements can also be taken into consideration in this way.

3 COMPUTATIONAL RESULTS AND ANALYSIS

In order to study the deformation behavior in construction period and the effects of considering the construction procedure and the supports themselves to the deformations, three computational plans are drafted. One-off excavation is named plan 1, sequential excavation (7 steps from top to the bottom) plan 2 and multiple step excavation (7 steps according to the simplification) plan 3. Comparison of results show that the states of strain and stress are better adopting plan 2 than that adopting other plans.

3.1 *Analysis of deformation of surrounding rock*

In order to investigate the rheologic properties of surrounding rock, the deformation behavior of plan one is analyzed. The displacement at the top of arch, section III, of the main powerhouse is shown in Figure 3

The rheologic displacements are listed in the Table 1.

From the Table 1 it is seen that the final stable rheologic displacement is 1.51cm and the time when the rheologic displacement becomes stable is around 240 days. During the early stage of excavation the rheologic displacement, which is 0.68cm and constitutes 45% of the total rheologic displacement in the first 30 days and 1.14cm, 75% in the preliminary 70 days, is quite obvious. The displacement increases slowly afterwards and tends to be stable in about 240 days. It indicates that it is appropriate to conduct support between 30 to 50 days after completing excavation to enable the surrounding rock and the support body to bear 50% of the rheologic deformation respectively. By doing so, the inherent stability can be made full use of and the support body is in optimum and reliable state at the same time. According to this, the support is conducted 40 days after excavation in the following analysis.

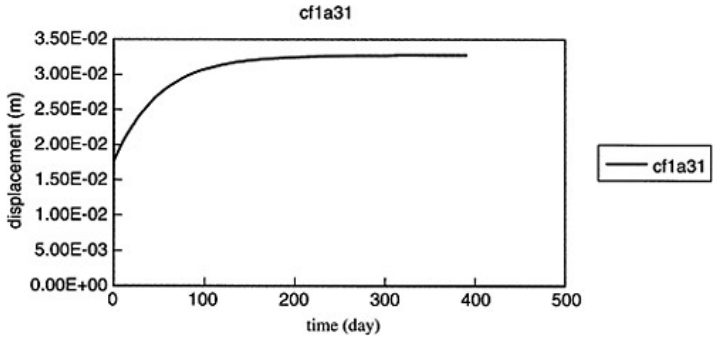

Figure 3. Displacement-time curve of section III at the top of arch, main powerhouse.

Table 1. Displacements of section III at the top of arch, main powerhouse.

Time (day)	Rheologic displacement (cm)	*Displacement 1/displacement 2
0	0	0
10	0.27	18%
20	0.49	32%
30	0.68	45%
50	0.95	63%
70	1.14	75%
90	1.26	83%
120	1.37	91%
150	1.43	95%
180	1.47	97%
210	1.49	99%
240	1.50	99%
270	1.50	99%
300	1.50	99%
330	1.51	100%
360	1.51	100%
390	1.51	100%
∞	1.51	

* Displacement 1 represents the rheologic displacements while displacement 2 the total rheologic displacements (1.51cm).

3.2 *Stresses of anchor bars*

The anchor bar support is conducted 40 days after excavation. When the second layer is excavated stresses of most anchor bars are in normal condition except that 4 of them, which are located at the left side of the top arch in the sidewall of the main powerhouse, are overstressed and the maximum value of stress is equal to or greater than 350 MPa. The position of these overstressed anchor bars are shown in Figure 4. The strength of anchor bars is supposed to be 350MPa.

When the last excavation is completed there exists some anchor bars in every chamber, shown in Figure 5, which are overstressed and most of them are in the left abutment and sidewall.

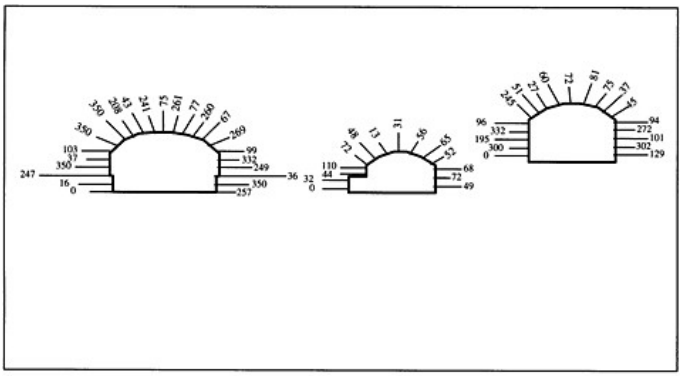

Figure 4. Stresses of anchor bars around chamber, section V, excavation step 2, sequential excavation.

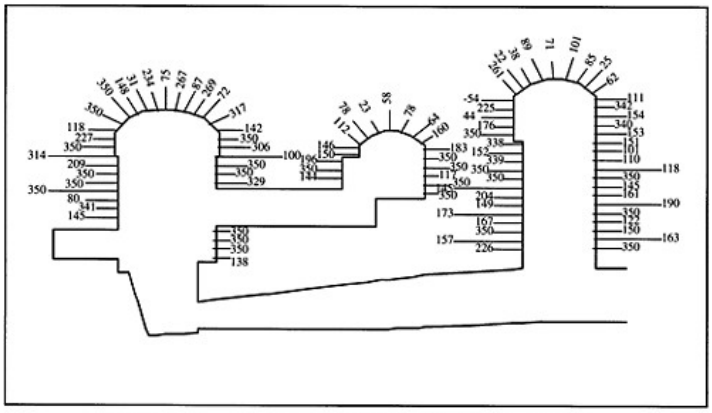

Figure 5. Stresses of anchor bars around chamber, section V, excavation completed, sequential excavation.

3.3 *Effect of anchor bars to the deformations*

Table 2 shows the effect of support body to the deformations and it is seen that rheologic displacements are reduced significantly when support is conducted. The total displacement at the top of arch in section V of the main building is 3.69cm (originally 3.95cm). The rheologic displacement is 1.39cm (originally 1.65cm).The rheologic displacement accounts for a proportion of 37% (originally 46%) and the descent is about 16%. It is obvious that support confines the rheologic displacements.

Table 2. Effect of support body to the displacements at the top of arch (cm).

	Section V	
Position	No support	Support
Main building	1.65	1.39
Main transformer room	1.51	1.27
Pressure well	1.70	1.42

4 CONCLUSIONS

4.1 The surrounding rock has distinct rheologic property. The rheologic displacement accounts for a large proportion of about 46%. The rheologic deformation tends to be stable in about 240 days. During the early stage of excavation the rheologic displacement, which constitutes 45% of the total rheologic displacement in the first 30 days and 75% in the preliminary 70 days, is quite obvious. The displacement increases slowly afterwards and tends to be stable in about 240 days. It indicates that it is appropriate to conduct support between 30 to 50 days after completing excavation to enable the surrounding rock and the support body to bear 50% of the rheologic deformation respectively. By doing so, the inherent stability can be made full use of and the support body is in optimum and reliable state at the same time. It is suggested that the support is conducted 40 days after excavation.

4.2 It is obvious that support confines the rheologic displacements and the descent is about 16%. The rheologic displacement at the top of arch in section V of the main building is reduced from 1.65cm to 1.39cm, about 16% descent. The proportion of rheologic displacement in total displacement decreases from 46% to 37%.

4.3 When the second layer is excavated 4 anchor bars, which are located at the left side of the top arch in the sidewall of the main powerhouse, are overstressed and the maximum value of stress is equal to or greater than 350MPa. When the last excavation is completed there exists some anchor bars in every chamber, which are overstressed and most of them are in the left abutment and sidewall. It is suggested that proper increase of anchor bars is needed for a good many of anchor bars are overstressed.

REFERENCES

Longtan Plant Area Rock Mass Mechanics Parameter Study Intermediate Result, National Electric Power Company Zhongnan Survey Research Institute, August, 2002.

Zhu Bofang, *Principle and Practice of Infinite Unit Method,* Water Conservancy and Electric Power press, 1998.

Chen Guorong, "Three-dimensional Rock Mass Viscoelasticity Parameter Inverse Analysis", Hohai University Journal, No. 6, 1996.

This page intentionally left blank.

New Developments in Dam Engineering—Wieland, Ren & Tan (eds),
© 2004 Taylor & Francis Group, London, ISBN 04 1536 240 7

Design and construction of impervious system in foundation of Yele embankment dam

Jianchun Chen
Sichuan University, China

ABSTRACT: Yele Dam is the highest embankment dam (125.5m) with asphalt concrete wall in Asia, located in the Nanya River in Sichuan Province south west of China, and is under construction. Due to the complicated geologic condition and high earthquake intensity (VIII), there are a lot of particular difficulties in design and construction of the foundation treatment. Yele Dam is placed on the highly asymmetrical ground bed. Its left abutment is on the quartz diorite, but the main body and the right abutment as well as the right upland plain is on the loam and sandy gravel interbedded strata with the depth of more than 420m.

To control the seepage of the foundation, compositive measurements in design have been adopted. From left to right, the curtain grouting in rock (left grouting gallery), cut-off wall plus lower curtain grouting in rock (left abutment), cut-off wall (in bed and right abutment) and cut-off wall plus lower curtain grouting (in the right bank upland plain) are used. The upland plain cut-off wall is 140 meters deep and is divided into two parts, the upper wall and the lower wall, connected by a construction gallery functioning as the work place to build the lower wall and the lower curtain grouting. The lower curtain grouting is 60 meters deep beneath the bottom of the lower cut-off wall, so the total depth of seepage control is 200 meters.

To build the cut-off walls in so deep overburden foundation, some difficulties must be resolved, such as bentonite slurry stable wall, hole deviation control and ring budding of the adjacent holes as well as the choose of proper drill machines (the twin wheels milling machine, chopping drill, and hammer drill with reverse circulation are adopted in different geologic condition). To execute the grout curtains, some difficulties such as the proper drilling equipment, the grouting pressure, water cement ratio, quality inspection and acceptance criterion, etc must be overcome.

Yele Dam and the power house will be completed and put into production in 2005.The total acreage of cut-off walls in the dam is 55000m^2, in which 30000m^2 has been completed and the tests demonstrated that results were satisfactory. This paper will detailedly describe the successful options in the design and construction of foundation treatment of Yele Dam

1 INTRODUCTION

Pivot Survey: Yele Hydropower Station locates at upstream of the Nanya River, which is the primary right branch river at middle reach of the Dadu River in Sichuan Province. The hydropower station, being combined developed, is the first one of series of power stations (six stages in one reservoir) in the Nanya Basin. The height of dam attains 125.5m, and diversion tunnel is 7119m in length. Plant situates 13km away from the dam. Two 120MW Pelton turbines are equipped in hydropower station. The reservoir is carry-over storage with total capacity of 2.98×10^9m^3 and regulating storage of 2.76×10^9m^3.

Climate Condition: Yele Project locates at the area with mountain humid climate, of which the character is low temperature and rainy. No summer here, and 6~7 months are in winter. Average temperature is 6.5°, with ultimate lowest temperature at −20°, while highest one at 27.5°. The mean

annual rainy day is 251 days, with average rainfall amount at 1830.9mm. Additionally, the max wind speed attains 20m/s.

Geologic Condition: The geologic structure of the dam site and reservoir area is Quaternary Period constructive faulted basin, with basin area of about 30km^2. The max deposit thickness at basin center is beyond 420m. Dam situates on downstream left bank of the basin. The underneath of stream bed and right bank is thick deposit of Quaternary System, whose distribution on the dam axis attains 2km. Due to thick deposit, the stratum structure is complicated. Through long-term sedimentation and over-consolidation, the interbedded strata of gravel, powdery loam and stereoplasm results in the complicated hydrologic and geologic structure.

Base rock consists of quartz diorite, above which is overburden with the thickness at 35m~60m. Burial depth of top layer of quartz diorite underneath the streambed is 55m to 60m. Thickness of overburden at right bank is beyond 420m.

From bottom to top, overburden of dam foundation can be classified into five fabrics:

The first is weakly bounded pebble and gravel, which consists mainly of thick-bedded pebble and gravel and minor of thin silty sand. This part is 15m to 100m in thickness, and possesses water-bearing and water permeability to some extent.

The second part is brown yellow and celadon soil aggregate with some tenacious clay in. In the space of this part is filled with tenacious clay with dense structure and over-consolidation. Its water permeability is very low. This layer, with thickness of 31m to 46m, is the main object of antiseepage treatment for dam foundation.

The third one is the interbedded strata of pebble and gravel layer and silty loam layer. It distributes at upside of dam foundation and underneath the right abutment, with the thickness of 46m to 154m. It is the important bearing stratum of dam foundation, and is the main stratum for which the imperious treatment is needed.

The fourth one is weakly bounded pebble and gravel layer, distributed at the top of the right abutment, with the thickness of 65m to 85m. It is weak permeability, so it is the main stratum of impervious treatment for right abutment.

The fifth one is the silty loam and silty sand loam with some charring plant debris in, distributed at the terrain of right abutment above normal pool level, with the thickness of 90m to 107m.

Generally speaking, these five fabrics belong to weak or extreme weak in water permeability. It can be classified into two types: one mainly consists of pebble and gravel whose permeability is relatively strong, with the value of K at 10^{-3}~10^{-4}cm/s, belonging to weak water permeability; the other one consists of silty loam and debris, whose permeability is relatively weak, with the value of K of 10^{-5}~10^{-6}cm/s. The K value for silty loam, belonging to extreme water permeability, is 10^{-7}~10^{-9}cm/s.

2 ANTISEEPAGE SYSTEM DESIGN FOR FOUNDATION

The combination scheme of concrete impervious wall and curtain grouting is adopted for foundation treatment for Yele Dam. From left to right, the whole antiseepage system can be classified into five types as following: curtain grouting for base rock on left bank (Pile No. 0−150~0+000), bank slope impervious wall and curtain grouting of base rock underneath the wall at A section on left bank (Pile No. 0+000~0+150; wall depth: 20m to 50m; wall thickness: 1m; intercalation into base rock; grouting depth: 80m), impervious wall at B section of stream bed (Pile No. 0+150~0+308; wall depth: 30m to 60m; wall thickness: 1.2m; intercalation into the second fabric at least 2m; being impervious wall of suspension type), bank slope impervious wall at C section on right bank (Pile No. 0+308~0+411), bench terrace overburden impervious wall at D section on right bank (Pile No. 0+411~0+710; wall depth: 60m to 78.5m; wall thickness: 1m).

Antiseepage treatment project for C section bank slope and D section bench terrace foundation on right bank can be divided into four layers: the first is concrete wall of ground surface open cut and on-site pouring type, with depth of 15m and thickness of 1m; the second layer is impervious

wall constructed on the flat bed at the elevation of 2639.5m, with the wall depth at 70.5m (in which at the section of 0+610~710, depth is 78.5m) and thickness at 1.0m; the third one is the 1.0m thick and 60m to 84m deep concrete impervious wall constructed in gallery with base plate of the elevation of 2562m, the fourth one is curtain grouting for overburden under impervious wall, and the max depth attains 120m. As gallery construction is beforehand with the construction of bench terrace impervious wall on the top of gallery, 3.0m~3.5m distance between bottom of impervious wall and the top of gallery should be dealt with curtain grouting (See Fig. 1 and Fig. 2).

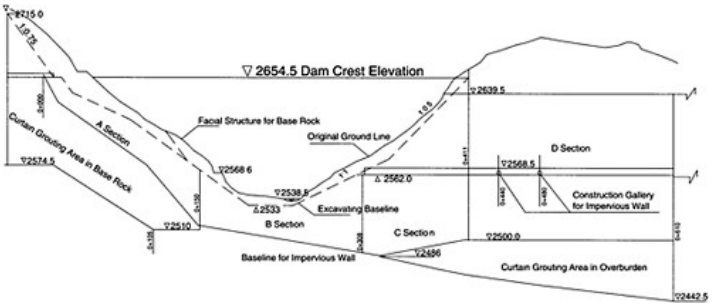

Figure 1. Layout of Antiseepage System of Foundation for Yele Hydropower Station Dam.

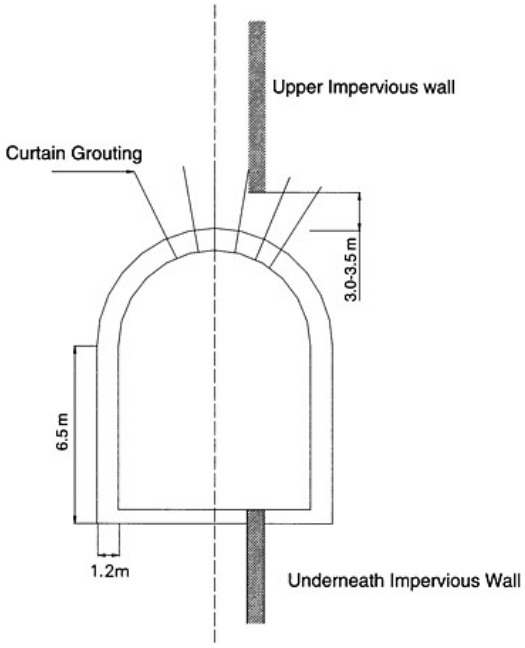

Figure 2. Sectional Drawing about Construction Gallery of Impervious Wall.

Table 1. Design parameters for impervious wall.

Segmentation	A section (left bank)	B section (streambed)	C section (right bank)	D section (bench terrace)
Pile No	0+00~0+150	0+150~0+308	0+308~0+411	0+411~0+710
Depth (m)	20~50	30~60	70.5~140	78.5~140
Thickness (m)	1.0	1.2	1.0	1.0
90d strength	≥300MPa			≥250MPa
Elastic modulus	≤28000MPa			≤21000MPa
90d antiseepage grade	≥W10			
90d freeze proof grade	≥F50			
Water injection of wall	Permeability coefficient $k \leq i \times 10^{-7}$cm/s (i=1~9)			
Connecting type	Drill method, double reverse-arc method, single reverse-arc method			
Bore slope	Termination main hole ≤2%, other slot ≤3%, other special conditions such as erratic or base rock declivity ≤4%,			

Table 2. Design parameter for curtain grouting.

Segmentation	Grouting adit on left bank	Bank slope at left bank	Bank slope and bench terrace at right bank
Pile No	0−150~0+000	0+000~0+150	0+308~0+610
Geological condition	Quartz diorite	Quartz diorite	Overburden
Max depth (m)	80	60	119.5
Bore rows (m)	2	2	3
Antiseepage Criterion (Lu)	3	3	5

Technical parameters of impervious wall can be seen in Table 1, and that for curtain grouting can be seen in Table 2.

3 IMPERVIOUS WALL CONSTRUCTION

3.1 *Construction arrangement for impervious wall*

Six flat beds of altar type are arranged from top to bottom for left bank, their respective elevations are as following: ▽2568.6 are constructed at the same time; impervious wall at other flat beds are constructed from top to bottom.

Flat bed of ▽2552 at stream bed section is a large one intersecting the whole couch (0+171~0+283).

Four flat beds of altar type are arranged or right bank slop from top to bottom, three of which the respective elevations are as following: ▽2602.5 is constructed simultaneously, and other impervious wall is constructed from top to bottom.

3.2 *Quality control index for impervious wall*

In the design, the performance of "high strength and low elastic modulus" is required for impervious wall, and acceptance is required to performed on the criterion of 90d strength of concrete.

Table 3. Designed mechanical performance index for impervious wall concrete.

Impervious wall segmentation	Pile No	28d index in construction period	Acceptance index of 90d	Antiseepage grade	Freeze proof grade
A, B, C	0+00~ 0+411	Compression strength ≧30 Mpa	Compression strength	W10	F50
		Elastic modulus ≦28000 Mpa	Elastic modulus		
D	0+411~ 0+710	Compression strength ≧25 Mpa	Compression strength	W10	F50
		Elastic modulus ≦21000 Mpa	Elastic modulus		

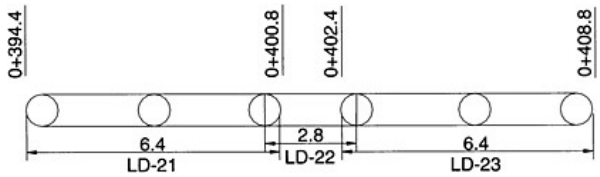

Figure 3. Typical Segmentation of Duct for 0+310–0+430 Impervious wall.

But taken the need of construction into account, after field test argumentation, 28d strength index instead of 90d index (Table 3) of concrete should be referred for quality control in construction process.

3.3 *Construction technique for impervious wall*

Impervious wall at abutments on both two banks, stream bed and bench terrace on right bank are constructed mainly by CZF-1500 Reverse Circulation Chopping Drill, and assistant by CZ-30 Chopping Drill (by drilling method). In stage I and II, duck length is 6.6m–7.4m (adaptor is included), with 3~5 main holes and 2~3 accessory holes. Adaptor is double reverse-arc type, with length between arc top at 1m.

The depth of overburden on right bank reaches more than 420m, in which the depth of important antiseepage treatment object attains 220m. At present, execution capacity for impervious wall both in home and abroad can not meet such requirement (Max wall depth of Manic-III Dam in Canada attains 131m, while the such depth of part of Xiaolangdi Project and Three Gorge Dam reaches 80m), so impervious wall project is divided into 2 parts (top and bottom) in design, and they are connected by the construction gallery for impervious wall. For this structure type, top impervious wall should be constructed first, and then, construction gallery for underneath impervious wall constructed, and last, underneath impervious wall constructed. But this way is adverse to shorten construction period. Therefore, the operational sequence is improved into a way: construction gallery is constructed first, and then, both top and underneath impervious walls constructed simultaneously. Thus, construction period can be shortened to a large extent.

Impervious wall construction in gallery is divided into two parts: for construction of the section of 0+310~0+430.0m, mainly the CZF-1500 Reverse Circulation Chopping Drill is used. When duct of stage I is constructed, BC120CBC25 Hydraulic Pressure Buggy Milling Adaptor is used. For the duct of stage I, the length is 6.4m, and 3 main holes (with hole length at 1.0m) and 2 accessory holes (with hole length at 1.7m) are included (See in Fig. 3); for construction of the section of 0+430~0+610m, mainly Hydraulic Pressure Buggy Miller is used, and assisted by Reverse Circulation Chopping Driller (See Fig. 4).

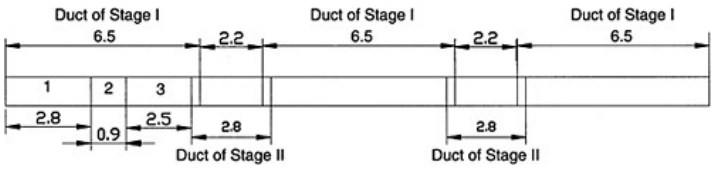

Figure 4. Typical Segmentation for Duct of 0+310~0+610 Impervious wall.

3.4 *Adaptor treatment of impervious wall*

In Yele Project, the depth of most parts of impervious wall is beyond 70m. For such deep impervious wall, the key is the connection among the duct sections. The typical driller-chiseling method and junction block (plate) method are not applicable here. Using driller-chiseling method for high strength concrete leads to low work efficiency and high cost. Additionally, using such construction method, quality is difficult to control owing to the large strength difference between wall and surrounding strata, which is prone to deflect boring. So, connecting of impervious wall is the key problem for Yele Project, and many treatment ways are introduced in construction such as ring budding driller chiseling, permutation, double reverse arc (DRA) method, single reverse arc (SRA) method and so on. Through many generalizations and practices, the connecting type of SRA connecting is adopted at last, and the reliable experience is achieved.

The connecting treatment of SRA is possessed of several advantages: 1.Adaptor and duct of stage II form block, thus adaptor quantity of wall can reduce to half; 2.Adjacent duct of stage I is constructed simultaneously, thus can void puncture caused by short size of connecting duct which usually occurs using the way of DRA, and shorten construction period.

3.5 *Quality inspection for impervious wall*

Impervious wall construction ofYele Hydropower Station started from July of 2001, and 88 duct sections (sum up to 28000m^2) had been completed till August of 2003, in which impervious wall for dam foundation had been completed, and construction of base plate connecting impervious wall and asphalt concrete of core had been started. Residual impervious wall mainly centers in bench terrace on right bank with Pile No. 0+414~0+610. Before impound and operation, quality control of impervious wall can be estimated technically by sampling at outlet of mixing machine and wall quality inspection. They mainly include: sampling check at outlet of concrete mixing machine, boring and coring check, boring and water injection test, mechanical property test for core sample and the like. The pass test criterion includes: mechanical property index and antiseepage criterion of wall material should reach design value, and qualified rate should attains 95%; mechanical strength index of unqualified part should attains 85% of design values, and these parts are not centered at adjacent slot-opening.

Concrete outlet sampling are performed in the lab, thus can avoid most of the disturbing factors that will influence appraisal results, and such tests can act as the main basis for quality evaluation for concrete. Statistics of sampling and appraisal results show as following: qualified rate with 90d strength index of C30 concrete is 99.2%, and only one group is found that its unqualified strength is just 94.3% of the design value; qualified rate with 90d strength index of C25 concrete is 100%; dispersion coefficient of C30 (C_v=0.141) is a little larger than that of C25 (C_v=0.116), mainly due to that some duct sections poured with C30 concrete started with productive test pouring, and thus experienced adjustment of mix ration of concrete; antiseepage index of concrete meets design requirement well. Coring and water injection for wall are disturbed by many factors, so they are only acted as reference for appraisal and evaluation of quality inspection of impervious wall. The test results show as following: average coring rate attains 95.1%; in the

whole water injection tests for 39 sections, no water is absorbed in 29 sections, and absorption value (k) for other 10 sections is at the magnitude of 10^{-7}cm/s; qualified rate with 90d strength criterion for core sampling is 100%, and the average reaches 41.6Mpa. With analyses of above statistical data, quality of constructed impervious wall meets design requirement well. Consulting reports issued at July of 2003 by the consultant team for Yele Hydropower Station hold the view that "impervious wall construction of Yele Hydropower Station Project conquered many technical difficulties, borne great fruit, and met the need of Yele Dam Project".

The whole impervious wall, which ranks first one over the nation, is 710m in axis length, with width of 1~1.2m. Most parts are at the depth more than 70m, and the deepest part attains 84m. The project scope, wall depth, structure type and construction difficulty are rare both at home and abroad.

4 CURTAIN GROUTING FOR THICK OVERBURDEN

4.1 *Design of curtain grouting for thick overburden*

At the impervious wall section with Pile No of 0+308~0+610 in construction gallery, the top elevation is 2561.5m, while bottom of impervious wall is at the elevation of 2486~2500m. Three rows of cores for curtain grouting are arranged underneath impervious wall. In these cores, two rows (A type) should be buried with grouting pipes in impervious wall in advance, and thus grouting can be performed through these pipes in construction gallery. The other row (B type) is arranged at the downstream of impervious wall, and thus grouting can be performed through these cores from base plate of construction gallery. Figures 5 and 6 show sectional drawing of Antiseepage Curtain.

- The depth of A type core into overburden is 0~57.5m.
- The depth of B type core into overburden is 75.7~119.5m.

4.2 *Productive test for curtain grouting in thick overburden*

Curtain grouting under impervious wall at construction gallery sums up to 20000m^2.The deepest core attains 119.5m, and all constructions proceed in overburden. Productive tests last from June 15, 2003 to Sep. 25, 2003, and up to 10 grouting test cores (sum up to 956m) had been completed, and all cores were drilled to the designed depth, which approved that aperture block up grouting is practicable in technique.

Using cement grouting, single core injection rate for I, II and III core are respectively 243kg/m, 194kg/m and 50kg/m, confirming to general rule, approved that grouting effect with cement is fine.

Proven by two seismic wave test holes, drilling with water by φ56mm adamantine driller can attain the design depth (96.29m). The problem of "drilling with water" in quality inspection of next stage is basically solved.

4.3 *Problems calling for solution*

Although productive tests have made great progress, many technical problems about curtain grouting for thick overburden still call for further solution owing to no criterion exists. The problems cried for solution include:

- construction of inspecting holes and method of water injection tests.
- antiseepage criterion of curtain grouting. The designed antiseepage criterion is q=3Lu, but the lap section between impervious wall and curtain is mainly formed by grouting in single row of hole, thus make it difficult to achieve design requirement.
- selection of grout mixture. Test of cement grout mixture have now been completed, and the grouting test of cement mixed with fly ash will be performed in the next stage. Thus the optimal grout mixture and its corresponding water cement ration can be obtained.
- grouting pressure. Test to acquire the most suitable grouting length and corresponding grouting pressure will be helpful to reduce damage in hole and improve work efficiency.

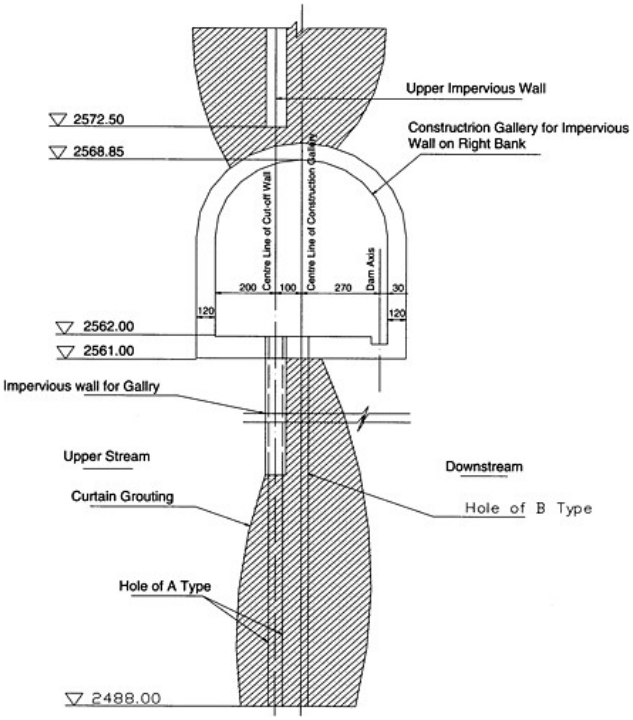

Figure 5. Sectional Drawing along River Direction of Antiseepage Curtain.

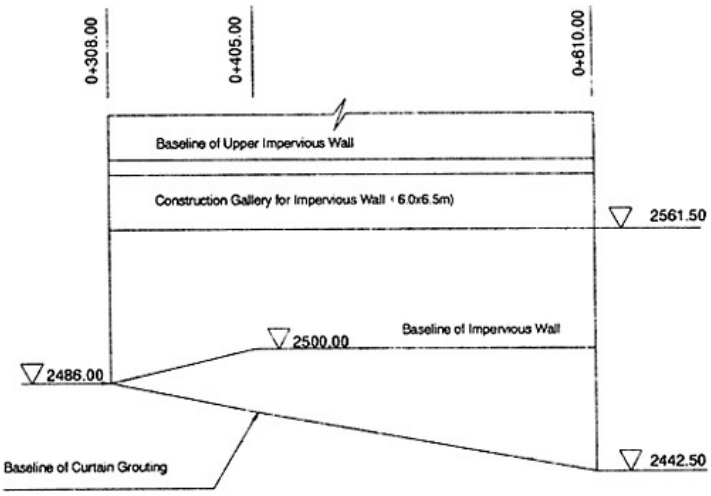

Figure 6. Cross Sectional Drawing of Antiseepage Curtain.

5 CONCLUSION

For antiseepage treatment of Yele Dam, the structure is complicated, and many difficult problems call for solution, and no related technical data or practical experiences can be referred. Especially for antiseepage structure on right bank, the wall connects with upper and underneath structures, and grouting is arranged underneath the wall, whose total depth beyond 200m. So it is extremely difficult in design or construction. Such difficulty ranks first around the nation and is rarely seen abroad. Therefore, solution of antiseepage treatment for foundation of Yele Hydropower Station will promote the development of foundation treatment, and serve as valuable reference for foundation design and construction for other projects.

This page intentionally left blank.

New Developments in Dam Engineering—Wieland, Ren & Tan (eds),
© 2004 Taylor & Francis Group, London, ISBN 04 1536 240 7

Applying hydrogen and oxygen isotope tracer method to study the seepage of dam and dyke

Jian-sheng Chen, Hai-zhou Dong, Zhe-chao Fan & Liang Chen
Hohai University, P.R.C

ABSTRACT: The theory of using hydrogen and oxygen isotope tracer method to study the seepage of dam and dyke is analyzed. As examples, the seepage of left dam abutment of Xiaolangdi reservoir and right dam abutment of Xin'anjiang reservoir is studied. The source of large volume of drain discharge in No. 30 drainage culvert of Xiaolangdi reservoir has been determined by the analysis of hydrogen and oxygen isotope. Moreover, artificial tracer and interconnection test proved this result. The by-pass seepage of right dam of Xin'anjiang reservoir is proved. All results are very important to the next reinforce work.

1 FOREWORD

Studying the seepage of the dam with environment isotope is an important content in isotope hydrology in the recent years. Stable isotopes D, T and ^{18}O of water have been broadly used in hydrogeologic investigation as important nature tracer. Much scientific research fruit has been attained about the analysis of stable isotopes and the application in the hydrology research. For example, Fontes, Edmunds, Coplen and Gat have systemically summarized about them, and latest papers include the ones of Mazor, Clark and Fritz. IAEA also has discussion meetings in scheduledtime (1966, 1970, 1974, 1978, 1984, 1987, 1992, 1996), and has specially published works about the isotopes of H and O.

The related information of the dam's seepage can be attained by the distributing law of the environment isotopes D, T and ^{18}O in the surface water and groundwater, by the comparison of the isotopic character in the precipitation, groundwater and seepage water, and by applying the altitude effect and the latitude effect of the occasional isotopes in the precipitation. So the recharge sources can be accurately separated, and the scientific reference can be put forward to supply the engineering cure of the dyke.

2 HYDROGEN AND OXYGEN ISOTOPE IN PRECIPITATION

The precipitation is the latest water that joins the atmospheric circulation, including rain, snow, glacial water, vapour, branch water, stream water, lake and most hypothermal groundwater. The compositions of hydrogen and oxygen isotope in the precipitation vary greatly, $\delta^{18}O$ varying from 0 to −60‰ and δD from +10 to −400‰. There exists a linear relation between the D and ^{18}O values in the precipitation. In 1961, Craig statistically attained the relation between the δD and $\delta^{18}O$ values in terms of the data of the global precipitation.

$$\delta D=8\ \delta^{18}O+10$$

So the isotopic compositions of water and ice are basically distributing along a line, which is called Craig precipitation line. The relation can be understood that the difference of D values

between water and vapour is 8 times that of the one of ^{18}O values in equilibrium condition. Because of the dynamics fractionation effect during the evaporation of the surface water over sea, the line don't pass the origin point which represents average isotopic composition of seawater ($\delta D=0$, $\delta\ ^{18}O=0$).

The environmental isotopic compositions of the water will depart the precipitation line equation because of evaporation. The degree of the departure can be expressed by the deuterium surplus ($d=\delta D-7.83\ \delta^{18}O$). d equal to 10‰ means δ value is just on the precipitation line; d exceeding 10‰ means δ value is at the right and below side of the precipitation line; d less than 10‰ means δ value is at the left and above side of the precipitation line. d equals δD axial intercept of the precipitation line in the $\delta D-8\delta^{18}O$ figure, which reflects the degree of the local region. The $\delta^{18}O$ value of the groundwater will increase when the isotopic exchange occurs between the rock and groundwater, which is called the ^{18}O's departure. The isotopic exchange can also occur between the groundwater and CO_2, so the isotopic composition of the groundwater will also depart the precipitation line equation.

3 PRINCIPLE OF APPLYING RELATION OF δD AND $\delta^{18}O$ TO ANALYZE SEEPAGE OF DYKE

3.1 *Judgment of groundwater recent recharge source*

Craigh precipitation line, available on IAEA web, can be used to judge recent recharge source of groundwater. Providing that several different regional precipitation recharge groundwater, and there are different evaporation and condensation conditions in different regions, different slopes and intercepts will occur in the Craigh precipitation lines, so different recharge sources of the groundwater can be determined.

3.2 *Determination of relation between groundwater, surface water and water reservoir*

Surface water and water reservoir exist obvious evaporation effect because of being exposed in the atmosphere, so δD and $\delta^{18}O$ of surface water are always greater than that of atmosphere and groundwater. The hydraulic relation can be determined according to δD and $\delta^{18}O$ values and the slope of the precipitation line. Generally, after precipitation converts into the surface water, the slope of line will change because of the evaporation.

3.3 *Determination of hydraulic relation between different aquifers*

Because different isotopic composition exists in different aquifers, the degree of their hydraulic relation can be determined according to δD and $\delta^{18}O$.

4 APPLICATION CASE ON THE LEFT DAM ABUTMENT OF XIAOLANGDI RESERVOIR

4.1 *Hydrogeological situation*

The seepage of the left dam abutment of Xiaolangdi reservoir has increasing trend with the increasing of reservoir water table. When reservoir water table exceeds EL235, the seepage has rapidly increasing trend, which mainly locates around No. 30 drainage culvert, the crown of the underground workshop, and the upstream abutment wall. Though there is sedimentation in front of the dam, and curtain grouting and remedial treatment have been made, the seepage is still rather large. So there probably exists a concentrated seepage passage leaking by pass the dam abutment.

The groundwater of Xiaolangdi reservoir dam site mainly includes porous unconfined water in Quaternary loose overburden aquifer, fissure unconfined water in bedrock, and confined water and perched water, etc. Porous unconfined water in Quaternary loose overburden aquifer mainly locates sand and gravel layer in riverbed and pluvial layer in bank slope, and its water table is close

to that of Yellow River, which means there exists close hydraulic relation between them. The hydraulic permeability of sand and gravel layer in riverbed is very inhomogeneous because of the change of percent sand and proluvial interlayer.

The seepage of groundwater in the research emphases areas has several characteristics:

1. The seepage layer is commonly uniformity structure, which is formed as a result of the discharge of the left dam abutment;
2. The seepage layer is zonary distributed and located along fault;
3. The seepage can be divided as follows: a. paralleling to dam axes; b. horizontal joint with permeable structure; c. impermeable in vertical direction, and water-resisting structure between the layers.

4.2 *The hydrogen and oxygen analysis in No. 30 drainage culvert of the left dam abutment*

The altitude of No. 30 drainage culvert is 117m, and the altitude of the drain hole bottom is 85m. The seepage source of No. 30 drainage culvert is found rather complicated through experiments. According to the runoff observation data, the discharge on the north side in the drainage culvert is far larger than that on the south side, on upstream side and on downstream side. For instance, when the head of the reservoir is around 233m, the discharge of No. 133, 143 and 169 drain hole is 3.5L/S, 2.2L/S and 3.5L/S respectively, while the discharge of other holes is less than 2L/S.

Five samples have been taken from No. 30 drainage culvert, and the hole numbers are 30RD-7, 30RD-37, 30D-18, 30D-133, 30D-194 respectively. In addition, from reservoir water, tail water No. 1 (rather far from dam) and tail water No. 2 (near dam), samples have been taken and analyzed. Data refer to Table 1.

Plot the data at corresponding location, referring to Figures 1, 2 & 3.

Table 1. Environment isotope data of part samples in the left abutment of Xiaolangdi reservoir.

Place	Reservoir water	Tail water No. 1	Tail water No. 2	30D-18	30RD-37	30RD-7	30D-133	30D-194
D(‰)	−69	−73	−66	−64	−61	−67	−68	−63
O^{18} (‰)	−9.4	−7.9	−8.5	−8.5	−8.9	−8.9	−8.6	−8.6
T (T.U)	18.73	17.14	16.96	33.65	14.15	44.19	18.95	8.61

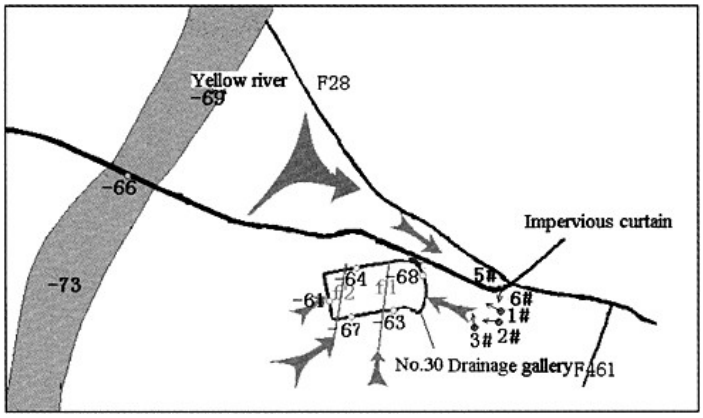

Figure 1. Distribution of δD value in No. 30 drainage gallery of Xiaolangdi reservoir (April, 2002).

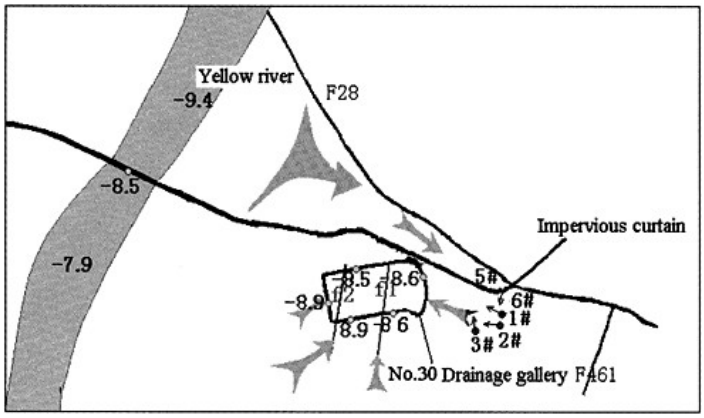

Figure 2. Distribution of $\delta^{18}O$ value in No. 30 drainage gallery of Xiaolangdi reservoir (April, 2002).

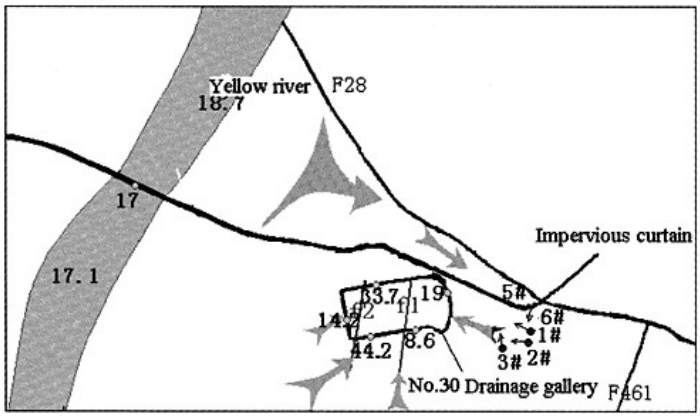

Figure 3. Distribution of T value in No. 30 drainage gallery of Xiaolangdi reservoir (April, 2002).

According to isotope data, the hydrogen and oxygen data of the 30D-133 drainage hole, which is on the north side of No. 30 drainage culvert, is very consistent to that of deep reservoir water, so it can preliminarily judged that there exists recharge from the bottom of the reservoir. The data of the environment isotope and chemical type of water shows that the leaking water is very close to the deep reservoir water. Water temperature in holes is 1~2°C higher than that of other holes in April, May and late July. Because the temperature of water, which is recharged by reservoir water, is commonly very low, seepage passage is probably rather long and deep. There probably exists by-pass seepage form the deep layer, which has been approved by the interconnection test.

Low temperature has also been detected around No. 7 drainage hole, which is on the upstream side of No. 30 drainage culvert. The temperature is the lowest in the drainage culvert, and preferably correlates with the seasons. The value of T is 44.2TU, and is concerned with shallow water, so the hole is recharged by shallow water. These show that there exists a complete seepage passage

at this point, and the seepage passage is not long, and may have relation with f1 fault. Reservoir water leaks into No. 30 drainage culvert along the fault.

The T value in the water of 30RD-37, which is on the side of No. 30 drainage culvert, is the mix of tail water and groundwater, equaling 14.15TU. Because the head of tail water is 135m, while the altitude of the bottom of No. 30 drainage culvert is 117m, the recharge of 30RD-37 comes from tail water. The water of downstream recharges No. 30 drainage culvert along the f_2 fault, and discharges through the drainage holes of the south side.

The T value in the water of 30D-194 of No. 30 drainage culvert is 8.61TU, so the supplying source is local precipitation. The recharge passage may be related with the f_2 fault.

4.3 *Verification of artificial isotope trace and interconnection test*

For the purpose of further finding out the source of drain water of No. 30 drainage culvert, artificial isotope test has been performed in the hole of left abutment to measure the seepage velocity and direction of the groundwater, and interconnection test has been performed between No. 3 hole and No. 30 drainage culvert. The result verifies the analysis of environment isotope.

The locations of the boring holes refer to Figures 1, 2 & 3. According to the seepage velocities of No. 1, 2, 3 holes, the one of No. 3 hole is far bigger than that of No. 1, 2 holes. The velocity of bottom of all holes is rather big. Especially in No. 3 hole, the seepage velocity is bigger than 0.2m/d, the maximum exceeding 0.4m/d. According to the average seepage directions, the angle of the No. 1 hole is 240°, and the one of the No. 2 hole is 180°, and the one of the No. 3 hole is 260°. Plot the directions in the figure, the seepage directions of No. 2, 3 holes points to the same direction, so the seepage passage is located between No. 2, 3 holes, but is closer to No. 3 hole according to the absolute seepage velocities value. No. 5, 6 holes are located on the point of intersection of F_{28} fault and impervious curtain. From the seepage directions of the two holes, the same phenomenon is reflected, and the angles of seepage directions of the No. 5, 6 holes are 180° and 300° respectively. The seepage directions of the two holes point to the same site, which is the site where F_{28} fault passes impervious curtain between No. 5, 6 holes. Plotting the directions in the figure, the by-pass seepage direction of left dam abutment is obvious, referring to the arrowheads of Figures 1, 2 & 3.

The interconnection test also shows there exists hydraulic relation between No. 3 hole and No. 30 drainage culvert. During 10:30–11:00a.m. on May 26, 2002, rose-colored tracer was put into No. 3 hole. There was red water draining out in the No. 119–No. 169 holes of No. 30 drainage culvert in the next morning. The depth of color achieved the maximum in the third day. These approve the analysis of the seepage directions.

During 9:30–10:00a.m. on July 29, 2002, rose-colored tracer was put in No. 5 hole. High-density red-colored water was attained in No. 3 hole, which shows the communicating relation between No. 3 and No. 3 holes, and No. 3 hole locating in the main seepage passage. Low-density red-colored water was attained in No. 1, 2 holes, which show the two holes are not in the main seepage passage. In the third day, the low-density tracer was attained in the north drain holes of No. 30 drainage culvert. These verify that there exists a deep bedrock seepage passage in the left dam abutment, which causes the rather-large volume of drainage water of the No. 30 drainage culvert.

5 APPLICATION CASE OF VERIFYING OF BY-PASS SEEPAGE OF XIN'ANJIANG RESERVOIR RIGHT DAM

5.1 *Leakage problem on the right dam abutment*

During 30-year running of Xin'anjiang dam, the heads of the observation R_4, R_5 and R_{16} holes are always around 10m lower than that of the reservoir, and correspondently fluctuate with the reservoir head, while the heads of the other holes always are higher than that of reservoir water. There

are three different opinions on the low head of the observation R_4, R_5 and R_{16} holes and their good correlation with the head of the reservoir. The first opinion says it was caused by the bad antiseepage effect of the curtain. In the second opinion, it was caused by the recharge of the precipitation. In the third opinion, there exists by-pass seepage passage on the dam abutment. Adopting which one is the key of the design of the reinforcement. For the purpose of verification, environmental isotope test has been performed. Environment isotopes D, ^{18}O and T are analyzed. The samples include reservoir surface water, 30m-deep reservoir water, tail water, observation holes water, drainage holes water, sector holes seepage water and concentrated seepage water, etc. The by-pass seepage is approved on the right dam abutment of Xin'anjiang dam.

5.2 *Analysis of environment isotope on the right abutment*

In China, the precipitation line equation is as follows:

$$\delta D=7.74\ \delta^{18}O+6.48$$

According to the analysis of local precipitation samples, the precipitation line equation of Xin'anjiang reservoir area is as follows:

$$\delta D=7.83\ \delta^{18}O+5.32$$

According to the precipitation line, the different sources of seepage can be analyzed on the right dam abutment of Xin'anjiang reservoir. Figure 4 is the sketch figure of the directions of the groundwater and the samples locations on the right dam abutment of Xin'anjiang reservoir.

The data for samples refer to Table 2.

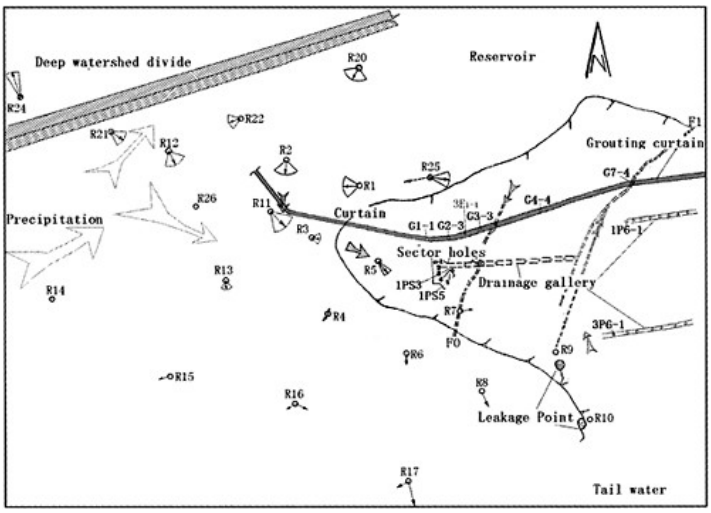

Figure 4. Sketch of sample locations and groundwater flow direction on right abutment of Xin'anjiang dam.

Table 2. Data of environmental isotope D, ^{18}O and T (November in 2002).

Sampling points	R_2	R_3	R_5	R_6	R_9	R_{10}	R_{14}	R_{21}	R_{22}	R_{26}	G_{1-1}
$\delta^{18}O$(‰)	−6.8	−6.8	−6.9	−7.6	−6.7	−6.9	−8.7	−8	−7	−7.3	−6.8
δD (‰)	−55.3	−52	−55.6	−52	−58.8	−58.4	−63.3	−59	−57.2	−56.3	−58.3
Content of reservoir water	≥0.35	≥0.67	≥0.32	≥0.67	Local groundwater	Local groundwater	Local groundwater	Local groundwater	≥0.17	≥0.26	≥0.07
T (T.U)	13.56±4.13	9.36±3.99	7.20±3.58	1.47±3.74	1.94±3.56	5.15±3.56	9.42±4.13	9.73±3.46	7.27±3.62	13.99±3.22	2.31±3.09
Sampling points	G_{2-3}	G_{3-3}	$G_4{}_{-4}$	$1P_{S-5}$	$1P_{S-5}$	Reservoir surface	Tail water	Reservoir 30m	$1P_{6-1}$	$3P_{6-3}$	G_{7-4}
$\delta^{18}O$(‰)	−6.8	−6.6	−6.5	−6.7	−7	−6.4	−6.5	−6.8	−7.2	−6.8	−6.4
δD(‰)	−59.4	−56.6	−57	−46.8	−48.4	−50.2	−48.5	−48.6	−45.8	−47.1	−47.4
Content of reservoir water	≥0	≥0.23	≥0.19	Reservoir water	Reservoir water	Reservoir water	Reservoir water	Reservoir water	Local precipitation	Local precipitation	Local precipitation
T (T.U)	7.54±3.13	3.84±3.49	<0.50	3.53±3.43	1.45±3.31	8.01±3.34	4.81±3.19	5.98±3.33	8.35±2.95	15.03±3.08	19.54±3.17

When there exists the mixture of reservoir water and local groundwater, the mixture proportion, denoted by the content of reservoir water in Table 2, can be calculated by the following method:

Supposing N_{rw} reservoir water molecules contain R_{rw} percentage of deuterium isotopes, there exist $N_m/(1+R_{rw})$ molecules, including R_{rw} $N_{rw}/(1+R_{rw})$ molecules of rarity isotope D. When the reservoir water is mixed with local groundwater, which containing N_{mw} molecules and ratio of the isotope D equaling R_{mw}, the isotope ratio can be attained by the equation of the mass conservation: $RN=R_{rw}N_{rw}+R_{mw}N_{mw}$, where R is the isotope D ratio of the mix water. Because N=N1+N2, the proportion of reservoir to local groundwater is: $N_{rw}/N_{mw}=R_{mw}-R/R-R_{rw}$, and the content of reservoir water is $N_{rw}/(N_{mw}+N_{rw})=1/(1+(N_{rw}/N_{mw}))$.

Figure 5 is the precipitation line and the distributing figure of environmental isotope data. According to the interrelation of the sample data and precipitation line, the source of groundwater can be determined:

(a) Precipitation is the main source of water in grouting gallery.

According to Figure 5, the seepage water of G_{1-1}, G_{2-3}, G_{3-3}, G_{4-4} holes in grouting galleries and the water of the R_2, R_5, R_{10}, R_{22}, R_{26} observation holes in the right dam abutment locate on the same right and below side of the precipitation line. These show that the seepage water of the area come from same source. The proportion of reservoir water in the grouting galleries is 0~23%, which shows that seepage water in grouting gallery is mainly recharged by the slope precipitation. Because T value is low, the retention time of groundwater is rather long, varying from several years to decades. Especially in G_{4-4} hole, the age of water exceeds 50 years. So there exists rather weak relation between the drain discharge volume and the head of the reservoir water. The isotope deuterium in grouting gallery is basically consistent to that of observation holes in the right abutment by the analysis of environment isotopes. These points locate on the right and low side of the local precipitation line, which shows that the drainage of grouting gallery mainly comes from by-pass seepage, and there occurs the interaction between rock and water in the groundwater according to the plus departure of ^{18}O.

(b) Reservoir water is the supply source of sector holes in drainage gallery.

The seepage water of $1P_{S-3}$ and $1P_{S-5}$ sector holes in grouting gallery and reservoir water locate in the same area in Figure 5, which shows that they have the same recharge resource. The bottom

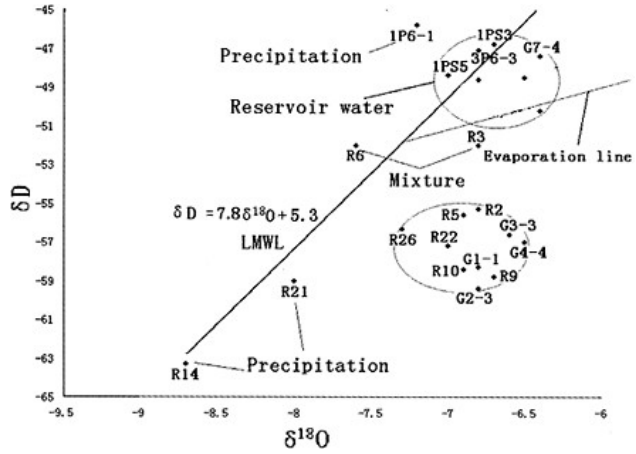

Figure 5. Distribution of environmental isotope data.

altitude of the two holes is around 55m, and the seepage water comes from the seepage along F_0 fault. Because the depth of the drain holes in grouting gallery are 20~45m, lower than the bottom altitudes of sector holes, and bottom altitude of the extended segment of right dam curtain is only 60m, there exists by-pass seepage around 60m altitude of right dam abutment.

(c) Analysis of seepage source around the R_9, R_{10} holes.

There exist two concentrated seepage areas around observation holes R_9 and R_{10} in the back area of right dam abutment (referring to Figure 5). δD of the seepage water are −58.8 and −58.4 respectively, so the source of water obviously comes from the slope precipitation. T of the water is 1.94±3.56 and 5.15±3.56 respectively. The age of the seepage water is old in the R_9 seepage areas, about 5~15 years. The average age of the seepage water is less than 5 years in the R_{10} seepage area. The content of reservoir water in the two seepage areas are low. But when the head of reservoir water is very high, the content of reservoir water in seepage water will increase.$\delta^{18}O$ values of the two holes are −6.7 and −6.9 respectively. According to the locations of the two areas in Fig. 5, there exist obvious plus departures of ^{18}O in the groundwater. The departure of the R_9 seepage area is rather large, because of its long average retention time of seepage water.

(d) R_{14} and R_{21} holes are completely recharged by the local hillside precipitation.

After No. 142 platform of the right dam abutment has been covered by concrete, the precipitation basically can't directly recharge the water in the bedrock under the platform, which is mainly recharged by the precipitation of higher slope. The value of R_6 hole locates on the right-above side of the precipitation line, having a little negative departure, which shows that the content of CO_2 is high in the local groundwater. There don't have by-pass seepage part.

(e) Precipitation in the back area of dam recharges G_{7-4} hole along F_1 fault.

Though the values of G_{7-4}, $3P_{6-3}$, $1P_{6-1}$ holes and reservoir water locate in the same area in the δD~$\delta^{18}O$ figure, their T values are as high as 19.54TU, 15.3Tu and 8.35TU respectively, while T of tail water and the bottom of reservoir water are 5.98±3.33 and 4.81±3.19 respectively. Obviously the seepage water can't directly come from reservoir along F1 fault. So the seepage water of F1 fault comes from the precipitation of the back area of dam, neither reservoir water nor local groundwater or by-pass seepage.

5.3 *By-pass seepage exists in the right dam abutment*

Considering the departure of $\delta^{18}O$ because of the interaction of water and rock, the altitude of precipitation can't be determined by $\delta^{18}O$. But the analysis of precipitation can be performed by applying δD. According to Figure 5, δD of R14 hole being −63.3 and R21 being −59, are completely different to reservoir water, which shows that their recharge altitudes are different. The values of observation holes in the right dam abutment insert the middle of the two parts in some different degrees. In fact, the water of right dam abutment comes from either slope precipitation or by-pass seepage of reservoir water, and there occurs their mixture. The content of reservoir water in the mixed water refers to Table 2. Contents of reservoir water have considerable proportions in the observation holes in the right dam abutment. The proportions are 32%~67% in R_2, R_3, R_5 and R_6 holes, while the water in No. 1 sector hole completely comes from reservoir water. The altitude of the bottom of the sector hole is 55m, while the one of the bottom of the curtain in the right dam abutment is 60m, so obviously there exists by-pass seepage below the 60m altitude of the extended part of curtain. By-pass seepage in the right dam abutment, a disputed issue, is tested by the analysis of environment isotopes.

6 CONCLUSION

The hydrogen and oxygen isotope is ideal nature tracer, because it is the component of water molecule itself marking the flowing of water. Much useful information of flowing of groundwater can be afforded by applying hydrogen and oxygen isotope to trace groundwater. Applying nature tracer method can make up the undiscovered issues, which are not discovered by the methods such as site

investigation, water pressure test and analysis of rock samples. So the research of the groundwater can further meet the objective fact. Applying more physical methods to the research of groundwater seepage system, the result will be more credible than the result got by simple research method.

By analyzing environment isotopes, much information can be got, such as the sources of seepage water, ages of groundwater and proportions of different source water in seepage water, etc. So it can be used to determine whether there exist hidden troubles of concentrated seepage in the stratums. These play crucial role in the proper engineering decision-making.

ACKNOWLEDGEMENTS

The work was jointly financed by the National Natural Science Key Foundation of China (Grant No.: 50139030) and academician foundation of Hohai University.

REFERENCES

Fontes J.-C., and Edmunds J.N. The use of environmental isotope techniques in arid zone hydrology. IHP-III Project 5.2 UNESCO, Paris, 1989.
Coplen T.B. Uses of environmental isotopes in Regional Ground-water Quality, ed. W.M.Alley, Van Nostrand Reinhold, NewYork, 1993:227–254.
Gat J.R. Oxygen and hydrogen isotopes in the hydrologic cycle. Annu. Rev. Earth Planet. Sci. 24, 1996:225–262.
Mazor E. Chemical and Isotopic Groundwater Hydrology: The applied Approach. M.Dekker, New York: 413.
Clark I. And Fritz P. Environmental isotopes in hydrology. Lewis, Boca Raton, Fl.
IAEA, Isotope Hydrology 1983. IAEA, Vienna, 1984.
Craig H. Isotopic variations in natural waters. Science 133, 1961:1702–1703.
Liu Guangyao, Chen Jiansheng. Detecting well by isotope tracing. Science and technology press of Jiangsu, October, 1999.
Liu Jinda, Zhao yinchang, Liu Enkai, Wang Dongsheng. Discussion on the stable isotope time-space distribution law of china atmospheric precipitation, Science and technology of investigation, 1997, 6:34–39.

New Developments in Dam Engineering—Wieland, Ren & Tan (eds),
© 2004 Taylor & Francis Group, London, ISBN 04 1536 240 7

Integrated tracer method in dam/dyke leakage investigation

Liang Chen & Jiansheng Chen
Geotechnical Institute of Hohai University, China

ABSTRACT: Leakage and unexpected seepage are serious problems for dam/dyke management. Firstly, a systemic summary is presented to describe the application of isotope tracer method in seepage investigation in single borehole. Secondly, the well flow theory is adopted to imitate the seepage field of groundwater. The methods of natural and isotope tracer using to detect seepage and leakage are also discussed in the paper. Finally, these methods are used to analyze an example of dam leakage, and the results perfectly verify the efficiency of the method.

FOREWORD: No matter what methods are adopted to study the seepage, all their purposes are to prevent dam or dyke from losing face, and to play a guide action in strengthening. For the relation between the seepage and the geological structure of each place is compact, so there is no catholicity in studying them respectively. Much research work about dyke seepage has been done, but there are no research articles so far about whether the concentrated leakage passage will be formed or if it's safety to dam or dyke. For only after knowing the distribution range of the soil particle brought out by the seepage in the layer and the progressively develop process of the seepage, can we have a definite object in dyke strengthening. The occurring of seepage in dam or dyke which maybe develop to leakage or piping is a complex mechanics process of reciprocity between water and soil mass, concerned with the factors such as the constituent, construction and grading of soil, hydraulic gradient, places and depth of the seepage, the internal friction angle of surface cover claypan, thickness of overburden layer, viscosity coefficient, saturation coefficient, solidification coefficient, soaking time etc. It is a complex multivariate problem.

At first we investigate all of the springs and wells to get the temperature field. Then we use steady flow theory to study the characteristic distribution of seepage field at initial seepage stage[1] (Liangtao Ge. 1984). And then we apply isotope tracer method[2] (Jiansheng Chen) to detect seepage flow in the borehole. This method has been researched for several decades, and has achieved great success. At present, this method has applied to such fields as hydraulic engineering, mining, survey of groundwater etc., and has solved many engineering problems successfully.

1 PRINCIPLE OF NATURAL TRACER METHOD

1.1 *The tracer principle of groundwater temperature*

We know that the density of water is maximum at 4°C, the water between 4~100°C obeys principle of heated to expand and cooled to contract, cold water's density is big than hot water's, and cold water is easy to go down while hot water goes up. This characteristic of water causes that temperature is highest at the surface layer and lowest at the bottom of the river water, reservoir water and lake water. But the trend of temperature in the geologic layer is reverse to water, as we know, the temperature on the surface of earth is lowest, while in the deep of earth where is in a

state of fusion, the temperature can achieve thousands degree. Along with the increase of the depth, the temperature will increase, commonly the depth increases 100m and the temperature increases 3°C.

Due to above mentioned reasons, the supply of river water to groundwater on both sides can be reflected by the change of temperature of the water in the layers behind dykes, and then the strong leakage area can be found out. In the observation well behind the dyke where there exists strong leakage, low-temperature areas always exist. The section with temperature abnormity is usually the strongest permeable section, is also the section where seepage may occur most probably. Using temperature abnormity to detect and check the permeability of the grouting under dyke is one of the most effective means.

Since the temperature transmits through medium, and under depth 4m in the borehole the influence of the earth's surface temperature can be excluded, the seepage field can be explored by installing temperature sensor. For those places where permeability of layer is strong, temperature-detecting method is correct under some certain depth. We install the temperature sensor at in the shallow hole behind the dyke, under the mutual supply of the river water and the groundwater, the sensitivity area of the temperature change can be found out, then strong leakage section can be determined preliminarily.

1.2 *The tracer principle of the groundwater conductivity*

The river water mainly comes from rainfall, so its mineralization degree is very low, and the conductivity of the water is also rather low. The forming of the groundwater is the rainfall that enters aquifers by vertical seepage flow. During the long-term moving process, some chemical or physical reactions such as dissolution, evaporation, concentration etc. take place between the groundwater and the minerals in layers, causing that mineral degree of the water increases gradually and the conductivity of the groundwater is rather high. The value of the conductivity is related to the time the groundwater stay in the layer, if the time is longer, the conductivity is higher. Moreover, the value of the conductivity is related to the rock ingredient of the layer the groundwater passing by and the effect of the pollution.

By determining the conductivity distribution in the river and the inland river under the natural flow field, we can make certain the mineral degree change at different position, different layer of the dyke, then ascertain the supply relation of the river water to the groundwater. So the conductivity of water can be regarded as another fine natural tracer to determine the leakage passage of the dyke, which can be used to explore not only the seepage of the dyke, but also the distribution of the groundwater flow field. It is very important to use conductivity tracer method to examine the results of isotope tracer method.

2 PRINCIPLE OF ISOTOPE TRACER METHOD

The principle and methods of measuring the groundwater flow direction in single borehole have been introduced in many literatures. Drost[3] thinks that once the isotope has been injected into the borehole, at the first time, the distribution of trace is equality, as the time go on, some trace enters into the aquifer with the flow, the concentration distribution of trace in the borehole or in the stratum around the borehole becomes inequality, the concentration in the flow direction is high, while the other is low. The flow direction can be determined though the measuring of the concentration in the borehole.

In single hole, the direction and velocity of seepage flow in soild-rock can be obtained with isotope infiltration method, and with tracer method the volume of vertical flow among soils can be known, then measuring the vertical flow repeatedly under the condition of projection or pumping, the non-disturbing well theory is been set up at last. Now we can determine many parameters such as the equivalent mechanical soil width, seepage coefficient, hydrostatic water level and so on.

2.1 *Using single well isotope tracer method to detect the dyke seepage field*

After using qualitative test with natural tracer method to find the larger area probably existing potential danger under dyke, quantitative test such as isotope tracer test must be done. Because seepage mainly takes place at the gravel bed, firstly we need to use experiment method to distinguish seepage soil and non-seepage soil. For the non-seepage soil, even under very high hydraulic gradient seepage cannot occur; on the contrary, for seepage soil, seepage will take place under very low hydraulic gradient.

With isotope tracer test, we can obtain such parameters as follows:

1. Seepage flow velocity: The distribution of seepage flow velocity along the depth can be detected. The bigger seepage velocity is at a certain layer, the more probability seepage occurs there.
2. Direction of flow: With the distribution of direction of flow, we can find out the concentrated leakage passage under the dyke.
3. Vertical flow: Usually in the low water period, there is no vertical flow, but sometimes leakage may be caused by the fault transmitting the water. When the borehole discloses the fault, upward or downward vertical flow may appear in the borehole. Through detecting the vertical flow we can judge whether strong flow exists in bedrock soil.

Sometimes, we need to do injecting test using isotope tracer, which is rather different from the common injecting test. Through the test the aquifer's soakage in separate layer can be determined, further, the smallest interval between the layers is less than 10cm. In the multi-aquifer system, the hydrostatic water head and hydraulic gradient of each aquifer can also be determined by using the test. Through water absorption test the continuous distribution of the permeability coefficient can be found out, we must pay much attention to the gravel layer where permeability coefficient >5m/d. Because the most permeable layer determined by injecting test is also the water rising layer of seepage, only the layers with strong permeability are dealt with and then the occurring of seepage during the flood period can be prevented.

2.2 *Measurement of seepage velocity by point dilution method in single borehole*

The principle of point dilution method is putting isotope tracer in the test point of the borehole, then the concentration of tracer will reduce with the seepage flow, so we can get the velocity of seepage flow through measuring the concentration of tracer in single borehole (Fig. 1).

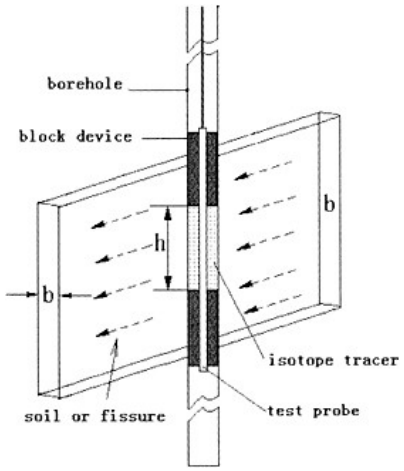

Figure 1. Measurement of the flow by isotope tracer method.

According to the three different cross of borehole and soil: vertical, parallel and bevel, there are different formulas of velocity as follows:

Given the borehole is vertical to the surface of the soil (Fig. 1), under laminar flow condition, the seepage velocity can be deduced as [4][5]:

$$V_f = \frac{\pi (r^2 - r_0^2) \cdot h}{2r \cdot \alpha \cdot b \cdot t} \ln \frac{N_0}{N_1} \quad (1)$$

where V_f seepage flow velocity; r, radius of borehole; r_0, radius of probe; N_0, primary concentration; N, concentration after time t; b, soil width; h, height of test; α, the correction coefficient.

After injecting a kind of soluble and weak sorption isotope tracer in the test segment of the borehole, if there is horizontal flow in the borehole (the probe must be added block-device if there is vertical flow in the borehole), the isotope tracer in the borehole will flow into soil. As a result, the isotope concentration near the soil in the block will be different: the inflow direction is the highest, and the outflow direction is the lowest. Detecting the distribution of isotope concentration, we will get the direction of groundwater flow.

The velocity of vertical flow can be calculated by measuring the peak value of tracer concentration. The isotope tracer is put into the point whose each side (above and below in vertical direction) has two calculators of concentration. With two calculators above or below detect the peak value, and the time of test is known, we will get the velocity of vertical flow.

2.3 *The selection of isotope tracer technique in single borehole*

The determination of permeability of rock soils in single borehole has great practical values, because the seepage field can be detected completely in the existed observing hole at the researching zone. The minimum diameter of the isotope tracer probe is only 30mm, which is suitable for the observing hole whose diameter ≥ 35mm, and the diameter of most existed observing hole is usually 75mm, so it needn't bore additional hole for detection.

The isotope tracer method in single borehole includes detecting vertical flow under the condition of injection. The purpose of injecting is to assure the groundwater flow is steady flow and usually its effect is good. Mostly the velocity of vertical flow is very low, even under the condition of injection, vertical flow velocity is less than 1m/h, so that other discharge instrument cannot detect the velocity accurately.

3 FIELD TEST

Samanalawewa dam is a important project in Sri Lanka (Fig. 2). The geologic condition of it is so complex, for there are many soils with different directions and intersections. The rock strata trend to downstream, so the seepage flow happens easily. The discharge of a leakage under the dam base reached 300L/s.

In order to ascertain the seepage field of Samanalawewa dam, nature tracer test and isotope tracer test have been done. After the demonstration in the field of Samanalawewa Dam, participants from different countries discussed the leakage reason and found:

1. According to the temperature distribution in the leakage area there is a low temperature zone (24.8°C) nearby the observation borehole No. 1 and No. 8. which is same as observed at the spot of leakage outlet. The temperature distribution measured in the tunnel drainage wells shows that there is a low temperature zone (24.9° C) between No. 5 to 9 and the other wells appear high temperature (>25.5°C).
2. Using the Point Dilution Probe, it is observed that there is an ascending vertical flow (0.35m/d at 380m elevation) in the observation borehole No. 8. It shows the pressure of the permeable stratum exploited is higher than the top aquifers. (Fig. 3)

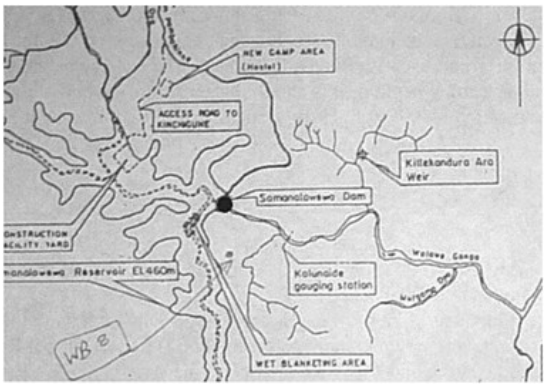

Figure 2. The site of Samanalawewa dam in Sri Lanka.

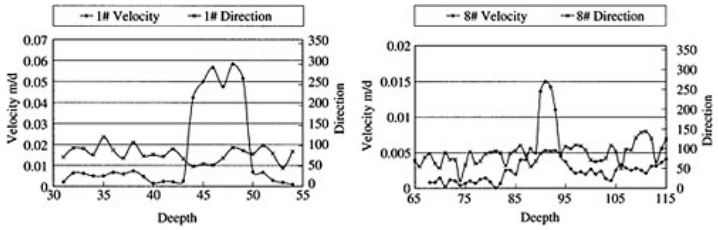

Figure 3. Velocity and Direction in borehole 1# and 8#.

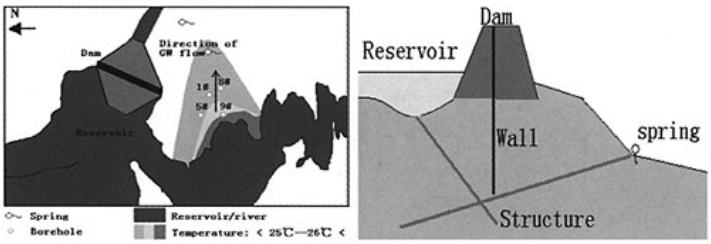

Figure 4. The leakage pathway of Samanalawewa Dam.

3. The groundwater flow direction detected from the boreholes No. 1 and No. 8 is about N90° (Fig. 3).

All of the above information shows that there is a big leakage pathway in this area and it is inclining. The elevation of the leakage pathway position crossing the tunnel is below 280m because the depth of the curtain wall is about 100m deep.

After analyzing the results of isotope tracer test, the main seepage passage is been found and the whole seepage flow field is clear (see Fig. 4 shows).

The leakage path comes from reservoir to spring about 50–100 degree (from N), and there have structures in the rock. Water come into the structures under the reservoir by the high pressure, and come through the cross structures, then flood out of a cave. The leakage path comes between borehole 1# and 8#, and the setting depth of it is about 40–50m from ground at the position 1#, 90m from ground at the position 8#. So, we get the exaltedly information to treat to the leakage with less money.

4 CONCLUSIONS

Tradition method in dyke/dam investigation have limited result even in not so bad conditions, these data always value in ten-meters depth.

With the rapid development of kinds of engineering, especially high dam, the study of seepage flow becomes increasingly important. Isotope tracer method is important tool for the investigation of leakage of dam and dyke, and this investigation is necessary for taking any repair work. Moreover, the nature tracer method is usually applied to investigate before to limit the possible area.

Isotope tracer method develops very fast. At present, many seepage flow models have been set up, which can be applied to obtain many hydraulic parameters. However, there are no seepage flow models applying isotope tracer method, while natural seepage is almost all in three dimensions, so that is a problem needed to be studied deeply.

We can use natural method to get a map of the problem, drain the borehole at possible positions, then use tracer method. With those we can got enough data such as velocity, direction, etc in borehole to get the seepage field, and to calculate the seepage path directions and depth. Finally we can analysis if there have structures harm to dam/dyke. If it exist, we can do a perfect job to fix it.

REFERENCES

[1] Ge, Liangtao. 1984. Flow principle of multi-layer aquifer in blended well and flow rate logging method. Geology Publishing House: Beijing.
[2] Chen, Jiansheng, Study of isotope tracer theory and method in rock hydraulics, Doctoral dissertation, Hohai university, 2000.
[3] Moser H, Drost W. Application of single and multi-well techniques in fractured rocks, Isotope techniques in the study of the hydrology of fractured and soild rocks. IAEA-AG-329.2/12. Vienna: IAEA, 1989:223.
[4] Chen, Jiansheng, Zhao Weibing, Study of permeability of fractured rock by isotope tracer.
[5] Xue, Yuqun, Zhu Xueyu. Groundwater Dynamics. Geology Publishing House.

New Developments in Dam Engineering—Wieland, Ren & Tan (eds),
© 2004 Taylor & Francis Group, London, ISBN 04 1536 240 7

Participation models for resettlement due to dam construction

Shaojun Chen, Guoqing Shai, Wenlong Zhu & Jiajun Xu
Hohai University, China

ABSTRACT: Participation is a means to promote social development and gain project success. Participatory approach is broadly understood as the active and all-around intervention of the development body in the process of relative decision-making that will affect the resettlers' production and livelihoods. Involuntary resettlers intervene in the resettlement activities democratically—deciding the general objective and the plan of resettlement, participating in the implementation of the resettlement, and sharing the interests and fruits of development—is the fundamental measure to safeguard resettlers' basic rights and interests. Starting with the problems existing in China's resettlers participation, then analyzing the factors affecting the participation, this paper brings forward the assumption of participatory capacity building for involuntary resettlers, and then combining with the Xiaolangdi Resettlement Project case to introduce the participatory models in different phases of resettlement relocation.

1 INTRODUCTION

Participatory development seems to be the most frequently used new concept in the research and practice fields such as current international development, international politics, economic policy, social policy and so on. Both the leaders from the World Bank who dominate the world development and the supervisors in a community who conduct development practice are using this concept. "Participation" is a process of endowing the mass with power, while "participatory development" is broadly understood as the active and all-around intervention of the development body in the development process that will affect persons' living condition or in the relative decision-making process of development project (Li xiaoyun, 2001). Participation is not only an objective of social development, but also a means to promote social development and gain project success. The stakeholders' participation in deciding, preparation and implementation stages will improve the project's implementation and gain support and cooperation from local residents.

Resettlers and their communities (villages or teams) are the host of resettlement activity and also primary stakeholders of the project, whose participation serves as one of the key factors of the project success. Resettlers' participation is the process of rights endowment caused by land requisition and house demolition, which could serve as an effective means of promoting participatory decision and social authorization and promote the transfer of right and control from external interveners to local residents.[1] In the 21st century, China will continue to make large-scale economic construction. Large number of highway, railway and city extension and rebuild projects and the projects of hydraulic, electric, environmental and agricultural construction will cause even larger resettlement problems and the estimated affected population will amount to

[1] Jennifer. Ritbagen-MacCracken, Depew. Lanier, Participatory Tools and Skills—Collection of Participation and Social Evaluation Method, Social Policy and Resettlement Department of World Bank, 1999.

annual several millions (Shi Guoqing, 2001). How to deal with these problems better, to make the resettlers restore their original income and living standard, to let resettlers participate in the project construction more broadly and deeply and enjoy interests and fruits are all theoretical and practical tasks of great importance deserving our deep research and settlement.

2 PROBLEMS EXISTING IN RESETTLEMENT PARTICIPATORY

There are still many problems needing to be solved in resettlers and communities' participatory capacity building. They are: (1) weak participatory system construction. There have been acquisitions about resettlers' participation in some current regulations,[2] but operational regulations and detailed rules are still lack; (2) resettlers and communities can't effective participate in many affairs during resettlement, especially the decision of compensation policy, relocation program and the construction of infrastructures and public facilities; (3) in resettlers' communities, resettlers broadly participation is lack of clear regulation, effective system and successful model and resettlers always make passive participation; (4) the participation capacity of resettlers and that of communities are very insufficient, effective capacity building activity is needed to inspire, promote and strengthen it; (5) research on theories and methods about participatory evaluation in resettlement activity and the development of successful case study is very weak; (6) the participatory evaluation capacity building of resettlement system is insufficient and the human resources are short.

3 FACTORS AFFECTING RESETTLEMENT PARTICIPATION

Factors affecting resettlers participation include objective environment and subjective conditions. The objective environment refers to all the external conditions affecting resettlers participation directly or indirectly, such as economic environment and social political environment. The subjective conditions refer to the desire of resettlers themselves, which are affected by their standard of education, mental quality, ability and so on.

Objective environment:

(1) *Social political environment.* The government's administrative system is the primary factor affecting resettlers effective participation.[3] Local governments sometimes believe that resettlement policy and program are under their control; they can provide resettlers with most favorable service. Under this kind of systemic framework, resettlers can only be passive receiver of the finial services. As society develops, people's consciousness of democracy, equitableness and legal system has been improved significantly; various participation channels have been built up and smoothened. Resettlers now can enjoy more freedom and rights and have more participation opportunity. They can join in various interest organizations and learn to take advantage of organizations to deal something they can't do by themselves.

(2) *Economic environment.* High regional economic development level, good resettlers' income and living standard and convenient transportation and communication conditions can eliminate the space difference of affecting the development of participation consciousness caused by the imbalance of economic development and increase participatory material resource. With the development of economics, economic structure is getting more complicated, multi-interest situation has

[2] "People's Republic of China Land Administration Law" empower those whose land are requisitioned to participate and supervise, demanding publication of land requisition scheme, land requisition compensation and the use of it. "Regulation for Urban House Demolition and Management" (2001, 6) states that once a house demolition lisence has been issued, the demolition sector should promulgate the demolition scope and deadline for relocation in the form of bulletin. House demolition management sector and removers should propagandise and explain well in time.

[3] Investment Research Institute of State Development Planning Commission, Criterion Ration Research Institute of Ministry of Construction, edited by social evaluation group: Economy Management Printing House, 1997, 45–50.

come into being and the economic difference has been broadened. All these have caused the emergence of different interest bodies and promote the resettlers' economy move toward multiple. More various contradictions and conflicts emerge and the degree of resettlers participation increase. With economic progress, people improve their expectation of spiritual demand when their material demand have been met, so resettlers' self-driving force to participation have been increased.

(3) *Social cultural environment.* Factors such as regional social structure, social rank classification, educational standard, social values, ethnic structure and right distribution involved in land requisition and house demolition have influence on resettlers participation. Advantage groups always have control over participation while vulnerable groups like the poor, women, the old and ethnic groups are voiceless, so the au pair participation is hard to achieve.

(4) *Information environment.* Government is the promulgator of resettlement policy, compensation, relocation, and administration who has the most authoritative, complete and precise information. However, because there is no standardization for information dissemination, resettlers are only provided with part of microcosmic and practical information relating closely to their production and livelihoods. Although they may try to understand available information, because of the lack of a routine channel they can only get incomplete information or even mingled with many hearsay and wrong information. The limited and insufficient information known by resettlers have greatly affected their participation.

Subjective conditions: people's desire of participation. Participation is a kind of high level demand of human,[4] resettlers' desire of participation, decided by educational standard, metal quality and ability, also has influence on participation degree.

(1) *Social psychology.* Social psychology guides resettlement participation. China has over 2000 years of feudal history. The psych that has developed within its traditional culture often appears to be incompatible with participation. A democratic society encourages members to participate, to stand up for their rights, while the psyche of traditional culture is such that most people want others to speak on their behalf so as to avoid possible risks caused by participation. A democratic society advocates independent thinking, but in the real life, where the traditional culture is still dominant, more people like to go with the stream and stand ready to submit to the authority, independent consciousness to develop individual never can get sufficient encourage. Some resettlers, especially vulnerable groups, sometimes have the desire to participate, but the increased economic costs and risks may discourage them. These factors seriously hamper the achievement of widespread resettler participation.

(2) *Participation ability.* There are obvious differences among resettlers in using participation skills. Resellters' ability to raise and communicate problems clearly and effectively can lead to activist roles within organizations, while other resettlers are able to contribute practical help. However, there are still some who can neither be useful part in the group nor offer any help. They can't participate in social activity effectively because of the failure to use any skill.

(3) *Educational standard.* With regard to resettlers participation, there is great difference between resettlers with different educational standards. Resettlers with high educational standard have clear sense of participation and strong influence power, they have the ability to call on and organize others to participate. On the contrary, resettlers with low educational standard are lack of sense of participation and have no opinions about widespread social issues; they are impossible and have no ability to influence the society.

Besides the above-mentioned important factors, wealth, occupation, experience, age, sex, nationality, religion and some other factors may also have influence on resettlers participation. Because a rich family may lose more than a poor family and has economic ability to pay participation cost, the former is often involved more in participatory activities with more enthusiasm. The heads of the village committee and village groups, as key community leaders, assist the local

[4] Maslow "Inspire Mechanism of Human".

government in undertaking the socio-economic survey, resettlement plan and implementation and may, therefore, obtain early details and broad information on resettlement policy, socio-economic results and potential resettlement sites. They have relatively broad, active relations with both internal and external of the community. Subjectively, they need to enhance selves or groups' authority by formal (community vote) or informal (recognized by community's internal members and families) ways in the process of resettlement, so as to cement their roles as decision makers in community affairs and resource management. They are the most active participants. Other stakeholders who are educated or have work experience, such as Teachers, doctors and village enterprises owners, may pay more attention to the future of communities, families, households and individuals, becoming very important stakeholders in the process. As far as gender is concerned, the idea that "men decide most issues outside the home, whilst women make most decisions on household issues" is still dominant in Chinese vast countryside, especially underdeveloped areas,[5] so women's level of participation is generally lower than that of men. Referring to age, young and medium-aged persons have participated more than the old and the children.

4 PARTICIPATORY CAPACITY BUILDING

Capacity building is main request in achieving three aims of project participation, which are sustainability, availability and extensibility (Janelle Plummer, 1999). Its main consideration is the sustainable functional system of resettlement, including participatory capacity building for resettlers, executives and administrative agencies.

(1) *To build up the host sense of affected groups.* In the traditional preparation and construction process of hydraulic projects, affected groups are always under domination with little influence on decision-making, thus forming a passive and negative situation. The primary aim of capacity building is to inspire the affected groups and foster their sense of responsibility and adscription to the project, to encourage them to combine the project's development with their own development, and with local social development. In this way, they can make sufficient mental preparation for effective participation.

At present, the formation of main body sense is still not a spontaneous process, whose impetus is largely external, so it is the interactional result between external impetus and affected groups. Under this circumstance, external impetus is not formal, bureaucratic, commanding but serves as prompter, propellent, incentive factor, changing power, which accelerates the community's organization and participation through guidance. It is the enlightenment of participants' capacity building and formation of internal impetus serving as the basis for the whole capacity building.

(2) *To eliminate the guard psychology of the affected groups.* It is emphasized in the participation approaches that executive agencies' behaviors must be changed to eliminate the guard psychology of the affected groups. It is usually believed by the owners, design institutes and executive agencies that only if the behavior is right and part of decision-making rights have been given to the affected groups, they will have no prejudice, but often it is not the case. No matter how good the performance of owners, design institutes and implementing agencies do, the affected groups always feel their interests being harmed and the result of participation is to accept arrangement unconditionally. Therefore, sound and equitable participation must adopt measures to eliminate the guard psychology of the affected groups.

(3) *To establish organizations capable of participation.* At present, no organization manages and organizes resettlers' overall participation. There are two ways to settle this problem: one

[5] In most rural regions in China, the traditional social work division is that women are responsible for internal household affairs (housework, agricultural work, caring for the old and young), and men are responsible for external affairs (discussing and deciding public affairs, heavy agricultural work, and outside contacting).

is to establish an independent agency to organize participation, which should be involved in resettlement from the project identification stage, organizing and developing various participatory activities. This agency should cooperate closely with other involved functional agencies, and should be responsible for all the participatory tasks undertaken by these agencies. By this means, participatory agencies take full time charge of participatory tasks from beginning to end and it can take complaints and appeals into its function. Another is way is to establish a special department in each functional agency to oversee each agency's participation instead of establishing an independent agency, and such departments should be responsible for fulfill participatory tasks of its own agency.

The initial form of resettlers participation organization can be small groups formed by kindred households with similar social and economic interests, similar economic activities, and from the same or contiguous village. Small group has the characteristic of sharing system; the members trust one another and make decisions together.

(4) *To mobilize resources.* Participation resources cover a biggish category, generally including human resource, fund and agencies resources. To establish organizations can assist the effective mobilization of the community's internal resources. As for collective activities, it can organize labor input, accumulate labor and collect limited funds to play convergency scale role. Self-mobilization is an important preparatory phase in organizing participatory activities, accumulating experience for the further extension of organizational management. With the extension of organization's longevity, participants can gradually build up confidence in jointly creating bigger changing power and gaining greater development.

The financial resource restriction of participation is ubiquity. First, it needs the changes in policy. There has no participation cost item in present reservoir submerge disposal budget criterion, but increasing expense has been put on participation, especially in some projects sponsored by foreign financial organizations, whose expense has account for considerable proportion of cost. So, it is necessary to modify relative policies and regulations to bring participation cost into budget. Second, it should make good control over participation in measure, and conduct appropriate participation. Excessive participation may not only increase the participation cost significantly but also make the decision-making difficult.

(5) *Skill training for participants.* To make participants master participation techniques and management skills. Assisting participants in learning how to participate is perhaps the most important issue of the whole participatory process. Usually the skills are divided into common skills and particular skills. Common skills include literacy, house health, family planning, community management and so on; particular skills include the production, the processing and marketing skills of agriculture, forestry, livestock, subsidiary production, and fishery. Training is an effective way to ensure the improvement of participants' ability.

The main current human resource problem is to increase people's capability to organize participation, and to create special organizers in relevant departments. Then sending these people to professional institutes to receive training, or to persuade the institute to provide on-the-job training that can be used into practical participation activities and to advance the quality and effect of participation. For the training of major stakeholders, one possible way is to select educated or highly motivated resettlers to receive training, so that they can teach others how to improve participatory skills in their own way. Only if the participation skills of both participation organizers and participants are improved, can the effect of participatory activities be ensured.

In conclusion, the effect and meaning of public participation couldn't be matched by superficial or formal participation. Public participation can't be contented with diverse forms. The same form may have quite different result just because the mastery of participation's core problems is different. Public participation with no effect and on emphasis is just a formality, with no promotion to the practical work. In addition, participation methods vary from projects to projects, from phases to phases. Therefore, in order to conduct real public participation activities, coordinate each party's interests and enhance their capacity, it is vital, on the basis of analyzing project's stakeholders and taking account of project's characteristics, to design different participation models for different project phases.

5 PARTICIPATION MODELS FOR DIFFERENT RESETTLEMENT PHASES

Participatory method can be used in the whole process of resettlement relocation, including socio-economic survey, resettlement planning, relocation, income restoration, monitoring and so on. Using participatory method in these activities can make the investigator understand the requisite information quickly and adjust resettlement activities in time because its characteristics of seeable, direct, opening and flexible.

5.1 *Participation in resettlement relocation planning*

(1) *Social-economic survey.* In order to draw out suitable rights qualification and relocation policy, resettlement planning and implementation should reflect the trusty and precise information of affected persons, while social-economic survey is the basis for resettlement planning.

In the social-economic survey of Xiaolangdi Reservoir Resettlement Project, municipal and county governments of affected areas, design institute, resettlement office and related functional departments at county level, township and county government, village and groups representative, resettlers and property right owners have broadly participated in the activities of investigation, measurement, registration and statistics. Village representatives (including women) confirmed details of affected collective land and property by signature and stamp, with householders confirming details of their homes and property in the same manner. Group, village, township and county stamped one by one. In the investigation, Requisite social-economic data had been collected broadly; the opinions of resettlers, village groups, township and local government on the resettlement plan had been considered.

(2) *Decision of resettlement relocation scheme.* Relocation is often the most difficult task, since rebuilding living conditions is a challenging and complex task involving the re-establishment of the community and its life style.[6]

In Xiaolangdi Reservoir Resettlement, the design institute, local government, resettlers and host community should combine to choose the relocation site, conduct on-the-spot investigations, compare and select schemes, and write the relocation report, so that the relocation plan adequately reflects resettlers' wishes, and coordinates local social-economic development. To program infrastructure construction needed in resettlement relocation and program agriculture, enterprises and the third estate can help production restoration and living standard restoration. At the same time, the town government, village team cadres and resettlers' representatives (including women) must participate in resettlement scheme decisions, relocation site choice, lay out and design, so as to make the resettlement scheme accepted by resettlers easily.

(3) *Compensation standard.* Compensation standard is an important task that resettlers pay most attention to in relocation planning. The failure of openness and transparence of it may lead to resettlers' nonconfidence on government, and then affect the whole resettlement process. Compensation policies and standards are based on Land Administration Law and Regulations for Land Requisition Compensation and Resettlement in Large and Medium Size Water Conservancy and Hydropower Prqjects, and based on the average output of the latest three years of the inundated land. In China, collective land requisition is national activity, but not land trade or compensation at "market value" under the consultation of government and resettlers (Bi baode, 1996). The principle of land compensation and relocation allowance is to ensure that farmers' living standards will not decline as a result of land requisition.[7]

In Xiaolangdi Reservoir Resettlement, the participatory process is: (1) to inform resettlers of state regulations governing land compensation; (2) to spend a substantial amount of time

[6] Resettlement Office of the Ministry of Water Resources, Resettlement Relocation and Compensation in Foreign Countries, 1994.

[7] Asia Development Bank, Resettlement Handbook, An Feasible Practice, 1995.

on resettlement sites, interviewing affected people (including women and vulnerable groups), to obtain information on output of the latest three years of the inundated land, house building costs, and affected people's income and expenditure; (3) the design institute, local government and community representatives must decide compensation standards, together, in compliance with state or local regulations; and (4) publish, disseminate and explain compensation standards at the village level.

After the relocation plan is established and approved, it should be made available to all, especially the major stakeholders in the form of an information booklet. The design institute and executive should also explain the main contents of this booklet to affected people[3].

5.2 *Participation in relocation*

(1) Resettlers' opinion should be considered sufficiently in choosing rehabilitation site and the method of land distribution for housing. The rehabilitation site should be decided with the sufficient participation of resettlers.
Participation of Xiaolangdi Reservoir Resettlement includes: (1) understanding the real opinions of resettlers and desires through meetings and interviews; (2) combining with resettlers' desires, executives published each potential scheme for resettlement sites; (3) organizing resettlers to inspect possible rehabilitation sites; (4) adjusting the rehabilitation site according to the resettlers' desire. On the premise of obeying unitive programming, resettlers chose land for housing by drawing lots in a process that is fair and open. When necessary, notarization can be done.

(2) *House reconstruction.* House reconstruction should take resettlers' desire into sufficient consideration, let resettlers participate the process of house reconstruction and the forms of it can vary from place to place.
Rural house reconstruction in Xiaolangdi Reservoir Resettlement adopts several forms, such as self-demolish and self-building, unified planning and self-building, unified planning, and so on. In the second form, the degree of participation is the highest and the self-decision is most sufficient within the general interest of whole community. When adopting the third form, a useful participatory style is to establish a "building inspection panel" (made up of house-constructing householders representatives), whose responsibility is to supervise the housing quality, progress and funding.

(3) *Compensation payment and use.* Land compensation and the rehabilitation allowance should be used to restore production, to re-employ labor made redundant as a result of land requisition, and to help those who cannot work. This fund should be used for these particular purposes, and should not be divided privately, or used for any other purpose. The use and ownership of the compensation belong to the resettlers, and resettlers also have the right to full information on compensation rates, to be involved in all decisions on compensation use, and in the management of resettlement activities.
In Xiaolangdi Reservoir Resettlement, on the premise of compensation fund publication, a fund supervisory group made up of representatives was established to take charge of the compensation fund supervision and management.

(4) *Infrastructure construction.* Infrastructure project construction should devote particular attention to mobilizing local government and resttlers' activities, and to the different organizational styles and types of management in use. The community should organize resettlers to participate in such labour-intensive construction activities as land levelling, water supply, electricity supply, traffic and other infrastructure areas. Professional project reconstruction such as irrigation works, roads, railways, electrical power, shipping, telecommunication and broadcasting should choose their mode of operation, based not only on project scale and extension, but also on the views of the resettlers. Professional project reconstruction with large scale and broad extension should be managed according to the process of infrastructure program, and resettlers may participate in part of the activities when possible.

5.3 *Participation in income restoration*

Income restoration strategies generally include two types: (1) strategies based on land, offering sufficient land to resettlers, restoring farmer's traditional production methods and sources of income; (2) non-farmer resettlement strategies, including a series of activities, such as occupational training, employment arrangement, direct loans, small rural stores, and enterprises providing employment. Affected persons should participate such activities actively.

Income restoration schemes. Under the guidance of executives and the organization of the village committee, resettlers (including women and vulnerable groups) discuss fully and decide on an appropriate scheme. *In Xiaolangdi Reservoir Resettlement, the opinions on usage of compensation fund from resettlers can be heard through village representative meeting and village meeting; technical personnel in agriculture, forestry, livestock and fishery helped resettlers and community organization with feasibility study of income restoration scheme; and then executives, technical personnel, village committee and resettlers decided the income restoration scheme together.*

Land adjustment is the most basic income restoration measure. It must be established on the basis of principles of fairness, openness and justice. The "Decide the area by production and decide the production by area"[8] model used in Xiaolangdi Resettlement Project is a fair method of land allocation, and a good means of enabling resettlers to participate in community construction. The method could usefully be used in other resettlement schemes.

Technical training is an indispensable aspect of income restoration. Training design should meet resettlers' needs, especially those of women and vulnerable groups. Since rural resettlers' qualifications are generally low, technical training or guidance should try and adopt a variety of forms, such as on-the-spot demonstration, for example.

Full participation in deciding on an income restoration scheme, together with active guidance from the government, can enable a successful restoration of resettlers' livelihoods and production.

5.4 *Monitoring and evaluation*

Monitoring and evaluation should include participatory monitoring of resettlers and community organizations and external independent monitoring.

Participatory monitoring and evaluation of resettlers and community organizations in Xiaolangdi Reservoir Resettlement was organized mainly by themselves, it aimed at the activities of inundated assets investigation, confirmation and compensation payment; land distribution for housing; house and public infrastructure reconstruction; cultivated land allocation and adjustment; public sanitation; community affairs management; community assets and fund management and so on. Monitoring and evaluation can be conducted by individuals, family members, and informal groups (such as cooperative teams comprising representatives from several households building houses together), formal organizations (village committee, village group, party branch), and temporary organizations. Their responsibility is to monitor, inspect, evaluate, accept, consult and decide activities to the benefit of the community and its constituent organizations.

Monitoring and evaluation by an equitable, independent organization is usually the responsibility of the project owner, and is conducted by an independent organization. It aims to periodically monitor and evaluate relocation activities and income restoration, in order to feedback complaints, problems and suggestions to proprietary and local executives, so that problems can be addressed as quickly as possible.[9]

Xiaolangdi external organizations adopted participatory evaluation methods in interviewing stakeholders, talking with resettlers, understanding local government's opinion of the project, compensation payments, and the restoration of their income, production, and livelihoods. Monitoring and evaluation provides an important platform and channel for resettlers 'participation and complaints.

[8] Shi guoqing, Yu wenxue, Xiaolangdi Reservoir Resettlement Evaluation and Analysis Report, 2000.

[9] World Bank, Directory of Resettlement Monitoring and Evaluation, 2001.

In conclusion, in diiferent phases of project cycle and different resettlement relocation activities it should be ensured that resettlers could participate sufficiently, and have the rights to know allocation policy and make decisions related to production and livelihood restoration and development.

REFERENCES

Bi debao (1996) *Land Economics.* Republic University of China Printing House, Beijing.

Dong ming (2002) Transaction of Hohai University (philosophy and social science edition). *Studies on the Application of Participatory Method in Involuntary resettlement.* Hohai University, Nanjing, China. Vol. 2.

Investment Research Institute of State Development Planning Commission, and Criterion Ration Research Institute of Ministry of Construction (1997) *Directory on Social Evaluation of Investment Project.* Economy Management Printing House. 45–50.

Janelle Plummer (1999) *Municipalities & Community Participation—A sourcebook for Capacity Building.* Earthscan Publication Ltd.

Li xiaoyun (2001) *Conspectus of Participatory Development, Theory—Method—Tools.* China Agricultural University Printing House.

Michael M.Cernea (1996) *Resettlement and Development, Studies on World Bank Resettlement Policies and Experiences.* Hohai University Printing House, Nanjing.

Shi guoqing, and Chen shaojun (2001) *China Resettlement Policies and Practices.* Republic Printing House Ningxia.

Tang chuanli (2002) Proceedings of International Symposium on Resettlement & Social Development. *China Resettlement Policies and Practices.* Hohai University Printing House, Nanjing. 3–8.

This page intentionally left blank.

New Developments in Dam Engineering—Wieland, Ren & Tan (eds),
© 2004 Taylor & Francis Group, London, ISBN 04 1536 240 7

Study on social assessment of dam projects

Shaojun Chen
University of Hohai, China

ABSTRACT: Social assessment of water conservancy and hydropower projects is to evaluate the contribution and impacts on social development objectives brought by the construction of such projects. It is to evaluate objectively the social effects from the angle of the whole society, so as to optimize the design and promote the implementation of the project. Social assessment should stick to the principle of "Put the person in the first place", putting human function and human development into primacy. And the detail principles are principles of multi-objectives comprehensive assessment, systematism, combining qualitative analysis with quantitative analysis, equity and justice, public support and participation, improving livelihood, welfare and sustainable development. The main methods in social assessment are quantitative and qualitative analysis, comprehensive assessment, comparison of socio-economic development with and without project, participation, stakeholders analysis, logic framework analysis, etc.. The social assessment should be carried out with three levels-nation, area and project. In detail, it includes social impact analysis, inter-adaptability analysis and social risk analysis. Based on the above, suggestion on optimizing design and measures on avoiding social risks are carried out.

1 INTRODUCTION

Water conservancy and hydropower projects, as effective means and main access to realize water resource development objective, play an important role in national economy and social development of China. New development stratagem of "based on human being" pays emphasis on that physical production is a means while human development is fundamentality. So the evaluation theory of investment project has experienced three main phases, with financial evaluation, economic evaluation and social assessment. Social assessment is trying to analyze some social problems occurred in water conservancy and hydropower projects by sociological theory and method, such as involuntary resettlement problem, poverty problem, social gender problem, minority problem, etc.. The function and development of human have been taken into account in social assessment. Carrying out social assessment in water conservancy and hydropower projects is a means to make scientific and democratic investment decision, to reduce bias in decision-making and to increase the benefit, adaptability and sustainability of the projects, which is still helpful in realizing the objectives of national economy and social development. Directory on Feasibility Study of Investment Project published in 2002 indicates definitely that social assessment, which include the analysis of social impacts caused by projects and the analysis of inter-adaptability between project and locus, must be carried out in the feasibility study of water conservancy and hydropower projects[1].

[1] *Directory on Feasibility Study of Investment Project.* China Electric Power Printing House. 2002, 198~208.

2 SIGNIFICANCE OF WATER CONSERVANCY AND HYDROPOWER PROJECTS SOCIAL ASSESSMENT

There have different understandings on investment project social assessment[2]: the first one is social assessment in social cost-benefit methods based on economics, usually including benefit analysis and equal distribution analysis. The second one is social analysis based on sociology and anthropology, analyzing the influence caused by social factor and cultural factor; and this method is adopted by most of the international organizations. The third one is social impacts assessment, including the influences on individuals, organizations and communities.

In *Social Assessment Capacity Building in China* published by ADB, social assessment is defined as a tool oriented by action[3] and the objective of it is to put the social factors into project cycle. Social assessment is both an analytic tool and a stratagem tool, which can find out, measure and adjust social impacts; can design specific benefit for specific beneficiary; can bring direct benefit for the poor and vulnerable group through participation; can identify potential negative effects caused by projects; and can avoid or decrease the negative effects on human.

Most scholars in China think that the social assessment in water conservancy and hydropower projects is to analyze the adaptability and acceptability of local social environment when investigating and forecasting the social impacts and social benefit caused by the project construction and operation. It is to analyze all kinds of social factors involved in project, study the feasibility and optimize the design; and then carry out a scheme to harmonize project with local society, to avoid social risks, to promote implementation of the project and to keep the social stabilization[4].

In penman opinion, water conservancy and hydropower projects social assessment is also a tool same as economic evaluation and financial evaluation. It is applying sociology methods to assess the contributions and impacts of the project construction in realizing social development objectives from the angle of sociology; to analyze the positive and negative effects on stakeholders, especially vulnerable group, and potential social risks in realizing project objective; to carry out suggestions to optimize the design, avoid social risks and promote the implementation of the project.

3 MEANING OF WATER CONSERVANCY AND HYDROPOWER PROJECTS SOCIAL ASSESSMENT

The development of the water conservancy and hydropower projects demands social assessment. And the economic growth is not in vacuum circumstance while goes with all kinds of social relations, which have affects on decision-making, scale and outcome of the project Social factors related to development should be taken into serious account if want to realize the established objectives of the project. For instance, economic, social and cultural characters of local area where project is constructed, including the possible negative impacts (such as resettlement); production activity of the social group; acceptability in culture and adaptability in special group when designing; social stratagem in project implementation and project operation, including the participation of the affected group; etc.

The emphasis of development stratagem in China has experienced the change from economy growth to harmonious social development. And social development has obtained the granted consideration[5]. Social assessment has carried out the viewpoint of "based on human" in social

[2] Wu heng'an. *Theory and Methods of Financial Evaluation, National Economic Evaluation, Social Assessment and Post-Evaluation*. China Water Conservancy and Hydropower Printing House. 1998.

[3] Shi guoqing. ADB TA3441: *Social Assessment Capacity Building in China.*

[4] *Directoiy on Feasibility Study of Investment Project.* China Electric Power Printing House. 2002, 73.

[5] Edit by Investment Research Institute of State Development Planning Commission, Criterion Ratio Research Institute of Ministry of Construction and Social Assessment Research Team. *Directory on Investment Project Social Assessment.* Economy Management Printing House. 1997.

development. To study the relation between project and human is in favor of coordinating the relationship among stakeholders and promoting the sustainability and adaptability of the project.

To carry out social assessment in water conservancy and hydropower projects helps to realize the harmony and coherence between national economic development objective and social development objective, avoid pursuing financial benefit merely; helps to realize the harmony and coherence between the project and local economy, decrease social contradictions, conflicts and disadvantageous social impacts caused by involuntary resettlement, promote social stabilization; helps to avoid or decrease social risks in implementing and operating project, improve the investment benefit.

4 PRINCIPLES OF SOCIAL ASSESSMENT

Social assessment should stick to the principle of "based on human", putting human function and human development into primacy. The detail principles are as follows:

Principle of multi-objectives comprehensive assessment. Social effect assessment should keep to the principle of multi-objectives comprehensive assessment. Each objective and its evaluation index have different position and different importance, so to evaluate the importance (weight) of each objective is necessary, and administrative levels analysis and the method of grading by experts can be adopted. That is the satisfactory degree of detail index may be quantitated or convert from qualitative description to quantity, then translate multi-objectives into single objective through certain mathematics methods, and obtain the evaluation result according to the value of single objective at last.

Principle of systematism. Systems analysis should be adopted in water conservancy and hydropower project. Not only the social effects brought by prospective project outcome, but also the social cost should be taken into consideration. Combining the source input and benefit output, it is to analyze systematically whether the social benefit can make for the social cost and how much net benefit can be obtain finally

Principle of combining qualitative analysis with quantitative analysis. Social effects of water conservancy and hydropower projects can be embodied from many aspects and their stand or fall can be evaluated by different criterions and indexes. Some indexes are difficult to quantitate exactly; while other indexes can be quantitated but cannot convert into a uniform unit. This makes the criterions separately and the inner relations are difficult to find out. So it cannot solve the problem effectively by using qualitative analysis merely or using quantitative analysis merely, only the combination of the two analyses can scientific and practical it is. Generally speaking, adopting quantitative analysis as much as possible is better; as to those indexes which cannot be quantitated, it had better be converted qualitative to quantitative by certain methods such as fuzzy mathematics, multi-objectives decision-making and other suitable methods.

Principle of equity and justice. This demands that the positive and negative impacts caused by project be taken into account sufficiently during planning, designing and implementing the project. All kinds of relations among stakeholders involved in project should be treated with equity and justice, so as to not prick up inequality, or even cut down the inequality as much as possible. Doing this is to ensure the interests of majority people with no loss of other people's interests.

Principle of public support and participation. This demands extensive public participation during planning, designing and implementing the project, so as to get extensive public support. Participation is not only an objective of social development, but also a means to promote social development and success of project. For example, Baise Water Conservancy Project involves broadly with large workload, the construction of the project must obtain the support and cooperation not only from local governments and local public, but also from related governments and public in higher and lower, left and right reaches of the river. To gain the supports from governments of each level, social communities and the public, extensive participation must be

organized to let stakeholders know the circumstance, declare themselves sufficiently and participate in decision-making.

Principle of improving livelihood. The prime objective of social development is to meet people's increasing demand of physical life and mental life to the utmost extent. For example, the prime objective of Baise Project is to safeguard the security of people's lives and properties, to promote economy growth and social development, to reduce poverty and to improve people's physical life and mental life. So, during the period of planning, designing and implementing of the project, special attention should be paid not only on how the project may help poverty reduction and life improvement in beneficial areas, but also on how to make PAPs share the benefits to restore their formal production and livelihoods level.

Principle of welfare. That is to say, various advantages and disadvantages to welfare brought by project should be paid attention to in planning, designing and implementing project, trying to eliminate the disadvantages to safeguard welfare. For instance, the affected areas in Baise Project are inhabited with Chuang; and beneficial areas of flood-control never be exempted from the threat on welfare. Because of the shortage of electricity and drinking water, the threat on safe industry-agriculture production is very serious. Besides, the inappropriate relocation and reconstruction of PAPs may lead to convulsions. All of the above should be taken into sufficient consideration in social development objective.

Principle of sustainable development. That is to say, the sustainability of social development should be considered in planning, designing and implementing project; the sustainability of project profit, economy growth and environmental function should be ensured to maintain or improve beneficiaries' livelihoods successively, to fix or increase pure income and welfare per capita, to meeting the present age peoples' demands with no loss of offspring.

5 METHODS OF SOCIAL ASSESSMENT

The methods of social assessment are not single and unalterable. Different methods may be adopted in different phases of different projects, and different valuators may adopt different methods. The main methods in water conservancy and hydropower projects social assessment are quantitative and qualitative analysis, comprehensive assessment, comparison between with and without project, participation, stakeholders analysis, logic framework analysis, etc.. what must be pointed out is that participatory method is an important means in social assessment, and the sufficient participation of stakeholders is the basis of social assessment.

5.1 *Qualitative and quantitative analysis*

The indexes of qualitative analysis in reflecting the social effects of water conservancy and hydropower projects are various. For instance, in analyzing the interest distribution relation between areas in higher reaches and lower reaches of the river, many fields including society, economy, culture, resource, environment and zoology are involved and it is impossible to weigh only by several quantitative indexes. So it must give priority to qualitative indexes, assisting with some quantitative indexes. Qualitative analysis is to adapt socio-economic statistic analysis and economic computation analysis as an approach to evaluate the effects of development resettlement in form of quantity. The main quantitative indexes are as follows:

Difference evaluation. It is to evaluate in the form of absolute value. The difference between labor output and labor input or between output and input can be used; and the difference between income and expense or the difference between capital inflow and capital outflow in a whole cycle can be used; and the net benefit of regular year can also be used.

Ratio evaluation. It is to evaluate in the form of relative value. The ratio of portion and whole, part and whole can be used; and the ratio of two quantitative indexes with different quantity can be used.

Increment evaluation. It is a comparison of quantitative indexes increments in different areas and different calculation periods; or a comparison of different quantitative indexes in same area and same calculation period.

5.2 *Comparison between with and without project*

Before the construction of the project, socio-economic survey (usually spot check) is carried out to investigate humanistic community, economy and natural resources of local areas. Such as investigation of population characters, nationality, culture and customs, resource, income, poverty, employment, infrastructure and commonweal establishment of local areas. And the result of the survey is regarded as the baseline of project assessment to forecast the socio-economic changes in local areas brought by the construction of project. Comparing with the baseline data collected before project construction, the social changes can be carried out. Such as the change of employment opportunity, the improvement of infrastructure, the extension of irrigation acreage, the increase of agriculture produce, the enhance of water supply and electricity supply, the decrease of disease, the reduction of poverty and so on.

5.3 *Stakeholders analysis*

Stakeholders are those who have direct or indirect relation with the project and have direct or indirect influences on the success of the project. In Baise Project, people of the higher and lower beach of the river and dam areas, resettlement institutes, governments of all levels and related sectors are all stakeholders. Their demands and attitudes to the project have direct or indirect influences on the success of the project. Stakeholders' analysis includes: deciding the stakeholders according to the objectives and contents of water conservancy and hydropower projects; analyzing both negative and positive effects on stakeholders caused by projects and the relationship among stakeholders; analyzing the participatory forms of all stakeholders.

5.4 *Participation*

"Participation", is a process of endowing the mass with power. "Participatory development" is broadly understood as the active and all-around intervention of the development body in the development process that will affect persons' living condition or in the relative decision-making process of development project[6].

From late 1980s, participatory method has been broadly applied in planning, designing and implementing some of the international development assist projects. This kind of apply is helpful to improve the design of project, and is helpful to obtain understanding, support and cooperation from stakeholders. Secondly, participatory method is helpful to enhance the social responsibility of each stakeholder, so as to decrease social contradiction and conflicts and to prevent negative effects and aftereffects. Thirdly, participatory method can also decrease social risks during construction and operation of the projects, playing an active role in realizing socio-economic objectives of the project.

The tools used in participatory method include tools used in rapid assessment and different research means. Such as Tools for Interview; Tools for Analysis; Tools for Ranking; Tools for Visualization; Tools for Recording; Tools for Mapping, Sketching and Modeling; Tools for Meeting and Workshop; Role Play; Direct Observation; Participant Observation and so on[7]. Specifically participatory tools can be chosen according to the detail of different project.

[6] Li xiaoyun. *Conspectus of Participatory Development, Theory—Method—Tools.* China Agricultural University Printing House. 2001, 21~28.

[7] Appliance Handbook of Participation. Proceedings of Symposium on Applying Participation into Project. 2001.

5.5 *Comprehensive assessment*

Considering most qualitative assessment and quantitative assessment evaluate social effects from a certain side, the final evaluation conclusion must be drawn by comprehensive assessment. There are various comprehensive assessment methods, such as grading by experts, administrative levels analysis and fuzzy comprehensive assessment. But the nature of them is to consider all kinds of qualitative and quantitative factors, to combine qualitative analysis with quantitative analysis, to convert qualitative indexes into quantitative indexes, convert multi-objectives into single objective by certain mathematics methods, and then make a final evaluation conclusion.

5.6 *Logic framework analysis*

Logic framework analysis is to decide objectives and relation between interior and exterior by causality, and then make sure the objectives and related hypothesis, so as to improve the design of the project. It is usually described by matrix.

6 CONTENT OF SOCIAL ASSESSMENT

Social assessment is different with economic evaluation and financial evaluation; it has no fixed contents and format. The contents of social assessment may vary from area to area, and vary from project to project. Generally speaking, the objectives of water conservancy and hydropower projects are to start water conservancy and get rid of water disaster, so the social assessment should be carried out with three levels—nation, area and project. In detail, it includes social impacts analysis, inter-adaptability analysis and social risks analysis[8]. Social problems caused by dam construction, such as involuntary resettlement, social gender problem, minority problem and poverty problem, are always important problems worth paying attention to during these analysis.

6.1 *Social impacts analysis*

This is to analyze the possible negative and positive impacts on stakeholder, the affected scope and degree, the potential aftereffect and measure after the construction of water conservancy and hydropower projects. It includes the impacts on: the interest distribution relation between areas in higher reaches and lower reaches of the river; equitable distribution of benefit (such as whether the poor household, women and minority have gotten benefit during the distribution of interest); income and employment of residenter; standard and quality of living; the vulnerable groups; infrastructure and commonweal establishment in local area; custom and religion of minorities; different stakeholder (organization or individual); and so on. The serious negative impacts caused by water conservancy and hydropower projects is involuntary resettlement, to eliminate the negative impacts of reservoir inundate, RAP should be carried out according to *Design Criterion of Disposing Reservoir Inundate in Water Conservancy and Hydropower Projects*.

6.2 *Inter-adaptability analysis*

This is to analyze the adaptability between the construction of the project and the main points of development in nation and area, and to analyze the adaptability between project and stakeholder, local institutes, local technological condition. Then point out the potential problems and put forward the countermeasures. This analysis can improve the participation degree and the capacity of institutes, so as to avoid social risks and promote the sustainability of the project. During the analysis, the adaptability and inter-confluence between resettlers and relocation areas should be put emphasis on and should be taken into account in the RAP.

[8] *Directory on Feasibility Study of Investment Project.* China Electric Power Printing House. 2002, 73~75.

6.3 *Social risks analysis*

Firstly, the potential social risks caused by water conservancy and hydropower projects should be recognized according to the nature of the project, such as the poverty risk of resettlers'; reduction in employment opportunity; inequity in distributing profit; nation contradiction and culture conflicts. Then the causes of formation and aftereffects of social risks should be analyzed and measures of risk management should be carried out. Special emphasis must be paid on poverty risk of resetters'. The construction of reservoir may bring many difficulties to resettlers individual and society, which may activate all kinds of contradictions and conflicts. So the uncertainty and after-effect of incidents which can damage the benefit of resettlers individual and society are called social risk of resettlers'. Furthermore, social risks of resettler' is the potential form and premonitory of serious social problem. To avoid the breaking out of social problems, it is vital to analyze social risks of resettler'. There are four types of risks according to the field—economic risk, political risk, social risk and environmental risk, which are all involved in reservoir resettlement.

7 OUTCOME OF SOCIAL ASSESSMENT

Both financial evaluation and economic evaluation can decide whether the project is feasible or not from the angle of financial and economic by basic principles of economic analysis and quantitated financial indexes and economic indexes. To social assessment, the circumstance is not the same. It adopts the theory and methods of sociology to analyze the social impacts, the interadaptability between project and society and the potential social risks, then find out the existing social problems and potential aftereffects and carry out measures and suggestions. It has put social factors such as the development of human into the project, so as to optimize project design and avoid social risks to promote the implementation of the project.

This page intentionally left blank.

New Developments in Dam Engineering—Wieland, Ren & Tan (eds),

Appraisal of ecological and environment protection works of the Three Gorges Project

Chen Yongbo
Institute of Hydrobiology, Chinese Academy of Sciences, China
China Yangtze River, Three-gorges Project Development Corporation, China

ABSTRACT: The Three Gorges Project (TGP) is the backbone project for the developing and harnessing of the Yangtze River, and it will result in a great deal of comprehensive benefits, such as effectively controlling the floods, generating powerful electricity, and improving the navigation condition. It has extensive function to the sustainable development of the Yangtze River basin and even the whole of China. It will also, however, exert far-reaching and profound impacts on the environment, which has brought ecological and environmental concerns both at home and abroad. The impact is one of the bone of contentions of the TGP.

The TGP' mainly adverse impacts on the environment and the ecology include in water quality, cultural relics and historic sites, sedimentation and species resources, etc.

Chinese Government and the unit of the project development attach great importance to the TGP' ecological and environmental protection work. Aiming at the possible adverse effect of the TGP constructing and running, that produce is at "Environmental Impact Statement For Yangtze Three Gorges Project". In terms of policy, engineering, supervision and management, scientific research and investment, etc., the effective measures are taken and fully implemented to prevent and minimize the negative impacts. At present, every job makes good progress and the achievement is remarkable.

1 INTRODUCTION

The Yangtze Three Gorges Project (TGP or the Project) is located in Xiling Gorge of the Three Gorges reaches of the Yangtze River main-stream, with the Dam at Sandouping in Yichang County, Hubei Province, about 40km upstream from the existing Gezhouba Project. The TGP is the backbone project for the developing and harnessing of the Yangtze River, and it will result in a great deal of comprehensive benefits, such as effectively controlling the floods, generating powerful electricity, and improving the navigation condition.

The construction of the Project will be in three phases. It started in 1993, and by 1997 the main river course has been closed; by 2003, i.e., the 11th year, the first batch of generating units has been put into operation and generated electricity; and by 2009 the construction will be completed. At that time, the Three Gorges Reservoir will have a capacity of $3.93\times10^{10}m^3$, of which $1.65\times10^{10}m^3$ will be a regulating storage, accounting for approximately 3.7% of the dam site's annual runoff. The 26 sets of hydraulic turbogenerators, with 700MW for each set, totaling 18,200MW in installed capacity, will produce an annual electricity output of 84.68TWh. Calculated in terms of the price in May 1993, the total fixed price estimate for the TGP will reach RMB 90.09 billions, of which 50.09 billions will be used for the TGP construction itself, and 40 billions will go for the compensation of inundation losses and resettlement about 1 millions persons.

Based on the Chinese laws and regulations related to environmental protection for construction projects, in December 1991, "The Environment Impact Statement (EIS) For Yangtze Three Gorges Project" for reviewing was finalized and submitted to the Ministry of Water Resources for

pre-reviewing. In February 1992, the China National Environmental Protection Agency (NEPA) formally approved EIS for the TGP.

On June 1 of 2003, the reservoir started to store water, and the pool level rose up to elevation 135m on June 10. The trial navigation of double-way and 5-step flight shiplock was run successfully on June 16. The first batch of generating units in the left bank power plant started to generate electricity from July By the end of 2003, there were 6 units formally put into use to generate electricity. So far, the three goals for the second phase construction of the TGP were achieved, which are water storage, navigation, and power generation.

2 THE TGP'S ENVIRONMENTAL IMPACT ASSESSMENT (EIA)

2.1 *Scope of assessment*

The impact of the Three Gorges Project on ecology and environment are widespread. Based on the Project's functions, characteristics, possible flow regime alteration to the Yangtze River to be caused by the Project, and the difference of environment in the regions to be affected by the Project, the scope of assessment was divided as follows:

1. The Three Gorges reservoir region, from the dam-site to the end of the backwater in Chongqing, covers the reservoir-inundated area and the resettled area for the people in inundated area.
2. The region covering the middle and lower reaches from the dam-site to Jiangyin in Jiangsu Province, including the Dongtin Lake area, Four Lakes area of Hubei Province and Poyang Lake area.
3. The estuary area from Jiangyin to Wusongkou.
4. Other regions: with considerations of the influences of soil erosion and the system of plantation of trees in the upper regions, and the effects of clear diluting water and tide intrusion in the lower region, the area of assessment has been extended to the upper part above the reservoir and surrounding sea area below the estuary.

2.2 *Hierarchic system of assessment*

Based on the characteristics of environmental impact of the TGP and the requirements for prediction and assessment, the system to be assessed is divided into the following four tiers in a hierarchy: Environmental factors, environmental components, environmental sub-systems, overall environment.

The environmental sub-system is divided into the natural environment and social environment. The environmental components to be assessed include local climate, water quality, water temperature, environmental geology, terrestrial plants, terrestrial animals, aquatic life fish, silting and scouring, water logging in plain & lake area of middle reaches, estuarine ecosystem, inundation and resettlement, public health, natural landscape, cultural relics and historic sites, project construction, flood control, power generation, navigation.

2.3 *Basic conclusions of EIA*

The impact of the TGP on environment and ecology is one of the major issues concerned both in China and abroad. Because a large number of agencies (more than 100) and technical personnel covering a wide range of disciplines, have long been engaged in the study on the ecological and environmental impact of the TGP for more than 40 years, a great deal of data have been accumulated in various monographic reports and books, which provide a solid foundation for conducting the environment impact assessment and compiling the EIS for the TGP.

The basic conclusions of EIA were:

1. For the middle and upper reaches or even the whole basin of the Yangtze River, the ecologic and environmental conditions have been improved to a certain extent only in limited areas, but a deterioration trend in the remaining large areas has not yet been under control. Therefore, even

if the TGP is not built, it is still urgent to have a comprehensive tackling and rehabilitation in the basin.

2. The TGP will bring about broad and profound impacts on ecosystems and the environment, covering various factors and vast areas and lasting a long time. The issues involved are complicatedly interpenetrated and have both positive and negative aspects.
   The TGP can effectively control the floods in upper reaches, enhance the capability of controlling floods, and significantly reduce the damage caused by floods and waterlogging hazards to ecosystems and the environment in the middle and lower reaches of the Yangtze River, especially in the Jingjiang reach. In addition it will also decrease the sediment deposition in the Dongting Lake and prolong its lifespan.
3. The ecological and environmental impacts of the TGP are featured by an uneven temporal and spatial distribution. The affecting period starts from the preparatory stage of the TGP and lasts for a long period. Some of the impacts, such as the impact caused by construction, will be shown only for a certain period, while some other impacts, for example, the sediment deposition will last a long time and have an accumulation. The factors and the extent to be affected are different in different time periods. The change in the impacts in each month of the year is closely related to the regulation of the water level in the reservoir. In terms of the spatial distribution, the main positive impacts will mainly occur in the middle reaches and the negative impacts will mainly be concentrated in the reservoir areas.
4. Of the ecological and environmental factors to be affected by the construction of the TGP, the environmental carrying capacity for resettlement is a relatively sensitive and restrictive one.

Generally, the ecological and environmental impacts of the TGP have both positive and negative aspects, to which adequate attention must be paid. Once the effective measures, in terms of policy, engineering, supervision and management, scientific research as well as investment, etc., are taken and fully implemented to minimize the negative impacts, none of the ecological and environmental issues will affect the feasibility of the TGP.

2.4 *The major environmental issues to be concerned*

2.4.1 *Water quality*

As a whole, the water quality in the TGP reservoir will not be significantly deteriorated and the reservoir will face no eutrophication, because the reservoir has a type of river channel where has rapid water flow. However, pollutant concentration will increase in the water body near shoreline due to the decrease of water flow velocity, and, as the result, the turbulent diffusion ability of water body. It is expected that the near shoreline pollution belt would develop to certain extents if the pollutant sources don't be controlled. In some local water body, especially in the small tributaries and reservoir bays, possible occurrence of eutrophication cannot be excluded.

Due to the regulation of the TGP reservoir, discharge in downstream reaches of the dam will be raised in dry season, and, the difference of releasing flow among the high, normal, dry years will become less, which will benefit the pollution control for cities in downstream reaches of the dam to improve and stabilize the water quality.

2.4.2 *Cultural relics and historic heritage*

Through the efforts of prominent experts, there were 1087 protection projects confirmed, with 335 in Hubei Province, 752 in Chongqing City. Among these projects, 364 are ground relics (118 in Hubei, 246 in Chongqing), 723 underground (217 in Hubei, 506 in Chongqing). The Three Gorges Project construction Committee authorized that all these projects would be brought into the protection plans of the TGP.

Based on the location and elevation, impacts of the Project on the cultural relics and historic heritage in the TGP reservoir region and its surrounding areas can be grouped into the following five types: completely submerged, partial submersion, Landscape alteration, potential discovery and not affected.

2.4.3 *Sedimentation issues*

The main sedimentation issues concerned in the TGP construction are as following:

1. Whether will the TGP reservoir lose its function due to siltation?
2. Will the sedimentation in the river channel and harbors in the fluctuated backwater regions block the navigation channel?
3. Will the rising of flood level caused by siltation at the reservoir tail imposes a threat on flood control in the city of Chongqing?
4. How will the sedimentation, the movement of bedload affect navigation and power generation?
5. What impact will be produced on the scouring of the downstream riverbed after the reduction of sediment content in the reservoir releasing flow?
6. What measures will be taken to tackle these issues?

After a series of extensive and detail studies which began in the early 1950's, sedimentation experts concluded that all the issues mentioned above have been clarified and can be solved by taking proper countermeasures.

2.4.4 *Species resources protection*

Disturbed by mankind for a long time, the primeval vegetation in the TGP reservoir region has been severely wrecked, and there is almost no primitive forests left. The fishery resources has also been decreased significantly.

Two rare and native plants species may be affected significantly by TGP, they are *Adiantum reniforme var.sinense* and *Myricaria laxiflora*. Reservoir impoundment will inundate most of their distributed sites. The relocation and resettlement is another main causing factor.

When TGP is completed, the fishes adapting to slow-flowing water will become the dominant ones in the reservoir. The native fishes adapting to lotic water will decrease or even disappear in the reservoir due to the change of the living environment. The TGP reservoir belongs to a seasonal regulated type one. The annual run off discharged to downstream of the dam basically remains unchanged and the amplitude of the discharge regulation is within the natural fluctuation range. Therefore, no major impacts on the fishery in lower reaches will be caused by formation of the reservoir. However, due to the reservoir's regulation in May and June, the releasing flow course from the reservoir may be not satisfy the demand for the family-fish's spawning, which may cause adverse impact on their natural reproduction.

For the migratory fishes, as the existing Gezhouba dam has already cut the migration route, TGP will not cause newly blocking of the route.

3 ENVIRONMENT PROTECTING WORK AND ITS PROGRESS

3.1 *Work assignment*

In order to strengthen the leadership to the environment protection of the TGP, guided by the State Council Three Gorges Project Construction Committee (TGPCC), a coordinating leadership group on eco-environment protection was founded to assign works of the TGP environment protection as follows:

The environment protection of the construction area, silt monitoring and investigation, and earthquake monitoring are taken charge of by the China Yangtze River Three Gorges Project Development Corporation (CTGPC). The Corporation has Environment and Cultural Relic Committee and Environment Protection Section.

Environment protection of resettlement is taken charge of by the government of Hubei Province and Chongqing City, and coordinated by the Office of TGPCC.

Sewage water treatment is taken charge of by the NEPC.

Geological Disaster monitoring and treatment is taken charge of by the Ministry of Land and Resources P.R.C.

Other special subjects related to environment protection are coordinated and organized by the Office of TGPCC.

3.2 *Project planning and policy support*

To fulfill countermeasures on EIS of the TGP, all authorities and undertakers of the TGP had made corresponding designs or plans on environment protection respectively, which were examined and approved by the corresponding authorities. They are: *The Primary Design of the TGP, including Environment Protection Section, The Implement Planning of Environment Protection of Construction Area of the TGP, The Ecology and Environment Protection Planning of ResettlementArea of the TGP (county as unit), The Implementing Planning of the Eco-Environment Monitoring System of the TGP, The Cultural Relic Protection Planning of Submerged area and RelocatingArea of the TGP,* and etc…

Because of the historically adverse base of and less investment to environment treatment of the reservoir area, some relevant government ministries had issued strategic plans and policies, and put in necessary supplement fund. These plans and policies are, for example, *The Water Pollution Treatment Planning along the Upstream of the Yangtze River, the Action Planning of Resettlement Environment Protection of the Three Gorges Reservoir, Related Technical Policies of Urban Sewage Water and Garbage Treatment at the Three Gorges Reservoir, the Strategic Planning of Environment Protection and Ecological Construction in the Three Gorges Reservoir, the Five-Year-Planning of National Environment Protection, and policy arrangement of 2010 long-term strategic planning.* In 2001, the State Council successively authorized *Water Pollution Treatment Planning in the Three Gorges Reservoir and its Upstream,* and *Prevention and Control Planning of Geological Disasters in the Three Gorges Reservoir*. Chinese government is investing a large amount of money in these projects to completely treat the regional environment pollution and geological disasters. The Government initiated the protective forest construction engineering in the middle and upper stream of the Yangtze River, which was as the prophase cooperative project of the TGP. The other projects, such as the protection engineering of the natural forest, and return to land from forest, also were granted priority to be carried out.

3.3 *Supervision and management of eco-environment protection*

In order to standardize and strengthen the management of eco-environment protection in the TGP, the related authorities have set up supervision and management system, and boosted the implementation of all plans and policies related to the eco-environment protection in the TGP

For the project management, we determined project undertakers by making and publishing project application guide (*scientific research subjects of eco-environment protection and their monitoring* as an example), or project biding documents (*engineering projects of eco-environment protection* as an example). These projects ware managed based on the contract. We also hired specialized consulting engineers to supervise the progress, quality, investment and their environmental impact of different projects. When projects finished, we would check them with an evaluating and checking system. For those long-term projects, we used a middle-term evaluation system to adjust the plan in time if needed.

For the construction of the TGP and resettlement arrangement, some administrative authorities often organized special checking to evaluate the progress of all works of eco-environment protection. In the finished check-and-accept procedure of different phases of the TGP, for example, the check-and-accept procedure of the first phase engineering, water storage and ship-locks trial navigation of the second phase, we will carry on a specialized check-and-accept procedure on ecoenvironment protection.

3.4 *Eco-environment monitoring*

The main goal of setting up the ecological and environmental monitoring system of TGP is to comprehensively watch and grasp the change of ecological and environmental factors influenced

by the TGP, especially those major factors and those seriously affected areas, to take countermeasures timely to tackle the problems.

The main task is to conduct systematic monitoring on ecology and environment in the reservoir region and the relevant areas before and after the TGP construction, and carrying out necessary research and experiments.

The monitoring system includes 11 subsystems, namely sub-system of water quality; pollution sources; local climate; fishes and other aquatic biota; terrestrial fauna and flora; public health; the reservoir area social environment; agricultural eco-environment; mountainous disasters; hydrology and silt; and construction site. Besides, it includes some experimental stations such as the ecoagriculture experimental station, the peculiar fishes experimental station, the terrestrial flora species resources experimental station and the comprehensive eco-environment experimental station of the Yangtze estuary.

The system started in 1996, running under the Implementation Planning of the Eco-Environment Monitoring System of the TGP and the progress of the TGP. On June 5th of each year from 1997, the *Bulletin on the Ecological and Environmental Monitoring Results of the Three Gorges Project* would be published by NEPC. All monitoring sub-systems had carried out stage sum-up.

3.5 *Work progress of related projects*

3.5.1 *Water quality protection*

According to *The Water Pollution Treatment Planning at the Three Gorges Reservoir and its Upstream,* Chinese government would invest RMB 39.2 billions for water pollution prevention and control in the Three Gorges Reservoir and its Upstream from 2002 to 2010. 20 of the planned 28 sewage water treatment factories which should be finished in 2003, were finished in June of 2003 and put into use, with a newly added water treatment ability of 490 k Ton/Day.The other 6 finished in the end of 2003 would add 190k Ton/Day more. 2 factories in the urban area of Chongqing City are expected in the end of 2004. By then, Chongqing City and the reservoir area would have a treatment ability of 1600k Ton/Day, which covers a population of about 9 million.

There are already 20 garbage treatment factories in the reservoir area, which locate at each county capital and major towns. Meanwhile, among 1959 enterprises that used to be in the submerged areas, those with serious pollution, out-of-date technology, adverse cost-efficiency would be closed and bankrupt (1012 planned to be closed) to ensure the environment of the reservoir area.

Based on related technical regulations of the reservoir clearing, the clearing work under water level of 135m had been finished by the end of 2002.

Some relevant scientific research subject had been finished, for example, the research of water pollution control in the reservoir (the first phase). The successive subjects are being implemented, for example, the coupling effect of major pollutants and silt in the Three Gorges Reservoir and its impact to water quality; the mechanism, forecasting and countermeasure of eutrophication in typical tributaries of the Three Gorges Reservoir, and the control of non-point sources pollution control in the Three Gorges Reservoir.

3.5.2 *Cultural relics protection*

Relic protection experts from about 30 authorities and institutions nationwide have been completely investigating, surveying and unearthing in small-scale ground and underground relics in the reservoir area since 1993. Based on the authorized protection outline on the relics of submerged and relocation areas, they made special protection plan for each relic site with the consideration of the preservation forms and characteristics of relics in these areas. For those underground relics, they instituted plans like unearthing, survey and archiving according to their values and places. For ground relics, on-site protection, relocating protection and keeping the copy of materials are planned.

By the end of 2003, RMB 339 millions was invested to carry out 302 ground protection projects, 531 underground relics unearthing projects. A survey area of 8.852 million m^2 and an unearthing area of 0.9327 million m^2 had been finished. Work on some major protection sites like

Baiheliang at Fulin City, Shibaozhai at Zhong County, and Zhangfei Temple at Yunyang County were smoothly implemented.

So far, a batch of achievements had been gained. The Chronicle of archaeological culture of the whole Three Gorges is gradually emerging, and will fill the archaeological empty of this area.

3.5.3 *Environmental geology*

Geological disasters: Chinese government attaches importance to geological disasters in the Three Gorges area, and had launched a special fund of 4 billion RMB Yuan for treatment and prevention from the TGP fund, which had been applied to 173 sites of rock-fall and landslide, 74 sections with an overall length of 70 Km of river bank collapse, 214 high slopes. Based on *Prevention and Control Planning of Geological Disaster at the Three Gorges Reservoir,* the first batch of geological disaster prevention and control projects, which are under the water level of 135 m, had been finished by May of 2003. Work on making the second batch of projects planning has started since July of 2003.

A geological disaster precaution network, which combines specialized monitoring and general monitoring, had been established. By now, 108 specialized monitoring sites and 1689 general sites have been confirmed. Once clues of disasters are reported, they must be submitted immediately as regulated procedure, and emergent treatment would be made in time.

Silt problem: Silt is one of key technical and ecological problems of the TGP construction. The silt expert group formed in 1993, when the TGP was in preparation, worked out scientific research plan on silt problem, which was based on the previous research. Jointing with relevant departments of Ministry of Water Resources, Ministry of Traffic, universities and Chinese Academy of Sciences, we have carried out research on silt problem of dam area, its downstream, and fluctuating backwater regions to optimize the design of the main engineering, the reservoir operation, and navigation requirements on water depth and flow, and provide basic data for the construction and development of harbors and docks. 5 special topics and 24 sub-topics were arranged, which involved 19 undertakers and more than 300 persons. 8 practical silt models and mathematical models had been established. The in-depth research on silt problem related to the TGP, which aimed on exploring silt movement rules and studying out corresponding countermeasures, was carried out. A large amount of works like model and prototype observation, calculation, analysis, and investigation had been implemented.

3.5.4 *Species resources protection*

Establishment of natural reserves is one of the main measure for protecting the species. Established reserves include “the Fingerlings Reserve for Chinese Sturgeon and Chinese PaddleFish in the Yangtze Estuary”, “Chinese Sturgeon Natural Reserve below the Gezhouba Dam”, “Yichang Dalaoling Plant Diversity Protection Project” and “Xingshan Longmenhe Evergreen Broadleaf Forest Reserve”.

Adiantum reniforme var.sinense and *Myricaria laxiflora* have been taken various protection ways like preservation of species resources, preservation in arboretum, wild relocation, on-site protection. For other plants at reservoir area, we have moved 30 rare plants and 73 major dominant plants.

As for public concerned *Craspedacusta ziguiensis,* we have organized experts to carry out corresponding protection and research.

We keep on implementing the *Chinese Sturgeon* artificial reproducing and releasing, organizing related research on species resources protection such as eco-hydrological mechanism and protection countermeasures behavior ecology research on reproducing and spawning of the *Chinese Sturgeon* and the famous “Chinese Four Family Fish” (black carp, grass carp, silver carp and bighead).

4 CONCLUSION

The TGP is the backbone project for the developing and harnessing of the Yangtze River, and it will result in a great deal of comprehensive benefits, such as effectively controlling the floods, generating powerful electricity, and improving the navigation condition. It plays important roles for the sustainable development of the Yangtze River basin, even the whole China.

On the basis of long-term and full argumentation and investigation on eco-environmental impacts, we have evaluated the environmental impacts of the TGP. Once the effective measures, in terms of policy, engineering, supervision and management, scientific research as well as investment, etc., are taken and fully implemented to minimize the negative impacts, none of the ecological and environmental issues will affect the feasibility of the TGP.

Chinese government and the TGP construction undertakers think highly of eco-environment protection. Based on the authorized to prevent and lessen the negative impacts, many effective measures from different angles including policy, engineering, supervision and management, scientific research as well as investment have been carried out. Currently, all works are moving forward smoothly and have already gained significant achievements.

REFERENCES

[1] The Environmental Impact Assessment Department, Chinese Academy of Sciences and the Research Institute for Protection of Yangtze Water Resources: Environmental Impact Statement for the Yangtze Three Gorges Project (a brief edition) Science Press 1995.
[2] Yangtze Valley Water Resources Protection Bureau: Questions and Answers on Environmental Issues for the Three Gorges Project Science Press 1999.
[3] Liu Jinrong, Chen Yongbo: Three Gorges Project and Sustainable Development (in Chinese) Urban Environment, Vol. 12, No. 4, 1998:7–10.
[4] Fang Ziyun, Cheng Yongbo: Research and Practice in Environment Protection for Three Gorges Project (in Chinese) China Three Gorges Construction, Vol. 9, No. 9, 2002:4–9.
[5] Pan Dazhong, Chen Yongbo: Discussion on the Environmental Supervision System in Three Gorges Project Construction (in Chinese) Environmental Protection, No. 3, 1998:11–13.
[6] Chen Yongbo: On Environmental management for Construction of Large Hydro Project (in Chinese) Yangtze River, Vol. 27, No. 3, 1996:20–22.

New Developments in Dam Engineering—Wieland, Ren & Tan (eds),
© 2004 Taylor & Francis Group, London, ISBN 04 1536 240 7

Overview on arch dam safety research

Chen Zaitie
Civil Engineering College, Hehai University, China
Shazhou Institute of Technology, China

ABSTRACT: Arch dams enjoy reasonable dam type, strong overload capacity and self-adjusting property, and outstanding predominance of safety/price ratio. The higher and larger the arch dam is built, the more complex the dam-site geologic conditions are and the greater the capacity of the reservoir is. Thus, in case any dam collapse should occur, the national economy would suffer greatly and people's life and property would be endangered. The great loss caused by arch dam collapse shows that great importance must be attached to the safety evaluation & monitoring of the arch dam. At present, the major approaches to arch dam safety research involve: strength theory, stability theory, reliability theory, damage fracture theory, as well as numerical simulation analysis, geomechanics model test, inverse analysis of the data monitored, etc. However, these approaches are far from both having scientifically theoretical basis and being generally accepted by dam engineering circles. This paper deals with the development of arch dams and the harmfulness of the dam collapse, summarizes the existing major theories and approaches to arch dam safety evaluation, analyses the weak points of these theories and approaches as well as the difficulties in the further researching, and comes up with such urgent issues and difficult points as the choice of arch dam safety evaluation norms.

1 INTRODUCTION

Arch dams are a type of economical and safe dams. Since the first arch dam in the world—Zola Dam—built in France in 1854 and the first high-arch dam in the world—Hoover Dam (with a height of 221m and a dam crest length of 372m)—built in the U.S.A. in 1936, arch dams, thanks to the unique strong overload capacity and the self-adjusting property, have been greatly developing in the practice of the dam engineering all over the world. At present, more than half of the great dams with the height being over 200m built all over the world are of arch type[1]. In the western region of China, a group of arch dams of top world grade are being built and to be built with the height being up to 300m or so. The practice of dam construction in all countries of the world has proved that the higher the dam is, the more outstanding the economic importance and its safety will be.

Generally speaking, arch dams are completed with large reservoirs such as the Malpasset arch dam of France, the Vaiont arch dam of Italy, etc. In case any dam collapse should occur, the consequence would be particularly serious and not only would the national economy suffer from a great loss but people's life and property would be endangered as well. In 1959, a dam collapse occurred on the Malpasset arch dam of France because of the sliding of the dam body together with the deeplayer rock foundation, resulting in the death of over 400 people as well as a great economic loss[2] Therefore, great importance has to be attached to the arch dam safety, and thorough research has to be conducted into the stress, deformation and destructive mechanism during the operation of the arch dam, and evaluation has to be made to the bulk safety of the arch dam (i.e. the minimum distance between the designed work state and the destroying state of the arch dam).

In general, most arch dams are of complex geologic conditions, adverse environmental conditions, and random physics & mechanics parameters, etc. All these factors result in the immaturity in the arch dam safety research. All the existing theories and approaches have both merits and weak points for which improvement and perfection are urgently to be made.

2 RESEARCH INTO THE ARCH DAM SAFETY BY MEANS OF STRENGTH THEORY

According to the strength theory, the destruction of the arch dam is caused by such factors as the dam heel crack resulting from excess tensile stress, the yield or even the conquassation of the dam shoulder or dam body resulting from excess compressive stress, the dam rock body's sliding along the soft & weak structure resulting from excess shear stress, etc. By means of the comparison between the resistance under limiting conditions and the design load action effect, it can be determined whether the structure has come into the strength destruction state. In such countries as the U.S.A., Japan, China, etc., it is stipulated that the tensile and compression resistance safety coefficient should be obtained through the analysis of arch dam stress and displacement by means of arch-beam load-division process, and then the shear resistance safety coefficient should be calculated according to the rigid-body limit balance principle[3]:

$$K=\frac{f\sigma+c}{\tau}$$

where K is the shear resistance safety coefficient, f and c are respectively the friction coefficient and cohesive force of the material on the sliding face, and σ and τ are respectively the normal stress and shear stress on the sliding face.

In the numerical calculation by using finite element process, etc., Mohr-Coulomb's and Drucker-Prager's criterion are generally used as the yield criterion for the rock-soil material, while quadruple-parameter-criterion is usually used for the concrete[4].

$$F=A\frac{J_2}{f_c^2}+B\frac{\sqrt{J_2}}{f_c}+C\frac{\sigma_1}{f_c}+D\frac{I_1}{f_c}-1=0$$

where A, B, C and D are material parameters, f_c is the uniaxial compression limiting strength, while I_1, J_2 and σ_1 are respectively the first invariant of the stress tensor, the second invariant of the stress deviator and the first normal stress.

The advantages of the strength safety coefficient process involve definite meaning, simple calculation, being based on years of dam engineering practice & experience, being widely familiar to the engineering & scientific personnel, as well as matching the allowed safety coefficient specified in the State Specifications of many countries[5]. The problem with this process is that insufficient local strength may not result in the entire destruction of the arch dam and, only when the sliding face is a plane or a circular arc and is given in advance, can we get the reasonable and sole calculation result of the shear stress safety coefficient. Besides, the strength theory process doesn't consider the dam body, the dam shoulder and the dam foundation as a whole system[6]

In order to perfect the strength safety coefficient analysis process, many scholars have made explorations from various aspects:

Zhang Jingjian, Sun Mingquan, etc. have researched the connectivity of the spot safety coefficient, and suggested the threshold resulting in the bulk destruction of the arch dam[7];

Wang Liangkui, Chen Jianping, etc. have studied the effect of cracks and the lengths of cracks on the destruction of the arch dam, and suggested the critical value of the connectivity for the cracks and crack lengths[8];

Huang Wei, Chen Jin, etc. have conducted analysis of the size of the cracking area, and suggested the cracking face connectivity concept as well as the critical index [9];

All the studies and researches mentioned above add to the content of the strength theory's analysis of the arch dam safety; however, the reasonability of choosing these connectivity thresholds deserves further study.

3 RESEARCH INTO THE ARCH DAM SAFETY BY MEANS OF STABILITY THEORY

According to the traditional mechanics, there exists no stability problem; arch dam's sliding along the foundation interface, the un-stability of the dam shoulder, and the rock block's sliding along the structure interface are all referred to the strength destruction. However, according to the definition of kinematic stability[10], any change of a state or a thing is a kind of motion and there exists a matter of stability. When the whole body of the dam is in the state of limiting equilibrium because of various reasons, only a slight disturbance will make it offset from its original equilibrium state, resulting in non-restorable destruction. In view of the fact that when the entire destruction of the arch dam occurs, the static state changes into the movable state, Ren Qingwen, on the basis of the study of "state" change of the system[11] suggested that the entire destruction of the arch dam may be regarded as the issue of stability, but unlike buckling un-stability this kind of un-stability belongs to the type of limit-point un-stability and the index for determining the arch dam safety property is the reliability of the arch dam.

As to the research into arch dam un-stability, so far there has been no approach which is not only based on an exact mechanics theory but also simple and practical. At present, there are following major approaches to the entire stability safety research of the arch dam: overload process, strength reserve process, integrated process combining overload with strength reserve, etc[12].

3.1 *Overload process*

According to the overload process, under the premise that the material strength parameters are constant, and under the combined action of normal operational loads, the horizontal load is increased by stages (by increasing the water level or reservoir capacity) until the un-stability & destruction of the arch dam occurs. The ratio of the destructive load to the normal load is referred to as the overload reliability K_p. The overload safety is general very high and can be worked out by means of geomechanics model or numerical simulation process[13][14]. However, during the normal operation of the arch dam, excessive overload is unrealistic. Besides, no consideration is taken into the effect on the strength by such factors as the rock foundation (esp. the weak zone of the rock foundation), the water corrosion, seepage and alkalization on the building materials, etc. [15]. However, the real peril is not from the doubled and redoubled load but from the strength insufficiency of the materials.

3.2 *Strength reserve process*

According to the strength reserve process, under the condition of keeping normal load unchanged, the strength of the dam body and the rock foundation is gradually reduced until the un-stability and destruction of the arch dam occurs, and the number of the times of half-reduction is referred to as the strength reserve reliability K_f. However, a number of models are needed for this process, which is practical in terms of both manpower and material resources and the precision and quality of the model fabrication is hard to be guaranteed. In general, the test is conducted on the equivalence principle, i.e. to keep the material strength unchanged and synchronously increase outside load and selfweight load until the destruction occurs instead of keeping the outside load unchanged and gradually reducing the material strength until the destruction occurs. For the test by equivalent strength reserve process, the difficult problem has to be solved in synchronously increasing the dam body, the rock foundation and outside loads. Gong Zhaoxiong, Guo Chunmao, etc., on the basis of satisfying the physics model similarity and by using centrifuge as the loading tool and substituting gravitational field with centrifugal force field, realized the synchronous increase of the dam body, rock foundation and outside loads and conducted the equivalent strength reserve process test on a single model. The result of the test[16] showed that the tendency of magnitude of the stress and the magnitude of the tensile & compression stresses are basically up to the general law.

To conduct the strength reserve process test on a single model, it is necessary to develop a new type of material that can reveal the gradual change in the shear strength of the dam foundation soft & weak structure interface or the rock as well as corresponding test technique. Li Chaoguo,

Lu Jinchi, etc., after years of exploration, have developed the "temperature-varying similar material" applicable to the models of fault interlayer and rock body. It is made of blanc fixe, engine oil, soluble high polymer material and admixture, blended in a certain proportion. During the test, the material strength is gradually reduced by means of temperature raising, realizing the strength reserve process test on a single model[17].

While the strength reserve reliability presents a clear conception, it is not the entire cause for the arch dam destruction. Moreover, when the *f* value decreases to the residual value, it is very difficult to decrease further; while *c* may totally disappear. Therefore, unequal-ratio strengthreduction is more reasonable and the equal-guarantee process[18] is often used.

3.3 *Integrated process*

The destruction of the arch dam is not due to the single factor of overload or material strength reduction, but because of the co-action of the both (factors of overload and material strength reduction). According to the integrated process combining Overload with Strength Reserve, when the arch dam reaches a specific overload coefficient K_p, the strength is to be reduced by K_f times, causing the destruction of the arch dam. The reliability of the integrated process is $K=K_pK_f$[19].

The integrated process is theoretically reasonable but the actual operation is rather completed, especially there is no uniform standard concerning to what degree should first overloaded before reducing the material strength.

At present, the study of the entire un-stability destruction is conducted mainly by means of the geomechanics model test, and certain achievements have been made in computerized simulation and numerical calculation of the destruction process of the arch dam[20] In terms of theoretical research, some arch dam entire un-stability criteria have been put forward such as calculation & iteration non-convergence, yield zone through, the second-order variation of the total potential energy is negative [21], etc., but the application of the stability theory to the research into the un-stability destruction of the arch dam is to be further deepened.

4 APPLICATION OF ARCH DAM RELIABILITY ANALYSIS IN ARCH DAM SAFETY EVALUATION

Widely existing in the objective world, randomness reflects the probability of the occurrence of things in a certain state. The randomness of the arch dam lies in the uncertainty in the material properties and the outside load. Reliability analysis based on probability theory and mathematical statistics presents a more advanced and reasonable approach to arch dam safety evaluation[22]. Reliability analysis will give us the answer about the probability, i.e. reliability of the normal operation of the arch dam under the specified operation condition and environment and within the operational life.

Given a group of basic random variables in the structure reliability analysis $X=(x_1, x_2,\ldots, x_n)^T$, the arch dam descriptive function $g(X)=g(R,S)=g(x_1, x_2,\ldots, x_n)$, and the limiting state equation $g(X)=0$. By standard normalizing the basic random variable *X,* we get a group of independent variables *Y,* then transform $g(X)$ into the standard normal space $G(X)$ and the shortest distance of the check calculation point Y^* on the design state face $G(X)=0$ from the original point can be determined by means of iterative method, and then by means of distance formula determine the reliability of the arch dam $\beta=\sqrt{Y^{*T}Y^*}$, and further determine the failure probability with the formula $P_f=1-\Phi(\beta)$[23].

Guo Huaizhi, Chen Zuping, Liu Ning, etc. in view of the randomness of the load (including temperature change) and material parameters, have conducted their research into the time-varying reliability of concrete arch dam and dam shoulder rock mass[24][25];

Huang Zhiquan, Wang Sijing, etc. have researched into the effect of rock mass un-stability probability and mechanics parameter variability on the structure[26];

Yang Lingqiang, Lian Jijian, etc., taking the load and material parameter as random variables and by means of random finite element and maximum entropy process, have worked out the reliability index distribution of the arch dam[27];

Chen Gang, Zhang Lin, etc. have applied the artificial nerve network technique in nonlinear analysis to the reliability analysis of the highly rolled concrete arch dam, and obtained the reliability index β on both upstream and downstream dam face as well as at the induced seam nodal[28];

Wu Qingxi, Lu Tairen, etc. have established mathematical model for the analysis of the static and dynamic reliability of the arch dam shoulder bulk stability, compiled corresponding calculating program, and obtained the reliability of all types of arch dams[29].

Although reliability theories and approaches have found relatively wide applications in arch dam safety analysis, they basically remain merely applicable to the "spot" reliability. Further effort is expected to realize the engineering design based on the systematic reliability analysis, especially to research and solve a series of theoretical and technical problems such as the method of analysis of the systematic reliability, the technique for practical probability network analysis, the expert decisionmaking supporting system, the distribution law of the statistics parameters, etc.[6].

5 OTHER THEORIES AND APPROACHES TO ARCH DAM SAFETY EVALUATION

Some scholars believe that the destruction of the dam and the rock mass results from the continuous expansion of the cracks formed by the constant accumulation of the initial damage and therefore, the processes of damage mechanics and fracture mechanics can be adopted to study the destruction of arch dams[30]. Huang Yun and others have studied the stability and expanding tendency of the upstream dam heel cracks of the arch dam by means of three-dimensional fracture boundary element process and minimum strain energy density factor theory, and pointed out that water splitting is the major factor contributing to the expansion of the initial cracks[31].

Other scholars look at the arch dam as a dynamic system and study the destruction from the viewpoint of nonlinear evolution. When the accumulative destruction and deformation of the arch dam system develop from disorderly to orderly and the system evolution curve develops from the linear & equal rate to nonlinear & acceleration, the entire destruction is about to happen to the system[32][33].

Based on the research into the cause of the accident occurred on the Ken double-convex arch dam in Austria, Switzerland dam engineering expert, Lombardi, put forward the idea of dam slenderness coefficient in 1986 and presented Lombardi Curve for the dam damage[34][35], which is a straight line only associated with the dam height. Ren Qingwen and others did a study of the shape and reason of this damage Curve by means of dam body strength and buckling stability theory, and suggested that Lombardi Curve should fall into two types[36]: the first type is a hyperbola with the dam body concrete strength as the parameter and related to the dam height and the dam body concrete strength; the second type is an exponential curve related to the buckling of the dam body, i.e. related to the modulus of elasticity of the dam body concrete, the dam height, etc.

6 CONCLUSION AND PROSPECTS

Characteristic of investment-saving, big overload capacity and high safety, arch dams, especially high-arch dams are being paid great attention to by all the countries in the world. Arch dams are built increasingly higher and the foundations are becoming increasingly complex. The complex and adverse geological conditions as well as the great loss in case of dam collapse force the scientific staff to research and solve the technical problems in the construction of arch dams and in the safety evaluation.

Although the existing Specifications of many countries are still based on the stress safety coefficient research approach of the traditional strength theory for checking the safety of the arch dam, the spot or local strength is not enough to result in the local crack or yield. However, arch dam is a kind of higher-order statically indeterminate structure and, under the strict restriction of its surroundings, is very sensitive to the overload or deformation. Splitting or yielding caused by excessive local stress is the normal response of the arch dam to adjust to the change by releasing the

restriction. Before the destruction of the arch dam, sure there exists a process of constant splitting or yielding and constant static determinacy, and in this very process, the potential of the arch dam still remains and thus safe operation continues[37]. Therefore, it is of extreme significance to study the evolution mechanism of the arch dam in the process from the spot or local strength insufficiency to the entire destruction[38].

Some countries including China have stipulated that the structure reliability theory should be adopted in the design of arch dams[39]. However, in the present evaluation of the reliability of arch dams by means of reliability theory, the functions chosen are mostly based on the arch dam strength destruction pattern and what is being studied is still the spot reliability. It is one of the key issues for the future study how to choose the random variables reflecting the state of the arch dam system as the basic variables for the analysis of the arch dam entire reliability[40].

Although definite achievements have been made in the research into the stability of arch dam's sliding along the foundation interface and into the un-stability of the dam shoulder rock body by means of motion stability theory[41], however, the arch dam consists of dam body, dam shoulder and rock foundation and their deformations are interacted and inseparable. Therefore, it will be a major direction worth researching to take dam body, dam shoulder and rock foundation as a whole to study the destruction mechanism of the arch dam, establish entire un-stability criteria and determine the safety of the whole arch dam[42].

The arch dam body and the foundation materials mostly are concrete, rock and soil, which belong to lower tensile or non-tensile materials with high randomness in terms of mechanics property and the stress & strain curve being obviously nonlinear. At present, Mohr-Coulomb & Drucker-Prager Yield Criterion and the Four-Parameter Criterion are generally adopted for the rock-soil and concrete. The yield face is mostly simplified as equal-direction intensive model, and relevance principle is adopted to determine the direction of the plastic strain increment. However, there is a big difference between the measured stress & strain relations of the arch dam material and these supposed relations[43]. It is not economically practical to infinitely increase dam foundation measuring points for the research into the constitutive model of the material; instead, it is of good & realistic significance to establish the constitutive model of the material based on the definite actually measured data and by means of reverse analysis process or nerve network adapting technique[44][45]. Thanks to such features as the lower testing cost, non-destruction, etc., microwave detecting technology and laser surveying technology will find wide applications in the arch dam safety evaluation.

Data show[46] that the operation of over 30% of the arch dams appears to be inconsistent with the expected operation by the design specifications. While studying the design safety of the arch dam, it is necessary to enhance the research into the safety of the actual operation of the arch dam.

To sum up, the research into the entire safety of the arch dam is far from mature, and up to now we lack practical methods that are based on scientific theory and also widely accepted by the dam engineering circle. Co-operation is expected to be enhanced in the academic world and in the dam engineering circle for the further exploring research.

REFERENCES

[1] *浙江大学学报*, 1999, 33(1):40–46.
[2] *水电站设计*, 1997, 13(4):1–6.
[3] *水力发电*. 2002, (12):10–13.
[4] *岩土力学*, 2000, 21(2):188–192, 21(3):305–308.
[5] *中国电力*, 1999, 32(12):12–19.
[6] *中国计算力学大会论文集*, 2003, 42–51.
[7] *华北水利水电学院学报*, 1997, 18(4):1–8.
[8] *煤田地质与勘探*, 2002, 30(1):41–44.
[9] .*长江科学院院报*, 1997, 14(2):27–30.

[10] 华超,任青文.有限单元法高拱坝坝肩稳定分析中的应用, 2003, 31(2):144–147.
[11] *水利学报*, 2002, (2):1–7.
[12] 任青文.现代水利水电工程中的力学问题[A].赵光恒.*力学——现代工业技术的支柱*.南京：河海大学出版社 2001. 258–282.
[13] *长江科学院院报*, 1997, 14(3):27–30.
[14] .*水利学报*, 1996, (7):67–74.
[15] *水利学报*, 2003, (3):55–62.
[16] 龚召熊,郭春茂等.地质力学模型新技术研究——用离心机作静力结构模型试验, 1991, (2):1–8.
[17] *四川联合大学学报*, 1997, 1(3):64–71.
[18] 北京:水利电力出版社, 1995, 16–78.
[19] *长江科学院院报*, 1995, (3):1–7.
[20] 陈建叶,胡成秋.碾压混凝土拱坝破坏试验中诱导缝相似模拟研究, 2003, 35(6):39–41.
[21] *四川大学学报*, 2002, 34(4):46–50.
[22] *力学进展*, 1993, 23(2):206–213.
[23] *重庆建筑大学学报*, 2002, 22(6):70–73.
[24] 与材料科学部, 1996:170–181.
[25] Liu Ning. Time-dependent reliability assessment for mass concrete structure. [J] Structure Safety, 1999.1.
[26] *岩石力学和工程学报*, 1999. 18(1):33–35.
[27] 杨令强,练继建等.随机有限元与最大熵法联合求混凝土拱坝可靠度, 2003, (2):24–28.
[28] *四川大学学报*, 2002, 34(4):34–37.
[29] 岩土工程学报, 1995, 17(3):51–59.
[30] *岩石力学与工程学报*, 1999, 18(3):245–249.
[31] *清华大学学报*, 2002, 42(4):35–37.
[32] *工程地质学报*, 1999, 7(1):9–14.
[33] *中国地质大学学报*, 1996, 21(6):604–606.
[34] 北京:*中国水利水电出版社*, 1995, 203–207.
[35] 北京:中国电力出版社, 1998, 40–41.
[36] *河海大学学报*, 2003, 31(1):1–4.
[37] *清华大学学报*, 2002, 42(4):35–37.
[38] Rocha M. Analysis and design of the foundation of concrete dams.Proc. Int. Symp. on Rock Mech.Related to Dam Foundation, Rio de Janeiro, 1978, 2(9).
[39] *河海大学学报*, 2000, 28(6):23–26.
[40] *河海大学学报*, 1995, 23(3):26–32.
[41] *河海大学学报*, 2003, 31(2):144–147.
[42] Souza Lima VM, et al. Rock foundations with marked discontinuities and assumptions for stability analysis. Trans.*14$_{th}$ ICOLD Congress,* Q.52-R.69, Rio de Janeiro, 1982.
[43] *岩土力学*, 2000, 21(2):188–192;21(3):305–308.
[44] *力学学报*, 1990, 22(4):429–437.
[45] *河海大学学报*, 1989, 17(5):23–31.
[46] *水利技术监督*, 2002, (2):32–38.

This page intentionally left blank.

New Developments in Dam Engineering—Wieland, Ren & Tan (eds),
© 2004 Taylor & Francis Group, London, ISBN 04 1536 240 7

Cameron Highlands/Batang Padang Hydroelectric Scheme: dam surveillance and performance review

Choy Fook Kun & Darul Hisham Saman
Tenaga Nasional Berhad, Malaysia

ABSTRACT: Cameron Highlands/Batang Padang Hydroelectric Scheme consists of two hydro projects with a total installed capacity of about 260 MW and is the first major hydro power development implemented by Tenaga Nasional Berhad (formerly known as National Electricity Board), a power utility company in Malaysia in the 1960s. A concrete buttress dam and three earthfill dams are four principal features among the many civil structures (e.g. power stations tunnels and intakes) and electrical and mechanical installations of the hydroelectric scheme. The reservoirs of Ringlet, Jor and Mahang created by the construction of these concrete dam (namely Ringlet dam) and three earthfill dams (namely Jor main, Jor saddle and Mahang dam) form an integral part of the hydro scheme. The Ringlet, Jor main, Jor saddle and Mahang dam are respectively 39.6m, 44.8m, 24.4m and 19.5m in height. Monitoring of the behaviour of the three earthfill dams is via the measurements of settlement, deflection, pore pressure, seepage and water table/pressure by means of the various types of instrumentation in the dams. The Ringlet dam behaviour is monitored by measuring uplift pressure at the foundation and seepage from adjoining structures at both ends of the concrete dam. There is presently no legislation requirement for dam safety assurance in Malaysia. Tenaga Nasional Berhad executes dam safety and surveillance works for its hydro dams in accordance with the dam designers' Operation and Maintenance Manuals and the Guidelines for Operation, Maintenance and Surveillance of Dams issued by the Inter-Departmental Committee on Dam Safety of the country. This paper gives a brief description of the surveillance aspect and a review of the performance of the four dams of the Cameron Highlands/Batang Padang Hydroelectric Scheme.

1 INTRODUCTION

The Cameron Highlands/Batang Padang Hydroelectric Scheme is located in the two states of Pahang and Perak in Malaysia. The Cameron Highlands development portion of the scheme utilises the hydro resources of the hill streams of Telom River and Bertam River in the Pahang state, and the Batang Padang development portion of the scheme utilises the Telom and Bertam waters (diverted from the Ringlet reservoir) together with the water of Batang Padang River and its tributaries.

There are seven power stations in the Cameron Highlands/Batang Padang Hydroelectric Scheme including Kampong Raja (0.8 MW), Kuala Terla (0.5 MW), Robinson Falls (0.9 MW), Habu (5.5 MW) and Jor (100 MW) of the Cameron Highlands Scheme, and Woh (150 MW) and Odak (4.2 MW) of the Batang Padang Scheme.

The construction of Cameron Highlands/Batang Padang Hydroelectric Scheme includes among others the building of the following four dams:

- The Ringlet dam—it impounds the water of Bertam River and the water diverted from Telom River, creating the Ringlet Reservoir for the Jor Power Station.
- The Jor main and saddle dam—the two dams impound the water of Batang Padang River and the water discharged from the Jor Power Station to create the Jor reservoir for the Woh Power Station.

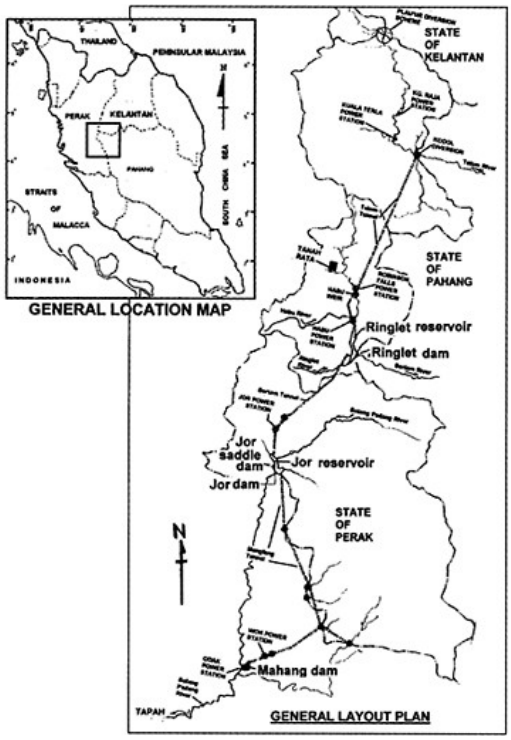

Figure 1.

• The Mahang Dam—it impounds the water discharged from the Woh Power Station and forms a pondage for the Odak Power Station.

Figure 1 shows the location and general layout of the Cameron Highlands/Batang Padang Hydroelectric Scheme.

2 BRIEF DESCRIPTION OF DAMS

2.1 *Ringlet dam*

The concrete Ringlet dam (also known as Sultan Abu Bakar Dam) was constructed in the years 1960–63, and a total of about 52,000m^3 of concrete and 19,000m^3 of rockfill was used for its construction. It is a concrete buttress dam with a mass concrete gravity section on the left bank and a rockfill section on the right bank. The rockfill is contained behind a mass concrete retaining wall and has an upstream concrete face as well as an upstream cut-off wall. The dam is about 39.6m high and 135m long (crest length) and has a 1,800mm diameter concrete-lined steel drain pipe (equipped with a downstream hollow jet regulator valve and an upstream butterfly valve) at El. 1037.64m. The gated spillway has one tilting and three radial gates, which are float-operated and can also be manually operated.

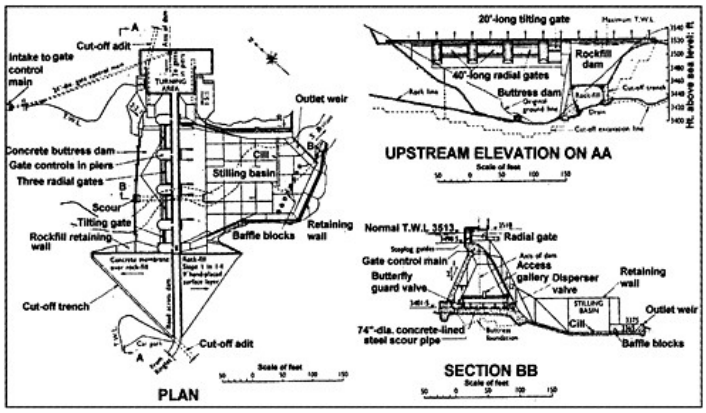

Figure 2.

The Ringlet reservoir has a useable storage of 4.7 million m^3 and a surface area of 60 ha at the normal top water level of El. 1071.71m. Instrumentations for monitoring the dam behaviour include:

- two number of 90° notch weirs each installed at the right bank and the left bank for measurement of seepage and ground water from the rockfill section and the area behind the left bank buttress respectively.
- a system of 76 number of inclined pipes installed on either side of buttresses to relieve uplift pressures beneath the buttress dam section.

Figure 2 shows a plan view and a cross-section of the Ringlet dam.

2.2 *Jor main and Jor saddle dam*

The construction of the Jor main and saddle dams was carried out in the years 1965–1967. Both dams are of earthfill construction with central clay core and the materials of the earthfill are of granite varying from fresh rock to decomposed granite. The total quantity of earthfill used in the dams is about 806,000m^3 including 680,000m^3 in the main dam and 126,000m^3 in the saddle dam. The material was rolled in 150mm consolidated layers by rubber tyred rollers on the clay cores and by 85 ton vibrating rollers on the shoulders and transition zone. Drainage mattress and drainage blankets were provided beneath the dams and across the shoulders and transition zones respectively. The height, crest length and crest elevation of the main dam are about 44.8m, 208.8m and El. 496.8m respectively, and those of the saddle dam are about 24.4m, 141.7m and El. 496.2m respectively.

The Jor reservoir at the normal fully supply level of El. 493.45m has a surface area of about 32ha and a gross storage of 3.85 million m^3 of which 2.1 million m^3 is the live storage. Excess water is discharged from the reservoir to downstream areas through the siphon bellmouth spillway and the 8.84m diameter concrete-lined spillway tunnel.

The types of instruments installed to monitor the dam behaviour are as follows:

- Jor main dam—53 number hydraulic piezometers, 2 number embankment internal settlement devices, 7 number dam crest settlement/deflection points, 4 number dam berm settlement/ deflection points, 9 number standpipe piezometers and a seepage measurement weir.
- Jor saddle dam—28 number hydraulic piezometers, 1 number embankment internal settlement device, 5 number dam crest/deflection points, 7 number standpipe piezometers and a seepage measurement weir.

Figure 3 shows a plan view of Jor dam and Jor reservoir plus a section through the dam.

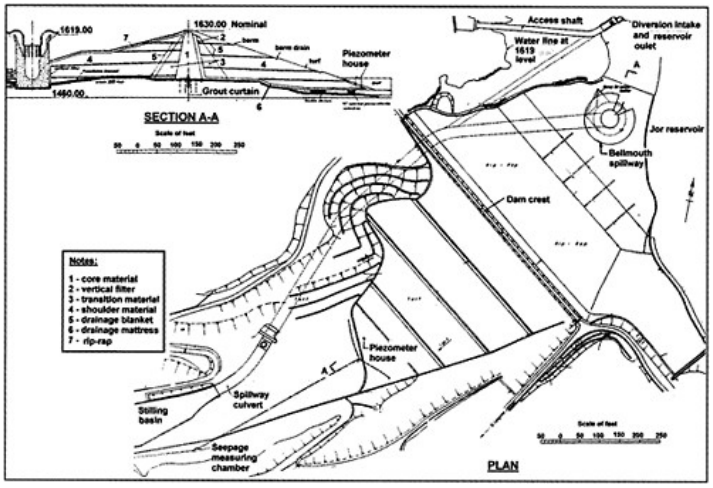

Figure 3.

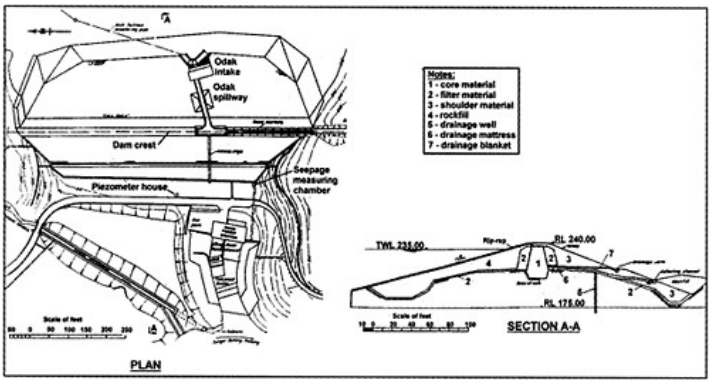

Figure 4.

2.3 *Mahang dam*

The Mahang dam is an earthfill dam with a central clay core and the volume of earthfill used for its construction is about 380,000m^3. It is about 19.5m in height and 228.6m in crest length. There are five reinforced concrete culverts located within the dam; three culverts are for conveying water from the Odak Intake to the Odak Power Station and two culverts function as overflow spillway culverts.

The Mahang reservoir at the full supply level of El. 71.65m has a surface area of about 8 ha, and a gross storage of 0.46 million m^3.

The types of instruments installed to monitor behaviour of the dam comprise 27 hydraulic piezometers, 1 number embankment internal settlement device, 5 number dam crest settlement/ deflection points, 11 number standpipe piezometers and a seepage measurement weir.

Figure 4 shows a plan view and sectional view of the Mahang dam.

3 DAM SURVEILLANCE AND MAINTENANCE

Dam safety assurance is not a statutory requirement by legislation in Malaysia, nevertheless the necessity and importance of dam surveillance works to monitor dam behaviour and to ensure dam safety is generally acknowledged by the relevant Government authority and all dam owners in Malaysia. The Guidelines for Operation, Maintenance and Surveillance of Dams (establishing procedures and practices for dam safety) was prepared/issued in October 1989 by an Interdepartmental Committee on Dam Safety in Malaysia that was formed in May 1986.

The surveillance and maintenance works of the four dams in the Cameron Highlands and Batang Padang Scheme are carried out in accordance with the abovementioned Guidelines (1989) and the designer's Operating and Maintenance Manual (PC & R, 1963 and 1968). Instrumentation data readings of seepage and piezometer (hydraulic and standpipe) are taken by trained personnel stationed at site. The readings are recorded on daily, weekly or monthly basis based on recommendations made in the O&M Manuals. The instrumentation data record and the observation report are forwarded to the head office for processing and analysing. Clearings of floating debris in the reservoirs and cutting of grass on the earth dams are carried out periodically as part of dam maintenance.

Dam inspection and deformation surveys are conducted quarterly by the dam surveillance section of the hydro engineering unit. The dam surveillance team consists of civil engineers, technicians and qualified surveyor. Annual inspection is headed by a registered Professional Engineer. Consulting engineers and dam experts are engaged to conduct independent review of the dam behaviours and safety once in every ten years or at an appropriate time.

4 DAM MONITORING RESULTS

4.1 *Embankment settlements and deflection*

The measured settlements on the mid-section of dam crest of the Jor main, Jor saddle and Mahang dams are respectively 100mm, 50mm and 20mm. These settlements correspond to about 0.22%, 0.20% and 0.10% of the respective dam height.

Figures 5 and 6 show the dam crest settlement and the trend of measured settlement on dam crest at mid-section over time respectively for the Jor main, Jor saddle and Mahang dams.

The average downstream horizontal displacements at about mid-section of the Jor main, Jor saddle and Mahang dams are about 50mm, 30mm and 10mm respectively.

4.2 *Internal settlements*

The measured internal settlements of central clay core for both Jor main and Jor saddle dams are shown in Figures 7 and 8 respectively. The results suggest that maximum settlements in the core occurred about mid-height of the dam.

4.3 *Porewater pressure*

The readings of some piezometers in the Jor main, Jor saddle and Mahang dams are shown in Figures 9, 10 and 11 respectively. The results generally suggest the followings:

- There is a drop in porewater pressure across the dam core.
- For piezometers installed at about same elevation the readings of piezometers at downstream are noticeably lower than those at upstream.
- Porewater pressure in the dam body has generally stabilised.

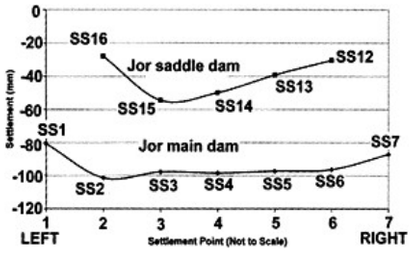

Figure 5.

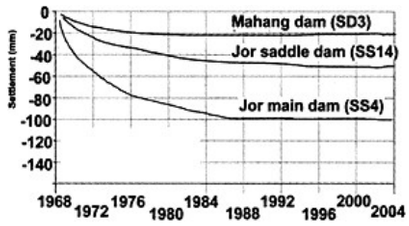

Figure 6.

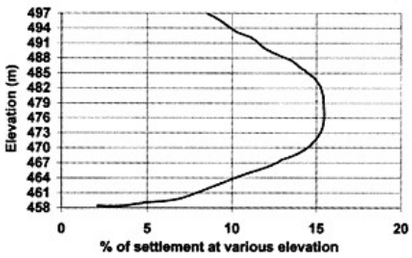

Figure 7.

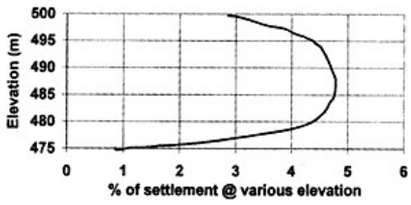

Figure 8.

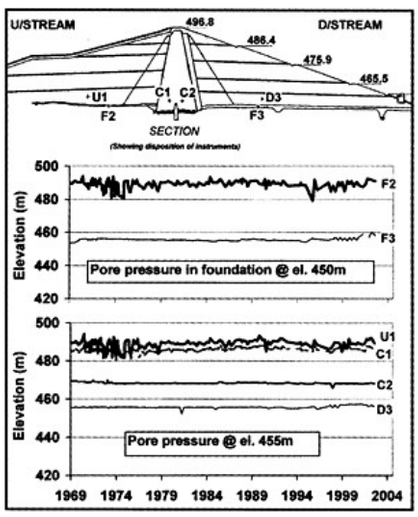

Figure 9.

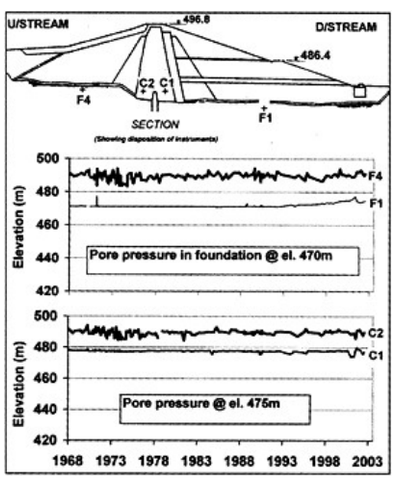

Figure 10.

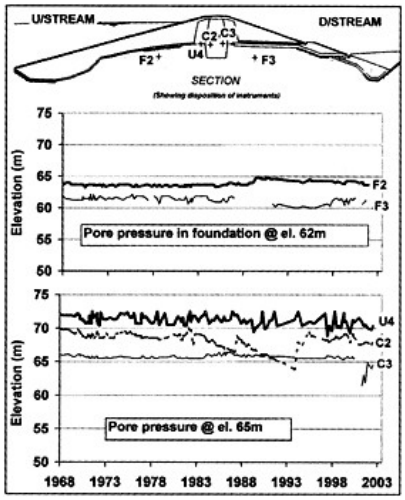

Figure 11.

4.4 *Standpipe piezometer readings*

The standpipe piezometer readings for the three earthfill dams are much influenced by rainfall. Nonetheless the following table gives a summary of the average readings of some standpipe piezometers (upstream standpipes followed by downstream standpipes) installed around the three earthfill dams.

The water table in the abutments of the three dams is generally shown to be descending from high ground to low ground and from upstream to downstream.

Dam	Abutment	Standpipe No.	Ground level, m	Water table, m
Jor main dam	Left	De 219	513	496
	Left	De 216	495	474
	Left	De 217	483	472
	Left	De 218	475	460
	Right	De 224	497	488
	Right	De 221	488	484
	Right	De 220	484	479
	Right	De 225	478	469
Jor saddledam	Left	DF 212	495	490
	Left	DF 213	483	475
	Right	DF 214	496	485
	Right	DF 226	488	476
Mahang dam	Left	Sl	80	68
	Left	S2	78	66
	Left	SIO	78	64
	Right	S9	77	68
	Right	S6	78	64
	Right	S5	67	63

4.5 *Seepage*

The Operating and Maintenance Recommendations (PC & R, 1968) highlight that the seepage flows of the three earthfill dams of Jor main, Jor saddle and Mahang would be influenced by rainfall and reservoir level. A statistical study of the seepages by Choy (1979) derives an equation/ expression for the relationship between monthly mean values of seepage Y, rainfall X and reservoir level Z in the form of $Y=A+BX+CZ^n$, where A, B, C and n are constants. The following three equations were obtained by regression:

(a)	Jor main dam	$Y=0.19175+0.00422X+0.00181((Z-1575)/10)^{2.5}$
(b)	Jor saddle dam	$Y=0.1235+0.0331X+0.0028((Z-1575)/10)^2$
(c)	Mahang dam	$Y=0.1461+0.0382X+0.0042(Z-228)$

5 DAM PERFORMANCE OBSERVATIONS

5.1 *Ringlet dam*

The Ringlet reservoir is badly silted. Accumulation of sediment in the reservoir is presently estimated to reach about 5.0 million m^3 reducing the originally designed live storage of 4.7 million m^3 to less than 2.0 million m^3. As a result, the maximum inflow with no spilling at the dam is reported (Teras & SNC, 2002) to be only $39m^3/s$ at the present days as compared with $80m^3/s$ in the early 1970's. However, overtopping of the dam is reported to be not likely to occur, as the spillway at the dam has been designed to pass $880m^3/s$ flood flow.

A preliminary study report of the sedimentation problem (SNC, 2000) highlights among others that the dam is safe and is able to sustain the combined pressure due to silt accumulation and high flood level or designed earthquake. The dam however has its capacity of flood flow regulation substantially reduced due to sedimentation. There is an increased risk of spilling, which will cause damages to crops and infrastructures and more importantly will endanger the lives of villagers in the Bertam Valley at the downstream area.

The spillway gates and the scour valve (butterfly) have been tested yearly as part of dam safety assurance program and the equipment is found to be in a satisfactory working condition.

The seepage is less than the allowable quantity and the uplift pressures have stabilised to establish a long term trend suggesting great stability and satisfactory performance of the data.

5.2 *Jor main, Jor saddle and mahang dam*

The designed maximum allowable settlement on dam crest of each Jor main, Jor saddle and Mahang dam is 1.5% of the respective dam height. This is obtained as 672mm for the Jor main dam, 366mm for the Jor saddle dam and 293mm for the Mahang dam. The measured total settlement for each of the Jor main, Jor saddle and Mahang dam (para 4.1) is therefore much less than the designed permissible value.

The average downstream horizontal displacement for each of the dams is considered to be small taking into consideration of the dam height/crest length of 44.8m/208.8m for the Jor main dam, 24.4m/141.7m for the Jor saddle dam and 19.5m/228.6m for the Mahang dam.

According to the measurement values of porewater pressure and seepage for the three earthfill dams, the central impervious cores of the dams have minimised the water seepage through the dams. The seepage pressures exerted by seepage water on the dams have generally stabilised and the measured seepage values are more influenced by rainfall than seepage water through the dams.

The findings/observations suggest that the cut-off structure, curtain grouting and blanket grouting at the foundation of each Jor main, Jor saddle and Mahang dam is performing satisfactorily. There is no or very low risk of slope failures by piping for the three dams and the performance of the three dams is generally satisfactory.

6 CONCLUSIONS

The Management of Tenaga Nasional Berhad (TNB) realizes the importance of dam surveillance works for dam safety assurance and has implemented dam safety assurance program for the hydro dams in Peninsular Malaysia. Monitoring of the dam behaviour is done in accordance with the dam designers' recommendations and the guidelines prepared by the Inter-departmental Committee for Dam Safety of the Country.

The performance of the four dams in the Cameron Highlands and Batang Padang Hydroelectric Scheme is generally concluded as satisfactory. Nonetheless, extensive and rapid land use change in the Cameron Highlands area has resulted in sedimentation of the Ringlet reservoir and reduction of the reservoir storage. This leads to, reduced flow regulation capability of the reservoir, and increased probability of water spilling and flooding of downstream area particularly during rainy days and wet season. While the Ringlet dam is reported to be still safe against the combined pressure of water and sediment, spilling of water laden with silt over the dam is a risk to the safety of the villagers living in the downstream Bertam valley.

In addition to structural stability, social and environmental aspects are oftenly necessary to be taken into consideration for dam safety evaluation. TNB is currently in the process to implement dam break study for its existing hydro dams and also plans to carry out risk assessment of failure for these dams.

ACKNOWLEDGEMENT

The writers would like to thank the President of Tenaga Nasional Berhad for his permission to publish this paper. All views expressed in the paper are the writers' and do not necessarily reflect those of the Management of Tenaga Nasional Berhad. The writers are fully responsible for any shortcomings of the paper.

REFERENCES

[1] Bjorn F Dahlen (1993) Hydro Power In Malaysia published by Tenaga Nasional Berhad.
[2] Choy Fook Kun (1979) Batang Padang Hydroelectric Scheme, Statistical Study on Underdrain Flow in the Three Earthfill Dams, Bulletin IEM, March Issue.
[3] Choy Fook Kun and Darul Hisham Saman. Upper Perak Hydroelectric Scheme, Dam Surveillance Aspect, Proceedings of 3rd International Conference on Dam Safety Evaluation, 11–14 December 2001, Goa, India.
[4] FK Choy & Fauzan Hamzah (2001) Cameron Highlands Hydroelectric Scheme, Land Use Change -Impacts and Issues. Proceedings of The 4th International Conference on Hydropower Development, Bergen, Norway.
[5] Inter-departmental Committee on Dam Safety in Malaysia (1989). Guidelines for Operational, maintenance and Surveillance of Dams.
[6] Perunding Teras and SNC-Lavalin Power (Malaysia). Flood Study for Ringlet Reservoir (2002).
[7] Preece, Cardew & Rider (1963). Cameron Highlands Hydroelectric Scheme. Operating and Maintenance Recommendations. Volume 3, Sultan Abu Bakar Dam.
[8] Preece, Cardew & Rider (1968). Batang Padang Hydroelectric Scheme. Operating and Maintenance Recommendations.
[9] Tenaga Nasional Berhad (2003). Cameron Highlands/Batang Padang Hydroelectric Scheme. Annual Inspection Report of Dams & Associated Civil Structures.
[10] SNC-Lavalin (2000). Cameron Highlands-Batang Padang Hydroelectric Rehabilitation Project, Sedimentation Study.

This page intentionally left blank.

New Developments in Dam Engineering—Wieland, Ren & Tan (eds),

Design calculation of "soft" gasket in penstock intended for replacement of the expansion joint in place of abutment of dam to power house

Dai Huichao
China Yangtze Three Gorges Project Development Corporation, China

Tian Bin
School of Civil Engineering, China Three Gorges University, China

ABSTRACT: The Yangtze Three Gorges Project (TGP) with the comprehensive benefits of flood control, power generation and navigation, a major project in developing and harnessing the Yangtze River in China, will have a great effect on the development of Chinese society and economy. The TGP consists of dam, hydropower station and navigation structure. The place of the abutment of the Dam to the Power House where the expansion joint is located is one of the most complicated parts of the TGP structures. In the place of passing the penstock from the dam section to the hydro power house it is necessary to provide the compensating portion within of which the penstock takes up the relative displacement of the dam and power house. Several variants of the execution of this transition zone are feasible. One of the design variants of the realization of the compensating portion for the TGP envisages the use of the so-called "soft" gasket. In so doing, the dam and the power house settles in joint zone and also the influence of the joint design on the stresses and strains at this portion were studied.

1 INTRODUCTION

The intake pipe of the power station of The Three Gorges Project, 12.4m in inner diameter, has the characteristics of large diameter penstocks and high HD values. Jointly stress-receiving structures by steel liner and reinforced concrete were adopted after comprehensive comparison and selection. Because of the extra big diameter of penstocks, it is difficult to meet the safety requirements by common expansion joints which, in the design, were replaced by cushion pipes. Based on calculations and analyses, the relative displacement and turning angle was small between the powerhouse and the dam in the section of Nos. 1–6 units of the left-bank powerhouse and the joining stress of steel pipes were within the allowable range at any season, therefore, it was determined to use cushion pipes instead of expansion joints. To ensure the safety of cushion pipes, the thickness of the cushion around the cushion pipe was increased from 3cm to 5cm; drainage was provided on the bottom of the cushion pipe and monitoring instruments were installed; the outside of the cushion pipe was wrapped by reinforced concrete which was designed on a total water head basis; no reinforced rings were provided for the cushion pipe for an axial length of 12m and thrust rings were provided for two sections of the steel pipe. The relative displacement in the riverbed section of Nos. 7–14 units was also within the allowable range of stress, only some local stresses beyond the allowable range where, if joining time is properly selected, expansion joints could also be cancelled. Considering the safety, a joint option of using corrugated pipes cased by common expansion joints was finally selected for the connection of the powerhouse and the dam of the Nos. 7–14 units. This new structural pattern is the biggest size corrugated-pipe expansion joint at home and abroad.

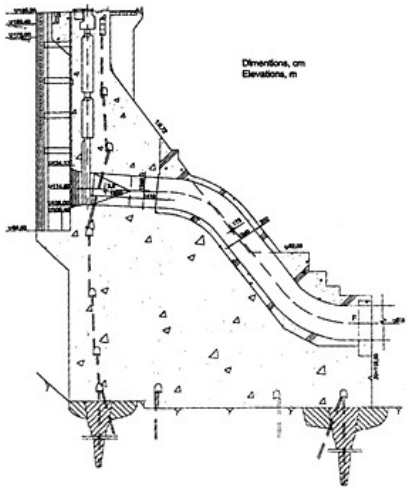

Figure 1. Layout of the dam section of TGR

The place of the abutment of the Dam to the Power House where the expansion joint is located is one of the most complicated parts of the Three Gorges Project structures. In the place of passing the penstock from the dam section to the hydro power house it is necessary to provide the compensating portion within of which the penstock takes up the relative displacement of the dam and power house. Several variants of the execution of this transition zone are feasible. One of the design variants of the realization of the compensating portion for the TGP envisages the use of the so-called "soft" gasket. At the portion of 10m long the inner steel lining of the penstock is separated from the concrete by the gasket made of material with low value of the deformation modulus. In so doing, the internal hydraulic pressure is completely taken by the inner lining. Within the scope of the present stage of work, the calculations aimed at reviewing the feasibility of the adopted design concerning the compensating portion in the connecting position of the dam with powerhouse were carried out.

The design studies have been fulfilled using the two-dimensional computational model (three dimensional structure is reduced to the two-dimensional model) of dam section including the hydro power house and massif of foundation rock, as well as using 3-Dimensional Model of the compensating portion, taking into account the reference characteristics and conditions. In so doing, the dam and powerhouse settlements in the joint zone and also the influence of the joint design on the stresses and strains at this portion were studied.

2 INITIAL DATA

For the performing the works on the review of the design of the "soft" gasket in the penstock within the abutment joint between the dam and powerhouse. The typical layout of the dam section of TGP is adopted in Fig. 1, the scheme of compensating portion including the "soft" gasket zone is taken from the Figure illustrating the layout of the lower section of penstock without compensating zone. The adopted scheme of the compensating portion with the "soft" gasket is shown in Fig. 2.

The geometric and physical-mechanical parameters of the reinforcing bars and steel lining, the physical-mechanical parameters of concrete and rock foundation, the physical-mechanical parameters of concrete and rock foundation, the hydraulic pressure with consideration for water-hammer pressure, the upstream and downstream water levels and the data regarding the temperature fields

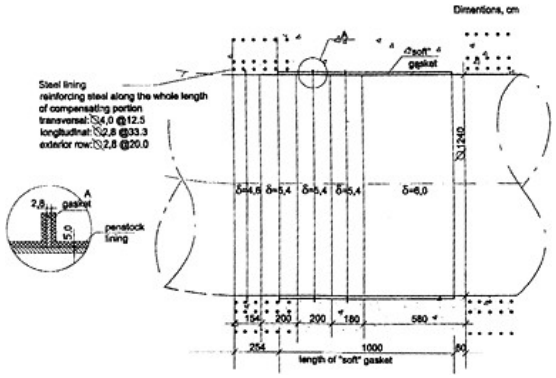

Figure 2. Scheme of the penstock portion in the soft gasket zone.

(water and ambient air temperature; temperature of inner and exterior surface of dam, machine hall and penstock, concrete temperature and temperature of water in proximity to upstream face, and etc.) are adopted from the Design Institute of the Yangtze Water Resources Commission. The rock foundation has been considered as a continuous elastic structure without fissure and faults. In temperature calculations, the variants in terms of assemble joint closure are adopted. The data on the expansion joint between the machine hall and dam in the river bed and bank slope dam sections are taken separately.

3 COMPUTATIONAL MODEL

3.1 *Computational two-dimensional finite element plane-reduced model of the "dam-power house-rock foundation" system*

The studies of the stress-strain state of the dam-power house-rock foundation system were made, using the plane-reduced model (three- dimensional structure was reduced to two-dimensional model), to calculate the tangential stress gradients along the whole penstock which are indispensable for taking into account the three-dimensional factor when calculating two-dimensional penstock sections, as well as for taking into account boundary conditions (displacements and stresses) when calculating three-dimensional fragmentary compensating portion of the penstock. Besides, some of stress-strain state characteristics like stresses along the penstock, penstock section thicknessaveraged vertical stresses (they are circular for diametrical plane), displacements of the boundary points of the compensating portion; strains in the joint between the dam and power house can be taken from the calculations made for the plane-reduced problem. The following loads were taken into account during the calculations:

– the weight of the dam, of the hydro power house, of the turbine and of the generator;
– hydrostatic pressure, upstream and downstream, at El. 175.0 and 62.0 respectively;
– seepage and uplift pressure to the dam foot and to the power house base;
– internal pressure in the penstock and in the spiral case including hydraulic hammer and centrifugal forces in the bending sections, taking into account in this case that the internal pressure in the penstock compensating portion and in the "soft" gasket zone of the spiral case upper part is taken up by the steel lining and it is not transmitted to concrete);
– influence of ambient winter and summer temperatures (water and air temperatures).

The design area was approximated by two-dimensional finite elements, four-cornered basically, and in some zones of the grid lines. The grid with finite elements includes 2001 nodes and 2676 elements. The loading scheme (hydrostatic pressure and concentrated forces resulting from the part of the building, above El. 82.0, not taken into account in the design area).

Uplift pressure was calculated by lowering the dam foot and power house up to downstream. The design area of the rock foundation was taken from the upper point of the dam foot upstream to the lower point of the power house downstream and at the 195.5m depth. The following boundary conditions were taken into account:

– the lower horizontal boundary is no vertical displacements;
– the upstream vertical boundary is free boundary;
– the downstream vertical boundary is no horizontal displacements.

The Finite element model of dam-hydro powerhouse-foundation system is shown in Fig. 3.

3.2 *Three dimensional computational model of the compensating portion of the penstock with "soft" gasket*

Special calculations were carried out for review of the design of the compensating portion of the penstock with "soft" gasket. The calculations of the stress-strain state were made on the basis of the 3-dimensional finite element model. A special structural dam and machine hall fragment restricted from the upstream by a vertical section crossing and by a vertical section within the machine hall was chosen for modeling. This design fragment was restricted in the upper part by a plane at El.67.0. The lower face of it was at E1.40.0m. Detailed 3-dimensional finite element model included:

– inner steel lining consisting of elements of 46mm, 54mm and 60mm thick;
– four ribs 30cm high and 28mm thick, strengthening the lining;
– "soft" gasket 10m long and 50mm thick;
– concrete part surrounding the "soft" gasket zone;
– expansion joint between the dam and machine hall (above El. 51.0m);
– reinforcing steel surrounding the "soft" gasket zone.

The width of the dam section fragment in the river bed was 25m, the width of the section fragment on the bank slope was 38.3m. Lateral faces of the river bed section fragment were assumed to be free from loads and boundaries; lateral faces of the bank slope section fragment consisting of rocks were bounded to prevent their displacements along the dam axis.

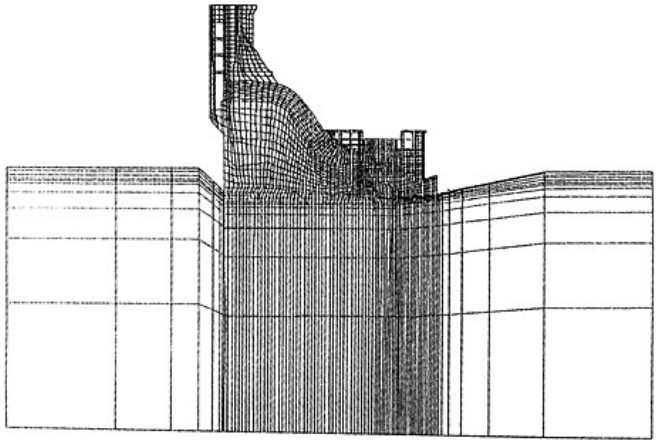

Figure 3. The Finite element model of dam-hydro powerhouse-foundation system.

The vertical faces of the model were subjected, from upstream and downstream, to forces and stresses (normal and tangential) calculated in solving appropriate plane-reduced problem (the three-dimensional structure is reduced to two-dimensional model). The upper horizontal face of the model (at E1.67.0m) was subjected to the vertical load equivalent to the weight of the above-arranged machine hall structures with its equipment. Special supporting boundary elements were placed on the lower face of the model; they simulated rock foundation massif situated lower. The expansion joint of the compensating portion of the fragmentary model was simulated in two different versions:

– joint is not grouted above El.51.0m;
– joint is completely grouted.

3.3 *Loads and effects*

The main design case was accepted as using the full-water penstock subjected to internal water pressure including water hammer. In so doing, forces and stresses in the steel lining and concrete surrounding the "soft" gasket were accompanied by temperature changes. The stresses in the steel lining and concrete, the settlements and displacements, as well as the influence of the expansion joint and "soft" gasket on the state of the penstock were studied using the 3-dimensional finite element model.

4 CALCULATION RESULTS

4.1 *Results of the calculations for the plane-reduced model of the "dam-power house-rock foundation" system*

The calculations were carried out for the riverbed and the bank slope dam sections. Main results regarding the bank slope section are tabulated. The strained state of the dam and the power house under main combinations of loads for the case when the joint is grouted within E1.50.8–67.0m. Maximum horizontal shift downstream is equal to 10.7mm and it is to be observed below the dam crest, is to 12.6mm. When the joint is not grouted within El.50.8–67.0m, the horizontal downstream shifts are equal to 11.5mm and the vertical shifts to 12.4mm. In case of non-grouted joint, the shifts in zone of the joint between the dam and the powerhouse are equal to 3.32mm for the rapprochement of the joint walls at El. 63.2m. The rapprochement of the penstock points, located within the "soft" gasket limits, is equal, at El.63.2, to 3.42mm for the non-grouted joint and to 0.75mm for the grouted joint.

The shift values of the penstock in the "soft" gasket zone of TGP calculated are shown in Table 1 (on the bank slope dam section) and Table 2 (on the river bed dam section) separately.

The principal stresses in the dam, the power house and adjoining foundation for the case of main combination of loads and grouted joint. Maximum principal stresses are as follows:

– at zone of adjoining of rock foundation upstream, they are equal to 1.33MPa for the rock element located below dam foot, and they are equal to 2.98MPa for the rock element adjoining to the upstream face of the dam.
– at the walls of the penstock part lying outside the downstream face of the dam, they may reach 3.0MPa.

Maximum calculated principal compression stresses can reach 5.16MPa in zone of the abutment of the downstream face of the hydro power plant pier with draft tube floor (the joint is grouted). In case of the non-grouted joint the compression stresses are equal to 4.00MPa.

The rated values of the temperature increment (summer and winter) in reference to the steady state temperature in the dam body, for which was determined the stress-strained state of the "dam-power house-rock foundation" system at season ambient temperature variations. The strained state of the dam and the power house under summer and winter temperature effect in reference to the structural state under average annual temperature. In summer, the upstream face of the dam is deviated in upstream direction, the downstream face of the power house is deviated in downstream direction.

Table 1. Shift values in the "soft" gasket zone (on the bank slope dam section).

Design versions	Shift values, mm	
	Horizontal shift	Vertical shift
The joint is grouted below El.51.0m	0.99	0.10
The joint is grouted above El.51.0m	0.11	0.05
Summer temperature	0.31	0.33
Winter temperature	0.22	0.22

Table 2. Shift values in the "soft" gasket zone (on the river bed dam section).

Design versions	Shift values, mm	
	Horizontal shift	Vertical shift
The joint is grouted below El.51.0m	2.34	0.59
The joint is grouted above El.51.0m	0.27	0.33
Summer temperature	0.32	0.30
Winter temperature	0.54	0.14

The joint between the dam and power house is closed, at E. 82.0m, by 3.79mm. In winter, the upstream face of the dam is deviated in downstream direction (the deviation of the crest is 7.06mm), the downstream face of the power house is deviated in the upstream direction at El.61.2m of 1.86mm). The joint between the dam and the power house is open by 0.58mm at El.82.0m. In case of grouting the joint within El.50.8–67.0m, the points of the steel lining (El.63.2) at the place of the "soft" gasket draw together by 0.34mm in summer and they draw apart by 0.28mm in winter; in this case in the lining the longitudinal compressive (298MPa) and tensile (26.1MPa) stresses develop respectively. In case of non-grouted joint, the compressive stresses appearing in the lining (El.63.2m) are equal to 62MPa in summer and with regard to the static stresses due to main combination of loads they reach 34MPa. When the joint is grouted, the adequate compressive stresses are not more than 46MPa. Consequently, the grouting of the joint permits to decrease Ingitudinal stresses in the steel lining of the penstock in zone of the expansion joint.

4.2 *Results of the calculations of compensating portion of the penstock with "soft" gasket*

The calculations of stress-strain state and strength of the penstock in this zone were performed. The reinforcement analysis was also made and a basic scheme of the reinforcing around the "soft" gasket was developed. The calculations were made on the basis of detailed 3-dimensional models of this zone for the bank slope and the river bed dam sections by using required results of calculations for two-dimensional plane-reduced model. Two alternatives regarding the expansion joint between the dam and the power house were considered, one is the joint grouted up to E1.51.0m, the other is the joint completely grouted above El.51.0m. The loads and effects taken into account in performing the calculations were as follows:

– loads at normal operation, including emergency closing of the gate with redard to the water hammer;
– loads at construction period, up to term of assemble joint closure;
– various variants of temperature effects.

The following cases of the temperature effects were considered:

– annual temperature changes of air, water, concrete, within housing; and etc (winter and summer temperatures) relative to corresponding average yearly temperature;
– three variants of temperature changes corresponding to 3 cases in design terms of assemble joint closure.

Table 3. Maximum stresses in the lining at the place of the “soft” gasket (on the bank slope dam section).

Type of loads and effects	Stress values, MPa	
	Annular stresses	Longitudinal stresses
Pression (the joint is grouted below El.51.0m)	222.9	60.1
Pression (the joint is grouted above El.51.0m)	222.8	43.2
Assemble joint closure (in July)	294.8	127.0
Assemble joint closure (in April, in October)	251.7	84.0

Table 4. Maximum stresses in the lining at the place of the “soft” gasket (on the river bed dam section).

Type of loads and effects	Stress values, MPa	
	Annular stresses	Longitudinal stresses
Pression (the joint is grouted below El.51.0m)	228.8	15.6
Pression (the joint is grouted above El. 51.0 m)	222.8	57.6
Assemble joint closure (in July)	294.8	123.0
Assemble joint closure (in April, in October)	261.5	75.5

In the last case, the initial stresses in the lining at this zone was assumed to be created in the moment of the assemble joint closure (April, July or October) and the design temperature difference is regarded to temperature of given month. The calculations made possible the determining of:

– stresses in lining, in surrounding concrete and in reinforcement;
– vertical and horizontal shifts in the joint zone (the joint is not grouted);
– vertical and horizontal shifts of ends of the portion with “soft” gasket;
– shifts of the lining at the place of contact with the “soft” gasket.

The stresses of the penstock in the lining at the place of the “soft” gasket zone of TGP calculated are shown in Table 3 (on the bank slope dam section) and Table 4 (on the river bed dam section) separately.

When performing calculations, the total settlements of the dam and the powerhouse in the expansion joint zone, as well as settlements developing after assemble joint closure were determined. Because of the absence of sufficient data on the rock foundation (jointing, faults, fracture, etc), in calculations the rock mass was assumed to be a continuous homogeneous structure, The settlement values obtained during the calculations comply with initial adopted data. The stress state in the “soft” gasket zone, due to temperature effect, as well as due to hydraulic pressure and weight of the machine hall and equipment, was assumed to be appeared after assemble joint closure. The influence of the dam and the power house on the given 3-dimensional design fragment at the place of the “soft” gasket was taken into account thus: the model faces were subjected to forces calculated for this zone with the use of two-dimensional plane-reduced model of “dam-machine hall-rock foundation” system. In other words, for each design case regarding the 3-dimensional fragment, the adequate problem has been previously solved by using the two-dimensional “dammachine hall-rock foundation” model. The forces obtained in the boundary points of the “soft” gasket zone were applied to the 3-dimentional fragmentary model.

When solving temperature problems, the shifts taken from the two-dimensional model were given at the ends of the penstock with “soft” gasket and the temperature fields and their associated fields of temperature stresses for the 3-dimensional fragment were then determined.

The analysis of the computation results shows that the complete grouting of the joint exerts a favorable effect on the state in the “soft” gasket zone. The complete grouting of the expansion joint above E1.51.0m is recommended. The analysis of the calculation results shown that the main

combination of loads involving internal pressure with regard to the water hammer, weight of the structure and equipment, temperature effect is the most dangerous. The value of the total stresses in the lining for the considered combinations of loads doesn't exceed the value of the design strength of the steel used for the lining portions.

In the concrete part of the penstock at the place of the "soft" gasket, both longitudinal tensile stresses and annular tensile ones develop. For their taking up, the placing of required quantity of reinforcement is necessary.

As the rated strength of the steel lining exceeds the acting tensile force, a minimum quantity of the reinforcement can be placed at the place of the "soft" gasket according to the Russian Specifications: for instance, annular reinforcement ∅ 25 A-II with a pitch of 50cm for each row of annular reinforcement. In so doing, in accordance with the Russian Specifications the reliable drainage and measures on the emergency gate closing can be provided. Such a quantity of the reinforcement conforms to so-called structural reinforcement (according to conditions for assemble joint closure and fissure limitation).

In case of the emergency loads (the discontinuity of the steel lining in the "soft gasket zone) the internal water pressure is completely transmitted to the reinforced concrete part and after cracking the tensile forces are taken up by the reinforcement. In this case it is necessary to use the following scheme of reinforcing. Annular reinforcement, two internal rows ∅ 28 A-II (two internal rows with a pitch of 33.3cm and one external row with a pitch of 20cm).

5 CONCLUSIONS AND RECOMMENDATIONS

The calculations of the stresses, strains and settlements in the penstock zone with "soft" gasket were carried out on the basis of two- and three-dimensional finite element models for all combinations of loads and effects predetermined above. Because of the absence of sufficient data on the rock foundation (jointing, faults, fracture), during the calculations the rock mass was assumed to be continuous homogeneous structure. The analysis of the calculation results have shown that the grouting of the joint above E1.51.0m exerts a positive effect. To increase the reliability of the TGP, it is advisable to make a complete grouting of joints above El. 51.0m at all the sections (in the river bed and on the bank slope).

The estimation of the terms of the assemble joint closure was made. The moment of the closure in July was found to be non-favorable supplementary temperature stresses in the steel lining. The assemble joint closure in April or in October is recommended. To improve the reliability and safety of the penstock the following scheme of reinforcing is recommended: three rows of circular reinforcement Φ40 with a pitch of 12.5cm, longitudinal reinforcement, respectively, 028A-II, two row with a pitch of 33.3cm and one row with a pitch of 20cm. A 50mm-thick "soft" gasket is recommended. The calculations confirmed the strength and reliability of the designed variant of the compensating portion with using the "soft" gasket. The arrangement of the "soft" gasket for the bank slope and the river bed dam sections of the Three Gorges Project is recommended.

REFERENCES

Zhang Chaoran 2003. Technical Break throughs in the Construction of TGR ENGINEERING SCIENCE, 5(2), 20–25.

Dai Huichao, Zhang Chaoran. 2002., New Technology adoped in high intensity concrete construction of the Three Gorges Projects. Journal of Hydraulic Engineering, 10, 91–95.

Dai Huichao, Zhou Hougui. Rapid Dam Concrete Construction at Three Gorges. China Three Gorges Construction, 2002, 9(7), 10–12.

New Developments in Dam Engineering—Wieland, Ren & Tan (eds),

Using in-situ dynamic tests for accurate seismic stability evaluation of embankment dam

M.Davoodi
Assistant Professor, Geotechnical Research Center of IIEES, Tehran, I.R.Iran
M.K.Jafari
Assoc. Professor, Geotechnical Research Center of IIEES, Tehran, I.R.Iran

ABSTRACT: In order to study the effect of in-situ dynamic tests for accurate seismic stability evaluation of embankment dams, modal and spectral analysis of the Masjed-Soleiman (MS) dam was performed. Based on the results of the forced and ambient vibration tests, modal frequencies of the dam were measured and the related mode shapes were identified. Although it is known that the dynamic behavior of embankment dams in strong earthquakes is affected by nonlinear behavior of the dam body's material, but in this study, the linear behavior of the materials is assumed for small to moderate earthquakes. Consequently, the 2-D spectral analysis using ANSYS software was carried out in the full reservoir condition and the stress distribution was evaluated based on the participation of fundamental mode.

These studies indicated the critical influence of foundation mass on modal frequencies and dam stability (during small and moderate earthquake) evaluation. Also, the in-situ dynamic soil properties were used for evaluating the stress distribution as calculating the modal frequencies of the dam body. It is evident that using the in-situ dynamic test results with improved numerical modeling (material properties and foundation mass) has an utmost importance in stability evaluation when an especial structure such as embankment dam is under investigation.

1 INTRODUCTION

Iran is a part of Alpine seismic belt and is considered as an earthquake prone region with a high seismic hazard level. Evaluation of the dynamic behavior of dams (both embankment and concrete) under earthquake loading is always the outmost concerns of the researchers and engineers in this country.

It is recommended to use the results of in-situ dynamic tests to check the mathematical model of embankment dams and as basic input data to predict how the dam will behave in an earthquake. Since real earthquakes are uncontrolled in terms of time, location, intensity and repeatability, the ambient and forced vibration tests (the most common types of vibration tests on prototype of dams) have been used frequently in the world since 1960s [Jafari, 2002].

Ambient and forced vibration studies have one draw back with regards to earthquake studies, and that is because they are concerned with vibrations of much smaller amplitude than those normally encountered in earthquakes. Consequently, the ambient and forced vibration studies must be used to confirm the linear elastic modeling of a dam, which can then be used in conjunction with non-linear extrapolations to predict how the dam would behave under earthquake loading.

In order to study the effect of in-situ dynamic tests for accurate seismic stability evaluation of embankment dams, a comprehensive study has been defined. Consequently, a complete ambient

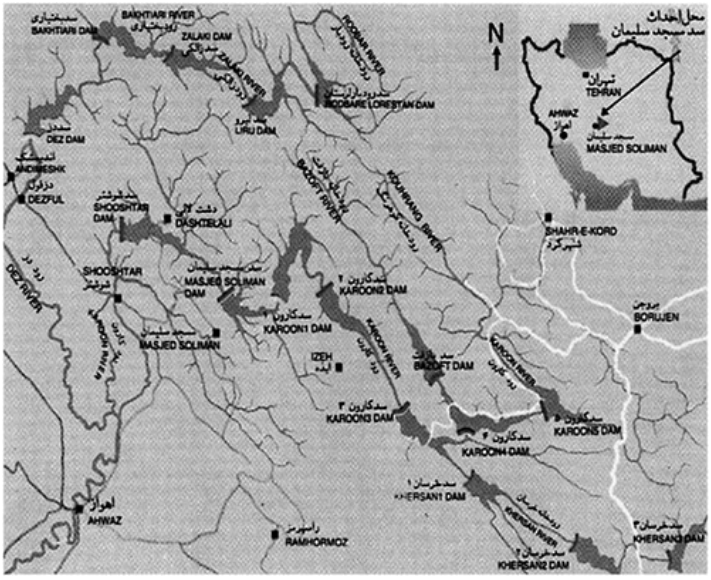

Figure 1. Outline of MS embankment dam position on Iran map.

(including explosion) and forced vibration testing program and numerical study on the highest embankment dam in Iran, named Masjed-Soleiman (MS), was performed. The MS dam is a rock-fill one with a clay core, which is located in south west of Iran (Khuzestan province) on Karun river (figure 1). The dam has a maximum height of 177m, a dam body volume of nearly 13.4 millions of m^3 and a reservoir capacity of about 230 millions of m^3. The length to height ratio (L/H) of the dam is 2.76, which is a small ratio in comparison with other large embankment dams. Therefore the 3D evaluation of the dam behavior under dynamic loading is important. The whole dam body lies on Bakhtiyari geological formation, which is marked by hard conglomerate and very thin clay intercalation. The construction of the dam body has been recently completed and first stage of powerplant project is under operation.

In this paper, the effect of boundary condition and material properties correction on dynamic characteristics and slope sliding stability evaluation of MS embankment dam will be presented.

2 IN-SITU DYNAMIC TESTS RESULTS

The response of the dam body in full reservoir condition to ambient vibrations, large explosives (in quarries and underground power plant house) and forced vibration tests (by three mechanical unbalance mass shakers) were measured. The instrumentation system used to measure the dam response to the mentioned excitations consisted of 9 SS-1 short period ranger seismometers [Kinemetrics(A), 1990], 4 SSR-1 solid-state recorders [Kinemetrics(B), 1990], AC-21 force balance accelerometers and CR-1 (and CR-2) portable digital central recording systems [GeoSig, 2001]. The complete description of the test procedures and signal processing techniques has been presented in [Jafari, 2003, 2004].

Table 1. Modal frequencies (HZ) and Corresponding mode shapes of the MS embankment dam due to ambient vibration (including explosion) and forced vibration tests, 2-D and 3-D FEM.

No.	1	2	3	4	5	6	7	8
Direction	U-D	L	U-D	V	L	U-D	V	L
Shape	First symmetric	First symmetric	First anti-symmetric	First symmetric	First anti-symmetric	Second symmetric	Second symmetric	Second symmetric
Measured value	1.45–1.5	1.7–1.8	1.75–1.8	2.0–2.1	2.1–2.25	2.9–3	2.9–3	3.3–3.4
	1.5	1.8	1.8	2.1	2.2	2.9	3	3.3
3-D	1.65	1.9	2.24	2.37	2.76	3.06	3.25	3.33
2-D	1.26	–	–	1.93	–	–	–	–

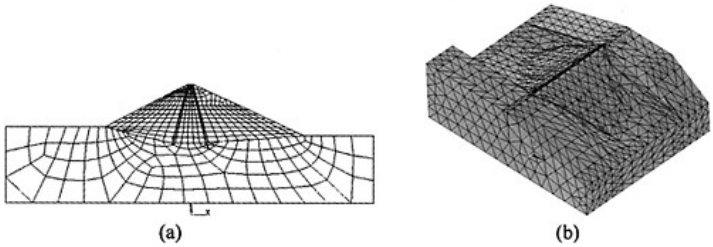

Figure 2. The final finite element model of MS dam body and foundation, a: 2D FEM, b: 3D FEM.

Based on the results of the in-situ dynamic tests, the first 23 modal frequencies of the dam were measured and the related mode shapes for the first 16 modes were identified. The first 8 modal frequencies and corresponding mode shapes of the dam body due to in-situ dynamic tests are presented in table 1.

3 MODAL ANALYSIS RESULTS AND ITS COMPARISON WITH MEASURED ONES

Using ANSYS software [Ansys, 1997], the 2-D & 3-D modal analysis of MS embankment dam was developed and the natural frequencies and mode shapes of the dam body were estimated. There has been used 516 PLANE 42 elements and 489 nodes for 2-D analysis, whiles in the case of 3-D analysis, 13189 SOLID 45 elements and 2865 nodes for the final model has been used. Figure 2 shows the final 2-D & 3-D finite element model of the dam body and the corresponding foundation.

The dynamic soil properties of the dam body and foundation materials were estimated based on consulting Eng. reports and appropriate seismic refraction investigations. Foundation-dam interaction effect was investigated by modeling 3 different inertial properties (massless, decreasing mass and complete mass model). In the decreasing mass model, the foundation inertia near the dam body is considered completely, whereas towards the outsiding boundaries it reaches to zero. Because of the low slope and high porosity of the shell, the hydrodynamic effects of the full reservoir on dynamic properties of the dam has been neglected, while the shear modulus and density values of the dam materials has been affected due to impounding effects.

The natural frequencies for 8 modes of 3-D FEM in full reservoir condition are presented in table 1. The flexibility of the foundation is characterized, but not its damping and inertial properties (i.e. massless condition as in common dynamic analysis). For comparison of the 3-D results

Table 2. Diiferent foundation Conditions effect on natural frequencies of the MS embankment dam in full reservoir condition due to 3-D FE analyses; f indicates frequency values (in Hz) and (Δ the percent of difference between each situation and the test results (in each column, from left to right: first U-D symmetric mode, first L symmetric mode and first V symmetric mode).

	Rigid foundation			Massless foundation			Foundation with decreasing mass			Foundation with complete mass		
Frequency (HZ)	1.98	2.24	2.87	1.65	1.9	2.37	1.51	1.72	2.10	1.44	1.63	1.96
Difference %	32	32	37	10	12	13	1	1	0	−4	−4	−7

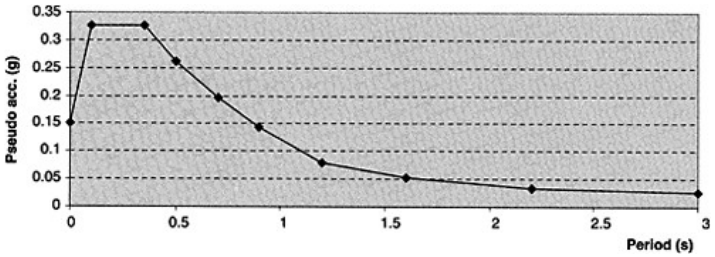

Figure 3. The input spectrum in dynamic analysis of the MS embankment dam.

with the 2-D simplified model, the first natural frequency of 2-D FEM in U-D and V directions are also presented in this table. Since various deformations along the crest cannot be represented in 2-D analysis, the other modes of vibration in this analysis are not comparable with the 3-D ones; therefore they are not presented in this table. Based on the presented results in table 2 and obtained mode shapes, the first natural frequency of 2-D analysis is 15% less than the measured one, whereas the corresponding 3-D analysis is 10% more than the test result.

In order to consider the effect of different foundation conditions on natural frequencies of the dam body, 3 first natural frequencies in 4 different cases are summarized in table 2. Based on the results of the analysis, the best compromise between the measured and 3-D computed values (specially in the low modes) occurred when decreasing mass foundation height became as the height of the dam. In this case, the calculated first natural frequencies is approaching the most to the measured one. In high modes of dam body, it seems that the results of massless foundation model fits better to measured one. In these cases, the optimum foundation height and abutment width were evaluated as the height of the dam.

4 SPECTRUM ANALYSIS

In order to study the effect of in-situ dynamic tests for accurate seismic stability evaluation and stress distribution of the dam body, dynamic analysis of the dam was performed. Although it is known that the dynamic behavior of embankment dams in strong earthquakes is affected by nonlinear behavior of the dam body's material, but in this study the linear behavior of the materials is assumed for small (and moderate) earthquakes. Consequently, the 2-D spectral analysis using ANSYS software was carried out in the full reservoir condition and the stress distribution was evaluated based on the participation of fundamental mode. The figures 3 to 5 show the input data on horizontal direction and some results of spectrum analysis including stress distribution due to static and dynamic loading. Based on the combined static and dynamic stress distribution, 4 most possible failure surfaces were

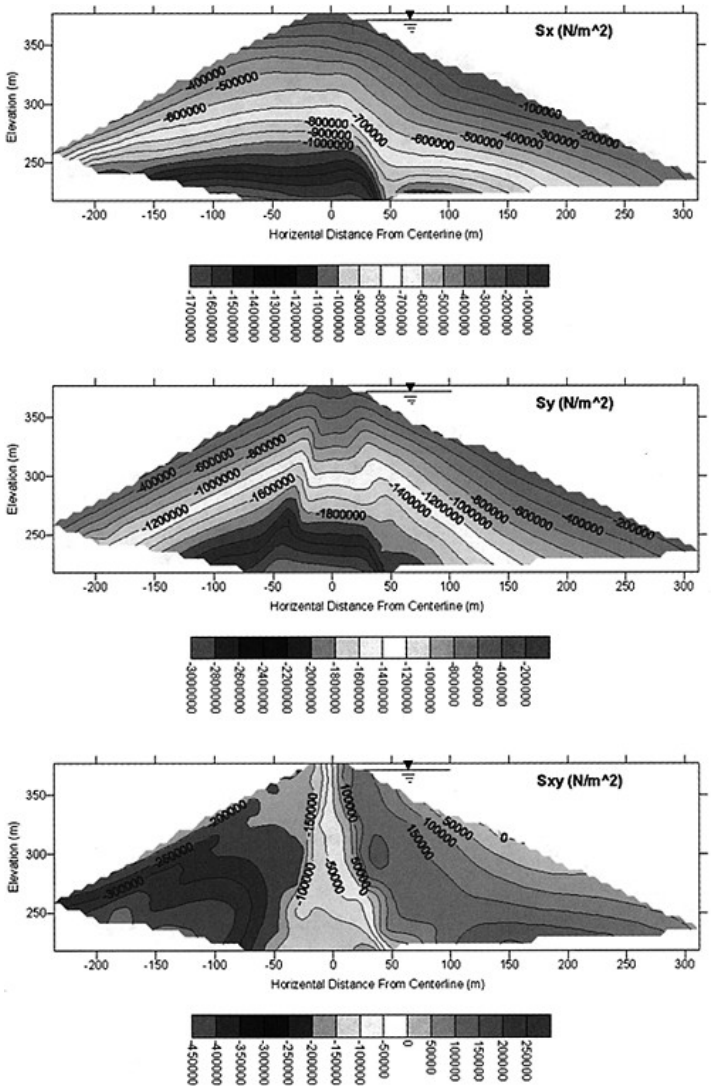

Figure 4. Static stress distribution on the MS embankment dam body in the first impounding due to static analysis; from top to bottom: horizontal, vertical and shear stress.

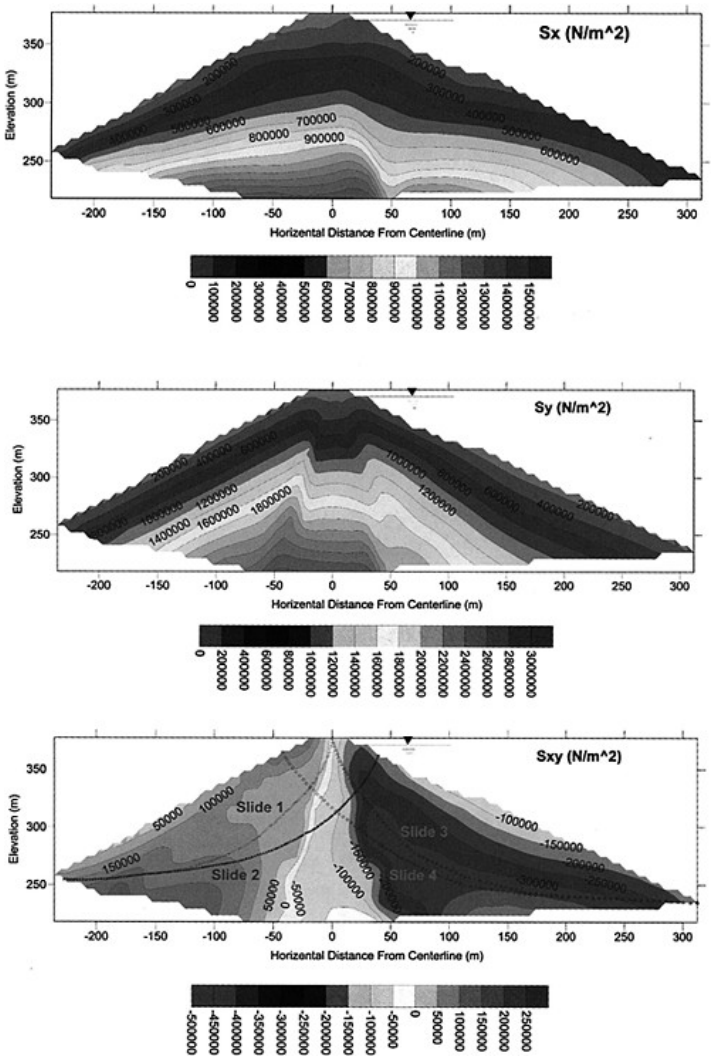

Figure 5. Horizontal, vertical and shear stress distribution (from top to bottom) on the MS embankment dam body due to static and dynamic (for input spectrum in X direction) analysis; the 4 assumed sliding surfaces can be shown in bottom picture.

assumed as can be seen in figure 5. In p-q (mean principal stress $q = \frac{\sigma_1 - \sigma_3}{2}$ based on the [lambe & Whitman, 1979]) diagram, the stress situation of the elements located on each assumed surfaces were obtained and corresponding sliding safety factor (SF) were calculated.

At the end of dynamic analysis, the effect of boundary condition (3 different inertial properties) and material properties correction (due to using the in place dynamic shear modulus of the dam body and foundation materials) on slope sliding stability of the dam body were evaluated and the following results were obtained:

1. Although the correction in dynamic material properties of the dam body leads to 5% increase in the first natural frequency of the dam body, but the dynamic stress distribution on the assumed sliding surfaces increases up to 70%. It is important to point that by increasing the same static stresses to the mentioned dynamic stresses and evaluating the safety factor (SF) on sliding slopes, the SF values decrease only 3%. This indicates the importance of correct static stress evaluation on the dam body in order to evaluate the stability of the embankment dams during weak to moderate earthquakes. In addition, the dynamic stresses has more important role during strong earthquakes, which has to be evaluated by nonlinear dynamic analysis.
2. The rigid foundation assumption in comparison with flexibility one increases the first natural frequency as 20% and the SF of downstream sliding slope as 7%. In this condition, the SF value of upstream sliding slope decreases as 6%.
3. In the case of foundation flexibility assumption, applying mass in the foundation model leads to not only 6% decrement in the first natural frequency of the dam body, but also 19% and 9% decrement in the SF of downstream and upstream sliding slopes, respectively. In other words, the mass of the foundation in the numerical model not only changes the natural frequencies of the dam body, but also has an important influence on the dam stability. Consequently, further investigation is necessary to reveal more accurate amount of mass in the foundation model.

5 CONCLUSION

A comprehensive study on the highest embankment dam ever constructed in Iran (at the ending stage of construction) including ambient vibration (including explosion) and forced vibration test and preparing appropriate numerical model was performed. Based on the results of this study, the following considerations can be revealed:

1. Detailed comparison between FE modal analysis and the in-situ tests results revealed that the best fit in low modes occurs when the decreasing mass foundation is used in numerical model. In high modes of dam body, it seems that the results of massless foundation model fits better to measured one. In these cases, the optimum foundation height and abutment width were evaluated as the height of the dam.
2. These studies indicate the critical influence of foundation mass in dam stability evaluation (during small and moderate earthquake).

Totally, these studies revealed that using the in-situ dynamic test results with improved numerical modeling (material properties and foundation mass) has an utmost importance in stability evaluation of an especial structure such as embankment dam.

6 ACKNOWLEDGEMENTS

The authors are grateful of the Iranian Water and Power Company IWPC (the owner of the MS dam) for excellent cooperation. Many people contributed substantially to the work described in this paper, specially from geotechnical department of IIEES for their effort during seismic refraction survey and from Electronic Instrumentation group of IIEES for their efforts during forced and ambient vibration tests.

REFERENCES

1. Jafari M.K., Davoodi M., “Forced and Ambient Vibration Tests of embankment Dams”, IIEES, I.R.Iran, 2002 (Report in Persian).
2. Kinemetrics (A), Manual of “Operating Instructions for Model SS-1 Ranger Seismometer”, Kinemetrics Systems, Pasadena, Calif., 1990
3. Kinemetrics (B), Manual of “SSR-lSolid State Recorder”, Kinemetrics Systems, Pasadena, Calif., 1990.
4. GeoSig, Technical Documentation of “SMACH CR-2 and CR-1 Central Recorders and AC-21 & AC-23 Accelerometers”, User Manual, www.geosig.ch,2001.
5. Jafari M.K., Davoodi M., “Dynamic Characteristics Evaluation of Masjed-Soleiman Embankment Dam by Ambient Vibration and Explosion Tests”, 4th International Conference on Seismology and Earthquake Engineering, Tehran, I.R.Iran, 12–14 May, 2003.
6. Jafari M.K., Davoodi M., “Dynamic Characteristics Evaluation of MS Dam by In-Situ Dynamic Tests”, Journal of Geotechnical and Geoenvoronmental Engineering, ASCI, 2004 (under publication).
7. ANSYS, “ANSYS Theory Manual, ANSYS Release 5.4”, ANSYS INC, Canon Sburg, USA, 8th edition, www.ansys.com, 1997.
8. Lambe T.W., Whitman R.V, “Soil Mechanics, SI Version”, John Wiley & Sons, P.P. (107,141), 1979.

New Developments in Dam Engineering—Wieland, Ren & Tan (eds),
© 2004 Taylor & Francis Group, London, ISBN 04 1536 240 7

Engineering properties of kaolinitic clay as core of Batutegi dam

D.Djarwadi
PT Pamapersada Nusantara, Jakarta, Indonesia

B.Suhendro & H.C.Hardiyatmo
Gadjah Mada University, Jogjakarta, Indonesia

ABSTRACT: This paper discussed the engineering properties of the proposed clay core materials for Batutegi dam, obtained from soil investigation on 140 test pits in the borrow area, before the construction stage of the dam. The impervious materials for core was obtained from tertiary sandstone and laharic breccias regions borrow area at downstream of the dam, and most of the materials are sandy clay with medium to high plasticity. The X-ray diffraction examination indicated that kaolin mineral dominated the proposed impervious embankment material; while a small portion of quartz and halloysite minerals was exist. The interrelation of the geotechnical parameters obtained from soil laboratory tests was analyzed in order to indicate the characteristic of the kaolinitic soils as core embankment materials.

The performance of the core indicated by dam instrumentation during construction and operation satisfactorily meet the prediction made using the laboratory test results.

1 INTRODUCTION

Batutegi dam was an earth-rockfill dam, was built on the Way Sekampung River, in Lampung province of Indonesia. The maximum height of the dam was 125meter, while the crest length was 700meter. The foundation of the dam was primarily quartzite with intrusion of volcanic conglomerate on the riverbed area. The embankment zone are central clay cored protected by filter, transition and rockfill and riprap at upstream side, while at downstream protected by double layer of filter, transition rockfill and riprap. The rockfill material was andesitic basalt rock obtained from Tangkit Kemuning quarry; a basalt peak of more than 200m in height stands up from a flat ground at right side of the dam. The impervious materials for core was obtained from tertiary sandstone and laharic breccia regions borrow area at downstream of the dam, and most of the materials are sandy clay with medium to high plasticity. The filter materials are crushed and screened basaltic rock obtained from quarry The gradation of the filter was controlled and shall fall in the filter envelopes in order to perform as critical filters. The embankment volume of the core was 1,500,200m^3, a filter both upstream and downstream was 624,400m^3, while rockfill, transition zones and riprap was 7,462,100m^3. All the embankment materials were sufficiently available around the dam site with maximum distance of 5km. The dam has an upstream slope of 2.25H: 1V, and downstream slope of 1.75H: 1V Blanket grouting were constructed in the foundation of the clay core at weak and fractured rock to a depth of 10m, while the three rows of curtain grouting were constructed from grouting gallery to a depth of 100m. The typical cross section of the dam was shown on Figure 1.

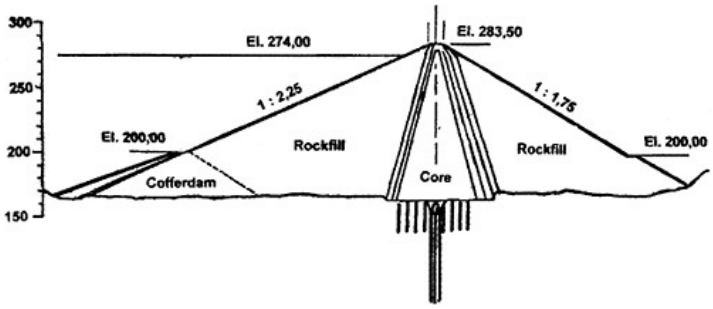

Figure 1. Typical cross section of Batutegi dam.

2 THE TEST PITS AND SOIL LABORATORY TEST PROGRAM

The identification of soils was done to select the suitable core embankment materials from borrow area. The Technical Specifications for core requires that when the core compacted by compaction effort of 600kN.m/m^3, as indicated in the ASTM Standards D 698–91, the optimum water content shall fall within the range of 18% to 28%, the maximum dry density shall fall within the range of 14kN/m^3 up to 17.5kN/m^3, and construction water content shall fall within the envelope of w_{opt} −2% <w<w_{opt}+3%. Provided that the field permeability usually less than the permeability obtained in the laboratory due to the nature of anisotropy of compacted soil, the permeability of compacted core I the laboratory shall not greater than 1×10^{-6}cm/sec.

The source of core materials was from borrow area at the downstream of the dam. The area of the proposed borrow area was 200 hectares. The number of test pit carried out in borrow area was 136 in a rectangular pattern of 100 meter. The depth of test pits varied from 1.00m to 4.00m. Most of the test pits have around 2.00m depth, and only 5 test pits have depth more than 4m. The test pits were carried out in the end of the rainy season. The natural water content, specific gravity, Atterberg limits, soil classification, gradation and compaction tests were carried out for all the samples obtained from test pits, while the consolidation, direct shear, triaxial, as well as permeability tests were carried out on selected and compacted samples in order to represent all the soil suitable for core materials from borrow area.

3 IDENTIFICATION OF CLAY MINERALS

The identification of clay minerals was carried out by chemical analysis, and X-ray diffraction. The scanning electron microscope was carried out on the natural samples taken from borrow area. The chemical composition of proposed core materials for Batutegi dam is presented in Table 1.

Table 1 indicated that SiO_2 and Al_2O_3 dominated the chemical composition of the proposed core material. It can be predicted that the clay mineral will be kandite group, such as kaolin, gibbsite and halloysite. Mineralogical analyses from X-ray diffraction confirmed that the coarser fractions are dominated by quartz, whereas; the finer fraction are dominated by kaolin. A trace of halloysite in a small portion was also acknowledged. Halloysite has a similar structure to kaolin, however it has water molecules occurring between the sheets. Figure 2 shows the examples of the X-ray diffraction traces of kaolin and quartz.

The soil sample for scanning electron micrograph (SEM) was done to follow Wong and Tovey (1975), while the technique to enhance the detail on scanning follow Tovey and Krinsley (1975). Figure 3 shows the image of kaolin mineral for proposed core materials of Batutegi dam.

Table 1. The chemical composition of proposed core materials for Batutegi dam.

Chemical composition	%
SiO_2	68.35
Al_2O_3	17.21
Fe_2O_3	3.98
CaO	0.14
MgO	0.12
Na_2O	0.47
K_2O	0.05
MnO	0.02
TiO_2	0.51
P_2O_5	0.69
Loss due to ignition	8.46

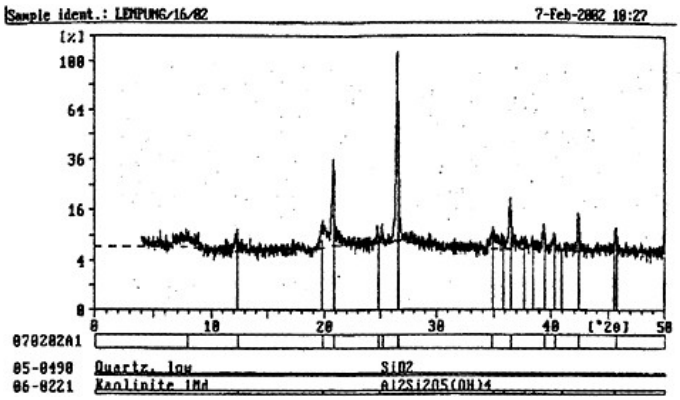

Figure 2. Image of clay mineral identification by X-ray diffraction.

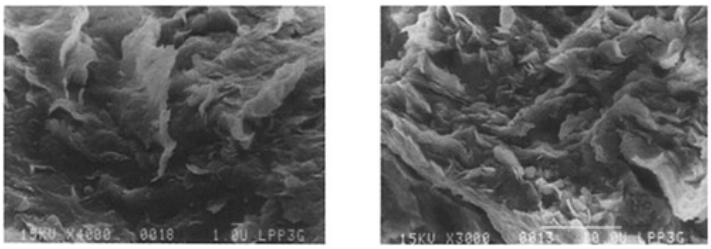

Figure 3. Image of kaolin mineral at nature condition from borrow area by SEM.

Kaolin, because it does not absorb water, does not expand when it comes in contact with water. Thus kaolinitic clay is one of the preferred types of clay for the core of the embankment dams. Mitchell (1993) stated that the engineering properties of soil depend on the composite effects of several interaction factors; there are environmental factors and compositional factors. The later

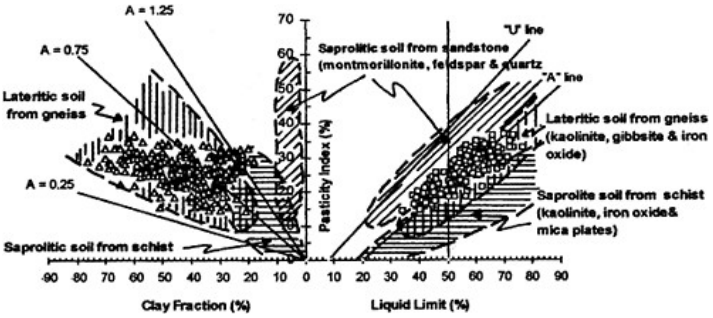

Figure 4. The position of the activity and plasticity of Batutegi core material on Vargas chart.

consists of type of minerals, amount of each minerals, shape and size distribution of particles and pore water composition. Skempton (1953) described that activity (A) of soil was the ratio of plasticity index/clay fraction, and Atterberg limits are related to the combined effects of particle size and mineral composition. Mineralogical analysis is not liable to be made by means of simple test in the soil mechanic laboratory, but the presence of the type and amount of clay minerals requires during establishing the engineering properties of soils. Vargas (1990) proposed combined charts of Casagrande's plasticity and Skempton's activity chart for identification of fine-grained tropical soils that included the mineral identifications. Figure 4 shows the activity and plasticity of proposed Batutegi core materials that plotted on the proposed Vargas chart. By neglected some points in the activity chart, the kaolinitic clay as core of Batutegi dam have an activity between 0.25 to 1.25, and its confirm that the clay can be classified into inactive to normal activity. Figure 4 also shows that the Plasticity Index and Liquid Limit of the proposed core materials were ranged between 14% to 37% and 35% to 76%.

4 TEST RESULTS AND ANALYSES

4.1 *Atterberg limits against optimum water content*

Figure 5, shows a graph in which liquid and plastic limits of the suitable core materials for Batutegi dam plotted against their optimum moisture content, obtained from laboratory compaction tests. It is confirmed that all the optimum moisture content of the core materials for Batutegi dam was 3% to 7% lower than their plastic limit. As the soils for Batutegi dam are compacted at 2% above and below the OMC, the compacted kaolinitic clay was in the semi-solid and friable state.

4.2 *Compaction test*

The compaction test results presented on Figure 6 shows the optimum moisture content against their maximum dry densities. The maximum dry densities and optimum moisture contents for proposed core materials for Batutegi dam ranged from 1.40t/m^3 to 1.75t/m^3, and 18% to 28% respectively. The materials that have maximum dry densities greater than 1.75t/m3, and optimum moisture content less than 18% will not be used as core materials provided that they are non-plastic materials. A small amount of materials that have maximum dry densities less than 1.40t/m^3, and their optimum moisture content up to 30% will be used as contact clay, the first layer of core that contact the foundations. The maximum dry densities is related to their optimum moisture content

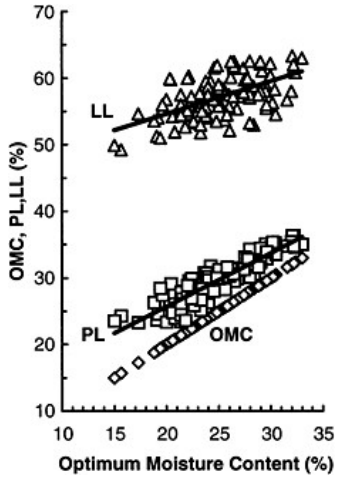

Figure 5. Comparison between Atterberg limits and optimum moisture content.

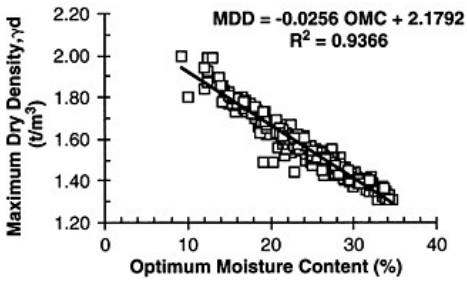

Figure 6. The relation of MDD and OMC for kaolinitic clay as core of Batutegi dam.

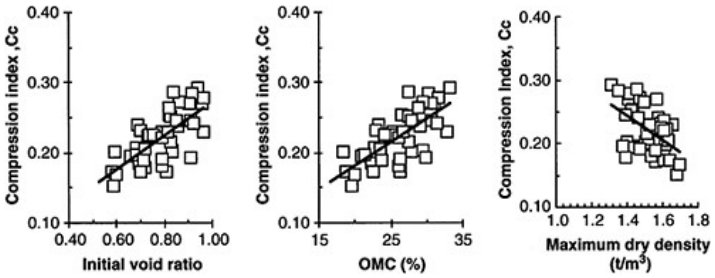

Figure 7. Correlation of C_c to compaction parameters of kaolinitic clay as core of Batutegi dam.

through the following;

$$MDD = -0.0256\ OMC + 2.1792 \quad (1)$$

where MDD is the maximum dry density and OMC is the optimum moisture content.

4.3 *Compressibility and consolidation characteristics*

The linear relationship between void ratio and log of effective consolidation pressure that defines the compression index (C_c) is simply a useful engineering approximation that applies over a range of stresses and void ratios of practical interest. Mitchell (1993) stated that value of C_c less than 0.2 are considered to represent soils of slight to low compressibility, values of 0.2 to 0.4 are for soils of moderate to intermediate compressibility, and greater than 0.4 indicates high compressibility. Correlations between compression index and compaction parameters for core materials have been reported by a number of investigators such as de Mello (1980). Figure 7 shows the correlations of

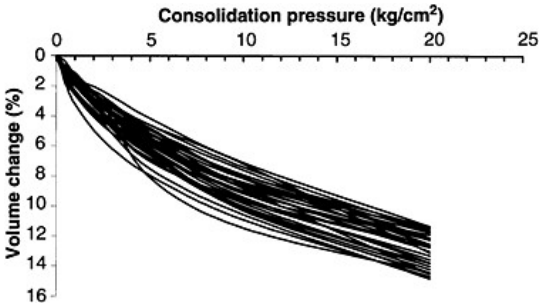

Figure 8. Consolidation characteristics of kaolinitic clay as core of Batutegi dam.

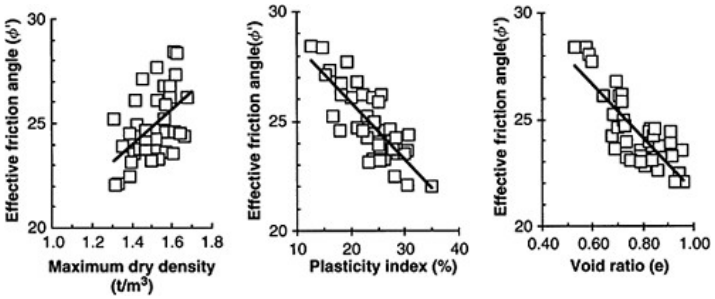

Figure 9. Correlation of effective friction angle (ϕ') to their maximum dry densities, plasticity index and void ratio of kaolinitic clay as core of Batutegi dam.

compression index against initial void ratio, optimum moisture content and maximum dry densities for kaolinitic clay as core of Batutegi dam.

As the core materials were considered as fine-grained soil, the long term settlement is primarily controlled by consolidation, a physical process in which the interstitial water that is under excess pressure slowly diffuses through the compressible matrix of soil particles. The properties that characterize the amplitude and rate of deformation for fine-grained soils are determined in the consolidation test. The consolidation characteristic of the kaolinitic clay compacted on their optimum moisture contents obtained from consolidation tests were shown on Figure 8.

4.4 *Undrained shear strength*

Two kind of triaxial test were carried in the laboratory, there were UU test and CU test with isotropic consolidation. The triaxial UU test indicated that the values of c (cohesion) and  (internal angle of friction) range from 0.50 to 1.70kg/cm^2, and from 18 to 26° respectively, while triaxial CU test indicated that the values of c′ (effective cohesion intercept) and ϕ' (effective friction angle) range from 0.40 to 2.10kg/cm^2, and from 21 to 28° respectively. As shown in Figure 9, the effective friction angle decrease from 29° to 22° when the plasticity index varies from 14% to 35%, void ratio varies from 0.52 to 0.96, and maximum dry densities varies from 1.70 to 1.30 t/m^3.

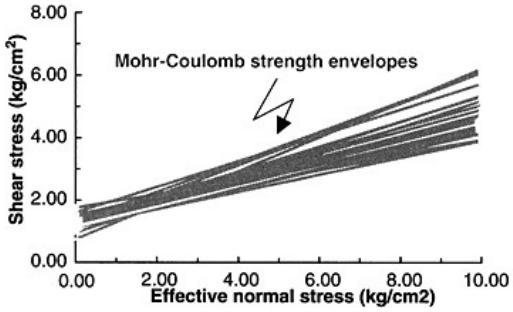

Figure 10. Mohr-Coulomb strength envelope of kaolinitic clay as core of Batutegi dam from CU tests.

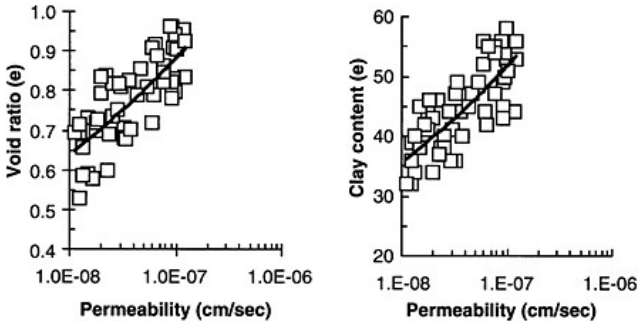

Figure 11. Correlation of permeability to their void ratio and clay contents of kaolinitic clay as core of Batutegi dam.

By definition, the shear strength *(τ)* is the shear stress at failure during undrained loadings. During consolidated undrained triaxial compression tests, shear strength may be expressed by Mohr-Coulomb criterion as follows:

$$\tau = c' + (\sigma - u)\tan\phi' \tag{2}$$

where: τ is the shear strength, c′ is the apparent cohesion, σ is the normal stress, u is the pore water pressure, and Φ' is the effective friction angle of soil.

The shear strength of soil may be presented in the form of Mohr-Coulomb strength envelope. Figure 10, shows the shear strength envelope of kaolinitic clay compacted on their optimum moisture contents obtained from CU triaxial tests.

4.5 *Permeability of soil*

Soils are permeable to water because the voids between soil particles are interconnected. The degree of permeability is characterized by the permeability coefficient, also referred to as hydraulic conductivity. Mitchell (1993) stated that for clay minerals compared at the same water content, the permeability are in the order of smectite (montmorillonite) <attapulgite<illite<kaolinite. Mineralogical composition, particle size, void ratio are some factors that influences the permeability of soils. As shown in Figure 11, the permeability increase from 1.110×10^{-8}cm/sec to 1.224×10^{-7}cm/sec, when the void ratio varies from 0.528 to 0.961, and void ratio varies from 32% to 58%.

5 DISCUSSION AND CONCLUDING REMARKS

The engineering properties of kaolinitic clay that intended to be used as core materials for Batutegi dam has been presented. The test results indicated that the proposed core materials were not homogeny, and shown that the proposed core materials have ranges in their optimum moisture contents, maximum dry densities, compression index, clay contents, effective friction angle as well as permeability. The test results also indicated that the kaolinitic clay can be classified into inactive to normal activities, and have a moderate compressibility as indicated in their compression index and settlement characteristics, and very low permeability when compacted by compaction effort of 600kN.m/m^3, as indicated in the ASTM Standards D 698–91. These test results indicated that the kaolinitic clay suitable to be used as core materials for the embankment dam. Based on the required volume of core for Batutegi dam, materials availability at borrow area and their engineering properties, the kaolinitic clay that used for core of Batutegi dam shall fall in the following ranges;

1. The clay contents of the core materials shall fall within 30 to 60% of the weight.
2. The liquid limit and plasticity index of the core materials shall fall within 30 to 60% and 15 to 45% respectively.
3. When compacted by compaction effort of 600kN.m/m^3 or equivalent during placement, the optimum moisture contents and maximum dry densities shall fall within 18 to 28% and 1.40 to 1.75 t/m^3 respectively.

Batutegi dam was constructed from January 1996 and the embankment was completed on October 2000. The average placement water content were 1.5% above their optimum moisture contents. Impoundment was started on August 2001. The maximum water level was reached on February 2003. The performance of the dam during construction and operation observed from dam instrumentation shows that the settlement of the dam was 10% greater than indicated in the consolidation characteristic shown on figure 8 due to the higher placement water contents. The measurement of seepage indicated that the average field permeability of the core was 5×10^{-6}cm/sec, and it is confirmed that the field permeability were a bit higher than obtained by laboratory tests due to the nature of anisotropy of compacted soil.

The Safety Dam Committee declared that the performance of the dam during construction first impounding, and operation indicated that the dam was in normal condition. Reference to the Safety Dam Committee statement, it is concluded that the kaolinitic clay was satisfactorily to be used as core materials for embankment dam.

REFERENCES

De Mello, V.F.B. 1980. Comparative behaviours of similar compacted earthrock dams in basalt geology in Brazil. *Proceedings Geotechnical Problems andPractice of dam Engineering.* pp 61–79.

Mitchell, J.K. 1993. *Fundamentals of Soil Behavior,* 2nd Edition. John Wiley & Sons, New York, pp 304.

Skempton, A.W. 1953. The colloidal activity of clays, *Proceedings 3rd International Conference on Soil Mechanics and foundation Engineering.* Vol. 1, pp 57–61.

Tovey, N.K, and Krinsley, D.H. 1975. A Technique to Enhance Detail on Scanning Electron Micrographs of Geological Materials. *Geotechnique.* Vol. 47, No. 3, pp 146–152.

Vargas, M. 1990. Characterization, identification and classification of tropical soils. *Proceedings 2nd International Conference on Geomechanics in Tropical Soils.* Vol. 1, pp 71–75.

Wong, K.Y, and Tovey, N.K. 1975. A New Specimen Preparation Technique for Scanning Electron Microscope. *Geotechnique.* Vol. 47, No. 3, pp 142–145.

New Developments in Dam Engineering—Wieland, Ren & Tan (eds),
© 2004 Taylor & Francis Group, London, ISBN 04 1536 240 7

Numerical simulation of static and dynamic mechanical behavior of mass concrete

DU Chengbin & Shang Yan
College of Civil and Eng., Hohai University, China

ABSTRACT: Mass concrete is taken as three-phase composites consisting of mortar matrix, aggregate and bond between matrix and aggregate in this paper. The cracking process of the three-grade concrete supported beam specimen under action of static and dynamic load is studied with nonlinear finite element method from the point of view of micro-scale. The aggregates, following a predefined size distribution, are placed randomly in the specimen. The shape of the aggregates is approximated by circles and their minimum diameter is 12.5mm. Nonlinear constitutive relations are proposed to model cracking, softening, yielding and crushing for the composites. The full curves of stress and strain at the key location of the beam are given, and the results are also compared with that of homogeneous materials. The results from numerical simulation show that mechanical behaviors are directly related to the microstructure of concrete and the interface is the weakest location where the cracking usually occurs first. The failure process of concrete reveals that the phenomenon of tensile strain softening and localization can be observed obviously. The ultimate loads of calculation are very close to those of the experiments.

1 INTRODUCTION

Static and dynamic mechanical properties of mass concrete are the basis of evaluating the safety of large dams. Due to the complexity of the problem, few achievements have been made so far. Because of the limitations of condition, few tests have been carried out focusing on wet-screened small specimens, in which the aggregates whose diameter greater than 40mm are removed. Dam concrete can be classified into three-grade concrete and four-grade concrete. The aggregate sizes of three-grade concrete usually include large aggregates, middle aggregates and small aggregates. The content of aggregate in dam concrete is generally from 60% to 70%. Obviously, because of wet screen, the proportions of composition of concrete have changed, especially that of the content of cement mortar and the aggregates, therefore mechanical properties from the specimens are different from those of actual cases. All kinds of mechanical indexes determined by the specimens can't be really represent those of the dam, thus will bring great inaccurate to the design and construction of the dam [1].

In this study, mass concrete is taken as three—phase heterogeneous composites consisting of mortar matrix, aggregate and bond between matrix and aggregate. The mechanical behavior of concrete is simulated numerically through the finite element method. The aggregates, following a predefined size distribution, are placed randomly in the specimen through Monte Carlo simulation. The number of each kind of aggregates is determined by actual aggregate gradation. A numerical model is developed to describe the constitutive relation of microelement and analysis of failure process, the mechanical properties and fracture process of three-grade concrete simply supported beam under action of static and dynamic load are conducted. Two concentrate forces are applied at the one-third of length of beam symmetrically. The bending moment is identical to the point at which the force applied to the other. Two kinds of dynamic load, such as triangular wave load and sine load, are considered in the study. The full curves of stress and strain at the key location of the beam are given, and the results are also compared with that of homogeneous materials. The ultimate loads of calculation are very close to those of the experiments.

2 MATERIAL MODEL

Components of mass concrete are basically quasi-brittle material, whose failure patterns are mainly brittle failure. Nonlinear constitutive relations are constructed to represent the mechanical performance of each phase of mass concrete, and an after peak behavior, the so-called softening is considered in the model [2]. A schematic constitutive relation is shown in Figure 1 where the input parameters for each phase are the critical cracking stress σ_{cr}, the yield stress σ_y, the limit tensile strain ε_u, the crushing strain ε_{crush}, the elastic modulus E, and the tension-softening modulus E_{soft}. Main features of the model are as follows: (a) Low tension cracking. (b) Tension softening. (c) Crack closure. (d) Crushing. The incremental strain after cracking can be described as follows:

$$\Delta\varepsilon=\Delta\varepsilon^{co}+\Delta\varepsilon^{cr} \tag{1}$$

where $\Delta\varepsilon^{co}$ is strain increment that is depended on elastic component and plastic component for continue medium, and $\Delta\varepsilon^{cr}$ is the cracking strain, which is the opening width of the crack at the integration point.

Materials of the element are assumed isotropic and no crack exists at first. Stress increment and strain increment at each integration point can be calculated according to the elastic plastic constitutive relation proposed above. The new principal stress at each point is obtained and transform matrix R can be formed. Stress and strain can be transformed from physical to principal coordinate system. Stress S and strain e of principal coordinate system are as follows:

$$S=R\sigma \tag{2}$$

$$e=R\varepsilon^{co} \tag{3}$$

where σ and ε^{co} are stress and strain of physical coordinate system respectively. Once principal stress at the direction θ_i (i=1, 2) exceeds the threshold value S^{cr}, the crack, whose opening width is ε^{cr} at the direction, is formed, and the stress at the direction will be released. The shear retention of a degraded zone is taken into account by a factor) β [3].

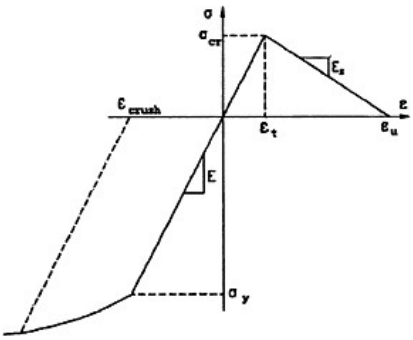

Figure 1. Constitutive model for materials.

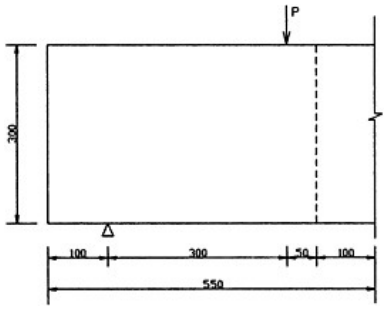

Figure 2. Specimen geometry and loading/mm.

In order to model the softening after cracking, the stress increment at the direction can be given by the softening modulus E_{soft}:

$$\Delta S_i = E_{soft} \Delta e_i^{cr} \tag{4}$$

3 SIMULATION OF THE THREE-GRADE CONCRETE BEAM

The proportion of the large aggregate, middle aggregate and small aggregate of the three-grade concrete of Xiaowan arch dam, which is being built in china, is 4:3:3. Representative sizes above three aggregates are 60mm, 30mm and 12.5mm respectively. The density of the aggregate is taken as2.8×10^3kg/m^3.The dimensions of the specimen bending are 300mm×300mm×1100mm. Plane problem is considered in this paper, and its size is 300mm×1100mm. The Schematic of the specimen is presented in Figure 2. The location the concentrate force applied is 400mm away from the near end. Half of specimen is given because of the symmetry.

In order to minimize the calculation and the maximum internal forces appear in the middle of the beam, 200mm in the middle part is chosen as emphasis for studying. The multiphase inhomogeneous material of the part is considered. The shape of the aggregates is approximated by circles. The large aggregates, middle aggregates and small aggregates are 3, 10 and 68 respectively. The aggregates are placed randomly in the specimen through Monte Carlo simulation, and the width of the interface of the aggregates is taken as 1mm.

The FEM mesh of the typical beam is generated by means of advanced method. The plane four-node element is chosen in the analysis. The element size of the fine mesh of the middle part is about 3mm, and the length of element of the interface is 1mm. The material of both sides from the edge of fine mesh to the near end is assumed isotropic, and the maximum element size is about 25mm. The fine mesh of the middle part includes 10510 elements and 10679 nodes. The FEM mesh of the beam is shown in Figure 3, which involves 12792 elements and 12937 nodes. The material parameters adopted in the analysis are shown in Table 1. The parameters are obtained from relevant experiments, and except the crush strain of concrete at the both sides is assumed 6 times of the critical tensile strain. The shear retention factor β=0.5.

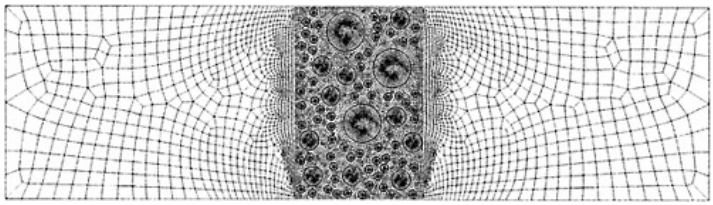

Figure 3. FEM mesh of the beam.

Table 1. The material parameters adopted in the analysis.

	Young's modulus/GPa	Soften modulus/GPa	Tensile strength/MPa	Critical tensile strain	Ultimate tensile strain	Crush strain
Aggregate	55.5	11.1	6.0	0.0001	0.0006	0.0015
Mortar	26.0	5.2	2.5	0.0001	0.0006	0.0015
Interface	25.0	5.0	2.0	0.0001	0.0006	0.0015
Concrete	30.0	6.0	2.8	0.0001	0.0006	0.0015

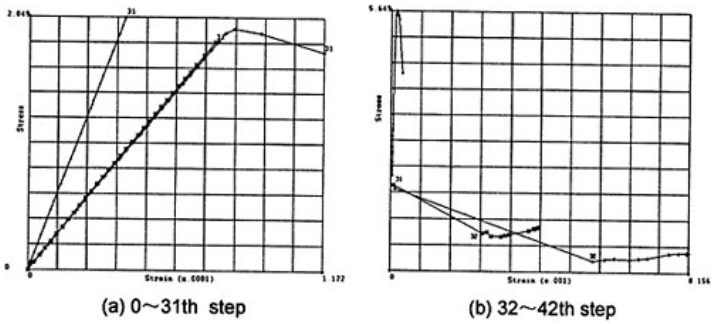

Figure 4. σ–ε curves considering material inhomogeneous/MPa. (+—+—+ Interface)

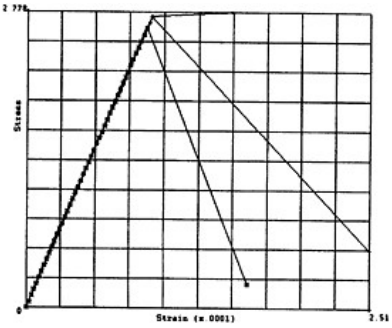

Fieure 5. σ–ε curves without considering material inhomogeneous/MPa. (+—+—+ Interface)

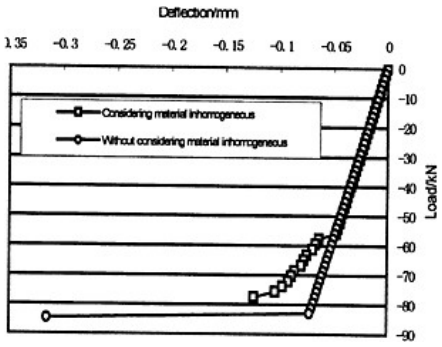

Figure 6. *P*–Δ curves of the two cases.

4 4 THE FAILURE PROCESS OF THE BEAM UNDER ACTION OF STATIC LOAD

The load is divided into 42 steps in the calculation, in the 29th step, the value of loading is 52.2kN. At this time, stresses in the elements of the interfaces of two aggregates near the bottom of the beam reach the tensile strength. Cracks occur first in these two elements and the turning point of the curves of the horizontal stress-strain of the elements can be observed in the Figure 4(a), while stresses of aggregate elements and mortar elements nearby are less than critical tensile stress. With the increase of the load, more cracks occur in the elements of the interfaces near the bottom of the beam at the 32nd step. These cracks have a great influence on the stresses of mortar elements, the tensile stresses of mortar elements near the cracks decrease obviously, while the aggregate stresses still remain increasing in this period. The decreases of tensile stresses of aggregates can be observed in the 39th step, and the time of the occurrence is obviously behind the mortar and interfaces. Strain soften of aggregates is obviously less than that of mortar and interface, which is shown in Figure 4(b). The reason why the first crack occurs in the interface rather than the mortar is that the strength of the interface is less than that of the mortar. For the comparisons, stress-strain curves without considering material inhomogeneous are given in Figure 5. The results show that three curves do coincide in the elastic region, and the turns appear at the last step but one.

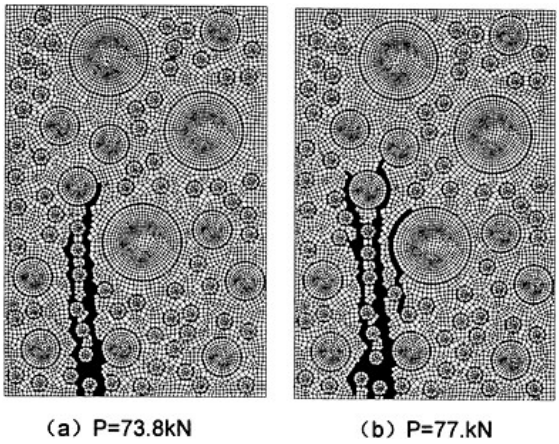

Figure 7. Propagation of cracks and cracking patterns at failure.

Different positions of turns are due to slight different points adopted in the analysis. The curves do have a great difference compared to the case of material inhomogeneous.

$P-\Delta$ Curves of the two cases are given in the Figure 6. The results show that turning point for the case of material inhomogeneous appears in the 29th step, while turning point for material homogeneous in the 41st step. It is apparent that the ultimate load of the former is less than that of the latter. Calculations from the former indicate that failure process of concrete start at one cracking element after another separately cracking element in the interface at first, it was only when the number of cracking elements of the interface is adequate, and the cracking would expand to the mortar. Propagation of crack and cracking patterns at failure are shown in Figure 7(a), (b). The two main cracks are formed after a certain load applied, propagation of crack is along the interface and mortar, and the bearing capacity of the beam is lost at last. Strain-softening behavior in the post-peak and strain localization phenomenon are apparent observed in the calculation. The ultimate load achieved in the numerical analysis is 77.4kN, which is very close to the result of the experiment, and average value of the test is about 75kN.

5 THE FAILURE PROCESS OF THE BEAM UNDER ACTION OF DYNAMIC LOAD

5.1 *Triangle wave load*

As the device of lab only generates the triangle wave load, in order to compare with the result of the lab, the numerical simulation of the specimen under action of the triangle wave load is carried out first. The shape of dynamic load used in the lab is plotted in Figure 8. The amplitude of dynamic load gradually increases with the time. In order to aim at Xiaowan arch dam, the period of load is taken as 1s, which is close to the first period of the dam. Two hoops are used to contact the loading force and the beam.

Newmark-β method is adopted in the calculation, the time step Δt=0.05s. Damping is determined by Rayleigh proportion supposition, and damping ratio ζ=0.05. Dynamic parameters, such as dynamic modulus, dynamic strength, are 1.3 times of the static value. Compared to measured displacement, strain achieved in the experiment is relatively accurate. Figure 9 shows the comparison of result of numerical simulation with the experiment, testing result was obtained after 0.25s. It is shown that the two curves are close well. Many vertical cracks can be observed near the top and bottom of the beam at failure. One or two of the cracks expands enough to run

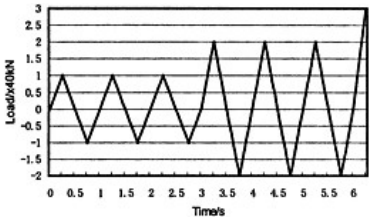

Figure 8. Dynamic load used in the experiment.

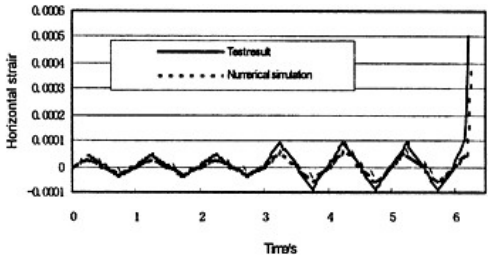

Figure 9. Horizontal strain curve at the mid-span of the bottom of the beam.

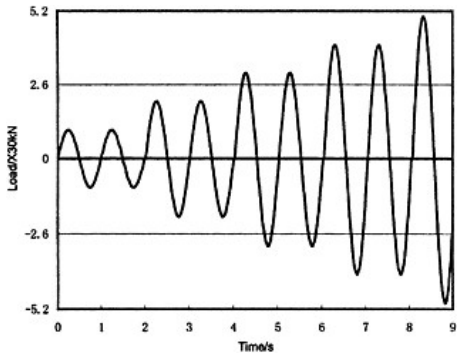

Figure 10. A time history of dynamic loading.

through the cross section of the beam. The ultimate load achieved in the numerical analysis is 120kN, value of test is about 115.6kN, and relative error is about 3.83%.

5.2 *Sine load*

To further study failure mechanism of the beam under action of dynamic load, the responses of the specimen under sine load are carried out. Figure 10 shows a time history of dynamic load, the period of vibration from 0 to 6s is about 1s, and that from 6s to 9s is slight greater than 1s. The amplitude of dynamic load was also adjusted to gradually increase with the time.

Two vertical displacement responses at the mid-span of the bottom of the beam are given in Figure 11: one with circles with consideration of material inhomogeneous and the other with rectangles without. The results show that responses are gradually increased with the increasing

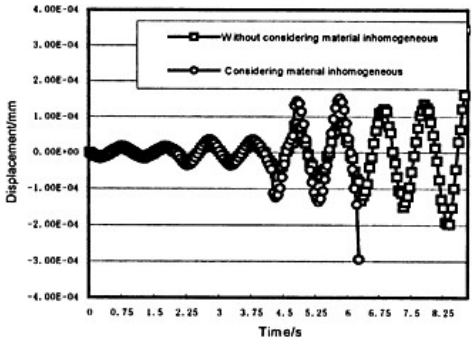

Figure 11. Vertical displacement responses at the mid-span of the bottom of the beam.

amplitude of load. No crack occurs in the concrete in the first 4s at beginning, linear elastic responses are observed and two curves do coincide. When the amplitude increases to 90kN, displacement response of the first case is greater than that of the second case. When t=4.35s, the displacement considering material inhomogeneous is −0.117mm, while the other is −0.0666mm. Cracking occurs in the interface of the bottom of the beam at this time in the first case. The maximum displacement in the first case is about −0.295mm at failure, while the other is −0.133mm at corresponding time. The ultimate load considering material inhomogeneous is significantly less than that without considering material inhomogeneous. The ultimate dynamic loads considering and without considering material inhomogeneous are 111.3kN and 137.04kN respectively. The time at failure in the first case (6.25s) is significantly prior to that in the second case (8.75s). Combination with the analysis of above triangle wave load, we can draw the conclusion that average value of ultimate dynamic load of the three-grade concrete beam is about 115.7kN, which is 1.49 times than that of static case.

When t=4.35s, tensile strain at the bottom increased sharply, compressive strain at the top increased also, but its value is much less than that of tensile strain. Cracking first appears near the bottom of the beam, once cracking occurs, tensile strain at the top is decreased. The failure of the beam is causes of the cracking that propagates from bottom to top. Five mainly cracks, whose length is about 2/3 height of the cross, are observed at failure [2].

6 CONCLUSIONS

Following conclusions can be drawn as follows: (1) The Numerical Concrete is a suitable tool to investigate the effective properties of concrete as a composite material. It is possible to study the mechanical behaviors of mass concrete by calculation micro-mechanics method. Ultimate static load of three-grade concrete beam of Xiaowan arch dam is about 77kN, while ultimate dynamic load is about 115kN. (2) Multiphase composite like concrete, mechanical performances are strongly associated with the internal microstructures, the assumption that concrete is regarded as a homogeneous material does not coincide with actual case. Usually, the ultimate load considering material inhomogeneous is less than the one without considering material inhomogeneous. (3) The characteristic of the concrete failure is cracking, which usually appears in the interface. It is observed that several main cracks at failure, and exhibits significantly tensile strain-softening behavior and strain localization.

The evaluation of effective properties of a composite material like concrete requires the consideration of many factors, such as shape of aggregate, initial damage, space distribution of aggregate strength, and combination static load with dynamic load. These should be further investigated in the future.

ACKNOWLEDGEMENTS

The authors are grateful to the support for this research by Academic fund from Hohai University, Creative fund from Hohai University. Besides the thanks will go to the Academician Chen Houqun for his guidance, and thanks will also go to Professor Wu Shengxing and Doctor Zhou Jikai for some results of their experiments.

REFERENCES

[1] Liu Wenyan & Xie Nianxiang. Experimental study on mechanical properties of fully graded aggregate concrete in Dongjiang arch dam, Water power, 1986, 5:8–14.
[2] Shangyan. Numerical simulation of static and dynamic mechanical performance of mass concrete, Nanjing: Hohai university, 2004.
[3] Du chengbin, Maliangjun & Renqingwen. Nonlinear seismic response analysis of high arch dams with joints. Journal of Hohai university, 1999, 6:40–43.

New Developments in Dam Engineering—Wieland, Ren & Tan (eds),
© 2004 Taylor & Francis Group, London, ISBN 04 1536 240 7

Structural measures for preventing reservoir water penetrating into dam-foundation interface of high gravity dams

C.Du
Lahmeyer International GmbH, Germany

ABSTRACT: In planning of high concrete gravity dams, a problem frequently encountered is that tension exists on the upstream face of dam heel area and in the immediate vicinity of foundation rock. In this case the dam-foundation interface may be detached due to its low bearing capacity of tensile stresses, and thus the high pressure reservoir water may penetrate into the interface. The interface crack feeds reservoir pressure as full uplift along the open interface and the uplift pressure in the crack would in turn assist propagation of the interface cracking, which will aggravate the working state of the dam, or even may render the dam unsafe. To cope with this difficult situation, various transit structures in the vicinity of dam heel, such as concrete plinths/platforms, concrete dragging plates, base joints and synthetic geomembrane sealing systems etc., may be considered as appropriate solutions used in practice to prevent water ingress. In the present paper, such structural measures are summarised and discussed on basis of the application experiences. An analysis for an ongoing high gravity dam is performed and observation results from an existing dam are presented. The results demonstrate that the transit structures mentioned above are suitable for solving this problem. These transit structures are easy to be constructed and can effectively relieve and solve the problem of water ingress into the dam-foundation interface after cracking to maintain the dam stability.

1 INTRODUCTION

In design of a high concrete gravity dam, it is usually required that no tension shall be allowed on upstream face of the dam in usual operation conditions. However, in many cases tensile stresses on the upstream face of high gravity dams could not be avoided [3]. In practice, tension may occur on the upstream face in the vicinity of dam heel due to seismic, thermal and other operation loads or their combination. It has been realised that thermal loads in a mass concrete block could frequently cause tensile stresses in the vicinity of block edges and compressive stresses in block interior [1].

Dam concrete can withstand tensile stresses to a limited extent. However, the dam-foundation interface can usually maintain on little tensile stresses because of existence of discontinuities in foundation rock and very low bonding effect [8]. As far as excessive tensile stresses occur at the interface, the bond between the dam and its foundation would be destroyed and cracking of the interface initiated. Another potential risk of the interface cracking at dam heel is that vertical longitudinal cracks (parallel to the dam axis) occur or the longitudinal construction joints are not properly grouted, so that the joints are open. The dam structure is thus divided into discrete masses and the excessive tensile stresses may appear in the mentioned area. As a consequence, the reservoir water with high hydrostatic pressure may penetrate into the cracking interface and then act as full uplift pressure which could assist for cracking propagation. The grout curtain may thus broken which could lead to dam instability. Certainly, the internal hydrostatic pressure can be assumed to be zero in the cracks caused by the seismic loads during earthquakes because of the rapidly cycling changes in stress. However, after earthquake the uplift and splitting/jacking effect

of the high water pressure in the interface cracks will aggravate the working conditions of the dam and create a potential failure mechanism in the dam. Planning, designing and constructing such a concrete gravity dam requires special care and suitable measures are to be taken.

In principle, there are two options to cope with the interface opening in the transit area at the dam heel. The first way is that cracking at the interface is not allowed in design. This implies a design criterion of no tension for any possible loading cases. Structural measures usually taken to avoid the occurrence of cracking include modifying the typical cross sectional shape like enlarging the dam cross profile, using pre-stressing tendons or hydrodynamic isolation [7]. The other way is that the interface cracking (i.e. the tensile stresses) is permitted in a limited extent for extreme loading combinations, while the high pressure reservoir water does not allowed to enter into the crack. From the point of view of project costs, the later way usually results in an economic design. For doing this, various structural measures for the transit area may be taken as follows:

- concrete plinths/platforms;
- concrete dragging plates;
- upstream base joints; and
- synthetic geomembrane sealing system.

These measures are taken with varying degrees to update existing dams and designing new dams. In the following, we will individually discuss these structures. Analysis is carried out to demonstrate the application and advantages of these structural measures. Although the discussions are initially for concrete gravity dams, the results can be used for arch dams as well as concrete-faced rockfill dams (CFRD) etc. both for design of new dams and for rehabilitation of existing dams.

2 CONCRETE PLINTHS/PLATFORMS

As shown in Figure 1, a plinth or platform is a strip of concrete constructed in the immediate front of dam heel with anchoring (e.g. rock bolts) into foundation rock. It looks like an apron of concrete at the dam heel. Between the dam and plinth concrete, a gap of 1.0~2.0cm shall remain to allow free movement of the dam without contact to the plinth. A sealing element (water stops) shall be installed in the gap to create a watertight connection between the dam and the plinth, for which two

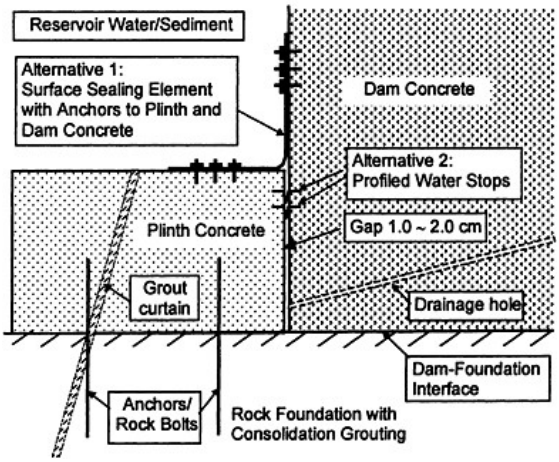

Figure 1. Concrete plinth/platform structure with sealing elements and anchors.

alternatives are suggested in Figure 1. In alternative 1 a sealing element from the plinth surface to the dam upstream face can be extended to a higher level if tensile stress exists in the lower portion of the dam facing concrete, while in alternative 2 the sealing element is embedded in the dam and plinth concrete. The sealing elements shall be able to withstand the full reservoir water and silt pressure. Meanwhile, consolidation grouting may be applied to the rock foundation beneath the plinth.

If the plinth is designed sufficiently wide (horizontal to upstream), the curtain grouting can be conducted from the plinth surface. In this case, the uplift pressure will be significantly reduced in the dam foundation and grouting work is facilitated as well. In order to drain the gap and to reduce the water pressure in the gap joint, drainage pipes/holes should be installed after grouting. Between rock and lower part of the plinth, backfill concrete can be first placed to compensate over excavation and to create an even working place. The alignment of the plinth in elevation more or less follows the course of foundation area of the dam smoothing out any irregularities at an adequate distance. Apparently, the plinth structure services as a surface sealing element to prevent the reservoir water penetrating into the dam-foundation interface in the case that the interface is cracking. In addition, if the grout curtain is arranged from the plinth surface, the plinth may serve as a platform for the grouting work, and the uplift pressure in the dam foundation is reduced.

The concrete plinth structures have been applied to many dams. In Mujib RCC gravity dam (64m high) of Jordan, the plinth is designed in a form of the reinforced concrete platform, while it provides meanwhile a platform for curtain grouting. The platform of 4.0m wide and 2.0m high is arranged in immediate front of the dam heel. Rock bolts of 4.0m long with spacing of 2.0m c/c bothway and staggered arrangement are installed to anchor the concrete platform onto foundation rock. As surface sealing element, a geomembrane on the RCC dam surface is extended and ended to the platform surface, so as to form a watertight seal between the dam and the platform. Due to the comprehensive bonding of the geomembrane to entire substrate, no mechanical fittings are necessary. The curtain grouting is conducted from the surface of the concrete platform, as shown in Figure 2.

In rehabilitation of existing dams, especially masonry gravity dams whose dam body and foundation often suffer a serious leakage, an alternative frequently used is to built a reinforced concrete sealing onto the upstream face of the old dams and a plinth in the dam heel area. In this alternative, the grouting and drainage gallery is usually arranged in the plinth for curtain grouting later and for drainage hole drilling. A typical reinforced concrete sealing-plinth system for

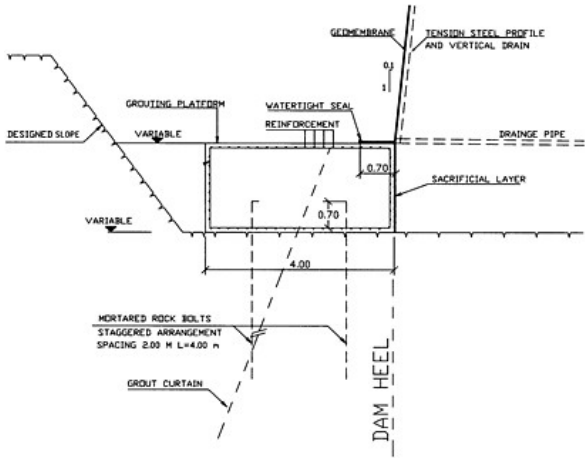

Figure 2. Concrete platform coupled with geomembrane for Mujib RCC dam.

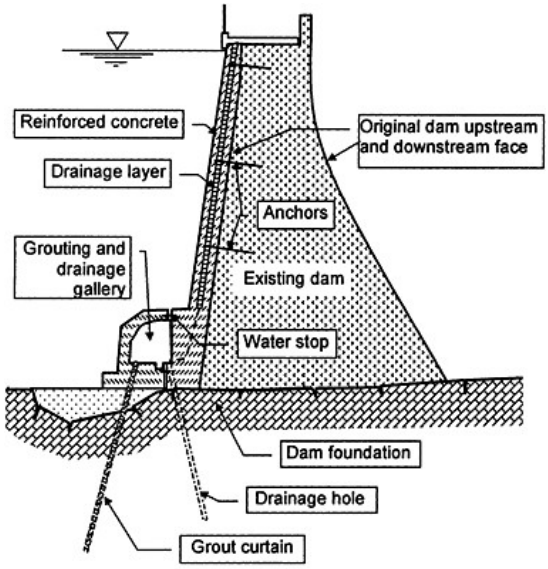

Figure 3. Typical reinforced concrete sealing-plinth system for rehabilitation of (masonry) gravity dams.

rehabilitation of old (masonry) gravity dams is shown in Figure 3. A typical example is the rehabilitation of Neunzehnhain II dam [9] of over 80 years old in Germany.

For earth dam and CFRD, the plinth is a necessary element. As an example, in the Africa's highest Mohale CFRD dam (145m high) of the Lesotho Highlands Water Project, a concrete plinth is arranged in immediate front of and coupled with the concrete face slab of the CFRD. The plinth serves as a working platform for the grouting work as well. The reinforced concrete plinth is 4.0 to 8.0m wide and 45 to 75cm high. Three rows of anchors of 3.5m long and 32mm diameter are arranged to fix the plinth onto its foundation rock. A profiled copper water stop and a rubber water stop are embedded in the plinth and face concrete to create an effective watertight connection between the two elements. Transverse contraction joints in spacing of 8.0m is placed. For details see Godde and Droste [2].

3 CONCRETE DRAGGING PLATES

A concrete dragging plate can be regarded as an enlarged plinth/platform structure. An example is the application of this structure in Rauschenbach concrete gravity dam of Germany. The dam has a maximum height of 47.9m and a crest length of 346m, and was completed in 1968. During dam construction after excavation of its foundation and just before commencement of concrete placement, *in situ* direct shear tests were performed. Unfortunately, the test results indicated that the shear parameters obtained from the direct shear tests were significantly smaller than those assumed in the design. This meant that the safety of the designed dam in the river bed portion of about 80m long would not be ensured if no proper measure was taken. For this reason, the concrete dragging plate was chosen to enhance the dam stability after comparison of various alternatives and in consideration of the local conditions and time schedule of the dam construction.

As shown in Figure 4, the dragging plate has a dimension of W×H×L=13.4×5.0× 87.5m. Five transverse contraction joints with a spacing of 15m divide the whole dragging plate

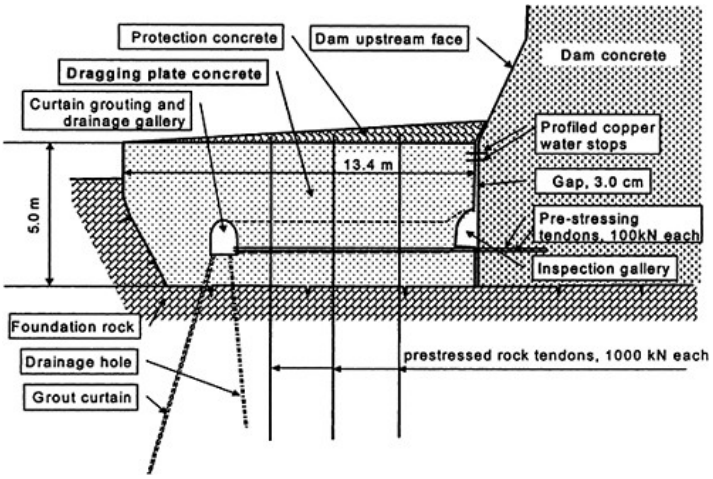

Figure 4. Dragging plate in Rauschenbach concrete gravity dam.

into six blocks. The grouting and drainage gallery is arranged in the dragging plate, in which the curtain grouting and drilling of the drainage holes were carried out. Between the dragging plate and the dam body a gap of 3.0cm was reserved and two profiled copper water stops were installed to seal the gap. An inspection gallery at the dam heel in the dragging plate and two access galleries on both sides of the dragging plate for connecting the grouting gallery and the inspection gallery were arranged. In order to create a dragging action of the plate to the dam body, totally 368 horizontal pre-stressing tendons with pre-stressing force of 100kN each were conducted. To fix the dragging plate onto its foundation and stabilize it, 80 vertical pre-stressed rock tendons with tension force of 1000kN each were performed. Therefore, the dragging plate has the following functions for the dam stability:

- providing horizontal dragging action;
- taking over a part of horizontal water and silt pressure;
- reducing uplift pressure; and
- preventing ingress of reservoir water into dam-foundation interface detached.

Calculation results showed that the dragging plate has a comparatively large effect on withstanding the horizontal water and silt pressure to the dam. Under usual operation conditions, the total water pressure on the main dam per meter length is 10280kN/ml, in which the part of water pressure maintained by the dragging plate amounts to 2140kN/ml, or 21% of the total water pressure. This will significantly improve the dam stability.

The uplift pressure on the dam-foundation interface is regularly observed and a cross section of the observed uplift pressure distribution is shown in Figure 5. It can be clearly seen that the uplift pressure under the dam body is substantially reduced. The effective coefficient is determined by the formula:

$$\lambda = \frac{H_{up} - H_{dw}}{H_{uw} - H_{dw}} \tag{1}$$

in which, H_{up} is the uplift pressure level; H_{uw} the upstream water level; and H_{dw} the downstream water level. It works out that $\lambda \approx 0.28$, which is lower than that assumed in the design.

Many instruments were installed in the dam, foundation and the dragging plate, and the inspection is regularly conducted. The inspection and observed data show a reasonable behaviour of the dam, the foundation and the dragging plate. In the last 35 years since the dam was put into operation in 1968, no stability problem was concerned. As an example, the observed variation of the width of the gap between the dragging plate and the dam body is shown in Figure 6. An annual seasonal periodical variation is clearly visible. An overall analysis demonstrates that the variation is mainly caused by the seasonal movement of the dam body due to seasonal temperature oscillation, while the dragging plate situates under deep reservoir water where the temperature remains almost constant.

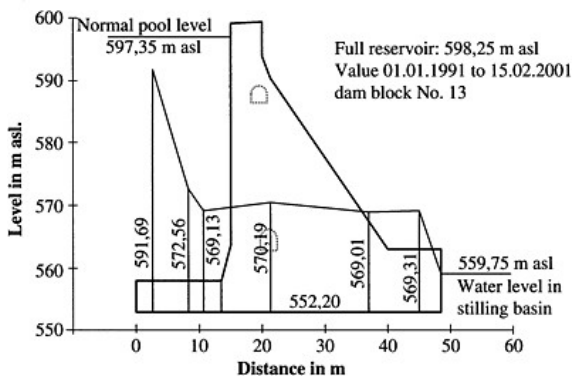

Figure 5. Observed uplift pressure distribution in Rauschenbach dam.

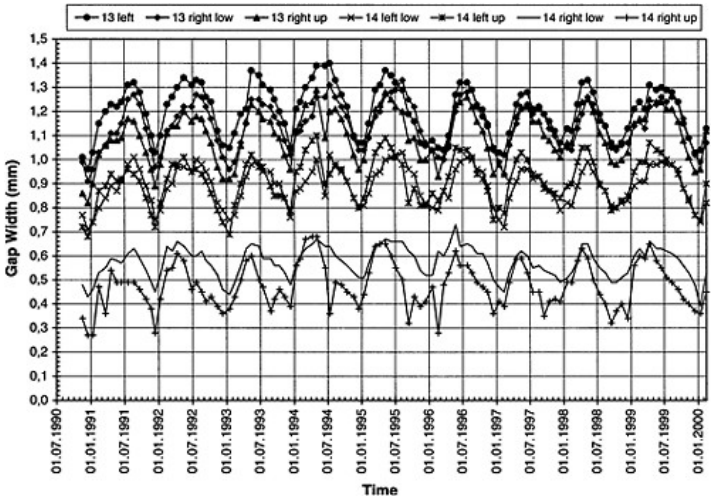

Figure 6. Observed variation of width of the gap between the dragging plate and dam.

4 UPSTREAM BASE JOINTS

An upstream base joint is a partial horizontal contraction joint with sealing elements on the upstream side. The base joint is built like a normal horizontal construction joint and usually cannot transmit shear and tensile stresses normal to the joint. For this purpose a thin layer of bitumen may be provided on the joint surface. If specified, a drainage system can be equipped to allow for drainage. It is apparent that the base joints are artificially created and properly treated horizontal cracks at the predetermined locations. The base joints are arranged near to the dam foundation and can create a sort of "cut-off" for tensile stresses to ensure that no uncontrolled cracking occurs due to excessive tensile stresses in the heel area of the dam-foundation. The joint is basically closed for usual operation conditions and during compression cycles of seismic loading, and may be open during tension cycles. Its length can principally be restricted to the tensile zone in the heel area. The main function of the base joints is to provide free movement of the dam without adversely affecting the dam and its foundation behaviours. The joints only open if required by the deformation process without unduly disturbing the monolithic action of the dam body. Figure 7 shows the application of the base joint in Baglihar high concrete gravity dam.

The base joints are frequently applied in arch dams for releasing excessive tensile stresses occurred in the area of dam-foundation interface. Rescher [7] summarised and studied the upstream base joints for arch dams. However, application of the base joint structure into concrete gravity dams has so far been little seen. Nevertheless, as an engineering solution, the concept of the base joint can be utilised for concrete gravity dams. Different from other structural measures for preventing the ingress of water into the interface discussed in this paper, using the base joint can modify the distribution of tensile stress in the heel area and improve the working condition of the dam. The possible uncontrolled cracking of the interface is therefore avoided by means of introduction of an artificial joint. In the following we will present this structure in example of use in Baglihar gravity dam.

The ongoing Baglihar hydroelectric project is situated on the river Chenab in Jammu and Kashmir state, India. The main barrier is a concrete gravity dam with a maximum height of 144.5m above the lowest foundation level and a crest length of 345m. The dam situated in a moderate seismic zone with a peak ground acceleration of 0.11g for OBE and 0.22g for MCE. 2D and 3D dynamic analysis indicated that the maximum tensile stresses up to 3.0MPa will occur in the upstream face in the case of MCE when the upstream base joint was not arranged. Thus cracking will occur in the heel area, especially the dam-foundation interface may be detached. As a consequence, the grout curtain may be broken or the upstream facing concrete near the grouting gallery

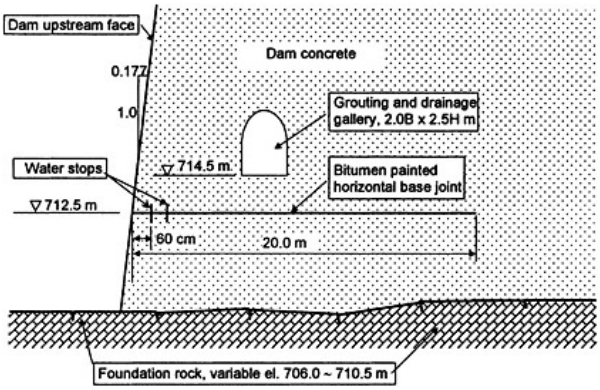

Figure 7. Upstream base joint for Baglihar concrete gravity dam.

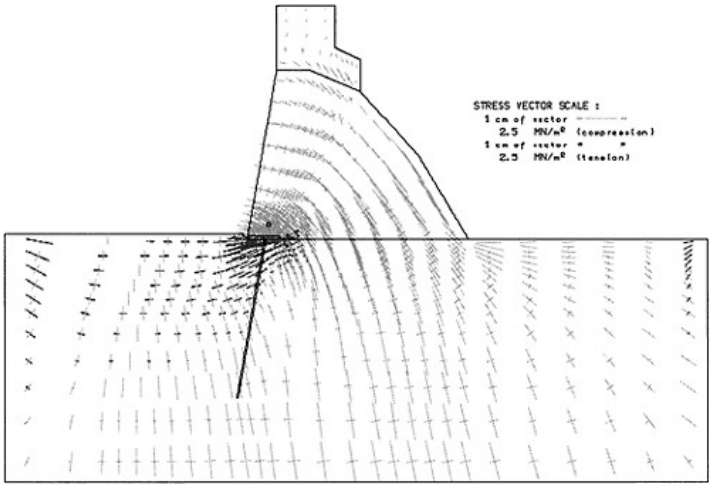

Figure 8. Stress distribution in Baglihar dam after application of the upstream base joint.

may be cracking, which will threaten the dam safety and disturb the operation of the structure. For this reason, a 20m long base joint from the dam upstream face is introduced into the dam heel area (see Figure 7) in consideration of the dam design/construction and local site conditions. The further 2D and 3D FE-analysis indicated that the tensile stresses in the heel and grouting gallery area are significant released, as shown in Figure 8. There is no tension in the facing concrete of the dam heel, and only very little "sub-horizontal" tensile stresses exist in the foundation rock, which is harmless to the dam safety. Meanwhile, the requirement for dam stability against sliding along the base joint can be satisfied as well. In addition, the base joint will eliminate the restraint of foundation causing thermal stresses in the upstream facing of the dam and thus the probability of the upstream vertical transverse cracking of the dam is significantly reduced.

5 SYNTHETIC GEOMEMBRANE SEALING SYSTEMS

According to the ICOLD's definition [4], "the term geomembrane is used here for polymeric membranes which constitute flexible watertight material with a thickness of one-half to a few millimeters". Owing to intensive research and a wide range of trials since the last three decades, great success has been achieved in developing and applying various synthetic geomembranes as dam sealing systems. The most commonly used types as base products in the manufacture of synthetic geomembranes include the thermoplastics, crystalline thermoplastics, elastomers and thermoplastic elastomers [4]. The geomembrane sealing systems mostly used in practice are, for instance, the PP-dam system [7], Carpi-system, UTG-system and so on. Usually the impervious material of geomembranes has high performance in water tightness for dam sealing, tensile, compressive, tear and bonding strength for withstanding loads and against mechanical damage, chemical resistance to chemical attacks, elasticity and ductility for fitting dam and foundation movements, as well as aging, UV radiation and frost resistance. They are suitable for various dam types such as gravity dams, arch dams, concrete-faced rockfill dams and earth dams as well.

The composite sealing elements can be produced either in a factory before use or manufactured *in situ* directly on dam/rock surface. The geomembranes being factory manufactured are usually

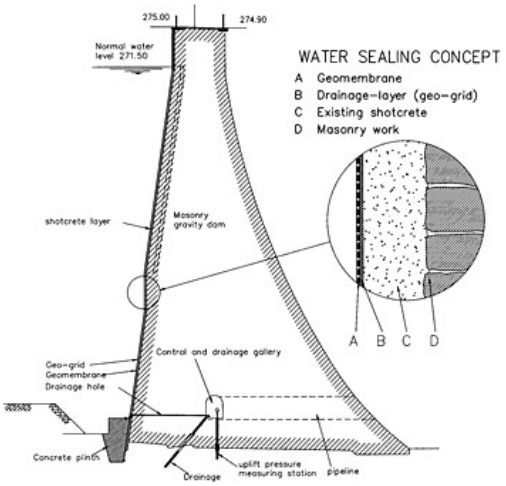

Figure 9. Application of geomembrane in Upper Herbringhauser masonry gravity dam.

formed in rolls for delivery and storage. Depending on the particular material, various chemical and thermal methods are available for seaming. The *in situ* manufactured geomembranes consist of products applied hot or cold in liquid form. Apparently, this method does not need for seaming roll widths or panels together. However, controlling the uniformity of the product and the thickness of the finished membrane by this method is frequently a challenge. Trained workers are usually required. The geomembrane sealing systems can be mechanically anchored or chemically/thermally bonded on the dam upstream face or put in the dam body. In principle, they can be applied for whole dam upstream face as a lining, or a part of the dam area. It is therefore understandable to take it as a sealing system for protection of dam heel from ingress of water into the interface.

The synthetic geomembrane sealing systems are successfully used in newly designed and especially for rehabilitation of existing dams world wide. The application can be found, for example, in Mujib RCC dam (Figure 2), Concepcion RCC dam (70m high) in Hondulas, Lago Nero concrete dam (40m high) in Italy [4], Bovilla CFRD dam (91m high) in Albania, Lago Bianco south and north dam in Switzerland [7] and Braendbach dam [5] etc. Figure 9 shows the application of the geomembrane sealing system for rehabilitation of the Upper Herbringhauser masonry gravity dam in Germany. The dam has a maximum height of 37m and a crest length of 215m. Construction of the original structure was completed in 1900. For its rehabilitation, various alternatives have been studied and found that the application of the upstream sealing geomembrane on the existing shotcrete layer is technically feasible and cost-effective.

6 CONCLUSIONS

It has been recognised that the dam-foundation interface in the heel area may be detached due to excessive tensile stresses in high gravity dams. Ingress of reservoir water with high pressure into the interface will aggravate the working conditions of the dam and may lead to propagation of the cracking. In the worst case it may threaten the dam stability. The transit connection structures discussed above are effective measures to prevent the infiltration of reservoir water into the interface. Successful applications of the structural measures demonstrated their effectiveness. The structures are suitable not only for gravity dams but for almost all dam types. Especially for construction of RCC dams and rehabilitation of existing masonry dams, the transit structures can easily be incorporated with other measures to solve the dam leakage/seepage problem as well. It is reasonable to believe that the transit structures have a great prospect of application in future.

REFERENCES

[1] Du, C.J., *Afinite element procedure for calculation of accumulated stresses in mass concrete structures and stresses in roller compacted concrete dams,* Master thesis, Tsinghua University, Beijing, 1988
[2] Godde, D. & Droste, M., CFRD Mohale, Lesotho- some aspects of face slab construction, *Proceedings of Workshop on Modern Techniques for Dams-Financing, Construction, Operation and Risik Assessment,* 14.Sept.2001, Dresden, Vol. I, pp. 99–118
[3] Hall, J.R, Dowling, MJ. & El-Aidi, B., Defensive earthquake design of concrete gravity dams, *Dam Engineering,* Vol. 3, Issue 4, 1992
[4] ICOLD Bulletin 78, *Watertight Geomembranes for Dams,* 1991
[5] Jaup, A. & Veyhle, D., Braendbach: Germany's first dam rehabilitation using a geomembrane, *International Journal on Hydropower & Dams,* June 2002, pp. 84–89
[6] Rescher, O.J., Arch dams with an upstream base joint, *International Water Power & Dam Construction,* March 1993
[7] Ruesch, C. & Scherrer, I., A new sealing system for dams, *Proceedings of Workshop on Modern Techniques for Dams-Financing, Construction, Operation and RisikAssessment,* 14.Sept.2001, Dresden, Vol. I, pp. 119–125
[8] United States Bureau of Reclamation, Department of the Interior, *Design ofGravity Dams,* United States Government Printing Office, 1976
[9] Zschammer, C. & Lengfeld, M., Rehabilitation of gravity dams at the example of Neunzehnhain II Dam, *Proceedings of Workshop on Modern Techniques for Dams-Financing, Construction, Operation and Risik Assessment,* 14. Sept. 2001, Dresden, Vol. I, pp. 151–162

New Developments in Dam Engineering—Wieland, Ren & Tan (eds),

Problems and experience in temperature control for mass concrete of Baglihar gravity dam with long construction blocks

C.Du & B.Stabel
Lahmeyer International GmbH, Germany

ABSTRACT: Thermal cracking in concrete of large dams depends mainly on the dimension and shape of construction blocks, materials used, temperature control measures taken in construction and construction methodology as well as local climate conditions. Long construction blocks are prone to cracking in comparison to the short blocks. Especially, when mass concrete experiences thermal shocks such as sudden air temperature drops or overtopping of river water with low temperature, the situation will be aggravated. Therefore, strict temperature control measures for construction of long blocks are to be taken. Otherwise, costly repairs for cracks may be required, which will offset the benefit from the saving of form works and grouting longitudinal construction joints for short block construction method.

The ongoing Baglihar dam is a solid conventional concrete gravity structure with a maximum height of 144.5m. The dam mass concrete is designed to be placed in full lift length as single monolithic blocks without longitudinal construction joints with a maximum block length of 137m. During the construction, serious cracking across the blocks was detected, especially after overtopping of the placed mass concrete by seasonal flooding with lower water temperature. In this paper, the temperature control measures implemented are summarised, the cracks detected and the remedial works taken are described. Special discussions are focused on the long construction blocks and thermal shocks caused by cold river water from the point of view of temperature control.

1 INTRODUCTION

As the ICOLD congress Q.57 expressed, cracking in concrete dams is an old problem always present [9]. Thermal cracking is a major part of mass concrete cracking. The heat generation of cement and the resulting thermal stresses in mass concrete are often decisive factors for a concrete structure rather than a high initial compressive strength. Dam mass concrete is plain concrete with little or even without steel reinforcement. The tensile stresses occurring in the structure must be maintained by the concrete itself. Due to its lower tensile strength, the tensile stresses might easily exceed the tensile strength and lead to cracking.

The causes of tensile thermal stresses in dam mass concrete can be briefly outlined as: (i) the volume changes due to temperature variation; (ii) autogenous volume shrinkage; and (iii) restraints to the volume change from exterior and interior of mass concrete structures. The problem of thermal cracking will be particularly severe when the concrete dams are constructed in regions with severe ambient conditions such as severe winters, hot weather and combination of the high air temperature with thermal shock caused by cold river water from near snow- and ice-clad mountains. The designer should account for probable ambient conditions in planning temperature control requirements.

Thermal cracking has plagued many large concrete dams. It may affect the watertightness, integrity, serviceability and durability, or even the stability of dams. Therefore, the tensile stresses

in mass concrete structures should be reduced to the minimum practicable level. Efforts to control the thermal cracking in mass concrete of large dams are directed mainly towards: (i) to choose appropriate structural shapes including introduction of proper transverse contraction and longitudinal construction joints and thereafter grouting them; (ii) to reduce maximum temperature rise in mass concrete recourse to choosing proper material and optimal mix design as well as reducing placement temperature and post-cooling; and (iii) to use special concrete which ensures optimal correlation prevailing to fit the deformation process, such as using shrinkage-compensating concrete [2].

For construction of high concrete dams, two construction methodologies related in temperature control have been developed and dominantly implemented [4]. The first is the blockwise placement of mass concrete with longitudinal (parallel to dam axis) construction joints and joint grouting, which was first implemented at Hoover dam by USBR in 1936. The world's highest gravity dams, such as Grande Dixence (285m, Switzerland) and Bhakra (226m, India) [8] have been built with two or more longitudinal construction joints. For joint grouting, the post-cooling by means of circulating cold water through embedded coils must be conducted before impoundment of reservoir. It can be seen that the philosophy of this method is that the cracks are artificially produced at predetermined locations and properly treated later. Performance of these high dams over a half of century demonstrated the efficiency of the longitudinal construction joints in preventing longitudinal cracks. Another method is the so-called full-lift-length placement by which the dam mass concrete is placed in full lift length as single monolithic blocks without longitudinal joints. This method was intensively studied by US Army Corps of Engineers and first implemented at Norfork dam of 71m high in 1943. Later this method was used to the record block length of 152m at Dworshak dam of 218.5m high [5]. By using this method the costs induced by the post-cooling with embedded coils and joint grouting work in the blockwise placement method are saved. However, strict temperature control measures such as comprehensive pre-cooling are essential to prevent concrete cracking. For construction of an individual concrete dam, which construction method will be adopted depends more or less upon the preference of the designer. No clear-cut line has been drawn to establish the criteria for choosing the methods. In this paper we will discuss the thermal problems related to the ongoing Baglihar Project with emphasis on the full-lift-length placement method and thermal shock caused by cold river water.

2 BAGLIHAR DAM AND MAIN CONSTRUCTION CONDITIONS

The Baglihar hydroelectric project is situated on the river Chenab in Jammu and Kashmir state of northern India. The project envisages construction of a concrete gravity dam, a 5-bay spillway and a 3-bay chute spillway integrated in the dam body with a maximum discharge capacity of 16 500m^3/s as well as an underground powerhouse. The installed capacity of the powerhouse is 3×150=450MW for the first stage and another 450MW for the second stage, in total 900MW. A 2.2km long head race tunnel carries water from reservoir to the underground powerhouse of Stage I. Its intakes lie separately on the right abutment upstream of the dam. The dam crest is at el. 844.5m asl. A plunge pool of 70m length is connected to the spillway. For river diversion, two horse shoe-shaped diversion tunnels of 10.48m (W) ×10.64m (H) with flat invert are arranged. The maximum diversion capacity is 3000m^3/s. The rockfill cofferdams with concrete core are located on the up- and downstream side of the main dam. A typical cross section of the barrier is shown in Figure 1. More project details are given in [13].

The project site is located in a subtropical climate region with high temperature in summer and mild temperature in winter. The observed maximum and minimum air temperature is 46.1°C and 0.1°C, respectively. The mean annual air temperature is 21.8°C. Daily air temperature difference between the maximum and the minimum temperature frequently reaches over 20°C. The river originates from the Himalaya snow- and ice-clad mountains about 250km from the dam site. Therefore, the temperature of snowmelt river water is quite low with an annual mean value of 10.4°C, or 11.4°C lower than that of the air. The observed mean monthly air and river water temperatures

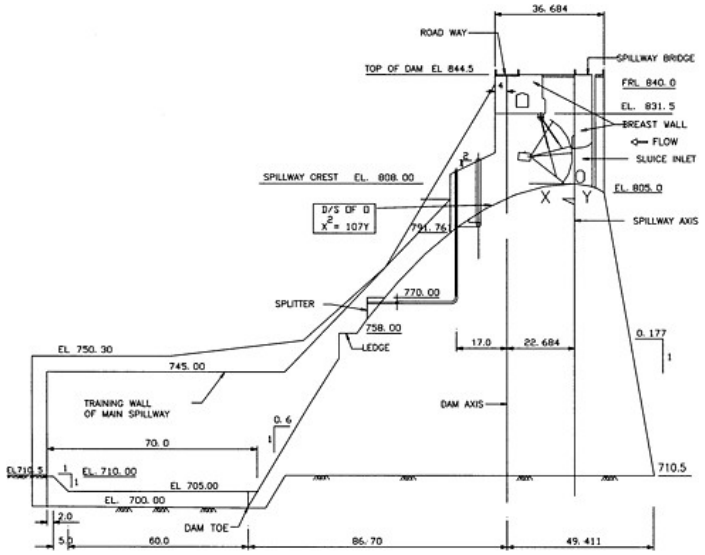

Figure 1. A cross section of the Baglihar concrete gravity dam.

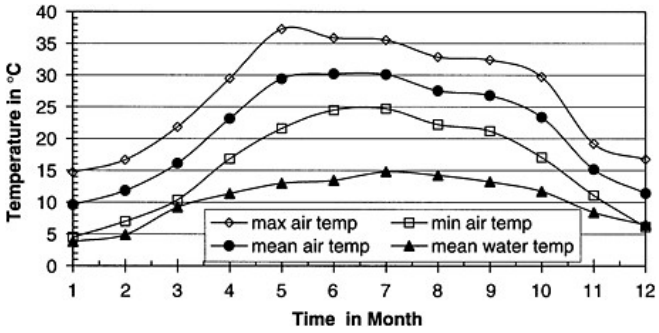

Figure 2. Observed mean monthly air and river water temperature.

are shown in Figure 2. It can be seen that the mean monthly temperature of the river water is 16°C lower than that of the air in summer months, while in winter months the temperature difference ranges from 5 to 7°C.

The gravity dam is a solid conventional mass concrete structure with a maximum height of 144.5m above the lowest foundation level. The typical up- and downstream slopes of the dam are 1 V: 0.177/0.35H and 1 V: 0.6H, respectively, resulting in a maximum base length of 137m in the river bed portion. The dam crest length is 335m. The total concrete quantity is in the order of 1.8 Miom^3. The project area lies in mountainous and rugged terrain in Middle Himalayas. The dam is founded on quartzite rock. Provisions have been conducted for consolidation and curtain grouting during the dam construction. The mean value of the modulus of deformation of the

foundation rock is 8GPa. The required strength of the dam concrete was determined by the stability and stress analysis. For the Baglihar dam three types of concrete have been used, namely:

(a) interior concrete of M15 grade with a cement content of 160kg/m^3 and a nominal maximum size of aggregate (NMSA) of 150mm, applied in dam interior;
(b) facing and base concrete of M20 grade with a cement content of 277kg/m^3 and NMSA of 40mm, applied for the dam upstream facing of 5.0m thick and for dam base of 2.0m thick on rock surface;
(c) sub-base concrete of M20 grade with a cement content of 220kg/m^3 and NMSA of 80mm, applied for sub-base area of dam of 4.0m thick between the base and interior concrete.

All strengths of concrete refer to an age of 91 days. The cement is the so-called Portland Pozzolana Cement, PPC, which contains about 23% fly ash as per Indian Standard IS 1489-1991. The heat of hydration of the cement is 56.0 and 61.0kcal/kg at 7 and 28 days, respectively. The adiabatic temperature rise of the concrete for dam interior is thus 23°C. The aggregates used for concrete production are mainly manufactured from quartzite with minor slate partings quarried at the project crushing plant in the near vicinity of the dam site. Processed aggregate is delivered to the batching plant bins by belt conveyor. The river sand is used in a very limited extent and gravel is not used for producing concrete due to the high content of mica and limited volume. All the principal concrete production facilities are located on the left abutment above the dam crest. The main concrete batching plant lies on left abutment about 150m to the dam top of the block 1 at left side. In the batching plant, four mixers with a capacity of 4.5m^3 each are installed. The capacity of the batching plant for producing concrete is 360m^3/hr. The fresh concrete from the batching plant will first be transported by a concrete bus to the delivery dock on the left dam top, where it is discharged into a bucket of 9m^3 and further transported by a cable crane to the placing spot in the dam. The cable crane has three lines installed between the fixed mast on left abutment and the tail track on the right abutment with a distance of 440m between the two end supports. The maximum vertical run of hooks is 190m and the useful length of the runway along the tail track between stops is 245m. Three buckets of 9m^3 each on the cable lines for carrying concrete mix can ply between placing spots and the delivery dock simultaneously. The capacity of concrete transport of each line of the cable crane is planed to be 90m^3/hr.

For the dam concrete construction, the full-lift-length placement method without longitudinal construction joints was chosen. As described above, the dam is divided into 18 monolithic blocks with a width of 17 or 18m for most blocks, and the maximum base length is 137m. It is apparent that for placement of such long concrete monoliths, strict temperature control measures must be taken to avoid concrete cracking. The thermal studies were followed as per the Indian Standard IS:14591-1999 [6]. The placement temperature is accordingly specified to 12°C, approximately 10°C lower than the mean annual temperature of 21.8°C. The fresh concrete at the main batching plant is thus produced at the temperature of 10°C or less. For achieving this degree of temperature, a comprehensive pre-cooling measures are taken, such as, (i) all coarse aggregates (>10mm in size) are to be cooled down to a temperature of 9°C in the inundation bins by feeding chilled water at 2°C from the chilling water plant; (ii) the chilling water of 2°C is used as mixing water; and (iii) the calculated quantity of ice flakes (up to a content of 44kg/m^3) of 0°C are added into the mixers at the batching plant as a replacement of partial mixing water.

The lift height of the mass concrete placement varies from 0.75 to 1.5m for base concrete in strong restraint zones and from 1.0 to 2.5m for upper part of concrete in weak restraint zones, depending on location and season that concrete is placed. The time interval for placing concrete is specified as 3 to 8 days, and the long time interruption (>15 days) shall be avoided as possible. Before concreting stared, the pit is thoroughly cleaned with high-pressure air/water jet. The concrete mix downloaded on the pit is spread in strips by an excavator or a bulldozer in layers of about 50cm thick each and thereafter vibrated with crawler-mounted distributors/vibrators (netter vibrators) of needle type (150mm in diameter). In corners and near form works where operation of the crawler-mounted vibrator is difficult, the large hand-operated vibrators of needle type (60mm in diameter) are used. After setting of the placed concrete, the green cutting is conducted to create a

roughened surface and thus obtain a better bonding between lifts. Curing the concrete with river water for 14 days or up to covering with the subsequent lift of concrete is then followed with seasonal adjustment. Since the river water comes from snowmelt of Himalaya snow- and ice-clad mountains near the dam site, its daily temperature variation is very little. In this way the cooling effect is achieved and heating up of concrete by solar radiation is counteracted. In addition, the tarpaulin is specified to protect concrete from thermal shock by sudden air temperature drops in the winter months. No post-cooling is specified.

The chilling water plant is located about 100m from the main batching plant and has a capacity of 11.80×10^6kJ/hr (940 TR, 1TR=3.489kJ/s) against the required capacity of 11.05×10^6kJ/hr (880 TR) for producing chilled water of 0°C, for which four 100 TR and two 220 TR chillers have been installed. The chilled water is stored in a pool of the chilling water plant and fed through pipelines with insulation to the inundation bins and the mixers. The temperature loss before use is assumed as 2°C. The ice plant lies between the chilling water plant and the main batching plant. Its capacity of production of ice flakes is 445 t/day against the required 245 t/day. Six ice makers with capacity of 37.7 t/day and twenty two 10 t/day have been installed. The ice flakes are transported from the storage in the ice plant directly to the mixers in the main batching plant by a conveyor belt.

3 THERMAL CRACKING PROBLEMS DURING DAM CONSTRUCTION

The placement of dam concrete commenced at the beginning of April 2002, an unfavourable season for dam concreting in this region. The observed mean monthly air temperature was 24.1°C and maximum air temperature reached to 40.7°C. Besides of this condition, the ice plant and the chilling water plant were not completed. The river water of about 11°C was used as mixing water. Therefore, the placement temperature of dam concrete is quite high, above 20°C.

Only after placement of base concrete with a volume of roughly $7000m^3$ for two dam blocks (Bl. 12 and 13) in one month, the pit was overtopped by the river water because only one of the planed two diversion tunnels was working and the other one was not yet completed. The thickness of the placed base concrete varied from 1.0m to 3.0m just covered the foundation rock. The concrete has been submerged under cold water with temperature of 11 to 15°C for four months long. After overtopping, four cracks in the dam block 13 (No. CR13–1–13–4) and three cracks in the block 12 (No. CR12–1–12–3) were detected, while in that time the concrete for block 12 was only placed from upstream face to the dam axis. Figure 3 shows the cracks that were detected in blocks 13, 12 and later placed block 11. The cracks are section-through from the block surface to the foundation rock and longitudinally (parallel to the dam axis) distributed, or in other words,

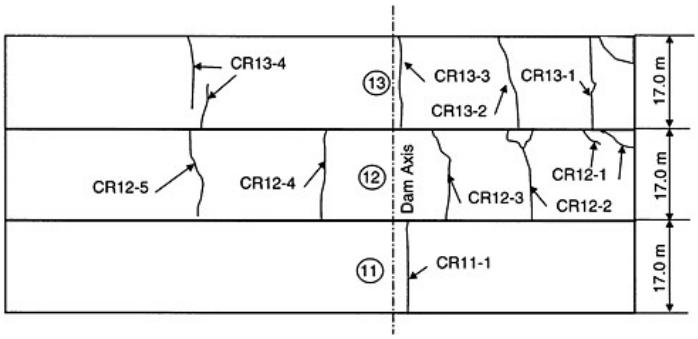

Figure 3. Cracks in base concrete of the dam blocks 11, 12 and 13.

perpendicular to the long edge of the blocks. Practically the distances of the cracks ranged from 10 to 20m. And the crack openings varied from 2 to 5mm.

It is apparent that the concrete cracking was mainly attributed to the too high placing temperature and the thermal shock by the cold river water to the young concrete. A back-analysis for the base concrete showed that the maximum temperature in the concrete raised to 37°C and the tensile stresses reached to 2.3MPa which obviously exceeded the young concrete tensile strength. Due to the thermal shock during the overtopping period, the concrete surface temperature and in turn the temperature in the interior dropped fast. Thus the cracks were initiated on the surface at first and quickly developed into the interior under restraints of foundation rock and internal concrete. Because of the fast temperature drop, the tensile stresses were developed so rapid that there was not sufficient time for concrete to adjust or relax the tensile stresses by means of its creep.

All cracks were grouted with epoxy resin by pressure vessel at a pressure up to 3.5 bar, as usual. After setting of the epoxy grout, drilling cores were extracted from the grouted cracks to visually inspect the quality of the grouting. The core recovery revealed good grout intake in the cracks. In addition, each crack was covered with a mesh of reinforcing bar of 32mm in diameter for steel at 20cm in spacing along the length and 2.5m long on either side of the crack in order to avoid crack extension to the overlaid lifts as a preventive measure.

After treatment of the cracks, the concrete placement was restarted from November 2002, the best season for dam concreting in this region. Up to this time, the ice plant and chilling water plant were put into operation. Therefore, the placement temperature could be controlled below the specified 12°C, usually at 10 to 12°C. The concreting was concentrated in block 11 and the downstream portion from the dam axis of the block 12. The quality of concrete placement was substantially improved as well. Unfortunately, after a cold air current of several days, cracks occurred in the newly placed concrete, namely, two cracks in block 12 (No. CR120-4–12-5) of 3.0m thick concrete and one in block 11 (CR11-1) of 6.0m thick concrete (see Figure 3). The cracks are section-through, but their distances are larger. An analysis showed that the cracks may be caused by the thermal shock of cold air current, because the placed dam blocks were exposed to air for a long time and the specified protection of concrete surface was not carried out. Certainly, there were a number of other uncertainties in the thermal design and concrete construction. Although the cracks are not significant to dam safety, they are objectionable as they may affect the integrity, durability and serviceability of the structure if not repaired properly. Although the surface protection measures are specified, they are difficult to be implemented in the construction environment. Instead, measures for reducing cement content in concrete by using big sizes of aggregates have been taken in order to lower the peak temperature of concrete and prevent further cracking.

4 DISCUSSIONS

In the following we will discuss the problems of the thermal shocks on mass concrete surface and long construction blocks.

4.1 *Thermal shocks and over-cooling caused by cold river water*

It has been realised that shape of temperature gradient near concrete surface plays a great part in thermal cracking of mass concrete. The mass concrete is susceptible to “shell” cracking when the temperature gradient changes sharply. Such steep temperature gradients between the interior and surface are usually caused by excessive change of the boundary temperature conditions, namely rapid cooling of the exterior relative to the interior of concrete by cold current from sudden ambient temperature drop or cold water by shortly overtopping and so on, while the thermal conductivity of concrete is comparatively low. This phenomenon is known as the thermal shock on concrete surface. The thermal shock frequently initiates surface cracking if the tensile stresses on the exterior exceeds the tensile strength of concrete. Although the surface cracks are usually harmless to the dam stability and integrity, special attention must be paid to their successive consequence that they

may easily extend into the interior and lead to more serious cracking, because the energy required to propagate a crack is much less than the energy required to initiate the crack. In order to prevent concrete cracking due to sudden air temperature drop, protective measures for insulation of exposed concrete surfaces and joint faces of previously constructed blocks are usually taken by using blankets, jute sheets or spray-on foam etc. These measures result in slowing the rate of cooling so as to reduce the temperature gradient. However, the surface insulation in the case of overtopping by river water is difficult to be economically carried out due to the high velocity flow with water bones.

When the thermal shock lasts a long period, the so-called "over-cooling" of mass concrete may happen. This over-cooling effect on mass concrete is significant. It leads frequently to seriously deeply extended or even full-section cracks.

Thermal design of mass concrete is usually based on the ground temperature differential, i.e. the difference between the maximum temperature rise and the stable temperature in concrete. The temperature of the cold river water from near snow- and ice-clad mountains is usually much lower than the stable temperature of dam concrete. In the case of Baglihar project, the river water temperature ranges from 3.8°C in winters and 14.8°C in summers with an average of 10.4°C, while the stable temperature of the dam concrete is specified as 21.8°C. Thus the annual mean air temperature is about 11°C higher than the mean annual temperature of river water. Especially in the summer months the mean monthly temperature difference between the air and river water reaches 16°C. In addition, the fresh concrete temperature is much higher its stable temperature. Hence, the temperature difference between the river water and concrete is sharp. Because overtopping of the dam concrete by the cold river water during construction in summer can take two to four months, it acts as the "over-cooling" to the mass concrete. The concrete is more brittle and more vulnerable to cracking by rapid temperature drop than that by slow temperature drop because the creep effect of concrete cannot take part in relaxing the tensile stresses. The over-cooling can create tensile stresses on the order up to 1.0~2.0 MPa which lies in the same order of the tensile strength of mass concrete. Thus the over-cooling itself can induce the concrete cracking. Besides of this, in mass concrete before overtopping, residue tensile stresses due to temperature variation or other loads exist unavoidably. Therefore, it is straightforward that the superposition of the tensile stresses exceeds the tensile strength of concrete and the mass concrete cracking occurs. The cracks in Baglihar dam during construction indicate the significant effect of over-cooling by cold river water.

Other portions in a dam which may experience the over-cooling of cold water include the dam upstream face, spillways, bottom outlets and other water releasing works. Several papers [1],[7], [11],[12] dealt with the concrete cracking induced by the over-cooling effect of cold air and water. A typical example of the over-cooling cracking is the vertical cracks in the upstream face of concrete dams after impoundment of reservoir. The reservoir water enters into the crack and develops a jacking force tending to further open the crack. The problem of over-cooling has been known for a while. However, the countermeasures are still missing except taking stricter and in turn more expensive and time-consuming temperature control measures during construction of dam mass concrete for the mentioned portions. This matter remains a research topic for concrete dam builders. In the author's opinion, the thermal studies for a concrete dam should also include the analysis of the shape of temperature gradient near the surface. The river water temperature should be taken as the stable temperature of concrete in analysis.

4.2 *Blockwise versus full-lift-length placement method*

As mentioned earlier, in current practice of concrete dam construction the blockwise placement method with longitudinal construction joints and the full-lift-length placement method without longitudinal construction joints are dominant. In comparison to the blockwise method, the fulllift-length method has the advantages that (a) owing to elimination of the longitudinal construction joints, form works, joint grouting work and equipment, cooling coils and post-cooling work are saved; and (b) for placement of "long blocks" of dam mass concrete by full-lift-length, the placing area is large, the construction procedure is simple and it is thus convenient to use heavy

machines. However, we should not overlook the following disadvantages (i) the zone of foundation restraint and the thermal stresses will be larger in the long blocks and thus more strict temperature control measures are necessary; (ii) temperature drop in the dam body is very slow and thus the mass concrete is vulnerable to the thermal shocks, as discussed above; and (iii) the concrete construction is not so flexible as that by the blockwise placement method, thereby cold joints might be formed due to interruptions during construction, which are definitely weak surfaces in the dam concrete.

Up to date, there is no clear-cut line for selecting between the two construction methods. The philosophy and criteria of temperature control for blockwise placement method are generally taken for the full-lift-length placement method. In practice, more strict temperature control measures, especially the placement temperature and the surface protection from the thermal shocks, are taken. For instance, in construction of Dworshak dam [5], the placing temperature was specified in the range from 4.6° C to 6.7°C; the cooling coils were embedded in the concrete in strong restraint zone of 0.4H (H=dam height) and the post-cooling was conducted for three weeks; the maximum lift height was specified to 1.5m; and the surface protection in the cold months was performed. From the construction of Dworshak dam, it can be seen that the strict temperature control measures should be taken as prerequisites for the full-lift-length placement, which will help for prevention of concrete cracking. However, in practice such preconditions frequently cannot be fulfilled on some dam sites, in the authors' opinion, the blockwise placement method should be considered as the first choice.

It is worth mentioning the Toktogulsky method for placement of dam mass concrete [10]. The core of the method consists of comparatively thin lift heights of 0.5 to 1.5m, a uniform placing schedule for lifts with short time intervals (3 to 7 days), continuous water curing of the lift surface during warm months and insulation of the exposed surfaces in cold seasons. Theoretical analysis and practice demonstrate that the thermal tensile stresses can be reduced to a low level by using this procedure so that no or little cracking occurs. In particular, the stress differential on lift joints between the upper and lower lift induced by temperature and by differential of the moduli of elasticity is dramatically reduced. The stress distribution in the dam concrete becomes more uniform, which favours for cracking resistance. Although the Toktogulsky method was originally developed for placement of concrete in cold weather regions, its principles may be generally suitable for concrete construction everywhere. Especially in hot weather regions, the flowing or pool water curing for concrete after placement can frequently not be undertaken in construction practice. Therefore, heat dissipation from the mass concrete is very little, or even heat absorption often happens. Long time intervals cause larger differential of moduli of elasticity and in turn larger stress differential between upper and lower lifts, which is unfavourable for preventing concrete cracking. The Toktogulsky method can balance the weather conditions and concrete hardening process and result in a better compromise.

In our earlier study on using the shrinkage-compensating concrete for construction of the spillway of Ankang gravity dam (128m high) with long construction blocks [2],[3], it has been found that continuous placement of the concrete without time interval results in the tensile stresses in the structure being smallest in comparison with other alternatives. This implies a procedure very similar to the Toktogulsky method of concreting and to the roller compacted concrete (RCC) construction. In fact, the RCC dam construction procedure is very similar to the Toktogulsky method. Although this result was obtained from the shrinkage-compensating concrete, its principle is useful for mass concrete with a low adiabatic temperature rise. The similar construction procedure is the full-lift-length placement with high lifts, like at the Rayher dam of 72m with a lift height of 19.5m [12].

From the discussions above it can be seen that the uniform construction with short time intervals, continuous construction and high lifts construction have the similar characteristics to the full-lift-length placement method. The Toktogulsky method for concreting can be taken as a reference for the full-lift-length placement method for placement of mass concrete from the point of view of cracking prevention. More studies should be carried out in the thin lifts uniform construction. By thermal studies for a concrete dam, it is suggested to consider this method.

5 CONCLUSIONS

Among various reasons causing thermal cracking of mass concrete, the thermal shocks on the concrete surface caused by overtopping of cold river water provoke steep temperature gradient on the surface at the beginning, and makes the concrete over-cooling later. In thermal design of a concrete dam, special attention should be paid to the problem of the thermal shocks. Protection of structures from thermal shocks caused by cold air remains another challenge to concrete dam engineers in construction practice. Rapid temperature drop leads to comparably larger tensile stresses in mass concrete, and the concrete behaves more brittle, because the creep effect of concrete cannot be utilised to relax the tensile stresses, which should be taken into account in the thermal design of mass concrete.

Dam concrete placement in short blocks with and in full-lift-length without longitudinal construction joints is dominant in current dam construction practice. However, there is no clear criterion for choosing the construction methods. The full-lift-length placement method requires strict temperature control measures. If the dam concrete is expected to experience severe ambient temperature conditions or overtopping by cold river water during construction, it is not suggested to use the full-lift-length placement method. At present, the temperature control theory of the short blockwise placement method is taken for the full-lift-length placement method. More criteria for the full-lift-length placement method should be established in consideration of its characteristics. This matter is also of great significance for the RCC dam construction—a typical full-lift-length placement.

REFERENCES

[1] Brunner, W.J. & Wu, K.H., Cracking of the Revelstoke concrete gravity dam mass concrete, *Fifteenth Congress on Large Dams,* Lausanne, Switzerland, Q.57-R.1, 1985, pp. 1–21
[2] Du, C.J., Mass concrete structures using novel shrinkage-compensating concrete, *The Indian Concrete Journal,* May 2003, pp. 1055–1059
[3] Du, C.J., Special cement concrete for Ankang Dam, *Concrete International,* September 1997, pp. 61–66
[4] Fujisawa, T. & Nagayama, I., Cause and cracks by thermal stress in concrete dam, *Fifteenth Congress on LargeDams,* Lausanne, Switzerland, Q.57-R.7, 1985, pp. 117–142
[5] Houghton, D.L., Measures being taken for prevention of cracks in mass concrete at Dworshak and Libby dams, *Tenth Congress on LargeDams,* Montreal, Q.39-R.14, 1970, pp. 241–271
[6] Indian Standard IS :14591-1999, *Temperature control of mass concrete for dams,* 1999
[7] Norman, C.D. & Anderson, F.A., Reanalysis of cracking in large concrete dams in the US Army Corps of Engineers, *Fifteenth Congress on Large Dams,* Lausanne, Switzerland, Q.57-R.9, 1985, pp. 157–171
[8] Palta, B.R., Aggarwala, S.K. and Rao, P.S., Prevention of cracks in concrete during the construction of Bhakra dam, *Tenth Congress on Large Dams,* Montreal, Q.39-R.32, 1970, pp. 599–614
[9] Philleo, R.E., General Report on Question 57: Concrete Dams—an Old Problems Always Present: Cracking—a New Technology: Rolled Concrete, *Fifteenth Congress on Large Dams,* Lausanne, Switzerland, GRQ.57, 1985, pp. 769–811
[10] Rosanov, N.S. et al, Temperature cracking in massive concrete dams-criteria of crack formation and preventive measures, *Fifteenth Congress on Large Dams,* Lausanne, Switzerland, Q.57-R. 43, 1985, pp. 755–765
[11] Tu, C.L., A study of the cracking of Zhexi diamond head buttress dam and its strengthening measures, *Fifteenth Congress on Large Dams,* Lausanne, Switzerland, Q.57-R.38, 1985, pp. 653–670
[12] Zhu, B.F., *Thermal Stresses and Temperature Control of Mass Concrete,* China Electric Power Press, 1999
[13] Stabel, B. & Lazaric, B., The 900 MW Baglihar Hydropower Scheme in Jammu & Kashmir India, Conference on Large Dams and Hydropower Development, 26–28. May 2004, Delhi, India

This page intentionally left blank.

New Developments in Dam Engineering—Wieland, Ren & Tan (eds),

Nonlinear seismic response analysis of arch dam-foundation systems—Part I*

Xiuli Du
Beijing Lab of Earthquake Engineering and Structural Retroflt,
Beijing University of Technology, China

Yanhong Zhang
China Institute of Water Resources and Hydropower Research, China

Boyan Zhang
China Institute of Water Resources and Hydropower Research, China

ABSTRACT: The arch dam-foundation rock dynamic interaction and the nonlinear effects of closing and opening of contracted joints of arch dams are important to the analysis of seismic response of arch dams. Up to date, there is not yet a reasonable and rigorous procedure including the two factors in the analysis of seismic response of arch dams. It is the reason that the methods used for analysis of the arch dam-foundation rock dynamic interaction in the frequency domain are not suitable to the problem with nonlinear behaviors. For the purpose an analysis method in the time domain is proposed by combining the explicit finite element method and the transmitting boundary, and by using a dynamic analysis method the static responses of arch dams is solved and a combination method is also proposed to calculate the nonlinear responses of arch dams under the actions of static and dynamic load, in this paper. The influences of the arch dam-foundation dynamic interaction with energy dispersion, local material nonlinear and non-homogeneous behaviors on the seismic response of arch dams have been also studied for the designed Xiaowan arch dam with maximum height of 292m in China. Moreover, the results obtained by the proposed method are compared with the ones obtained by the conventional method with the massless foundation. The influences of the closing-opening effects of contracted joints of arch dams on the seismic response of arch dams will be considered in another paper.

1 INTRODUCTION

Reliable analytical procedures of the seismic response of arch dams are foundational to the seismic design of arch dams to be constructed and the earthquake safety prediction of existing arch dams. Many researches have been done and many developments have been achieved for a reasonable, full and rigorous representation of the actual problem. From the results obtained it is shown that a reasonable and rigorous model to simulate the seismic response of arch dams should include the factors as follows, 1. the arch dam-foundation rock dynamic interaction, 2. the impounded water with compressibility-arch dam dynamic interaction, 3. the impounded water with compressibility-foundation rock dynamic interaction, 4. the effects of closing-opening of contracted joints of arch dams, 5. the effects of traveling-waves, 6. the effects of local topographical and geological behaviors of foundation rock. Prof. R.W.Clough (1973) developed one of the earliest computer programs ADAP based on the finite element method for calculating of the seismic response

* Sponsored by National Natural Science Foundation for Distinguished Young Scholar of China, Grant No. 50325826.

of arch dams, in which the massless foundation rock model with fixed boundaries was adopted and the influences of impounded water on the seismic response of arch dams were not considered. Based on ADAP, J.S.-H.Kuo (1982) and Y.Ghanaat and R.W.Clough (1989) studied the influences of the hydrodynamic effects with added mass approximation on the seismic response of arch dams and developed a computer program EADAR In order to consider the hydrodynamic effects of impounded water with compressibility and the reservoir boundary absorption effects, a substructure technique in the frequency domain was developed by J.F.Hall and A.K.Chopra (1983) and K.-L.Fok (1986a, 1986b, 1986c, 1986d, 1987). O.Maeso and J.Dominguez (1993) and J.Dominguez and O.Maeso (1993) used the boundary element method in the frequency domain for considering the arch dam-foundation rock dynamic interaction and the traveling-waves effects of arch dam systems under the action of the harmonic seismic motion input. H.Tan and A.K.Chopra (1995a, b) also used the boundary element method to calculate the foundation impedance matrix and developed a substructure technique considering the foundation rock-arch dam dynamic interaction, impounded water with compressibility-arch dam dynamic interaction and the reservoir boundary absorption effects, in which for simplicity the foundation impedance functions are assumed as the 3-order curves and the seismic input motions along the interface between foundation rock and arch dam are uniform. G.L.Fenves (1989), M.J.Dowling (1987) studied the influence of contracted joints of arch dams on the seismic response of arch dams, in these researches, the arch dam-foundation rock dynamic interaction and the traveling-waves effects are not considered. As mentioned above, at the present there is yet not a method to include the influence of the six factors stated above, there are especially the some difficulties to consider the foundation rock-arch dam dynamic interaction and the effects of the closing-opening of contracted joints of arch dams and the local nonlinear and non-homogenous behaviors in foundation rocks in the meanwhile. It is the reason that the methods used for analysis of the arch dam-foundation rock dynamic interaction in the frequency domain are not suitable to the problem with nonlinear behaviors. In this paper, an analytical technique in the time domain has been proposed for considering the foundation rock-arch dam dynamic interaction and the nonlinear effects of materials mentioned above.

The many important developments have been achieved on studying of the topic called as the dynamic soil (or rock)-structure interaction in which the one key problem is to simulate scattering wave propagation in infinite foundation media. At the present, there are mainly the two classes of method to simulate scattering wave propagation in infinite media, the one class satisfies all the differential equations of motion and the radiation conditions at infinite region in the exterior of discrete models exactly, such as the boundary element method seen in Ref. by J.P.Wolf (1985) and X.L.Du (1987). They couple in space and time, and are usually formulated in the frequency domain, in which the shortcomings are that computing costs are high and it is difficult to simulate the local nonlinear and non-homogeneous features in the foundation near structures. The other class satisfies approximately the non-reflection condition at the artificial boundary of the finite discrete models to be used to simulate the effects of infinite foundation, in which the assumption of outgoing plane waves is mostly made, such as a transmitting boundary suggested by Z.P.Liao et al (1984), an absorbing boundary suggested by R.Clayton and B.Engquist (1977), a viscous boundary suggested by J.Lysmer and R.L.Kuhlemeyer (1969), they are all local non-coupling in space and time, and have the advantages for solving of the near field wave motion problems with local nonlinear behaviors. J.P.Wolf (1986) compared the accuracy of these artificial boundary methods for the simple one-dimensional case and pointed that the well-known viscous boundary and the transmitting boundary lead to good accuracy. Due to the feature of multi-times transmitting, the high-order transmitting boundary methods lead to good accuracy for two-and-three dimensional cases also.

In this paper, an analysis method in the time domain used for computing the seismic responses of arch dams with consideration of the dam-foundation rock dynamic interaction and the local nonlinear behavior in the near-field foundation rock has been developed by combining the explicit finite element method with the transmitting boundary proposed by Z.P.Liao, et al (1984). It is noticed that there is a high frequency unstable phenomenon at artificial boundaries by use of the transmitting boundary. A method to eliminate the phenomenon has been proposed by Z.P.Liao (1996a), in which the damping forces of media are related to the stiffness of media. Therefore, Rayleigh damping assumption was used here. The some results obtained by applying of the approach for the analysis of seismic responses of a designed arch dam with a maximum height of 292m in China are illustrated, and are compared with the ones of the conventional method with massless foundation proposed by R.W.Clough, et al (1973).

2 FUNDAMENTALAPPROACH

In this paper, an arch dam-foundation system is divided into an interior region with dam body and its adjacent near-field foundation with important local topographical and geological features and an infinite far-field foundation region with homogenous and linear features. The interior region is meshed by using of finite element method. The infinite exterior region is simulated by setting a set of artificial boundaries to simulate propagation of outgoing scatter waves from the interior region to the infinite exterior region. To obtain a non-coupling method for the finite discrete dynamic model with artificial boundaries mentioned above, the motions of the nodes of the discrete finite element model in the interior region are calculated by the explicit finite element method and the motions of the nodes at the artificial boundaries are solved by the transmitting boundary. Next, the brief descriptions of the two ways are given.

2.1 *Solving of the interior nodal motions*

From the explicit FEM, the motion of equation of j direction at any node i in the discrete model of arch dam-foundation systems can be written as

$$R_{ij} = \sum_{l=1}^{n_e} \sum_{k=1}^{n} k_{ijlk} u_{lk} \tag{1}$$

where, m_i the mass of the node i, $\ddot{u}_{ij}$ is the acceleration of j direction at the node i, $\ddot{u}_{ij}$ is the velocity of k direction at the node l which is around the node i and belongs to the same element with the node i, R_{ij} and F_{ij} are the restoring force and the external force of j direction at the node i respectively, C_{ijlk} is the damping influence coefficient of k direction at the node l on j direction at the node i, n_e is the nodal number related to the node i, n is the number of freedom degree, R_{ij} may be determined by an elastic-plastic constitution model.

If R_{ij} is an elastic restoring force, it is expressed by

$$\begin{cases} c_{ijlk} = 0 & l \neq i \\ c_{ijlk} = c_{ij} & l = i \end{cases} \tag{2}$$

In which, u_{lk} is the displacement of k direction at the node l, k_{ijlk} is the stiffness coefficient of k direction at the node l on j direction at the node i.

Assuming that the damping force of any direction at the node i is only relative to itself velocities at the node i, thus

$$m_i \ddot{u}_{ij} + c_i \dot{u}_{ij} + R_{ij} = F_{ij} \tag{3}$$

When $C_{ij}=c_{ik}=c_i$, the formula (1) may by written as

$$m_i \ddot{u}_{ij} + c_i \dot{u}_{ij} + R_{ij} = F_{ij} \tag{4}$$

It is known that the formula (4) is a special example of the formula (1), this is, when the damping force is only relative to the velocity of the node/and every direction damping coefficient is the

same, there is the formula (4). Substituting the central difference formulations for acceleration and displacement into the formula (4), the explicit integration formula of Eq. (4) can be obtained. Generally, the assumption from the formula (1) to the formula (4) is not reasonable. Thus, an explicit integration formula can't be obtained by introducing the central difference method. XJ. Li, et al (1992) derived a explicit integration formula with the accuracy of 2-order ($O(\Delta t^2)$), it can be expressed as

$$u_{ij}^{t+\Delta t}=\left(F_{ij}^{t}-R_{ij}^{t}-\sum_{l=1}^{n_e}\sum_{k=1}^{n}c_{ijlk}\dot{u}_{lk}^{t}\right)\Delta t^2/2m_i+u_{ij}^{t}+\Delta t\cdot\dot{u}_{ij}^{t} \tag{5}$$

$$\dot{u}_{ij}^{t+\Delta t}=\dot{u}_{ij}^{t}+\left(F_{ij}^{t+\Delta t}-R_{ij}^{t+\Delta t}+F_{ij}^{t}-R_{ij}^{t}\right)\Delta t/2m_i-\left(\sum_{l=1}^{n_e}\sum_{k=1}^{n}c_{ijlk}\left(u_{lk}^{t+\Delta t}-u_{lk}^{t}\right)\right)/2m_i \tag{6}$$

From Rayleigh damping assumption, c_{ijlk} may be written as

$$c_{ijlk}=\alpha m_l+\beta k_{ijlk} \tag{7}$$

where, α and β are constants decided by experiences.

The formulations introduced above is conditional stable, the time step Δt is limited as

$$\Delta t\le\min\left(\Delta R_{\min}^{1}/c_{\max}^{1},\cdots,\Delta R_{\min}^{s}/c_{\max}^{s},\cdots,\Delta R_{\min}^{m}/c_{\max}^{m}\right)/\gamma \tag{8}$$

In which, m is the number of media of the system to be solved. $\Delta R_{\min}^{s}$ are the minimum element size and maximum wave speed of mediums, respectively, and γ is a constant coefficient related to damping ratio, the determination of the constant coefficient is given by X.L. Li, et al (1992).

In general, in order to obtain enough accuracy solutions, it is required

$$\Delta R_{\max}\le(1/8\sim1/12)\lambda_{\min} \tag{9}$$

where, $\Delta R_{\max}=\max(\Delta R^{1}_{\max},\ldots,\Delta^{s}_{\max},\ldots,\Delta R^{m}_{\max})$, $\lambda_{\min}$ is the minimum wavelength of incident waves, $\Delta R^{s}_{\max}$ is the maximum element size of mediums.

2.2 *Transmitting boundary*

As seen from Fig. 1, any outgoing plane sub-wave with wave speed c_i and incident angle θ_i from the interior region impinging upon the artificial boundary L can be expressed by it's apparent propagation along the X-axis (normal to the boundary L) as follows

$$u_i(x,y,z,t)=u_i(x-c_{xi}t,y,z) \tag{10}$$

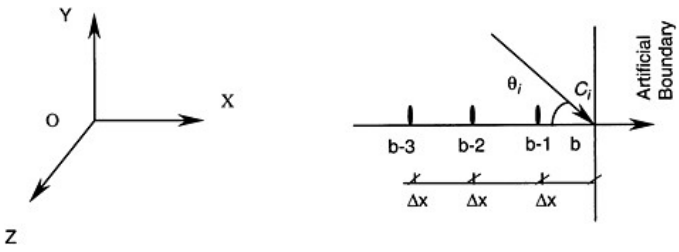

Figure 1. Artificial boundary and outgoing plane sub-ware.

$$c_{xi}=c_i/\cos\theta_i \tag{11}$$

c_{xi} is called as apparent wave speed.

Assuming that the media of the artificial boundary region are all linear, the total motion of outgoing plane waves can be expressed as

$$u(x,y,z,t)=\sum_{i=1}^{n_s}u_i(x-c_{xi}t,y,z) \tag{12}$$

where, n_s is the number of outgoing plane sub-waves.

A constant value of wave speed c_a called as artificial wave speed is taken to replace c_{xi} in the formula (12) approximately, we can have

$$u(x,y,z,t)\approx\sum_{i=1}^{n_s}u_i(x-c_at,y,z)=u(x-c_at,y,z) \tag{13}$$

There may be different speeds of wave types (P, S, Rayleigh, Love) and different angles of incidence in a problem to be solved, therefore, c_a is generally decided by experiences and it's range of values is between S wave speed and P wave speed, the influence of different speeds of wave types and different angles of incidence on the accuracy of the transmitting boundary may be decreased through considering high-order items seen in Ref. Z.P.Liao, et al (1984).

As seen from Fig. 1 again, from the propagation identity of plane wave and the formula (13), the motion of the node b at time $t+\Delta t$ can be expressed as

$$u(x_b, y_b, z_b, t+\Delta t)\approx u(x_b-c_at, y_b, z_b, t) \tag{14}$$

$u(x_b-c_at, y_b, z_b, t)$ may be obtained by interpolating between the node $(b-1)$ and the node b, thus, $u(x_b, y_b, z_b, t+\Delta t)$ can be calculated by the motions of the node $(b-1)$ and the node b at time t. The formula (14) is called as the 1-order transmitting formula and it's error can be expressed as

$$\begin{aligned}&\Delta u(x_b, y_b, z_b, t+\Delta t)=u(x_{b,}y_{b,}z_b, t+\Delta t)-u(x_b-c_a\Delta t, y_b, z_b, t)\\&=\Delta u(x_b-c_at, y_b, z_b, t)\end{aligned} \tag{15}$$

From the plane wave propagation behaviors, the formula (15) may be transformed into

$$\Delta u(x_b-c_at, y_b, z_b, t)=u(x_b-c_at, y_b, z_b, t)-u(x_b-2c_a\Delta t, y_b, z_b, t-\Delta t) \tag{16}$$

Substituting the formula (16) into the formula (15), there is

$$u(x_b, y_b, z_b, t+\Delta t)=2u(x_b-c_at, y_{b,}z_b, t)-u(x_b-2c_a\Delta t, y_b, z_{b,}t-\Delta t) \tag{17}$$

The formula (17) is called as the 2-order transmitting formula. Based on the same concept and way, the N-order transmitting formula can be derived as follows:

$$u(x_b,y_b,z_b,t+\Delta t)=\sum_{n=1}^{N}(-1)^{n+1}C_n^Nu(x_b-nc_a\Delta t,y_b,z_b,t-(n-1)\Delta t) \tag{18}$$

where, $C_n^N=N!/[(N-1)!n!]$

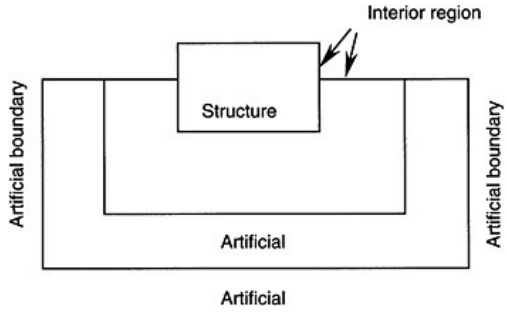

Figure 2. Sketch of the simulation model.

By using a quadratic interpolation, the motion of the node *b* in the finite element discrete model can be written as

$$u(x_b, y_b, z_b, t+\Delta t)=\sum_{n=1}^{N}(-1)^{n+1}C_n^N \overline{T}_n \overline{U}_n \tag{19}$$

In which,

$$\overline{U}_n=[u(x_b, y_b, z_b, t-(n-1)\Delta t), u(x_b-\Delta x, y_b, z_b, t-(n-1)\Delta t), \cdots, u(x_b-2n\Delta x, y_b, z_b, t-(n-1)\Delta t)]^T \tag{20}$$

$\overline{T}_n$ is a function of c_a, Δt, and Δx, and can be obtained by using the formula given by Z.P.Liao et al (1984). The detailed introduction on the accuracy and the efficiency of the transmitting boundary can be seen in the references given by Z.P.Liao (1992, 1996b, 1997a, 1997b).

2.3 *Input method of incident seismic waves*

As seen from Fig.2, the total calculation region is divided into the two sub-regions: the interior calculation region, the artificial boundary region. In order to separate the outgoing wave from the total wave motion field in the artificial boundary region, the total motion field u is divided into the two parts: the free field motion u_f of semi-infinite space with vertical incident seismic wave and the scattering wave field motion u_s induced by having of structure, local topography and inhomogeneous, nonlinear media. It is written as

$$u=u_s+u_f \tag{21}$$

u_f may be gained by analytic method or solving of the one-dimension finite element discrete model and u_s at artificial boundary nodes is calculated by the transmitting formula stated above. The input earthquake motions at the artificial boundary regions are determined by analysis of the one-dimensional elastic semi-space model from the free field motions at the ground surface of foundation rock given by the earthquake risk analysis method. Due to the existence of structure, non-homogeneous media and local irregular topography in the interior region, the propagation of the outgoing scatter waves from the interior calculation region to the infinite semi-space region in the calculation model will be induced by the factors, therefore, the motions of the interface between arch dam and foundation rock will are non-uniform. Moreover, the incident motions are only exerted at the artificial boundary regions according to the one-dimensional wave propagation theory Hence, the effects of traveling-waves in the interior region can be simulated in the proposed model.

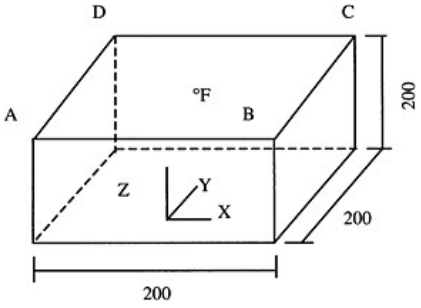

Figure 3. Sketch of the finite element calculation model of 3D-semi-infinite medium.

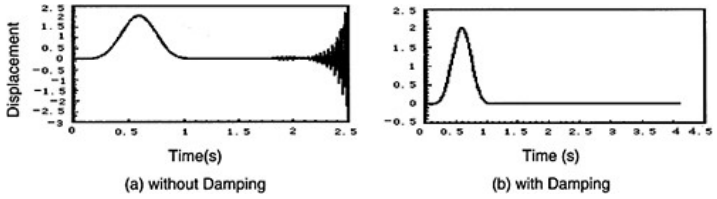

Figure 4. Displacement response histories of node E.

2.4 *Simple example*

For verification of this program and approach developed in this paper, a simple example is examined here, in which the displacement responses in a three-dimensional semi-infinite medium induced by a vertical incident pulse wave with a unit peak of displacement are calculated. Fig.3 is the sketch of the calculation model of the example. The displacement response histories of the calculation output node E are shown in Fig.4. The results without damping in the medium are shown in Fig.4(a), the ones with damping $c_{ijlk}=\alpha_{mi}+\beta k_{ijlk}$, ($\alpha=0$, $\beta=0.0001$ are taken here) are shown in Fig.4(b). It can be seen that the high frequency unstable phenomenon (seeing Ref. By Z.P.Liao, et al (1992)) induced by the transmitting boundary has eliminated by considering a very little damping related to stiffness. The maximum displacement response at the node E on the ground surface obtained by the proposed method is 2, it is equal to the result of analytic method.

3 COMPUTING OF THE COMBINATIVE RESPONSES OF ARCH DAM-FOUNDATION SYSTEMS DURING STATIC LOADS AND EARTHQUAKE

The influences of faults, cracks etc in the foundation rock on the seismic response of arch dams during the action of strong earthquake have not seriously yet been paid attention. In this paper, the faults, cracks etc are treated as elastic-plastic media with a nonlinear constitutive relation with Druker-Prager Cap model adopted here. Due to the nonlinear effects of material behaviors, the seismic response of arch dams is related to the static response of ones subjected by static loads. Such as self-weight, impound water and sediment etc. Therefore, the static response of arch dams should be firstly calculated, then, the static actions and the static response are taken as the initial conditions for computing of the dynamic response of arch dams. In this paper, a technique of calculating the static responses by the dynamic method has been adopted, in which the static loads are regarded as the step loads exerted at the initial time and the artificial damping are exerted during the step loads.

It is noticed that the scattering wave of propagation in the semi-infinite foundation are only treated in the transmitting boundary as the plane waves outgoing through the artificial boundaries, the attenuation phenomenon of outgoing scattering waves in the infinite domain can't be considered in the transmitting boundary. In reality, the constrained effect of the stiffness supplied by the infinite domain for the finite model of the near-field medium is neglected. While the elastic restore behavior of the artificial boundaries of the finite model is needed in order to keep the equilibrium of the calculation model, the transmitting boundary may lead to drift instability. In order to overcome the instability, a constrained artificial boundary on which the elastic coefficients are given by experiences is introduced for computing of the static response of the problem.

4 APPLICATION TO ARCH DAM-FOUNDATION SYSTEMS

The proposed method is used to calculate the seismic dynamic responses of an arch with height of 292m called as Xiaowan arch dam located in the upper reach of the Lanchuang River in Yunnan province in China. The design earthquake intensity for the arch dam is IX degree with a horizontal peak acceleration of 0.290g, while the vertical peak acceleration is 2/3 of the horizontal one. The geological and topographical conditions of the site are very complicated. The finite element model containing the arch dam and the foundation region to be calculated has the total element number of 20107 and the total nodal number of 22878, and there are the material kinds of 22 in the model. The sketch of the finite element discrete model except the artificial boundary region is shown in Fig.5. The altitude at the bottom of the dam is 953m, the altitude at the top of the dam is 1245m. The arc length at the top of the dam is 935m, the thickness at the top of the dam is 12m, and the thickness at the bottom of the dam is 73m. The dynamic elastic modulus is 27.3GPa, the density is 2400N/m^3, and the Poisson ratio is 0.189 in the concrete of dam body. The material constants in the foundation region are shown in Table 1. Here, the dynamic elastic modulus is 1.3 times the static elastic modulus. For simplicity, the influence of arch dam-reservoir water dynamic interaction was modeled through added mass with neglect of the compressibility of reservoir water. The acceleration histories of incident seismic waves are shown in Fig.6 (incident S waves for stream-wise component and cross-stream component, incident P wave for vertical component). In the model the most fault located apart from the dam heel is also considered with a nonlinear constitutive relation with Dmker-Prager Cap model adopted here. In the fault, the two group material parameters are given out according to the distance from the valley site. In the group 1, the static elastic modulus is 3500MPa, the Poisson ratio is 0.3, the density is 1900N/m^3, the friction coefficient f=1.00, the cohesive force C=0.5MPa. In the group 2, the static elastic modulus is 1400MPa, the Poisson ratio is 0.31, the density is 1900N/m^3, the friction coefficient f=0.85, the cohesive force C=0.35MPa. In order to analysis the effects of the nonlinear behaviors of the

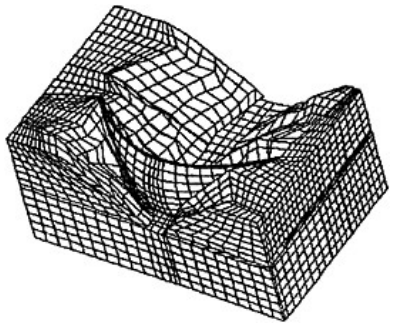

Figure 5. Finite element discrete model of Xiaowan arch.

fault, the two different foundation models were adopted here, the model-1 with the fault of linear behaviors, the model-2 with the fault of nonlinear behaviors.

In the finite element discrete model, the minimum element size is 3m, Δt is determined as 0.0004 second according to the computational requirements given by the formula (8). The stress and displacement fields induced by gravity load, temperature load and hydrostatic load of normal water lever are considered during the calculation process of seismic action.

4.1 *The comparison between the proposed method and the conventional method*

In the conventional method with the massless foundation model the influences of the elasticity of the foundation are considered. Due to neglecting the influences of the mass of the foundation, there are mainly the two shortcomings of no considering the arch dam-foundation dynamic interaction and the phase and amplitude differences of input earthquake motion on dam site along valley in the method. As an example, the seismic stresses of Xiaowan arch dam are compared by the conventional method and the proposed method as follows.

The arch and cantilever peak dynamic stress absolute values at the different heights of the crown cantilever calculated by the proposed method and the conventional method are shown in Table 2 and Table 3. We can see that the peak dynamic stresses obtained by the proposed method with consideration of energy dispersion in infinite foundation through the transmitting boundaries are more less than the ones obtained by the conventional method with the assumptions of a massless foundation with fixed boundaries and uniform input seismic motion along the interface of dam-foundation on an average.

The principal stresses of the upstream and downstream surfaces at the top altitude (1245m) near the abutments are illustrated in Table 4. It can be seen that the maximum principal stresses by the two methods are roughly identical. The minimum principal stress absolute values by the

Table 1. Material constants of the foundation region media (SI units).

Group No.	Density (N/m^3)	Dynamic elastic modulus ($\times 10^{11}$Pa)	Poisson ratio	Group No.	Density (N/m^3)	Dynamic elastic modulus ($\times 10^{11}$Pa)	Poisson ratio
1	2630.00	0.3250	0.2200	12	2630.00	0.2210	0.2600
2	2630.00	0.2600	0.2500	13	2630.00	0.7150	0.3000
3	1900.00	0.4550	0.3000	14	2630.00	0.2990	0.2300
4	1900.00	0.1820	0.3100	15	2630.00	0.3250	0.2200
5	2000.00	0.5070	0.3000	16	2630.00	0.2600	0.2500
6	2630.00	0.1170	0.2650	17	2630.00	0.2860	0.2400
7	1900.00	0.2600	0.3000	18	2630.00	0.3380	0.2100
8	1900.00	0.1326	0.3100	19	2630.00	0.2730	0.2500
9	1900.00	0.3900	0.3500	20	2630.00	0.2470	0.2500
10	1900.00	0.7150	0.3000	21	2630.00	0.2340	0.2500
11	1900.00	0.1040	0.2900				

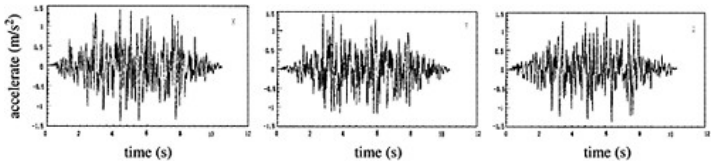

Figure 6. Incident seismic waves of Xiaowan arch dam.

Table 2. Dynamic arch stress of crown cantilever of Xiaowan arch dam (MPa).

Altitude (m)	▽953							
Upstream								
B	4.18	3.47	3.05	2.39	1.83	1.11	0.79	1.25
A	4.70	4.02	3.28	2.53	1.85	0.95	0.51	0.72
Downstream								
B	3.38	2.39	1.62	1.10	0.80	0.77	0.41	0.26
A	3.80	2.88	2.25	1.83	1.27	0.85	0.46	0.29

Table 3. Dynamic cantilever stress of crown cantilever of Xiaowan arch dam (MPa).

Altitude (m)	▽953							
Upstream								
B	1.29	1.86	2.19	2.32	1.92	2.57	3.43	4.82
A	1.32	2.52	2.92	2.77	2.45	2.58	3.52	4.36
Downstream								
B	0.94	2.03	2.26	2.04	1.83	1.51	1.55	1.65
A	1.15	2.21	2.44	2.16	1.87	1.72	2.52	3.09

Table 4. Dynamic principal stresses near the abutments (Mpa).

			Right Abutments	Left Abutments
Upstream surface	Maximum	A	1.82	1.40
		B	1.93	1.13
	Minimum	A	−0.13	−0.12
		B	−1.85	−1.14
Downstream surface	Maximum	A	2.10	1.80
		B	1.49	1.56
	Minimum	A	−0.10	−0.08
		B	−1.53	1.17

Table 5. Nonlinear and Linear Effects of the Fault on Peak Synthetical arch Stress of Crown Cantilever of Xiaowan Arch Dam (MPa).

Altitude (M)	▽953							
Upstream								
Linear Fault	11.45	11.25	10.38	9.04	7.64	5.75	3.64	1.58
Nonlinear Fault	11.61	11.09	10.32	9.17	7.74	5.88	3.70	1.57
Downstream								
Linear Fault	8.42	6.04	4.86	4.18	3.21	2.15	1.32	1.63
Nonlinear Fault	8.77	6.28	4.99	4.20	3.11	1.99	1.24	1.53

proposed method are obviously larger than the ones by the conventional method. A and B represent the results of the conventional method and the proposed method here, respectively.

4.2 *The effects of the fault*

In order to study the effects of the fault with the different mechanical behaviors, the comparison calculations have been carried out for the two foundation models with the fault of linear and nonlinear

Table 6. Nonlinear and linear effects of the fault on peak Synthetical Cantilever Stress of Crown Cantilever of Xiaowan Arch Dam (MPa).

Altitude (M)	▽953							
Upstream								
Linear Fault	2.36	3.64	4.42	4.62	4.72	4.12	3.30	8.59
Nonlinear Fault	2.58	3.87	4.55	4.66	4.77	4.26	3.29	8.52
Downstream								
Linear Fault	1.35	2.79	3.33	3.42	3.70	5.35	9.10	10.26
Nonlinear Fault	1.40	2.79	3.41	3.56	3.79	5.25	8.95	10.11

behaviors. The results are illustrated in Table 5 and Table 6, respectively. It can be seen that with consideration of the nonlinear behaviors of the fault, the influences on the arch and cantilever stresses at the different parts of the upstream and downstream of the crown cantilever are less. It may be reason that the fault located apart from the dam heel is not across the interface between the arch dam and the rock foundation.

5 CONCLUSION

In this paper, a nonlinear seismic response analysis method of arch dam-foundation systems in which the effects of energy radiation in infinite foundation and nonlinear behaviors in local near field media have been considered is proposed by combining the explicit finite element method and the transmitting boundaries. The proposed method has been applied to obtain some results for Xiaowan arch dam, and a comparison of the proposed method and the conventional method was made. Some conclusions as an aid to further understanding the important influences of the foundation model with energy dispersion, local inhomogeneous and nonlinear behaviors on seismic responses of arch dams have some reference for engineers.

Some conclusions for the analysis of seismic responses of Xiaowan arch dam can be drawn as follows:

1. With consideration of the energy dispersion in infinite foundation and the effects of non-uniform motion at dam base along the canyon, the arch and cantilever stresses in the central and upper part of the arch dam are obviously reduced by (20%~40%), and the minimum principal absolute stresses on the upstream and downstream surfaces near the two abutments are significantly increased.
2. The influence of the fault with nonlinear behaviors on the seismic stresses of the arch dam is very little.

ACKNOWLEDGEMENTS

I am grateful to Professor Anil Chopra for his critical reading and very helpful suggestions. This research has been supported by CNSF grant (No. 59739180).

REFERENCES

[1] Clayton, R., and Engquist, B. (1977). “Absorbing Boundary Conditions for Acoustic and Elastic Wave Equations.” *BSSA,* 67(6), 1529–1540.
[2] Clough, R.W., Raphael, J.M., and Mojtahedi, S. (1973). “ADAP-A Computer Program for static and Dynamic Analysis of Arch Dams.” *Report No. EERC 73–14,* Earthquake Engineering Research Center, University of California, Berkeley, California.

[3] Dominguez, J., and Maeso, O. (1993). "Earthquake Analysis of Arch Dams II. Dam-Water-Foundation Interaction." *J. Eng.Mech., ASCE,* 119(3), 513–530.
[4] Dowling, M.J. (1987). "Nonlinear Seismic Analysis of Arch Dams." *Report No. EERL-87/03,* Earthquake Engineering Research Laboratory, California Institute of Technology, Pasadina, California.
[5] Du, X.L., and Xiong, J.G. (1987). "Application of Boundary Element Method to Soil-structure Interaction." *Proc. Int. Sym. on Geomechanics,* Bridges and Structure, Lanzhou, China, 357–366.
[6] Fenves, G.L., Mojthahedi, S., and Reimer, R.B. (1989). "ADAP-88: A Computer Program for Nonlinear Earthquake Analysis of Concrete Arch Dams." *Report No. UCB/EERC-89/12,* Earthquake Engineering Research Center University of California, Berkeley, California.
[7] Fok, K.L., and Chopra, A.K. (1986a). "Earthquake Analysis of Arch Dams Including Dam-Water Interaction, Reservoir Boundary Absorption and Foundation Flexibility." *Earthquake Eng. Struct. Dyn.,* 14(2), 155–184.
[8] Fok, K.L., and Chopra, A.K. (1986c). "Frequency Response Functions for Arch dams: Hydrodynamic and Foundation Flexibility Effects." *Earthquake Eng. Struct. Dyn.,* 14(5), 769–795.
[9] Fok, K.L., and Chopra, A.K. (1986d). "Hydrodynamic and Foundation Flexibility Effects in Earthquake Response of Arch Dams." *J.Struct Eng.,* ASCE, 112, 1810–1828.
[10] Fok, K.L., and Chopra, A.K. (1987). "Water Compressibility in Earthquake Response of Arch Dams." *J. Struct. Eng.,* ASCE, 113(5), 958–975.
[11] Fok, K.L., Hall, J.K., and Chopra, A.K. (1986b). "EACD-3D: A Computer Program for three-dimensional Earthquake Analysis of Concrete Dams." *Report No. UCB/EERC-86/09,* Earthquake Engineering Research Center, University of California, Berkeley, California.
[12] Ghanaat, Y., and Clough, R.W. (1989). "EADAP Enhanced Arch Dam Analysis Program, User's Manual." *Report No. UCB/EERC-89/07,* Earthquake Engineering Research Center, University of California, Berkeley, California.
[13] Hall, J.F., and Chopra, A.K. (1983). "Dynamic Analysis of Arch Dams Including Hydrodynamic Effects." *J. Eng.Mech.,* ASCE, 109(1), 149–167.
[14] Kuo, J.S.H. (1982). "Fluid-Structure Interaction: Added Mass Computations for Incompressible Fluid." *Report No. UCB/EERC-82/09,* Earthquake Engineering Research Center, University of California, Berkeley, California.
[15] Li, X.J., Liao, Z.P., and Du, X.L. (1992). "An Explicit Finite Difference Method for Viscoelastic Dynamic Problem, Earthquake Engineering and Engineering Vibration." 12(4), 74–80 (In Chinese).
[16] Liao, Z.P. (1996a). "An Introduction to Wave Motion Theories in Engineering." Beijing, China, Academic Press, 165–322 (In Chinese).
[17] Liao, Z.P. (1996b). "Extrapolation Non-reflecting Boundary Conditions." *Wave Motion,* 24, 117–138.
[18] Liao, Z.P. (1997). "A decoupling Numerical Simulation of Wave Motion." *Proceedings of the Chinese-Swiss Workshop on Dynamic Soil-Structure Interaction,* Edited by Zhang C.H. and Wolf J.P., Beijing, 125–140.
[19] Liao, Z.P. (1997). "Numerical Simulation of Near-Field Wave Motion." *Advances in Mechanics,* 27(2),, 193–216 (In Chinese).
[20] Liao, Z.P., and Liu, J.B. (1992). "Numerical Instabilities of a Local Transmitting Boundary." *Earthq. Eng. Struct. Dyn.,* 21(1), 65–77.
[21] Liao, Z.P., Wong, H.L., Yang, B.P. and Yuan, Y.F. (1984). "A Transmitting Boundary for the Numerical Simulation of Elastic Wave Propagation." *Soil Dyn, Earthq. Eng.,* 3(4), 174–183.
[22] Lysmer, J., and Kuhlemeyer, R.L. (1969). "Finite Dynamic Model for Infinite Media." *J. Eng. Mech. Div.,* ASCE, 95(4), 859–877.
[23] Maeso, O., and Dominguez, J. (1993). "Earthquake Analysis of Arch Dams, I. Dam-Foundation Interaction." *J. Eng. Mech.,* ASCE, 119(3), 496–512.
[24] Tan, H. and Chopra, A.K. (1995). "Earthquake Analysis of Arch Dams Including Dam-Water-Foundation Rock Interaction." *Earthquake Eng. Struct. Dyn.,* 24(11), 1453–1474.
[25] Tan, H. and Chopra, A.K. (1995). "Dam-Foundation Rock Interaction Effects in Frequency-Response Functions of Arch Dams." *Earthquake Eng. Struct. Dyn.,* 24 (11), 1475–1489.
[26] Wolf, J.P. (1985). "Dynamic Soil-Structure Interaction, Prentice-Hall, Englewood Cliffs." Prentice-Hall, Englewood Cliffs, *NJ.*
[27] Wolf, J.P. (1986). "A Comparison of Time-Domain Transimitting Boundaries." *Earthq. Eng. Struct. Dyn.,* 14(4), 655–673.

New Developments in Dam Engineering—Wieland, Ren & Tan (eds),
© 2004 Taylor & Francis Group, London, ISBN 04 1536 240 7

Nonlinear seismic response analysis of arch dam-foundation systems—Part II*

Xiuli Du
Beijing Lab of Earthquake Engineering and Structural Retrofit, Beijing University of Technology, China
Jin Tu
China Institute of Water Resources and Hydropower Research, China

ABSTRACT: The influences of opening and closing of contactable joints of arch dam and arch dam-foundation rock dynamic interaction on the seismic response analysis of arch dams under strong earthquake are all very obvious. The present some models simulating the contact process of contactable joints used in the seismic response analysis of arch dams, such as Fenves' model and Dowlings' model, are also based on the penalty parameter method, it is trouble that the penalty parameters are determined. In addition, the two effects mentioned above have not yet been considered together in the present seismic response analysis of arch dams, and it is difficult to consider the two effects together by the methods in the frequency domain. Therefore, a combination method in the time domain of the explicit FEM and a transmitting boundary have been proposed for the analysis of the seismic response of arch dams by X.L.Du et al (2000). In this paper, the first effect stated above is studied by introducing a contact force model into the combination method. Through comparing with the results obtained by the model tests on vibration table, the simulation accuracy for contact state between the interfaces of contactable joints by the contact force model is verified. By using a dynamic analysis method the static responses of arch dams is solved, and a combination method is also proposed to calculate the nonlinear responses of arch dams under the actions of static and dynamic load. Finally, some results have been obtained by using this approach for the designed Xiaowan arch dam with maximum height of 292m in china.

1 INTRODUCTION

The fact that the effects of energy radiation in infinite foundation and opening and closing of contactable joints of arch dams are important to the seismic response of arch dams under strong earthquake has become a common view in academic and engineering circles, and many researches have been done and many developments have been archived. Recently, the influences of local topographical and geological conditions, especially faults, cracks etc., on the seismic response of arch dams have been paid attention by X.L.Du et al (2000). The influences of energy radiation in infinite foundation on the seismic response of arch dams were studied by O.Maeso, J.Dominguez (1993), J.Dominguez, O.Maeso (1993), H.Tan and A.K.Chopra (1995a, b) through the combination method of BEM and FEM in frequency domain, which is not suitable for the nonlinear problems and is complicated in calculation. Taking consideration of the effects of faults and cracks existed in near-field foundation on the seismic response of arch dam, X.L.Du et al (2000) studied the non-linear seismic response of arch dam-foundation systems by use of the explicit FEM and a transmitting boundary in time domain. In this way some advantages are very obvious for solving the nonlinear

* Sponsored by National Natural Science Foundation for Distinguished Young Scholar of China, Grant No. 50325826.

problems with large freedom degrees due to the uncoupling feature. As far as the influence of simulation of opening and closing of contactable joints of arch dams on the seismic response of the arch dams during strong earthquake is concerned, some developments have been achieved. D.Row and V.Schricker (1984) proposed a contact element model with two nodes. G.L.Fenves, S.Mojthahedi and R.B.Reimer (1989) used a block contact element model without thickness. M.J.Dowling (1989) presented a three parameter contact model with rotational angle spring, transnational spring and position of it. The models mentioned above are based on the penalty parameter method. J.F.Hall (1996) used a smear crack method for simulating the influences of contactable joints on the seismic response of arch dams, which is suitable for simulating the stress response of arch dams. In this paper, a dynamic contact force model proposed by J.B.Liu, S.Liu and X.L.Du (1999) is used to analysis the seismic responses of arch dams with contactable joints, meanwhile, the energy radiation in infinite foundation and the local topographical and geological feature in near-field foundation are also considered.

2 WAVE MOTION SIMULATION METHOD

2.1 *Calculating of the interior nodes of arch dam-foundation systems*

From the explicit FEM, the motion of equation of j direction at any node i in the discrete model of arch dam-foundation systems can be written as

$$m_i \ddot{u}_{ij} + \sum_{l=1}^{n_e} \sum_{k=1}^{n} c_{ijlk} \dot{u}_{lk} + R_{ij} = F_{ij} \tag{1}$$

Where, m_i is the mass of the node i, $\ddot{u}_{ij}$ is the acceleration of j direction at the node i, $\dot{u}_{ij}$ is the velocity of k direction at some node l which is around the node i and belongs to the same element with the node i, R_{ij} and F_{ij} are the restoring force and external force of j direction at the node i respectively, c_{ijlk} is the damping influence coefficient of k direction at the node l on j direction at the note i, n_e is the nodal number related to the node i, n is the number of freedom degree, R_{ij} may be determined by an elastic-plastic constitution model.

If R_{ij} is an elastic restoring force, it is expressed by

$$R_{ij} = \sum_{l=1}^{n_e} \sum_{k=1}^{n} k_{ijlk} u_{lk} \tag{2}$$

In which, u_{lk} is the displacement of k direction at the node l, k_{ijlk} is the stiffness coefficient of k direction at the node l on j direction at the node i.

Assuming that the damping force of any direction at the node i is only relative to itself velocities at the node i, thus

$$\begin{cases} c_{ijlk} = 0 & l \neq i \\ c_{ijlk} = c_{ij} & l = i \end{cases} \tag{3}$$

When $c_{ij}=c_{ik}=c_i$, the formula (1) may by written as

$$m_i \ddot{u}_{ij} + c_i \dot{u}_{ij} + R_{ij} = F_{ij} \tag{4}$$

It is known that the formula (4) is a special example of the formula (1), this is, when the damping force is only relative to the velocity of the node i and every direction damping coefficient is the the same, there is the formula (4). Substituting the central difference formulations for acceleration and displacement into the formula (4). the explicit integration formula of Eq. (4) can be obtained. Generally, the assumption from the formula (1) to the formula (4) is not reasonable. Thus, an

explicit integration formula can't be obtained by introducing the central difference method. X.J.Li et al (1992) derived a explicit integration formula with the accuracy of 2-order ($O(\Delta t^2)$), it can be expressed as

$$u_{ij}^{t+\Delta t} = \left(F_{ij}^{t} - R_{ij}^{t} - \sum_{l=1}^{n_e} \sum_{k=1}^{n} c_{ijlk} \dot{u}_{lk}^{t} \right) \Delta t^2 / 2m_i + u_{ij}^{t} + \Delta t \cdot \dot{u}_{ij}^{t} \tag{5}$$

$$\dot{u}_{ij}^{t+\Delta t} = \dot{u}_{ij}^{t} + \Delta t \left(F_{ij}^{t+\Delta t} - R_{ij}^{t+\Delta t} + F_{ij}^{t} - R_{ij}^{t} \right) / 2m_i - \left(\sum \sum c_{ijlk} \left(u_{lk}^{t+\Delta t} - u_{lk}^{t} \right) \right) / 2m_i \tag{6}$$

From Rayleigh damping assumption, c_{ijlk} may be written as

$$c_{ijlk} = \alpha m_i + \beta k_{ijlk} \tag{7}$$

Where, α and β are constants decided by experiences.

2.2 *Computing of responses of artificial boundary nodes*

The key of simulation of wave motion of near field is to simulate scattering wave propagation in infinite foundation media. Of course, scattering wave propagation should also satisfy the radiation regularity in the infinite domain. The viscous damping boundary suggested by J.Lysmer and R.L.Kuhlemeyer (1969), the absorbing boundary proposed by R.Clayton and B.Engquist (1977), and the transmitting boundary proposed by Z.P.Liao et al (1984) may simulate the fact not generating reflection wave on the artificial boundaries. The simulation accuracy of the latter two methods may be increased through considering high-order items. It is difficult to obtain the single-side wave motion of equations for general vector wave motion of equations, therefore, the transmitting boundary based on the physical motion regularity of waves proposed by Z.P.Liao et al (1984) is wider than the absorbing boundary set up from the single-side wave motion of equations in adaptability for application of various wave propagation. The three methods mentioned above may be all in the time domain and may be used to solve the response of the artificial boundaries explicitly. Combining them with the explicit FEM is a very important development way for solving the large and complicated nonlinear wave motion problems. Here, the transmitting boundary is used for computing of the motion values at the artificial boundary nodes, the unstable phenomenon of the transmitting boundary are eliminated by introducing the damping in proportion to the stiffness seen in Ref. by Z.P.Liao (1996).

3 DYNAMIC CONTACT FORCE MODEL

A contactable interface S is shown in Fig.l, the two side surfaces of S are called as S^+ and S^-, they are coincident each other, and assuming that S is a smooth curve or curve surface. The finite element nodes between S^+ and S^- are a pair of nodes. The sliding deformation along the direction of interface of the contactable joints is too little to be considered. Hence, the contact process between the surfaces of the contactable joints may be simulated by the contact process between the two nodes of the pairs of nodes simply.

For any pair of nodes, *i* and *i,* the node *i* is located on the side of S^+ and the node *i'* is located on the side of S^-, $\vec{n}$ of normal direction of S^+ is positive. From the formula (5), by neglecting the effects of damping force, the displacement of *j* direction at the node *i* can been written as

$$u_{ij}^{t+\Delta t} = ((F_{ij}^{t} + N_{ij}^{t} + \tau_{ij}^{t}) - R_{ij}^{t}) \Delta t^2 / 2m_i + u_{ij}^{t} + \Delta t \dot{u}_{ij}^{t} \tag{8}$$

In which, N_{ij} and τ_{ij} are a projection of $\vec{\tau}_i$ on *j* direction, respectively.

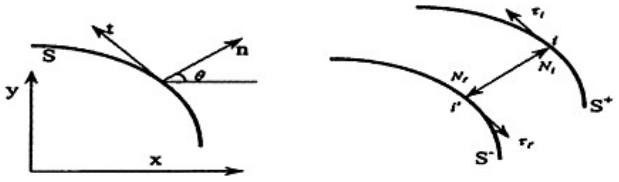

Figure 1. Model with joints and two side of contactable interface.

From the motion of equilibrium equations of *j* direction at the node *i* at time *t,* it can be known that $u_{ij}^{t+\Delta t}$ is unknown. Usually, the formula (8) may be solved by the iteration method. Fortunately, because of the characteristic of the explicit method, the tedious iterative process may be avoided through determining the contact state between the interfaces of the contactable joints at the time *t* while neglecting the damping at the nodes on the interface S.

For convenience to derive, the formula (8) is written as:

$$u_{ij}^{t+\Delta t} = \bar{u}_{ij}^{t+\Delta t} + \Delta u_{ij}^{t+\Delta t} + \Delta v_{ij}^{t+\Delta t} \tag{9}$$

$$\bar{u}_{ij}^{t+\Delta t} = (F_{ij}^{t} - R_{ij}^{t})\Delta t^2 / 2m_i + u_{ij}^{t} + \Delta t \dot{u}_{ij}^{t} \tag{10}$$

$$\Delta u_{ij}^{t+\Delta t} = N_{ij}^{t} / M_i \tag{11}$$

$$\Delta v_{ij}^{t+\Delta t} = \tau_{ij}^{t} / M_i \tag{12}$$

$$M_i = 2m_i / \Delta t^2 \tag{13}$$

Similarly, for the node i' there are the formulas as follow:

$$u_{i'j}^{t+\Delta t} = \bar{u}_{i'j}^{t+\Delta t} + \Delta u_{i'j}^{t+\Delta t} + \Delta v_{i'j}^{t+\Delta t} \tag{14}$$

$$\bar{u}_{i'j}^{t+\Delta t} = (F_{i'j}^{t} - R_{ij}^{t})\Delta t^2 / 2m_{i'} + u_{i'j}^{t} + \Delta t \dot{u}_{i'j}^{t} \tag{15}$$

$$\Delta u_{i'j}^{t+\Delta t} = N_{i'j}^{t} / M_{i'} \tag{16}$$

$$\Delta v_{i'j}^{t+\Delta t} = \tau_{i'j}^{t} / M_{i'} \tag{17}$$

$$M_{i'} = 2m_{i'} / \Delta t^2 \tag{18}$$

$$N_{ij}^{t} = -N_{i'j}^{t} \tag{19}$$

$$\tau_{ij}^{t} = -\tau_{i'j}^{t} \tag{20}$$

Next, the computation methods of τ_{ij}^{t} are introduced, respectively.

3.1 *Computing of* N_{ij}^{t}

N_{ij}^{t} is dependent on the contact state between the interfaces of the contactable joints. By the geometric conditions of not intruding into each other, there is

$$\vec{n}_i^T \cdot (\vec{u}_{i'}^{t+\Delta t} - \vec{u}_i^{t+\Delta t}) = 0 \tag{21}$$

The formula (21) represents the normal contact condition between the pair of the nodes *i* and the node *i'*.

While to satisfy

$$\vec{n}_i^T \cdot (\vec{u}_{i'}^{t+\Delta t} - \vec{u}_i^{t+\Delta t}) \geq 0 \tag{22}$$

The contacting occurs between the nodes *i* and the node *i'*, otherwise, the node *i* and the node *i'* keep separating.

When the separating between the node *i* and the node *i'* occurs, there is

$$N_{ij}^t = N_{i'j}^t = 0 \ , \quad \tau_{ij}^t = \tau_{i'j}^t = 0 \tag{23}$$

$$u_{ij}^{t+\Delta t} = \bar{u}_{ij}^{t+\Delta t} \ , \quad u_{i'j}^{t+\Delta t} = \bar{u}_{ij}^{t+\Delta t} \tag{24}$$

When the contact between the node *i* and the node *i'* occurs, there is the formula (21). Substituting the formula (9) and (14) into the formula (21), there is

$$\vec{n}_i^T \cdot (\vec{\bar{u}}_{i'}^{t+\Delta t} + \Delta\vec{u}_{i'}^{t+\Delta t} + \Delta\vec{v}_{i'}^{t+\Delta t} - \vec{\bar{u}}_i^{t+\Delta t} - \Delta\vec{u}_i^{t+\Delta t} - \Delta\vec{v}_i^{t+\Delta t}) = 0 \tag{25}$$

Because that the displacement of normal direction induced by the tangential force is zero, there exists

$$\vec{n}_i^T \cdot \Delta\vec{v}_i^{t+\Delta t} = \vec{n}_{i'}^T \cdot \Delta\vec{v}_{i'}^{t+\Delta t} = 0 \tag{26}$$

Substituting the formula (26) into the formula (25), there is

$$\vec{n}_i^T \cdot \left(\Delta\vec{u}_i^{t+\Delta t} - \Delta\vec{u}_{i'}^{t+\Delta t}\right) = \vec{n}_i^T \cdot \left(\Delta\vec{\bar{u}}_{i'}^{t+\Delta t} - \Delta\vec{\bar{u}}_i^{t+\Delta t}\right) \tag{27}$$

Let us order

$$\Delta_{1i} = \vec{n}_i^T \cdot \left(\Delta\vec{u}_i^{t+\Delta t} - \Delta\vec{u}_{i'}^{t+\Delta t}\right) = \vec{n}_i^T \cdot \left(\Delta\vec{\bar{u}}_{i'}^{t+\Delta t} - \Delta\vec{\bar{u}}_i^{t+\Delta t}\right) \tag{28}$$

Substituting the formula (11) and (16) into the formula (27) again, there exists

$$\vec{N}_i^t = \left(M_i M_{i'} / (M_i + M_{i'})\right)\Delta_{1i} \cdot \vec{n}_i \tag{29}$$

3.2 *Computing of* τ_{ij}^t

When the contact between the node *i* and the node *i'* occurs, the sliding between the node *i* and the node *i'* along tangential direction may be generated or not be generated. When there is not the relative sliding, the static friction state is generated. When there is the relative sliding, the dynamic friction state is generated. μ_s and μ_d are the static friction coefficient and the dynamic friction coefficient, respectively.

For the static friction state, there is

$$\vec{t}_i^T \cdot \left(\vec{u}_i^{t+\Delta t} - \vec{u}_{i'}^{t+\Delta t}\right) = \vec{t}_i^T \cdot \left(\vec{u}_i^t - \vec{u}_{i'}^t\right) \tag{30}$$

Where, $\vec{t}_i$ is the tangential vector at the node *i* on S^+.

Substituting the formula (9), (14) into the formula (30), there is

$$\vec{t}_i^{\,T}\cdot\left(\vec{\bar{u}}_i^{\,t+\Delta t}+\Delta\vec{u}_i^{\,t+\Delta t}+\Delta\vec{v}_i^{\,t+\Delta t}-\vec{\bar{u}}_{i'}^{\,t+\Delta t}-\Delta\vec{u}_{i'}^{\,t+\Delta t}-\Delta\vec{v}_{i'}^{\,t+\Delta t}\right)=\vec{t}_i\cdot\left(\vec{u}_i^{\,t}-\vec{u}_{i'}^{\,t}\right) \tag{31}$$

Noticing the condition, $\vec{\bar{u}}_i^{\,t+\Delta t})-(\vec{u}_{i'}^{\,t}-\vec{u}_i^{\,t})]$, thus, from the formula (31), we can obtain

$$\vec{t}_i^{\,T}\cdot\left(\Delta\vec{v}_i^{\,t+\Delta t}-\Delta\vec{v}_{i'}^{\,t+\Delta t}\right)=\Delta_{2i} \tag{32}$$

Substituting the formula (12) and (17) into the formula (32), there is

$$\vec{\tau}_i^{\,t}=-\vec{\tau}_{i'}^{\,t}=\left(M_iM_{i'}/(M_i+M_{i'})\right)\Delta_{2i}\cdot\vec{t}_i \tag{33}$$

For the dynamic contact state, there is

$$\left|\vec{\tau}_i^{\,t}\right|=\mu_d\left|\vec{N}_i^{\,t}\right| \tag{34}$$

During the calculation process, it is firstly assumed that the friction state between the node i and the node i' is the same as the former time step. If the friction state at the former time step is static, $\vec{\tau}_i^{\,t}$ can be solved by the formula (33), then, the assumption is examined

$$\left|\vec{\tau}_i^{\,t}\right|\le\mu_s\left|\vec{N}_i^{\,t}\right| \tag{35}$$

If the formula (35) is not satisfied, $\left|\vec{\tau}_i^{\,t}\right|$ is calculated by the formula (34), the sign of $\vec{\tau}_i^{\,t}$ is determined by Δ_{2i}.

If the contact state between the node i and the node i is dynamic, the next sufficient and necessary conditions are observed

$$\text{If } \operatorname{sgn}(\Delta 2i)=1,\ \vec{t}_i^{\,T}\cdot(\vec{u}_i^{\,t+\Delta t}-\vec{u}_{i'}^{\,t+\Delta t})>\vec{t}_i\cdot(\vec{u}_i^{\,t}-\vec{u}_{i'}^{\,t}) \tag{36}$$

$$\text{If } \operatorname{sgn}(\Delta 2i)=-1,\ \vec{t}_i^{\,T}\cdot(\vec{u}_i^{\,t+\Delta t}-\vec{u}_{i'}^{\,t+\Delta t})<\vec{t}_i\cdot(\vec{u}_i^{\,t}-\vec{u}_{i'}^{\,t}) \tag{37}$$

The calculation accuracy of the dynamic contact force model has been verified by the some typical examples with analytic solution case in the research work of J.B.Liu, S.Liu and X.L.Du (1999). In the dynamic contact force model, the equilibrium conditions on mechanics and the contact conditions on geometry are only considered. Therefore, it is also suitable for the contact problems with nonlinear material media.

For three-dimensional problem, S is a curve surface. The tangential sliding direction in the tangential plane at any contact point at time t is unknown. Therefore, the tangential sliding direction at any contact point should firstly be determined, then, the tangential friction force is determined by the same method for two-dimensional problem. The tangential sliding direction at the time t can be determined by the way of neglecting the friction force at the time t.

4 COMPUTING OF THE COMBINATIVE RESPONSES OF ARCH DAM-FOUNDATION SYSTEMS DURING STATIC LOADS AND EARTHQUAKE

Due to the nonlinear effects of contact and material behaviors, the seismic response of arch dams is related to the static response of ones subjected by static loads, such as self-weight, impound water and sediment etc. Therefore, the static response of arch dams should be firstly calculated,

then, the static actions and the static response are taken as the initial conditions for computing of the dynamic response of arch dams. In this paper, a technique of calculating the static responses by the dynamic method has been adopted, in which the static loads are regarded as the step loads exerted at the initial time and the artificial damping are exerted during the step loads.

It is noticed that the scattering wave of propagation in infinite foundation are only treated in the transmitting boundary as the plane waves outgoing through the artificial boundaries, the attenuation phenomenon of outgoing scattering waves in the infinite domain can't be considered in the transmitting boundary. In reality, the constrained effect of the stiffness supplied by the infinite domain for the finite model of the near-field medium is neglected. While the elastic restore behavior of the artificial boundaries of the finite model is needed in order to keep the equilibrium of the calculation model, the transmitting boundary may lead to drift instability. In order to overcome the instability, a constrained artificial boundary on which the elastic coefficients are given by experiences is introduced for computing of the static response of the problem.

5 COMPARISON OF THE DYNAMIC CONTACT FORCE MODEL AND THE TEST OF A SCALE MODEL ON VIBRATION TABLE

To verify the accuracy of simulation of the dynamic contact force model for opening and closing of the contactable joints, the results calculated by the dynamic contact force model are compared with the ones obtained by the test of a scale model with the five stripes of contraction joints of an arch dam with fixed interface assumption between dam and foundation.

The test is carried out on the large vibration table at China Institute of Water Resources and Hydropower Research, the sketch of the 1/292 scale model with the joints of Xiaowan arch dam to be constructed in China is shown in Fig. 2. The finite element model of the scale model has the total element number of 264 and the total nodal number of 396 while without joints on the scale model dam. The average value of the dynamic elastic modulus is 250MPa, the density is 2400N/m^3, in the materials of the scale model dam.

The proposed method in this paper is used for computing the response of the scale model during scale artificial seismic motions with the same motions on the vibration table, in which the self-weight of the scale model and hydrostatic pressure exerted on the dam face are considered and the influence of hydrodynamic pressure is also considered by the way of adding mass. After the scale model of arch dam is cut by thin handsaws to form the joints on it, plaster mortars are backfilled in the saws. Since contracting of plaster mortars, it is not avoidable to generate the initial gaps. Hence, the two kinds of initial condition between the interfaces of the joints, having the initial gaps with 0.02mm (case B) and having no initial gaps (case A) have been considered in the calculation model in this paper. The initial gaps are all taken as 0.02mm from measuring and repetitive trial calculation. It is an average value of estimating.

5.1 *Opening and closing of the joints*

The comparison of the calculation results and the test results for the maximum opening degree of the joints is shown in Table 1 for the lower water level. It can be seen that the calculation results taking consideration of the initial gaps are more close to the test results, which means that it is necessary

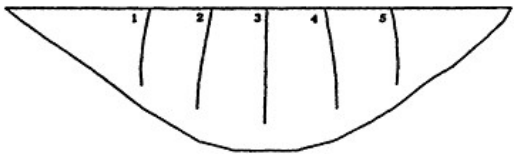

Figure 2. Location of transverse joints in the scale model.

Table 1. The maximal opening degree of transverse joints (mm).

	Position	Joint 1	Joint 2	Joint 3	Joint 4	Joint 5
CaseA	US	0.015	0.025	0.028	0.013	0.025
	DS	0.010	0.019	0.024	0.010	0.022
CaseB	US	0.054	0.096	0.072	0.093	0.078
	DS	0.057	0.099	0.071	0.088	0.076
Experiment	US	0.063	0.065	0.076	0.039	0.087
	DS	–	–	0.070	–	0.120

Note: US=upstream surface, DS=downstream surface.

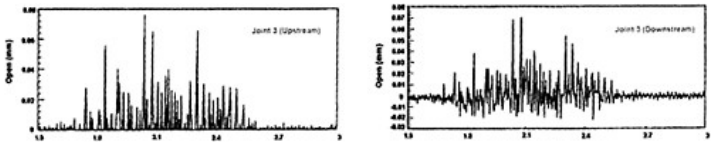

Figure 3. Opening and closing degree histories on top of upstream and downstream at joint 3 (Experiment).

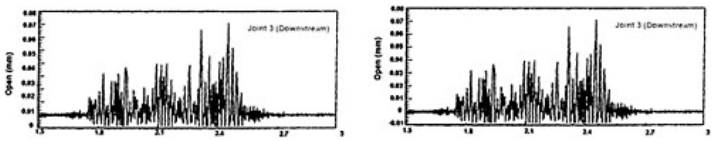

Figure 4. Opening and closing degree histories on top of upstream and downstream at Joint 3 (Calculation).

to establish the methods in which the initial gaps can be considered. It is noticed that the degree of opening and closing are defined as the difference between the real calculation gap and the initial gap in this paper, positive values represent opening, negative values represent closing. The opening and closing degree histories on the top of upstream and downstream at the joint 3 by the test on the vibration table and by computing by the dynamic contact model are shown in Fig. 3 and Fig. 4, respectively. It can be seen in Fig. 3 and Fig. 4 that there are positive and negative values on the opening and closing degree histories on the top of upstream and downstream at the joint 3, but, due to the huge initial gap in the case B, the contact between the pair of nodes at the joint do not occur. Of course, the precise prediction of the initial gaps is very important for practical engineering problem.

5.2 *Comparison of stress*

The comparison of the cantilever peak stresses at the different heights of the crown cantilever is shown in Table 2. We can see that the influences of the initial gaps on the maximum stresses are less. The results obtained by the two calculation models in this paper are approximately coincided with the results obtained by the tests.

Table 2. The cantilever peak dynamic stresses at different height of the crown cantilever (MPa).

Scale	Altitude	∇87 cm	∇63 cm	∇35 cm	∇12 cm
Case A	US	0.007	0.010	–	–
	DS	0.005	0.016	–	–
Case B	US	0.013	0.013	0.012	0.013
	DS	0.011	0.017	0.013	0.010
Test	US	0.009	0.010	0.011	0.010
	DS	0.011	0.024	0.007	0.006

Note: US=upstream surface, DS=downstream surface, low level water condition.

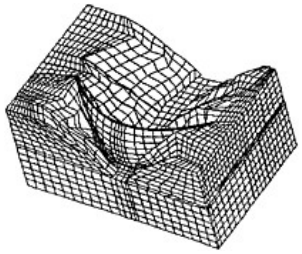

Figure 5. Finite element discrete model of Xiaowan arch dam-foundation.

Table 3. The material constants of the foundation region (SI units).

Group no.	Density (N/m^3)	Dynamic elastic modulus ($\times 10^{11}$Pa)	Poisson ratio	Group no.	Density (N/m^3)	Dynamic elastic modulus ($\times 10^{11}$Pa)	Poisson ratio
1	2630.00	0.3250	0.2200	12	2630.00	0.2210	0.2600
2	2630.00	0.2600	0.2500	13	2630.00	0.7150	0.3000
3	1900.00	0.4550	0.3000	14	2630.00	0.2990	0.2300
4	1900.00	0.1820	0.3100	15	2630.00	0.3250	0.2200
5	2000.00	0.5070	0.3000	16	2630.00	0.2600	0.2500
6	2630.00	0.1170	0.2650	17	2630.00	0.2860	0.2400
7	1900.00	0.2600	0.3000	18	2630.00	0.3380	0.2100
8	1900.00	0.1326	0.3100	19	2630.00	0.2730	0.2500
9	1900.00	0.3900	0.3500	20	2630.00	0.2470	0.2500
10	1900.00	0.7150	0.3000	21	2630.00	0.2340	0.2500
11	1900.00	0.1040	0.2900				

6 ANALYSIS EXAMPLE OF THE SEISMIC RESPONSE OF AN ARCH DAM WITH JOINTS

Xiaowan arch dam with height of 292m will be located at the upper reach of the Lanchuang River in Yunnan province in China, the design earthquake intensity is IX degree with a horizontal peak acceleration of 0.290 g, while the vertical peak acceleration is 2/3 of the horizontal one. The geological and topographical conditions of the site are very complicated. The finite element model containing the arch dam and the foundation region to be calculated has the total element number of 20 107 and the total nodal number of 22 878 while without joints on the dam, and there are the material kinds of 22 in the model. The sketch of the finite element discrete model except the artificial boundary region is shown in Fig. 5. The altitude at the bottom of the dam is 953m, the altitude at the top of the dam is 1245m. The arc length at the top of the dam is 935m, the thickness at the top of the dam is 12m, and the thickness at the bottom of the dam is 73m. The dynamic elastic modulus is 27.3GPa, the density is 2400N/m^3, and the Poisson ratio is 0.189, in the concrete of dam body. The material constants in the foundation region are shown in Table 3. Here, the dynamic elastic modulus is 1.3 times the static elastic modulus.

The acceleration histories of incident seismic waves are shown in Fig. 6 (incident S wave for stream-wise component and cross-stream component, incident P wave for vertical component).

The four different kind of analytical cases considered here are illustrated in Table 4. For simplicity, the influence of arch dam-reservoir water dynamic interaction was modeled through added

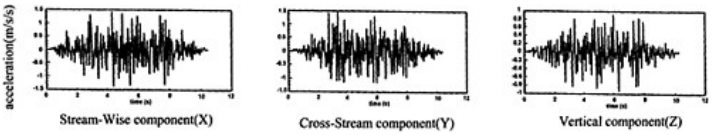

Figure 6. Incident seismic waves of Xiaowan arch dam.

Table 4. The four different kinds of analytical cases.

Case	Water level	Strips of joints	Bottom crack
A	Low water level	5	Without
B	Low water level	Without	Without
C	Normal water level	5	With
D	Normal water level	5	Without

Table 5. The influences of transverse joints to stresses of X direction in main location (MPa).

			Dam crest			Mid dam	Dam bottom
	Location		Left abutment	Crown	Right abutment	Crown	Crown
Maximum	CaseA	US	1.21	0.76	−0.17	−1.69	0.44
		DS	0.42	0.75	0.63	−0.18	–
	CaseB	US	1.20	2.20	−0.28	−1.45	0.30
		DS	0.47	3.10	0.68	−0.50	–
Minimum	CaseA	US	−0.33	−6.10	−1.88	−6.23	−1.96
		DS	−0.43	−5.69	−0.18	−2.86	–
	CaseB	us	−0.20	−6.02	−1.76	−5.96	−2.05
		DS	−0.42	−5.70	−0.14	−2.80	–

Note: US=upstream surface, DS=downstream surface.

mass with neglect of the compressibility of reservoir water. The influences of gravity load, temperature load, hydrostatic load, and sediment load have been considered. Five strips of joints are set up in the arch dam for Case A, C, D.

6.1 *The influence of the contraction joints on the seismic response of the arch dam*

The comparison of X direction stresses and Z direction stresses at the different heights on the surface of the arch dam with joints and without joints are shown in Table 5 and Table 6, respectively. It can be seen that the effect of the joints make X direction stresses (approximate arch stresses) lower obviously, Z direction stress (Cantilever stresses) increase roughly.

Table 7 shows the maximum opening degree of the joints for the case A, the total relative slid between a pair of nodes at the top of upstream and downstream of the middle joints are illustrated in Fig. 7 and Fig. 8 respectively.

Table 8 shows the maximum dynamic stresses at the different heights on the surface of the crown cantilever given by the paper method. The maximum opening on the upstream and downstream surfaces of the joints are shown in Table 9.

Table 6. The influences of transverse joints to stress of Z direction in main location (MPa).

Location			Dam crest			Mid dam	Dam bottom
			Left abutment	Crown	Right abutment	Crown	Crown
Maximum	Case A	US	0.16	1.07	−0.67	−1.40	2.75
		DS	−0.58	0.31	0.07	−0.79	–
	Case B	US	0.15	1.10	−0.64	−1.30	2.50
		DS	−0.58	0.05	0.10	−0.75	–
Minimum	Case A	US	−1.08	−2.01	−2.17	−5.25	−6.99
		DS	−1.36	−0.93	−0.47	−2.68	–
	Case B	us	−1.00	−1.60	−2.12	−5.25	−7.20
		DS	−1.35	−0.84	−0.47	−2.75	–

Note: US=upstream surface, DS=downstream surface.

Table 7. The maximal opening degree of joints (mm).

Location	Joint 1	Joint 2	Joint 3	Joint 4	Joint 5
US	4.06	4.67	11.05	3.56	8.65
DS	5.05	3.65	10.25	4.22	6.21

Note: US=upstream surface, DS=downstream surface.

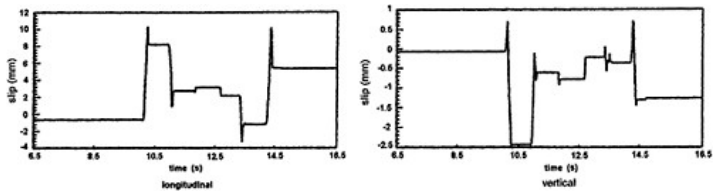

Figure 7. Tangential summating slippage histories of upstream surface of joint 3 (Case A).

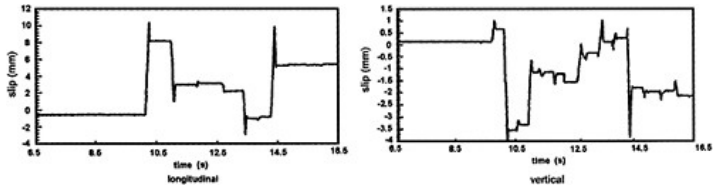

Figure 8. Tangential summating slippage histories of downstream surface of joint 3 (Case A).

Table 8. Effects of radiant damping to maximal dynamic stress (MPa).

Altitude (m)	Location	Arch stress	Cantilever stress
▽1210	US	3.186	1.176
	DS	1.900	0.827
▽1170	US	3.034	1.559
	DS	2.008	1.654
▽1130	US	2.579	1.750
	DS	1.761	1.958
▽1090	US	2.024	1.664
	DS	1.450	1.774
▽1050	US	1.441	1.646
	DS	1.215	1.361
▽1010	US	0.883	2.055
	DS	0.960	1.347
▽975	US	0.818	3.460
	DS	0.639	1.382
▽953	US	1.409	5.196
	DS	0.359	1.378

Note: US=upstream surface, DS=downstream surface.

Table 9. Effects of radiant damping to the opening degree of joints (mm).

Case	Location	Joint 1	Joint 2	Joint 3	Joint 4	Joint 5
A	US	5.05	3.65	10.25	4.22	6.21
	DS	4.06	4.67	11.05	3.56	8.65
B	US	0.70	0.00	0.00	0.09	0.75
	DS	0.47	0.67	0.98	0.04	0.00

Note: US=upstream surface, DS=downstream surface.

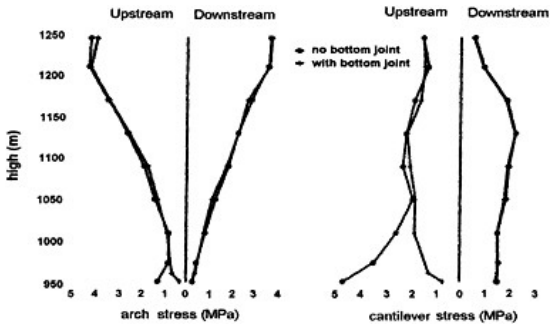

Figure 9. Arch and cantilever stresses at crown of arch dam with and without bottom crack.

6.2 *The influence of bottom joint on the seismic response of arch dam*

A strip of joint at the bottom of dam is set up for comparison of the influences at the bottom joint on the seismic responses of arch dams. The comparison of dynamic arch and cantilever stresses at the crown of the arch dam with bottom joint and without bottom joint for normal level of water is shown in Fig. 9. It can be seen that the bottom joint makes the cantilever dynamic stresses lower obviously.

7 CONCLUSION

In this paper, a calculation method has been established for solving the nonlinear seismic responses of the arch dam-foundation systems by combining of the dynamic contact force model with the explicit FEM, in which a dynamic method is presented for solving of the static response of the systems, and a combinative calculation of the static and dynamic response of the arch dams with joints has also been proposed. By comparing with the results of the vibration table test, the simulation accuracy of the dynamic contact force model for the contact state between joint interfaces is verified. As an example, the influences of contraction joints and bottom joints on the seismic response of Xiaowan arch dam are calculated by the use of the proposed method in this paper, and some results are obtained for reference to engineering design.

The study was supported by CNSF grant (No. 59739180).

REFERENCES

[1] Clayton, R., and Engquist, B. (1977). "Absorbing Boundary Conditions for Acoustic and Elastic Wave Equations." *BSSA,* 67(6), 1529–1540.
[2] Dominguez, J., and Maeso, O. (1993). "Earthquake Analysis of Arch Dams, II, Dam-Water-Foundation Interaction." *J. Eng. Mech., ASCE,* 119(3), 513–530.
[3] Dowling, M.J. (1987). "Nonlinear Seismic Analysis of Arch Dams." *Report No. EERL-87/03,* Earthquake Engineering Research Laboratory, California Institute of Technology, Pasadena, California.
[4] Du, X.L., Zhang, Y.H., and Zhang, B.Y. "Nonlinear Seismic Response Analysis of Arch Dam-Foundation Systems Part I." has been tentatively approved for Journal of Engineering Mechanics, ASCE.
[5] Fenves, G.L., Mojthahedi, S., and Reimer, P.B. (1989). "ADAD-88: A Computer Program for Nonlinear Earthquake Analysis of Concrete Arch Dams." *Report No. UCB/EERC-89/12,* Earthquake Engineering Research Center University of California, Berkeley, California.
[6] Hall, J.F. (1996). "Efficient Nonlinear Seismic Analysis of Arch Dams-Smeared Crack Arch Dam Analysis." *California Institute of Technology, Pasadena, California,* April.
[7] Li, X.J., Liao, Z.R, and Du, X.L. (1992). "An Explicit Finite Difference Method for Viscoelastic Dynamic Problem." *Earthquake Engineering and Engineering Vibration,* 12(4), 74–80.
[8] Liao, Z.P. (1996). "An Introduction to Wave Motion Theories in Engineering." *Academic Press,* Beijing, China, 165–322.
[9] Liao, Z.R, Wong, H.L., Yang, B.R, and Yuan, Y.F. (1984)."A Transmitting Boundary for the Numerical Simulation of Elastic Wave Propagation." *Soil Dyn, Earthq. Eng.,* 3(4), 174–183.
[10] Liu, J.B., Liu, S., and Du, X.L. (1999). "A Method for the Analysis of Dynamic Response of Structure Containing Non-Smooth contactable Interfaces." *ACTA Mechanic Sinica* (English Series), 15(1), 63–72.
[11] Lysmer, J., and Kuhlemeyer, R.L. (1969). "Finite Dynamic Model for Infinite Media." *J. Eng. Mech. Div.,* ASCE, 95(4), 859–877.
[12] Maeso, O., and Dominguez, J. (1993). "Earthquake Analysis of Arch Dams, II, Dam-Water-Foundation Interaction." *J. Eng. Mech.,* ASCE, 119(3), 496–512.
[13] Row, D., and Schricker, V (1984). "Seismic Analysis of Structures With Localized Nonlinearities." *Proc. 8th WCEE,* San Francisco, California.
[14] Tan, H., and Chopra, A.K. (1995a). "Earthquake Analysis of Arch Dams Including Dam-Water-Foundation Rock Interaction." *Earthquake Eng. Struct. Dyn.* 24 (11), 1453–1474.
[15] Tan, H., and Chopra, A.K. (1995b). "Dam-Foundation Rock Interaction Effects in Frequency-Response Function of Arch Dams." *Earthquake Eng. Struct. Dyn.* 24 (11), 1475–1489.

This page intentionally left blank.

New Developments in Dam Engineering—Wieland, Ren & Tan (eds),
© 2004 Taylor& Francis Group, London, ISBN 04 1536 240 7

Design and study of Jinggangchong double curvature stone masonry arch dam

Duan Shaohui
Hohai University, Nanjing, Jiangsu, P.R. China
Mid-South Design & Research Institutefor Hydroelectric Projects, Changsha, P.R. China

ABSTRACT: Jinggangchong stone masonry arch dam is a double curvature arch dam with multiple arc-centers. It is 92m high with a thickness-height ratio of 0.261, a maximum arc angle of 99.9 degrees, and a maximum arc radius of 160m. The shape of the arch dam was optimized by ADCAD developed by MSDI. The structure analysis shows that the stress meets the norm requirement, and the capability of over loading isn't high. The abutment stability just meets the norm requirement, so drainage tunnels in abutments are set up to reduce the permeated water stress in abutments, and some observation apparatuses are buried to observe the deflection of abutment. The dam body is composed of impervious concrete face slab on upstream face, cement and rag masonry on downstream face, and fine-aggregate concrete and stone masonry in between. The dam body is divided per 72m by a grouted transverse joint, and the face slab is divided per 18m by a 0.8m wide gap. Cement grouting in the joints and swell concrete filling in the gaps were performed in low temperature season. The tests of stones with rust and immerged cracks at the laboratory and concrete masonry with the stones at the quarry site were carried out. Through design and test research, narrow outlet energy dissipators are taken for the surface bays.

1 GENERAL

Jinggangchong Hydropower Project, located in Jinggangchong City in Jiangxi Province, was developed mainly for power generation, concurrently with multipurpose benefits of water supply and tourism. The hydro complex consists of a masonry double curvature arch dam, a power intake system including a 4, 245.15m long headrace tunnel and 804.55m long penstock, and a powerhouse. The power plant has an installed capacity of 12MW, a design water head of 284m. The catchment area above the damsite is 48 km^2, and the reservoir, with all-year-around regulation property, has a total storage capacity of $18.70\times10^6m^3$.

The Jinggangchong masonry double curvature arch dam, located at the east side of the main peak of Jinggangshan mountains, is a four arc-centered double curvature stone masonry dam. The foundation for the arch dam is blastosandstone, silicarenite and sandy slate of Ordovician System O_2. The arch dam has a crest elevation of 730.00m, a maximum height of 92m, an arch crown cantilever thickness of 5m for the crest and 24m for the base, a thickness-height ratio of 0.261, a maximum arc angle of 99.9°, and a maximum arc radius of 160m. An emptying outlet is provided at the arch crown, which is controlled by a cone valve. The water flow from the valve is dissipated by spraying. A surface bay with a net width of 8m, with narrow slot and flip bucket dissipater, is provided at each side of the arch crown. The power intake for the water diversion type plant is located on the left of the arch dam. A foundation grouting gallery and a dam drainage and inspection gallery are provided respectively at the bottom and middle dam body. The layout of the arch dam is shown in Fig. 1. The project commenced construction in September 1989 and the first

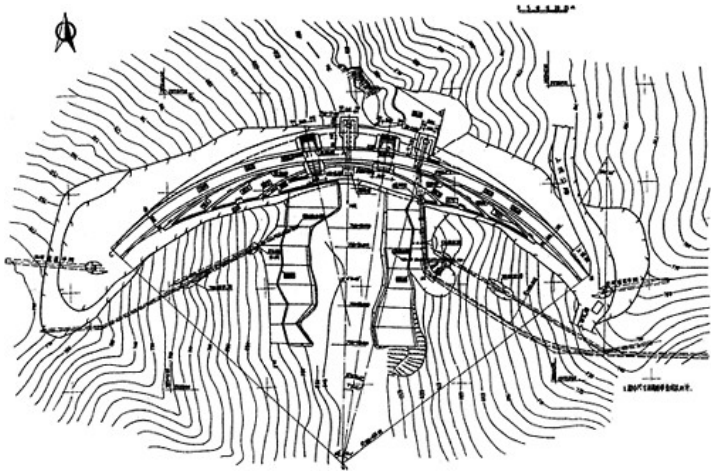

Figure 1. Layout of Jinggangchong dam.

unit was put into operation in October 1992. However, due to difficulty in fund raising, the arch dam was not completed until the end of 1998.

Design and study for the Jinggangchong double-curvature arch dam covers configuration design and structural analysis, abutment stability analysis, masonry arch dam joint design, rock material and masonry, and flood discharge and energy dissipation.

2 CONFIGURATION DESIGN AND STRUCTURAL ANALYSIS

2.1 *Configuration design*

(1) *Restraint condition and assumption*

Stress control conditions for dam body: the maximum compression stress of the dam is not greater than 4.0MPa and the maximum tensile stress is not greater than 1.2MPa for the bottom of the central cantilever and 1.0MPa for the other locations.

Geometrical restraint conditions: the intersection angle of the arch ring and the contour of available bed rock on both banks shall not be less than 30° and the maximum overhang of the cantilever shall not be greater than 0.26.

Assumption of dam material: For the convenience of calculation of the double-curved stone masonry arch dam, at the conditions in 1989, the material is assumed isotropic linear elastic material.

(2) *Configuration design*

The optimized design for the configuration of the dam body has been carried out by ADCAD programme developed by MSDI. The 4-arc-centered double-curved arch dam body has been adopted for the Project. During construction period, based on the practical excavation for the dam foundation, some modifications have been made for the configuration of the dam body. The final configuration is: 4-arc-centered arch with different thickness at El. 638m–680m; single-centered arch with equal thickness at El. 680m–730m; the maximum arc angle is 99.9° (at dam crest), with

a corresponding outer radius of 160m and inner radius of 155m; the minimum arc angle is 26° (at bottom of dam) with a corresponding outer radius of 62.3m and inner radius of 38.3m; the crown cantilever is 92m high with a crest thickness of 5m and a base thickness of 24m; the formula for the upstream and downstream faces of the crown cantilever are $Tu=154.104-(27544.6975-(Z-61.617)^2)^{0.5}$, $Td=186.253-(33578.84471-(Z-26.948)^2)^{0.5}$ respectively; the ratio of thickness and height of the arch dam is 0.261 and the max. overhang of the cantilever is 0.252.

2.2 *Structural analysis*

(1) *Basic data*

Mechanical properties of materials for dam and its foundation: the physical mechanical property of the dam body is as follows: overall density 23kN/m^3, overall elastic modulus 10.5GPa, Poisson's ratio 0.20, linear expansion coefficient 8.0×10^{-6}°C and heat diffusion coefficient 0.1m^2/d; The performance of dam foundation's deformation is as follows: elastic modulus 5.0−12.0 GPa and Poisson's ratio 0.35−0.26.

The seismic intensity: the basic seismic intensity in the Project area is less than VI.

(2) *Load combinations*

Basic combination:

Operating condition 1: hydrostatic pressure+design normal temperature drop load+dead weight+sediment pressure as the dam is at normal pool level.

Operating condition 2: hydrostatic pressure+design normal temperature drop load+dead weight+sediment pressure as the dam is at the minimum operating level.

Special combination:

Operating condition 3: hydrostatic pressure+design normal temperature drop load+dead weight+sediment pressure as the dam is at check flood level.

(3) *Stress calculation*

Multiple arch-cantilever method and finite element method have been used for stress calculation of this double-curved arch dam. The calculation programme of the multiple arch-cantilever method has adopted the stress calculation programme ADTRLC-90 of multi-centered archcantilever load distribution method of the ADCAD system. The calculation result obtained by multiple arch-cantilever method indicates that the radial displacements at dam crest would develop towards downstream for the 3 operating conditions with a corresponding value of 71.8mm, 10.7mm and 48.0mm respectively. Under the action of hydraulic pressure and temperature load, the law that dam displacement varies with the operating condition is reasonable.

The principal stresses of the dam under the 3 different operating conditions are all within the allowable limit. The max. compression stress is 3.98MPa (operating condition 1), close to the allowable stress 4.0MPa. The max. tensile stress is-1.00MPa (operating condition 3), equal to the allowable tensile stress. From the point of view of stress distribution pattern of dam face, the changes of the principal stress and its orientation are even and regular. Operating conditions 1 and 3 are the controlling conditions for the configuration and stress of the dam. The extreme principal stresses of dam body at the main effects of hydraulic load and temperature load (σ_{1max}=3.98MPa, σ_{1min}=−1.00MPa) are below 1/3 of dam height. The hydraulic load is small for operating condition 2. Under this condition, the stress distribution of the dam body is represented mainly by the effect of the temperature drop load. Therefore, the tensile stress zone has appeared along the arch on the upstream and downstream faces of the upper part of the arch dam, but the tensile stresses are not great.

(4) *Overload test for structure model of dam body*

In consideration that Jinggangchong stone masonry double-curved arch dam is 92m high and it was the highest of its kind in China at the beginning of construction design stage and it is also the highest double-curved masonry arch dam existing. Therefore, the overload test has been done for

the integral structure model of brittle material by MSDI to understand its overload capability and failure mechanism. The test model is 1:200 on scale. The simulated thickness of the foundation is 1.2 times of the dam height. The simulated length of the downstream river channel is 2 times of the dam height. The simulated horizontal depth of mountain on either bank is over 100m. Fault F9 and the loosened argillaceous interbedded layers PN9 and PNIO in the right abutment have been simulated. The material for dam body is simulated with single-overall elasticity modulus. The model material is gypsum. The factor of temperature load has not been considered in the overload test.

The overload test has indicated that the potential failure of the arch dam including 3 stages, i.e., tensile failure, compressive failure and bearing capacity failure. The coefficients of overload obtained from the test are k1=1.6 for tensile failure, k2=4.1 for compressive failure and k3=5.1 for bearing capability failure. These have indicated that the overload capacity of the arch dam is not high.

3 STABILITY ANALYSIS FOR ARCH ABUTMENTS

The Jinggangchong arch dam lies on the rock formation of silicarenite and blasto-sandstone intercalated with sandy slate of Ordovician System O_2, and in the east limb of an overturned anticline, with an attitude of 350°–355°/NE∠50°. The construction of the stable boundary planes of the abutments is basically identical, with that on the right bank more developed. The strata at the left abutment are of counter-inclined laminar structure. The left crown arch end is about 60m away from the open face of a valley slope at the downstream river bend, so the rock mass of the left abutment is slightly thin. However, no boundary conditions constituting a threat to the stability against sliding of the left abutment has been found. The calculation results show that rigid block of the left abutment is of sufficient stability against sliding. The strata at the right abutment is of bedding structure. The natural slope at the right abutment is over 40 degrees. There exists a gully downstream the right abutment, and the right crown arch end is about 60m away from the open face of the gully. The gully at El. 641m is 170m away from the dam axis. The rigid block consisting of faults, bedding planes and low-angle joints is very unfavorable for the stability against sliding of the right abutment. Based on the requirements of the specifications, the safety factor against sliding k1 of abutments shall meet the following: k1≥3.0 for basic combination, and k1≥2.5 for special combination. The stability against sliding of the right abutment is presented as follows.

3.1 *Boundary conditions*

(1) *Boundary conditions of rigid block of abutment*

The boundary conditions of rigid block of the right abutment of Jinggangchong arch dam are as follows:

Side fracture plane: A continuous side fracture plane composed of faulted bedding planes, fracture interbeds and fracture sludging interbeds exists with an attitude of 355°/NE∠50°. Mechanical parameters of the side fracture plane are taken from the average values of those of the bedding planes and faulted bedding planes (τ=0.4a+0.15MPa).

Base fracture plane: The base fracture plane is composed of a set of low-angle joints which are very developed, with an attitude of 50°–75°/NW∠20°–35°, and filled with redeposited loess and katamorphic feldspath (accounting for 30% of the total area), fresh feldspath, quartz or closed plane (accounting for 40%), and fresh rock (accounting for 30%). The mechanical parameters are taken from a communication rate of low-angle joints of 30% for the planes above El. 670m (τ=0.76a+0.79MPa); and from a communication rate of low-angle joints of 50% for the planes below El. 670m (τ=0.667σ+0.61MPa).

Upstream pull-apart plane: The parting plane is composed of F9 and high-dip-angle joints. Fault F9 runs through the reservoir and upstream side of the crown arch end, with an attitude of 60°–85°/SE(NW)∠45°–85°.

Downstream open face: The downstream open face is composed of the gully and F12 (50°/ SE∠85°). F12, consisting of crushed block, is 15–40m away from the dam site, with a fracture zone width of 0.2–0.5m.

(2) *Seepage pressure*

The seepage pressure is considered based on the net head of the reservoir, and is reduced based on section load, with a coefficient of reduction of 0.4.

3.2 *Computation and analysis on stability of arch abutments*

The abutment stability analysis program ADSTAB of the ADCAD system has been employed for the stability calculation for the arch abutments of the Jinggangchong arch dam. The program was prepared with rigid block limit equilibrium method. The arch abutment was subjected to stability computation by two methods, i.e., two-dimensional stability analysis, and three-dimensional integral stability analysis (vector algebraic method). The load transferred from the arch end to the abutment was taken from the computation results by ring-cantilever load distribution method. The arch end action under the operating condition 1 (normal pool level+temperature decrease) and operating condition 3 (check flood level+temperature rise) was adopted to conduct stability analysis for the arch abutments. The computation results indicate that K1 for the rigid block below E1. 664m (obtained by the method of two-dimensional stability calculation) and below E1. 651m (obtained by the method of three-dimensional integral stability calculation) where F12 is the downstream open face can not meet the requirements of specifications. In case the downstream gully is the open face, k1=3.05 for operating condition 1 and k1=2.99 for operating condition 3, meeting the stability requirements. F12 consists of crushed block, and joints are dense along some sections of the fault, with low compressibility. F12 and the downstream rock mass can provide some counter force for the abutment rigid block to resist sliding. The computation results of stability against sliding of the abutment with F12 as the downstream open face indicate that there is still some safety margin, but it is not sufficient to justify the stability of the abutment. The synthetic assessment concludes that the right arch abutment is stable, but with low safety margin.

In view of the low safety margin of the arch abutments, the following three safety measures were designed to take for the arch abutments: 1) six drainage tunnels (three in each bank) were arranged respectively at El. 650m, 670m & 700m in the left and right banks 31 to 53m downstream of the dam axis so as to lower the seepage pressure at the arch abutments and improve the stability against sliding; 2) eleven observation holes were arranged at the two arch abutments (5 at the left abutment and 6 at the right abutment) to timely understand the variation of the ground water level and guide the safe operation of the arch dam; and 3) six displacement gauges were designed to arrange at the right arch abutment to monitor the displacement of the right arch abutment. However, due to fund shortage, the displacement gauges have not been arranged yet.

4 STRUCTURE AND JOINT DESIGN FOR THE ARCH DAM

4.1 *Dam structure*

A 2m-thick concrete bed was provided above the foundation surface of the arch dam. The concrete face slab is 0.8–3.0m thick (with a corresponding elevation of 730–640m), consisting of Φ12 reinforcement mesh with a mesh size of 0.15m×0.15m and C20 concrete. Granite rag (with a thickness of 0.3–0.6m) with MIO mortar was provided on the dam downstream side. The placement technology was: laying two pieces of granite rags along the horizontal direction of dam axis then laying one piece along the vertical direction of the dam axis. C15 fine-aggregate concrete and rubble were placed in the middle part of the dam body and the rubble were mostly fresh Granite and partly weakly-weathered silicarenite. $\Phi 22/m^2$ connecting dowel bar was provided between the upstream face slab and the rubble masonry. A drain hole curtain was arranged in the location 2m far away from the concrete face slab inside the masonry with a drain hole interval of 3m. The seepage is drained out of the dam body through the foundation-grouting galley and the drainage and inspection galley at El. 685m.

4.2 *Joint design*

The joint and block design for previous masonry arch dam was as follows: slots were arranged in the dam, with the slots on upper and lower layers staggered, which was unfavorable for the construction progress. With the consideration of the requirements of continuous raising of dam body and the reliable connection with the upstream concrete slab joints, grouting transverse joints (totally 3) were arranged with an interval of 72m along the dam axis after some studies on constitution of masonry materials and masonry construction technology were carried out. A 0.8mwide slot was provided on the concrete face slab at every 18m interval, totally 11 slots arranged. The transverse joint in the dam joined the transverse joint on the slab to form an integrity. The grouting technology of using plastic pipe withdrawing method to ascend and distribute grout was firstly employed for masonry arch dam in the design. The grouting operation for transverse joint to form an arch and swell concrete backfilling in the slot of the face slab were carried out in low temperature season. The joint design has accelerated the construction progress, and enabled the dam body to raise continuously and be free from the adverse impacts of slot backfilling operation, thus ensuring that the first unit of the power station was put into operation on time. Although the work suspension, down time and slow construction progress frequently occurred due to studies on the stone quarry and transportation problem, the dam body was raised by 63m during the period from January 1991 when concrete bed commenced to September 1992.

5 TESTS AND STUDIES ON STONE MATERIALS AND MASONRY OF DAM BODY

Selection of source of stone materials was critical to the high stone masonry arch dam. According to the design requirements, the allowable compression stress was up to 4MPa. In the preliminary design stage, the Xiazhuang limestone quarry, 13.5km far away from the dam site, was selected as the quarry for the project; but in the examination stage for the preliminary design, a quarry nearby the dam was required to select, therefore the Xianfoqiao silicarenite and siltstone quarry, 3km far away from the dam site, finally was selected as the quarry in the supplementary stage for preliminary design. Although the rolled concrete aggregate from the rock materials of this quarry could meet the requirements, the rock was deeply weathered and stripping of the unavailable rocks was great. In addition, the joint fissure of rock was very developed, with weathered joint plane, and the size, shape and quality of the block stones were not ideal for the masonry. In the detailed design stage, uniaxial ultimate compressive strength test, weathered joint plane laboratory test and large masonry in-situ compression test were carried out on the rock materials of the Xianfoqiao quarry. The wet and dry compressive strength tests were carried out according to different combinations with obvious blind joints, unobvious blind joints and different stressed direction for the uniaxial ultimate compressive strength test. The saturation compressive strength was the minimum value (77.6MPa) in case the stressed direction was oblique to the joint plane with a skew angle of (30°−45°); it was the medium value (89.5MPa) in case the stressed direction was parallel to the joint plane; and it was the maximum value (105.8MPa) in case the stressed direction was normal to the joint plane, which indicated that the existence of blind joint would decrease rock strength by no more than 27%. The weathered joint plane laboratory test indicated that the values f’ and c’ of rust joint plane decreased by 7% and 22% respectively as compared to those free of rust, which indicated that the rust had obvious adverse impacts on the bonding strength between the joint plane and the concrete. The size of the specimen for in-situ masonry compressive strength test was 800mm×800mm×800mm, with the same laying technology and joint between blocks as that of the masonry of the dam body. Strongly weathered rock with iron rust joint plane was selected for the test. The tests indicated that the masonry’ strength can reach or exceed the strength grade of the fine-aggregate concrete C15, but the test results could not reflect the changes in bonding strength between the iron rust joint plane and the concrete under long-term seepage action. According to the above mentioned test results and consultants’ comments, a great quantity of strongly-weathered rock materials in Xiafoqiao quarry could not be used for the masonry. The rock materials in Xiazhuang quarry was also abandoned due to low block rate and content of magnesium oxide obtained from blasting test. Finally, the dam was built with the following rock materials: weakly-weathered silicarenite selected from dam foundation clearing for the lower part of the dam, granite from downstream Granite rag quarry (45km far away from the dam site) for the dam body from the lower part to 2/3 dam height, and rock materials from the Xianfoqiao quarry partially for the part above 2/3 dam height.

6 STUDY ON FLOOD DISCHARGE AND ENERGY DISSIPATION

In the preliminary design stage, it was proposed to provide two overflowing surface bays, which have equal width all the way (with a net width of 8.0m, and a radial gate height of 5.0m) on either side of the arch crown 20m away from the crown. The weir crest elevation was 722.5m, and two flip buckets with equal height was employed for the energy dissipation. A secondary dam was proposed to build at the downstream riverbed for auxiliary dissipation. In the detailed design stage, with the consideration of the narrow riverbed at the dam site, bedding plane and shallow creeping mass on the right bank as well as stability safety of the right abutment of the arch dam, it was considered in the design to make the two deflecting flows jump to the center of the river as far as possible and stagger them longitudinally along the river flow direction, so as to avoid considerable scoured pit and consequently avoid affecting the stability of the right abutment. On the basis of design, study and optimization by hydraulic tests, a dissipater combined with differential flip-buckets plus narrow outlets was employed for the two surface bays. The flip buckets (with equal height) of the left and right surface bays was changed to have different elevations as 710.218m and 704.974m respectively; 2 surface bays with equal width was changed to narrow outlet dissipater, where the width of the left and right surface bay at the corresponding flip bucket was narrowed from the original 8m to 6.25m and 4.45m respectively. After cancellation of the secondary dam and optimization of the dissipater, 2 deflecting nappes are staggered along the river flow direction and sprays evenly down into the river. Strong return flow field would exist in the stilling basin formed by the original secondary dam and there would be a zone with large flow velocity immediately behind the secondary dam (14m/s). After cancellation of the secondary dam, as the downstream river channel has a large gradient, up to 4.9%, such problems as strong returning flow field and the high velocity zone were completely resolved. Operation over the years indicates that the narrow outlet and flip bucket dissipater functions fairly well.

REFERENCES

1. SL25–91, *Design Specifications for Stone Masonry Dams;*
2. SD145–85, *Design Specifications for ConcreteArch Dams (Tentative);*
3. SD120–84, *Specifications for Construction Technology of Stone Masonry Dams (Tentative);*
4. SDJ341–89, *Design Specifications for Spillways;*
5. East China Institute for Hydraulic Engineering, Sichuan Provincial Electric Power Bureau, and Guangxi University, *Design of Stone Masonry Dam;*
6. Bureau of Reclamation, USA, *Design of Arch Dams;*
7. East China Institute for Hydraulic Engineering, *Handbook of Hydraulic Engineering (Volume 6)—Water Release Structures and Dam Passing Structures;*
8. Duan Shaohui, *Design and Test Study on Flood Discharge Dissipation for Jinggangchong Stone Masonry Double Curvature Arch Dam, Masonry Dam Technology, Issue 2 of 1992*.

This page intentionally left blank.

New Developments in Dam Engineering—Wieland, Ren & Tan (eds),
© 2004 Taylor & Francis Group, London, ISBN 04 1536 240 7

Study on seismic safety performance of Longtan high gravity RCC dam

Feng Shurong[1,2], Xiao Feng[1] & Ou Hongguang[1]
[1]*Mid-South Design and Research Institute for Hydroelectric Projects, Changsha, Hunan, P.R. China*
[2]*College of Civil Engineering, Hehai University, Nanjing, Jiangsu, P.R. China*

ABSTRACT: Longtan Hydropower Project has a high gravity RCC (roller-compacted concrete) dam with a maximum height of 216.5m. It is to be constructed in two stages and the dam height in Stage I is 196m. The study on the seismic safety performance of the dam is carried out mainly by Dynamic Material Mechanical Approach and Dynamic Finite Element Approach. Dynamic Non-linear Finite Element Analysis based on strain-rate-related concrete constitution and seismic safety performance analysis based on Discontinuous Deformation Approach are also used. The study findings indicate that Longtan dam has comparatively good seismic safety performance and be capable of considerably overloading.

1 PROJECT DESCRIPTION AND LAYOUT

Longtan Hydropower Project (HPP) is located on the upper Hongshui River. It is designed with a normal pool level of 400m and to be constructed in two stages. In the first stage it will have a normal pool level of 375m. Nine units, of which seven will be installed in the first stage, with a total installed capacity of 5400MW, are to be installed. The project buildings consist of a dam, a spillway, a power system and a navigation structure.

The dam is a gravity RCC dam, with a maximum dam height of 192m and a crest elevation of 382m in the first stage and a maximum dam height of 216.5m and a crest elevation of 406.50m in the second stage. The dam consists of 35 dam blocks. In accordance with the features of the dam structure and layout, the typical dam sections are the highest spillway dam section, the highest water retaining dam section, the low level outlet dam section, the elevator shaft dam section, unit 1 intake dam section, unit 7 intake dam section, the delta turning dam section, the navigation dam section etc. This paper only introduces the findings of research on seismic safety performance of the spillway dam section in the middle of the riverbed. The spillway section is shown in Figure 1.

2 SEISMIC DESIGN STANDARD AND ANALYSIS APPROACHES

The Longtan damsite is located in a comparatively stable massif, belonging to a weak seismic circumstances. In accordance with the review and approval of China Earthquake Administration, both the basic seismic intensity and the potential reservoir-inducing seismic intensity are 7 degrees. As specified in *Seismic Design Specifications for Hydraulic Structures* (DL5073-2000), the seismic design for Longtan Dam shall be classified as Class A, for which the design earthquake intensity shall be the basic seismic degree plus one degree, and shall be designed with an earthquake intensity of 8 degrees. The basis for dam seismic design shall be determined by a monographic study on seismic hazard. The probability level of the seismic acceleration representative value for

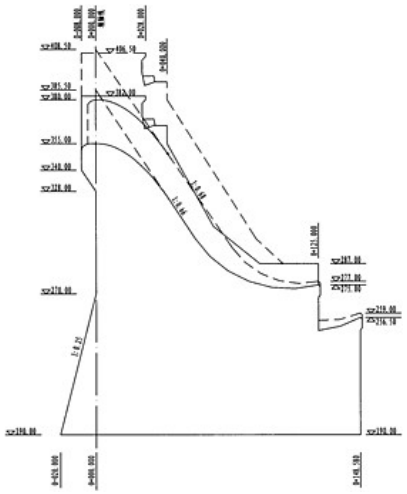

Figure 1. Spilway section.

dam design shall take the exceedance probability within the basic period of 100 years, $\mathbf{P}_{100}$, which is equal to 0.02.

The study on seismic safety performance is done mainly by analysis using Dynamic Material Mechanical Approach and Dynamic Finite Element Approach, and also by Dynamic Non-linear Finite Element Analysis based on Strain-Rate-Related Concrete Constitution and Seismic Safety Performance Analysis based on Discontinuous Deformation Approach.

The combinations of actions used for the dam seismic safety performance analysis mainly consider two occasional cases as only the earthquake and the normal pool level plus the earthquake. The actions effecting on the spillway dam section consist of gravity, static water pressure, uplift, sediment pressure, wave pressure, acting force of the radial gate hinge and the earthquake.

Except for the conventional concrete for the foundation cushion, the dam crest and locations where conventional concrete is necessary by the structural requirements, RCC shall be used at all the locations where RCC construction can be done. Generally, the dam is of RCC in full height and full section.

In dynamic calculation, the dynamic tensile strength and dynamic elastic modulus of the concrete increase by 30% in comparison with the static standard values and the dynamic tensile strength of the concrete takes a value of 10% of the dynamic compressive strength.

3 ANALYSIS BY MECHANICAL DYNAMIC METHOD OF MATERIALS

A principle of probabilistic ultimate status design is followed. Check is done with ultimate status of the bearing capacity by using design expression of ultimate status of itemized factors. The dynamic approach used is vibration resolution response spectrum approach.

Design expression: $\gamma_o \cdot \psi \cdot s(\cdot) \leq R(\cdot)/\gamma_d$

γ_o – structural importance factor;

ψ – design case factor of earthquake situation;

γ_d – tructural factor;

$s(\cdot)$ – action function;

$R(\cdot)$ – resisting function under ultimate compressive strength status (or ultimate anti-sliding stability status);

Table 1. Check calculation results of ultimate bearing capacity status of downstream compressive strength of spillway dam section (design expression: $\gamma_o \cdot \psi \cdot S(\cdot) \leq R(\cdot)/\gamma_d$) (Unit: MPa).

El. of calculated section (m)	Section of stage I			Section of stage II		
	$\gamma_o \cdot \psi \cdot S(\cdot)$	$R(\cdot)/\gamma_d$	Acceptability	$\gamma_o \cdot \psi \cdot S(\cdot)$	$R(\cdot)/\gamma_d$	Acceptability
190	4.448	12.333	acceptable	5.798	12.333	acceptable
230	2.753	9.533	acceptable	1.844	9.533	acceptable
270	5.383	9.533	acceptable	5.921	9.533	acceptable
342	3.209	6.533	acceptable	3.089	6.533	acceptable

Table 2. Check calculation results of ultimate anti-sliding stability status of lift joints of spillway dam section (design expression: $\gamma_o \cdot \psi \cdot S(\cdot) \leq R(\cdot)/\gamma_d$) (Unit: kN).

El. of calculated section (m)	Section in stage I			Section in stage II		
	$\gamma_o \cdot \psi \cdot S(\cdot)$	$R(\cdot)/\gamma_d$	Acceptability	$\gamma_o \cdot \psi \cdot S(\cdot)$	$R(\cdot)/\gamma_d$	Acceptability
190	242.837	544.540	acceptable	291.224	618.512	acceptable
230	175.043	219.494	acceptable	152.716	307.580	acceptable
270	83.584	147.197	acceptable	117.823	203.822	acceptable
342	10.933	44.206	acceptable	30.856	52.907	acceptable

The analysis findings on the ultimate status of compressive strength and anti-sliding stability of the foundation construction face and the internal lift joints of the spillway dam section are shown in the following Table 1 and Table 2:

In order to analyze the sensitivity of the dam anti-sliding stability impacted by the dam foundation anti-shear reference under an earthquake case, it is considered to reduce the anti-shear reference of the foundation construction joint by 20%. The review results indicate that the stability of the construction foundation plane against sliding can still meet the requirements.

4 ANALYSIS BY DYNAMIC FINITE ELEMENT APPROACH

The dynamic seismic analysis of the spillway dam section uses vibration resolution and response spectrum approach (VRRSA) and timescale dynamic analysis approach (TDA). In the vibration resolution and response spectrum approach the seismic effects are applied separately in a direction along the water flow (forward direction) and a direction opposite to the water flow (reverse direction). The timescale curves used for TDA are one artificial seismic wave produced by the design response spectrum and 2 measured Koyna seismic waves. The coordinates system for calculation takes the horizontal water flow direction as the X axis positive and the vertical upward as the Y axis positive.

4.1 *Vibration Resolution and Response Spectrum Method (VRRSM)*

The displacements of the characteristic dam points under the dynamic and static combined actions are shown in Table 3.

The Calculation indicates:

1) The displacement of the dam body mainly appear as vertical displacement and horizontal displacement along the river direction. The horizontal displacement of the dam body is larger under forward seismic action and the vertical displacement is larger under reverse seismic action;

Table 3. Displacements of characteristic dam points of spillway dam section under normal pool level + earthquake case (Unit: cm).

Time period	Seismic direction	Upstream crest face		Upstream slope turning point		Dam heel		Dam toe	
		Horizontal displacement	Vertical displacement	Horizontal displacement	Vertical displacement	Horizontal displacement	Vertical displacement	Horizontal displacement	Vertical displacement
Stage I	Forward	9.44	−1.15	5.01	−1.67	2.34	−0.90	1.82	−2.62
	Reverse	1.97	−4.62	2.47	−3.68	1.41	−2.03	0.92	−3.56
Stage II (After heightening)	Forward	9.89	2.14	6.08	−1.88	2.76	−0.97	2.19	−3.18
	Reverse	−1.16	−1.82	3.36	−4.01	1.78	−2.18	1.23	−4.23
Constructed in one time	Forward	13.22	−0.98	6.35	−1.68	2.82	−0.85	2.26	−3.30
	Reverse	4.25	−4.95	3.66	−3.77	1.87	−2.04	1.32	−4.32

Table 4. Stress values of characteristic lift joints of spillway dam section under normal pool level + earthquake (Unit, MPa).

Time period	Seismic action direction	Foundation construction face		Initial RCC lift		Lift joint at El. 250m		Lift joint at El. 270m	
		Maximum positive stress σ_y	Maximum shear stress τ_{xy}	Maximum positive stress σ_y	Maximum shear stress τ_{xy}	Maximum positive stress σ_y	Maximum shear stress τ_{xy}	Maximum positive stress σ_y	Maximum shear stress τ_{xy}
Stage I	Forward	2.25	3.63	1.02	2.77	2.06	2.28	1.50	2.4
	Reverse	0.197	2.15	−1.57	1.03	0.197	1.13	−0.2	1.13
Stage II (after heightening)	Forward	1.05	4.19	0.18	3.44	0.10	2.70	1.20	2.30
	Reverse	−2.5	2.75	−2.0	2.17	−0.15	1.59	−0.50	1.10
Constructed in one time	Forward	2.80	4.57	2.32	3.52	2.32	2.33	1.60	2.92
	Reverse	−2.10	2.84	−1.85	2.24	0.404	1.57	−0.70	1.90

2) Under the reverse seismic action, the horizontal displacement in Stage I and in construction in one time increases along with the dam height, and reaches the maximum value in the upper middle dam, the vertical displacement distribution shows a increasing trend along with the dam height, and reaches the maximum value at the dam top;

3) Under the forward seismic action, in Stage I and in construction in one time the horizontal displacement increases along with the dam height, and reaches the maximum value in the top of the dam, the maximum vertical displacement occurs close to the downstream. In Stage II (after heightening) the maximum displacement occurs at the elevation of the dam crest of Stage I, the horizontal displacement is up to 11cm at the elevation of the dam crest of Stage I, and only 9.89cm at the dam crest of Stage II. The vertical displacement is 2.14cm (upward) at the dam crest of Stage II and −4.06cm (downward) at the downstream face of Stage I.

The stresses of the typical dam lift joints are shown in Table 4.

The calculation indicates:

Both the maximum normal stress and the maximum shear stress of the typical lift joints occur under the forward seismic action. Except for some local stress concentration zones, maximum normal stress value of each lift joint is not very large. Generally, the maximum shear stress of each lift joint decreases gradually inward from the dam face, and the shear stress gradient has considerable variation close to the dam face and gradually slows down inward the dam. Therefore, under

Table 5. Dynamic stress values of characteristic points and typical lift joints of spillway dam section (calculation results by timescale dynamic approach) (Unit: MPa).

Location	Stage I		Stage II (after heightening)		Construction in one time	
	Max. stress	Min. stress	Max. stress	Min. stress	Max. stress	Min. stress
Primary stress at upstream face of crest	2.16	−1.98	2.33	−2.75	2.33	−2.75
Primary stress at dam heel	4.31	−4.66	5.56	−4.67	5.56	−4.67
Primary stress at dam toe	3.15	−2.86	2.98	−2.84	2.98	−2.84
Construction foundation plane						
Maximum normal stress	3.2	−3.2	2.62	2.62	2.62	2.62
τ_{xy}	2.0	−1.4	1.8	1.8	1.8	1.8
Initial RCC lift						
Maximum normal stress	3.0	−3.0	3.2	3.2	3.2	3.2
τ_{xy}	0.9	−0.9	1.1	1.1	1.1	1.1
Lift at El. 250m						
Maximum normal stress	1.4	−2.0	1.5	1.5	1.5	1.5
τ_{xy}	0.6	−0.8	0.5	0.5	0.5	0.5
Lift as El. 270m						
Maximum normal stress	2.5	−2.0	2.3	2.3	2.3	2.3
τ_{xy}	0.9	−0.8	0.7	0.7	0.7	0.7

dynamic actions, the shear stress may exceed the shear strength in some locations (mainly close to the upstream and downstream faces), however, the scope is very small, and the total shear strength of the entire lift joint still exceeds the shear stress and the anti-sliding requirements for lift joints can be met.

4.2 *Timescale dynamic analysis*

The dynamic displacements of characteristic dam points obtained by calculation using Timescale Dynamic Analysis matches those of the calculation results by VRRSA. The calculation results indicate that the displacements within the dam follows the deformation law of a gravity dam, the horizontal displacement increases gradually with the dam height, the maximum horizontal displacement occurs at the top of the dam; the maximum vertical displacement occurs at the upstream crest face.

The dynamic stress values of characteristic dam points and typical lift joints under various operating cases, obtained by calculation of using Timescale Dynamic Approach are shown in Table 5.

The calculation indicates:

1) Analysis from distribution of maximum primary stress: In addition to the stress concentration at the dam heel and toe, tensile stress concentration zone of maximum positive primary stress also occurs close to the abutment wall turning point, where the tensile stress in Stage I is up to some 4.0 MPa, and the tensile stress in Stage II (after heightening) and in construction in one time is up to some 3.0MPa; compressive stress concentration zone of maximum negative primary stress occurs close to the abutment wall turning point, where the compressive stress in Stage I is up to some 2.0 MPa, and the compressive stress in Stage II (after heightening) and in construction in one time is up to some 0.3 MPa.
2) Analysis from distribution of minimum primary stress: In addition to stress concentration at the dam heel and toe, tensile stress concentration zone of minimum positive primary stress also occurs close to the abutment wall turning point, where the tensile stress in Stage I is up to some

2.0MPa, and the tensile stress in Stage II (after heightening) and in construction in one time is up to some 0.3MPa; compressive stress concentration zone of minimum negative primary stress occurs close to the abutment wall turning point, where the compressive stress in Stage I is up to some 4.0MPa, and the compressive stress in Stage II (after heightening) and in construction in one time is up to some 3.0MPa.

3) After superimposition of the stress generated by the static load, most of tensile stress values within the dam decrease in a large degree. Only the tensile stress at the dam heel increases by some, and certain tensile stress occurs close to the upstream turning point.

5 OTHER DYNAMIC ANALYSIS

5.1 *Dynamic non-linear finite element analysis based on strain-rate-related concrete constitution*

Seismic analysis based on the linear elastic model cannot reflect the seismic safety performance of the dam in an all-round way. Due to the influence of high stress and stress concentration at the dam heel and toe, the materials are in a non-linear status. Some sections subject to high stress may have cracks, which results in redistribution of stress. Meanwhile, under the action of earthquake, the dam is under various strain rate and historical strain conditions at different locations, so the strength and stiffness of different locations will change accordingly. Consequently, it is indispensable to consider the influence of materials' dynamic features in seismic analysis of the dam.

Deformation features of concrete is treated by stage according to the status of loaded concrete:

(1) Under low stress and unloading situations, materials, treated as being elastic, have continuous, harmonious and isotropic features;
(2) When the stress rises to a certain degree, materials feature in non-linear isotropy;
(3) When the stress continues to increase up to 70% of the compressive strength, materials feature in non-linear orthotropy owing to the development of microfissuring inside concrete;
(4) Materials are in a softened state when the compressive stress exceeds compressive strength;
(5) As the tensile stress exceeds tensile strength, cracks occur at right angle to principal stress and materials are orthotropic.

The computation uses the model of elasticity and plasticity and variable damage (based on strain-rate-related concrete) proposed by Dalian University of Technology. Following factors were considered in computation: (1) Influence of strain rate on concrete stress-strain curve (strength and stiffness); (2) Effects of loading and unloading; (3) Difference of being subject to tensile or compressive force.

Main results of analysis

Under the action of static forces and earthquake load, the maximum horizontal displacement of cross-sections in Stage I and in construction in one time, which is about 10 (13.7)cm, occurs at the dam crest, of which 6.5 (6.8)cm is caused by the earthquake load alone, and the relative displacement of crest to dam base is about 5.7 (6.0)cm. The maximum vertical displacement of dam body is 4.9(6.0)cm, the relative displacement of crest to dam base about 2(3)cm.

Compressive stress is the dominant horizontal stress acting on dam body. During the earthquake, the maximum horizontal tensile stress in Stage I and in construction in one time occurs at the dam heel, which is about 0.1 (0.2) MPa; and the maximum tensile stress around the dam heel, which is less than 1MPa, is at the rock face at the dam bottom close to the dam heel; The maximum compressive stress on the dam body occurs at the dam toe, which is some 4.3(4.8) MPa. The stress at the turning point of lower middle section of the guide wall is quite high but decreases quickly inwards the dam with the large gradient.

Under the combined action of static and dynamic loads, the maximum vertical tensile stress in Stage I and in construction in one time, up to about 1.1 (0.6) MPa, occurs at the middle of the upstream face. There is also some 0.5 (0.47) MPa of tensile stress on the inclined plane of upper

middle section of the guide wall. The maximum vertical compressive stress, which is about 6.8 (8.9) MPa, occurs at the dam toe.

The strain rate under earthquake has a high magnitude, 10^{-3} level, at the dam heel and the middle part of downstream face of dam body, and has a low magnitude, 10^{-4} level, inside the dam, at the upstream face and dam toe. That indicates the dynamic concrete strength and module at those positions raise only a little.

As for the damage, damage of the whole dam body caused by compressive stress is as small as about 2~3% (3~4%). Damage caused by compressive stress is most serious at dam toe, up to 6.8% (10%), and is about 3.0% (5.0%) at the middle of the guide wall. Under the action of design earthquake wave, the whole dam has no damage. Only except the small cracks occurring at the dam heel, damage caused by tensile stress develops into the foundation, so the most serious situation is at the dam bottom around the dam heel. It is the development of fissures and cracks of the rock at the dam bottom around the dam heel that relieves the tensile stress at the dam heel.

Under the action of design earthquake, the shear stress for RCC lift joints on the lower middle part of dam body, especially at the downstream face, is relatively high. Whereas the normal positive stress is always of compressive stress, so the demands of shear strength can be satisfied and no shear yield will occur. The normal positive stress for lift joints on the upper middle part of dam body includes tensile stress of small magnitude, and shear stress of lift joints is very small. Therefore, it can be ensured that no lift joints have shear yield.

5.2 *Seismic safety performance analysis of spillway dam based on discontinuous deformation method*

Since Longtan Dam is of RCC gravity type, discontinuous deformation may occur in the lift joints and different zones of material. By employing coupling method of Discontinuous Deformation Analysis (DDA) and Finite Element Method (FEM), dynamic computation was conducted on the deformation and stability of spillway dam section to verify the rationality of taking RCC as a continuous medium in the linear elastic finite element analysis under design earthquake motion action. Meanwhile, preliminary analysis was conducted on the seismic safety performance and overload potential of the dam.

Coupling Method of DDA and FEM is a method that divides the blocks in DDA by finite element mesh and describes the displacement field and stress field inside the blocks through finite element, with the movement of blocks and the contact between the blocks being simulated by DDA. The Coupling Method combines well the advantages of DDA and FEM because it can improve the precision of stress field in the blocks through good simulation on the complicated deformation of blocks and can simulate the discontinuous deformation among blocks.

Peak earthquake accelerations of 0.2g, 0.4g, 0.6g, and 0.8g were considered in computation. The calculation is for the cross-sections of Stage I. The four input earthquake waves are Longtan artificial, Xiluodu artificial, Koyna and El-Centro respectively. 0.01s is taken as time step, 0.0016 as stiffness damping, and 2.2 as quality damping.

Under the action of design acceleration, points at datum plane, El. 270m, and other planes are in an adhesive state during the whole computed period, and there is no sliding between the RCC lift joints.

A tensile stress zone occurs on the upstream face at El. 326m, with a maximum tensile stress of 2–3MPa. However, the zone is quite small and the acting time is very short, so the whole lift joint is still in a stable state.

Consequently, under the action of design earthquake motion, the continuous medium model can rationally reflect the response to earthquake.

Overload capacity and failure pattern of the dam

For the sake of studying the overload capacity and failure pattern of the dam, dynamic dam responses to the four earthquake waves were calculated under peak earthquake accelerations of 0.4g, 0.6g, and 0.8g. The displacement-duration curves at dam crest and El. 270m are shown in Fig. 2.

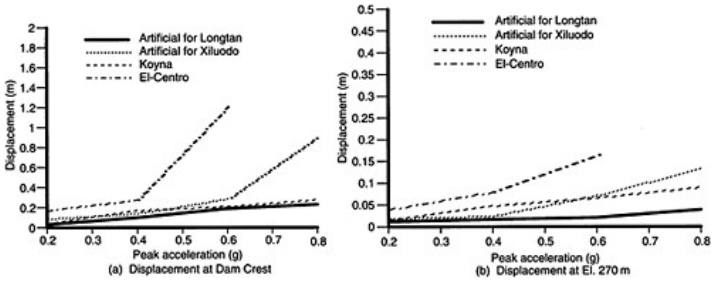

Figure 2. Comparison on dam displacements at various earthquake motion inputs.

It can be seen in Fig. 2 that under design earthquake motion the dynamic reactions of dam body is basically linear elastic to various wave inputs and no big sliding occurs between the RCC lift joints; At peak accelerations of 0.4g and 0.6g, some RCC lift joints on the upper part of the dam have slight sliding. The loss of cohesive force for the sliding planes results in the drop of stability against sliding. The maximum horizontal displacement on the dam crest is up to 10cm and 19cm respectively. However, in general, the dam maintains its integrity and thus the basic functions of the dam can be ensured.

Since El-Centro wave has more low-frequency components, it brings on quite large displacement of the dam. According to the comparison on the dam displacement with different earthquake motion input, the earthquake motion input greatly affects the dynamic responses and failure mode of the dam. The failure of the dam occurs mainly at the RCC lift joints at the upper middle section of the dam. Under the joint action of upstream hydrostatic pressure and earthquake motion, the sliding upper dam blocks gradually slide towards downstream and finally will cause dam failure.

6 CONCLUSIONS

(1) The analysis on the basic type of Longtan dam by dynamic material mechanical method shows that the stress and stability of the dam construction foundation joint and typical lift joints can satisfy the requirements under the joint action of normal pool level and earthquake, and both the stress and the stability are controlled by the cross-sections of Stage II.

(2) Linear elastic finite element analysis on the spillway dam section indicates:

(a) Displacement distribution rules: Horizontal displacement increases upwards along the dam height and vertical displacement increases along the water flow direction. Normally, the maximum horizontal and vertical displacements occur on the upstream face of the dam crest. The maximum displacement in Stage II after heightening will occur at the crest of Stage I instead of that of Stage II, and the displacement at joints of fresh and old concretes is discontinuous.

(b) As for the stress distribution, the stress on the dam body and datum rises greatly under the action of earthquake, and stress concentration occurs at the dam toe and heel but decays quickly at vicinity, Superposed by static loads, the dam heel is subject to large tensile stress, which does not reach the curtain line and will not damage the impervious curtain. In addition, since earthquake action is instantaneous, once the stress on bedrock at the dam heel exceeds the tensile strength and therein slight fissures develop, the dynamic stress at the dam heel will reduce significantly. That will not affect the safety of the dam as a whole.

(c) The point of gradient change at El. 270m and other sharp figure transition positions are subject to stress concentration. Superposed by static stress, a vertical tensile stress zone occurs cross to the point of gradient change at El. 270m and the dam section upper to it.

(d) Spillway dam section: The guide wall, located at the diffluent point of high and low sills, is subject to a certain stress concentration with a stress of 3MPa. Through superposition of maximum dynamic and static principal stresses, the point of gradient change of guide wall has stress concentration to a large extent, and a long tensile stress zone exists at the whole guide wall. Consequently, such measures as enhancing reinforcement shall be taken at the joints between the guide walls and between the guide wall and the spillway face.

Analysis on the spillway dam section by Coupling Method of DDA and FEM shows:

(a) The maximum tensile stress of the spillway dam section occurs at the rock face on the bottom of the reservoir cross to the dam heel. Tensile stress develops to the foundation and the dam body itself has almost no damage due to tensile stress. The middle part of upstream dam face and the upper part of the guide wall have tensile stress of small magnitude; which usually does not exceed the concrete tensile strength. After earthquake damage of a certain degree caused by compressive stress occurs at the dam toe and the lowest RCC lift joint.

(b) Through seismic safety performance analysis based on discontinuous deformation method, when different earthquake waves are input at design acceleration, the dynamic responses of the spillway dam section is generally linearly elastic and the lift joints are in a stable state. When the peak acceleration is raised to 0.4g and 0.6g, some RCC lift joints in the upper middle dam have slight sliding, but the integrity of the dam can still be maintained. That shows the dam body is capable of considerable overloading.

In conclusion, Longtan dam has fairly good seismic safety performance as a whole under the action of design earthquake. Although stress concentration occurs at the dam heel, toe, and sharp figure transition positions, a tensile stress zone occurs at the upstream and downstream faces of dam body, and the dam body will have cracks and shear failure partially, the failure is in a shallow area and the dynamic stress will be released quickly once the failure occurs. The integral dam safety will not be affected. It is in favor of further improving the dam performance against earthquake to take anti-crack measures partially such as improving the tensile strength of concrete and furnishing a certain number of anti-crack reinforcement.

REFERENCE

[1] Lin Gao, Zhou Jing, Chen Jianyun etc., FEM Computation on Spillway of Longtan Hydropower Project [M], School of Civil and Hydraulic Engineering, Dalian University of Technology, 2002.

This page intentionally left blank.

New Developments in Dam Engineering—Wieland, Ren & Tan (eds),
© 2004 Taylor& Francis Group, London, ISBN 04 1536 240 7

Seepage parameters back analysis for dam foundation based on bionics algorithm

Wei Gao
Department of Civil Engineering, Wuhan Polytechnic University, P.R.China

ABSTRACT: The seepage of dam foundation is very important for dam stability. But selection the seepage parameters is a very hard task. The back analysis is a practical method to solve this problem. But back analysis of seepage parameters for dam foundation is a complicated optimum problem. To solve this problem, there exist a lot of shortcomings to use traditional optimum methods, and also genetic algorithm. So, in this paper, a more suitable bionics algorithm that is called immunized evolutionary programming is used to solve this problem. At last, this new back analysis method is verified by a typical engineering example.

1 INTRODUCTION

The seepage of dam foundation is very important for dam stability. But the reliability of seepage computation relay mainly on seepage parameters. So, selection the suitable seepage parameters is a very important task in seepage computation. Nowadays, the most direct method to select the seepage parameters is site test that is based on statistics and the cubic law. This method is very easy to use, but its precision is very low. Because the distribution of fractures in dam foundation is very complicated, the measured fracture parameters from the outcrop and the borehole are not the typical parameters of fractures. And the seepage parameters computed with the cubic law is the direct proportion to the cube of the fracture space, so the little error of fracture space will lead to big error of seepage parameters. Also there are many other test methods to determine the seepage parameters, but the parameters decided by those methods can only describe the fractures near the testing site. So a few site testing can not get the seepage parameters which describes the whole dam foundation, while a large numbers of site testing will need a lot of money and a lot of time, and can not used in real practice. And then there does not exist a method to select the seepage parameters accurately, reliably and economically. But the same as other geotechnical engineering, the back analysis is a suitable method to determine the seepage parameters [1–7].

The problem of parameter back analysis generally can be divided into two methods, which are direct back analysis and inverse back analysis [8]. For some shortcomings of inverse back analysis, this method is applied little. The most widely used method is direct back analysis based on optimization method. In this back analysis, the generally used optimization method is traditional optimization method, such as simple method, gradient method and complex method, et al. But these methods belong to local optimization method, and have many shortcomings, such as relying on initial values severely, the weak stability and the low efficiency, et al. In order to overcome those shortcomings, the global optimization methods, such as evolutionary algorithm, neural network and simulated annealing et al. have been applied into the back analysis field, and proposed a kind of intelligent back analysis method [4–8]. But those intelligent back analysis methods also have the shortcomings of low efficiency and weak stability. Here, based on the new bionics algorithm-immunized evolutionary programming proposed in [9–10], a new back analysis method for seepage parameters is proposed.

2 BASIC BACK ANALYSIS MODEL OF SEEPAGE PARAMETERS

The permeability coefficient of rock mass controls the seepage analysis mainly, so it should be inversely calculated by water head values of site testing. When there are L groups of different fractures in rock mass, from the Snow theory and tensor theory, the permeability tensor can be described as follows,

$$k_{ij} = \sum_{l=1}^{L} k_{fl}(\delta_{ij} - n_{li}n_{lj}), \quad i = 1,2,3 \tag{1}$$

where, k_{ij} is permeability tensor, k_{fl} is permeability coefficient of fracture l, n_{li} is unit normal vector of fracture surface.

The stable seepage controlling function is as follows,

$$(k_{ij}H_f)_i=0,\ i=1,\ 2,\ 3,\ j=1,\ 2,\ 3 \tag{2}$$

The whole analysis field of dam foundation is brook into computing zones which number is NM according to character of hydrologic geology and distribution of fractures. The permeability coefficient of the fracture l in zone i is described by k_{fl}^{i}, whose constraint condition is as follows,

$$k_{fl}^{id} < k_{fl}^{i} < k_{fl}^{iu}, \quad (i = 1,2,\Lambda\ ,NM; l = 1,2,\Lambda\ ,L) \tag{3}$$

where, k_{fl}^{iu} is parameters to be identified;

k_{fl}^{iu} and k_{fl}^{id} are upper and lower range of parameters respectively, which can be determined by engineering experience or site testing, et al.

According to the principles of direct back analysis, the inverse back analysis model for seepage parameters can be constructed. The error between calculated water head and measured water head on measured points, which coordinate location are known is taken as the optimal objective. And the objective function is based on least squares method, and which is as follows,

$$E(k_{fl}^{i}) = \sum_{m=1}^{M} \omega_m^2 \left[\frac{H_m - H_m^{obs}}{H_m^{obs}}\right]^2 \tag{4}$$

where, H_m is calculated water head value on measured point m, H_m^{obs} is its measured value, M is the total number of measured points, ω_m is the corresponding weight coefficient.

The above objective function takes the relative value of water head, and makes the objective function a nondimensional numerical function. So, some illogical phenomena from the dimensional problem can be avoided, and makes the judgment of convergence of algorithm easy. And then, from the above analysis, the inverse problem of seepage parameters can be transformed to a typical optimization problem.

3 INTRODUCTION OF BIONICS ALGORITHM

Evolutionary programming was proposed as a Finite State Machine (FSM) model by L.J.Fogel in 1960s'. In that model, the mutation operator of the state of machine is a kind of uniform distribution [11–12]. In 1990s', the thinking of evolutionary programming was extended by D.B.Fogel, and then evolutionary programming was made to an optimization tool. And also, the normal school mutation was introduced into evolutionary programming by D.B.Fogel, so the evolutionary programming has been become a general optimization tool and been applied in many real problems [12].

Different from genetic algorithm, there is only one evolutionary operation in evolutionary programming, which is the mutation operation. In reference [12], D.B.Fogel has drowned the conclusion that, the complicated evolutionary operations are not superior to simple mutation operation, and the crossover operation is a subset of mutation operation.

The main construction of evolutionary programming is as follows.

3.1 *Mutation operator*

Different from genetic algorithm, evolutionary programming mimics the evolutionary process from colony aspect, and it emphasizes the evolution of the whole colony. So, the crossover operator that describes the evolution of individual is not used. Generally, the Gauss mutation is applied. But compared with Cauchy distribution, the range of Gauss distributions is very narrow, and then the probability of jumping out from the local extreme area is very low. In order to overcome this problem, here the Cauchy mutation is applied.

3.2 *Selection operator*

In evolutionary programming, the selection operator is a kind of stochastic tournament model that is called random competition with parameter q. The basic process of this operator is as follows:

(a) Calculate the fitness of each offspring.
(b) Conduct pairwise comparison over the union of parents and offspring. For each individual, q opponents are chosen uniformly at random from all the parents and offspring. For each comparison, if the individual's fitness is no smaller than the opponent's, it receives a "win."
(c) Select the individuals out of the parents and offspring, that have the most wins to be parents of the next generation.

From the above analysis, we can conclude that, compared with genetic algorithm, the operations of evolutionary programming is very simple, and it can avoid the difficulties for selection of some controlling parameters, such as selection probability and mutation probability, et al.

Considering the shortcomings of losing population diversity and premature of evolutionary programming, we improve the evolutionary programming by principles of artificial immune system [13].

In artificial immune system, to one antigen, the immune system can produce corresponding antibody to resist it adaptively. After the antibody combines with the antigen, the antigen can be destroyed through a series of reaction. At the same time, the stimulative reaction and restraining reaction can be occurred among antibodies, and this kind of reaction take place according to thickness of antibodies. So, the diversity of population can be maintained through the immune process. And then, through stimulative reaction and restraining reaction among antibodies, the adaptive power to circumstance of the antibody can be improved.

From above principles, we take the problem to be solved as antigen and solution as antibody. And then, the adjustment mechanism based on thickness is introduced into evolutionary programming. Then a new bionics algorithm-immunized evolutionary programming is proposed here.

The basic flow chart of immunized evolutionary programming is as Fig. 1.

4 BIONICS ALGORITHM FORINVERSE PROBLEM OF SEEPAGE PARAMETERS

Individual Expression. In immunized evolutionary programming, the vector of identified parameters is taken as the individual expression.

Creation Initial Population. If the performance of the initial population is poor, the algorithm will have a slow convergence, or no convergence at all. To overcome this difficulty, a new method to create the initial population, called Small Region Creation Method (SRCM) is proposed here. In this method, the range of each parameter is divided into small regions. The number of the small regions is equal to the population size. In each small region, an initial individual is created randomly Using

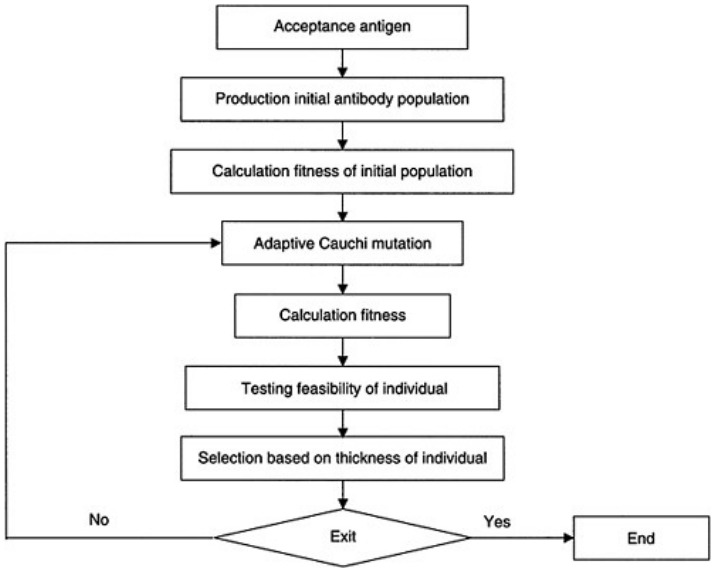

Figure 1. Basic flow chart of immunized evolutionary programming.

this method, the created initial individuals will have the apparent diversity, and distribute evenly on the solution space. So, the probability to find the optimal solution will be improved.

Fitness Function. The fitness function is the power of evolution in an algorithm. Here we define the objective function as above equation (4).

The fitness function can then be expressed as,

$$F(i) = 1.0 / (1.0 + f(i)) \tag{5}$$

After the fitness is computed, in order to reduce the needed FEM computations, one method to increase the computation speed is proposed. After the mutation operation (see below) is completed, we search the individuals mutated in parent population. If the individual is found, its fitness is copied from the parent population directly, otherwise its fitness is computed.

Mutation Operation. Here, the adaptive Cauchi mutation is applied, which form is as follows.

Suppose one individual of the population is $X=(a_1,\ldots, a_1)$, its mutated individual is $X'=(a'_1,\ldots, a'_1)$, then the component of the new individual can be described as follows,

$$a'_i = a_i + \sigma_i \cdot T \cdot C_i(0,1) \quad (i=1\sim l) \tag{6}$$

where,

$$\sigma_i = 1.0 / \sqrt{\beta_i F(X) + \gamma_i} \quad (i=1\sim l) \tag{7}$$

where, σ_i is the standard deviation of the parameters; $C_i(0, 1)$ is the Cauchi random number; $F(x)$ is the fitness of individual; β_i, γ_i are two parameters, here β_i=1, γ_i=0; T is a adaptive parameter, which description is as follows,

$$T = \frac{T_0}{F_{max} - F_{avr}} \tag{8}$$

where, T_0 is the initial parameter, which value is 2.5; F_{max}, F_{min} are the maximum and minimum fitness of the current population.

The adaptive mutation can make the disturbing extent of mutation adaptively changeable through the evolutionary extent, so the search performance of the whole algorithm can be improved.

Individual testing. The suitable ranges of seepage parameters are not the whole field of real number, so, after mutation, the parameters must be tested. If the parameter mutated is not in its suitable range, then a random number in suitable range is selected to replace the parameter mutated.

Selection Operation. In immunized evolutionary programming, the adjustment mechanism based on thickness in artificial immune system is introduced to improve the selection operation of evolutionary programming.

According to the stimulative reaction and restraining reaction in immune system, one kind of thickness factor is introduced into selection operation to adjust the score of individual. The details is as follows, the adjustive modification based on thickness and fitness of individual is added to the score of individual, which is as follows,

$$p'(i).scores = p(i).scores + \alpha \cdot C \cdot (1 - \frac{F(i)}{\max F}) \cdot p(i).scores + \beta \cdot \frac{F(i)}{\max F} \cdot p(i).scores \tag{9}$$

where, $p'(i)$.scores and $p(i)$.scores are the individual scores after and before mutation, respectively. α and β are the testing parameters between 0 to 1, and here α=β=0.5. $F(i)$ is the fitness value of an individual whose sequence number is i and max F is the maximum fitness of the population. Parameter C is the thickness of individual, whose definition is the ratio of number of individuals whose fitness is highest or near highest to total number of population, and can be expressed as follows,

$$C = \frac{t \cdot (0.8 \cdot \max F \rightarrow \max f)}{N} \tag{10}$$

where, the numerator is the summation of individuals whose fitness is between max F and 0.8 times of max F, and N is the total number of the population.

From the above score formula equation, we can see that, as to the individuals whose thickness is high and total number is t, if their fitness is high, their scores are little (this can be seen from second term of score formula). While if the thickness of individual is low, the score of individuals whose fitness is high must be higher due to the third term of score formula.

5 NUMERICAL EXAMPLE

In order to verify this algorithm, here the example in reference [6] is used. Suppose there is a gravity dam. The water height on its upstream side and downstream side are 20m and 5m respectively. The rack mass of dam foundation is divided into three computing zones from up to down. The distribution of fractures in dam foundation is as follow Fig. 2.

There are two groups of fractures in each computing zone, so there are six groups of fractures in the whole computing zone. Here the seepage of dam foundation is mainly analyzed. Before back analysis, the seepage parameters values of each fracture groups are supposed. Through FEM,

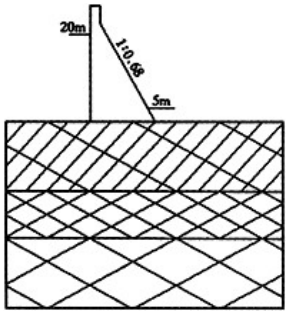

Figure 2. Fracture distribution of dam foundation.

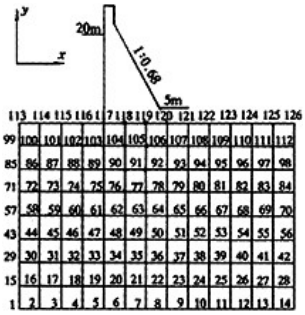

Figure 3. FEM map of dam foundation.

Table 1. Information of rock fractures in dam foundation.

Zone number j	Fracture group l	Relative value of seepage parameters k_{fl}^{j}	Upper bound of seepage parameters k_{fl}^{ju}	Lower bound of seepage parameters k_{fl}^{jd}	Normal angle/O θ_x	Normal angle/O θ_y
a	1	1.0	1.0	1.0	60	30
	2	5.0	10.0	1.0	120	30
b	1	10.0	20.0	5.0	60	30
	2	10.0	20.0	5.0	120	30
c	1	30.0	60.0	15.0	60	30
	2	100.0	200.0	50.0	135	45

Note: θ_x express the angle between normal direction and x axis. θ_y express the angle between normal direction and y axis.

Table 2. Water head on measured points.

Measured points	118	119	104	105	90	91	76	77	62	63
Water head values/m	14.37	10.44	11.91	8.64	10.33	8.35	9.30	7.81	9.97	8.84

the node water head of dam foundation is calculated. Then some values of water head on some nodes are supposed as measured ones to identify the seepage parameters of fracture in dam foundation. The FEM map of dam foundation is showed in Fig. 3. The size of element is 6m×6m. The supposed measured points are showed by black nodes in Fig. 3. Now, according to the above conditions, the seepage parameters of dam foundation are analyzed inversely. Because only measured water head are known, only the relative values of each group fractures can be identified.

Before computation, the information, the calculated seepage parameters and range of seepage parameters of each group of fractures must be given. The above information is showed in table 1.

For computation simple, the seepage parameters of first group fractures in zone are supposed as 1.0. So, the seepage parameters of the other five group fractures showed in table 1 are actually the scale factor according to the above one. Using the values given in table 1, we can get the water head values of each node in dam foundation through FEM. The water head values on supposed measured points are showed in table 2.

Table 3. Results of some inverse methods.

Parameters	k_{f2}^3				
Truth value	5.0	10.0	10.0	30.0	100.0
Result 1 by simple method	4.99075	10.0096	10.0116	29.9541	99.9508
Result 2 by simple method	5.04233	10.9489	11.019	32.8379	109.448
Result 3 by simple method	5.14196	15.0734	15.4469	45.1836	150.593
Result by genetic algorithm	5.00784	10.0884	10.0012	30.0202	100.17
Result by bionics algorithm	5.00054	10.0078	9.99335	30.0154	99.9984

Table 4. Initial values in simple method.

Initial value	k_{f2}^3				
Value 1 (error is 5%)	5.25	10.5	10.5	31.5	105.0
Value 2 (error is 10%)	5.5	11.0	11.0	33.0	110.0
Value 3 (error is 50%)	7.5	15.0	15.0	45.0	150.0

Here X is the parameters vector to be identified, which can be described as $k_{f2}^3)^T$. The above conditions are put into our algorithm for parameters identification, and the results are showed in table 3. In order to compare the identification results with other methods, the identification results by genetic algorithm and results by simple method are also showed in table 3. Also, in order to verify the initial value dependence, we take three initial values in simple method. The three initial values are showed in table 4.

From table 3, we can conclude that, the results of simple method rely on the initial values seriously, and only when initial values are suitable, the results of inverse problem may be accurate. When initial value 1 is used, the error of inverse results is little, while when initial value 3 is used, the error of inverse results is big. But the results of two other methods are all good. So, the inverse results through traditional optimization method are affected by initial values very seriously, while the ones of global optimization method are not, and reliability of inverse results by global optimization method is higher. Also, we can find that, the accuracy of genetic algorithm is poor compared with that of bionics algorithm.

Also, we compare the efficiency of our bionics algorithm with that of genetic algorithm, and find that, our bionics algorithm can improve the computing efficiency of genetic algorithm by 1.5 times. So, the accuracy and efficiency of our bionics algorithm are all better than that of other methods in inverse problems for seepage parameters.

6 CONCLUSIONS

The inverse problem for seepage parameters is a very complicated optimization problem. To solve that problem, the traditional optimization methods have many shortcomings, such as initial value dependence, local optimization, et al. Especially when information of parameters is deficient and unsafe, the reliability of inverse problem will be very poor. But the global optimization method, such as evolutionary algorithm can solve this problem very well. Now, the generally used global optimization method in inverse problem is genetic algorithm, but for the shortcomings of genetic algorithm, the results of inverse problem by genetic algorithm are not satisfactory. So, here a more suitable bionics algorithm to solve inverse problem, which is called immunized evolutionary programming is proposed. And the results of numerical example show that, the accuracy and efficiency of our bionics algorithm are all better than that of other methods, and our bionics algorithm is a more suitable method for seepage parameters identification problem.

REFERENCES

[1] M.Dennis, L.R.Townly, A reassessment of the groundwater inverse problem, *Water Resource Research,* 1996, 32(5):1131–1161
[2] N.Z.Sun, W.G.Yeh, Identification of parameter structure in groundwater inverse problem, *Water Resource Research,* 1985, 21(6):869–883
[3] J.M.Cheng, W.G.Yeh, A proposed quasi Newton method for parameter identification in a flow and transport system, *Advances in Water Resource Research,* 1992, 15(4):239–250
[4] M.Davey, An inverse technique for developing models for flow in fracture systems using simulated annealing, *Water Resource Research,* 1993, 29(11):3775–3789
[5] J.Morshed, J.J.Kaluarachchi, Parameter estimation using artificial neural network and genetic algorithm for free-product migration and recovery, *Water Resource Research,* 1998, 34(5):1101–1113
[6] J.Liu, Y.Wang, J.G.Yang, Back analysis of seepage parameters for fractured rack mass using accelerated genetic algorithm, *Chinese J. Hydraulics,* 2003, 33(2):55–60
[7] J.G.Wang, W.Li, Z.F.Zhou, et al, Back analysis for seepage parameters of fissured rock based on evolutionary algorithm and its application, *Int. J. Hydroelectric Energy,* 2002, 20(2):33–35
[8] W.Gao, Y.R.Zheng, Back analysis of geomechanics and its intelligent study, *Rock and Soil Mechanics,* 2001, 22(1):114–116
[9] W.Gao, Y.R.Zheng, A new evolutionary back analysis method in geotechanical engineering, *Chinese J. of Rock Mechanics and Engineering,* 2003, 22(2):192–196
[10] W.Gao, Y.R.Zheng, A bionics algorithm for parameter identification in underground engineering and its application, *Chinese J. of Rock Mechanics and Engineering,* 2002, 21(s2):2521–2526
[11] D.B.Fogel, K.Chellapilla, Revisiting Evolutionary Programming, In: S.K.Rogers, D.B.Fogel, J.C. Bezdek, et al (Eds.), *Proc. of Applications and Science of Computational Intelligence,* Orlando, Florida,pp. 2–11, 1998
[12] D.B.Fogel, L.J.Fogel, An Introduction to Evolutionary Programming, In: J.M.Alliot, E.Lutton, et al (Eds), *European Conf. on AE'95.* Berlin: Springer, pp. 21–33, 1996
[13] K.Kumar, J.Neidhoefer, Immunized Artificial Systems-Concepts and Applications, In: D.Quagliarella, J.Periaux, et al (Eds.), *GA and ES in Engineering and Computer Science,* London: John Wiley & Sons Ltd., pp. 85–104, 1997

New Developments in Dam Engineering—Wieland, Ren & Tan (eds),
© 2004 Taylor& Francis Group, London, ISBN 04 1536 240 7

Seismic safety evaluation of Sanmenxia Longgou flyash storage dam

GengYe
Yellow River Institute of Hydraulic Research, YRCC, China

Li Ning
Xi'an Science University, Shanxi, China

Wang Yibo
Henan Electric Power & Survey Institute, Henan, China

Pan Shu
Yellow River Institute of Hydraulic Research, YRCC, China

ABSTRACT: This article shows that through an analysis of the dynamic characteristic of the Long'gou Ash Dam in the Sanmenxia Thermal Power Plant under the earthquake effect with adopting Equivalent visco-elastic FEM model and principle effective stress method, it proves that under the effect of a 7° earthquake intensity, the dam's stability cannot be endangered as the liquidating area of the dam locates mainly in the natural coal ash settling area far from the dam top and simultaneously the depth of liquidation is relatively shallow.

1 INTRODUCTION

The yearly wasted coal ash of our country totals up to 100 million tons, and the safety of ash dam situated in earthquake regions has always been paid great attentions by designers. Because of the big void ratio and easy liquefaction of fly ash, it is of great significance to investigate the seismic stability of such ash dam with the height over 100m, as Sanmenxia Longgou Ash dam.

In the paper, static and dynamic triaxial tests were conducted on materials at Sanmenxia Longgou Ash Dam, and the static and dynamic parameters of fly ash were obtained. Thirdly the 2 dimensions static analysis of the ash dam was conducted based on Biot's consolidation theory and Duncan's nonlinear stress-strain model. Finally the plane dynamic behaviors of the ash dam during earthquake of intensity 7 were analyzed based on the exponent function model of excess pore water pressure aroused by earthquake.

2 CONSTRUCTION OUTLINE

The Sanmenxia Thermal Power Plant is the key construction project in our country's "8th five year plans". The first phase of ash storing yard is built in Long'gou, Dawang Town, Lingbao County, Henan Province and the Long'gou ash dam there is in the area with possible 7° earthquake intensity. The ash blocking dam of such ash storing yard is designed to comprise primary dam and some post sub-dams. The primary dam is the well-proportional loess dam with adopting piled rock's prism as the seepage draining facility and the post sub-dams are built with the scheme of heightening the part before the dam, i.e. adding up grade by grade the part before the dam with heaping and grinding loess on the powder coal ash. The seepage draining measure is done with setting four rows

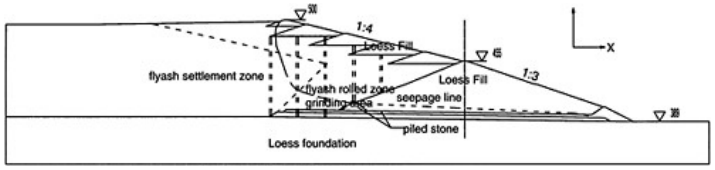

Diagram 1. Chart of ash dam's transversal section plane.

of vertical seepage draining wells basically parallel to dam axis between the post dam axis and the draining prisms in the primary dam's upstream position, the depth of which should extend unless going through the coal ash layer. The designed primary's altitude is 64.5m, the inclination ratio of both dam's upstream and downstream side slops is 1:3 and that of each grade of sub-dam is 1:4, and the altitude of chief dam is 109.5m. The area of 100–150m before dam is the area of grinding coal ash and the rest is the natural coal ash settling area for receiving the hydraulically transmitted ash slurry. The chart of ash dam's transversal section plane is seen in Diagram 1.

According to the datum provided by the designing department, the construction term of such ash dam's primary dam is two years beginning from 1993 and completing by 1995 and after such completion, the dam began to run and functioned well. At present, the inside of the primary dam has been almost full with the coal ash and it is necessary to build sub-dam to heighten it on the powder coal ash before the dam and the construction term of each grade of sub-dam is 3–4 months and each service term is 2 years.

3 ANALYSIS TO THE MODEL AND NUMERICAL SOLUTION

3.1 *Calculation on static*

As to the problem on static, it is available to adopt the relation of incremental stress and strain to conduct a finite element splitting to the calculated area with parameter unit such as plane 4 crunodes and with combining the principle of effective stress, the relationship formula of the soil's incremental stress and strain and the geometrical relation of the incremental distortion so as to gain the balanceable equation and seepage continuity equation, i.e. Biot's consolidation equation. From such equation, if is applicable to gain the crunod's displacement and pore water pressure and then gain the element stress from the stress and strain relationship formula. The calculation is done with adopting Duncan's nonelinear stress-strain model (E-μ model).

3.2 *Calculation on dynamic*

When the soil-stone made dam's foundation system receives vibrating load, the basic equation for the dynamic after the finite element dispersed is as follows:

$$[M]\{\ddot{\delta}\}+[C]\{\dot{\delta}\}+[K]\{\delta\}=\{F(t)\}$$

In the equation: [M], [C] and [K]—the system's quality matrix, damp matrix and stiffness matrix; {F(t)}—crunode's dynamic load column matrix; {δ}, $\{\ddot{\delta}\}$—the column matrix of the crunode's displacement, velocity and acceleration to the base rock.

3.3 *Calculation model on dynamic*

1. The system's damp matrix is set by adopting Rayleign theory[2], among it each unit's damp is gained with using the interpolating value of the average shearing strain (equal to $0.65|\gamma_{max}|$,

γ_{max} is the maximum shearing strain of such unit in such time period) of all the units in such time period upon the dynamic character of their material. Each unit's maximum shearing module is set upon following equation:

$$G_{d\max} = k_d \cdot Pa\,(\sigma_0 / Pa)^{n_d}$$

In the equation, σ_0 is the average static positive effective stress, k_d, n_d is testing constant, Pa is atmosphere pressure. The ratio of each unit's actual shearing module vs the maximum shearing module is gained with using the interpolating value of all the units' average shearing stress upon the dynamic character of their material.

2. The dispersing calculation is done with adopting none-linear Duncan E-JJL model and taking the unloading effect in count, and the model expression and its parameter can be seen in Reference Literature[1].
3. The model for the liquefiable soil's excess pore water pressure increment is designed with adopting the index function[3] model involving the effect of primary shearing stress presented by Mr. Pan Shu etc., and its mathematical expression is:

$$U=1-(1-U_0)10^{-k\xi/(1-\xi)}$$

In the expression, $U=u_N/u_f$—relative pore pressure ratio; $U_0=u_1/u_f$—relative pore pressure ratio in first turn, it is set by following expression: $U_0 = \gamma N_f^{-\theta}$.

$\xi=\log N/\log N_f$—logarithmic ruin vibrating time ratio. The testing constant K is set upon the following expression: $K = \alpha N_f^{-\beta}$.

The ruin vibrating time N_f is set by the following expression: $\alpha_d = AN_f^{-B}$

The seven constants such as γ, θ, α, β, u_f, A, B are set by the experiment to the dynamic without in water draining state.

4 FINITE ELEMENT MODEL AND ITS PARAMETER

4.1 *Finite element model*

Considering the character of Long'gou ash dam, the calculating extent covers the upstream area of 250m in length from the primary dam's foot to the ash reservoir orientation and downstream area of 280m in length from the primary dam's dam foot to the ash reservoir orientation, and the dam foundation is set to the surface of basic rock with distance of 60m. On each border surface, the bottom is set as fixed holding, the upstream and downstream border faces are set as the connecting rod holding, which is vertical to the border surface. The soakage line position's seepage is gained by calculation, and the calculating section includes split elements of 1673 and crunodes of 1688 in total.

4.2 *The time vs space of earthquake's acceleration*

There is no actually tested earthquake record in the Long'gou Ash Yard. In this article, we try to provide an man-made acceleration's process curve of basic rock which is synthesized with adopting the designed reflecting lineage and peak value acceleration a_{max} and the characteristic period Tg in "The Designing Specification for the Water Conservancy Construction against Earthquake", and the finally synthesized curve is seen in the Diagram 2, the peak value acceleration is 0.15g and the earthquake extends for 25 s.

4.3 *Calculating parameter*

The calculating parameters adopted in this article are gained through sorting out the result of the static and dynamic triaxis experiment and they are seem in Table 1–Table 3.

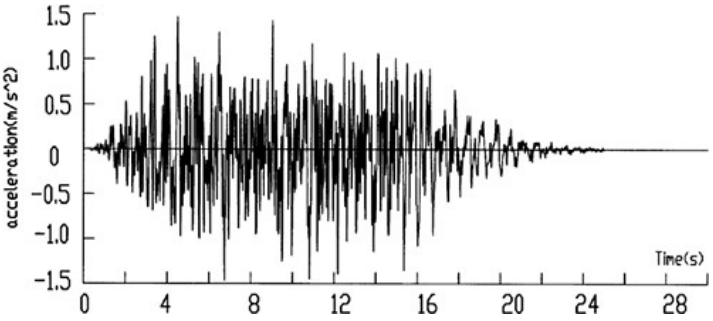

Diagram 2. The acceleration process curve.

Table 1. Static non-linear calculating parameter

Soil sorts	Dry weight (kN/m^3)	c′ kPa	φ′0 degree	k	n	R_f	D	G	F
Saturated loess	16.6	6.0	32.0	303.3	0.569	0.9	0.295	0.27	13.2
None saturated loess	16.6	19.6	33.1	444.4	0.424	0.89	0.27	0.28	31.0
Piled stone	20.6	0.0	42.0	1000.0	0.50	0.93	0.00	0.42	0.00
Grinded powder coal ash (Saturated)	9.41	3.0	32.9	142.9	0.564	0.75	0.316	0.16	4.73
Grinded powder coal ash (No Saturated)	9.41	6.0	32.1	384.6	0.447	0.88	0.28	0.15	10.46
Settled powder coal ash	8.5	0.0	30.7	66.7	0.792	0.75	0.23	0.15	5.0

Table 2. Each material's k_d and n_d value.

Material sorts	Loess (satd)	Loess (no satd)	Piled stone	Grinded ash (satd)	Grinded ash (no satd)	Settled ash (satd)
k_d	760	840	1400.0	520	620	430
n_d	0.504	0.574	0.5	0.475	0.5	0.446
Seepage coefficient (cm/s)	5×10^{-6}	5×10^{-6}	1.5×10^{-1}	$K_h=1\times10^{-4}$	$K_h=1\times10^{-4}$	$K_h=1\times10^{-4}$
				$K_v=2\times10^{-5}$	$K_v=2\times10^{-5}$	$K_v=2\times10^{-5}$

5 RESULTS ANALYZING

5.1 *Static stress analyzing*

The final result of the static calculation on the Long'gou ash dam is seen in Diagram 3–Diagram 6 and it includes horizontal displacement, vertical displacement, horizontally positive stress σ_x, vertically positive stress σ_z, shearing stress τ_{xz} and dam body's extra static pore pressure isoline. It can be seen in the diagram that the max vertical displacement is 2.91m, occurred in the position of 1/3 of the ash dam body's altitude. The horizontal and vertical stresses distribute evenly and they increase gradually from up position to down one. The max vertical stress is 2.104 MPa, max horizontal stress 0.799MPa and max shearing stress 0.249 MPa, occurred in the part of dam foundation, but the shearing stress in the ash's up part is less and such case shows that farther the ash placed is apart from the dam's top, nearer its stress state is adjacent to the free field. It can be also seen in the Diagram 6 that the extra static pore pressure in the ash dam's body is less and it cannot

Table 3. The calculating parameter of remained pore pressure increment model.

Soil name	Dry weight (kN/m^3)	Static shear stress ratio *a*	Static positive stress (kPa)	Calculating parameter						
				A	B	γ	θ	α	β	U_f
Grinded powder coal ash	9.41	0.0	100.0	0.184	0.069	0.81	0.397	0.163	0.258	1.0
		0.0	300.0	0.184	0.069	0.244	0.632	0.163	0.258	1.0
		0.188	111.4	0.392	0.126	0.508	0.585	0.214	0.335	0.729
		0.188	334.3	0.392	0.126	0.508	0.585	0.214	0.335	0.729
		0.342	122.8	0.369	0.108	0.73	0.483	0.325	0.348	0.485
		0.342	368.5	0.369	0.108	0.19	0.354	0.325	0.348	0.485
Settled powder coal ash	8.5	0.0	100.0	0.146	0.135	1.26	0.778	0.19	0.306	1.0
		0.0	300.0	0.146	0.135	0.16	0.463	0.19	0.306	1.0
		0.192	112.2	0.284	0.136	1.04	0.552	0.33	0.331	0.744
		0.192	336.7	0.284	0.136	0.113	0.163	0.33	0.331	0.744
		0.345	124.5	0.279	0.13	0.97	0.419	0.5	0.366	0.527
		0.345	373.4	0.279	0.13	0.94	0.128	0.5	0.366	0.527

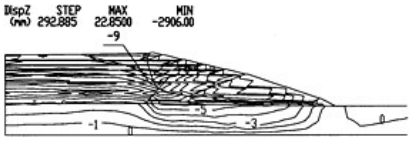

Diagram 3. Isoline chart of the ash dam's vertical displacement.

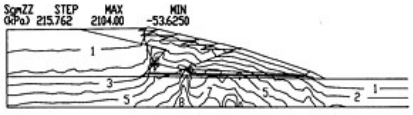

Diagram 4. Isoline chart of the ash dam's vertical Strees

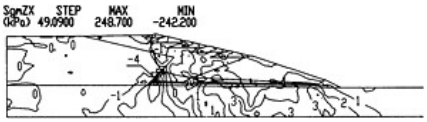

Diagram 5. Isoline chart of the ash dam's shearing stress.

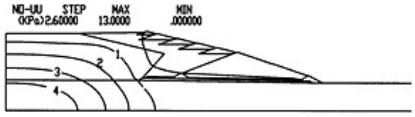

Diagram 6. Isoline of the ash dam's extra static hole pressure.

bring forth obvious effect to the dam's stability. Generally speaking, the stresses in the dam body distribute reasonably and the ash dam's static stability is relatively fine.

5.2 *Analysis on dynamic calculation*

The analysis on earthquake response with the effective stress method is done on the base of calculation on static added with the earthquake acceleration input wave in the basic rock shown in Diagram 3 in the condition that the earthquake orientation is along riverwise. The calculation adopts time pace of 0.02s. In order to reduce calculating workload, an iterative calculation is done with choosing 10 longer time paces and setting iterative precise of 5% upon the external frame line of the earthquake input's acceleration process.

5.2.1 *Method of estimating the saturated soil's liquefaction*

Estimating whether the saturated soil is liquefied or ruined is the key point for analyzing earthquake response with the effective stress method. This article adopts two kinds of estimating methods.

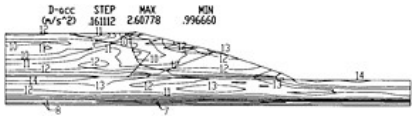

Diagram 7. The isoline of the ash dams max acceleration

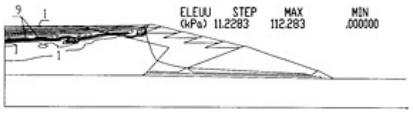

Diagram 8. The isolne of the ash dam's pore water (No. 9s).

One method is to adopt the experienced Seed Safety coefficient to estimate the earthquake resistance performance of the liquefiable soil. Generally, the area with the Seed Safety coefficient less than 1.3 may be regarded as liquefiable area, the area with such coefficient between 1.3–1.5 belongs to ruin area and the area with such coefficient more than 1.5 belongs to none liquefiable area. Another method is to introduce the pore pressure level (equal to the ratio of such element's pore pressure value vs its static vertical valid stress) to estimate the element pore pressure's relative value. When the hole pressure level is more than 0.9, such element can be regarded as being liquefied, and when the pore pressure level is between 0.5–0.9, such element may be regarded as being ruined.

5.2.2 *Dynamic response*

Under the earthquake effect, the max acceleration absolute value of the dam body are seen in Diagram 7. It can be seen in the diagrams that the distribution case of the dam body's acceleration is somewhat different with the horizontal earthquake distribution coefficient of the dam made by the grinded soil and stones provided in the specification and shows no regular inverse trapezium distribution, and its value at the joint position between the loess foundation of the dam's middle part and ash dam as well as on the top of primary dam is comparatively more, and after passing through the effect of foundation loess, in the ash reservoir, again the acceleration increases gradually. Why such phenomenon occurs is mainly as the different intensity between the loess and ash, and such phenomenon also shows the characters of powder coal ash's lower intensity in all, stronger material none-linearity and weaker response to earthquake.

5.2.3 *Pore water pressure distribution*

Diagram 8 show the distribution chart of the remained pore water pressure isoline in the dam body at No. 9s of the earthquake period. In the diagram, it can be seen that at No. 9s, the pore pressure extends to the down part of the natural ash settling area, and the max value then is 112.28kPa, at No. 12s, the pore pressure value gets a little less, but its extent continuously extends to the down part and is adjacent to the level when the earthquake ends. Such phenomenon shows that the increment of remained hole pressure mainly occurs between No. 3s and No. 9s. Why the pore pressure gets a little less is that in the earthquake period, the problem concerning pore pressure's dissipation is taken in count and it relates to the dam's water draining condition and the ash's seepage coefficient.

5.2.4 *Liquefied area's distribution*

The distribution of the area (i.e. liquefied area) where the dam body's Seed Safety coefficient is less than 1.3 can be seen in Diagram 9 and the distribution of the area (i.e. liquefied area) where the hole pressure level is more than 0.9 can be seen in Diagram 10. It can be seen in the diagram that the liquefied area's extant is in the ash's up part. According to the result of estimating the liquefied area with Citer Safety coefficient, the max depth of liquefied area is about 23m, and there still exist liquefaction units in the grinded area, and the liquefied area is quite adjacent to the five grades of sub-dams; if estimating the liquefied area with adopting the method of hole pressure level, the extent of liquefied area is comparatively less and the distance between it and the sub-dams is comparatively farther, about 40m, and its liquefied depth is about 19m. If estimating the liquefied area under the earthquake with adopting both methods, its both tendencies are coincident and the only difference is that the method with Seed Safety coefficient is relatively a little more conservative.

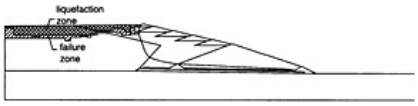

Diagram 9. The distribution of the ash dam's liquefied area with the Seed method.

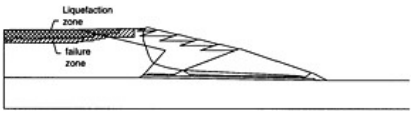

Diagram 10. The distribution of the ash dam's liquefied area with the pore pressure level method.

5.3 *Seismic stability analysis of the dam's slope*

According to the designing specification of earthquake resistance, when doing an analysis to the stability of the ash dam's downstream side slop against earthquake with adopting the imitative static method, the result shows that the dam slop's minimum safety coefficient is 1.34, and it can meet 1.25, the designed standard on slip-proof stability, the safety coefficient.

6 CONCLUSION

The result of analyzing dynamic response on effective stress with adopting the remained pore pressure model presented in this article shows that no matter whether it is in the earthquake acting period or earthquake ceasing period, the pore pressure's distribution, value magnitude and tendency are in accordance with the law. Though when estimating the liquefied area with adopting both the method of Seed Safety coefficient and the method of pore pressure level, the both results are not completely coincident, the both tendencies are adjacent. As the method of Seed Safety coefficient is a better experienced one and it is also relatively more conservative, so this article recommends to adopt the method of pore pressure level for estimating the liquefied area distribution of the saturated soil under the earthquake effect as its result may be more reasonable and creditable. Therefore, it is acceptable that the dam body's liquefied area locates mainly at the natural coal ash settling area far away form the dam top and its liquefied depth is shallower, and it cannot bring forth danger to the dam body. The analysis to the dam slop's stability shows that its minimum safety coefficient is 1.34, reaching to the requirement regulated in the specification. Whereby, it is ensured that the dam body of Long'gou Ash Dam of Sanmenxia is safe in case it is subject to 7° earthquake effect.

REFERENCES

[1] "Soil Mechanics Calculation" written by Zhu Baili and Shen Zhujiang etc. published by Shanghai Science and Technique Pb. House in 1990.
[2] "Analysis to the Power Coal Ash Dam's Dynamic Response" written by Wang Guixuan and Wang Zhongzheng, published in the Rock and Soil Engineering Journal No. 5 issue, 1988.
[3] "Analysis to the Power Coal Ash's Dynamic Character and Dynamic" written by Guo Peijiu and Hu Cheng published in Rock and Soil Engineering Journal No. 5 issue, 1988.
[4] "Analysis to the Valid Stress of Stone Piling Dam of the Inclined Wall of Xiaolangdi Reservoir" written by Shen Fengsheng, Fan Shu and Geng Hua published in the People Yellow River Paper, No. 5 issue, 1994.

This page intentionally left blank.

New Developments in Dam Engineering—Wieland, Ren & Tan (eds),
© 2004 Taylor& Francis Group, London, ISBN 04 1536 240 7

Concrete model for analysis of RCC dam

Gu Chongshi, Zhu Guojin & Nie Xuejun
College of Water Conservancy and Hydropower Engineer, Hohai University, Nanjing, China

ABSTRACT: Based on the characteristics of series-wound and shunt-wound connection, the gradual formula for the calculation parameters is derived, and the method of determining the effect zones is put forward. The three-dimensional viscoelastic model of RCC dam is established and the corresponding finite element program is developed. This case shows the model can be applied to the analysis of RCC dams.

RCC dams have the virtues of saving a great deal of concrete, building quickly, making project cost down and early bringing into playing project advantages and so on. Hence, the technique of constructing dams has been quickly spread and applied since it came out. But due to rolling layer by layer in the construction of RCC dam, its body has many horizontal construction planes. And the cementation between layers affects directly dam's quality. Meanwhile, an interim zone appears between layers in the process of rolling, and the property of RCC also changes gradually in the interim zone. In the past, the researches' emphasis was put on the property of the construction planes between layers, and little attention was paid the effect zones. In fact, the influence of the effect zones on dam body is notable. Based on the study of the experimentations and theories, the paper researches deeply the principle of gradual change of the calculation parameters of the effect zones for RCC dam. Besides, based on the characteristics of series—wound and shunt-wound, the gradual formula for the calculation parameters is derived, and the method of determining the effect zones is put forward. The three-dimensional viscoelastic model of RCC dam is established, and the corresponding finite element program is developed.

1 DETERMINE YOUNG'S MODULUS AND THE THICKNESS OF THE EFFECT ZONES FOR RCCD

Figure 1 shows the structure model of RCC layers, in which B represents the thickness of RCC layer, b_a and b_c denote the thickness of effect zone and RCC noumenon ($b_c=B-ba$). Assume that Young's modulus and Poisson's ratio of RCC noumenon and effect zone are E_c, μ_c and $E_a(x)$, $\mu_a(x)$ respectively, where x represents the distance between any point and the central lager of effect zone.

RCC layers can be considered as composite material, and the series-wound and shunt-wound models are established according to the idea of composite material. They are respectively used to calculate the Young's modulus (E_v and E_l) which are respectively vertical and parallel form the construction interface.

When RCC layer stretches homogeneously at the vertical direction, the same stress a appears on the cross-sections of noumenon and effect zone. According to the series-wound model, the tensile quantities (Δb_c and Δb_a) of noumenon and effect zone can be expressed as

$$\left.\begin{aligned}\Delta b_c &= \frac{\sigma b_c}{E_c}\\ \Delta b_a &= 2\int_0^{\frac{b_a}{2}} \frac{\sigma}{E_a(x)}dx\end{aligned}\right\} \tag{1}$$

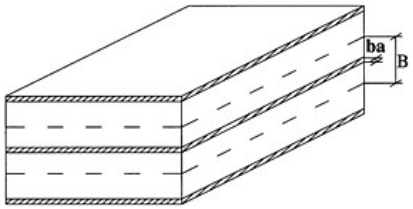

Figure 1. Structure model of RCC layers.

Then, the total tensile quantity (ΔB) of RCC layer is

$$\Delta B = \Delta b_c + \Delta b_a = \sigma\left(\frac{b_c}{E_c} + 2\int_0^{\frac{b_a}{2}} \frac{1}{E_a(x)}dx\right) \tag{2}$$

Furthermore,

$$\Delta B = \frac{\sigma}{E_v} B \tag{3}$$

Then from Eq. (2) and (3), the following equation can be obtained:

$$\frac{B}{E_v} = \frac{b_c}{E_c} + 2\int_0^{\frac{b_a}{2}} \frac{1}{E_a(x)}dx \tag{4}$$

the thickness *(b_a)* and Young's modulus *($E_a(x)$)* of effect zone can be calculated from Eq. (4), in which b_a relates not only to the thickness of RCC layer but to E_c, E_v and E_a, especial the change rule of $E_a(x)$.

Similarly, according to the shunt-wound model, the relationship of E_l and E_c, E_a can be obtained as follows

$$E_l B = E_c b_c + 2\int_0^{\frac{b_a}{2}} E_a(x)dx \tag{5}$$

From Eq. (5), the thickness *(b_a)* and Young's modulus *($E_a(x)$)* of effect zone can be calculated. E_v, E_l and E_c can be easily determined with experiment methods, the Young's modulus of the central layer ($E_a(0)$) can also be obtained by experiment. (Generally, $E_a(0)$ takes the minimum value of the Young's modulus of effect zone). Then, E_c and $E_a(0)$ are upper and low limit of $E_a(x)$.

$$E_a(0) \leqslant E_a(x) \leqslant E_c \tag{6}$$

in which, if x takes 0, the Young's modulus of effect zone is $E_a(0)$, and if x takes $b_a/2$, it is E_c.

b_a can change with the change rule of $E_a(x)$, so if the change rule is determined, b_a can be easily obtained. Generally, assume that E_a changes according to some rules (for example linearity, logarithm, power series and so on), then b_a can be obtained with Eq. (4) and (5). If the approximation value of b_a satisfies the need of accuracy, the above assumption is appropriate and b_a is considered as the undetermined thickness.

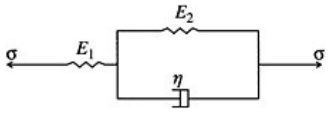

Figure 2. Generalized Kelvin model.

2 THE 3D VISCOELASTIC ANALYSIS MODEL

RCC apparently has rheotogical behavior at permanent loads, especially in continuous compression. Viscoelastic model can usually describe the rheotogical behavior, and it chiefly reflects viscose flow of material. Figure 2 is the generalized Kelvin model that can reflect the viscose flow behavior.

From Fig. 2, the total strain can be divided into elastic and viscous parts as follows

$$\{\varepsilon\}=\{\varepsilon^e\}+\{\varepsilon^{ve}\} \tag{7}$$

where $\{\varepsilon\}$ is the total strain $\{\varepsilon^e\}$ and $\{\varepsilon^{ve}\}$ denote the elastic and viscous strain respectively.

The elastic strain satisfies Hooke's law, and the viscous strain can be acquired from the generalized Kelvin model as follows

$$\{\sigma\}=\mathrm{D}\,(\{\varepsilon\}-\{\varepsilon^{ve}\}) \tag{8}$$

$$\{\dot{\varepsilon}^{ve}\}+E/\eta\,\{\varepsilon^{ve}\}=1/\eta\,\{\sigma\} \tag{9}$$

where $\{\sigma\}$ is the stress matrix, D is the elastic matrix, $\{\dot{\varepsilon}^{ve}\}$ denotes the time derivative of the viscous strain and E, η represent Young's modulus and viscosity coefficient.

$$\mathrm{D}=\begin{bmatrix} \lambda+2G & & & & & \\ \lambda & \lambda+2G & & \text{对称} & & \\ \lambda & \lambda & \lambda+2G & & & \\ 0 & 0 & 0 & G & & \\ 0 & 0 & 0 & 0 & G & \\ 0 & 0 & 0 & 0 & 0 & G \end{bmatrix}$$

in which λ and G are Lame's constants, the relationship of which and Young's modulus and Poisson's ratio can be expressed as follows

$$\lambda=\mathrm{E}\mu/(1+\mu)(1-2\mu),\quad \mathrm{G}=E/2(1+\mu)$$

Assume that, in the time step (Δt_m) under considered the increment of the viscous strain is

$$\{\Delta\varepsilon^{ve}\}_m=\{\dot{\varepsilon}^{ve}\}_{m+\theta}\,\Delta t_m \tag{10}$$

Because

$$\{\dot{\varepsilon}^{ve}\}_{m+\theta}=(1-\theta)\,\{\dot{\varepsilon}^{ve}\}_m+\theta\,\{\dot{\varepsilon}^{ve}\}_{m+1} \tag{11}$$

where the subscripts (m and m+1) denote the time of t_m and t_{m+1} respectively. If θ takes 0, Eq. (11) is Euler's integral, by which the implicit escalator style is acquired, and if θ gets 1, that is implicit. So the stress increment is determined thought the strain ratio of the time step end.

Because the amount of calculation is large during the structural analysis of RCCD, the escalator style of constant stiffness is adopted in the developed FEM program. Therefore, if the time step is properly limited the convergent result can be obtained.

If θ gets 0, Eq. (10) can be expressed as follows

$$\{\Delta\varepsilon^{ve}\}_m = \{\dot{\varepsilon}^{ve}\}_m \Delta t_m \tag{12}$$

Then, the strain of t_{m+1} can be expressed as follows

$$\{\varepsilon^{ve}\}_{m+1} = \{\varepsilon^{ve}\}_m + \{\dot{\varepsilon}^{ve}\}_m \Delta t_m \tag{13}$$

The above equation is suitable for any viscoelastic model. For increasing integration accnracy, from Eq. (9) calculated, $\{\varepsilon^{ve}\}_{m+1}$ can be obtained as follows

$$\{\varepsilon^{ve}\}_{m+1} = \{\varepsilon^{ve}\}_m e^{-\frac{E}{\eta}\Delta t_m} + D^{-1}\{\sigma\}_m \left(1 - e^{-\frac{E}{\eta}\Delta t_m}\right) \tag{14}$$

Because

$$D^{-1} = \frac{1}{E}\begin{bmatrix} 1 & & & & \\ -\mu & 1 & & \text{对称} & \\ -\mu & -\mu & 1 & & \\ 0 & 0 & 2(1+\mu) & & \\ 0 & 0 & 0 & 2(1+\mu) & \\ 0 & 0 & 0 & 0 & 2(1+\mu) \end{bmatrix}$$

If the viscous cubic strain isn't considered, Eq. (14) can be expressed as follows

$$\{\varepsilon^{ve}\}_{m+1} = \{\varepsilon^{ve}\}_m e^{-\frac{G}{\eta}\Delta t_m} + 1/2G\{S\}_m \left(1 - e^{-\frac{2G}{\eta}\Delta t_m}\right) \tag{15}$$

where $\{S\}$ is the deviator.

According to the above method of determining Young's modulus and the influence, the 3D viscoelastic model is established and the corresponding FEM program is developed.

3 EXAMPLE

3.1 *Calculation parameter and work condition of FEM model*

For some RCCD, the elevation of the crest is 146m, the maximum height of the dam is 57m, and the thickness between two construction layers. The Young's modulus (E_c), Poisson's ratio (μ) and viscosity coefficient (η) of RCC noumenon are 20.4 GPa, 0.167 and 2.3×10^7GPa.s respectively. The thickness and Young's modulus of effect zone can be obtained with Eq. (4) and (5), and

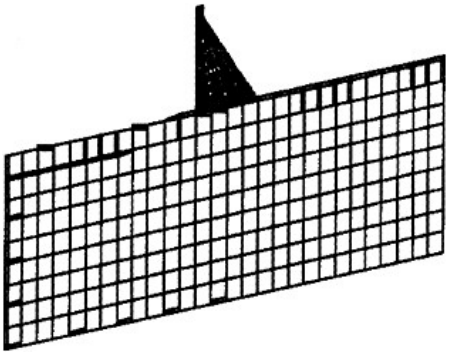

Figure 3. FEM model of the RCCD.

Table 1. Calculation results of the horizontal displacements of the crest.

Reservoir level (m)	135.0	140.0	144.5
Analysis methods			
Statistic model*	1.17	1.52	1.59
FEM	1.19	1.56	1.63

* Hohai university, Shuidong hydroelectric CO., LTD Positive and Inverse Analysis of The Observation Data and Structures for Shuidong Dam 1998.

its Poisson's ratio (μ) and viscosity coefficient (η) are 0.169 and 2.3×10^7GPa.s respectively. Figure 3 shows the FEM model of the dam. The range of FEM model is that 2-fold height of the dam upstream, 1.5-fold downstream and 2-fold under the foundation. There are 3749 elements and 4918 nodes. In addition, the water loads are s forced in steps from 100.0m to 144.5m.

3.2 *Comprehensive analysis results*

According to the above method, 3D FEM program is developed and the analysis to the RCCD is made. Table 1 is the horizontal displacements of the crest correspond to three reservoir levels: 135.0m, 140.0m and 144.5m. In addition, the water constituents of the horizontal displacements by statistic model are listed.

The statistic model is established according to the observation data, so its results agree with the fact. The results of FEM are near to that of statistic model, thus the method of determining the parameters and analysis model are feasible.

4 CONCLUSIONS

The paper studied the behavior of effect zone and analyze in detail the principle of gradual change of the calculation parameters for RCCD. On the other hand, the viscoelastic analysis model is established, and the following conclusions can be obtained.

1. Based on the series-wound and shunt-wound model, the principle of gradual change of the calculation parameters is put forward, and the corresponding formula is derived.

2 The 3D viscoelastic analysis model is established, which can reflect the principle of gradual change and the change of the influence thickness with the parameters foe example Young's modulus and so on.
3 The case shows the analysis model can preferable apply to the analysis to the behavior of RCCD, furthermore to the work condition of these dams with fault and sandwich.

ACKNOWLEDGEMENT

Financial support for this paper was provided by Natural Science Fund of China (50139030) and 973 Project Fund of China (2002CB412707).

REFERENCES

[1] Wu Zhongru, Gu Chongshi and Wu XiangHao. Safety Monitoring Theory and Its Application of RCCD. Science Press. Beijing; China. 2001
[2] Shen Guanling. Composite Material Mechanics. Qinghua University Press. Beijing, China. 1996
[3] Wu XiangHao. Transferring Attribute of Shapai RCCD. Water and Electricity Energy Science. 2002, 20 (2):10–12
[4] Wu Zhongru. Safety Monitoring Theory and Its Application of Hydraulic Structures, Higher Education Press, Beijing, China. 2003
[5] Wu Zhongru, Gu Chongshi. Prototype Back Analysis and Its Application for Dam Jiangshu Science and Technology Press, Nanjing, 1999

New Developments in Dam Engineering—Wieland, Ren & Tan (eds),
© 2004 Taylor & Francis Group, London, ISBN 04 1536 240 7

Study on special tailrace system of Xiangjiaba Hydroelectric Project

Gu Xiaoyuan, Li Foyan & Yu Zhiwen
Mid South Design & Research Institute for Hydroelectric Projects, Changsha, Hunan, P.R. China

ABSTRACT: In order to meet the regulation guarantee requirements, and minimize the size of underground cavern complex, the special tailrace system scheme (i.e., roof elevation of the tailrace tunnel will increase with the increase of its length toward downstream and no surge chamber will be arranged) has been adopted for the Xiangjiaba Hydroelectric Project. This paper presents the basic working principle and design philosophy of the special tailrace system, and justifies the viability and rationality of the scheme.

1 GENERAL

In accordance with the development tasks of the project, the hydro complex will be arranged as follows: flood-releasing works at the middle of the riverbed, powerhouse at dam toe at the left riverbed, underground powerhouse at the right bank, and navigation works at the left riverbed. Four 750MW generating units will be installed in each powerhouse, and the total installed capacity will be 6000MW.

The caverns of underground powerhouse will be located in thick sandstone of T_3^{2-6} rock cover should be remained for the cavern complex, and the size of the cavern complex should be minimized.

2 ARRANGEMENT AND CONFIGURATION DESIGN FOR THE SPECIAL TAILRACE SYSTEM

The water conveyance system of the underground powerhouse will be an arc in the plane view. The headrace conduits will range from 326.915m for Unit 1 to 220.338m for Unit 4, and the tailrace sections from 384.292m for Unit 1 to 309.542m for Unit 4. The rated head of the turbine is 95.0m, and the unit discharge 893m^3/s. The study and analysis on the transition process of the water conveyance system show that vacuity at the draft tube can hardly meet the requirements of specifications. If the topographical and geological conditions are permissible, the tailrace length should be minimized, and rational arrangement of the tailrace structures should be selected so as to meet the regulation guarantee requirements. Considerable variation of the tailwater level will occur during the operation of the power plant. The tailrace system is designed to operate with a variation of tail-water level up to 29.18m. However, the tailwater level is relatively stable in wet or dry season.

The special tailrace system can achieve that the tailwater will connect one point of the tunnel roof, and the tailrace tunnel will be divided into two sections, one pressure flow and the other free flow. In low-level season, the tailwater will connect the low-level point of the tunnel roof, which will result in a short pressure section and a long free flow section. In this case, the vacuity at the draft tube inlet would not exceed the specified value. With the raising of the tailwater level, the

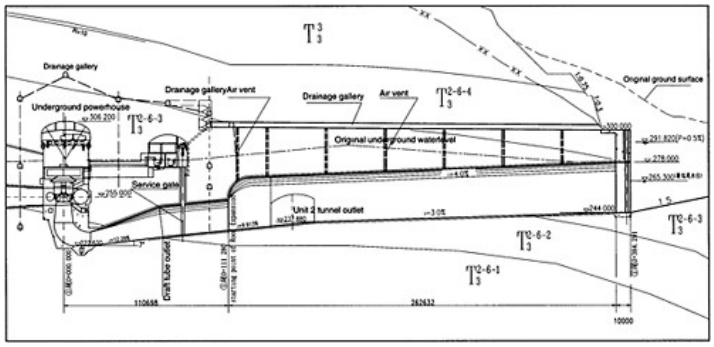

Figure 1. Layout of the special tailrace system.

pressure section will become longer and the free flow section shorter. The negative water hammer pressure will increase in the transition process. However, raising of the tailwater level will bring a bigger submersible depth of the turbine. Accumulation of the two pressures can achieve that the vacuity at the draft tube inlet would not exceed the specified value.

The working principle of the special tailrace system is as follows: Based on the variation of tail-water level (i.e., variation of submersible depth of turbine), the length of the pressure section will be determined not to exceed the limit so that the vacuity at the draft tube inlet would not exceed the specified value in the transition process and the surge chamber would not be necessary. The maximum cross section (D-shaped outlet section) of the tailrace system will be 20m wide by 34m high. The tailrace tunnel will have an outlet invert elevation of 244.000m and an outlet roof elevation of 278.000m. The tailrace tunnel will be 263m long for Units 1 & 2, and 199m long for Units 3 & 4. The invert and roof grades will be 0.03 and 0.04 respectively.

3 NUMERICAL CALCULATION AND MODEL TESTS

Study on the special tailrace system mainly consists of: (1) configuration of the special tailrace system without a surge chamber; (2) operating characteristics and stabilizing process of the hydraulic-mechanical-regulating system in transition process such as major fluctuation, minor fluctuation and hydraulic disturbance by means of numerical calculation and model test; and (3) the model test parameters were input the numerical calculation program to verify the dependability and rationality of the results obtained by the two methods.

The study scope of numerical simulation calculation and prototype model test covered the same unit with a long tailrace system (i.e., the water conveyance system of Units 1 and 2). An integral normal model was adopted for obtaining the performance relating to the transition process. The model turbine has a minimum runner diameter of 250mm and a scale of 1:38. Numerical calculations and model tests were conducted for the operating conditions of 18 major fluctuations, 17 minor fluctuations and 5 hydraulic disturbances, including the controlling operating conditions of the first units in service, special tailrace system and surge chamber, as well as the operating conditions which may be encountered in low-flow and high-flow seasons of a normal year.

(1) Numerical calculation on hydraulic transition process

The numerical calculation results for major fluctuation transition process are shown in Table 1. The results indicate that all the regulation guarantee parameters can meet the requirements of pertinent

Table 1. Summary of the numerical calculation results on major fluctuation transition process.

Calculator	Max. pressure rise at the spiral case (m)				Max. speed rise rate of generating unit		Max. vacuity at the draft tube inlet	
	No. of operating condition	Absolute value	ζ_{max} (%)	ζ'_{max} (%)	No. of operating condition	β_{max} (%)	No. of operating condition	B ($-mH_2O$)
Advisory firm	D37	163.69	40.72	30.95	D9	45.620	D13	4.34
Tsinghua University	D4	156.73	30.00	25.38	D16	51.902	D5	5.05
Hehai University	D13	151.28	27.66	21.00	D4	50.430	D6	5.57
Wuhan University	D4	160.56	28.50	28.45	D9	51.810	D6	8.17
Liu Baohua	D46	157.96	44.98	26.37	D49	49.492	D6	4.629
Design requirements	≤168.75			≤35		≤52		≤7.5

Notes: 1. ζ_{max} herein was obtained by the calculator based on his own initial pressure value; 2. ζ'_{max} herein was obtained based on the reference initial value H_0=125m.

specifications and project design if appropriate closing law is adopted for the wicket gate. Although different computation programs were used by different calculators, some boundary conditions were dealt with different methods, and the calculation results were slightly different, the variation tendency of main parameters like pressure under the same operating condition was almost consistent; and operating conditions in which extreme values occurred in major fluctuation were basically consistent. The operating condition with a minimum pressure at the draft tube inlet occurred under the following conditions: minimum operating level, minimum tailwater level, full load of the two units rejected successively, and the maximum vacuity no more than 7.5m head. The operating condition with the maximum speed rise rate occurred under the following conditions: rated load rejected under the operation at rated head, and the speed rise rate P≤52%. The special tailrace system converged the major fluctuation transition process in a relatively quick speed, and that is why the surge chamber should be cancelled.

For the minor fluctuation transition process, the operation conditions of load increase from zero under various reservoir and tailwater levels, and load increase or decrease by 10% were studied. The numerical calculation results indicate that fluctuation of pressure at spiral case, pressure at draft tube inlet and power of generating unit will decay with the time, and dynamic performance of the regulation system will conform to the specifications. Regardless of the regulating factor of the power grid, ±0.2% frequency range will be achieved in a short period of time. Under the operating condition of load increase from zero, the generating unit will operate in a stable manner with quite good regulating performance. The fluctuation of tailwater will be minor and quick to be converged. Hence the minor fluctuation will be of good stability and regulating property.

The calculation results on hydraulic disturbance transition process indicate that in case load of adjacent generating units of one unit varies, the fluctuation of pressure at spiral case, pressure at draft tube inlet and power of generating unit will decay with the time, and the regulating system will be stable. Therefore, hydraulic disturbance will not be a controlling factor.

(2) Modeltests

The hydraulic characteristics of the special tailrace system will be closely related to the tailwater level. The tested operating conditions include the tailwater levels which will have considerable impacts on the hydraulic characteristics of the special tailrace system and regulating guarantee parameters of the generating units, i.e., low level (266.5m when two generating units operate at rated flow), medium level (273.15m when 8 generating units operate, which will touch the middle of tunnel roof), and high level (278.0m, flush with the roof of tunnel outlet; and 294.22m, the downstream check flood level).

The model test results indicate that at the steady flow through the turbine, the flow pattern in the tailrace tunnel will vary with the variation of the tailwater level. At low tailwater level, the flow in

the tailrace tunnel will be mostly free and steady, and the intersection of pressure flow and free flow will be located at the curve arch section. At medium tailwater level, flow in the tailrace tunnel will be partly pressurized and partly free, and will be subject to some disturbance due to operation of the generating unit. The water level at the tailrace gate shaft will vary in a range of 0.2m~0.4m, and the intersection of pressure flow and free flow will move upstream and downstream in a range of 8m, consistent with the fluctuation cycle of water level in the tailrace gate shaft. No alternation of pressure flow and free flow will be formed, so no damage to the structure will occur. At high tailwater level, the tailrace tunnel outlet will be submerged, and the flow in the tailrace tunnel will be pressurized and will be steady. In this case, the average flow rate will be 2.78m/s or so, and the water surface in the tailrace gate shaft will be subject to a slight fluctuation, 0.1m or so, which will be lower than that at medium tailwater level.

The model test results indicate that under various transition process operating conditions, the tailrace tunnel can operate normally, steadily and reliably, with a roof pressure variation ranging from 6m to 10m head. No abrupt pressure variation occurred in the tailrace tunnel due to collapse of vacuum air mass, nor did alternation of pressure flow and free flow. The magnitude of water hammer pressure and moving range and rate of intersection of pressure flow and free flow were all in a reasonable range. No hydraulic phenomena affecting the steady operation of the power plant occurred due to the abrupt pressure variation, and all the controlling parameters can meet the design codes and specifications. All these indicate that the configuration design of the special tailrace system is reasonable and viable, and can effectively deal with the major fluctuation transition process, and replace the surge chamber. The test results show that pressure distribution on the cross section of the draft tube inlet will be uneven, with the maximum pressure on the side wall, the medium pressure in the center and the minimum pressure at two-thirds of the radius from the center.

The test results indicate that whether air vents are arranged at the tunnel roof or not will have minor impacts on the regulation guarantee parameters. However, the air vents can accelerate to stabilize the major fluctuation transition process, reduce the pressure at the tunnel roof and invert by 0.5 m head, decrease the water level variation in tailrace gate shaft by 1.2m, and make the transition process relatively flat. In addition, air vents would be beneficial for improving the transition process and increasing the safety margin.

The test results also show that the selected governor parameters are basically rational. The minor fluctuation transition process can not only modify the disturbance due to load increase or decrease of the generating units, and also be convergent. All the fluctuations caused by hydraulic disturbance will be convergent. Therefore, the generating units will operate steadily.

(3) Comparison and verification of numerical calculation results and model test results

In order to verify the dependability of numerical calculation software, numerical calculation was conducted based on the operating conditions of physical model test, i.e., the parameters obtained from model tests such as the conduit parameters and unit characteristic parameters, and the corresponding curves for boundary conditions and closing law of wicket gate obtained from the model tests were input the numerical calculation program. Analysis and comparison of calculation results obtained from numerical calculation program based on boundary conditions of model test and the data obtained from model tests were conducted.

The contrast of controlling parameters for major fluctuation transition process obtained from model tests and numerical calculation is shown in Table 2.

Under the same operating condition, most of the controlling parameters for major fluctuation transition process obtained from model tests and numerical calculations are very close, with a difference within 10% or 5% and minor error. Therefore, the two methods can verify each other, and the results are believable.

As for minor fluctuation and hydraulic disturbance, the controlling parameters obtained from model tests and numerical calculations share the same variation tendency, with the magnitude in the same class. Hence, the results are reasonable.

As the one-dimensional unsteady flow mathematic model and characteristic method were used for numerical calculation, the turbine boundary condition was obtained by the model synthetic

Table 2. Contrast of controlling parameters for major fluctuation transition process obtained from model tests and numerical calculation.

Controlling parameters	Operating condition	Model test results	Calculation results
Closing law and time (s)	–	Brokenline 12.0	Broken line 12.0
Max. dynamic pressure at	13TSD2 (Unit 1)	146.28	147.35
spiral case end (m)	13TSD2 (Unit 2)	145.77	147.64
Min. dynamic pressure at	811J2SD2 (Unit 2)	−6.71	−1.17
draft tube (m)	20TJSD2 (Unit 2)	−5.62	−7.65
Max. speed rise rate of	821J2SD3 (Unit 2)	43.9	46.4
generating unit (%)	20TSD3 (Unit 1)	41.2	48.1
Max. surge at the gate shaft (m)	14TSD2 (Unit 1)	299.98	300.30
Min. surge at the gate shaft (m)	5TSD6 (Unit 2)	262.41	261.35
	651J2SD2 (Unit 2)	262.58	259.45
Max. displacement toward upstream of the intersection of pressure flow and free flow (m)	81U2SD2	140.88	165.33
Max. displacement toward downstream of the intersection of pressure flow and free flow (m)	8TSD2	37.66	30.06
Max. fluctuation at intersection of pressure flow and free flow (m)	8TSD2	171.30	195.15

Table 3. Impacts of sectional area of tailrace gate shaft on regulation guarantee calculation (Unit 1).

No.	Sectional area of gate shaft	Area of spiral case inlet H_{max} (m)	Max. speed rise $\beta max_{(\%)}$	Vacuity at the draft tube inlet H_{Dmin} (m)	Min. surge level at gate shaft (m)
1	55.00	157.95	49.517	4.643	262.74
2	62.56	157.96	49.492	4.629	262.72
3	100.00	157.99	49.422	4.459	262.88
Operating condition		Two generating units reject the rated load at normal pool level	Two generating units reject the rated load at rated head	Two generating units reject the rated load successively at operating level	

curve and interpolation method, and the mixed flow of pressure flow and free flow was dealt with the modified fictitious slit method, simplification and assumption which are different from the actual conditions, are unavoidable for the mathematic models and handling methods. In addition, unavoidable error might occur in the test. All these are attributable to the difference of the results obtained from numerical calculation and model tests.

In view of the physical model tests, the tests were of good repetition and gave out the regulation guarantee parameters with high accuracy, especially the speed rise of generating unit and the min. dynamic pressure at the draft tube inlet, which are critical for modification of the numerical simulation, error analysis and mutual verification of numerical calculation results and model test results.

The comparison and mutual verification indicate that model test results are tally with the numerical calculation results. The numerical calculation program can be used as an effective tool for research and design work and for alternative comparison and configuration optimization.

(4) Impacts of sectional area of tailrace gate shaft on regulation guarantee calculation

The tailrace gate shaft can reduce the adverse impacts of the pressure fluctuation in the tailrace tunnel on the generating unit to some extent. Impacts of the increased sectional area of tailrace gate shaft on regulation guarantee calculation are shown in Table 3.

As shown from Table 3, appropriate adjustment of the sectional area of the gate shaft will have minor impacts on the regulation guarantee calculation result and the min. surge level. Therefore, it is not necessary to further increase the sectional area of the tailrace gate shaft.

4 CONCLUSIONS

Based on study on the special tailrace system scheme of Xiangjiaba Hydroelectric Project, the following can be concluded:

(1) With the help of variation of the tailwater level, the special tailrace system can effectively solve the transition process and meet the min. absolute pressure requirements of the draft tube inlet. Under various operating conditions of major fluctuations, all the controlling parameters can meet the design codes or specifications. Hence, the surge chamber may be cancelled. Under the transition process of minor fluctuation and hydraulic disturbance, fluctuation of the speed of generating unit, pressure at the spiral case, and pressure at the draft tube inlet will decay and converge with the time and finally flatten at a new steady flow. The regulation performance will be better than that of the surge chamber. This is why the surge chamber can be replaced.

(2) Under normal operation of the power plant, and steady flow or minor fluctuation in the tailrace tunnel, no alternation of pressure flow and free flow will occur in the full length of the tailrace tunnel, nor will air mass. Therefore, there will be no worries that the special tailrace tunnel will have any adverse impacts on the steady operation of the generating units and the roof structure.

(3) In view of the hydraulic performance of transition process in the special tailrace tunnel, corresponding mathematical model and calculation method were established, and the computation program was prepared. The numerical simulation calculation results are comparable with the model test results. Hence, the mathematical model and computation program can be used as effective tools for the design of the project and for alternative comparison and configuration optimization.

(4) In comparison with the impedance surge chamber scheme, the special tailrace system scheme can reduce mass excavation, favorable for lowering damage to the surrounding rock of the underground powerhouse, and reducing work quantities of the underground powerhouse; and reduce the head loss by 0.406m, hence reducing the energy loss in long-term running.

(5) Considering the factors of the regulation capacity, cost effectiveness, impacts on the stability of the surrounding rock of the cavern complex, and the potential risks, the special tailrace system scheme is superior to the impedance surge chamber scheme. Therefore, the special tailrace system scheme has been adopted for the Xiangjiaba Hydroelectric Project, and the tailrace surge chamber cancelled.

New Developments in Dam Engineering—Wieland, Ren & Tan (eds),
© 2004 Taylor & Francis Group, London, ISBN 04 1536 240 7

Rheological model of rockfill for analysis of Concrete Face Rockfill Dam

Xing-wen Guo, De-xin Wang & Xin Cai
College of Civil Engineering, Hohai Univ., P.R. China

ABSTRACT: In this paper, a rheological model for rockfill is proposed and a method for solving is suggested. Based on the 3-dimensional finite element methods, the model is applied to analyse the influence of the rheology of rockfill to the Shuibuya concrete face rockfill dam. The calculation result indicates that the rheology of rockfill has effects on the dam, especially on the concrete face slab. Some characteristics of the influence caused by the rheology of rockfill to the SHUIBUYA CFRD are expatiated. It is necessary to consider the rheology of rockfill material in large dam design in various stages including construction and reservoir impounding period.

1 INTRODUCTION

Concrete face rockfill dam (CFRD) has many advantages, such as the available of local material, short construction period, convenient construction, low cost, etc. It has developed rapidly during the past few decades, and become a widely used type of dam in the world. But now the design and the construction of CFRD are still at the empirical stage, and theory of design at the stage of development. Although, nonlinear finite element method (NFEM) and elastoplastic finite element method (EPFM) have been employed to simulate the behavior of the CFRD, they cannot adequately predict the behavior of the CFRD [1]. The results obtained from the observation of the built CFRD indicated that rockfill may produce rheological deformations which cannot be simulated by using NFEM or EPFM. But this kind of rheological deformation of the rockfill will significantly influence the behavior of the CFRD [2,3]. So, it is necessary to consider the rheology of rockfill in large dam design in various stages including construction and reservoir impounding period.

In this paper, a rheological model for rockfill is proposed and a method for solving is suggested. Based on the 3-Dimension finite element methods, the model is applied to analysis the influence of the rheology of rockfill to the SHUIBUYA CFRD. Some characteristics of the influence caused by the rheology of rockfill to the SHUIBUYA CFRD are expatiated.

2 CONSTITUTIVE MODELS OF ROCKFILL FOR CONSIDERING RHEOLOGY OF ROCKFILL

At present the studies of the rheology of rockfill is not sufficient, some researchers simulate the rheology of rockfill with experimental model expressed as [2]

$$\varepsilon(t)=\varepsilon_f(1-e^{-ct}) \tag{1}$$

where ε_f is the ultimate rheology of rockfill when time $t \to \infty$ and which is associated with the stress of the rockfill element; c is the ratio of the rheology of rockfill occurred in the first day.

The volume rheology and shear rheology of the rockfill are different. According to formulas suggested by Shen Z.J. [2], the author revamps the formulas, which can be expressed as

$$\varepsilon_{vf} = b\left(\frac{\sigma_3}{Pa}\right)^n \quad , \quad \varepsilon_{sf} = d\frac{SL}{1-SL} \tag{2}$$

where b, n and d are parameters, and their meaning are as follows: b is the ultimate volume rheology of rockfill when confining pressure σ_3=1 *Pa;* n is the index indicating the variation of volume rheology of rockfill with changing of the confining pressure σ_3; d is the ultimate shear volume creep of rockfill when stress level SL=0.5.

In the computation the ultimate shear rheology of rockfill ε_{sf} may be an unlimited value if stress level of rockfill reached value 1.0. In this case the stress level of rockfill element may be taken as SL=0.95 for the computation.

Supposed that the volume rheology of rockfill and the shear rheology of rockfill can be simulated with formula (1), and also supposed that the two kinds of rheology of rockfill have similar reducing features, thus the speed of volume rheology and the rheology of shear rheology can be respectively expressed as

$$\dot{\varepsilon}_v = c\varepsilon_{vf}e^{-ct} \, , \quad \dot{\varepsilon}_s = c\varepsilon_{sf}e^{-ct} \tag{3}$$

3 METHOD FOR CONSIDERATION OF THE RHEOLOGY OF ROCKFILL

The rockfill material is compacted in layers in CFRD construction and the impounding procedure is completed gradually. In different stages, the element's rheology time in different places is different. The procedure of track time will be complicated using uniform time when using increment FEM to analyses the rheology of rockfill. Idea of relative time is proposed and is used for solving this problem. In the program, time is reckoned in when every load procedure completed and current load procedure commenced.

3.1 *The equation transform with the relative time*

Change the equation (3) as following

$$\dot{\varepsilon}_v = c\varepsilon_{vf}\left(1-\frac{\varepsilon_{vt}}{\varepsilon_{vf}}\right); \quad \dot{\varepsilon}_s = c\varepsilon_{sf}\left(1-\frac{\varepsilon_{st}}{\varepsilon_{sf}}\right) \tag{4}$$

ε_{vt} and ε_{st} are accumulated volume strain and the shearing strain, they can be calculated by formulas (5).

$$\varepsilon_{vt} = \sum \dot{\varepsilon}_v \Delta t \, ; \quad \varepsilon_{st} = \sum \dot{\varepsilon}_s \Delta t \tag{5}$$

The corresponding increment of ε_{vt} and ε_{st} in the period Δt can be calculated by formulas (6).

$$\Delta\varepsilon_{vt} = \dot{\varepsilon}_v \Delta t \, ; \quad \Delta\varepsilon_{st} = \dot{\varepsilon}_s \Delta t \tag{6}$$

Thus, in the computation we can use the increment Δt, not the total time t in the whole calculations through the transformation. The relationship between volume rheology and shear rheology of rockfill and stress of rectangular Cartesian coordinates can be changed with Prandtl-Reuss's flow criteria and can be expressed as following

$$[\Delta\varepsilon] = \frac{1}{3}\dot{\varepsilon}_v[I] + \frac{1}{2}\frac{\dot{\varepsilon}_s}{q}[s] \tag{7}$$

where [$\Delta\varepsilon$] is the strain increment tensor, *[I]* is unit tensor, *[s]* is derivative stress tensor and q is general shear stress.

3.2 *The steps of increment FEM*

In FEM calculation, we can follow the steps:

1. We first do the work of calculating the instantaneous nonlinear elastic deformation or elastoplastic deformation of the corresponding load using nonlinear model or elastoplastic model, and get the result of the element stress and the stress level according to the constructing and the impounding course.
2. We confirm the loading time T_i of this level by the construction schedule and separate the T_i to a few of period of time Δt_i (the equal one and the not equal one).
3. Supporting that the stress doesn't change during the period of the time Δt_i, we can get the shearing theology ε_{sf} and the volume strain ε_{vf} by the formulas (2). We can also get the strain rate by formulas (4), the cumulative theology by formulas (5), the corresponding rheology increment by formulas (6), and strain increment in the rectangular Cartesian coordinates by formulas (7).
4. Do structural FEM analysis by the primary strain method, and get corresponding displacement increment, stress increment, and cumulate total displacement and stress.
5. Do judgment of the time during the period of loading, if completed and then to circulation [1], else to circulation [3].

4 RHEOLOGICAL ANALYSIS OF SHUIBUYA CFRD

SHUIBUYA CFRD with height 233m located on qinjiang river in hubei province, P.R. China. It is the highest CFRD under construction in the world.

4.1 *Material consititutive relation and material parameters*

The rockfill deformation is composed with instantaneous deformation and rheological deformation. The rockfill instantaneous deformation is calculated with Duncan's *E-B* model [3], The rheological deformation is simulated with four-parameter model proposed in [2]. The material model parameters are listed in table 1.

The stiffness of the rockfill in cushion zone is very smaller compared with that of concrete face slab, so when load is applied on them, the contact part between the cushion and concrete face slab may occur displacement. In order to simulate this kind of interaction between them one type of contact element is adopted in the computation. In this paper the Goodman contact is applied.

Water stop materials are placed in the joints in order to prevent water seepage, however the water stop materials can produce deformation when load applied. According to the test result, the deformation of water stop can be simulated by applied no thickness connect element. The no thickness connect element is similar to Goodman interface element. The modulus coefficient of

Table 1. Parameters of rockfill for Duncan's *E–B* model and rheologic model.

Materials	Parameters											
	(γkN/m^3)	φ/°	k	n	R_f	k_b	m	Δ/°	b	c	d	n
Cushion	22.0	56	1200	0.45	0.78	750	0.20	8.6	0.0003	0.005	0.004	0.5
Transition	21.8	54	1000	0.40	0.85	450	0.15	10.5	0.0002	0.005	0.003	0.5
Mainrockfill	21.5	52	1100	0.35	0.82	600	0.10	8.5	0.0002	0.005	0.003	0.5
Downstream rockfill	21.5	50	850	0.25	0.80	400	0.05	8.4	0.0005	0.007	0.004	0.5

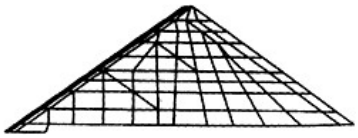

Figure 1. FE mesh for typical section.

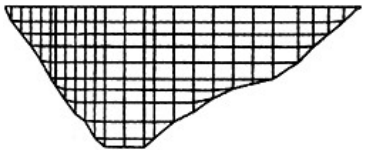

Figure 2. FE mesh for the face slab.

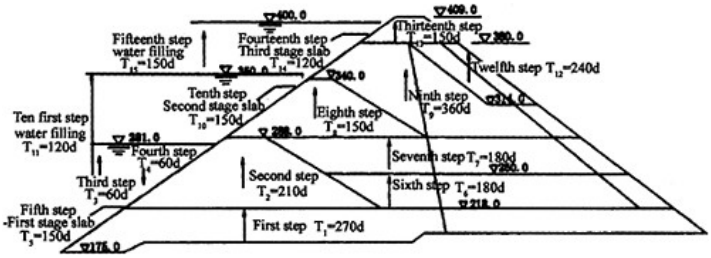

Figure 3. Loading procedure and time schedule (d means days).

connected element is determined by test with waterproof materials. To study the deformation of joints in CFRD, a serials of tests of copper waterproof, rubber waterproof and stainless steel waterproof had been carried out by Hohai University, and relationship between the stress and relative displacement of connect element is also derived [3].

Concrete materials such as concrete face slab and plinth adopt the linear elastic model and do not consider their rheology.

All parameters of contact, wateproof and concrete can be found in reference [3].

4.2 *Structure meshing, calculate loading procedure and time schedule*

In 3-D FE model, the structure are divided into 2007 elements with 2245 nodes, in which the number of rockfill element is 1535, the number of concrete face slab element is 152, the number of contact element between slab and cushion is 152, and the number of water proof joint element is 168. Figures 1 and 2 show the FE mesh for typical section and the face slab.

In combination with provided dam construction and impounding procedure, loading procedure and time schedule are simulated, shown in Figure 3.

4.3 *The results and discussions*

Owing to limit of paper size, we can only list partial results, and we will mainly discuss the influence caused by the rheology of rockfill on the concrete face slab. Other detailed results can be found in reference [3].

Figure 4 shows displacement contours of face slabs without considering rheology of rockfill. Figure 5 shows displacement contours of face slabs with considering rheology of rockfill. Figure 6 shows stress contours of face slabs without considering rheology of rockfill. Figure 7 shows stress contours of face slabs with considering rheology of rockfill.

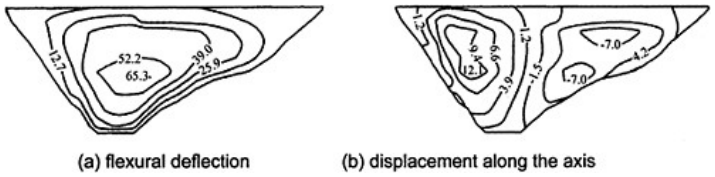

Figure 4. Displacement contours of face slab without considering the rheology of rockfill (unit: cm).

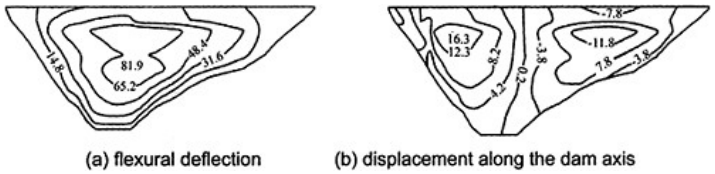

Figure 5. Displacement contours of face slab with considering the rheology of rockfill (unit: cm).

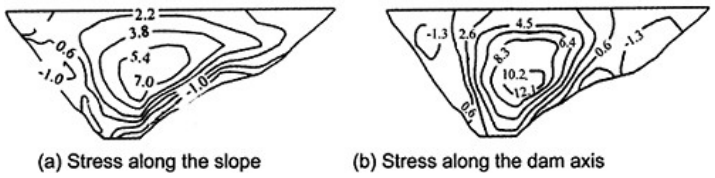

Figure 6. Stress contours of face slab without considering the rheology of rockfill (unit: MPa).

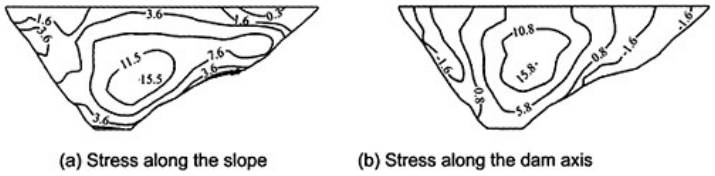

Figure 7. Stress contours of face slab with considering the rheology of rockfill (unit: MPa).

According the results we can find that the influence caused by the rheology of rockfill to the face slab are as following:

(1) Rheology of rockfill increase the displacements of face slabs both flexural deflection and displacements along the dam axis. The general trend of displacements of face slabs along the dam axis is valley-oriented deformation. The maximum displacement of face slabs toward

right bank is 12.1cm, toward left bank is 9.0cm without the rheology of rockfill being considered. The maximum displacement of face slabs toward right bank is 16.3cm, toward left bank is 12.3cm with the rheology of rockfill being considered. The maximum flexural deflection of face slabs is 65.3cm without the rheology of rockfill being considered. The maximum flexural deflection of face slabs is 81.9cm with the rheology of rockfill being considered.

(2) Rheology of rockfill increases the compression stress value of face slabs along slope and decreases the tension stress value of face slabs along slope. The maximum compression stress value of face slabs along slope is 7.0MPa and the maximum tension stress value of that is 4.1MPa without the rheology of rockfill being considered. The maximum compression stress value of face slabs along slope is 15.5MPa and the maximum tension stress value of that is 0.3MPa without the rheology of rockfill being considered. At the same time the areas with tension stress also decrease.

(3) Rheology of rockfill increases the compressing stress of face slabs along the axis in the valley, whereas increase extension stress of face slabs near banks regions. The maximum compression stress value of face slabs along the axis is 12.1MPa and the maximum tension stress value of that is 2.3MPa without the rheology of rockfill being considered. The maximum compression stress value of face slabs along the axis is 15.8MPa and the maximum tension stress value of that is 3.1MPa without the rheology of rockfill being considered. At the same time the areas with tension stress changes little.

5 CONCLUSIONS

According to the partial test results and results obtained from the observation of the built CFRD, a rheological model for rockfill is proposed and a method for solving is suggested. Based on the 3-Dimension finite element methods, the model is applied to analysis the influence of the rheology of rockfill to the SHUIBUYA concrete face rockfill dam. Some characteristics of the influence caused by the rheology of rockfill to the SHUIBUYA CFRD are expatiated. It is necessary to consider the rheology of rockfill material in large dam design in various stages including construction and reservoir impounding period.

REFERENCES

[1] Fu Zhian, Fen Jiaji. Concrete Faced rockfill dam. Press of Huazhong University of Science & Technology, Wuhai, P.R.China, 1993 (in Chinese).

[2] Shen zhujiang, Zhao kuizi. Back analysis of creep deformation of rockfill dams, Journal of Hydraulic Engineering, 1998, 6(1):1~6 (in Chinese).

[3] Guo Xingwen. Numerical analysis of rockfill dams and test research of waterstop structures. Dissertation for the degree of Doctor of Engineering. Hohai Univ., P.R. China, 1999, 6: 41~70 (in Chinese).

New Developments in Dam Engineering—Wieland, Ren & Tan (eds),

Experimental investigation of rubber liner

Hao Yuan, Xie Yibing & Wang Aiping
Yellow River Institute of Hydmulic Research, YRCC, China

ABSTRACT: As for the static and dynamic test of coarse-grained soils, in order to prevent the rubber membrane from being penetrated by coarse-grained silt, many methods to reinforce the rubber membrane are widely adopted at home and abroad to sure the test going on smoothly but the methods will produce certain constraints on the tested samples. Here a series of comparative tests on the static and dynamic characteristics with or without rubber liners were carried out. Initial analysis and study are carried out on the impact of rubber liner on the test results. And according to the results, the empirical formula to eliminate the impact of rubber liner is produced.

FOREWARD: In the indoors static and dynamic test of the coarse-grained soil, as for its big grain size, edges and corners and rather high intensity, the rubber membrane is liable to the penetration by the convexes of sharp silts during preparing of the samples. In order to ensure the seal of the sample and prevent the rubber membrane from being penetrated, a lot of methods are adopted at home and abroad to reinforce the rubber membrane[1], such as (1) double or multiple rubber membranes, (2) rubber sheets between rubber membrane and sample, (3) three membranes of internal, central and external ones with rubber hexagons (thickness 8mm, side length 40mm and interval 5mm) mounted on the central membrane, (4) filling sand of 50mm thick between the internal and external rubber membranes, (5) insert galvanized paper between the sample and internal rubber membrane, stick on oiled PVC sheet (100mm×100mm× 1mm) on the internal membrane and then put on the external membrane, etc. The first and second methods are widely adopted to reinforce the rubber membrane in China. Though the reinforced rubber membranes ensured the smooth test operation, it increased the binding of the samples and could produce certain influence on the test results. Here a series of comparative tests on the static and dynamic characteristics initially show the influence of the rubber sheets on the test results.

1 TEST EQUIPMENT, MATERIALS AND METHODS

Test equipment is the 1000 kN electrohydraulic Servo Dynamic & Static Triaxial Tester. The geometrical size of the sample is: 30cm × 75cm (diameter×height); the maximum surrounding pressure: 2MPa; the maximum axial static load: 1000kN; and excitation frequency: 0.01~5Hz.

1.1 *Test materials*

The comparative test adopted two kinds of materials. One is a kind of fine grain material, the standard sand from Pingtan, Fujian Province. Its grain grade is as Table 1. Another is a kind of coarse grain material, the gravel from the flood land of Xiaolangdi. Its grain grade is as Table 2.

Table 1. Grain gradation of standard sand.

Grain size (mm)	1~0.5	0.5~0.25	0.25~0.1	0.1~0.074	<0.074
Content (%)	11.7	58.0	28.1	0.5	1.7

Table 2. Grain gradation of Xiaolangdi gravel.

Grain size (mm)	60~40	40~20	20~10	<2
Content (%)	25.5	28.7	25.5	20.3

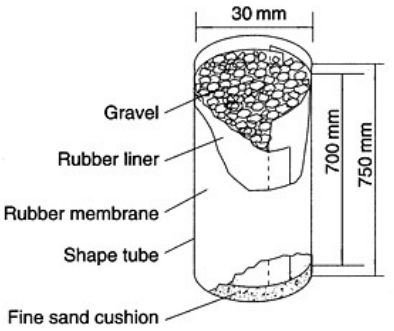

Figure 1. Diagram of sample with rubber liner.

1.2 *Test method*

The comparative test adopted the whole test method[2] i.e. two paralleled groups of tests with standard sand and gravel are carried out. The samples of Group 1 are covered with a coat of rubber membrane, and the binding force of the rubber membrane is supposed as zero. The samples of the other group are lined with three rubber sheets (each: length: 70cm, width: 35cm, thickness: 5mm) between the sample and rubber membrane. In order to minimize the binding force of the rubber sheets, a layer of fine sand 2.5cm thick is paved inside the rubber membrane, then three rubber sheets are overlapped inside the rubber membrane, gravels are filled in and at last another layer of fine sand (as Figure 1). The comparative tests are carried out under related side pressure of various classes, the test results of the two groups are compared to study the influence of the static and dynamic test results by the lined rubber sheets.

The same method and process of manufacture are adopted in the same humidity for the comparative tests. For the sample with rubber liner, when the material is taken, the volume of the rubber sheet is first deducted and the material is taken as per the controlled density. See test content and conditions in Table 3.

2 STATIC TEST RESULTS

2.1 *Influence on stress, strain and volumetric strain*

Figure 2 shows the relation curve of stress, strain and volumetric strain in the comparative tests of standard sand. Table 4 shows the comparison of change of the main stress difference in the static

Table 3. Test content and conditions.

Test item	Test material	Controlled humidity ρ_d (g/cm^3)	No. of test groups	Concretion ratio Kc	Pressure of concretion σ_3 (kPa)				
Shear stress at concretion without drain	Standard sand	1.55	1 with liner and 1 without			400	600	800	1000
Shear stress at concretion without drain	Standard sand	1.64	1 with liner and 1 without		200	400	600	800	
Shear stress at concretion & drainage	Standard sand	1.55	1 with liner and 1 without		200	400	600	800	1000
Shearing stress at concretion & drainage	Gravel	2.1	1 with liner and 1 without		100	200	300	400	
Dynamic intensity	Standard sand	1.55	2 with liner and 2 without	1.0	600	1000			
Dynamic intensity	Standard sand	1.55	2 with liner and 2 without	2.0	600	1000			
Dynamic intensity	Gravel	2.10	1 with liner and 1 without	1.0	600				

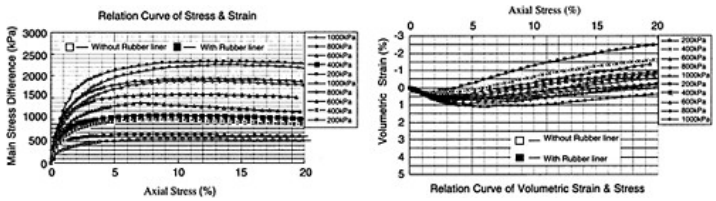

Figure 2. Medium density of standard sand ρ_d=1.57g/cm^3, comparative chart of stress, strain and volumetric strain with or without rubber liners at consolidation & drainage.

tests. It is known that under the same surrounding pressure the main stress difference of samples of the different density and different materials with lining rubber is all bigger than that without lining rubber, which shows that the lining rubber enlarges the failure strength of the soil material. The main stress difference shall gradually decrease with the increase of the surrounding pressure, which shows that under the low surrounding pressure the binding function of the lining rubber on the samples is stronger.

The relations between surrounding pressure and axial strain and volumetric strain in Figures 3 and 4 show that under the same surrounding pressure, the axial failure strain with lining rubber is bigger than that without lining rubber, the shear expansion in volumetric strain with lining rubber is bigger than that without lining rubber and will gradually decrease with the increase of the surrounding pressure. It is shown that the lining rubber has the function of delaying the failure of the test samples and the influence on axial strain is bigger than that on the volumetric strain.

2.2 *Influence on parameters of strain and stress*

Take K and n of the initial tangent modulus as an example (Table 5), the K and n values with lining rubber are always bigger that without lining rubber. K value is enlarged as 3.9~18.3% and n value is enlarged as 5.5~20%, which shows the samples are stiffer with lining rubber.

Table 4. Comparison of the main stress differences in the static tests.

Surrounding pressure (kPa)		100	200	300	400	600	800	1000
Standard sand	Shear force at concretion without drainage, p_d=1.57g/cm^3 Main stress difference when destroying without rubber plate (kPa)				1250	1600	1990	2380
	Shear force at concretion without drainage, p_d=1.57g/cm^3 Main stress difference when failure with lining rubber (kPa)				1307	1767	2125	2564
	Shear force at concretion without drainage, p_d=1.67g/cm^3 Main stress difference when failure without lining rubber (kPa)		760		1340	1900	2190	
	Shear force at concretion without drainage, p_d=1.67 g/cm^3 Main stress difference when failure with lining rubber (kPa)		870		1430	1950	2510	
	Shear force at concretion with drainage, p_d=1.57g/cm^3 Main stress difference when failure without lining rubber (kPa)		548		997	1372	1884	2251
	Shear force at concretion with drainage, p_d=1.57g/cm^3 Main stress difference when failure with lining rubber (kPa)		651		1097	1578	1934	2338
Gravel	Shear force at concretion with drainage, p_d=2.1g/cm^3 Main stress difference when failure without lining rubber (kPa)	517	925	1195	1662			
	Shear force at concretion with drainage, p_d=2.1g/cm^3 Main stress difference when failure with lining rubber (kPa)	629	998	1422	1691			

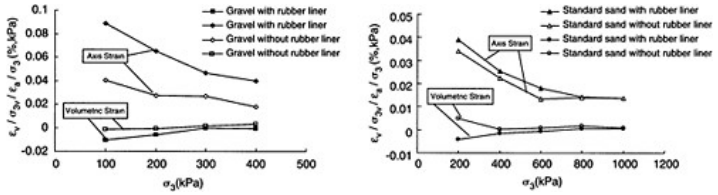

Figure 3. Relation between surrounding pressure and axial strain and volumetric strain of standard sand.

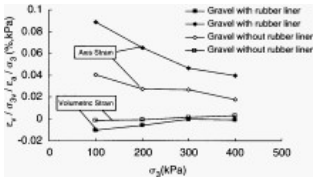

Figure 4. Relation between surrounding pressure and axial strain and volumetric strain of gravel.

3 DYNAMIC TEST RESULTS

3.1 *Influence on the dynamic ratio curve*

In Figure 5, the relation between dynamic stress and failure vibration times of standard sand is sorted out with strain of 5% as the failure standard. The figure shows that when Kc=1 consolidation at equal directional pressure, the test points under the same failure standard basically fall on the same curve. When Kc=2 consolidation at unequal directional pressure, the test points with rubber liner are a little higher than that without rubber liner. Take the dynamic strain ratio under 10, 20 and 30 vibration times as examples, the dynamic stress ratio with rubber liner are higher by 8.5~9.3% than that without rubber (as in Table 6). It is possibly because the dynamic strength test is under the condition of consolidation without drainage, when test sample in the state of Kc=1 consolidation at equal directional pressure under the action of cyclic load, the soil framework has the trend of continuous shrinkage, the pore water pressure increases rapidly, and rises up sharply at last and the liquefaction failure happens in short time, the lining rubber has no influence on the development of pore pressure.

Table 5. Parameters of strain & stress.

Tested material	Dry density controlled ρ_d (g/cm^3)	k	n
Standard sand (without rubber)	1.55	630	0.55
Standard sand (with rubber)	1.55	745	0.66
Gravel (without rubber)	2.10	1505.7	0.50
Gravel (with rubber)	2.10	1563.3	0.58

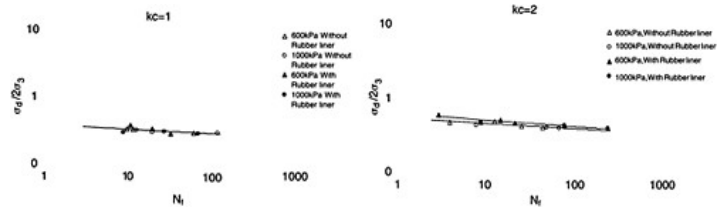

Figure 5. Relation between dynamic stress ratio & failure vibration times of standard sand.

Table 6. Dynamic stress ratio value.

Test material	Controlled dry density p_d (g/cm^3)	Concretion dry density p_d (g/cm^3)	Concretion ratio Kc	Surrounding pressure (kPa)	Dynamic stress ratio $\sigma_d/2\sigma_3$ N_f=10	N_f=20	N_f=30
Standard sand (with & without rubber)	1.55	1.59	1.0	600	0.33	0.31	0.30
	1.55	1.59	1.0	1000	0.33	0.31	0.30
Standard sand (without rubber)	1.55	1.59	2.0	600, 1000	0.47	0.45	0.43
Standard sand (with rubber)	1.55	1.60	2.0	600, 1000	0.51	0.49	0.47
Gravel (with & without rubber)	2.10	2.10	1.0	600	0.255	0.21	0.190
	2.10	2.10	1.0	600	0.255	0.21	0.190

While test sample is consolidated under Kc=2 unequal directional pressure, rather big initial shear stress is already in the soil; when cyclic load is added, the trend of volumetric shrinkage and expansion continues alternately. The binding function of rubber liner increases the trend of volumetric expansion; therefore, slight influence on the dynamic strength occurs under unequal directional pressure.

4 CORRECTION OF THE TEST RESULTS

The static and dynamic comparative test results show if the influence of the rubber plate is not considered, the shear strength of the sample measured is relatively high and unsafe and not suitable for the project. Thus, the influence with lining rubber shall be corrected.

4.1 *Correction of the static test results*

The static comparative test shows: the enlargement of failure main stress difference with lining rubber can be judged with the normalized failure main stress difference ratio (i.e. the failure main stress difference ratio is divided by surrounding pressure.), as shown in Figure 6. It is known from the figure that the relation between normalized failure main stress difference ratio and surrounding pressure is satisfactory, the following formula can be used:

$$\alpha/\sigma_3=1.5128\sigma_3^{-1.0523} \tag{1}$$

$$\alpha=1.5128\sigma_3^{-0.0523} \tag{2}$$

in which: α is enlargement times of failure main stress difference with rubber; $\alpha=(\sigma_1-\sigma_3)$ with/ $(\sigma_1-\sigma_3)$ without; $(\sigma_1-\sigma_3)$ with: failure main stress difference with rubber; $(\sigma_1-\sigma_3)$ without: failure main stress difference without rubber.

The figure shows that with the surrounding pressure increasing, failure main stress difference is gradually minimizing; which shows that the lining rubber has rather big influence on surrounding pressure.

4.2 *Correction of dynamic test results when Kc=2*

The dynamic test shows lining rubber only has influence on the test results when Kc=2. Figure 7 shows the normalized dynamic stress enlargement ratio has good linear relation with failure vibration times; the following formula can be proposed:

$$a_d/N_f=1.1276N_f^{-1.0116} \tag{3}$$

$$a_d=1.1276N_f^{-0.0116} \tag{4}$$

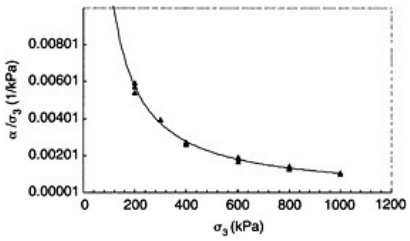

Figure 6. Relation between normalized failure main stress difference ratio.

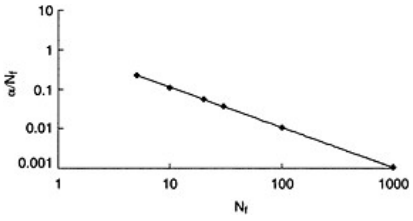

Figure 7. Relation between normalized dynamic stress ratio and failure vibration times of standard sand when Kc=2.

in which: α is enlargement times of dynamic stress ratio with lining rubber $\alpha_d=(\sigma_d/2\sigma_3)$ with/$(\sigma_d/2\sigma_3)$ without; $(\sigma_d/2\sigma_3)$ with: failure dynamic stress ratio with rubber; $(\sigma_d/2\sigma_3)$ without: failure dynamic stress ratio without rubber.

The figure shows that with failure vibration times increasing, the dynamic stress ratio minimizes; which shows that the lining rubber has bigger influence on the dynamic stress ratio at small number of vibration times.

The enlargement times of the test results with lining rubber can be estimated with formula (2) & (4), which can be adopted to correct the influence on the static and dynamic test results with lining rubber.

It is a pity that with influence of various reasons, the parallel test was not carried out for each group in this comparative test, which has brought certain limit to sort out and sum up the test results. But the test results show better law. With lining rubber, the trend of strength increasing under different test conditions is the same. The relationship of regression equation of fitting curves in the test is good and the relative factor is 0.996~1.0, which can be used to correct the static and dynamic test results with lining rubber.

5 CONCLUSIONS

1. The static test study shows that under the same surrounding pressure and with different densities and different materials, the failure main stress difference with lining rubber is always bigger than that without lining rubber, which shows the failure strength of soil material is enlarged with lining rubber.
2. The axial failure strain with lining rubber is bigger than that without lining rubber, which shows the lining rubber has the function to delay the failure of the samples.
3. Dynamic test shows that lining rubber has a little influence on the test results when Kc=2, and correction is needed; lining rubber has no influence on the test results when Kc=1, and correction is not needed.
4. Empirical formula (2) and (4), which are produced from the comparative test, can reflect the change of enlargement ratio of main stress and dynamic stress ratio with surrounding pressure and the number of failure vibration with lining rubber. They can be used to correct the static and dynamic test results with lining rubber.

REFERENCES

[1] Trade standard of P.R. China, Soil Test Rules (SL237–1999).
[2] Si Hongyang, Issues on Large Tri-axial Test of Earth Rockfill Dam Material, Earth and Rockfill Dam Project, April of 1987.
[3] Han Yuming, An Approach to Liquefaction of Saturated Sand, Journal of Geotechnical Engineering, March (4) of 1980.

This page intentionally left blank.

New Developments in Dam Engineering—Wieland, Ren & Tan (eds),
© 2004 Taylor & Francis Group, London, ISBN 04 1536 240 7

3-D seepage analyses on limb-grouting design by FEM

Chihiro Hayashi, Takahiko Tateishi & Michimasa Menjo
Nippon Giken Inc., Japan

ABSTRACT: A two-dimensional or quasi-three dimensional seepage analysis by FEM is one of useful method to evaluate a design of limb-grout that aims to mitigate leakage in foundation of dam abutment. However, this analysis is not fully effective for a dam foundation that has complicated geological formation in hydraulic conductivity aspect. Our study has applied a three-dimensional seepage flow analysis, which is by a method of saturated—unsaturated steady flow condition, for the foundation of the Rockfill dam that is under-construction in Kyushu, Japan as of Dec. 2003.

Then trial-and-error calibrations of modeling were conducted to simulate the hydraulic model on the original underground water condition. In order to a modified formation of plural ground-water tables were represented as accurate as natural figure through several trials of the calibration for hydraulic model, seepage flow analysis was conducted for several cases of limb-grout design. As a result of this analysis, a reasonable design of limb-grout was obtained.

We confirmed that this study has shown the effectiveness of the three-dimensional seepage flow analysis by FEM for the grout design of dam foundation that has the complicated geology and plural water tables. Because this analysis has a system for visualization of seepage trace in foundation, detouring flow beyond the limb-grout curtain can be shown visually in the model. We got the conclusion that this result can comprehensively evaluate the effectiveness of the limb-grout with the calculation of the leakage amount.

1 INTRODUCTION

It has been the general design that limb-grout curtain extends up to the intersect point of water table and designed normal full water level so far. However recent dams are often constructed on the foundation composed of some intricate groundwater conditions due to complicated hydrogeological structures. In the case of that water table of dam abutment and limb were much lower than the normal full water level, limb-grout would be designed much longer than usual.

The dam mentioned in this report is central core zone type of rock-fill dam of which main features are; height 69.9m, crest length 312.5m, full reservoir area 0.28km^2, gross reservoir capacity 4,310,000m^3, effective reservoir capacity 4,250,000m^3, normal full water level (FWL) 354.0m, and water depth of reservoir 66.5m. The right hillside limb consists of complicated geological structures, which has plural water tables being lower than its normal full water level of dam. Tateishi et al (2001 and 2003) had already studied the left hillside limb where water table was single, and decided its optimal limb-grout range applying three-dimensional seepage analysis with a method of saturated—unsaturated condition. Our study has applied to right hillside limb again, where water tables exist at many levels and we got its optimum grouting range to mitigate leakage effectively considering the relationship between its grouting range, seepage condition, hydraulic stability, and the cost. Plural water table conditions in the right hillside limb were shown by computer graphics on a system of three-dimensional analysis and detouring condition of seepage lines beyond the limb-grout curtain was also shown visually in the model. Those results comprehensively evaluated the effectiveness of the limb-grout with the calculation of the leakage amount.

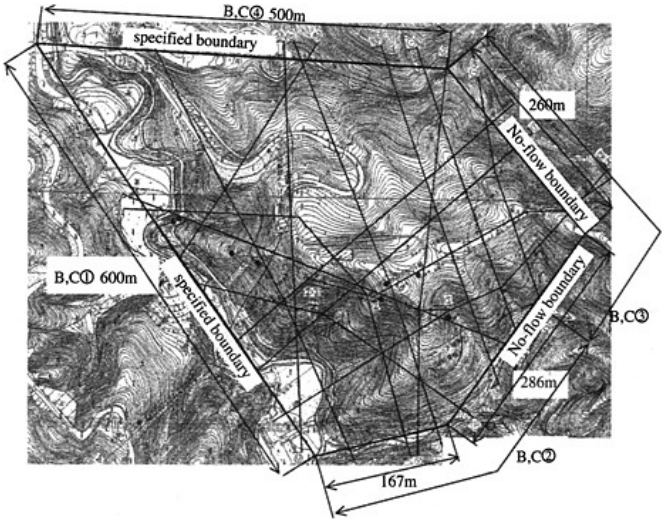

Figure 1. Locations of geological investigations and lines for geological sections.

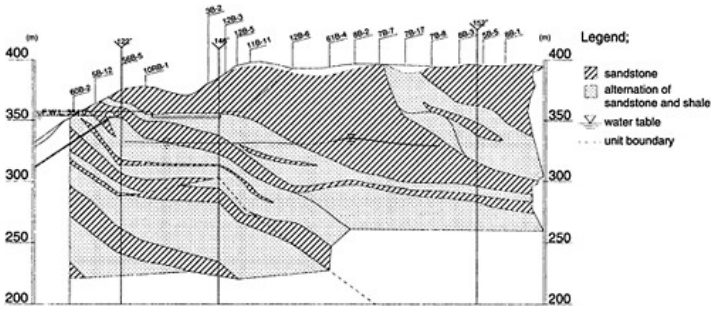

Figure 2. Geological section along limb-grout line.

2 GEOLOGICAL STRUCTURE ALONG RIGHT HILLSIDE LIMB

Geological structures and respective hydraulic conductivities were clarified by investigations and tests in situ such as drillings, Lugeon Tests, water pressure tests, simultaneous water table measuring at every boreholes, and so on. Sixteen geological sections and sixteen Lugeon maps were drawn. Figure 1 shows topographical condition and lines of drawn geological sections in the area, and Figures 2 and 3 show the geological section and the Lugeon map of the right hillside limb.

Main geological feature in the area is such multiple rock mass units called as accretionary prisms.

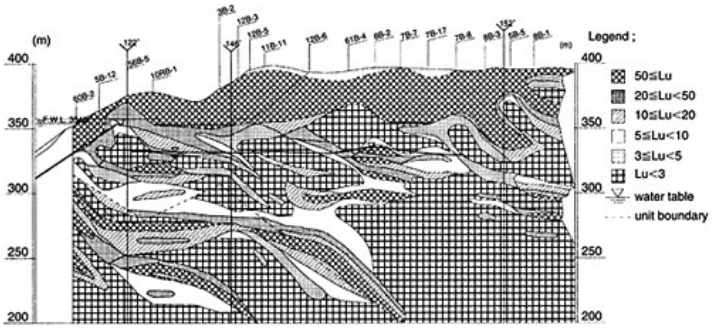

Figure 3. Lugeon map along limb-grout line.

In respect to hydrogeological feature, the highly pervious strata exist widely in the area and near the dam make it complicated. Adding to this, multi layers of water level exist in the area because of their multi hydrogeological properties.

3 BASIC EQUATIONS, BOUNDARY CONDITIONS AND FORMULIZATION FOR SEEPAGE FLOW

Basic equation for saturated—unsaturated steady seepage flow in a case without sink or source is expressed as follows.

$$\frac{\partial}{\partial x_i}\left(K_{ij}(\varphi)\frac{\partial h}{\partial x_j}\right)=0 \tag{1}$$

where h: total head ($=\varphi+x_3$), φ: pressure head, $K_{ij}(\varphi)$: hydraulic conductivity tensor, x_i, x_j: (i,j=1,2,3) shows regular coordinates which (i,j=1,2) are horizontal and $(i,j=3)$ is vertical as the positive takes to the upper. Horizontal plane of coordinate system (x_3=0) is considered as standard plane of total head. Hydraulic conductivity tensor $K_{ij}(\varphi)$ is the hydraulic conductivity K^s_{ij} in saturated zone, while in unsaturated zone it is the function $K_{ij}(\varphi)$ of pressure head φ. Assuming the hydraulic conductivity tensor $K_{ij}(\varphi)$ can be expressed as follows the relative hydraulic conductivity $K_r(\varphi)$,

$$K_{ij}(\varphi)=K_r(\varphi)K^s_{ij}(\varphi)\ (I,j=1,2,3) \tag{2}$$

where, $K_r(\varphi)$=1 when φ>0 and 0<$K_r(\varphi)$<1 when φ<0, basic equation regarding pressure head φ is expressed as

$$\frac{\partial}{\partial x_i}\left(K_r(\varphi)K^s_{ij}(\varphi)\frac{\partial \varphi}{\partial x_j}+K_r(\varphi)K^s_{i3}(\varphi)\right)=0 \tag{3}$$

substituting (2) for (1).

And, the discharge velocity *(vi)* is expressed as follows from Darcy-Buckingham's kinetic equation.

$$v_i = -K_{ij}(\varphi)\frac{\partial h}{\partial x_j} \tag{4}$$

Further, boundary conditions become as follows.

1. Boundary Γ_1 when pressure head is known: letting φ_b substitute for known pressure head

$$\varphi=\varphi_b \tag{5}$$

2. Boundary Γ_2 when flow quantity is known: n_i sets as the component of normal vector facing to outside of Boundary Γ_2, and v_b as known discharge velocity of Boundary Γ_2,

$$K_r\left(K_{ij}^s\frac{\partial\varphi}{\partial x_j}+K_{i3}^s\right)n_i=-v_b \quad \text{(non-flow boundary; } v_b=0\text{)} \tag{6}$$

FEM and Galerkin method are adopted when formulizing these basic equations.

4 ANALYSIS MODEL

4.1 *Range of analyses and Mesh Model*

Analysis has been carried out in the area enclosed by the river, the streams and ridges putting the right dam axis line and the right hillside limb-grout line around its center, where is assumed to be closed domain without any inflow from or outflow to adjoining area and only to be recharged from rainfall. However, to keep water balance in that closed domain, water can be allowed to flow in or out through the elements of near riverbed even at the head-known boundary, but deeper portion along that boundary is kept completely closed. Analyzed range dimension is 675m×429m×225m as shown in Figure 4. The type of element used in this analysis is hexahedral 27 nodes and Lagrangian second isoparametric. Total number of elements is 139, 815, and number of nodes is 130, 304. Size of respective elements is 10m×10m×5m except the portion near limb-grout line, while along grouting line it is 1.25m×10m×5m and limb grouting width is 5.0m. Three-dimensional Lugeon map block model is processed visually in the optimizing theory applicable system software after some sections of Lugeon map drawn from the result of the investigation in situ and input them in it. General view of three-dimensional block model is shown in Figure 5. Directional hydraulic conductivity of

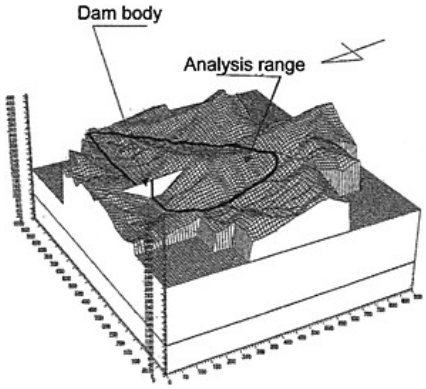

Figure 4. Range of analyses.

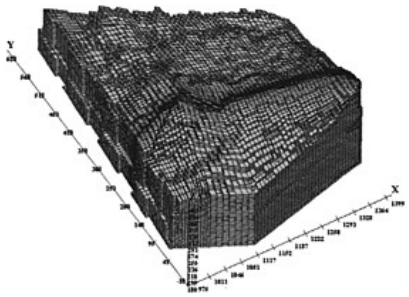

Figure 5. Three-dimensional block model.

each element is assumed to be isotropic, because remarkable anisotropic properties thorough rock mass could not be found according to the result of the pulse test in situ carried out at dam abutment.

4.2 *Boundary condition*

Boundary condition is as follows (refer to Figure 1)

(i) Boundaries B,C④

Head-known boundaries are aligned along River Oyodo and the streams of the upper and lower. Water can flow in or out through elements just under the riverbeds or the streambeds along the boundaries, but deeper portions are completely impervious.

(ii) Boundaries B, C③

The behind ridge is considered as groundwater ridge, and then assumed to be impervious boundary.

(iii) Ground surface plane of analysis model: recharged from rainfalls.

Recharged volume from rainfalls to respective elements is assumed to be equal because geography in this area shows generally gentle without any large streams. Its volume is 5.4mm/day, which is simulated from three-stories Tank Model.

5 RESULTS AND CONSIDERATION

5.1 *Consideration regarding trial-and-error calibration*

(1) Analysis Method

To get appropriate analysis model (parameters), the condition of plural water tables are simulated and visualized and the trial-and-error calibration to converge the differences between borehole water level and simulated water level into the allowable value were executed. Though Lugeon value is divided into six ranges in the original Lugeon map, it is into four ranges in the model due to avoid complication. Lugeon value *(Lu)* is converted into saturated hydraulic conductivity *(k),* that is, Lu=1 is k=1.31×10^{-5}cm/s, Lu<3 is k=3.0×10^{-5}cm/s, $20 \leq Lu$ is k=1×10^{-3}cm/s. While, unsaturated properties of fissured rock has one value in analysis domain, trial-and-error calibration was carried out. First those calibrations started referring to the curve of Nakagawa et al (1982), and were finally carried out according to such characteristics shown in Figure 6.

(2) Natural Condition regarding Water tables

Figure 7 show the free water tables of which pressure head is zero (equal to atmospheric pressure). Figure 8 shows the comparison the simulated water tables with the measured borehole water level at the depth such levels changes suddenly on drilling excavation going. From these analyses, the groundwater in the peripheral area of analysis range has the condition having multiple levels intercalated with unsaturated zone. While in the central area, it exists as the continuous saturated body like a mushroom shape. The reason why borehole water level at 7B-1 changed suddenly on the time drilling excavation going may be due to its location. These kinds of condition are not fully expressive in the analysis by two-dimensional system. Then, we have considered the importance of the analysis by three-dimensional hydraulic models with a system for 3 D graphics visualization of seepage flow in foundation by a saturated—unsaturated steady flow analysis.

(3) Evaluation of Simulated Water tables

To evaluate the simulated water tables comparing with measured borehole water levels, Anderson et al (1992) enumerated such factors as the maximum absolute value of the differences *(ME),* the mean absolute value of the differences *(MAE),* and the square absolute value of the differences *(RMSE)*. *ME, MAE,* and *RMSE* are expressed as the following equation, where n is the sample number, h_0 is measured levels, and h_c is the simulated levels;

$$ME=\max\{|h_0-h_c|\} \tag{7}$$

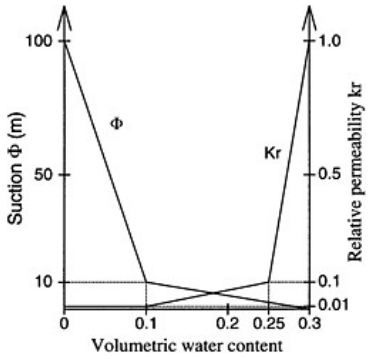

Figure 6. Unsaturated properties of fissured rock.

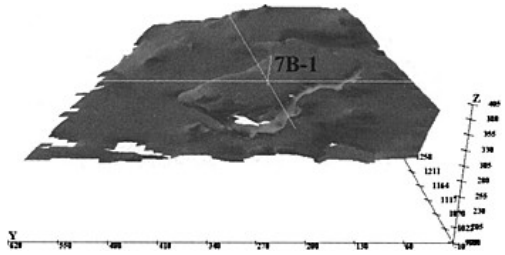

Figure 7. Condition of free water table (view from reservoir side).

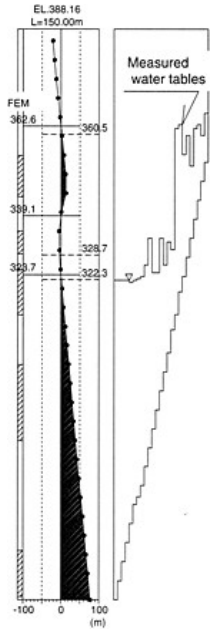

Figure 8. Water tables on drilling and simulated (7B-1).

$$MAE = \frac{1}{n}\sum_{i=1}^{n}\left|(h_0 - h_c)_i\right| \tag{8}$$

$$RMSE = \left[\frac{1}{n}\sum_{i=1}^{n}(h_0 - h_c)_i^2\right]^{0.5} \tag{9}$$

Calibration in this analysis was carried out to converge the allowable difference between measured borehole water levels and simulated levels into the value *MAE* within 3.0 m. Final result of simulated levels h_c and measured levels h_0 are shown in Table 1 and Figure 9. The h_0 is measured borehole water levels on the time of drilling excavation (or measured levels after drilling) along dam axis, limb-grout line or spillways. Figure 10 shows their relationship where the values disperse evenly and do not rely on their elevation. As shown in Table 1, *MAE* is 2.7m which is recognized to be fit in the first setting value *MAE* 3.0m. Distribution of hydraulic conductivity in the model shall be concluded to be appropriate enough from their accuracy.

5.2 *Consideration regarding water impounding simulation*

Water impounding simulations were conducted for some cases using calibrated model that could obtain basic hydrogeological parameters. Six cases are shown in the following Table 2 and Figure 10 on condition that high pervious portions from reservoir to downstream crossing through the limb

Table 1. *hc* and h_0

Br.No.	h_0 EL. (m)	h_c EL. (m)	h_0-h_c EL. (m)
56B-4	309.6	312.5	−2.9
61B-4	345.5	341.0	4.5
1B-2	307.7	310.0	−2.3
3B-2(Uppertable)	359.0	360.4	−1.4
3B-2(Lower table)	320.2	321.2	−1.0
7B-1(Uppertable)	360.5	362.6	−2.1
7B-1(Lowertable)	322.3	323.7	−1.4
7B-4	311.6	313.5	−1.9
7B-7	335.5	340.3	−4.8
7B-8	357.8	353.4	4.4
		MAE	2.7

h_0; measured value, h_c; simulated value.

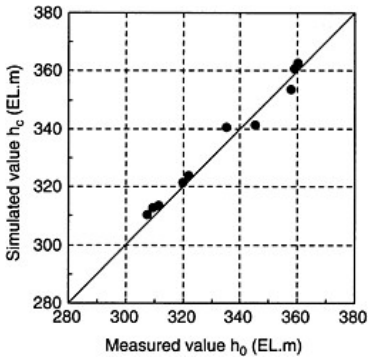

Figure 9. Relationship between measured and simulated water tables.

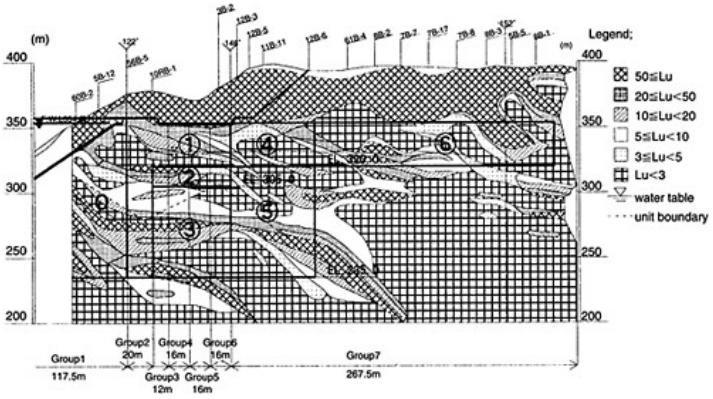

Figure 10. Analyzed cases to decide ranges for limb-grout (when impounding water).

be improved by grouting. From these cases, the effectiveness of the limb-grout with the calculation of the leakage amount can be totally evaluated.

(1) Leakage Characteristics

Leakages (amount of seepage flow) Q (m^3/day) in each case are shown in Figure 11. Gross leakages decrease little by little from *Case A* to *Case D* and almost same between *Case D* and *Case F* according to the Figure. These may be due to the effect detouring flow beyond the limb-grout curtain. Leakage at *Case D* and *Case F* show the minimum (767m^3/day) in total. In the case the section of seepage length shorter and hydraulic gradient larger (Group 1~6: L=80m), *Case C* shows the least leakage and higher grouting effect. While in *Case F* which grout up to the intersecting point of water table and F.W.L 354.0m, though total leakage is lower than *Case C,* the leakage from the section Group 1~6 is higher than *Case C*. From the viewpoint of hydrologic stability, *Case C* is considered to have a advantage.

Table 2. Analysis cases.

Case	Portion in the following figure	Range and purpose of limb-grout
Case A	0	To compute the leakage without any limb-grout as a guide value for the effect of limb-grout
Case B	0, ①, ②	To reduce the uplifting pressure being harmful to the facility of spillway (up to EL.310m) and to supplement to curtain-grout (EL.240~EL.270m)
Case C	0, ①, ②, ③	To refrain from leakage through high pervious section in deeper portion (EL.230~EL.240m)
Case D	0, ①, ②, ③, ④	To reduce the uplifting pressure to the facility of spillway
Case E	0, ①, ②, ③, ④, ⑤	To refrain from leakage through high pervious section in deeper portion (EL.240~EL.270m)
Case F	0, ①, ④, ⑥	To intersect groundwater table to F.W.L. 354 m
Case G	Without grouting	The case for reference

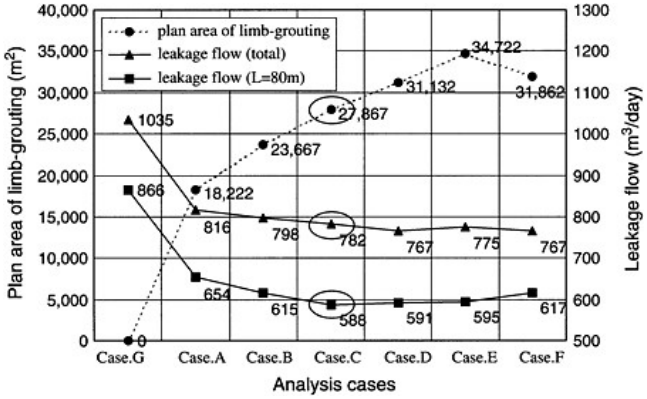

Figure 11. Leakage amount and grouting effectiveness.

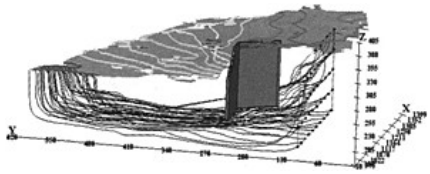

Figure 12. Seepage flow detouring limb-grout (view from reservoir side).

From the total consideration based on these analyses, *Case C* shows the most appropriate range of limb-grout. It is limb-grout range L=80m and grouting depth 119m. Comparing to *Case F,* the limb-grout ranges can be reduced to 63% (from 260m to 96m), and its area is reduced 13%.

(2) Particle Tracking Simulation

Figures 12 and 13 show three-dimensional groundwater flow condition tracing hypothetical particles arranged at some point in the side of reservoir in *Case C*. If comparing the seepage flow

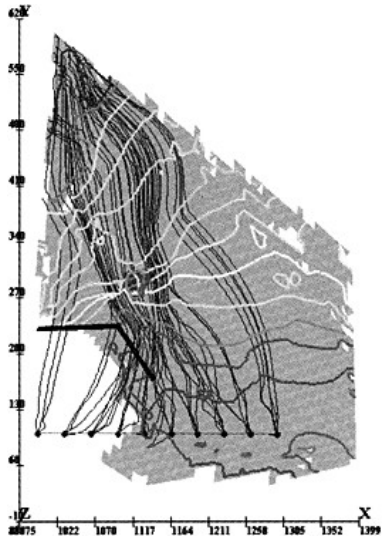

Figure 13. Seepage flow detouring limb-grout (two-dimensional view).

from reservoir to downstream that goes under the curtain-grout and detours beyond the limb-grout curtain and that goes through curtain-grout and/or limb-grout, the former is much distinguished from the latter. This result show the one of a condition that even if grouting range is made longer, the effect of mitigation leakage does not become larger.

6 CONCLUSION

The mitigation effect of leakage was studied when some limb-grout is carried out in the area having complicated hydrogeological structures with plural water tables in case that those levels are lower than full water level of the dam reservoir. Three-dimensional seepage flow analysis by FEM, which is by a method of saturated—unsaturated steady seepage flow analysis, shows natural groundwater condition and the mitigation effects of leakage in some cases of limb-grouting design.

The content and the result of the studies are as follows.

1. We have attained to the fruitful results to show three-dimensional visualization of the domain having plural water tables by trial-and-error calibration in accurate through the modeling hydrogeological conditions based on the information from the investigations and tests in situ.
2. As a result of water impounding simulations conducted for some cases, the effectiveness to mitigate leakage can be recognized when grouted extending to limb 1.5 times as long as water depth (54m), but further long grouting is not so effective. This is due to detouring seepage flow gathers to the adjoining area around the end of limb-grout resulting seepage flow increase and offsetting the detouring effect of limb-grout.
3. The effectiveness of limb-grout can be totally evaluated quantitatively with seepage amount to clarify detouring flow lines from reservoir beyond the limb-grout curtain shown visually in the model by the particle tracking simulation.

Three-dimensional seepage flow analysis by FEM has demonstrated its effectiveness for the limb-grout design even the target domain has very complicated condition such as plural water tables existing and being lower than designed normal full water level of reservoir.

REFERENCES

[1] Tateishi, T., Hasegawa,T., Yoshitake, Y. and Kobayashi, N. 2001: Three Dimensional Seepage Analysis to Estimate Limb Grouting Effects on Detouring Flow, Trans. JSIDRE, No. 215, pp. 125–133.
[2] Tsateishi, T., Kobayashi, N., Hasegawa, T. and Yoshitake, Y. (2003): Effects or Limb Grouting on Seepage Loss Reduction, JRCS, Vol.8, No.2, pp. 41–50.
[3] Nakagawa, K. and Komada, H. (1982): Analysis of Pressure Behaviour of Rockfill Dam During Construction and Reservoir Filling, Civil Engineering Laboratory Rep., No. 382007, pp. 1–16.
[4] Anderson, M.P. and Woessner, W.W. (1992): Applied Ground water Modeling: Simulation of Flow and Advective Transport, Academic Press, pp. 236–246.
[5] Kobayashi, N., Tateishi, T., Yoshitake, Y. and Ikegashira, J. (2003): Effects of Length of Limb Grouting Works on Seepage Loss Reduction, Trans. JSIDRE, No. 227, pp. 41–47.

New Developments in Dam Engineering—Wieland, Ren & Tan (eds),

Flood discharge and energy dissipation design of Goupitan hydropower station

Hu Zhongping, Xiang Guanghong & Ban Hongyan
Changjiang Institute of Survey, Planning, Design and Research, Hubei China

ABSTRACT: Goupitan hydropower station is at the dam site where the river valley is very narrow and the flood peak discharge is tremendous. The maximum flood discharge power of project is 42000MW which is the highest inside and outside of China. Flood discharge and energy dissipation design is one of the key technical problem of the project. By scheme comparison, the layout scheme is recommended to adopt orifice discharge of dam body, plunge pool behind the arch dam, flood discharge tunnel at the river bank and pre-excavated scour pit and ejaculate flow energy dissipation.

1 INTRODUCTION

Goupitan hydropower station comes out top inside and outside of china with arch dam 232.5m heigh, flood of high peak and tremendous quantity, maximum check flood of project being 35600m^3/s,water level distance between upstream and downstream being 150m, appoximately and maximum flood discharge power being 42000MW. Besides, the valley is very narrow, topography and geology condition is complicated, the rock at the tail and downstream of the energy dissipation area is soft rock like clay rock. Therefore, the flood discharge and energy dissipation design of the project is very complicated and one of key technical problem of the project. By scheme comparison, the layout scheme is recommended to adopt 6 superficial orifices and 7 medium orifices in the dam body, closed pumping drainage plunge pool, behind the arch dam, one discharge tunnel at the river bank and pre-excavated scour pit and ejaculate flow energy dissipation. The result of the hydraulic model test indicates that all hydraulic indexes of the scheme are content with the design.

2 GENERAL SITUATION OF PROJECT

Goupitan hydropower station is situated midstream on Wujiang main river of Yuqing county Guizhou province, which is the biggest hydraulic power source of Wujiang river and has such functions as power generation, flood control, navigation etc. This project began to be constructed in November 2003. The reservoir's normal water level is 630m and its relevant reservoir volume is 5.564 billion m^3. The electric generator capacity of the power station is 3000MW with a 751.8MW guaranteed output and a 9.667 billion Kw·h perennial average electric power output. The main buildings of the project include concrete hyperboloidal arch dam, closed pumping and drainage plunge pool, left bank flood discharge tunnel, right bank underground powerhouse and diversion structures.

At the dam site, the downstream river valley is very narrow and straight. The water surface width is 30~60m in low water period and is 100~120m in flood period. The slope of both river

Table 1. Storage routing data of Goupitan hydraulic powerhouse.

Flood frequency (%)	Flood peak discharge (m^3/s)	Reservoir water level (m)	Regulated discharge (m^3/s)	Downstream water level (m)
0.02	35600	638.36	28900	490.23
0.1	30300	634.56	24400	484.66
0.2	27900	632.89	23600	483.59
1	22500	630.49	21200	480.25

banks are abrupt with angles exceed 60° mostly. The rock of both banks and river bed is made up of hardy Maokou and Qixia group limestone. Meanwhile the river valley becomes broad at dam site downstream 300~350m and its water surface width is 200~250m in flood period, where the slope of both banks is moderate and its rock belongs to clay stone in Silurian period, which is on same attitude with limestone. The natural bayonet which is control section of water discharge at dam site downstream 1000m is a natural terrain advantage for flood discharge and energy dissipation because of its uplift water effect and deep tail water formation. Such geologic problems exist in flood discharge and energy dissipation zone as listed below: (1) unloaded crevasses and small faults which are full of mud are developed on both bank slopes and intense dissolve-erosion effect appears. (2) The rock of energy dissipation tail zone and downstream river bed belongs to clay stone which has low anti-scour capacity.

The flood which is primarily formed by rainstorm rises and falls abruptly and its peak discharge form appears lanky. This project belongs to grade I, which its design flood criterion of flood discharge buildings is 0.2% and its check design criterion is 0.02% as well as its design can avoid flood brimming over dam when 0.01% flood discharge appears. For energy dissipation buildings, flood design and check criterion is 1% and 0.1% respectively. Flood peak discharge, upstream and downstream water level, regulated discharge are listed in Table 1.

3 DESIGN CRITERION OF FLOOD DISCHARGE ANG ENERGY DISSIPATION

(1) It can meet normal flood discharge requirement and has definite capacity for over discharge and predischarge. At the same time 5% flood peak discharge can be released safely at flood control limit level during flood period.
(2) To reduce the difficulty of dam body flood discharge and energy dissipation, appropriate bankside diffluence method and diffluence discharge should be chosen.
(3) Based on terrain and geologic condition, deconcentrates water flow falling points to reduce unit area energy dissipation power of energy dissipation zone.
(4) Guarantees good flow pattern to reduce scour on downstream river bed and bank slopes and reduce protection work amount.
(5) Guarantees energy dissipation buildings operating safely and reliably and provides checkrepair qualification.

4 FLOOD DISCHARGE SCHEMES STUDY

Check flood peak discharge of Goupitan hydropower station is $35600m^3/s$. After regulating and reducing peak discharge, there will be still $28900m^3/s$ flood need to be released by flood discharge facilities and its maximum discharge power is 42000MW, unit water body energy dissipation rate of energy dissipation zone is $13.5kw/m^3$. The amount and the power is the highest inside and out-side of China. Flood discharge indenes for some of the heigh arch dams inside and outside of china are listed in Table 2. To reduce concentrated discharge of river bed, to reduce energy dissipation

Table 2. Flood discharge and energy dissipation index of some high arch dam of China for check condition energy dissipation power in pool.

Project	Height of arch dam (m)	Discharge quantity of dam body (m^3/s)	Water level (m)	Flood discharge power of dam body (MW)	Energy dissipation power in pool (KW/m^3)
Xiaowan	292	15260	226.6	33900	12.3
Xiluodu	273	31496	188.6	58750	10.3
Laxiwa	250	6000	213	12500	20.5
Ertan	240	16300	166.3	26600	13.5
Goupitan	232.5	28900	148.1	42000	13.5

difficulty, as well as to improve safety and agility of operation, extra bankside diffluence facility is necessary to be installed.

4.1 *Bankside diffluence discharge and diffluence facilities*

On left bank of the project, two diversion tunnels are installed and the space for installation of vertical ship lift is reserved beforehand. On right bank, a diversion tunnel, water transportation system and underground powerplant should be installed. If diffluence facilities are installed on right bank, it will be incompatible with water transportation system by all means. Therefore bankside diffluence facilities can only be installed in limited space between left abutment and ship lift.

In order to reduce discharge times of dam body, ordinary flood should be released by bankside diffluence facilities as possible. For Goupitan hydraulic project, if it is to be requested that 20% flood can be released by bankside diffluence facilities, three diversion tunnels need to be constructed on left bank. Neither diffluence facilities installation condition nor rock condition (soft rock) of energy dissipation condition can be bearable for this plan. Therefore bankside diffluence facilities can only be a passage for auxiliary flood discharge.

Two schemes including $3000m^3/s$ and $6000m^3/s$ discharge are studied for bankside diffluence facility. In order to reduce energy dissipation load of plunge pool, increase its chek-repair time period and reduce construction cost, recommended bankside diffluence discharge is $3000m^3/s$.

Based on terrain and geologic condition, two schemes of re-bulided open flow tunnel and discharge tunnel revised from diversion tunnel are studied for bankside diffluence facilities. “Longtaitou” scheme and whirl-flow vertical well scheme are considered in diversion tunnel revision. Because of high speed and bend outgate of great submerge, such hydraulic problems as high speed water flow and outgate energy dissipation are too difficult to resolve in “Longtaitou” scheme. Because of great downstream water depth, too many hydraulic problems exist in whirlpool vertical well scheme. Meanwhile this construction design of whirl-flow vertical well has not appeared in practical application in these days and it is not a mature technic application. So two diversion tunnel revision scheme should not be adopted. Open flow discharge tunnel is recommended as bankside diffluence facility.

4.2 *Dam body discharge scheme*

Three schemes are studied in orifice collocation of dam body which includes six surface orifices adding seven middle orifices, six surface orifices adding five middle orifices with two emptier bottom orifices and six surface orifices adding seven middle orifices with two emptier bottom orifices. Comparing discharge capacity, energy dissipation effect, sand washing during flood season, emptier check-repair, metal structure and engineery quantities, six surface orifices adding seven middle orifices with two emptier bottom orifices scheme is recommended. The recommended storage routing data is listed in Table 1.

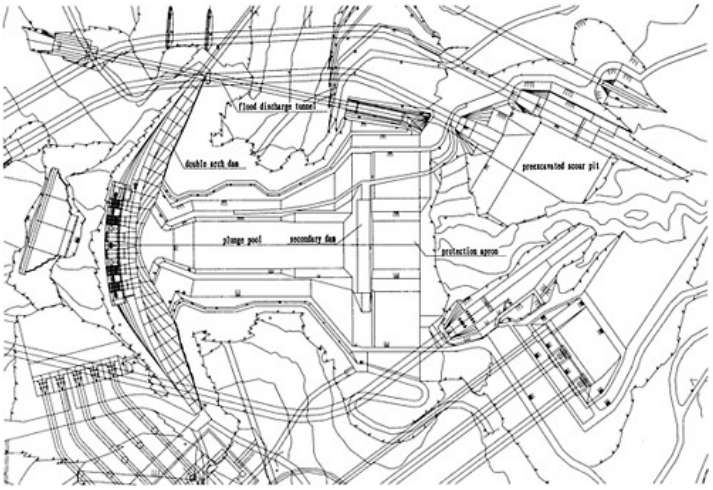

Figure 1. Flood discharge and energy dissipation buildings plane collocation.

5 ENERGY DISSIPATION SCHEMES STUDY

5.1 *Energy dissipation of dam body discharge*

Two energy dissipation schemes including closed pumping and drainage plunge pool and ejaculation dissipation facility are studied for dam body discharge. Hydraulic model test data indicates that ejaculation dissipation can result in more than 30m scour depth in natural river bed because of soft rock distribution located in tail section of energy dissipation zone. In energy dissipation zone, falling flow exceeding natural river bed, that has bad effect on its stability of abutment and bank slopes. Preexcavated scour pit and anti-scour protection can increase great construction cost. Closed pumping and drainage plunge pool can guarantee bank slope stability and its hydraulic parameters is satisfying. This energy dissipation facility has been applied successfully in many projects of China. It is mature in technic and reliable in operation and it is convenient for checking and repair. Therefore closed pumping and drainage plunge pool scheme is recommended.

5.2 *Bankside tunnel energy dissipation scheme*

Two energy dissipation schemes including bottom flow and ejaculation flow are studied for bankside tunnel. Bottom flow dissipation is advantageous to reduce scour on energy dissipation zone and reduce effect on powerplant tail water. However because of great water head difference between upstream and downstream, high water speed on pool bottom board (soft rock ground-work), there is too much difficulty in design and it is too hard to guarantee safety for long-term operation. Ejaculation flow dissipation can disperse water flow and reduce downstream scour by advantage of wide water field and deep water with low construction cost. With generalization comparison, ejaculation flow dissipation scheme is adopted for bankside tunnel outgate energy dissipation.

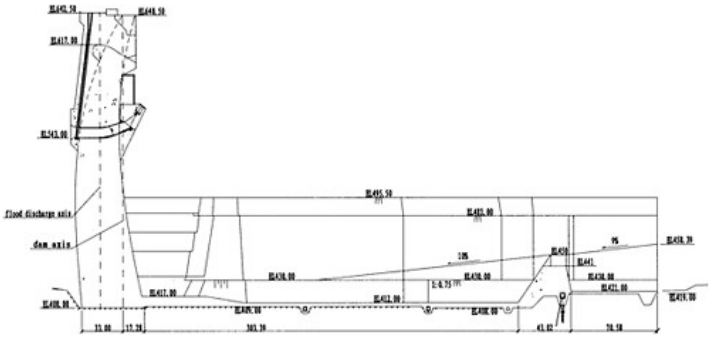

Figure 2. Flood discharge and energy dissipation buildings vertical lateral section.

6 FLOOD DISCHARGE AND ENERGY DISSIPATION BUILDINGS DESIGN

6.1 *Surface orifices*

Surface orifice crests adopt open WES practical crest and its elevation is 617m. The orifice dimension is 12m width and 13m height. The upstream crest adopts 1/4 ellipse curve and is downwards joint with WES crest curve. The crest curve equation is y=0.03918×1.85. In order to reduce water flow centripetal concentration effect and disperse water flow falling points as possible, outgate angle of surface orifices adopts variate value, viz 0° for 1# and 6# orifice, −20° for 2# and 5# orifice, −30° for 3# and 4# orifice. Meanwhile different diffluence toothed sills are installed on their outgates to increase water flow falling stratification. All toothed sills' angle is 20°. In order to utilize front lip of main river bed effectively, middle orifices are installed in gate walls of surface orifices whose width is 12m. In order to disperse water flow in limited river bed space adequately, outgate section of surface orifices adopts plane diffusion form. Inlet width of surface orifices is 12m and outgate width is increased to 18m. Brim surface orifices' outgate width is designed as 15m to avoid falling water flow impinging on pool slopes.

6.2 *Middle orifices*

The inlet and outlet of middle orifices adopt pressure flow form. The inlet pressure straight line section dimension is 6m width and 8m height. The outlet forms include up-raise form (for 2#, 4# and 6# orifice) and flat bottom form (for 1#, 3#, 5# and 7# orifice). The outlet dimension is 7m width and 6m height. The inlet bottom board elevation of flat bottom and up-raise orifices is 550m and 543m respectively. Their outlet angle is 25°. The outlet bottom joint with straight line section bottom by 30m radius reverse arc section. The inlet roof and side wall curve adopts ellipse curve. The pressure section downstream check-repair groove is reinforced with steel liner. In order to disperse water flow, the outlet section of middle orifices adopts plane diffusion form and its diffusion angle is 5.71°. That appears constringent form in sectional view.

6.3 *Flood discharge tunnel*

Flood discharge tunnel adopt short pressure inlet joint with open flow tunnel and its axis line is a straight line whose full length is 580m. The inlet adopts bank tower structure and its bottom board

elevation is 590m. Control section dimension of inlet is 11m wide and 12m high. Flood discharge tunnel adopts “Longtaitou” open flow form. Tunnel body adopts city gate hole form and its section dimension is 11m width and 17~13m height. The tunnel includes parabola section, inclined tunnel section, reverse arc section and water-retreating tunnel section. The parabola equation is X^2=230Y. The inclined tunnel section gradient is 1:1.5. The reverse arc section radius is 80m. The water-retreating tunnel section gradient is 0.08 and it joints downwards with open channel. The outlet adopts inclined diffused bucket lip. The rock located in energy dissipation zone of the tunnel is weak and fragmentized. In order to guarantee stability of bank slope and avoid scour substance blocking powerplant tail water outlet, preexcavated scour pit is installed in energy dissipation zone. The upstream borderline of scour pit is 130m away from the outlet bucket lip. The scour pit is 130m length and its maximum width is 175m. The bottom elevation of scour pit is 425m and the sour pit bottom is unshielded. Anti-scouring toothed wall is installed on left side and upstream side of preexcavated scour pit and its bottom board elevation is 420m.

6.4 *Plunge pool*

The transection of plunge pool is compound trapeziform. The length of closed pumping drainage section is 304m and its bottom width is 70m. Its bottom board elevation is 412m. The roof width of the pool is 174~181m and the roof elevation is 481m. The bottom board of limestone section is 3m thick and that of clay stone section is 4m thick. The protection slope below 481m elevation is 3m thick. The protection slope of 481m~495m elevation is 1.5m thick. Anchor rods or anchor piles (soft rock section) are installed in bottom board and protection slope below 481m elevation. The closed pumping drainage section joints downwards with secondary dam. The secondary dam installment is combined with downstream RCC cofferdam. The roof elevation of secondary dam is 441m and its roof width is 19m. The upstream and downstream gradient is 1:0.7 and 1:0.2 respectively. The secondary dam joints downwards with water-penetrated protection-apron of 71m length. The bottom width of protection-apron is 71m and 2m thick and its bottom board elevation is 421m. The protection slope of both banks below 481m elevation is linered with 2m thickness concrete and it has anchor rods installment. The protection slope whose elevation is 481~495m is linered with 1.5m thicks concrete and it has not anchor rods installment. Toothed slot is installed on downstream section of protection-apron and the slot bottom elevation is 410m. In some range of downstream protection-apron below 481m elevation, protection slope of both banks are reinforced with 1.0~1.5m thickness concrete.

7 CONCLUSION

(1) In order to adapt the topography and geology condition of the project and flood discharge and energy dissipation characteristic, Goupitan power station adopts dam body orifice discharge, closed pumping drainage plunge pool behind the arch dam, one discharge tunnel at the river bank, ejaculate flow energy dissipation and antiwashing mode with downsteam pre-excavated scour pit and anti-scour toothed wall.

(2) Surface orifice outlets adopt plane diffusion and variable angle. Middle orifice outlets adopt flat bottom and up-raise forms with plane diffusion and transection compression. All these installments resolve centripetal concentration flow problem of arch dam effectively. The flow entering pool can be dispersed breathwise and pulled apart lengthways. Hydraulic model test data indicates that maximum dynamic water pressure on pool bottom board is 12.52×9.81kPa, flow velocity on protection-apron tail section is 4.38m/s, scour pit depth is 5.75m and its back slope gradient is 1:8.6, downstream flood discharge tunnel maximum scour pit depth is 2.85m and its back slope gradient is 1:6.74. All these show that flood discharge energy dissipation of dam body and bankside tunnel achieves good effect.

New Developments in Dam Engineering—Wieland, Ren & Tan (eds),

Design for Goupitan arch dam

Hu Zhongping, Cao Quxiu & Wang Zhihong
Changjiang Institute of Survey, Planning, Design and Research, Hubei China

ABSTRACT: Goupitan arch dam is 232.5m high, the geological condition of dam foundation is complicate and there are many orifices in the dam body with large scale. The scale and technical difficulty of the arch dam go beyond the control of the active arch dam design criterion. Through referring domestic and overseas design experience and up to date research fruit of high arch dam, many analysis methods and model experiments are adopted, and through the analogy of other engineering, Goupitan arch dam's figure, stress, abutments stability, the whole safety, anti-seism and foundation treatment and so on are studied and analyzed. Finally the arch dam design meet safety, reliability, technical feasibility, economy and rationality.

1 INTRODUCTION

Goupitan arch dam is 232.5m high whose base lies on grey rock. The geological condition of dam foundation is complicate and there are many orifices in the dam body with large scale. The scale and technical difficulty of the arch dam go beyond the control of the active arch dam design criterion. Through referring domestic and overseas design experience and up to date research fruit of high arch dam, many analysis methods and model tests are adopted, and through the analogy of other engineering, Goupitan arch dam's figure, stress, abutments stability, the whole safety, antiseism and foundation treatment and so on are studied and analyzed. Finally the arch dam design meet safety, reliability, technical feasibility, economy and rationality.

2 ENGINEERING GENERAL SITUATION

Goupitan Water Power Station is located at Wujiang River in Yuqing County in the middle of Guizhou Province and is the biggest water power station in the step development plan of Wujiang River. The main task of engineering development is generating electricity, the other aims are shipping, flood controlling and other multipurpose. The average current over many years at the dam site is 716m^3/s, the average runoff over many years is $226\times10^8m^3$. The design flood (0.2%) and the check (0.02%) are 27900m^3/s and 35600m^3/s respectively. The normal conservation level is 630.0m and the storage is $64.51\times10^8m^3$. The power station installing capacity is 300MW and the design annual quantity of generating electricity is 96.67×10^8KW·h. The power station is composed of concrete double arch dam, dam body's orifices, energy dissipation pool, flood discharge tunnel, underground workhouse, shipping structures (reserved) and grouting curtains. The engineering started in 2003 and will generate electricity in 2009.

The V-shaped canyon's across section at dam site is symmetric. The elevation of riverbed is 410.00 to 425.00m and the overlay is 2 to 8m thick. The slope of the bank above 550.00m is 30 to 40 degree, otherwise, it is 55 to 65 degree even to 90 degree. The bedrock at the dam site is changing from Permian's lower part to Cambrian's upper and medium part from upstream to downstream. The terrain's orientation nearly orthogonalizes the river, that is NE 30 to 35 degree

for most cases and NE 40 to 50 degree at the right bank. The terrain inclines to NW (upstream) and the obliquity is 45 to 55 degree. The dam foundation is seated on the lower segment of Maokou group (P^{l}_{1m}) that has high compressive strength, with wet compressive strength being nearly 70MPa and modulus of deformation being 15 to 30GPa. The main geological defects at the foundation are as following: small faults along the river, deep inclined cranny with NW and NWW orientation, interbedded large soft structure plane with the same formation and lay, weathered to water eroded strip developing along the lay and water eroded cave.

3 FIGURE DESIGN OF ARCH DAM

3.1 *Bed rock selection*

The bed rock selection is mainly depends on the bed rock's carrying capacity and slide stability. Goupitan arch dam's base is mainly seated on the lower segment of Maokou group (P^{l}_{1m}). There are obvious unloaded zone at the abutment whose horizontal width decreases when the elevation goes down. In most cases, the horizontal depth is smaller than 15m for the zone below 460.00m, otherwise, it's larger than 20m. The test of seismoscope shows that in unloaded zone the rock's seismic wave velocity is 2.1 to 4.6km/s, the integrity coefficient is 0.2 to 0.48. The rock is classified as IV rock and should be excavated rather than used as bed rock.

The principle of defining the bed rock at the abutments is as following: excavate the rock of unloaded zone, partially treat the geological defect of erosion and fracture zone instead of controlling the embedded depth, adjust properly considering the figure's change along peripheral zone in partial range and stability of resistance to slide. Based on it, the embedded depth of downstream abutments is 27 to 43m and the elevation of the bed rock in the riverbed is chosen as 408.00m.

3.2 *Design for arch dam shape*

The factors mainly considered in the figure design of the arch dam are as following: ④ the dam's maximum thickness and overhang are controlled to be convenient to the construction and no construction longitude joint is set.

Based on above principles, the linetype of the arch rings are compared and chosen firstly

Under the same design conditions, five kinds of arch rings such as three center round arch, parabolic arch, elliptic arch, logarithmic spiral arch and hybrid arch are chosen in the figure design. The result shows that: ③ slide resistance stability: below the elevation 500m, the arch end thrust angle of the parabolic arch, elliptic arch, logarithm spiral arch, three center round arch are almost the same, but that of the hybrid arch is obviously smaller. Synthetically considering of all the above factors, five kinds of arch all can adapt to the Goupitan's geology and topography condition and there are no essential difference. The parabolic arch has stronger adaptability, so the parabolic arch ring is chosen in Goupitan arch dam.

After the kind of arch ring has been chosen, optimization is carried out for many times and the design is modified. Combining with the adaptability of arch dam to the foundation, the characteristic parameters of the parabolic double arch dam finally recommended is listed in Table 1.

Table 1. Characteristic value of figure parameter for Goupitan arch dam.

Item	Parameters
Dam crest level (m)	640.5
Dam height (m)	232.5
Top thickness of arch crown (m)	10.25
Bottom thickness of arch crown (m)	50.28
The maximum thickness of arch end (m)	58.43
Center angle of crest arch (°)	79.25
The maximum center angle (°)	88.56
The upstream arc length of crest arch	552.55
The ratio of arc to height	2.38
The ratio of thickness to height	0.216
Average curvity radius at crest	
Center axis (m)	298
Upstream overhang	0.19
Downstream overhang	0.30
Flexibility coefficient	12.1
Quantity of dam body concrete (10^4m^3)	242.00

4 ANALYSIS OF ARCH DAM STRESS

4.1 *Controlling criterion for arch dam stress*

According to the criterion, controlling index for Goupitan arch dam stress should be studied specially. Referring the domestic and overseas experience of designing and constructing high arch dam, combining with the engineering character of Goupitan arch dam, stress control criterion of arch cantilever method in Goupitan arch dam can be seen in Table 2, and the stress control criterion of finite element method (equivalent stress method) can be seen in Table 3.

4.2 *Dam body stress analysis by arch cantilever method*

The stress calculation of arch dam primarily adopts Arch Cantilever Method. For Goupitan arch dam, using ADCAS program (developed by Zhejiang University) as main tool, stress calculation analysis of various operating conditions are carried out. At the same time, RCT program (compiled by Institute of Beijing survey and Designing) and SAADPV program (compiled by Institute of Changjiang Science and Research) are also applied in comparison. The main conclusions are as following:

(1) Under basic combination, dam body's maximum main pull stress and compression stress are controlled by the combination of normal impounding water level and temperature rising. The above value are 1.17MPa and 7.45MPa respectively. Under Special combination (non-seism), the maximum main pull and compression stress are 1.37MPa and 7.95MPa respectively. Dam body's stress meets stress control criterion and distributes evenly and has good symmetry for both abutment.
(2) When simulating the construction process, the results of the dam stress are as following: for all stages encountering construction period flood, the maximum main compression stress is 5.35MPa and the maximum main pull stress is 0.86 MPa., which are all under the criterion and the proposed construction process is suitable.
(3) The main result of arch dam dynamic calculation is that the dam's first rank vibration form is asymmetric, the basic frequency of empty reservoir is 1.85Hz, the basic frequency of full reservoir is 1.35Hz, the maximum main pull stress of dam is 2.01MPa, the maximum main compression stress of dam is 8.64MPa. The result basically meets the demand of design.

Table 2. Arch dam stress control criterion in arch cantilever method.

Forces combinations	Permitted stress value		Safety factor of concrete compression
	Main compression stress (MPa)	Main pull stress (MPa)	
Basic combination	8.50	1.20	4.00
Special combination			
Non-seism	9.50	1.50	3.50
Seism	11.00	2.00	3.00

Table 3. Arch dam stress control criterion in finite element method.

Forces combinations	Permitted pull stress coefficient	Safety factor of compression
Basic combination	0.08	4.00
Special combination		
Non-seism	0.09	3.50
Seism	0.13	3.00

(4) The comparison between different programs indicates that the dam stress distribution pattern is almost the same, the maximum main stress is relatively close to each other, under the basic combination, the maximum main pull stress of dam is 1.0 to 1.38MPa and the maximum main compression stress of dam is 7.45 to 8.60MPa, under special combination (non-seism), the maximum main pull stress of dam is 1.09 to 1.37MPa and the maximum main compression stress of dam is 7.95 to 8.66MPa.

4.3 *Analysis of dam body stress with FEM*

Using P type FEM program, FIESTA, 3-D finite element stress of Goupitan arch dam are analyzed. In order to eliminate the stress concentration at the upstream and downstream points of the section, equivalent stress method is adopted where equivalent inner forces are obtained through integral along the dam thickness. The calculation result shows that under basic combination, the maximum main pull stress of dam is 1.55MPa, under special combination (non-seism) the maximum main pull stress is 1.71MPa. The maximum compression stress under basic combination of normal water level and temperature rising is 8.93MPa while that under special combination is 10.09MPa. According to the division of the concrete grade in Goupitan arch dam, $C_{180}35$ concrete is adopted in high pressure stress zone of dam base with standard compression strength within 180 days is 35.0MPa. Therefore, for the maximum main compression stress, the compression safety factors are 3.92 and 3.47 for basic combination and special combination respectively, which is content with the stress criterion roughly.

4.4 *Analyzing the effect of orifice on dam stress*

Goupitan arch dam has 6 surface orifices, 7 middle orifices and 2 empty bottom orifices. The dimensions of the orifices are large. Affected by dam body gravity, water pressure, temperature load and so on together with the factor of own structure, there are such problems as partial stress concentration, complicate force state near the orifices. For the effect of orifice size and layout on dam stress, 3-D finite element method are studied and analyzed. The result indicates that dam body near orifice has obvious stress concentration phenomena and the effect of the orifice on dam stress reduces very rapidly when the distance between the orifice and the studied zone increase. The maximum main stress at the surface of the arch dam appears near the arch end, which is affected smaller by the orifices due to the long distance to the orifice.

4.5 *Sensitive stress analysis for arch dam*

Goupitan arch dam base's geological condition is very complicate. In the arch dam design, that the foundation modulus adopts certain value can not really reflect the actual deformation character of dam base. So the effect of foundation modulus on the dam stress should be analyzed sensitively. According to actual geological condition of Goupitan arch dam, the total tendency of modulus variation of bed rock is that the modulus of bed rock at the lower foundation is high while the modulus at the upper foundation is low and the geology defect such as interbedded movements has larger effect on the medium foundation. In carrying out the sensitive analysis of the foundation, the foundation is simplified to upper, medium, lower parts. The modulus of each part changes according to the same scope, with positive or negative scope of 40%. The effect of modulus on the dam's body is analyzed according to the combination of modulus of different parts.

The result shows that adaptability of Goupitan arch dam's figure to foundation is strong and dam body stress are only sensitive to the modulus of the medium part. Because the medium part is affected by soft structural plane such as interbedded movement and weathered and water eroded strip, its complex modulus is low, and it needs to be treated properly.

5 ABUTMENT STABILITY ANALYSIS

The abutment stability analysis is performed mainly through limit stability method of rigid body and validated by FEM, the synthetical judgement on the abutment stability is provided.

5.1 *Analysis of slide resistance stability of abutment*

The analysis of the slide resistance stabiliy for the abutment includes plane and block analysis, where the block analysis is emphasized. According to the geology condition of the abutment, two calculation models are adopted in the stability analysis. The first model is that the parted plane is assumed to be plumb cybinder along the dam heel, the side slide plane is a discontinuous incisal plane composed of small faults near the skewback whose orientation is close to direction of the thrust at the arch end. The bottom slide plane is a horizontal plane whose elevation is selected for safety according to the formation and distribution of the small faults; The down stream empty plane is the ground surface. The second model is the same as the first one except that the downstream empty plane is a soft structural plane of large scale developing along the layer at the downstream of the abutment.

The calculation result indicates that for the first model the safety factor of the abutment slide resistance stability is larger than 3.5 and content with the criterion because it's impossible to form the bottom slide plane due to transverse vale at the dam site, rock body inclining upstream with obliquity of 40~50° and undeveloped geology structure with slow obliquity and the side slide plane is a discontinuous incisal plane composed of small faults. For the second model, the safety factor is smaller than 3.5 and can't meet with the criterion because when the empty plane is assumed to be the soft structural plane developing along the layer at the downstream abutment, the bottom and side slide planes are all short and resistant force is small, the soft structural plane forming the empty plane need to be treated in order to reinforce the effect of passing force.

5.2 *Deformation stability analysis of abutment*

The large soft structural plane along the layer at the abutment will have some effect on the stress, deformation and stability of the arch dam, research and analysis are conducted by 2D and 3D linear, nonlinear FEM. The major conclusion is as following:

If the overall deformation modulus of the soft structural plane is upto 2.0 GPa, it's unnecessary to treat it, otherwise it need to be treated according to the geology condition and the load status despite of the relative location to the arch dam.

When the soft structural plane is at the upstream of the dam heel, it has small effect on the stress and deformation of the arch dam, and if it's harmless to the pervasion resistance, it need not to be treated.

For the soft structural plane at the base of the dam, when its overall modulus is 1.0 GPa~2.0 GPa, the shallow layer treatment depth will be only 4m; When the overall modulus is smaller than 1.0 GPa, the treatment depth will be about 40m to increase the modulus upto 2.0 GPa.

For the soft structural plane at the downstream of the base, the treament depth will be about 40~100m to increase the modulus upto 2.0 GPa.

Adopting the concrete pillar passing force to treat the soft structural plane can enhance the passing effect efficiently.

6 WHOLE SAFETY ANALYSIS OF ARCH DAM

Combinating the research results of the national "85", "95" technology breakthrough with the high arch dam design experience of Ertan and Xiaowan, the whole safety analysis of the arch dam is performed by 3D nonlinear FEM, engineering analogy and geology mechnical model test.

(1) 3D nonlinear FEM

3D nonlinear FEM is applied in the research and analysis to investigate the safety of the arch dam, surcharging capacity and the treatment effect for the soft structural plane at the abutment. The result shows that the safety of the dam and foundation increases at a certain amount after the soft structure plane is treated, especially that at the right abutment increases obviously from 1.5~2.0 to 2.0~3.0. The safety at both abutment after consolidation is almost the same while the symmetry is enhanced. The surcharge coefficient before consolidation is 6.0~7.0 P_0, it reaches up to 8.0~9.0 P_0 after consolidation.

(2) Engineering analogy method

The crack stability of the dam heel is investigated by engineering analogy method and the crack possibility of the dam heel for Goupitan is evaluated with the monitory data and joint deformation data at the dam heel after impounding in Ertan arch dam. The result indicates that the main pulling stress at the dam heel of Goupitan arch dam is a bit larger than that of Ertan, but the attenuation speed of the main pulling stress at the crack end after cracking is better than that of Ertan. The crack resistance capability of the two arch dam is almost at the same level. Even if provided that the dam heel of Ertan arch dam is under cracking critical status, the upper limit of the cracking depth is only 1.0~1.5m for Goupitan arch dam heel corresponding to the assumption and it will not destroy the grout curtain. Therefore the operation safety of the dam is guaranteed.

(3) Geology mechanical model test

The result of the 3D geology mechanical model test shows that the failure of Goupitan arch dam belongs to strength failure form, and has strong surcharging ability due to elastic surcharge coefficient being 2.2 and failure surcharging coefficient being 8.5.

7 ASEISMATIC ANALYSIS OF ARCH DAM

The basic intensity at the dam site is 6 degree. According to the fortified standard of the dam, the horizontal seismic maximum acceleration is 0.06g corresponding to surmounted probability 0.02 within 100 year basic norm period, which is at low level and the seismic force is not the decision factor for the stress of arch dam and stability of abutment. However, because there are so many orifices in the dam body, the scale is large, the quantity of the flood discharge comes out top among the high arch dam inside and outside of the country, vibration caused by flood discharge is one of the major problem to be investigated in the arch dam design. Hence water elastic model test during flood discharge and numerical back analysis are performed. The results indicated: ① the self-vibration frequency of the arch dam is low, adjoining vibration form is dense, the arch effect is

obvious, with the basic frequency under empty and full reservoir being 2.0Hz, 1.6Hz respectively; ④ The magnitude of the seismic stress produced by the flood discharge vibration is very small and it will not destroy the structure.

8 FOUNDATIONTREATMENT

8.1 *Consolidation grouting and grout curtain for the dam site*

The bedrock is seated in the lower segment of Maokou group (P^{1}_{1m}), mainly made up of I, II and III category rocks. The range and depth of the consolidation grout depends on the stress status and geology condition at different part of the base. The range of the consolidation grout at the riverbed and right abutment extend to 5m away from the outline of the dam base, that of the downstream left abutment extend to 10m away from the base while that of upstream left abutment 5m away. The depth of the consolidation grout at the riverbed is 12m, and that at both abutment is 15~25m. Two rows of deep consolidation grout are layed in the front of the grout curtain to enhance the seepage resistance effect of the grout curtain, with depth 25~35m.

The grout curtain is layed along the foundation corridor at the riverbed, folding toward down-stream and connecting waterproof rock body at both abutments after it comes out of the abutment and extends certain distance. Two rows of grout curtains are set at the base of the dam and the nearby area, the standard of the pervasion resistance is that the leakage of the bed rock is smaller than 1.0Lu. One row of grout curtain is layed at other places, the standard is that the leakage of the bedrock is smaller than 3.0Lu. There is drainage system behind the grout curtain.

8.2 *Geology defect treatment at the bedrock and abutment*

The geology defect at the bedrock and abutment needs to be treated in order to ensure the stability of the abutment and decrease the effect of uneven deformation on the arch dam, synthetical treatment method of combinating excavating, backfilling and grouting should be adopted besides normal consolidation grouting. For the geology defects at the bed rock, water-eroded cave, reconnoitering tunnel and hole, backfilling with concrete is mainly adopted. For the soft structural plane such as relative movements between layers that affect the slide resistance and deformation stability of the abutment, systemic deep-seated treatment is necessary. Transpositional horizontal tunnel is set at every 15~20m along the geology defect structural plane according to elevation, inclined well is layed properly along the orientation (visual incline direction) of the structural plane among the wells so that the transpositional tunnel are arranged in “grid” form to enhance the overall effect of passing force in the rock body.

9 STRUCTURE DESIGN OF DAM BODY

9.1 *Parting and division of dam body*

With temperature control analysis and adopting relevant temperature control measure, there will no construction longitudinal joints, but there are transverse joints. The layout of the transverse joint adopts vertical joint between different parts, that is, it’s plumb joint between elevation 408m~505m and 535~640.5m. while it’s transition joint between elevation 505m and 535m. The upstream length is 552.55m at the top arch of the dam body. There are 26 transverse joints in the dam body all together form left to right abutment and 27 dam blocks, with maximum width 24m. The transverse joint has key slot and joint grouting system.

9.2 *Transportation layout inside the dam*

Foundation grouting corridor are set at elevation 413.0m of dam body and both abutements and 3 layers longitudinal horizontal corridor at different elevations in the dam body in order to meet with foundation grouting, joint grouting in the dam body. Dramage observation and check and transportation. The elevation difference between different horizontal corridor at different elevation is about 50~60m, and the horizontal corridor connects with foundation corridor at the obutment. An elevantor is set in the dam and used as vertical passage, which is connected with horizontal corridor through connective corridor.

9.3 *Concrete division of dam body*

Based on stress condition of the dam, orifice layout in the dam and stress calculation result of dam body, considering of different requirement for concrete strength at different parts of the dam body, the concrete of dam body is divided into 3 parts, with $C_{180}35$ at high stress zone near foundation and orifice zone, $C_{180}25$ at low stress area in the dam body, $C_{180}30$ at other zones.

10 CONCLUSION

(1) Figure design is one of the most key and basic technical problem in the arch dam design. In the design of Goupitan arch dam, based on the topography and geology condition at the dam site, considering of the selection of foundation for arch dam and the layout of flood discharge structure of the dam body, the linetype comparison for the arch dam and optimizing design for the figure of the dam are conducted. The recommended figure of the arch dam with parabola double arch dam proves to be economic, high overall reliability and strong adaptability by sensitive analysis and validation of various kinds of programmers and methods.

(2) With reference to the high arch dam design and construction experience inside and outside of the country and considering of the engineering characteristic of Goupitan arch dam, stress control standards corresponding to arch dam partaking load method and FEM are provided here. The stress analysis of the arch dam indicates that the standards are feasible for Goupitan arch dam and also can be regarded as a reference to other high arch dam design.

(3) The overall safety analysis for Goupitan arch dam has been carried out by 3D nonlinear FEM, engineering analogy and geology mechanical model test. The result shows that Goupitan arch dam has high overall safety. It's necessary to do the overall safety analysis in the design of high arch dam.

(4) Flood discharge vibration has been researched and analyzed for Goupitan arch dam by water elastic model test and numerical back analysis. The result reveals that for Goupitan arch dam the flood discharge vibration is one kind of sensible vibration, with very small dynamic stress in scale produced by vibration. And the vibration will not destroy the structure. The method can be regarded as normal method for research of flood discharge vibration.

(5) Considering of the unevenness and complexity of the bedrock. It's necessary to carry out the adaptability analysis of the figure according to different foundation in the figure design of the arch dam. The analysis is important for evaluating the advantage and disadvantage and rationality of the arch dam figure.

New Developments in Dam Engineering—Wieland, Ren & Tan (eds),
© 2004 Taylor & Francis Group, London, ISBN 04 1536 240 7

Waterproofing technique for a sand dam on sand foundation using geomembrane

K.E.Jiang & Shi Feng Jun
Research Institute of Water Resources and Hydropower, Liaoning Province China Shenyang

Gu Gan Chen
Hohai University Nanjing China

ABSTRACT: The paper introduces a dam project on a river. The dam can only be built using fine sand, because the surrounding area and the foundation are all covered with sand. In seepage prevention design, the geomembrane is adopted. The paper presents the design method and the structure details. The dam was completed in 1994 and has successfully performed for ten years.

1 INTRODUCTION

Xiaoqinggou River located in Zhangwu District, Liaoning, Kerqin Meadow, Inner Mongolia is formed by being cut of the sand dune. The cutting depth at No. 2 dam site is about 40m. The runoff entering the reservoir comes from the underground flow of sand dune. The foundation is winddeposited fine sand and within 50km no cohesive soil is available. The bedrock is 40m deep. So the dam can only be constructed using fine sand with coefficient of permeability 5×10^{-3}cm/s. The sand dam on porvious foundation must have flatter downstream slope. For example, Daqinggou Reservoir Dam, 10km apart and completed in 1976, had an original slope of 1:6, but during its performance, the seepage water continuously seeped out from downstream slope. The slope angle was changed repeatedly, until finally the slope was reduced to two steps of 1:8 and 1:10, and seepage water led to downstream prism, the slope became stable. The original design of No. 2 Xiaoqinggou Dam was similar to that of Daqinggou. After using geomembrane instead, the downstream slope changes to 1:3 and 1:3.5, hence about 166,300m^3 of earth work is saved.

2 THE DETERMINATION OF SLOPE OF SAND DAM

The upstream slope is determined according to the coefficients of friction between sand and the geocomposite geomembrane, which were obtained by tests and listed in Table 1.

3 SEEPAGE PREVENTION OF DAM AND ITS FOUNDATION

The geomembrane is installed on both upstream slope and upstream blanket, it is impervious in vertical direction, so the hydraulic design may assume that dam is on the impervious ground surface. The calculation was based on Darcy's Law and Dupit's Assumption. The entrance head loss of flow into blanket, Δh, is substitued by a extension of seepage path 0.44T, where T is the thickness of pervious foundation, see Fig.1. In Fig.1, in section I and section II the flow are under pressure, and in section III, the flow is free and there is a free surface. When the blanket is considerably

Table 1. Test and calculation results.

Item	Dry sand	Saturated sand
Dry density of sand (γ_0)	15.4kn/m^3	15.4
Cohesion of sand (c)	0.07	0.02
Friction angle between sand and geomembrane (ϕ)	25.5°	21°
Coef. of friction (f)	0.477	0.384
Factor of safety (k)	For 4th grade structure, standard k=1.0~1.05 take k=1.1 in calcadation	
Calculated upstream slope	1:2.31	1:2.86
Adopted slope	1:3 (upper)	1:3.5 (lower)

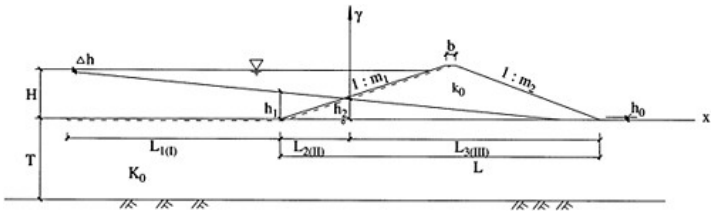

Figure 1. Sketch for seepage calculation.

long, the height exit point on downstream surface is very low, so it may be neglected. According to previous experience, the total flow may be calculated as the summation of the flow of foundation under pressure and that of the dam body without pressure. The seepage calculation used section method and followed law of continuity.

The parameters used in calculation: k_0=k=5×10^{-3}m/s, T=40m, H=20m, h_0=1m, L_1=100m, L=L_2+L_3=147.05m, m_1=m_2=3.25. Solve the following simultaneous equations for all sections, and substitute the results into equations (1) through (4), and check the gradients in dam body and foundation, they must be not larger than [i_{found}]=0.1 and [i_{dam}]=0.105.

Section I: $\frac{H-h_1}{L_1+0.447T} = 0.073 \le 0.1$ (1)

Section II: $\frac{h_1-h_2}{m_1 h_2} = 0.095 < 11.1 < 11.105$ (2)

Section III: $\frac{h_2-h_t}{L-m_1 h_2} = 0.064 < 0.1$ (3)

at the end of phreatic line of dam body: $\frac{k(h_2-h_t)}{2(L-m_1 h_2)} \quad 0.015 \le 0.105$ (4)

It may be seen, when the length of the geomembrane L_1=100m, the conditions in all equations shown above may be satisfied.

Table 2. Main properties of geomembrane.

Item	Unit	Test value
Thickness of PE geomembrane	mm	0.5
Tensile strength	kN/m	11.81
Elongation	%	20–22

4 THICKNESS OF GEOMEMBRANE UNDER PRESSURE

The properties of geomembrane are shown in Table 2.

The coefficients of permeability on both banks of Xiaoqinggou No. 2 Dam are larger, so it is necessary to take measure in both sides of blanket to prevent seepage. If the concrete revetment is built on the dam and bank, the geomembrane may be cracked by the deformation of sand and the internal and external water pressure. So according to the suggestion of Prof. Gu Ganchen, the required strength of geomembrane over strip seam crack was calculated using his formula.

$$T = \frac{0.204Pb}{\sqrt{\varepsilon}} \tag{5}$$

The parameters used in calculation are tensile strength T=11.81kN/m, elongation ε=20%, assume seam width 0.005m, 0.01m, the pressure exerted=196kP_a, factor of safety k=5. Substitute all parameters in equation (5), we obtain $T_1 = 0.2/\sqrt{\varepsilon_1}(b = 0.005\,m)$; (b=0.01m).

The results show that the geomembrane with thickness of 0.5mm is sate for seam crack 0.01m.

5 THE DESIGN FOR BANK PROTECTION AND SEEPAGE PREVENTION

After reservoir filling, the water heads on both sides of geomembrane are high. During reservoir drawdown, the water pressure beneath geomembrane will push up the geomembrane, hence may easily make it unstable. Especially at the beginning of the geomembrane, the problem is most serious. So the preventive measure must be taken to overcome it. According to the condition of reservoir water level change, the woven geotextile wrapping sand, non-waven geotextile and geonet were used in conjunction with geomembrane. In order to reduce the pore water pressure in bank, weep holes were installed, so that the water level in sand on geomembrane could drawdown simultaneously with the lowering of reservoir water level.

6 DRAINAGE OF WATER AND RELIEF OF GAS BENEATH BLANKET AS WELL AS OVERBURDEN ON IT

For the geomembrane installed on original dry ground, after filling the water entering into sand under geomembrane will replace the air entrapped. The air squeezed out in turn pushes up the geomembrane. If no relief facility and overburden is provided, the geomembrane will be likely floated or bursted. If the reservoir level drawdown follows, the water beneath geomembrane cannot drain out in time, the water pressure would act be applied upward, causing geomembrane floating. There are many such failure case records. For ouch preventing failure, Xiaoqingou No. 2 Dam takes the following measures.

(1) Installation of “non-reversible valve” on geomembrane

Here the “non-reversible” means the water can only flow through the valve in one direction. According to the permeability of the sand layer, the valves are fixed on geomembrane for

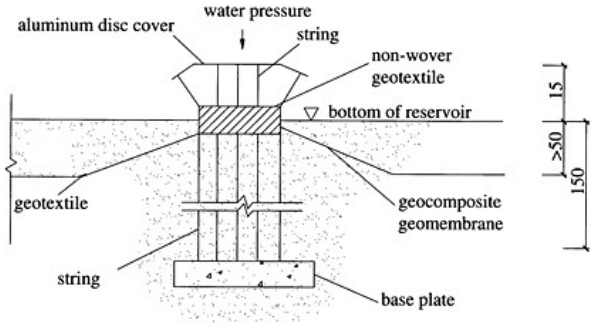

Figure 2. Structure of "non-reversible valve" Unit: cm.

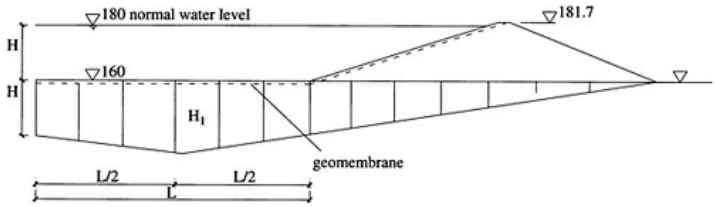

Figure 3. Seepage water pressure distribution beneath geomembrane before drawdown.

every 20–30m. The structure of valve is shown in Fig. 2. First a hole of dia.30cm is cut in geomembrane, then the valve is welded on it. The top of the valve is an aluminum discover, which is connected with durable strings. Strings penetrate geotextile and are attached to a base plate buried in ground. Upon filling the cover rests on geotextile due to water pressure above. When the water and air pressure exceeds the water pressure above, the cover lifts or opens upward automatically, the pressure below geomembrane gradually relieves, then the cover falls down again due to its self-weight.

(2) Overburden on geomembrane

Sand is used as overburden on geomembrane to prevent it from floating. The overburden pressure needed for different parts of geomembrane may be estimated by hydraulic computation. Before reservoir level drawdown, the seepage water pressure distribution beneath geomembrane is shown in Fig. 3. At the beginning of drawdown, the water head at upstream end of the geomembrane is equal to the reservoir water depth, because the water below the geomembrane flows out very quickly. But in the central part, the water head is higher than reservoir water depth because of time lag of flowing out. Even when the reservoir lowers to the lowest level, the pressure in central part still slightly higher at this time, h_2-h_0 may reach to a max. value, see Fig. 4. At this time, the pressure h_2, h_0 must be balanced by sand overburden, otherwise the geomembrane will be pushed up. The max value of h_2-h_0 may be evaluated by successive calculation is connection with the process of reservoir drawdowns. Its value may also be assumed approximately as H_1-h_0, where H_1 is the pressure head in central part before drawdawn. So the height of sand fill needed on geomembrane may be determined by the method mentioned above. The height needed is maximum is central part it may be gradually reduced to upstream and downstream ends. It may be seen that "overburden" method requires

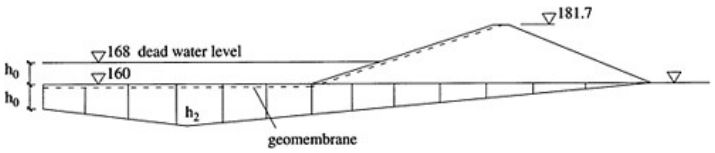

Figure 4. Seepage water pressure distribution beneath geomembrane during lowest reservoir level.

a large amount of soil and hence uneconomic, so sometimes, it may be adopted in conjunction with the "non-reversible" valve method. Farthis dam the combined method gives the height of sand fill 1.5m in central part, and 0.5m, 1.0m at upstream and downstream end respectively.

7 PERFORMANCE

The dam was completed in 1994 and has been working successfully for ten years. The seepage quantity is 40 L/s, mainly comes from bypassing flow.

8 CONCLUSION

(1) Xiaoqinggou Dam saves large amount of earthwork, shortens the length of water conveyance tunnel and saves 37% of the total engineering investment because it utilizes the geomembrane for seepage prevention.
(2) The length of geomembrane is equal to about five to six times of water head, which is coincident with the calculated value and those successfully used in the similar projects.
(3) The adoption of deformed structure of geomembrane on both upstream banks may keep banks stable during reservoir drawdown.
(4) "Overburden" method combined with "non-reversible" valve may guarantee geomembrane working well.

This page intentionally left blank.

New Developments in Dam Engineering—Wieland, Ren & Tan (eds),
© 2004 Taylor & Francis Group, London, ISBN 04 1536 240 7

On wireless pore water transducer for fill-type dams

Y.Kohgo, I.Asano & Y.Hayashida
National Institute for Rural Engineering, Japan

A.Takahashi
Tokyo Electric Power Company, Japan

R.Towmezuka
Sakata Denki, Japan

ABSTRACT: The purposes of this paper are to introduce the wireless transducer and to express the performance of the transducers installed within an embankment of dam. Some experimental tests were conducted to investigate the performance. It was confirmed from these tests that the transducers could express more than 100m underground-communication, the lives were more than 10 years, and the waterproof was more than 3MPa etc. The pore water pressure values measured by these wireless transducers were compared with those of conventional pressure gauges with cables. It was found from the results that both values measured were consistent.

1 INTRODUCTION

It is very important to measure pore water pressures within embankments and foundations in order to monitor the stabilities of fill dams. In the measurement of pore water pressures, pore water pressure gauges, which were connected with cables to the data loggers located on the ground surfaces, were used. The cables were utilized to transfer measurement data and supply power sources. However, there are following shortcomings in the use of the gauges with cables.

(1) To reduce stabilities of embankments: Cable trenches become weak points because of lack of compaction and in some cases, water paths may form along the trenches.
(2) To become a cause of breakdown of gauges: Breakage and insulation reduction of cables, and lightning surge trigger breakdown of the gauges.
(3) To be obstacles against construction: It takes long time to install the gauges.
(4) Low cost performance: The more cost takes when the total length of cables becomes longer.

In order to overcome these shortcomings, we developed a type of wireless pore water pressure transducers. In this transducer, a low frequency electromagnetic wave (8.5kHz) and the latest digital transfer technique were used.

The purposes of this paper are to introduce the wireless transducer and to express the performance of the transducers installed within an embankment of dam. Some experimental tests were conducted to investigate the performance.

2 OUTLINE OF WIRELESS PORE WATER PRESSURE TRANSDUCER DEVELOPED

2.1 *Wireless pore water pressure transducer*

In this design concept, the performance of the transducers required is as follows. The distance of transmission within soils is more than 100m, the dimensions of the transducer are smaller than the

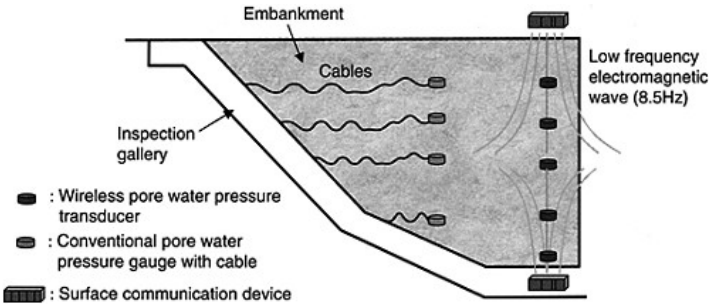

Figure 1. Difference between wireless pore water pressure transducers and conventional gauges with cable.

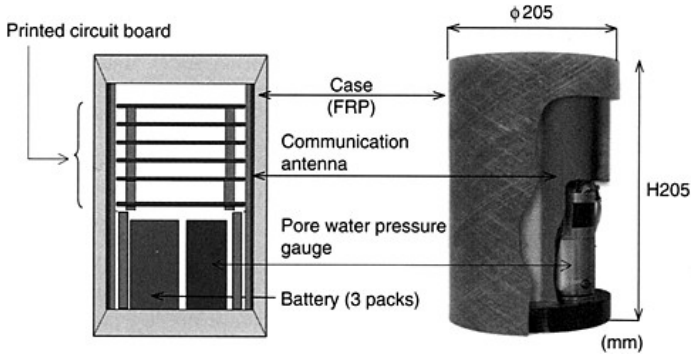

Figure 2. Structure of wireless pore water pressure transducer.

maximum particle size of impervious core materials, the life is more than 10 years, waterproof is more than 3MPa, and the density of the transducer is almost the same as that of gravels. In order to satisfy the specifications, we utilized 8.5kHz electromagnetic wave, latest digital transfer technique, power-saved electric circuit, lithic batteries and FRP (Fiber Reinforced Plastics) case. Figure 1 shows an illustration of difference between the wireless transducers and conventional gauges with cables installed in an embankment dam. The wireless system consists of data communicate devices (surface device), which set on an embankment surface and or in an inspection gallery, and transducers installed within an embankment dam.

Figure 2 shows the structure of wireless transducer developed. The dimensions are 125mm in diameter and 205mm in height. The transducer mainly consists of a pore water pressure gauge, printed circuit boards, three size D batteries, and an antenna coil. It has functions of storing, transmitting and receiving of data. Once the transducer received commands from the surface device, it can send data stored to the surface device.

Figure 3 shows a schematic figure for the underground communication system developed here. The communications between wireless transducers and the surface device are conducted with 8.5kHz electromagnetic wave. The digital signals (0 or 1 figures) are identified using phase shift keying (PSK) technique. The S/N ratio (signal-to-noise ratio) needs to be more than 2. In reality, the most efficient communications can be conducted when the antenna in the wireless transducer is set parallel to that in the surface device as shown in this figure. The vertical axes of both antennas are namely parallel each other. It is found from some experimental data that in this case, the receiving voltage is

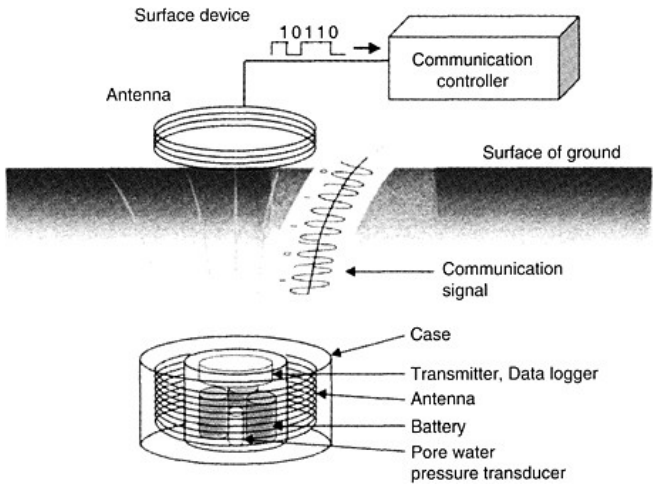

Figure 3. Schematic view of underground wireless communication system.

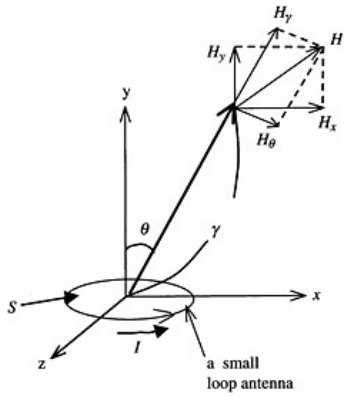

Figure 4. A small antenna.

almost equal to the theoretical value (kH_y: referring next section). In order to obtain the sufficient communications, we investigated the setting procedure of wireless transducers where the inclines of the transducers become as small as possible when setting them. This will be described in section 4.1.

2.2 *Transmission principles within soils*

The wireless transducer can communicate to the surface device with a low frequency electromagnetic wave. In order explain the transmission principles, let us now consider a small loop antenna for transmission, which has area S and current I, as shown in Figure 4. The intensities of magnetic field H_θ (for θ direction) and H_r (for r direction) at a point with distance r and angle θ from the center of the small antenna are obtained as follows [1].

$$H_\theta = \frac{j}{2\lambda}\frac{1}{\eta_0}\left(1+\frac{1}{jkr}+\frac{1}{(jkr)^2}\right)\frac{\exp(-jkr)}{r} j\omega\mu IS\sin\theta \quad (1)$$

$$H_r = \frac{1}{\lambda}\frac{1}{\eta_0}\left(\frac{1}{jkr}+\frac{1}{(jkr)^2}\right)\frac{\exp(-jkr)}{r} j\omega\mu IS\cos\theta \quad (2)$$

$$k = w\sqrt{\varepsilon\mu} = \frac{2\pi}{\lambda} \quad (3)$$

$$\eta_0 = \sqrt{\frac{\mu}{\varepsilon}} \quad (4)$$

where j is imaginary unit, λ wave length, ε dielectric constant, μ permeability, and ω angular velocity. As described in the previous section, the receiving voltage is almost equal to kH_y, so we address to the value of H_y. The intensity of magnetic field for y direction H_y is given referring Figure 4,

$$H_y = H_r\cos\theta - H_\theta\sin\theta. \quad (5)$$

As value of θ is usually small, the value of H_y depends mainly on the value of H_r. If a high frequency of wave is used, value of kr could be remarkably larger than 1. Then the terms of $1/jkr$ and $1/(jkr)^2$ in Equations (1) and (2) may vanish, and the value of H_r is almost equal to 0. Communication with high frequency wave cannot be established. Meanwhile supposing a frequency of wave used is very low, value of kr could be sufficiently smaller than 1. Then the terms of $1/(jkr)^2$ in Equations (1) and (2) may only remain. The value of H_r is inverse proportion to r^3 and the absolute value is given as,

$$|H_r| = \frac{IS\cos\theta}{2\pi r^3}. \quad (6)$$

It is obviously found from Equation (6) that the absolute value of H_r is independent of properties of propagation media. Thus, if you use a low frequency electromagnetic wave, the attenuation due to distance is remarkably high, but the affection of the properties of propagation media to the attenuation is small.

3 VARIOUS TESTS FOR VERIFICATIONS OF PERFORMANCE [2]

Five kinds of tests were carried out to investigate the specifications shown in Table 1. They are tests for transmission change due to temperature, mechanical tests for FRP case, waterproof tests, life tests for battery and tests for property of transmission.

Table 1. Design specifications for wireless pore pressure transducer.

Carrier frequency	8.5kHz
Communication distance	100m (Underground)
Size	Less than Φ 125mm×H205mm
Measurement frequency	1/day (Automatic mesurement)
Communication frequency	1/week+1/month (Periodical)
Battery life	Over 10 years

3.1 *Transmission change due to temperature*

We investigated the lags of the internal timer installed within the transducer due to environmental temperature changes from 0 to 40°C. It was found that the lag in a day was about 2 seconds and this value was within an adjustable range. Transmission tests were carried out within −10 to 50°C. It was found from the test that the transmission was normal.

3.2 *Mechanical tests for FRP case*

When the transducers are installed within a more than 100m embankment dam, they may be applied more than 2MPa earth pressures. It is necessary for the FRP case of the transducer to bear such earth pressures. We have also to consider whether the FRP case is safety or not in such a special situation as that it touches gravels. In such a case stress concentration occurs. So we conducted some experimental compression tests shown in Figure 5. Figure 5 shows three loading patterns that will really occur. Pattern 1 is vertical point loading tests where vertical point loads are applied at the center of the cap and large deformations occur around the connecting part between the cylinder part and the cap of the FRP case. We investigate from the tests whether a leakage through the connecting part occur. Pattern 2 is a line loading that can be normally seen. Pattern 3 is a special case such as that the FRP case touches gravels. Strains were only measured during the tests with strain gauges stuck on the surfaces of the FRP case. A scene of tests is shown in Figure 6.

It was found from Pattern 1 tests that (1) the maximum strain appeared around the connecting part, (2) the strain increased about 1000μ each 10kN, (3) the strain expressed about 4000μ at the maximum load applied, (4) the maximum load was about 40kN, (5) the load-strain relationships were linear elastic, and (6) exceeding 35kN, strains concentrated the loading point.

Pattern 2 tests showed the following results. (1) The maximum strain was recorded in the gauge stuck vertically at the center of the cylinder. (2) The strain expressed about 2000μ at the maximum

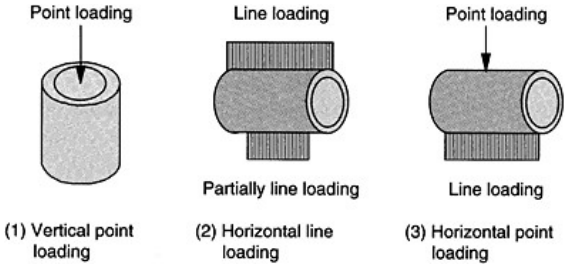

Figure 5. Test conditions (Loading patterns).

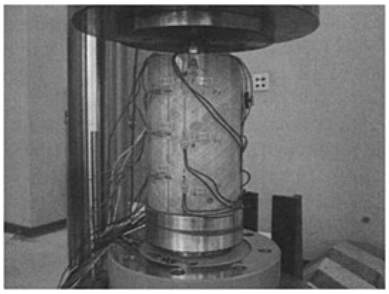

Figure 6. A scene of point loading test.

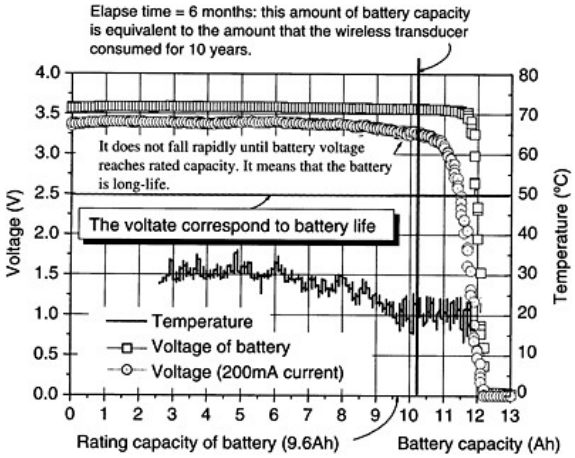

Figure 7. Relationship between voltages and battery capacities for 6 months discharge test.

load applied, and the maximum load was about 50kN. (3) The load-strain relationships were linear elastic. (4) Any collapse cannot be seen.

It was found from Pattern 3 tests that (1) the maximum load was about 40kN, and (2) exceeding 35kN, strains concentrated the loading point.

3.3 *Waterproof test*

The transducer was set in a pressure chamber filled with water and was subjected up to 3MPa water pressure in order to check if water came into the transducer. The water pressures were gradually applied and 1, 1.5 and 3MPa pressures kept for 12, 43 and 7 hours, respectively. It was found from the test results that water did not come into the transducer and the FRP case was compressed by about 1700μ strain when 3Mpa pressure applied. The amount of the strain occurred was 14% of the limit strain for FRP. Then, the transducer has a sufficient waterproof.

3.4 *Life tests for battery*

The required life of the transducer is more than 10 years. Then, batteries, which can steady supply powers for more than 10 years, are necessary. We used lithic batteries. In order to investigate if the batteries can steady supply powers for more than 10 years, we conducted haste electric discharge tests. These tests were carried out so that regulated discharges were applied to the batteries and the amount of discharges for terms (1/12, 1/2, 2.5 and 10 years adopted) was almost equal to the amount of power consumption of the transducer for 10 years. The batteries used have the capacity 13.0Ah, the self-power consumption less than 2% of the capacity, and the maximum discharge current 2000mA. The amount of power consumption of the transducer for 10 years is 10.18Ah that was calculated under the condition that pore water pressures were measured once a day.

Figure 7 shows the result of 1/2 (6 months) year discharge test. The voltage of the battery kept more than 3V and was steady after 6 months. Then, batteries used satisfy our specifications.

3.5 *Property of transmission*

In order to obtain a fundamental propagation characteristic, communication tests, where media, direction of antennas and transmission power were constant and transmission distances were

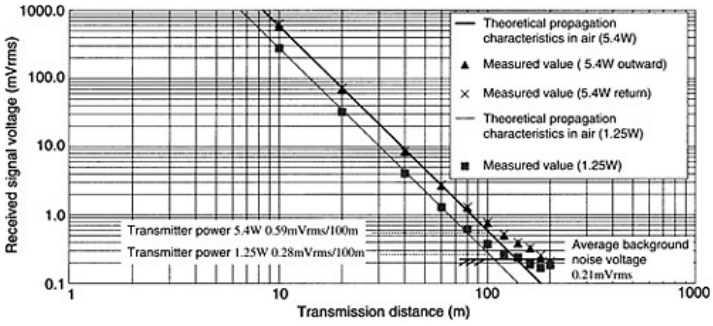

Figure 8. Relationship between received signal voltages and transmission distances in the air.

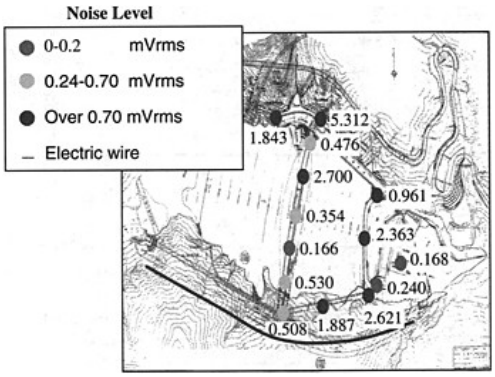

Figure 9. An example of the noise level in a dam site.

changed, and measuring noises at the receiving points may be conducted. Figure 8 shows an example of such communication tests in the air. The solid lines are theoretical and symbols are measured values. Two transmission powers (5.4W and 1.25W) were used. As the mean noise level was 0.21mVrms in these cases, the S/N ratio at the point with 100m distance for 5.4W case was 2.8 that was larger than 2. Then, we could obtain that the communication distance was more than 100m.

Figure 9 shows noises measured in a dam site. The noise levels were very different at each point. It is very important to survey noise levels around receiving points, for the communication distances depend on propagation characteristics and noise levels at receiving points.

4 PERFORMANCE OF THE WIRELESS TRANSDUCERS INSTALLED IN A REAL EMBANKMENT

4.1 *Setting procedure for wireless transducer [3]*

In order to obtain the sufficient communications, we investigated the setting procedure of wireless transducers where the inclines of the transducers become as small as possible when setting them. Here we conducted in situ install tests of the transducers. Two procedures (Conventional method and Core boring method) were adopted. In the Conventional method, a transducer lies on a setting level and is installed by compacting thin layers surround it as shown in Figure 10(a), while in the

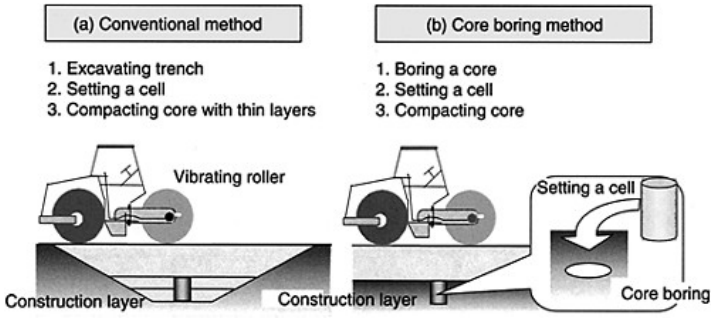

Figure 10. Setting procedures of wireless pore water pressure transducer.

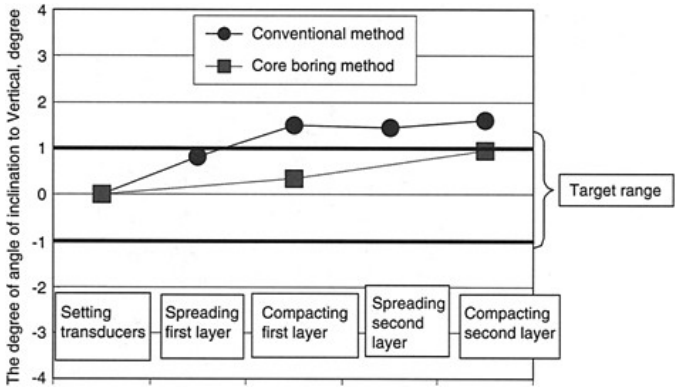

Figure 11. The degree of angle of transducer inclines from vertical direction at every work stages.

Core boring method, a compacted layer is cored out, the transducer is put into the hole and the space between walls of the hole and the transducer is filled with the fill material passed through 2mm sieve as shown in Figure 10(b). In these tests, two transducers are installed within an embankment (Height=90cm, Crest width=8m and Crest length=15m with 1:1 slopes). The height of points installed was 30cm. During the tests, inclines of transducers were measured.

Figure 11 shows the incline changes at every work stages. The inclines with Core boring method were smaller than those with Conventional method. When we install the transducers within real embankment dams, we will employ the Core boring method.

4.2 *Installing transducers within a real embankment dam and measuring results*

Three wireless transducers developed here were installed within a real embankment dam (H=69.9m, total storage volume=4.31Mm^3) in order to investigate their real behavior. Figure 12 shows their setting points on the maximum close section. The No. 49 transducer was installed within the filter zone and other two (Nos. 45 and 46 transducers) were in the impervious core zone. The conventional pore water pressure gauges Nos. P-18 and P-19 were installed associated with Nos. 46 and 45 wireless transducers, respectively. The setting level was EL. 337.5m below about 20m of the crest.

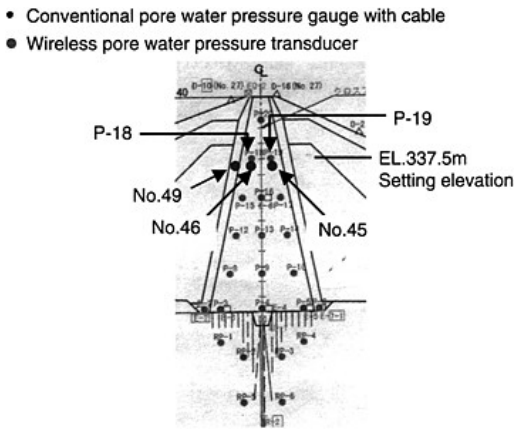

Figure 12. Setting points of wireless pore water pressure transducers on the maximum cross section.

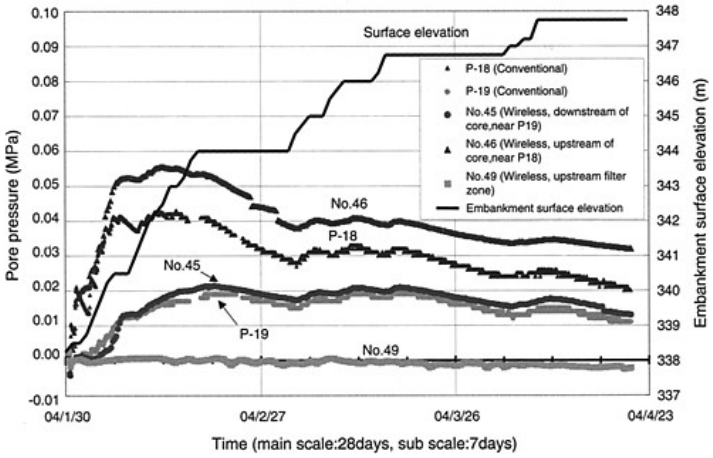

Figure 13. Comparison between pore water pressure values measured with wireless transducers and conventional gauges with cables.

Figure 13 shows comparison between pore water pressure values measured with wireless transducers and conventional gauges with cables. It was found from this figure that there was little bit difference between values of No. 46 and P-18 but the changing patterns were almost the same. The values of No. 45 and P-19 were well consistent each other. The values of No. 49 were almost 0. As the wireless transducer was installed within the filter zone, the values were reasonable.

5 CONCLUSIONS

We developed wireless pore water pressure transducers that can communicate with a surface devise by using a low frequency electromagnetic wave. We investigated through various experimental tests if the transducer satisfied their design specifications. It was confirmed from these tests that the transducers could express more than 100m underground-communication, the lives were more than 10 years, and the waterproof was more than 3MPa. The pore water pressure values measured by these wireless transducers were compared with those of conventional pressure gauges with cables. It was found from the results that both values measured were well consistent.

REFERENCES

[1] Matsumoto, K. (1978). Introdution to electromagnetic wave engineering, Asakura-shoten (in Japanese).
[2] Kohgo, Y., Asano, I. and Hayashida, Y. (2003). Development of wireless pore water pressure transducers and their application to fill-dams, *SDERD* Vol. 57, 7–18 (in Japanese).
[3] Takahashi, A., Kohgo, Y., Endoh, S., Kakuei, T. and Ohtsuki, T. (2003). Application of wireless pore water pressure transducers to a fill-dam, *Proc. 38th Congress on Geotechnical Engineering,* JGS, 1271–1272 (in Japanese).

New Developments in Dam Engineering—Wieland, Ren & Tan (eds),
© 2004 Taylor & Francis Group, London, ISBN 04 1536 240 7

Steel lining of sluice spillways for 92m high Wangkha dam in Bhutan Himalayas

Swaraj B.lalit., V.K.Verma, D.P.Goyal & R.N.Khazanchi
Tala Hydroelectric Project Authority, Bhutan

ABSTRACT: This paper presents a case study of steel lining of sluice spillways provided in 92m high concrete gravity dam under advanced stage of construction across river Wangchu in Eastern Himalayas. Five sluice spillway openings of 6.5m width and 13.15m height have been provided at lower level to serve dual purpose of providing free passage to the probable maximum flood of 10,600m^3sec^{-1} and to restore the live storage regularly by flushing out sediments deposited upstream of the dam each year for the purpose of maximum generation during peak hours throughout the life of the project. These sluice spillways are thus quite diiferent from the normal overflow spillways which during the floods pass relatively clear water from the top layer of the reservoir. The sluice barrels have been steel lined in the reach upstream of the radial gates to take care of any susceptible damage to the concrete surfaces due to movement of heavy sediment load, boulders, so as to minimize post operation maintenance. The paper outlines the need of providing Sluice steel lining as against other options. Spillway glacis protection, piers & divide walls steel cladding on the downstream of radial gates has also been brought out.

1 THE TALA PROJECT

Tala Hydroelectric Project (1020MW), a joint venture between the Royal Government of Bhutan and Government of India is located on the river Wangchu in South Western Bhutan in Eastern Himalayas and envisages utilization of gross head of 861.5m available in 30km stretch of this river between TRT outfall of existing upstream 336MW Chukha Power House and TRT outfall of Tala Hydroelectric project. Key features of the Project are:

- Head works consisting of a diversion structure in the form of 92m high concrete gravity dam at Wangkha located about 3km downstream of Chukha Project TRT outfall, to divert a design discharge of 172m^3sec^{-1} through three Power Intakes, feeding three underground Desilting Chambers each 250m long, 13.9m wide and 18.5m high for removal of suspended sediments of 0.2mm size and above.
- Water Conductor System consisting of a 6.8m diameter 23km long Head Race Tunnel terminating into a 184m high, 15m/12m diameter surge shaft followed by two 4m diameter and 1.1km long pressure shafts trifurcating into penstocks of 2.3m diameter each.
- An underground Power House Complex consisting of a Machine hall cavern of 206m× 20.4m×45.5m size to house 6 Pelton turbo generators of 170MW capacity each; a Transformer hall cavern of 190m×16m×27m size to accommodate 19–70MVA 13.8/400kV transformers and 3.1km long Tail Race Tunnel of 7.75m diameter to discharge the water back into river Wangchu.
- It will generate 4885Gwh of energy annually on an average besides 1122MW of peaking power (with 10% continuous overload capacity). The surplus power after meeting the demand of Bhutan will be transmitted to India through a double circuit 400kV transmission lines of 140km circuit length from Tala Power House to Indo-Bhutan border to evacuate Power to India.

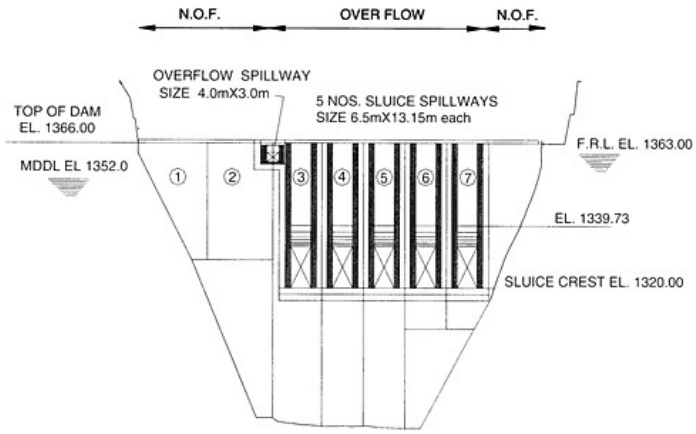

Figure 1. Wangkha dam—upstream elevation.

2 WANGKHA DAM

It is a 92m high concrete gravity dam having a crest length of 129.5m at top EL. 1366.00m. There are seven dam blocks containing five sluices and one overflow spillway as shown in Fig. 1. The Full Reservoir Level (FRL) would be at EL. 1363.00m and Minimum Draw Down Level (MDDL) would be at EL. 1352.00m.

Five deep-seated sluice spillways 6.5m (wide)×13.15m (high) presently under construction[1] have crest at EL. 1320.00m. An auxiliary overflow spillway 4m (wide)×3m (high) with crest at EL. 1360.00m has been envisaged to take care of daily minor fluctuations in the reservoir besides passing logs & trash. This has been located towards left bank such that the floating debris remain away from the Intake Structure on the right bank.

The energy dissipation arrangement is in the form of ski jump bucket having 39m radius. Maximum sluice section is shown in Fig. 2. The horizontal throw of the water jet will extend up to about 100m downstream of bucket lip into the Plunge Pool. The axis of the dam has been provided 11° curvature with radius of 607.347m, in order to compress the width of ski-jump jet at bucket lip and consequently reducing excavation of banks. The toe of the ski jump bucket has been protected by providing minimum 1.5m thick concrete apron founded on rock all along the river cross section, up to 20m length, downstream of toe of spillway portion of dam.

2.1 *Sediments in River Wangchu*

The river drains a catchment of 4028km^2 at Wangkha dam site. The catchment has mountainous rugged terrain with elevations ranging from 7000m to 1300m, and is covered with dense vegetation growth except at higher elevations, which is snow bound for most of the year and is barren. The Wangchu river, like all Himalayan rivers, carries a heavy bed load in the monsoon months from June to September, which includes moving boulders & suspended silt load containing hard particles like quartz.

Total annual sediment load in river Wangchu at Wangkha dam site has been estimated as 1.45 million-t (0.8 million m^3). Around 90% of this sediment load is transported in the river during June to October in the monsoon period. The storage area behind the dam, being meager, would tend to get filled up quickly by the sediments.

Analysis of sediment constituents in the river water on ten samples for Moh's hardness scale showed that particles having Moh's hardness greater than 7 varied from 34.51% to 54.49% with an

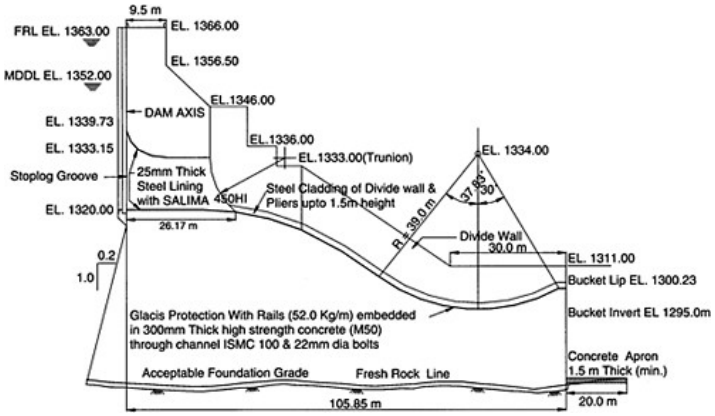

Figure 2. Wangkha dam—maximum sluice section.

average of 45.66%. Quartz constituted 43.16% of the total sediments on an average. The petrographic analysis to determine the shape of the particles revealed that percentage of angular/ sub-angular particles varied from 10.30% to 37.03% with an average of 16.76%. These angular/ sub-angular particles having Moh's hardness greater than 7 are apprehended to inflict maximum damage to the concrete surfaces in the sluices and on the Divide walls and Training wall especially during the heavy floods and during the flushing operation of the reservoir.

Model studies carried out at Central Water & Power Research Station, Khadakwasla, India by creating natural flow conditions for assessing effectiveness of flushing out of reservoir through sluices provided near the bed level, have indicated that most of the incoming accumulated sediments can be flushed out in one day with a discharge of about $300 m^3 sec^{-1}$. During flushing operation of the reservoir, sediment concentration passing through the sluices will be very high.

3 STEEL LINING OF SLUICE OPENINGS

These sluice spillways are thus quite different from the normal overflow spillways, which during the floods pass relatively clear water from the top layer of the reservoir. Maximum discharge intensity through sluice spillways would be of the order of $324 m^3 sec^{-1} m^{-1}$ of spillway width during the PMF conditions. While undertaking the flushing operation of the reservoir to recoup the live storage of the reservoir, it is apprehended that the concrete faces of the sluices are highly vulnerable to the abrasive action of the silted reservoir and impact of flowing boulders and bed material. Therefore, these need to be protected against any eventuality of damage to the concrete surfaces, exposing the reinforcement especially upstream of the gates, minimizing the post operation maintenance. Exposed areas of the sluices upstream of the stoplog gate cannot be repaired which have higher probability of getting damaged during flushing operation of reservoir.

4 DESIGN, FABRICATION & ERECTION OF STEEL LINERS

The following aspects have been considered;

(i) Stability of liner for all loading conditions.
(ii) Selection of suitable steel in view of (i), and its capability to withstand heavy abrasion and impact.

(iii) Construction sequence to ensure uniform distribution of loads & monolithic behaviour of the pier section to transfer stresses developed on the skin plate to concrete systematically and uniformly through combination of stiffeners.

4.1 *Design consideration*

Looking at different conditions that may exist, the worst conditions seems to exist during the maintenance & operation of radial gates, when the stoplogs are closed, the sluice liner has to be designed for external pressure due to pore water pressure in the surrounding concrete mass. The steel liner should not buckle against external pressure. Stiffeners are provided to take care of such eventualities. The shape of the sluice liner being rectangular, deflection/buckling in the liner due to external loads would be far more severe than in circular section. Though, subsurface drainage (formed drains) could reduce the external pressure, in worst conditions, it is not accounted for due to the fact that drains tend to get choked due to calcination. Even the weep holes, if provided may get choked, as highly silted water shall be flowing through the sluices.

As such, provision of stiffeners is essential for safety of liner against external pressures. Provision of stiffeners also ensures sound integration of liner with surrounding concrete. The following three types of loads have been considered while designing the sluice liner system:

(i) Water Load—Under the full reservoir level the water pressure on the sluice liner act all around, when the stop-logs are in position and sluices are empty. This is the worst case and results in maximum deflection at the sides.
(ii) Concreting at top—Loading due to weight of fixed depth of concrete slab on top of the sluice liner is taken in this case. Liner deflection is not much.
(iii) Concreting on sides—Concreting on sides of sluice opening causes a loading over the whole height of the sidewalls. This causes maximum lateral deflection.

Though conditions at (ii) & (iii) exist temporarily during construction only. As per design requirement, following mechanical properties were specified for steel plate.

(a)	Ultimate Tensile Strength	–	570–720 MPa
(b)	Yield Strength	–	450MPa
(c)	Elongation (%age)	–	19%
(d)	Hardness	–	160BHN (Minimum)
(e)	Impact Proportion	–	90 Joules to 20 Joules at 0° to 20°C.

Steel plate SAILMA 450 HI manufactured by SAIL (India), which fulfills these requirements has been chosen for use as steel lining plate.

4.2 *Arrangement of sluice liner*

The selected arrangement gives due care to proper anchoring of steel plates into piers through stiffeners and total integration of stiffeners, reinforcement and concrete so as to distribute the loads uniformly and monolithic behaviour of pier is ensured. Construction methodology has accordingly been planned envisaging erection of steel liner in single stage.

The arrangement envisaged fixing skin plate with an elaborate arrangement of transverse stiffeners and longitudinal stiffeners welded to the skin plate and embedded in concrete. The transverse stiffeners are provided across the flow at a spacing of 800mm c/c as indicated in Fig. 3. The 500mm deep longitudinal stiffeners provided along the flow are spaced at 1000mm c/c and interconnects each set of adjacent transverse stiffeners. The transverse stiffeners are 1000mm deep at top and bottom and 1200mm deep on sides and are provided with a 300mm wide flange at the ends. The flanges of transverse stiffeners are spliced in the middle, top & bottom corners for additional strength requirements in these areas.

Total weight of one liner, as per this arrangement, works out to be 7301. The skin plate, the transverse stiffener and the longitudinal stiffeners accounts for around 28%, 58% and 14% respectively.

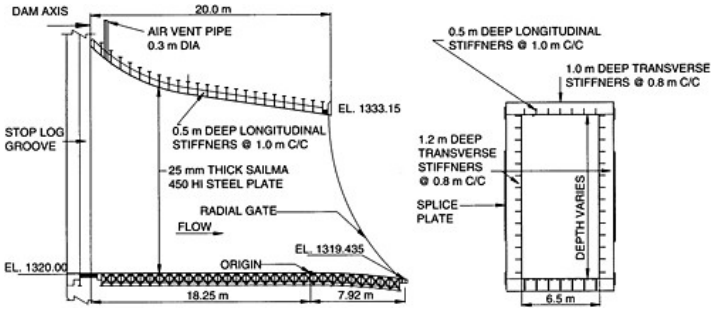

Figure 3. Longitudinal section & cross section through center line of sluice.

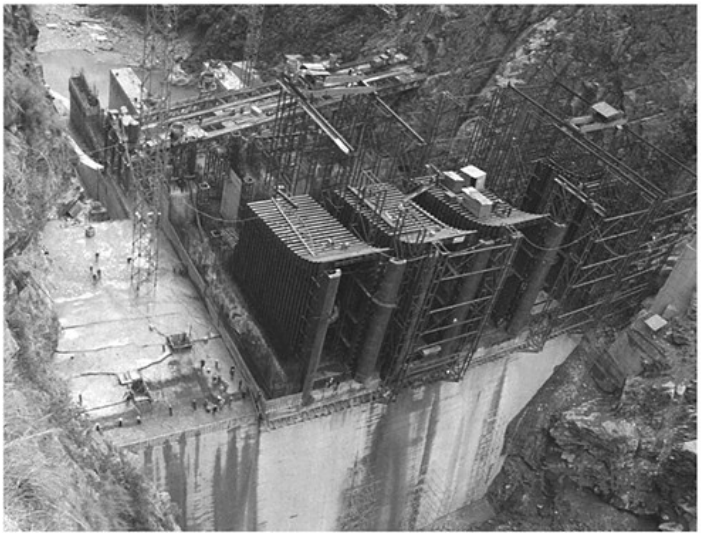

Figure 4. View of sluice liner under construction.

4.3 *Fabrication & erection*

Some important aspects, which needed consideration are as under:

- Fabrication of liners had to be planned & co-ordinated with load carrying capacity of the Potain crane arrangement provided at site. Fabrication at yard was accordingly divided into about 600 sub assemblies for all the five liners with total weight as 3650t in view of load carrying capacity of tower cranes being 101 at maximum reach of 30m and available manufactured size of the plates. A view of sluice liners during erection is shown in Fig. 4.
- Erection of liners is a time consuming activity, involving stoppage of concreting of dam blocks to take up erection of each unit till its completion in all respects including testing. After erection

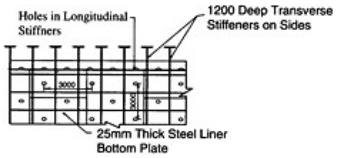

Figure 5. Concreting/grouting hole pattern.

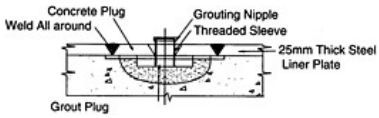

Figure 6. Details of concreting/grouting Plug in liner plate fitted with the grouting nipple.

is over liners need to be embedded in concrete upto a safer height before onset of monsoons, as the flood is planned to pass through these openings.

- From experience it is observed that minimum length shall be left for field butt weld joint for fast erection at site and better welding of skin plate.
- All weld joints in skin plates shall be staggered. Though, it will pose difficulties in alignment during erection work, it will automatically increase precision required during fabrication.
- For effective concreting beneath the sluice invert longitudinal stiffeners were replaced by x-bracing. Cut outs in transverse stiffeners were provided in the sides for avoiding air entrapment during concreting and better concrete flow. For proper integration of concrete between stiffeners and rest of the concrete, additional reinforcement loops in various forms have been provided.
- Further to ensure proper contact of skin plate especially bottom plate with concrete, contact grouting has been done through 165mm dia holes provided @ 3000mmc/c in the bottom plate as indicated in Fig. 5, which were first used for pouring concrete beneath the sluice invert. These holes were then sealed with a circular plate, which contained another 20mm dia threaded hole at the center for carrying out contact grouting through a threaded nipple as indicated in Fig. 6. The grouting work was carried out at a maximum pressure of 4kg/cm^2, after the side piers have been raised by atleast 3.0m. Microsilica @ 4% by weight of cement and non-shrink compound @ 1.5% was used for better results. After completion of grouting, nipples were replaced by grout plug and the hole cut in skin plate was sealed with filler weld material up to the top. The importance of this job can be judged from the fact that till now two of the blocks in which this activity of contact grouting of bottom plate has been completed has taken on an average 2t of cement per block.

5 PROTECTION OF GLACIS

In case of Wangkha dam, the glacis drops from a sluice crest elevation of 1320.00m at Chainage 18.5m to the bucket invert level of 1295.00m at chainage 85.5m from where it rises up to EL.1300.23 (Bucket Lip) for facilitating a ski-jump of the water jet. The velocity of the moving jet will rise to more than 30m sec^{-1} at bucket invert.

Since abrading and subsequent damage to the glacis is generally caused by eddy currents coupled with high velocity flow and impact due to debris, glacis protection works envisage provision of closely spaced steel rails along the glacis embedded in abrasion resistant Concrete. The rails (R-52) having weight 52kg/m are being provided along the flow direction at 300mm c/c spacing. The arrangement of rails supported on channels (ISLC 100×50) @ 2000mmc/c is anchored deep inside the concrete with the help of 22mm diameter 1.1m long bolts. The arrangement of downstream protection works is shown in Fig. 7.

As main consideration for top layer of concrete was to achieve lowest abrasion loss & high resistance to impact, high performance abrasion resistant 300mm thick concrete (M:50) layer was specified at top which also embeds the arrangement of rails on channels. This was considered in view of experience from the upstream Chukha dam, wherein M20 A20 concrete used between rails has been eroded to the extent of 10mm to 150mm during last about 18 years of operation, when no major flood has occurred. However, conditions at Wangkha dam will be more

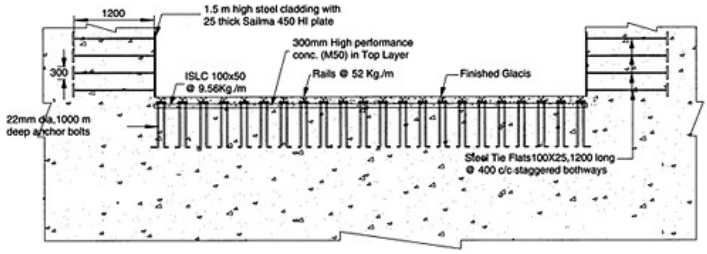

Figure 7. Wangkha dam—cross section showing protection works downstream of radial gates.

severe as higher velocities will prevail in the bucket portion due to the designed drop for facilitating ski-jump.

It was decided to evaluate abrasion resistance of concrete using cement and aggregates available in and around the project site[2] and microsilica (grade 920D, Elkem make) conforming to ASTMC 1240 (2001) and CAN/CSA-A23.5 M86 (1986). Admixture Rheobuild 1100, Glenium 51M and Glenium 51 were tried which have water reducing capacity of more than 20%. To ensure that there is no shrinkage of concrete near rails and its embedments, non shrink compound (NSC) was recommended by the Designer. However, the dosage was limited to 0.3% as field tests proved that use of NSC reduces the compressive strength and increases the abrasion loss. Concurrently water permeability and chloride penetration tests were also done. These showed remarkable reduction in the depth of water penetration & rapid chloride penetration, which are the main requirements for durability of the concrete.

The final mix contained 400kg of cement and 40kg of microsilica per m^3 of concrete and 1.1% Glenium 51M by weight of cement and microsilica as admixture. Glacis surface being curved, only low-slump concrete ranging from 0–10mm slump was poured to avoid sagging of concrete on the inclined curved glacis. A view of glacis showing part finished glacis and erected rails arrangement along with steel cladding is shown in Fig. 8.

Since the lower most layer of water jet contains maximum concentration of sediment load, the divide walls and piers have been cladded upto a height of 1.5m from glacis level with abrasion resistant 25 thick, SAILMA 450HI steel plate anchored with 1.2m deep tie flats. The lip of the bucket has also been cladded with the same steel plate.

6 CONTROL OF ABRASION EROSION—OTHER OPTIONS

Some of the abrasion resistant concrete mixes used in hydraulic structures, though not very sound, which could be considered for lining of such structures are:

(i) Polymer impregnated concrete (PIC), Polymer concrete (PC) and Polymer modified cement concrete (PMCC).
(ii) Aluminous cement + Artificial aggregates
(iii) Cement based concrete with silica fumes
(iv) Steel Fibre reinforced concrete.

The abrasion erosion resistance of Polymer based concrete is significantly superior to that of comparable conventional concrete due to a stronger cement matrix. However, its application could only be found to be mostly in bridge deck overlays & parking garages in columns, beams, slabs and floors of industrial buildings.

Figure 8. View showing part finished glacis and erected rails arrangement.

Abrasion resistant concrete made out of aluminous cement & artificial aggregates appears to have been extensively used on spillways/sluice aprons, pier faces and other locations susceptible to damage by high velocities & silt loads. No direct application for lining of under sluices upstream of the gates could however be located. Further, rate of abrasion of this material is more as compared to steel lining and accordingly requires to be made up regularly through annual maintenance. An idea regarding extent of annual wear which can be expected with respect to this abrasion resistant material is about 1cm with following parameters; constant angle of attack of the stream of 45°, a water velocity of 10m sec^{-1}, fine particle (<2mm), sand load of 50%, as quoted in technical paper[3]. However, the actual wear when highly silted water containing boulders as well moves on these surfaces would be more.

Silicafume based High Performance Concrete (M:70) is although more effective in offering better resistance to abrasion yet it falls short of abrasion erosion offered by granite blocks and steel plate.

Steel Fibre Reinforced Concrete is although good in mechanical strength but steel fibres do not enhance abrasion resistance.

It is pertinent to mention that in Wangkha dam spillway sluices, conditions are far severe, where bed load comprising both fine and coarse sediments containing quartz along with boulders need to be passed/flushed through the sluices. Moreover, bell mouth area upstream of stoplogs, which would also be subjected to abrasion, would not be available for maintenance once the project is commissioned, and it would be difficult to undertake repairs in that region without suffering huge power generation losses. Since the steel parts of the gates like sill beam and gate guides would tend to get protruded when the concrete wears out, these are susceptible to damage and would need to be profiled suitably from time to time.

As per ACI210[4] "The rate of erosion is dependent on a number of factors including the size, shape, quantity, and hardness of particles being transported, the velocity of the water, and the quality of the concrete. While high-quality concrete is capable of resisting high water velocities for many years with little or no damage, the concrete cannot withstand the abrasive action of debris

grinding or repeatedly impacting on its surface. In such cases, abrasion erosion ranging in depth from a few centimeters to a meter or more can result depending on the flow condition. Under appropriate flow conditions and transport of debris, all of the construction materials currently being used in hydraulic structures are to some degree susceptible to abrasion. While improvements in materials should reduce the rate of damage, these alone will not solve the problem. Until the adverse hydraulic conditions, which can cause abrasion erosion damage are minimized or eliminated, it is extremely difficult for any of the construction materials currently being used to perform in the desired manner."

Out of all other options, steel lining thus seemed to be most reliable and durable in the vulnerable area upstream of sluice radial gates for minimizing post operation maintenance, whereas a combination of rails embedded in High performance concrete (M:50) in the glacis portion and steel plate cladding on piers/divide-walls upto 1.5m height was selected for area downstream of the radial gates.

7 CONCLUSIONS

Depending upon severity of the operating conditions similar to one described in the present case, it is essential that sluices in dams, to cater to very high discharge intensities need to be protected against abrasion, erosion and impact action of the flowing debris with high velocity water. Out of all the options presently available, provision of steel lining appears to be the best as even stronger concrete (M:70) would also get abraded with time and the steel guide plates of the gates would protrude in the waterway and are likely to get dislodged with time. Though provision of steel lining is a costly proposition involving longer time for its fabrication and erection but it ensures its sturdiness against all eventualities. However its proper fixity with the surrounding concrete has to be duly ensured.

REFERENCES

[1] Devendra, K.Sharma, V.K.Verma, D.P.Goyal and R.N.Khazanchi, "Design and construction of sluice spillways for reservoir flushing for 92m high Wangkha Dam in Bhtuan" *Hydro Africa 2003, International Conference on Hydropower, Arusha, Tanzania, 17–19 Nov 2003.*

[2] Rajbal Singh, A.K.Sathapak, R.K.Vishnoi, N.E.Joshi, S.A.Hasbi and C.J.Jones, "Abrasion and erosion resistant concrete with silica fume ". *International Conference on Accelerated construction of Hydro Power Projects, 15–17 October, 2003, Gedu, Bhutan.*

[3] Jean-Louis Cabiron, Sylvain Lavigne, "Research on the use of Alag Concrete for Hydraulic Abrasion and Cavitation Protection in Dam structures", *International symposium on Rehabilitation of Dams organized by INCOLD (4–6th November, 1998), New Delhi*

[4] ACI 210 (1998): "Erosion of concrete in Hydraulic Structures", *American Concrete Institute (ACI), Report no. ACI 210-IR-93.*

This page intentionally left blank.

New Developments in Dam Engineering—Wieland, Ren & Tan (eds),
© 2004 Taylor & Francis Group, London, ISBN 04 1536 240 7

Eeperimental study and design aspects of morning-glory spillways

M.Leopardi
University of L'Aquila, Italy

ABSTRACT: The tested models reproduce some small-scale morning-glory spillways of artificial reservoirs realized in the last few years. Every experimental apparatus shows differences both in the design criteria which govern the crest and the meridian profile of the spillways, and in the geometrical characteristics of the shaft and the transitional vertical curve between the former and the outlet tunnel. The difference between the spillway crest elevation and the bank level which defines real operating terms moving away from the results of ideal conditions experiments, have been finally considered.

1 INTRODUCTION

Morning-glory spillways, whose first realisation dates in 1896 and 1908 in England, are generally made up of a circular horizontal crest that carries on to the bottom as far as the throat, with a progressive decreasing diameter, whereas the throat is called shaft and is the starting section of a vertical part, generally working with a constant diameter. The shaft is followed by a curved part, the elbow, with the axis in the vertical plane and an angular diversion of about 90°. The elbow, whose section is progressively decreasing or uniform with a sharp reduction at the end, terminates at the control section, the area of which is smaller than the flow section area of the outlet tunnel.

By the vertical generators of the spillway profile, we have arranged some anti-vortex devices, overhanging the crest and jointing the shaft at the bottom, in order to avoid the reduction of the discharging capacity, produced by both rotating components and non-uniform stream getting to the spillway, caused by both unevenness of the ground and location of the discharge.

In Figure 1 there is an outline of the main symbols concerning the terminology of morningglory spillways, whose first realization dates in 1896 and 1908, in England.

2 OPERATING TERMS

Through the study of a large technical literature on the subject *(Gourley [1911], Wagner [1914], Creager [1923], Scimemi [1930–1937–1946] Camp e Howe [1939], Gardel [1949], Lazzari [1954–1959], Marchi Rubatta [1959], Rubatta [1962], Arredi [1988]* depending on the water level makes it possible to distinguish two types of working widely observed both in physicalmodel experiments, and in prototype situations (e.g.):

1. *Freeflow* (Figure 2): the rate of flow is a function of the hydraulic load on the spillway crest; the nappe, after getting over the crest, goes down along the shaft, while adhering to the wall and leaving the shaft aerated. At the bottom, in different depths varying according to the flow, the nappe closes at the centre while making a "fungus". The estimated relation of the spillway flow is:

$$Q = \mu \cdot 2\pi \cdot Rh \cdot \sqrt{2gh} \tag{1}$$

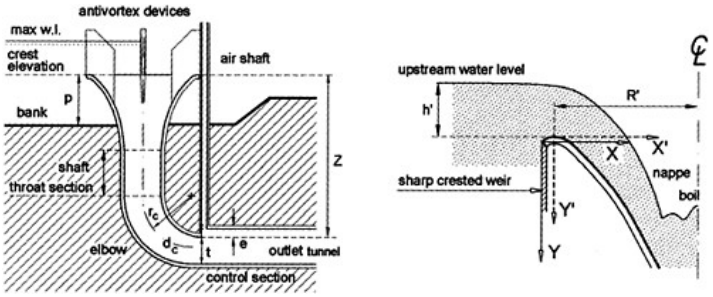

Figure 1. Characteristics of a morning glory spillway.

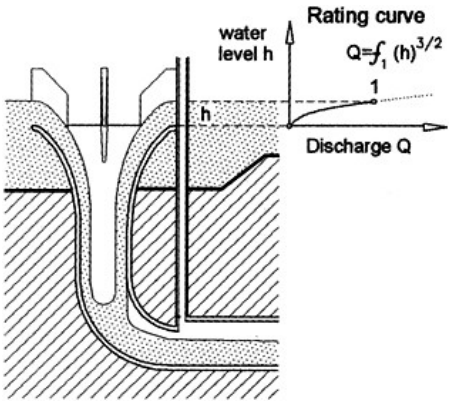

Figure 2. Free overfall over the spillway crest.

where μ is equal to the discharge coefficient, depending on geometrical characteristics of the crest and on h. The flow is not conditioned by shapes and sizes of the morning-glory at the end of the crest.

2. *Saturated flow* (Figure 3) concomitant with the *pressure operation* of both all shaft pipe and the curve situated on the base, as far as the control section which is placed on the starting section of the outlet tunnel, connected with which the discharge can be expressed as:

$$Q = C_m \omega \sqrt{2g(h+Z)} \tag{2}$$

where C_m is equal to the experimentally definable discharge coefficient. On the basis of model tests, Gardel suggested the following equation:

$$Q = \omega \sqrt{2g\eta(H+h-0{,}5t-\Delta)} \tag{3}$$

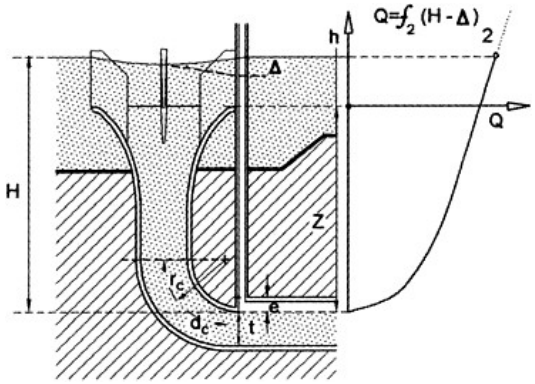

Figure 3. Submerged shaft spillway.

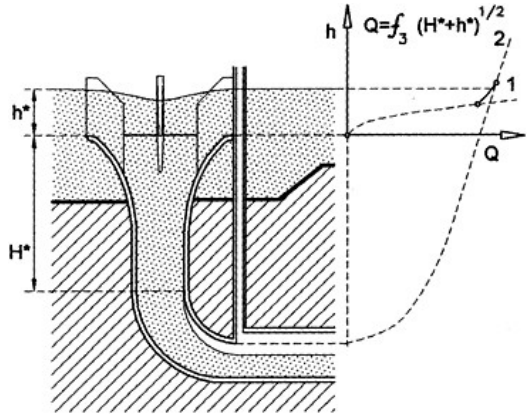

Figure 4. Transition between condition 1 and 2

where η is the *efficiency coefficient,* $\eta = 0{,}133 \cdot \left(4 + \frac{r_c}{d_c}\right)$ with validity limits:

$$1 < \frac{r_c}{d_c} < 2 \qquad 0{,}18 < \frac{e}{d_c} < 0{,}5$$

with Δ, as the friction loss along the shaft, estimated by ordinary formulas of permanent turbulent motion.

The converging solution of (1) and (3) is called *"engulfing point"*

Transition from an operating condition to the other is not sudden, since there is an intermediate operation, called *engulfed flow operation* or orifice control operation, with concomitant occlusion of the shaft pipe upper zones and no total engagement of the terminal control section ω. Sewage flow grows according to the difference between the reservoir free surface level and the throat section shaft level and is conditioned by shapes and sizes of the spillway single components.

Hydraulic model tests, carried out on models geometrically similar to different spillways, made it possible to point out the parameters marking the transition regime between condition 1 and 2 in the rating curve (Figure 4).

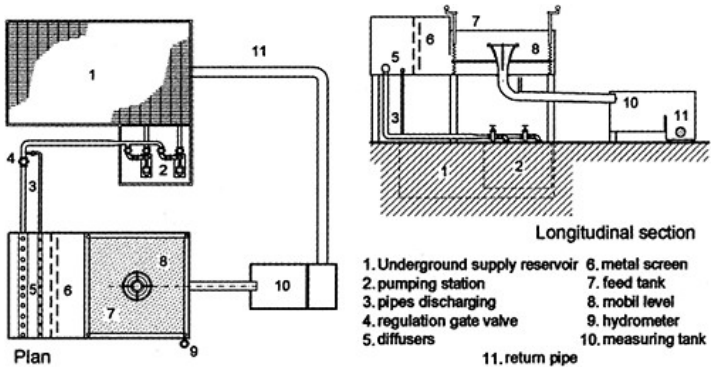

Figure 5. Experimental installation.

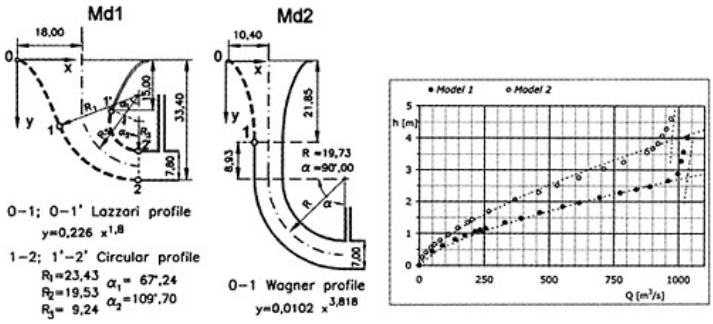

Figure 6. Models 1 and 2.

3 EXPERIMENTAL INSTALLATION, GEOMETRICAL CHARACTERISTICS OF THE SPILLWAYS AND OBTAINED RATING CURVES

The main characteristics of experimental installation are schematically represented in Figure 5.

Five models of morning-glory spillways have been submitted to hydraulic tests. The following outline is a short description of each tested model and its pertinent variants, together with its geometrical characteristics, its theoretical and its experimental data discharge curves (Figures 6–9).

Data are shown in real terms, in order to allow a quicker interpretation.

Model 1: The spillway crest of the manufacture is geometrically defined in conformity with Lazzari's directions. Some circular bends with appropriate radius join the profile to the outlet tunnel. In this case both the cylindrical shaft, and the control section are absent while the antivortex device corresponds to only one *fin,* whose orientation depends on the longitudinal axis of the outlet tunnel.

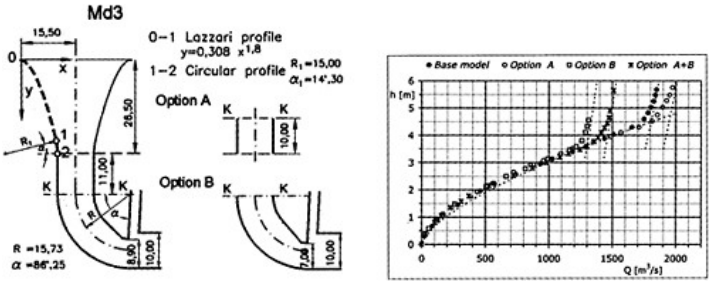

Figure 7. Model 3.

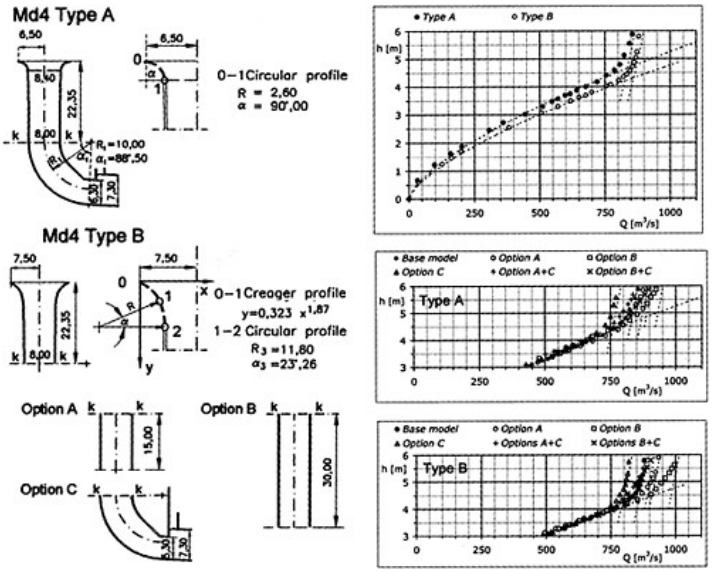

Figure 8. Models 4 Type A and 4 Type B.

Model 2: The meridian profile follows Wagner's directions. As everybody knows, although these profiles give the advantage of increasing the discharge coefficient with consequent considerable discharge increase (a 10% depression tallies with a discharge increase of about 2%, a 30% depression corresponds with an increase of about 8%), they also produce some depressions causing small traction stresses, well absorbed by the structure (a 30% depression on a load of 3m provokes a traction stress of ≅10kPa).

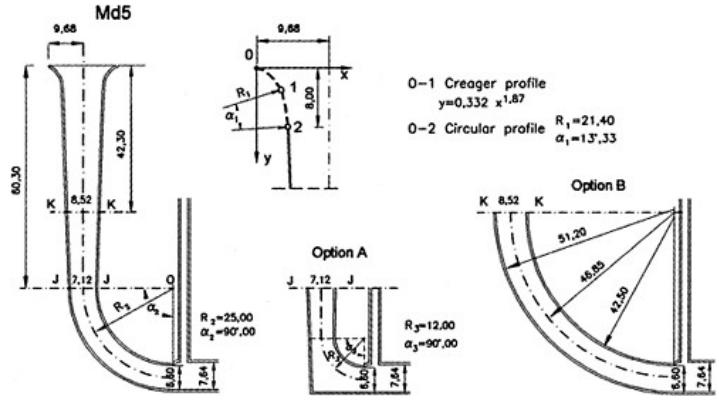

Figure 9a. Geometrical characteristics of Models 5.

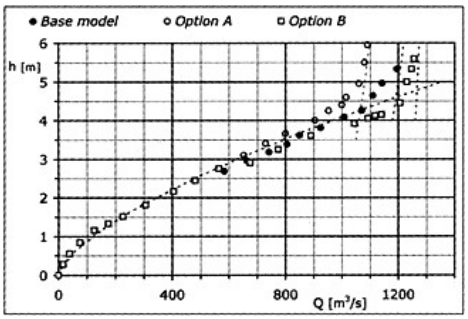

Figure 9b. Theoretical and its experimental data discharge curves of Models 5.

Model 3: the whole funnel is sized according to Lazzari's directions; the shaft is located between the funnel and the elbow. Two significant variants have been included in this model:

– the doubling of the shaft pipe length;
– a 15% reduction of the control section area, compared to that of the basic model, and a 33% reduction, compared to that of the outlet tunnel.

Model 4: the model has been realized with a double layout of the spillway crest. Whilst type A plans a simple circular connection between the spillway crest and the shaft throat, type B links up with the shaft by a first part according to a Creager profile, followed by a circular curve, besides having the radius 1m longer.

In both models, we have introduced some variants increasing the shaft length of about 1,75 and 2,5 times the basic model and reducing the control section area to about 13%, compared to that of the basic model, and to about 24%, compared to that of the outlet tunnel.

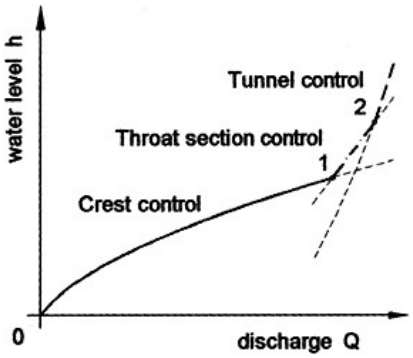

Figure 10.

Model 5: The basic layout consists of a very long shaft joining to the spillway crest, first by a curvilinear part with a circular radius and then by a Creager profile. The layout shows a constant reduction of the spillway section, ending downstream on the elbow tangent which gets into the outlet tunnel together with the control section. Two further elbow layouts have been tested using this model: the first one is characterised by a reduction of the elbow radius of curvature and by a peculiar geometry, adopted in the overflow spillway plan of Pontesei's dam, in the drainage area of the river Piave.

The second variant plans a considerable increase of the elbow radius of curvature with consequent decrease of both shaft elevation and tunnel length.

4 FIRST OBSERVATIONS

Operation working between free flow and saturated flow (Figure 10) mainly depends on:

- the marked presence of the shaft vertical part (option A, for model 3, option B, for model 4a and 4b);
- the ratio of shaft diameter to morning-glory diameter (the width increases in relation to the ratio reduction);
- the ratio of control section area, situated in the shaft-tunnel transition point, to shaft area (the width increases in relation to the ratio increase).

Tests on model 5 point out that option B showed a wide field of working in engulfed regime, in the presence of a very high shaft (about 110m), whose reducer part is characterised by the values of 0,56–0.44 of the ratio dc/2R, and by the value of 0,85 of control section area to shaft area and to an elbow area with the high ratio rc/dc.

5 INFLUENCE OF SURROUNDING TOPOGRAPHIC LAYOUT

In the free flow field, further surveys concerned the influence of the morning-glory surrounding topographic layout on the discharge coefficient values. At the design stage, real operating terms moving away from the results of ideal conditions experiments come about when the foreseen hypotheses and conditions concerning the surrounding do not happen.

As for model 3, we have hypothesized and realized 5 different layouts of the ground. The first one plans a 30° inclined plane with the morning-glory coming to the surface, downstream, at a level equal to the diameter (Figure 11).

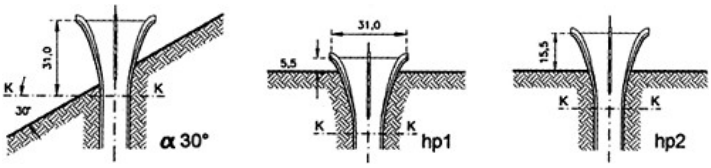

Figure 11.

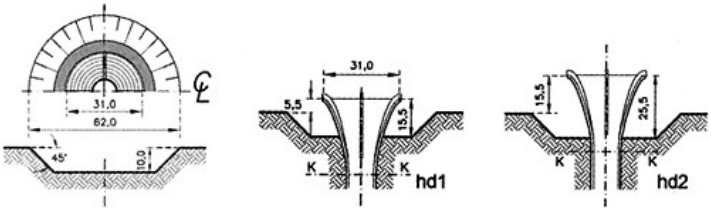

Figure 12.

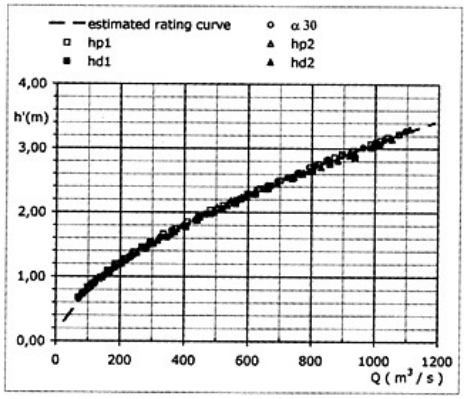

Figure 13.

The second one, hp1, and the third one, hp2, plan an extra storey on a horizontal plane, respectively a fourth and a half of the morning-glory diameter (Figure 12).

In the end, the last two layouts, hd1 and hd2, vary compared to the foregoing ones because of the realisation of a circular-shaped depressed area, 10m depth in comparison with the datum plane, whose diameter is twice the morning-glory diameter (Figure 13).

Figures 13 and 14 graphically facsimile the rating curve, with the heads h′ referring to the crest elevation and the correlated discharge coefficient values μ′ calculated as follows

$$\mu' = \frac{Q}{2\pi R' \cdot \sqrt{2g} \cdot h'^{1,5}}$$

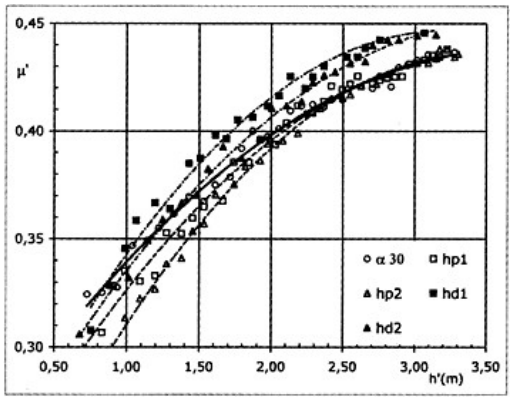

Figure 14.

6 SECONDS OBSERVATIONS

Through the distinct comparison of the diagrams and correlated conditions surrounding the first three conditions and the remaining two, we can see that the acquired data with values of h′ in proximity to the plan ones do not stress a discharge coefficient variation depending on the inclination. On the contrary, in the transition between the hp and the hd condition, an increase of the discharge coefficient in relation to the variation of the dock geometry is obvious.

In the design discharge, both of them coincide with two only discharge coefficient values μ moving away from each other of about 1,6%. At a parity of load h′ on the crest, all this means a slight discharge increase Q that, according to the different conditions, takes the following values:

$$\frac{Q_{hd1}}{Q_{hp1}} = 1{,}028 \qquad \frac{Q_{hd2}}{Q_{hp2}} = 1{,}049$$

As far as the influence of anti-vortex devices on flow conditions is concerned, all the surveys did not point out any considerable alteration of the function μ′=μ′(h′). It must be noticed that all the surveys have been carried out in the presence of four and two devices, and have been compared to the solution deprived of these components.

7 NOTATIONS

Q	design discharge
C_m	discharge coefficient
h'	overfall head
R'	radius of the circular shaft spillway crest
r_c	radius of curvature of the axis of the bend in the vertical section
d_c	diameter of the shaft
Δ	friction loss along the shaft
ω	terminal control section
μ	discharge coefficient
μ'	discharge coefficient referring to the crest elevation
η	efficiency coefficient

REFERENCES

Allen J., *Scale Models in Hydraulic Engineering,* Green & Co, 1947.

Arredi F., Note di caratterizzazione degli sfioratori a calice in rapporto alla loro funzione, *Idrotecnica,* 1988, 291–304.

Bovolin V., Marone V., Sul proporzionamento degli scaricatori di superficie a calice prossimi alla saturazione, *Idrotecnica,* 1992, 31–43.

Bovolin V., Marone V., Influenza delle dimensioni delle luci di scarico sui sovralzi massimi nei serbatoi artificiali, *Idrotecnica,* 1992, 145–149.

Camp C.S., Howel J.W., Tests of circular weirs, *Civil Engineering,* Vol. 9 n. 4, 1939.

Creager W.P., Justin J.D., Hinds J., *Engineering for Dams,* John Wiley & Sons, 1945.

Gardel A., Les évacuateurs de crues en déversoirs circulaire, *Bulletin Tecnique de la Suisse Romande,* 1949, 341–349.

Langhaar H.L., *Dimensional Analysis and Theory of Models,* Krieger Publishing Company, Huntington, 1980.

Lazzari E., Ricerca sperimentale sullo sfioratore a pianta circolare, *L'Energia Elettrica,* 1954, 838–849.

Lazzari E., Ricerca sperimentale sugli sfioratori a calice, *L'Energia Elettrica,* 1959, 641–651.

Leopardi M., Remedia G., Indagine sperimentale sul coefficiente di efflusso di sfioratori a calice. *Scritti in onore di Girolamo Ippolito,* Associazione Idrotecnica Italiana, 1991, 207–222.

Leopardi M., Limite di saturazione degli sfioratori a calice, *Idrotecnica,* 1995, 273–291.

Leopardi M., Morfometria delle darsene e coefficienti di efflusso di sfioratori a calice, *Scritti in onore di Mario Ippolito,* Associazione Idrotecnica Italiana, 1995, 441–452.

Marchi E., Rubatta A., Ricerca sperimentale sugli sfioratori a calice, *Atti VI Convegno di Idraulica e Costruzioni Idrauliche,* 1959.

Peterka A.J., Morning-glory shaft spillways: performance tests on prototype and model, *Trans. A.S.C.E.,* Vol. 121, 1956.

Rubatta A., Gli sfioratori a calice. Conclusioni di una ricerca sperimentale, *L'Energia Elettrica,* 1962, 109–119.

Viparelli R., Proporzionamento di un imbocco a calice. *Atti XXII Convegno di Costruzioni Idrauliche,* 1990.

Wagner W.E., Morning-glory shaft spillways determination of pressure-controlled profiles, *A.S.C.E. Proceedings* vol. 80, 1954.

Wagner W.E., Morning-glory shaft spillways determination of pressure-controlled profiles, *A.S.C.E. Trans,* vol. 121, 1956.

New Developments in Dam Engineering—Wieland, Ren & Tan (eds),
© 2004 Taylor & Francis Group, London, ISBN 04 1536 240 7

Numerical simulation of quality inspection on concrete diaphragm wall

Li Bin, Song Haiting & Pan Shu
Yellow River Institute of Hydraulic Research, YRCC, China

ABSTRACT: With more and more application of concrete diaphragm wall in projects, its quality has received much attention. However, nondestructive inspection technique for the concrete diaphragm walls has left a blank in the world currently. Both concrete pile and diaphragm wall are the structures in soil foundations and can be simplified as a dimensional pole and 2-dimensional plate respectively. But the nondestructive inspection on a concrete pile as a dimensional pole has become relatively mature at present, that is to make use of reflection and transmission laws of stress wave to analyze quality characteristics of the pile body. Therefore, an assumption can be made to popularize the stress wave theory in the inspection of 2-dimensional plates. This paper, based on the assumption, simulates the transmission law of stress wave in medium by means of finite element method so as to predict the problems that may occur in actual inspection. To simulate the transmission law of stress wave has been carried out by applying different exciting forces on supposed pile and plate. By doing so, the law of interfaces such as plate bottom that produces influence on the wave has been found out and the layout pattern of exciting forces and sensors for diaphragm walls inspection has been worked out preliminarily, which has offered the theoretic basis for the implementation of nondestructive inspection.

1 PREFACE

With more and more application of concrete diaphragm wall in projects, its quality has received much attention. However, nondestructive inspection technique for the concrete diaphragm walls has left a blank in the world currently. The concrete pile and concrete diaphragm wall are both concrete structure in the soil foundation and they can be simplified as one-dimensional pile and two-dimensional plate. The technique of nondestructive inspection concrete diaphragm pile called as one-dimensional pole is relatively mature at present, i.e. it is available to analyze the pile's quality character with using the reflecting and transmitting laws of the stress wave transmission. Therefore, it may be possible to extensively apply such stress wave theory into the two-dimensional plate inspection. Upon such idea, this article hereof tries to forecast the problems which are possibly occurred in the actual inspection process with adopting the method of finite element to imitate the transmitting law of the stress wave in medium.

2 NUMERICAL SIMULATION METHOD

As to the structure effected by exciting forces, the outside force and displacement are both time's function. In the case of existing damp, the force equation of such structure is as follows:

$$[M]\{\ddot{\delta}\}+[C]\{\dot{\delta}\}+[K]\{\delta\}=\{F(t)\} \tag{1}$$

In the equation: [M] is integral mass matrix, consisting of each unit mass matrix;
[K] is integral rigid matrix, consisting of each unit rigid matrix;
[C] is integral damp matrix, generally taking Rayleigh damp,
i.e.: $[C]=\alpha [M]+\beta [K]$
$\{F(t)\}$ is force loading column array at node;
$\{\delta\}$, $\{\ddot{\delta}\}$ is the column array of the displacement, velocity and acceleration of node to rocky base.
In the damp matrix expression, α and β are damp coefficient, they can be gained from structural basic frequency ω: $\alpha=D\omega$, $\beta=D/\omega$
D is each unit's damp ratio.
Load column array $\{F(t)\}$ is varied upon time going, if giving a periodically intensive vibrating force onto No. i node: $Fi=FCos(t)$
Bring it into (1), to solve such equation, may gain the value of displacement, velocity and acceleration of each node at each time. Wilson—θ can be used as solving method.

3 THE NUMERICAL SIMULATION FOR PILE INSPECTION

In order to check the correctness of abovementioned numerical simulation method, we conduct a numerical simulation to the pile inspection, the technique of which is relatively mature at present. In order to calculate easily, when calculating the simulation, we adopt a kind of rock inserting pile, the bottom of which is fixed in the rock. The parameter of the pile body is: 20m in length, $\phi 400$ in diameter and concrete mark is C25.

Giving a exciting force onto the top of a pile:

$$F=\begin{cases}\dfrac{200}{0.7}t & (0<t<0.7\ \text{ms})\\ \dfrac{200}{0.7}(1.4-t) & (0.7<t<1.4\ \text{ms})\\ 0 & (t>1.4\ \text{ms})\end{cases} \tag{2}$$

Upon the transmitting theory of stress wave in the one-dimensional pole, the obtained theory curve on the reflection of the velocity vs time on the top of pile after the exciting force is transmitted in the pile body is shown in fig. 3-1.

The aim of finite element simulation is at producing the abovementioned reflecting process through calculation.

Giving a exciting force shown in the Expression (2) onto a certain node of a pile's top end, then to solve Expression (1), one can gain the curve reflecting velocity vs time on the node of the pile's top end. The fig. 3-2 show the curve of velocity vs time on the node of the pile top end under the case of different structure damp ratios ($\Delta t=50\mu s$).

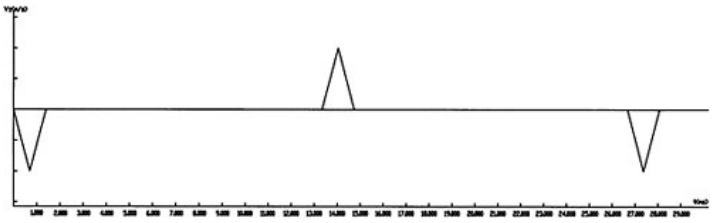

Figure 3-1. The theory curve reflecting velocity vs time on the top of pile effected by the exciting force.

It can be seen in the figure that besides the curve may be distorted by the force effect at the time when the exciting force acts, the general law of velocity variety of the pile's top end at other time is coincident with the theory curve, the reflection at pile bottom is visible. In case damp is less, there is more high frequency wave and in case damp is more, the high frequency wave may be filtered, but the reflection in the pile bottom end is also relatively lessened. Generally, the finite element numerical simulation may basically reflect the effect of the pile body's border.

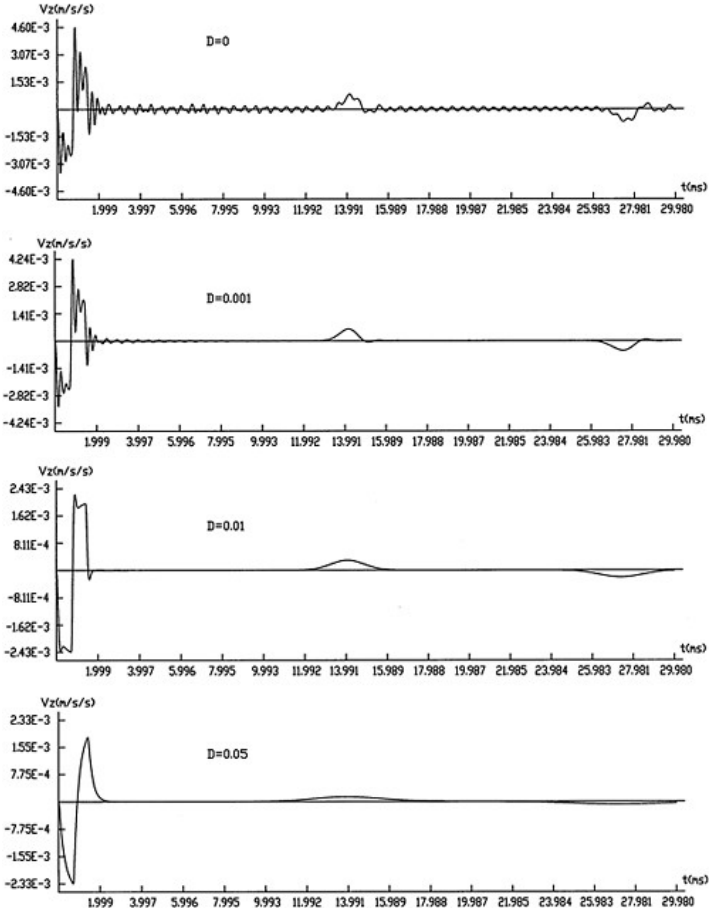

Figure 3–2. The curve of velocity vs time on the node of the pile top end in the case of different structure damp ratios.

4 THE NUMERICAL SIMULATION OF INSPECTION PLATE WITH FORCING ONCE AND RECEIVING MORE TIMES

Supposing taking a bottom-fixed plate, parameter of which is 20m in depth, 20cm in thick and 100m in width, as sample, if providing a exciting force F (same as that in Expression (2)) onto the top of the sampled plate's middle part and then conducting an simulation of transmitting such exciting force in the plate with the finite element method.

When damp ratio is D=0.005, the curve of velocity vs time on each node of the plate top is seen in fig. 4-1~fig. 4-3.

It can be informed by the curve in the figure that the time when the first wave arrives onto each node keeps a direct ratio to the distance between such node and the exciting force node and the vibrating direction of the first wave keeps inverse to the initiative one of the forced node, it seems relating to the surface wave. In about 13ms at each node, there appears a velocity reflecting peak

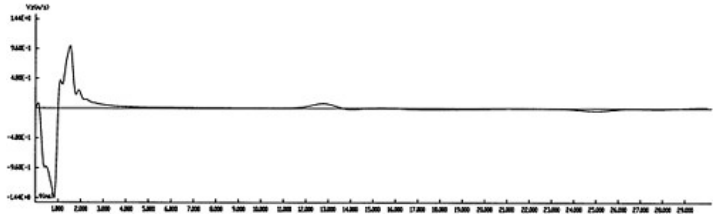

Figure 4-1. The curve of velocity vs time on the node of the plate top face's center.

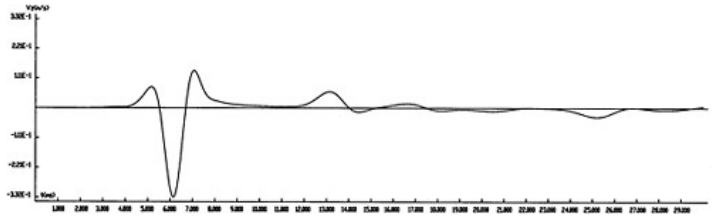

Figure 4-2. The curve of velocity vs time on the node 10m far from the plate top face's center.

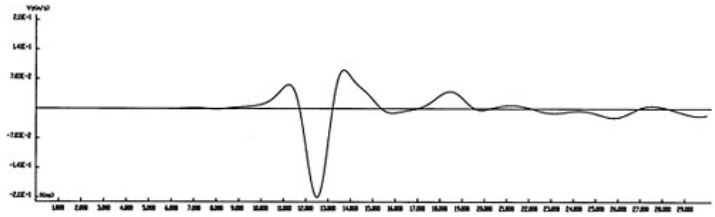

Figure 4–3. The curve of velocity vs time on the node 20m far from the plate top face's center.

brought by the effect of plate bottom's border. The time of peak value point is respectively: 12.8ms, 13.05ms and 13.25ms, the velocity value is respectively: 0.076m/s, 0.060m/s and 0.088 m/s.

5 THE NUMERICAL SIMULATION OF INSPECTION PLATE WITH FORCING MORE POSITIONS AND RECEIVING ONCE

It can see from above that as being effected by damp, the velocity reflecting peak occurred by the effect of the plate bottom's border is very weak and is easy to be covered by other sundry waves. Therefore, it is necessary to solve the problem on the energy for reflecting stress wave. For such case, it is possible to solve it with increasing the exciting force energy. There are two methods for increasing such energy, one is to increase the exciting force's amplitude and another is to increase the force's effecting extent. Increasing the exciting force's amplitude may possibly do partial damage to the concrete structure, so it is acceptable to increase the force's effecting extent for increasing the exciting energy. Such so called increasing exciting energy means taking same size and frequency forces to effect onto a definite extensive area so as to use the joint effect of each force to increase the reflecting energy.

Supposing to use a plate with the same condition as the abovementioned one, firstly providing a exciting force in different width F (same with that in Expression (2)) onto the top of plate's middle part, and then conducting an simulation of transmitting such exciting force in the plate with the finite element method.

When the width of the exciting force F is only 0.2m, the curve of velocity vs time on the node of the plate top face's center is shown as fig. 5–1. Whereby, such velocity reflection is as the same as that occurred by forcing once and receiving more times. A velocity reflecting peak may be brought by the effect of the plate bottom's border, its peak value point time is: 13.35ms and its velocity value is 0.077m/s.

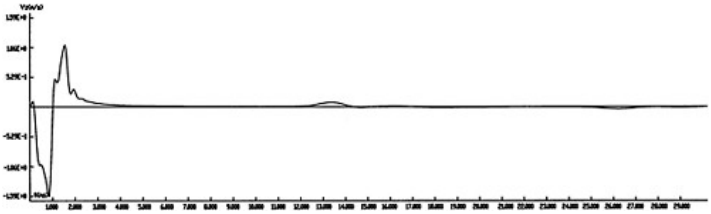

Figure 5–1. The curve of velocity vs time on the node of the plate top face's center when the width of the exciting force is only 0.2m.

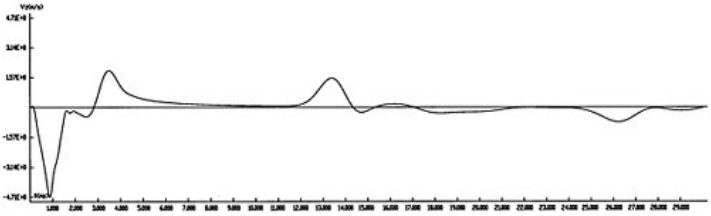

Figure 5–2. The curve of velocity vs time on the node of the plate top face's center when the width of the exciting force is only 4m.

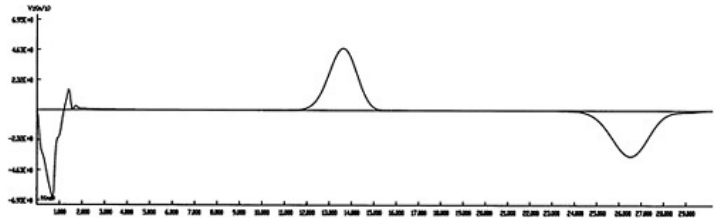

Figure 5–3. The curve of velocity vs time on the node of the plate top face's center when the width of exciting force is as wide as the whole area of plate top face.

When the width of the exciting force F is 4m, the curve of velocity vs time on the node of the plate top face's center is shown as fig. 5–2. As to the velocity reflecting peak brought by the effect of the plate bottom's border, its peak value point time is: 13.35ms and its velocity value is 1.52m/s.

When the width of exciting force F is as wide as the whole area of plate top face, the curve of velocity vs time on the node of the plate top face's center is shown as fig. 5–3. As to the velocity reflecting peak brought by the effect of the plate bottom's border, its peak value point time is: 13.65ms and its velocity value is 4.78m/s.

6 CONCLUSION

Viewing the transmitting law of the stress wave in the pile obtained from the finite element numerical simulation, it basically reflects the effect at the pile body's border, so it is feasible to apply the finite element method to imitate the transmitting law of the stress wave in a concrete structure.

Supposing taking a bottom-fixed plate, the parameter of which is 20m in depth, 20cm in thick and 100m in width, as sample, if providing a exciting force F onto the top face of the sampled plate's middle part, the time when the first wave arrives onto each node keeps a direct ratio to the distance between such node and the exciting force and the vibrating direction of the first wave keeps inverse to the initiative one of the forced node, it seems relating to the surface wave. In about 13ms at each node, there appears a velocity reflecting peak as the effect of plate bottom's border, and its peak value point time is respectively: 12.8ms, 13.05ms and 13.25ms.

As to a plate with the same condition as the abovementioned one, firstly providing a exciting force in different width onto the top face of plate's middle part, when the width of the exciting forces is only 0.2m, 4m and as wide as the whole area of plate top face, an velocity reflecting peak may occur by the effect of plate bottom's border, its peak value point time is about 13.35ms and its velocity value is respectively: 0.077m/s, 1.52m/s and 4.78m/s, the reflecting energy may increase with the increment of width of exciting force F.

According to the above conclusion, when conducting the concrete diaphragm wall inspection, it is absolutely available to apply the method of stress wave reflection. If finding the energy of reflecting wave deficient, it is applicable to reinforce the energy feedback with the inspection point arrangement of the numerical simulation of inspection plate with forcing more positions once and receiving once so as to achieve better inspection effect.

REFERENCES

[1] Wan Jingtao, "The Theory on Inspection the Stress Wave in Pile and Its Engineering Application", Earthquake Publishing House, 1998.
[2] Liu Jinli etc., "Technique for Inspection Pile Construction", China Construction Material Industry Publishing House, 1998.

New Developments in Dam Engineering—Wieland, Ren & Tan (eds),
© 2004 Taylor & Francis Group, London, ISBN 04 1536 240 7

Liquefaction analysis of the foundation of Erwangzhuang reservoir dam in Tianjin

Li Sa, Li Jingmei & Yang Jinliang
Geotechnical Engineering Institute of Civil Faculty, Tianjin University, China
Yu Ziming
Erwangzhaung Reservoir Administrative Office, China

ABSTRACT: The dam of Erwangzhang reservoir is the key engineering of proj ect leading water of Luan river into Tianjin. There are saturated silt and silty sand that can be liquefied within 15m depth in the foundation of the dam. In this paper, the liquefaction evaluation of silt and silty sand was made according to the results of tests indoors and in situ. At the same time, the FEM method was used to analyze the effect of seepage to the zone of the liquefaction.

1 INTRODUCTION

There are many earthquakes occurring in China, the accurate evaluation and forecast of the seismic behavior of the dam is promoted by the enormous destroy made by earthquakes, especially there are saturated silt and silty sand in the soil layer. Investigating the potential of liquefaction in high seismic areas has become commonplace in the pratice of geotechnical engineering. Standard penetration together with geological factors have permitted the assessment of liquefaction potential. At the same time, various types of laboratory tests such as dynamic triaxial test (Seed and Lee, 1966), cyclic simple shear test (Seed and Peacock, 1971) are used to do the same thing. A comprehensive literature review of the behavior of the silt and silty sand assessment under earthquake indicates tremendous efforts have been carried out for the assessment of liquefaction problems (Castro, 1976; Tokimatsu, 1986; Singh, 1994; Yoshimi, 1994, etc.).

In this paper, we present the approach for liquefaction potential by the different kinds of tests and FEM analysis. The standard penetration tests in-situ and dynamic triaxial tests indoor are done, the results of them are compared. According to the tests results, we make the dynamic FEM analysis calculating and not calculating the seepage.

2 BACKGROUND

Erwangzhang reservoir is the key project leading water of Luan river into Tianjin. It locates the Erwangzhuang village south of the Baodi country, Tianjin city. It was built in 1983 and is having been worked about 20 years until now.

The water collecting area of the reservoir is 11.03km^2, the total reservoir capacity is 4530× 10^{4}m^3, the useful storage is 3868×10^{4}m^3, the dead storage is 662×10^{4}m^3. The normal water level of the reservoir is 5.5m, the dead water level is 2.0m, and the average elevation of the bottom of the reservoir is 1.4m. The plan of the Erwangzhuang reservoir dam is shown in the figure 1.

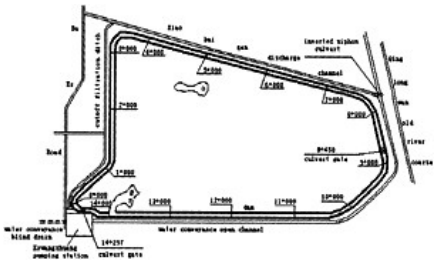

Figure 1. The plan of the dam.

3 SITE GEOLOGICAL SETTING

The site is located on the alluvial plain, and the topographical feature is flat. There is the manmade top layer above the in-situ soils. This top layer is comprised by clay. It is mixed with silty sand somewhere. This layer formed the dam.

The in-situ ground can be classified into the six soil layers. The first in-situ soil layer, 1, was the first continental deposit(alQ_4^3) of 2.00–5.00m thick. This layer can be furthered divided into two sub-layers according to their physical and mechanical properties. The upper sub-layer, 1-1, was a clay soil. Its distribution was continuous. Occasionally, silty clay could be found in this sub-layer. The second sub-layer, 1–2, was a silty clay soil. It distributed near 0+250–3+650,4+500–6+500,9+150–9+700, 10+400–11+300, 11+700–12+200, 13+150–14+000 (see figure 1).

The second in-situ soil layer, 2, was the first marine deposit(mQ_4^2) of 5.50–10.50m thick, and can be furthered divided into three sub-layers. The upper sub-layer, 2-1, was a silty sand soil. Occasionally, it mixed with the thin clay and silty clay seam. It distributed near 0+200–5+250, 7+500–8+950, 9+150–9+650, 11+200–14+000. The middle sub-layer, 2-2, was silt. The thin silty sand, clay seam and shells could be found occasionally in this sub-layer. It distributed near 2+200–2+850, 4+500–7+800, 8+600–8+950, 10+400–13+150. The bottom sub-layer, 2-3, was clay or silty clay. It appeared as lens and distributed near 2+850–3+700, 6+500–8+600, 8+950–10+400, 12+150–2+200.

The third in-situ soil layer, 3, was the second continental deposit(alQ_4^1) of 4.50–9.50m thick. It can also be furthered divided into three sub-layers. The upper sub-layer, 3-1, was clay or silty clay. It occasionally mixed with thin silty sand or silt seam. It distributed near 13+150–2+850, 3+700–5+250, 9+650–12+150. The middle sub-layer, 3-2, was silty sand. It occasionally mixed with thin clay or silty clay seam. It distributed near 2+850–3+650, 6+500–9+650, 12+100–14+000. The bottom sub-layer, 3-3, was silt. It mixed with thin silty sand seam. It distributed near 2+200–2+850,4+500–6+500,9+650–10+400, 11+200–11+700, 12+150–13+100.

The fourth in-situ soil layer, 4, was the third continental deposit(mQ_3^4) It mainly comprised by clay or silty clay.

Table 1 summaries the representative values for the soil shear strength from the laboratory tests that were carried out on the soil samples obtained in the boreholes. In addition, Table 1 also lists the soil compressibility and the coefficient of permeability.

4 ASSESSMENT OF LIQUEFACTION POTENTIAL BY TESTS

In order to make discrimination of liquefaction of the site soil, standard penetration test in-situ and dynamic triaxial test indoor were done. We chose the bore hole 11+800 to show the results of tests. Figure 2 shows the blow count in standard penetration test.

Table 1. The soil shear strength values.

Soil layer		Direct shear test QDST		Triaxial test CD		α_{1-2}(1/MPa)	Permeability coefficient $K_v \times 10^{-6}$ (cm/s)
		φ°	c (kPa)	φ ‘°	c ‘(kPa)		
Surface layer		16	36	18	30	0.30	400
First layer	1–1	11	14	22	30	0.49	307.3
	1–2	6	19	23	26	0.33	40.0
Second layer	2–1	28	14	36	8	0.1	3098.2
	2–2	33	6	36	8	0.2	1624.3
	2–3	9	21	23	26	0.43	9.24
Third layer	3–1	10	20	25	29	0.35	30.1
	3–2	19	4	37	10	0.26	4149.0
	3–3	10	22	22	30	0.12	387.4

Note: α_{1-2}=soil compressibility.

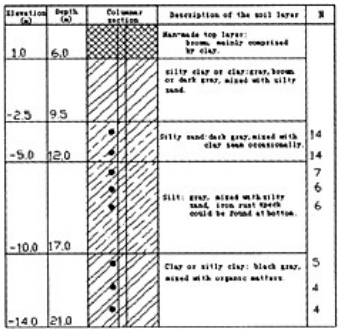

Figure 2. The blow count in standard penetration test.

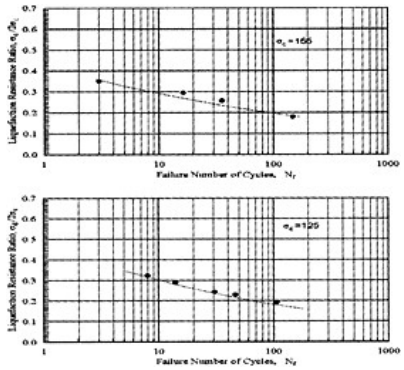

Figure 3. The curve of liquefaction defense shear stress.

According to the 》(GB 50287–99), the assessment of liquefaction potential is shown in table 2. It can be seen that according to the results of standard penetration test, the silty sand layer (9.5m~12m) will not be liquefied under 7.5 earthquake intensity, but the silt layer (12m~15m) will be liquefied.

At the same time, the soil sample at depth 10m~12m and 12m~14m in this borehole were fetched and the dynamic triaxial tests were done. The results of the tests are shown in the figure 3.

The assessment of liquefaction potential is shown in the table 3. The tests results show that the silty sand and silt layer are all liquefied under 7.5 earthquake intensity.

The different tests draw the different conclusion. The reason should be that the soil samples were disturbed when they were fetched from the soil mass. So the strap of liquefaction determined by the dynamic triaxial tests is larger than that by standard penetration test.

5 FEMANALYSIS

In order to make clear the location of the liquefaction zone, the FEM is used to do the dynamic analysis. The analysis is divided into two steps. The first step is the initial static analysis. The linear-elastic model is used. The second step is the dynamic analysis. The equivalent-linear model is choice.

Table 2. The assessment of liquefaction potential by the blow count in standard penetration test.

Depth (m)	Blow count N	Critical blow count N_{cr}	Assessment	Liquefaction index I_{IE}	Class of liquefaction
10	14	7.2	Not liquefaction	– –	
11	14	7.7	Not liquefaction		
13	7	8.8	Liquefaction		
14	6	9.4	Liquefaction		
15	6	10	Liquefaction	6.57	Moderate liquefaction

Table 3. The assessment of liquefaction potential by the dynamic triaxial test.

Depth (m)	Equivalent seismic shear stress τ_c(kpa)	Equivalent number of cycles $\bar{N}$	Liquefaction defense shear stress τ_d(kPa)	Assessment
12~14	22.8	20	21.3	Liquefaction
10–12	19.5	20	17.9	Liquefaction

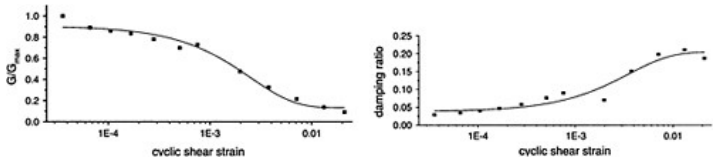

Figure 4. G/G_{max} and damping ratio changing with shear strain of the silty sand.

The procedure for the FEM analysis involves use of the shear modulus and damping ratio of soil layers. As the magnitude of shear strain increases, the value of shear modulus G of a soil decreases, and the damping ratio increases. The dynamic trixial tests were done to determine these relationships of the silty sand, silt and clay. The results are shown as in figures 4, 5, 6. In equivalent linear analysis, the shear modulus G and damping ratio is computed from the cyclic shear strain obtained in the dynamic analysis. Then a new dynamic analysis starts with the new G and damping ratio. This iterative process repeats until changes in displacements within two successive iterations are small.

Excess pore water pressure builds up under earthquake condition. In the FEM analysis, the level of excess pore water pressure is calculated based on the equation as follow:

$$\frac{u_{excess}}{\sigma'_{3c}} = \frac{1}{2} + \frac{1}{\pi}\arcsin\left(2\left(\frac{N}{N_L}\right)^{\frac{1}{\alpha}} - 1\right)$$

where, α—constant, α=0.7; N_L—stress cycles required to produce liquefaction; N—stress cycles.

During the FEM analysis, it is necessary to define the boundary conditions. In this analysis, we allow the left and right vertical boundaries to move freely in the horizontal direction. The boundaries

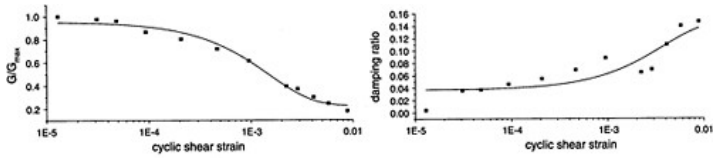

Figure 5. G/G_{max} and damping ratio changing with shear strain of the silt.

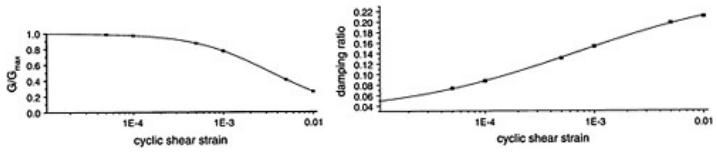

Figure 6. G/G_{max} and damping ratio changing with shear strain of the clay.

Table 4. The parameters using in the finite element analysis.

Soil type	Compression modulus (kPa)	Poisson's ration	G_{max}(kPa)	Damping ratio	Unit weight (kN/m^3)
Man-made soil	5600	0.3	8084	0.04	19.92
Clay	5370	0.4	5099	0.05	18.25
Silt	10225	0.4	45546	0.04	19.35
Sand	13260	0.4	48395	0.04	20.35
Silty clay	5250	0.4	21692	0.04	19.78

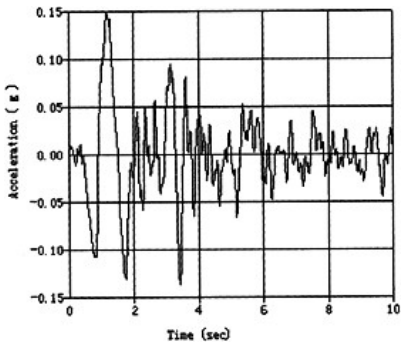

Figure 7. The earthquake wave.

at the bottom cannot move in two directions. The indexes used to do FEM analysis are shown in the table 4 and the earthquake record used is the aftershock wave of Tangshan earthquake. The maximum horizontal acceleration is 0.15g which is equivalent 7.5 earthquake intensity. The earthquake wave is shown in the figure 7. The soil layers of section 11+800 is shown in the figure 8.

In the analysis, first we do not consider the effect of the seepage, it is said that the initial water pore pressure is the static water pressure. By the dynamic analysis, the liquefaction zone can be obtained. It is shown in the figure 9. It can be seen that the liquefaction zone appears mainly under the dam. At the same time, small liquefaction zone can be found near the water conveyance open channel. The liquefaction zone is all in the slity sand layer and silt layer. This result is the same as the results obtained by the dynamic triaxial tests discussed above.

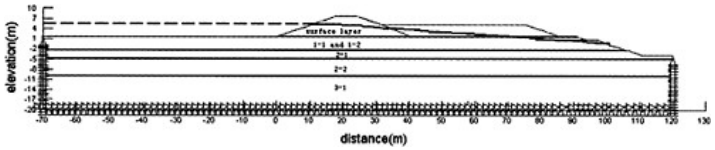

Figure 8. The soil layers of section 11+800.

Figure 9. The liquefaction zone not calculating seepage of the section 11+800.

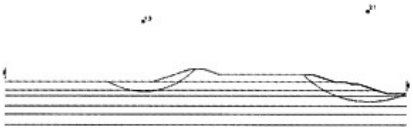

Figure 10. The safety factor of the upstream slope and the downstream slope.

Figure 11. The velocity vector of section 11+800.

Figure 12. The total head contour of the section 11+800.

Figure 13. The liquefaction zone calculating the seepage of the section 11+800.

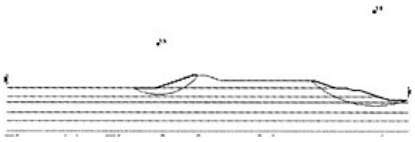

Figure 14. The safety factor of the upstream slope and downstream slope.

Furthermore, the safety factor of the upstream slope and the downstream slope are calculated by pseudostatic method. In the pseudostatic analysis, the horizontal seismic coefficient is 0.15. The shear strength is calculated by the static effective friction angle and cohesion. The pore water pressure is determined by the results of dynamic finite element analysis. It is said that we find the element that exists at the center of the slice base, then finds the corresponding local coordinates of the center of the slice base, and the matrix of the interpolation functions. Finally, computes the pore-water pressure at this location based on the nodal total head at the element nodes. By this method, the safety factor of the upstream slope and downstream slope and the location of the slip circle are shown in the figure 10.

Then, we do dynamic FEM analysis calculating the seepage through the soil mass. This has the advantage of computing more realistic effective stress in areas where there is some vertical flow. The downward seepage has the effect of increasing the effective stress. In the case of upward flow, it decreases the effective stress below the hydrostatic case. The velocity vector caused by the seepage is shown in the figure 11 and the total head contour is shown in the figure 12.

The liquefaction zone calculating the seepage is shown in the figurelS. Comparing with two cases, it could be found that the liquefaction zone changes small. If the seepage is considered, the liquefaction zone near the upstream decreases, and the liquefaction zone in the silt layer increases.

Also, the safety factor is calculated by the same method. The results are shown in the figure 14. The results show that if the seepage is considered, the safety factor of the upstream slope increases and the safety factor of the downstream slope decreases.

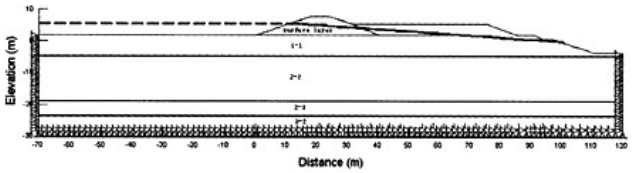

Figure 15. The mesh of the finite element of the section 9+350.

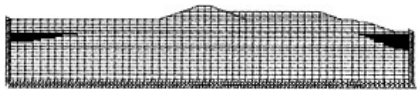

Figure 16. The liquefaction zone not calculating the seepage of the section 9+350.

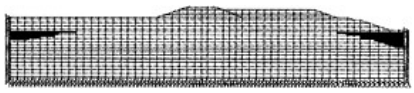

Figure 17. The liquefaction zone calculating the seepage of the section 9+350.

We do dynamic analysis by FEM for other sections. It is found that if the distribution of the soil layers changed, the location of the liquefaction zone changed. The figure 15 shows the section 9+350. The liquefaction zone of section 9+350 effecting or not effecting by the seepage are shown in the figures 16 and 17. It can be seen though the location of the liquefaction zone changed, the change of the scale of the liquefaction zone effecting by the seepage is small.

6 CONCLUSION

In the above, we have assessed the liquefaction potential by the tests indoor and in-situ. At the same time, we do the dynamic analysis by FEM. The safety factors are obtained by the effective stress analysis.

We have found that the liquefaction potential assessed by dynamic triaxial tests is more dangerous than that by the standard penetrate test. The reason should be that the soil samples were disturbed by the tests indoor. The results of the dynamic finite analysis are the same as that by the indoor tests.

The location of the liquefaction zone effected by the distribution of the soil layers, and the change of the liquefaction zone effected by the seepage is small. For section 11+800, the safety factor of the upstream slope change from 1.3 to 1.5 and the safety factor of the downstream slope change from 2.1 to 1.8 if the seepage effect is considered.

REFERENCES

Seed, H.B. and Lee, K.L., Liquefaction of Saturated Sands During Cyclic Loading, *Journal of the Soil Mechanics and Foundation Division,* ASCE 92 (SM6), 1966, pp. 105–134

Seed, H.B. and Peacock, W.H., The Procedure for Measuring Soil Liquefaction Characteristics, *Journal of the Soil Mechanics and Foundation Division,* ASCE 97 (SM8), 1971, pp. 1099–1119

Castro, G. and Poulos, J., Factors affecting Liquefaction and Cyclic Mobility, *Liquefaction Problems in Geotechnical Engineering,* Annual Convention and Exposition, ASCE, 1976, pp. 105–138

Tokimatsu, K., Yamazaki, T. and Yoshimi, Y., Soil Liquefaction Evaluations by Elastic Shear Moduli, *Soils and Foundations,* Vol. 26, No. 1, 1986, pp. 25–35

Singh, S., Liquefaction Characteristics of silts, *Ground Failures Under Seismic Conditions,* ASCE National Convention, Geotechnical Special Publication, No. 44, 1994, pp.91–105

Yoshimi, Y., Tokimastu, K. and Ohara, J. “In situ Liquefaction Resistance of Clean Sands over a Wide Density Range”, *Geotechnique,* 1994, 44(3), pp. 479–494

》, GB 5028-99, The hydraulic department of China

This page intentionally left blank.

New Developments in Dam Engineering—Wieland, Ren & Tan (eds),
© 2004 Taylor & Francis Group, London, ISBN 04 1536 240 7

Cracking mechanism of concrete dam piers and rehabilitation techniques

Li Shouju & Liu Yingxi
State Key Laboratory of Structural Analysis for Industrial Equipment, Dalian University of Technology, Dalian, China

ABSTRACT: Under extreme cold weather conditions, there appeared some cracks at some piers of Fengman concrete gravity dam. The maximum length of the cracks was approximately 15m, which had directly threatened dam safety. In order to investigate the cracking mechanism of concrete dam piers, finite element simulation are carried out. Numerical analysis shows that the thermal stresses in the concrete piers have exceeded the tensile strength of concrete. A study concerning the application of some repair techniques on damaged concrete piers is proposed. The rehabilitation techniques performed at Fengman concrete dam include the installation of pre-stressed anchoring cables, grout injection, and surface concrete coating. The application results indicate that the proposed techniques are able to control the growth and size of the cracks in the concrete pier and to ensure dam safety.

1 INTRODUCTION

Most civil engineers and construction industry experts have recognized the deterioration problem of aged infrastructures around the world. The freezing and thawing problem of concrete dam is of utmost importance in countries having subzero temperature conditions. The deterioration of concrete dams is particularly accelerated when heat and moisture are readily available. The high internal humidity in the concrete dam can supply the necessary moisture to sustain numerous deterioration mechanisms. Cracking in concrete dams can be expected to occur for a number of reasons, including plastic and drying shrinkage, thermal effects, fatigue, reactive aggregates, and excessive loads. Freeze-thaw damage to concrete structures is caused by the pressure resulting from the increase in volume[1]. It can result in severe deterioration of concrete structures. The first one to study freezing and thawing of concrete structures was T.C.Powers[2]. He presented a theory of hydraulic pressure in which the pore water in the largest pores freezes first during cooling and only after the smaller pores have been frozen would the expansion be hindered causing large hydraulic pressure and subsequent paste destruction. In order to repair damaged structures effectively, many repair materials and techniques have been developed to provide strong, longer lasting rehabilitation[1,3,4]. Some continues cracks were observed along the gate slot of dam piers at Fengman concrete dam. The maximum length of some cracks was approximately 15m, from elevation 253m to dam crest (267.7m), its maximum width 10mm, which had directly threatened dam safety service. The main objective of the study is to investigate the cracking mechanism of concrete dam pier by means of finite element method and to propose the reasonable and economical measures to deal with the pier crack rehabilitation for Fengman dam.

2 ESTIMATION OF ATMOSPHERIC AND CONCRETE DAM SURFACE TEMPERATURES

Fengman concrete gravity dam was built in the years 1937 to 1943, shown in figure 1. It has a maximum height of 92m and a crest length of 1080m. The crest width is 11.4m and maximum base width is 67m.

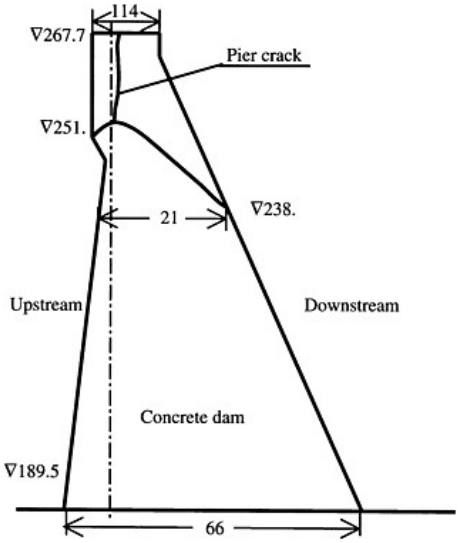

Figure 1. Cross-section of block 14.

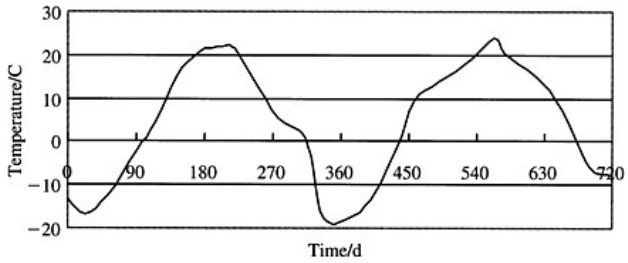

Figure 2. Change of air temperature versus date.

The temperature field of concrete dam will change annually with the change of air temperature. Parameters of the annual atmospheric temperature cycle are estimated by the following periodic regression equation[5]

$$T_{air}=T_m+A\cos(\omega\times t_i-\theta) \tag{1}$$

where T_{air} denotes atmospheric temperature (°C) on day i, T_m denotes mean atmospheric temperature (°C), A denotes amplitude of the cosine curve (°C), ω is constant converting time t_i to angular frequency(2π/365 radians per day), t_i is number of days since January 1 (i.e. t_1=January 1), θ is phase coefficient of the cosine curve (radians). Figure 2 shows the change of air temperature versus date at Fengman dam location.

According to measured air temperatures, the equation constants are got as follows: T_m=2.0°C, A=20.0°C, θ=195. The correct modeling of the boundary conditions on the upstream and downstream faces of the dam is very important for the accurate computation of the temperature distribution within the dam. The surface processes, i.e. convection and radiation, determine the

relation between the air and concrete surface temperature. On the sunny side, the relationship between the surface temperature and air temperature is established as follows[6]:

$$T_{csu}=0.937\times T_{air}+7.2 \tag{2}$$

where T_{csu} denotes the concrete surface temperature on the sunny side, T_{air} denotes the air temperature. For the shady side:

$$T_{csd}=0.905\times T_{air}-0.4 \tag{3}$$

where T_{csd} is the concrete surface temperature on the shady side.

3 FINITE ELEMENT ANALYSIS OF THERMAL STRESS FOR CONCRETE DAM PIERS

The three-dimensional finite element model is performed. The ordinary heat transfer equation for a three-dimensional concrete dam is expressed as follows:

$$k_x\partial^2T/\partial x^2+k_y\partial^2T/\partial y^2+k_z\partial^2T/\partial z^2+q=\rho c\partial T/\partial t \tag{4}$$

where T denotes temperature, k_x, k_y, k_z are the thermal conductivity coefficients in x, y and z direction, respectively; c is the specific heat per unit mass, ρ is the mass density, q is source-sink term(known); t denotes time. Let the weighting function equal the shape function. Then, the heat transfer finite element model can be obtained by means of the Galerkin method[7]:

$$[K_\theta]\{\theta\}+[K_c]\{\frac{\partial\{\theta\}}{\partial t}\}=\{F_t\} \tag{5}$$

where $\{\theta\}$ is the temperature of element node, $[K_\theta]$ is the stiffness matrix for heat transfer, $[K_c]$ is the capacitance matrix and $\{F_t\}$ is the temperature load matrix. The relation between element stress and nodal displacement can be written as

$$\{\sigma\}=[De](\{Bd\}\{d\}-\{\varepsilon'\}) \tag{6}$$

where $\{\varepsilon^t\}$ is the nodal initial thermal strain, $[D^e]$ is the elastic stiffness matrix and $[B_d]$ is the strain-displacement relation matrix, $\{d\}$ is the element's nodal displacement. The initial and boundary conditions are shown as follows:

$$T(x, y, z)=T_0(x, y, z)\ t=0,\ (x, y, z)\in\Omega \tag{7}$$

$$T(x, y, z)=T_b\ (x, y, z)\ (x, y, z)\in\Omega_1 \tag{8}$$

$$Q_0(x,y,z)=k_x\frac{\partial T}{\partial x}l_x+k_y\frac{\partial T}{\partial y}l_y+k_z\frac{\partial T}{\partial z}l_z \qquad (x,y,z)\in\Omega_2 \tag{9}$$

The thermal parameters of concrete dam are shown as follows: the thermal conductivity coefficient 2.9J/(m·s·°C), the specific heat per unit mass 1047J/·(kg·°C), the mass density 2350kg/m^3. The temperature fields of dam pier in different season are shown in figures 3 and 4. The horizontal tensile stress distribution of dam pier in different season is shown in table 2. Mechanical parameters of concrete dam pier are shown in table 1.

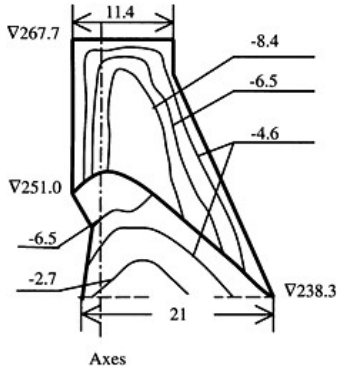

Figure 3. Temperature field of dam pier in March [°C].

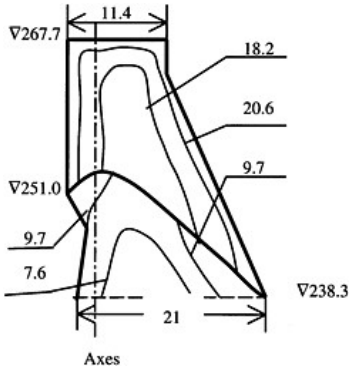

Figure 4. Temperature field of dam pier in July [°C].

Table 1. Mechanical parameters of concrete dam pier.

Young's modulus/MPa	Poisson coefficient	Thermal expansion coefFicient/°C
20000	0.167	10^{-5}

Table 2. Horizontal tensile stress at location of dam pier crack.

	Horizontal tensile stress/MPa		
Elevation/m	January	May	August
253	1.77	−0.23	−0.25
255	1.93	−0.07	−0.02
257	1.36	−0.06	−0.45
259	1.16	−1.70	−0.12
261	0.67	−1.08	0.33
263	0.80	−0.25	−1.34

4 REHABILITATION TECHNIQUES OF DAM PIERS

According to investigating in field and finite element analysis, the repair measures are performed with pres-stressed cables and high cement content and high strength mortars for pier cracks. The pier cracks are injected with mortars, and then compressed with pre-stressed cables, shown in figure 5. The grouting pressure is controlled at 0.22MPa. The upper cable load is 294kN, the other cable load is 981kN. A plan of dam pier rehabilitation is shown in figure 6. In order to improve the strengthening result, 0.4m thick old concrete at the gate slot of pier was moved and then substituted by new reinforcement concrete.

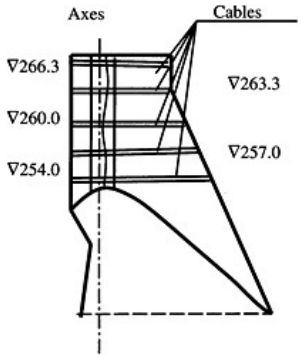

Figure 5. Location of pre-stressed cables for dam pier rehabilitation.

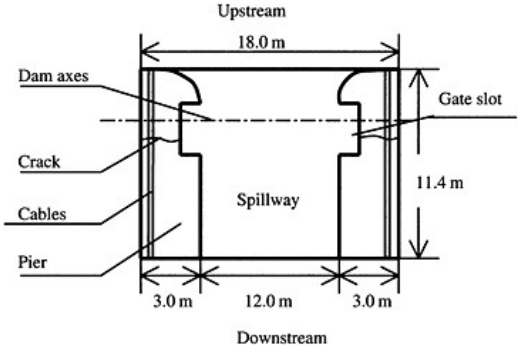

Figure 6. A plan of dam pier rehabilitation.

5 CONCLUSION

By three-dimensional finite element analysis, the maximum horizontal tensile stress at location of dam pier crack can be 1.8MPa in January. It has been predicted that the changes of air temperature will lead to unacceptable cracking of the concrete dam piers at Fengman hydropower station. The calculating results also show that the mass concrete constraints will result in crack initiation and development of dam piers. The pre-stressed cables, grout injection, and surface concrete coating method were applied to prevent cracks from widening and lengthening. The application results indicate that the proposed techniques are able to control the growth and stretch of concrete pier cracks and to ensure dam safety service.

REFERENCES

[1] P.D.Krauss Repair materials and techniques for concrete structures in nuclear power plants. Nuclear Engineering and Design, 1998, 181:71–89
[2] Vesa Penttala Stress and strain state of concrete during freezing and thawing cycles, Cement and Concrete Research, 2002, 32:1407–1420
[3] L.G.Verhoef Restrengthening of brickwork to reduce crack width, Advances in Engineering Software, 2002, 33:49–57
[4] M.O.Jannadi A concrete pier: case history of failure and repair, Construction and Building Materials, 2000, 14:7–16
[5] R.M.Preeece The effect of Keepit dam on the temperature regime of the Namoi river, Australia, River Research and Applications, 2002, 18:397–414
[6] S.Malla Analysis of an arch-gravity dam with a horizontal crack, Computers and Structures, 1999, 72:267–278
[7] Z.C.Lin 3-D finite element simulation of water thermal distortion and stress fields in exposure process, International Journal of Heat and Mass Transfer, 2002, 45:619–630

This page intentionally left blank.

New Developments in Dam Engineering—Wieland, Ren & Tan (eds),
© 2004 Taylor & Francis Group, London, ISBN 04 1536 240 7

Estimation of permeability of foundation of gravity dam with artificial neural network

Li Shouju & Liu Yingxi
State Key Laboratory of Structural Analysis for Industrial Equipment, Dalian University of Technology, Dalian, China

ABSTRACT: The mathematical model of underground water flow is introduced as basis to identify the permeability coefficients of rock foundation by observing the water heads of the underground water flow. The artificial neural network is applied to estimate the he permeability coefficients. The weights of neural network are trained by using BFGS optimization algorithm which has a fast convergent ability. The parameter identification results illustrate that the proposed neural network has not only higher computing efficiency but also better identification accuracy According to identified permeability coefficients of the rock foundation, the seepage field of gravity dam and its rock foundation is computed by using finite element method. The numerically computational results with finite element method show that the forecasted water heads at observing points according to identified parameters can precisely agree with the observed water heads.

1 INTRODUCTION

A common use of groundwater flow models is to predict the response of an aquifer. While the mathematical and computational aspects of such response predictions are reasonably well developed, the question of how to choose appropriate parameter values for a specific aquifer has not been completely resolved[1]. Traditionally, the determination of aquifer parameters is based on trial-and-error and graphical matching techniques under the assumptions that the aquifer is homogenous and isotropic and a closed-form solution for the governing equation exists[2]. The inverse problem of aquifer parameter identification is often ill-posed. The ill-posedness is generally characterized by the nonuniqueness and instability of the identified parameters. The instability of the inverse solution stems the fact that small errors in heads will cause serious errors in the identified parameters. Classical identification procedures are based on the optimization algorithm. Their drawbacks lie in lacking robustness and global convergence property. With the development of artificial intelligence, artificial neural network has been widely applied in the inverse problem domain[3,4,5]. Artificial neural networks have gradually been established as a powerful tool in pattern recognition, signal processing, control and complex mapping problems, because of their excellent learning capacity and their high tolerance to partially inaccurate data[6,7].

2 CALCULATION OF GROUNDWATER FLOW MODELS

Consider a three dimensional steady seepage field, its governing equation can be written as follows:

$$k_x \partial^2 h/\partial x^2 + k_y \partial^2 h/\partial y^2 k_y + \partial^2 h/\partial z^2 + q = 0 \quad (1)$$

Where k_x and k_y are permeability coefficient in x and y direction, respectively, h is the water head, q is the source-sink item. The first kind boundary condition is expressed as the following:

$$h(x,y,z)|_{\Gamma_1} = h_0(x,y,z) \tag{2}$$

Where $h_0(x,y,z)$ is the already known head. The second kind boundary condition is written as the following:

$$Q_0(x,y,z)|_{\Gamma_2} = k_x \frac{\partial h}{\partial x} l_x + k_y \frac{\partial h}{\partial y} l_y + k_z \frac{\partial h}{\partial z} l_z \tag{3}$$

Where $Q_0(x,y,z)$ is the drainage already known, l_x, l_y and l_z are the direction cosines of the exterior normal of the boundary in x, y and z direction, respectively. The following infinite element equation can be derived by the principle of the variational method:

$$[G]\{h\}=\{F\} \tag{4}$$

Where $[G]$ is the matrix of the water transmissibility coefficient, which is already known, and $\{F\}$ is the free item. When the boundary condition and the predicted permeability coefficient are determined, the infinite element equation is adopted to compute the distribution of the water head and the drainage in the whole seepage field, which provides modal data to the analysis of the inversion problem of the permeability coefficient.

3 ARTIFICIAL NEURAL NETWORKS FOR THE PARAMETER IDENTIFICATION

An artificial neural network model is a system with inputs and outputs based on biological nerves. The system can be composed of many computational elements that operate in parallel and are arranged in patterns similar to biological neural nets. A neural network is typically characterized by its computational elements, its network topology and the learning algorithm used. Among the several different types of ANN, the feed-forward, multilayered, supervised neural network with the error back-propagation algorithm, the BPN, is by far the most frequently applied neural network learning model, due to its simplicity.

The architecture of BP networks, depicted in Figure 1, includes an input layer, one or more hidden layers, and an output layer. The nodes in each layer are connected to each node in the adjacent layer. Notably, Hecht-Nielsen proved that one hidden layer of neurons suffices to model any solution surface of practical interest. Hence, a network with only one hidden layer is considered in this

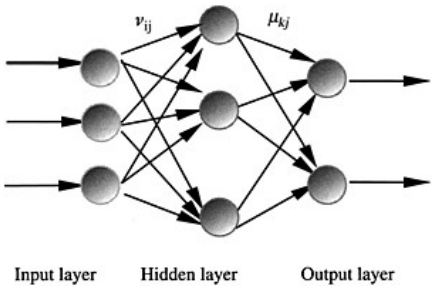

Figure 1. Topography structure of artificial neural network.

study. Before an ANN can be used, it must be trained from an existing training set of pairs of input-output elements. The training of a supervised neural network using a BP learning algorithm normally involves three stages. The first stage is the data feed forward. The computed output of the i-th node in output layer is defined as follows [6]:

$$y_i = f(\sum_{j=1}^{N_h}(\mu_{ij} f(\sum_{k=1}^{N_i} v_{jk} x_k + \theta_j) + \lambda_i)) \quad i = 1,2,...N \tag{5}$$

Where μ_{jk} is the connective weight between nodes in the hidden layer and those in the output layer; v_{jk} is the connective weight between nodes in the input layer and those in the hidden layer; θ_j or λ_i is bias term that represents the threshold of the transfer function f, and x_k is the input of the kth node in the input layer. Term N_i, N_h, and N_o are the number of nodes in input, hidden and output layers, respectively. The transfer function f is selected as Sigmoid function:

$$f(\cdot)=1/[1+\exp(-\cdot)] \tag{6}$$

The second stage is error BP through the network. During training, a system error function is used to monitor the performance of the network. This function is often defined as follows:

$$E(w) = \sum_{p=1}^{P}(\sum_{i=1}^{N_o}(y_i^p - o_i^p)^2 \tag{7}$$

Where o_i^p denote the practical and desired value of output node i for training pattern p, P is the number of sample. Training methods based on BP offer a means of solving this nonlinear optimization problem based on adjusting the network parameters by a constant amount in the direction of steepest descent, with some variations depending on the flavor of BP being used. The BFGS algorithm is a quasi-Newton optimization technique, in which curvature information is used to prove a more accurate descent direction, without actually calculating the second derivatives. A sequence can be computed according to the formula[7]:

$$w(k+1)=w(k)+\alpha(k)d(k) \tag{8}$$

Where $w(k)$ is the vector of network parameters(net weights and element biases) for iteration k, $d(k)$ is the search direction used for iteration k, and $\alpha(k)$ is the step length for iteration k. The search direction will be determined by the following formula[8]:

$$d(k)=-H(k)g(k)+\beta(k)d(k-1) \tag{9}$$

Where $H(k)$ is the current approximation to the inverse of the Hessian matrix, and $g(k)$ is the current gradient vector. The approximation to $H(k)$, $g(k)$ and $\beta(k)$ in detail is presented in the references[6,8].

4 APPLICATION OF ANN TO IDENTIFICATION OF PERMEABILITY COEFFICIENTS OF DAM FOUNDATION

Baishan Hydropower Station is located in the Second Sonhuajiang River in Jilin province, China. It consists of a 149.5-meter-high concrete heavy-pressure dam, a weir with four 12×13 meter tunnels on top of the 404-meter-high spillway dam, three 6×7 meter tunnels for discharging water are 350 meters high, an underground powerhouse with an installed generating capacity of 900,000KW and

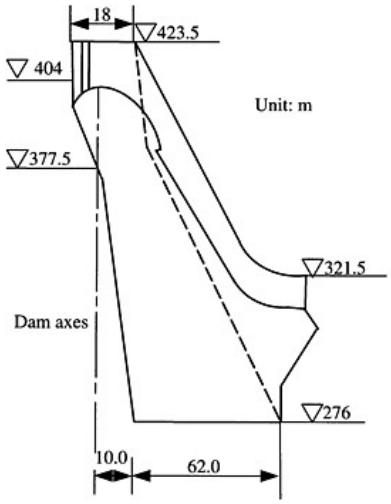

Figure 2. Cross-section of Baishan dam at block 18.

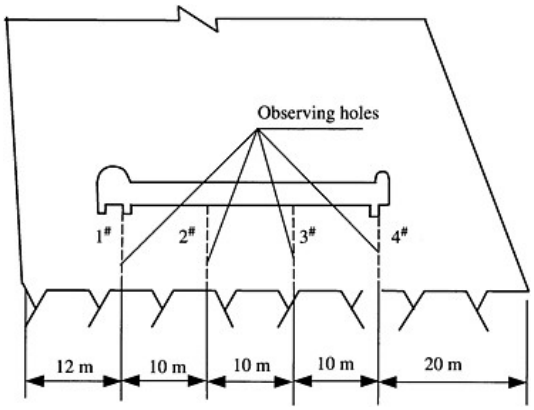

Figure 3. Disposition of observation holes for dam uplift pressure at block 18.

another powerhouse on the surface with an installed generating capacity of 600,000KW. The dam is 423.5 meters high and the reservoir has a storage capacity of 6.812 billion cubic meters. Its highest normal storage water level is 413 meters. The capacity for water control storage is 3.54 billion cubic meters while the flood control storage capacity is 950 million cubic meters. Cross-section of Baishan dam at block 18 is shown in Figure 2. Figure 3 shows the disposition of observation holes for dam uplift pressure at block 18.

In order to identify the permeability coefficients of rock foundation, the three-dimensional finite element model for seepage calculation is carried out. The seepage fields of the dam and its rock foundation at different load cases are computed. According to the prior information of pumping water test in field, the domains of identification parameters are determined. The training sample

Table 1. Measured data of water heads in the observation holes.

Measuring date	Upstream water elevation	Downstream water elevation	Measure head			
			h_1	h_2	h_3	h_4
19980910	413.00	290.80	291.82	283.59	284.74	281.72

Table 2. Identification results of permeability coefficients.

Rock base before concrete certain $k_1/10^{-9}m{\cdot}s^{-1}$	Concrete certain $k_2/10^{-9}m{\cdot}s^{-1}$	Rock base after concrete certain $k_3/10^{-9}m{\cdot}s^{-1}$
44.05	6.16	52.80

Table 3. Comparison between measured and forecasted water heads.

Measuring date	Measured point			
	No. 1	No. 2	No. 3	No. 4
19971015	291.82/291.78	283.54/283.49	284.23/283.19	281.72/281.13
19980108	291.31/291.29	283.59/283.44	282.19/283.15	281.82/282.14
19980901	291.82/291.78	283.59/283.49	284.74/283.19	281.72/282.12
19981012	291.82/291.78	283.49/283.49	284.74/283.19	281.72/282.12

Note: Measured water heads/computed water heads.

pairs are got basing on finite element analysis. The rock foundation is divided into 3 sub-regions, rock base before concrete certain, concrete certain and rock base after concrete certain. The number of input neurons is determined as 4 according to the number of observing points. And the number of hidden neurons is equal to 8. The number of output neurons is equal to 3, which is equal to the number of sub-regions for back-analysis. After training ANN with BFGS optimization algorithm, based on measured data of water heads in the observation holes, shown in Table 1, the permeability coefficients of rock foundation are obtained. Table 2 is identification results of permeability coefficients. Table 3 is the comparison between measured and forecasted water heads.

5 CONCLUSION

Based on the finite element model of groundwater flow and the measured water heads of uplift pressure at dam tunnel, artificial neural network is applied to estimate the permeability coefficients of rock foundations of concrete dam. The BFGS optimization method is used to train and adjust the weights of neural network. It was found that this algorithm can improve the rate of convergence of neural network. According to the identified permeability coefficients of rock foundations of concrete dam and finite element analysis, the forecasted water heads can precisely agree with the observed water heads.

REFERENCES

[1] J.Carrera Estimation of aquifer parameters under transient and steady state conditions Water Resources Research, 1986,22:199–210
[2] W.Yeh Review of parameter identification procedures in groundwater hydrology: the inverse problem Water Resources Research, 1986, 22:95–108

[3] Yi Huang Application of artificial neural networks to predictions of aggregate quality parameters, Int. J. of Rock Mechanics and Mining Sciences, 1999, 36:551–561
[4] Y.M.Najjar Utilizing computational neural networks for evaluating the permeability of compacted clay liners, Geotechnical and geological Engineering, 1996, 14:193–212
[5] X.Cao Application of artificial neural networks to load identification. Computers & Structures, 1998, 69: 63–78
[6] C.S.Huang A neural network approach for structural identification and diagnosis of a building from seismic response data. Earthquake Engineering and Structural Dynamics, 2003, 32:187–206
[7] G.Lightbody Multi-layer perceptron based modeling of nonlinear systems Fuzzy Sets and System, 1996, 79:93–112
[8] J.W.Denton A comparison of nonlinear optimization methods for supervised learning in multilayer feedforward neural networks European Journal of Operational Research, 1996, 93:358–368

New Developments in Dam Engineering—Wieland, Ren & Tan (eds),
© 2004 Taylor & Francis Group, London, ISBN 04 1536 240 7

Study on formation cause of cracks for Shuanghe Arch dam

Li Tong-chun & Chen hui-fang
Hohai University, China

Zhang Hang-hui
TAIHU Basin Authority of Ministry, China

Niu zhi-wei
Hohai University, China

ABSTRACT: Shortly after construction of the Shuanghe Arch dam, substantial perforative cracks were observed on the upstream and downstream faces of the arch dam, and these cracks would threaten the stabilization of the dam. The load combination analysis method and the emulation analysis method are carried out to evaluate the formation cause of cracks in this paper. The results from the two analysis methods are compatible, and the following conclusions are obtained from the analysis: Temperature drop is the main external cause of crack growing, and the extremity of asymmetry of the foundational material is the important internal reason resulting in crack producing.

1 INTRODUCTION

Shuanghe Arch reservoir is located at debouch of Shuanghe river which is a branch of Guixi river in Xinming town, Dianjiang country, Sichuan province, China. The reservoir is dominated with irrigating agricultural lands, together with controlling flood, supplying water to towns and generating electricity. It is a median size reservoir with a gross reservoir capacity of 1257.3mm^3, for irrigation of 2723.3 ha of agricultural lands, supplying water from 3000 to 10000m^3 to the towns every day. The hydroelectric capacity is 640kw.

The characteristics of Shuanghe Arch dam are as follows: The dam is a hyperbolic concrete arch dam of masonry structure with a maximum height of 64.56m; crest elevation of 552.26m and normal high water level elevation of 548.60m; the thickness of 2.5m at the crest and 15m at the bottom; the chord length of 137m at the crest and 15m at the bottom; a central angle varying between 84° and 30° (from top to bottom); span-depth ratio of 2.12 and thick-depth ratio of 0.23. There is no sluice-gate on the crest spillway, and overflow weir is set in the middle of the dam crest. The weir crest elevation is 548.60m, and spillway length is 32.5m.

The dam was started building in June 1990, and finished on December 5, 1992. Shortly after construction in the middle December on the condition of reservoir-empty, six vertical perforative cracks developed on the downstream face of the arches. In January 1993 the cracks were propagating with two cracks through the crest of dam and four through the foundation. The total length of the cracks on downstream face exceeds 184m, and the general width of the cracks is almost 1.5mm but the maximal width is 8mm. The longest crack is 54m long to the right section 2.7~3m of the arch crown. The total area of cracked sections is about 900m^2. The order of the crack developing is that the cracks generate from the middle height of dam, and propagate towards the dam crest or bottom. Figure 1 shows the specific positions of the cracks on the downstream face of the dam.

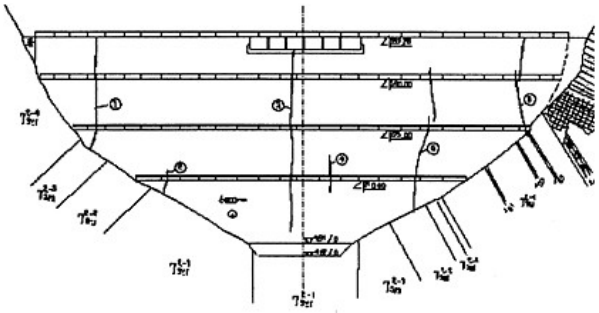

Figure 1. Cracks on the downstream face of the dam.

2 FORMATION CAUSE OF CRACKS

Shuanghe Arch dam is a thin low dam, and it is a masonry structure, composed of the rocks in the main body of the dam with the rate of the rocks is from 10 percent to 20 percent. Extensive field measurements and analytical studies were initiated to understand and evaluate the structural behaviour of the dam, and the temperature load was found as the main load on this thin low arch dam, moreover the variety of temperature load was large in a year. Because the dam had no transverse joints, the temperature stress gathered in the dam body in the process of construction would not be released, so the adaptability of the dam to temperature change would decrease. The cross-bedded pouring was used to Shuanghe Arch dam, and the deficiency of the method was that the restraint of each layer was much large, which would be very adverse to resist the cracking of the concrete during the construction period.

The temperature control was not studied generally during the design period of dam and the valid measures of the temperature control were not adapted during construction period, thus the dam body cracked to different degree in course of the construction, and the cracks were propagating far more after the reservoir was impounded.

The analytical study is performed in two methods. The first is the load combination analysis method which is used to analyze the temperature load, the temperature stress, the basal capability of material, the temperature variety during construction period, and so on. The second is the emulation analysis method consisting of applying the finite element program to calculate the temperature and stress fields and to simulate approximately the process of cracks producing and growing.

2.1 *Analysis of the temperature load*

Shuanghe Arch dam is a thin arch dam, and the temperature field is not steady. The influence of the ambient monthly temperature variation is not obvious to the temperature of dam body.

For studying the influence of the temperature load to the stress and strain of dam body, the dam structure must be calculated with the annual temperature load variation of the dam body. In order to know the influence of temperature load variety in a year to the dam stress and strain, three conditions of load combination are used: the all loads do, all do but the temperature load and only the temperature load does. The load combination conditions are as follows:

- Load combination 1: upstream design water level load and downstream design water level load; and silt load; and self-weight; and monthly temperature load.
- Load combination 2: upstream design water level load and downstream design water level load; and silt load; and self-weight.
- Load combination 3: monthly temperature load.

Table 1. Maximum stress variety in a year (MPa).

	Maximum compressive stress on upstream face				Maximum tensile stress on upstream face			
	Load combination				Load combination			
Month	1	2	3	Temperature influence (%)	1	2	3	Temperature influence (%)
1	2.91	3.18	0.23	91.51	−1.55	−1.39	−0.66	111.51
2	2.74	3.18	0.16	86.16	−1.68	−1.39	−0.72	120.86
3	2.62	3.18	0.58	82.39	−1.79	−1.39	−0.74	128.78
4	2.61	3.18	1.11	82.08	−1.83	−1.39	−0.88	131.65
5	2.70	3.18	1.42	84.91	−1.79	−1.39	−0.95	128.78
6	2.86	3.18	1.42	89.94	−1.70	−1.39	−0.84	122.30
7	3.06	3.18	1.16	96.23	−1.56	−1.39	−0.59	112.23
8	3.23	3.18	0.82	101.57	−1.42	−1.39	−0.38	102.16
9	3.34	3.18	0.56	105.03	−1.32	−1.39	−0.19	94.96
10	3.35	3.18	0.39	105.35	−1.28	−1.39	−0.53	92.09
11	3.27	3.18	0.37	102.83	−1.32	−1.39	−0.84	94.96
12	3.11	3.18	0.33	97.80	−1.41	−1.39	−0.84	101.44
Maximum	**3.35**	**3.18**	**1.42**	**105.35**	**−1.83**	**−1.39**	**−0.95**	**131.65**
Minimum	**2.61**	**3.18**	**0.16**	**82.08**	**−1.32**	**−1.39**	**−0.19**	**92.09**
	Maximum compressive stress on downstream face				Maximum tensile stress on downstream face			
	Load combination				Load combination			
Month	1	2	3	Temperature influence (%)	1	2	3	Temperature influence (%)
1	3.63	3.43	0.35	105.83	−1.01	−0.99	−0.31	102.02
2	3.72	3.43	0.45	108.45	−0.83	−0.99	−0.33	83.84
3	3.88	3.43	0.58	113.12	−0.63	−0.99	−0.29	63.64
4	4.07	3.43	0.90	118.66	−0.45	−0.99	−0.23	45.45
5	4.16	3.43	1.10	121.28	−0.46	−0.99	−0.25	46.46
6	4.12	3.43	1.11	120.12	−0.52	−0.99	−0.24	52.53
7	3.95	3.43	0.96	115.16	−0.56	−0.99	−0.19	56.57
8	3.70	3.43	0.68	107.87	−0.65	−0.99	−0.21	65.66
9	3.45	3.43	0.44	100.58	−0.85	−0.99	−0.21	85.86
10	3.27	3.43	0.21	95.34	−1.02	−0.99	−0.39	103.03
11	3.33	3.43	0.10	97.08	−1.12	−0.99	−0.51	113.13
12	3.49	3.43	0.21	101.75	−1.11	−0.99	−0.47	112.12
Maximum	**4.16**	**3.43**	**1.11**	**121.28**	**−1.11**	**−0.99**	**499**	**113.13**
Minimum	**3.27**	**3.43**	**0.10**	**95.34**	**−0.52**	**−0.99**	**−0.19**	**45.45**

The results are shown in Tables 1, 2 and 3. The values of the temperature influence are the ratio of the load combination 1 and the load combination 2, with which the influence of temperature load to the stress and strain of dam body can be known.

The results show that the dimension of the maximum compressive stresses in a year is from 2.27MPa to 4.16MPa under all the loads, and that of the maximum tensile stresses is from 1.32MPa to 1.83 MPa, and that of the radial displacement is from 1.93cm to 2.78cm. When only the temperature load does, the dimension of the maximum compressive stresses in a year is from 0.16MPa to 4.421MPa, and that of the maximum tensile stresses is 0.19MPa to 0.95MPa, and that of the radial displacement is −0.01cm to 0.89cm. From the analysis of the stress, the ratios of the compressive stresses due to the change of the temperature change from −18% to 22%, and those of the tensile stresses change from −55% to 31%. Considering the strain, the ratio of the axis displacement changes from −17% to 17%, and the rate of what is caused by the temperature

Table 2. Annual average radial displacement of the crown cantilever (cm).

Month	1	2	3	4	5	6	7	8	9	10	11	12
Load combination 1	−1.94	−1.80	−1.56	−1.32	−1.11	−1.01	−1.03	−1.18	−1.41	−1.66	−1.86	−1.97
Load combination 2	−1.60	−1.60	−1.60	−1.60	−1.60	−1.60	−1.60	−1.60	−1.60	−1.60	−1.60	−1.60
Load combination 3	−0.34	−0.19	0.04	0.29	0.49	0.60	0.57	0.42	0.19	−0.06	−0.26	−0.37
100* (3)/(1)%	17.53	10.56	−2.56	−21.97	−44.14	−59.41	−55.3	−35.59	−13.48	3.61	13.98	18.78

Table 3. Annual maximum radial displacement (cm).

	Load combination			
Month	1	2	3	Temperature influence (%)
1	−2.78	−2.37	−0.68	117.30
2	−2.64	−2.37	−0.34	111.39
3	−2.46	−2.37	−0.12	103.80
4	−2.30	−2.37	−0.07	97.05
5	−2.14	−2.37	−0.03	90.30
6	−2.02	−2.37	0.01	85.23
7	−1.97	−2.37	0.00	83.12
8	−2.01	−2.37	0.00	84.81
9	−2.12	−2.37	−0.08	89.45
10	−2.34	−2.37	−0.39	98.73
11	−2.60	−2.37	−0.78	109.70
12	−2.77	−2.37	−0.89	116.88
Maximum	**−2.78**	**−2.37**	**−0.89**	**117.30**
Minimum	**−1.97**	**−2.37**	**0.01**	**83.12**

load in the all loads is from −59% to 19%. Viewing on the time, in summer the temperature load reduces the water pressure, but in winter it matches with the water pressure. From the absolute values of the temperature load affects the stress and the strain, the values are further large in June and July than those in December and January. It is concluded therefore that the temperature load is the main load that affects the stress and strain of the dam body strongly, and the temperature changing is the main cause that makes the stress and strain of the dam body change.

In a word, because the dam body is very thin, the influence of the ambient temperature to the dam is acute, and the temperature load is the main load that influences the stress and strain of the dam body. Compared with the water and silt load the temperature load is dominating to affect the dam body, so the displacement direction of the dam crest tends to the upstream direction under high water level in summer.

2.2 *The emulation analysis method*

In order to meet with the continuum of the temperature fields and the displacement fields, compatible displacement method of incompatible mesh is presented in this paper for the nodes of the contact layer of the dam body and the foundation. The mesh of the dam body may be generated by 3D hexahedron elements and that of dam foundation may be generated by 3D tetrahedron elements. The mesh is shown in Figure 2, which involves 6609 nodes and 12447 elements. The positive direction of the x and y axis point to the left bank and the upstream respectively, and the positive direction of the z axis point upwards.

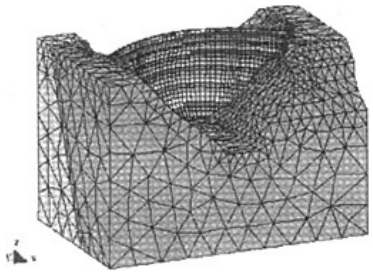

Figure 2. Finite element mesh.

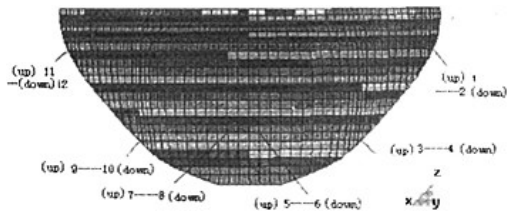

Figure 3. Layout of analyzed dots on arch dam.

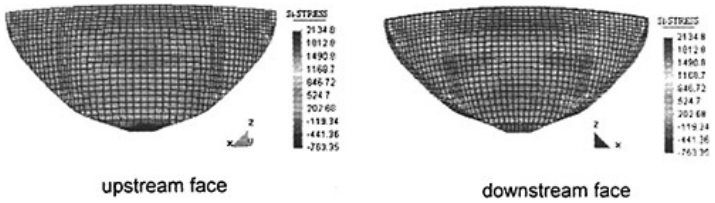

Figure 4. First principal stress after 702 days of dam poured (KPa).

The analyzed dots in the middle and down sections of the dam body and in the crest of upstream are shown in Figure 3, and the positions of the six pairs analyzed dots are similar to those of the six cracks observed. Figures 6, 7 and 8 show the maximum principal tensile stresses of the six pairs dots. It can be seen that the values of the maximum tensile stresses of the dots 3, 4 and the dots 9, 10 on upstream face on the 348 day surpasses 1.1MPa, which are less than that on the downstream face, so the feasibility of cracking nearly at the same time is large in the two pairs dots. It is shown in the figures of the temperature change course that the temperature drop are great at this time. This indicates that the temperature drop contribute the major of the tensile stress. After 702 days of the dam starting being poured the principal tensile stresses of the six pairs dots are rather large, and exceed 1.0MPa except for the middle two pairs ones. But when the cracking effect caused by the dots 3, 4 and dots 9, 10 are considered, the stresses of the middle two pairs dots will increase. Figures 4 and 5 show the maximum and minimum stresses on the upstream and downstream dam face, and the positions of the computed maximum principal tensile stresses are reasonably close to those of the cracks. The maximum principal tensile stresses on the middle

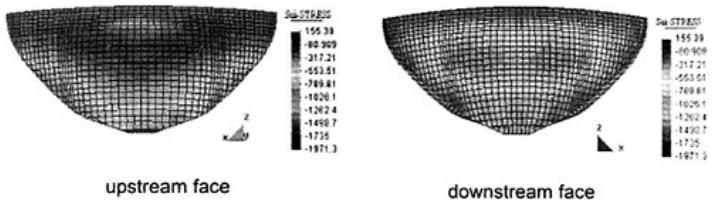

Figure 5. Third principal stress after 702 days of dam poured (KPa).

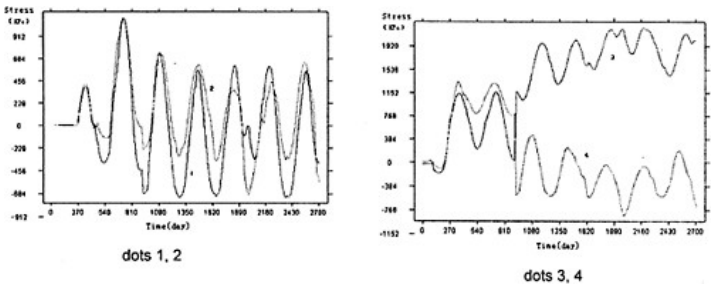

Figure 6. Change of maximum principal tensile stress with time going.

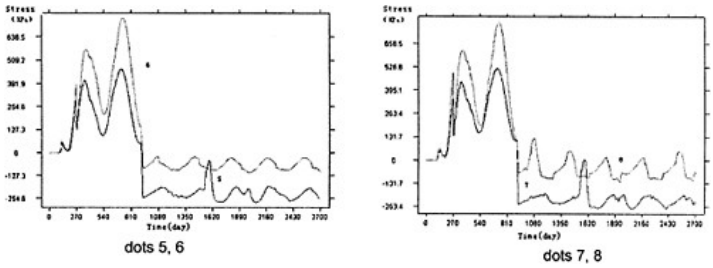

Figure 7. Change of maximum principal tensile stress with time going.

section of the dam are less than those on the left and right sides, so the cracks on the middle section of the dam form after that on the left and right sides, which is consistent with the results of observation.

From the Figures 6, 7 and 8, it can be shown that times of the larger principal tensile stresses correspond with that of temperature drops, while times of the smaller principal tensile stresses correspond with that of temperature rises. After 922 days of dam poured the changes in the stresses of the dots 1, 2 and dots 11, 12 caused by the impounding are barely noticeable, but those to the dots 3, 4 and 9, 10 are largish. And the water compressive stresses make the maximum principal tensile stresses of the two pairs dots increase rapidly to about 2.5MPa on the dam upstream face, while

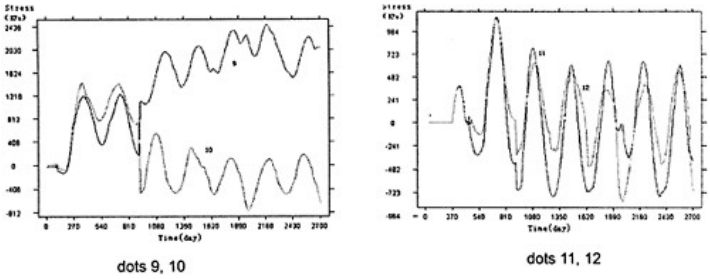

Figure 8. Change of maximum principal tensile stress with time going.

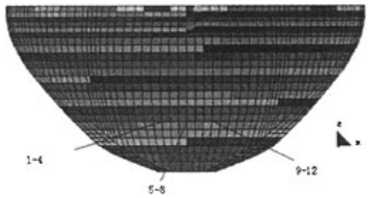

Figure 9. Layout of analyzed dots.

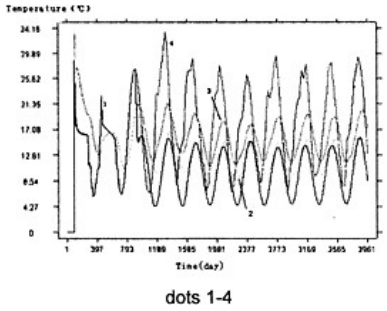

Figure 10. Change of temperature with time going.

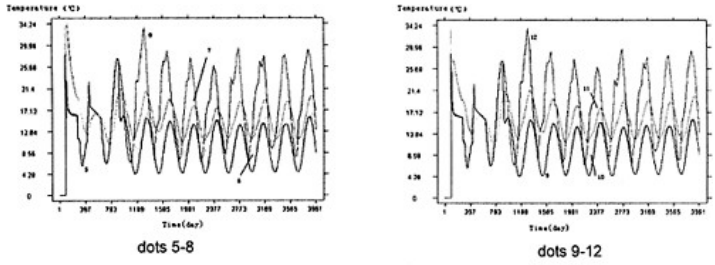

Figure 11. Change of temperature with time going.

descend to negative value on the dam downstream face. The two pairs dots 5, 6 and 7, 8 locate the 1/4 dam height, and without consideration of the dam cracking effect before the dam impounded these two pairs dots affected by the water load are completely in compression after the dam impounded.

Figures 9, 10 and 11 show the temperature of the analyzed dots changing with time going. It can be seen that the temperature of the dam body concrete changes with time going, then matches with

the external temperature step by step. After 730 days of the dam body starting pouring, the temperature of the dam body concrete stabilizes on the whole.

It is concluded that mostly areas are in compression after the dam is impounded. The larger tensile stresses were only occurred on the local part of dam heel on upstream surface and the local part of dam toe on downstream surface. The cracks on the middle section of the downstream side will remain closed under water loading condition, which explains why the water leakage does not occur in the arch dam after the dam impounded.

3 CONCLUSION

The analytical results of the finite element emulation analysis are similar to those of the load combination analysis. The results from the two analysis methods are followed:

- Shuanghe Arch dam is a thin arch dam, and the temperature load almost equal to the water which is the predominant load on the dam. With the great variation of the temperature load in a year, the stress and strain of the dam will change periodically During December 1992 to January 1993, under the reservoir-empty condition the dam temperature dropped with that of surroundingenvironment falling down, and the range of the temperature dropping is large. At that time the strength and the crack resistance of the concrete were low without the proper protective measures on the dam face, so the perforative cracks on the arch dam were caused by the combination of self-weight and temperature load with the residual temperature stress during construction. This indicates that temperature drop is the main external cause of crack growing.
- The tensile stress is not very large comparatively under the combination of the self-weight, water load and the temperature load, but the shear stress is great comparatively. So the cracks will not open under these loading conditions, but the shear crack can generate. The position of the shear stress great comparatively is the edge of the soft and hard rock stratum in the foundation, which shows that the extremity of asymmetry of the foundational material is the important internal reason resulting in crack generating.

REFERENCES

Bofang, Zhu (1999) *Temperature stress and control of mass concrete.* China Electric Press, Bei-Jing, China.

Hanghui, Zhang (2003) *Study on the Emulation Analysis of Danger Removing and Reinforcement on Sickdangerous Concrete Arch Dams.* Master Degree thesis, College of Water Conservancy and Hydropower Engineering, Hohai University, Nanjing, China.

Veltrop J.A., Yeh C.H. and Paul W.J. (1994) Evaluation of cracks in a multiple arch dam. *Dam Engineering,* Vol 1, 3–13.

New Developments in Dam Engineering—Wieland, Ren & Tan (eds),

Equivalent stress analysis method based on finite element solution for arch dams

Li Tong-chun & Liu Xiao-qing
Hohai University, China

Zhang Hang-hui
TAIHU Basin Authority of Ministry, China

ABSTRACT: The stresses based on the trial load method are used to evaluate the arch dam safety in the design criteria in all Countries. Due to the well-known disadvantages, many researchers try to use finite element method to compute the arch dam stresses. But up to now, the stresses based on FEM are only taken as references because of the stress concentration at the dam heel or the dam toe. The stresses equivalent to that of trial load based on FEM makes the real application of FEM on arch dam stress analysis to be possible. The arch dam equivalent stress analysis method based on the finite element internal forces is developed in this paper. Based on the bilinear distribution assumption of the normal and shear stresses in the plane elements on the arch or beam sections, the formulas are obtained to solve the nodal stresses according to the constraining forces on the given internal sections. Further more, computation equations and corresponding formulas of equivalent stresses on upstream and downstream surfaces are derived by assuming linear distribution of stresses in the arch and beam sections along the radial direction. In addition, the equivalent stresses of a typical cylindrical arch dam is analyzed to prove that the method proposed in this paper is reasonable. The effect of mesh sizes on equivalent stresses of arch dams is also studied. And it indicates that equivalent stresses of arch dam are not very sensitive to the mesh sizes.

1 INTRODUCTION

Trial load and finite element methods are the main existing stress analysis methods for arch dams. With the trial load method, an arch dam is divided into a series of arch and beam elements. The distributions of water pressure in arch and beam elements are solved according to the translation and rotation displacement compatibility conditions at the intersection nodes of arch and beam elements. The stresses are calculated according to the obtained internal forces in arches and beams by assuming linear distribution of the main stresses along the radial direction. Up to now, the stresses based on the trial load method are used to evaluate the arch dam safety in the world. The main reason is that the stresses obtained by this method are corresponding to the concrete strengths calculated from the formulas of material mechanics according to the action loads on standard test specimens. It is well known that the conventional trial load method has the following obvious disadvantages.

1) The formulation and solution are based on some hypothesis so that the results are reasonably approximate in some extent.
2) It is difficult to tackle some problems in the calculation procedure such as an arbitrary initial distribution of the exterior loads between the arches and the beams. For examples, there are approximate that the self-weight is assumed to completely act on beams and the temperature load is assumed to act on arches or beams individually.
3) The method is usually impracticable used to deal with dynamic analysis and nonlinear analysis.

4) It is difficult to reasonably simulate the cases such as dam bodies with big holes, especially those with intermediate and bottom outlets, and those with complex geologic conditions.

To overcome these assumptions and drawbacks, a lot of researchers have been preserving in this field, for example, Lin Shaozhong and Yang Zhonghou presented load distribution displacement method to deal with dynamic analysis and nonlinear analysis [3].

The finite element method is used in stress analysis of arch dams more and more universally It takes the translation nodal displacements as the variables and the elements can be shell or isoparametric. The isoparimetric elements are widely used in view of their simplicity, easily fitting the dam shape and conveniently simulating the interaction between the dam and its foundation. The method can overcome the intractable difficulties involved in the trial load method. But there always exists an intractable problem of stress concentration at the dam heel or the dam toe of an arch dam. In addition, existing strength criterion needs to be advanced because of the effect of mesh size and types of element. Therefore it is difficult to evaluate the stress given by the classical finite element method. Besides, the conventional isoparametric elements are not so good to simulate the bending behaviors of the arch dams.

The author presents the concepts of named strength and the named stress in 1989 [1]. It indicated that the straight linear stress distribution assumption is consistent with that of material mechanics while it is the basis to determine the concrete strengths. The equivalent stresses for arch dam presented by Fu Zuoxin in 1991 [2] is similar to that by author. Fu determines equivalent stresses as follows. (1) The stress curves are fit at a given section that passes through the line connected by the central points along the radial direction. (2) The moment, shear force and axial force in the unit width are obtained by integration of the curves. (3) The equivalent stresses are calculated according to the formulas of material mechanics. Although this method gave an idea to determine the equivalent stresses, the force equilibrium equations are incompletely satisfied because the internal forces of given sections are obtained from the fitted stress curves.

This paper presents a simple and complete method to determine the equivalent stresses for arch dams. The principle of the method is as following. First of all, finite element equilibrium equation of dam body and dam foundation under water pressure and body force is established to solve nodal displacements and element stresses. Then according to the force equilibrium equations of the arch system and the beam system, constraining internal forces of given sections are solved by dividing the dam body into an arch system and a beam system. Assuming the bilinear distribution of the normal and shear stresses in the plane elements on the arch or beam sections, the formulas based on the principles of static equilibrium are obtained to solve the nodal stresses according to the constraining forces on the given internal sections. Further more, computation equations of equivalent stresses on upstream and downstream surfaces are derived by assuming straight-linear distribution of stresses in the arch and beam sections along the radial direction. For simulating the bending behaviors of the arch dams properly, the enhanced assumed strain elements developed by J.C.Simo and M.S.Rifai [6] and modified by U.Andelfinger and E.Ramm [7] are used in this paper.

The equivalent stresses of a typical cylindrical arch dam is analyzed to prove the method proposed in this paper. The effect of mesh sizes on equivalent stresses is also studied.

2 BASIC FORMULATION

2.1 *Internal forces of given sections*

For a given structural systems with the known constrained boundary conditions, the finite element equation is

$$[K]\{\delta\}=\{F\} \tag{1}$$

in which the matrix $[K]$ is structural stiffness matrix, $\{\delta\}$ is the vector of unknown nodal displacement and $\{F\}$ is vector of applied loads.

Suppose the structural system is divided into two parts (namely substructure I and substructure II) by the given section π. It is naturally that there is a pair of constraining internal forces acting on the given sections of the two substructures, which have the same magnitude and the opposite direction.

Therefore, the equation (1) can also be expressed as follows:

$$\begin{bmatrix} k_{ii} & k_{ic} \\ k_{ci} & k_{cc} \end{bmatrix}_{I,II} \begin{Bmatrix} \delta_i \\ \delta_c \end{Bmatrix}_{I,II} = \begin{Bmatrix} F_i \\ F_c + f_c \end{Bmatrix}_{I,II} \tag{2}$$

where the subscript c refers to those nodes on the given section π, and the subscript i refers to the others. F_c is the nodal load vector on the given section π, and F_i is the nodal load vector for the others; $\{f_c\}_I$ $\{f_c\}_{II}$ are respectively the constraining internal forces on the given section π between substructure I and substructure II. It is obvious that the following equation is automatically satisfied.

$$\{f_c\}_I+\{f_c\}_{II}=0 \tag{3}$$

As a consequence, the nodal displacements can be obtained via equation (1) because it is equivalent to equation (2) completely. Then introducing the nodal displacements into equation (2), the constraining internal forces on the given section π are as following:

$$\{f_c\}_1=-\{f_c)_{11}=[k_{c,}]_1\{\delta,\}_1+[k_{cr}]_{11}\{\delta c\}_1-[k_{cr}]_{11}\{\delta_i\}_{11}-[k_{cc}]\{\delta_c\}_{11} \tag{4}$$

After circling all elements of substructure I (or substructure II), the right term of equation (4) is obtained by superimposing all unknowns. Because displacement of finite element method is expressed with fractional interpolating function, the constraining internal forces on the section π are only related to those elements including any nodes on the section π of substructure I (or substructure II). Therefore, in the practical procedure of solution, only those elements at least contain one of the nodes on the section π are circled.

2.2 *Nodal equivalent stresses*

Assuming the bilinear distribution of the normal and shear stresses in the plane elements on the arch or beam sections, the formulas based on the principles of static equilibrium can be obtained to solve the nodal stresses according to the constraining forces on the given internal sections. Further more, computation equations of equivalent stresses on upstream and downstream surfaces can be derived by assuming straight-linear distribution of stresses in the arch and beam sections along the radial direction. In the analysis, normal stress along arch and vertical directions and shear stress along arch direction are assumed to be distributed straight-linearly in the radial direction. Thus, according to equilibrium condition of infinitesimal mass, shear stresses are in parabolic and normal stress is in cubic along the radial direction. These assumptions are the same as that of trial load method. As a consequence, for the stresses on the upstream and downstream surfaces, the normal stresses along the arch and vertical directions and the shear stress along the arch direction are solved by the analysis method mentioned above and others can be obtained according to stress boundary conditions on the upstream and downstream surfaces.

3 EXAMPLES

3.1 *Example 1—a cylindrical arch dam*

As the first test of this method, a very simple cylindrical arch dam of constant thickness, a typical one studied by many researchers [5], is investigated. The shape is defined in Figure 1. The elastic

modulus and Poisson's ratio for the dam material are 20000MPa and 0.15. The bulk density of the cylindrical arch dam is 2.4kN/m^3. The elastic modulus of the dam foundation is assumed to be rigid, equal to 10.0×106MPa. For being convenient to compare the results with others, only water-pressure is considered. The configuration of finite element mesh is shown in Figure 2 and computation results are given in Figure 3 and 4.

As shown in Figure 3 and 4, the hoop and the vertical equivalent stresses compare favorably with the results obtained by O.C.Zienkiewicz with shell finite element or by U.S. B.R. with the trial load method [5].

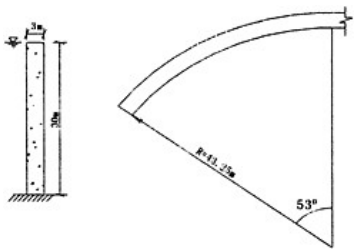

Figure 1. Shape of a cylindrical arch dam.

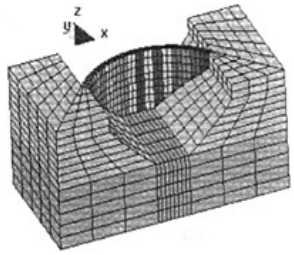

Figure 2. Finite element calculation model.

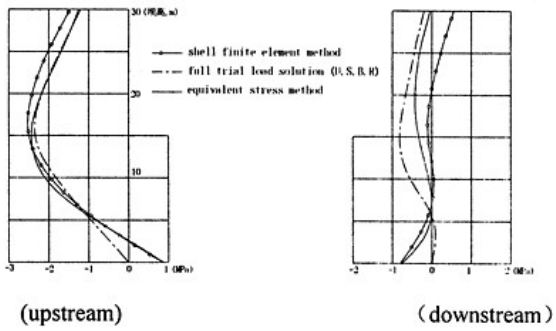

Figure 3. Hoop equivalent stress on central "Cantilever".

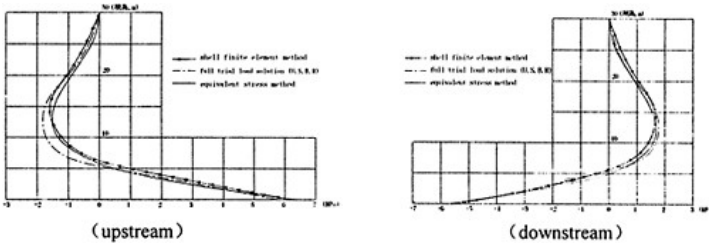

Figure 4. Vertical equivalent stress on central "Cantilever".

4 EFFECT OF MESH SIZE ON ARCH DAM EQUIVALENT STRESSES

The stresses at the heel or the toe of an arch dam from conventional FEM are very sensitive to the mesh size. Could the situation be changed by use of equivalent stresses? The answer will be obtained in this section. In order to explain the effect of mesh size clearly, the same dam with various meshes is used in the radial, arch axial and vertical directions.

4.1 *Effect of mesh size in the radial direction*

The calculation models respectively have four different meshes, namely 1 to 4 elements in the radial direction and the same elements in other directions. Table 1 shows the maximum and the minimum principal stresses on the upstream and downstream surfaces of the cylindrical arch dam.

As for the cylindrical arch dam, it is evident that the results are of excellent computation accuracy even with a quite coarse mesh, in which the maximum of the first principal stress is 6.623MPa and the minimum of that is 6.555MPa. Their relative error is only 1.03%. Similarly, the relative error of the third principal stress is also slight with the value of 1.07%. Both of them lie within engineering accuracy.

4.2 *Effect of mesh size in the arch axial and vertical directions*

In this section, the same example is given to test the effect of mesh size in the arch axial and vertical directions again. Original computation mesh is with two elements in the radial direction and relatively coarse elements in the arch axial and vertical directions. Here we change the original elements into 2×2, 3×3 and 4×4 in arch axial and vertical directions while the elements numbers along radial direction is unchanged for the cylindrical arch dam.

In Table 2, the maximum and the minimum principal stresses on upstream and downstream surfaces of the cylindrical arch dam are given for the different finite element meshes. In general, the relative errors also lie within engineering accuracy. The result shows that the equivalent stresses are not very sensitive to the mesh size although there is a visible difference between the normal stresses on central “Cantilever” of original mesh and those of fine meshes.

Table 1. Maximum principal stress on upstream and minimum principal stress on downstream surfaces for the cylindrical arch dam.

Number of elements in radial direction	1	2	3	4
σ1 (MPa)	6.613	6.623	6.578	6.555
σ3 (MPa)	−5.873	−5.876	−5.836	−5.813

Table 2. Maximum principal stress on upstream and minimum principal stress on downstream surfaces for the cylindrical arch dam.

		Fine mesh		
Principal stress	Original mesh	2×2	3×3	4×4
σ1(MPa)	6.623	6.443	6.408	6.401
σ3(MPa)	−5.876	−5.732	−5.705	−5.696

5 CONCLUSION

Based on the finite element analysis, the equivalent stress computation method developed in this paper combines the advantages of FEM and trial load method. The arbitrary geometries, and arbitrary thickness and material property variations, as well as arbitrary loading conditions can be considered in this method with the advantages of conventional FEM. Moreover, the enhanced assumed strain elements developed by J.C.Simo and M.S.Rifai can be used to simulate the bending behavior of an arch dam properly. The equivalent stresses are consistent with that of the trial load method because of the straight-linear distribution assumption of main stresses along the radial direction. One example mentioned above demonstrate the practicability of this method. The equivalent principal stress formulas on upstream and downstream surfaces are also given in this paper. In addition, the examples also demonstrated that equivalent stresses of arch dam are not very sensitive to the mesh sizes. The study on effect of mesh size shows that the equivalent stresses can be used to evaluate the arch dam safety as those of trial load method.

REFERENCES

[1] Li Tong-chun (1989) *Study on limit state design criterion for arch dams.* PhD thesis, Hohai University.
[2] Fu Zuo-xin (1993) The analysis and computation of structure mechanics in hydraulic structure engineering. *The application of finite element method on design of arch dams.* Hohai University Press, 28–43.
[3] Lin Shao-zhong, and Yang Zhong-hou (1987) Load distribution displacement method for arch dam stress analysis. *Journal of Hydraulic Engineering.* 1:17–25.
[4] The United States Bureau of Reclamation for the Arch Dam Committee. The group of arch dam, translators. *Design of arch dams.* Beijing: Hydroelectric Press, 1984.6:129–145.
[5] O.C.Zinkiewicz, and Y.K.Cheung (1664) *Finite element method of analysis for arch dam shells and comparison with finite difference procedure,* In J.R.Rydzewski: *Theory of arch dams,* symposium publications division Pergamon Press, 1664.4:123–140.
[6] J.C.Simo, and M.S.Rifai (1990) A class of mixed assumed strain methods and the method of incompatible models, *Int. j. numer. methods eng.* 29:1595–1638.
[7] U.Andelfinger, and E.Ramm (1993) *EAS-elements for two-dimensional, three—dimensional,* plate and shell structures and their equivalence to HR—elements, *Int. j. numer. methods eng.* 36:1311–1337.

New Developments in Dam Engineering—Wieland, Ren & Tan (eds),
© 2004 Taylor & Francis Group, London, ISBN 04 1536 240 7

Seismic strengthening of embankment dam with sandy shell material

Li Wanglin, Li Zongli & Yin Zongze
College of Civil and Engineering, Hohai University, Nanjing, China

ABSTRACT: Core dam with sandy shell is a primary type of earth dam of large reservoirs in Shangdong province of China. The main characteristics of this kind of earth dam are its body with wide core wall, loose sandy shell, and usually existing possibility of liquefaction and instability at dam slope and foundation. Through practice of two typical projects that were strengthened by different methods, the paper introduces the seismic strengthening effect of core dam with sandy shell. The main methods applied in projects include vibroflotation, vibro-roller and riprap compaction. Finally, the opinions and experiences on seismic strengthening design of core dam with sandy shell are proposed.

1 INTRODUCTION

A great number of reservoirs had been built at Shangdong province of China in last century 60's, most large reservoirs earth dam were core dam with sandy shell. Most of them kinds of dam are about 40m in height, 6~8m in crest, up slope 1:2.75~1:3.25, down slope 1:2.5~1:3. The core walls are 3~6m in dam crest, 50~85m in bottom width, core wall slope 1:0.75~1:1.5. The dam shell material is usually made of coarse sand, a few of dam is medium fine sand or mixed material by sand and clay. The core wall material is made of clay. The type of cut-off is usually trench made of clay, 6~10m in bottom width.

The primary problems of core dam with sandy shell: (1) the compactness of dam shell and base are smaller than original design values. The relative density in there is only 0.3~0.4, and dry density 14.0~15.5kN/m^3. So, dam body occurs easily crack, slump and slip, and is likely to take place seismic liquefaction and instability. (2) The dam body exists permeable deformation that threatens dam safety due to imperfect cut-off trench, or no cut-off building in some project. (3) After great flood "75.8" happened in Henan province of China, most of reservoirs had been raised height of dam. But construction quality of core wall is poor, or joint location of new and old core wall is not correct. Above of problems, many reservoirs were listed as key large danger reservoirs in China. The seismic strengthening design is needed for key large danger reservoirs.

2 SEISMIC STRENGTHENING DESIGN METHOD

The task of seismic strengthening design of earth dam is to eliminate liquefaction of dam shell and foundation, and to enhance stability capability of resistance earthquake.

2.1 *The evaluation method of seismic capability of earth dam*

The evaluation method of seismic capability of earth dam includes seismic liquefaction method and dam slope stability analysis method under seismic load.

The seismic liquefaction evaluation method includes site test judgment method and finite element dynamic analysis method. The site test judgment method mainly includes standard penetration test and shear wave velocity test method, and so on. The finite element dynamic analysis method includes total stress method and effective stress method. The standard penetration test evaluation method is to judge possibility of sand liquefaction by contrasting of standard penetration test blow count and critical value. The shear wave velocity judgment method is to judge by contrasting of investigation shear wave velocity and critical value of sand liquefaction. The total stress method is to judge possibility of liquefaction by contrasting of shear strength from liquefaction experiment and dynamic shear stress obtained from total stress analysis method. The effective stress method is to judge possibility of liquefaction by liquefaction index from effective stress analysis method.

The dam slope seismic stability evaluation method includes quasi-static and dynamic stability analysis method. The principle of quasi-static method is to add seismic inertia force to slope as static load, then to analyze according to static method. The principle of dynamic stability analysis is to obtain static, dynamic stress and dynamic pore water pressure, then to analyze. Because dynamic stability analysis method can take consideration of dynamic pore water pressure of saturation sand during earthquake, its method can obtain true evaluation for core dam with sandy shell.

2.2 *Seismic strengthening design method*

The step of seismic strengthening design includes evaluation of seismic performance of dam body and analysis existing problem firstly, then making a strengthening scheme, finally, evaluating feasibility.

The strengthening method to eliminate liquefaction of sand and slope slip includes densification and kentledge method. The aim of densification method is to raise degree of compaction in order to enhance seismic performance of sand itself. This method is usually used to strengthen loose sandy dam slope. The practical densification method includes vibroflotation and vibro-reller compaction method. The aim of kentledge method is to raise surrounding pressure of sand in order to enhance seismic performance of sand itself. This method is usually used to strengthen loose sand slope and dam foundation. The practical method is riprap method.

According to characteristics of core dam with sandy shell built in Shangdong province of China, combined strengthening schemes are proposed in this paper. The common combined types are vibroflotation-kentledge, vibro-roller-kentledge and kentledge method. The seismic strengthening design method is introduced in lower section according to practical projects of Andi reservoir and Yanma reservoir at Shangdong province.

3 SEISMIC STRENGTHENING DESIGN PRACTICAL PROJECTS

3.1 *The project application of combined of vibroflotation and kentledge method*

Andi reservoir with capacity of 7.49 hundred million cubic meters is located at Mengying county of Shangdong province, 7 seismic intensity region. The type of dam body is core dam with sandy shell. The traverse section is seen as Figure 1. Its foundation of dam toe and heel were made of loose

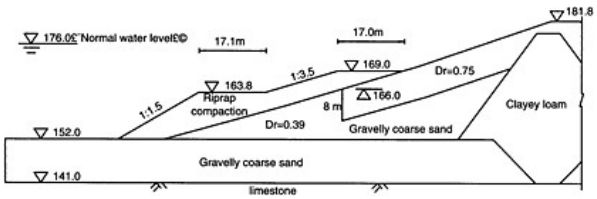

Figure 1. The transverse section of Andi reservoir earth dam.

gravelly coarse sand, and its shell was divided into coarse sand region and medium sand region which relative densities are approximate 0.4. Andi reservoir, which was listed as one of the first group of key large danger reservoir in China, was a first strengthening and eliminating danger project by virboflotation method.

During period of strengthening design the seismic performance of current dam section is evaluated by total stress analysis method and effective stress analysis method respectively. The result from total stress analysis shows that surface layer of up slope of dam is likely to occur liquefaction, maximal depth 8m, as well as local region at up and down foundation outward dam toe and heel. The result from effective stress analysis shows that surface layer of up slope is likely to occur liquefaction as same as total stress analysis, but maximal depth 6m, and that down slope is not satisfy demand of seismic stability and the maximal depth at instability scope is about 8m.

Strengthening scheme: (1) Dam slope up level 166.0m is strengthened by vibroflotation method. Strengthening depth is 8m. (2) Dam slope below level 169.0m and dam heel foundation are strengthened by riprap compaction. Weight flats are built at level 163.8m and 169m respectively. Above scheme is demonstrated on Figure 1.

After dynamic analysis for design scheme, the results shows that dam slope and foundation will eliminate possibility of liquefaction and satisfy demand of seismic stability.

The site vibroflotation test had made before strengthening construction. The test had divided into 5 group taking considerations of two kinds of vibration depth (6.5m, 8.0m) and of three kinds of vibroshockor power (30, 55 and 75KW). The test results are followed: (1) The relative density of sand strengthened by vibroflotation method can be raised from 0.22 to about 0.75. So dam slope stability can be enhanced significantly (2) The strengthening effect is better when sand is at saturation condition. Under same conditions of vibroflotation power and depth, the strengthening density of saturation sand is high about 15% than that of instauration. So, the dam slope above saturation line should add water to saturation condition during construction. (3) According to shock hole spacing and depth, the vibroshockor power should chose properly in order to get optimum effect, short time and economy. The parameters chosen in test are outlined in Table 1.

After construction the standard penetration tests were made at strengthening region. The check results are seen in Table 2. The test shows that both gravelly coarse sand region and gravelly medium sand region reaches design demand. The pass percent of 39 checking points relative density distributed at gravelly sand region is 96.8%.

Table 1. Vibroflotation parameters.

Scheme	Soil type	Pole depth/m	Power/kw	Longitudinal spacing	Transverse spacing
A	Coarse sand	6.5	55	1.5	1.3
B	Coarse sand	8.0	75	2.0	1.73
C	Medium sand	6.5	30	1.5	1.3
D	Medium sand	8.0	75	2.0	1.73

Table 2. Check results.

		Before strengthening		After strengthening	
Scheme	Soil type	Relative density	Standard penetration blow count	Relative density	Standard penetration blow count
A	Coarse sand	0.39	4~7	0.75	14~28
B	Coarse sand	0.39	4~7	0.75	16~27
C	Medium sand	0.42	4~6	0.75	11~23
D	Medium sand	0.42	4~6	0.75	14~28

3.2 *The project application of combined of vibro-roller and kentledge method*

Yanma reservoir with capacity of 2.03 hundred million cubic meters is located at Zaozhuang municipality of Shangdong province, 7 seismic intensity region. The type of earth dam is core dam with sandy shell. The shell and foundation are all made of gravelly coarse sand, and its relative density is only 0.36. This dam appeared two times of dam slope slip in past. This reservoir was listed as one of the secondary group key large danger reservoir in China. The current transversal section of dam is seen Figure 2.

In seismic strengthening design, current seismic performance of dam body was evaluated by using the shear wave velocity judgment method and effective stress method respectively. The shear wave velocity at depth 7m is 140 m/s~160 m/s under condition of 7 seismic intensity, but the correspond critical value is 145~165m/s. The results show that the possibility of liquefaction inside depth 7m at up dam slope exists, but that there is no possibility below 7m and dam foundation. The results from effective stress analysis shows that up dam slope is likely to occur liquefaction, depth 3~4m, but that dam foundation is no possibility. The safety coefficient of seismic stability is less than 1.0. The instability region locates at level 113~128m.

Dam strengthening scheme: The dam shell above level 117.8m is to strengthen by vibro-roller compaction method. The shell below level 120.8m is to strengthen by riprap method and to build two additional weights flat at level 120.8m and 117.5m respectively. The detail scheme is seen Figure 2. Using dynamic analysis the liquefaction will be eliminated after strengthening, and dam slope satisfies demand.

The vibro-roller parameters are 13t vibrating compactor, the thickness of 40~50cm each compaction layer, and 6,7 times compacting. The site quality check shows that the dry density exceeds 18kN/m^3 and relative density of gravelly coarse sand exceeds 0.75 after strengthening.

3.3 *The seismic strengthening scheme of kentledge method*

The application of riprap method had researched in detail during of Yanma reservoir strengthening design. The detailed design scheme is to build a additional weight flat with width 7m at level 128m, to riprap stone along slope below that flat, and to build a flat at level 115.0m also. The sandy shell above level 126m is to take away old, lay and compact again, the relative density of new shell reaches and exceeds 0.75. The detail scheme is seen Figure 3.

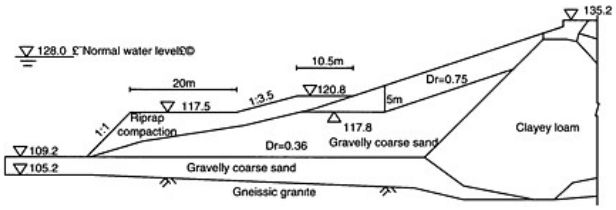

Figure 2. The transverse section of Yanma reservoir earth dam.

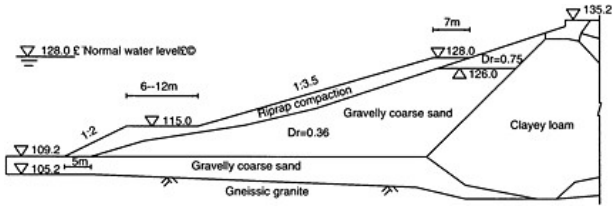

Figure 3. The other transverse section of Yanma reservoir earth dam.

After analysis the liquefaction of dam sand will be eliminated after strengthening, and dam slope satisfies demand. This confirms that it is effective to strengthen core dam with shell by kentledge method.

4 OPINIONS AND CONCLUSIONS

4.1 *The opinions on evaluation method*

Through the seismic liquefaction evaluation of Yanma reservoir earth dam, the result shows that the liquefaction scope of saturation sand obtained from site shear wave velocity test method and effective stress analysis method is agreed. This confirms that the shear wave velocity method is reliable to evaluate saturation sand liquefaction, but this method is only applied to site and not to design scheme. The finite element dynamic analysis is an effective method, especial effective stress method because of consideration of dynamic pore water pressure.

The stability safety coefficient of up dam slope of Yanma dam is 1.32 by quasi-static method analysis, and satisfies stability demand. But the safety coefficient is less than 1.0 by dynamic analysis, and its is not satisfies demand. Two conclusions is not agreed. The reason is that the quasi-static analysis method is not consider the dynamic pore water pressure effect to shear strength. In fact, dynamic pore water pressure can affect shear strength of sand, and lead loss of shear strength in some condition. This confirms that quasi-static analysis method is not rational, and that conclusion from this method is incredulous.

4.2 *Advantages and shortcomings of various strengthening method*

The principle of vibro-roller method and vibroflotation method is to increase density degree in order to eliminate sand liquefaction. The investment of vibro-roller method is low, but vibroflotation is high. Construction condition of both methods is poor. Both method constructions need long time, affect reservoir storage, and is not applied to strengthen loose sandy shell and foundation below dead water level. The investment of the kentledge method is low comparing with other method. Its construction time is short, procedure is simple, and is not affect reservoir storage. Although the kentledge method is not direct applied to compact loose sand, it can increase initial stress so that the resistance capability of liquefaction would be raised. The kentledge method is a familiar method to strengthen dam slope and foundation below dead water level in practice, kentledge at dam heel is helpful for dam slope seismic stability.

4.3 *Experience*

When strengthening scheme is combined by kentledge method and another, designer should pay more attentions to joint region of two method, and ensure enough overlapping length in order to satisfy seismic demand at joint region. The double step flat scheme is reasonable compared with single step. Its scheme can not only adjust initial stress and raise resistance capability of liquefaction, but save investment.

REFERENCES

[1] Li Wanglin. The effective dynamic stress analysis of Yanma reservoir earth dam[A]. The 3rd national youth Geotechnical mechanics and engineering proceeding—geomechanics theory and practice[C]. Nanjing, China: Hohai publisher, 1998, 415–419.

[2] Li Wanglin. The practice of Andi reservoir earth dam strengthening using vibroflotation method[A]. earth dam and geotechnical mechanics[C], Beijing, China: Earthquake publisher, 2001, 315–317.

This page intentionally left blank.

New Developments in Dam Engineering—Wieland, Ren & Tan (eds),
© 2004 Taylor & Francis Group, London, ISBN 04 1536 240 7

Multi-objective linear programming method of optimizing foundation deformation modulus for high arch dam

Liu Defu & Peng Hui
China Three Gorges University, China

ABSTRACT: The good deformation characters of foundation are severely requested when a high dam especially high arch dam is constructed on the foundation. But it does not mean the higher modulus the better working condition of arch dam. It is a big difficult problem for designers to rationally make a design which not only does good to the stress, stability and deformation for arch dam, but also can save a large sum of money on treating foundation through man-made methods. This paper establishes an optimization model for multi-objective linear programming of deformation modulus for arch dam foundation based on the unit deformation modulus method for calculating the stress of arch dam. In the optimization model, the deformation modulus E which varies with different elevation for arch dam foundation is chosen as design variable and through using multi-objective linear programming method the optimal deformation modulus is solved which on the one hand avails the best working condition of arch dam and on the other can reduce the treatment costs to the minimum within the value bound of deformation modulus that artificial methods can reach. The model created in this paper is used to solve the optimal deformation modulus of a high arch dam in China. The calculated results indicate that the optimization model is reasonable and practical and also provides strong technique support to designers and foundation treatment.

1 INTRODUCTION

As a kind of safe and economic type of dam, more and more arch dam will be constructed in China hydroelectric engineering project, especially high arch dam. It is well known that arch dam has strict demand for terrain and geological condition. Under common circumstance, the natural condition often can't directly meet the requirement of arch dam constructing. As a result, foundation treatment, such as excavation, grouting and so on, is needed to improve the adaptability of foundation to arch dam. However, foundation treatment so far mainly depends on experiences and field test because of lacking viable and effective methods. Similarly, the depth and strength of foundation treatment is often decided by the height of arch dam rather than considering the distribution of stresses and displacement in arch dam. In fact, the stresses and displacement in arch dam not only has relation with the value of foundation modulus, but also has close relation with the modulus distribution in foundation. The aim of foundation treatment mainly focuses on the adaptability between foundation deformation and upper dam structures. But the aim does not mean the higher strength of foundation modulus the better working condition for arch dam. This paper establishes an optimization model for multi-objective linear programming of deformation modulus for arch dam foundation based on the unit deformation modulus method for calculating the stress of arch dam. In the optimization model, the deformation modulus E which varies with different elevation for arch dam foundation is chosen as design variable and through using multi-objective linear programming method the optimal deformation modulus is solved which on the one hand avails the best working condition of arch dam and on the other can reduce the treatment costs to the minimum within the value bound of deformation modulus that artificial methods can reach. The model is used to solve the optimal deformation modulus of a high arch dam in China. The calculated results indicate that the optimization model is reasonable and practical and also provides strong technique support to designers and foundation treatment.

2 THE OPTIMIZATION MODEL FOR MULTI-OBJECTIVE LINEAR PROGRAMMING OF DEFORMATION MODULUS FOR ARCH DAM FOUNDATION

2.1 *Design variable and unit deformation modulus method for calculating the stress of arch dam*

Because arch dam design criterion so far about stresses calculating (according to references [2] and [4]) based on the linear-elastic supposition, the stresses, internal forces and displacement of arch dam will take proportional change with the foundation modulus if maintaining the size, shape, materials and loads of arch dam unchangeable. Supposed that the foundation rock mass can be divided into n areas and each area the natural modulus defines as E_{0i}(i=1, 2,…, n). After manual treatment, the modulus of each area become E_i(i=1, 2,…, n), thus:

$$E_i = (1+\lambda_i) E_{0i} \quad (i=1, 2,\ldots, n) \tag{1}$$

where λ_i(i=1, 2,…, n) is design variable. When the value of λ_i is confirmed, the aim of treatment in each area will be known.

Under the condition of natural modulus E_{0i}, σ_{ij}^k in k point and ij direction equals:

$$\sigma_{ij}^k = \sigma_{ij}^{k0} + \sum_{m=1}^{n} \Delta\sigma_{ij}^{km} \lambda_m \tag{2}$$

Similarly, under the condition of natural modulus E_{0i}, internal force Δf_i^{km}. According to principle of superposition, after manual treatment, the internal force in k section and i direction will be expressed by formula (3) as follows:

$$F_i^k = F_i^{k0} + \sum_{m=1}^{n} \Delta f_i^{km} \lambda_m \tag{3}$$

At the same time, Δu_i^{km} means displacement increment in k section and i direction brought by the increment modulus $\Delta E_m = \lambda_m E_{0m} = 1$. So, after manual treatment, the displacement in k section and i direction changes into:

$$U_i^k = U_i^{k0} + \sum_{m=1}^{n} \Delta u_i^{km} \lambda_m \tag{4}$$

Before doing optimization analysis of foundation modulus, Δu_i^{km} should be calculated in advance then given any kind of modulus distribution (given λ_i (i=1, 2,…, n)) in foundation the field of stresses, displacement and internal forces in arch dam can be obtained.

2.2 *Objective function*

The goal of optimization is to find such kind of foundation deformation modulus that optimizes the situation of stresses, stability and deformation in arch dam and reduces the cost of foundation treatment. Clearly, such problem belongs to multi-objective optimization problem.

Supposed that the maximum compressive stress in arch dam is σrmax and the maximum tensile stress is $\sigma_{l\max}$. Obviously, normal stresses in any point of arch dam have to meet the demand of formula (5) as follows:

$$-\sigma_{l\max} \le \sigma_{ij}^{k} \le \sigma_{r\max} \tag{5}$$

the less value of $\sigma_{r\max}$ and $\sigma_{l\max}$, the higher degree of safety of arch dam as well as the better situation of stresses.

As far as stability and safety are concerned, in order to search for stability and safety expressed by linear design variable, the traditional coefficient of stability and safety is clearly not applicable. From analyzing $(S^k - N^k)$ (here S^k stands for composition of forces along downstream direction in the No. k layer of spandrel, N^k means composition of forces along vertical direction of downstream in the No. k layer of spandrel) we can know that the less value of $(S^k - N^k)$ the higher stability of the No. k layer of arch dam. Supposed that the maximum value of $(S^k - N^k)$ in each arch layer is $SJN_{\max}$, then we can know:

$$S^k - N^k \le SJN_{\max} \tag{6}$$

Therefore, $SJN_{\max}$ can be used to assess the general stability of arch dam. The less $SJN_{\max}$, the better stability of arch dam.

Some arch dam are constructed in the places where the geometric shape of foundation is asymmetric. As a result, the deformation of arch dam often shows asymmetry. Sometimes distorted deformation which does harm to arch dam will take place. In order to make the deformation in arch dam symmetrical, we can suppose that the distance between center point of one certain arch layer with elevation z_i and the point which appears the maximum displacement at the same elevation and arch layer is l_i (i=1, Λ, A, n). The maximum value of l_i (i= 1, 2, Λ, n) at different elevation can be defined as $l_{\max}$. Apparently, the less $l_{\max}$, the more symmetrical deformation will be gained in arch dam.

$$l_i \le l_{\max} \tag{7}$$

Concretion grouting is a main method to be used to treat the foundation in order to improve the value of foundation deformation modulus. Hence, the cost of foundation treatment is largely decided by the fee consumed by grouting. Supposed that the unit cost of grouting is C_0 (here C_0 stands for the grouting fee used by per cubic meter foundation rock mass with an increment of modulus 1Gpa), then the total fee C of foundation treatment can be expressed as follows:

$$C = C_0 \sum_{m=1}^{n} \Delta E_m V_m = C_0 \sum_{m=1}^{n} \lambda_m E_{0m} V_m \tag{8}$$

The aim of optimization is to make $\sigma_{l\max}$, $\sigma_{r\max}$, C, $SJN_{\max}$ and $l_{\max}$ to the minimum. Therefore the objective function can be written as follows:

$$f(x)\rightarrow \begin{cases} \min\limits_{x\in X}\sigma_{l\max}(x) \\ \min\limits_{x\in X}\sigma_{r\max}(x) \\ \min\limits_{x\in X}C(x) \\ \min\limits_{x\in X}l_{\max}(x) \\ \min\limits_{x\in X}SJN_{\max}(x) \end{cases} \tag{9}$$

2.3 *Constraint condition*

Through manual treatment of foundation, the foundation modulus can be improved. But it can't be improved discretionarily. In order to realize the optimization of modulus in real project, the maximum value of λ_i (i=1, 2, …, n) should be limited. Clearly, under any circumstances the foundation modulus after manual treatment cannot but improve. Therefore, the constraint condition of λ_i (i=1, 2, …, n) will be as follows:

$$0\leqslant \lambda_i \leqslant \lambda_{i\max}\ (i=1,\ 2,\ \ldots\ldots,\ n) \tag{10}$$

Here $\lambda_{i\max}$ (i=1, 2, …, n) is defined as the maximum percentage of foundation modulus which can be improved in No. i area by use of treatment. In reference [6] a lots of real projects and its' corresponding grouting methods and effects are enumerated. From this reference, after concretion grouting,, the foundation modulus can be improved from percentage 10 to 80 and in most real projects it can be improved 45% in average. For some real projects lacking of experiment materials, the value of $\lambda_{\max}$ can be chosen from section 0 to 0.8.

2.4 *The education of optimization model*

For the sake of simplifying formula (9) from multi-objective optimization function to single-objective optimization problem, the method of linear weighting sum is applied to construct objective function as follows:

$$Obj(x)=k1\frac{\sigma_{r\max}}{[\sigma_r]}+k2\frac{\sigma_{l\max}}{[\sigma_l]}+k3\frac{l_{\max}}{l_f}+k4\frac{C}{C_j}+k5\frac{SJN_{\max}}{SJN_f} \tag{11}$$

In formula (11), k1~k5 here are weighting coefficients for branch objective, $[\sigma_l]$ is the maximum allow tensile strength and $[\sigma r]$ stands for the maximum allow compressive strength, l_f is defined as $l_{\max}$ which takes place under certain foundation modulus and different kinds of external loads, C_j is norm value of foundation treatment fee, SJN_f represents $SJN_{\max}$ which appears under certain foundation modulus and different kinds of external loads.

The aim of optimization is to make *Obj(x)* much less as soon as possible, namely:

$$\min Obj(x),\ \ x\in X \tag{12}$$

Here X meets the demand of constraint condition in formula (10).

From formula (11) and (12) it is obvious that this optimization problem is nonlinear program-ming problem. Before optimization calculation the maximum value should be selected at first, then minimum calculation takes place. For transferring nonlinear programming problem into linear programming problem, four other design variables are needed. So the design variable changes into:

$$x=\{x1, x2\} \tag{13}$$

Here: $x_1=\{\lambda_1, \lambda_2, \Lambda, \lambda_n\}$ and $x_2=\{\sigma_{r\max}, \sigma_{l\max}, l_{\max}, SJN_{\max}\}$

$x1$ meets requirement of formula (10) and $x2$ meets demand of formula (5), (6) and (7).

Now the optimization model of multi-objective linear programming of deformation modulus for arch dam foundation can be constructed:

$$minObj(x), \tag{14-1}$$

$$\text{s.t. } \sigma_{ij}^k(x1) \le \sigma_{r\max} \quad -\sigma_{l\max} \le \sigma_{ij}^k(x1) \tag{14-2}$$

$$l_i \le l_{\max} \tag{14-3}$$

$$0 \le x1_i, x1_i \le \lambda_{i\max} \tag{14-4}$$

$$S^k(x_1)-N^k(x_1) \le SJN_{\max} \tag{14-5}$$

2.5 *The solution of the optimization model of multi-objective linear programming of deformation modulus for arch dam foundation*

According to formula (14), there are many kinds of methods can be used to solve this linear programming problem. In formula(11) applying different weighting coefficient k1~k5 will obtain different optimization results. The method of selecting weighting coefficient is plentiful (according to reference [5]). In this paper, the value of weighting coefficient can be used to indicate the importance of respective branch objective. For example, if the main aim is to reduce the maximum tensile strength, then the value of k2 equals 1.0 and other weighting coefficient equals 0. By the same token, if the main objective is to not only reduce the stresses but also reduce the foundation treatment fee, then you can choose $k1$, $k2$, $k4=1$, $k3=0$, $k5=0$. Of course you can select different kinds of combined weighting coefficient in order to get different optimization situation and results.

3 CONCRETE APPLICATION AND CALCULATION EXAMPLE

There is a high bi-curvaceous arch dam with the maximum height of 305m. The elevation of construction foundation is 1580m and the elevation of dam crest is 1885m. The valley of dam site appears apparently asymmetrical with slight slope in left side and steep slope in the right. The foundation rock in dam site mainly consists of metamorphosis rock. The main geological disfigurements include f_5, f_8, f_{13}, f_{14} faults and different kinds of cracks and crevice. Furthermore, because the both sides of dam site appear asymmetrical and deformation modulus in left bank is low and high in right bank, under action of external loads the asymmetrical deformation and displacement have taken place in dam. In order to change the asymmetrical displacement and stresses situation in dam, in this paper the method of optimization model of multi-objective linear programming of deformation modulus for arch dam foundation is put forward and applied.

According to geological investigation and rock mechanics experiment, the natural deformation modulus of foundation rock near dam site is confirmed. The modulus distributed with elevation is listed in table 1.

The calculation condition which consists of normal water level in upstream and corresponding water level in downstream, silt pressure, dam gravity, falling temperature is selected as initial calculation condition. In terms of initial calculation condition and natural deformation modulus in table 1, the maximum compressive stress $\sigma_{r\max}$ of dam is $9.2MPa$ and the maximum tensile stress $\sigma_{l\max}$ equals $-1.22MPa$. From calculation results, both of $\sigma_{r\max}$ and $\sigma_{l\max}$ exceed the limitation

Table 1. The natural deformation modulus of dam foundation unit: GPa.

Elevation (m)	1885.0	1870.0	1830.0	1790.0	1750.0	1710.0	1670.0	1630.0	1600.0	1580.0
Leftbank	10.0	10.0	10.0	13.0	13.0	12.0	13.0	18.0	17.0	17.0
Rightbank	13.0	16.0	19.0	19.0	19.0	17.0	13.0	13.0	13.0	13.0

Table 2. The eigenvalue of optimization results.

k	Elevation(m)	1885	1870	1830	1790	1750	1710	1670	1630	1600	1580	σ_{max} σ_{min} l_{max}, SJN_{max}
1,0	Left bank	14.2	14.0	13.8	16.6	16.7	15.6	16.6	18.0	19	19	8.89
0,0,0	Right	13.2	16.4	19.0	19.0	19.0	19.0	17.1	13.5	13.4	13.4	−1.3 7.4, 9215
0,1	Left	14.2	12.3	11.0	13.5	16.7	16.3	13.0	18.2	18.3	17.8	9.3
0,0,0	Right	13.0	18.8	19.0	20.2	20.5	21.0	20.4	19.7	18.1	18.3	−0.05 6.48, 7438
0,0	Left	14.3	13.7	13.9	17.3	17.4	16.3	17.1	18.1	18.4	18.3	9.4
1,0,0	Right	13.0	16.45	19.8	19.8	20.3	20.6	21.1	18.3	18.3	18.5	−0.09 5.5, 8380
1,1	Left	14.4	13.8	14.2	16.9	16.7	16.3	16.8	18.2	18.2	18.2	9.17
0,1,1	Right	13.5	16.5	19.2	19.4	19.3	19.3	17.6	13.5	18.1	18.3	−0.081 7.66, 9320
0,0	Left	14.3	13.7	14.3	17.6	17.4	16.6	16.8	18.1	18.3	18.3	9.44
1,1,1	Right	13.4	17.2	20.1	20.3	20.5	21.1	19.8	18.2	18.3	18.3	−0.11 5.39, 7290
1,1	Left	12.6	13.1	14.3	16.2	16.4	16.2	16.3	18.1	18.5	18.4	8.94
1,1,1	Right	13.3	16.3	19.0	19.0	19.0	19.5	18.3	17.5	17.5	17.4	−0.052 6.79, 8945

Here: Plus stands for compressive stress, minus stands for tensile stress (unit: Mpa); the unit of l_{max} is meter and the unit of SJN_{max} is 10kN.

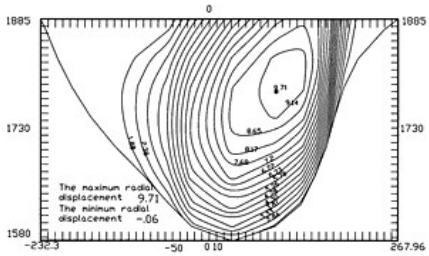

Figure 1. The radial displacement under condition of initial calculation situation with natural deformation modulus (unit: centimeter).

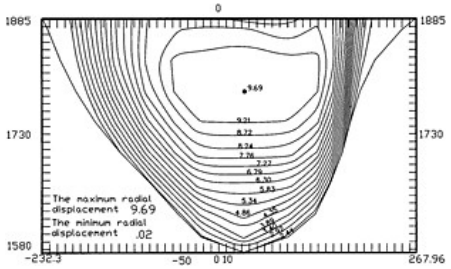

Figure 2. The radial displacement under condition of initial calculation situation with optimized deformation modulus (unit: centimeter).

value of design criterion ($[\sigma_{r\max}]$=9.0MPa and $[\sigma_{l\max}]$=−1.2MPa). When $\lambda_{i\max}$ equals 0.8, under condition of different weighting coefficient the optimized foundation deformation modulus and the eigenvalue of stresses, displacement of dam are illustrated in table 2 by application of this optimization model. According to table 2, different weighting coefficient will lead to different optimization results.

4 CALCULATION RESULTS AND CONCLUSION

From above-illustrated calculation results, we can clearly know that:

(1) When the shape, size, materials, loads of arch dam are confirmed, the stresses and displacement of dam have close relation with foundation deformation modulus. Therefore, through manual treatment to regulate the deformation modulus can ameliorate the field of stress and displacement of dam.
(2) After optimization calculation, the maximum tensile stress of dam can be apparently reduced as well as the maximum compressive stress. Especially, the distribution of displacement of dam appears clearly symmetrical when uses optimized deformation modulus to calculate.
(3) From optimized modulus, foundation rock in left arch spandrel needn't much more grouting to improve the strength and modulus of rock. Similarly, in right spandrel hardly need grouting to change the character of foundation rock. As a result, a great deal of treatment fee can be saved.
(4) In order to get different optimization situation and results it's flexible to select different kinds of combined weighting coefficient.
(5) The optimization model put forward in this paper is worthy of popularizing because the calculation results are reasonable and calculation speed is fast.

REFERENCES

[1] Zhu Bofang, Discussing temperature loads on arch dam, Waterpower, 1984(2).
[2] Liu defu, Multi-objective linear programming method of determining joint closure temperature field for arch dam, Water Conservancy Journal, 1998(8):77–81.
[3] Liu defu Chen guoqi, Optimization of closure temperature field for arch dams, Proceedings of international symposium on arch dams, Hohai University Press, 1992, 10.
[4] Liu defu, Multi-objective nonlinear programming method of determining joint closure temperature field for arch dam, People's Yangtse River, 1997(5):29–31.
[5] Hu Yuda, Practical multi-objective optimization, Shanghai Scientific Technology Publishing House, 1990,4.
[6] Yu Shengbin, Foundation concretion grouting of high arch dam, Waterpower of Yunan, 1996, Vol.15, No. 3:53–58.
[7] Pan Jiazheng, Chen Shihui, Discussion on some problems of high arch dam construction, Scientific Technology Guidance, 1997(2): 17–19.

This page intentionally left blank.

New Developments in Dam Engineering—Wieland, Ren & Tan (eds),
© 2004 Taylor & Francis Group, London, ISBN 04 1536 240 7

Time history analysis of high earth-rockfill dam seismic stability

Liu Hanlong[1], Fei Kang[1], Gao Yufeng[1], & Aly H.Mahfouz[1,2]
[1]*Research Institute of Geotechnical Engineering, Hohai University Nanjing, China*
[2]*Geological & Geophysical Dept., Engineering College, Suez Canal University, Suez-Egypt*

ABSTRACT: The change of high earth-rockfill dam factor of safety of its slope stability during the earthquake can be predicted by nonlinear dynamic finite element method. The minimum factor of safety of slope stability occurs at one moment during the process of earthquake, it is unsuitable to evaluate the anti-slide stability of the slope under seismic load using this value. In the paper the minimum mean safety factor is presented as evaluating index. The 0.65 times of maximum amplitude of vibration is taken as the mean amplitude of vibration to evaluate changes of safety factor with the ground motion time history. The anti-slide stability of a high earth-rockfill dam is evaluated by using the minimum mean safety factor. The result is compared with one of the pseudo-static methods.

1 INTRODUCTION

Stability analysis of earth-rockfill dam resisting earthquake is a very important task in geotechnical engineering. Usually, seismically induced permanent displacements of earth dams or the safety factor of slope are used to estimate the stability of an earth-rockfill against earthquake loads.

The first method to predict seismically induced permanent deformations of slopes was developed by Newmark (1965)[1]. Newmark made an analogy between the soil in a potentially unstable slope and a rigid block resting on an inclined plane. The assumption of material rigidity implies that the shear strength of the soil is equally mobilized along the critical failure plane. It is also assumed that the interface between the block and inclined plane exhibits rigid-perfectly plastic stress-displacement behavior. As the rigid block is subjected to dynamic motion, it will slide down the inclined slope when a certain level of acceleration is exceeded, and there will be a permanent displacement of the sliding mass in the downslope direction. The concept of this acceleration level, termed the yield acceleration is commonly based on pseudostatic slope stability analysis. The Newmark method has been modified to account for time varying shear strengths and strain hardening or strain softening behavior.

A more elaborate method to obtain permanent deformation of dams due to earthquake was proposed by Lee (1974)[2]. The method is based on the assumption that seismically induced deformations are due to a softening of the soil by seismic shaking so that following the earthquake the dam will settle or deform to a new condition compatible with the new softened stiffness of the soil. Somewhat different methodology was employed by Seed (1979) [3] based on the strain potential concept. In the method, the nodal forces necessary to produce the given amount of strain potential are computed for each element and with these forces being applied to the nodes of the finite element grid, the static analysis is made to determine the continuous configuration of the dam deformed by the earthquake. Similar method of analysis was used by Taniguch et al. (1983)[4] to predict the settlement of embankment during earthquake. Though it is reasonable to use the total permanent displacement during the earthquake as a parameter for evaluating dam stability than use the safety factor of slope, the specific limit value cannot be decided in China due to few engineering experiences.

Nowadays, the factor of safety is usually calculated by pseudo-static analysis or finite element method. The pseudo-static method assumes that the load induced by an earthquake can be regarded as inertia force acting on the earth structure. This inertia force is described by multiplying the mass by the enforced acceleration due to an earthquake. Considering the fact that the acceleration of an earth-rockfill dam changes with height during an earthquake, the acceleration distribution along the height of dam is proposed in "Specifications for seismic design of hydraulic structures (SL203-97, China)" [5]based on the results of nonlinear dynamic analysis of earth-rockfill dam by shear beam method. But sometimes the acceleration distribution decided by this way may have great difference with the actual case, especial to the high earth-rockfill dam. The pseudo-static method using seismic coefficient employs a simple assumption and only considers a particular instant of successive motion of the earth structure in a certain acceleration time history. These defects largely affect the accuracy and reliability of the seismic coefficient method. Therefore this method cannot consider the effect of both enforced acceleration time history and vibration properties of the earth structure, originally.

The finite element method can simulate the process of an earthquake and provides the capability of modeling complex geometries, boundary conditions and wide variations in material properties. Based on the calculated stress histories, the factor of safety at each time can be decided. During the earthquake the factor of safety may drop below one, however, because acceleration reverse during an earthquake, the factor of safety would be less than one for only an instant. So the stability of a slope during an earthquake excitation cannot be reflected by the minimum safety factor.

Recently, in order to estimate the slope stability during earthquake, several stochastic methods were developed[6,7]. Based on the stochastic finite element dynamic analysis, the earthquakeinduced permanent displacement and slope stability under seismic load can be obtained. However, the stochastic method can only get the magnitude of the stress, the direction of the stress cannot be decided. So all possible directions combination must be take into account to find the minimum factor of safety against sliding or shear failure. But the stress directions at the dangerous case may be difference with the fact. In this paper, a method to evaluate seismic stability of high earthrockfill dam is proposed.

2 DYNAMIC SEISMIC RESPONSE ANALYSIS

The analysis of dynamic response using finite element method requires the solution of the global dynamic equation of motion as given by the following equation:

$$[M]\{\ddot{\delta}\}+[C]\{\dot{\delta}\}+[K]\{\delta\}=P(t) \tag{1}$$

where *[M], [C]* and *[K]* are the global mass, damping and stiffness matrices for the assemblage of elements, respectively; $\ddot{\delta}$ $\{\delta\}$ are the relative nodal acceleration, velocity and displacement vectors and *P(t)* is the load vector, that, for base excitation can be presented as:

$$P(t)=-[M]\{I\}\ddot{\delta}_g \tag{2}$$

where *{I}* is the identity (i.e., column) vector and $\{\ddot{\delta}_g\}$ is the input base acceleration time history. The absolute displacement, velocity and acceleration can be found directly by adding the corresponding value at the bedrock. The Wilson direct integration is used to solve equation 1 in the time domain.

The nonlinear behavior of soils during seismic excitation are modeled by equivalent linear model. The damping matrix in the equations of motion is obtained through the assemblage of the element damping matrices which are individually based on the Rayleigh damping formulation:

$$[C]^i=\alpha_e[M]^i+\beta_e[K]^i \tag{3}$$

where $[M]^i$, $[C]^i$ and $[K]^i$ are the mass, damping and stiffness matrices for element i, and α_i, β_i are the mass and stiffness proportional Rayleigh damping coefficients, respectively. The selection of Rayleigh damping coefficients α_i, β_i determines the variation of damping with respect to the frequency as expressed by:

$$\lambda_i = \frac{1}{2}(\frac{\alpha_i}{\omega} + \beta_i \omega) \tag{4}$$

where λ_i is the hysteretic damping for element e based on the shear strain level of the material. α_i, β_i, are computed based on the fundamental frequency of the system, ω_1

$$\alpha_i = \lambda_i \omega_1,\ \beta_i = \lambda_i / \omega_1 \tag{5}$$

In recognizing the increasing nature of dynamic shear modulus with increasing confining pressure, the shear modulus is expressed in the following equation:

$$G = kP_a^{1-n}\sigma_m'^n \frac{G}{G_{\max}} \tag{6}$$

where P_a is the atmospheric pressure, $\sigma_m'^n$ the effective mean normal stress, k is the shear modulus constant, n is the shear modulus exponent, G/G_{max} based on shear strain.

3 SLOPE STABILITY ANALYSIS

The slope stability analysis during the earthquake is based on the static stress analysis and dynamic response analysis. Based on static stress σ_{xs}, σ_{ys}, τ_{xys} and dynamic stress σ_{xd}, σ_{yd}, τ_{xyd} computed at each instant of time, both total normal stress σ_i, and shear stress τ_i at any location on the slip surface are calculated according to expression(7)~(11):

$$\sigma_{si} = \frac{\sigma_{xs}+\sigma_{ys}}{2} + \sqrt{(\frac{\sigma_{xs}-\sigma_{ys}}{2})^2 + \tau_{xys}^2}\cos(2\alpha - arctg\frac{2\tau_{xys}}{\sigma_{xs}-\sigma_{ys}}) \tag{7}$$

$$\tau_{si} = \sqrt{(\frac{\sigma_{xs}-\sigma_{ys}}{2})^2 + \tau_{xys}^2}\sin(2\alpha - arctg\frac{2\tau_{xys}}{\sigma_{xs}-\sigma_{ys}}) \tag{8}$$

$$\sigma_{di} = \frac{\sigma_{xd}+\sigma_{yd}}{2} + \sqrt{(\frac{\sigma_{xd}-\sigma_{yd}}{2})^2 + \tau_{xyd}^2}\cos(2\alpha - arctg\frac{2\tau_{xyd}}{\sigma_{xd}-\sigma_{yd}}) \tag{9}$$

$$\tau_{di} = \sqrt{(\frac{\sigma_{xd}-\sigma_{yd}}{2})^2 + \tau_{xyd}^2}\sin(2\alpha - arctg\frac{2\tau_{xyd}}{\sigma_{xd}-\sigma_{yd}}) \tag{10}$$

$$\sigma_i = \sigma_{si} + \sigma_{di},\ \tau_i = \tau_{si} + \tau_{di} \tag{11}$$

Then the factor of safety at every time interval is given by:

$$F_s = \frac{\sum \tau_{fi} l_i}{\sum \tau_i l_i} \tag{12}$$

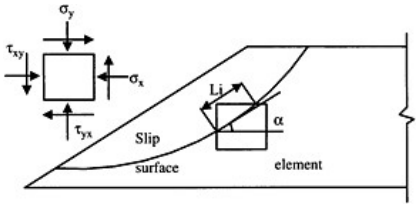

Figure 1. Sketch of the sliding surface.

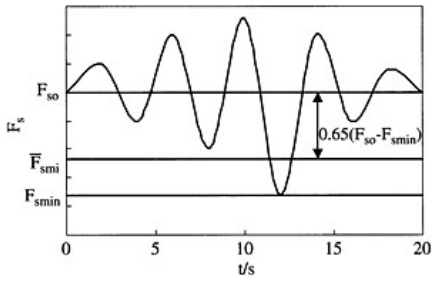

Figure 2. Sketch of the minimum average safety factor.

where l_i is the length of the slip arc segment across the element i (Fig. 1), τ_{fi} is shearing strength of the element i, τ_i is shear stress along the tangent direction of slip arc segment i.

F_{s0} represent the factor of safety before the earthquake, the safety factor changes with time due to earthquake excitation, the minimum value of factor of safety is F_{s0}. Considering the acceleration reverse during an earthquake, the factor of safety drops below one at some time it does not necessarily imply a serious problem, (see Fig. 2). The 0.65 times of the maximum amplitude of vibration of the safety factor is taken as the mean amplitude of vibration to evaluate the change of the safety factor with time period of the ground motion. Then minimum mean safety factor is given as:

$$\overline{F}_{s\min} = F_{s0} - 0.65 \times (F_{s0} - F_{s\min}) \tag{13}$$

4 EXAMPLE

4.1 *Summary*

To illustrate the use of the present procedure, a numerical example is worked out in detail.

A high earth-rock dam with a core wall, locating at Simao City and the boundary of Lancang County Simao Region, Yunnan province-China, which belonging to strong earthquake ward, the dam has a height of 260m. The cross sections of the dam is presented in Fig. 4. During construction period and circulating period, the problem about stability of the dam slope stands out, need the thorough analyse argument.

According to the seismic risk analysis, the horizontal peak acceleration is 0.283g, the vertical acceleration component is taken as 2/3 of the horizontal component, and a coupling coefficient 0.5 is considered. Input base seismic acceleration is shown in Fig. 3.

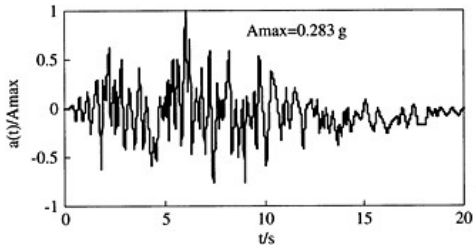

Figure 3. Input base seismic acceleration.

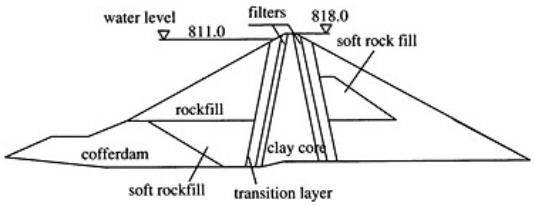

Figure 4. A cross section of the rockfill dam.

Table 1. Dynamic material parameters vs. shear strain.

Shear strain		10^{-6}	5×10^{-6}	10^{-5}	5×10^{-5}	10^{-4}	5×10^{-4}	10^{-3}	5×10^{-3}	10^{-2}	5×10^{-6}
Cofferdam	G/G_{max}	1.00	0.98	0.92	0.56	0.44	0.28	0.22	0.16	0.10	0.13
	λ	0.010	0.010	0.016	0.032	0.054	0.096	0.154	0.192	0.246	0.228
Soft	G/G_{max}	1.00	0.99	0.98	0.90	0.82	0.705	0.538	0.188	0.105	0.085
Rockfill	λ	0.001	0.003	0.007	0.030	0.055	0.075	0.123	0.210	0.228	0.23
Rockfill	G/G_{max}	1.00	0.98	0.92	0.56	0.44	0.28	0.22	0.16	0.10	0.13
	λ	0.010	0.010	0.016	0.032	0.054	0.096	0.154	0.192	0.246	0.228
Transition	G/G_{max}	1.00	0.99	0.98	0.90	0.82	0.705	0.538	0.188	0.105	0.085
Layer	λ	0.001	0.003	0.007	0.030	0.055	0.075	0.123	0.210	0.228	0.23
Filter	G/G_{max}	1.00	0.99	0.98	0.90	0.82	0.705	0.538	0.188	0.105	0.085
	λ	0.001	0.003	0.007	0.030	0.055	0.075	0.123	0.210	0.228	0.23
Core	G/G_{max}	1.00	0.98	0.92	0.56	0.44	0.28	0.22	0.16	0.10	0.06
	λ	0.010	0.010	0.016	0.032	0.054	0.096	0.154	0.192	0.246	0.325

A two-dimensional static stress analysis was carried out first, using a computer program "WWCC"[8]. The program takes into account the nonlinear behavior of soils by using the nonlinear elastic model developed by Duncan. The dynamic seismic response analysis is performed by using the same program "WWCC". The nonlinear behavior of soils is simulated by an equivalent model in the program. The dynamic properties of soils are determined laboratorial and are given in Table 1 and Table 2.

4.2 *Results*

The peak acceleration is increased with the increase of the dam elevation. The maximum dynamic amplification coefficient is about 2.0. The maximum dynamic shear stress occurs at the middle and

Table 2. Maximum shear module parameters.

Material	Cofferdam	Soft rockfill	Rockfill	Transition layer	Filter	Core
K	1580	490	1580	1520	1460	400
n	0.69	0.50	0.69	0.63	0.60	0.51

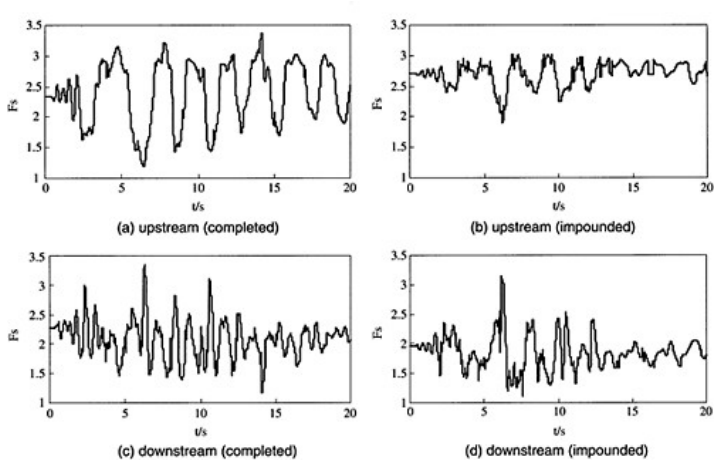

Figure 5. Safety factors time histories.

Table 3. Results of computation.

	Upstream		Upstream	
	Completed	Impounded	Completed	Impounded
The minimum factor of safety	1.193	1.906	1.170	1.089
Time history analysis method	1.594	2.184	1.558	1.393
Pseudo-static method	1.675	2.257	1.616	1.426

under part of dam, the value of maximum dynamic shear stress is about 700–800kPa. And, near the dam slope of upstream and downstream, the value of maximum dynamic shear is about 50–100kPa. When the dam is impounded, the contour law is primarily consistent to that of final completion.

The stability against sliding histories of upstream and downstream dam slope when the dam is completed and is impounded are showed in Fig. 5. When the dam is completed, the safety factor of upstream slope is minimum, the value occurred at 6.40s is 1.193. When the dam is impounded, the safety factor of downstream slope is minimum, the value occurred at 7.82s is 1.089. the minimum safety factors are less than the code value of 1.20. The minimum slope stability safety factor occurs at one moment during the process of earthquake, it is unsuitable to evaluate the anti-slide stability of the slope under seismic load. The minimum mean safety factor is calculated and given in Table 3. The results of pseudo-static method are also listed. Because the pseudo-static method cannot consider both the acceleration time history of earthquake and the dynamic properties of subsoil and earth structures, the factor of safety calculated is different with that provided by the time history analysis method.

5 CONCLUSION

Stability analysis of earth-rockfill dam resisting earthquake is a very important task in geotechnical engineering. The stability of slope during an earthquake excitation cannot be reflected by the minimum safety factor. In this paper, the 0.65 times of the maximum amplitude of vibration of the safety factor is taken as the mean amplitude of vibration to evaluate the change of the safety factor with the ground motion time history. The anti-slide stability of a high earth-rockfill dam is evaluated by using the minimum mean safety factor. The result is compared with one of the pseudo-static method. The results indicate that the proposed method to evaluate the slope stability in this paper is feasible, but the worth standard of stability safety factor, still need be examined and corrected by lots of cases before used for actual engineering.

REFERENCES

[1] Newmark N M. Effective of earthquake on dams and embankments [J]. Geotechnique, 1965, 15(20) 139–159.
[2] Lee K L., Albaisa Aurelio. Earthquake induced settlements in saturated sands [J]. Journal of the Geotechnical Engineering Division, 1974, 100(4):387–406.
[3] Seed, H B. Considerations in the earthquake-resistant designs of earth and rockfill dams [J]. Geotechnique, 1979, 29(3):215–263.
[4] Taniguchi, Whitman R V, Marr W A. Prediction of earthquake induced deformation of earth dams [J]. Soils and Foundation, 1983, 23(4): 126–132.
[5] Specifications for seismic design of hydraulic structures (SL203-97, China)[S]. Beijing: Water Resources and Hydro Power Press of China 1998. (In Chinese)
[6] Liu Hanlong, Permanent deformation of foundation and embankment dam due to stochastic seismic excitation[J]. Chinese Journal of Geotechnical Engineering, 1996,18 (3): 19–27. (In Chinese)
[7] Shao Longtan et al. Finite element analysis for slope stability of earth rock dam under the action of stochastic seismic [J]. Journal of Hydraulic Engineering, 1999, (11): 66–71. (In Chinese)
[8] Qian Jiahuan, Yin Zongze. Theory and Computation of Soil Engineering [M]. Beijing: Water Resources and Hydro Power Press of China, 1996. (In Chinese)

This page intentionally left blank.

New Developments in Dam Engineering—Wieland, Ren & Tan (eds),
© 2004 Taylor & Francis Group, London, ISBN 04 1536 240 7

Design and study for orifice tunnel with multi-stage energy dissipation

Qingliang Liu, Yali Liu & Hao Du
Reconnaissance, Design & Research Institute, YRCC, Zhengzhou, China

Haiting Song
Hydraulic Scientific Research Institute, YRCC, Zhengzhou, China

ABSTRACT: Xiaolangdi Multipurpose Dam Project on the Yellow River, which is an important project in the "eighth five-year-plan" of the country, is one of the most challenging projects acknowledged by the experts both at home and abroad. One of the quite key and contentious design schemes in resolving the challenging technical problems is to convert the division tunnel to orifice tunnel with multi-stage energy dissipation. The arguing is that the accepted dissipation mode inside the tunnel by stages is the first case in the world dam history. If it is not successful, the result cannot be imagined. This article introduces the developing background, research status, key techniques, project design, prototype excess flow observation for orifice tunnel with multi-stage energy dissipation, etc. in details, with the reference to project practice. The practice improves that the orifice tunnel with multi-stage energy dissipation converted from diversion tunnel in Xiaolangdi Project is successful. It stops the gap in energy dissipation inside tunnel in China, makes contribution to the development of the world dam work and puts our theoretical research and project practice in pressure energy dissipation at the advanced level in the world.

1 INTRODUCTION

Xiaolangdi Multipurpose Project, which is national "Eighth Five-year Plan" key project, lies at the outlet of the last gorge situated on the middle reach of the Yellow River, and 130km apart from Sanmenxia Reservoir; it is the key to control flood and sediment of the lower Yellow River. The project is constituted of 17 buildings for retaining dam, flood diversion, water diversion, power generation and irrigation. The dam basically is inclined core rockfill dam, which crest is above EL.281 meters, and the most height of dam is 154 meters. The total discharge capacity is designed to be 17063 cubic meters/s. The underground powerhouse has total installed capacity of 6×300,000kW.

Because of critical sediment problem, complicated geological conditions and rigid application term, the project must find the solutions to a series of most challenging technical difficulties. So, domestic and abroad experts generally regard it as one of the most challenging projects in history of world dam construction. In course of solving these numerous challenges, the key and disputed design program is to adopt energy dissipation spillway tunnels instead of diversion tunnels. It is key because adoption of this program makes the total arrangement come of predicament and it is disputed because the precedent adoption of gradual energy dissipation in tunnel. The result of failure of this precedent technique in such a significant project is out of imagination. Luckily, the successful application of 3 energy dissipation spillway tunnels of multi-stage orifice plates with diameter of 14.5 meters, which replace the diversion tunnels, has already been a successful example.

According to the planning of flood control and regulation of water and sand, total discharge capacity of the project shouldn't be less than 17000 cubic meters/s; at emergency dead water level

of 220 meters, discharge capacity not less than 7000 cubic meters/s. The location is only suitable for local material and takes the specific characteristics of tunnel diversion and deep intake mass tunnels. With regard of the topographic and geologic conditions, all the buildings of flood diversion and sediment ejection and power generation are in the weak left mountains only. In accordance with storage of pure water and ejection of the muddy, together with regulation of water and sand, all the building inlets must adopt concentrated arrangement, so that they will protect each other from being be filled up with sediment. Such was another distinctive characteristic—inlet concentration, chamber concentration and outlet concentration of these buildings.

Xiaolangdi Project is designed to meet the flood standard in 100 years. After the considerable scheme comparison, 3 circular diversion tunnels with diameter of 14.5 meters are in use with maximum releasing capacity of 8270 cubic meters/s. These three diversion tunnels suitable to be situated in the left mountain only occupy much space of the weak left mountain and bring great difficulties for the arrangement of permanent mass tunnels. So, recycle of diversion tunnels is the key technique problem in the general layout and scheme comparison. Originally, changing the diversion tunnel into open spillway tunnel has been in research, but the drawback is that the diversion tunnel is so low that the flow velocity will be up to between 45 and 48 meters, which is far beyond the limits of engineering example. But if pressure spillway tunnel is accepted, we may install sector gate at outlet of diversion tunnel, and control flow velocity. The problem is that 130 to 140 meters high-pressure water head makes the weak left mountain in danger; especially the infiltration of high-pressure water will make the mountain lose stabilization. In order to find the solution to these problems, we have studied steel plate lining and complex lining schemes. For such a great diameter tunnel, whatever a scheme is costly. And also, the drawbacks are thoroughly clear: the construction full of difficulties, the construction time is too long, and the quality is uncertain. On the other side, if discarding the existing three diversion tunnels and creating new relatively large permanent spillway tunnel, it will be hard to come true the general layout, and hard to perfectly meet the demand of application with reluctance.

In 1985, ratified by State Development Planning Committee, Yellow River Water Conservancy Commission together with Bechtel Company, U.S.A., put up the united contour design. On account of inspiration of fishpass hole, the American experts put forword progressive orifice plate energy dissipation. From then on, coordinating with domestic universities and polytechnics and scientific research institutes, the design unit, that is Reconnaissance Planning & Design Institute of Yellow River Water Conservancy Commission put up long-term research and proof about the key technique to orifice plate energy dissipation which is paid much attention by experts. During this period, with scale of 1 to 3.8, the research stuff makes on-the-spot test in Bikou hydropower station sediment tunnel, and get hundreds of first-hand research reports. Based on the tests and in accordance to the general layout of the buildings, a flood of scheme comparison and design optimization has been carried out. The last implement scheme put forward gets the approval of authorized experts headed by academician, Pan Jiazheng and the ratification by State Development Planning Committee.

2 RESEARCH ON ENERGY DISSIPATION SPILLWAY TUNNEL OF MULTI-STAGE ORIFICE PLATE AND ITS DEVELOPMENT

2.1 *Energy dissipation mechanism and its effect*

The research began in 1950s that energy dissipation is created with help of artificial shear friction by swift contraction and expansion of waterflow, which is called pressure dissipater. In 1970s, Canadian Mica Dam took adoption of such technique: two concrete cocks with length of 49 meters and 37 meters respectively and with partition of 104 meters established in the diversion tunnel with diameter of 13.7 meters. The upper cock has three triangle-arranged steel pipes in it and the lower cock has three parallel steel pipes. They are in the control of gate valve respectively. With swift contraction and expansion of waterflow at concrete cocks, the diversion tunnel with water head of 180 meters

reconstructed into permanent bottom outlet. This is lucrative trial and successful fulfillment in test of energy dissipation. American New Don Pedro Reservoir has also a set of spillway bottom outlet with pressure energy dissipation. Above two spillway bottom outlets with pressure energy dissipation were the only examples then and were rarely operated. Especially the New Don Pedro reservoir, it was thoroughly in-tunnel energy dissipation with three-meter-diameter bottom outlet hole.

With a host of airflow and waterflow model tests, water head is reduced by water whirling, mixed water, and shear friction when orifice plates with swift contraction and expansion and forced shear friction after orifice plates. Energy dissipation effect is related with ratio of orifice diameter and tunnel diameter: smaller the ratio is, the more significant the effect becomes, but the longer the water regime recovering even flow. In certain shape, when waterflow Renault number larger than 10^5, energy coefficient is near to a constant. Examined by pure and muddy water tests, sediment concentration puts no effect on energy dissipation coefficient.

2.1.1 *Research on distance between orifice plates*

Choosing of distance between orifice plates is related with orifice-diameter and tunnel-diameter, which regards relative stability of waterflow pressure after orifice plates as principle. A flood of trials show that energy can't fully dissipate between orifice plates, coefficient turns down, and the loss of total water head becomes smaller when distance between orifice plates is too small. Take orifice-diameter ratio of Xiaolangdi, the distance between orifice plate is decided to be three times of tunnel-diameter, just because when distance between orifice plate is more than 3 times of tunnel-diameter, the total quantity of energy dissipation doesn't increase.

2.1.2 *Measures on protection of cavitations and corrosion*

According to specifications, energy dissipation orifice tunnel corresponds to non-cavitation. In so doing, a large number of vacuum tank model tests have been consigned to domestic research institutes in order to testify mechanism of cavitation creation and orifice plate of cavitation cancellation. The results are satisfactory: when cavitations number of waterflow is larger than initial cavitation number, the orifice plate tunnel will not cavitate; cavitation can be cancelled by changing gate opening area and shape of orifice plate; waterflow cavitation number and initial cavitation number both are related with orifice-diameter ratio, orifice-edge radius, flow regime, gate scale and shape of orifice plate. Because of progressive energy dissipation and progressive change of waterflow cavitation number together with energy dissipation, the adjustment of multi-stage orifice-diameter ratio, orifice-edge radius and shape may realize the optimum combination. According to project experience and rectification of Bikou experimental research, when model design is non-cavitation or slight cavitation, the prototype will not be in erosion damage.

2.1.3 *Research on induced vibration*

If every orifice tunnel may dispel 55 meters water head with flow velocity of 1500 cubic meters/s, the total energy dissipation is about 800,000kW. Experts care much about whether the enormous energy will induce waterflow pulsating pressure and then do damage to lining structure and surrounding rock? Still a flood of tests prove that waterflow pulsating pressure becomes maximum in about one time tunnel-diameter downstream of orifice plate; the maximum value is in direct proportion to section average velocity head; when spotted pulsating pressure margined as 6 to 8 meters of water head, and convert to prototype energy of 95%, the frequency range is from 0 to 2Hz, and excellence frequency is less than 1Hz. Prototype observation in Bikou sediment tunnel shows that excellence frequency of waterflow pulsating is 1.25Hz; the ratio of overall pulsating intensity of pressure to spotted pulsating intensity pressure is 1/10~1/30; the lining structure and surrounding rocks have slight vibration; waterflow pulsating pressure cannot induce resonance because of the high inherent vibration of orifice plate and the lining structure.

2.1.4 *Effect of energy dissipation in pure and muddy water*

Xiaolangdi Project is located on the Yellow River, and influence of waterflow with high sediment cannot be ignored. Tests of pure and muddy water proves that when Renault number is larger

than 10^5, waterflow is in resistance square area with complete turbulent motion, and the flow regime of pure water and muddy water is the same. As for Xiaolangdi Project, the Renault number is not less than 10^7 when in minimum discharge, and waterflow is in strong turbulent motion, so regardless of difference between pure and muddy water when in hydraulic design.

2.1.5 *Research on similarity of prototype and model*

Keeping in mind the primary characteristic of energy dissipation of orifice plate, considering the general layout of the buildings, we studied orifice plate with cofferdam and energy dissipation with 3-stage or 4-stage orifice plate. The tasks we want to testify in the tests are: the aeration and erosion control when the high-speed waterflow generates swift expansion and drop in mid-gate chamber outlet, the rapid flow vibration, the transfer of open flow and full flow when emergency gate is opening in moving water. All these provide scientific data. Though testing data makes it feasible that changing diversion tunnel into orifice tunnel, the professionals still fear that only the model tests cannot display all technical problems because of scale effect of hydraulic tests. To make it better, supported and coordinated by associated units, Reconnaissance Planning & Design Institute of Yellow River Water Conservancy Commission makes use of sediment tunnel with diameter of 4.4 meters of Bikou Hydropower Station. In the test, we add two-stage orifice plates to carry out comparison tests between prototype observation and model test. The sufficient data show that prototype and model match well in pressure distribution, cavitation characteristics, and waterflow pulsation. These data is the key to decision of tunnel of orifice plate scheme. This makes the scheme based on full demonstration, advanced technique, and credible safety.

3 DESIGN ON ORIFICE TUNNEL

3.1 *Design principle*

(1) When water level in reservoir is 275 meters, flow velocity at mid-gate chamber outlet is less than 35 meters/s;
(2) When water level in reservoir is 220 meters, discharge capacity should be 1270 cubic meters/s≤Q≤1300 cubic meters/s;
(3) When all-stage water level operates, orifice plate model designed in non-cavitation, prototype is without erosion;
(4) When all-stage water level operates, excellent flow regime and enough aeration at mid-gate chamber outlet avoid erosion damage.

3.2 *Arrangement characteristics*

According to the requirement of total discharge capacity, the highest applied water level of No.1 orifice tunnel is 250 meters, simultaneously, the water head drop between upper reaches and lower reaches is 115 meters; the highest applied water level for No. 2 and No. 3 is 275 meters, the water head drop is 140 meters.

The three diversion tunnels in the utmost scheme all are in circular section with diameter of 14.5 meters. No. 1 diversion tunnel tied to original riverbed, with intake at EL.132 meters; the intake elevation of No. 2 and No. 3 is 141.5 meters; the total length of the three is 1100 meters. Plane axis distance of every tunnel is 68 meters. The arrangement type of the three orifice tunnels after reconstruction is basically the same. Orifice tunnel is made up of intake tower, raising connection, multi-stage energy dissipation of orifice plate, mid-gate chamber, open flow after mid-gate chamber and outlet.

When diversion tunnel is out of function, it will be plugged and reconstructed. At raising stage, the intake will be raised up to EL. 175 meters; the intake tower, with service gate and emergency gate, is connected with original diversion tunnel with 14.5-meter-diameter raising section; the diversion

tunnel is installed with 3-staged orifice plates in distance of 3 times of tunnel-diameter with orificediameter ratio of 0.689, 0.724, 0.724 and with orifice edge radius of 0.02 meters, 0.2 meters, and 0.3 meters respectively; pressure side flow velocity is not more than 10 meters/s, and velocity through orifice is more or less 20 meters/s. After 3 times of tunnel distance of the third orifice plate ring, i.e., 43.5 meters, the diversion tunnel contracts from circular to square section, with mid-gate chamber set up. Before the mid-gate chamber, waterflow is in pressure and energy dissipation is through orifice plate; out of the gate, with sudden breadth and sudden fall, jet waterflow flows into slower reaches with open flow regime, and then flows into the stilling pool just at tunnel outlet. The reutilization ratio of the three diversion tunnels is about 85%, total maximum discharge capacity is 4826 cubic meters/s. Total energy dissipation of water head after the three-staged orifice plate ring is about 55 meters, the maximum flow velocity through gate is 35 meters/s. Thus, these three diversion tunnels come into use effectively and are reconstructed into permanent orifice tunnels.

The following are elevational sections of orifice tunnel. (unit:meters)

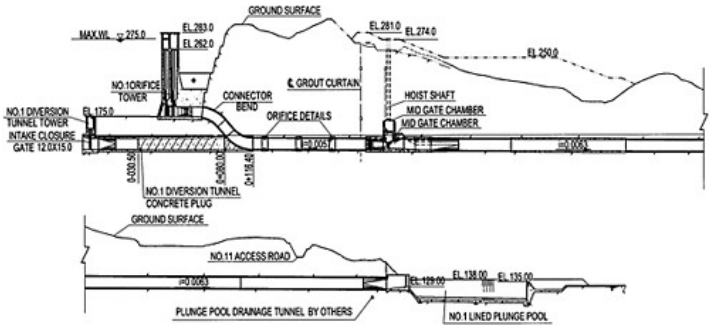

4 PROTOTYPE OBSERVATION OF ORIFICE TUNNEL

In April 26th, 2000, No. 1 orifice tunnel carried out hydraulic prototype observation test. Testing reservoir water level is 210.2 meters. The test lasted 24 hours, and total discharge capacity is 1200~1300 cubic meters/s. In November of the same year, when water level in reservoir rose to 234 meters, No. 1 orifice tunnel carried out hydraulic prototype observation test once again. The test is to get on-the-spot information about energy dissipation effect, waterflow cavitation, vibration of lining structure and surrounding rocks induced by pulsating waterflow, aeration and hollow pressure in mid-gate chamber outlet, rapid flow vibration when opening the gate and stress on orifice plate rings and lining structure. The test results are: the time-average pressure and pulsating pressure in the pressure part of orifice tunnel are excellent between the prototype observation and model test results, and total percentage of energy dissipation of the three-staged orifice plates is 46.6%; when gate is fully open, No. 2 and No. 3 orifice plates are in state of slight cavitation; the maximum acceleration of mountain vibration induced by No. 1 is 4.91cm/s^2 and generally is senseless vibration; It is supposed that when at high water level, the three tunnels may induce slight vibration when discharging simultaneously; safety measures for lining structure of tunnel are sufficient, and slight vibration when the gate is partially open. All in all, the prototype observation result is of great significance in guidance of the safe operation of Xiaolangdi spillway tunnel of multi-stage orifice plate, and it has vital reference value in popularization of changing diversion tunnel into permanent spillway tunnel and its orifice energy dissipation form.

5 CONCLUSION

We may ratify and deduce from a host of model and on-the-spot tests that the energy dissipation effect of orifice plates is of significance. When water level in reservoir is 275 meters, total dispelling water head passing through three-staged orifice plates is 55 meters; when No. 1 is in the highest applied water level of 250 meters, No.2 and No.3 in the highest applied water level of 275 meters respectively, slightly cavitate in the orifice and no erosion, no resonance of structure and mountain.

In July 5th, 2002, the orifice tunnels were put into function in the first “artificial flood peak” tests to adjust water and sediment. It is true that spillway tunnel of multi-stage orifice plate is successful design, which is in the leading level in energy dissipation domestically and does a great contribution to the development of world dam projects. It pioneers a new method in reconstruction and utilization of diversion tunnels, which makes China to be in the lead of theoretical research in pressure energy dissipation and engineering practice over the world.

New Developments in Dam Engineering—Wieland, Ren & Tan (eds),
© 2004 Taylor & Francis Group, London, ISBN 04 1536 240 7

Key technical problems of the Three Gorges Project construction

Liu Shaoling
Changjiang Institute of Survey, Planning, Design & Research, China

ABSTRACT: The Three Gorges Project (TGP) has huge work load, amounts to about $2.8\times10^7m^3$ concrete, $1.04\times10^8m^3$ earth-rock excavation and 7.2×10^5t metal structures and reinforcing steel bars. TGP is constructed in three stages, 5 years preparative and the first stage, 6 years the second stage and 6 years the third stage. Main river closure of the second stage and diversion channel closure of the third stage were orderly actualized. In the second stage, from 1998 to 2003, poured $1.846\times10^7m^3$ concrete and installed 1.92×10^5t metal structures and embedded elements of mechanical and electrical equipments. The new world's record of $5.4285\times10^6m^3$ concrete-placing in one year was created in 2000.

1 CLOSURES AND COFFER DAMS CONSTRUCTION IN THE SECOND AND THIRD STAGE

The three stage diversion is adopted in the Three Gorges Project construction. The first stage, right riverbed was enclosed. The diversion channel was excavated and the longitudinal concrete coffer dam on left side of the diversion channel was built under the protection of the first stage earth-rock coffer dams. In the second stage, the main river was closured and the left riverbed was enclosed. Under the protection of the second stage earth-rock coffer dams and the longitudinal concrete coffer dam, spill dam monoliths, power house dam monoliths and power house of hydropower station on the left of the river were constructed. The third stage, the diversion channel was closured. The dam monoliths with power house and power house of hydropower station on the right of the river were constructed under the protection of the third stage coffer dams. Closures and the second and third stage coffer dams construction can be the most difficult technique and highest construction intensity of hydraulic projects in the world.

The design discharge of main river closure in the second stage is 14000~19400m^3/s, the maximum closure flow depth reaches 60m and average velocity of gap section is 3.33~4.16m/s. These exceed the maximum closure practice discharges and flow depths of constructed hydraulic projects in the world. Further more navigation cannot be interrupted during the period of closure work. The upstream banquette of the second stage closure began to closure at 8 o'clock on October 26 in 1997. Very big block rocks and medium block rocks were threw at the embankment head of upstream gap section and formed shoulder angle which solved the difficult problem that embankment head incidental slough off when throw loose materials into deep water. The gap section was narrowed from 130m to 40m which lasted 22.5 hours and used 369 large equipments. The practice closure flow is 11600m^3/s and day throw intensity reaches $1.21\times10^5m^3$. Employing large scale equipments and the high construction intensity is infrequent in the world closure works.

The design discharge of the diversion channel closure in the third stage is 9010~10300m^3/s, the maximum closure flow depth is 20~30m, the closure fall is 3.26~4.06m and the total closure energy of gap section reaches 410.2MW. These are number one in the world closure works. Further more rock bottom surface of open channel is flat and smooth that makes against stability of block rocks. Gap sections of upstream and downstream banquettes closure at the same time

which share in closure fall. The means of setting block rock bank at gap section of upstream banquette and throwing very big block rock clusters and concrete tetrahedron with burying iron were adopted to improve stability of closure block rocks. The upstream and downstream banquettes began to closure on October 27 in 2002. And the gap sections were narrowed to 20 and 30m on Novermber 3. The width of difficult gap section (70~30m) was broke through successfully, and two banquettes stand closure succeeded for the first time.

The maximum height of the second stage earth-rock coffer dams is 85.2m, and 80 percent of $1.06\times10^7m^3$ filling materials were constructed underwater with 60m maximum depth. It is maximum deep water coffer dam in the world. The maximum height of cut-off wall is 74m, and geologic foundation of coffer dam is complex. At the construction time, fill rubble enrockment of both sides firstly, fill weathering sands on the midst and built cut-off wall next. The rubble enrockment of the back water side concurrently act as closure banquettes and drain corner. Fill weathering sands under-water with vibration, impact and compaction technique that can reduce transmutation of coffer dam and cut-off wall. The construction fetched in hydraulic pressure grab bucket, hydraulic pressure milling slit and other advanced equipments from abroad, and adopted the milling slit technique for building cut-off wall of "two drill and one grab (milling)", "two drill and three grab (milling)" and "milling, grab, drill, explode and smash". The technique fits the TGP coffer dam character of stratum complex and project time limit pressure, and the constructed maximal cut-off wall area of upstream coffer dam reaches $6440m^2$ every month. It is invention that using plasticity wall materials which make up of weathering sand, granite chip, cement and bentonitic clay. And waterproofing effect is excellent; it is safety and credibility proved by construction and practice.

The third stage lateral RCC coffer dam must be constructed within 4 months. The maximum height is 121m, length of coffer dam crest is 580m and the volume of concrete is $1.67\times10^6m^3$. It is the key that coffer dam constructed quickly with the precondition of ensuring it work safely. The structure of coffer dam can be designed as simple as possible, the slope with gradient 1:0.75 on the back water side was changed into steps, and complex foundation gallery was laid in the construction section of first stage possibly. The whole section of coffer dam is RCC, tip cars enter working face under level 90m, and tower-belt conveyer was used over level 90m. The overturn moulding panels were used for concrete placing of upstream face, and precast panels were used for pouring downstream face concrete. The techniques are adapted to construct coffer dam quickly. The concrete-placing intensity of peak months reached $4.76\times10^5m^3$, and the maximum rise height of working face in one month was 27.9m.

2 CONCRETE-PLACING WITH HIGH INTENSITY AND ARRANGEMENT OF PLACING EQUIPMENTS INTHE SECOND STAGE

The second stage is 6 years with the most difficult and highest pressure construction and the most complex technique in TGP. The state of high construction intensity and great concrete-placing gross lacks precedent. The main control schedule as follows:

(1) Concrete-placing at deep trough of riverbed begin in January, 1999;
(2) Water filling in upstream foundation ditch in May, 2002, and in downstream foundation ditch in September, 2002;
(3) Gates are closed and reservoir accumulate water from the first ten days of June, 2003, and ship lock began to work in the same month;
(4) The first group power units began to generate electricity in October, 2003.

In 1999, the second year of the second stage, the new world records of $4.585\times10^6m^3$ concrete-placing in one year and $5.535\times10^5m^3$ concrete-placing in one month were created. The year of 2000 is the highest construction intensity year in the TGP schedule construction. The project poured $5.4285\times10^6m^3$ concrete and installed 3.2×10^4t metal structures and embedded elements of mechanical and electrical equipments in this year. The compare between the TGP concrete-placing intensity and peak concrete-placing intensity of oversea projects is showed as the following Table 1.

Table 1. The compare between TGP concrete-placing intensity and other projects.

Project	Nation	Amount of concrete ($\times10^4m^3$)	Intensity of peak month ($\times10^4m^3$)	Intensity of peak year ($\times10^4m^3$)	Remark (primary machines)
TGP	China	2800	55.35	542.85	Tower belt, portal hoist and cord machines
Kuibisev	Russia	734	38.9	313.4	Tip cars
Itapú	Brazil, Paraguay	1228	33.9	302.8	5 parallel translation cord machines
Grand Coulee	U.S.A	809	37.8	270.0	High pile trestle and double arms cranes
Dvorak	U.S.A	512.5	18.3	221.0	3 table cord machines
Whist	Mexico	280	24.8	206.4	3 tower belt machines
Ge Zhouba Dam	China	1048	23.94	202.9	Portal-tower hoist machines
Hoover Dam	U.S.A	339.0	15.0	120.0	5 cord machines

The conceptual construction methods of using tower belt, cord, portal hoist and tower machines were used during the construction of dam and power house of hydropower station. Four TC2400 fixation tower belt machines produced by ROTEC Corp., U.S. were arranged at spill dam monoliths, and they are laid at the middle of No. 21, No. 14, No. 7 and No. 1 spill dam monoliths. No. 5 and No. 6 MD2000 fixed tower belt machines were produced by POTAIN Corp., France were laid at the middle of entity and no steel tube monoliths of No. 12 and No. 3 power house dam monoliths. Two swing tower type cord machines can lift 461 heavies. The height of tower mast on side banks is 125m, span is 1416m, swing is ±20m and hoisting capacity is 201. Two pile trestles are built on the downstream dam surface with level 120m and out of the downstream spill dam with level 45m. Portal hoist, tower machines for pouring concrete and installing metal structures are laid on the pile trestles. The portal hoist and tower machines are used in the concrete placing of power house. Seven MQ2000 elevated portal hoists are specially manufactured for the TGP which are used for the construction of dam and power house. Each elevated portal hoist can lift $6m^3$ concrete pot, and its maximum work range is 71m. The homemade portal hoist and tower machines under the level of 1.26×10^7N.m were used during the ship lock concrete construction.

3 BLASTING CONTROL OF THE SHIP LOCK EXCAVATION AND DISMANTLING OF EARTH-ROCK COFFER DAMS OF THE SECOND STAGE

The principal part length of ship lock is 1607m, the maximum height of side slope reaches 170m and the range of side slope height continue over level 120m is 460m long. There is a 54~57m high rock separation pier in the middle of two line ship lock. It brings the difficult problems of figuration excavation and high side slop excavation blasting control. The excavation procedure is mid pioneer groove primarily and side protective layers next. The blasting parameters are confirmed by field blasting experiments which adapt to the construction procedure of ship lock groove excavation blasting and kinds of different blasting type (groove excavation—long borehole bench blasting, side protective layer blasting, base rock protective layer blasting etc.). Smooth blasting and pre-shearing blasting were practiced successfully which reduce side slope (side wall) rock disturb farthest. The configuration of construction foundation and gradient of side slope after excavation achieved the design requirement.

The second stage earth-rock coffer dams are requested to be dismantled $2.43\times10^6m^3$ at least before the closure in the third stage, and $6.0\times10^6m^3$ in April, 2003. The dismantling of coffer dams has limited work time and are underwater excavation. The dismantling blasting of coffer dam has no precedent that grouting steel tubes and holding shelf for fixing the steel tubes embedded in the cut-off wall of the second stage coffer dam. In order to reduce underwater dismantling difficulty and accomplish the task in the scheduled time, the cut-off wall and steel tube and holding shelf must be broken by once blasting. Because the steel tube blasting, meshwork blasting, explosive material capability and dip in deep water test and cut-off wall field dismantling blasting were experimented orderly, the best blasting parameters were obtained. The blasting was once and successful on July 1, 2002. The total delay time of the blasting is 9.5s, the weight of total explosive is 19.24t, and the total segments are 375. The blasting achieved expectable results that the cut-off wall became loose and broken bits and no obstacle in shovel excavation process was met because of appearing hard barrier in cut-off wall or long steel tube link with holding shelf together.

4 CONCRETE PRODUCTION AND TEMPERATURE CONTROL

The manual aggregate is used in the concrete of the second stage. The coarse aggregate is new granite which is crushed at Gu Shuling aggregate plant and comes from the excavation of ship lock, the second stage dam and power station. It is transported to each concrete system by adhesive tape machines, and the production capacity per month is 7.6×10^5t. The sand is manufactured from porphyritic granite of Xia Anxi material yard. It is transported by trucks, and the production capacity per month is 3.91×10^5t.

Nine mixing plants are distributed into five concrete mixing systems. The total production capacity of 7°C low temperature concrete is 1720m^3/h and the normal temperature concrete is 2530m^3/h. The allocations of the mixing plants are shown as Table 2.

The 52.5 moderate heat Portland cement, 42.5 low heat scoria Portland cement, and the first level of pulverized fuel ash are adopted. Experiment shows that manual aggregate has no active reaction. But considering the importance of the TGP, three measures for restraining or avoiding aggregate active reaction are under the strict control of the concrete design which is cement alkalinity, concrete alkalinity and pulverized fuel ash mix quantity. Based on a great lot of experiments after the project start working, design index and mix proportion of concrete are optimized.

Concrete temperature control of the TGP is difficult, so the owner, consultant, engineering supervisor composed a temperature control group in order to strengthen harmony and management of concrete temperature control and crack prevention. The group holds regular meeting termly, organizes field inspection, guides and supervises the concrete placing temperature control, edits and perfects temperature control standard, and organizes study on concrete temperature control and correlative quality problems need for solving imminently. All of these go along under the requirement of 7°C project standard.

Table 2. The concrete production systems allocation of the second stage in TGP.

System	Mixing plant		Production capacity of normal temperature concrete (m^3/h)	Design temperature of low temperature concrete (°C)	Production capacity of low temperature concrete (m^3/h)	Refrigerating capacity (×10^{4}kJ/h)	
	Model (m3)	Amount (set)					
EL79m	4×4.5	2					320×2 7 250×2 8987
EL90m	4×6	1	360	7	250	6688	
	4×3	1	240	7	180		
EL120m	4×Z3	2	240×2	7	180×2	5747.5	
EL82m	4×3	1	240	7	180	3135	
	2×4.5	1	330	7	250		
EL98.7m	4×3	1	240	2×4.5m^3 mixing plant can change to produce 7°C low temperature concrete		5525	
Total			2530		1720	29782.3	

For satisfying the requirements of concrete temperature control and joint grouting, cooling pipes are laid in big volume concrete. It sorts into initial, mid and late stage cooling according to pipe water action and cooling characteristic. The main effect of initial stage cooling is decrease of temperature increment of heat of concrete hydration and control of the highest concrete temperature; the mid stage cooling is for avoiding excessive difference in temperature between inside and outside of concrete dam; the aim of the late stage cooling is to reduce dam temperature to joint grouting temperature (or steady temperature).

5 TWICE AIR COOLING TECHNIQUE AND 7°C PROJECT

A set of advance cooling establishment for 7°C pre-cooling concrete at outlet of the mixing plant in summer called 7°C project. It had been used in Ge Zhouba Dam Project and the water cooling—air cooling—adding ice refrigerating technology (called "three cooling technique" for short) are used.

The basic flow of "three cooling technique" is that the aggregate is sprayed using 2~4°C cooling water on the transport belt, next transported into the storage bin after dehydration and refrigerated by air cooling, and added ice when mixing concrete. The technique achieved success in Ge Zhouba Dam Project, but there are many difficult problems to work out. First, dehydration effect of water cooling aggregate in working procedure is not good that aggregate surfaces contain water (water ratio is 2~4%). The aggregate is easy to freeze when it is refrigerated by air in mixing plant. Because the main air cooling action is to keep cool, the capability of more deep cooling get limit. Second, a 200~300m watering gallery need to be built for water cooling, the refrigeration establishment occupies too large field to arrange the concrete production system. Third, many refrigerating equipments bring complex management. The refrigeration water contains a great deal of sediment, so waste water plant needs to be built. Further, water cooling aggregate has high water radio and ice quantity of mixing is limit.

The main difference between twice air cooling and "three cooling technique" is that the first working procedure of refrigerating aggregate, water cooling, is changed to first air cooling. The aggregate after washing and size classification is refrigerated by 0~5°C cold air in the ground regulative bin. The air after decalescence is refrigerated again by cold air machine and used in circular aggregate cooling. After the first air cooling, the water radio of aggregate surfaces reduces in evidence, aggregate surfaces water radio is near to 0 except gravelstone has lower water radio, and four class aggregate can be refrigerated to 5~8°C. The aggregate after the first air cooling is transported into mixing plant bin by heat preservation belt machine and refrigerated by second air cooling. The next refrigeration procedure is similar with latter two courses of "three cooling technique". The difference is that aggregate refrigeration final temperature can reduce greatly; the coarse aggregate can be refrigerated to −2°C or lower in the −10~ −15°C cold air (Only gravelstone needs to keep positive temperature in order to avoid freezing bin). In addition, the aggregate after the second air cooling has dry surfaces and no water which affords good condition for mixing with adding ice.

After the test of high production intensity of the second stage pre-cooling concrete in the summer of 1999, concrete temperature at outlet of the mixing plant is steadily controlled under 7°C. This proved that 7°C project adopted twice air cooling technique is entirely feasible and successful. The twice air cooling technique has many advantages which "three cooling technique" has not. It occupies less area field, has less links of management and lower cost of establishment and work. The twice air cooling technique for 7°C pre-cooling concrete production has already been used in TGP.

6 CONSTRUCTION OF METAL STRUCTURES AND MECHANICAL AND ELECTRICAL EQUIPMENTS

During the second stage construction 1.48×10^5t metal structures and embedded elements of mechanical and electrical equipments need to be installed. There are 22 diversion outlets, 23 flood discharge oulets, 22 spill ways, 2 floater sluice outlets, 2 sediment flushing outlets and 14 power

house water intakes. The gates operate with high water head, and headstock gears work with great force. In order to ensure storage water on time, the gate grooves of working and access and accident gates at frontage of blocking water would be tested before closing the gates and accumulating water.

The length of steel penstock is 122.175m with 13.2m diameter, 28~60mm steel thickness and the total weight is 21126t. The 6 top sideling and straight steel pipe segments are designed according to the buried penstock in dam; the top curve segments, sideling and straight segments, and bottom curve segments are designed according to steel liner and reinforced concrete pipe associated bear force; and bottom horizontal segments are designed according to exposed pipe. There is a steel penstock manufactory lies in the dam region. The steel plates are machined to slice, next rolled and welded to single section steel pipes. The section pipes are transported by special low gravity center trolley. The MQ6000 special portal hoist lies on the pile trestle with level 82m between dam and power house was used during the primary hoisting and installation.

The power units are turbine generators with 700MW capacity of single unit, and the operation water level is level 135~175m. Not only super capacity of single unit but also great water head bound farther exceeds oversize power units with similar capacity in the world. By the international bidding, GEC-ALSTOM of France and ABB of Switzerland accommodate 8 set of units together. The group accommodates 6 set of units which is composed of GE of Canada, VOITH and SIEMENS of Germany. Harbin Electric Machine Limited Liability Corporation and Oriental Electric Machine Stock Company respectively are the subcontractors of the two groups. The subcontracts account 31% of the total amount.

The amount of ship lock metal structures installation is 4.32×10^4t. The installation of 24 leaf gates, 24 ogee gates and bridge machine tramroads of the No.1 lock head are the most difficult. The arrangement of cranes and installation procedure need to adapt to the two line steps of ship lock chamber.

Navigation of the Yangtse River is restricted by working of the ship lock on schedule after closing gates and reservoir storage water. The debugging before opening to navigation is necessary, and it divides into no water debugging and water debugging two steps. The main items of the no water debugging step are every lock head's leaf gate system, lock valve system, headstock gear, and lock chamber bollards. The aim is to inspect status of every lock valve's water seals, groove test, operation of single unit and single gate, and work of main mechanical and electrical equipments control system. Teamwork debugs based on these and achieves whole linkage control equipments can work elementarily. Except continuation to inspect and adjust items above, the water debugging step mostly debug single and combined option of every lock head's leaf gate with different water design heads and various water level combination. Under the different work conditions, the debugging inspects the manipulative time of water transfer valves with single side or two sides water transfer, checks the single and combined debugging of hydraulic machines and correlative mechanical and electrical equipments, and prepares for opening to navigation of ship lock. Water fills the lock chamber by pump water system in the water debugging step.

7 CONCLUSION

The TGP construction is characterized with huge project scope, great work quantity, high construction intensity, complex technique and many construction items. The twice closure and concrete placing both exceed world level. The construction of metal structures, mechanical and electrical equipments and embedded elements are cross and parallel busywork with concrete placing. Navigation must be considered in stage of construction because of the long work time. Navigation is by diversion channel and temporary ship lock in the second stage, with the help of dock-transfer and cross dam during the flood season. The originate twice air cooling technique, produce 7°C concrete at outlet of the mixing plant during concrete construction, and a great deal of experiments and analysis researches for improving quality and durability of concrete are quite useful. The construction worker ability and labor capacity is improved more than before. The new world record of 5.4285×10^6m^3 concrete-placing in one year was created in 2000, and in the same year 3.2×10^5t metal structures and mechanical and electrical embedded elements were installed.

New Developments in Dam Engineering—Wieland, Ren & Tan (eds),

Large-scale in-situ direct shear tests on rockfill materials of upper reservoir dam in Yixing pumped storage power station

S.H.Liu[1], G.Y.Xiao[2], J.Z.Yang[3] & G.Y.Wu[4]
[1] *College of Water Conservancy and Hydropower Engineering, Hohai University, Nanjing*
[2] *Shanghai Investigation, Design & Research Institute, Shanghai*
[3] *Jiangsu Pumped Storage Power Co. Ltd, Yixing*
[4] *Sinohydro Engineering Bureau, Chendu*

ABSTRACT: A new in-situ direct shear testing method for large-grained rockfill materials is introduced. The distinctive feature of this new in-situ direct shear testing method is to pull the shearing frame with a flexible chain, which causes the mutual movement of the shearing frame and the specimen during shear. Thus, the wall friction of the shearing frame has little influence on the normal stress on the shear plane and the accurate measurement for the shear strength becomes possible in the new direct shear test. There have been many applications of this new testing method abroad, but it is the first time in China to be applied in the construction field of the upper reservoir of Yixing pumped storage power station.

1 INTRODUCTION

The direct box shear test, with both an upper shear box and a lower shear box, is very popular in the laboratory testing of soils owing to its simplicity. However, it is usually criticized that the real normal stress on the shear plane cannot be correctly measured because it is affected by the frictional forces between the sample and the internal surfaces of the shear box. There may be two ways to minimize the effect of these frictional forces. One is to set a reaction platen on the opposite side of the loading platen and then to measure the normal force by a load cell that is set on the reaction platen, as standardized by the Japanese Geotechnical Society [1]. The other is to pull a shearing frame, which is equivalent to the upper shear box as used in conventional direct box shear test, with a flexible rope or chain. By using the latter way, a new in-situ direct shear testing method, possibly for testing soils ranging from clay to large-grained rockfill materials, was developed [2,3,4]. This new in-situ testing method has been widely applied in Japan in dam and road construction projects [5]. This paper reports its application in the construction field of the upper reservoir of Yixing pumped storage power station, the first application in China.

2 PRINCIPLE OF NEW IN-SITU DIRECT SHEAR TEST

Figure 1 shows the schematic view of the new in-situ direct shear test along the shear direction. In general, four latticed shearing frames with a size of 120cm square and 17cm high are directly buried into the actual ground in advance before the tests, and then the ground is compacted in the same way as the real construction. The reason of burying four shearing frames at one site is to enable shear strengths be determined quickly from four tests under the same testing conditions except for the different normal stresses. In this test, the vertical force (normal load) on the specimen is applied by dead loads, and the horizontal (shear) force on the specimen is applied by

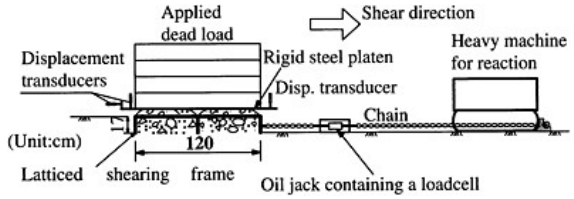

Figure 1. Schematic view of the newly developed in-situ direct shear test [2–4].

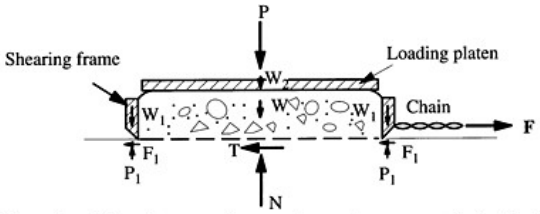

N, T – Normal and shear forces acting on shear plane, respectively; A – Area of shear plane; P – Applied dead load; F – Measured shear force; W – Weight of specimen inside shearing frame; W_1 – Dead weight of shearing frame; W_2 – Dead weight of rigid steel platen; P_1, T_1 – Normal and frictional forces on contact plane between shearing frame and specimen

Figure 2. Forces acting on specimen of new in-situ direct shear test.

pulling the shearing frame horizontally with a flexible chain through an oil jack. The chain is reacted against a heavy machine like bulldozer, or against a concrete pier. The shear force is measured by a load cell, which is contained in the hollow center of the oil jack. The shear displacement is measured with a displacement transducer that is set in the middle backside of the rigid steel platen, and the normal displacement is obtained from the average of the measured values by two displacement transducers that are set diagonally on the rigid steel platen. As shown in Fig. 1, the rigid steel platen is not directly set on the latticed shearing frame, but on the raised specimen among the meshes of the shearing frame. This is an important point in this test to ensure the normal load be transmitted uniformly into the shear plane; otherwise, the normal load will be transmitted into the sample mainly through the ribs of the shearing frame and the applied normal stress will be concentrated just under the ribs, resulting in the breakage of grains.

Figure 2 shows the forces acting on the specimen of this new test (for simplicity, only one mesh of the latticed shearing frame is illustrated). From the equilibrium of the forces, we get the following equations:

$$\left.\begin{aligned} &N = P + W + W_1 + W_2 - P_1 \\ &T = F - T_1 \\ &P_1 \cong 0, T_1 \cong 0 \quad (\textit{when the sample dilates}) \\ &\sigma = N / A, \qquad \tau = T / A \end{aligned}\right\} \tag{1}$$

All the symbols in Eq.(1) are explained in Fig. 2, where P, W, W_1, W_2, A and F are known in advance or can be measured exactly. Because the normal force is not directly applied on the ribs of the shearing frame and the sample of granular materials usually dilates up to the peak strength, the shearing frame is almost floating over the shear plane, especially at the peak strength. Thus, the forces P_1 and T_1 between the base of the shearing frame and the sample are nearly equal to zero. In addition, our measurements up to date show that the shearing frame does not tilt so much during

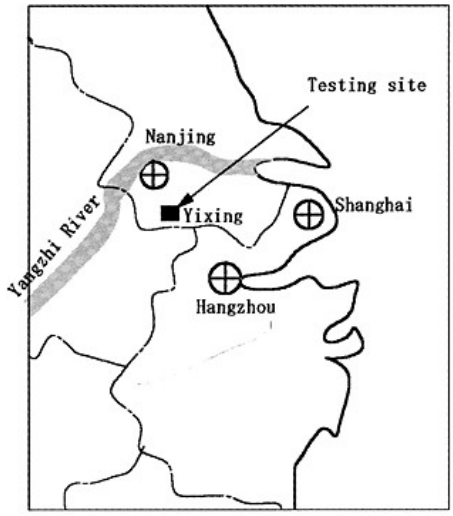

Figure 3. Location of the in-situ direct shear tests in the construction field of Yixing pumped storage power station.

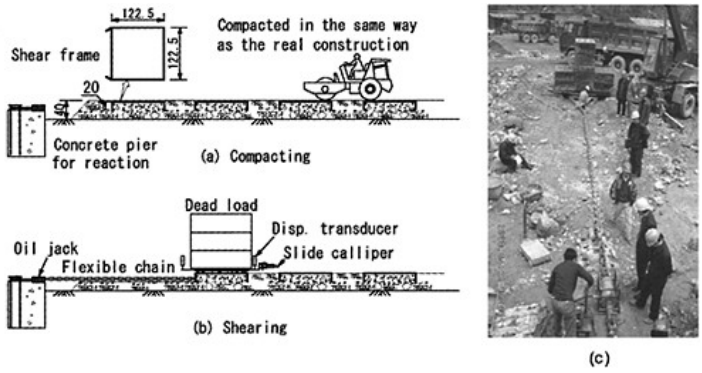

Figure 4. Schematic view and picture of the in-situ direct shear tests on rockfill materials at Yixing pumped storage power station construction site.

shear up to the peak strength (the actually measured max. angle of inclination is about 0.8°). Therefore, it is known from Eq.(1) that the real stresses, σ and T, on the shear plane can be measured exactly in this new direct shear test.

3 TESTS AT YIXING PUMPED STORAGE POWER STATION CONSTRUCTION SITE

The site where the in-situ direct shear tests were carried out is located in the vicinity of Yixing city, Jiangsu Province, near to Nanjing, Shanghai and Hangzhou cities (Fig. 3). Now, a large pumped storage power station with a total installed capacity of 1200MW is under construction there.

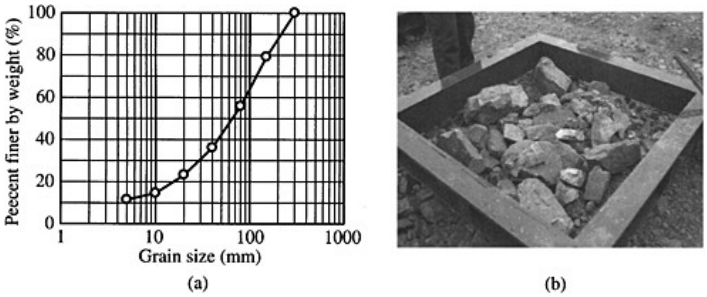

Figure 5. (a) Gradation of the tested samples and (b) the large-grained sample into the shearing frame.

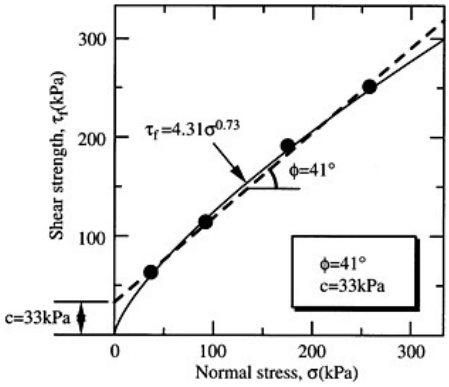

Figure 6. Measured peak shear strengths vs. normal stresses.

Figure 4 shows the schematic view and picture of the tests. In the same way as performed in Japan, four shearing frames were used in the tests, which enable the shear strength to be determined quickly from four tests under similar conditions except for the applied normal stresses. One shearing frame has the inner dimensions of 122.5cm wide by 122.5cm long by 20cm high. The shearing frame is not reinforced with two latticed ribs as commonly done in Japan, but it is reinforced with a H-shaped steel around the frame. As the maximum normal load to be applied is as high as 387.91kN, a concrete pier with a capacity of resisting the horizontal force of 600kN was cast for the reaction. The tests were carried out in a 40cm thick layer of the rockfill material with a maximum grain size of 300mm and an average grain size of about 60mm (Fig. 5). The testing procedures are as follows: (1) Setting four shearing frames with their centers located on the same straight line as the concrete pier. Each shearing frame was lifted up 20cm high in advance over the ground with some stones. (2) Filling the testing materials into the shearing frames. The intervals between the shearing frames were filled with other materials available at the site. (3) Compacting the testing area, where the shearing frames are embedded, with a vibrating roller of 181 weight. The compaction was performed by two static passes and six vibrating passes, which is the same as the actual construction. (4) Raising some crushed stones up on the tested material inside the shearing frame to ensure the normal load be transmitted uniformly into the shear plane of the sample. (5) Setting the displacement transducers. The vertical displacement was measured with two digital displacement transducers that were set in the front and back of the shearing frame, respectively; while the horizontal displacement was measured with a slide calliper that was set at the back of the

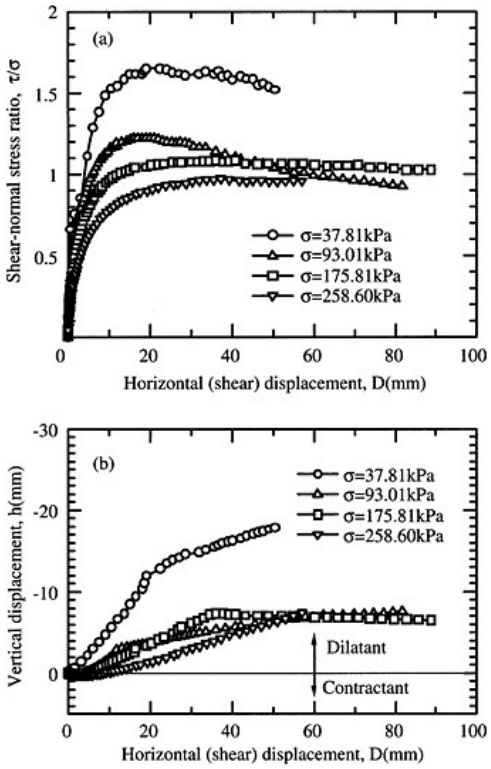

Figure 7. Relationships among stress ratio, horizontal and vertical displacements.

shearing frame. (6) Applying dead loads on the sample and shearing the sample by pulling the shearing frame with a flexible chain. Four normal stresses of 37.81kPa, 93.01kPa, 175.81kPa and 258.60kPa were respectively applied on the shear planes of the four samples.

The measured peak shear strengths are plotted against the applied normal stresses in Fig. 6. If the four plots are characterized with a straight line as shown in the dash line in Fig. 6, then we can obtain the angle of internal friction $\varphi=41°$ and the apparent cohesion c=33kPa. As granular material cannot bear any extensive forces, namely, $\tau_f=0$ when $\sigma<0$, its shear strength should develop continuously from zero at $\sigma=0$ to its intrinsic value at $\sigma>0$. Thus, the failure envelope of granular materials should pass through the origin, as has already been verified by this new insitu direct shear tests [2–5]. Numerous test results indicate that the failure envelope of granular materials can be best represented by the curvilinear exponent expression of $\tau_f=A\sigma^b$. The fitting for the four test plots in this exponent expression is given in Fig. 6 by the solid curve with A=4.31 and b=0.73.

The measured relationships among stress ratio, horizontal (shear) displacement and vertical (dilatant) displacement are shown in Fig. 7. The pressure-dependent characteristic of granular materials is well illustrated in these results. In Fig. 7(b), the evolution of vertical displacement for $\sigma=37.81$kPa and 175.81kPa changes suddenly at certain horizontal displacements after the peak shear strengths. This is because one of the vertical displacement transducers exceeds its measurement range during the tests, which should be overcome in any tests.

4 CONCLUSIONS

(1) The new in-situ direct shear testing method introduced in this paper is very simple in its principle and easy to be performed. It can be used to determine the shear strength of large-grained rockfill materials directly in-situ that have experienced an actual construction compaction.

(2) It is the first application of this new in-situ direct shear testing method in China. In comparison with the applications abroad, there are two different points: one is to eliminate the latticed ribs of the shearing frame, which may benefit the test performance; the other is that the normal stress on the shear plane is applied as high as 258.60kPa, which is the highest for this insitu testing method.

Finally, the authors would like to acknowledge Prof. H.Matsuoka of Nagoya Institute of Technology, Japan, for his great support in these tests. The strong recommendation for this new testing method by Prof. Z.Y.Chen of China Institute of Water Resources and Hydropower Research (IWHR) is also greatly acknowledged.

REFERENCES

[1] The Japanese Geotechnical Society. 1997. Method for consolidated constant pressure direct box shear test on soils. *Tsuchi-to-Kiso, JSSMFE,* Ser. No. 468, Vol. 45, No. 1:70–74 (in Japanese).

[2] Matsuoka H, Liu S H. Simplified direct box shear test on granular materials and its application to rockfill materials. *Soils and Foundations,* 1998, Vol. 38, No. 4:.275–284.

[3] Liu S H. Development of a new in-situ direct shear test method and its application to problems of slope stability and bearing capacity. *Dr. Eng. Thesis,* Nagoya Institute of Technology, 1999.

[4] Matsuoka H, Liu S H. A new in-situ direct shear testing method for sands and clays. *Proc. of the 10th International Conf. on Computer Methods and Advances in Geomechanics, Tucson, USA,* 2001: 963–966.

[5] Matsuoka H, Liu, S H, Sun D, Nishikata U. Development of a New In-situ Direct Shear Test. *Geotechnical Testing Journal,* GTJODJ, American Society for Testing and Materials (ASTM), 2001, Vol. 24, No. 1:99–109.

New Developments in Dam Engineering—Wieland, Ren & Tan (eds),
© 2004 Taylor & Francis Group, London, ISBN 04 1536 240 7

A three-dimensional (3D) coupled nonlinear K-G model for granular material

S.H.Liu[1] & Y.S.Wang[2]
[1] *College of Water Conservancy and Hydropower Engineering, Hohai University, Nanjing*
[2] *Water Resources and Hydropower Planning and Design General Administration, MWR, Beijing*

ABSTRACT: In this paper, a modified version of the simplified *K-G* constitutive model is presented to predict the nonlinear behavior of granular soils with reasonable accuracy. In the modified model, the Spatially Mobilized Plane (SMP) criterion [1,2] is incorporated into the tangent shear modulus G_t through a transformed stress tensor to account for the effect of the intermediate principal stress σ_2 on the deformation and strength of soils and a coefficient including the deviatoric stress q is multiplied to the tangent bulk modulus K_t to reflect approximately the effect of dilatancy of granular soils and to consider the coupling between shear and volumetric strains. The model performance has been illustrated through the comparison of the prediction results with the results of triaxial compression and extension tests on clays and sands.

1 INTRODUCTION

Finite-element methods are frequently used in the analysis of geotechnical engineering problems. In finite-element analysis, the selection of an appropriate constitutive model primarily involves balancing simplicity with accuracy. A number of soil constitutive models have been developed for finite-element analyses. Those models may be roughly classified into advanced elastoplastic models, represented by the Cam-clay model [3] and its numerous modifications (e.g. [4]), and simple nonlinear elastic or hyperbolic models, represented by the Duncan-Chang's E~v model [5] and the Naylor's *K~G* model [6]. The former can simulate realistically nonlinear stress-strain behavior, plastic deformations, and volume change caused by changes in shear stress, as well as the behavior of soils at high stress levels [7]. The latter simulates nonlinear behavior, irrecoverable strains, and stress-dependent stiffness, but it does not model plastic deformations or volume changes due to shear stress because it relates strain increments to stress increments through the extended Hooke's Law [8]. Elastoplastic models can model more realistically the soil behavior than nonlinear elastic ones, especially at high stress levels close to failure, at failure and after failure. However, the nonlinear elastic constitutive models are still widely used due to their simplicity and the well-accumulated experience. Experience has shown that there may be little advantage in using elastoplastic analyses rather than the nonlinear or hyperbolic analyses if the soil mass is not close to failure, for instance, in most earth or rockfill dams, embankments and stable slopes [9].

It is considered that nonlinear elastic isotropic stress-strain laws are more properly defined by the tangent bulk modulus K_t and the tangent shear modulus G_t, as the behavior of soil in the separate modes of volume change and shear are reasonably well understood [6]. However, in the existing *K-G* models, the formulation of the shear modulus G usually uses the Mohr-Coulomb criterion. Besides, the intermediate principal stress σ_2 is not involved. It is thus unreasonable to use this formulation in three-dimensional finite-element analyses. In this paper, the Spatially Mobilized Plane (SMP) criterion [1,2], which is regarded as a three-dimensional (3D) modified version of the Mohr-Coulomb criterion, is incorporated into the tangent shear modulus G_t through

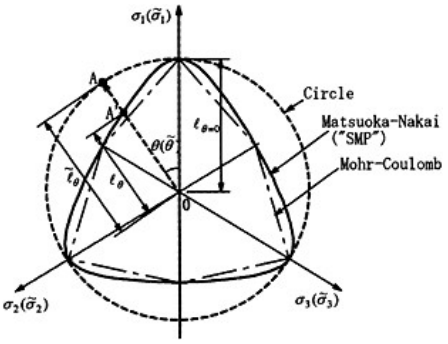

Figure 1. Shapes of the SMP criterion on π plane before and after the stress is transferred.

a transformed stress tensor [4] to account for the effect of the intermediate principal stress σ_2. Moreover, following the methodology of elastoplastic model, the formulation of the tangent bulk modulus K_t is modified to reflect the effect of dilatancy of granular soils and to model the coupling between shear and volumetric strains. The modified *K-G* model accurately predicts the stress-strain behaviors of Toyoura sand measured in triaxial compression and extension tests as well as plane strain tests.

2 A TRANSFORMED STRESS TENSOR FOR THE SMP FAILURE CRITERION

The SMP criterion [1,2] can explain realistically the failure of soil in 3D stress state, which is expressed as:

$$\frac{\tau_{SMP}}{\sigma_{SMP}} = \sqrt{\frac{I_1 I_2 - 9I_3}{9I_3}} = const.. \tag{1}$$

where I_1, I_2 and I_3 are the first, second and third effective stress invariants. On the π-plane (the plane in principal stress space at right angles to the line $\sigma_1=\sigma_2=\sigma_3$), the SMP criterion is a smoothly convex curve circumscribing the regular hexagon of the Mohr-Coulomb criterion, as shown in Fig. 1. In most 3D constitutive models of soil, the Extended Mises criterion, which is a circle on the π-plane, is commonly used. Compared to the Extended Mises criterion, the SMP criterion can reflect more realistically the failure of soil in 3D stress state. Especially, it can reflect the larger shear strength at triaxial compression ($\sigma_2=\sigma_3$, Lode's angle θ=0°) than that at triaxial extension ($\sigma_2=\sigma_1$, Lode's angle θ=60°). Moreover, the shape of the SMP criterion on the irplane develops subsequently from a circle at low stress state to a smoothly convex curve at high stress state, so that it is better than the Mohr-Coulomb criterion in consistency and continuation of the shear deformation and the shear failure. In order to adopt the SMP criterion into 3D constitutive models, a transformed stress tensor $\tilde{\sigma}_{ij}$, as expressed in Eq. (2), has been proposed on the conditions that the stress tensor at triaxial compression and the mean effective stress at any Lode's angle hold the same before and after the transformation, while the shape of the SMP criterion on the π-plane is converted from the smoothly convex curve (the solid curve in Fig.1) to a cone (the broken circle in Fig.1) [4].

$$\tilde{\sigma}_{ij} = p\delta_{ij} + \frac{\ell_0}{\ell_\theta} s_{ij} = p\delta_{ij} + \frac{\ell_0}{\sqrt{s_{kl}s_{kl}}} s_{ij}, \qquad \ell_0 = \sqrt{\frac{2}{3}} \frac{2I_1}{3\sqrt{(I_1 I_2 - I_3)/(I_1 I_2 - 9I_3)} - 1} \tag{2}$$

where s_{ij} ($=\sigma_{ij}=p\delta_{ij}$), is the deviator stress tensor; and δ_{ij} is Kronecker's delta. With this transformed stress tensor $\tilde{\sigma}_{ij}$, the SMP criterion can be adopted into any constitutive models similarly as the Extended Mises criterion.

3 THREE-DIMENSIONAL NONLINEAR *K*-*G* MODEL

3.1 *Tangent shear modulus* G_t

The tangent shear modulus G_t is usually determined from conventional triaxial tests (σ_3=constant) in a similar way as the Duncan-Chang's hyperbolic model [4], which may be expressed as

$$G_t = G_i \cdot \left(1 - R_f \frac{\tau}{\tau_f}\right)^2 = G_i \cdot \left(1 - R_f \frac{q}{q_f}\right)^2 \tag{3}$$

where G_i is the initial tangent shear modulus. τ_f and q_f are the shear stress τ and the deviator stress q at failure, respectively. R_f is defined as the ratio of the deviator stress at failure to the asymptotic value of deviator stress at large axial strains. The adoption of the SMP criterion into the tangent shear modulus G_t requires the deviator stresses in Eq. (3) to be expressed in terms of the transformed stresses as defined by Eq. (2).

$$G_t = G_i \cdot \left(1 - R_f \frac{\tilde{q}}{\tilde{q}_f}\right)^2 \tag{4}$$

As the shape of the SMP criterion on the π-plane is a cone in the transformed stress space (*see* Fig.1), the deviator stress at failure $\tilde{q}_f$ is given as follows:

$$\tilde{q}_f = M_f \cdot \tilde{p} \tag{5}$$

in which

$$\left.\begin{aligned} &\tilde{p} = \frac{1}{3}\tilde{\sigma}_{ii},\quad \tilde{q} = \sqrt{\frac{3}{2}(\tilde{\sigma}_{ij} - \tilde{p}\delta_{ij})(\tilde{\sigma}_{ij} - \tilde{p}\delta_{ij})} \\ &M_f = \frac{6\sin\phi}{3 - \sin\phi},\quad \phi - Angle\ \ of\ internal\ \ friction \end{aligned}\right\} \tag{6}$$

Substituting Eq. (5) into Eq. (4) yields

$$G_t = G_i \cdot \left(1 - R_f \frac{\tilde{q}}{M_f \cdot \tilde{p}}\right)^2 \tag{7}$$

The initial tangent shear modulus G_i is computed in a similar way as the Duncan-Chang's model:

$$G_i = k \cdot p_a \cdot \left(\frac{p}{p_a}\right)^n \tag{8}$$

where k=nondimensional primary-loading modulus number; n=nondimensional modulus exponent; p_a=atmospheric pressure (1000kPa).

3.2 *Tangent bulk modulus* K_t

For granular materials, experiments [10] show that the volumetric strain ε_v under isotropic compression may be properly expressed as a power function of the effective mean stress p:

$$\varepsilon_v = c \cdot \left(\left(\frac{p}{p_a} \right)^m - \left(\frac{p_0}{p_a} \right)^m \right) \tag{9}$$

in which p_0 is the initial mean stress before isotropic compression, c and m are two material parameters under initial isotropic compression.

Differentiating Eq. (9) yields

$$d\varepsilon_v = c \cdot m \cdot \left(\frac{p}{p_a} \right)^{m-1} \frac{dp}{p_a} \tag{10}$$

The volumetric strain increment $d\varepsilon_v$ calculated by Eq.(10) only involves the portion under isotropic compression (change in the mean normal stress p). That is to say, Eq.(10) doesn't involve the volumetric strain increment caused by the change in the deviatoric stress q. Also, it cannot consider the dilation of granular materials, which is one of the most important characteristics of granular materials. To solve these problems, Eq. (10) is modified as follows, inspired by a hardening parameter H proposed by Yao et al. [11]:

$$\frac{M^4}{M_f^4} \frac{M_f^4 - (\tilde{q}/\tilde{p})^4}{M^4 - (\tilde{q}/\tilde{p})^4} \cdot d\varepsilon_v^{dila} = c \cdot m \cdot \left(\frac{p}{p_a} \right)^{m-1} \frac{dp}{p_a} \tag{13}$$

where M and M_f are the stress ratios of $d\varepsilon_v^{dila}$ $d\varepsilon_v$.

Thus, the tangent bulk modulus K_t is obtained as

$$K_t = \frac{dp}{d\varepsilon_v^{dila}} = \frac{M^4}{M_f^4} \frac{M_f^4 - (\tilde{q}/\tilde{p})^4}{M^4 - (\tilde{q}/\tilde{p})^4} \cdot \frac{p_a^m}{c \cdot m} \cdot p^{1-m} \tag{12}$$

Similar to the shear modulus, the bulk modulus is also dependent on the stress history, as pointed out by [12]. For unloading-reloading stress changes, the bulk modulus K_{ur} is assumed to have a similar expression to Eq. (12) but replace the soil parameter c under initial isotropic compression with c_e under swelling.

4 PREDICTION VERSUS EXPERIMENT

Figs. 2 and 3 show the results of the triaxial compression and extension tests on Fujinomori clay and Toyoura sand (from [10] and [13]), respectively, together with the predicted results by the original *K-G* model (in dash lines) and by the proposed *K-G* model (in solid lines). The original *K-G* model means that the intermediate principal stress σ_2 is not involved in the tangent shear modulus G_t and the dilation of granular material is not reflected in the tangent bulk modulus K_t. The model

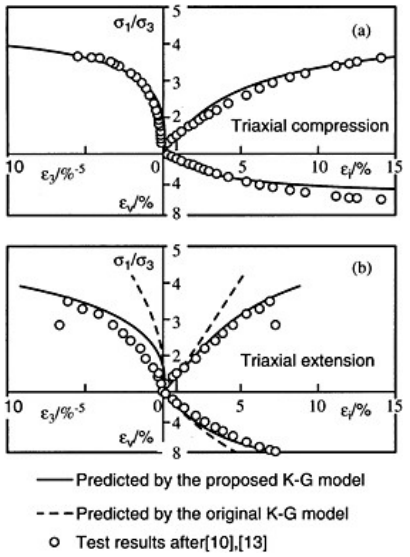

Figure 2. Comparison of predicted and measured results of triaxial compression and extension tests on Fujinomori clay under σ_3=196 kPa.

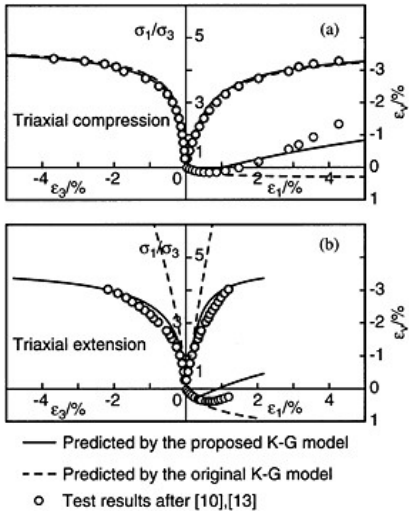

Figure 3. Comparison of predicted and measured results of triaxial compression and extension tests on Toyoura sand under σ_3=196 kPa.

parameters used in the prediction are determined from the triaxial compression tests. For Fujinomori clay, they are: R_f=0.85, k=40.0, n=0.99, M=M_f=1.4 and $(1+e_0)/\lambda$=1/0.0508. For Toyoura sand, they are: R_f=0.99, k=290.0, n=0.99, M=0.95, M_f=1.66, m=0.008 and c=0.5. It is seen from Figs. 2(b) and 3(b) that the shear strengths of both the Fujinomori clay and the Toyoura sand under the extension condition predicted by the proposed *K-G* model agree well with the experimental results, while the shear strengths predicted by the original *K-G* model are much higher than the experiments under the extension condition. Also as shown in Fig. 3(b), the dilation of granular sand can be approximately predicted by the proposed *K-G* model.

5 CONCLUSIONS

The nonlinear *K-G* constitutive model is easily understood and suitable to analyze most earth/rockfill dams, embankments, stable slopes because the soil mass in those cases is not close to failure. In order to accurately predict the deformation and strength behaviors of soils, a modified version of the *K-G* constitutive model has been proposed in the paper. The proposed model can account for the effect of the intermediate principal stress σ_2 on the deformation and strength of soils and reflect approximately the effect of dilation of granular soils.

REFERENCES

[1] Matsuoka, H., Nakai, T. (1974): Stress-deformation and strength characteristics of soil under three different principal stresses, *Proc, JSCE,* 232, pp. 59–70.
[2] Matsuoka, H. (1976): On the significance of the spatial Mobilized Plane, *Soils and Foundations,* Vol.16, No.1, pp. 91–100.

[3] Roscoe, K.H., Burland, J.B. (1968): On the generalized stress-strain behavior of 'wet' clay, *Engineering Plasticity,* Cambridge University Press, pp. 535–609.
[4] Matsuoka, H., Yao, Y.P., Sun, D.A. (1999): The Cam-clay models revised by the SMP criterion, *Soils and Foundations,* 39(1), pp. 81–95.
[5] Duncan, J.M., Chang, C.Y. (1970): Nonlinear analysis of stress and strain in soils, *J. Soil Mech. Found. Div.*, ASCE, 96, pp. 1629–1653.
[6] Naylor, D.J. (1978): Stress-strain laws for soils, *Developments in soil mechanics,* pp. 39–68, Edited by C.R.Scott, Applied Science Publishers Ltd.
[7] Chen, W.F., Mizuno, E. (1990): *Nonlinear Analysis in Soil Mechanics: Theory and Implementation,* Elsevier, New York.
[8] Duncan, J.M. (1994): The role of advanced constitutive relations in practical applications, *Proceedings of XIII ICSMFE,* New Delhi, India, pp. 31–44.
[9] Duncan, J.M. (1996): State of the art: limit equilibrium and finite element analysis of slopes, *J. Geotech. Engrg., ASCE,* 122, pp. 577–596.
[10] Nakai, T. (1989): An isotropic hardening elastoplastic model for sand considering the stress path dependency in three-dimensional stresses, *Soils and Foundations,* 29(1), pp. 119–137.
[11] Yao, Y.P., Matsuoka, H., Sun, D.A. (1999): A unified elastoplastic model for clay and sand with the SMP criterion. *Proceedings of 8th Australia New Zealand Conference on Geomechanics.* Rotterdam: Balkema, pp. 997–1003.
[12] Rodriguez-Roa, F. (2000): Observed and calculated load-settlement relationship in a sandy gravel, *Can. Geotech. J.,* 37, 332–342.
[13] Nakai, T., Matsuoka, H. (1986): A generalized elastoplastic constitutive model for clay in threedimensional stresses. *Soils and Foundations,* 26(3), pp. 81–98.

New Developments in Dam Engineering—Wieland, Ren & Tan (eds),

Geomechanical model test study on stability of concrete arch dam

Xiaoqiang Liu, Lin Zhang, Jianye Chen & Lin'guang Liu
Sichuan University, China

ABSTRACT: With the method of the combination of overload and strength-decreasing, the geomechanical model test about the stability of base and abutment is applied in this paper, and combined with the concrete double arch dam in Sichuan province. The destruction test is made to discuss the failure pattern, process and mechanism of the base and abutment stability, with the temperature analogous material simulating the weak structural planes. The degree of safety of the dam and the abutment is achieved. And the security of the project is evaluated.

1 INTRODUCTION

The key project of Tongtou hydroelectric station lies in the Yaan of Sichuan province. It is one of rundle power plants on the branch of Qingyi river, which is built for irrigation, flood prevention, aquiculture, tourism, and so on, but mostly for generation of electric. The total reservoir capacity is 2,250m^3, with the installed capacity of 60MW. The project is composed of concrete double arch dam, discharging flood tunnels on both side banks, power house and diversion system. The maximum height of dam is 77m; the crest width is 3.5m, while the width of dam base is 15.3m.

The topographic form on dam site is similar to "V", with degree of slope of 60°~80°, and the aspect ratio of valley is 1~1.2. The rock mass is mainly calcarenite and conglomerate intercalations and siltstone intercalations. There are four structural fractures near the dam site, L_{13}, L_{12}, L_{11}, L_{47} which are high dip angle. They cut cross the valley parallelly on the whole.

The distributing status of intercalations.

Fractures	Status	Width of fissure erosion (m)	Fillings
L_{13}	N5° E/SE ∠81°	0.01~0.2	Clay, adarce
L_{12}	N15° E/EW ∠87°	Right bank: 0.1~0.3	Clayey
L_{11}	N10° E/SE ∠85°	Left bank: 0.05~0.2	
L_{47}	N25° E/SE ∠86°	Left bank: 0.01, 0.2	Siltstone

There are many weak intercalations distributing in the gravel stone of the dam site, among which there are mud quality conglomerate intercalations A_1 and cobble mud quality siltstone intercalations A_2. Between top and bottom wall A_{1-9} in dam base, for the existence of ground-water, rock strength will decrease in a long time. The distributing status of intercalations can be seen in Fig. 1.

For the complexity of topographic form and geology condition, the weak structures distributing in the base and abutment of dam affect the stability of dam greatly. To discuss the failure pattern, process and mechanism of the base and abutment, to determine the degree of safety of the dam, to evaluate the security of the project and to put forth the reference for design and construction of the project, in this article, the three-dimensional geomechanical model test was made, by simulating

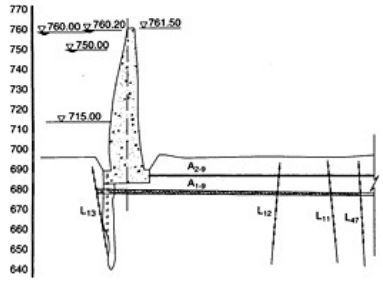

Figure 1. Four structural fractures of high angle.

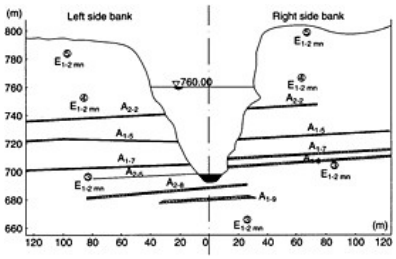

Figure 2. Weak intercalations on dam site.

the action of normal water load and sand load applied in the dam, with the method of the combination of overloading and strength-decreasing.

2 A DESCRIPTION OF SUB-SOIL

2.1 *The similarity theory*

Considering the fact that geomechanical model test is destructive experiment, the model was designed as Fig. 2 according to the similarity theory and the condition of the project synthetically.

The design of the model.

Items	Designs	Principles
Law of similarity	$CE=C_Y \cdot C_L$	(1) Geometrical similarity
	$C_\varepsilon=1, C_f=1, C_\mu=1$	(2) Similarity of mechanical and deformation characteristic
	$CE=C_\sigma=C_c=C_\tau$	(3) Similarity of shear strength parameter of rock masses, weak intercalations and faults
	$C_F=C_Y.C_L^3=C_E.C_L^2$ If $C_{Y=}1$, $C_E=C_L$, $C_F=C_L^3$	(4) Similarity of load and boundary conditions
Geometric proportion	150	(1) To meet the precision demand of the test
		(2) To consider modeling workload and economic effects synthetically
Simulation context	$200\times250m^2$, E.L.: 655.00m	(1) Undistorted edge-restraint condition
		(2) Propitious to dispose system of loading, measuration, and so on
Geological structures	L_{13}, L_{12}, L_{11}, L_{47} structural fractures	(1) To emphasize the major element, and to ignore the minor element properly
	Left bank: A_{2-5}, A_{1-7}, A_{1-5}, A_{2-2} Right bank: A_{1-8}, A_{1-7}, A_{1-5}, A_{2-2}	(2) Considering the worst-case factor
Model materials	To mix barite powder, gypsum, adhesives, additive according to certain proportion	To meet the demand of the similarity theory

Note: C_E, C_γ, C_L, C_σ, C_c and C_F stand for the proportion of modulus of deformation, bulk density proportion, geometric proportion, stress proportion, binding power proportion and concentrated force proportion. C_μ, C_ε, C_f stand for proportion Poisson's ratio, deformation proportion, friction coefficient proportion.

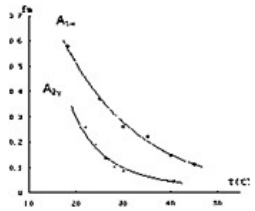

Figure 3. Intercalations' relation curves between f and T.

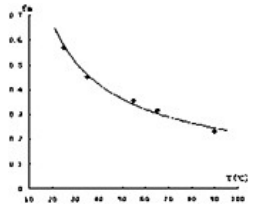

Figure 4. Rock's relation curves between f and T.

The method of the combination of overloading and strength-decreasing is applied in this test. First, decreasing the shear strength of weak structure in the dam base and abutment; second, over-loading on the dam upstream face by the water pressure continuously until destabilization and wreck happened to the dam base and abutment entirely. Strength-decreasing is realized through temperature analogous material. So according to test tasks, to simulate intercalations ($A_{1\text{-}I}$, $A_{2\text{-}j}$) by temperature analogous materials (No.1, No.3), which relation curves between f and T is showed as Fig. 3, structural fractures by model materials is mixed with a certain temperature analogous materials, showed as Fig. 4.

2.2 *Loads on the model and loading system*

Considering test tasks and condition synthetically, water load, sand load and osmotic pressure are determined to be simulated in the test. According to the similarity theory, similarity of load between the prototype and model must be satisfied. The method of applying loads by aerifying bags. The water and sand loads are applied through latex rubber bags distributed in the different elevations, which are aerified to apply pressures on the model. The osmotic pressure is also realized through latex rubber bags and spreading-load board as the mode of the surface force.

2.3 *The measuring system of the model*

The measuring system includes displacement measuration and deformation measuration. In this test, the latter gives priority to the former which includes dam surface displacement measuration, rock mass displacement measuration and intercalations measuration of interior relative displacement. Following the principle that it is able to not only reflect the dam's comprehensive distributing character of the displacement and deformation, but also monitor local position, 47 displacement measuring points and 22 deformation measuring points are installed.

2.4 *The test procedure*

Considering the stress difference of embankment and dam abutment during operation, also the influence of floodwater and rock strength of dam abutment and base, in this test, three steps are divided as follows.

Step 1: Preloading dam body with minor load, lifting pressure to the level of normal load to measure, then overloading to 1.2 multiple normal load to measure.

Step 2: Maintaining the loading level and rock body deadweight of the former step, warming up rock body in dam abutment and base by 10-stage, and measuring the measuration point. At this step, shear strength is reduced at the half of design value.

Step 3: Maintaining the temperature level and rock body deadweight of the former step, continuing to overload on the dam upstream to measure until destabilization and wreck happen.

3 TEST RESULTS AND ANALYSES

3.1 *Test results*

Test results include: the displacement developing process of embankment surface, abutment and base of dam; the interior relative displacement developing process of weak intercalations; the deformation developing process of typical sites of dam surface; the failure pattern and process of rock mass.

3.2 *Analyses of results*

3.2.1 *The distributing character of measured value*

(1) The distributing character displacement

Dam displacement distributing character accords with general law in sum. But for the reason of complexity of rock structure, weak lithologic characters, soft intercalations' distributing in the rock and the existence of L_{11}, L_{12}, L_{47} fractures of high dip angle, the particularities is that the displacement of left dam abutment is bigger than that of right one.

The displacement distributing character, of rock surface and interior one of soft intercalation, is also that the displacement of left side is bigger than that of right one. As for the displacement of rock surface, the maximal displacements are found in the position near the outcrops of intercalation A_{1-5}. Under the action of arch thrust, osmotic pressure, deadweight and boundary constraint, rock of dam abutment shows the tendency of motioning toward channel, character that measuring points' displacements of downstream are bigger than that of upstream. Because of intercalations' structural character, intercalations' relative displacement show specific character that higher elevation points' displacement are bigger than lower ones, that maximal displacement appears when rock strength decreases, which can be found near intercalations A_{1-5}, A_{1-7} in the left side bank, near intercalations A_{1-5} in the right one.

(2) Distributing character of deformation

It can be concluded from test that deformation distributing character accords with general law before decreasing rock strength. When rock strength decreases, there is a great adjustment of stress. Especially for the existence of plastic deformation, measured values increase significantly and conversion between compression deformation and tensile deformation happens.

In all, the course of deformation's development is similar to the one of displacement's.

3.2.2 *The course of failure's development*

The measured values' curves of development figured as Figs 5~6

(1) Step 1:

All the measured values are not obvious, included in the displacement of dam, the rock's displacement of dam abutment, the intercalations' relative displacement and deformation of dam surface. It shows that the dam can operate safely in this step.

(2) Step 2:

Although all the measured values go on increasing, the structure can still bear load with fissures' going on developing. It is left side bank that fissures first appear in, then vertical tension crack in the upstream of dam abutment, and then shear crack in the down stream of dam abutment.

(3) Step 3:

This step is characterized with outstanding plastic deformation, increasing displacement of dam accelerating, until the failure of the structure happens.

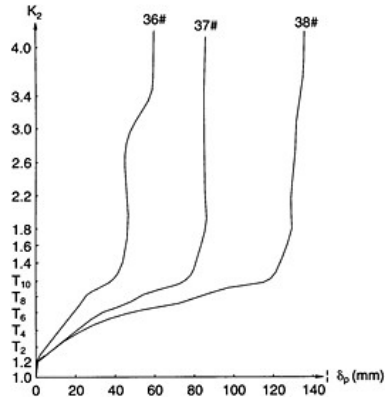

Figure 5. Displacement curves of measuring points on left side bank rock.

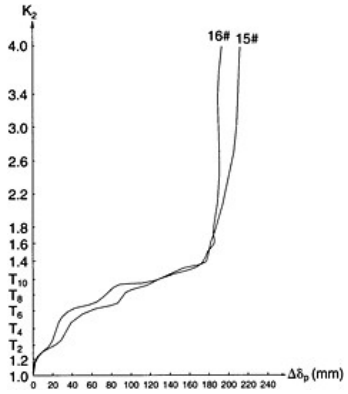

Figure 6. Relative displacement curves of intercalations A_{1-5}.

3.3 *Integrative safety degree of stability*

The integrative safety degree of stability of dam abutment can be assessed from 5 aspects as follows: all measured points' displacements course curves of development, all intercalations' interior relative displacement course curves of development, all measured points' deformation course curves of development on the dam's surface, the on-site record of failure course and pattern, and all temperature analogous materials' calibration curves achieved from material tests. The strength reserving factor, K_1 is determined as 1.95, and K_2, overloading factor as 1.6~1.8.

So the integrative safety degree of stability of dam abutment can be got according to Formula 1:

$$K_C=K_1\times K_2$$

That is the integrative safety degree of stability is determined as 3.12~3.51.

4 CONCLUSIONS

(1) Under the condition that normal load is applied and strength of abutment rock is kept, that is normal operation, the abutment and base can keep stable.
(2) When load arrives at 1.2 times of normal load, that is special operation, which might be caused by the emergence of superflood, the displacement and deformation is still not obvious. It shows that the dam can still operate safely.
(3) To maintain the level of load and decrease mechanical properties synchronously, and all measured values increase gradually. And obvious fissures appear in abutments, especially in the left abutment. So the reinforcement to the dam abutments especially to the left abutment is necessary.
(4) The result shows that the integrative safety degree of stability, K_C is 3.12~3.51.

Since having considered the emergence of superflood and the evolvement course of strength's decrease during the long running, the test can reflect the status of the project with a more intuitionistic and actual form.

REFERENCES

[1] E.Fumagalli. Statical and Geomechnical Models. Springer-Verlag/Wien, 1973.
[2] Xinghua Chen. The Structural Model Test of Brittle Materials. Water Conservancy and Power Poublishing House, 1984.
[3] Lin Zhang. The Failure Mechanism of Arch Dam Abutment Including in intermittent Joins. Sichuan University, Jou.1, 2000.
[4] Chaoguo Li, Chengqiu Hu. The 3-dimension Geomechanical Model Test Research of Baise RCC Gravity Dam Base Stability. HongshuiRiver, Vol.16, Jou.2.
[5] Chaoguo Li, Lin Zhang. The Destructive Test Research of Puding RCC Arch Dam. Hydroelectric Power Publishing House, Jou.1,1996.

New Developments in Dam Engineering—Wieland, Ren & Tan (eds),

Application of combined Discrete Crack and Non-Orthogonal Smeared Crack model in seismic response of arch dams

V.Lotfi
Amirkabir University of Technology, Iran

R.Espandar
Shahid Beheshti University, Iran

ABSTRACT: There are different techniques to examine the nonlinear seismic behavior of concrete arch dams, among which, Discrete Crack (DC) method is the most popular. A more recent option introduced for this purpose, is the Non-Orthogonal Smeared Crack (NOSC) approach. In this paper, a special finite element program is developed based on the combined Discrete Crack and Non-Orthogonal Smeared Crack (DC-NOSC) technique. Using this method, the nonlinear dynamic behavior of a typical thin arch dam is considered, and the results are compared against other simpler methods.

1 INTRODUCTION

Discrete Crack (DC) modeling is a very common technique for investigations regarding nonlinear seismic behavior of concrete arch dams [1–2]. Non-Orthogonal Smeared Crack (NOSC) approach is another more recent method, developed [3–4] as an alternative to avoid complex mesh definitions and inefficient algorithms for treating probable extensive cracking in analysis of complex structures such as concrete arch dams.

In this study, a special finite element program is developed [5] based on the combined Discrete Crack and Non-Orthogonal Smeared Crack (DC-NOSC) technique. It also includes Linear (LN) analysis, Discrete Crack (DC) method, and Non-Orthogonal Smeared Crack (NOSC) approach as its particular cases.

The basic concepts and the nonlinear models employed in the program are explained briefly at first. Then, the nonlinear dynamic behavior of a typical thin arch dam is considered by utilizing this program, and the results are discussed in comparison with other simpler options mentioned above.

2 MODELING STRATEGIES

In this study, three approaches are considered in the nonlinear modeling of concrete arch dams, which are briefly explained below.

2.1 *Discrete Crack (DC) model*

In this approach, two types of elements are utilized, the linear 20 noded isoparametric solid elements and the nonlinear 16 noded isoparametric interface elements. In general, interface elements could be used in this technique to model cracking at weak surfaces such as contraction, working, and perimetral joints, or even any pre-defined surfaces in mass concrete which are deemed to be the possible cracking surfaces. However, by discrete crack modeling, it is assumed herein that non-linearities are limited exclusively to contraction and perimetral joints. This is to avoid complex mesh definitions and inefficient algorithms for treating probable extensive cracking. Therefore, in this manner it is clear that solid elements can be taken as usual 20 noded linear isoparametric elements whose stiffnesses are calculated once at the beginning, assembled and stored for recursive application throughout the analysis. While, interface elements stiffnesses need to be updated at each iteration.

2.1.1 *Isoparametric interface element*

Each interface element consists of two spatial 8 noded isoparametric layers placed originally on top of each other with potential for being separated partially or completely. In the special finite element program developed, MAP-76 [5], there are two nonlinear options available for these elements. A separation alternative, which simply models joint opening and closure while shear stresses in the joint are assumed to behave linearly (NCRIT =1), and the second option which is separation along with shear stresses release mechanism (NCRIT=2). Both available models are relatively simple and efficient with no convergence problems.

2.2 *Non-Orthogonal Smeared Crack (NOSC) model*

In this type of analysis, the whole dam body is merely modeled by solid elements having smeared crack behavior with softening imposed for the constitutive relations. In this technique, several non-orthogonal cracks at each sampling point are allowed. This would be an ideal cracking model if the dam body is assumed to be a monolithic structure and the perimetral joint is disregarded. The main deficiency of this model in its usual form is that, it cannot recognize pre-defined weak surfaces and treat them in a special manner.

2.2.1 *Non-Orthogonal Smeared Crack (NOSC) constitutive relationship*

In the pre-cracked phase, there are several possibilities for modeling concrete. However, for simplicity and without loss of generality, a linearly elastic stress-strain relationship is adopted herein.

Following the details given elsewhere [3–4], the incremental stress-strain relation at a crack sampling point can be written as:

$$\Delta\sigma = \{(\mathbf{D}^{co})^{-1} + \sum_{i=1}^{NCRACK}[(\mathbf{T}_{\varepsilon}^{*})_i(\mathbf{D}^{cr})_i^{-1}(\mathbf{T}_{\varepsilon}^{*})_i^{T}]\}^{-1}\Delta\varepsilon \tag{1}$$

in which $\Delta\sigma$ is the incremental stress vector, and $\mathbf{D}^{co}$ is the elastic constitutive matrix of intact concrete. Meanwhile, NCRACK is the number of cracks (a maximum number of NCRACK=10 is allowed), and $(\mathbf{T}_{\varepsilon}^{*})_i$ is a 6×3 matrix transforming increments of ith crack strains from local to global system of coordinates. Also, $\mathbf{D}^{cr}$ relate the stresses along the n, s, and t directions of each crack to their corresponding local crack strains. This is a 3×3 matrix, which in general distinguishes among mode I and mode II types of failure. However, it is normally assumed that there is no interaction between these two modes of failure, thus the coupling among normal and shear components in the crack traction-strain expression may be neglected. As a result, the crack interface operator reduces to the diagonal format as follows:

$$\mathbf{D}^{cr} = \begin{bmatrix} D_c & 0 & 0 \\ 0 & \beta_c G & 0 \\ 0 & 0 & \beta_c G \end{bmatrix} \tag{2}$$

where β_C is assumed to be a constant, referred to as shear retention factor (here assumed as 0.1), G is the usual uncracked concrete shear modulus, and D_c is the cracked concrete modulus, normal to the crack plane defined as follows:

$$D_c = -\frac{\alpha_2 f_t^2 l^*}{2G_f} \tag{3}$$

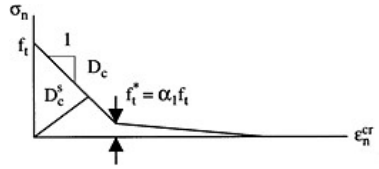

Figure 1. Bilinear idealization of strain softening branch.

in which f_t and G_f are tensile strength or crack initiation stress and fracture energy release rate, respectively. These parameters are material constants. α_2 is a factor which is different for each region of the softening curve, i.e. it changes in the second part of this curve which starts at a reduced tensile strength of $f_t^*=\alpha_1 f_t$ (Fig. 1). Of course, the factor α_2 should be determined such that the total area under the softening curve becomes equal to fracture energy density of the material. In this study, it was decided to use values of 0.01 for α_1 and 1, 0.0001 for α_2 in the two regions of softening branch, respectively. *l** is crack bandwidth, however, in finite element analysis this is taken as a characteristic length to overcome the objectivity with respect to the mesh size. One can find different alternatives in defining *l**. Here, characteristic length is chosen as the side of an equivalent cube having the same volume as the tributary volume at the cracked sampling point of a 20-noded solid isoparametric elements [6].

2.3 *Combined Discrete Crack and Non-Orthogonal Smeared Crack (DC-NOSC) technique*

In this method, the above two nonlinear approaches are combined. Another words, the dam body is modeled by solid elements with smeared crack mechanism specified for them. At the same time, interface elements are used for the contraction and perimetral joints. Therefore, it is obvious that it is a step toward reducing the deficiencies of the other two nonlinear alternatives mentioned above.

3 APPLICATION ON CONCRETE ARCH DAMS

In this section, the nonlinear behavior of Shahid Rajaee arch dam is being studied by application of the models discussed above. The dam is 130m high, with the crest length of 420m and it is located in north of Iran in the seismically active foothills of Alborz Mountains, near the city of Sari.

3.1 *Finite element idealization*

3.1.1 *Selected models*

Four cases are considered. Case A, a linear model (LN), which is mainly used for comparative purposes, and three nonlinear cases defined as follows: Case B is based on the Discrete Crack (DC) model. Case C is the analysis relying on non-orthogonal smeared crack (NOSC) approach, and case D is utilizing the combined discrete crack and Non-Orthogonal Smeared Crack (DC-NOSC) model.

The finite element mesh for cases B and D where discrete crack elements are used (Fig. 2), include 76 isoparametric 20 noded solid elements, and 84 isoparametric 16 noded interface elements. These models consists of a total of 873 nodes and 2316 degrees of freedom. The mesh for the cases A and C (LN and NOSC models) are similar to the other two cases except that, interface elements are excluded. Although the geometry of the dam is not exactly symmetric, but it was decided to idealize it as a symmetric model based on average parameters of the two sides. It is clear in this case, discretization might be performed on one half of the dam and conditions of symmetry or anti-symmetry would be applied in the mid-plane for different components of earthquake excitations. However, this was disregarded and the whole dam is discretized in this study. Therefore,

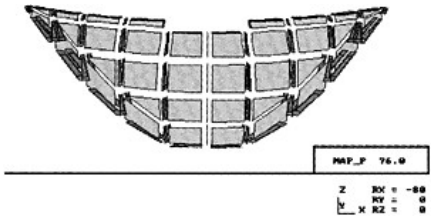

Figure 2. The finite element mesh for cases B and D (shrunken model).

symmetric results are expected throughout the analyses knowing that cross canyon excitation is also neglected, and this fact is used as an additional check for the accuracy of obtained results.

Dam-reservoir interaction is considered based on modified Westergaard's method [7]. Meanwhile, the foundation is taken as rigid. Both of these idealizations were decided to reduce computational efforts. Of course, it is clear that rigid foundation assumption would create large tensile stresses near the boundaries for linear analysis. However, for nonlinear cases considered, these high tensile stresses are expected to release, and this can be envisaged as challenging tests for these nonlinear models.

In the analyses carried out, the Rayleigh damping matrix is applied and the corresponding coefficients are determined such that equivalent damping for frequencies close to the first and sixth modes of vibration would be 10% of the critical damping.

3.1.2 *Basic parameters*

The concrete is assumed to have the following basic properties:

- Elastic modulus E_c=30.0GPa
- Poisson's ratio v_c=0.18
- Unitweight γ_c=24.0kN/m^3

The additional concrete parameters required for smeared crack modeling (cases C and D) are:

- Fracture energy release rate G_f=2400.0N/m
- Initial tensile strength f_t=3.0MPa
- Threshold angle α=15.0 degrees

Interface elements utilized for cases B and D are applied with the following conditions:

- Joint tensile strength σ_n^*=0.5MPa
- Ratio of normal stiffness coefficient to concrete elastic modulus k_n/E_c=4.0
- Ratio of tangential stiffness coefficient to concrete elastic modulus $k_{s,t}/E_c$=2.0
- Nonlinear model specified for contraction joints NCRIT=1
- Nonlinear model specified for perimetral joint NCRIT=2

The water is taken as incompressible, inviscid fluid, with weight density of 10.0kN/m^3 and the water level to be at elevation 485.0masl (h=122.0m).

3.1.3 *Loading*

It should be mentioned that static loads (weight, hydrostatic pressures) are visualized as being incrementally increasing in time until they reach their full magnitude. Therefore, the same time step of 0.01 second, which is chosen in dynamic analysis, is also considered as time increment of static loads application. It is noted that time for static analysis is just a convenient tool for applying the load incrementally, but it is obvious that inertia and damping effects are disregarded in the process. In this respect, the dead load is applied in ten increments and hydrostatic pressures thereafter in another ten increments at negative range of time. At time zero, the actual nonlinear dynamic analysis begins with the static displacements and stresses being applied as initial conditions.

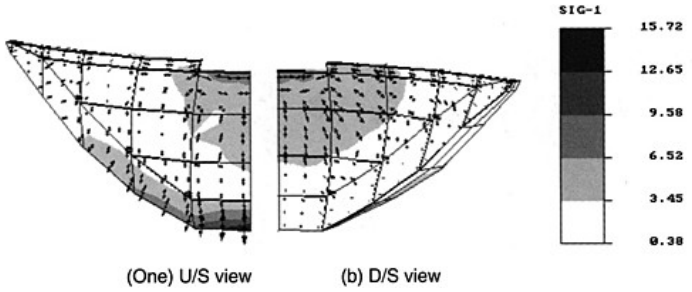

Figure 3. Envelope of maximum tensile stresses (MPa) for the LN model (Case A).

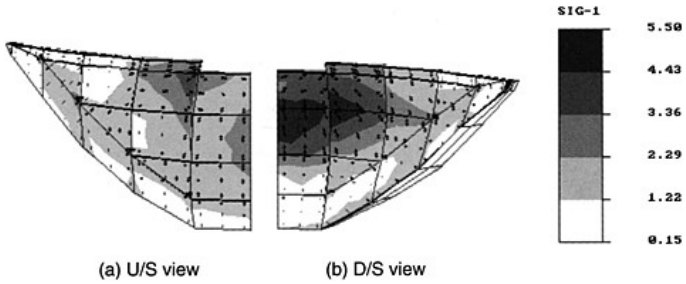

Figure 4. Envelope of maximum tensile stresses (MPa) for the DC model (Case B).

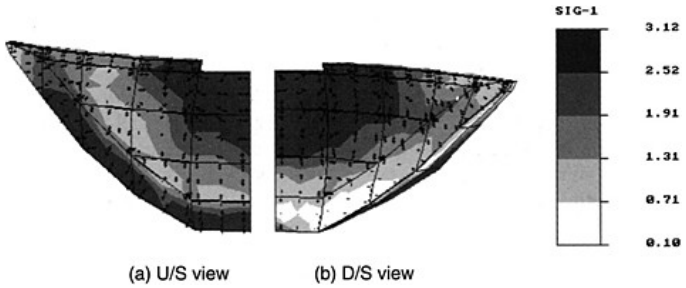

Figure 5. Envelope of maximum tensile stresses (MPa) for the NOSC model (Case C).

The dynamic excitations include two components of Friuli-Tolmezzo earthquake records (cross-canyon excitation neglected to have a symmetric loading) normalized based on the frequency content for MDE condition with a peak ground acceleration of 0.56g in the horizontal direction. The time duration considered is 12 seconds in each case.

3.2 *Numerical results and discussion*

As mentioned in the previous section, four cases are considered, the linear model (LN), and three nonlinear models. In each case, envelopes of maximum tensile stresses are obtained (Figs 3–6), and the results of maximum stresses occurring on both faces are summarized on Table 1 below.

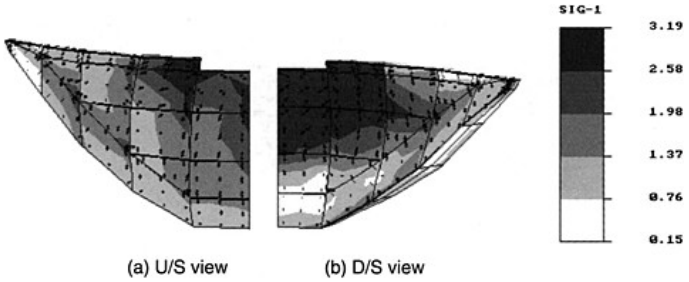

Figure 6. Envelope of maximum tensile stresses (MPa) for the DC-NOSC model (Case D).

Table 1. Maximum tensile principal stresses (MPa) for different cases.

		Maximum tensile principal stress (σ1)			
		Spillway and middle portion		Base and abutments	
Case	Model	U/S	D/S	U/S	D/S
A	LN	8.90	8.90	15.72	2.09
B	DC	4.31	5.50	1.93	2.53
C	NOSC	3.12	3.12	3.12	2.45
D	DC-NOSC	3.19	3.19	1.84	2.18

For the linear (LN) model, case A, it is observed that maximum tensile stresses for the spillway and abutments regions reach to maximum values of 8.9MPa and 15.72MPa, respectively (Fig. 3). The maximum tensile principal stresses of these zones occur in the arch direction and perpendicular to the abutments as expected.

For the case B, which is a Discrete Crack (DC) model, it is noted that maximum tensile stress for the whole analysis is limited to 5.5MPa, which is occurring approximately 25 meters below the spillway on the downstream face (Fig. 4). It is clear that high tensile stresses in the spillway and abutments regions observed in the linear case, are released in this case by opening of the joints. However, as the central cantilevers move toward upstream, a maximum tensile stress of 5.5MPa develops in the cantilever direction on downstream face. Of course, this limited stress is still higher than the tensile strength of concrete lifts or mass concrete itself. At the base and abutments, the maximum tensile stress observed is a much lower value of 2.53MPa.

Case C is based on the Non-Orthogonal Smeared Crack (NOSC) model. The joints are not considered in this case. The plots corresponding to envelopes of maximum tensile stresses for this case are depicted in Fig. 5. It is observed that maximum tensile stresses are limited to 3.12MPa. This is slightly higher than the tensile strength of mass concrete considered (3.0MPa). However, the amount of overstressing is negligible (4%). This overstressing is due to the fact that additional cracks are not allowed unless minimum angle between the new crack and previous crack directions at a sampling point is larger than the threshold angle.

Case D represent the combined Discrete Crack and Non-Orthogonal Smeared Crack (DC-NOSC) model. As for the envelopes of maximum tensile stresses (Fig. 6), it is noted that the distribution on the upstream face is different with NOSC model and similar to DC model. However, for downstream face it is closer to the NOSC results. This means that opening of contraction and perimetral joints are influencing this distribution significantly on the upstream face. The maximum tensile stress on the whole dam body is 3.19MPa, occurring in the spillway and middle portion of

Table 2. Maximum displacements (cm) at crest of the dam.

		Right 1/4 point			Center point		
Case	Model	U	V	W	V	W	
A	LN		−2.84	6.40	−0.54	11.71	−1.30
B	DC		−2.76	6.79	0.97	11.64	1.89
C	NOSC		−2.73	6.40	0.63	11.31	1.38
D	DC-NOSC		−2.90	6.79	0.84	11.23	2.23

Table 3. Maximum joint openings (cm) at crest of the dam.

		Left and Right 1/4 joints		Middle joint		
Case	Model	Upstream	Downstream	Upstream	Downstream	
B	DC	0.29	0.78	1.65	2.14	
D	DC-NOSC	0.29	0.61	2.10	2.16	

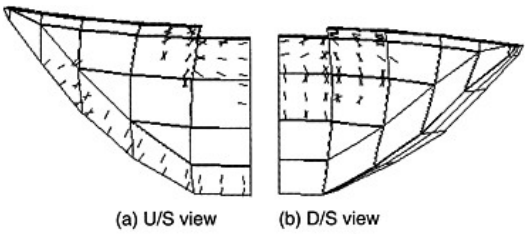

Figure 7. Crack pattern for the NOSC model (Case C).

the dam body on both faces. The amount of overstressing (6.3%) is slightly greater than similar value for case C (NOSC model), but still not significant. Meanwhile, the magnitude of maximum tensile stress on the upstream face of the base and abutment regions is much lower than for case C, and it is close to the case B (DC model). This reveals that opening of perimetral joint is the dominant behavior for limiting tensile stresses in this region.

The history of displacements at the right quarter point and the central point at the dam crest are also monitored through time and the maximum values are summarized in Table 2.

It is noted that maximum values, which correspond to stream component of center point displacement, are almost similar in all four cases. However, a major drift toward the upstream direction is observed in the displacement history for the NOSC model. The amount of drift is decreased for the DC-NOSC model, but it is still noticeable.

Furthermore, values of maximum joint openings at the crest for the middle and 1/4 point's joints can be found in Table 3 for the cases which joints are modeled (Cases B and D). It is observed that maximum value of joint opening in the upstream face of middle joint increases significantly for the case D (DC-NOSC) in comparison with case B (DC).

It is also interesting to compare crack patterns at the end of analyses for cases C and D that utilize smeared crack mechanisms. These are shown in Figs 7 and 8. The plots exhibit similar numbers and cracking extent on the downstream face, which is concentrated in the middle portion

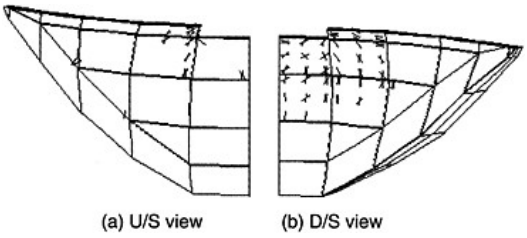

Figure 8. Crack pattern for the DC-NOSC model (Case D).

and adjacent to the spillway region. However, for the upstream face, case D (DC-NOSC) shows much less cracks in the spillway region. Meanwhile, there are no cracks in the upstream face of the base and abutment regions for case D, even though significant cracking occurred in this region for case C (NOSC).

4 CONCLUSIONS

The nonlinear dynamic behavior of Shahid Rajaee concrete arch dam is considered due to the Friuli-Tolmezzo earthquake records. Four cases are analyzed, a linear model and three nonlinear cases based on Discrete Crack (DC), Non-Orthogonal Smeared Crack (NOSC), and combined Discrete Crack and Non-Orthogonal Smeared Crack (DC-NOSC) models. Overall, the main conclusions obtained can be listed as follows:

- Although, the usual DC model cannot effectively limit the maximum tensile stresses to the concrete tensile strength, both NOSC and DC-NOSC models are approximately successful in this task.
- Having the practical limiting value of concrete tensile strength for maximum tensile stresses perceivable on the dam body, it is observed that, there is slight overstressing in the range of 4% and 6.3% for NOSC and DC-NOSC models, respectively. However, from practical point of view this minor amount is negligible.
- The maximum tensile stresses on the upstream face of the base and abutments regions for the DC-NOSC model is much lower than similar value for the NOSC approach, and it is close to the DC model. This reveals that opening of perimetral joint is the dominant behavior for limiting tensile stresses in this region.
- The major drift toward upstream which is usually noticed as the prominent characteristic of displacements history in NOSC approach, is decreased in the case of DC-NOSC model.
- The maximum value of joint opening at mid-crest on the upstream face increases significantly for the DC-NOSC model in comparison with DC technique.
- Comparing NOSC and DC-NOSC models from point of view of crack patterns, it is observed that, DC-NOSC model shows much less cracks in the spillway region. Furthermore, there are no cracks in the upstream face of the base and abutment regions for this case, even though significant cracking is observed in that region for the NOSC model. Therefore, it could be concluded that in general, NOSC approach results in unrealistic crack patterns and overestimates the degree of damage occurring in the dam body.
- Overall, DC-NOSC model is proved to be a more consistent and realistic approach from different aspects in comparison with both DC and NOSC models alone. This combined model is certainly a step toward reducing the deficiencies of other simpler approaches discussed in applications regarding nonlinear seismic analysis of concrete arch dams.

REFERENCES

[1] Hohberg, J.M., “A joint element for the nonlinear dynamic analysis of arch dams”, Report No. 186, Institute of Structural Engineering, ETH Zurich, Switzerland, 1992.
[2] Lotfi, V., “Application of discrete crack in nonlinear dynamic analysis of Shahid Rajaee arch dam”, Int. Journal of Engineering, Vol. 14, No. 1, 2001.
[3] Espandar, R., “A study of nonlinear dynamic response of concrete arch dams”, Ph.D. Dissertation, Dept. of Civil Eng., Amirkabir University of Technology, Tehran, Iran, 2001.
[4] Lotfi, V. and Espandar, R., “A study of nonlinear seismic response of concrete arch dams”, Report No. 31305301, Amirkabir University of Technology, Tehran, Iran, 2001.
[5] Lotfi, V., “MAP-76: A program for analysis of concrete arch dams”, Amirkabir University of Technology, Tehran, Iran, 2001.
[6] Cervera, M., “Nonlinear analysis of reinforced concrete structures using three dimensional and shell finite element models.” Ph.D. Dissertation, Dept. of Civil Engr., Univ. Coll. of Swansea, Wales, 1986.
[7] Clough, R.W., Chang, K.T., Chen, H.Q. and Ghanaat, Y., “Dynamic interaction effects in arch dams”, Report No. UCB/EERC 85/11, University of California, Berkeley, Calif., 1985.

This page intentionally left blank.

New Developments in Dam Engineering—Wieland, Ren & Tan (eds),

On stability of dam body and abutment rock mass of Xiluodu arch dam

Lu Xiaomin, Ren Qingwen & Wang Ailing
Hohai University, P.R. China

ABSTRACT: In this paper for the stratified structure of the arch dam abutment rock mass in Xiluodu hydropower station, we adopted the method of non-linear block element method to simulate the discontinuous deformation of interface between stratified rocks. Through the degree of safety of points and the destroy of the interface, we analyzed the most dangerous part in arch dam rock mass, and adopt overload method to study the holistic degree of safety of the arch dam.

1 INTRODUCTION

Xiluodu hydropower station is sited at the Xiluodu valley which is at downstream reach of the main river of Jinshajiang River, according to the terrain and the geology condition of the site and the arrangement of the hinges, we adopt double-curvature concrete arch dam, which is 285m in height and the crest elevation is 610m, there are a underground plant and spillway tunnels in the rock mass on both left and right banks.

The abutment rock body of Xiluodu arch dam is made up of rock layers, which ranges from 3 to 10 (named p_2/β_3 to p_2/β_{10}). Its character is stratified structure. The relative disturbance between the layers may lead to the potential danger for the stability of dam, there is a soft stratum under the elevation of 332m, and the influence of deformation to the stability of dam body is to be studied. The interface of layers is thin in strength. Under the action of arch thrust, the interfaces of the rock near to abutment have the possibility of occurring yielded, cracked destroy, which can cause excessive deformation of abutment rock mass, and farther affect the stability of the dam. Nonlinear block element method can comparatively conveniently simulate the discontinuous deformation and destroy between the layers. In this paper, we adopt nonlinear block element method[1] to analyze the deformation and stability of dam and abutment rock mass, which can reduce the workload, relative to FEM when meshing.

2 COMPUTATIONAL THEORY AND MODEL

2.1 *The basic theory of block element method*

It is not described in detail about the theory of block element method here, readers can refer to the literature[1]. Of which the basic idea is regarding the displacement of rigid body as the basic unknown variable. Considering the deformation energy of the interface element at the same time, it is educed that the dominating equation to solve the structure-displacement field through principle of minimum potential energy. The displacements between block interfaces are discontinuous.

In block element, we can take the non-linear material model of the blocks or the interface between the blocks into account. Here we choose the latter to simulate mainly two kinds of destroy forms of materials: shear yielded and cracked. The former is judged by M-C criterion and the latter by criterion of normal tension.

If the normal tension of interface $\sigma_z > \sigma_t$ (tensile strength), and interface element is cracked, it is thought to be losing of rigidity; if the yielding function is

$$F = \sqrt{\tau_{xz}^2 + \tau_{yz}^2} - C = \sigma_z f > 0 \tag{1}$$

Then, shear yielding of the interface is engendered. According to the flow principle we can deduce its plastic matrix

$$[D]_p = \frac{1}{G + f^2 G\lambda} \begin{bmatrix} \frac{G^2\tau_{xz}^2}{B^2} & \frac{G^2\tau_{xz}^2\tau_{yz}^2}{B^2} & \frac{f\lambda G^2\tau_{xz}^2}{B^2} \\ \frac{G^2\tau_{xz}\tau_{yz}}{B^2} & \frac{G^2\tau_{yz}^2}{B^2} & \frac{f\lambda G^2\tau_{yz}}{B^2} \\ \frac{f\lambda G^2\tau_{xz}}{B^2} & \frac{f\lambda G^2\tau_{yz}}{B^2} & G^2\lambda^2 f^2 \end{bmatrix} \tag{2}$$

where $B = \sqrt{\tau_{xz}^2 + \tau_{yz}^2}$, c is the cohesion of interface materials, f is friction coefficient.

2.2 *Method of stability analysis*

It is a complicated and difficult problem to distinguish the stability of rock mass, at present, the stability analysis methods of rock slope fall into two kinds. First is referred as direct method. Safety coefficient of sliding resistance can be directly obtained by resistance and sliding force. The second is indirect method First of all the numerical analysis methods (FEM, DEM, DDA etc.) are used to determine displacement and stress field, then method of overload or strength reserve is adopt to calculate safety coefficient indirectly. In this method, not only the equilibrium of the forces of the sliding body, but also the displacement coordination condition and material character is taken into account, which is a more exact method for stability analysis, only that it needs to establish criterion of losing stability when reaching limit equilibrium. At present, the criterion of losing stability falls into two kinds: convergent and abrupt criterion. They are more about theory of sudden transition of displacement, or the connectivity of yielded field etc.

As for the local stability of abutment rock mass, which can be studied by the safety degree of points obtained through the first method. The formula to calculate the degree of safety k follows:

$$k = \frac{c + f\sigma}{\tau} \tag{3}$$

where σ, τ are respectively the normal compressive stress and shear stress on the layer.

In order to analyze the holistic safety degree of stability of arch dam and abutment rock mass, indirect method is applied here. Using the method of overload to make the system of arch and foundation reach limit equilibrium, we adopt convergent and sudden transition of displacement criterion to judge losing stability

3 COMPUTATIONAL RESULTS AND ANALYSIS

3.1 *Computational parameters*

Mechanics parameters of the materials of concrete and base rock are showed in Table 1.

The buoyant unit weight of sand accretion is 5.0×10^3T/m^3, and the inner frictional angle is 0°. The linear expansion coefficient of concrete is 1.0×10^{-5}/°C. Seismic design intensity: the acceleration of horizontal seismic peak value of the base rock is 0.321g.

There are 5 kinds of load:

A: normal water level 600m (upstream), the corresponding water level downstream 375.5m.
B: the elevation of upstream silt 490m.

Table 1. Mechanics parameters of the materials.

Materials	Bulk density kN/m^3 (10^4)	Modulus kN/m^3 (10^4)	Possion's ratio μ	C′(Mpa)	f
Dam concrete	2.40	24	0.167	2.50	1.00
Plm limestone	2.60	15	0.22	1.20	1.10
Slightly rock mass	2.85	14	0.20	2.50	1.35
Airslaked rock mass	2.80	9	0.25	1.70	1.18
Interface of rock mass	2.30	1	0.30	0.15	0.50

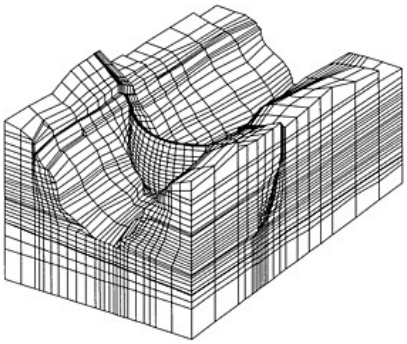

Figure 1. FEM mesh.

C: design temperature rise.
D: design temperature drop.
E: design flood water level 609.69m (upstream), the corresponding water level downstream 408.95m
F: seismic inertia force.

3.2 *Computational cases*

There are 6 computational cases, named Case1 to Case6:

Case1: A+B+C; Case2: A+B+D; Case3: E+B+C; Case4: E+B+D; Case5: A+B+C+F; Case6: A+B+D+F.

The seismic inertia force is determined by design standard, using pseudo-static method, and only along river.

Fig. 1 is FEM mesh. Coordinate origin is set at the arch crown of dam crest, x axis points to downstream, y axis points to left bank, z axis is the elevation, upwards vertically. Some meshes simulate all the interlays and the disturbed belt inside the layers, there are 13330 nodes in total, and elements 11302, among which dam elements 2134. The schematic diagram of geologic profile of the location of the interlayer disturbed belt is shown in Fig. 2.

3.3 *Computational results and results analysis*

3.3.1 *Displacement*

In this paper, we calculated the deformation and stress of cases from 1 to 6, and point safety of stability against sliding between the layers of abutment rock mass.

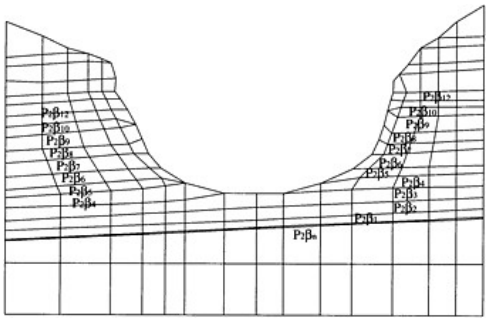

Figure 2. Rock layers.

Table 2. Maximum displacement of dam (cm).

			Direction of y			
	Displacement in the direction of x		Left	Right	Directionof z	Direction of x upstream arch crown face
Case1	Upstream	12.38	2.97	−3.18	−3.38	11.93
	Downstream	12.39	2.04	−2.60	−3.80	
Case2	Upstream	10.94	2.74	−2.67	−3.62	7.29
	Downstream	10.98	1.43	−1.57	−3.78	
Case3	Upstream	12.70	3.06	−3.32	−3.43	12.31
	Downstream	12.72	2.18	−2.79	−3.88	
Case4	Upstream	11.15	2.80	−2.77	−3.63	7.66
	Downstream	11.20	1.49	−1.66	−3.86	
Case5	Upstream	14.16	3.14	−3.33	−3.30	13.88
	Downstream	14.18	2.07	−2.64	−3.89	
Case6	Upstream	12.41	2.90	−2.82	−3.48	9.26
	Downstream	12.46	1.45	−1.59	−3.86	

The maximum displacement of dam body and the displacement of upstream arch crown face along the river are showed in Table 2.

The table 2 indicates that the displacement of the dam is not large due to the good quality of abutment rock. Under Case1, the upstream face displacement along river is about 12.4cm, while it is 12.7cm when under Case3. The maximum is about 14.2cm in Case5. The vertical displacement of dam body is mainly the settlement deformation caused by its gravity. Its magnitude is between 3.4cm and 3.9cm. In seismic case, there is obvious increase of displacement deformation along river, which is 2cm or so, and it is slightly increased in transverse and vertical direction. In the condition of temperature drop, the displacement at the arch crown is close to the maximum. The maximum locates near to the arch crown at elevation 600m or so; In the condition of temperature rise, the maximum differs from the displacement at the arch crown, which is located at elevation 510m.

3.3.2 *Stress*

The maximum stress (σ_1), the minimum stress (σ_3), and stress along the beam (σ_2) are listed in Table 3.

The upstream and downstream faces are in pressure. Principal compressive stress ranges mainly from 16 to 19Mpa. The maximum principal tension stress occurs at the upstream face, whose value is 1.19Mpa, at the right bank of dam heel (▽ 332m). The maximum compressive stress occurs on the downstream face whose value is about 19.06Mpa. At the abutment and dam heel there exists stress concentration phenomenon.

Table 3. The maximum and minimum stress on upstream and downstream faces of dam (MPa).

	Case1	Case2	Case3	Case4	Case5	Case6	
Upstream σ_1	1.0	1.16	1.04	1.19	1.11	1.08	
Downstream σ_3	−16.64	−18.46	−17.07	−18.41	−17.31	−19.06	
Upstream maximum σ_z	0.15	0.16	0.25	0.24	0.57	0.70	
Downstream minimum σ_z	−13.46	−14.35	−13.58	−14.49	−13.97	−14.85	

Table 4. Minimum safety coefficients of points of rock layers near abutment.

Case	$p_2\beta_n$ & β_1	$p_2\beta_2$ & β_3	$p_2\beta_3$ & β_4	$p_2\beta_4$ & β_5	$p_2\beta_5$ & β_6	$p_2\beta_6$ & β_7	$p_2\beta_7$ & β_8	$p_2\beta_8$ & β_9	$p_2\beta_9$ & β_{10}	$p_2\beta_{10}$ & β_{12}
Case1	4.0	3.2	8.7_L	3.6_L	3.3_L	1.9_L	1.6_L	2.0_L	1.9_L	2.7_L
			2.4_R	2.2_R	1.6_R	2.0_R	2.7_R	2.8_R	1.5_R	2.2_R
Case2	4.1	3.4	8.1_L	3.5_L	3.2_L	1.7_L	2.1_L	1.8_L	2.0_L	2.5_L
			2.8_R	2.1_R	1.5_R	2.3_R	2.7_R	2.8_R	1.6_R	2.3_R
Case3	3.9	3.2	8.3_L	3.4_L	3.2_L	1.9_L	2.1_L	1.9_L	1.9_L	2.6_L
			2.4_R	2.1_R	1.5_R	1.9_R	2.7_R	2.6_R	1.5_R	2.1_R
Case4	4.1	3.3	7.9_L	3.5_L	3.0_L	1.7_L	1.6_L	1.7_L	1.9_L	2.2_L
			2.7_R	2.1_R	1.5_R	2.2_R	2.5_R	2.7_R	1.5_R	2.1_R
Case5	3.9	2.6	8.1_L	3.1_L	3.3_L	1.9_L	2.0_L	1.6_L	1.9_L	2.3_L
			2.4_R	2.1_R	1.4_R	1–9_R	2.5_R	2.3_R	1.5_R	2.0_R
Case6	3.9	2.9	7.6_L	3.4_L	3.1_L	1–5_L	1.6_L	1.4_L	1.8_L	2.2_L
			2.6_R	2.0_R	1.4_R	2.0_R	2.3_R	2.7_R	1.5_R	2.1_R

3.3.3 *Safety coefficients of point*

The stability of the dam depends mainly on the stability of the abutment rock and foundation. The minimum safety coefficients of points for stability against sliding of layers are listed in Table 4. Subscrip L means safety coefficient of left bank, and R right bank.

At the left abutment the point safety coefficients at elevation about 520m are small, ranges from 1.4 to 1.6. At the right bank, the point safety coefficients of some area at elevation from 400m to 500m are small too, but all are above 1.4. k>1 indicates that it is in elastic state. The abutment rock is stable, but the complement degree of safety of local rock mass in arch support is not so big. It is suggested that grouting reinforcement be carried out.

3.3.4 *Destroy state of the dam body*

The calculation results indicate that the dam heel on upstream face appears cracking destroy, and the phenomenon of yielded and cracked destroy occur at the dam heel of downstream face too, which is most serious in seismic case.

3.3.5 *Ovaerload safety coefficient of the system*

In order to determine the holistic degree of safety, we adopt indirect method, and make the system reach limit equilibrium by overloading, and judge if the system reach the limit equilibrium with convergent and sudden transition criterion. The multiple of overload is the holistic degree of safety of the system.

Now we calculate the overload safety coefficient in case 1, keep the parameter of materials unchanged, and only change the bulk density of upstream water, i.e. overload coefficient k_O is the multiple increased of the water bulk density. 3 representative points on the foundation of the dam are selected to study the relationship between k_O and displacement along the river. Its results are showed in Fig. 3. Fig. 4 presents the relationship between k_O and displacement of arch crown on dam top.

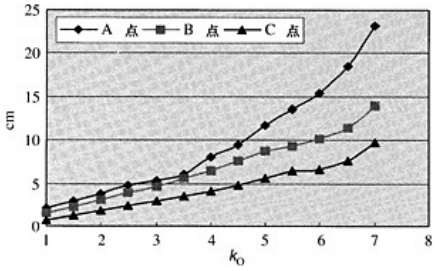

Figure 4. k_o and x-displacement.

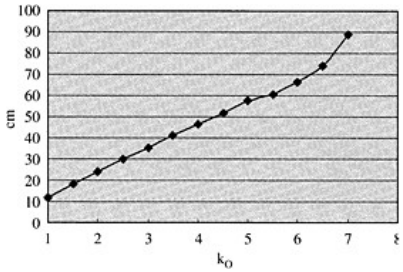

Figure 3. k_o and x-displacement.

It can be found out that when the overload coefficient is below 6, the displacement of dam and abutment rock mass is in linear relationship with overload coefficient; when beyond 6, the displacement takes on accelerating tendency. The load-displacement curves occur turning point when k_o is near to 6.5. when it reaches 7, the program is no longer convergent, so 6.5 is determined as the overload coefficient of the system.

4 CONCLUSIONS

In this paper, according to the structure characters of the abutment rock mass of Xluodu dam, we established the numerical model by the block element method, and studied the stability of the dam and foundation, conclusions are as follows:

In normal load case, the maximum displacement of the dam in the direction of the river is ranging from 10 to 14cm, and 2 to 3cm on the foundation of dam. The maximum principal tensile stress on upstream face is 1 to 1.3MPa, and the maximum principal compressive stress on downstream face is 16 to 19MPa. There are cracked and yielded elements near the foundation of dam, and the rock of abutment (foundation) is in elastic state. These indicate that the Xiluodu dam is in normal work condition.

In all load cases, the point safety coefficient of stability against sliding of abutment rock layers is above 1.4, which indicates that there is no yielding destroy, and in elastic state. The point safety coefficients of the left abutment are larger than those of the right, those near the face on foundation of dam are smaller than the far.

Using overload method make the system of dam-foundation of Xiluodu arch dam reach the limit equilibrium, we obtained holistic overload safety coefFicient by sudden transition criterion, which is about 6.5. The results show that the dam system is more safe.

REFERENCE

1. Ren Qingwen, Yu Tiantang, Theory and Computational Model of Elastic and Plastic Block Element, ENGINEERING MECHANICS, 1999 (1), P67–77.
2. Ren Qingwen, Numerical Analysis and Experiment Study of the Stability of Number 3 Monolith on the Left Bank of Three Gorges Dam, ENGINEERING SCIENCE OF CHINA, 1999 VOL.1 the third chapter, P41–49.
3. Ren Qingwen, Block Element and Its Application in Stability Analysis, JOURNAL OF HOHAI UNIVERSITY, 1995, Vol.23, No.1, P1–7
4. Sun Jun etc. Finite Element Resolution of Underground Structure, Shanghai: Tongji University publishing company, 1988.
5. Ren Qingwen, etc, Analysis of Destabilization and Treatment of High Rock Slope, JOURNAL OF ROCK MECHANICS AND ENGINEERING 1991, 10(1): P33–42.

New Developments in Dam Engineering—Wieland, Ren & Tan (eds),

Use of artificial neural network and genetic algorithms for prediction of stresses and deformations in rock-fill dam

Luo Xianqi & Liu Sifeng
China Three Gorges University, Yichang, China

ABSTRACT: Artificial neural network (ANN) and genetic algorithms (GA) were applied to Shuibuya concrete face rock-fill dam (CFRD) project. On the one hand, the paper provides a method for control and prediction of stresses and deformations depending on BP network, and rock-fill modulus of compressibility is controlled by the standard of face slab bending deformation with the trained BP network. Then other deformations of concrete face rock-fill dam are predicted by the controlling value. On the other hand, based on conclusion of BP network learning, multi-parameters of the design of Shuibuya project were controlled with genetic algorithms for the controlling condition of dam deformation.

1 INTRODUCTION

Shuibuya concrete face rock-fill dam, 233 meter high, is the highest concrete face rock-fill dam in the world. The project has complicated geologic environment, large scale and much technical problems. Furthermore, up to the present there is limited experience and very good computing method about concrete face rock-fill dam.

At present, the theories that are often used in concrete face rock-fill dam in China are as follows: Duncan's E-B model, Nalor's K-G model and Shen Zhujian's double yield surface elastic plastic model. The models are used to reflect the relation between stress and stain. However, the models are affected by material character, test conditions, and so on in the application. Furthermore, models have much shortcoming such as complex operation and high experiment cost.

With the project scale becoming large gradually, all kinds of methods are applied to make the engineering design better and more rational. For instance, such as FEM et al many methods and models have been used in the analysis of stress-strain of Shuibuya concrete face rock-fill dam, the Brazil COPEL Corporation also was commissioned to predict and analyze its deformation on the basis of dam datum.

At present, there are many data concerning design, stress-strain and other data of concrete face rock-fill dams that have been built.

Because it is difficult to know how some factors affect the stress-strain of the dam at present, the relationship between these data with the deformation of the dam is difficult to express in formula. However, ANN (Artificial Neural Network) that has widely applied in each science field at present. Therefore the application of ANN to predict the deformation of concrete face rock-fill dam is discussed. The design parameters are controlled using the training results of BP network and genetic algorithms.

2 PREDICTION AND CONTROL OF STRESS-STRAIN OF SHUIBUYA CONCRETE FACE ROCK-FILL DAM WITH BP NETWORK

BP network[1,2] is consist of input layer, output layer and hidden layer, which may include one or many layers, each layer is consist of a number of neural units.

2.1 *Selection of sample*

On the basis of project experience, the main factors that affect distortion of the concrete face rockfill dam[4] are x{H, W/H, r_d, E}, where H is height of the dam, W/H is the ratio of width to height of the vale, r_d is dry density of the rock-fill, E is modulus of vertical compressibility of the rockfill. The selected distortion data are y{Δh, δ, u1, u2, u3}, where Δh is sedimentation of the dam (stage of construction and impoundment stage), δ is deflection of the concrete face slab, u (u1, u2, u3) is three direction displacement of the peripheral joint.

According to present available data and material about the concrete face rock-fill dam, more representative and more comprehensive and better data and materials are selected as the sample [4], They are shown in table 1.

2.2 *Structure of BP neural network*

According to input and output variable number, the neural unit number of input and output layer is determined to be respectively 4 and 6. It is proved[5] that one BP network with M input layer units, 2M+1 hidden layer units and N output layer units is capable of approximating any continuing function F: I^M → R^N, Y=F(X), (0<I<1). In order to remain surely plentiful amount, the number of hidden layer unit is 10.

Therefore the architecture of the network is "4–10–6", transfer function is sigmoid function: f(x)=1/(1+exp(−x))

2.3 *Pretreatment of the sample and train of network*

2.3.1 *Pretreatment of the sample*

In order to improve the speed of the train and to converge, usually, the sample BP network is pretreated. The usual preprocessing method is normalization. For instance, normalization formula is:

$$x^{q}{}'_i = \frac{x^q{}_i - x_{i\min}}{x_{i\max} - x_{i\min}} \quad \text{or} \quad x^{q}{}'_i = \frac{x^q{}_i}{x_{i\max}}$$

where x_i^q is i variable of the q sample.

Because the dam is highest, the concrete face rock-fill dam at present in the world, the method above-mentioned is unsuitable. The preprocessing method in this paper is to change counter method of sample, that is to say, each kind of variable of sample separately rides to or eliminates by 10 integral multiples. In this paper, variables is eliminated by 100 (H), 10 (W/H), 1 (r_d), 100 (E), 100 (Δh1), 10 (Δh2), 10 (δ), 10 (u1), 1 (u2), 1 (u3) respectively.

2.3.2 *Train of BP network*

Momentum coefficient mc is 0.9, initial learning rate is 0.01, the learning increase rate is 1.05, learning decrease rate is 0.7, maximal error ratio is 1.04, error aim is 0.001. Through network training result comparison, we find six "4–10–1" the model convergence rate to be quicker, the precision is higher.

2.4 *Parameter control and deformation prediction based on the result of BP network*

According to the training result of BP network on bending deformation, change E value of Shuibuya concrete face rock-fill dam only and predict the bending deformation δ of the face slab, then the relationship between E & δ can be portrayed as figure 1.

Table 1. Samples describing the relationship between dam deformation and its main effect factor.

Serial number	Project name (country)	River valley (W/H)	Height of dam H (m)	Characteristic of rock-fill		Vertical modulus of compressibility (MPa)	Subsidence of top of dam (mm)		Deflection of faceplate (mm)	Deformation of peripheral slot (mm)		
				Lithology	Dry density (g/cm^3)		Completion	Remaining		Opening	Subsidence	Shearing
1	Foz do Areia (Brazil)	5.18	160	Basalt	2.12	37.5	3580	288	775	24	55	25
2	Salvajina (Colombia)	2.40	148	Sandstone	2.24	49	400	100	100	9.7	19.5	15.4
3	Segredo (Brazil)	4.86	145	Basalt	2.13	40	2220		340	10		
4	Anchicaya (Colombia)	1.86	140	Diorite	2.28	140	630	140	160	125	106	15
5	Golilas (Colombia)	0.90	127	Sand gravel	2.25	139	390	130	36	100	30	
6	Shiroro (Nigeria)	4.60	125	Granite	2.28	76	940	66	90	30	75	21
7	Reece (Australia)	3.10	122	Basalt	2.30	160			206	7	70	
8	Khao laem (Thailand)	7.70	115	Limestone	2.05	50			125	5	8	
9	Cethana (Australia)	2.00	110	Quartzite	2.10	185	449	114	140	12		7.5
10	XiBeiKou (China)	2.30	95	Limestone	2.15	91	320		43.3	6.8	10.4	
11	Murchison (Australia)	2.20	94	Rhyolite	2.20	225		50	44	12	9.6	7
12	Kotmale (Sri Lanka)		90	Granite	2.32	50				2	20	5
13	Machintosh (Australia)	6.00	75	Graywacke	2.30	40		187	200	4.8	20	2.8
14	Basryan (Australia)	2.90	75	Rhyolite	2.20	160			52	4.8	21.5	
15	ChengPing (China)	2.92	74.6	Tuff	2.00	73	282	35.2	104	11.1	22.6	−18.6
16	LongXi (China)	2.24	58.9	Tuff	1.89	67				0.38	5.53	3.93
17	GuanMenShan (China)	3.10	58.5	Andesite	2.00	148	67	15	41.8	−2.4	4.4	1.7

Comments: Opening—the deformation of perpendicular to slot, subsidence—the deformation of perpendicular to faceplate, shearing—the deformation of parallel to faceplate slope.

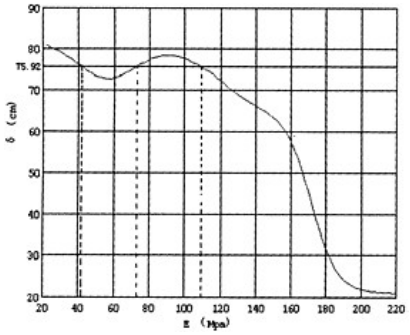

Figure 1. Relation curve between dam verticality modulus of compressibility and concrete slab bending deformation.

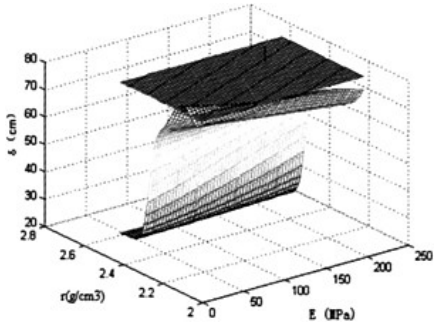

Figure 2. Relation surface between rock-fill dry density, dam verticality modulus of compressibility and concrete slab bending deformation.

Table 2. Comparing the prediction result of BP model with result of COPEL Co.

Prediction method	Deflection of face slab (cm)	Opening (cm)	Subsidence (cm)	Shearing (cm)
COPEL Co.	70.0~90.0	5.0	5.5	3.0
This article	75.52	3.10	3.66	2.67

From figure 2 (curves showing relationship among r_d, E & δ on bending deformation controlling plane 75.92cm), we find that only when 110MPa is adopted as control value, the predicted value of bending deformation of face slab will meet the demand of the criterion as r_d value and E value increasing. Thus, here we choose 110MPa as controlling value of E.

Choosing E which is determined by BP network as the design parameter of Shuibuya project, after pretreatment, the corresponding input value is that X is {2.33 0.256 2.18 1.10}, the results of prediction with trained network as shown in Table 2.

For the commission of Qingjiang Hydroelectricity Exploiture Co. Ltd, COPEL Co. of Brazil studied data of deformation of face slab derived from more than ten projects including internal and abroad. According to information of Shuibuya, the experienced formula $E_T=0.003H^2/D$(MPa) was adopted and prediction of bending deformation of face slab was about 70.0~90.0cm. The conservative deformation at the boundaries is that patulousness value is 5.0cm, sedimentation value is 5.5cm, shear value is 3.0cm. The comparing of prediction result of BP model with result of COPEL Co. is shown in Table 2.

3 PARAMETER CONTROL BASED ON GENETIC ALGORITHMS & THE RESULTS OF BP NETWORK

The main factors effecting deformation of face rock-fill dam include the height of the dam, the ratio of width and height of river valley, dry unit weight r_d, and modulus of compressibility E. when the location, height and material of dam is certain, the main factors effecting deformation of the rock block will be dry unit weight r_d, and modulus of compressibility E. Following, we study the multi-parameter control of face rock-fill dam with genetic algorithms. The controlling parameters are dry unit weight r_d and modulus of compressibility E. Aim function is the deformation of face rock-fill dam.

3.1 *Generation of initial group*

There are two variables in initial individual (chromosome). One is denoted as dry unit weight r_d. another is unit modulus of compressibility E. Ascertain the range of controlling result according to the range of r_d and E of existing engineering. Wide-spreading coding method of real number is used here. N unit vectors consisting of initial group are generated at random within the range of result. N is the size of initial group.

3.2 *Selection operation*

According to its adaptation, chromosome of the initial group is sequenced from large to small (namely, according to objective function value from small to large). The objective function is determined according to the expected value of deformation of the dam in this article. On the base of BP network, The objective function is the sum of error square between prediction result with expecting of corresponding individual (chromosome). Standard adapting function is: $F(x)=1/(1+f(x))$, where f(x) is the value of the objective function.

The proportion ($Fi/\Sigma Fi$) is calculated, and take it as the corresponding choice probability ($Pi=Fi/\Sigma Fi$) after the total sum (ΣFi) of all individuals adaptation in the chromosome group is calculated. A gambling wheel may be divided into N sector with this method, then turn the gambling wheel N times, The difference value may be obtained each time, chromosome of the sector take as choice object. In order to improve algorithmic convergence, best adapting chromosome in father generation directly is retain to next generation.

3.3 *Intersection operation*

Choose intersectional individuals according to the probability of Pc. Select two of chromosomes $\times 1$ & $\times 2$ at random and calculate. α is an random figure ranging from 0 to 1. Then we can get the new chromosomes as next generation $\times 1'$ & $\times 2'$ from formulas $\times 1' = \alpha \times 1 + (1-\alpha) \times 2$, $\times 2' = (1-\alpha) \times 1 + \alpha \times 2$.

3.4 *Variation operation*

Choose variable units according to probability of P_m and replace it with new one generated at random.

3.5 *Confirmation of the parameters and operation result*

Algorithms are edited with MATLAB language. According to the experience, some parameter values are as following: initial size of the groups N is 50, intersectional probability P_c is 0.6, variation probability P_m is 0.2.

The number of proliferous era is 400 and the result is that r_d is 2.15g/cm^3, and E is 105MPa. The result is preferable, and it shows the feasibility to apply genetic algorithms in this area.

4 CONCLUSION

4.1 BP network has the merit of rapid convergence, the high non-linear characteristic, the result reliability and so on. Compares with the finite element method, it has the merit of the short training and studying time (only needs several minutes), low spends, easy realization and so on. Compares with the method of COPEL Corporation, it is more rational, intuitionistic, as well as effective, because it bases on more than ten project which already completed as a sample, considers the many kinds of influence factors, and uses the neural network method which is similar to human brain.

4.2 Improved BP algorithm is used to enhance and improve the BP network performance in this paper. Furthermore, six "4–10–6" models is replaced with "4–10–1" model. On the one hand, the convergence is more quickly, and the precision is higher. On the other hand, it may fully use the incomplete data to enhance the result the reliability.

4.3 According to the results of BP network trained, and permit deflection of concrete face slab, it is determined that the control value of E is 110MPa. Then deformations of concrete face rock-fill dam are predicted by applying BP network. The predicting result is that maximum subsidence of dam in construction period and retaining water period respectively is 180cm and 204cm. Maximum deflection of face slab is 75.52cm, Deformation of peripheral slot: opening 3.10cm, subsidence 3.66cm, shearing 2.67cm. Through the predicting result, we know that control value of E may guarantee concrete face rock-fill dam project security in the course of work.

4.4 The genetic algorithms do not rely on the gradient information, so it has better overall situation search ability and convergence quickly, and the result is reliable. This article applies this method and BP network to control design parameter Shuibuya concrete face rock-fill dam project. The control result is that r_d is 2.15g/cm^3, and E is 105MPa. On the base of the predicting result, selection of design parameter of the Shuibuya concrete face rock-fill dam project is feasible, and the genetic algorithms may apply to control of more design parameter.

REFERENCE

1. Lou Shuntian, Shi Yang. System analysis and design based on MATLAB. Publishing company of Xian electron technology University, 1995.
2. Wen Xin, Zhou Lu, Wang Danli, Xiong Xiaoying and so on. Application Design of MATLAB neural network. Scientific publishing company, 2000.
3. Chen Guoliang, Wang Xufa and so on. genetic algorithms and its application. China post publishing company, 1996.
4. Jiang Guocheng, Fu Zhi'an, Feng Jiaji. Concrete Face Rock Fill Dam construction. Publishing company of Tsinghua university, 1997.
5. Xia Yuanyou and so on. Engineering Geology Evaluation Method for Slope Stability Based on Artificial Neural Network. Rock and Soil Mechanics, 1996. 9, 17(3).
6. Study of Concrete Face Rock Fill Dam of 200m height: staggered report of analysis on stress and strain of shuibuya face slab dam. the Yangtze River Conservancy Commission, 1998. 11.

New Developments in Dam Engineering—Wieland, Ren & Tan (eds),
© 2004 Taylor & Francis Group, London, ISBN 04 1536 240 7

Prevention of chemical suffosion of grout curtain

Ma Xiaohui, Zhai Liquen, Yang Guangzhong & Peng Hanxing
Hohai Engineering & Technical Corporation, Hohai University, Nanjing, China

ABSTRACT: After beginning of dam operation the water environment around the dam site changes greatly. The enrichment of organic materials in reservoir can enhance the erosive capacity of lower layer reservoir water and part of groundwater in dam foundation. It makes the capacity of seepage prevention of cement grout curtain turn weak, even results in changes of character of weak sandwich in dam foundation. According to the water quality data measured many years from some dams grout curtain of dam foundation should be made of grout cement modified for erosive resistance. This kind of cement consists of Portland cement mixed with 30% ground slag and additives. The experiment presents evident effect.

1 INTRODUCTION

After a dam has been built the torrential river water becomes relatively quiet reservoir water and a huge amount of organic matter enriches in the lower layer of the reservoir. This makes the environmental water of dam site form some new characteristics.

2 BASIC CHARACTERISTICS OF ENVIRONMENTAL WATER OF DAM SITE

2.1 *Reservoir water in front of a dam*

The water temperature of a reservoir is gradually getting lower from the surface to the bottom due to the thermal and gravity convection between the reservoir water layers. The bottom water is in a state of low temperature and in most instances lower than 12°C. Reservoir water quality possesses layered character. The water quality in the upper layer of a reservoir is almost the same as that in river. It belongs to neutral or weakly basic water. Along with the increasing of water depth the pH value of the water turns down gradually[1].

In most instances the pH value of water in bottom layer of a reservoir is less than 6.5 and belongs to weakly acid. The contents of erosive CO_2, HCO_3^- and Ca^{2+} are getting increasing from the surface to the bottom of a reservoir. Among them the increase of erosive CO_2 is the largest, reaching 16–17mg/l, which is 7–10 times larger than that in the surface water. This is due to the results of enrichment and decomposition of organic matter in the bottom layer water. That is:

$$CH_2O+H_2O \rightarrow CO_2+4H^+$$

During the reaction some deoxidized substances H_2S, CH_4, etc. can be released. It is lack of oxygen in the environment of reservoir bottom that organic matter decomposes incompletely. The content of CO_2 in water of bottom layer is restricted[1].

Table 1. Water quality analyses of dam foundations.

Dam	Site of samples	pH	Total hardness (H°)	Erosive CO_2 (mg/l)	K^++Na^+ (mg/l)	Ca^{2+} (mg/l)	HCO_3^- (mg/l)	Note
Dan	Grout U27–1 (riverbed)		12.46	51.6	2.25	57.3	270	
Jiang	Grout 27–11*(riverbed)	8.16	5.15	2.77	74.0	18.8	277	
Kou	Grout 26–7 (riverbed)	8.50	1.68		164.0	6.41	372.0	
	13(gallery)-19(rightbank)	7.77	12.05		93.25	64.46	464.39	An average of two times
Mei	13(gallery)-34(rightbank)	8.0	6.47	11.63	112.75	36.43	354.74	
Shan	13(strengthened arch)	7.43	5.38	62.79	68.75	31.53	257.99	
	12(rightbank)							
Mozi	10–3 (right bank)	7.02	5.40	32.54	26.63	38.57	174.15	
Tan	4–5 (riverbed)	7.27	4.17	4.65	17.88	26.24	122.70	
Xin	Drain 2-C (right bank)	5.15	0.78	50.5	/	2.0	6.1	An average of many years
An	Grout 2–3 (right bank)	6.31	2.13	41.79	2.67	9.62	46.97	
Jiang	Grout 24–1 (left bank)	11.59	22.02		80.59	154.13	10.07	

* Note: The letter 'U' expresses a uplift pressure borehole, Grout 27–11 means a drain borehole in grout gallery numbered 11 in dam section 27.

2.2 *Characteristics of water quality in dam foundation*

During the process of its transfer towards the dam foundation, as a solution, reservoir water produces interactions with dam foundation rock, grout curtain and concrete. The formation of water quality components in drain boreholes of dam foundation is the results of these interactions. The water quality characteristics of the groundwater in dam foundation can reflect the strength and property of these interactions.

The water quality components are complex. Apart from general major ions there are some components such as colloids, gases, etc. As to the major ion components in groundwater of dam foundation their contents vary a lot. The variation of water pH value in dam foundation is very much too (Table 1). For example, in Xinanjiang dam the variation range of water pH value is between 5.15 and 12.6 (the value of grout 24–1 is the largest). So the groundwater quality in dam foundation presents variety of character from weak acid through basic to strong basic. From the point of view of water chemistry there are a variety of types. With regard to anions, apart from type HCO_3 and $HCO_3 \cdot SO_4$, because of abundance of CO_3^{2-} and OH^- in the water, type OH, type CO_3 and type $CO_3 \cdot OH$ appear too, but they rarely appear in mountain bedrock type of groundwater. As to the components of cations the majority are type Ca or type K+Na, or both of them.

The water in part of drain borehole of dam foundation contains abundant colloid. Varieties of colored colloidal educts, such as red, black, white and sometimes yellow color, often formed around the mouths of drain boreholes[2]. According to X-ray diffraction analysis most of the educts are noncrystal colloids that did not create diffraction peaks. But sometimes some fine pulverous-grain minerals such as quartz, feldspar, kaolinite, etc. can be analysed from some educts. From the point of view of chemical analysis most of the colloids consist of elements of iron, manganese, calcium, etc. but much less silicon and aluminum (Table 2). Only minority of educts contains abundant silicon and aluminum. Iron and Manganese mainly come from bottom water of the reservoir and deposition on the face of rock fissures. Calcium mainly come from concrete and cement stone of grout curtain. So the changes of their quantities are little relative to the changes of rock characters. But Silicon and Aluminum are main components making up rocks and their large transfer is closely relative to the changes of rock characters.

Table 2. Chemical components of colloidal educts around the mouths of drain boreholes in some dam foundation (%).

Dam	Number of drain boreholes	SiO_2	Fe_2O_3	Al_2O_3	CaO	MgO	MnO	Loss of ignition	Feature of educts
Xin	Grout 4–6	4.0	75.90	1.17	0.36	0.06		19.20	Reddish brown
An	Grout 3–2	29.89	30.74	5.78	9.92		0.20		Reddish brown
Jiang	Drain 11–2	59.57	7.34	6.47	9.85	1.35	0.31	17.71	Brown
Shi	Middle 16–8	28.21	13.05	5.88	13.21	0.32	7.49	29.78	White
Tang	Middle 16–4	30.19	8.55	10.92	15.81	0.95	7.55	22.49	Black
Dan	Grout 28–4	3.58	0.49	1.39	50.35	0.63	0.24	42.69	White
Jiang	Grout 28–10	11.47	48.63	15.37	1.11	0.25	0.10	21.74	Red
Kou	Grout 30–10	56.62	22.89		5.01				Fulvous

The reservoir water of middle and lower layers contains erosive CO_2 and its pH value is often less than 6.5. So it is erosive. The content of erosive CO_2 increases obviously and its capacity of erosion becomes greater where the environment changes acutely. For example the position of dam foundation on riverbank slope is more in favor of decomposition of organic matter in water, where the hydraulic grade is larger, groundwater runoff is expedite, the groundwater is often in oxidative environment (see table 1). Hence during the process of seepage of reservoir water towards dam foundation physical chemistry reaction is sometimes violent between the water with curtain, concrete and soft bedrock. It means that sometimes the chemical suffosion is very violent.

3 PHYSICAL CHEMISTRY REACTIONS AMONG WATER-DAM-ROCK

3.1 *Physical chemistry reaction among water-dam (concrete, curtain)*

The reaction equation between cement and water is

$$\mathbf{3CaO{\cdot}SiO_2+Z\,H_2O=Ca(OH)_2+}\boldsymbol{x}\mathbf{\,CaO{\cdot}}\boldsymbol{y}\mathbf{\,SiO_2{\cdot}}\boldsymbol{aq}\mathbf{\,Ca(OH)_2+Ca(HCO_3)_2=2\,CaCO_3+2H_2O}$$

The hydrolyze process of Calcium carbonate is quickened while the acid water with abundant CO_2 presents.

The Ca^{2+} transfer of groundwater in dam foundation mainly comes from the interaction between water and cement stone. It is one of the main modes of chemical suffosion in dam foundation and it is one of the signs that the curtain is suffering from chemical suffosion. Under the circumstance of dam site the total hardness of water is often consistent with its temporary hardness. The quantity of carbonate transfer in curtain concrete stone (including carbonate minerals in bedrock) can be evaluated with total hardness combined with quantity of seepage. Table 1 shows that the reservoir water of lower layer is ultra-soft water containing little CaO. But a part of water from drain boreholes is slightly hard water or hard water that contains amount of CaO reaching 100~200 mg/l (German degree 10~20°) or higher. It says that the CaO in water of these boreholes transfers larger. Combining with averagely annual quantity of seepage an averagely annual quantity of erosion of cement stone can be calculated (generally in chemical components of cement the content of CaO is 64~67%). The bedrock of Fengman Dam foundation is metamorphic conglomerate. The quantity of erosion of dam foundation curtain was observed during 1983~1985. The averagely annual quantities of erosion in most of 54 dam sections were not large. But the quantities were large in a few sections (400~1900kg/year). Among them the largest reached 1923.8kg/year. The total of annual quantities of erosion in dam sections of Nos. 22, 36,

37, 38 and 39 is 56.9% of that of whole dam. It indicated that a concentrative suffosion took place in these sections and the function of foundation curtain has attenuated in different extent.

In recent years it was found from investigation that seepage suffosion is one of the most important and prevalent problems. Due to seepage suffosion large amounts of Calcium ions are dissolved from concrete, which largely weakens the density and erosion prevent of concrete and causes increase of seepage. Some water pressure tests were conducted in bedrock and concrete in dam section (No. 0–2) of right bank of Xinanjiang Dam. In the 251 test sections there were 19 sections of that the unit water absorptivity was ω>1 Lu. They belonged to strong seepage sections and were mainly distributed in concrete section of dam foundation. This phenomenon accounted for that the small openings or cracks in the concrete have developed. This was consistent with the conclusion from observing drill cores of boreholes, which offered evidence that the dam foundation concrete has suffered from suffosion.

3.2 *Physical chemistry reaction among water-rock*

The minerals of silicate and aluminum silicate are the main components of most of rocks. Their hydrolytic speed is low but it can be accelerated when carbonic acid participating in. The cation on the surface of crystal lattice of silicate mineral (K, Na, Ca, and Mg) can easily be replaced by H^+ of water and the minerals are then decomposed to soil. Taking sodium felspar as an example, i.e.

$$Na_2Al_2Si_6O_{16} + CO_2 + 2H_2O \longrightarrow H_2Al_2Si_2O_8 \cdot H_2O + Na_2CO_3 + 4SiO_2$$

Potassium and sodium are two important components in felspar kind of minerals and the felspar kind of minerals is main component of crystalloid rocks (magmatic rock, metamorphic rock). Their migration is closely related to the change of rock character. The dam foundation of Danjiangkou hydraulic power project belongs to metamorphic diorite and metamorphic diabase. The water in part of drain boreholes of dam foundation contains abundant K^++Na^+, up to 100~200mg/l, but the water in reservoir less than 5mg/l. The components of potassium and sodium were tested in a laboratory. The analysis showed that Na^+ in water of drain borehole of dam foundation accounts for more than 95% while K^+ is the main component in reservoir water. The chemical analysis of bedrock showed that the main component was Na_2O too. There into the strong weathered diabase K_2O accounts for only 0.5%, but Na_2O reached 5.0%, almost ten times larger. As to the distribution, the drain boreholes in which the water contains more K^++Na^+ mainly locate on the left bank. According to primary analysis the K^++Na^+ in groundwater of dam foundation comes mainly from weathered stone of survival upstream cofferdam on the left bank. The monitoring in this aspect is carrying on.

The dam foundation of Meishan hydraulic power project is granite. The seepage in arcade No. 13 is large in which the average seepage of drain borehole No.34 is up to 570ml/min (in the year 1998). The content of K^++Na^+ in groundwater is up to 112.75mg/l, 13.8 times as large as the content of reservoir water. The K^++Na^+ in water of dam foundation comes from bedrock. This data show that in certain sections the water in dam foundation erodes the rock violently so some active prevention and cure measures should be taken.

In the process of decomposition of silicate minerals the loss of SiO_2 is mostly due to colloidal eluviation and partly due to ion migration while the loss of Al_2O_3 is due to colloidal eluviation, i.e.

$$H_2Al_2Si_2O_8 \quad 2SiO_2 \cdot H_2O + Al_2O_3$$

From the water in a few of drain boreholes of dam foundation or the educt around a few of mouths of drain boreholes we can find the evidence that the components of silicon and aluminum have

largely migrated. For example, in 42 educt samples of chemical component analysis collected from the foundation of Xinanjiang Dam there are 5 samples in which the sum of SiO_2 and Al_2O_3 is the main component (see Table 2). The highest content of SiO_2 is up to 59.57% and Al_2O_3 6.47%. The larger sums of SiO_2 and Al_2O_3 are more than 66%. This indicates that the amount of migration is larger[3].

The foundation of Xinanjiang Dam on the right bank is quartz-sandstone sandwiching with thin shale. The foundation of the riverbed and the foundation on the left bank (dam section No. 8~26) are sandstone. The sandstone is hard and the migration of a small amount of component of silicon and aluminum affects its strength little. The thin shale on the right bank is a soft and weak sandwich. Some drain boreholes distributed in the shale are collapsed. The maximum thickness of deposit in these drain boreholes is 27.27m (drain borehole No. 3–9). The drain borehole No. 2–3 was cleaned continually for 11 days and reached to the depth of 29.56m, but deposited again to the depth of 27.05m later. The results and data above show that in part of right bank foundation of Xinanjiang Dam the elements of silicon and aluminum are migrated and the soft and weak sandwich arises softening argillazation phenomenon. The extent changed is expected to be surveyed.

The lithology of bedrock in the site of Shitang Dam is simplex Jurassic volcaniclastic rock. There is some amount of educt in the gallery of guide wall of stilling pool of dam foundation. The contents of silicon and aluminum in the educt are higher. The content of SiO_2 is 28%~31% and Al_2O_3 5%~11%. After several analyses to the water samples taken from drain boreholes here it was found that the content of soluble SiO_2 was always higher one time more than that in reservoir water and the average value is 11.86mg/l. This indicated that the migration of silicon and aluminum was obvious in a certain part of dam foundation. The results of X-ray diffraction analysis to the educts showed that there were minerals of quartz, felspar, kaolinite, etc. This was the evidence of migration of fine particle material. The results indicated that there was mechanical suffosion accompanying during the process of chemical suffosion. The chemical suffosion took the leading place while mechanical suffosion was less important. As a consequence the variation of lithology of local zone in dam foundation has been paid great attention and further close observation is conducted.

4 PREVENTION AND CURE MEASURES

1. Strengthening observation: The chemical suffosion of the water environment around the dam site is firstly reflected in the changes of components of water quality. This is the basis that is used to evaluate the changes of dam concrete, grout curtain and character of soft rock of dam foundation. Therefore it is necessary to strengthen periodic observation of water quality of dam foundation. On this base the eroded location of the concrete, grout curtain and soft rock should be thoroughly investigated and reinforcement measures should taken.
2. Using erosion-resisting grout cement: The grout curtain of dam foundation around bank slopes should be made of erosion-resisting grout cement. Because in dam foundation of the bank slopes there is lateral seepage pressure with high gradient (the pressure increases along with the height of the dam) and the water here often possesses strong acidity and carbonated erosion. The erosion-resisting grout cement is made of Portland cement added with 30% of ground slag. Its erosion-resisting factor is higher 14% than that of Portland cement and its seepageresisting characteristic is far lower than Portland cement. So this kind of cement can be used for fine fissure grouting.
3. Constructing an effective drainage of dam foundation around bank slope: An effective drainage of dam foundation can evidently reduce hydraulic gradient and runoff strength of dam foundation, lateral seepage pressure, the strength of water dynamic and chemical suffosion. Some active measures can be used to drain the groundwater in runoff expedite strips of dam foundation of bank slope, such as multiple-layer drainage level cavern or fan-shaped drain boreholes.

REFERENCES

[1] Peng Hanxing, Shi Xijing, Liu Jianging: Environment water action around dam site in Wanzhe mountainous area of China, 7th International AGE Congress 1994 Balkema [C], Rotterdam, 1994.
[2] Zeng Kaihua, et al.: Some Questions in Analysis of educts from Dam Foundation, J. Dam Observation and Geotechnical Teats, 2000.3. pp. 10–12.
[3] Ma Xiaohua, et al.: Discussion on Characteristics of Shale under Xinanjiang Dam Foundation [J], Journal of Hohai University (natural sciences), 1999, 27(4): 101–106 (in Chinese).

New Developments In Dam Engineering—Wieland, Ren & Tan (eds),
© 2004 Taylor & Francis Group, London, ISBN 04 1536 240 7

Stability analysis of earth dams by the method of determination

MD. Zakaria Hosaian & Inoue Sohji
Mie University, Japan

Menjyo Michimasa
Nihon Giken Ltd., Japan

ABSTRACT: This paper presents a new technique for stability analysis of earth dams based on the moment equilibrium of simultaneous blocks consisting of the circular slip lines. It is demonstrated that the whole slope can be constituted of two major portions namely block of left-hand-side and block of right-hand-side in which both portions maintain the equilibrium conditions by their acting and reacting moments on the dividing plane. Both these major portions (left and right blocks) are further divided into some small vertical slices. The major dividing plane is sequentially located at the interface of each slice continuing demonstration from left to right or vice versa i.e. the whole slope under treatment is undergone to the moment equilibrium conditions as of the number of slices. The formulation shows that the number of equations obtained by this technique are equal to the number of unknown parameters in the slope stability problems which makes the method as a determinate one where the ordinary method of slope stability analysis still has some shortage number of conditional equations than the number of variable needed to be determined remains the problem as indeterminate one. The validity of the proposed method is made by comparing it using the results based on non-parallel internal forces as well as ordinary method of slope stability analysis. It is concluded that the value of the factor of safety obtained by the proposed method, in general, is a little bit bigger one as compared to other methods those are based on some assumptions.

1 INTRODUCTION

It is well known that the slope stability analysis considering circular slip line usually begins from dividing the whole slope into few numbers of small vertical slices. Then, the internal forces acting on the interface on these small vertical slices as well as the factor of safety of the whole slope is to be found out from the equilibrium relationships of forces acted on each small vertical slice and from the moment equilibrium of the whole slope. On that occasion, when the number of divided small slices is made *(n),* the number of conditional equations are shortage by ($n-2$) and it becomes the so-called indeterminate problem. So, a trial of introducing some supposition to solve these kinds of problems has been made since long ago [1], [2]. The internal forces obtained in this way are usually termed as "determinate internal forces". However, it is difficult to expect the rigorous analytical results even if it is based on any kind of supposition to solve this type of slope stability problem.

This paper proposed a new method of slope stability analysis using determinate technique based on some ideas introducing in the derivation of force equilibrium equations particularly in moment equilibrium equations. Consequently, the internal forces obtained by that technique can be said as the determinate internal forces and also the slope safety factor may finally be regarded as the value based on the precise analysis. The points of action of the internal forces obtained by this new method (hereafter, named as determinate method—DM) are plotted in the different figures for better comparison with the other methods (hereafter, named as indeterminate method—IM). Positions of the internal forces, their connecting lines and the value of the factor of safety obtained by the proposed method are illustrated in details. In addition with these, detailed conditions of the internal forces and techniques that possessed basic characteristics of this new method are also demonstrated in this paper. The results showing the horizontal component of internal forces, vertical component at the bottom of the slices and the distribution of resultant are also presented and discussed.

2 DERIVATION OF FUNDAMENTAL EQUATION

2.1 *When empty of water storage*

The earth slope (the part surrounded by a slip line and the slope surface line) is divided into *n* small slices as shown in the Fig. 1. Then, these are separated into two groups (left-side and rightside soil-blocks) by taking the border at the boundary slice referred as *i-slice*. At first, giving attention on the left-side soil-block from the i-boundary, it can be think that the internal forces such as *Hi* (horizontal component of internal force) and *Vi* (vertical component of internal force) are acting at the vicinity of *i*-slice owing to the self weight of the right-side soil block.

In the same way, the *Hi* and *Vi* in the opposite direction are acting against the right-side soilblock. Now, putting α_{ir} is the center angle formed by the lines connecting to the center of the arc and the point which is cross-section of slip line and acting line of self-weight W_{ir} of whole right side slices group, X_{ir} is the horizontal distance between the surface of *i-slice* and the acting line of self-weight W_{ir}, L_i is the vertical distance at the surface of *i*-slice from the point of action of internal forces to the slip line. For the slices group at the left side of *i,* the terms W_{il}, α_{il}, X_{il} are defined in the same manner.

The L_i is common for both left and right group. The radius of the circular arc is *r*. The horizontal distance between the bottom edge of the slip circle and the vertical surface of *i*-slice is defined as *Xi* and the angle with the vertical direction at the center of the slip circle formed by the line passing to the cross section of *i*-surface and slip line is defined as α_i.

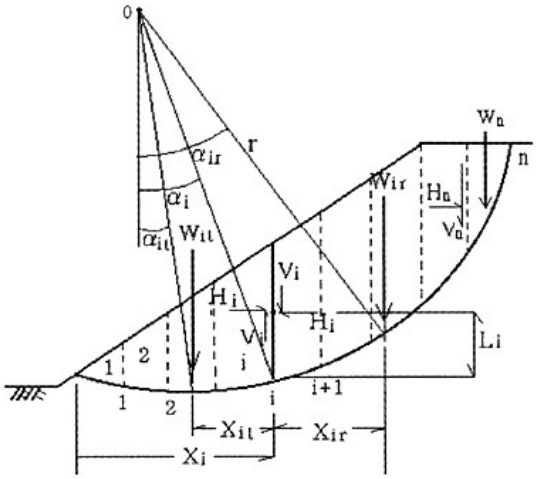

Figure 1. Symbols used in the analysis.

Based on the moment equilibrium for the soil-block on the right-side of the surface of *i-slice,*

$$\frac{V_i}{H_i} = \frac{L_i + r(\cos\alpha_{il} - \cos\alpha_i)}{X_{il}} \tag{1}$$

Based on the moment equilibrium for the soil-block on the right-side of the surface of *i-slice,*

$$\frac{V_i}{H_i} = \frac{r(\cos\alpha_i - \cos\alpha_{ir}) - L_i}{X_{ir}} \tag{2}$$

From Equation 1 and 2, the acting point of internal forces L_i which is independent of H_i and V_i is obtained as of following Equation

$$Li = \frac{r\{(\cos\alpha_i - \cos\alpha_{ir})X_{il} - (\cos\alpha_{il} - \cos\alpha_i)X_{ir}\}}{X_{il} + X_{ir}} \tag{3}$$

In the next, thinking the equilibrium of forces about the slice j ($j\,(1 \leqq j \leqq i \text{ or } i \leqq j \leqq n)$). Referring to Fig. 2, based on the equilibrium of forces in the horizontal direction

$$H_j - H_{j-1} = T_j\cos\alpha_j - P_j\sin\alpha_j \tag{4}$$

Here, by accounting the pore water pressure acting at the bottom of the slice and noting the vertical force Pj in effective pressure, it can be shown that $P_j = P'_j + u_j l_j$

Again, by using safety factor F_s and strength parameters c and ϕ, the shear force Tj can be written as $Tj=(c'l_j+P_j \tan\varphi')/Fs$.

Substituting these in Equation 4 results as Equation 5

$$H_j - H_{j-1} = \frac{c'l_j + P'_j\tan\phi'}{F_s}\cos\alpha_j - (P'_j + U_j)\sin\alpha_j \tag{5}$$

In the same way, Equation 6 can be obtained from the force equilibrium condition in the vertical direction

$$W_j + V_j - V_{j-1} = \frac{c'l_j + P'_j\tan\phi'}{F_s}\sin\alpha_j - (P'_j + U_j)\cos\alpha_j \tag{6}$$

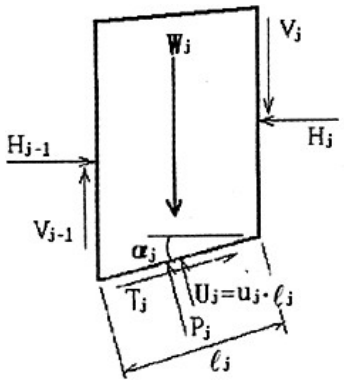

Figure 2. Forces acting on *j*-slice.

Besides, in Equation 5 and 6, it is $H_0=V_0=L_0=0$ at $j=0$ and $H_n=V_n=L_n=0$, at $j=n$. Here, putting θ_j at the right side of either Equation 1 or 2 (showing j in place of i for equal number of slice and planes)

$$V_j = \theta_j \cdot H_j \tag{7}$$

Substituting H_j and V_j of Equation 5 and 6 in Equation 7 and calculating P_j which takes as the following form

$$P'_j = \frac{\theta_j H_{j-1} - V_{j-1} + W_j + \theta_j F_{mj} - F_{kj}}{(\sin\alpha_j - \theta_j \cos\alpha_j)F_\phi + \cos\alpha_j + \theta_j \sin\alpha_j} \tag{8}$$

But, putting the following values for Equation 8

$$F_\phi = \frac{\tan\phi'}{F_s},\quad F_{mj} = \frac{c'l_j}{F_s}\cos\alpha_j - u_j l_j \sin\alpha_j,\quad F_{kj} = \frac{c'l_j}{F_s}\sin\alpha_j + u_j l_j \cos\alpha_j$$

substituting P'_j of the above equation in Equation 5, it takes the form as Equation 9

$$H_j = H_{j-1} + F_{mj} + \frac{\theta_j H_{j-1} - V_{j-1} + W_j + \theta_j F_{mj} - F_{kj}}{(\sin\alpha_j - \theta_j \cos\alpha_j)F_\phi + \cos\alpha_j + \theta_j \sin\alpha_j}(F_\phi \cos\alpha_j - \sin\alpha_j) \tag{9}$$

Applying the condition $H_j=H_n=0$ at $j=n$ in the above equation and after some calculations, the following equation can be obtained.

$$F_S = \frac{\{H_{n-1}\sin\alpha_n + (W_n - V_{n-1})\cos\alpha_n - u_n l_n\}\tan\phi' + c'l_n}{(W_n - V_{n-1})\sin\alpha_{n-1} - H_{n-1}\cos\alpha_n} \tag{10}$$

After calculating the factor of safety by Equation 10, the horizontal component of internal forces H_i by Equation 9 and the vertical component of internal forces V_i by Equation 7 can be calculated. The angle of the resultant force θ_i with the horizontal component calculated by either Equation 1 or 2 and its acting point fixed by Equation 3 can be obtained accordingly.

Here, it is examined about the problem of determinate and indeterminate cases. Considering a total of n number of slices of the whole slope, the number of unknown equations is given in Table 1. It is observed from this table that the problem is a determinate one in the proposed method even without setting any particular assumptions relating to the distribution of internal forces.

Table 1. Number of equations and unknowns in slope stability analysis.

	Number of equations		Number of unknowns	
Usual consideration method for internal forces	At single slice		Horizontal and vertical	
	$\Sigma H=0$, $\Sigma V=0$, $\Sigma M=0$	…$3n$	component of internal forces	
	strength condition	…n	H_i, V_i	…$2(n-1)$
	Total	…$4n$	Point of action	
			L_i	…$n-1$
Proposed method	Equation 1 or 2	…$n-1$	Strength component	
	Eqation for L_i	…$n-1$	T_i, P_i	…$2n$
	At single slice	Safety factor F_s		…1
	$\Sigma H=0$, $\Sigma V=0$	…$2n$	Total	…$5n-2$
	strength condition	…n		
	Total	…$5n-2$		

2.2 *When full of water storage*

Considering still water pressure acts on the plane at the toe of the slope OA in the submerged slope as shown in Fig. 3. At first, discussion is made about the left-side soil-block from *i-slice*. At this time, still water pressure in the opposition direction acts on the BD plane of the *i-slice*. Discussion is advanced by using the symbol shown in the following Fig. 3. From the equilibrium of the forces in the horizontal direction of whole part of OABD including soil,

$$\frac{1}{2}\gamma_w(d_l^2 - d_i^2) + T_{il}\cos\alpha_{il} - P_{il}\sin\alpha_{il} - H_i = 0 \tag{11}$$

In the similar way, from the equilibrium of the forces in the vertical direction,

$$W_{il} - T_{il}\sin\alpha_{il} - P_{il}\cos\alpha_{il} - V_i = 0 \tag{12}$$

From the moment equilibrium condition of this part in respect to the center of the arc,

$$(r\cos\alpha_i - L_i)H_i + (X_{il} + r\sin\alpha_{il})V_i + r\sin\alpha_{il}W_{il} - rT_{il} - \frac{1}{2}a_l\gamma_w d_l^2 + \frac{1}{2}a_i\gamma_w d_i^2 = 0 \tag{13}$$

Besides, γ_w: unit weight of water, Calculating T_{il} by Equation 11 and 12 and substituting this in Equation 13, the following equation is obtained

$$\begin{aligned}&(r\cos\alpha_i - L_i)H_i + (X_{il} + r\sin\alpha_{il})V_i + r\sin\alpha_{il}W_{il}\\ &-(W_{il} + V_i)r\sin\alpha_{il} - H_i r\cos\alpha_{il} + \frac{1}{2}r\gamma_w(d_l^2 - d_i^2)\cos\alpha_{il}\\ &-\frac{1}{2}a_l\gamma_w d_l^2 + \frac{1}{2}a_i\gamma_w d_i^2 = 0\end{aligned} \tag{14}$$

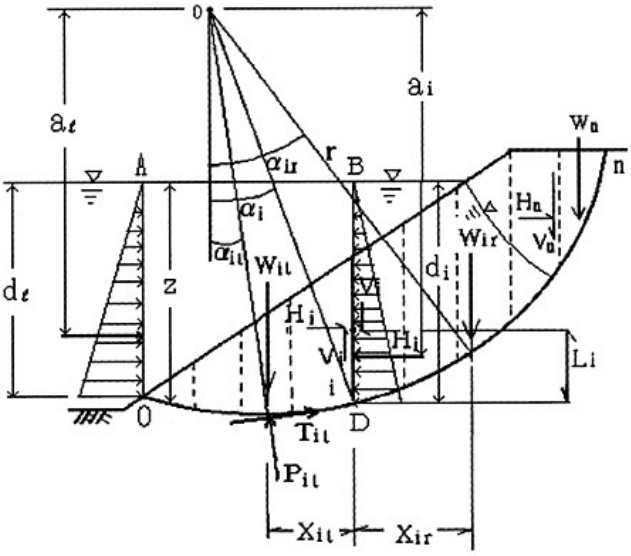

Figure 3. Graphical explanation of submerged slope.

Here, because of the water in part OABD of Fig. 3 is connected by still water pressure condition, the moment equilibrium condition of this water pressure in respect to center of the arc must be satisfied. That is,

$$r\gamma_w\sum_{j=1}^{i} b_j z_j \sin\alpha_j - \frac{1}{2}\gamma_w d_i^2 a_i + \frac{1}{2}\gamma_w d_l^2 a_l = 0 \tag{15}$$

Here, $W_{il} = W'_{il} + \gamma_w \Sigma_{j+1}^{i} b_j z_j$.

Moreover, the force equilibrium condition in the direction of α_{il} can also be kept. That is,

$$\frac{1}{2}\gamma_w d_l^2 \cos\alpha_{il} - \gamma_w\sum_{j=1}^{i} b_j z_j \sin\alpha_j - \frac{1}{2}\gamma_w d_i^2 \cos\alpha_{il} = 0 \tag{16}$$

By applying Equation 15 and 16 in Equation 14, it becomes

$(r\cos\alpha_i - L_i)H_i + X_{il}V_i - H_i r\cos\alpha_{il} = 0$

and Equation 2 can be derived. In the similar fashion, Equation 1 can also be derived.

After all, the Equations 1, 2 and 3 shown previously are constituted in the case of submerged slope during water storage. Derivation of equilibrium equations considering water pressure in each slice is similar to the procedure of submerged slope as usual. The indication of these equations is omitted here owing to the reason of the limited space.

3 RESULTS AND DISCUSSION

At first, concerning the empty of water storage, the validity of the proposed method is made using the results on nonparallel internal forces shown previously by one of the authors of this paper[3]. This is, an introduction of the following assumption, such as, $V_i = \lambda H_i \tan\alpha_i + \beta$ within the horizontal component and vertical component. where, λ and β are the constants and it coped with this indeterminate problem (hereafter, called as indeterminate method—IM). A model section used in this calculation is shown in Fig. 4.

The slope of the fill dam is considered as uniform type (half section of upstream portion is shown in figure). The wet unit weight of the dam material (γw) equal to $1.75\times9.81\text{kN/m}^3$, the angle of internal friction ($\frac{1}{2}\gamma_w d_l^2 \cos\alpha_{il} - \gamma_w\sum_{j=1}^{i} b_j z_j \sin\alpha_j - \frac{1}{2}\gamma_w d_i^2 \cos\alpha_{il} = 0$) equal to 32 degree and the value of cohesion force (c') equal to $0.2\times9.81\text{kN/m}^3$ are used, and the pore water pressure (u_i) equal to zero is taken.

The value of the factor of safety and the distribution of internal forces regarding the slip line of same radius which passes to the center of the arc with x=44.0m, y=55.0m is depicted in Fig. 5 (IM) and in Fig. 6 (DM).

As it is clear from these figures, the points of action of the internal forces are much more downward for DM than that for IM. The thrust lines (connecting lines of internal forces) are also comparatively more smoothen for DM than for IM. Little more discussions are added on the condition of internal forces that possesses basic characteristics of both the methods.

Figure 7 depicts the circumstances of variation of the horizontal component of internal forces H_i, the vertical component of internal forces formed with the horizontal component V_i plotted in accordance with the slice number (the number increases from toe to top of the slope). As observed, the value of H_i is almost the same pattern for both the methods with maximum value at the vicinity of the mid section. The value is slightly smaller in the case of determinate method. In comparison with this, the value of V_i at the bottom section of the slope i.e. at the starting numbers of the slices becomes smaller value for DM than that for IM. Furthermore, getting a look at the distribution of θ_I (angle of resultant force), it is obvious that there is a smooth increase gradually toward the right side of the slope in the case of DM, whereas, it changes violently at the bottom and top part of the slope in the case of IM. Thinking trend for V_i and θ_i the circumstances of the distribution of internal forces are somewhat unnatural characteristics for the case of IM than for

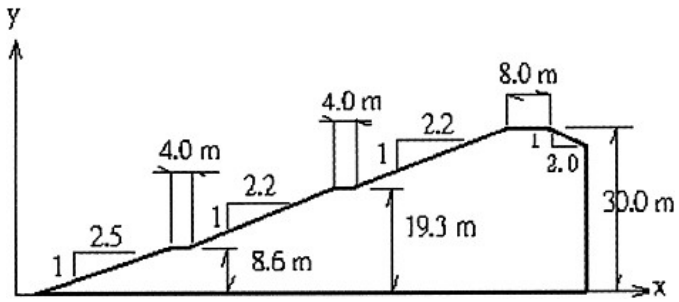

Figure 4. A model cross-section for calculation.

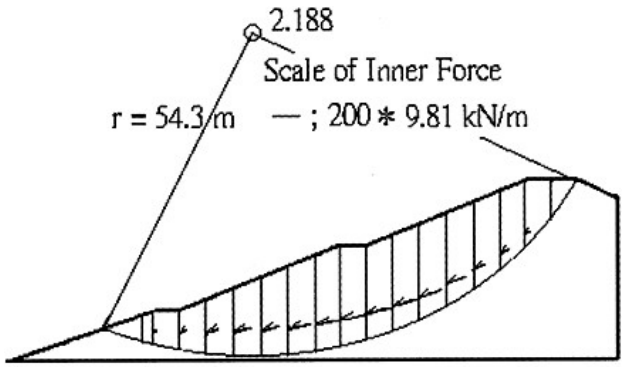

Figure 5. Distribution of internal forces and slip line by indeterminate method.

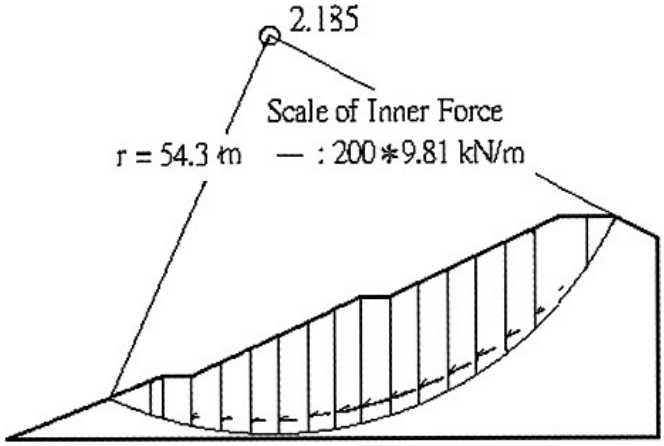

Figure 6. Distribution of internal forces and slip line by determinate method.

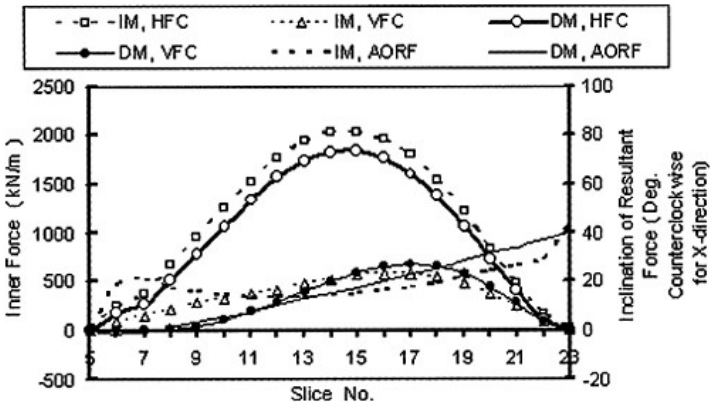

Figure 7. Comparison of each values in DM and IM (HFC and VFC are horizontal and vertical components, and AORF is angle of resultant force).

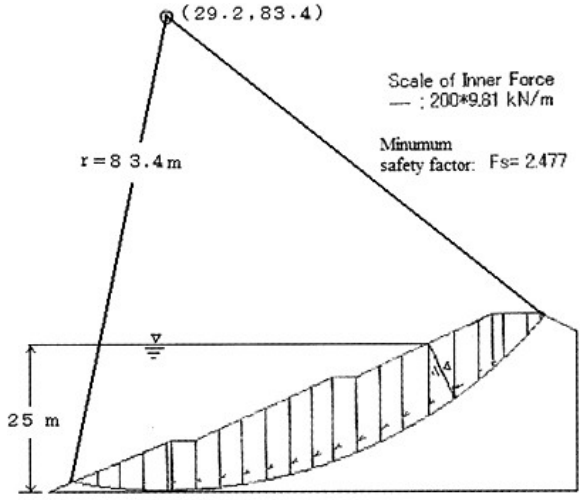

Figure 8. Internal for component and slippage circular arc in DM during the water storage condition.

the case of DM. It is guessed that there is a big chance of influence occurred due to the introduction of some assumptions used to cope with the devotion to indeterminate problems.

In the next, the circumstances of the connecting lines based on the determinate method of water storage condition at water head of 25 meter is shown in Fig. 8. In this case, the size of the crosssection to be calculated is the same as of empty condition, however, because it shows the cross-section which gives minimum factor of safety; the size of the slip line is little bit different from the earlier. From this figure, the size of the internal forces within the water storage area is reduced once, but, while it just cross the seepage line (unsaturated domain), it again getting large and then be converged to zero and the development of the internal forces at the toe of the slope is extremely little, etc. are the particular characteristics of the proposed method. Finally, in this case, the minimum

factor of safety obtained by the determinate method is compared to the analytical results of previous methods those are represented by circular slip surface such as Swedish and Bishop methods and the following results are obtained (Swedish method, F_s=1.688; Bishop methods, F_s=1.963; Determinate method, F_s=2.477). The differences of these values are varied depending on the calculating cross-section. However, it is clear that considerably a big value of the factor of safety is calculated in the determinate method, it can be thought that it is necessary to pay attention in this trend at the time of stability analysis of the dam body.

4 CONCLUSIONS

1) In contrast to the slope stability analysis method as of indeterminate problem given in the past, a new analytical method showing to be determinate is noted here based on the derivation of Equations (1), or (2) and (3).
2) In the results obtained by the determinate method proposed in this paper, the acting point of all the internal forces is located at slightly lower side below the one-third of the height of the divided slices.
3) The following trend is observed in the submerged part in the case of water storage condition, such that, the distribution of internal forces within the slope is changed as small□ big□ small, but, while it exceeds the seepage line, it again increases and then finally, it converged to zero.
4) The minimum factor of safety is bigger value as compared to Swedish and Bishop methods.

REFERENCES

[1] Morgenstern, N. and Price, V.E.: The Analysis of the Stability of General Slip Surfaces, *Geotechnique,* 1955, Vol. 5, No. 1, pp. 7–17.
[2] Spencer, E.: A Method of Analysis of the Stability of Embankments Assuming Parallel Inter-Slice Forces, *Geotechnique,* 1967, Vol. 17, No.1, pp. 11–26.
[3] Inoue, S.: The Stability Analysis of Circular Slip Surfaces Considering Inter-Slice Forces, *The Japnese Soc. of Soil Mechanics and Foundation Eng.,* 1986, Vol. 34, No. 4, pp. 35–39, (in Japanese).

This page intentionally left blank.

New Developments in Dam Engineering—Wieland, Ren & Tan (eds),

Geotechnical parameters effect on embankment dam analysis and design—applied to four case studies

M.A.Mehrdad & A.Eslami
Assistant Professor, Civil Engineering Department, University of Guilan, IRAN

J.A.Taghavi
Lecturer, Civil Engineering Department, University of Guilan, IRAN

M.Veis Karami
Research Assistant, Civil Engineering Department, University of Guilan, IRAN

ABSTRACT: In analysis and design of earth fill dams, shear strength and pore water pressure parameters are considered as substantial factors. Slope stability analysis for selecting and finalizing dam geometry is performed by analytical softwares which are based on limit state equilibrium approach and significantly dependent on geotechnical parameters.

In this paper, variation of strength parameters are discussed when soil is sheared in different situations and stress-strain levels. Four dam case histories located in Iran were compiled and investigated. The cases include earth fill dams varied in geometry and geomaterials and referenced to a case, which has been studied by USBR.

Current customary programs such as SLIDE, STABL and PCSTABL were implemented to study of shear strength parameters effects on safety factors. Also, FEADAM 84 was applied to evaluate stress-strain behavior of dams. Results have indicated that the method of analysis and the type of software were highly reliant on strength parameters. Finally, utilizing elaborated engineering judgment can be lead to safe, practical and optimum embankment dam projects.

1 INTRODUCTION

Among various engineering projects, dams construction and their industry involves major challenges. Since 1980 construction of earth and rock fill dams are more common than other type of dams. The reasons for this common usage are: the method of construction is based on ordinary technology with utilization of cheap raw soil materials, subsurface materials, and does not depend on particular valley shape. Also, geometric design of embankment dams depends on barrowed soil materials, subsurface conditions and type of construction. Consequently feasible design can cause significant reduction on construction time, materials and costs.

Along with the growth of technology, monitoring and surveying devices in earth fill dams have been developed. Such devices can produce relatively accurate geotechnical parameters, which can be used in analysis and design of earth dams. Data from four dams located in Iran were compiled applying computer and related softwares based on advanced methods of analysis (algorithms) puts a suitable tool on the hand of dam designers. The stability analysis of embankments, specially the control of slopes stability, is based upon parameters such as the shear strength parameters of dam's body and foundation materials, level of the reservoir water, region seismic properties, dam's geometry, topography of dam construction site and economical considerations of design [1]. By using suitable geotechnical parameters such as soil mechanical properties and the circumstances

Table 1. Requires factor of safety factors and strength conditions for embankment dams.

Case	Loading condition	Required factor of safety	Shear strength for evaluation*
1	Steady seepage at high pool level	1.5	S* strength
2	Rapid drawdown from pool level	1.2	Minimum composite of R* and S
3	Earthquake reservoir at high pool for downstream slope reservoir to intermediate pool for upstream slope	1.1	R tests with cyclic loading during shear

* S=Effective stress shear strength from CU or CD shear tests; R=Total stress shear strength from UU or CU.

of pore water pressure in dam's body; their decisive role will be investigated. The errors in stability analysis arise from three sources: the method of analysis, circumstances of pore water pressure in the dam body and employed soil strength parameters. The stability analysis of dam embankments should always be carried out using effective stress method in long-term analysis and for the short time condition or quick loading, it is recommended to use total stress approach. It is also recommended that the analysis must be checked using residual strengths, and the highest possible pore water pressure, with a factor of safety of at least 1.1 for extraordinary conditions. This is particularly important where large differential strains may be encountered, or the dam may be damaged by earthquake (Fell et al., 1992). The foregoing principles are emphasized by National Research Council (1983) and US Corps of Engineers as quoted the Table 1 [2].

Determination of accurate parameters and applying suitable software, leads to optimal and accurate design of embankment dams. Usually calculations are made by considering the worst conditions, that is, the lower limit shear strength parameters and higher pore water pressures. To demonstrate the dependency of embankment design to soil parameters, first the variation of shear strength parameters are discussed. Then, parametric study on safety factors is made by implementing common software in dam industry and four case studies [2].

2 VARIATION AND SELECTION OF SOIL SHEAR STRENGTH PARAMETERS

The major factor in embankment design, which strongly affects the economy of project, is dam geometry. Measurement and selection of shear strength soil parameters has a significant role in optimum design regarding volume of geomaterial, financial costs and duration of time of construction. Shear strength parameters of soil can be determined by considering following main approaches: drained or undrained, peak or softened or residual strengths, total or effective stress, normally consolidated or over consolidated, confined or unconfined, static or dynamic, small strain or large strain conditions.

Since cohesive soils extremely used in construction of homogeneous and cored embankment dams the following discussions concentrated on investigation of some forgoing criteria. An undisturbed sample of soil may behave in an over consolidated manner at low normal stress and in a normally consolidated manner at high normal stresses. This phenomenon affects the pore pressure response of the soil during shear and also the load-deformation behaviour as shown in Fig. 1-a.

Peak strength is obtained at a small displacement, then a reduction of strength to the critical stale or fully softened strengths occurs with farther displacement. The residual and fully softened strengths are significantly different for high clay fraction content soils (Fell et al., 1992). Sands behave similarly to the low clay fraction soils. Since indicated in Fig. 1-b for peak to residual stress and strain levels, the C and φ parameters are different. For slope stability analysis, selecting suitable strength parameters depends the presence or absence of existing slide planes and fissuring [2].

When several triaxial tests have been carried out on the soil, it is recommended that the design shear strength parameters are obtained from p-q plot of the test results, rather than by averaging the individual C′, φ' values from each test or plotting Mohr's circles on one diagram. (Fell et al., 1992).

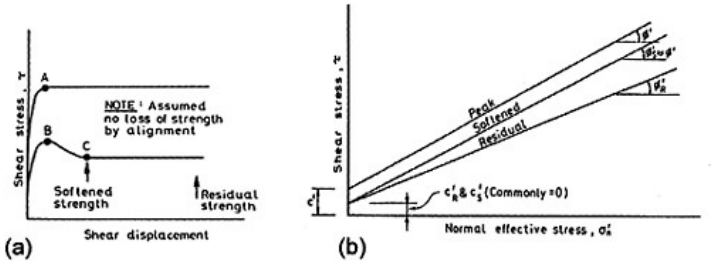

Figure 1. (a) Diagrams of stress-displacement behavior, (b) Relationship between peak, softened and residual strengths.

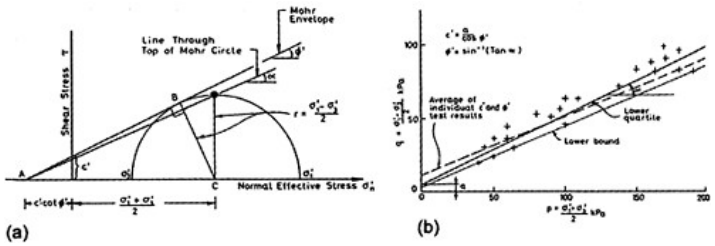

Figure 2. (a) Basis of p-q diagram, (b) Typical p-q diagrams of triaxial test results (Fell et al., 1992) [2].

This is also important to use results from effective stress range applicable to the field problem. The p-q plot is a graph of the apex points of the Mohr's circles from the test results as shown in Fig. 2-a.

The average of C′ and φ' values from which the p-q plot was derived is also shown in Fig. 2-b. It can be seen that using averages tends to give larger C′ and lower φ' than using the p-q diagram. This is generally unconservative for smaller dams and landslide stability because the strength is overestimated in the working stress range. Therefore, in any slope stability analysis, it is good practice to check the calculated factor of safety for a range of strength, e.g. lower quartile and lower bound to determine the sensivity of the factor of safety to the assumed strength. Moreover, engineering judgement is necessary due to poor individual test results, general curvature of the Mohr's circle envelope and etc. [2].

3 METHODS OF STABILITY ANALYSIS

The embankment dams are divided into three main types: homogeneous dams, core dams and diaphragm dams. Each of these three types has its unique properties and may be used in accordance with the case specifications. The main considerations in the design of earth dams are seep-age control through the body of dam, slope stability analysis, proper geometrical design and the determination of the reservoir water level to withstand overtopping. Many parameters and states of analysis should be considered and best estimated to perform analysis of embankment dams. Usual methods of earth dams stability analysis are:

1. Limit equilibrium methods: The analysis of stability of dams is almost always carried out using limit equilibrium methods. These methods are well established and described extensively in

textbooks and other literatures. These methods are usually based on the Mohr-Coulomb failure criteria through out a failure surface that may be straight or curved. In these methods the factor of safety is strongly influenced by the direction of forces acting on the sliding portion.
2. Numerical methods: Such finite element methods that can incorporate nonlinear behavior of materials and are more precise.
3. Stress-strain control: This method does not present a general factor of safety and only checks the stresses and strains and also displacements throughout dam body. Some computer programs use this method to calculate the settlement of the foundation and main mass.

Some important parameters in stability analysis of embankment dams are stated as below:

(a) The geotechnical properties of embankment and foundation: The embankments can generate the stability factors as well as instability factors. These factors are strongly related to the consisted materials and the properties that can be tested by laboratory tests and in situ tests.
(b) The influence of the water level and rate of water drawdown: This parameter is very important because in homogeneous dams it has been theoretically shown that the more critical state is when the reservoir is completely empty whereas calculations show the minimum factor of safety just when the reservoir is half empty. This phenomenon is due to the variations of the specific gravity of the materials as a result of submerging. Also the rate of water drawdown may affect on the factor of safety.
(c) The effect of slope gradient variation versus dam height: usually in high dams with weak foundations, the gradient of slopes decreases with the increase in the height of the dam and in highest elevations, steep slopes are designed by a constant factor of safety. This is because of the economical purposes and leads to decrease the body volume.
(d) The influences of drain and filter layers: because of their little volume in compare with the whole body of the dam, in compare to other parts it can be neglected.
(e) The effect of the type of the core in stability: theoretically, thin cores are more suitable though in highly seismic regions, thick cores are more stable under earthquake loading.
(f) The effect of the analysis method: The method of analysis, because of not considering any parameters or using lower-hand parameters, will contain some errors [3].

4 ASSESSMENT OF COMMON ANALYTICAL COMPUTER PROGRAMS

The stability analyses of slopes are usually done with the limit equilibrium methods. Such analysis can be performed manually as well as by computer. In this investigation, five computer programs are selected to compare the results of methods of analysis and the parameters, which have been proposed to design. Later on these methods are compared and the parameters, which have a main role in analysis and design of earth dams, will be introduced. The computer software that were used in this investigation are listed below:

1. PCSTABL 5: A 2-D computer program for analysis of both reinforced and unreinforced slopes. Based on limit equilibrium method, the factor of safety is calculated against failure in three different ways by modified Bishop, Janbo and Spencer methods. This program is able to model the heterogeneous soils, non-isotropic materials, surface and underground waters and earthquake loads.
2. STABL: This software is only used for unreinforced slopes stability analysis and based on limit equilibrium approach. Two methods to estimate the factor of safety in this program are modified Bishop method with a circular failure surface and the method of analysis of disordered failure surfaces. This is a 2-D analytical software [3].
3. STABGM: This is used for analysis of reinforced and unreinforced slopes based on modified Bishop method. The failure surface could be generated by the program or prescribed by the user [4].
4. SLIDE: This program is only used for unreinforced slopes and is a 2-D software which works by limit equilibrium approach. The program is capable of generate some random failure surfaces

or the user is able to impose some failure surface in the input data of the program. This program is able to contribute the inhomogeneous soil profile, surface and ground waters and also the increase of pore water pressure induced by the shear stresses.

5. FEADAM 84: Is a shareware, which is engaged to determine the stresses, strains and displacements of any points of a dam and works based on Non-Linear Finite Element Method (FEM). This program is also able to analyze the soil slopes in stage construction steps or multi loading steps and then provide total super positioned results in the last stage of construction and after construction loading steps. So the user can model the constructional stages of the dam as well as staged loads, which are applied to the dam like as multi stage filling the reservoir. Rigid and flexible foundations can be modeled as well as any layers in the dam [5]. A general factor of safety is not provided by this program and only the stress-strain and displacement pattern in the mass may be developed. But as proposed by Donald and Giam (1988), it is possible use of finite element techniques for analysis of the stability of slopes. This describes the use of displacements as a guide to incipient failure is used to allow calculation of a "factor of safety" and the uses of stress distribution to better predict the critical failure surface. The analysis of non-linear behavior of materials is based on the geotechnical parameters like as C, and φ, and some parameters referred to soil stiffness parameters [1].

5 CASE STUDIES

To evaluate the role of strength parameters in stability analysis of dams, based on suitable computer programs and method of analysis, four practical cases plus a USBR case have been studied.

5.1 *Sufisheikh dam*

Sufisheikh dam is constructed on Gorgan-Roud River in Golestan State of Iran. As criteria for uniformity of site materials, the type of the dam was taken as a homogeneous earth dam. Three types of drains are placed in the dam body that are chimney drain, blanket drain and toe drain. The elevation of the crest is 22m from the ground surface and the inclination of the slopes is 1v:6h for upstream and 1v:5h for downstream slopes sequentially [6]. In primary site investigation, three types of soil strata were distinguished. They are silty and clayey materials above water table as A-materials, silty and clayey soils below water table as B-materials and coarse grained materials as C-materials. These materials were selected to use in the main body. Fig. 3 shows cross section of Sufisheikh dam. Some unconfined compressive tests were established on undisturbed samples and a wide range of compressive strength tests performed to evaluate different part of the dam. For Sufisheikh dam the stability analysis was performed in the longest and highest cross section of the dam and among four state of loading, after construction conditions, rapid drawdown of reservoir,

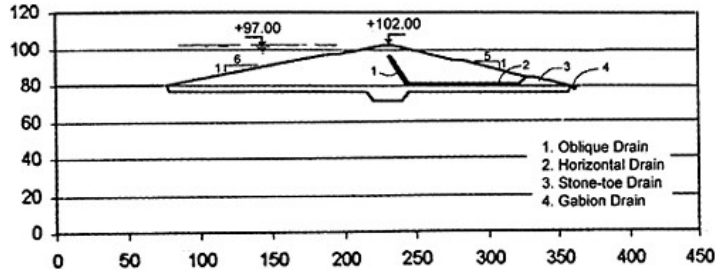

Figure 3. Illustration of analyzed cross section of Sufisheikh dam.

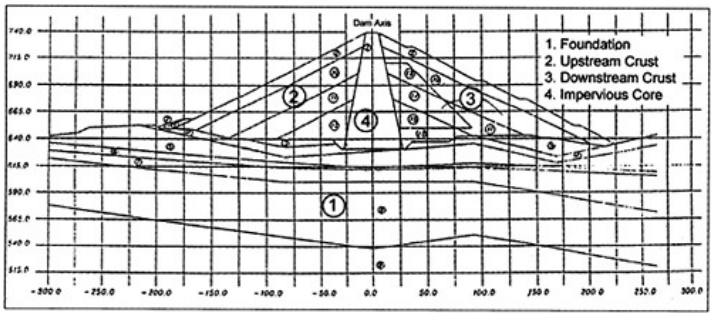

Figure 4. Illustration of analyzed Glevard dam's cross section.

steady state seepage and steady state seepage with earthquake loading (ANCOLD, 1969) [7], where the first two states were the critical conditions. According to performed site investigations and laboratory testing, the variations of cohesive strength of materials were very little in compare to friction angle parameter.

As there were some different values of C and φ parameters for site and working materials, an analysis based on the maximum and minimum values of C for the dam region was performed to investigate the effect of C parameters on factor of safety and dam economy. Results of analysis showed that a little changes in cohesive strength leads to a significant effect on the dam volume (about 20% variation in material usage and dam volume in this case) and also affects very much the factor of safety. Such a result, more or less, is obtained for variations of φ value in dam analysis. Therefore an accurate evaluation of geotechnical parameters may preserve the use of excessive materials.

5.2 *Glevard dam*

Glevard dam is a rockfill dam placed on the Glevard River in Mazandaraan State of Iran. It is also a clayey core dam. Due to the high seismic risk of this region, a thick vertical core is placed in this dam. An analyzed cross section of this dam is shown in Fig. 4.

Stability analysis for upstream and downstream slopes were performed based on Janbo and Modified Bishop methods for several conditions; end of construction, after construction with seismic loads, steady state seepage with and without earthquake, rapid drawdown and maximum probable flood conditions. The steady state seepage with earthquake is the most critical condition for Gelevard dam and the factor of safety from Janbo and Bishop methods were about 1.25 and 1.3 sequentially, which are close to the minimum factor of safety, required to be achieved for this condition (1.1 is proposed by US Corps of Engineers, 1983). A circular sliding surface was recognized as the critical stability condition. Using two softwares, PCSTABL 5 and STABL, a computer based stability analysis was performed. The results show that if the proper and accurate laboratory parameters (i.e. C and φ parameters) were used, more than 10% of rock materials would be saved while a proper factor of safety provided. More than geotechnical parameters, the type of software, which determines the stability analysis method, can affect the design. The results of stability analysis with different computer programs are presented in Table 2 [8].

5.3 *Polroud dam*

Polroud dam is designed to be constructed on Polroud River in Guilan State of Iran. It is an earthfill dam with a clayey core. The crest length is 530m and the highest elevation of dam is about

Table 2. Stability analysis results for Glevard dam by different programs.

Program used	Analysis method	After construction	Steady seepage	Steady seepage with earthquake	Rapid drawdown
PCSTABL	Spencer	2.45	1.98	1.36	2.41
	Janbo	2.20	1.83	1.28	1.98
	Bishop	2.40	1.96	1.40	2.40
	Random	2.24	1.93	1.34	2.16
STABL	Bishop	2.34	1.79	1.27	1.97
	Random	2.41	1.98	1.40	2.11

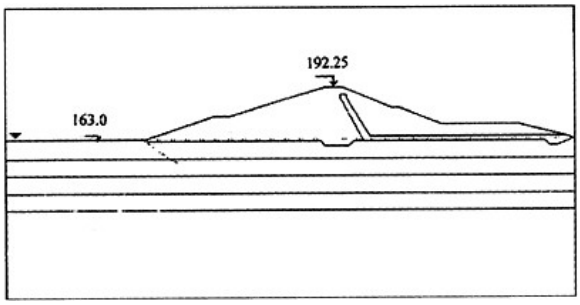

Figure 5. Illustration of analyzed Kaboudwal dam's cross section in the highest level.

109m above the base level. Four borrowed resources are selected to provide the materials used in the body. A pseudo dynamic and a static analysis for upstream and downstream slopes are performed. Among many different conditions, the steady state seepage with earthquake is the most critical condition. Because of high permeability of the materials, other loading conditions were not critical and large factors of safety were achieved in those conditions.

The results of stability analysis using a circular and a random failure surfaces, obtained by different methods in different softwares, show that the factor of safety that is obtained by analysis based on a circular failure surface is more than for the random failure surface, used in different sotfwares. It is apparent that the factor of safety for a random failure surface is less than a circular surface. The internal friction angle is obtained by the results of tests obtained from proportional confining pressures to consider the effect of all around pressure on internal friction angle. The use of total and effective stresses methods is shown to have similar results for this case [9].

5.4 *Kaboudwal dam*

Kaboudwal dam is going to be constructed on Qaressou-Zarringol River in Golestan State. This dam is designed to be a reservoir homogeneous dam by a crest elevation of about 31m above the ground surface. Three cross-section of this dam as critical sections was analyzed and outputs indicated sensitivity of results with variations of geotechnical parameters. Fig. 5 illustrates of Kaboudwal dam in its highest cross section [10].

Since little site investigations were done for Kaboudwal dam's abutments, the shear strength parameters used in analysis of abutments' sections were based conservatively on the results of minimum values obtained from other parts. However, if the results of geotechnical parameters for abutments are applied in abutments cross-sections analysis, the safety factor will increase very remarkably. It shows that if proper and sufficient geotechnical investigations are performed, geometric design will be economically sound and more precise [11].

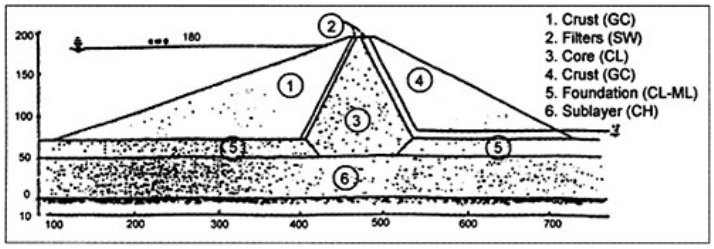

Figure 6. USBR investigated dam typical section.

5.5 *USBR investigated dam*

A non-homogeneous dam with 6 types of materials in foundation and body is investigated in USBR for end of construction, steady state seepage and rapid drawdown conditions. Also based on Spencer's method, for specified failure surfaces of three prementioned conditions, the factors of safety were evaluated. Fig. 6 shows a typical cross section of analyzed USBR dam [12, 13].

5.6 *FEADAM 84 stress-strain analysis*

A typical rockfill dam with two materials, clayey elasto-plastic core and an elastic gravelly shoulder was analyzed using FEADAM 84 program. Three construction stages and two load conditions were considered for this analysis: when the reservoir is in half level and when it is completely filled with water. A non-linear 2-D elasto-plastic analysis was performed for these stages of construction and load conditions. For investigation of the effect of shear strength parameters on stability analysis, other parameters were held constant. Changes in cohesion and internal friction angle, have a significant effect on stress-strain behavior of elements in nodal points and, as it is proposed by Donald and Giam (1988), the factor of safety may be affected by changes in these strength parameters. The results of FEADAM 84 analysis show that the effect of φ parameter is more than C in stress-strain behavior of earth dams. Therefore any changes in selected geotechnical parameters may lead to miscalculating of stresses and displacements in this dam. Calculations show that variations of cohesive parameter have little effect on stress and strain values in compare with internal friction angle parameter, that may be due to the failure criterion and nonlinear model used by FEADAM 84 program that is the hyperbolic model represented by Duncan et al., 1980. However, for practical purpose, it is recommended that to use the best estimated values for C, as well as that for internal friction angle according to those proposed by US Corps of Engineers (represented by Fell et al., 1992), when a FEADAM 84 analysis is performed.

6 CONCLUSIONS

For stability analysis of embankment dams pore pressure and shear strength parameters are critical issues as well as the stability analysis method used in each case. In real procedure, the design of an earth fill dam is based on the lower bond values of strength components. However, the geotechnical parameters involve a wide range as function of different conditions. To demonstrate the effect of strength values on stability and geometry of embankment dams, a parameter study has been performed employing four case studies by implementing current software. The results of investigations are as follows:

1. In earth fill dam slope stability analysis; it is superior practice to check the calculated factor of safety for a range of strength parameters. These parameters probably may occur in dam life and

structure to determine the sensitivity of safety factor to the assumed values. In addition, engineering judgement is essential for selecting the design parameters in order to achieve technical, stable and optimum project.

2. There are some approximations in static analysis methods regarding assumptions, inputs and principles of analysis. Therefore, it is recommended to use the methods by means of maximum correlation with the case in order to reach more accurate results.
3. The studies show that for linear sliding surface, the effect of cohesive intercept is more important than internal friction angle. Also for stress-strain analysis performed by FEADAM 84 analysis, φ parameter has more significant role in final results.
4. For homogeneous earth dams, programs have close results but in other cases, the type of computer software and method of analysis influence the results. It is recommended to use more than one computer program and/or analysis method. To average results of different methods of analysis and softwares, will lead to better estimation of safety factor for stability analysis of an earth dam.
5. Selection of design parameters is related to test and operation conditions, stress, and strain levels and it is highly recommended that laboratory tests to be performed in accordance with materials real (in-place) conditions. Sufficient and proper site investigation programs can affect the design of earth dams also. The type of the test and data interpretation has significant effects on outputs.

REFERENCES

[1] Sherard, J.L., Woodward, R.J., Gizienski, S.F. and Clevenger, W.A., *Earth and Rock Dams,* John Wiley and Sons, 1963.
[2] Fell, R., Mc Gregor, P. and Stapledon, D., *Geotechnical Engineering of Embankment Dams,* A.A.Balkema, 1992.
[3] Fattahi, A., *The Effect of Selective Shear Strength Parameters for Design of Earth Dam—Investigation of Three Case Studies in Iran,* M.Sc. Thesis, University of Guilan, IRAN, 2001.
[4] Duncan, J.M., *STABGM User Manual,* Department of Civil Engineering-VirginiaTech, Blacksborgh, 1985.
[5] Duncan, J.M., Wong, K.S. and Ozawa, Y., *FEADAM: A Computer Program For Finite Element Analysis of DAMs, Users Manual,* College of Engineering, University of California, Berkley, California, 1980.
[6] *Geotechnical Investigations Report of Suflsheikh Dam, 2nd phase,* Tehran-Berkley Consulting Engineers, 1999.
[7] ANCOLD, *Current Technical Practices for Design, Construction, Operation and Maintenance of Large Dams in Australia,* Australians National Committee on Large Dams, 1969.
[8] *Geotechnical Investigations Report of Reservoir Dam of Glevard and Other Establishments, 2nd phase,* Water and Soil Resources Consulting Engineers, 1999.
[9] *Geotechnical Investigations Report of Polroud Dam, 1st phase, vol. 2,* Mahab Ghods Consulting Engineers (MG), 1998.
[10] *Geotechnical Investigations Report of Kaboudwal Dam, 2nd phase, vol. 2,* Pajoohaab Consulting Engineers, 2001.
[11] Mehrdad, M.A., Eslami, A. and Veis Karami, M., Effect of Shear Strength Parameters on Design of Earth Dams: Several Case Studies, *Proceeding of 3rd Iranian International Conference on Geotechnical Engineering and Soil Mechanics,* (ICGESM), vol. 3, pp. 161–169, Dec. 9–11, Tehran, IRAN, 2002.
[12] USBR, *Design of Small Dams,* 3rd Edition, United States Government Printing Office, Denver, Colorado, 1987.
[13] USBR, *Design Standards of Embankment Dams,* No. 13, Chapter 4, United States Department of Interior Bureau of Reclamations, Colorado, 1987.

This page intentionally left blank.

New Developments in Dam Engineering—Wieland, Ren & Tan (eds),

Analysis of local stresses in gravity dam caused by drilling of hole

Mei Mingrong & Zhou Zhengdong
Hohai University, China

ABSTRACT: In making more electric power, engineers are planning to drill a hole on the built gravity dam for water turbine. It is concerned that drilling a hole in a built gravity dam will danger the safety of the dam. The paper analyzes aperture stress through nonlinear FEM in accordance with the rebuilding plan of a certain power station. Willam-Warnke concrete yield model is adopted in the processing. The result shows that concentrations of local stress around the hole occur after drilling. However, the safety of the dam will not be threatened by the concentrations for the maximum stress is not beyond the allowable concrete strength. The sensitivity analysis shows that if the concrete strength parameter is suppositively decreased, the localized cracks showing up near the hole tend to be stable.

With the nonlinear FEM, the dam working principles after drilling holes on it can be easily understood, which is beneficial to providing the reasonable rebuilding project of a dam.

1 FOREWORD

Power is key to the modernization of agriculture in a remote country. A hydropower station located in the south of China, whose installed capacity is 2×50MW, has been run smoothly since it was built in 1980. In 1995, taking advantage of the flood-discharge bottom intake on the 10# sluice section, the station laid pressure steel conduit to the diversion channel on the right bank 11# dam section. Thus the station built up workshops to form a new small hydropower station, whose installed capacity is 5MW. Owing to being occupied by the pressure steel conduit, the formerly designed lower flood-discharge function of button intake on the sluice section failed to realize. Now, to satisfy the requirement of the flood prevention, the flood-discharge function of the bottom intake should be restored by dismantling the pressure steel conduit of the latterly built station. In the July 2001, the concerned departments put forward the plan named "The plan of opening holes on detain section of the dam by the steel tubes through the reservoir". Figure 1 is the sketch of the designing plan. The advantage of the plan is that for one thing, the formerly designed flood-discharge fUnction can be restored, and for another, the lately built small hydropower station's generation of electricity will be preserved.

Nowadays, it is rare to practice drilling holes on the built gravity dam in China. The designers are concerned with the following questions: After drilling, whether cracks occur on the upstream surface of the dam? Whether the concrete around the hole crazes? How is the stability of the crack? What influence is imposed on the wholeness of the dam body? All the above questions directly concern the feasibility of drilling holes on a dam. It is essential to adopt nonlinear FEM to make emulational calculation on the localized stress around the hole so as to work out comparatively clear answers to guarantee the smooth expansion of the project [1].

2 ANALYSIS METHODS

Increment theory is adopted in solving the nonlinear equation [2].

$$K\Delta\delta = \Delta R = \Delta R_d + Q_d^0 + \Delta R^p \tag{1}$$

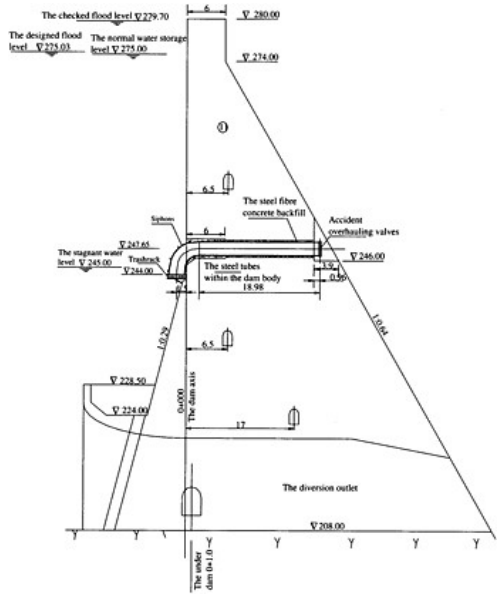

Figure 1. The sketch of the designing plan.

In the above equation, K refers to the stiffness matrix; ΔR_d refers to loading increment matrix; Q_d^o used to demonstrate unbalanced force matrix; ΔR_p is the loading matrix reflecting the flexible effect under the increment loading. When the material is in the stage of the initial flexibility, of the flexible unloading in the plasticity area and of the neutral changing loading, the stress relations are shown in the following equation.

$$\Delta\sigma=D\Delta\varepsilon \tag{2}$$

D is the stress-strain matrix.

When the material is in the stage of plasticity, the deformed increment includes the two aspects of the elasticity and plasticity, while the plasticity increment satisfies the demands of the following flow rule:

$$\Delta \varepsilon^p = d\lambda \frac{\partial F}{\partial \sigma} \tag{3}$$

In the above equation, $d\lambda$ is undetermined; F is the loading function. To be simplified, F can be adopted the same form as the yield function.

When the material is in the stage of plasticity, the relations of the stress-strain can be reflected in the following equation:

$$D_p = \frac{D\frac{\partial F}{\partial \sigma}\left(\frac{\partial F}{\partial \sigma}\right)^T D}{A+\left(\frac{\partial F}{\partial \sigma}\right)^T D\frac{\partial F}{\partial \sigma}} \tag{4}$$

$$A = -\frac{1}{d\lambda}\frac{\partial F}{\partial k}dk$$

In the above equation, k is used to demonstrate the hardening parameter of the material.

The phenomenon of hardening doesn't occur to the ideal elasticity and plasticity materials. By then, k is a constant, A=0. When the material is in subsequent yield surface, A is obtained from the experiment. The appropriate loading functions are used in the equation (4) to gain a plasticity matrix, thus the nonlinear iteration can be made.

The result of the experiment on the gradual destruction of the concrete under the complex loaded condition suggests while under the stress, the material's initial yielding surface and destruction surface share the same shape. The area between the yielding surface and the destruction surface is plastic. The area beyond that of the destruction is anisotropic and broken without any rigidity. The expression is following when William-Warnke yield model is adopted.

$$f(\sigma_m,\tau_m,\theta)=\frac{1}{r(\sigma_m,\theta)}\frac{\tau_m}{f_c'}-1=0 \tag{5}$$

$$r(\sigma_m,\theta)=\frac{2(r_c^3-r_c r_t^2)\cos\theta+(2r_t r_c-r_c^2)\left[4(r_c^2-r_t^2)\cos^2\theta+5r_t^2-4r_t r_c\right]^{1/2}}{4(r_c^2-r_t^2)\cos^2\theta+(r_c-2r_t)^2} \tag{6}$$

In the above expression, σ_m=1/3 I_1 is average normal stress; f'_c refers to the concrete uniaxial compressing intensity.

When θ=0° and θ=60° in the meridian, the function of yield is parabolic:

$$\frac{\tau_{mt}}{f_c'}=\frac{r_t}{\sqrt{5}f'}=a_0+a_1\frac{\sigma_m}{f'}+\left(a_1\frac{\sigma_m}{f'}\right)^2 \quad when\theta=0^0$$
$$\frac{\tau_{mc}}{f_c'}=\frac{r_c}{\sqrt{5}f'}=b_0+b_1\frac{\sigma_m}{f'}+\left(a_1\frac{\sigma_m}{f'}\right)^2 \quad whe\theta=60^0 \tag{7}$$

In the above equation, among a_0, a_1, a_2 and b_0, b_1, b_2, only 5 of them are individuals, which are concerned with the concrete ultimate uniaxial compressive strength, ultimate uniaxial tensile strength, ultimate biaxial compressive strength, ultimate uniaxial compressive strength.

3 THE COMPUTATION

3.1 *The computation model*

The dam body is supposed to be fixed to the base of the rock, while the lateral joint of the either side end freely [3]. Figure 2 is that of the finite element mesh of the dam section 11#, in which the total number of the elements and nodes are separately 4938 and 6155 respectively. The computation is carried out by famous software ANSY5.6.

3.2 *The computation cases*

To satisfy the practical needs of the project, we analyze the period of construction and operation stage. And the analysis of the construction stage also includes: (1) The excavation of the hole section on the rear part has been finished, while the steel tubes have yet to be installed and the block head segment of the hole has yet to be opened. Under such condition, when the water levels are 275m and 245m separately, Case #1–275 and Case #1–245 are adopted respectively to make computation. (2) The excavation of the hole section on the rear part has been finished. The blockhead segment of the hole has been opened. The siphons have yet to be installed. Under such conditions, when the water level is 245m, the computation of which is named by Case #2–245. When the working period has approached after the construction period has come to an end, the holes have been drilled and the

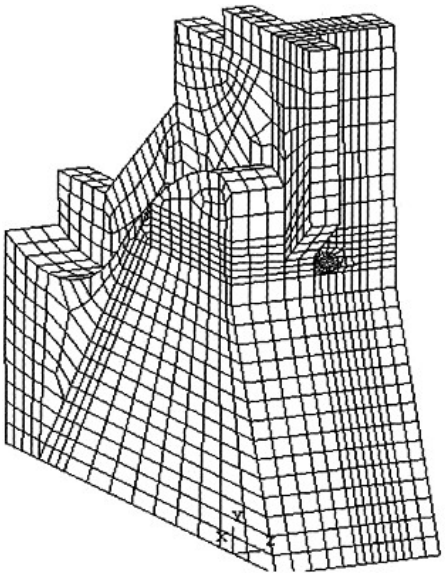

Figure 2. Finite element mesh of the dam.

Table 1. The divisions of dam body materials and their parameters.

The divisions of dam body materials	Modulus of elasticity (Mpa)	Possion's ratio	Capacity (kN/m)	Tensile strength (Mpa)	Compressive strength (Mpa)
C8	1.66×10^4	0.167	24	0.8	5.5
C12	1.97×10^4	0.167	24	1.05	8.5
Speciality C18	2.55×10^4	0.167	24	1.3	10.0

installation of steel tubes has been finished. The power station is functioning normally when the water passes through the tubes. By then, the water level used for computation is 275m. The above condition is labeled as Case #3–215. In view of the above 4 cases, the analysis of the stress distribution around the hole is made to judge whether the concrete around the hole cracks, what the stability of the cracks is like, the possibility of the cracks caused by the upstream surface of the dam body, and the influence on the wholeness of the dam section imposed by the hole-drilling.

3.3 *The computation parameters*

The materials of the dam body falls into the following parts: (1) The concrete that is within the 3-meter thickness on the dam body facing the water and the concrete on the foot of the slope on the upstream surface is labeled as C12. (2) The remaining part is marked as C8. (3) The backfill concrete between the wall of the hole and the steel tubes is marked as the Speciality C18. The other detailed parameters are illustrated in Table 1.

The shearing stress transmission coefficient of the opening cracks of the concrete is 0.4, while that of the closing cracks is 1.0. The other parameters in the Willam-Warnke yield model can be

Table 2. The results of the stress around the hole.

Cases	Max. principal stress	The range of the stress	Min. principal stress
#1–275	0.58	0.3~0.8	−1.24
#1–245	0.59	0.3~0.8	−1.47
#2–245	0.79	0.5~1.0	−2.23
#3–275	0.58	0.1~0.3	−2.02

Note: The range of the principal stress refers to the radial depth along the edge of the hole.

educed through the ratios between the tensile strength and compressive strength by means of the empirical formulas.

4 THE RESULT ANALYSIS

4.1 *Stress analysis*

In the article, the author only gives the computation results of Case #1–215, #1–245, #2–245 and #3–215. The Figure 3(a) and 3(b) illustrate the contours of the part stress and the whole stress on the mouth of the hole. The Figure 3(c) and (d) illustrate the contours of Case #3–275.

From the results of the computation, it is clear that the stress around the hole after the drilling makes redistribution. That is to say, the stresses concentrate on the partial area, the tensile stress concentrating on the hole bottom while the compressive stress on the middle of the hole. The farther away from the hole, the more greatly the phenomenon of the stress concentration lessens. And the stress of the dam body approaches the original state before the hole-drilling. No matter during the construction period or the operation period, the tensile principal stress of the hole mouth is within the limit of the materials' tensile strength. The unfavorable influences caused by the hole drilling is local and partial, that is to say, the whole security of the project is safeguarded [4].

The results of the computation from the said 4 cases make it known that in Case #2–245, when the water level of the reservoir reduces to 245m and the upstream and the downstream of the hole have been linked up, the state of the construction stress is the most unfavorable due to the fact that the hole endures only the outer pressure. In Case #3–275, the hydraulic pressure within the hole counterbalances part of the outer pressure, so as to make the stress lessen. Besides, the comparison between Case #1–275 and #1–245 shows that the stress of the former is a little smaller than that of the latter. The reason responsible for it is that the higher water level makes the dam body backward to some extent. Thus the stress of the hole mouth may lessens. By contrast, when the water level reduces to 245m, the stress around the hole mouth will increase accordingly.

4.2 *The sensibility analysis*

The sensibility analysis is made by supposing less the tensile strength and compressive strength to make it known the safety reserve of the construction. Among the above 4 cases, the state of the construction stress is the most unfavorable in Case #2–245, owing to which, the sensibility analysis is made by reducing 1.4 times and 2.8 times the strength in the case. The results show that when the strength is reduced 1.4 times, the structure trends to initial failure. By then, the most elements are within the elastic limits, the cracks happening on only a few units. (In Figure 4, the vacuum wafer illustrates the cracks element.) When the strength is reduced 2.8 times, more elements are on damage mode. By then, the cracks and crushes show up both the top and bottom of

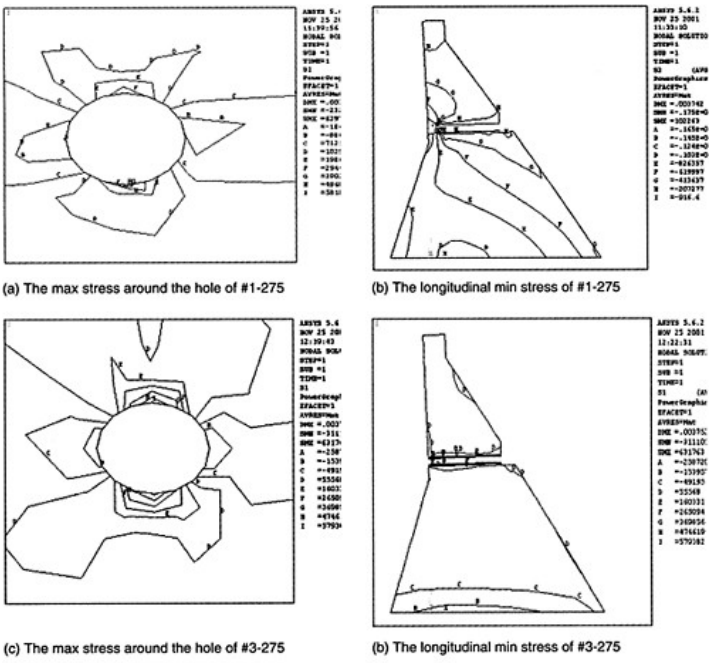

Figure 3. The contours educed from the computation.

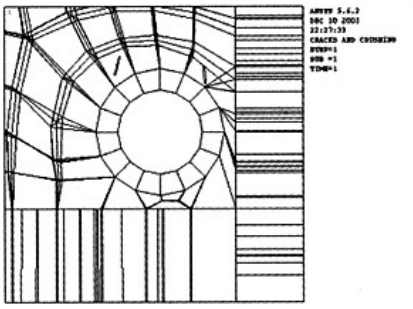

Figure 4. The circumstance of the ripping areas around the hole (1.4 times).

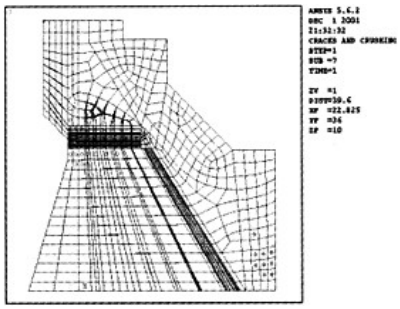

Figure 5. The circumstance of the integral rip (2.8 times).

the hole. The crushes element can also be seen on the downstream of dam body. (In Figure 5, the rhombi are used to illustrate the crushes element.) The sensibility analysis makes it clear that when the strength is reduced, the local ripping areas will arise around the hole, but they tend to be stable.

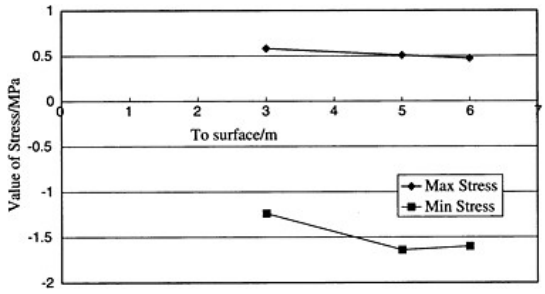

Figure 6. The relations between the excavation process of the block head and the main stress.

4.3 *The simulated analysis of the construction*

As far as Case #1–275 is concerned, we simulated the excavation process of the blockhead on the upper reach of the hole. The change of the stresses is under study when the distances from the forepart face are 6m, 5m, and 3m respectively. Figure 6 illustrates the change of the construction maximum stress along with the excavation process of the blockhead on the upper reach. From Figure 6, it is clear that with the increase of the hole depth, the stress increases slowly. In other words, the excavation process imposes no great influence on the whole dam body. However, the process of the hole-drilling should be in strict accordance with the rules of operation, especially when the shattering process is adopted in the construction.

5 CONCLUSIONS

When a hole is drilled on the built gravity dam, the stress around the hole will redistribute and the concentration of stress will take place on the local areas, the tensile stress concentrating firstly on the hole bottom and secondly on the hole middle. The farther away from the place of hole drilling, the more quickly stress concentration will decrease. From the results of stress analysis, it is clear that drilling a hole on a dam body will result in stress concentration on local areas. However, no great unfavorable influences will be imposed on the whole construction of a dam body. Besides, the maximum tensile stress resulted from the hole drilling is not beyond the allowable tensile strength of the concrete on the said place. The sensibility analysis shows that some local ripping areas will appear around the hole, but tend to be stable. The simulated analysis of the construction shows that the excavation process of the hole imposes no great influence on the whole dam body.

REFERENCES

[1] Lin Keji, *Holes and Galleries in Dam* [M]. Beijing: China Water Conservation and Power Press, 1984:120–132. (in Chinese)
[2] Gong Xiaonan, Ye Qianyuan, Xu Riqing, *Constitution Equation of Engineering Materrials* [M]. Beijing: Press of China Architectural Industry, 1995:136–145. (in Chinese)
[3] Zuo Dongqi, Wang Shixia, Lin Yicai, *Hydraulic Structure (I)* [M]. Nanjing: Press of Hohai University, 1995:184–190, 392–393. (in Chinese)
[4] Chen Jing, Huang Wei, Ding Qian, *Aperture Stress Analyzes to Rectangle Hole in Dam* [J]. Hydraulic Power, December 2000, 12:21–24. (in Chinese)

This page intentionally left blank.

New Developments in Dam Engineering—Wieland, Ren & Tan (eds),

Application of distributed visual simulation technology in hydropower engineering construction

Meng Yongdong[A1,A2], Tian Bin[A2] & Cai Yizhou[A2]

[A1] *Hubei Key Laboratory of Construction and Management in Hydropower Engineering,*

[A2] *College of Civil & Hydropower Engineering, Three Gorges Univ., China*

ABSTRACT: This paper applied Virtual Reality Modeling Language (VRML) and Java programming technology to distributed visual simulation of the dam concrete building of Hydropower project, and realized interactive query information of hydropower engineering construction (for instance: concrete construction intensity, total amount of construction, etc.) in virtual 3D scenes. This simulation system offers sustaining information to administrator in order to facilitate the scientific decision-making process, that in favor of advancing technology of hydropower engineering construction and improving the level of management. All above-mentioned are realized on Internet.

1 INTRODUCTION1

With the development of construction technologies in hydropower engineering, it is one of the keys that how to describe construction course and construction image directly, and to manage, analyses and deals with the information from the project construction for offering the decision information for designing and making policy to a administrator to support effectively, to improve design efficiency and construction management level, at the same time, it is convenient to compare different construction schemes and choose the superior, because it receives restriction and influence of many kinds of factors, such as complicated construction course, large amount of information of construction, and so on. In the past, visual simulation system in the field of hydroelectric project is mostly the concentrating type structure that is developed to individual PC running environment [1]. At present, computer network technology has already been applied to each field. Client/server the distributed structure became the mainstream of computer application and development progressively. It has the extensive one in conformity with the prospect and demand to set up a three-dimension visual simulation system of hydropower engineering construction based on Web for offering long-distance decision support to policymaker.

Some present interactive simulation software tools, can't be used in the distributed network simulation environment directly, must work out the interface program of network in addition. They also can't offer realistic 3D render. And the graphics is relatively coarse [2]. With the development of compute graphics technology and Internet technology, three-dimension visual technology based on Web (Web3D) is becoming riper. VRML is a network 3D technological international standard which was made first. At present, it has the ability to render 3D graphics with ultra sense of reality based on Web. Furthermore, it provides technical support of three-dimension interactive operation and information obtaining, which make it possible to set up distributed three-dimension visual simulation system.

The article proceeds from project practice, combining the visual simulation research of concrete dam on divided block construction course, uses VRML and Java programming technology to develop hydropower engineering construction visual simulation system based on Web3D, also discusses the communication method that dynamic webpage technology and VRML target, offers the basis for other relevant fields to popularize and use this technology.

2 THREE-DIMENSIONAL TECHNOLOGY OF THE WEB

Visualization techniques used in science and project for showing the calculation result with the graphics or figure information, it is a result combined with the computer graphics technology and the scientific calculation, so it can describe the physical phenomenon or physical parameter of varying with time and space more ocularly.

With the development of network technology of the computer, Internet applied to fields of the global extensively. The three-dimensional technology of the network (Web3D) as information carrier of Internet has already become developing direction with new present visual technology.

Virtual Reality Modeling Language (VRML), as the earliest international standard of 3D technology of the network, is one kind simple text language used for describing the 3D modeling and interactive environment. With the VRML, you can incorporate high-quality, scalable, platform-independent 3D graphics into applications and Internet, it have become an opening standard of setting up 3D multimedia and sharing virtual world on Internet at present. VRML program is that a kind of explanation execution, real-time modeling rendered text codes, and the extension is named to. WRL (a kind of ASCII file), or the file is zipped and named to. WRZ (binary file), it has two main points: (1) Node, as key element forming the virtual world scene; (2) Route, convey the way of information among the nodes.

It generally includes the following 4 parts: (1) File head, lie in the first trip of VRML file, provide the edition information of the file for browser, it is '#VRML V2.0 utf8' in VRML 2.0 edition; (2) Explanatory note, a section of characters begun with '#' symbol; (3) The node, the unit of scene information, Can describe modeling, light and sound in the scene, etc. with it; (4) Field value, for describing and changing nodal attribute, field value has reflected the size of the field. VRML1.0 can only establish 3D scenery of taking a stand and move between them, to have a look around three-dimensional world, there is no interactive function. VRML2.0 has enormous changes, includes 54 kinds of standard nodal types.

The most attractive place of VRML is its interactive dynamic scene. Such interactive realization that is exposed to of the scene and user needs two basic factors: First, behavior (whether one description happen anything, what must change, by any method that change); Second, the execution pattern (a kind of method to convey the scene entity back and forth). In VRML, basic mechanism composed of behaviors, and behavior to change the state of VRML target of scene through execution pattern. The execution pattern regards the event as changing tool and acts on the section which keep the status, can be divided into two kinds: static behavior and dynamic behavior. The so-called static behavior means that the behavior takes place in a place: The event source (EventOut Field) and target (EventIn Field) are connected together in order to change the scene view. The dynamic behavior different from static behavior, it can do the route event more than route of the original definition. The dynamic behavior has ability to inquire state, then make the decision based these states, change the state of the scene on the basis of these decisions.

X3D is an open standard for 3D content delivery. It is not a programming API, nor just a file format for geometry interchange. It combines both geometry and runtime behavioral descriptions into a single file that has a number of different file formats available for it, including the Extensible Markup Language (XML). It is the next revision of the VRML97 ISO specification. There are both major and minor differences between the VRML97 and X3D. X3D takes the work of VRML97 and clarifies all the grey areas in the previous specification that have been uncovered thorough years of use. It has then taken the basic premise and extended it to provide greater flexibility. Major changes include the complete revamp of the specification into three separate specifications dealing with abstract concepts, file format encodings and programming language access. Other modifications include being more precise with the lighting and event models, and changing some field names for consistency.

3 THE REAL-TIME STRUCTURE OF VRML SCENE

The visual simulation of hydropower project construction involves a large amount of data information, such as DEM data of construction zone, building size and attribute message datum, etc. How to collect, save and manage the data, and the correct choices of visual expression method are the key to setting up a high performance visual simulation system.

Hydropower project construction is a dynamic course, construction zone topographical ground form and building form change constantly with lapse of time, the structure of its visual simulation scene needs to consider the time characteristic. Supporting the mergence of a lot of scenes in VRML, in order to make it convenient for operated and improve the efficiency that the scene structure, can divides the whole simulation scene into unchangeable part and variable part. Using External Authoring Interface (EAI) of VRML and network database technology can realize VRML dynamic scene structure in real time.

3.1 *Source of the data*

Concrete dam construction is a course that from preparing and transporting the concrete to building the concrete block. According to the Systems Engineering principle, the concrete dam construction as a complicated system, can be regarded as formed by three subsystems (mix and stir concrete, transport concrete and build the concrete block), the whole system is influenced by synthesis of external factor and inside factor. Utilizing the systematic analytical method, under the situation of dam body size and section divide certain, the definitely scheme of machinery and various kinds of condition with restrictions and restrains, can arrange to each order of concrete block and calculate the time limit for a project construction through calculating in emulation [3], carry on many kinds of construction scheme select excellent relatively.

Through system emulation analysis, export the calculation result of each block geo-information and decision variable (for instance: construct machinery, build time, etc.), as the data source of structuring the variable scene and interactive inquiry attribute information. As to the unchangeable scene, its data source is mainly CAD modeling software.

3.2 *The way and structure of data storage*

The commonly used ways of data storage have an ordered text file and database file. Text file has simply store method, but unable to punish magnanimity datum. Database is suitable for storing the magnanimity data, such advantages as swift acquirement, flexible and the record is easy to operate, already become the first-selected way in which the data stored.

The concrete blocks include space geometry information and attribute information, the data amounts are great and interrelations are complicated. Considering that two kinds of information data need flexible logic to be matched and joined when the variable scene is structured and inquires interactively that is operated, choose to adopt the form of the database to be stored, keep geometry information and attribute information in different data lists respectively, the record of geometry information and attribute information of same block joined through the same word relatively, as Figure 1 shows.

3.3 *Structure VRML scene based on Java EAI*

The VRML97 Java EAI allows a Java applet to control a VRML97 plug-in, running on the same HTML page. The applet can use Java user-interface elements, threads, sockets, etc. The applet can interact with the VRML world in the following ways [4]:

- accesses the functionality of the browser interface (e.g. to create new geometry),
- sends events to eventIns of nodes inside the scene (e.g. to change positions or colors of objects),
- reads the last value sent from eventOuts of nodes inside the scene (e.g. to find the last position of an object),

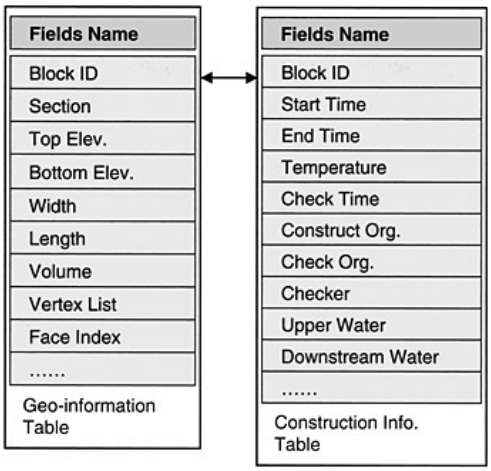

Figure 1. The database structure of concrete blocks.

• is notified when events are sent from eventOuts of nodes inside the scene (e.g. when an object is being clicked).

An applet is a small Internet-based program written in Java, which can be downloaded by any computer. The applet is also able to run in HTML. The applet is usually embedded in an HTML page on a Web site and can be executed within a client browser.

JDBC technology is a Java API that provides cross-DBMS connectivity to a wide range of SQL databases and access to other tabular data sources, such as spreadsheets or flat files. With a JDBC technology enabled driver, Java program can connect all corporate data even in outside environment [5]. Figure 2 shows the relation of different technology involved for structure VRML scene.

Utilize Java applet to connect concrete block information database, read all record that accord with the specified conditions in the information data table of geometry, the geometry information of concrete block will be written into VRML scene, output. WRL format scene file finally, realize a certain time concrete dam construct image of appearance. Figure 3 shows the diagram of program which structure VRML scene.

Concrete block can be described with hexahedron in VRML scene, description method as follows codes:

```
Geometry IndexedFaceSet{
    coord Coordinate {
        #Vertex list of hexahedron
        point [25.0 86.0 0, …]
    }
    #Vertex index of each face
    coordIndex 3,2,1,0,-1, …]
}
```

The unchangeable scene that modeled under the enviroment of CAD software mainly include DTM model of construction zone, water field model and permanent building, etc. it can be changed into WRL file format through third party's software. Because the changes of scene appearance which caused by excavating, backfill, etc. is considered, can produce a lot of different WRL file of unchangeable scene separately for using the scene mergency, and each of them represent the

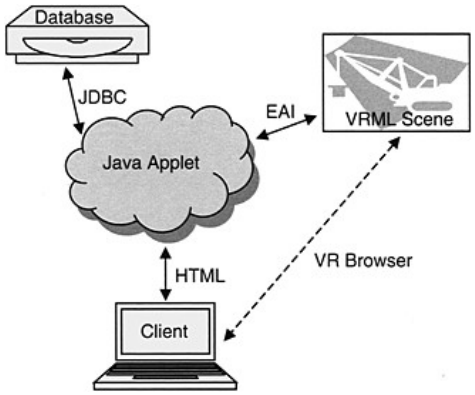

Figure 2. The relation of each different technology.

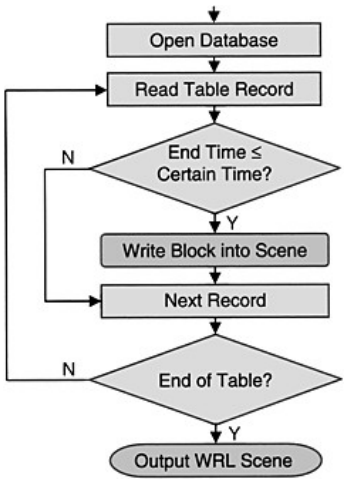

Figure 3. Program diagram of structure VRML scene.

image of the crucial moment. While producing the whole scene, utilize Java Applet program to judge according to certain time at first, confirm the unchangeable scene which merge with variable scene, then use Inline node to merge the unchangeable scene into variable scene, finish forming the whole scene at last.

4 REALIZATION OF THE INTERACTIVE FUNCTION

VRML scene offers simple interaction to what user's needs punish, including the event and route, but must have interface to realize interaction between VRML and other specific applacation, can use Script node and JavaScript programming realize interaction of VRML and external information. There are Script nodal main functions: (1) Can respond to the change of the environment and users' operation; (2) Receive the event and carry on some treatment from other nodes; (3) The

inside code can finish some calculating work; (4) Make some changes of the external world through sending event. Using Script node can write complicated VRML program [6], the grammar of Script node as follows:

```
Script {
    Field SFBool directOutput FALSE
    Field SFBool mustEvaluate FALSE
    exposedField MFString url []
    "http://foo.com/fooBar.class", # JavaApplet
    "http://foo.com/fooBar.js", # JavaScript
    "Javascript:
    function start(value, timestamp) {…}"
    #And the following fields of any nodes
    field fieldTypeName fieldName initialValue
    eventIn eventTypeName eventName
    eventOut eventTypeName eventName
}
```

Each scripting language provides a mechanism for allowing scripts to send a value through an eventOut defined by the Script node. For example, one scripting language may define an explicit function for sending each eventOut, while another language may use assignment statements to automatically defined eventOut variables to implicitly send the eventOut. The results of sending multiple values through an eventOut during a single script execution are undefined—it may result in multiple eventOuts with the same timestamp or a single event out with the value of the last assigned value [7].

In the concrete dam construction visual simulation system, it mainly include interaction which between VRML scene and HTML webpage, and connecting to the information database of concrete block use JavaScript in VRML scene.

4.1 *Interaction between VRML and HTML*

While structuring VRML scene, transmit HTML form message that user referred (for instance: Project position, simulation time, etc.) to Java applet which can operate the VRML scene through using EAI, thus can realize interaction between HTML and VRML. But transmission information through 3D interactive from VRML to HTML is the key of getting message of concrete block, can realize it through attach an Anchor hyperlink node to each corresponded Geometry node of block, the grammar is as follows:

```
Anchor {
  description "Tooltip text"
  parameter "target=_Blank"
  url "JavaScript:dofunc(Block_ID);"
  children [Shape {geometry IndexedFaceSet {…}}]
}
```

The Url field of the above-mentioned Anchor node can transmit the value of concrete BlockJD to applet through parameter of dofunc() function that defined in HTML, then Java applet finishes reading the attribute information that corresponding Block_ID is written down in the database, output to HTML page finally.

4.2 *Connect database using JavaScript*

When simulate the construction course of concrete dam at a certain time using animated pictures, need to use Script node to increase and build the node of geometry in VRML scene. The geometry information of concrete block needs obtaining from the database, and the data operation to the

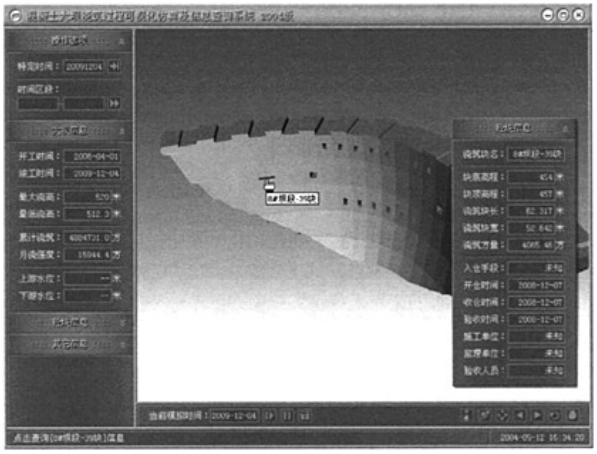

Figure 4. The interface of distributed visual simulation system.

database can be realized through JavaScript script language which inside in Script node, the program code is as follows:

```
DEF DataOperate script {
   url "Javascript:
   # Connect the database
   this.database.connect(databasetype,servername,username,password,databasename)
   # Operate data
   temp=this.database.execute(select * from …)
   # Convey the data to the export interface
   stockindexes changed = temp"
}
```

5 APPLICATIONS EXAMPLE

According to the above technological train of thought, combining the Xiluodu arch dam construction, we developed the distributed visual simulation system based on Web3D and VRML browser.

This system has better interaction and vivid 3D animation effect. It can show realtime 3D scene of different construction process. The project policymakers and construction administrators can inquire about construction image of any moment in the areas far away from construction site. Through this software, the dam construction image of any certain time section can be simulated dynamically, and they can get the construction information, such as concrete construction intensity, total amount of construction, the highest elevation, the lowest elevation, water level, etc. For example, in Figure 4, they can operate interactively on choosing any dam section to show single dam section in detail and inquire information of each concrete block.

6 CONCLUSION

Directed against visual simulation of hydropower engineering construction, using VRML and HTML (the Java applet embedded) webpage technology, we developed a visual simulation system of concrete dam based on VRML and its browser. We succeeded in applying to concrete construction course simulation of the second stage of dam and power station of CTGP (China Three Gorges Project) and Xiluodu arch dam (located at Jinshajiang River in China). It offers reference for the application in other fields (such as the construction of underground complicated hole-room group, the layout of construction site, earth and stone project, etc.) of hydroelectric project of technology of distributed visual simulation. Compared with commonly used visual simulation system at present, its outstanding advantage is to support distributed interactive simulation. Furthermore, the simulation equipments can be distributed in the wide long-distance area. Visual simulation of hydroelectric engineering construction course and interactive information inquiry based on three-dimensional technology of the network, can offer real-time long-distance decision information support for administrators and policymakers. This system helps to advance management level and construction technology of hydropower engineering, and to improve long-distance networked management level of hydropower engineering. It has far-reaching meanings in improving the management level of engineering construction.

REFERENCES

[1] Zhong Denghwa, Zheng Jiaxiang, Liu Donghai, Zhang Weibo. *Visual simulation technology and application.* Chinese water conservancy and power publishing house, Beijing, 2002.
[2] Wang Li, Feng Wu. Application in the visual simulation system of VRML. *Simulation of the computer,* 2001,18(3), p 50–52.
[3] Sun Xiheng, Wang Donghai. *Computer simulation and program designing of the hydropower project construction.* Chinese water conservancy and power publishing house, Beijing, 1997.
[4] Chris Marrin. *Proposal for a VRML 2.0 Informative Annex: External Authoring Interface Reference.* Silicon Graphics, Inc. November 21, 1997.
[5] *JDBC API Speciflcation.* Sun Microsystems, Inc. 2003.
[6] *VRML97 Standard.* International Standard. ISO/IEC 14772–1:1997.
[7] Boon-Hee Kim, Jun Hwang, Young-Chan Kim. The Design of High-Level Database Access Method in a Web-Based 3D Object Authoring Tool. *Lecture Notes in Computer Science,* 2002, p 204–214.
[8] Anima Gupta, Paul Tarau. Logic Programming Techniques for Dynamic VRML Web Content Generation. *Lecture Notes in Computer Science,* 2001.
[9] Huang, Bo. Web-based dynamic and interactive environmental visualization. *Computers, Environment and Urban Systems,* November, 2003, p 623–636.
[10] Hong, Z. Shi, J.J. Tam, C.M. Visual modeling and simulation for construction operations. *Automation in Construction,* January, 2002, p 47–57.
[11] Au, Grace. Paul, Ray J. Visual interactive modeling: A pictorial simulation specification system. *European Journal of Operational Research,* May 24, 1996, p 14–26.
[12] Tamura, Yoshiaki. Development of visual computing systems for fluid dynamics simulations. *JSME International Journal, Series B,* February, 2000, p 1–11.

New Developments in Dam Engineering—Wieland, Ren & Tan (eds),
© 2004 Taylor & Francis Group, London, ISBN 04 1536 240 7.

Results and experiences obtained from chemical grout testing in part of conglomerate foundation of Karkheh dam—Iran

Ali Asghar Mirghasemi
Univ. of Tehran and Mahab Ghodss Consulting Engineers, Iran

Mohammad heidarzadeh
Univ. of Tehran, Iran

Mansour Etemadzadeh & Mehdi Pakzad
Mahab Ghodss Consulting Engineers, Iran

ABSTRACT: Chemical grouts were developed in response to a need to develop strength and control water flow in geologic units where the pore sizes in the rock or soil units were too small to allow the introduction of conventional Portland cement suspensions. Important advantages of chemical grouts are very high penetration power, less pumping pressure required for the same rate of grout injection, controllable setting time, severalty of commercial chemical grouts with different quality characteristics and quick action of grout in seepage control.

Seepage control system of Karkheh dam is cutoff wall that is executed in all over the dam axis using plastic concrete. In part of conglomerate foundation of Karkheh dam, in region named gallery 950, is considered to create a water seal curtain due to impossibility of cutoff wall development. Because of the choice of cement grout curtain was not completely successful, therefore a water seal curtain using chemical grouts for first time in the country was designed by Mahab Ghodss consulting engineers to remove the problems arised from seepage in this part of dam foundation. Chemical grout testing in Karkheh dam proved the efficiency of the method in seepage control as well as resulted in valuable and unique experiences, among them are design of correct program for chemical grouting, mix design, solving execution problems and selection of proper preparation and grouting system. In this paper chemical grouting is briefly introduced then results and experiences obtained from chemical grout testing in Karkheh dam is presented.

1 INTRODUCTION

Nowadays grouting is used in many projects and different purposes. In some cases it is used to develop soil consistency, to reduce the effect of vibrations in the soil, to decrease soil settlement under static and dynamic loads and similar objectives. In other cases the objective of grouting works is water sealing, which based on this purpose grouting is used in dam construction. Grouting is a procedure in which grout is injected into pores, voids or fissures of the rock and soil formations and improves systems characteristics, so that permeability of layers reduces, their strength improves and their deformability decreases.

Chemical grouting is the practice of injection liquids (chemical grouts) that solidify to form strong water impermeable barriers into soil, rock or concrete. First studies about chemical grouts started around 1900, but really became popular in stabilization and water tightening from the 1950s onwards. Francois introduced the use of sodium silicate in conjunction with other reactive chemicals for strengthening sandy foundations in 1914 [1]. With a view to the history of grouting

technology, pure Portland cement, approximately was the only grout material until 1925 [2]. But for some soil mass conditions, cement suspensions can not solve all leakage problems. The problem appeared in grouting of sandy and gravely formations, when cement was not able to pass the narrow channels between the pores of the soil. In fact the pores were blocked by coarse particle of the cement grouts and grouting range was been limited. Consequently grout materials become useless. To remove this problem Yoosten for first time in the history of grouting, invent the method of chemical grouting. His procedure was based on successive grouting of sodium silicate and a salt solution such as calcium chloride. In the Yoosten procedure sodium silicate was injected into one borehole and a coagulant (strong calcium chloride) into an adjoining borehole with the mixing of these two substances forming the grout. Blocking and obstruction of grout flow was prevented by using these materials.

Although chemical grouts may be more expensive than conventional particulate grouts, they posses the following several important advantages [1].

- The absence of particulate material in the grout means, theoretically, that a chemical grout can be injected into any formation with a reasonable average size opening
- Chemical grouts generally have a lower viscosity, indicating that for the same rate of grout injection, less pumping pressure will be required
- Setting time can be controlled in chemical grouts, allowing the grout to gel at the right place at the right time
- Severalty of commercial chemical grouts with different characteristics

In spite of extensive usage of chemical grouts in five recent decades in all over the world, Karkheh dam chemical grouting is the first experience of chemical grouting in Iran. The water tightening method of Karkheh dam foundation is cutoff wall, which is performed all over the dam axis using plastic concrete [3]. In part of conglomerate foundation of dam, in the region named gallery 950, is considered to create a grout curtain due to impossibility of cutoff wall development. Also the cement grout curtain was not completely successful [4]. Therefore after various technical, economical and environmental studies a chemical grout curtain for the first time in the country was designed by Mahab Ghodss consulting engineers to remove the problems arising from seepage in this part of dam foundation. The importance of Karkheh dam chemical grouting design appears when we know that there was no practical experience and local technology and expertness in this field in the country before Karkheh experience. Results and experiences obtained from Karkheh chemical grout testing showed that grouting procedure will be successful, if correct grouting program is used. Chemical grout testing of Karkheh dam proved the efficiency of this method in seepage control, as well as resulted in valuable and unique experiences. From most important of them the following cases can be mentioned.

- Experiences obtained in the context of mix design selection
- Experiences obtained in the context of preparation and grouting system
- Design of correct grouting program
- Solving of execution problems

In other words Karkheh chemical grouting experience is a great step in order to localize the technology of chemical grouting in the country. In this paper at first chemical grouting is briefly introduced. Then results and experiences obtained from Karkheh chemical grouting is presented.

2 BRIEF INTRODUCTION TO CHEMICAL GROUTING

2.2 *Different types of chemical grouts*

For many years the term chemical grouts was synonymous with sodium silicate and Yoosten process [1]. Sodium silicate accompanied by an activator was used in the first half of century 20. This set as a whole was named two component grout. The last three decades have witnessed the

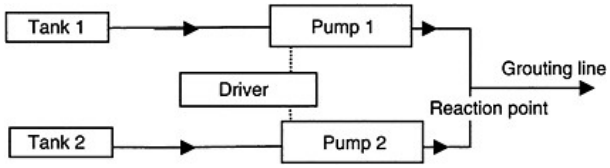

Figure 1. A system used for chemical grouting, including two tanks and two pumps.

introduction and use of many chemical compounds as commercial chemical grouts, covering a wide range of chemical grout system, namely, sodium silicate, acrylamide, acrylate, aminoplast, phenoplast, crome lignin, polyurethane, epoxy resin, acetone formaldehyde, furan resin etc., which provide a wide selection for the grouting engineer, who must choose a grout according to specific job requirements. Among them, sodium silicate and acrylamide have been used more. So that nowadays sodium silicate and acrylamide are used in 90 percent of projects in the United States [5].

2.2 *Preparation and grouting system of chemical grouts*

The common system used for conventional portland cement grouting is batch system. In the batch system all of the components including the catalyst are mixed together at the same time, generally in a single tank. But often we can not use batch system for chemical grouts. In chemical grouts the entire batch must be placed during the established gel time. However, because pumping rates often decrease as injection continues, this is not always possible, and the danger of gelation in the equipment is always present. Nowadays due to the nature of chemical grouts, which it is possible to separate the main grout from its additive (or activator); various systems are invented for preparation and injection of these materials. A system including two tanks is the most common system used for chemical grouting. In this method, one tank contains the catalyst and the other tank contains all of the other components. Using this method, two chemicals that must react for creation of silica gel, will not meet each other until they do not come to the grouting pipe. Consequently the gel time can be controlled better. In the Figure 1 a common system used for chemical grouting, including two tanks and two pumps is presented [6].

2.3 *Chemical grouting equipment and execution method*

In chemical grouting generally grouting pipes in holes are used. In this case tube with protective cover named moanchette tube is the most technical and most modern system of pipe-laying that today widely is used in chemical grouting. The spaces between moanchette tube and hole are filled by a weak mortar that generally is made of cement and bentonite. Chemical grout is injected into soil formation through pores of the moanchette tube. In this process a system including two packers is travelled to a certain depth of the hole. Then desired pores of moanchette tube are separated from other parts of the pipe. Due to pumping pressure that is exerted to the rubber tube around pores from the ground level, the rubber tube opens. So that chemical grout breaks the weak mortar around the moanchette and penetrates into the soil (Figure 2) [7].

3 THE FIRST CHEMICAL GROUTING IN THE COUNTRY IN THE KARKHEH DAM

3.1 *Karkheh reservoir dam*

Karkheh earthfill dam, as the largest dam in the country, is located on north of the Khuzestan province at southwest of Iran. Karkheh is the first dam that is constructed on Karkheh River, the

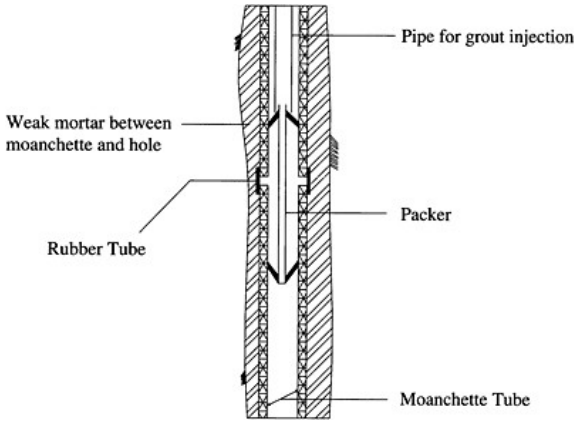

Figure 2. A typical chemical grouting hole.

Figure 3. Karkheh reservoir dam, Andimeshk—Iran.

third largest river in Iran. The dam height is 127m, the crest length is 3030m, the crest width is 12m and the reservoir capacity at normal reservoir level is $5.6\times10^{9}m^{3}$.

3.2 *Geology*

Karkheh River in the location of Karkheh dam axis is located in an unsymmetrical valley in Bakhtiary aquifer. Bakhtiary aquifer is composed of mudstone and conglomerate layers (Figure 4). Bakhtiary conglomerate is subdivided into two units, including lower Bakhtiary conglomerate and upper Bakhtiary conglomerate in the karkheh dam location. Lower conglomerate has relatively lower cementation and is located from level 165 to down. Upper conglomerate is located from level 165 to up and has better cementation conditions. Dam foundation is located on lower Bakhtiary conglomerate and alluvial terraces that covered it in the middle portion and parts of left and right abutments [8]. Existence of very weak grains with open gravels is from most important characteristics of Bakhtiary aquifer in the location of Karkheh dam. These layers have very low cementation and gravel grains freely placed on each other.

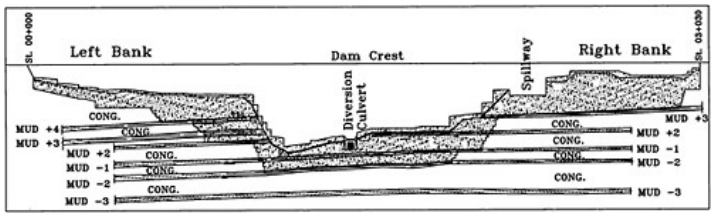

Figure 4. Karkheh dam geology condition.

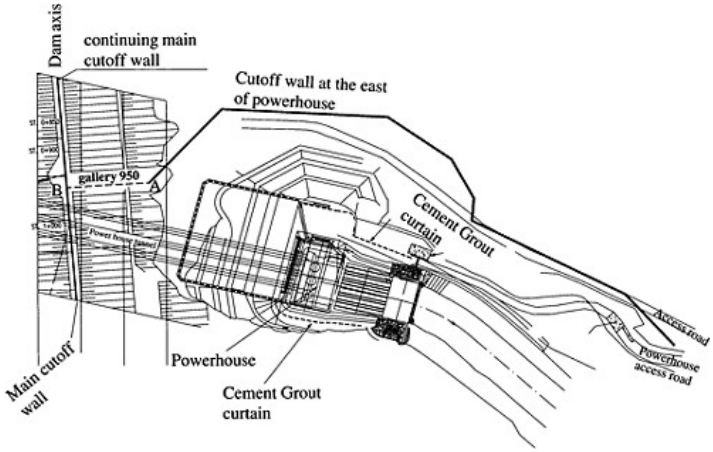

Figure 5. Plan of dam, power hose and cutoff walls.

3.3 *Site of chemical grouting and necessity of it*

Karkheh dam foundation water sealing system is plastic concrete cutoff wall that is executed all over the dam axis. Also another cutoff wall is performed around power house for water tightening the power house in the downstream of dam. The plan of dam, power house and cutoff walls can be seen in the Figure 5. One of the access galleries of dam, named gallery 950 is located between these two cutoff walls, in region specified by dashed line AB in the Figure 5. Due to lock of cuttoff wall in this zone of dam foundation, a concentration of seepage is established, and creation of a water sealing system is indisputable. With regard to insufficient space in the gallery, construction of a cuoff wall is impossible. Also execution of a cement grout curtain was not completely successful. Therefore, finally a grout curtain using chemical grouts is considered.

3.4 *Chemical grout testing in Karkheh dam*

Two series of holes with different grouting programs were tested to obtain some primary objectives of chemical grouting, such as amount and performance of chemical grouts penetration in the Bakhtiary conglomerate, radius of influence and effects on rock permeability. These holes were drilled near a conglomerate trench, located in the vicinity of gallery 950.

Table 1. The final chemical grout used in chemical grout testing in Karkheh dam.

Material properties			Mix design	
Gel time (min)	Viscosity (c.p)	Water (ml)	Acethat ethil (ml)	Sodium silicate (ml)
40	2–3	93	21	60

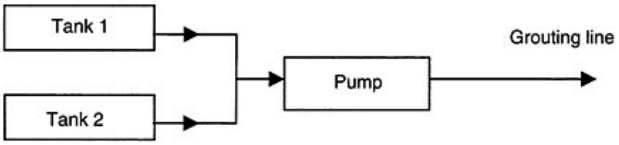

Figure 6. System of chemical grouting in Karkheh dam, including two tanks and one pump.

3.5 *Chemical grout used in Karkheh*

The grout components and mix design were determined, after about two months various laboratorial studies. The final design is composed of sodium silicate as main grout and acethat ethil as additive. Mixing ratio and material properties are presented in Table 1. Also economical consideration is regarded in selection of grout components.

3.6 *Preparation and grouting system used in Karkheh*

At first due to adequate gel time of the grout (40 min), batch system was used. While one batch was exhausting, the next batch was prepared. Considering sufficient gel time of the grout, it was been seem that there was no problem. But after some batch observed that gel time is strongly reduced. Therefore regarding the danger of clogging of the pumps, pipes and flow channels, chemical grouting procedure stopped. Consequently a system including two mixing tanks and one pump was used for chemical grouting. In this system one tank contains the catalyst and the other tank contains all of the other components (Figure 6).

3.7 *Discussion about results obtained from preparation and grouting system*

Until now it was imagined that batch system, which is the cheapest and the easiest system for grouting, is applicable in grout with adequate gel time. But Karkheh experience showed that very little amount of grout from previous batch acts as a accelerator for the next batch grouts and strongly reduces the grout gel time. Therefore the danger of gelation in the equipment is always present. Karkheh experience shows that batch systems are not useful for chemical grouting, unless for the case of small projects that amount of grout materials is only one batch.

3.8 *First series of test holes*

First series of holes, at first were injected by chemical grouts. Then they were grouted by cement grouts. Meanwhile in each stage, permeability test was accomplished before and after any grouting. The arrangement of first series of holes was triangular. The triangle was isoside, wich each side had 1.5m length. These holes had a depth of about 5m. At first primary holes, located at corners of triangle (S1, S2, S3) were drilled and grouted. Then secondry holes (S5, S6, S7) (Figure 7), between primary holes as linear control holes are drilled and recovery specimens from these holes are investigated and effect of grouting in primary holes is studied and then they were grouted.

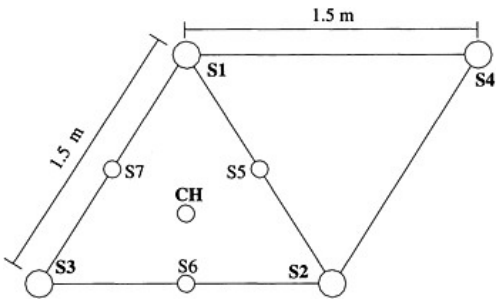

Figure 7. Position of first and second series of test holes.

Table 2. Complete results of chemical grouting in first series of holes.

Comments	Permeability		Depth (m)	Hole name
	Lu	cm/s		
Before any grouting	163	2.1×10^{-3}	5	S1
Before any grouting	239	3.1×10^{-3}	5	S2
Before any grouting	225	3.3×10^{-3}	4	S3
After chemical grouting in s1, s2, s3	102.5	1.3×10^{-3}	4	S5
After chemical grouting in s1, s2, s3	89	1.1×10^{-3}	5	S6
After chemical grouting in s1, s2, s3	70	9.1×10^{-4}	5	S7
After chemical grouting in all hole	73	9.4×10^{-4}	4	CH
After chemical and cement grouting in all	16	2.0×10^{-4}		

Table 3. Complete results of chemical grouting in second series of holes.

Permeability after cement and chemical grouting		Permeability after cement grouting		Permeablity before any grouting		
Lu	cm/s	Lu	cm/s	Lu	cm/s	Hole
1.2	1.5×10^{-5}	29	3.7×10^{-4}	70	9.1×10^{-4}	S4

Finally control hole (CH) is drilled at the centre of secondary holes and its permeability is determined. Complete results of chemical grouting in first series of holes, is presented in Table 2.

As can be seen from Table 2, chemical grouting alone is not efficient. In this case soil permeability from about 219 Lu, reduced to 73 Lu, whereas generally the objective of grouting programs is to reduce soil permeability to the down of 5 or 10 Lu. The reason can be related to the geology of Karkheh dam, which are included open gravels. Therefore created gel loses it's durability due to water flow. Also this result shows that the method of chemical grouting at first, and then cement grouting is not adequately efficient.

3.9 *Second series of test holes*

Second series of test holes, in contrast with series one, at first were injected by cement and bentonite (8 percent of cement) groutes and then they were grouted by chemical grouts. Second series of test holes were included of a hole named S4, with depth of 4m, which its position comparing with first holes is shown in Figure 7. Complete result is presented in Table 3.

Table 3 shows the method of cement grouting at first, and then chemical grouting has better performance than the method of chemical grouting at first, and then cement grouting. In this case, at first large pores are blocked by cement grouts and then small pores would be blocked using chemical grouts.

4 CONCLUSION

For first time in the country chemical grouting is used to remove problems arised from seepage in part of gonglomerate foundation of Karkheh dam. Karkheh chemical grout testing proved the high performance of the method of chemical grouting in seepage control, as well as, resulted in valuable and unique experiences, which most important of them are:

- Batch system is not useful for chemical grouting. Karkheh experience showed that very little amount of grout from previous batch acts as a accelerator for the next batch grout and strongly reduces the grout gel time. Therefore the danger of gelation in the equipment is always present.
- Chemical grouting alone is not efficient. In this case soil permeability from about 219 Lu, reduced to 73 Lu, whereas generally the objective of grouting programs is to reduce soil permeability to the down of 5 or 10 Lu.
- A compostion of cement grouting and then chemical grouting is the best grouting program for conglomerate foundation of Karkheh dam. In this case, at first large pores are blocked by cement grouts and then small pores would be blocked using chemical grouts.

ACKNOWLEDGMENT

The authors would like to thank Iran Water and Power Resources Development Company and C.S.C. Company for their help.

REFERENCES

[1] A.V.Shroff, D.L.Shah [1999]. *"Grouting Technology in tunneling and dam construction",* second edition, A.A.BALKEMA/Rotterdam/BrookField.
[2] Christian Kutzner [1996]. *"Grouting of Rock and Soil",* A.A.BALKEMA/Rotterdam/Brookfield.
[3] Karkheh dam section engineers [1995]. *"Karkheh dam cutoff wall technical specification",* Mahab Ghodss consulting engineers, Tehran.
[4] Karkheh dam section engineers [1995]. *"The engineering geological report of the Karkheh storage dam",* Mahab Ghodss consulting engineers, Tehran.
[5] E.Nonveiller [1996]. *"Grouting theory and practice"*, Translation to Persian by "Zayand ab consulting engineers", science and technology press, Esfahan, Iran.
[6] US Army corps of engineers [1995]. *"Engineering and Design, CHEMICAL GROUTING",* Engineer Manual, EM 1110–1–3500, Washington, DC.
[7] Ructures Raymod W.Henn, Thomas Telrord [2001]. *"Practical guide to grouting",* American Society of Civil Engineers (ASCE) Press, New York.
[8] Iran Water and Power Resources Development company [2001]. *"Summary of phase one of Karkheh project",* Tehran.

New Developments in Dam Engineering—Wieland, Ren & Tan (eds),

Nonlinear seismic response of concrete gravity dams using damage mechanics including dam-reservoir interaction

H.Mirzabozorg & M.Ghaemian
Department of Civil Engineering, Sharif University of Technology, Tehran, Iran

ABSTRACT: A local anisotropic damage mechanics model based on energy equivalence was used for evaluating the nonlinear static and dynamic response of concrete gravity dams. The cracks within the elements was formulated as coaxial rotating cracks and the effect of hydrodynamic pressure was included using the staggered displacement method. The features of strain rate effects; strain softening and closing/reopening of cracks were included in the model. The mesh objectivity of the nonlinear model was satisfied by the fracture energy conservation technique. The Pine Flat dam was chosen to investigate the performance of the proposed algorithms. It was found that the resulted crack profiles when including dam-reservoir interaction is less diffused in comparison when the reservoir is modeled as added mass and also there is not any numerical instability during dynamic analysis.

1 INTRODUCTION

Recently, the seismic safety of concrete dams is one of the important problems in engineering field due to vast socio-economic disasters caused by collapse of these infra-structures. Several numerical models have been developed for seismic safety evaluation of concrete dams in two and three-dimensional space. In the early stage of nonlinear analysis, Chopra and Chakrabarti [1] predicted the location of crack profiles using linear elastic analysis excluding the dynamic interaction of the reservoir and foundation. Pal [2 and 3] analyzed concrete gravity dams using nonlinear models for the first time in which the foundation was assumed rigid and the dynamic interaction effect of the reservoir was excluded. The smeared crack was used to model the nonlinear behavior. Shrikrud and Bachmann [4] used discrete crack model in seismic analysis of concrete gravity dams. In this study, the strength criterion was used for crack initiation and propagation. Webf et al. [5] used the discrete crack to model seismic response of concrete gravity dams. The reservoir was modeled by boundary element method and the aggregate interlock was modeled by special elastoplastic springs. El-Aidi and Hall [6 and 7] considered the nonlinear seismic response of concrete gravity dams using the smeared crack model. The effect of the reservoir interaction was rigorously accounted for and the foundation was modeled as a rectangular mass-less region connected to a semi-infinite visco-elastic half space. It was found that the resulted crack profiles are unrealistic due to using the size reduced strength criterion (SRS) in the proposed smeared crack model. Vargas-Loli and Fenves [8] considered the seismic response of Pine Flat dam using the smeared crack model with the brittle fracture criterion. The resulted crack profiles were too diffused and numerical instability was encountered due to sudden release of energy in small fractured elements.

Feltrin et al. [9] used the discrete crack model in association with the Hillerborg's fictitious crack model and considered the Pine Flat dam under seismic loads. Bhattachrjee and Leger [10–12] used a smeared crack model to analyze concrete gravity dams under static and dynamic loads. In seismic analysis, the reservoir was modeled by added mass approach. Ghrib and Tinawi [13 and 14]

used the damage mechanics theory in static and seismic analysis of concrete gravity dams. It was found that the proposed numerical model can simulate the nonlinear behavior of two-dimensional concrete structures in static and dynamic conditions. In their study, the reservoir was modeled using added mass approach. Ghaemian and Ghobareh [15] developed a solution scheme to analyze concrete gravity dams under seismic loads. This method is called staggered method. The developed method was used in nonlinear seismic analysis of concrete dams in two-dimensional space successfully [16]. Guanglun et al. [17] used the smeared crack model developed in [10]. However, the model has re-meshing capability in the crack tip. Horii and Chen [18] presented a paper in which advantages and disadvantages of the smeared crack, damage mechanics and discrete crack approaches are discussed. In their work, an embedded crack element was developed to simulate the nonlinear behavior in dynamic loads.

In the present article, an anisotropic damage mechanics model has been used to analyze concrete gravity dams under static and dynamic loads. The effect of reservoir interaction has been accounted for rigorously using the staggered displacement method. The Pine Flat dam was analyzed using the proposed numerical algorithms and the effect of dam-reservoir interaction on the nonlinear response was considered in comparison with the results obtained when the added mass technique is used.

2 CONSTITUTIVE MODEL OF MASS CONCRETE

2.1 *Pre-softening stress-strain relationship*

The relationship of the stress and strain vectors at the pre-softening phase is given as:

$$\{\sigma\}=[D]\{\varepsilon\} \tag{1}$$

where $[D]$ is the elastic modulus matrix; $\{\sigma\}$ is the vector of stress components given as $(\sigma_{xx}\ \sigma_{yy}\ \sigma_{xy})^T$; and $\{\varepsilon\}$ is the vector of strain components including the corresponding three components of the strain. Assuming plane stress behavior at the pre-softening phase, the modulus matrix of $[D]$ is given as:

$$[D]=\frac{E}{(1-\upsilon^2)}\begin{bmatrix} 1 & \upsilon & 0 \\ \upsilon & 1 & 0 \\ 0 & 0 & \frac{1+\upsilon}{2} \end{bmatrix} \tag{2}$$

where E and v are Young's modulus and Poisson's ratio, respectively Generally, in nonlinear analysis the strain rate effect on Poisson's ratio and Young's modulus is neglected [11].

2.2 *Softening initiation criterion*

In the present study, the area under the stress-strain curve up to the peak stress (apparent tensile stress), is used as softening initiation index [11 and 16]. The crack initiates when uni-axial strain energy density, $\sigma_1\varepsilon_1/2$, is greater than U_0 which is a material parameter given as:

$$U_0=\int_0^{\varepsilon_i}\sigma d\varepsilon=\frac{\sigma_i\varepsilon_i}{2} \tag{3}$$

where σ_i and ε_i are apparent tensile strength and its corresponding strain, respectively.

Under dynamic loads, the material parameter U_0 is multiplied by a dynamic magnification factor DMF_e as following:

$$U_0' = \frac{\sigma_i'^2}{E} = DMF_e^2 U_0 \tag{4}$$

where the primed parameters correspond to dynamic loads. The dynamic magnification factor DMF_e is applied on the apparent tensile strength.

2.3 *Stress-strain relationship in softening phase*

In this article, the secant modulus stiffness (SMS) approach was used for stiffness formulation in which the constitutive relation is defined in terms of total stresses and strains. Based on the energy equivalence principle and neglecting the coupling between the principal fracture modes, the following modulus matrix is obtained [13]:

$$[D] = \frac{E}{1-\upsilon^2}\begin{bmatrix} (1-d_1)^2 & (1-d_1)(1-d_2) & 0 \\ (1-d_1)(1-d_2) & (1-d_2)^2 & 0 \\ 0 & 0 & \dfrac{(1-\upsilon)(1-d_1)^2(1-d_2)^2}{(1-d_1)^2+(1-d_2)^2} \end{bmatrix} \tag{5}$$

where d_1 and d_2 are damage variables in local principal directions. Satisfying the principle of energy equivalence and assuming linear stress-strain curve in the post-peak phase, d_i is given as:

$$d_i = 1 - \sqrt{\frac{\varepsilon_0}{\varepsilon_i} - \left(\frac{\varepsilon_i - \varepsilon_0}{\varepsilon_f - \varepsilon_0}\right)\cdot\frac{\varepsilon_0}{\varepsilon_i}} \tag{6}$$

where ε_0 and ε_f are the strain corresponding to crack initiation and no resistance strain, respectively and ε_i is the principal strain of the element in the considered direction.

The constitutive matrix given in eqn. (5) in global coordinate system can be obtained conventionally as following:

$$[D]_S = [T]^T [D]_d [T] \tag{7}$$

where $[T]$ is the strain transformation matrix in two-dimensional space. In the proposed formulation, co-axial rotating crack model has been used to simulate the behavior of the cracked element. Satisfying the fracture energy conservation principle in static and dynamic conditions, the no resistance strain is defined as:

$$\varepsilon_f = \frac{2G_f}{\sigma_0 h_c} \text{ and } \varepsilon_f' = \frac{2G_f'}{\sigma_0' h_c} \tag{8}$$

where h_c is the characteristic dimension of the element and assumed equal to the square root of the element's area. The primed quantities show the dynamic constitutive parameters. The strain-rate sensitivity of the specific fracture energy is taken into account through a dynamic magnification factor DMF_f as follows:

$$G_f' = DMF_f G_f \tag{9}$$

It is worth to note that DMF_f is mainly contributed by DMF_e and is assumed equal to it.

2.4 *Crack closing/reopening criterion*

In the present article, the crack opening and closing criterion is based on the principal strains. It has been shown that under the cyclic loads there is residual strain in the closed element. Based on this concept, the total strain can be decomposed into two components of elastic and residual strain given as [13]:

$$\varepsilon=\varepsilon^{e}+\varepsilon^{in}=\varepsilon^{e}+\lambda\varepsilon_{max} \tag{10}$$

where ε_{max} is the maximum principal strain which the element has reached during the previous cycles and λ is the ratio between the residual strain in the closed element and the maximum principal strain ε_{max} and is given as 0.2 usually. The element is closed when the considered principal strain reached in the current state is less that $\lambda\varepsilon_{max}$ and it is reopened when the principal strain is greater that this value.

2.5 *Finite element implementation of the proposed model*

In the present article, plane stress 4-node iso-parametric element has been used in finite element implementation. The stiffness matrix and all of the other related components have been computed based on 2*2 Gaussian integration points. All of the related algorithms and state determination of elements are based on the average response of the element which is computed with averaging the computed strains within Gaussian points. The staggered displacement method introduced in [15] was used to solve the coupled equilibrium equations of the structure and the reservoir.

3 NUMERICAL RESULTS

The tallest monolith of the Pine Flat dam with the height of 122m was selected for evaluation of the proposed model. Modulus of elasticity, unit weight and Poisson's ratio of the concrete were taken as 27850MPa, 2400Kg/m^3 and 0.2, respectively. The tensile strength of the concrete was assumed 2.7MPa which is about 10% of the compressive strength. Fracture energy of the concrete was 150N/m. A dynamic magnification factor of 1.2 was taken for both of the tensile strength and the specific fracture energy. The stiffness proportional damping equivalent to 5% damping in the first mode of the dam structure with empty reservoir was applied on the system. Elasto-brittle damping mechanism was used in dynamic loading.

The two approaches were used to consider hydrodynamic pressure effect. In the first approach, the Westergaard's added mass technique was used and in the second model, hydrodynamic pressure effect were modeled rigorously using the staggered displacement method. The far-end truncated boundary condition was located at a distance of 5 times of the height of the dam, from upstream face. The depth of the reservoir was chosen 116.88m and the pressure wave velocity was taken as 1438.66m/s. The finite element model of the dam body included 1984 4-node iso-parametric plane stress elements with 2101 nodes and the reservoir had 2065 4-node iso-parametric fluid elements with 2160 nodes. Figure 1 shows the dam-reservoir system used in the present article.

The first 10 sec of the horizontal S69E component of the 21 July 1952 Taft Lincoln earthquake, Kern County site record shown in Figure 2 was used as upstream-downstream excitation of the system in which the peak ground acceleration is 0.179g. This component was scaled by the factor of 1.5 in order to develop crack profiles in the dynamic analysis. The time step was taken as 0.001s.

Figure 3 compares the time history of the crest displacement in upstream-downstream direction in the two considered cases. The crest displacements from the two approaches are in close agreement before cracks are formed at the top part of the dam body. After initiation of the crack at the neck of the dam, the responses resulted from the two approaches are different. Comparing with the results reported in [16], the proposed numerical algorithms are more stable during closing/reopening of cracked elements.

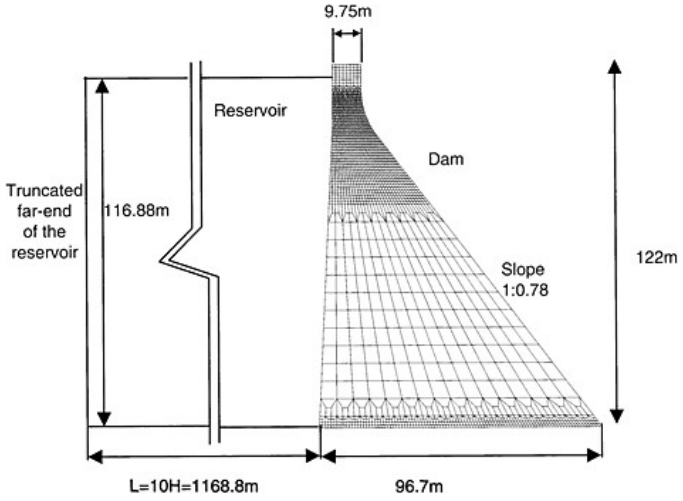

Figure 1. Considered dam-reservoir system.

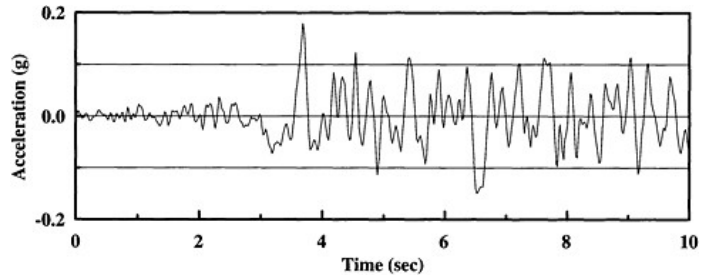

Figure 2. S69E component of the 21 July 1952 Taft Lincoln earthquake, upstream-downstream excitation.

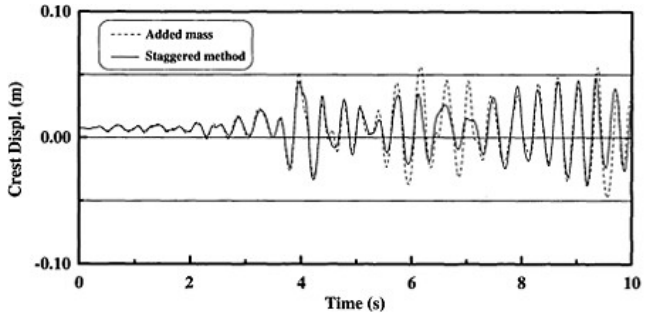

Figure 3. Crest displacement in upstream-downstream direction, comparing the two cases of including dam-reservoir interaction and added mass approach.

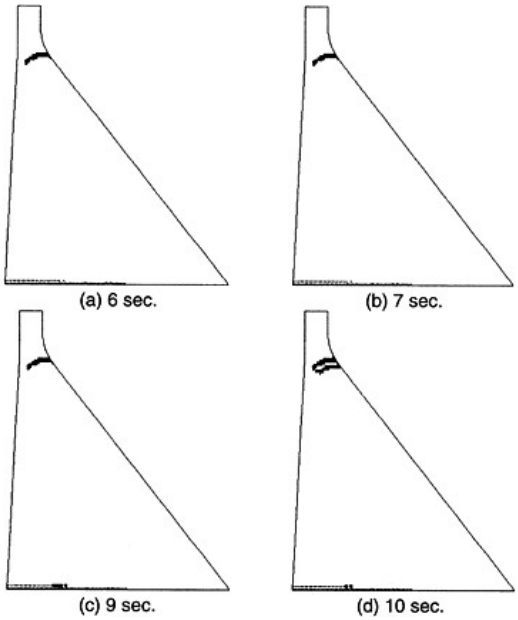

Figure 4. Crack profiles of the Pine Flat dam including dam-reservoir interaction.

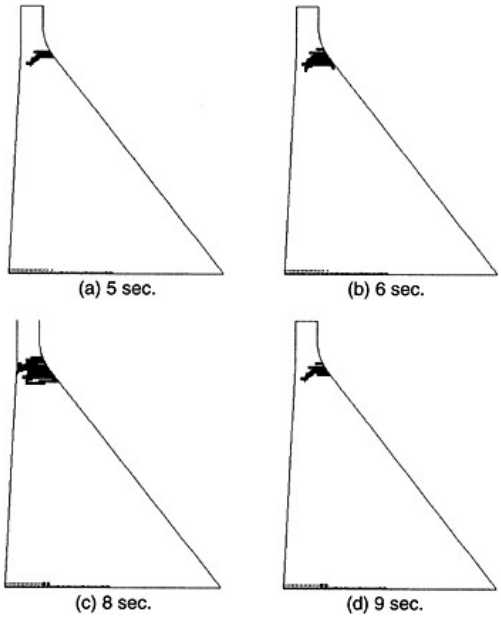

Figure 5. Crack profiles of the Pine Flat dam, added mass approach.

The cracked configuration of the dam body was shown in Figures 4 and 5 at different times for the two cases of dam-reservoir interaction (staggered method) and the added mass approach. Clearly, including the dam-reservoir interaction yields different crack pattern than in the case of the added mass approach.

As shown in Figures 4 and 5, when the reservoir interaction effect is modeled by added mass technique, the resulted crack profiles are much more diffused. The resulted crack profiles when including dam-reservoir interaction are localized as shown in Figure 4 and at the end of the time history, at the upper part of the dam body, there is only a crack profile which includes two branches. It is worth to remind that the elasto-brittle damping mechanism was applied in all of the analyses in the present article. This damping mechanism can lead to localized crack profiles due to omitting of damping of the cracked elements.

4 CONCLUSIONS

The nonlinear seismic fracture analysis of a typical concrete gravity dam based on two-dimensional anisotropic damage mechanics model was conducted to investigate the performance of the proposed numerical algorithms under dynamic loads. It was found that the proposed model gives more localized crack profile when includes dam-reservoir interaction in comparison with the case of added mass approach. Generally, the crack pattern predicted when the dam-reservoir interaction is included is different with that obtained from added mass and in comparison with the other investigations, the proposed algorithm is more stable and leads to more localized and reliable dynamic responses.

REFERENCES

[1] Chopra, A.K. and Chakrabarti, P., *The earthquake experience at Koyna dam and stresses in concrete gravity dams,* Earthquake Engineering & Structural Dynamics, 1972, 1, 151–164.
[2] Pal N., *Nonlinear earthquake response of concrete gravity dams,* Report No. EERC 74–14, Earthquake Engineering Research Center, University of California, Berkeley, 1974.
[3] Pal, N., *Seismic cracking of concrete gravity dams,* Journal of the Structural Division, ASCE, 1976, 102(9), 1827–1844.
[4] Skrikemd, P.E. and Bachmann, H., *Discrete crack modeling for dynamically loaded un-reinforced concrete structures,* Earthquake Engineering & Structural Dynamics, 1986, 14, 297–315.
[5] Webf, D.H., Feltrin, G. and Bachmann, H., *Influence of time domain dam-reservoir interaction on cracking of concrete gravity dams,* Earthquake Engineering & Structural Dynamics, 1993, 22, 573–582.
[6] El-Aidi, B. and Hall, J.F., *Non-linear earthquake response of concrete gravity dams, part 1: modeling,* Earthquake Engineering and Structural Dynamics, 1989, 18, 837–851.
[7] El-Aidi, B. and Hall, J.F., *Non-linear earthquake response of concrete gravity dams, part 2: behavior,* Earthquake Engineering and Structural Dynamics, 1989, 18, 853–865.
[8] Vargas-Loli, L. and Fenves, G., *Effects of concrete cracking on the earthquake response of gravity dams,* Earthquake Engineering & Structural Dynamics, 1989, 18, 575–592.
[9] Feltrin, G., Wepf, D. and Bachmann, H., *Seismic cracking of concrete gravity dams,* Dam Engineering, 1990, 1(4), 279–289.
[10] Bhattacharjee, S.S. and Leger, P., *Application of NLFM Models to Predict Cracking in Concrete Gravity Dams,* Journal of Structural Engineering, ASCE, 1994, 120(4), 1255–1271.
[11] Bhattacharjee, S.S. and Leger, P., *Seismic cracking and energy dissipation in concrete gravity dams,* Earthquake Engineering & Structural Dynamics, 1993, 22, 991–1007.
[12] Bhattacharjee, S.S. and Leger, P., *Fracture response of gravity dams due to rise of reservoir elevation,* Journal of Structural Engineering, ASCE, 1995, 121(9), 1298–1305.
[13] Ghrib, F. and Tinawi, R., *Nonlinear behavior of concrete dams using damage mechanics,* Journal of Engineering Mechanics, ASCE, 1995, 121(4), 513–526.
[14] Ghrib, F. and Tinawi, R., *An application of damage mechanics for seismic analysis of concrete gravity dams,* Earthquake Engineering & Structural Dynamics, 1995, 24, 157–173.

[15] Ghaemian, M. and Ghobarah, A., *Staggered solution schemes for dam-reservoir interaction,* Journal of Fluids and Structures, 1998, 12, 933–948.
[16] Ghaemian, M. and Ghobarah, A., *Non-linear seismic response of concrete gravity dams with damreservoir interaction,* Journal of Engineering Structures, 1999, 21, 306–315.
[17] Guanglun, W., Pekau, O.A., Chuhan, Z. and Shaomin, W., *Seismic fracture analysis of concrete gravity dams based on nonlinear fracture mechanics,* Engineering Fracture Mechanics, 2000, 65, 67–87.
[18] Horii, H. and Chen, S.C., *Computational fracture analysis of concrete gravity dams by crack embedded elements-towards an engineering evaluation of seismic safety,* Engineering Fracture Mechanics, 2003, 70, 1029–1045.

New Developments in Dam Engineering—Wieland, Ren & Tan (eds),

Shahid Rajaee dam and its effects on water resources of Tajan valley

J.Najihammodi & H.Khadir
PWIT, Iran

ABSTRACT: Shahid Rajaee is a double curved arch dam with a reservoir of 139MM cubic meter that was constructed in 1996 at a distance of 40 kilometer south of Sary City on Dodanke River (one of Tajan River Branches). This dam was built to control flood and to supply enough water for the valley (for drinking, industry and agriculture) and to control its distribution over the year in a proper way. The dam is actually fulfilling its aims in preventing seasonal floods, generating energy and maintaining a suitable quantity of water with a relatively high quality of both surface and ground waters for all the time of the year. Moreover, the ground water potential and quality are increasing markably because of the surface water penetration in to ground. As a result, the agriculture production of the valley (especially the rice) is increasing every day making at present time a pleasant environmental valley.

1 INTRODUCTION

Tajan Valley is located in north Iran in Mazandaran District (between Naka River at east and Syaroud River at west), which is located south of the Caspian Sea. The valley and surrounding mountains are evergreen with a relatively high rainfall of about 700mm annually that brings a continuous flowing river into the valley. This district is very suitable for agriculture and can be said to be one of the main agricultural producing area in Iran (Figure 1).

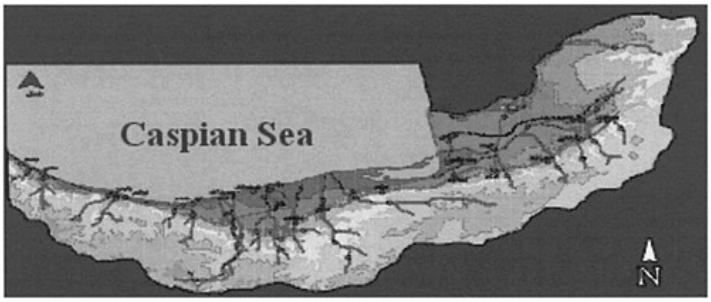

Figure 1. Mazandaran valley in north Iran.

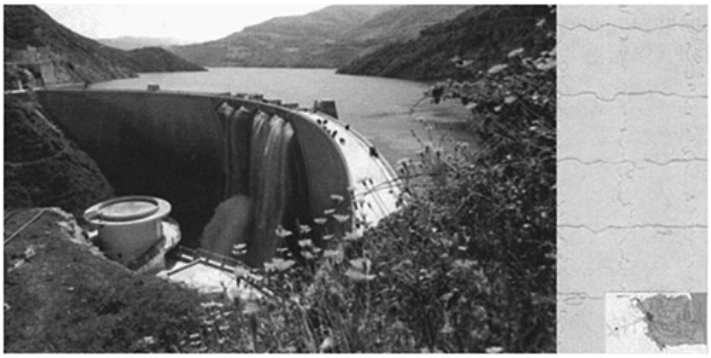

Figure 2. Shahid Rajaee Dam in Mazandaran, Iran.

2. SHAHID RAJAAI'S DAM

2.1 *Location*

Shahid Rajai's Dam is located on Dodanke River about 40 kilometer south of Sary City at the mountain basis of the Alborz, south of the valley in Mazandaran District.

2.2 *Dam history and goals*

Eleskender Gieb Engineering Company studied this project in the 1970's, thenafter two other companies, namely Mahab Khodss and Waner Kopprojet proposed a final phase of the project in 1985 as a concrete dam, which was built later on in 1996.

This dam was constructed to control floods and to supply enough water (for drinking, industry and agriculture) for the valley. It was also sought to control the water flow and its distribution over the year in the valley.

2.3 *Dam description*

This is two curves concrete dam, which is located about 490 meter above sea level with a total useful reservoir volume of about 139MM cubic meter. The dam crest length is 427 meter with a seven meter width (Figure 2).

3 VALLEY'S ENVIRONMENT AND GEOENVIRONMENT

3.1 *Valley's environment*

The evergreen environment of the valley and surrounding are due to the continuous rainfalls and a good soil of the valley. By studying the water properties in two points above and below the dam (near the river deposition into Caspian Sea), the effect of which upon the ecology of the valley and thereafter upon its environmental conditions can be verified. In the above dam where it is mountains, the rainfalls and therefore the water wash up the mountains down into the dam reservoir. Here, the water is relatively very good. Moreover, at the northern part of Tajan River about 100 meters south of the Caspian Sea where the river flow is a minimum and it has maximum contaminations, the

water quality, here, is decreasing but it does not reach the critical point that affect the ecology of the valley. Moreover, the existence of sea fishes and other sea livings in a greater number in this area to lay their eggs prod cast good news of the environment.

However, the water quantity as well as the quality of the river and ground waters is improved greatly as compared before constructing the dam due to a continuous and controlled water flow. It seems also that the sea livings have already adapted themselves for the new ecosystem of the area after constructing the dam. All in all, the environment so far is improving greatly.

3.2 *Valley's geoenvironment*

Activities such as mining, drilling, building, dam building planting and many others can affect the geoenvironment of any place. Therefore, by building Shahid Rajai's Dam the geoenvironment of the area is changed where the dam and its reservoir caused a compaction of soil underneath. Drilling a great number of wells in the valley, the soil under the reservoir being always fully saturated with water and the water levels in the aquifers being rising to reach the surface, all of which will have a negative effect upon planting process. Therefore, it is advisable to maintain the geo-environmental engineering of the area to safe guard it from future damage.

4 WATER RESOURCES

The valley is dominated by a local sea humid wind (i.e. normally hot in Summer and moderate in Winter) with an average rainfalls of 700mm (and higher in the mountains), which is mainly under the effect of the continental weather.

There are seven weather stations in the valley that record rainfalls, temperatures and humidity all the year around. The average temperature of the valley is 16.5 Centigrade, while the humidity is relatively high (80%).

4.1 *Surface water*

The area under this study is located between Nakaroud at the East and Syaroud at the West.

Shahid Rajai's Dam is located on Tajan River that is flowing in between the above mentioned rivers, whose water comes from Alborz Mountains. So Tajan River and Shahid Rajai's Dam Reservoir are the main surface water resources for Tajan Valley; and therefore all the three rivers enrich the valley and its aquifers with water. Moreover, Tajan River flows into about 4000 square kilometers before ending into Caspian Sea.

The surface water quality in the upper and middle stream of the valley is good (EC between 650 and 690 micro mhos per square centimeter); while this becomes more near the sea, but it still good for irrigation (of rice).

The dam reservoir increases the available surface water resources to reach up to 300MM cubic meter annually.

4.2 *Ground water*

The sediments of the aquifers in the valley are mainly alluvium. A surface unconfined aquifer at the south of the valley with an average thickness of about 20 meter and a deeper confined aquifer at the middle of the valley, which are fed by the rainfalls and the rivers.

There are 18000 wells, 31 springs and 33 canals in the valley to produce about 240MM cubic meter annually (i.e. 40% of the amount of water needed by the agriculture).

The quality of the ground water is improved due to the construction of the dam to reach an average EC of about 1200 micro mhos per square centimeter.

5 CONCLUSIONS

1. The quality and quantity of the surface and ground waters are improved specially after building the dam. However, it was advised to check the water intensively in Summer time to allocate the exact amount of poisons from agricultural fertilizers that may in due time have negative effects upon the soil and thereafter, the environment and/or the geoenvironment of the valley.
2. It was advisable to check the surface water, likewise the ground water for microbiological contamination for the area where native fertilizer is used.
3. It is suggested that the agriculture people do wash their lands from contamination elements at the time when Tajan River Flow is maximum (in March and April of every year).
4. Since ground water level is rising, it is suggested that more water from the surface aquifer produced to bring its level down.
5. It is suggested to use more sophisticated management software to control the quality of the water and to prod cast any anomalies in water quality (surface and ground), since this area and its rice products are very sensitive to salinity.
6. Shahid Rajai's Dam helped in preventing floods and generating power and also in maintaining suitable and controllable of enough amount of water for the valley even so there is drought time, and therefore agriculture products (specially the rice) are increasing continuously.

REFERENCES

[1] Balance, R. (1996), *Studying the Monitoring of Water Quality,* MOE, Tehran, Iran.
[2] Lar Nespark (1998), *Quarterly Monitoring Report,* Irrigation Improvement Project, Ministry of Energy (MOE), Tehran, Iran.
[3] Justin and Courtney (1986), *Reconnaissance Report on Five River Basins in the Main Doab Plains Area,* MOE, Tehran, Iran.
[4] Khadir, H. (2002), *Effects of Shahid Rajaee's Dam on Water Resources of Tajan Valley,* MS-Thesis, PWIT, Tehran, Iran.
[5] Kazarab (1990), *Studying the Environment of Tajan Valley,* Kazarab Interior Report, MOE, Tehran, Iran.
[6] Mahab Khodss (1986), *Studying the Required Water for Tajan Valley,* Mahab Khodss Interior Report, MOE, Tehran, Iran.
[7] Mahab Khodss and MMP (1992), *Tajan River Operational Study,* Proposal for Consultancy, Interior Report, MOE, Tehran, Iran.
[8] Tanji, K. (...), *Agricultural Salinity Assessment to Management,* Ministry of Agriculture, Tehran, Iran.

New Developments in Dam Engineering—Wieland, Ren & Tan (eds),

Improvement of impervious asphalt mixture for high ductility against earthquake excitation

Y.Nakamura
Aico Co., Ltd, Japan

T.Okumura, K.Narita & Y.Ohne
Aichi Institute of Technology, Japan

ABSTRACT: In the design and construction of embankment dam with an asphalt facing impervious zone, it is important to confirm that the facing material of asphalt mixture can adequately follow static and dynamic deformation of main embankment body. It is known that deformability of asphalt mixture shows a considerable decrease under a low temperature condition in winter and under a high loading rate of earthquake excitation. This paper concerns an improvement of asphalt mixture as a flexible facing material with high ductility against earthquake loading under low temperature conditions. Series of cyclic loading tests were carried out to investigate the influence of temperature and cyclic loading conditions on the dynamic deformation characteristics of the newly developed asphalt mixture, and the results were compared with those of usual straight asphalt mixtures. It is revealed that the critical dynamic strain of the improved asphalt mixture can be six to nine times as large as that of straight asphalt mixture.

1 INTRODUCTION

An earth dam about 25m high with asphalt facing impervious zone was attacked by an earthquake with a medium intensity to cause severe damages on the facing, where many surface cracks appeared in the whole area of the project, especially near the crest of the dam [1]. It is inferred that dynamic deformation induced by the earthquake exceeded an allowable strain of asphalt mixture of the facing material. Asphalt mixtures that have been used for facing materials are in general impervious, and to have high flexibility to adapt a large deformation without cracking. It has well been known, on the other hand, that cracking damages are ready to develop under the conditions of low temperature in winter and of high loading rate of cyclic earthquake excitation.

A newly developed asphalt mixture, having high ductility against earthquake excitation, is introduced in the present paper. The mixture, which is called by "Superflex-phalt" in this paper, has high flexibility, stress relaxation effects, and high ductility under the conditions of low temperature and high loading rate of cyclic excitation. It, on the other hand, has much toughness to prevent flow under a high temperature. Some laboratory physical and mechanical tests were carried out on the new asphalt mixture to examine those advantageous properties mentioned above by comparing the results with those of the straight asphalt one usually used for facing materials.

Binder properties were first examined on such items as penetration, softening point, viscosity and bending strain. Creep characteristics under a low temperature were also evaluated by Bending Beam Rheometer (BBR) test. The results revealed that the binder properties of Superflex-phalt are improved by several times as compared with those of the straight asphalt.

Table 1. Basic properties of binders.

Properties	Unit	Straight Asphalt (60/80)	Superflex-phalt
Penetration	1/10mm	69	187
Softening point	°C	48	84
Viscosity (60°C)	Pa·sec	208	11,300
Bendingstrain(−10°C)	$(\times 10^{-3})$cm/cm	49	384

In order to investigate fundamental mechanical properties of the asphalt mixture, axial static tensile strength tests were conducted, and an elasto-plastic FEM analysis was made for the specimen by using the law of n-power hardening. The measured and calculated results were compared to investigate uniformity of stress and strain in the specimen, and some discussions were made on applicability and reliability of the testing procedure.

Series of cyclic loading test were then performed to investigate the influence of temperature and cyclic loading conditions on the dynamic deformation characteristics of the newly developed asphalt mixture, and the results were compared with those of the usual straight asphalt mixture. It was verified that the critical dynamic strain of the improved asphalt mixture can be six to nine times as large as that of straight asphalt one.

2 OUTLINE OF BINDER TEST

2.1 *Basic properties of the binder*

Table 1 shows the basic properties of binders of straight asphalt and Superflex-phalt, respectively. The testing procedures of the respective measured items were referred to the Handbook of Pavement Test Method [2]. Superflex-phalt indicated larger values for penetration and bending strain (−10°C) even when softening point and viscosity at 60°C become equally high compared with straight asphalt. This means high flexibility under low temperature and much less deformability due to flow.

2.2 *Binder properties under low temperature*

The creep characteristics under a low temperature of asphalt binders were evaluated by BBR test. It is considered that the creep characteristic under a low temperature is related to crack generation. In this test, bending creep stiffness (S-value), an index of hardness, and the m-value, an index of deformation rate, are determined. The S-value expresses deformation resistance and is calculated as a function of time from the relationship between load and deflection. The m-value is calculated from gradient of the curve of the S-value versus time relation plotted in the logarithmic scale. Therefore the smaller the S-value the smaller the stress produced at shrinkage, and the larger the m-value the higher the capacity of relieving the stress produced.

Figure 1 shows variations of the S-value and the m-value with temperature at a loading time of 60 seconds. It is seen in these figures that the S-value increases and the m-value decreases as the temperature decreases in both binders. If the relation curve of the S-value versus temperature of the Superflex-phalt is shifted to the high temperature side by approximately 10°C, the curve will almost lie on that of straight asphalt. It is considered that Superflex-phalt has similar properties as straight asphalt in lower temperature regions. The m-value also shows a similar tendency as that of the S-value. It is readily recognized by comparing the m-value and the S-value, respectively, at the same temperature that binder properties of Superflex-phalt is improved several times as those of straight asphalt.

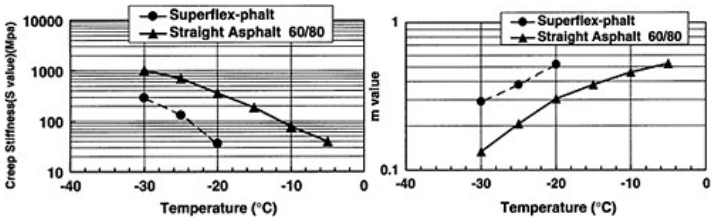

Figure 1. Results of BBR test.

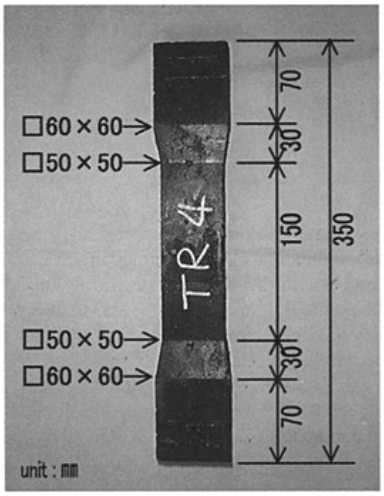

Figure 2. Shape of specimen.

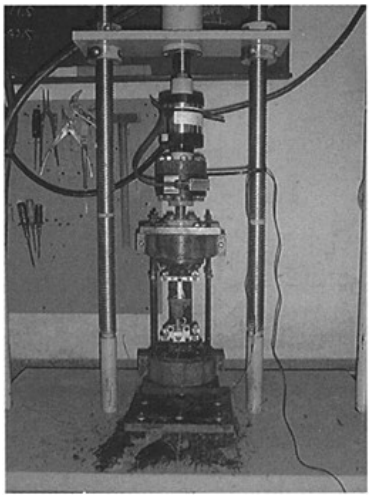

Figure 3. Test apparatus.

3 OUTLINE OF MECHANICAL TESTS

3.1 *Test apparatus and procedures*

The specimen is prepared in the shape of dumbbell as shown in Fig. 2 to avoid stress concentration at the loading ends. Samples measured and adjusted to have standard density are uniformly laid in 2 layers, and compacted with a small tamper. The specimen is attached at both ends to a fixed frame by using sulfur mortar, and is cured in 24 hours under the temperature of 0°C in a curing tank. The loading system is shown in Fig. 3, where a specimen is loaded in the vertical direction, statically in tension and/or cyclic by sine wave. Both loadings are controlled by means of an electrohydraulic servo system. The load is measured through a load cell of a capacity of 29.4kN and the axial displacement of the specimen is measured by a non-contact deformation gauge having a resolution of 0.001mm, which is mounted on the side face in the middle part of the specimen.

3.2 *Materials and test conditions*

In this series of mechanical tests, two different types of asphalt (binder) are compared; straight asphalt (60/80) which is used as a usual binder of the asphalt mixture and Superflex-phalt developed for

Table 2. Blending of mixtures.

		Blending ratio of aggregate (wt %)				
Asphalt content (%)	Cellulose fiber (%)	Grade 6	Grade 7	Coarse sand	Fine sand	Stone powder
8.5	0.15	24.0	16.5	37.5	8.0	14.0

Note. ARBOCEL ZZ 8/1 is used as cellulose fiber. The value of its content is represented by the ratio to the total weight of aggregates in percent.

the purpose of improving deformation performance under a low temperature. The blending of the mixtures is the same for these binders, as shown in Table 2.

The axial tensile strength test is conducted with a constant strain rate of approximately 10^{-4} to 10^{-1} (1/sec) under the temperature of 0°C. The cyclic loading tests are done by strain control in sine wave, by changing the loading rate of frequency in three different levels as 1Hz, 2Hz and 4Hz. The test temperature is set also in three levels as 4°C, 0°C and −5°C.

4 TEST RESULTS AND DISCUSSIONS

4.1 *Axial tensile test*

Figure 4 shows stress-strain curves of three specimens of Superflex-phalt mixture tested at a strain rate of $\bar{\sigma} = c(a + \bar{\varepsilon}^p)^n$. An elasto-plasticity analysis is then made by introducing this stress-strain behavior and applying an isotropic hardening rule using the von Mises condition as a yield function. The results are compared in Fig. 5, where the test result of No. 3 specimen is drawn by a solid line and the computed values are represented by open circles. It is recognized in the figure that the measured and the computed values are in a fairly good agreement and reproduction of stress-strain relationship by the presented analysis procedure is successful.

Figure 7(b) shows contour lines of equal normal stress in the axial direction (σ_y) in the specimen and the values of the normal strain (ε_y) along the center line (x=30mm) of the specimen, at the axial tensile strain of the specimen of ε_y=6.16×10^{-3}. The value of the normal strain (ε_y) is calculated by dividing the relative displacement between neighboring nodal points on the center line by the length of respective sections. It is well recognized that uniformity of both stress and strain distributions is maintained in approximately 80% of the section of minimum width. Distribution of principal stresses is presented in Fig. 7(c) for the same stress level. It is seen that principal tensile stresses distributed in the section of minimum width coincide well with the applied axial tensile stress and another principal stresses in the orthogonal direction are almost equal to zero.

While the axial tensile test is most simple in mechanism as similar as the unconfined compression test, it is believed from a technical point of view that the method may be the most difficult among all tensile tests, because treatment at the loading ends of the specimen gives severe influence on the test result. In the tensile test presented here, it was confirmed that uniformity of stress and strain is maintained in approximately 80% of the middle reduced section, although this applies only under limited test conditions.

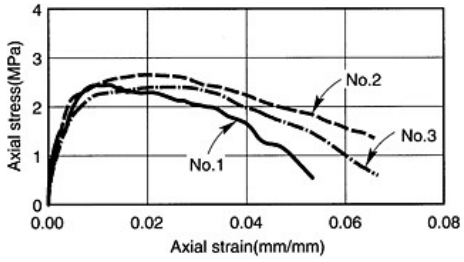

Figure 4. Stress-strain curves (Superflex-phalt).

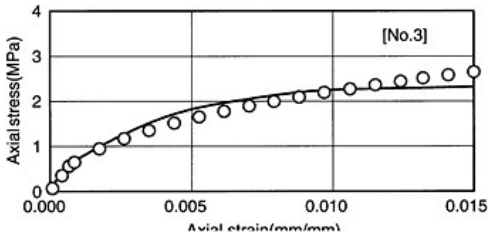

Figure 5. Comparison of test and analysis.

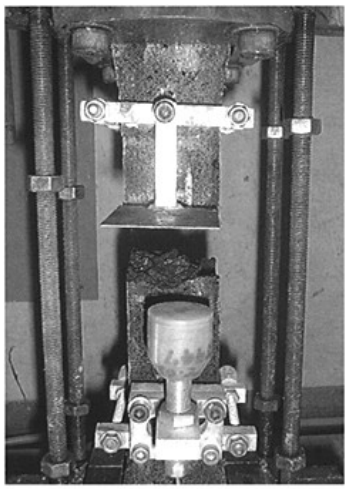

Figure 6. Broken specimen.

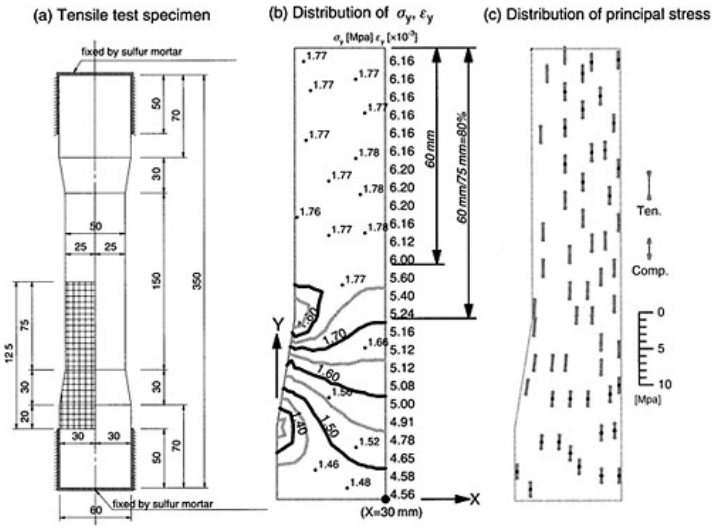

Figure 7. Results of FEM analysis.

Stress-strain curves obtained in the tests at the strain rate of 10^{-2} (1/sec) under the temperature of 0°C are compared in Fig. 8, where those of the straight asphalt mixture are drawn by solid lines and those of the Superflex-phalt mixture by broken lines. Stress-strain relations of the straight asphalt mixture show considerably large initial tangent modulus of elasticity and brittle failure accompanied by abrupt decrease of stress after the peak tensile strength. Those relations of the Superflex-phalt mixture, on the other hand, show apparent non-linear characteristics and comparatively low modulus of deformation in the small strain range and little stress drop in the range up to the strain of about 0.04. It is thus concluded that the Superflex-phalt mixture is much more ductile than the straight asphalt one under a low temperature and high loading rate of earthquake excitation.

Figure 9 shows a relation between the strain rate in loading test and the axial tensile strain at failure. It is noticed in the figure that the failure strain of the Superflex-phalt mixture is much improved, having high failure strain of more than 10 times as compared with the straight asphalt one under various strain rate of loading.

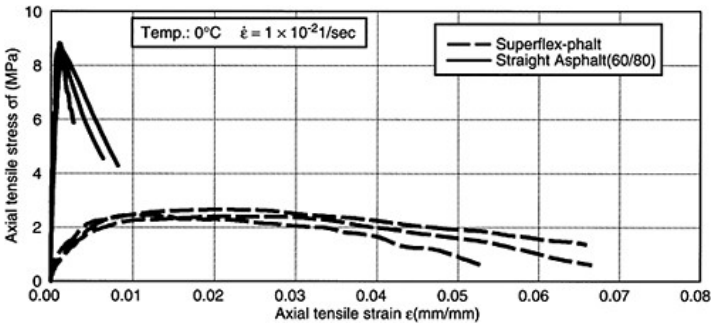

Figure 8. Comparison of stress-strain behavior of superflex-phalt and straight asphalt mixtures.

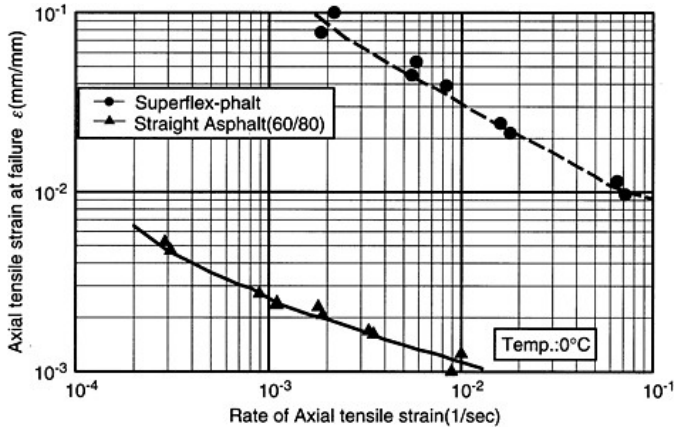

Figure 9. Relation of axial tensile strain at failure to strain rate of loading.

4.2 *Cyclic loading test*

(1) *Determination of dynamic deformation parameters*

From the measurement of the axial load (P) and the axial displacement (d) of a specimen, the axial stress and strain (σ, ε), shear stress and strain (τ, γ), Young's modulus (E), and the modulus of rigidity (G) are determined, respectively, in the followings, where (A) and (H) are the sectional area and the height of the specimen, and Poisson's ratio *(ν)* is assumed to be 0.5 in the calculation.

$$\sigma = \frac{P}{A}, \quad \tau = \frac{\sigma}{2}, \quad \varepsilon = \frac{d}{H}, \quad \gamma = (1+\nu)\varepsilon, \quad E = \frac{\sigma}{\varepsilon}, \quad G = \frac{\tau}{\gamma} = \frac{E}{2(1+\nu)} \tag{1}$$

Another deformation parameter, the damping coefficient h, is evaluated from τ~γ cyclic hysteresis loop as follows, where ΔW is the plastic shear strain energy consumed during one cycle of loading, being expressed by an area of τ~γ loop, and W is the strain energy corresponding to the shear strain amplitude γ_a as $W=G\gamma_a^2/2$

$$h = \frac{1}{2\pi} \cdot \frac{\Delta W}{W} \tag{2}$$

(2) *τ~ γ relation*

Figure 10 shows a τ~γ relationship of the Superflex-phalt mixture at the strain level of $\gamma \fallingdotseq 4 \times 10^{-3}$. It is recognized in the figure that the hysteresis curves are to be a visco-elastic ellipse in shape, and the value of G becomes greater and to be more dependent on frequency as frequency increases. τ~γ curves in Fig. 10 are re-drawn in Fig. 11 by normalizing shear stress and strain with their respective amplitudes. It is clearly seen that the normalized hysteresis loops are almost the same in shape and size regardless of frequency adopted, and it is therefore inferred that the asphalt mixtures have viscous damping characteristics which are not easily affected by frequency.

(3) *G, h~γ relation*

Figure 12 and Fig. 13 show G, h~γ relations of the Superflex-phalt mixture and the straight asphalt mixture, respectively, obtained under the temperature of 4°C. It is commonly seen in both mixtures that the value of G increases and conversely the value of h decreases as the frequency of loading increases. It should be noted here that the value of G has a very great difference in these two mixtures, the order of the difference being more than 10 times. For example, at $\gamma \fallingdotseq 1 \times 10^{-4}$,

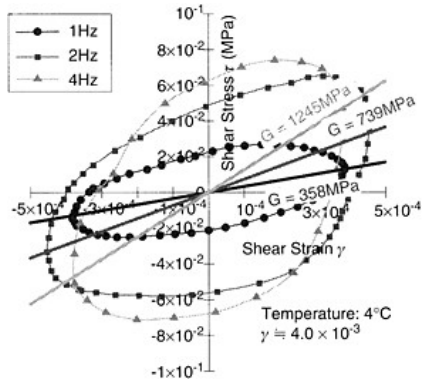

Figure 10. τ~γ relation (Superflex-phalt).

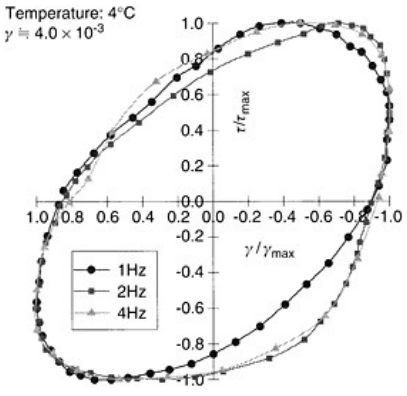

Figure 11. Normalized τ~γ relation (Superflex-phalt).

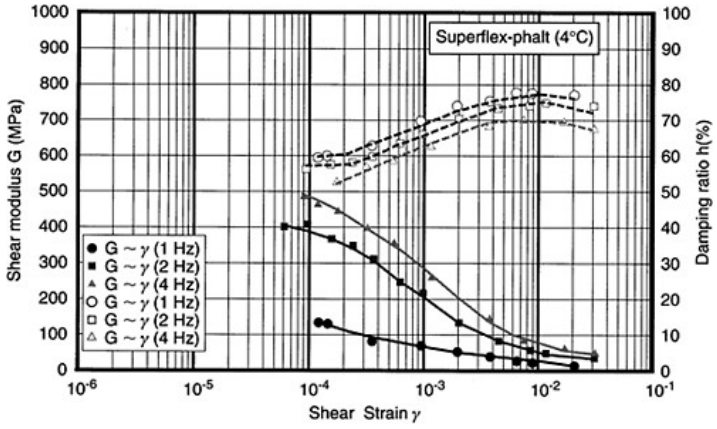

Figure 12. G, h~γ relation (Superflex-phalt mixture).

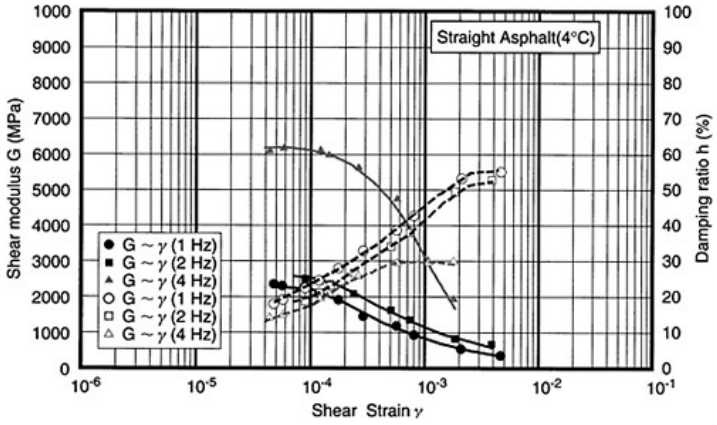

Figure 13. G, h~γ relation (straight asphalt mixture).

the Superflex-phalt mixture has G=150~500MPa and the straight asphalt one has G= 2,500~6,000MPa, the difference being about 10 to 20 times. The damping coefficient h has also a great difference in two mixtures, showing h=50~60% and h=20~30%, respectively, for the Superflex-phalt and the straight asphalt, and the difference being 2 to 2.5 times. As mentioned above, frequency dependency of h is not so remarkable.

(4) *Characteristics of skeleton curves*

Figure 14 shows τ~γ hysteresis loop of the two mixtures at the condition of temperature of 0°C and frequency of 1Hz; τ~γ loop and skeleton curve are drawn by solid line for the straight asphalt mixture and by broken line for the Superflex-phalt mixture. The skeleton curve is composed of

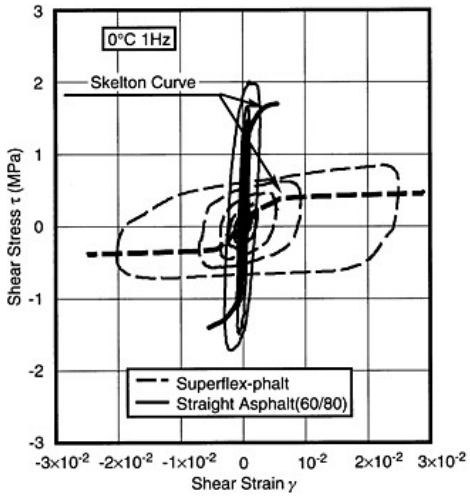

Figure 14. τ~γ Relation and skeleton curve.

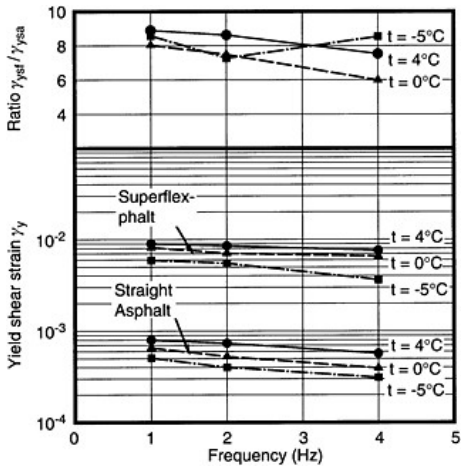

Figure 15. Dynamic yield strain.

successive points of stress and strain amplitude of cyclic loading. It is noticed that both skeleton curves are similar in shape to respective tensile stress-strain curves presented in Fig. 8. The skeleton curve of the straight asphalt mixture shows linearly elastic behavior having a high modulus of elasticity like a brittle material, and that of the Superflex-phalt mixture much more large plastic deformation over the yield point to failure like a ductile material. A turning point of strain on the skeleton curve, where tangential modulus of stress and strain changes abruptly, is defined as the yield shear strain (γ_y), which should be regarded as a symptom of failure. Fig. 15 shows relationships of the yield share strain to the rate of loading in frequency under three different temperatures. It is

seen that the value of γ_y decreases with the decrease in the temperature (t) and the increase in frequency (f). The ratio of γ_y values of the two mixtures, shown on the upper part in Fig. 15, reveals that the dynamic yield strain of the Superflex-phalt mixture can be 6 to 9 times as large as that of straight asphalt mixture.

5 CONCLUSIONS

Concluding remarks drawn from the present study are summarized in the following.

(1) The newly developed binder, Superflex-phalt, has much improved basic binder properties and showed different behavior as compared with the usual straight asphalt in BBR test.
(2) While the straight asphalt mixture is linearly elastic and behaves like a brittle material, the new mixture shows much more large plastic deformations over the yield point like a ductile material.
(3) The dynamic modulus of rigidity G of asphalt mixture is strongly dependent on frequency and the shear strain γ. The damping coefficient h is also dependent on the shear strain and shows viscous damping characteristics which are not easily affected by frequency.
(4) The dynamic deformation characteristics of the newly developed mixture takes considerably smaller value of G, 1/10 to 1/20 times as compared with the straight asphalt mixture, and larger value of h, 2 to 2.5 times, showing great improvement for deformation performance during cyclic excitation.

ACKNOWLEDGMENT

The authors wish to express their gratitude to Mr. Masaru Shimazaki for his kind assistance in experiments.

REFERENCES

[1] Ohne, Y. et al.: Earthquake Damage and its Remedial Measure for Earth Dam with an Asphalt Facing, *3rd U.S.-Japan Workshop on Advanced Research on Earthquake Engineering for Dams,* 2002.
[2] Japan road association: *Handbook of Pavement Tests Method,* Maruzen, 2002 (in Japanese).
[3] Inoue, T. et al.: *Solid mechanical and analysis of phase transformation,* Ohkawa Shuppan, 1995 (in Japanese).

New Developments in Dam Engineering—Wieland, Ren & Tan (eds),
© 2004 Taylor & Francis Group, London, ISBN 04 1536 240 7

Centrifuge tests on seepage behavior in embankment dam during rapid draw-down

K.Narita, T.Okumura, K.Kimura & Y.Ohne
Aichi Institute of Technology, Japan

ABSTRACT: Embankment dams for power generation and irrigation purposes have often experienced severe damages of slope failure due to a rapid draw-down of the reservoir water in seasons of full operation. This paper concerns seepage behavior in embankment dam during a rapid drawdown of the reservoir water. Distribution of the residual pore water pressure generated in the dam body and its influence on instability of the upstream slope are important points to be discussed. Centrifuge model tests were carried out on several model fills with different permeability to understand the mechanism of seepage flow during draw-down and variation with time of the residual pore water pressure accumulated in the embankment. Sliding failure of the upstream slope was also realized in the tests to discuss an appropriate procedure of evaluating the residual pore water pressure and its influence on slope stability. The test results and associated analysis of slope stability revealed that the residual pore water pressure generated during rapid draw-down directly leads to a serious damage of the upstream slope, and the procedure of pore water pressure estimation currently adopted in the design gives a safe side value as compared with the test results.

1 INTRODUCTION

Embankment dams for power generation and irrigation purposes have often experienced severe damages of slope failure due to a rapid draw-down of the reservoir water in seasons of full operation. This is principally caused by the residual pore water pressure generated in the fill during drawdown and also by the loss of confining effect of the reservoir hydrostatic water pressure. The drainage rate of seepage water from the upstream slope and the decreasing rate of the reservoir water level are then considered to be correlating influential factors.

Behavior of seepage flow and pore water pressure in embankments during a rapid raw-down has been studied through such analytical and experimental approaches as the finite difference method, the flow net diagram and the Hele-shaw model [1]. In recent studies, more refined approaches, the finite element analysis of saturated and unsaturated seepage, centrifuge model tests and data analysis of field observation [2], [3], have developed. Much consideration is still required, however, to understand the mechanism of this unsteady seepage flow, and to propose more precise practical method of estimation for the residual pore water pressure in the routine design of slope stability

This paper concerns seepage behavior in embankment dams during a rapid draw-down of the reservoir water. Distribution of the residual pore water pressure generated in the dam and its influence on instability of the upstream slope are important points to be discussed. Centrifuge model tests were carried out on several model fills with different permeability to understand the mechanism of seepage flow during draw-down and variation with time of the residual pore water pressure accumulated in the embankment. Sliding failure of the upstream slope was also realized in the tests to discuss an appropriate procedure of evaluating the residual pore water pressure and its influence on slope stability.

2 OUTLINE OF CENTRIFUGE TEST

2.1 *Test apparatus and procedures*

The major specifications of the AIT centrifuge apparatus are listed in Table 1, and setup for a centrifuge rapid draw-down test is illustrated in Figure 1. A model embankment dam is constructed in an aluminum container of W460×D200×H460mm in size, which has an acrylic fiber transparent plate on the front face. Water is supplied from the upper storage tank attached to the container to fill the upstream reservoir space. A draw-down of the reservoir water is then realized under constant centrifuge acceleration by pumping out of water from the lower drainage hole.

An earth dam model of 250mm in height, with a 20mm wide crest and slopes of 1:0.8 on both sides, is made on a steel circular spacer by compacting the fill material in 10 layers with 30mm in thickness to a required placement condition. In order to adapt to centrifuge test, the circular spacer is set to realize equal acceleration along the base of the dam, and the compacted fill is scraped down along both side slopes to form log-spiral curves. For pore water pressure measurement, total eight small transducers are set in the fill in three different heights, as shown by solid circles in Figure 1. A vertical drain of crushed sand is made on the downstream side, and a clayey soil is filled in spaces between the container wall and the model dam to prevent water flow from the reservoir.

After making the model dam, a pore water pressure transducer is set on the circular spacer on the upstream side to measure the water level of the reservoir. A water tank is set on the upper frame of the container, which supplies water in the reservoir. The amount of water supply is controlled by opening and closing the bulb attached to the tank through air pressure. The reservoir water is drained from the lower hole to realize draw-down operation, and the water is again supplied to the upper storage tank through a diaphragm pump. In order to make water supply and draw-down operations easier, the reservoir capacity is reduced by setting many wooden boards in the reservoir space.

In this series of draw-down test, centrifuge acceleration of 30G is applied to the 250mm high model dams, and draw-down of the reservoir water is realized in several different conditions from the target water level of 200mm (±). These correspond to the dam height of 7.5m and the water level of 6.0m (±), respectively, in prototype scale. The test proceeds first to increase the centrifuge acceleration up to a value of 30G at the bottom of the dam. Water is then supplied from the upper storage tank, and the reservoir level is controlled with the bulb to keep the target level, by watching a CCD camera and the indication of the pressure transducer on the bottom. After a state of steady seepage is confirmed in the dam through the measurement of pore water pressure distribution, draw-down test starts by opening the lower drainage bulb. Variation of pore water pressure with time is traced during the test for every transducer in the fill, and sliding failure of the upstream slope is observed by use of a CCD camera through the transparent plate of the container.

2.2 *Fill materials and test conditions*

Some physical and mechanical properties of the fill materials used in the model tests are summarized in Table 2. The material A is sand with a little silt (S-M), which is used as a main fill material. The material B is clayey sand (SC), which is used as a material for a surface soil layer in a test of dam with an inclined impervious zone. Other material called as C, which is a mixture of the materials A and B with the ratio of 10:1, is also used for a surface soil layer. Grain size distribution curves are drawn in Figure 2 for these three materials. The material C is very close to the material A.

Test conditions are summarized in Table 3. Draw-down tests are conducted for three different model dams, by keeping the time of draw-down from the target level to empty constant as 36 seconds, which corresponds to 9 hours in prototype scale. In CASE 1, the model is a homogeneous dam of the material A. In CASE 2 and 3, models have thin impervious zones on the upstream slope, with different materials and thickness, to investigate the influence of surface zone.

Table 1. AIT centrifuge specifications.

Item	Capacity
Radius of rotation	1360mm
Max. acceleration	200G at payload 75kg
Max. payload	200kg at acc. 75G
Loading capacity	15g-ton
Motor type	11.0kw inverter motor
Loading type	Swing platform
Platform space	W660×D500×H770

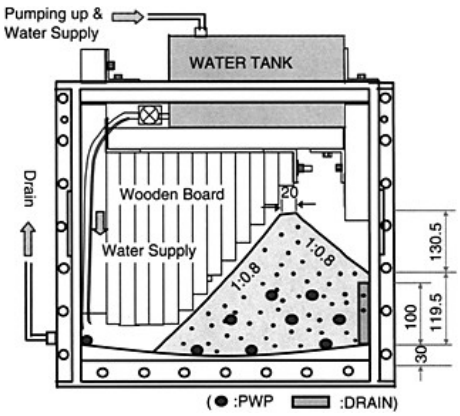

Figure 1. Setup for rapid draw-down test.

Table 2. Material properties.

Material parameters	A	B	C
Japanese unified soil classification	S-M	S	C
Maximum grain size, d_{max} (mm)	2.00	2.00	
Density of solid particle, ρ_s (g/cm^3)	2.564	2.496	
Max. compaction dry density, ρ_{dmax} (g/cm^3)	1.798	1.665	
Optimum moisture content, w_{opt} (%)	12.5	15.3	
Compaction dry density of model, ρ_d (g/cm^3) (Degree of compaction, ρ_d/ρ_{dmax} (%))	1.546 (85%)	1.415 (85%)	
Moisture content of model, w (%)	6.0	13.0	
Saturated coefficient of permeability, k (cm/s)	6.08×10^{-3}	1.90×10^{-5}	

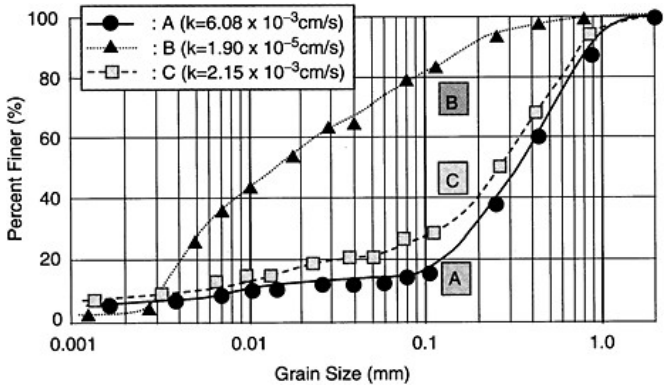

Figure 2. Grain gradation of fill materials.

Table 3. Test Conditions.

Case	Material	Type of embankment
1	A	Without a surface layer
2	B	With a surface layer of width 10mm (top), 40mm (bottom)
3	C	With a surface layer of width 10mm (top), 20mm (bottom)

3 TEST RESULTS AND DISCUSSIONS

3.1 *Seepage behavior during a rapid draw-down*

From the measurement of pore water pressure, the value of the total head in the embankment is obtained at each point of the buried 8 transducers. Seepage behavior can then be traced with time by drawing a flow net diagram, in referring to the phreatic surface observed by the CCD camera.

Flow net diagrams are drawn in Figure 3 for three different situations in CASE 1 (homogeneous dam), Figure 3(a) at a steady seepage state immediately before draw-down operation, Figure 3(b) at a state of an intermediate water level, about 3.0m high from the base in prototype scale, and Figure 3(c) at a state of the final water level, where about 19 hours (76 seconds in model scale) have passed after the water level reached to 0.6m. In Figure 3(a), a parabolic phreatic surface proposed by Casagrande is also drawn for reference by a dotted line. As can be seen in this figure, the measured phreatic surface closely resembles to the proposed parabola, which assures validity in accuracy of the present testing procedure of using pore water pressure transducers and a CCD camera as main measurement devices. As the water level goes down and seepage flow arises from the interior to the upstream face, as is seen in Figures 3(b) and 3(c), the phreatic surface becomes to be a convex curve with a peak at the center of the dam. It is noted in these figures that the head difference between the reservoir water level and the peak of the phreatic surface tends to increase as the reservoir level decreases. The difference is larger in the state (c) than in (b). This suggests that the influence of the residual pore water pressure on slope stability becomes notable as the draw-down operation proceeds.

Figure 4 shows flow net diagrams in CASE 2 (dam with a surface layer of the material B), for three different states of (a) steady seepage, (b) an intermediate water level and (c) the final water level. Because the coefficient of permeability of the surface layer (k_1) is about 1/300 of that of the main fill material (k_2), discontinuous head difference appears in every state between the reservoir water level and the phreatic surface in the fill. The phreatic surface indicated by a chained line in Figure 4(a) is drawn by use of an estimation method for a dam with an inclined impervious core zone, which has been proposed in the governmental design standard for small scale reservoir [4], as illustrated in Figure 5.

In the inclined core, the phreatic surface is given by a circular arc PQ with a center at point R, which is located below the seepage-in point P by the length of $(B_1+B_2)/2$ along the upstream slope, where B_1 and B_2 are width of the core at the base and at the reservoir level, respectively. On the downstream side, the phreatic surface is drawn by use of the basic parabola, given by Eq. (1), which has a pole at the height Y_0 on the seepage-out surface.

$$y=\sqrt{2Y_0x+Y_0^2} \tag{1}$$

The value of Y_0 is determined from the height h of the point Q from the foundation and the ratio of the coefficient of permeability of impervious core material (k_1) to main fill material (k_2), as

$$Y_0=(k_1/k_2)h \tag{2}$$

Because phreatic surfaces obtained above separately for the inclined core and the downstream part of the fill are discontinuous, two curves are smoothly connected with a tracing line passing

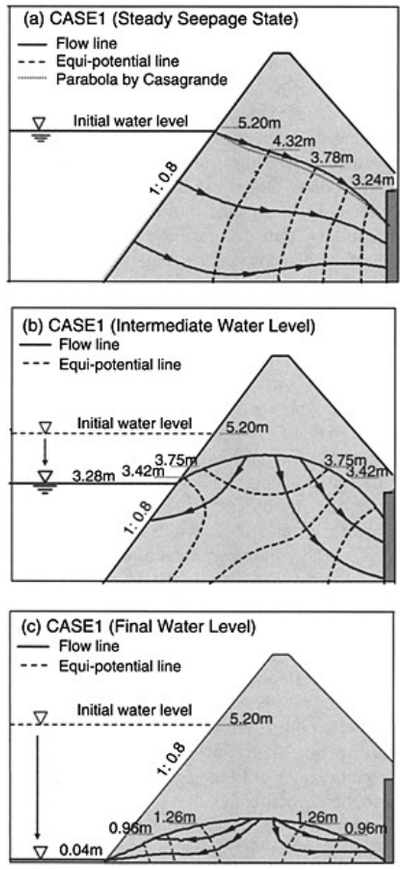

Figure 3. Seepage behavior (Case 1).

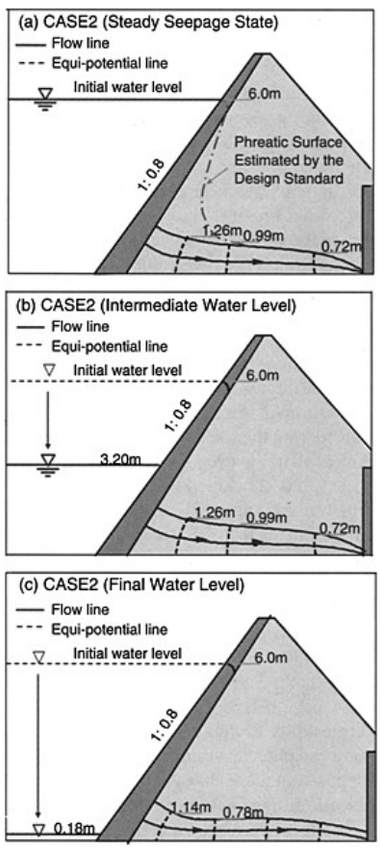

Figure 4. Seepage behavior (Case 2).

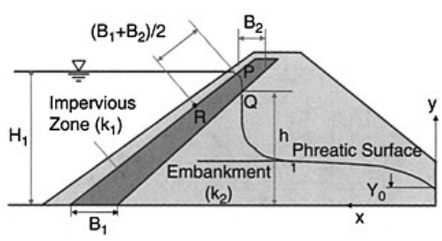

Figure 5. Phreatic surface in inclined core dam.

through the point Q to complete a continuous phreatic surface. In case of $k_2/k_1<10$, the dam can be treated as a homogeneous dam in the standard.

Comparing, in Figure 4(a), the phreatic surface observed in the test with that calculated by the design standard, it is clearly understood that the observed phreatic surface has an apparent large difference in level between the up- and down stream sides of the impervious zone, and a continuous phreatic surface is therefore not expected to form as supposed in the theory. It is believed that discontinuity of the observed phreatic surface is properly supported through measurement and calculation of pore water behavior, as insisted in the following two points. One is validity of measurement of pore water pressure; i.e., the measured values below the phreatic surface showed a good correlation to the values estimated from the flow net analysis, and two transducers above the phreatic surface indicated negative values as expected in the area of capillary water. The negative pore water pressure noticed in the latter, however, is considered to be still controversial to discuss its absolute value because of a few technical problems. The other point is a good correlation of the discharge through the impervious zone to that through the main dam body. The discharge Q_1 which flows in through the impervious zone below the reservoir level is roughly estimated from the difference between the up- and down stream water levels, as $Q_1=0.838m^3$/day. The discharge Q_2 which flows through the dam body can be calculated from the flow net diagram, as $Q_2=0.474m^3$/day. Considering their accuracy in evaluation, it is not unreasonable to say $Q_1 \fallingdotseq Q_2$, and continuity of flow is affirmed even though the phreatic surface is regarded discontinuous in the test.

It is thus concluded that in the present study a fairly good accuracy is maintained in the pore pressure measurement, offering a sufficient basis for the discussion of seepage behavior in embankment. If the discontinuity of the observed phreatic surface is justified, soil should be in unsaturated state in a triangle-like area, which is surrounded by the lower face of the impervious zone, the assumed chained phreatic line and the observed phreatic surface in the downstream dam body, as indicated in Figure 4(a). In the stability analysis based on the design standard for small scale reservoir, however, the triangle domain is treated as in a saturated state, so that the weight of soil and the pore water pressure may be overestimated along a sliding plane. It is then necessarily to say that the governmental design standard tends to offer a safe-side design.

Seepage behavior during draw-down in CASE 2 are shown in Figures 4(b) and 4(c). Because permeability of the impervious zone is considerably low as compared with that of the main dam body, the phreatic surface on the downstream side does not quickly follow the reservoir level. It is supposed in these states that very little water flows from the interior to the upstream face, and the phreatic surface goes down gradually as water flows to the downstream side.

Figure 6 shows flow net diagrams in CASE 3 (dam with a surface layer of the material C), for three different states as presented in Figures 3 and 4. The material C is a mixture of the materials A and B, blended in the ratio of 10:1, which has a little more fine content than the material A. The material is used to construct a surface layer with the lower width of 20cm, half of CASE 2, and compacted in a dense condition to have permeability of about one-third of the material A. The aim of the CASE 3 test is to realize an intermediate seepage behavior of CASE 1 (homogeneous dam) and CASE 2 (dam with an impervious zone), in order to investigate the influence of the surface impervious zone.

In a steady seepage state, Figure 6(a) the flow net diagram can be drawn similarly as a homogeneous dam (CASE 1), and the phreatic surface closely resembles to the parabolic one proposed by

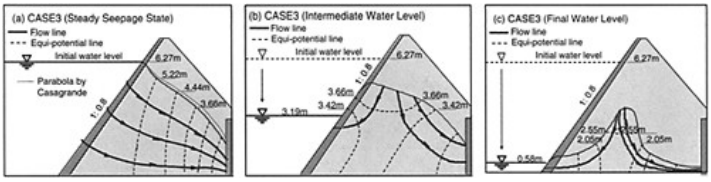

Figure 6. Seepage behavior (Case 3).

Casagrande. It is therefore noted that this kind of thin surface layer with relatively high permeability ($k_1/k_2 \fallingdotseq 1/3$) has little influence on seepage behavior as far as the steady state is concerned. In an intermediate water level of Figure 6(b), however, drainage water from the interior to the upstream face is restricted by the surface layer and much pore water remains in the upstream part of the dam, which results to form an asymmetric phreatic surface unlike a homogeneous dam in CASE 1. In the final water level, Figure 6(c), though the phreatic surface goes down naturally on the downstream side following the reservoir level, much more pore water remains on the upstream side due to the increase of the thickness of the surface layer, and a convex shape phreatic surface lasts in the center of the dam. Distribution of this type of the residual pore water pressure may bring about undesirable situation in circular sliding of the upstream slope.

3.2 *Slope failure during a rapid draw-down*

Figure 7 shows photographs of the interior of the container during the CASE 3 test, taken by a CCD camera for three different stages of (1) immediately after the start of draw-down, (2) start of slope failure and (3) final state of draw-down test. Outline and shape of the embankment, the upstream water table, phreatic surfaces and sliding planes read from these photographs are traced by a marker. It is seen in the stage (1) that the water flow from the interior to the upstream face is restricted by the impervious surface layer, which results in the presence of the residual water in the upstream part of the slope. As the reservoir level goes down further, the increase of the residual pore water pressure, together with the loss of confining effect of the hydrostatic pressure on the upstream face, causes a circular sliding failure passing through the crest in the upstream slope, as shown in the photo (2). The sliding plane is not so large at this time, because the lower part of the dam body below the sliding plane is restrained by the water pressure and the collapsed fill material. In the final stage of draw-down, the photo (3), a successive large and deep sliding failure takes place, including the former slide, to the extent that produces a little deformation in the downstream part of the dam. Generally speaking in the CASE 3 test, though some confining effect of the reservoir water pressure is expected by the presence of the surface layer, the residual pore water pressure tends to concentrate in the central part of the dam, as is seen in Figure 6, so that a large sliding failure which affects on the whole dam body will be anticipated to occur.

In order to investigate whether or not the routine design method of stability analysis can be used with a sufficient accuracy to evaluate slope failures as reproduced in the above centrifuge tests, another failure test is conducted for a simple homogeneous embankment dam. The material and the shape of the model dam is the same as in the CASE 1 test, and reservoir draw-down is done from the initial water level of 6.3m by setting the operation time as 6.75 hours (27seconds in model).

Distribution of the pore water pressure observed in the model dam is drawn in Figure 8, at the time of slope failure of the water level of 5.1m. It is recognized in this test, unlike the CASE 1 test in Figure 3, that water goes down a little slower and the residual water pressure develops in the upstream slope. An asymmetric phreatic surface is therefore formed having a time-lag from the reservoir

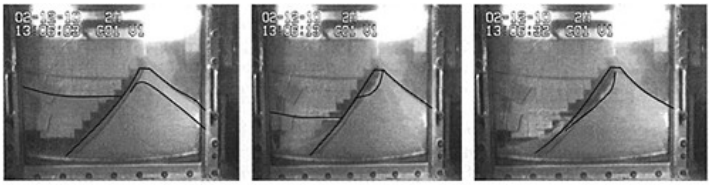

Figure 7. Slope failure (CASE 3).

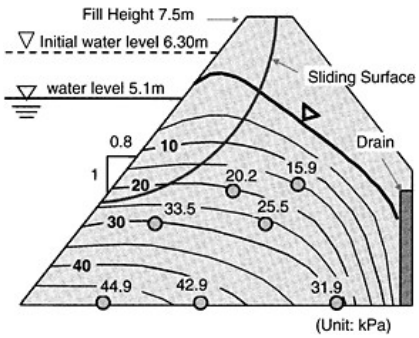

Figure 8. Pore pressure distribution at failure.

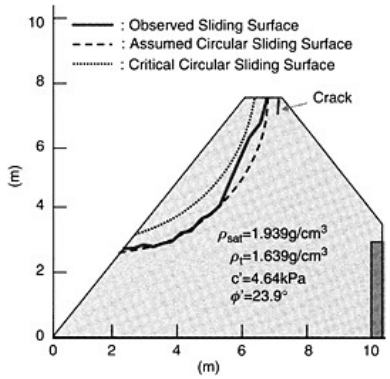

Figure 9. Comparison of sliding surfaces.

Table 4. Results of stability analysis.

Factor of safety		F_s
①	Observed circular sliding surface	0.921
②	Critical circular sliding surface	0.828

level. This is supposed to be due to the fact that the initial reservoir level is higher by 1.1m and the rate of draw-down is faster by about 1.3 times than the CASE 1 test, which results in a delay of drainage water flow to the upstream face.

Sliding surfaces are compared in Figure 9, where the observed real sliding surface is drawn by a solid line, an assumed one which traces the real one as a circular plane by a broken line, and the critical circular sliding surface obtained in the slope stability analysis by a dotted line. Stability analysis is made for these circular sliding surfaces, by using the simplified Bishop method, with strength constants in terms of effective stresses of c'=4.64kPa and [×] degrees. These ([×]) values were determined from tri-axial SCU tests on specimens prepared in the same compaction condition as in the model dam. It is assumed for convenience that the values of strength constants are the same for both soils in saturated and unsaturated states. The results are summarized in Table 4, where values of safety factor are compared for cases of ① the observed sliding surface assumed by a circle and ② the critical circular sliding surface calculated by iteration. At the time a sliding failure appeared in the experiment, some of soil along the sliding plane is supposed to approach a state close to the residual strength after exceeding the peak strength. It is therefore believed that the safety factor of ①, a little smaller than unity, has interpreted the observed sliding failure with a comparatively good accuracy. Although the critical sliding surface of ② becomes to be shallower than the observed one, such a shallow failure is not expected to occur in practice, because compacted soils in general preserves pre-compression effects, that is to say, strength increase in cohesion in the surface part of the slope.

4 CONCLUSIONS

Concluding remarks drawn from the present study are summarized in the following.

(1) In the cases where the rate of draw-down of the reservoir water is considerably high and the slope surface is covered by a thin impervious layer, drainage water from the interior to the upstream face is restricted even in an almost homogeneous dam, and the residual pore water pressure develops in the upstream slope to have a large influence in slope stability.
(2) In a dam with a thick impervious soil layer on its surface, a discontinuous head difference appears in every state between the reservoir water level and the phreatic surface in the dam, due to little flow of drainage water to the upstream face. The design standard for small scale reservoir proposed by the government tends to offer a safe side design in the evaluation of the pore water pressure in the dam.
(3) Slope failures due to a rapid draw-down of the reservoir water are satisfactorily reproduced in the present centrifuge tests, and a sufficient accuracy is obtained in slope stability evaluation.

ACKNOWLEDGMENT

The authors wish to express their gratitude to Mr. Naoki Sadaoka, AICO co. Itd, for his tremendous assistance throughout this centrifuge study. This research was undertaken with the financial support of Grant-in Aid for Science Research of the Ministry of Education.

REFERENCES

[1] Yamaguchi, H. and Ohne, Y.: *Design and construction of fill dams,* Giho-do, 1973, pp. 238–244 (in Japanese).
[2] Ohmori, K., Okumura, T., Kimura, K., Narita, K. and Ohne, Y.: Stability evaluation of fill-type dams due to a rapid draw-down of the reservoir water, *Technical Report of Aichi Institute of Technology,* No. 37, 2002, pp. 115–122 (in Japanese).
[3] Kudo, A., Nishigaki, M., Torii, T. and Asada, S.: The effects of saturated-unsaturated hydraulic properties on residual water level in upper zone of rock-fill dam due to rapid draw-down, *Dam Engineering,* Vol. 13, No. 3, 2003, pp. 137–151 (in Japanese).
[4] The Ministry of Agriculture, Forestry and Fisheries in Japan: *Design standard for small scale reservoir,* The Japanese Society of Irrigation, Drainage and Reclamation Engineering, 2001 (in Japanese).

This page intentionally left blank.

New Developments in Dam Engineering—Wieland, Ren & Tan (eds),

Analysis of vertical dam deformation using geodetic measurements

Gh.Nistor
Technical University of Iasi, Romania

I.Nistor
University of Ottawa, Canada

ABSTRACT: The information concerning the vertical displacements and deformations (in the form of either settlement or uplift) is of crucial importance for the study of dams' behavior. The high precision geodetic leveling methods are a key procedure when it comes to obtaining the values of the vertical deformations. Their magnitude and extent can be obtained through the cyclic processing of the leveling measurements using rigorous methods such as the method of the weighted indirect observations. The principle of measuring the dam deformations consists in the cyclic determination of the elevations of the control points located on the dam crest and at the foot of its downstream slope with reference to several control points located on non-deformable soil and outside of the direct influence zone of the dam. Several elements of the sequence of measurement operations are common to all observation cycles. Based on this fact, the current paper proposes a new calculation algorithm of the vertical deformation vector of a dam. The calculation procedure is directly depending on the variation of the measured elements in the field and comprises a mathematical estimation model coupled with an accurate estimation procedure for the results.

1 INTRODUCTION

The magnitude of the vertical deformations and displacements are of crucial importance when analyzing the in-situ behavior of a dam. By convention, the settlements are assigned negative values while uplifts are assumed to have positive values. Since the geodetic measurements conducted with by means of high precision geodetic measurements enable the analysis of the structure's behavior only based on the magnitude of the deformation vector, it is necessary to relate them to other field data and investigations concerning soil properties, the groundwater characteristics, etc. The association of all available and collected data allows the identification of the causes that induced the deformations and the eventual mitigation measures and/or restoration programs to be taken [1].

Employing the least square method and based on the known elevations of the fixed points of the reference network, the field leveling measurements are corrected during each cycle of measurement. As a result of this operation, the elevations of the control points (settlement marks) located on the dam are obtained. Further on, analyzing the distribution of the elevations of the control points corresponding to each measuring cycle, the vector of vertical deformations is obtained. However, this solution is not efficient, especially when time is a constraining factor. During the rigorous processing of the collected data within each measurement cycle, a number of elements remain constant. Consequently, the current paper proposes an algorithm for the determination of the vertical deformation vector as a direct function of the variation of the cyclically determined elements in the field.

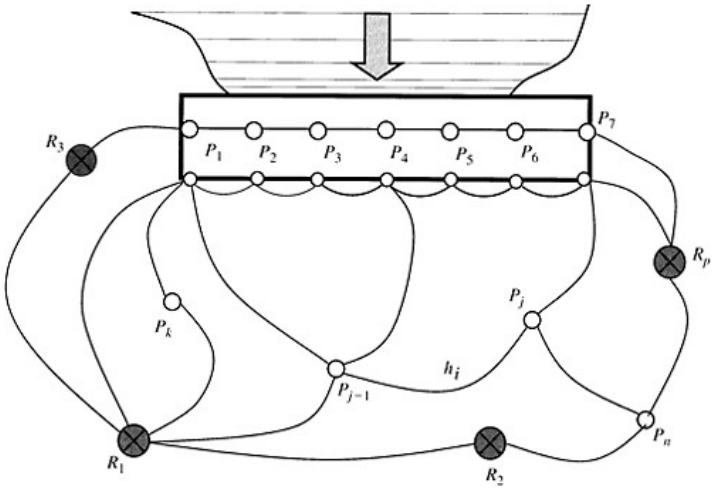

Figure 1. Typical localization of the fixed *(R_i)* and control points *(P_i)*.

Since several elements concerning the processing of the geodetic measurements are identical for all measurement cycles, the paper is presenting an algorithm for computing the vector of horizontal deformations, directly based on the variation of the cyclically measured elements. Due to difficult often encountered during measuring procedures, the method of weighted indirect measurements is assumed to give the best results under such circumstances [1].

2 STRUCTURE OF THE PROPOSED ALGORITHM

The purpose of the algorithm is to calculate the vertical deformation of n control points—with respect to a p number of fixed points of the reference network—on the basis of level differences measured during a number, r, of direct field observations (Fig. 1). The geometrical leveling measurements are performed using high accuracy levels equipped with optical micrometers employing high precision measuring rods. Each leveling line is measured using one or more elevations of the instrument.

Each level difference is obtained as an arithmetic mean of the field measurements as follows:

$$h_i = \frac{1}{2}\left(h_i' + h_i''\right),\ i = \overline{1,r} \tag{1}$$

During the first measuring cycle (also known as the 'zero' cycle), the initial elevations of all control points are calculated with respect to the elevations of the fixed points, H_k—where $k = \overline{1,p}$—and of the level differences.

$$H_{0j} = H_k + h_{0,kj},\ j = \overline{1,n} \tag{2}$$

where $h_{0,kj}$ represents the level difference—indicated in Eq. (1)—measured within the space interval connecting the points of the fixed network whose elevations are H_k and H_j.

Since processing of the measurement results is conducted using the method of the indirect weighted observations, the linear system of the corrections can be expressed in matrix form as,

$B_{rn}X_{n1}{}^0+L_{r1}{}^0=V_{r1}{}^0$, with the weight matrix P_{rr} (3)

where the following notations are considered: r—the number of level differences measured in the field which is equal to the number of correction equations; n—the number of indirectly determined parameters which represents also the number of corrections to be added to the initial elevations of the control points, leading thus to their compensated values which are, in fact, the unknowns; B_{rn}—the matrix of the coefficients of the correction equations *(r<n);* the elements of the matrix have the following values: (+1) if the control point represents the beginning of the leveling section, (−1) if it represents its end and (0) if it is situated between the two; $\mathbf{L}^0_{r1}$—the vector matrix of the free terms which are obtained from the differences between the calculated and the measured values during the initial observation cycle.

$$l_{0i}=(H_{0j}-H_{0,j-1})-h_{0i} \tag{4}$$

In Eq. (4), $H_{0,j}$ and $H_{0,j-1}$ are the provisory elevations, h_{0i} is the average difference in elevation measured in section i. Further on, in Eq. (3), V^0_{r1} is the correction vector for the provisional differences used to obtain the compensated level differences; P_{rr} represents the weight matrix whose elements are calculated—for the case of equal leveling intervals—using one of the following relations [2].

$$p_i=\frac{1}{D_i}=\frac{K}{D_i} \text{ or } p_i=\frac{1}{R_i}=\frac{K}{R_i} \tag{5}$$

where: K represents the proportionality coefficient, D_i is the length of section i and R_i represents the number of stations in section i.

The matrices can be presented in extended form as follows:

$$\begin{cases} B_{rn}=\begin{bmatrix} a_1 & b_1 & .... & h_1 \\ a_2 & b_2 & .... & h_2 \\ . & . & . & . \\ a_r & b_r & . & h_r \end{bmatrix}, \quad X^0_{n1}=\begin{bmatrix} H_{11}-H_{01} \\ H_{12}-H_{02} \\ ..... \\ H_{1n}-H_{0n} \end{bmatrix}=\begin{bmatrix} \Delta h_{01} \\ \Delta h_{02} \\ ..... \\ \Delta h_{0n} \end{bmatrix}, \quad L^0_{r1}=\begin{bmatrix} l_{01} \\ l_{02} \\ ..... \\ l_{0n} \end{bmatrix} \\ V^0_{r1}=\begin{bmatrix} v_{01} \\ v_{02} \\ ..... \\ v_{0n} \end{bmatrix}, \quad P_{rr}=\begin{bmatrix} p_1 & 0 & .... & 0 \\ 0 & p_2 & .... & 0 \\ . & . & . & . \\ 0 & 0 & . & p_r \end{bmatrix} \end{cases} \tag{6}$$

For the second measuring cycle, the linear system of corrections is expressed by the following equation (in matrix form):

$$B_{rn}X_{n1}{}^{1}+L_{r1}{}^{1}=V_{r1}{}^{1}, \text{ with the weight matrix } P_{rr} \tag{7}$$

where matrices B_{rn} and P_{rr} are identical to the ones used during the initial (zero) cycle while the other ones are detailed below:

$$X^1_{n1}=\begin{bmatrix} H_{21}-H_{01} \\ H_{22}-H_{02} \\ ..... \\ H_{2n}-H_{0n} \end{bmatrix}=\begin{bmatrix} \Delta h_{11} \\ \Delta h_{12} \\ ..... \\ \Delta h_{1n} \end{bmatrix}, \quad L^1_{r1}=\begin{bmatrix} l_{11} \\ l_{12} \\ ..... \\ l_{1n} \end{bmatrix}, \quad V^1_{r1}=\begin{bmatrix} v_{11} \\ v_{12} \\ ..... \\ v_{1n} \end{bmatrix} \tag{8}$$

In the vector of the unknowns in Eq. (8), the following notations were made: H_{0j}—the provisory elevations of the control points; H_{1j} and H_{2j}—the compensated elevations from the initial (zero)

and the current measurement cycles, respectively. Further on, one tries to directly relate the magnitude of the vertical deformations to the variation of the magnitudes of the level differences obtained during the two cycles. Consequently, Eq. (3) is subtracted from Eq. (7):

$$B_{rn}\left(X_{n1}^{1}-X_{n1}^{0}\right)+\left(L_{r1}^{1}-L_{r1}^{0}\right)=V_{r1}^{1}-V_{r1}^{0}\text{, with the weight matrix} \tag{9}$$

which is rewritten as

$$B_{rn}X_{n1}+L_{r1}=V_{r1}\text{, with the weight matrix } P_{rr} \tag{10}$$

The matrices B_{rn} and P_{rr} remain the same as Eq. (6) while the rest of the matrices are given as:

$$\begin{cases} X_{n1}=X_{n1}^{1}-X_{n1}^{0}=\begin{bmatrix}\Delta h_{11}-\Delta h_{01}\\ \Delta h_{12}-\Delta h_{02}\\ \cdots\cdots\\ \Delta h_{1n}-\Delta h_{0n}\end{bmatrix}=\begin{bmatrix}\Delta H_1\\ \Delta H_2\\ \cdots\cdots\\ \Delta H_n\end{bmatrix} \\ V_{r1}=V_{r1}^{1}-V_{r1}^{0}=\begin{bmatrix}v_{11}-v_{01}\\ v_{12}-v_{02}\\ \cdots\cdots\\ v_{1r}-v_{0r}\end{bmatrix}\begin{bmatrix}v_1\\ v_2\\ \cdots\cdots\\ v_n\end{bmatrix} L_{r1}=L_{r1}^{1}-L_{r1}^{0}=\begin{bmatrix}l_{11}-l_{01}\\ l_{12}-l_{02}\\ \cdots\cdots\\ l_{1r}-l_{0r}\end{bmatrix}\begin{bmatrix}l_1\\ l_2\\ \cdots\cdots\\ l_r\end{bmatrix} \end{cases} \tag{11}$$

The free terms are represented by the following differences:

$$l_i=l_{1i}-l_{0i}=\left[\left(H_{0j}-H_{0,j-1}\right)-h_{1i}\right]-\left[\left(H_{0j}-H_{0,j-1}\right)-h_{0i}\right]=h_{0i}-h_{1i} \tag{12}$$

In the new system shown in Eq. (10), the vector of the unknowns is represented by the vertical deformation vector while the free terms are represented by the level differences measured during the initial (zero) and current cycle. Therefore, the system is denoted by the vertical deformations equation system. The vector V_{ri} represents the corrections to be brought to the differences of the provisory level differences in order to obtain their compensated values. Since the number of equations is smaller than that of the unknowns X_{n1} and $V_{r1}(n<(n+r))$, the solution of the system of equations is obtained by introducing the following condition of minimum:

$$V_{1r}^{T}P_{rr}V_{r1}\rightarrow\min \tag{13}$$

Replacing the corrections, the minimum condition will be expressed as:

$$V_{1r}^{T}P_{rr}V_{r1}=X_{1n}^{T}B_{nr}^{T}P_{rr}B_{rn}X_{n1}+2X_{1n}^{T}B_{nr}^{T}P_{rr}L_{r1}+L_{1r}^{T}P_{rr}L_{r1}\rightarrow\min \tag{14}$$

The above condition will be fulfilled once the partial derivatives with respect to the unknowns are set equal to zero as:

$$\frac{1}{2}\frac{\partial\left(V^{T}PV\right)}{\partial\left(X\right)}=B_{nr}^{T}P_{rr}B_{rn}X_{n1}+B_{nr}^{T}P_{rr}L_{r1}=0 \tag{15}$$

The following notation is adopted: $N_{nn}=B_{nr}^{T}P_{rr}B_{rn}$ and therefore,

$$N_{nn}X_{n1}+B_{nr}^{T}P_{rr}L_{r1}=0 \tag{16}$$

Equation (16) which depicts the minima of the Gauss-Legendre function is known as the system of normal equations. Its solution is obtained by multiplying the left-hand side of the equation with the inverse of the coefficients matrix.

$$X_{n1} = -N_{nn}^{-1} B_{nr}^{T} P_{rr} L_{r1} = -\tilde{Q}_{nn} B_{nr}^{T} P_{rr} L_{r1} \tag{17}$$

The product of the matrices from the initial cycle is written as:

$$Z_{nr} = \tilde{Q}_{nn} B_{nr}^{T} P_{rr} \tag{18}$$

The elements composing matrix Z_{nr} remain constant for all subsequent measurement cycles. Therefore, the vector of the unknowns will be directly expressed as a function of the magnitudes of the level differences.

$$X_{n1} = -Z_{nr} Lr_1 \tag{19}$$

Equation (19) can be expressed in its extended form as:

$$\begin{bmatrix} \Delta H_1 \\ \Delta H_2 \\ \cdots\cdots \\ \Delta H_n \end{bmatrix} = - \begin{bmatrix} z_{11} & z_{12} & \cdots\cdots & z_{1r} \\ z_{21} & z_{22} & \cdots\cdots & z_{2r} \\ \cdots\cdots & \cdots\cdots & \cdots\cdots & \cdots\cdots \\ z_{n1} & z_{n2} & \cdots\cdots & z_{nr} \end{bmatrix} \begin{bmatrix} l_1 \\ l_2 \\ \cdots\cdots \\ l_r \end{bmatrix} \tag{20}$$

Thus, the vertical deformations of the control points located on the dam are expressed as a direct function of the variation of the measured level differences. Using Eq. (19), one can obtain either the vertical deformations between two subsequent measuring cycles, when the free terms are calculated using the subsequent level differences,

$$l_i = h_{t-1,i} - h_{t,i} \tag{21}$$

where t represents the number of the measurement cycle, $t = \overline{1, T}$ or the total vertical deformations, when the free terms are calculated with respect to the initial cycle as

$$l_i = h_{0,i} - h_{t,i} \tag{22}$$

Based on the vertical deformations, ΔH_f the final settlement charts and graphs can be drawn up.

3 ESTIMATION OF THE ALGORITHM ACCURACY

In order to estimate the accuracy of the results, several factors are calculated as follows:

a. The error of the weight unit calculated with the Bessel formula [2].

$$\mu = \pm \sqrt{\frac{V_{1r}^{T} P_{rr} V_{r1}}{r - n}} \tag{23}$$

where

$$V_{1r}^{T} P_{rr} V_{r1} = V_{1r}^{T} P_{rr} L_{r1} = L_{1r}^{T} P_{rr} L_{r1} + X_{1n}^{T} B_{nr}^{T} P_{rr} L_{r1} \tag{24}$$

b. The mean square errors of the vertical deformations and their correlation matrix

$$\mu_X^2 = \mu^2 \tilde{Q}_{nn} \tag{25}$$

where $\tilde{Q}_{nn}$ represents the matrix of the weight coefficients of the unknowns (in this case, the deformations). The mean square error of the vertical deformation of the control point j is therefore:

$$\mu_{\Delta H_j} = \pm\mu\sqrt{Q_{jj}}\text{, where } j = \overline{1,n} \tag{26}$$

Based on Eq. (26), the confidence interval within whose limits the true values of the vertical deformation can be found will be:

$$\Delta H_j - \mu_{\Delta H_j} \le \overline{\Delta H_{j,P=67.3\%}} \le \Delta H_j + \mu_{\Delta H_j} \tag{27}$$

Other statistical methods such as the method of the confidence intervals can also be used. However, such a method has the advantage that it covers both the theoretical value of the weight unit as well as the magnitude of the vertical deformations of each control point, especially the ones whose positions are significantly affected by displacement.

4 CONCLUSIONS

The presented algorithm enables the fast and reliable determination of the vector of vertical deformations of all control points installed on a dam. The vector is directly obtained from the elements measured in the field, whose magnitude changes over time. The most probable values of the vertical deformations of the dam are found using the method of the least squares.

The calculations are conducted either by using specific software or by determining only the elements of the constant matrix Z_{nr} and then directly computing the deformation vector in the field using a simple scientific calculator.

A complete estimation of the accuracy of results can be conducted in the field during each measuring cycle for all control points. According to Eq. (25) and (26), since the weight coefficients depend on the configuration of the local topographic network, one can establish beforehand the required accuracy for the leveling measurements in the field.

The proposed algorithm has a general character and can be applied to the analysis of any large structure.

REFERENCES

[1] Nistor, Gh.,—*Applied geodesy for the Study of Constructions,* "Gh. Asachi" Publishing House, Iasi, Romania, 1993.
[2] Nistor, Gh.,—*The Theory of Geodetic Measurements Processing,* "Gh. Asachi" Publishing House, Iasi, Romania, 1996.
[3] Nistor, Gh., Braier, A.,—Étude anticipé de la precision du nivellement géométrique utilisée pour determiner les deformations verticales des constructions, *Bulletin. of the Polytechnic Institute,* XXXII (XXXVI), 1–4, Section V, 1986, pp. 43–48.

New Developments in Dam Engineering—Wieland, Ren & Tan (eds),
© 2004 Taylor & Francis Group, London, ISBN 04 1536 240 7

Design on navigation structures of the Three Gorges Project of Yangtze river

Niu Xin-Qiang & Song Wei-Bang
Changjiang Institute of Survey, Planning, Design & Research, CWRC, China

ABSTRACT: The Yangtze river is the largest navigation waterway in China and the navigation development is one of comprehensive benefits of Three Gorges Project's (TGP) construction. The TGP's navigation structure consists of three works, i.e. the large type of double lane and five-step ship lock with the largest designed water head and operation water head of valve, the large type of vertical ship lift with largest lifting height and weight, the temporary ship lock during construction period. This paper concisely presents several key points of designing navigation structures of TGP, locations of navigation structures in TGP, the arrangement of structures, mechanical and electric equipments, water convey system in the double-lane, five-step flight ship lock, the design of lock head, lock chamber and high slope in ship lock, the arrangement of structures, mechanical and electric equipments in the vertical ship lift and temporary ship lock and the design of its main structures and equipments.

1 INTRODUCTION

Yangtze river, the largest navigation waterway in China. Due to current and depth restriction, about 660km long waterway from Chongqing to Yichang can only pass less than 3000t-grade fleet, and its annual capacity is about 10 million tons before Three Gorges Project is built. Once TGP is accomplished, this waterway would be improved entirely: 10-thousand-ton fleet could sail to Jiulongpo port in Chongqing directly about six months every year; also its downstream waterway would be improved obviously by controlling discharge, i.e. it would be increased from nowadays 3000m^3/s to more than 5000m^3/s in low flow period. The annual navigation capacity would be increased to 50 million tons.

According to Gezhouba's two-lane and three-lock navigation structure, TGP should have the same capacity with two-lane ship lock and one-lane vertical ship lift. On the whole, TGP couldn't break the waterway during construction: in first stage, fleet can go through the main sea-route; in second stage, they can go through open channel on right side in most time and temporary ship lock on left side sometime; in third stage, the open channel is closed and the temporary ship lock stops, before reservoir water level rises to cofferdam generation level 135m, passengers and goods pass by port over TGP, shortly after the water level rises to 135m, fleet can go through two-lane five-step ship lock.

2 TWO-LANE FIVE-STEP SHIP LOCK

2.1 *Layout of ship lock*

The design water head and valve operation water head of ship lock are 113m, and its planning capacity is: 50 thousand tons annual goods transportation for single line, 3.9 million person-time

annual passengers transportation for double line. The upstream design water levels are: 135m in cofferdam generation period, 135m~156m in early stage,145m~175m in late stage. Downstream design water levels are from 63.0m to 73.8m. 12-thousand-ton fleet is designed to pass ship lock. Maximum fleet grade in planning is 12 thousand tons. Maximum discharge is: 45,000m^3/s for double line 10-thousand-ton fleet, 56,700m^3/s for one-way 3-thousand-ton fleet.

According to water levels and site topography, continuously five-step ship lock is selected for it has obvious advantages in BOK, cost, management, relations to layout of project, etc.

The effective size of ship lock chamber is 280m×34m×5.0m. Comparing with four routes, the ship lock route is finally determined on the left side of Tanziling mountain, the summit on the left side of riverbed. The principle part of ship lock is 1621m long, joined to bending breakwater both its upstream and downstream, whose length are 2670m and 3700m respectively. The upstream and downstream approach channel are 2113m and 2708m long respectively, and the total length of ship lock route is 6442m.

Normally, the ship lock runs as one lane up and the other down. When one of ship lock lanes is in examination, the other could pass ships groups by groups in single direction and could change directions timely. Fleet may enter ship lock every an hour, and pass the ship lock for 2.4 hours totally. It may spend a ship 3.1 hours going from entrance to exit. The annual one-way capacity of ship lock is 51.52 million tons with 1.7 billion m^3 water consumption except overflowed in flood season.

2.2 *Main structure*

Ship lock structures lies in a deeply excavated slot in the left side mountain rock, where reserved a 57m wide middle dividing rock wall between two lanes. Each lane of lock consists of six lock heads, five chambers, two guide walls, breasting dolphins, and dams on two sides of NO.1 lock head.

The lock heads and chambers are all separate structures. Most of chamber walls are lining structure, and some are mixed structures with gravity structures above and lining structures below. The lock heads and bottom boards are all gravity lining structures.

Upstream guide wall is floating structure and downstream guide wall is lining structure. On two sides of straight line segments of approach channels, there are some breasting dolphins which are solid cylinders.

Constant-inertia water convey systems are adopted for the locks. Two water conveyancy tunnels are installed symmetrically on two sides of each lane of locks, with the upstream inlets positioned within the access channel and most water release at the last lock directly to Yangtze River, only a small portion of water release to the downstream access channel. The layout of water conveyance galleries in the chambers is all in type of eight pips in four sections, with energy dissipating cover plates, releasing water dispersively on the top of branch galleries.

The main gallery of water conveyance system is a reinforced concrete lining tunnel excavated in rock. Two adjacent galleries of two lanes in middle dividing rock are constructed in one large excavated section.

2.3 *Arrangement of equipments*

From upstream to downstream in turn on ship lock, there are: emergency gate with its bridge type gears in NO.1 lock head, NO.1 to NO.6 leaf gates with its hydraulic pressure gears and opposite arc gates with its hydraulic pressure gears for filling and draining water, plain emergency valves for repairing opposite arc gates, plate gates with its gears for supplementary drainage, emergency gate for repairing plain gate. There is a floating emergency gate behind NO.6 lock head, a set of anti-collision alert apparatus on NO.2 and NO.3 lock head, and floating bollards and emergency ladders on waterside of every chamber.

The leaf gate is 37.5m high normally except that NO.3 and NO.4 leaf gate is 38.5m high. The single leaf is 20.2m wide. The intersection angle between leaf gate axis and ship lock's transverse axis is 22.5°. According to reservoir water level stages, NO.1 lock head is used as an open channel during the initial stage and NO.1 leaf gate is assembled as later water level stages. NO.2 leaf

gate, assembled as initial stage, should be reassembled and the bottom sills of NO. 1 and NO. 2 leaf gate should be heightened before later stages. The maximum submerge depth of NO. 1 leaf gate is 35m. The opening size of opposite arc gates in NO. 1 and NO. 6 lock head are 4.5×5.5m (width×height), and that in NO. 2 to NO. 5 lock head are 4.2×4.5m (width×height).

Leaf gates are made and broken by horizontal hydraulic pressure hoist, and opposite arc valves are done by vertical hydraulic pressure hoist. Those two gears share one hydraulic pressure system. All the gates are controlled by PLC.

2.4 *Ship lock*

2.4.1 *Lock head*

The side walls in the first lock head are gravity lining structures. And that of NO.2 to NO.4 lock head are thin lining structures above their supports, which are gravity lining structures also, and that of NO. 5 lock head is a mixed structure with gravity structure above and gravity lining structure below. Due to the three dimensional stress in lock head, the outlook size and interior layout of lock head are determined by water levels, rock foundation, stability and layout of equipments. The lengths of lock heads are: 70m for NO. 1 lock head, 43.5m for NO. 2 and NO. 3 lock head, 41.5m for NO. 4 lock head, 52.8m for NO. 5 lock head and 56m for NO. 6 lock head. The widths of lock heads are: 12m for NO. 1 to NO. 5 lock head and 14m for NO. 6 lock head. There are strengthened bolts and drainages on the interfaces between linings and rocks.

The lock head is analyzed by principle that it works together with rocks anchored to be stable enough.

The lining structure at the upstream of the support is analyzed in plane assume. Ignoring the bolts' action, the concrete supports should keep stable against sliding and over turning themselves under working loads. But in repairing load case, the bolts' action should be considered in stability against over turning. Furthermore, the contact forms between concrete and rocks, the stress and deformation of bolts should be analyzed when temperature changes. And the strength of both bolts and concrete should be checked in repairing load case.

The leaf gate sill, which is a mixed structure, is divided into two parts to be analyzed. The upper gravity part is considered as a gravity structure on rock foundation assuming that the interface takes all the sliding loads and ignoring the help of the lower lining structure. As well as dead weight and water pressure behind lining, the analysis of lower lining structure should be concern loads from upper structure in order to check bolts and concrete walls whether they are strong enough or not. Assuming the contact interfaces have enough shear strength to avoid shear fractures, the integer stability against sliding and over turning of the supports should be checked with cohesiveness of interfaces and lower bolts' action ignored.

2.4.2 *Ship lock chamber*

According to the stability of deeply excavated rock, anti-permeability and flatness of walls, chambers have two structure types, one is lining structure, the other is mixed structure. The minimal width of lining is 1.5m, and bottom width of gravity structure part is usually more than 0.8 times of its height. The side walls of chambers are divided by gaps every 12m along the current direction, as well as few is divided every 22m or 24m. The stability, strength and fracture width of the chambers should be checked according to structure type, loads and usage requirement.

2.4.3 *High excavated slopes*

According to the rocks cut by geologic structures and blatts, great height, long extensions, complex outlines, excavated rocks working together with structures and severe deformations control request, the high excavated slopes on two sides of ship lock should keep stable enough and little deformation. Many technologies applied to solve high excavated slopes mainly include a reasonable trench shape, proper construction program and blasting technology, water treatment of cutting, defending and draining with bolts auxiliary, necessary surveillance equipments.

The standard outlines of excavation section is vertical in the lower part. But in need of construction equipment, there are 30 cm-wide altars on the rock wall every 15m and a 15m-wide platform on the top of chamber, upon where there is a 5m-wide packway every 15m; the rates of slopes are: 1:0.3 in tiny fresh rocks, 1:0.5 in slightly weathering rocks, 1:1.0 in intense weathering rocks and 1:1.0~1.5 in entirely weathering rocks.

The excavation program of high slopes consists of two stages: regular excavation stage and protective layer excavation stage. According to excavation shapes and rocks, many blasting control technologies are required, such as multi-segment short delay blasting, smooth blasting, stress relieving blasting, slashing blasting, etc. And the turn between open and underground excavation, the turn between left lane and right lane, the turn between open excavation and construction of bolts and anchorage cables are all determined in detail.

Shotcrete is applied in some area on the top of slopes for anti-seepage. There are intercepting ditches on every packway and along the peripheries of slopes. And in rocks beside ship lock, there are seven layers of drainage holes, with 20m elevation difference between adjacent layers, and there is a drainage curtain in each layer. Between lining and rocks, there is a drainage pipes net cutting the water coming from the rocks of two sides.

During excavation, some instable or potentially instable rocks are fastened by bolts and 100t or 300t anchorage cables which are 4157 bunches in total.

Blasting vibration, deformation, wave velocity in rocks, gaps, ground stress and seepage are all under monitor during excavation and post-excavation.

The surveillance data show: the total value of deformation inclining to chamber is in the scope from 20mm to 60mm and it declines every year till into allowed error scope in the third year after excavation was over. The gaps, appearing on the top of slopes and middle dividing wall, stop stretching after they anchored by cables. The prestress loss of anchor cables is low enough to meet design request. The slopes are dry at present and the underground water level is to some extent below what was planned. The conclusions drawn from those surveillance data are that the high excavated slopes and the middle dividing wall rocks are stable.

2.4.4 *Water conveyance system*

The maximum water head of a single step ship lock in TGP is 45.2m. The design of water conveyance system includes: properly determining the request for filling time and ship berthing, system arrangement to meet the upstream and downstream approach channels, researching to eliminate cavitation erosion in valves and galleries, and researching to resolve overfilling and over-releasing issue, water complementarity issue and sediment issue.

In order to inlet water at any water levels with no whirls, no time controlling, good conditions for navigation and ship berthed, seldom silting and keeping bed load sediment out of galleries, there are four inlet galleries, which can inlet water along itself, at some distance from each other perpendicular to the chamber axis, each for main gallery in approach channel.

The main galleries, symmetrically set on two sides of ship lock, are in gate-shape section, and change to rectangle section near valves. The section size of filling gallery in NO.1 chamber and of draining gallery in NO.5 chamber near valve are 4.5m×5.5m (width×height), as well as 4.2m×4.5m (width×height) in other parts. The minimum submerge depth of valves is 26m. The gallery behind valve is enlarged with the slope of 1:10 on top and a 3.1m-high vertical sill. Tunnels in rocks are reinforced by 0.6m-thick RC lining. The two galleries in middle dividing wall are in one excavated section, and its lining is 1.0m thick except 1.5m thick in dividing slab. Near the valves and emergence gates, the galleries are protected by steel liners.

There are two steps of diversion among main gallery and its brunches, one is set in the center of chamber and another is set in one fourth of chamber. There are eight brunches of gallery divided in four areas under every chamber, and on the top of galleries, there are outlets set equidistantly and covered by dissipation slab with crinolines.

The two main galleries in each lane ship lock unite into one rectangle culvert, whose section size is 9.6m×9.6m, in the downstream of NO.6 chamber. Two culverts, under the approach channel, wind its way practically downstream from breakwater to river.

Taking full advantage of the tunnel in rocks, designers drop the elevation of galleries near the valves as possible in order to improve valve hydraulic conditions. In addition, many technologies are applied to control or eliminate cavitations such as opening valves quickly, enlarging the gallery behind valve gradually on its top and enlarging it suddenly at its bottom, steel liner and ventilation behind valve, etc.

The water conveyance system in ship lock were verified by several hydraulic models. The results of filling debugging indicate: the hydraulic conditions are good and the system efficiency is very high, the time for filling or draining is 10min in usual less than designed time which is 12min~13min, ship berthing conditions in chamber is good, overfilling and over-draining are all under control with the opposite water head of leaf gate less than 20cm. However, the water inlet and complementary should be verified in trial navigation because of condition restriction.

2.5 *Metal structures*

2.5.1 *Upstream emergency gate*

The emergency gate consists of 11.5m high plate gate above and eight stoplogs, 3.7m high each, below. There are two bi-directional bridge winches with capacity of 2×2500kN complimentarily for two lanes of ship lock. The maximal height of winch is 76m. The lift speed of winch is 6m/min, and its walk speed is 20m/s for big wheels and 5m/s for small wheels.

2.5.2 *Leaf gate*

The normal water head of leaf gate is in scope of 26m to 36.75m, and its submerge depth is in scope of 14.17m to 35m. 2000kN collision loads, deformations of rocks in anaphase, deformations of leaf caused by water pressure and 1000kN silting weight are concerned when leaf gate is being designed.

The leaf gate is a cross beam structure. The gateposts and diagonal staffs are in uncorked I-shape section set with 5 longitudinal clapboards between them according to stability request. There are hypo-beams among main beams, whose web plate is reinforced by rib bars. There are two layers of back tie rods on the downstream side of leaf. The leaf gate is analyzed as a plane structure and verified by 3-dimension FEM. The top pivot is adjusted by a sprag. The included angle between A, B straining frame and currency are 80° and 10° respectively. The bottom pivot is a settled structure with a sole plate for adjustment. The coping of bottom pivot is joined to the web plate of the bottom main beam on leaf gate by refined bolts and tightened by shearing plates after it is fixed. The diameter of the spherical gatepost bottom, welded with stainless steel on its surface, is 1.0m. The pivots can lubricate automatically, and there is an oil pumped lubricating device on the top of leaf preparing for lubrication.

The horizontal hydraulic pressure gears, used for leaf gates, is designed in load of 2700kN and verified in load of 5400kN.

2.5.3 *Opposite arc valve*

The opposite arc valve is a packaged cross beam structure and its leaf is 700mm thick. The valve is designed to stand 1.8 times of water head in valve wells. The downstream face plate of valve is made of stainless clad steel plate. And the joint of valve is a self-lubricating bearing with oil pipe lubricating system prepared.

The capacity of hoist of valve is 1500kN. The derrick boom, connecting the piston rod and valve, is 72.48m long. And it is connected by several poles in hinge joints with idler pulleys and sliding bearings.

2.6 *Electric dragging and automatic control*

The leaf gates shares the hydraulic pressure pump with valves. The dragging electric machines for pumps are: five 75kw machines in NO.1 lock head, five 45kw machines each in from NO.2 to NO.6 lock head, and one machine in each lock head is used for preparing.

There are two PLC apparatus complementarily for stepless speed regulation in control rooms standing on the two sides of each lock head. The control apparatus protects the valves and gates by the means of shutting them of adjacent steps complementarily.

The centralized control system of each lane of ship lock consists of supervisory computer control system, navigation signal and broadcasting command system, supervisory video control system, etc. Moreover, this system should include automatic detect apparatus for water level, gate opening and ship detecting.

3 VERTICAL SHIP LIFT

3.1 *Main structures and equipments*

The vertical ship lift, cooperating with ship lock, is mainly used as an express for passenger ships and other special ships. The water level conditions of vertical ship lift are the same to that of ship lock. Concerned that 3000t-grade passenger ships and freighters, sailing between Shanghai and Chongqin, climb over TGP, the effective size of the ship lift chamber of vertical ship lift should be 120m×18m×3.5m, the same as NO.3 ship lock in Gezhouba.

Many types of vertical ship lift were researched in different design periods. In initial design period, the type of one-step steel rope hoisted balance heavy is adopted, but in technical design period, this type is substituted by the type of gear-rack climbing finally.

The ship lift lies in left riverside and it is about 1km far from the right side of ship lock. It consists of upper lock head, lower lock head, ship lift chamber, approach channel sharing with ship lock, guide walls, breasting dolphins. On the upper lock head, there a traffic bridge, emergency gate, working gate and their hoistes in turn. The ground elevation of ship lift chamber is 50m. Four columns, whose section size is 16m×50m and top elevation is 196.0m, stand symmetrically along two sides of ship lift chamber. In each column, there are balance well, emergency ladder and lift. On each side of ship lift chamber, there is machine room, sized 120m×20.4m×20m, where the balance rollers and bridge hoist lie.

The outline of ship lift chamber is 132m×23.4m×10m. It weighs 13000 tons lift by 256 steel ropes which are divided into 16 teams and turn over rollers to connect 16 balance units with a balance chain hanging on each unit.

There are four sets of drive systems in the ship lift chamber in total, forming a rigid synchronization system by machine shaft. Also, there are four sets of safe systems in the ship lift chamber. The racks of drive system and the long nuts of safe system are installed in the grooves on the wall of column. The rest apparatus of drive system and the short nuts of safe system are symmetrically installed on the steel platform inserted into grooves on the walls of column on two sides of ship lift chamber. Moreover, there are locking apparatus, tightening structures, portrait guide apparatus, U-shape seal frames, anti-collision apparatus, fire control, transformers, switchboards, hydraulic system and safe evacuation, etc in the ship lift chamber.

The centralized control room is built at the downstream side of columns.

From up to down, there are working gate, emergency gate and hoist on lower lock head in turn. The ship lift chamber ascends from bottom to top or descends oppositely for 9 min.

3.2 *Metal structure*

3.2.1 *Gates and hoist in upper lock head*

The working gate consists of a 17m high plate gate in upper with an U-shape navigation gap controlled by an overturning plate gate, seven stoplogs in lower, each of 3.75m high. The maximum water head of working gate is 15m but it is lift and dropped down in no water head by a single-direction bridge hoist with capacity of 2×2500kN.

The emergency gate, 41.5 high, consists of a plate gate in upper and eight stoplogs in lower. The plate gate is 11m high, weighs 160t. The stoplog is 3.75m high and weighs 90t maximally. The emergency gate is controlled by a single-direction bridge hoist with capacity of 2×2500kN and maximum lift of 70m.

3.2.2 *Ship lift chamber*

The ship lift chamber, a slot-shape steel structure, mainly stands dead weight of water and equipments in chamber and deadweight of itself. The chamber consists of bottom plank, crossbeams and inclined braces.

3.2.3 *Gates and their hoists in lower chamber head*

The working gate in lower chamber head is a sinkage plate gate with a small horizontal gate. It is a double faces structure with multi main beams. And it is supported by a trolley with the span of 27m. The working gate is operating in pressure with two hydraulic locks on its outside and a emergency lock on its top. The small horizontal gate is 18m in clear span and 6.7m in height. The working gate weighs approximately 450t.

The emergency gate in lower chamber head consists of 6 stoplogs which are truss structures, each of 4m high and 50t weighing, totaling in 24m high. It is operated by a crane with capacity of 120t.

3.3 *Machinery equipments*

3.3.1 *Chamber drive system*

The chamber drive system is designed in error depth of 0.1m, and it climbs by gears on racks. This system consists of opening gears, speed reducer, brake, hydraulic springs, ranging arms, alternating current machine, flexing universal joints and hydraulic pumps.

The opening gears are drove by double electric machines and double speed reducers. The gears mesh with the racks laid on the tower columns when chamber is driven up or down. The opening gear box and a set of corresponding safety device are joined by a machinery shaft and a reversing bevel gear box. They are insured in same speed by the means of strictly configuring the speed ratio of main speed reducer.

The speed reducer is a planet gear speed reducer, taking advantage of compact structure, slight weight and large capacity.

There are two sets of brakes in chamber drive system. One is working brake, which is hydraulic handspike type, installed between each electric machine and speed reducer, the other is safety brake, which is hydraulic disk type, installed on the shaft of the end step of speed reducer. There are two types of hydraulic springs in system. One is vertical hydraulic spring used to limit the climbing force of system, the other is horizontal hydraulic spring used to make gears meshed with racks reliably. Sharing a hydraulic pump, those two hydraulic springs work independently. The mechanism of vertical hydraulic spring is described as below: as the meshing force of gears increases because of seepage and overload of chamber, the loads on oil tank and oil pressure increase proportionally. When the meshing force reaches the limit value and the loads on oil tank reach the designed value, the piston rod begins to move. As the piston rod moves to a certain distant, the travel switch on oil tank is started and it sends out signals to shut off the power supply of electric machines automatically. Immediately, the brake works so that the gears and the screw connecting to gear shaft stop rotating. As the piston rod moves, the ranging arm rotates around the central hinge joint in vertical plane. Thus, the vertical displacement of chamber opposite to gears, racks and nut shaft comes forth. As the chamber moves till the threads both on screw and nut shaft contact each other, the chamber is locked safely and the vertical hydraulic spring stops. The horizontal hydraulic spring is maintained in a certain pressure so as to overcome the horizontal component meshing force of gears as they are climbing and horizontal wind loads.

3.3.2 *Accident safety system*

The safety lock mechanism is by the means of “long nut shaft-short screw”, in which many accident cases are concerned in design such as chamber’s leaking dry, water filling, wreck accident happened as chambers are docking, water entering chamber, chamber’s dry overhaul, etc.

The safety system of chamber consists of nut shaft, rotatable short screw, guiding dolly, knight-head, alter angle gears case and transmission shaft. The short screw, installed on the chamber, is connected to gears in the drive system by a mechanical shaft.

The long nut shaft is a hollow notched structure. It is 6.5m long and installed on tower column by a steel adjustment beam. The screw is installed on the chamber by the upper and lower knight-heads and connected to the drive system by the transmission shaft.

3.3.3 *Balance heavy system of chamber*

The balance heavy system consists of heavy team, balance sheave, steel rope and balance chain. There are 16 heavy teams, in same structure, symmetrically arranged on two sides of chamber, each consisting of heavy, additional heavy, guiding frame and connecter and each hung by a balance chain.

3.3.4 *U-shape seal frame in chamber*

In the U-shape seal groove in chamber, there is a seal mechanism, consisting of a seal frame, hydraulic cylinders and the rubber water seal system. There are two layers of U-shape rubber water seal on flanges of the seal frame close to the lift head side, and a C-shape rubber belt, which can shift with frames, close to chamber head side. And there are hydraulic rams installed on the flanges of chamber, several rows of angle wheels installed on the outside wall, top and bottom board of U-shape seal groove.

3.3.5 *Docking lock device*

There are four sets of docking lock devices by the means of “tightening lock”, symmetrically arranged on two sides of the chamber. And there is a steel railway installed on the tower column in the navigation water level variation.

3.3.6 *Longitudinal guiding device*

There are two sets of longitudinal guiding devices symmetrically installed on two sides of chamber center, each including two flexible guiding wheels. And there are two steel railways installed on the division walls of chamber.

3.3.7 *Power supply device*

The total power load of ship lift is about 2000kw. In order to reduce voltage loss in favor of power supply, the high voltage supply is adopted.

3.4 *Civil work*

3.4.1 *Ship lock head*

The upper head, which is a monolithic structure, is 125m long and 62m wide. Its top elevation is 185.0m, and its foundation elevation is 95.0m mostly in upstream side and declined to 48.0m by a slope of 1:0.3. The navigation groove inside chamber is 18m wide, and elevation of its sill is 141.0m. The bottom board of ship lift head is a prestressing reinforced concrete structure.

During construction, two longitudinal and three transversal construction joints are applied in ship lift head temporarily. The longitudinal construction joints are 8m far above the sill. Two upstream transversal construction joints are width slots, which are 0.5m and 1m wide respectively, above the sills and on their watersides. The transversal construction joint on downstream side of lift head is a width slot all along. The others are all keyway joints.

The foundation of upper ship lift head is plagiogranite accompanied with dykes and transversed by the largest blatt F23 and the worst blatt F215 in dam site. There is an impervious curtain in the foundation of ship lift along the dam axis. The criterion of impermeability is described in following: permeability is less than 1 Lu, single or double rows of curtain should insert 5m depth into the impermeable rocks, the back row of curtain should not be deeper than two thirds of the front and the grout boring hole should be 10m to 20m deeper than the lowest excavation elevation of downstream foundation when the impermeable bed is too deep to be touched.

The degree of safety of structure is analyzed by some deterministic generalization models with their corresponding criterions. Analyzed by rigid body limiting balance method, the value of safety factor (kC) of upper lift head should be: KC≥3.0 in normal case, and KC≥2.3 in special case.

3.4.2 *Tower column structure*

The foundation of the tower column is at 48.0 elevation, and its top is at 196.0m elevation. The tower column is a massive concrete structure below 60.0m elevation, above this elevation, it is the balance heavy well which is a membrane structure. There are rack rails of climbing mechanism and nut shaft of safety mechanism installed inside of each column and stairs and lift for traffic and evacuating installed outside of each column. It is 20m far between the front and back column, where a supporting wall with a horizontal section of 9m×2m is arranged and connected to columns by sixteen stringers. On the side of supporting wall facing to chamber, there installed the longitudinal guiding rails of chamber.

There are 12 crossbeams, with net span of 25.8m, arranged from 193m elevation to 196m elevation between the right and left column. The crossbeams are also used as the support of the bridge linking the right and left machine rooms.

Analysis on static, temperature and dynamic by finite element method shows that the stress and deformations in tower column are all in allowance.

4 TEMPORARY SHIP LOCK

The temporary ship lock is a single lane, one step ship lock. The effective size of chamber is 240m×24m×4m, determined by the demand of 3000t fleet at present. Its navigation discharge is 45000 m^3/s. The temporary ship lock is suitable for the following water levels: from 75.5m to 65.7m in upstream and from 71.8m to 65.6m in downstream. It is located on the right side of vertical ship lift. It consists of upper and lower chamber head, chamber, approach channels, guiding structures and breasting dolphins. The upstream approach channel is excavated specially for temporary ship lock while the downstream approach channel is shared with permanent navigation structures.

The main body of temporary ship lock is basically in a slot excavated in rocks. The upper chamber head is a gravity structure. The two vertical side walls of chamber are 0.5m thick reinforced concrete lining structures, of which are impermeable on left and permeable on right. The walls work together with rocks joined by bolts.

The working water head of temporary ship lock is 3.7m normally, but it may be maintained in its maximum value of 6m for a short span before reservoir inpoured. The water conveys in the short gallery centralized in head water convey system. The working valve of system is a plate valve with sharp edges driven by a vertical hydraulic hoist. The chamber's filling or draining is about 8 min per once. The temporary ship lock runs by two means: single or double directions. The interval is 75 min when it runs in double directions while it is 40 min in single direction. The capacity of ship lock in single direction is about 12 million tons annual.

5 CONCLUSION

The navigation structures in TGP include two ship locks and a ship lift. A lot of technical issues were solved during the design and construction periods. The reservoir in TGP has been inpoured to 135m and the two-lane, five-step ship lock has been in operation for almost a year, while the temporary ship lock was dismantled and the ship lift is under building. The adventures of operation of ship locks show that the behaviors of five-step ship lock and temporary ship lock are the same to what they are expected. The ship lift is resisting water but its upper lock head has not been accomplished yet.

This page intentionally left blank.

New Developments in Dam Engineering—Wieland, Ren & Tan (eds),

Hydraulic fracturing of a rock-fill dam during the 1995 Hyogoken-Nambu earthquake

Y.Ohne, K.Narita & T.Okumura
Aichi Institute of Technology, Japan

Y.Nakamura
Aico co., ltd, Japan

ABSTRACT: A large quantity of leakage was detected along the downstream slope of a central core type rock-fill dam, at about one-third of the height from the crest, just after the HyogokenNambu earthquake of January 17, 1995 (M=7.2). Hydraulic fracturing was considered to be the most provable cause of the damage: i.e. Erosion of the core material and successive leakage may have taken place through open cracks, which were generated by shear deformation and/or differential settlement in embankment during the earthquake.

This paper concerns the mechanism and its possibility of occurrence of hydraulic fracturing in rock-fill dam during earthquake. Laboratory seepage fracture tests were conducted on the core materials under various conditions of pore water pressure, overburden confining pressure and dynamic shear stress induced by earthquake, to know what are to be influential factors on seepage failure. FEM dynamic response analysis was also made for different cases of embankment and abutment configuration, to study development process and the extent of damage of hydraulic fracturing during earthquake. The damaged rock-fill dam has already been repaired based on the discussions presented in this investigation, so that the remedial measures taken in the field are briefly reviewed in the paper.

1 INTRODUCTION

An earthquake of magnitude 7.2 happened to occur in the early morning on January 17, 1995, which was given a name as Hyogoken-Nambu earthquake, the epicenter being located in the northern part of Awaji Island. The Hanshin and Awaji area has suffered severe damages by the earthquake, and structures especially near the epicenter, such as buildings, houses, railways, highways, harbors and other public facilities, were destroyed completely.

More than 3,000 dams are located within 200km from the epicenter. About 95 percent of them (about 2,900) are small earth dams and remaining are large dams. Immediately after the earthquake, visual inspections were conducted to confirm safety for 251 dams within a distance of about 200km from the epicenter. The locations of the inspected dams are shown in Fig. 1 [1].

According to the results of inspections, most of small earth dams constructed on soft foundations were damaged by liquefaction of the foundation and/or sliding failure of slopes. On the other hand, severe damages to require emergency protective countermeasures were not reported for large fill-type and concrete dams, except for slight damages of minor cracks near the crest and the increase in leakage observed in several earth and rock-fill dams. The amount of leakage was small enough, and decreased and stabilized within a few weeks. It is naturally accepted for these reasons, however, that the water level was less than one-third from the reservoir bottom when earthquake happened.

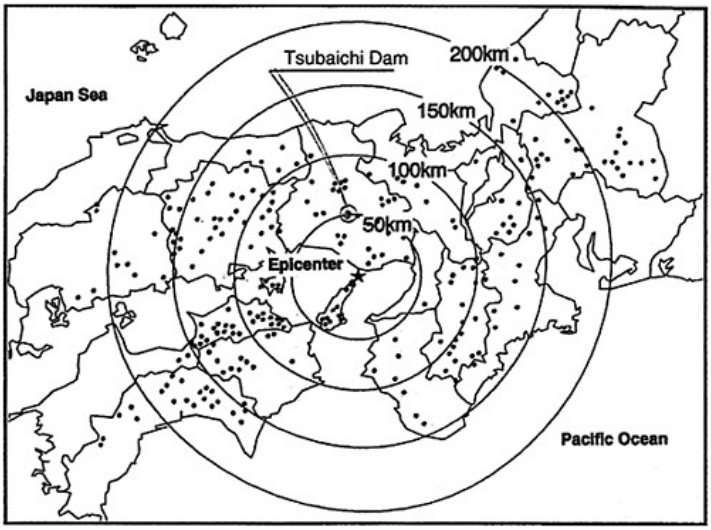

Figure 1. Location of dams.

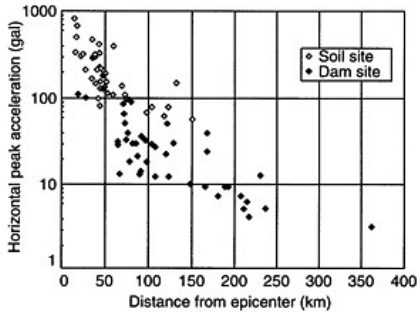

Figure 2. Attenuation of horizontal peak acceleration with distance from epicenter [1].

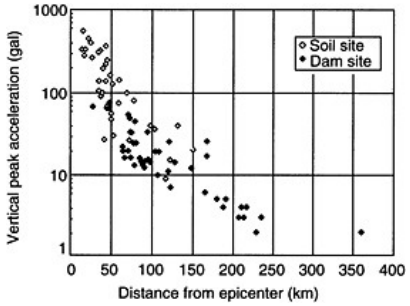

Figure 3. Attenuation of vertical peak acceleration with distance from epicenter [1].

Earthquake motions were recorded at the dams and in the areas of dam-site, as shown in Figs. 2 and 3, presenting the relation of the maximum horizontal and vertical accelerations to the distance from the epicenter. It is noticed in these records that the maximum acceleration was about 185 gals on the rock foundation and about 818 gals on the soil foundation.

2 SEEPAGE PROBLEM

As the amount of leakage water was small and the safety was confirmed in the dams, as mentioned above, impounding of reservoir water started in the early March in most of the dams. Special problem was not found except for a rock-fill dam with central core. The standard cross section of the

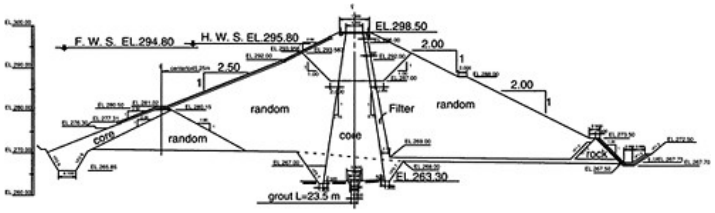

Figure 4. Standard cross section of Tsubaichi dam.

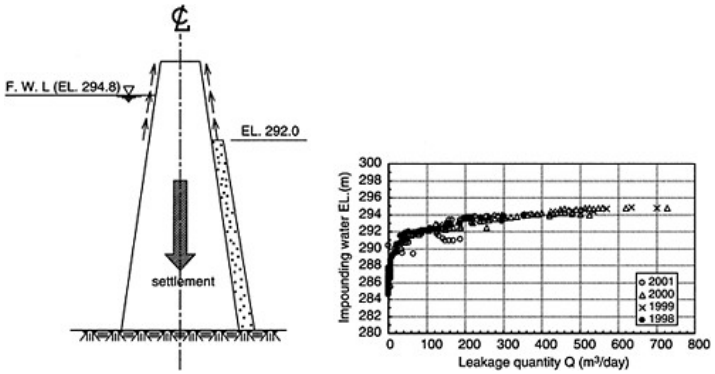

Figure 5. Relation between water level and leakage quantity.

dam is shown in the Fig. 4. The event happened when the water level reached up to about El.292m, where a large amount of leakage appeared unexpectedly. The quantity was not so large, however, to anticipate a dam failure. Figure 5 shows the relation between elevation of the impounded water and the quantity of leakage. This could be considered as a phenomenon accompanied by the settlement of the core.

3 DAMAGE OF FILL-TYPE DAMS CAUSED BY EARTHQUAKE

According to the recent reports on the damages of fill-type dams caused by big earthquakes, seismic damages can be classified into two categories; (1) the transverse cracking at the crest of the dam near the abutment foundation and (2) the longitudinal cracking appearing along the crest of dam. The former type of cracking could lead leakage of the reservoir water and internal erosion through the core and the latter can be causes of sliding failure of slopes.

4 MECHANISM OF HYDRAULIC FRACTURE [2],[3]

Hydraulic fracturing takes place due to the decrease in confining stress acting on the soil, which in turn is caused by the differential settlement in the core. In Fig. 6(a), for instance, differential

settlement is induced by the earthquake force and/or some other causes near the abutment foundation, and it causes reduction in the lateral confining pressure (σ_3). In Fig. 7(a), settlement near the turning point of the core width induces arching action and decrease in the vertical confining pressure (σ_1), which must be the cause of hydraulic fracturing. Figure 6(b) and Figure 7(b), respectively, represent these stress conditions by Mohr's stress circles. As indicated by the dotted lines, reduction in the confining pressure may shift the stress circle to the left and get it closer to the failure envelope to lead a state of hydraulic fracturing.

4.1 *Laboratory tests on hydraulic fracturing*

In order to discuss the possibility of hydraulic fracturing for situations mentioned above, the following two series of laboratory seepage tests were carried out in this study.

Test-1 realizes the stress states shown in Fig. 6. From the initial uniform stress state of $\sigma_1=\sigma_3$ in the tri-axial compression apparatus, the minor principal stress σ_3 is decreased gradually, under a seepage condition of constant hydraulic gradient, to produce the final state of seepage fracture.

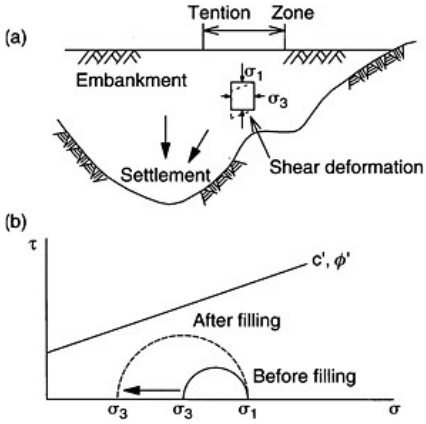

Figure 6. Stress change due to differential settlement.

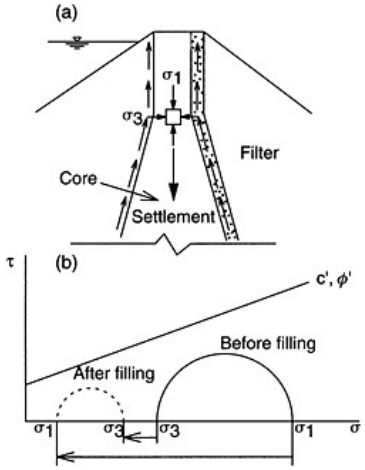

Figure 7. Stress change due to arching.

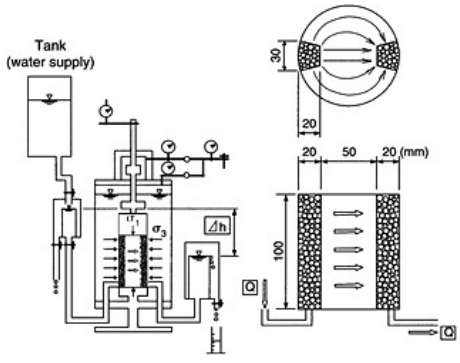

Figure 8. Seepage test apparatus for Test-1 series.

Test-2 realizes the stress state presented in Fig.7. Seepage fracture tests are conducted under a constant effective vertical stress (σ'_v), by increasing the hydraulic gradient step by step, to obtain the final value of hydraulic gradient (i_f) at fracture.

4.2 *Apparatus and samples*

The testing apparatus for Test-1 and Test-2 series are schematically illustrated in Fig. 8 and Fig. 9, respectively. Water flows from one side to the other as shown in Fig.8 and from the center to the two end points in Fig.9, with a head difference of Δh.

Grain size distribution curves of the materials used in the test are shown in Fig.10, in which the material of (a) SM and (b) SC are used for Test-1 and Test-2, respectively. The specimens are

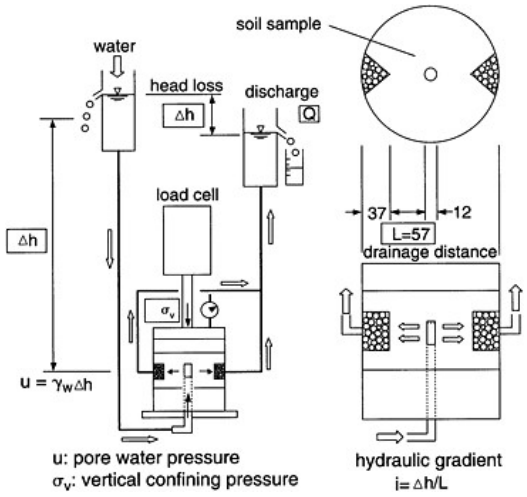

Figure 9. Seepage test apparatus for Test-2 series.

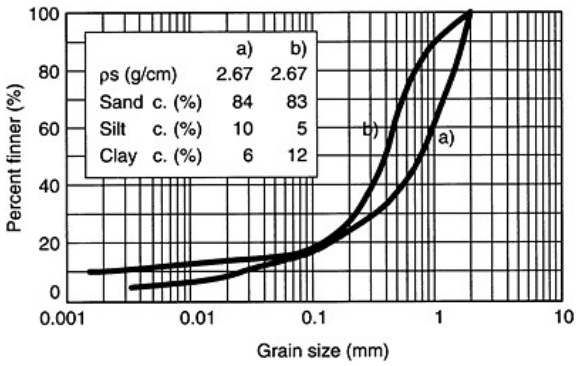

Figure 10. Grain size distribution of fill materials used in tests.

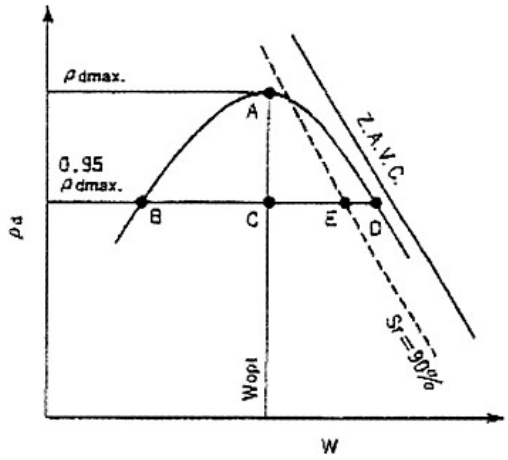

Figure 11. Compaction conditions of test specimens.

Table 1. Summary of seepage test conditions.

	Test-1	Test-2
Stress and seepage conditions	Initial state: $\sigma_1=\sigma_2$; σ_1=100, 200, 300 (kPa) i=5, 10, 20 σ_3: gradually decreasing	σ_v=50 (kPa); σ'_v =10, 20, 40 (kPa) i: gradually increasing
Specimen		
Test point	B C D	E
Density	0.95×ρ dmax (ρ dmax=1.86g/cm3)	0.95×ρ dmax (ρ dmax=1.85g/cm3)
Water content W (%)	9.4, 13.7, 16.8	17.6
Deg. of sat. Sr (%)	49.1, 71.6, 87.8	90.0

prepared in the laboratory to satisfy the specified compaction conditions of dry density and water content, as shown by points B, C and D for Test-1 and the point E for Test-2 series in Fig. 11. Details of the test conditions are summarized in Table-1.

4.3 *Test result in Test-1 series*

The results of the Test-1 series are summarized in Figs 12 and 13. The relationship between the discharge (Q) and the effective stress ratio (ob/oc) defined in the column is shown in Fig.13. It is clearly seen in the figure that the discharge from the specimen increases due to the increase in the stress ratio, showing an abrupt change at a certain stress condition. The value of the critical stress ratio $(ob/oc)_f$ defined by the point is plotted against the value of the hydraulic gradient at failure (i_f) in Fig. 13 for different compaction conditions. It is recognized in the figure that for samples having the same dry density a higher resistance can be expected to achieve against hydraulic fracturing as the wet side of the optimum.

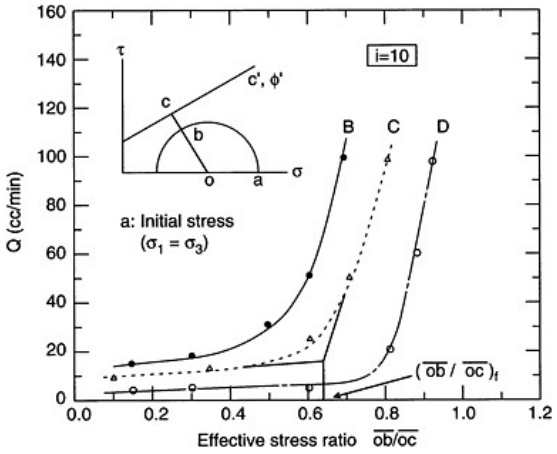

Figure 12. Discharge vs. stress ratio (Test-1).

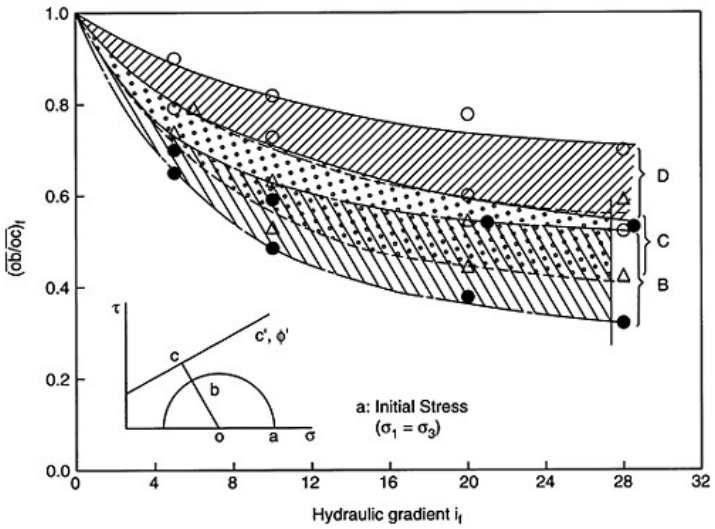

Figure 13. Stress ratio at failure (Test-1).

4.4 *The test results in Test-2 series*

A representative test result of σ'_v=40kPa is shown in Fig.14, taking the discharge (Q) from the specimen on the ordinate and the hydraulic gradient (i) on the abscissa. Solid lines are drawn in reference to the constant coefficient of permeability, where the Darcy's law of v=ki for the state

of the laminar flow is satisfied. It is seen that solid circles move along these straight lines of constant k-value in the early stage of the test, showing however an abrupt change in the discharge (Q) at around i=40. The critical value of the hydraulic gradient (i_f) can then be defined at the point of i_f=40 for the case of σ'_v is summarized in Fig. 15, for the results of the present study by solid circles and for other tests on SM to CL materials by open circles.

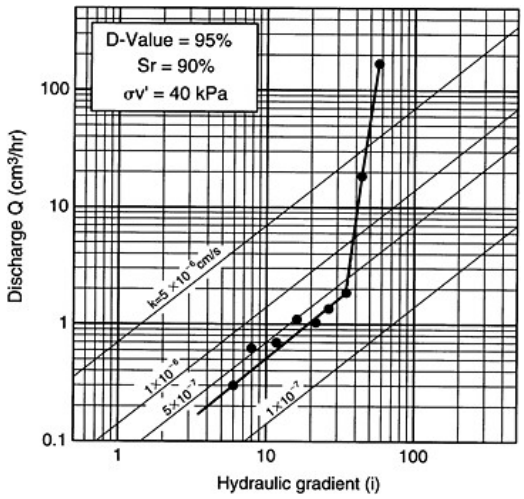

Figure 14. Discharge vs. hydraulic gradient (Test-2).

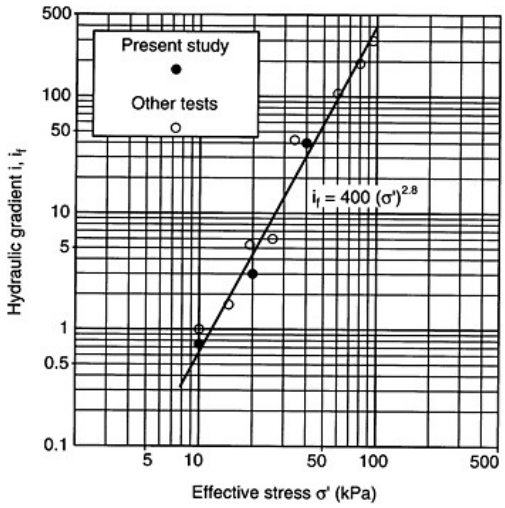

Figure 15. Hydraulic gradient at failure (Test-2).

5 FEM DYNAMIC RESPONSE ANALYSIS

Analysis procedures and conditions employed here are summarized below.

(1) The analysis is done for Tsubaichi rock-fill dam with a centrally located core shown in Fig. 4.
(2) Two dimensional analysis may be reasonable as a first step to understand dynamic behavior of the dam and to evaluate their possibility of hydraulic fracturing during earthquake.
(3) The analytical procedure adopted here is basically the same as the QUAD-4 program, where non linear material properties of dynamic behavior are represented by the Hardin-Drnevich model.

6 EVALUATION OF HYDRAULIC FRACTURING AND DISCUSSIONS

Evaluation of safety against hydraulic fracturing is made here by using the results of the dynamic analysis, as shown in Fig.16, where the relationship between the critical stress ratio $(ob/oc)_f$ and the hydraulic gradient at failure (i_f) presented in Fig. 13 is redrawn in a more precise form. In this figure, the stress ratio which leads to hydraulic fracture is obtained corresponding to the value of the hydraulic gradient at failure (i_f), and the safety factor can be evaluated as the ratio of the stress ratio at failure to that at the present state. Assuming that i_f=2.0 for the soil compacted in the state of B, for example, the value of the stress ratio at failure can be determined from the upper solid line as $(ob/oc)_f$=0.95. If the value of the stress ratio calculated in the dynamic response analysis is taken as (ob/oc)=0.93, the safety factor (F_s) becomes to be F_s=0.95/0.93=1.02. This suggests a little safety against hydraulic fracturing, however, as this value is almost equal to F_s=1.0, so that possibility of fracture can be anticipated on this dam. It can thus be considered that the

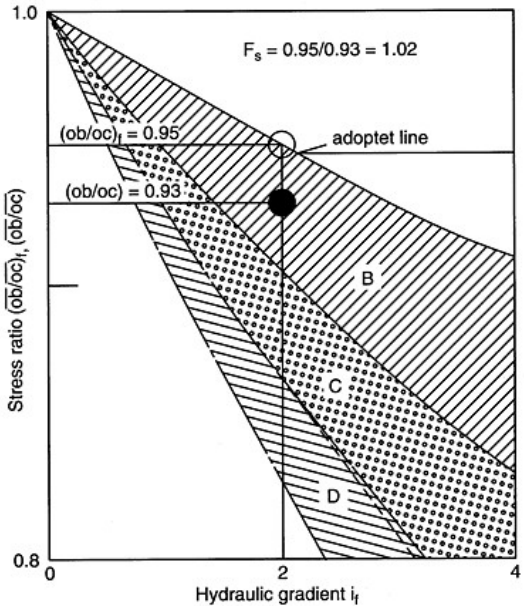

Figure 16. Safety evaluation with stress ratio.

proposed method is in general appropriate. More details on the evaluation of hydraulic fracturing and remedial measures taken in the dam will be reported at the conference.

7 CONCLUSIONS

(1) Hydraulic fracturing in embankment dams can be reproduced in the laboratory by two types of seepage fracture tests, which realize different situations of stress states in the field at failure.
(2) In the evaluation of the possibility of hydraulic fracturing, a practically useful procedure is presented by combining the results of FEM analysis and those from laboratory seepage tests, by examining the relationship between the critical stress ratio and the hydraulic gradient at failure.
(3) The proposed evaluation method of hydraulic fracturing indicates critical value for a rock-fill dam with a high leakage after the earthquake, suggesting its satisfactory application in practice.

REFERENCES

[1] Suzuki, A. (1996): Characteristics of Hygoken-Nambu Earthquake Motion, *US-Japan Earthquake Engineering Workshop.*
[2] Ohne, Y. and Narita, K. (1978): Some Considerations on the Teton Dam Failure. *Technical report of Aichi Institute of Technology,* No.13: pp. 217–229 (in Japanese).
[3] Murase, Y. et al. (1995): Study on Hydraulic Fracturing of Core-type Rockfill Dams. *The MWA Int. Conf. on Dam Eng.,* pp. 363–371.

New Developments in Dam Engineering—Wieland, Ren & Tan (eds),
© 2004 Taylor & Francis Group, London, ISBN 04 1536 240 7

Evaluation of in-situ strength of rock fill material taking into account of in-situ density and strength by laboratory test

T.Okamoto
Central Research Institute of Electric Power Industry, Japan

ABSTRACT: The density of rockfill material heavily affects on the mechanical property because of non-cohesive material, but evaluation of in-situ density of rockfill material has been difficult issues due to large particle size. This paper studies compaction degree of rockfill material by the existing results of several in-situ rolling compaction tests, and density and confining pressure dependency of already tested strength data of rockfill material. Rockfill material of older dams were dumped, so the density was loose or medium dense. Crest settlements after embankment of dams, which are constructed after almost 1960, were greatly smaller because of heavy compaction roller. Investigated tests consist of large triaxial compression test, and most of Japanese strength tests are based on 30cm of diameter and Marsal, RJ. (1973) with 1130cm of diameter is contained. Rockfill material strength in Japan indicates higher than other countries especially in case of very dense density, and rockfill material strength consisting of shale and slate shows lower. Internal friction angle of rock material except shale and slate shows higher than 40° even with loose condition.

1 INTRODUCTION

In Japan 2 kinds of dam design codes have been applied, one is "Design standard of dam" (Japanese Conference of Large Dam: 1978, called "basic standard" below) and "Draft on technical standard of river disaster prevention by Japanese construction ministry" (Japanese association

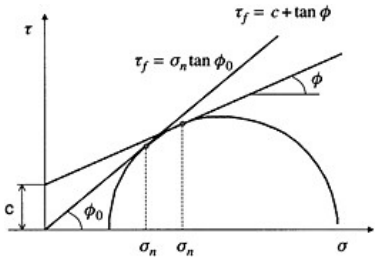

Figure 1. Expression methods of strength of rock fill material.

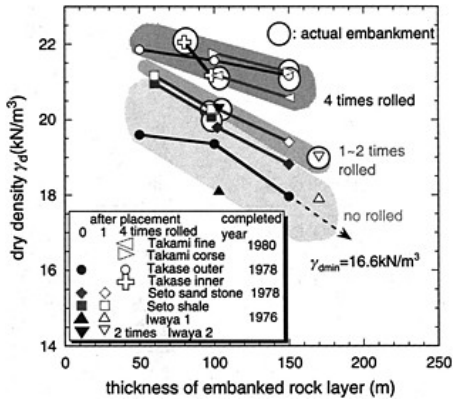

Figure 2. In-situ density by rolling compaction test.

of river: 1986, called “ministry standard”), another is “Draft on guideline of seismic design of fill dam” (Development division of river department of Japanese construction ministry: 1991, called “new seismic code”). “Basic standard” is an original code of “ministry standard” and based on static equivalent seismic coefficient. And “new seismic code” is based on modified static seismic coefficient.

“New seismic code” suggests 3 following expression methods of strength of rock fill material.

(3)

τ_f: shear strength, σ_n: normal stress at failure, *c:* cohesion, φ: internal friction angle *A, b:* material constants.

$$\phi_0 = \sin^{-1}\{(\sigma_1-\sigma_3)_f/(\sigma_1+\sigma_3)_f\} \quad \sigma_1,\sigma_3 : \text{maximum and minimum principal stress}$$

σ_1, σ_3 : maximum and minimum principal stress

Then expression (3) is based on the following relation.

$$\phi_0 = \phi_{max} - a\log(\sigma_n/\sigma_{n0}) \quad (\sigma_n \geq \sigma_{n0})$$

$$\phi_0 = \phi_{max} \quad (\sigma_n \leq \sigma_{n0}) \quad \sigma_{n0}: \text{unit stress } (\sigma_{n0} = 0.3\times 9.8kN/m^3 \text{ by "new seismic code"})$$

$$\phi_{max}: \ \phi \text{ if } \sigma_n = \sigma_{n0} \quad a: \text{material constant}$$

“Basic standard” and “ministry standard” regard c=0 in many cases even if laboratory test shows $c\neq 0$, so design strength of rock fill material is c_{de}=0 $\phi_{de} = \phi$ by equation (1). “New seismic code” recommends (2) and (3), and their material constants based on laboratory test. Therefore 2 kinds of Japanese dam design codes apply different strength and different seismic force.

There is an important item to determine design strength and it is to apply the strength corresponded to in-situ density. However strength of rock fill material is investigated in laboratory and in-situ density is evaluated by in-situ rolling compaction test. And design strength is usually determined by laboratory test result before rolling compaction test and embankment work.

In this study, already done result of in-situ rolling compaction test and laboratory triaxial compression test are reviewed and dependency of confining pressure and density is discussed. Finally design strength of rock fill material is considered.

Table 1. Estimation of in-situ density.

Dam material rock type	Takase outer granite	Takase inner diorite	Seto sand stone	Seto shale	Iwaya I rhyolite	Iwaya II rhyolite
Minimum dry density γ_{dmin}	16.64	17.84	17.84	17.84	17.64	17.64
Maximum dry density γ_{dmin}	21.85	22.54	21.56	21.56	21.76	21.76
In-situ dry density γ_{dmax}	21.17	22.05	20.19	20.19	19.01	20.19
Maximum void ratio e_{max}	0.561	0.456	0.456	0.456	0.472	0.472
Minimum void ratio e_{min}	0.188	0.152	0.205	0.205	0.194	0.472
In-situ void ratio e	0.227	0.178	0.286	0.286	0.366	0.286
In-situ relative density D_r %	90	91	65	65	38	67
In-situ compaction degree D %	97	98	94	94	87	93

Unit of dry density: kN/m^3 assumed to be G=2.65.

2 CONSIDERATION ON IN-SITU DENSITY

2.1 *Density degree by rolling compaction test*

Figure 1 and Table 1 shows already done results of rolling compaction test for 4 dams in Japan (Kansai Electric Power Company, 1970–1992; Tokyo Electric Power Company, 1979; Chubu Electric Power Company and Japanese agency of water resource development, 1977; Hokkaido Electric Power Company, 1981; Kyushu Electric Power Company, 1986). According to them, it found that thickness of rock fill layer and rolling number are important parameters and 4 dams applied different actual embankment method.

Also it found that older dam applied thicker layer and smaller rolling number such as Iwaya. Before 1975 many dams adopted dumped method, and for example high lift dump means dropping from 10–30m height and low lift dump from almost 5m.

Let's try to estimate density degree although maximum and minimum densities are not clarified except Takase dam. Minimum density is assumed to be one in 2m of thickness of embankment layer and no rolled case, and maximum density is assumed to correspond to 0.5m of thickness of embankment layer and 4 times rolled case. Calculated result is indicated in Table 1. Here 2 parameters selected to evaluate density degree are

$$\text{compaction degree } D=\gamma_d/\gamma_{d\max} \tag{4}$$

and

$$\text{relative density } D_r=\frac{e_{\max}-e}{e_{\max}-e_{\min}}=\frac{\gamma_d-\gamma_{d\min}}{\gamma_{d\max}-\gamma_{d\min}}\cdot\frac{\gamma_{d\max}}{\gamma_d} \tag{5}$$

Here, $\gamma_{d\max}$, $\gamma_{d\min}$: maximum and minimum dry density, $e_{\max}$, $e_{\min}$: maximum and minimum void ratio.

According to calculated result shown in Table 1, it is found that most of calculated Ds are larger than 90%, and this is empirically acceptable. On the other hand, D_r=38~91 and is sensitive to density condition, so it is easy to recognize density conditions such as very dense, dense, medium dense or loose as mentioned later in Table 2.

Also it is noted that D_r can clarify the influence of embankment method as above mentioned such as Fig. 3 basing on the result of Fig. 2. Especially placement work heavily affects on D_r rather than number of rolling compaction, because rockfill material is compacted with placement work so as to make the placed layer thin.

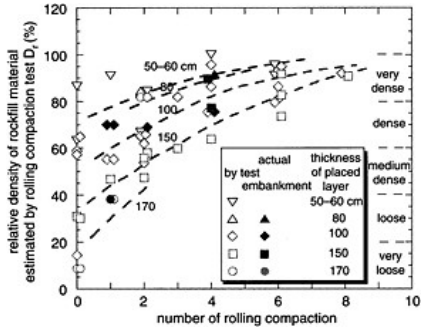

Figure 3. Relative density and number of rolling compaction.

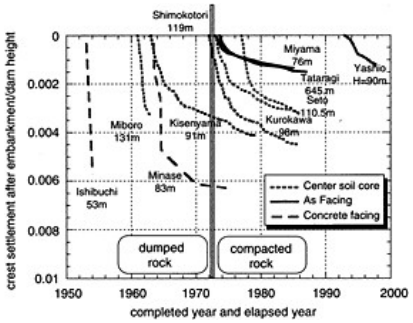

Figure 4. Crest settlement of Japanese dams after embankment and embankment method.

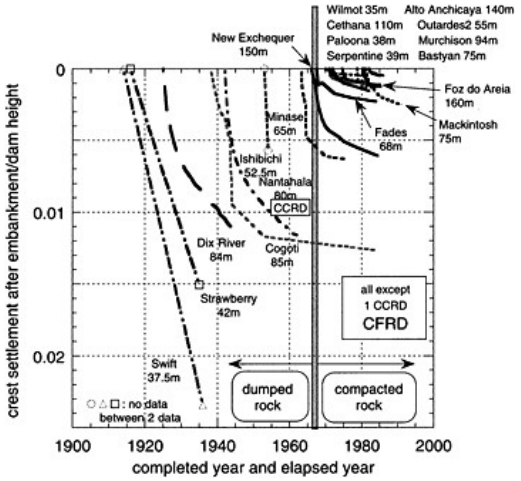

Figure 5. Crest settlement of CFRD after embankment and embankment method.

2.2 *Effect of embankment method on in-situ density and long-term settlement*

It found that embankment method affects on density of rockfill material in previous section. The density leads the deformation and strength property, so in this section long-term settlement after embankment is investigated. Figures 4 and 5 show crest settlement after embankment and embankment method for Japanese dams and CFRD (Concrete Facing Rockfill Dam) except one.

Figures 4 and 5 indicates that embankment method greatly affects on the settlement after embankment, and crest settlement of compacted rock zone ceased till 10 years after completed embankment although dumped rock zone continued to settle almost for 2 decades. Crest settlement after embankment/dam height reached almost 0.005–0.02 in case of dumped rock and it became to be smaller for newer dam. On the other hand Crest settlement after embankment/dam height in case of compacted rock is almost 0.001–0.003 for several years elapsed.

Figure 4 includes center soil core type rockfill dam. Rock zone was dumped before 1972 and compacted after 1973, however each soil core was compacted. But ceased value of crest settlement/dam height before 1972 is a little bit larger than that after 1973. So there is some affect of embankment method of rockfill on crest settlement.

It is noted that changed time from dumped to compacted method in Fig. 3 is different from that in Fig. 5, it is 1972 in Japan and 1967 in other countries. Finally it concluded that density condition can be assumed to be loose to medium dense in case of dumped rock and medium dense to dense in case of compacted rock by embankment method.

3 STRENGTH BY LABORATORY TEST

3.1 *c, ϕ and design strength*

Individual sample strengths are collected in Japan and other countries and Japanese data are divided to 2 for dam owners of Electric Power Company and others (Kansai Electric Power Company, 1970–1992; Tokyo Electric Power Company, 1979; Chubu Electric Power Company and Japanese agency of water resource development, 1977; Hokkaido Electric Power Company, 1981; Chubu Electric Power Company, 1991; Kyushu Electric Power Company, 1986) (Kaneko et al. 1988, Kawaguchi et al. 1986, Terakawa et al. 1986, Kishi 1986, Committee of test and design

Table 2. Density and sample preparation to evaluated test result.

Density condition	Relative density	Compaction energy (E_{cJIS})
Very loose	<20%	–
Loose	20–40%	0–0.3
Medium dense	40–60%	0.3–0.5
Dense	60–80%	1.0–1.5
Very dense	80–100%	2.0<

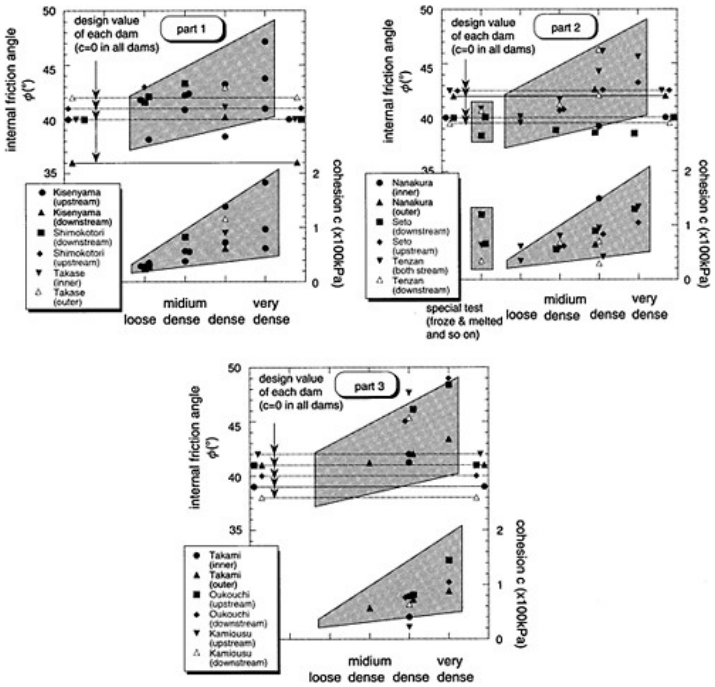

Figure 6. Internal friction angle and cohesion by large triaxial compression test.

strength of rock fill material: 1982, Nagai, 1976, Komyouji et al. 1975, Nagano 1975, Ukaji 1975). Data in other countries are referred from Marsal, R.J. 1973, Zeller et al. 1957, Lowe: 1964, Leps 1970. All test methods are based on triaxial compression tests and Most of their diameters are larger than 30cm and all diameters in Japan are 30cm. Rockfill materials are classified according to their placement position such as upstream or downstream side and inner or outer.

2 sample preparation methods are applied and they are vibration and compaction method. So 2 parameters of relative density and compaction energy are selected to evaluate density condition, such as Table 2 referring Meyerhof's classification. Table 2 does not contradict with Akashi: 1985,

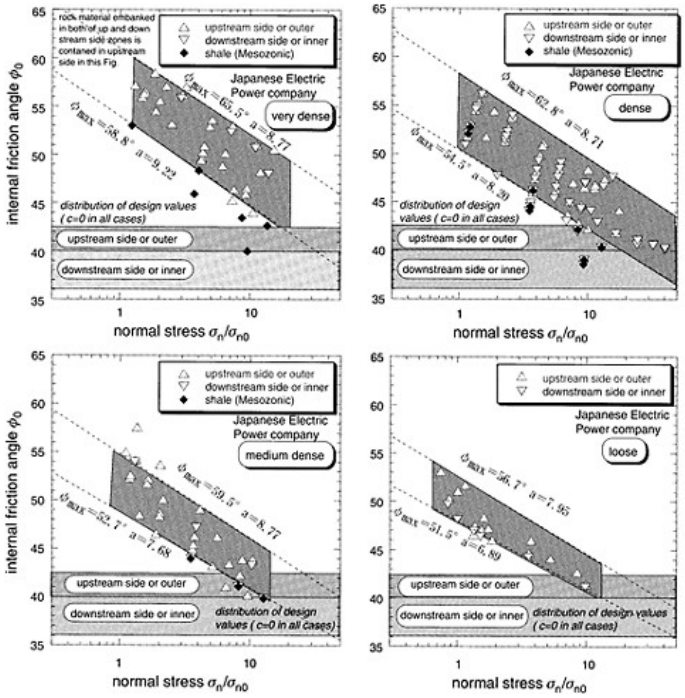

Figure 7. Strength of rock materials of Japanese Electric Power companies dams.

which concluded that rock material had high density close to the density corresponding to 1.0 E_{cJIS} if adequate in-situ rolling compaction was applied as embankment method. Besides "very loose" of density condition is not applied later because placement work of rockfill material does not lead to very loose condition.

Figure 6 presents *c*, ϕ obtained by triaxial tests, and therefore design strengths are lower than strengths obtained triaxial tests. However in-situ density condition were not clear. It is concluded that in-situ density condition should be investigated and appropriate strength expression should be applied instead of expression (1) because there is some possibility to overestimate strength at low confining pressure if applying expression (1).

3.2 *Detailed strength distribution*

Strength expression (2) and (3) are appropriate to evaluate detailed strength, and $\tau_f = \sigma_n \tan \phi_0$ (3) can evaluate individual strength. So (3) is applied here.

3.2.1 *In Japan*

Figures 7 and 8 indicate sample strengths for dam owners of Electric Power Company and others each other. Classifying density condition strength of rockfill material in Fig. 7 distribute in agreement

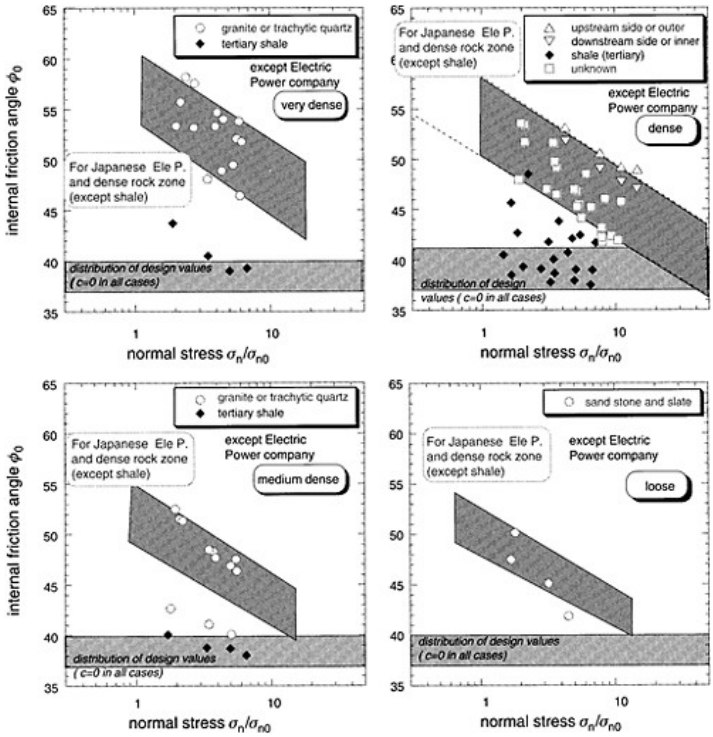

Figure 8. Strength of rock materials of Japanese dams except J. Ele. P.companies.

with that in Fig. 7. Strength of shale is lower than other rock types, which are sandstone, granite, schist, rhyolite, and diorite.

Also Strength of rockfill material placed in upstream side or outer is a little bit higher than that in downstream side or inner. Because rock zone in upstream side or outer always suffer some weathering from high and low temperature, snow, rain, drying and so on, so rockfill material with higher strength were usually placed in upstream side or outer.

They have C_H and/or C_M class rock in many cases, although many of rockfill material placed in downstream side or inner has C_M and/or C_L class rock. C_H class rock is a little bit soft and weathered, D class means heavily soft and weathered, C_L soft and weathered and C_M medium soft and weathered.

3.2.2 *In other countries*

Figure 9 shows results of Marsal: 1973, Zeller & Wullimann: 1957 and Lowe: 1964 corresponding to density condition, and also includes the review by Leps: 1970 and the result in Fig. 7 and 8.

Figure 9 makes clear following things. One is that strength of very dense and dense material in Japan is higher than that in other countries, and strength of medium dense and loose material in Japan has good agreement with that in other countries. Two is that rockfill material consisted of shale and slate has lower strength comparing with other rock types, and rockfill material consisted of shale and slate in other countries has same strength as rockfill material consisted of shale in Japan.

The reason why strength of very dense and dense material in Japan is higher than that in other countries is not clear even by checking test method and so on in detail. It may be sample preparation

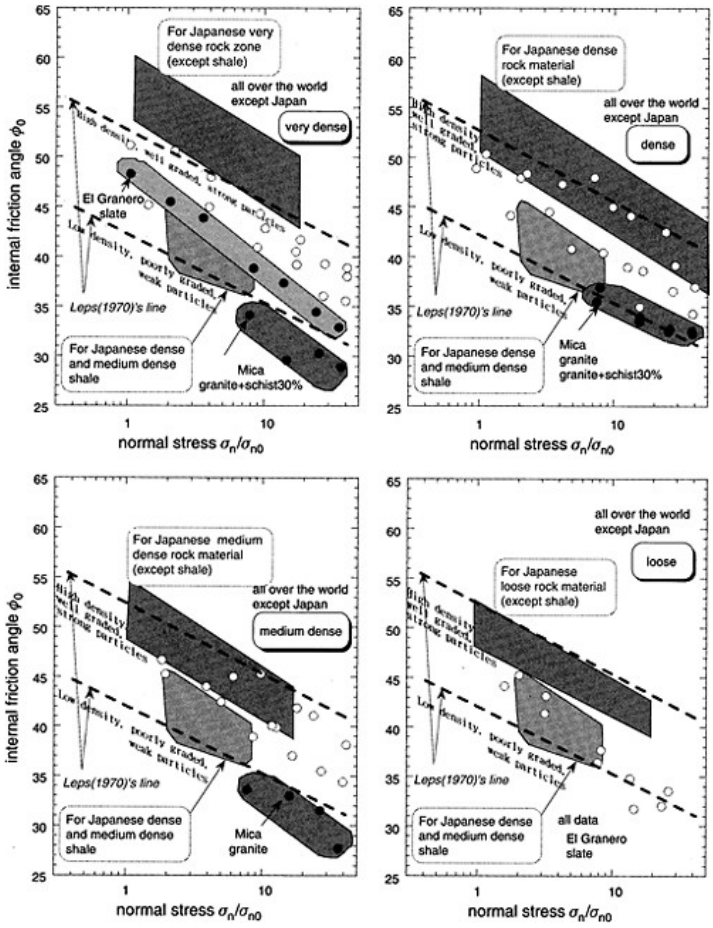

Figure 9. Strength of rock materials of all over the world dams except Japanese dams.

method and rock class including weathering. Especially in Japan rockfill material usually was selected corresponding to placement position such as outer or inner and upstream or downstream side. And the reason why rockfill material consisted of granite of Mica dam is not clear, it may relate weathering, because granite is usually very hard or very soft if weathered.

3.2.3 *Summary*

Figures 10 and 11 indicate the summary of strength distribution and average of all over the world each other. Strength distribution and average strength in other countries has good harmony with them in Japan excluding that strength of very dense and dense material in Japan is higher than that in other countries.

Table 3 summarizes constants of upper, lower and average strength for density and embankment placement position in Japan.

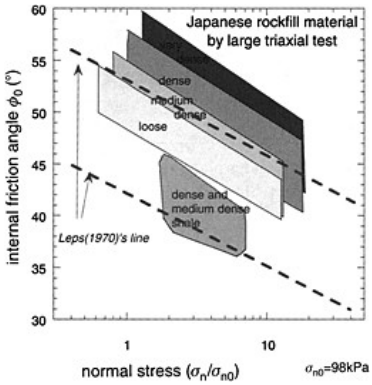

Figure 11. Average strength of all over the world.

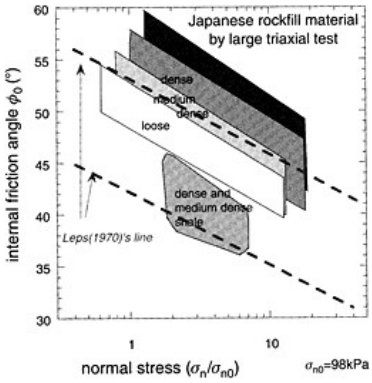

Figure 10. Strength distribution of all over the world.

Table 3. Strength constant for density and embankment placement in Japan.

Density condition	Upper/lower/ average	Upstream side or outer		Downstream side or inner		Downstream side or inner shale	
		ϕ_{max}	a	ϕ_{max}	a	ϕ_{max}	a
Very dense	Upper	65.5	8.77	–	–	–	–
	Lower	–	–	58.8	9.22	–	–
	Average	64.2	10.6	58.9	8.30	59.7	11.4
Dense	Upper	62.8	8.71	–	–	–	–
	Lower	–	–	54.5	8.20	–	–
	Average	60.8	9.90	58.2	9.10	59.7	13.1
Medium dense	Upper	59.5	8.77	–	–	–	–
	Lower	–	–	52.7	7.68	–	–
	Average	61.0	13.0	60.7	12.7	51.8	7.40
Loose	Upper	56.7	7.95	–	–	–	–
	Lower	–	–	51.5	6.89	–	–
	Average	54.4	8.60	52.1	7.30	–	–

4 DESIGN STRENGTH OF ROCKFILL MATERIAL

4.1 *Applicability of* c=0 *method*

c=0 method is applying for static seismic coefficient method, but design strength is not reduced for static modified seismic coefficient method in Japan. And both of final safety coefficients are 1.2. Generally speaking 3 factors of strength, stability evaluation method and safety coefficient must have good harmony. However strength of embankment material can correctly have been evaluated, because test apparatus and other test method have been revised. Besides the reason why design strength is not reduced for static modified seismic coefficient method depends on recent revised technique as above mentioned. Therefore it is necessary to evaluate the correct strength of embanked material.

Table 4. Difference between actual and laboratory strength.

	Difference between actual condition and laboratory		
	Related factor	Content	Should take into account
Test method	Actual shear mechanism	Actual shear mode is close to direct shear and under plane strain, althogh usual test mode is triaxial compression. Strength by direct shear is generally larger than that by triaxial compression and the difference is usually a margin.	Δ
	Earthquake	The difference between actual strength and laboratory strength based on dynamic cyclic test and monotonic static test has been evaluated, it found that the material with loose density exhibites the strength decrease under undrained condition and drained strength is close to monotonic static strength.	Δ
Test condition	Stress	The dependency of confining stress is mainly evaluated in design. Stress history does not affect the strength.	×
	Drainage	Drainage condition affects strength decrease in case of loose condition and also permeability affects drainage condition.	Δ
Sample	Rock type rock class	Effect of rock type on strength is important and CM and CH class are usually applied and sometimes CL.	◎
	representation	Mechanical change exhibites in in-situ because of a large quantity.	×
	durability	Rock zone is exposed to temperature, sun, weather, snow, freezing and drying. Freezing is prohibited in surface shallower than 1m.	□
Specimen	Grading/D_{max}	Maximum particle size D_{max} is usually 400~1500mm, the effect on strength is not so large in case of D_{max} >500mm and the rock material with $D_{max} \fallingdotseq 500\,mm$.	Δ
	Embankment method	To take in to account of roller type rolled number and density distributed with depth.	◎
	Density	To evaluate density condition because D_{max} and embankment method affect in-situ density D_{max}.	◎
	Water content	To take into account the placement at upstream or downstream side.	◎

4.2 *Factors to evaluate strength of rockfill material*

Some factors are picked up to evaluate design strength of rockfill material as show in Table 4 referring to Japanese Geo-technical society: 1986. Table 4 especially focuses on the difference between actual and laboratory strength for their factors and whether it should be taken in account to evaluate design value of rockfill material from view point of recent technical advance.

Many factors should be taken into consideration to evaluate strength of rockfill material, however density-dependency, confining pressure-dependency of the strength and rock class including weathering are most important.

4.3 *Design strength*

In-situ rolling compaction tests indicate that dumped method leaded to loose or medium dense condition and compacted method leaded to medium or dense condition as above mentioned. However detailed density degree will be evaluated. So some item is suggested in present time.

Figure 12 summarizes dependency on normal stress and density of rockfill material except for rockfill material consisted of shale and slate. Due to Fig. 12, it found that internal friction angle

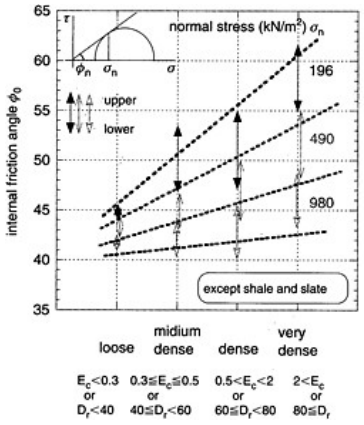

Figure 12. Dependency on normal stress and density.

shows bigger than 40° even for loose condition. Usually very loose condition shows residual strength, so it can be applied bigger strength than 40° as design strength.

Usually static critical slip line is close to embankment surface for granular soil and residual deformation by earthquake shows bigger surface strain (T.Okamoto et al., 2004). Usually seismic slip circle by static seismic coefficient method has 20m of depth at maximum deep position, so normal stress is almost 400 kPa in maximum. As design strength 40–45° can be applied taking in account of density and confing pressure.

5 CONCLUSION

Conclusion is summarized as followed.

(1) Embankment method affects on the density of rockfill material and it changed at 1960's and/or 1970's. And it reflected the long-term settlement of rockfill dam. Embankment method is classified to dumped and compacted method with the boundary of 1960's and/or 1970's, and in-situ rolling compaction tests indicate that dumped method leaded to loose or medium dense condition and compacted method leaded to medium or dense condition.
(2) Laboratory tests results shows that rockfill material in very dense and dense condition in Japan has higher strength than in other countries, however rockfill material in medium dense and loose condition has no difference of the strength between in Japan and other countries. And rockfill material consisted of shale and slate and so on shows lower strength than granite, sandstone and so on.
(3) Many factors should be taken into consideration to evaluate strength of rockfill material, however density-dependency, confining pressure-dependency of the strength and rock class including weathering are most important.

REFERENCES

1) Japanese Conference of Large Dam (1978): Design standard of dam
2) Japanese association of river (1986): Draft on technical standard of river disaster prevention by Japanese construction ministry, Sankai-dou
3) Development division of river department of Japanese construction ministry (1991): draft on guideline of seismic design of fill dam

4) Japanese Geo-technical society (1986): deformation and strength of coarse particle material
5) R.Akashi (1985): control of the density of rock material and confirmation of the strength, Tuchi-to-kiso, vol. 33, No. 6, pp. 19–24
6) Kansai Electric Power Company (1970–1992): Construction records of Kisenyama, Shimokotori OkuYoshino and Oukouchi electric power plants
7) Tokyo Electric Power Company (1979): Construction records of electric power development of Takase river
8) Hokkaido Electric Power Company (1981): Construction records of Takami and Kyougoku electric power plant
9) Chubu Electric Power Company and Japanese agency of water resource development (1977): Construction records of Iwaya dam
10) Japanese society of electric civil engineering (1981): Recent fill dam engineering, Sankai-dou
11) T.Okamoto (2001): Recent measurements of residual settlement of rockfill dams induced by earthquakes and some consideration of their influenced effects, 46th geo-technical engineering symposium, Japanese society of geo-technical engineering, pp.65–70
12) Kyushu Electric Power Company (1986): Construction records of Tenzan and Omarugawa power plant
13) Chubu Electric Power Company (1991): Construction records of Oku-Mino power plant
14) T.Kaneko, Oomoto, and E.Sumitani (1988): On the design and embankment work (part 2)—property of excavated material, symposium of dam technique, Japanese society of large dam, pp.12–29
15) T.Kawaguchi and Y.Kougo (1986): Static shear strength of rock fill material, Symposium of deformation and strength of coarse material and test method for it, Japanese society of soil engineering, pp.61–68
16) Y.Terakawa, H.Hasegawa and K.Honda (1986): A example of strength change of rock fill material from saturation to instauration, Symposium of deformation and strength of coarse material and test method for it, Japanese society of soil engineering, pp.81–84
17) Y.Kishi (1986): A example of rock fill material using soft rock—On the test and design strength of M dam applying shale, Deformation and strength of coarse fill material, Japanese society of soil engineering, pp.373–390
18) Committee of test and design strength of rockfill material (1982): test and design strength of rockfill material, Japanese society of soil engineering
19) K.Nagai (1976): Investigation and design of Terauchi dam, Dam Japan, No.386, pp.13–32
20) H.Komyouji, Y.Yoshida and M.Yamashita (1975): Design and work of Daisetu dam, Dam Japan, No.367,pp.17–45
21) A.Nagano (1975): On the design and work of Hirose dam, Hydraulic generation, No.139, pp.9–22
22) F.Ukaji (1975): Property and evaluation of fill dam material, Japanese association of dam, Symposium of dam work, or Dam Japan, No.399, pp.31–63
23) R.J.Marsal (1973): Mechanical Properties of Rock Fill Embankment-Dam Engineering, ed. Hirschfelt and Poulos, John Wiley
24) J.Zeller and R.Wullimann (1957): The Shear Strength of the Shell Materials for the Goschenenalp Dam, Switzerland, Proceedings of 4th I.C.F.F.E, vol.2, pp.399–404
25) J.Lowe (1964): Shear Strength of Coarse Embankment Dam Materials, Pro. Of 8th ICOLD, R.l 1, Q.31, pp.745–761
26) T.M.Leps (1970): Review of shearing strength of rockfill, Proc. of the American Society of Civil Engineers, SM 4, pp.1159–1170
27) T.Okamoto, Y.Uchita, S.Tsuruta, Y.Hoshino and T.Matsuda (2004): Centrifuge test of rockfill dam and seismic stability evaluation basing on seismic response and residual, 13th World Conference on Earthquake Engineering, Paper No. 199

New Developments in Dam Engineering—Wieland, Ren & Tan (eds),
© 2004 Taylor & Francis Group, London, ISBN 04 1536 240 7

Recent trend for earthquake induced residual settlement of rockfill dam and some consideration on affecting factors

T.Okamoto
Central Research Institute of Electric Power Industry, Japan

ABSTRACT: The author has analyzed the seismic acceleration response and the earthquake induced residual deformation of rockfill dams and it found that they have been affected by earthquake property including base acceleration and duration but also slope gradient and embankment method and so on. This study will clarify the effect of embankment method basing on the analysis of completed year, embankment method, long-term settlement after construction and embanked density of rock material.

1 INTRODUCTION

The seismic acceleration response and the earthquake induced residual deformation of rockfill dams has been analyzed by some researchers (Bureau, G. et. al. 1985, Okamoto, T. 1999). Bureau, G. et al. 1985 suggested the relation between residual crest settlement of rockfill dam and the earthquake property including maximum base acceleration and duration. Okamoto, T. 1999 also studied the relation and considered the necessity to take into account of other factors. And as a result, it found that there is some effect of slope gradient and embankment method and so on but it is not detailed. This study will clarify the effect of embankment method basing on the analysis of completed year, embankment method, long-term settlement after construction and embanked density of rock material.

2 OBSERVED EARTHQUAKE RESPONSE ACCOMPANYING RESIDUAL DEFORMATION

Table 1 shows observed earthquake response of rockfill dams accompanying residual deformation and outline of dam property. References 1)–19) are same as those in Okamoto, T. 1999. Leakage increment occurred by earthquake at 2 CFRDs (Concrete Facing Rockfill Dam) of Cogoti and Minase and many other dams did not damage and kept poundage function. Fig. 1 shows the relation between observed residual settlement and maximum base acceleration.

Fig. 2 indicates the amplifier between crest and base foundation maximum accerelation basing on the results of Table 1. Also Fig. 2 contains the amplifier of smaller maximum accerelation without residual deformation observed recently in Japan (21)–30)). The amplifier widely distributes because of dam structure, material property, site character and so on. However the amplifier decreases when maximum accerelation is bigger or residual deformation occurs. Average amplifier is followed from small to strong earthquake.

$$A_c = 1{,}165 A_b / (A_b + 271) \quad (1)$$

Average amplifier under small earthquake is 4.3 (=1,165/271).

Table 1. Observed residual deformation and dam property.

Dam	Nation	Earthquake (Magnitude)		Based accerel. A_b (gal)	Crest accerel. A_c (gal)	Crest resid. settlement S_v (cm)	Crest resid. horiz. def. S_h (cm)	Dam height H (m)	Completed year	Type	Gradient		Leakage or other damage
											Upstream	Downstream	
Malpasso	Peru	1938.10.10		*100	–	7.6	5.1	78	1936	CFRD	0.5	1.33	
Cogoti	Chile	Illapel 1943	(8.3)	*190	–	60		83.8	1940	CFRD	L6	1.8	leakage gradually increased slide occurred
Miboro	Japan	Kita-Mino 1961	(7.0)	*200	–	3	5	131	1960	IECRD	2.5	1.75	
Minase	Japan	Niigata 1964	(7.5)	55		13.9	11.4	65	1963	CFRD	135	L4	leakage increased 2)
LaVillita	Mexico	75.10.11	(5.5)	72.8	300.2	2.5	2	60	1968	CECRD	2.5	2.5	
LaVillita	Mexico	75.11.15	(6.5)	40.8	191.6	2.5	2	60		CECRD	2.5	2.5	
LaVillita	Mexico	79.3.14	(7.6)	17	371	5	2.5	60		CECRD	2.5	2.5	
LaVillita	Mexico	81.10.25	(8.1)	85	338	11	4.5	60		CECRD	2.5	2.5	
LaVillita	Mexico	85.9.19	(8.1)	125	450	32	11.5	60		CECRD	2.5	2.5	
Infiernillo	Mexico	75.11.15	(5.5)	52.9	130.1	0.54		148	1963	CECRD	1.75	1.75	
Infiernillo	Mexico	79.3.14	(7.6)	105	355	7.55	12.9	148		CECRD	L75	1.75	
Infiernillo	Mexico	85.9.19	(8.1)	125	303	10.6	10.7	148		CECRD	1J5	1.75	
Namioka	Japan	Nihon-kai Chubu 83	(7.7)	79	223	5.7		52.4	1982	CECRD	3.47	2.072.7	settlement was observed near abutment
Makio	Japan	Nagano-ken Seibu 84	(6.8)	*400	*750	50		105	1961	CECRD	3	2.25	
Anderson	USA	Morgan-Hill 1984	(6.2)	410	630	1.5	0.9	71.6	1950	CECRD	2.5	2.5	
Anderson	USA	Loma Prieta 1989	(7.1)	78	421	3.9	2.4	71.6	–	CECRD	2.5	2.5	
Matahina	New Zealand	Edgecumbe 1987	(6.3)	324.7	764.8	80	26.8	86	1967	IECRD	2.5	2.3	
Ambuklao	Philippine	85.4.24	(6.3)	–	–	40	9	129	1956	CECRD	1.75	L75	
Ambuklao	Philippine	1990Ruzon	(7.8)	*200		68	28	129		CECRD	1.75	1.75	
Los Angel	USA	Northridge 1994	(6.7)	270	600	8.89	3.81	46.5	1977	CECED	3.5	3.0	

Dam	Embankment method and other character 9)	Reference
Malpasso	dumped at downstream side and placed by human power or hanging heavy machine	7)
Cogoti	dumped	3), 6)
Miboro	thin layer compacted soil core, dumped rock	1), 6)
Minase	dumped, sprinkled 7), 10)	2), 10)
LaVillita	compacted by roller, river deposit with 70m of depth	9), 15)
LaVillita		9), 15)
LaVillita		5), 9), 15)
Lavillita		9), 15)
Lavillita		9), 12), 15)
Infiernillo	compacted inner shell and dumped outer shell 7)	9), 15)
Infiernillo		5), 9), 15)
Inf fiernillo		9), 12), 15)
Namioka		11)
Makio	dumped rock, soil core, filter and transition compacted with thin layer	8), 13), 15)
Anderson	dumped rock and sprinkled, compacted soil core 7)	7)
Anderson		15), 16), 17)
Matahina	compacted rock by tractor, some problem of settlement and leakage during construction and filling	14)
Ambuklao		18)
Ambuklao		18)
Los Angels	soil core and sand gravel shell well compacted compaction degree 93%	19), 20)

CECRD: center soil core type RD
CECED: center soil core type earth dam
IECRD: inclined soil core type RD
CFRD: concrete facting TD
: special characted

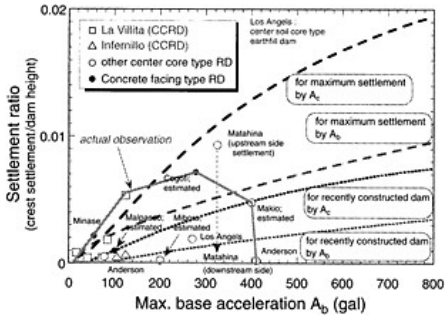

Figure 1. Relation between observed residual settlement and maximum base acceleration.

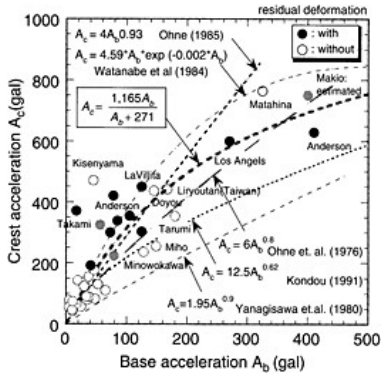

Figure 2. Base and crest acceleration and residual deformation.

Fig. 1 concludes that there are 3 regions which are no-residual deformation, no and sometime residual deformation and all residual deformation. Three regions correspond to (a) $A_b \leq 100$*gal and* $A_c \leq 200$ *gal,* (b) $A_b \leq 200$ *gal and* $A_c \leq 500$ *gal,* (c) 200 *gal*$\leq A_b$ and 500 *gal*$\leq A_c$ here A_b*:* maximum base acceleration, A_c*:* maximum crest acceleration.

According to recent data, Liyutan dam by Taiwan Jiji earthquake and Doyou dam by Tottori-ken seibu earthquake did not show residual deformation even though observed maximum acceleration were larger comparing with existing data in Fig. 2. Fig. 2 concludes that (b) region is wide, there is a possibility to take into account of residual deformation from viewpoint of design under even small acceleration and only some specified dams showed residual deformation under (b) region.

3 EVALUATION OF RESIDUAL SETTLEMENT AND EARTHQUAKE PROPERTY BY REGRESSION ANALYSIS

3.1 *Regression analysis*

Basic equation follows equation (2) in regression analysis for Table 1 to take into account of earthquake property.

$$\varepsilon_v = \ell \cdot A^m D^n \tag{2}$$

Here ε_v*:* crest settlement ratio (=S_v/H, S_v*:* crest settlement, *H:* dam height), *A:* maximum acceleration (A_b at base foundation or A_c at crest), *D:* duration, ℓ*, m, n:* constant.

Duration is estimated by following equation (3) suggested by Japanese electricity association: 1986. Here *M* is magnitude.

$$\log D = 0.31M - 0.774 \tag{3}$$

Final results are followed.

$$\varepsilon_v = 9.24 \times 10^{-7} A_b^{0.68} D^{1.14} \qquad \varepsilon_v = 1.19 \times 10^{-9} A_c^{1.83} D^{0.84} \tag{4}$$

Some result is close to Bureau, G. et al. 1985 because *m:n*=1:2 for A_b. However it found that crest settlement ratio depends on A_c rather than A_b.

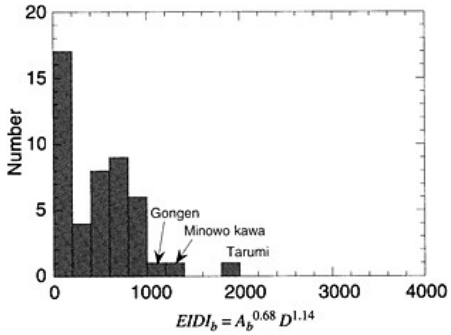

Figure 3. Frequency of $EIDI_b$ for non-residual deformation in Japan.

3.2 *Effect of some factors*

Equation (1) does not take into account of the effects of structual mechanics and material property. Structual mechanics means slope gradient and dam type and material property includes density, embankment method, rigidity, confining pressure and strain dependency of strength and deformation and so on. Now detailed consideration on structual mechanics and material property is difficult, so first of all some consideration will be done classifying dams in Table 1. Two kinds of dams in Table 1 are introduced to recongnize quantity of residual deformation, one is "easily deform" and another is "not easily deform". Criteria are followed to judge which is each dam classified to. (I) adequate compaction (Malpasso, Cogoti, Minase, Ambuklao, Makio), (II) gentler slope gradient than 1:1.8 (Malpasso, Cogoti, Minase, El Infernillo), (III) no anything wrong in embankment or filling (Matahina), (IV) rock foundation (La Villita), (V) others (local residual settlement, Minase) Dams inside ( ) are not corresponded to each criteria.

Equation (4) expresses average relation among crest settlement, acceleration and duration, therefore we can recongnize that there are some effect of structual mechanics and material property if some data are far from equation (3). Now Earthquake Induced Deformation Index *(EIDI)* is defined to:

$$EIDI_b = A_b^{0.68} D^{1.14}$$
$$EIDI_c = A_c^{1.83} D^{0.84} \quad (5)$$

3.2.1 *Base foundation acceleration*

Fig. 3 shows frequency of *EIDI* for dams wthout residual deformation in Japan and many of these dams in Fig. 3 were constructed recently. Fig. 4 indicates the relationship between crest settlement ratio and *EIDI* for dams with residual deformation in Table 1. A group of "not easily deform" shows smaller residual settlement than a group of "easily deform". Two equations are derived from Fig. 4 for maximum settlement and recently constructed dams.

$$\varepsilon_v = 2 \times 10^{-6} EIDI_b$$
$$\varepsilon_v = 9.24 \times 10^{-7} \left(EIDI_b - 1{,}000 \right) \quad (6)$$

3.2.2 *Crest acceleration*

Fig. 5 shows frequency of EIDI for dams wthout residual deformation in Japan and many of these dams in Fig. 5 were constructed recently such as in Fig. 3. Fig. 6 indicates the relationship between crest settlement ratio and EIDI for dams with residual deformation in Table 1. A group of "not easily

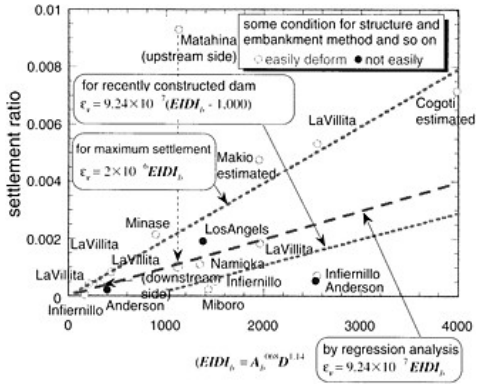

Figure 4. Settlement ratio and $EIDI_b$ for residual deformation in Japan.

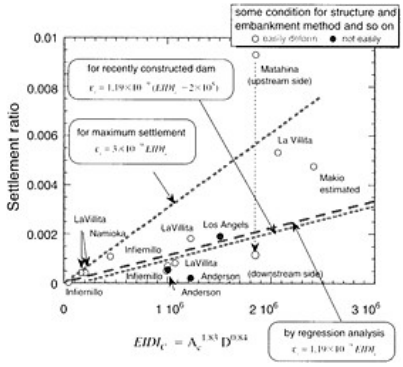

Figure 6. Settlement ratio and $EIDI_c$ for residual deformation in Japan.

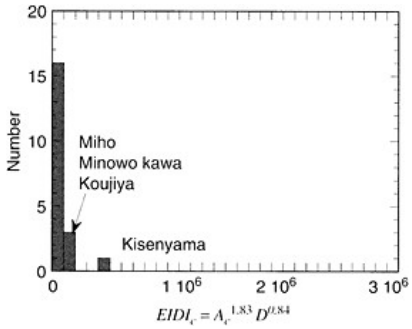

Figure 5. Frequency of $EIDI_c$ for non-residual deformation in Japan.

deform" shows smaller residual settlement than a group of "easily deform". Two equations are derived from Fig. 6 for maximum settlement and recently constructed dams.

$$\varepsilon_v = 3\times10^{-9}\times10^{-6}\,EIDI_c$$
$$\varepsilon_v = 1.19\times10^{-9}\left(EIDI_c - 2\times10^5\right) \qquad (7)$$

4 EFFECT OF COMPLETED PERIOD AND EMBANKMENT METHOD

Criteria applied in previous chapter (I) and (III) relate to embankment performance, and (II) and (IV) to seismic design. And chapter 2 leads that only some specified dams showed residual deformation under (b) region, those specified dams include La Villita and El Infernillo, which rockfill material were dumped. First of all let us check some change accompanying with completed year.

Figs 7 and 8 show observed base and crest maximum acceleration and the presence of residual deformation accompanying with completed year each other. And Figs 9 and 10 indicate embankment method of rockfill material. It found that there are few examples to observe big acceleration and

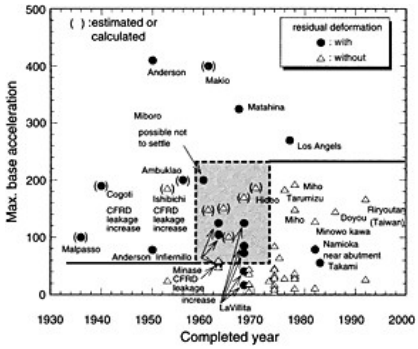

Figure 7. Base acceleration and the presence of residual deformation accompanying with completed year.

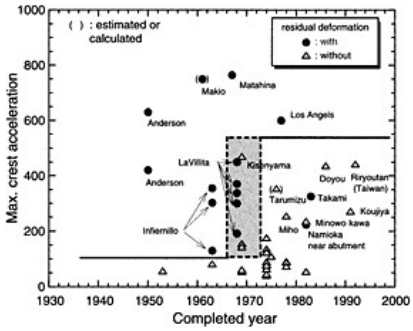

Figure 8. Crest acceleration and the presence of residual deformation accompanying with completed year.

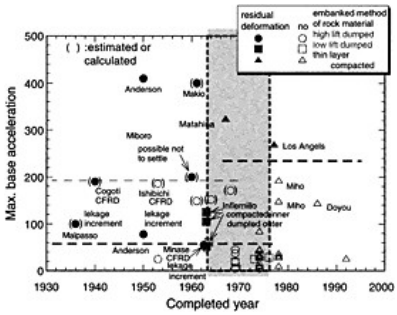

Figure 9. Base acceleration and embankment method accompanying with completed year.

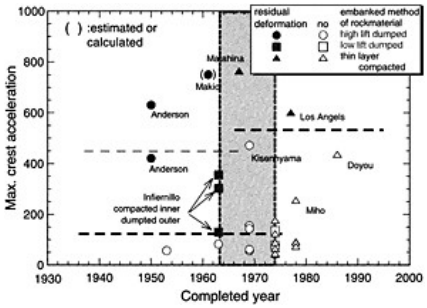

Figure 10. Crest acceleration and embankment method accompanying with completed year.

show residual deformation. However it can be recognize that (b) region changes accompanying with completed year and the change depends on embankment method of rockfill material.

5 LONG TERM SETTLEMENT AND ROCKFILL MATERIAL DENSITY

Previous chapter concludes that it is embankment method to change accompanying completed year. And embankment method affects on the settlement of fill dam. Figs 11 and 12 show long-term crest settlement after embankment of CFRD and in Japan each other. Due to Figs 11 and 12 it found that all of recently constructed dams show smaller settlement than older dams, it depends on embankment method and the time changed embankment method is almost 1950–1963 in all over the world and almost 1972 in Japan.

Figs 13 and 14 indicate settlement ratio 5 and 10 years after embankment due to data in Fig. 11. Also Figs 15 and 16 indicate settlement ratio 5 and 10 years after embankment due to data in Fig. 12. Embankment method of rockfill material affects on crest settlement. However it is not clear whether embankment method of core material affects on crest settlement.

Okamoto T. 2004 studies in-situ density of rockfill material and presents Fig. 17 for relative density basing on several in-situ rolling compaction tests in Japan. Maximum and minimum density are

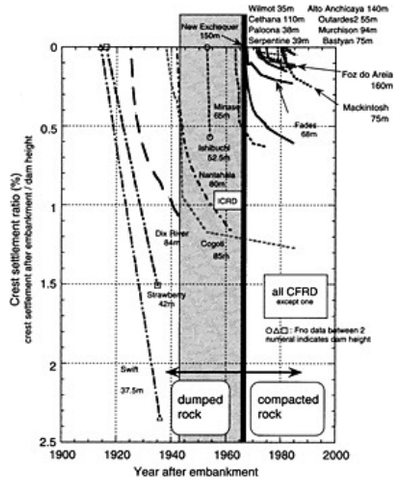

Figure 11. Long-term crest settlement ratio of CFRD.

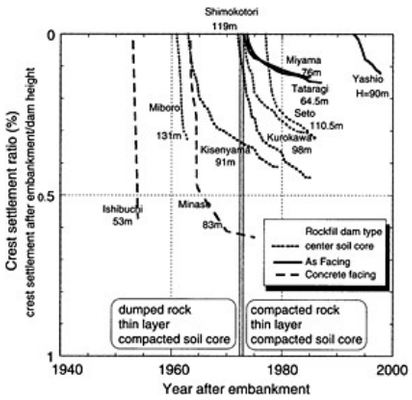

Figure 12. Long-term crest settlement ratio in Japan.

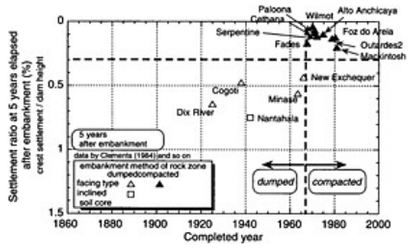

Figure 13. Settlement ratio 5 years after embankment due to data in Fig. 10.

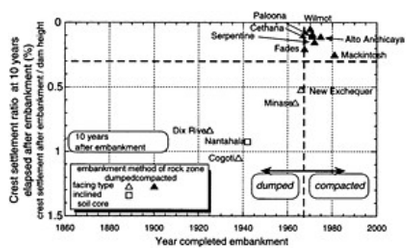

Figure 14. Settlement ratio 10 years after embankment due to data in Fig. 10.

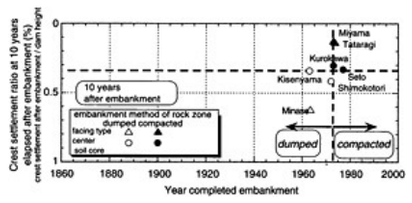

Figure 15. Settlement ratio 5 years after embankment due to data in Fig. 11.

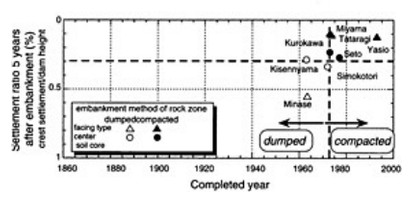

Figure 16. Settlement ratio 10 years after embankment due to data in Fig. 11.

estimated the results of in-situ rolling compaction test. And density condition is based on Table 2. According to Fig. 17 it found that in-situ relative density has wide range and placement work to maintain the thickness of compacted layer leads to have an important role rather than rolling number. Therefore dumped rockfill has low relative density and it influences on long-term settlement.

Table 2. Outline of relation between density condition and relative density (Okamoto T. 2004).

Density condition	Relative density	Compaction energy (E_{cJIS})
Very loose	<20%	–
Loose	20–40%	0–0.3
Medium dense	40–60%	0.3–0.5
Dense	60–80%	1.0–1.5
Very dense	80–100%	2.0<

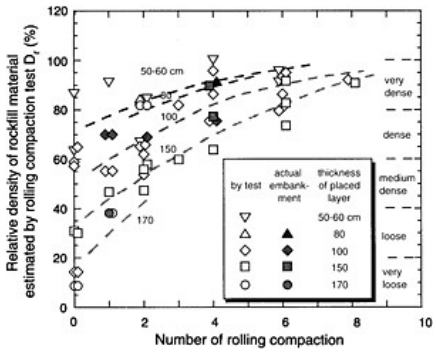

Figure 17. Estimated relative density of rockfill material and in-situ rolling compaction (Okamoto T. 2004).

6 EFFECT OF DENSITY ON RESIDUAL SETTLEMENT

Density dependency on mechanical property is most important for granular assembly such as sand. Okamoto T. et al. 2004 studied the effect of density of rockfill material on residual settlement by centrifuge test and concluded the result of Fig. 18. Also the range of in-situ observation for actual dams in Fig. 18 is based on Table 1 and the detailed range is showed in Fig. 1. In Fig. 18 Minowo wave has small magnitude although 10 cycles sine wave has large magnitude. According to the result of Okamoto T. et al. 2004, following equations are derived.

For large magnitude

$$\text{loose: } (\varepsilon_v + 0.013)(550\text{-}A_b) = 6.24$$
$$\text{dense: } (\varepsilon_v + 0.015)(722\text{-}A_b) = 9.45$$

For small magnitude

$$\text{loose: } (\varepsilon_v + 0.016)(780\text{-}A_b) = 10.4$$
$$\text{dense: } (\varepsilon_v + 0.020)(1{,}130\text{-}A_b) = 19.0 \quad (8)$$

However Okamoto T. et al. 2004 showed the result of rockfill dam with 1:1.4 of slope gradients for both of upstream and downstream side. And the dam model consists of only rockfill material, so resultant residual deformation should be applied to facing type rockfill dam. Therefore detailed study is necessary to evaluate residual deformation for center soil core type and for many factors as mentioned in 3.2.

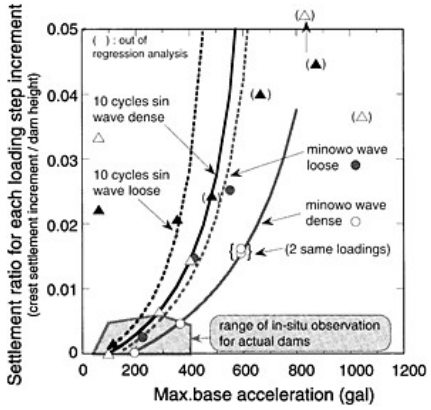

Figure 18. Residual settlement of rockfill dam by centrifuge test (Okamoto T. et al. 2004).

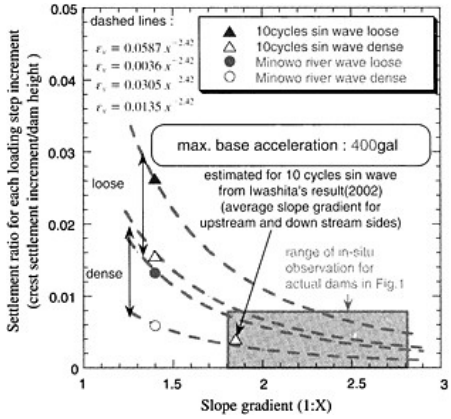

Figure 19. Effect of slope gradient on residual settlement by centrifuge test (Okamoto T. et al. 2004).

Fig. 19 showed the effect of slope gradient on residual deformation by centrifuge test and observation results such as Fig. 1 (Okamoto T. et al. 2004). Estimated curves in Fig. 18 are expressed as followed:

$$\varepsilon_v = 0.0587x^{-2.42}\ 0.0361x^{-2.42}\ 0.0305x^{-2.42}\ 0.0135x^{-2.42} \tag{9}$$

here x:slope gradient 1:x Now $\varepsilon_{v1.4}$ is defined to settlement ratio obtained by equation (8), settlement ratio with slope gradient 1:x. ε_{vx} is estimated by

$$\varepsilon_{vx} = \varepsilon_{v1.4}\left(\frac{x}{1.4}\right)^{-2.42} \tag{10}$$

Fig. 1 shows the relation between observed residual settlement and maximum base acceleration and equations (6) and (7). Applying equation (7), base maximum acceleration is calculated by

equation (1). Equations (6) and (7) does not take into account of the effect of density, but they correspond to equation (8). Equations (6) and (7) shows that the increment of ε_v decreases as A_b increases, although equation (8) shows that the increment of ε_v increases as A_b increases. However the relation by equations (6) and (7) almost agrees with that by equation (8) at small acceleration.

7 CONCLUSION

Conclusion is summarized as followed. (1) According to recent data, Liyutan dam by Taiwan Jiji earthquake and Doyou dam by Tottori-ken seibu earthquake did not show residual deformation even though observed maximum acceleration were larger comparing with existing data. And only some specified dams showed residual deformation under small acceleration region. (2) It found that there are few examples to observe big acceleration and show residual deformation. However it can be recognize that small acceleration region changes accompanying with completed year and the change depends on embankment method of rockfill material. (3) Embankment method affects on the settlement of fill dam. And all of recently constructed dams show smaller settlement than older dams. (4) It found that in-situ relative density of rockfill material has wide range and placement work to maintain the thickness of compacted layer leads to have an important role rather than rolling number. Therefore dumped rockfill has low relative density and it influences on long-term settlement. (5) For the effect of density of rockfill material on residual settlement some relations are derived for large and small magnitude and for loose and dense density condition using already done centrifuge test.

REFERENCES

Okamoto, T. (1999): Evaluation of measured vertical and horizontal residual deformation at crest of rockfill dam under earthquake, IS-Shikoku 99, I.S. on Slope Stability Eng.

Bureau, G., Volpe, R.L., Roth, W.H. and Udaka, T. (1985): Seismic analysis of concrete face rockfill dams, Concrete Face Rockfill Dams—Design, Construction and Performance, ASCE, pp. 479–508

Japanese electricity association (1987): Technical guideline for seismic design of nuclear power plant (JEAG 4601)

Okamoto, T. (2004): Evaluation of in-situ strength of rockfill material taking account of in-situ density and strength by laboratory, 4th Dam Engineering

Okamoto, T., Uchita, Y., Tsuruta, S., Hoshino Y. and Matsuda T. (2004): Centrifuge test of rockfill dam and seismic stability evaluation basing on seismic response and residual, 13th World Conference on Earthquake Engineering, Vancouver, B.C., Canada, August 1–6, Paper No. 199

Iwashita, T. (2002): Centrifuge shaking table test of rockfill dam and elasto-plastic effective stress dynamic analysis, j. of Dam technology, No. 184, pp. 32–42

REFERENCE FOR RESIDUAL DEFORMATION AND RESPONSE BY EARTHQUAKE

References 1)–19) are same as those in Okamoto, T. 1999

20) Davis, C.A. and J.P.Bardet (1996): Performance of Two Reservoirs during 1994 Northridge Earthquake, J. of Geotechnical Engineering, August, pp. 613–622

21) Edited by Technical research center of Japanese land development (1982): Seismic design of dam

22) Matsumoto, N., N.Yasuda and M.Shiga (1984): Property of earthquake motion observed at dam site, J. of Japanese large dam, No. 108, pp. 61–83

23) Matsumoto, N. and S.Kondo (1979): Report of damage investigation of 1978 Miyagi-ken oki earthquake, chapter 7 damage of dam, Report of civil engineering of Japanese construction ministry

24) Technical center of land development (1996): Report on evaluation of seismic stability of dam

25) Japanese society of civil engineering (1998): Chapter 6 facility of river and erosion control, Report on disaster investigation by Hanshin-Awaji earthquake—damage of civil engineering structure—

(26) Hasegawa, T. and A.Murakami (1997): 7.6 agricultural facility, Report on disaster investigation by Hanshin-Awaji earthquake, committee on disaster investigation by Hanshin-Awaji earthquake, Japanese society of geotechnical engineering, pp. 342–352
(27) Hasegawa, K. and A.Murakami (1996): Damage to agricultural facilities, Special issues on Geotechnical Aspects of the January 17 1995 Hyougoken-Nanbu, Soils and Foundations, pp. 255–262
(28) Kusunoki, H. (1995): damage of agricultural facility and its feature, Hyougoken-Nanbu Earthquake, J. of performance work of civil engineering, vol. 36, No. 9, pp. 105–109
(29) Investigation committee of Japanese society of civil engineering (1999): Report on disaster investigation by Taiwan Jiji earthquake
(30) Touma, et al. (2000): investigation report on Heisei 12 Tottori-ken Seibu Earthquake, Investigation report of CRIEPI

REFERENCE FOR LONG-TERM SETTLEMENT

1 Sherard, J.L. and J.B.Cooke (1987): Concrete-Face Rockfill Dam: I. Assessment, J. of Geotechnical Engineering, ASCE, vol. 113, No. 10, pp. 1096–1112
Following 2–7 are referred on Cooke, J.B. and J.L.Sherard (1985): Concrete-Face Rockfill Dam—Design, Construction and Performance, Proc. Of Symposium, ASCE
2 Arrau, L., I.Ibarra and G.Noguera: Performance of Cogoti Dam under Seismic Loading, pp. 1–14
3 Leps, T.M, C.A.Cashatt and R.N.Janopaul: New Exchequer Dam, California, pp. 15–26
4 Millet, J.C., F.Louis and F.Robert: Design, Construction & Performance of Fades Dam, pp. 27–39
5 B.Marteron: Alto Anchicaya Dam—ten years Performance, pp. 73–87
6 O.Dascal: The Outardes 2 Concrete-Faced Rockfill Dam, pp. 121–139
7 N.L.de S.Pinto, P.L. M.Filho and E.Maurer: Foz do Areia Dam-Design, Construction and Behavior, pp. 173–191
8 Honma, S. and Y.Miyata (1956): design and performance of rockfill dam, Kokuminn-kagaku-sha
9 Matsumoto, N., M.Takahashi and F.Sato (1985): Repairing the concrete facing of Minase rockfill dam, 15th ICOLD, Q59, R. 13, pp. 203–225
10 Kondou, N. (1991): Study of behavior of rockfill dam basing on long-term observation, doctor thesis
11 Hasegawa T. and M.Kikusawa (1988): Long-term Observation of Asphalted Concrete Facing Dam, ICOLD, Q. 61, R. 13, pp. 205–226
12 Nose, M. and K.Baba (1981): Dynamic behavior of rockfill dams, Dams and earthquake, TTL, London, pp. 69–78
13 Sugai, M., K.Ishiguro, E.Hibino, Y.Mori and H.Oota (1999): Consideration on long-term behavior asphalt facing fill dam—part 2 long-term deformation after filling, 54th annual meeting of Japanese society of civil engineering, III–B340, pp. 680–681
14 Clements (1984): Post-Construction Deformation of Rockfill Dams, J. of Geotechnical Eng. vol. 110 , No. 7, pp. 821–840

New Developments in Dam Engineering—Wieland, Ren & Tan (eds),
© 2004 Taylor & Francis Group, London, ISBN 04 1536 240 7

Test and research on seismic characteristics of sand gravel and gravel earth of Xiaolangdi earth rockfill dam

Pan Shu, Chang Xiangqian & Xu Gang
Yellow River Institute of Hydraulic Research, YRCC, China

ABSTRACT: The consolidated undrained triaxial vibration test was made on sand gravel for dam foundation and gravel earth for inner blanket, being prepared with three kinds of sediment concentration, by using of a large sized hydraulic servo triaxial tester developed first by the Chinese people. Based on the testing results, the dynamic strength and deformation features of sand gravel have been studied and its strength that might be impacted by different sediment content, relative density and grain gradation has also been reviewed.

In accordance with the above studies, index and function computation models for both pore water pressure of saturated nonclay soil by vibrating and residual deformation of anisotropic consolidated soil by vibrating have been brought forward. In order to satisfy the testing requirements of high stress condition, technical renovation on the above mentioned triaxial tester had been carried out.

1 PREFACE

The Xiaolangdi Dam is an earth rockfill dam with inclined core, and its height is 154m. The dam is situated in an area with strong earthquake. Its design intensity is VIII. The thickness of the sand gravel layers at the foundation is 70m, and the content of gravel is different from 20 to 50%. Therefore the stability of the Xiaolangdi Dam to resist the earthquakes is an important issue.

Therefore, tests on two kinds of sand gravel mixtures with different ratios and coarse grain sizes in the Xiaolangdi Dam project are carried out. The characteristics of the nonclay sand gravel are thoroughly studied on its dynamic strength, relation between dynamic stress and dynamic strain, vibrating pore water pressure, development law of residual deformation, etc. For gravel earth, a kind of coarse clay earth, study focuses on the test technology, mainly sample saturation, methods of different consolidations at unequal compressions, as well as its dynamic strength and residual deformation.

The tests were carried out with the large-scale Electrohydraulic Servo Dynamic & Static Triaxial Tester. In order to keep stable performance on the conditions of high pressure, a series of technical improvement was carried out on the tester. In order to study the saturation technology of large-scale gravel earth samples, special equipment was examined & manufactured.

Two items of research are introduced here:

A. Dynamic strength of sand gravel (different sand content) and gravel earth mixture;
B. Pore water pressure of sand gravel under the action of dynamic load, the residual deformation law of coarse earth and their mathematical model.

2 TEST CONDITIONS AND METHODS

2.1 *Test materials*

(i) Sand gravel (pebble) The test material is selected from the Xiaolangdi upper gravel alluvium, which is widely spread in the upper & medium layer of the riverbed with top level of 130~135m. Coarse grains

contain a small portion of floating ones, with grain size of 40~10mm and the biggest one can reach 300mm. Filling material is silt sand or fine silt sand. The sand content is different from 20~50%.

In order to select the representative material, as per the sand gravel gradation of Group192, a group with grain size <5mm and content of 47% was selected, named Base-1; a group with grain size <5mm and content of 35% was selected, named Base-2; and a group with grain size <5mm and content of 25% was selected, named Base-3. The grain size bigger than 60mm, which is the limit of the tester, was got rid of and substituted with equal amount; and then the gradation of tested material was got.

(ii) Gravel earth

Gravel earth is a mixture of sand gravel and earth in Siyuanpo at the ratio of 3:7. Siyuanpo was the main borrow site for the inclined core. The material is mainly heavy silty loam, covering 70%; the others are medium and light silty loam and a small amount of clay. The permeability coefficient of the material is $k=0.52\times10^{-8}$~3.5×10^{-7}cm/s. The sand gravel mixed in was confirmed as per the average of the grain gradation in the static test. The oversized part was also treated with equal substitution and then the gradation of tested material was got.

2.2 *The large-scale Electrohydraulic Servo Dynamic & Static Triaxial Tester (hereafter called tester)*

The tester is the main equipment for this research. It is first researched and manufactured in China specially to carry out dynamic test of coarse grains. Its main technical features: max. axial static load is 1000kN; max. axial dynamic load is ±30kN; max. pressure around is 2.0MPa; and the size of test sample is Φ300×750mm.

In order to get good functions at the conditions of high stress, the key part of three-stage electrohydraulic servo valve was replaced by D079–210 three-stage electrohydraulic servo valve manufactured by MOOG Company of USA and also equipped with MKZ-201A servo-controller.

The survey magnifying unit, dynamic control unit, signal unit, figure display unit, etc. were renewed.

2.3 *Test method*

The saturation of the test sample for the tester is rather difficult, especially for gravel earth, which has great influence on the test results. Some measures were taken to make the saturation of the test sample up to 95%.

The tests of dynamic features are carried out on the conditions without drainage; axial reciprocating load is put on the test sample; vibration frequency is 0.33Hz and at the same time stress, strain, curve of pore water pressure, load and deformation hysteresis loop are surveyed and noted down. Before test, the survey and measure system shall be corrected with undamped ring and the survey value marked.

3 DYNAMIC STRENGTH OF SAND GRAVEL AND GRAVEL EARTH

3.1 *Failure standard*

To determine the failure standard reasonably is the basis to discuss the soil dynamic strength. Here when the consolidation ratio of sand gravel Kc=1, the standard that the pore pressure ratio equals the surrounding pressure is selected. When Kc≠1, the failure standard that axial strain εa=5% is selected. For the clay earth such as gravel earth and the earth from Siyuanpo, the failure standard is always εa=5%. The test data show for sand gravel of Kc=1, when pore pressure ratio equals the surrounding pressure σ_3, the axial strain basically reaches about 5%.

3.2 *Relation between failure vibration times and dynamic stress ratio*

According to the selected failure standard, the relation curve of vibration times, NL, and dynamic stress ratio $\sigma_d/2\sigma_3$ (σ_d: amplitude value of axial dynamic stress) is set up. According to the curve, dynamic stress ratio relative to any failure vibration times can be obtained.

If double logarithmic coordinates are adopted to show the relation $\sigma_d/2\sigma_3 \sim N_L$ of soil, their relation of beeline can be got. Therefore the relation of $\sigma_d/2\sigma_3$ an N_L can be shown with power function, i.e.

$$\sigma_d = AN_L^{-B} \tag{1}$$

in which, $\alpha_d=\sigma_d/_2\sigma_3$; A and B are two test constants.

There is no difference of the results between this method and curve of semi-logarithmic coordinates and this expressing method is much more simple.

4 VIBRATION PORE WATER PRESSURE AND COMPUTATION MODEL OF RESIDUAL STRAIN

Two phenomena shall not be neglected in the triaxial vibrating test of saturation consolidation without drainage. One is when the pore water pressure of the nonclay soil increases remarkably and the consolidation stress ratio Kc>1, the range of pore pressure increase shall minimize with Kc being enlarged. The other is when consolidation stress Kc>1, either clayey or nonclay soil will produce obvious residual deformation.

Much study was carried out on the fine grain soil before. This study is carried out on sand gravel and gravel earth and introduced computation model for pore pressure and residual strain.

4.1 *Model of vibration pore water pressure increase*

According to the test records, the following characteristics of pore pressure increase of sand gravel were found: First, pore pressure and number of vibrating times would not form direct proportion; under the action of the small dynamic stress, the initial pore pressure increases slowly; during vibration, it will speed up in the medium and later stages and become slow near the failure and approximately near a fixed value. While under the action of high dynamic stress, the pore pressure can reach a great numerical value in the first week. Secondly, the maximum value of pore pressure has relation with consolidation ratio Kc, the big the consolidation ratio, the smaller the value. The third, the process of the pore pressure increase cannot be described with the existing simple models, otherwise the divergence is too big. In reality, the process of the pore pressure increase is rather complicated. Even if it is with the same surrounding pressure and same consolidation ratio, under the function of different dynamic stress, the vibrating pore pressure can not be simply shown with a curve of pore pressure ratio and vibrating period ratio.

As per the analysis of the recorded curve of pore pressure increase, if the logarithmic failure vibration times ratio $\xi=\lg N/\lg N_L$ (N is number of vibration times and N_L is number of failure vibration times) as the variable, and the relative ratio of pore pressure $U=u_N/u_L$ (u_N pore pressure ratio of vibrating N times, u_L pore pressure ratio when the sample fails) is introduced, the soil sample with the same surrounding pressure and same consolidation ratio, under the function of different dynamic stresses, the relation curve of U and ξ will form a fine dissymmetrical “S” curve. In order to eliminate the influence of the elastic pore pressure of the dynamic stress, during data processing, when the dynamic stress $\sigma_d=0$, the corresponding pore pressure value is the residual pore pressure value. Regression analysis shows an index function can be adopted to describe the curve:

$$(1-U)=C\cdot 10^{-K/(1-\xi)} \tag{2}$$

in which: $\xi=\lg N/\lg N_L$ logarithmic failure vibration times ratio

N number of vibration times

N_L number of failure vibration times

$U=u_N/u_L$ relative pore pressure ratio

u_N pore pressure ratio after N times vibrating

u_L pore pressure ratio when it fails

C has relations with the relative pore pressure ratio produced from the first vibration ($U_0=u_1/u_L$); because: let N=1, take $\xi=\lg 1/\lg N_L=0$ into formula (2), have

$$(1-U_0)=C\cdot 10^{-K}$$
$$C=(1-U_0)\,10^{K} \tag{3}$$

Taken into formula (2), get:

$$U=1-(1-U_0)10^{-K\xi/(1-\xi)}$$
$$U=1-(1-U_0)e^{-2.303K\xi/(1-\xi)} \tag{4}$$

or while K, U_0 can be shown with power of N_L:

$$K=NL^{-\beta} \tag{5}$$

$$U_0=\gamma N_L^{-\beta} \tag{6}$$

As the above mentioned, in the triaxial vibrating test, dynamic stress ratio α_d has the following relation with number of failure vibration times N_L:

$$\alpha_d=AN_L^{-B} \tag{7}$$

So the pore pressure increasing process of the triaxial vibrating test can be expressed with the index function model of Formula (4). Among them, A, B, α, β, θ, γ, u_L are 7 test constants, which have relations with surrounding pressure, consolidation ratio and the characteristics of the soil. As per the test results, the parameters of the computation model of the pore pressure of the three kinds of sand gravels are got in Table 1.

4.2 *Model of residual strain*

For the consolidated soil sample at unequal compressions, in the triaxial vibrating test without drainage, not only pore pressure is produced but also residual strain. It is found from the test records that the residual strain enhances with the increase of number of vibration times and continues to increase after failure. Secondly, at the time of failure the residual strain reaching failure is basically the same if their consolidation ratio is the same. It can be described with an index function model:

$$\bar{\gamma}=c10^{b\xi} \tag{8}$$

Table 1. Calculation parameters of pore pressure model of 3 kinds of sand gravels.

Soil	Kc	A	B	α	β	θ	γ	u_L
Base-1	1.0	0.280	0.071	0.550	0.683	0.93	0.701	1.00
	1.5	0.440	0.087	1.400	0.676	0.998	0.568	0.854
	2.0	0.660	0.078	2.32	0.684	1.04	0.443	0.749
Base-2	1.0	0.410	0.166	0.315	0.569	0.93	0.521	1.00
	1.5	0.657	0.145	0.743	0.621	1.03	0.364	0.948
	2.0	1.11	0.159	1.210	0.643	1.03	0.168	0.706
Base-3	1.0	0.640	0.143	/	/	/	/	/
	1.5	1.050	0.202	3.300	0.794	0.98	0.327	0.888
	2.0	1.45	0.202	4.700	0.774	1.06	0.168	0.780

$\bar{\gamma} = \gamma_N/\gamma_L$ relative shearing strain;

γ_N residual strain after N times of vibration;

γ_L residual strain when it fails;

$\xi = \lg N/\lg N_L$ the same meaning as pore pressure model

b and c are two parameters but not independent.

Let N=1, ξ=0, therefore $c = \gamma_1/\gamma_L = \bar{\gamma}_0$, $\bar{\gamma}_0$ relative shearing strain produced in the first time. That is c is the relative shearing strain produced in the first week.

$$\bar{\gamma} = \bar{\gamma}_0 10^{b\xi} \tag{9}$$

As per the definition of the relative shearing strain, when reaching failure $\bar{\gamma} = 1$, at this time ξ=0, therefore, from Formula (9), we get

$$\bar{\gamma}_0 \cdot 10^{b} = 1$$
$$\bar{\gamma}_0 = 10^{-b} \tag{10}$$

take Formula (10) into Formula (9):

$$\bar{\gamma} = 10^{b(\xi-1)} = \bar{\gamma}_0^{(1-\xi)} \tag{11}$$

In the same way, the number of failure vibration times N_L relates to dynamic strain by $\alpha_d = ANL^{-B}$. Therefore Formula (11) only includes four constants determined in the test:

A, B the same as pore pressure model;

b related to shearing strain in the first week;

y_L failure shearing strain, the values of soil samples with the same consolidation ratio are basically the same.

While b can show power function of N_L:

$$b = \alpha_0 N_L^{\beta_0} \tag{12}$$

Table 2. Calculation parameters of the soil residual deformation.

Material item	Consondation ratio	Consolidation Pressure σ_3 (kPa)	Calculation model parameter $b = \alpha_0 N_L^{\beta_0}$	
			α_0	β_0
Base-1 Sandgravel	1.5	600	0.62	0.37
	1.5	800	0.62	0.37
	1.5	1200	0.62	0.37
	2.0	600	0.36	0.403
	2.0	800	0.36	0.403
	2.0	1200	0.36	0.403
Base-2 Sand gravel	1.5	400	0.56	0.349
	1.5	800	0.56	0.349
	1.5	1200	0.56	0.349
	2.0	400	0.44	0.424
	2.0	800	0.20	0.477
	2.0	1200	0.20	0.477
Base-3 Sand gravel	1.5	400	0.58	0.435
	1.5	800	0.58	0.435
	1.5	1200	0.50	0.428
	2.0	400	0.42	0.430
	2.0	800	0.30	0.452
Gravel mixture	1.5	600	0.44	0.436
	2.0	600	0.62	0.530

Because Formula (11) expresses shearing strain ratio, when the data of triaxial vibration test were treated, b, α_0, β_0 can be directly shown by the axial strain value without conversion. α_0, β_0 of various soil materials are shown in Table 2. Similarly, parameters of α_0, β_0 got relation with the property, surrounding pressure and consolidation ratio of the soil.

5 CONCLUSION

From the test and research of the earthquake-resistant characteristics of sand gravel and gravel earth in the Xiaolangdi Dam Project, the following can be obtained:

(1) The dynamic strength of sand gravel has close relation with its density. With the increase of the relative density, the dynamic intensity shall increase. For Xiaolangdi Dam sand gravel with relative density of 50~70%, the liquefaction resistance is the same as that of the heavy silty loam. Under the earthquake intensity of VIII the places without good drainage conditions are liable to liquefaction.

(2) Under different consolidation conditions, the dynamic strength ratio of sand gravel $\sigma_d/2\sigma_3$ got relation curve with failure vibration times N_L. When the surrounding pressure $\sigma_3 \leq 1.2$MPa, the relation curve does not get lower remarkably.

(3) The static and dynamic strength of the gravel earth with the design mix ratio does not show increase. The main reason is that the content of coarse grain is low (<45%).

(4) The index function model of the vibrating pore pressure and residual strain can describe the increasing process of the vibrating pore pressure and residual strain more carefully and accurately than any models before. It has the characteristics of suitable lines and simple expression, its parameters have clear physical meaning and it forms relation with dynamic strength.

REFERENCES

[1] Pan Shu and Yang Zhongmao, Test & Study Report on the Earthquake Stability of the Saturated Soil of Xiaolangdi Dam and Foundation, 1989.
[2] The Ministry of Water Conservancy & Electricity of P.R. China, Soil Test Rules, SD128−87, SDSO1−79, Volume B.
[3] Pan Shu, Total Dynamic Shear Strength, A Method for Slope Stability against Earthquake, Oct.1988.
[4] Wang Wenshao, Strength, Liquefaction and Failure of Saturated Soil under Hysteresis Load, Journal of Water Conservancy, Jan.1980.
[5] Yang Zhongmao, Comparative Test Report on Standard Sand for the Large-scale Electrohydraulic Servo Dynamic & Static Triaxial Tester, Sept.1987.
[6] Liu Ying and Xie Junfei, Sand Liquefaction under Vibration, Earthquake Publishing House, 1984.3.
[7] Pan Shu and Shen Fengsheng, Analysis of 3D Seismic Response to Effective Stress of Earth and Rockfill Dam, Final report of eighty-five years' national scientific and technological projects, Hydraulic Scientific Research Institute of the Yellow River Water Conservancy Commission, Dec.1994.

New Developments in Dam Engineering—Wieland, Ren & Tan (eds),
© 2004 Taylor & Francis Group, London, ISBN 04 1536 240 7

Three-dimensional non-linear analysis on the reinforcement in the opening of diversion pipe for Three Gorges dam

Xuanmao Peng & Weijian Chu
University of Hohai, China

ABSTRACT: The reinforcement arrangement in the opening of diversion pipe in the spillway dam section and powerhouse dam section of Three Gorges Project was calculated and studied by using the three-dimensional non-linear FEM and taking the elasto-plastic behavior of rebar and softening damage behavior of concrete and the joint action of steel bar and concrete into account. The scope of crack and yielding of concrete and rebar in the surrounding of the opening of diversion pipe under the design working conditions was got. Through increasing gradually the water pressure in the opening, the overload coefficient of internal water pressure was calculated when the stresses of rebar reached yielding limit, in order to assess the safety degree of the strength of the opening of powerhouse dam section after reinforcement.

1 INTRODUCTION

The dam of the world-famous Three Gorges Project is concrete gravity dam, with axis 2309.47m long. The altitude of the dam is 185m, and the maximum height of the dam is 175m. Applying overflow dam and deep outlet staggered arrangement, 23 deep outlet, 22 overflow surface holes and 22 diversion bottom hole are set. The water inlet and transition orifice is giant in size, and the stress condition of the orifice is very complicated. Consequently, the research of the reinforcement arrangement in the orifice is an important and complicated task. In this paper, the reinforcement arrangement in the opening of diversion pipe on the spillway dam section and powerhouse dam section of Three Gorges Project was calculated and studied by using the three-dimensional non-linear FEM and taking the elasto-plastic behavior of rebar and softening damage behavior of concrete and the joint action of steel bar and concrete into account. The scope of crack and yielding of concrete and rebar in the surrounding of the opening of diversion pipe under the design working conditions was got. Through increasing gradually the water pressure in the opening, the overload coefficient of internal water pressure was calculated when the stresses of rebar reached yielding limit, in order to assess the safety degree of the strength of the opening of powerhouse dam section after reinforcement.

2 METHOD AND MODEL FOR CALCULATION

2.1 *Increment three-dimensional elasto-plastic FEM*

An increment form of three-dimensional elasto-plastic FEM is applied to analyse the non-linear behavior of the concrete dam and the rebar material. According to requirement of the load process and overload analysis, load over the structure is subdivision into some different level increment. Now, considering a typical level load increment $\{\Delta R\}$, there is a summation load $\{R_m\}$ before

application the load, corresponding displacement and stress is $\{\delta_m\}$, $\{\sigma_m\}$. System generate a new displacement increment and stress increment, $\{\Delta\delta\}$, $\{\Delta\sigma\}$ due to $\{\Delta R\}$. So the new accumulated load is as follows:

$$\{R_{m+1}\}=\{R_m\}+\{\Delta R\} \tag{1}$$

The accumulated displacement and stress is:

$$\{\delta_{m+1}\}=\{\delta_m\}+\{\Delta\delta\} \tag{2}$$

$$\{\sigma_{m+1}\}=\{\sigma_m\}+\{\Delta\sigma\} \tag{3}$$

By the acting of $\{R_{m+1}\}$, the equilibrium equation is as follows:

$$\varphi(\{\delta_{m+1}\}) = \sum_e [C^e]^T \int [B]^T \{\sigma_{m+1}\} dv - \{R_{m+1}\} = 0 \tag{4}$$

The upper equation could be expressed in increment format:

$$\varphi(\{\delta_{m+1}\}) = \sum_e [C^e]^T \int [B]^T \{\Delta\sigma\} dv - \{\Delta R\} + \varphi(\{\delta_m\}) = 0 \tag{5}$$

Here $[C^e]$ is selectivity matrix of element, $[B]$ is geometric matrix of element, $\varphi(\{\delta_m\})$ is the accumulative unbalance force before this level load is applied.

Considering geometric relationship in small-strain condition

$$\{\Delta\varepsilon\}=[B](C^e]\{\Delta\delta\} \tag{6}$$

and elasto-plastic constitutive relationship,

$$\{\Delta\sigma\}=[D]_{ep}\{\Delta\varepsilon\}=([D]-[D]_p)\{\Delta\varepsilon\} \tag{7}$$

$$\{\Delta\sigma\}=[D]_{ep}[B][C^e]\{\Delta\delta\} \tag{8}$$

substituting the relations (8) into (5) leads to FEM governing equation of increment format:

$$([K]-[K]_p)\{\Delta\delta\} = \{\Delta R\} + \{\bar{R}\} \tag{9}$$

with

$$[K] = \sum_e [C^e]^T \int [B]^T [D][B][C^e] dv \tag{10}$$

$$[K]_p = \sum_e [C^e]^T \int [B]^T [D]_p [B][C^e] dv \tag{11}$$

$$\{\bar{R}\} = -\varphi(\{\delta_m\}) \tag{12}$$

Here relation (9) is a non-linear equation about $\{\Delta\delta\}$ and $\{\sigma\}$, which iterative method always been used to get the solution. We apply sub-increment variation $[K]_p$ iterative method that adapt to crack and yield failure module. It derived from normal stiffness variation $[K]_p$ method.

2.2 *Constitutive relationship of material*

Assume rebar to be ideal elasto-plastic material, which yield criterion is as follows when applying an axial direction force:

$$F=|\sigma|-\sigma_t \tag{13}$$

Here σ is the stress of rebar, and σ_1 is material yield limit.

As for the concrete of dam, we adopt isotropic elasto-plastic brittle tension fracture. Its failure and yield criterion is as follows:

$$F_i=\sigma_i-\sigma_t \ (i=1,2,3) \tag{14}$$

$$F=\tfrac{1}{2}(\sigma_1-\sigma_3)+\tfrac{1}{2}(\sigma_1+\sigma_3)\sin\varphi-c\cdot\cos\varphi \tag{15}$$

The relation (14) is the maximum tensile stress criterion. Here σ_i is principal stress, σ_t is tensile strength of material. The relation (15) is Mohr-Coulomb yield criterion, where σ_1, σ_3 is 1st and 3rd principal stress, c, φ is cohesive force and internal frictional angle.

When $F_i<0$ and $F<0$, material is in elastic condition, the relation between stress and strain is as follows:

$$\{d\sigma\}=[D]\{d\varepsilon\} \tag{16}$$

Here $[D]$ is elastic matrix of material.

When $F_i>0$, brittle tension fracture occurs in the material. After crack, the material lose its stiffness along cracked face, and became transversely isotropic. In the local coordinate system, assume x', y' in the plane of crack face, and z' is consistent with the normal line of the crack face. So the relation between stress and strain in the local coordinate is as follows:

$$\{d\sigma'\}=[\bar{D}]\{d\varepsilon'\} \tag{17}$$

Here $[\bar{D}]$ is a corrected elastic matrix. The relation between stress and strain in the global coordinate system as follows:

$$\{d\sigma\}=[T]^T[\bar{D}][T]\{d\varepsilon\} \tag{18}$$

Here $[T]$ is a coordinate transformation matrix.

When $F_i<0$ and $F_i>0$, plastic shear yielding occurs in the material, thus the relation between stress and strain as follows:

$$\{d\sigma\}=[D]ep\{d\varepsilon\}=([D]-[D]p)\{d\varepsilon\} \tag{19}$$

Here $[D]_{ep}$ is an elasto-plastic matrix of material, $[D]_p$ is a plastic matrix of material. According to the orthogonal normal regulation and flow theory, the expression of $[D]_p$ as follows:

$$[D]_p=\frac{[D]\left\{\frac{\partial F}{\partial\{\sigma\}}\right\}\left\{\frac{\partial F}{\partial\{\sigma\}}\right\}^T[D]}{\left\{\frac{\partial F}{\partial\{\sigma\}}\right\}^T[D]\left\{\frac{\partial F}{\partial\{\sigma\}}\right\}+H} \tag{20}$$

Here H is related to soften and harden regulation of material.

As to three-dimension Mohr-Coulomb yield criterion, the corner singularity will appear in using relation (20). Therefore we use a simple practical processing method instead of expression (20). Though reducing the stiffness of yield concrete, the residual stiffness after reduced as follows:

$$[D]_{ep}=(1-\beta)[D] \tag{21}$$

Here β is a number bigger than 0 and less than 1. We always set β equal 3/4 according to experience.

2.3 *Assessing the safety degree of the strength on the orifice after reinforcement*

The distribution of stress on the orifice is obvious different from common pressure piping. The main load is internal water pressure in the common pressure piping, and the distribution of stress caused by it is similar to the distribution of thin and thick cylinder. The load affect the stress of orifice in the opening of diversion pipe include the weight of dam, water pressure on the dam face, internal water pressure in the orifice etc. The variation of the dam weight and dam normal water storage is inferior, but the variation of internal water pressure fluctuation is in a wider margin due to the state of the gate. Considering all above conditions, we regard the dam weight and design water load as constant in calculating the ultimate capacity of orifice after reinforcement. After the load (weight, water and sand pressure on the dam face, internal water pressure) over the dam hit its design value, we increase the water pressure in the orifice gradually until the rebar of orifice yield. Consequently, the dam will crack along the symmetric plane of upper hole and lower hole. The condition could be defined as load capacity after reinforcement, and the corresponding overload coefficient of internal water pressure is defined as the safety degree coefficient of the strength in the orifice after reinforcement, which used to assess the safety degree in the orifice after reinforcement.

2.4 *Generalized the rebar*

It is impossible to simulate detailed layout of rebar in the Three-dimension calculating model because of the number of the rebar is huge and the density is large. Thus, an equivalent calculate rebar area method is adopted. This method merge the multi-layer rebar along the orifice into a single layer, the merged rebar mesh sited on the gravity center of multi-layer rebar mesh. In this case, the crosswise and longwise rebar formed a spatial grid, which nodes are concurrent to the nodes of concrete element. The density of mesh drop a lot, the rigidity and strength of rebar still be kept, the efficiency of calculation increase obviously by using this kind of method.

3 CALCULATION OF DEEP OUTLET ON SPILLING DAM SECTION

Take a spilling dam into account, the maximum of the dam is 175m high, the length of dam along stream current is 134.5m long, the width of dam is 21m, the altitude of the dam foundation is 185m.The cambered gate of diversion bottom hole is installed in the lower river.

According to the real area of reinforcement in the orifice and layout of rebar, the shape of the rebar mesh look like a ‘U’ on the gate groove and work well.

Divide load in 12 increments. The first increment is gravity; the second is water pressure in orifice and on dam surface under design water height, cambered gate pressure, sediment pressure, and water pressure on lateral dam; from the third to twelfth is internal water pressure by 20 percent increment. Table 1 list the stress of rebar element under each loading step in rebar mesh 2m from the orifice.

According to the table, the inner force of rebar on the upper surface and lower surface is tensile stress, and the inner force on lateral surface is compression stress. Under the design load (k=1.0), the rebar stress is small, it doesn’t reach the yield limit of rebar. With the increasing of

Table 1. The rebar stress of deep outlet on typical spilling dam section (MPa).

Rebar number	Load level.											
	1	2	3	4	5	6	7	8	9	10	11	12
1	10.4	9.0	9.6	10.4	14.8	22.4	27.7	41.9	112.0	197.9	300.0	300.0
2	8.0	9.5	10.3	15.8	23.0	34.9	42.7	62.9	126.7	211.0	300.0	300.0
3	6.6	12.8	20.6	31.6	62.9	77.9	88.2	105.5	165.2	250.1	300.0	300.0
4	5.6	6.4	8.6	6.9	8.0	8.0	8.9	11.9	13.6	18.0	17.9	32.4
5	−22.1	−22.1	−12.8	−12.0	−12.3	−13.1	−13.0	−23.6	−54.4	−62.9	−87.6	−99.6
6	−26.2	−13.6	−13.5	−13.5	−14.4	−14.8	−14.9	−15.5	−16.4	−15.6	−8.2	−4.2
7	−27.7	−14.9	−15.2	−15.6	−16.7	−17.5	−18.1	−19.0	−20.5	−20.6	−11.6	0.3
8	−26.6	−12.4	−12.0	−11.6	−11.8	−11.8	−11.8	−12.2	−12.5	10.6	−2.2	1.4
9	−22.0	−10.5	−9.2	−9.2	−7.8	−8.6	−8.6	−9.6	−41.2	−83.4	−103.0	−80.6
10	5.8	4.8	7.2	8.9	5.7	7.2	7.6	8.0	8.4	10.2	28.9	28.1
11	5.5	8.7	17.5	20.0	51.7	64.4	74.6	89.9	135.7	216.1	258.0	300.0
12	7.1	9.6	8.9	12.5	11.7	22.2	33.6	51.3	101.9	179.5	228.9	300.0
13	9.8	8.9	8.0	11.1	10.1	12.6	13.2	22.0	65.3	72.8	144.5	215.7

water pressure, the tensile stress on the upper surface and lower surface begin to increase; and the compression stress on lateral surface start to decrease. As the load reach eleventh step, a portion of rebar reached yield limit (300MPa). As the load continue increase, more and more rebar element reached yield limit. The rebar start to yield when the load reached eleventh step and the corresponding overload coefficient of internal water pressure is 2.8.

Under the design load, only a small portion of concrete element on the orifice cracked, and the rebar stress is small. With the increasing of the load, the concrete crack region around the orifice start to enlarge gradually, and move from edge of orifice to inside, and the concrete crack will not appear on the orifice behind cambered gate even with the increasing of the internal water pressure. In response to the distribution of rebar stress under each overload step, we can see, with the increasing of load, the rebar stress on the upper and lower orifice increase too, at the same time, the concrete crack region move inside. It indicates that the rebar begin to exploit obviously when concrete crack appear, and reach yield limit when crack appear on large acreage concrete region.

For the typical reinforcement program on spilling dam section under the design load, the crack only appear on partial region of orifice, the maximum depth of crack is about 0.5m. The upper orifice rebar begin yield when overload coefficient of internal water pressure reach 2.8, and concrete generate several deep flaws. This kind of situation is called load capacity after reinforcement, and the corresponding safety degree coefficient of the strength in the orifice after reinforcement is 2.8.

4 CALCULATION OF WATER DIVERSION CONDUITS ON POWERHOUSE DAM SECTION

Take a typical powerhouse dam section as a research object, the maximum of the dam is 175m high, the length of dam along stream current is 123.2m long, the width of dam is 25m, the altitude of the dam foundation is 29m. Applying single hole arrangement on deep outlet, the radius of water diversion conduits is 12.4m. According to the real area of reinforcement in the orifice and layout of rebar, the arrangement of rebar is a spatial rebar mesh. Divide load in 12 increments. The first increment is gravity; the second is water pressure in orifice and on dam surface under design water height, sediment pressure; from the third to twelfth is internal water pressure by 20 percent increment. Table 2 list the stress of rebar element under each loading step in rebar mesh 2m from the orifice.

According to the table, the inner force of rebar on the upper surface and lower surface is tensile stress, and the inner force on lateral surface is compression stress. Under the design load (k=1.0),

Table 2. The rebar stress of water diversion conduits on typical powerhouse dam section (MPa).

Rebar number	Load level											
	1	2	3	4	5	6	7	8	9	10	11	12
1	10.0	22.3	30.4	40.7	57.0	82.1	122.5	172.0	240.0	300.0	300.0	300.0
2	8.9	21.4	30.1	38.6	55.9	81.8	123.1	172.2	247.2	300.0	300.0	300.0
3	6.1	23.6	31.7	39.0	54.2	79.6	117.6	168.9	250.6	300.0	300.0	300.0
4	5.5	18.8	25.0	31.4	42.3	62.0	84.6	112.4	163.8	210.2	233.2	264.4
5	−25.9	−14.6	−15.3	−14.5	−14.6	−15.4	−21.0	−23.1	−26.7	−40.0	−82.4	−139.5
6	−26.9	−16.6	−17.3	−17.8	−19.1	−20.8	−19.0	−18.2	−17.4	−19.7	−38.0	−93.0
7	−25.5	−18.3	−19.5	−20.7	−22.5	−25.0	−26.7	−26.5	−26.5	−22.5	−19.8	−33.8
8	−25.6	−19.2	−20.8	−22.4	−24.4	−27.2	−29.3	−30.3	−31.7	−34.3	−35.9	−38.4
9	−25.7	−19.1	−20.7	−22.4	−24.3	−26.8	−28.6	−29.8	−31.9	36.3	−38.6	−42.2
10	−26.7	−18.1	−19.5	−21.1	−22.6	−24.5	−24.8	−25.4	−27.5	−32.9	−33.1	−31.0
11	−20.4	−14.4	15.1	−16.2	−17.3	−15.5	−10.0	−13.5	−16.7	−22.5	−28.0	−36.2
12	−26.9	−10.1	−9.9	−9.8	−9.4	−10.3	−14.8	−32.9	−62.5	−98.2	−135.0	159.2
13	6.1	19.7	28.4	37.2	47.4	57.3	77.4	102.2	129.9	148.0	185.1	230.6
14	5.1	16.8	23.7	30.8	30.4	50.9	72.0	101.2	135.4	164.8	190.0	210.4
15	7.7	13.4	15.3	21.8	31.3	46.6	71.3	99.8	135.4	169.9	203.2	238.0
16	8.7	12.7	15.7	19.6	26.7	43.3	69.9	98.5	133.0	165.3	199.1	234.6

the rebar stress is small, it doesn't reach the yield limit of rebar. With the increasing of water pressure, the tensile stress on the upper surface and lower surface begin increase; and the compression stress on lateral surface start to decrease. As the load reach the tenth step, a portion of rebar reached yield limit (300 MPa). As the load continue increase, more and more rebar element reached yield limit. The rebar start to yield when the load reached the tenth step, and the corresponding overload coefficient of internal water pressure is 2.6.

Under the design load, only a small portion of concrete element on the orifice cracked, and the rebar stress is small. With the increasing of the load, the concrete crack region around the orifice start to enlarge gradually, and move from edge of orifice to inside, and the concrete crack will not appear on the orifice behind cambered gate even with the increasing of the internal water pressure. In response to the distribution of rebar stress under each overload step, we can see, with the increasing of load, the rebar stress on the upper and lower orifice increase too, at the same time, the concrete crack region move inside. It indicates that the rebar begin to exploit obviously when concrete crack appear, and reach yield limit when crack appear on large acreage concrete region.

For the typical reinforcement program on powerhouse dam section under the design load, the crack only appear on partial region of orifice, the maximum depth of crack is about 0.5 m. The upper orifice rebar begin yield when overload coefficient of internal water pressure reach 2.6, and concrete generate several deep flaws. This kind of situation is called load capacity after reinforcement, and the corresponding safety degree coefficient of the strength in the orifice after reinforcement is 2.6.

5 CONCLUSIONS

We have presented a three-dimensional non-linear FEM method for study the safety degree problem of the strength after reinforcement arrangement in the opening of diversion pipe in the spillway dam section and powerhouse dam section of Three Gorges Project. The model of calculation take elastic-plasticity of material and the joint action of rebar and concrete into account, the outcome of calculation including the scope of crack, the depth of flaw and yielding of concrete and rebar in the surrounding of the opening of diversion pipe. The research indicate that as for deep outlet on spilling dam the corresponding safety degree coefficient of the strength in the orifice after reinforcement is 2.8 when applying typical reinforcement program; as for water diversion conduits on powerhouse dam section, the corresponding safety degree coefficient of the strength in the orifice after reinforcement is 2.6. Consequently, the typical reinforcement program on powerhouse dam section and spilling dam section is feasible and suitable considering the strength design.

REFERENCES

The engineering technique report of hydro-junction dam in Three Gorges, The long river committee of water conservancy, 1994
Shenxing Wu, The study of reinforcement on the orifice of deep outlet, Civil engineering department of Hohai university, 1996
Xuanmao Peng, Three-dimension linear FEM for Three Gorges spilling dam, The mechanical research institute of Hohai university, 1996

This page intentionally left blank.

New Developments in Dam Engineering—Wieland, Ren & Tan (eds),
© 2004 Taylor& Francis Group, London, ISBN 04 1536 240 7

Design criteria for remedial works for a 75-year old earthfill dam

N.Petrovic
Hydro Tasmania, Australia

N.Vitharana
Sinclair Knight Merz Pty Ltd, Australia

ABSTRACT: The safety of existing dams is a major issue faced by today's dam engineers not only in Australia but also in other countries, both developed and developing. Churchman Brook Dam is a 26m high earthfill dam with a puddle clay core and impounds a reservoir of 2.2GL. Various remedial works have been undertaken since completion of construction in 1928. In September 2000, a sinkhole in the right abutment was observed during a routine dam inspection. Following this incident, detailed site investigations were carried out. These investigations revealed that there are soft zones and possibly voids formed in the upper part of the clay core.

A comprehensive dam safety study and a risk workshop undertaken in 2002/2003 showed the dam to be deficient in aspects associated with piping, spillway adequacy and outlet works condition. It was agreed at the early stages of the design phase that a rational set of design criteria be developed considering both safety and economical aspects. A rational geotechnical model was developed for the foundation utilising triaxial test data from 1980s and recent investigations. The existing spillway chute will be upgraded with a concrete liner attached to the existing chute incorporating no-fine concrete as a free-draining medium.

This paper presents the various aspects of the remedial works with main emphasis on the development of the design criteria considering both safety of the dam and economy of the proposed remedial works.

1 INTRODUCTION

Churchman Brook Dam is a 26m high earthfill dam with a puddle clay core and it impounds a reservoir of 2.2 GL at its Full Supply Level (FSL). The dam is located on the Darling Scalp approximately 30km south east of Perth and was constructed between 1924 and 1928. The dam supplies a yield of 2.75 GL per annum to Perth's Integrated Metropolitan Water Supply Scheme.

In 2000, during a routine inspection, a sinkhole was observed on the right abutment. In 1997 and 1998, damp patches had been observed on the downstream face. Following the sinkhole observation, detailed investigations were carried out to establish the cause for these incidents in particular the sinkhole formation. As an interim risk management measure against possible piping failure, the storage was maintained at a lower level. A comprehensive dam safety review in conjunction with a risk workshop identified key issues related to the safety of the dam. The following remedial works will be undertaken:

- Construction of a downstream filter/drain on the downstream slope of the dam with an overlying stabilisation fill. The thickness of the stabilisation fill is designed to meet embankment stability and to avoid blowout through the filter.

- Removal of the existing (constructed in 1989) downstream toe weighting. The existing foundation filter comprises a crushed rock aggregate sandwiched between geotextiles. Stability analyses showed that, with the proposed downstream stabilisation fill, adequate factors of safety can be achieved without the toe weighting. Part of this excavated material will be used in the stabilising fill above.
- Demolish the existing stilling basin and construct a new one. The existing structure is capable of sustaining a flood event with Annual Exceedence Probability (AEP) of 1:600. The new stilling basin should be able to contain a flood event with AEP=1:10,000 without sweep-out (erosion) and be stable against flotation for a flood event with AEP =1:1,000,000.
- Upgrade the existing spillway chute so that it is stable against seepage and flow-induced uplift pressures.
- Upgrade the outlet pipeworks to have downstream emergency control.
- Upgrade the dam instrumentation. Install piezometers in the upstream shoulder of the dam and replace a selected group of the existing pneumatic piezometers with vibrating-wire piezometers connected to a SCADA system. Construct additional seepage weirs.

2 HISTORY OF DAM UPGRADES

Construction of the Churchman Brook Dam was completed in 1928 after a 5-year investigation and construction period. The design comprised an earthen dam with a maximum embankment height of 26m. The crest width is 4.6m and the upstream face has a slope of 1 v:3 h and the down-stream face has a slope of 1 v:2h. Figure 1a shows the cross section of the dam.

The clay for the puddle core was excavated by hand from a pit at the dam site. According to Parr (1927), it was sprinkled with water, and after conditioning it was well cut up and mixed. The placing of the puddle was by hand with conveyance to the bottom of the trench by galvanised chutes. The exact details of the placement method was not known but it is believed it was placed in 150mm thick layers rammed with 17-pound hammers. The total quantity of puddled clay placed is 12,335 cubic yards to stream bed level and 26,928 cubic yards in total.

The construction progress had been documented accurately at each cross section and a snapshot of the record is reproduced in Figure 2 for reader's interest as it is believed that there are other dams throughout the world with similar construction undertaken in that era. The progress records showed when the construction was interrupted during the winter and rainy seasons, sometimes for prolonged periods.

In 1989, 25,000m^3 of earthfill weighting was placed at the downstream toe (Fig. 1b) following a major investigation on the adequacy of slope stability. The weighting included a foundation drain consisting of crushed rocks sandwiched between geotextiles. This toe weighting was required to achieve adequate factors of safety. The size of the weighting was controlled by assumed low effective friction angle of the foundation materials. These were interpreted from CU triaxial tests (effective friction angle of 16 degrees was used on the critical slip circle).

In September 2000, a sinkhole appeared on the upper right abutment of the dam. A program of cone penetrometer testing, test-pitting and drilling was undertaken in the area around the sinkhole and along the length of the dam crest. These investigations targeted the consistency of the puddle core. Laboratory testing was also undertaken: triaxial tests, Atterberg limits, piping tests, particle size distributions, etc.

These investigations and laboratory testing consistently showed that the clay core had a zone of very soft material at depths of 4 to 8m below the crest. The test pit in the right abutment, adjacent to the sinkhole also exposed voids in the clay. It was postulated that this softening and formation of voids was occurring due to processes of consolidation and settlement below the phreatic surface. Due to the narrow profile of the clay core, the stiffer puddle clay above the phreatic surface was able to arch between the embankment shoulders or stiff abutment materials. As a short-term piping risk mitigation measure, the maximum operating level of the reservoir was reduced by 6.6m.

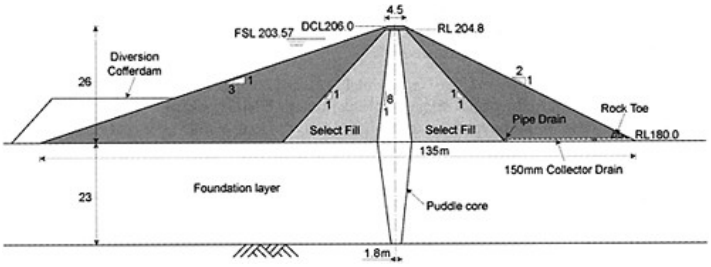

Figure 1a. Original dam profile when constructed in 1928.

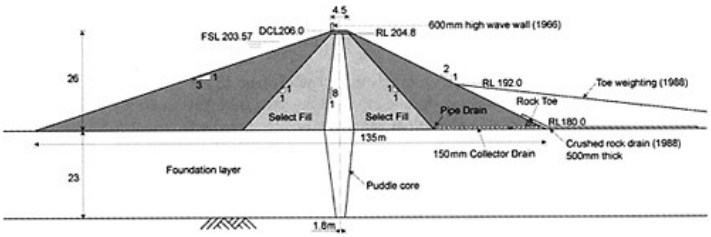

Figure 1b. Toe weighting stabilisation undertaken in 1988.

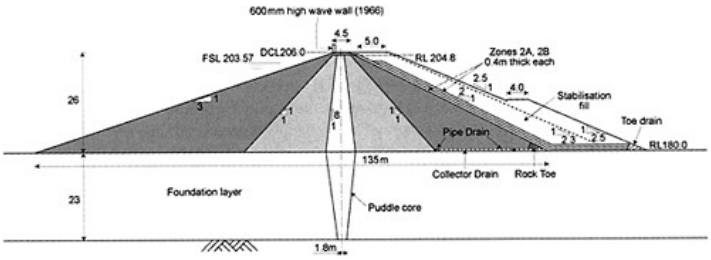

Figure 1c. Planned filter construction and stabilisation works.

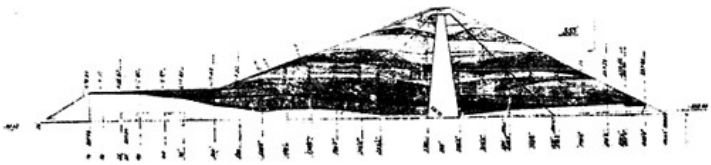

Figure 2. Construction progress in 1920s (note the inward slope of the shoulder construction).

3 REMEDIAL WORKS

3.1 *Piping potential and filter construction*

The risk assessment for the dam safety review included an event tree analysis considering various reservoir operation scenarios and reservoir water levels. This assessment showed that piping potential at the dam would be unacceptably high due to the soft puddle core and possible voids (mainly above RL 198m, 8m below the crest). Due to the construction method adopted in the 1920's, it is considered likely that there are lenses in the shoulder material that are poorly compacted. These lenses may have relatively higher permeability and be more susceptible to internal piping erosion. On this basis, it is highly likely that a concentrated leak through hydraulic fracture or void in the clay core would progress rapidly.

The predicted annual probability of failure value for piping-induced failures is in the order of 6×10^{-3} for the desired operation mode of the dam (i.e. annual filling to FSL). This exceeds the guideline for societal and individual risk as given in ANCOLD's Guidelines on Risk Assessment (August 2001).

Remedial work proposed is the placement of filters on the downstream shoulder of the dam with a stabilisation fill to avoid the uplift of the filter. This will require the removal of the crushed rock filter and toe weighting placed in 1989.

An assessment was made to determine whether replacement of the 1989 toe weighting was required. In this assessment, it was considered that the selected foundation strength parameters in 1987 were too low. Based on the revised soil strength parameters and geometry of the proposed stabilisation fill, the toe weighting was not required.

Figure 1c shows the proposed remedial works associated with the filter placement and downstream stabilisation. The filter/drain provided consists of 2A/2B/2A with each layer of 400mm in thickness designed according to USDA (1994).

In Figure 1c, two downstream profiles are shown corresponding with "average" and "lowerbound" values for foundation strength parameters. The slope with the lower-bound strength values (finally adopted) has a 4m wide berm at the mid-height. Associated design details and geotechnical model developed are given in Section 4.2.

3.2 *Spillway chute*

The PMPDF inflow flood is 219m^3/s for an AEP=1:1,000,0000 event. The flood attenuation in the storage is negligible with the reservoir level at the full supply level before the storm. The spillway crest discharge (capacity) with the storage at the dam crest level (RL 205.96m) is 268m^3/s. This corresponds to a 900mm freeboard below the wave wall crest for the PMPDF.

The existing spillway chute floor (the retained section from 1926) is only 250mm thick and has cracks up to 3–5mm wide. There is no sub-floor drainage system under the chute slab.

It was considered that this part of the floor slab may fail due to the uplift pressures generated by spillway flow. When the high-velocity water enters through these cracks and openings, uplift pressures would occur. According to McLellan (1976), the uplift pressures would exceed the weight of the structure at chute velocities of 6.5m/s, corresponding with a flood event with AEP=1:30.

A comparison of the cost of constructing a new spillway chute against upgrading the existing spillway chute showed the upgrade to be cost effective. Accordingly, it was decided to undertake the following main remedial works for the spillway chute at an estimated cost equal to about 30% of a new spillway chute:

- Drill 75mm dia and 600mm long drain holes in the existing slab and fill them with fine filter to act as pressure-relief holes for under-seepage from the storage or runoff from the hillside;
- Construction of a 250mm thick no-fines concrete slab on the existing 1926 spillway chute;
- Placement of 100mm dia transverse coil pipes at 10m spacing along the chute;

- Construction of a 200mm thick reinforced concrete liner (slab) continuous over the whole spillway length (i.e. no contraction joints). This slab is separated from the no-fines concrete slab with a layer of geofabric to avoid the flow of cement paste into no-fines concrete;
- Anchor the 200mm thick concrete liner to the existing spillway walls with 24mm dia anchors at 2m spacing;
- Excavate behind and place 900mm wide free-draining earthfill on either side of the chute walls.

With the proposed design, the no-fine concrete will act as a free-draining layer to avoid build up of any flow-induced pore pressures resulting from defects in the concrete liner or poor bond at the interface of the new slab and existing walls. This was considered necessary despite the concrete liner being continuous with reinforcement designed for fully-restrained thermal contraction. Drainage is accommodated with 75mm drain holes.

3.3 *Stilling basin*

It is somewhat difficult to ascertain a value for the probability of failure due to dam breach following the failure of the stilling basin. However, considering that the existing stilling basin is designed for an AEP of 1:170, and is constructed on soft soils, it was recommended to construct a new stilling basin.

The criteria adopted for the design of the stilling basin considering both dam safety and economical aspects are:

- Serviceability/unusual condition: During small-medium floods, the hydraulic jump turbulence is contained within the stilling basin with respect to length and height. The selected flood event has an AEP of 1:10,000.
- Extreme/ultimate condition: At large-extreme floods, the hydraulic jump could form beyond the stilling basin length resulting in erosion (sweep out) but the collapse of the stilling basin should not occur. The stilling basin should be stable against flotation with supercritical flow depth inside and tailwater depth outside.

At Churchman Brook, stability against flotation was achieved by providing enough mass for the structure as the provision of grouted dowels is not possible due to lack of rock strata near the ground surface. Undermining will be minimised by constructing a concrete cutoff under the endsill of the stilling basin and by providing rock protection in the streambed downstream. Three AEPs (10,000, 40,000 and 1,000,000) were considered in designing the structure against uplift and for extent of erosion protection. The selected flood event is 1:1,000,000.

The rock protection was provided downstream of the stilling basin to control the erodibility of the material once the flood exceeds the 1:10,000 event. A row of sheetpiles was provided under the sill of the stilling basin to avoid the undermining of the stilling basin. The pullout resistance of the piles was neglected in the flotation assessment of the stilling basin.

4 DAM STABILISATION DESIGN

4.1 *Geotechnical model*

4.1.1 *Material types*

A number of foundation investigations at Churchman Brook Dam have been carried. The results of these were used to develop a comprehensive geotechnical strength model for the foundation and embankment materials.

The upstream and downstream fill consists of compacted sandy/silty clay material which is assessed as firm. The puddle core consists of high plasticity clay which has low dry density with high moisture content. The foundation material consists of three basic formations as follows:

- Alluvium/colluvium layer varying in the depth from 2m to 3m.

• Residual (granites and dolerites) soils overlaying bedrock at the depth of 20m to 25m below surface level.
• Bedrock (granite gneiss with the dolerite dykes at depth of 20m to 25m.

4.2 *Main features of the approach adopted*

4.2.1 *1980s triaxial results*

The 1980s triaxial tests were consolidated undrained multi-stage tests with pore pressure measurements. Effective stress Mohr-circles were drawn to determine the c′ and Φ' values. The major drawback with the 1980s tests is that they are tested at a high strain rate (in the order of 2.0mm/min). At high strain rates, the shear-induced pore pressures may not be picked up instantaneously by the pore pressure cells. This occurs because shearing takes place at the middle of the sample in a rapid manner and pore pressure dissipation is much slower than the testing rate in clayey materials having low permeability [Fell, 1992].

Many of the 1980s triaxial tests show a high cohesion value (interception at zero normal stress) and it is highly likely that there are three reasons:

High strain rate during testing: The triaxial tests carried out in 1980s were consolidated undrained tests with pore pressure measurements. At low triaxial stresses, the samples behave as an over-consolidated material (test pressure lower than the preconsolidation stress) and the measured pore pressures are higher than the negative pressures generating at the shearing. This situation is not critical at high triaxial stresses as the soil behaves as a normally-consolidated material. These aspects have been discussed in Fell (1987).

Testing at high strain rates therefore results in high c' and low Φ' apparent values. High cohesion values are usually associated with "undrained" strength parameters of over-consolidated clays due to negative pressures associated with shearing. Consequently, undrained shear strength can be higher than drained strength in over-consolidated clays.

High triaxial testing stresses: It is known that effective stress friction angle is higher at low normal stresses. Therefore it is important to carry out triaxial tests in a stress range close to the stresses existing in the structure.

High cohesion value shown in the 1980s tests would be an apparent cohesion value due to the linear shear strength-stress model drawn from a limited number of high testing stresses. The actual shear strength-stress relation may curve back through the origin. This trend can be generally observed in the higher p′ values in p′–q′ plots.

Use of multi-stage testing: If the initial stage is strained too far, the Mohr circles of the later stages may be smaller than they should be due to earlier over-working (strain softening) of the test specimen.

4.2.2 *Recent laboratory tests*

Drilling and sampling was undertaken to target areas where soft clay had been logged in the 1980s. However, samples retrieved did not include clays of similar consistency to those reported previously. The recent sampling and testing procedures were in accordance with current best practices. The five triaxial tests performed didn't show effective angles of friction and are close to 30 degrees.

4.2.3 *The model adopted*

The main drawback with the 1980s triaxial results is the "high" effective cohesion values c′ and "low" Φ' values quoted. Therefore, the cursory use of high c′ values could result in unsafe designs at low stress levels whereas the use of only low Φ' values would result in over conservative results. The latter may have been the reason for the 1989 toe weighting design. The current recommendation is to use zero c′ values as this is not an intrinsic property of a non-cementitious soil mass [Schofield, 1998]. Even if some cohesion (or tension) capacity exists in heavily overconsolidated soil, it can be lost at very small strain levels due to its brittle behaviour.

The approach adopted in developing the model herein is very simple in concept and results in a bi-linear shear strength-stress relationship to describe the effective stress parameters of the soil.

In the low stress range, c′=0kPa and representative Φ' values were determined from other means such as (1) PI values, (2) SPT-N correlations, with some reservations, and (3) five test results from the 2002–2003 triaxial tests done at 0.05mm/min strain rate.

At high stress levels, the shear strength was limited to that given by the 1980s c′-Φ' relationship. This was to safeguard against overestimating the shear strength at high stress levels in impervious soils (shear strength relationship is close to undrained behaviour).

Similarly, undrained p_u–q_u values were calculated without excluding the pore pressures but with corrections for the initial back pressures.

The foundation was divided into 5 layers due to 3 primary reasons: (a) it would represent the variation of the foundation strength in a better way in the stability analysis model; (b) it would represent observed variation in the parameters shown from correlations with SPTs and PIs and (c) observations made in the boreholes for a possible layering system.

The p–q plots were used to determine the best-fit curve and then the average c and Φvalues for both effective stress and undrained strength conditions. It was considered that plasticity index (PI) would also provide a reasonable indication of the effective stress parameters of a "clayey" soil. PI correlations given by Kenney (1953) were used. Drained residual strength values were obtained from reported correlations, Lupini (1981).

4.3 *Stability analysis*

Phreatic surface: The phreatic surface developed by the maximum recorded values showed that the clay core is effective in lowering the phreatic surface. It is considered unlikely that the piezometers would pick any localised areas with high pore pressures (perched water tables) due to concentrated leaks in the clay core.

Stability analysis method: Limit equilibrium analysis in Slope/W software package was used with the Morgenstern-Price method. The critical slip circles were selected from a range of slip circles, generally the ones passing at the upstream crest of the embankment.

The relevant ANCOLD Guidelines related to dam stability assessment was issued in 1969 and it is outdated and would not reflect on the current level of understanding of the loading conditions, soil behaviour and interpretation of test results. Consequently, the following design criteria were developed for the Churchman Brook dam upgrade design.

Filter criteria: A sandwich filter (2A, 2B, 2A) is to cover the downstream face of the dam and wrap partially around the abutments. The maximum seepage value of 1 litres/s measured during Churchman Brook surveillance was considered. The filter discharge capacity was designed with a FOS of at least 10.0. The filter materials used in the design shall comply with the criteria set out by [Sherard, 1984; Fell, 1992].

Filter extents: The filter dimensions (2A/2B/2A) were determined by the required discharge capacity and convenience of placement and construction. The thickness of each filter (i.e., dimension perpendicular to the dam slope) is 400mm. The sandwich filter is to extend vertically to the Full Supply Level. The 2A filter shall be extended through to the underside of the crest paving. The filters were also extended over the left abutment to the spillway and a nominal distance over the right abutment to reduce risk of piping through the abutment.

Weighting over the filters: There are no accepted or reported criteria in this regard within the dam design practices. Sufficient weighting should be placed over the filters to avoid filter uplift or blow out. Sherard's filter design mechanism [Sherard, 1984] assumed that any minute pipes (concentrated leaks) formed in the clay core (base material) would be blocked by the filter and then the base material would collapse into the pipe thus creating a self-sealing process. Under the above conditions, weighting over the filters was not probably an issue in new dams due to "small" cross-sectional area of the concentrated leak. However, at Churchman Brook, it is highly likely that there are preexisting soft area and voids in the clay core. In the absence of any reported precedented cases, the following criteria were used for dimensioning the fill above the filter for Churchman Brook dam:

General criteria: The minimum horizontal width of the weighting over the filters was 5m (1.5×the compactor width).

Between Dam Crest and RL=198mAHD

Deficiencies are believed to exist in the dam core between RL 201 and RL 198m AHD. The simple overburden total stress (=∑vertical heigth×density) shall be equal to 1.2 times the maximum head (from FSL) on the filter/embankment interface. This "implicitly" assumes that soft zones and defects exist throughout the dam body in this region. A FoS of 1.2 would allow for the uncertainty in the density in the weighting material.

Below RL=198mAHD down to the toe of the dam.

Below RL 198m AHD, it is highly unlikely that continuous voids exist below RL=198m AHD.

In order to arrive at a conservative but a realistic size for the downstream fill, it was assumed that the weighting+filter material shall be able to sustain the corresponding head (from FSL) acting through a void of 1.0m^2 cross-sectional area on the underside of the filters. The stabilising weight is assumed to be provided by a truncated push-out cone with an apex angle of 40 degree and saturated density. The selected apex angle of 40 degree is indirectly related to the friction angle of the weighting+filter. A FoS of 1.5 should be used to allow for uncertainty in the density and friction angle of the material.

At Churchman Brook, the downstream slope required to satisfy the above filter-blowout criterion is 1 v:2.3 h with a minimum fill width of 5m at the dam crest and this profile is used in the following stability analyses (Fig. 1c).

Steady state seepage: The soil strength parameters to be used are the "effective" (drained) stress parameters. There are 3 processes in which pore pressure is developed in a dam body: (1) seepage from the upstream storage, (2) pore pressure-induced by loading (change of total stress in an elastic state), and (3) shear-induced pore pressures in the shearing planes.

In a dam body, both gravity and water load on the upstream face are long-term loadings and therefore it is reasonable to assume that pore pressures induced by loading and shearing have been dissipated. However, seepage pressures should be considered in the slope stability analysis. Factor of Safety of at least 1.5 using limit equilibrium methods.

The calculated FoSs for two slip surfaces (through the dam body and foundation) are 1.86 and 1.78 respectively.

Seismic load case (MDE): Use consolidated undrained shear strength parameters in conjunction with steady-state seepage pressures (i.e. use effective stresses after allowing for steady state pore pressures). The use of undrained shear strength parameters recognises the development of pore pressures during seismic excitation and also acknowledge that it is somewhat difficult to predict what these seismic-induced pore pressures are theoretically. This also implicitly assumes that seismic-induced pore pressures will not be dissipated (i.e. undrained conditions during the seismic excitation). This approach can be treated as a hybrid analysis method and would be more accurate than a traditional undrained analysis in conjunction with total stresses.

Carry out a simplified dynamic analysis of MDE seismic load using Makdisi & Seed (1978) method if the pseudo-static FoS falls below unity. Reduce the above strength parameters by 20% to allow for strain softening if large deformations take place under the earthquake loading. At Churchman Brook, it was conservatively assumed that the seismic coefficient is equal to the peak ground acceleration (PGA) for the pseudo-static analysis.

Limit crest settlement to 1m and ensure that shear displacements are less than the proposed filter thickness so that potential post-earthquake piping is avoided. The seismic event (MDE) considered has an AEP of 1:10,000 with a PGA of 0.2g for the Churchman Brook Dam site. Also the crest deformations were calculated for MDE=1:100,000 (PGA=0.4g) to ensure that the settlement is less than the existing freeboard.

The calculated FoS with a seismic coefficient=0.2 g (AEP=1:10,000) are 1.28 and 1.42 and these values are greater than unity thus indicating that there may be only small permanent displacements under the MDE event of 1:10,000.

To estimate the performance of the dam under AEP=1:100,000 (PGA=0.4 g), a similar pseudostatic analysis was undertaken and the resulting FoS value is 0.90. A Makdisi-Seed deformation analysis showed that the maximum crest displacement is about 30mm.

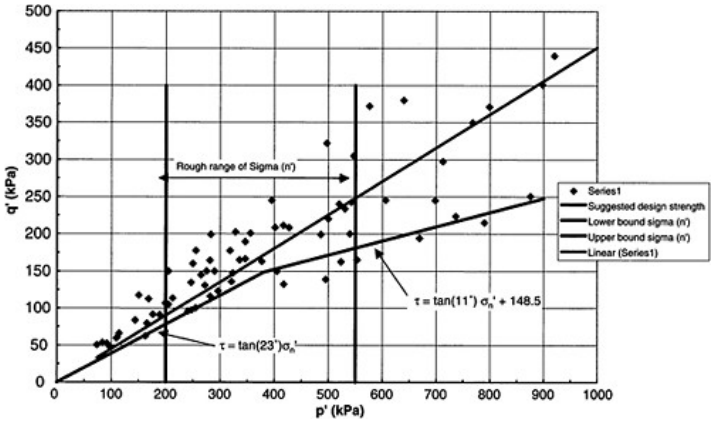

Figure 3. Shear and confining stress plots (p′–q′ plots) for triaxial data and selected lower-bound curve.

It was also assessed that the transverse cracking of the dam due to seismic excitations would be small and the underlying filters of the new fill would provide protection against this cracking.

4.4 *Lower-bound FoS assessment*

At the beginning of the detailed design, it was decided to add a 4m wide berm at the mid-height for the convenience of dam inspections and erosion control due to rainfall runoff. The slope was made at 1 v:2.5 h to minimise the slipping of topsoil under wet conditions.

To obtain a ower value FoS for the dam stability, it was decided to adopt a "lower-bound" strength (bi-linear) model incorporating all the available p′–q′ data points Figure 3. The calculated FoS value for the steady-state seepage condition with water level at the FSL is 1.55. Finally, adopted shape for the fill is shown in Figure 1c.

5 CONCLUDING REMARKS

A comprehensive dam safety study and a risk workshop undertaken has showed the dam to be deficient in aspects associated with piping, spillway adequacy and outlet works condition.

Considering the nature of the foundation materials and past stabilisation works undertaken due to apparent low strengths of the foundation material, a comprehensive model was developed to represent the foundation strength parameters. This utilised a large number of triaxial tests carried out in 1980s and recent investigations. Based on this rational geotechnical model, it has been decided to remove the 1989 toe weighting and replace it with a fill with a smaller extent downstream. Part of this excavated material will be used in the filter stabilisation fill.

The upgrading of the existing spillway chute will be undertaken at an estimated cost equal to about 30% of a new spillway chute.

The planned upgrading works are designed to ensure the safety of the Churchman Brook Dam in accordance with modern dam practices.

REFERENCES

Australian National Committee on Large Dams, ANCOLD, (1984): "Churchman Brook Dam installation of removable piezometers", Bulletin No. 69.
Australian National Committee on Large Dams, ANCOLD, (2000): "Guidelines on Assessment of Consequences of Dam Failure".
ANCOLD Guidelines, (1969): "Current technical practices for design, construction, operation and maintenance of large dams in Australia".
Australian National Committee on Large Dams, ANCOLD, (1998): "Guidelines for Design of Dams for Earthquakes".
Fell, R., MacGregor, P. & Stapledon, D. (1992): "Geotechnical Engineering of Embankment Dams", Balkema, Rotterdam.
Kenney, T.C., "Discussion", ASCE, Vol. 85, No. SM3, 1953.
Lupini, J.E, Skinner, A.E. & Vaughan, P.R. (1981): "The drained residual strength of cohesive soils", Geotechnique 31, No. 2, pp. 181–213.
McLellan, G. (1976): "Chute spillway sub-drainage and anchorage", 12th ICOLD Congress, Mexico, Vol. IV, C16, pp. 1029–1037.
Makdisi, F.I. & Seed, B.H. (1978): "Simplified procedure for estimating dam and embankment earthquakeinduced deformations", Journal of Geotechnical Engineering, ASCE, Vol. 104(7).
Parr, J. (1927): "Perth Water Supply", Institution of Engineers Australia.
Schofield, A.N. (1998): "Don't use the c-world", Ground Engineering.
Sherard, J.L., Dunnigan, L.P. & Talbot, J.R. (1984): "Filters for silts and clays", Journal of Geotechnical Engineering, ASCE, Vol. 110.

New Developments in Dam Engineering—Wieland, Ren & Tan (eds),
© 2004 Taylor & Francis Group, London, ISBN 04 1536 240 7

Nonlinear parameter identification of geo-materials

Xiangdong Qian, Yin Zhao & Qingwen Ren
Hohai University, China

ABSTRACT: Material parameters such as elasticity module, cohesion and friction angle are very important for dam engineering or slope engineering, which directly affect the safety and economy of a project. But the parameter values used in design time may be not the actual because of the complexity of geologic condition and the construction disturbance. Therefore, how to get the reliable material parameters becomes more and more significant. With the development of field test and observation, the parameters can be identified by back analysis with observed deformation, stress or other responses of a geo-structure during construction. Because the responses, usually, are nonlinearly relative to the material parameters, the analyses are all nonlinear in the identification, and the procedure can be expressed as the solution of a nonlinear optimization problem. In this paper, the back analysis model is presented to be a nonlinear least square problem which solved with the LMF (Levenberg-Marquardt-Fletcher) method. And the parameters to be identified are classified several sets according to their sensitivity to the response, which can improve the convergence and accuracy of the solution. Two examples, a dam foundation and a rock slope, are presented in this paper, and the result shows that the model and implement presented is reasonable and effective for nonlinear parameter identification of geo-materials.

1 INTRODUCTION

For geo-engineering projects, physical and mechanical parameters such as elasticity module, cohesion and friction angle are very important, which directly affect the safety and economy of a project. But the parameter values adopted in design time may be not the actual because of the complexity of geologic condition and the construction disturbance. A way to get the reliable material parameters is back analysis. With the development of modern measuring technique, computing technique and field observing and monitoring technique since 1970's, the field measuring data in construction time are widely used in modern engineering design (especially in underground engineering) to identify the parameters of materials, and furthermore improve the design.

At present, the determined model is generally used in the back analysis of civil engineering [1]~[5]. The model is based on stable data and suits to the cases in which the measuring means are accurate or the system output is rather little disturbed by external factors (such as the unstable input disturbance of a system). In the determined model, the direct method based on optimization program is suitable to nonlinear problems.

The direct method originates from the concept of system identification, and its basic procedure, for an observing or monitoring object, is as follows:

(1) building a theoretic model to describe the system behaviors, in which the parameters to be identified are supposedly expressed $\mathbf{X}=[E, C, \varphi]^T$ express the material parameters;
(2) describing the external loads acting on the system;
(3) observing the structural response $\mathbf{u}^*$(displacements, strain, temperature, frequency and so on) caused by loads with field measuring system made up of measuring instruments;

(4) analyzing the response $\underset{\sim}{X}$:

$$\underset{\sim}{u} = f(\underset{\sim}{X}) \tag{1}$$

where f usually a nonlinear function;
(5) building the objective function, $\underset{\sim}{X}$ to be identified;
(6) selecting an optimal method to search the $F(\underset{\sim}{X}^*)$ minimum, i.e.,

$$F(\underset{\sim}{X}^*) = \min F(\underset{\sim}{X}) \tag{2}$$

where $\underset{\sim}{X}$.

It can be seen that the direct method is factual an optimization procedure in which a series of normal analyses are proceeded and owing to the unity of its mathematical model, the direct method made it easy to program and also it can solve more complex problems.

2 OPTIMIZATION METHOD

It is important to select a good optimization method for improving the efficiency of back analysis and obtaining reliable and sensible result. It can be seen from the procedure of direct method introduced above that the mathematical model of back analysis is minimum squares problem and the most effective method solving the problem of this kind is Levinberg-Marqardt-Fletcher method (LMF method).

LMF method is an improved method of Gauss-Newton method and its iterative form is as follows:

$$\underset{\sim}{X}_{k+1} = \underset{\sim}{X}_k + \underset{\sim}{P}_k \tag{3}$$

where, $\underset{\sim}{P}_k$ the solution of the equation:

$$(\underset{\sim}{T}_k + \alpha_k \underset{\sim}{W}_k)\underset{\sim}{P}_k = -\underset{\sim}{g}_k \tag{4}$$

And $\underset{\sim}{X}_k$

$$\underset{\sim}{g}_k = \nabla F(\underset{\sim}{X}_k) = 2\underset{\sim}{R}_k^T r_k \tag{5}$$

$$\underset{\sim}{r}_k = \underset{\sim}{r}(\underset{\sim}{X}_k) = \underset{\sim}{u}(\underset{\sim}{X}_k) - \underset{\sim}{u}^*(\underset{\sim}{X}_k) = (r_1(\underset{\sim}{X}_k), r_2(\underset{\sim}{X}_k), \cdots, r_m(\underset{\sim}{X}_k))^T \tag{6}$$

$$\underset{\sim}{R}_k = \begin{bmatrix} \dfrac{\partial r_1(\underset{\sim}{X}_k)}{\partial x_1} & \cdots\cdots & \dfrac{\partial r_1(\underset{\sim}{X}_k)}{\partial x_n} \\ \cdots\cdots & \cdots\cdots & \cdots\cdots \\ \dfrac{\partial r_m(\underset{\sim}{X}_k)}{\partial x_1} & \cdots\cdots & \dfrac{\partial r_m(\underset{\sim}{X}_k)}{\partial x_n} \end{bmatrix} \tag{7}$$

$$\underset{\sim}{T}_k = 2\,\underset{\sim}{R}_k^T\,\underset{\sim}{R}_k \tag{8}$$

When computing, $\underset{\sim}{T}_k$ But the selecting of α_k is complex and it can be referred to reference [6].

The convergence criterion of iterative form is $F(\underset{\sim}{X}_k)\leq\varepsilon_1$ or $||gk||\leq \varepsilon_2.\varepsilon_1$ and ε_2 are pre-assigned accuracy tolerances.

3 RESPONSE ANALYSIS METHOD

In the process of back analysis with optimal iteration, the system responses should be computed for a serial supposed material parameter $\underset{\sim}{X}_k$. The process to get system responses with given material parameters is called normal analysis. If only the displacement responses are considered, the above back analysis process is named displacement back analysis.

The nonlinear finite element method (NFEM), seen in [7], is efficient for resolving displacement responses of complex nonlinear structural or geo-engineering system. But in the NFEM model, the constitutive relation selected for the system must show its physical and mechanical properties and include all the material parameters to be identified.

4 GROUPING IDENTIFICATION TECHNIQUE

Usually, the sensibility of the objective function $F(\underset{\sim}{W}_k)$ to each material parameter is different. The objective function made up of system displacements is usually sensitive to deformation modulus of material, but not so to strength parameters (such as friction coefficient f, cohesion c). So, in order to improve the accuracy of the optimal computing and accelerate the convergence in practical back analysis process, the material parameters to be identified are divided into groups according to their sensibility, and each group parameters are identified in the sequence of high sensibility to low sensitivity.

5 EXAMPLES

5.1 *Dam foundation*

A supposed concrete gravity dam and rock system is shown in Figure 1. The dam is 50m in height and 40m wide at bottom. There is a weak joint with an incline angle of 45° in the bedrock. Loads up on the system are gravity, full reservoir water pressure, and osmotic pressure in rock.

The design values of material parameters are as follows:

Elasticity modulus of dam concrete $E_c=2.0\times10^4$MPa, and Poisson's ratio $\mu_c=0.167$; Elasticity modulus of rock $E_r=3.0\times10^4$MPa, and Poisson's ratio $\mu_r=0.25$; Elasticity modulus of weak joint $E_w=2.0\times10^2$Mpa, Poisson's ratio $\mu_w=0.30$, friction coefficient f=0.557, and cohesion c=0.1 Mpa.

The displacements at three points A, B and C computed from the design value are supposed to be taken as field measuring displacements. And the elasticity modulus of concrete and rock, friction coefficient and cohesion of weak joint can be identified with these measured displacements. The initial values supposed and the final values identified of the parameters are listed in table 1.

5.2 *Rock slope*

Figure 2 shows a high slope of a hydroelectric engineering in China. The slope is about 100m in height. It contains five principal faults and six groups of fracture. According to the display of the pre-assigned observing instruments, the slope has given rise to rather big deformation under the

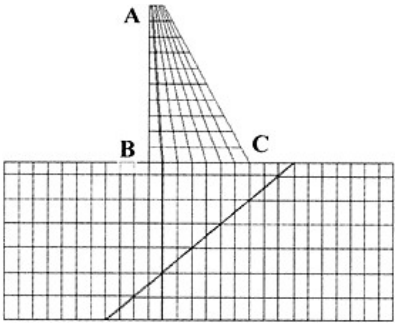

Figure 1. Concrete gravity dam-bedrock system.

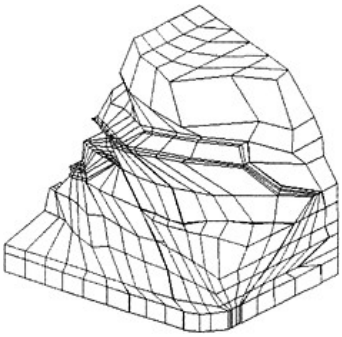

Figure 2. Rock slope of a hydroelectric engineering.

Table 1. List of material parameters.

Name	Initial value	Final value	Design value
Elasticity modulus of dam/Mpa	10000	20070	20000
Elasticity modulus of rock/Mpa	40000	30020	30000
Friction coefficient of joint	1.0	0.492	0.577
Cohesion of joint/Mpa	0.2	0.109	0.10

Table 2. Displacements of measuring points. (Unit: mm)

Point	Computing value	Measuring value	Point	Computing value	Measuring value
1	1.256	1.020	9	2.283	
2	1.309	1.870	10	2.590	
3	2.671	3.140	11	8.999	
4	4.333	4.330	12	11.773	
5	4.828	3.660	13	12.544	
6	1.195	0.660	14	10.756	
7	1.635	1.190	15	12.158	
8	2.008	1.690	16	1.772	

effect of excavation and ground water. The purpose of the research is to identify the factual deformation modulus of rock after excavation according to existed observing deformation data. By so, the stability of the slope can be further predicted and controlled.

By the sensibility analysis of the material parameters, it shows that the displacements at measuring points are sensitive to the rock deformation modulus of the two main loose zones located in the upstream and downstream of outside of the faults along the river, but basically not so to other parameters. So, the deformation modulus of rock in the two loose zones is selected as the parameters to be identified, denoted as E_1, E_2. Their initial values are taken as E_2^*=2369 Mpa. The displacements of observing points computed from above identified values and field measuring displacements are listed in table 2.

6 CONCLUSIONS

(1) The problem of parameter identification of geo-materials can be reduced to a problem of the minimum squares with the material parameters as its variables and it can be solved by high efficient classical algorithm (such as LMF method).
(2) Owing to the different sensibility of each material parameter to the objective function, the material parameters can be made grouping iteration according to the level of their sensibilities. The parameters with high sensibility can be identified firstly, and then the parameters with lower sensibility.
(3) Examples show that the parameter identification method presented in this paper is high efficient and practical and has good accuracy.

REFERENCES

[1] Maier G, Gioda G. Optimization methods for static parametric identification of geomechanics system. Numerical Method in Geomechanics, Boston, 1981, 273–304
[2] Li Suhua, Zhu Weisheng. Application of optimization methods in back analysis of deformation monitoring in elastic, transversally isotropic and elasto-plastic surrounding rocks. Chinese Journal of rock mechanics and engineering, 1993, 12(2): 105–114
[3] Yuan Yong, Sun Jun. Theory of model recognition for back analysis the constitutive relationship of rock mass and its application. Chinese Journal of rock mechanics and engineering, 1993, 12(3): 232–239
[4] Wang Qixing. Back analysis of mechanical parameter of weak fault face in slope engineering. Advances in rock and soil mechanics. China prospect press, Beijing, 1988, 131–137
[5] Cen Z Z, Shen X P, Xu B Y. A numerical method of material identification in rock engineering. Siriwardan, Zama, Computer methods and advances in geomechanics, 1994, 2229–2234
[6] Den Neiyang, et al. Algorithm of non-restriction optimization. China science press, Beijing, 1982
[7] Yin Youquan. Introduction of nonlinear finite element method of solid mechanics. Peking University press and Tsinghua University press, Beijing, 1987

This page intentionally left blank.

New Developments in Dam Engineering—Wieland, Ren & Tan (eds),
© 2004 Taylor & Francis Group, London, ISBN 04 1536 240 7

Assessment of dam foundation improvement based on strain energy*

Qingwen Ren
Hohai University, China

Bin Hu
China Yangtze Three Gorges Project Development Corporation, China

ABSTRACT: In order to improve the safety of dam, the rock foundation of it is usually strengthened. The most treatment measures are grouting, replacement of concrete (e.g. plug, frame), anchor or prestressing anchor. It is difficult to compare the different strengthening schemes from technique and economy for lack of the index to weigh up the strengthening effect scientifically. The Least Strain Energy Principle is presented in this paper. It points out that the best dam-foundation system strengthened has the least strain energy. And the relationship between the energy and some factors, e.g. Young's modulus, friction coefficient, cohesion, strengthened area etc., has been studied. It shows that strengthening effect increases quickly first and then the effect increasing speed becomes slow when the factors go up. Moreover the changing law of the strain energy during the failure process of dam-foundation system is found. It is beneficial to determine the reinforce scheme and parameters, which ensures safety and economy of the system.

1 INTRODUCTION

By the end of last century, there had been more than 40,000 dams all over the world which played an important role in the economy and development of society China has rich water resource and hydro energy, and nearly half of total dams were built for the development of economy. In recent years, dams built in China are becoming higher and higher. For example, the height of Three Gorges Dam and Longtan dam reaches 200m around, and the height of arch dams such as Xiaowan, Xiluodu and Jinping reaches about 300m. With the increase in the height of dams, the safety of dams is paid more attention, and the requirement for dam rock foundation is stricter than before. In order to improve the dam safety, the strengthening of the rock foundation is usually done. The most treatment measures are grouting, replacement of concrete (e.g. plug, frame), anchor or prestressing anchor. It is difficult to compare the different strengthening schemes from technique and economy for lack of the index to weigh up the strengthening effect scientifically The Least Strain Energy Principle is presented in this paper which can be used in comparing of strengthening schemes and verifying the strengthening effect.

2 LEAST STRAIN ENERGY PRINCIPLE

Besides the excavation of surface crushed rock, the most treatment measures (Dl 5108–1999, 2000) to strengthen the dam foundation is grouting, such as backfill grouting in karst cavity,

* Sponsored by NSFC (50379005).

consolidation grouting in fissured rock and etc. For the fault fracture zone and the weak structural surfaces, properties of rock can be improved by replacement of concrete, such as concrete plugs, resisting piles and key wall. Moreover, bolts and prestressed cables are more and more widely used in protecting surface of rock and improving stability against sliding of dam rock foundation (abutment) and dam itself.

For strengthened dam foundation, the strengthening effect is obtained by physical test such as measurement of sound wave speed by physical detection, the change of quantity of grouting material and water by grouting and water pressure test, measurement of physical and mechanical parameters like bulk density, porosity, Young's modulus, shear strength, and compression strength, etc by sampling of rock. Moreover, the change of microstructure of rock can be known by stereo scan, and the change of composition of rock can be studied by atlas analysis and differential thermal analysis (Liu, 2000 and Zhu, 2002). Of all the method, the most direct is to find out the improvement of quality of rock mass by observing the deformation of dam.

For the design of foundation treatment, strengthening schemes of dams to be built should be compared. The methods referred above is not feasible, and numerical analysis can be used instead. At the present time, the most popular method is comparing the maximum displacement and stress, stress distribution and the area and distribution of failure zone after strengthening with before or between different strengthening schemes according to the result of numerical analysis of damfoundation system (Chen, 2002 and Ren, 2002). In theory, the strengthening scheme with less displacement, stress and area of failure zone is better. But displacement and stress are all local variation, and the maximum displacement, maximum stress and the failure zone may appear at different parts in different strengthening schemes, so the function that they characterize the dam safety is different. Moreover, as the calculation indicates, the displacement and stress are insensitive to different strengthening schemes and the variation of displacement and stress caused by different strengthening schemes is very small. So it is hard to compare strengthening effect through displacement and stress. The same problem also exists when the dam safety coefficient of stability is used to compare strengthening effect, and moreover the stability analysis method of damfoundation system is still controversial, especially for the arch dam.

The strain energy reflects the deformation of the system. It is well known that the stronger the system is, the less deformation and strain energy it has. If the system is strengthened to a rigid body, its strain energy becomes zero. The Least Strain Energy Principle is as follows:

The Least Strain Energy Principle: in view point of deformation, the less the strain energy the strengthened system has, the better the strengthening scheme is.

According to the Least Strain Energy Principle (LSEP), strengthening schemes can be optimized by the use of the strain energy as the object function of the strengthened system and the strengthening support parameter as design variation.

3 RELATIONSHIP BETWEEN STRAIN ENERGY AND SHORING PARAMETERS

3.1 *Strengthened area*

Firstly suppose that an axial symmetrical circle tunnel in infinite homogeneous rock is bearing uniform pressure p, with the inside radius of tunnel being a, the radius of strengthening circle being b, Young's modulus and Poisson's ratio of strengthened circle being E', μ' respectively, and those of unstrengthened rock being E and μ'. Suppose that the tunnel rock is in elastic stage, so when the ground stress is ignored, the stress in the strengthened circle is:

$$\sigma_r' = -p\left(\frac{m_1 b^2}{m_2 r^2} - \frac{1-n}{m_2}\right)$$
$$\sigma_\theta' = p\left(\frac{m_1 b^2}{m_2 r^2} + \frac{1-n}{m_2}\right) \quad (1)$$

the stress in the unstrengthened rock is:

$$\sigma_r = -\sigma_\theta = -2(1-\mu)np\frac{b^2}{m_2 r^2} \tag{2}$$

where $n=E(1+\mu')/E'(1+\mu)$, $m_1=1+(1-2\mu)n$, $m_2=m_1 b^2/a^2-(1-n)$.

For the plane strain problem, stress can be expressed as:

$$\varepsilon_r = \frac{1-\mu^2}{E}(\sigma_r - \frac{\mu}{1-\mu}\sigma_\theta)$$
$$\varepsilon_\theta = \frac{1-\mu^2}{E}(\sigma_\theta - \frac{\mu}{1-\mu}\sigma_r) \tag{3}$$

for axial symmetrical problem, the elastic strain energy can be calculated by the following equation:

$$U = \frac{1}{2}\int \sigma\varepsilon dv = \pi\int(\sigma_r\varepsilon_r + \sigma_\theta\varepsilon_\theta)rdr \tag{4}$$

Substituting equation (1), (2) and (3) into (4), the strain energy in strengthened circle U_1 and unstrengthened rock U_2 are:

$$U_1 = A_1\frac{(1+\mu)\pi p^2 a^2}{E}, \qquad A_1 = \frac{n}{m_2^2}(\frac{b^2}{a^2}-1)[m_1^2\frac{b^2}{a^2}+(1-2\mu)(1-n)^2] \tag{5}$$

$$U_2 = A_2\frac{(1+\mu)\pi p^2 a^2}{E}, \qquad A_2 = \frac{4(1-\mu)^2 n^2}{m_2^2}\frac{b^2}{a^2} \tag{6}$$

the total strain energy of the system U is:

$$U=U_1+U_2 \tag{7}$$

Suppose that $\mu=\mu'=0.2$, then $n=E/E'$. According to equation (5)–(7), the total strain energy of the system is calculated when n equals 0.5 and 0.8, as Figure 1 shows. When n is set as 0.5 and 0.8, which shows that Young's modulus in the strengthened circle is increased by 100% and 25% than that of the material in the unstrengthened rock respectively. It is shown that the system strain energy is decreasing with the increase in the Young's modulus of the material in the strengthened

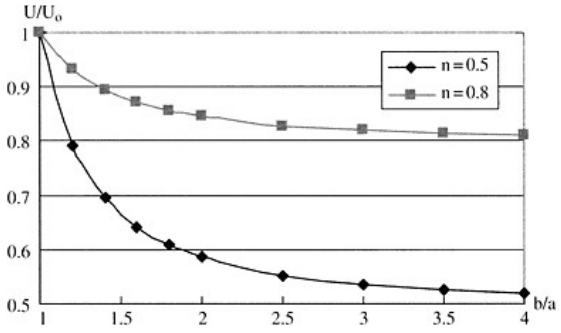

Figure 1. U/U_o vs b/a for circle tunnel.

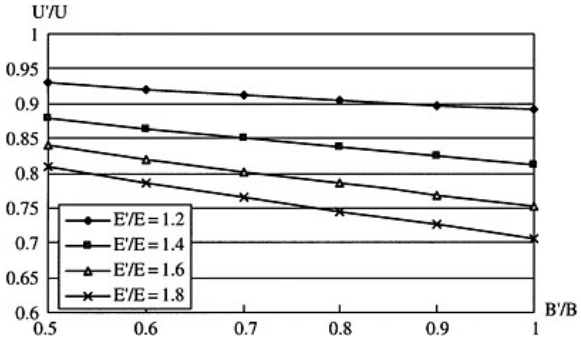

Figure 2. U′/U vs B′/B for dam foundation.

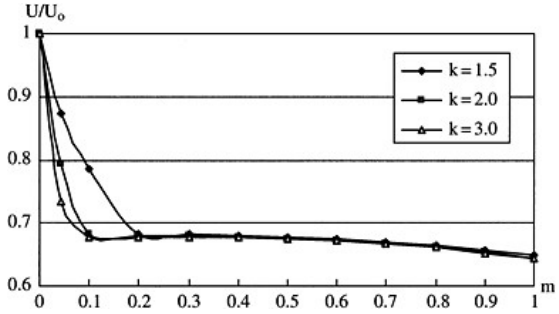

Figure 3. U/U$_o$ vs m for dam base surface.

circle. With the expansion of the strengthened area, the strain energy of the system decreases sharply. But after *b/a*>3, the change of the strain energy of the system is very slight. So when the strengthened area is expanded to a certain degree, the strain energy of the system tends to be steady and the further expansion is ineffective.

For the gravity dam based on the infinite foundation, it is difficult to calculate its strain energy by analytic method, so numerical analysis method can be used instead. The curve of the relation between the strengthened area of the gravity dam foundation and the strain energy of the damfoundation system is shown in Figure 2, where B is the bottom width of the gravity dam, B′ is the strengthening area expanding from the dam base surface to upstream, downstream and underground, E, U are the Young's modulus and the system strain energy of the unstrengthened dam foundation rock, and E′, U′ are the Young's modulus and strain energy of the system of the strengthened dam foundation rock. It is shown that with the expansion of the strengthened area, the decrease of the strain energy in the system is very obvious. Although the strain energy has a linear decrease approximately with B′/B increasing from 0.5 to 1.0, the calculation shows when the strengthened area is further expanded (B′/B>2.0), the strain energy of the system tends to be constant.

The above is the effect of the increase in the Young's modulus of the strengthened material on the strain energy, and Figure 3 shows the effect of the change of shear strength of the gravity dam base surface on the system strain energy. Suppose that the shear strength of the foundation material is less than that of dam concrete and foundation rock, and the gravity dam has a possibility to slide along the base surface. The dam is strengthened by increasing the shear strength (friction coefficient *f* and cohesion *c*) of the base surface. In Figure 3, m and k represent the ratio of the

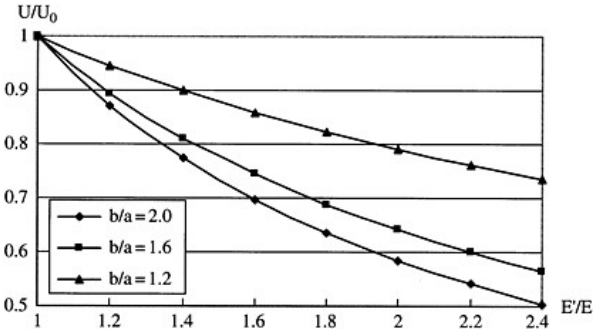

Figure 4. U/U_o vs E′/E for circle tunnel.

strengthening area of the base surface to the bottom width of a gravity dam and the shear strength of the base surface strengthened to that unstrengthened respectively. It is obviously seen that the system strain energy decreases significantly with the increase in the shear strength of the base surface.

3.2 *Strengthening level*

The above two examples are used to study the effect of strengthening level on the system strain energy.

For the axial symmetrical circle tunnel in infinite homogeneous rock, considering that the Young's modulus in the strengthened circle is increased at different level comparing with that in unstrengthend rock, the relationship between the system strain energy and the strengthening level of the material in the reinforcement circle can be obtained by calculating system strain energy according to (5)–(7). Figure 4 shows that the system strain energy initially decreases sharply, and then slowly with the increase in the strengthening level E′/E.

The same rule is also seen in Figure 2 and Figure 3. With the increase in strengthening level E′/E or k, the distance between the adjacent strain energy curve becomes smaller and smaller, which indicates that the variation of the system strain energy is gradually unobvious with the increase in strengthening level.

4 STRAIN ENERGY DURING STRUCTURE FAILURE PROCESS

4.1 *Thick-walled cylinder*

An axial symmetry thick-walled cylinder with inside radius *a* and outer radius *b* is bearing uniform internal pressure. Supposing that *p* is increased form zero gradually, so the thick-walled cylinder is initially in elastic stage, but when *p* is increased to a certain value, the inner part of the cylinder firstly enters into plastic stage and the plastic area gradually expanded until the whole cylinder is under plastic failure.

Supposing that the cylinder is made of the ideal elastic-plastic material with yield strength σ_s, which can be regarded as plane problem. When the radius of the plastic area is *c,* the stress in the elastic area can be expressed by formula (8).

$$\sigma_r = \frac{\sigma_s c^2}{\sqrt{3}b^2}\left(1-\frac{b^2}{r^2}\right)$$
$$\sigma_\theta = \frac{\sigma_s c^2}{\sqrt{3}b^2}\left(1+\frac{b^2}{r^2}\right) \quad (8)$$

the stress in the plastic area *(a≤r≤c)* is as follows:

$$\sigma_r = -p + \frac{2}{\sqrt{3}}\sigma_s \ln\frac{r}{a}$$
$$\sigma_\theta = -p + \frac{2}{\sqrt{3}}\sigma_s(1 + \ln\frac{r}{a}) \tag{9}$$

where the radius of the plastic area *c* can be defined by equation (10)

$$\ln\frac{c}{a} + \frac{1}{2}(1 - \frac{c^2}{b^2}) = \frac{\sqrt{3}p}{2\sigma_s} \tag{10}$$

When the cylinder is under plastic condition, the elastic and plastic strain energy should be calculated by increment method. As the load is increased from p to $p+\delta p$, the increment of the elastic strain energy δU^e and the plastic strain energy δU^p is:

$$\delta U^e = 2\pi\int_a^b(\sigma_r\delta\varepsilon_r + \sigma_\theta\delta\varepsilon_\theta)rdr = \frac{\pi\sigma_s c^2}{\sqrt{3}G}\delta p \tag{11}$$

$$\delta U^p = 2\pi\int_c^b(\sigma_r\delta\varepsilon_r + \sigma_\theta\delta\varepsilon_\theta)rdr = \frac{2\pi\sigma_s b^2c^2}{\sqrt{3}G(b^2-c^2)}\ln\frac{c}{a}\delta p \tag{12}$$

respectively, the total strain energy can be obtained by the sum of the both:

$$\delta U = \delta U^e + \delta U^p \tag{13}$$

For example, there is a thick-walled cylinder with the inner radius a=1m, outer radius b=1.2m, the Young's modulus E=2×10^5MPa, Poison's ratio μ=0.2 and the yield stress σ_s=250 MPa. Analysis shows that p=44.10MPa when the cylinder firstly enters into plastic stage, and p=52.63 MPa when it is plasticity wholly. According to equation (11)–(13), the strain energy is calculated and the corresponding curve is shown in Figure 5, where U_o is the strain energy when p=40 MPa. It is shown, the increment of the strain energy in plastic stage is greater than that in elastic stage and it increases rapidly with p increasing. When p≥ 52.63 MPa, the strain energy goes to infinite characterizing the structure is thoroughly destroyed.

4.2 *Gravity dam*

For the gravity dam, the same conclusion can be drawn that when sliding failure occurs to it along the base surface, the system strain energy goes to infinite. For example, there is a 100m high and 70m wide in bottom gravity dam with the shear strength of base surface is f=1.0, c=20MPa. Using Strength Reserve Method that f, c are reduced by K times at the same time, the ratio F of the sliding resistance of the dam base surface to sliding force and the system strain energy are calculated according to the stress on base surface obtained by nonlinear element method. The change of F and U/U with that of K is shown by the curve in Figure 6, where U_o and U are the system strain energy without and with decrease in f and c respectively. It can be seen that when no decrease occurs to f and c, F≈3.6; with K increasing, F decreases rapidly, while U/U changes slightly. When K approaches 5.6, the system strain energy goes to infinite and F closes to 1.0 gradually characterizing the whole base surface is in plastic stage, and sliding failure occurs.

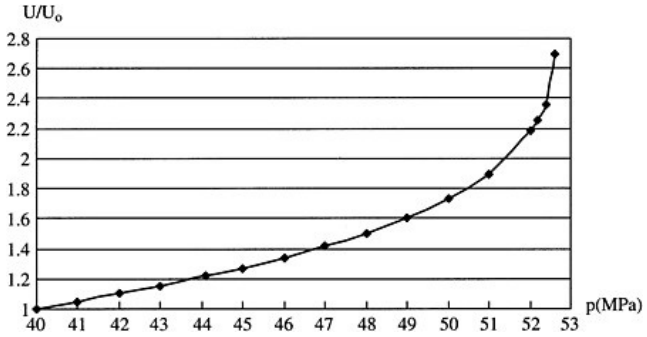

Figure 5. U/U$_o$ vs p for thick-wall cylinder.

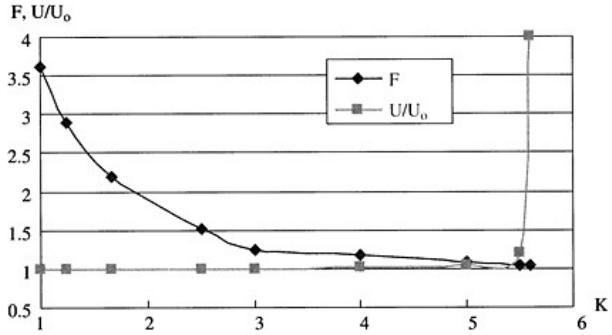

Figure 6. F and U/U$_o$ vs K for dam base surface.

5 CONCLUSION

In the paper, the Least Strain Energy Principle is presented, the relation between the system strain energy and supporting parameters is studied and the rule of the change of the system strain energy in the process that the structure is destroyed is investigated.

In view point of deformation, the less the strain energy of the strengthened system is, the better the reinforcement scheme is.

With the expansion of the reinforcement area and the upgrade in strengthened level, the strain energy of the dam-foundation system initially decreases rapidly, afterwards slowly and even tends to be constant.

When the strain energy of the dam-foundation system goes to infinite, the dam approaches sliding failure.

REFERENCES

[1] Chen Weizhong, Zhu Weisheng, Qiu Xiangbo, Yang Jialing and Zhang Qiangyong. Research on Reinforcement Scheme for Xiaowan Abutment. *Chinese Journal ofRock Mechanics and Engineering,* Wuhan, China, 2002, Vol. 21(3), 374–378. (in Chinese)

[2] *Dl 5108–1999. Design specification for concrete gravity dams.* China Power Press, China, 2000. (in Chinese)
[3] Liu Chang-wu and Lu Shi-liang. Reinforcement Eifect of Cement Grouting on Engineering Rock Mass, *Journal of China University of Mining & Technology,* Xuzhou, China, 2000, Vol. 29(5), 454–458. (in Chinese)
[4] Ren Qingwen, Qian Xiangdong, Zhao Yin and Fu Shuhong. Methods for analyzing s sliding resistance stability along the base surface of high arch dam. *Journal of Hydraulic Engineering,* Beijing, China, 2002, (2), 1–7. (in Chinese)
[5] Zhu Jiebin, Han Jun, Cheng Liangkui and Xiao Guoqiang. Research on Rock Mass Properties near Anchor with Prestressing for TGP Permanent Shiplock, *Chinese Journal of Rock Mechanics and Engineering,* Wuhan, China, 2002, Vol. 21(6), 853–857. (in Chinese)

New Developments in Dam Engineering—Wieland, Ren & Tan (eds),
© 2004 Taylor & Francis Group, London, ISBN 04 1536 240 7

Analysis of impacts of large dams on river ecosystems

Ruan Xiaohong & Qi Jiying
Hohai University, China

ABSTRACT: Large dams are one of the symbols of civilization. Nowadays, dams play an important role in river basin management and flood control. In addition, they are used to generate electricity and get clean and cheap energy. At the same time they will affect the river system significantly. Unlike rivers, reservoirs greatly reduce the flow velocity of water. Although builders and managers of dams do their best to alleviate the negative effects of large dams on river ecosystems, they cannot restore the original state. In this study, several cases of long term effects of dams on physical, chemical and ecological characters of river system (downstream, estuary and estuary wetland and so on are discussed). The effective strategies and critical points are summarized to protect river ecosystem in dam construction.

1 INTRODUCTION

Large dam is one of the symbols of human civilization, which is a project for assorting with the relation between human and water. Meanwhile it can protect ecological environment. It can regulate and store up unbalanced water source, and alleviate flood disaster. Potential water energy can be transformed to electric energy by dam and hydropower station, which offers cost saving and clear energy Dam project is an important infrastructure for every country. Nothing can replace dam project, even in the 21th century.

However, dam construction is producing global-scale effects on the environment. Reservoir is opposite to river. River makes water flowing, while reservoir makes water standstill. River is dynamic and mutable. There is sedimentation associated with erosion. Dam is static permanently. It is used to control river, regulate seasonal mode of flood, decelerate flow rate, hold up sedimentary deposit, cut off relation of life in river valley, change temperature and chemical component of river water, disarrange geological course of corrosion and deposit. Although builders and managers of dams do their best to alleviate impacting of large dam on river ecosystem, they cannot restore the original state. The effects of large dam on catchment environment mainly include two aspects, one is resulted from dam construction itself, the other is resulted from the operation mode of dam. They are mainly effects on geological environment, terrestrial hydrological condition, water quality, and ecological environment and so on.

In the study, the effects of dam construction on physical characters, chemical characters and ecological characters of river system are analyzed. The effective strategies and critical points are summarized to protect river ecosystem in dam construction.

2 IMPACTS OF LARGE DAM ON RIVER ECOSYSTEM

The river ecosystem includes the riverheads, rivers between riverhead and estuary, riparian area, estuary area, groundwater and wetland and floodplain area, and nearshore area. Considering the whole ecosystem the effects of large dam include the changes of non-ecological variants and ecological

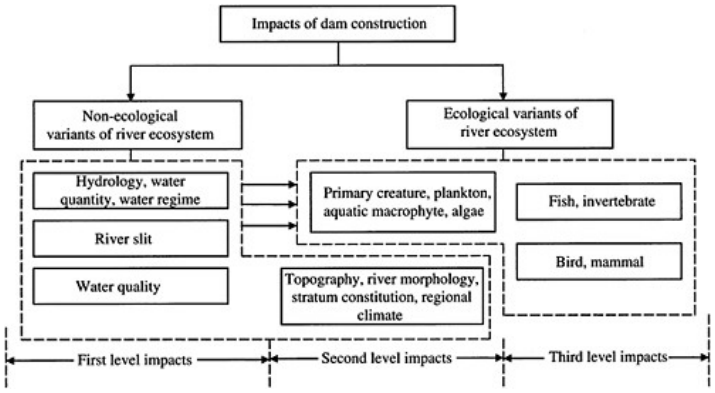

Figure 1. The effects of dam construction on river ecosystem.

variants of a river. The two aspects are related and influenced mutually. Dam construction first has effects on non-ecological variants, including hydrology, water quantity, water potential, silt, water quality etc. These are the first level impact. The second level impact includes catchment land form, topography and primary yield etc. Furthermore, changes happen at higher nutrient level (the third level impact). Usually, the mutual relations between different factors become more and more complicated from the first level to the third level (see Fig. 1).

2.1 *Impacts of dam construction on non-ecological variant of a river system*

2.1.1 *Effects on hydrology of river system*

Dam construction changes the original flow regime of a river. The main alteration is as the following.

(1) Decrease of peak flow and reducing of lake and sea area
Dam construction on a river alters the natural seasonal flow regime of the river. The peak flood flow is decreased. Accordingly, water quantity discharging to lake and sea decreases and water area of downstream reduces. At the same time, the salinity of downstream lake water increases. For example, considering the 139 regulated and free-flowing rivers in the United States, Canada, Europe, and former USSR, that exceed 350 m^3/s in mean annual discharge, eighty-five of them, representing 77% of the total water, were strongly or moderately regulated and fragmented by dams[1]. Quarter of scale of peak flow is averagely decreased after dam building the Nile and the Colorado Rivers seldom discharge fresh water into the sea[2].

(2) Alterationof water level of downstream
After dam is constructed, water level does not change with precipitation amount as usually, but with other factors such as the demand for electricity. The water level even changes within an hour. The discharged water for meeting peak requirement for electricity can even change the water level for several meters at times.

(3) Alteration of groundwater level of upstream and downstream of dam site
Groundwater has close hydraulic relation with surface water. Groundwater is affected by the condition of river hydrology. At the upper reaches of dam site, water is stored in reservoir. So the groundwater level around the reservoir increases. This results in the expansion of inundated area, resulting in soil salinization and swampiness. 1/5 of irrigated land of the whole world has

been polluted by salt. Nearly 2~3 million ha of land is not proper for cultivation because of high salt concentration[3] Meanwhile, dam construction decreases the supply to downstream groundwater. Therefore, the groundwater level falls and lots of land lose the gravitational flow condition, which affects irrigation of downstream land and reduces using rate of water resource.

2.1.2 *Effects on landform and physiognomy of river system*

(1) Backwater sedimentation of reservoir

After river is cut by a dam, slit will settle down to the bottom of reservoir and form backwater delta. This delta elevates towards the dam. For example, dam built across the Maujira River, a tributary to the Godavari River in India, lost 60% of its storage capacity in 43 years because of siltation[4]. It is roughly estimated that 50km^3 silts is settled all over the world every year. In china, there are 80,000 reservoirs and the total storage capacity is nearly 500 billion m^3, which was decreased by 40% because of sedimentation[3].

(2) Downstream narrowing and river morphology simplification

Soil and rocks at areas where water flows through are eroded and moved, parts of which settle down in reservoir and upstream of the dam, especially cobbles and pebbles. Meanwhile, downstream riverbed and bank can be eroded by water discharged from dam. This makes rivers near dam narrower and deeper, and makes wriggle rivers with shoals and river beaches single and straight.

(3) Floodplain and estuary

The intercepting sediment by dam has significant effects on floodplain, delta and nearshore area. Delta is formed by sedimentation and the interaction between sediment crushing and sea water erosion along hundreds and thousands of years. Delta and shoreline will be eroded because of decrease of sediment flowing to the sea, associated with the increment of salinity. For example, before the Aswan High dam was built, 124 million tons of silts flowed to the sea though Nile, and 9.5 million tons of slits settled down at narrow floodplain and the delta area every year. Now, 98% of silts flow into the Nasser reservoir. Sediments in Nile don't flow into the Mediterranean Sea any more. This results that the shoreline of the Mediterranean Sea was backward for about 6000m between 1900 and 1991[3].

2.1.3 *Effects on water quality of river systems*

The chemical, physical and biological changes of flowing water resulted from dam construction can alter the original water quality. The extent of water quality degradation is related to the water retention time in reservoir. The main phenomena caused by water quality degradation include the increment of salinity, changes of water temperature, over growth of algae and the effects of these changes on downstream water quality.

(1) Increment of salinity of water Impounding by dam construction forms expansive reservoirs, which increases the water areas exposed to the sun. At arid regions, reservoir water can evaporate greatly from the surface of reservoirs, resulting in the increment of salinity. At the mean time, salinization of land caused by the increasing of groundwater level by the dam has direct effects on river water quality. Groundwater with high concentration of salt can react with surface water and pollute water quality.

(2) Changes of water temperature of reservoirs Generally, the water discharged from the deep layer of reservoirs is cooler than river water in summer, but warmer in winter. However, the water discharged from top layer is always warmer than river water. The changes of river water temperature can affect the dissolved oxygen and suspended solids in river water, and the chemical reactions happens in water. The water stored in reservoirs for several months or even several years is fatal to the creatures in lower reaches several decade kilometers far from the reservoir.

(3) Changes of the chemical composition of waters At the upper reaches of large dams, the inundated plants consume the dissolved oxygen in water, and release a great amount of greenhouse gas and CO_2. This increases the acidity of water, resulting in the dissolving of mineral matters such as Fe and Mn in lake bed. Besides,

the domestic wastewater from upper reaches can be intercepted in reservoirs, which deteriorates water quality. The self-purification ability of intercepted water is also relatively weak. For the rivers at arid and semi-arid areas, the natural runoff is rare. After interception, the lower reaches are nearly cut ofF. River water loses its dilution and purification ability. Due to a great amount of wastewater discharged from cities and counties along the river, river becomes wastewater ditch losing the original ecological functions.

(4) Propagation of algae in reservoir water

In the mean time of sediment interception by large dams, nutrients are also entrapped. Eutrophication is easy to happen in reservoirs. When the weather is warm, algae can propagate quickly at the water surface where nutrients are sufficient. The over growth of algae produces offensive odor, alters the concentration of dissolved oxygen and results in the lost of the functions of waters. Eutrophicated water is not suitable for using of people and industries.

2.2 *Effects on ecological variables of river systems*

The functions of river systems are affected by non-ecological variables related to hydrology, water quality and silts etc. Furthermore, these will affect ecological variables of river systems. The main effect of dam construction on upstream is the inundation of forest, swamps and the habitats for wild animals by reservoir. For downstream, dams decrease the biodiversity of river systems.

2.2.1 *Effects on the ecological environment of downstream*

Dams disconnect the life network in river valleys. They also affect the ecological environment for the living and propagation of wild lives. Meanders are regulated to be straight, which significantly affects the biodiversity of rivers.

In terms of hydropower dams, the water level changes with the requirement for electricity, resulting in many negative effects on aquatic environment. The rapid fluctuation of water level accelerates the erosion of downstream river valleys. The shallow habitats for fish stocks are inundated or exposed alternatively, affecting egg laying. The life cycle of aquatic lives is sensitive to water temperature, which changes with the temperature of water discharged from reservoir. For example, the propagation, incubation and metamorphosis of larval always depend on the changes of temperature. The main effect of reservoir on terrestrial plants and animals is the inundation of their habitats, while the effects on aquatic plants and animals are much more complicated. Besides the inundation of habitats, reservoir also separates the migration pathways for migratory fish, affects the exchange of different fishes etc.

Large dams change and weaken the hydraulic connection between downstream and groundwater. The water level of groundwater is then decreased, with the result of disappearance of riparian wetlands.

- Plankton: Because large dams control flood, adjust the water temperature, decrease the turbidity of river water, and weaken the dilution of polluted water in downstream, the number of planktons is increased greatly.
- Aquatic macrophytes: Plants with roots are increased. Since large dams can reduce inundation and substrate erosion, more eutrophicated sediments can be accumulated. In the mean time, because large dams can decrease the flood peak flow, the sands in rivers cannot be flushed. Thus, the number of floating plants is increased.
- Riparian plants: The species, such as riparian forest, depending on the changes of flood are affected negatively by the decrease of inundation.
- Invertebrates: The distribution and number of minitype invertebrates change significantly because of the changes of water regime and physio-chemical conditions (e.g. water temperature, turbidity and dissolved oxygen etc.). Large number of cobbles and sand stones are intercepted by large dams, resulting in the lost of living habitats for salmons and the invertebrates living on river beds (e.g. insects, mollusk, and mussel animals etc.).
- Fish: Because of the blockage of migration pathways and the changes of water regime, physiochemical conditions, primary life-forms and morphology of rivers etc., the amount of fish is changed significantly.

2.2.2 *Effects on the wetlands at floodplains*

(1) Lost of wetland landscape

Because of the construction of water conservancies such as dikes and dams, the spatial connection between floodplain wetland and river is cut. The hydrological regime and water cycle of floodplain wetland is then changed, which will result in the degradation of its ecological environment. For example, at the Yangtze River Watershed, nearly 46,000 dams and more than 7,000 sluices were constructed to control flood. They disconnect the relations between rivers and lakes, and have serious negative effects on the ecological environment of floodplain wetlands. With the combined effects of water conservancies and land reclamation, 82% of floodplain wetlands at mid and lower Yangtze River were lost from 1950s till now. Besides the lost of wetland landscapes at floodplains, the regulation and storage ability of lake wetland for river runoff is decreased greatly[5]

(2) Decease of biodiversity of floodplain wetland

The environmental changes of the animal habitats at floodplain area and the separation of river pathways can change the number of birds and mammals. Associated with the lost of wetland landscape, more and more plant and animal species are endangered or even extinct because of the lost of living habitats. The propagation ability and population of plants and animals are decreased. The biodiversity is negatively affected.

(3) Degradation of ecological environment of floodplain wetlands

The structure and function of floodplain wetlands are mainly affected by the hydrological and hydrodynamic conditions at floodplain area. The relative changes and instability of these conditions make the ecosystem to be fragile.

3 STRATEGIES TO ALLEVIATE THE NEGATIVE EFFECTS OF LARGE DAMS ON RIVER ECOSYSTEMS3

Large dams have positive effects on flood control, water amount regulation and energy source supply etc., while also have negative effects, such as population migration, inundation of culture and remainders, and the natural environment changes of upper and lower reaches etc. Therefore, people have tried to attenuate the negative effects of dam construction for a long time, in order to balance the ecological environment improvement and sustainable development.

3.1 *Application of modern techniques*

The modern scientific and technical technologies should be applied in the planning, design, construction and operation of large dams. At the planning period, more remote sensing technologies should be used to collect the environmental, hydrological and geological data of the whole watershed and region. The foundation of large dams and the natural conditions of reservoirs can be studied using modern geophysical prospecting techniques. Numerical and physical models can be applied to analyze the environmental changes before and after dam construction. Computer expert decision making system is effective for the selection of dam shape and construction site, and the design of complicated dam structure etc. Such kind of system can help people to make the optimal decision. New raw materials can be used to improve the quality of dams. Information techniques can be used to establish integrated safety operation monitoring system for large dams, each hydraulic structures and reservoirs. Modern management science and electronic commerce system can be applied to manage the whole process of large dam construction.

3.2 *Environment impact assessment of large dam construction*

The function of environment impact assessment should combine environment requirement into project planning and design, which reflects the principle of sustainable development. During the process of development, the effects of large dam construction on ecology should be assessed, so as to minimize the negative effects.

In the environment impact assessment, economic estimation should be put more emphasis. The changes of environment, resource utilization etc. induced by project construction will definitely affect economic development. Thus, the changes of resources and environment induced by project construction should be evaluated as one of the cost factors for social economic development. Large dam construction has wide effects on ecology and environment. For the positive effects, we should try to exert more of its economic benefits. For the negative effects, we should try to answer the following questions: how to investigate and control these effects? What will be the environmental status after investment and control? What are the benefits of control measures? Based on these answers, the target, direction, items and region of investment can be determined further. Finally, the optimal investment benefits can be gained.

Environment impact assessment should be carried out in the long term, but not be stopped at the period of feasibility validation period. The effects of large dams on ecology and environment are long-term and potential. Many problems, particularly the structure of estuary ecology, reservoir area ecology and aquatic ecosystem, and the changes of functions and benefits, cannot be understood and mastered within a short period of time. The inherent principles can only be found out gradually through long-term monitoring, investigation and research. Therefore, the environmental problems induced by water conservancies cannot disappear at the end of construction, but exist with the life of the project itself. The ecological and environmental benefits should be regarded as the long-term benefits and targets of a project.

3.3 *Establishment of water discharge control regulations beneficial to ecological environment*

Flood regulation refers to discharge water from reservoir and inundate specific range of floodplain or delta area at lower reaches according to special regulations, in order to maintain the ecological process and natural resources. Traditionally, flood was considered as negative effects merely. However, many ecological functions beneficial for humans can be maintained due to the periodical inundation. Regular discharge can attenuate the negative effects of dam construction. Therefore, discharge regulation is an effective measure to rehabilitate downstream ecosystem or maintain it to be at an ideal status.

According to the frequency, duration, time and flow rate of discharge, the relations between production, functions and characters of floodplain (include silt and water quality) can be determined. Particularly, the required amount of inundation to maintain partial ecosystem should be quantified. The discharge and storage of floodwater by reservoir should consider the water usage at upper and lower reaches, including the requirement of water supply and electricity generation, and the demand for maintaining the living environment for aquatic lives. Discharge regulation is a part of the integrated watershed development. It combines traditional and modern consciousness. Its target is to get the maximal benefits (including currency and non-currency benefits) of the development of water resourses.

3.4 *Pollution control of upstream water resources*

Dam construction intercepts the upstream water resources. At the mean time, pollutants in water are also intercepted to the reservoir. Pollution control of upstream has significant values for water resource protection of the whole river system. The domestic, industrial, agricultural and aquacultural wastewater at upstream areas should be collected and discharged after proper treatment. Then, pollutant concentrations associated with river water can be decreased, avoiding the degradation of water quality. Finally, the damages of dam construction to river ecosystems can be attenuated.

3.5 *Construction of water conservancies beneficial for ecological environment protection*

The flow rate of current flowing through dams is increased, which impedes fish from swimming back. The rare fishes may be extinct because of the lost of habitats. Considering the propagating and growing conditions of fishes, establishment of fishway is a good measure to protect fish resources. They can let the fishes run back to the egg laying areas at upstream. The hydraulic calculation and structure design of these fishways are based on the living habits of fishes and requirements of hydraulic structures. In addition, sound facilities can be set at the fishways to guide the migratory fishes to direct to these special structures.

3.6 *Integrated managing proposals for floodplain wetlands*

Inundation is the natural character of rivers and floodplains. Flood is not only one of the manifestations of water resource, but also one of the movement forms of water resource. It plays significant role in the sustainable utilization of regional water resource, maintaining the landscape and maintaining functions of rivers, floodplains and their connection. The reclamation of natural floodplains without limitation restricts the function of inundation, resulting in the degradation of ecological environment of floodplain wetlands. The floodplains should be regulated scientifically. The spatial ranges of inundation for different floods with different frequencies should be determined according to the frequency, intensity and historical characters of flood. The land use patterns at different floodplains should be divided and managed strictly. For example, some of the states in America regulated that the floodplains for the floods with the frequency of 10 years are prohibited to develop. The original ecological environment should be maintained.

4 CONCLUSIONS

During the planning and design of large dam projects, scientific demonstration systems should be established. Every possible negative effect of large dam project on environment should be studied. Environmental feasibility of dam construction should be proved sufficiently. What's more, the possible changes of human culture, society, ecology of plants and animals, natural resources, climate, land resources and silts in rivers etc. should be analyzed. The positive effects should be maximized, while the negative ones should be minimized. If all of the above can be fulfilled, the new project not only has great economic benefits, but also can promote the sustainable development of economic and society, and the harmonious relations between human and the nature. Thus, the near term and long term final aims of large dam construction can be achieved.

REFERENCES

[1] David M.Rosenberg, Patrick McCully, and Catherine M. Pringle. Global-scale environmental effects of hydrological alterations: introduction. *Bioscience.* American institute of biological sciences. 2000, p. 746–751.
[2] Dynesius M., Nilsson C. Fragmentation and flow regulation of river systems in the northern third of the world. *Science 266,* 1994, p. 753–762.
[3] Patrick McCully. *Silenced River,* Zed Books Ltd, 1996.
[4] Christer Nilsson, Kajsa Berggren. Alterations of riparian ecosystems caused by river regulation. *Bioscience.* American institute of biological sciences. 2000, p. 783–792.
[5] Zhai Jinliang, Deng Wei, He yan. Flood-plain wetland ecoenvironmental functions and its management counter measures. *Advances in Water science.* China waterpower press. 2003, p. 203–208.

This page intentionally left blank.

New Developments in Dam Engineering—Wieland, Ren & Tan (eds),
© 2004 Taylor & Francis Group, London, ISBN 04 1536 240 7

Dam maintenance and management: an overview of Chamera dam (Stage-I)

A.K.Sachdeva & Virender Salman
Region-II, NHPC, India

ABSTRACT: Chamera Power Station-I lies in high seismic zone of lower Himalaya range and is prone to earthquake and floods, as such to meet such like eventuality disaster plan have been prepared and are revised annually to reduce the response time in organizing the assistance and improving state of preparedness to meet any contingency and define the role of Project Management, identification of manpower, major resources and equipment needed without any lose of time.

This paper brings out in detail the practices being followed in respect of Dam Maintenance & Management Plan bringing out periodicity & aspects of inspections & monitoring for the structures & components of Chamera Dam during the O&M stage to meet contingency of any nature.

1 INTRODUCTION

Chamera Power Station is located in district Chamba of Himachal Pradesh. It is a run of the river with pondage type scheme, which uses the combined flow of Ravi and Siul rivers to generate power. It consists of 141m in height and 285m in length, an arch concrete gravity dam to store 39130 Hectare meter of water incl. Of live storage of 10955 Hectare meter. One 9.5m dia horseshoe shaped 6.4 Km. long tunnel, one surge shaft of 25m dia., 85m in height, one pressure shaft of 8.5m dia and 157m long trifurcate into 5m penstock at the bottom with an underground power house having three machines of 180 MW each. The water joins the main river through 9.5m dia., 2.5. Km. long tail race tunnel and 550m cut & cover section and 100m open channel.

The Dam is located at Chaurah, 20 Km. from Banikhet. Power House/Switchyard, Workshop stores, Residential colony, Office, Guest Houses etc. are located further 16Km. downstream on left & right banks of Ravi near the confluence of Sewa & Ravi river at Khairi.

The safety of the dams is often taken for granted until certain events reveal the associated risk causing loss of life, property in the downstream. Unsafe dams may result in loss of life, destruction of property, harm downstream river environment. Safety is key to the effectiveness of dam. Dams are not designed to last forever, their deterioration is inevitable over time and risk of failure is of top most concern of all. As such, well planned and coordinated safety measures are essential. Dam safety measures are subjected to numerous recommendations and in many countries, it is regulated by rigorous administrative standards.

The primary requirement for ensuring safety is regular inspections & monitoring. Inspection & Monitoring plays a fundamental role during construction. It enables the verification of design hypotheses and the control of the construction methodology and quality. Inspection & Monitoring are particularly crucial during the initial filling of the reservoir, a critical phase in the life of a dam. Inspection & Monitoring during operation and maintenance phase must enable the timely detection of any signs that could lead to deterioration of the dam.

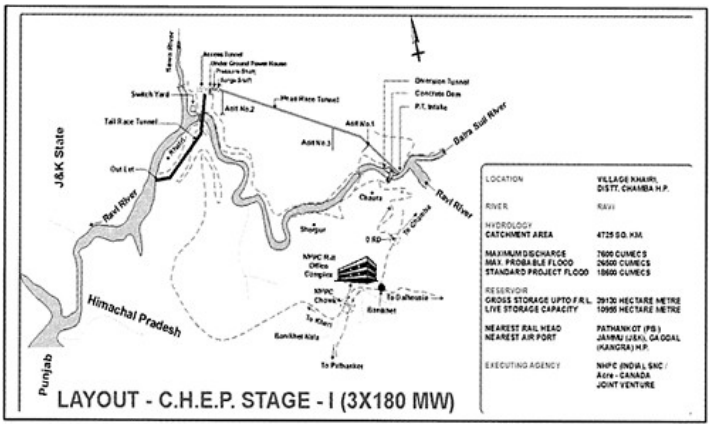

Inspection & Monitoring involves numerous steps including direct or remote visual inspection, as well as topographical measurements and instrumentation. The scope of the monitoring methods employed depends on the risk potential associated with the dam and site characteristics.

2 DAM SAFETY ASPECTS

As the concept of safety applies from the day the work on any dam is started but the safety aspects differ from the measures being taken during the construction period and in the operation period. NHPC has formulated a Dam Safety Group for its projects in operation that visits different Project sites prior to monsoon and after the monsoon period and the members are drawn from Design Wing—For inspection of civil structures, Hydro Mechanical Wing—For inspection of gates, Geologist—Engineering geologist to have an overview of the area, Hydrologist—To assess the hydrological data.

3 INSPECTION

Monitoring of dam safety surveillance criteria is based on the risk potential perceived to the downstream area and level of consequences.

4 INSPECTION OF DAMS TO COVER

Status of instruments
Instrumental data
Seepage in the downstream
Seepage through dam body/joints
Seepage quantity
Seepage water quality
Condition of inspection galleries
Status of flood protection works
Condition of downstream channel
Reservoir level and discharge inflow
Weeds and plants in the dam area
Access roads
Communication facilities

Condition of drain holes
Status of re-drilling
Condition of glacis and bucket
Condition of outlet structure, its sealing
Condition of embedded parts
Alternate operation facilities for outlets
Erosion in the downstream
Dam slope
Settlement/cracks/opening up of joints
Operating trials of gates
Reservoir rim stability
Floating debris/wood/logs reservoir
Floating debris against intake structures
Equipment for maintenance works
Lift/stair cases/approaches
Inspection galleries
Differential head across the trash racks.

5 REPORT OF PERIOD INSPECTION

The group prepares a written report and photographic record of the inspection. The report must contain the following:

- The date and the detailed findings of the inspection and an assessment of the conditions of the dam and reservoir based on the visual observations, instrumentation data, operational records, review of available data on the design, construction, operation and maintenance of the structure including hydrologic, hydraulic, stability and other considerations.
- Recommendations for any critical or emergency measures or actions.
- Recommendations for corrective measures or actions relating to design, construction, operation, maintenance and other aspects of inspection of the structure.
- Recommendations for time periods appropriate for implementing any necessary emergency or corrective measures or actions to improve the safety of the dam to an acceptable level.
- Recommendations for additional detailed studies, investigations and analysis.
- Recommendations for the safe storage level of the reservoir and recommendations for the time of the next inspection by an engineer.

View of Chamera dam

6 MONITORING DURING O&M PHASE

All performance monitoring records are reviewed by a qualified and experienced dam performance monitoring group of Corporate Office and findings reported. Any data or observations appearing to indicate unusual or unacceptable dam performance are thoroughly investigated. Unacceptable dam performance are considered a dam safety issue and are processed in a timely manner.

7 GENERAL MAINTENANCE AND ORDINARY REPAIRS

The major preventative maintenance measure taken in Chamera Dam are:

A. *Reservoir*

- Silt-Silt data is collected daily and twice daily during monsoons.
- Reservoir run inspection are done before monsoons and the safety requirement of check dams, plugging of gullies etc. are done i.e. periodical reservoir run inspection and remedies thereof.
- The water level gauges are properly painted and the cross sections are checked.
- A network of rain gauges, discharge sites with reliable communication system and the data of discharge of the Hydro Project running in the upstream of this Project is regularly sent to the Control Room of Power House & Dam and this is maintained hourly during monsoon period and twice in a day in lean season. This results in deciding the regulation of supplies from the reservoir from time to time and to regulate the flow of water judiciously for maximum benefit of the water as well as minimum silt accumulation in the reservoir when the silt load in the upstream is high.

The water levels in the reservoir are generally maintained as shown below during the periods. The FRL of Chamera-I Dam is 760m.

1st Nov to 31st May	EL 757 to 760M
1ST June to 20th June	EL±757M
21st June to 30th June	EL 757 to 753M
lst July to 5th July	EL 750M
6th July to 15th Sep	EL 750M
16th Sep to 30th Sep	EL 750 to 753M
1st Oct to 15th Oct	EL 753 to 755 M
16th Oct to 31st Oct	EL 755 to 757M

- A network of seismological observatories around the Dam i.e. at Dam site, Dralka, Banikhet, Dalhousie, Power House site of Chamera-I & Chamera-II have been established to assess & monitor the seismic behaviour of the structures and also to find out the effect of the impounding of water in the reservoir on the seismicity of the area. This is done in consultation with School of Earthquake Engineering, Roorkee.
- Reservoir silt survey is done by taking cross sections of the reservoir before the onset of monsoons and the same are repeated after the monsoon period is over. During this period desilting operation is carried out by keeping reservoir level at 750M and discharging through under sluices when the inflow is generally more than 400 cumecs. The data is fed and the area capacity curve of the reservoir is framed and revised accordingly. This also indicates the quantum of silt cleared from the reservoir.
- The siltation of the reservoir is done by operation of under sluices so that there is minimum effect on the dead storage and no effect on live storage. In addition to this, the floating debris i.e. logs are lifted out of Dam through cleaning trash rack machine in front of the intake and by deploying of labour and boats for manual uplifting of material from the reservoir/and in front of the Dam.

B. *Dam hill slopes*

The Dam Hill slopes upstream & esp. downstream right side of the spillway are checked monthly and the movement is monitored by tell-tales etc. Remedial measures like checking the vegetation growth, proper rock bolting and shotcreting are adopted and in slope stabilization wherever necessary plantation of required specimen like robino psendo alongwith proper drainage facilities are provided.

C. *Instrumentation*

The various types of instruments provided in the Chamera Dam for gathering essential behavioural information include:

1. Embedded instruments for internal measurements of strain, stress, joint opening, temperature, pore pressure and foundation deformation, direct and reverse pendulum;
2. The measurement of frequency of each instrument is fixed and measurement are taken accordingly & evaluated once in a month.

D. *Hydromechanical equipments*

1. Intake structures

The intake service and bulk head gates are checked for seals, gate rollers & lubrication of rollers and other routine maintenance once in a year and before the onset of monsoons.

2. Spillway radial gates

The gates are maintained once in year especially in the months of November–March and generally checked for painting/Lubrication of trunnion pins, checking/replacement of seals/slide rollers and fasteners as per requirement.

Status of instruments inside dam

S No.	Name of instruments	Total	Working	Not working	% working
1	Strain meter	330	181	149	54.84
2	Piezo meter	12	10	2	83.33
3	Joint meter	45	26	19	57.77
4	Uplift	17	16	1	94.11
5	Stress meter	4	4	Nil	100
6	Pendulum	3	3	Nil	100

3. Anchorage system

- 10% of the prestressed anchorage system is tested for the load carrying capacity and if there is variation, the same are tensioned to its required tension load.
- The anti greasing compound used in the prestressed anchor bolts is tested for its chemical & physical property every year in the lean season and the results evaluated.

4. Low level sluice gate

These gates are used for silt flushing & reservoir management. The major maintenance check list is attended once in a year & generally the check points are:

- Checking & replacing of seals.
- Checking & Lubrication of gate rollers.
- Checking/repair/building up of roller tracks & seal seats.
- Torque checking/replacement of nuts & bolts.

5. Hydraulic system

The major maintenance is done once in a year preferably during November–March & mainly focuses on:

- The physical & chemical properties of hydraulic oil in hydraulic cylinders.
- Cleaning of main oil filter, return filter & replacing after 100 operating hours.
- Checking up the operation of gate through manual/remote control system.
- For the emergency purposes one number gasoline engine with quick coupling for operation of spillway radial gates is tested every month in the monsoon period also in addition to regular maintenance & testing during the lean season.

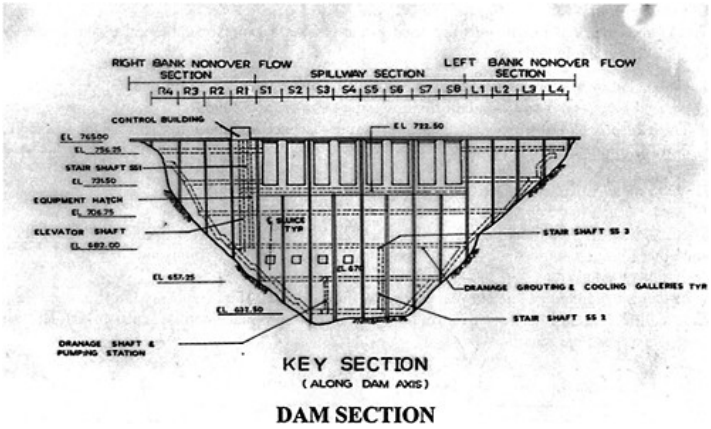

DAM SECTION

E. Electrical installations
The electrical installations have been grouped into following components:

i) Transformers.
ii) Control Panels.
iii) Motors.
iv) DGSets.
v) LT Panels.

The inspection, checking, cleaning, rectification, replacement is done according to the requirements and most of the activities are taken up during the month of Nov-March of each year.

F. *Civil maintenance*
For the civil maintenance, overall cleaning of drains and painting of structures and drilling of Poros drains between seven galleries at different elevation and pressure relief holes are checked up and drilled wherever required. Seepage in Dam is checked from Gallery E, F, G & DR-5 through calibrated V-notches once in a day. The seepage varies from 88 lit/sec with Reservoir level at ±749 to 235 lit/sec with Reservoir level at ±760. Any variation if found can be taken care accordingly.

8 O&M MANUAL

A pocket hand book on operation & maintenance of civil, electromechanical and hydraulics installations has been prepared for all the equipments installed at Dam and is provided to all the Engineers/Foremen working at Dam site. The gate operation schedules that clearly indicates the complete sequence and stages of operation of various gates corresponding to various pondage levels alongwith the various operation modes i.e. manual as well as remote are demonstrated & tested before the onset of monsoons to all the staff in the control room. The hand book gives daily, weekly, monthly and yearly schedules of maintenance for each component as well as key functioning operations & circuit diagram and main salient feature of the equipment.

9 EMERGENCY PREPAREDNESS

The emergency preparedness plan has been prepared for both natural & man-made disaster.

A proper plan with well defined measures that will help to reduce the risk of the disaster have been formulated.

All operation plans contain emergency procedures and warning plans to be used in the event of any emergency.

The plan includes but is not limited to:

1. A map of the evacuation area downstream of the dam based on the estimated inundation caused by a sudden breach of the dam during the design flood and non flooding failure conditions. The evacuation area is depicted on a map with the approximate travel time indicated at significant locations.
2. Proper communication network with wireless/Motorola/WLL of all important gauges & discharge sites with control room of Dam & than to PH.
3. Proper information to the locals downstream of the opening of gates by Public Address Systems, alarm sirens etc.
4. Adequate POL in stock & proper maintenance of the essential equipment, machinery & D.G. sets.
5. A directory of tents, bedding & blankets and other materials (ration, drinking water, fuel etc.) that will be required in emergency/evacuation and proper identification of buildings/rooms etc. for relief measures.
6. An up-to-date notification directory with phone numbers of key district or municipal and emergency management officials, departmental officers/engineers familiar with the Dam's characteristics, downstream residential localities/establishment requiring immediate notification within the inundation area (listed in order by those affected first).
7. The name of the nodal official responsible for giving notification of a threat of failure.
8. The general sites and availability of construction materials for emergency repairs.
9. A list of contractors and other sources that could provide assistance before, during and after a Dam failure.
10. Arrangement required for proper law & order and prevention to spreading of any fatal disease, proper security arrangements, identification of the dead, cremation of the dead and proper medical facilities are identified to be provided.

This plan is updated every year especially in the month of April in consultation with State Govt. authorities under the Chairmanship of District Commissioner so that all the resources available in the district are clubbed & synerzed to meet any such eventuality.

10 CONCLUSION

Effective maintenance and management of the Dam is thus being carried out at Chamera Power Station-I through combination of well planned activities involving scheduling/budgeting, monitoring, inspections, repair/upkeep, appropriate upgrading of operation and maintenance instructions to meet the latest state of art technological improvements/developments, conformance to the requirements of operating and maintenance procedures and periodicity. For effective and efficient utilization of inflow and stored water & maintaining quality and improved performance of outcome/results and efficiency of all the associated components, it is essential to retain/maintain/ restore these components to acceptable/fittest possible physical conditions to improve their working life, within optimum O&M costs, keeping all the safety aspects intact. In addition to the above, ensuring preparedness for any emergent exigencies as a result of likely disaster due to failure of any of the components is also taken care of.

The systematic approach & continuing education and training is used as key for development of appropriate skills & creative contribution by individuals/groups/teams are rewarded.

This page intentionally left blank.

New Developments in Dam Engineering—Wieland, Ren & Tan (eds),

Behaviour of cut-off wall of a large dam during construction

J.Sadrekarimi
Faculty of Civil Engineering, University of Tabriz, Iran

ABSTRACT: Arasbaran dam is a large earth dam, with a 26m deep plastic concrete cut-off wall, being constructed in the north west of Iran. The results of during construction analysis reveals that the stress level in the cut-off wall may double when the friction angle increases from 0 to 10 degrees. While the stress level in the cut-off wall increases due to the embankment construction, it also relaxes gradually and at the same time due to the visco-elastic behaviour of the plastic concrete; and it may decrease to less than 50% of that obtained from the elastic analysis.

1 INTRODUCTION

1.1 *Background*

It is some long time that the significance of application of visco-elastic and non-linear models have been revealed for engineers and scientists. However, there are two basic key questions that spring into the designer's mind. First, what are the loads that the proposed structure will support, and second, what will be the magnitudes of the produced deformations and stresses. At this stage, it is necessary to establish an appropriate model that represents the material behaviour due to the applied loads as precisely as possible. One crucial reason for this is that if components of stress produced by the external loads exceed a certain level, the stress-strain response may no longer be linear elastic and a new behaviour, that may be irreversible, may dominate the material behaviour. In this case, the behaviour will be stress level dependent and may be linear elastic and then elastoplastic and so on [1].

Amongst the techniques that have been employed to control seepage pressure and exit gradient, the cast-in-place plastic concrete diaphragm wall technique has been considerably developed during recent years [2]. Plastic concrete is an appropriate mixture of aggregate, Portland cement, bentonite and water. It is quite clear; if the produced stresses and/or strains in the cut-off wall exceed a certain level, the wall may fail. However, prediction of such a failure condition still is uncertain and a matter of suspect and question for most engineers. Because, plastic concrete is not fully elastic and the creep properties of plastic concrete may cause a considerable stress relaxation with time.

This paper presents results of the analysis of a plastic concrete cut-off wall as a visco-elastic body. In order to evaluate the plastic concrete- surrounding ground mechanical interaction, and for deformation analysis, the mechanical properties of both ground and plastic concrete are required. However, very limited guidelines are encountered in the literature. ICOLD (1985) and many other designers and investigators consider plastic concrete as an elastic body [3,4,5]. ICOLD (1985) suggests an unconfined compressive strength of 1 to 2MPa and modulus of elasticity not exceeding five times that of the surrounding soil. Xanthakos suggests an upper limit of 2MPa for the unconfined strength [6]. Recent investigations reveal that there is an acceptable level of agreement between the plastic concrete mechanical behaviour and Burgers visco-elastic model, and that the plastic concrete elastic modulus is considerably stress dependent [2,7].

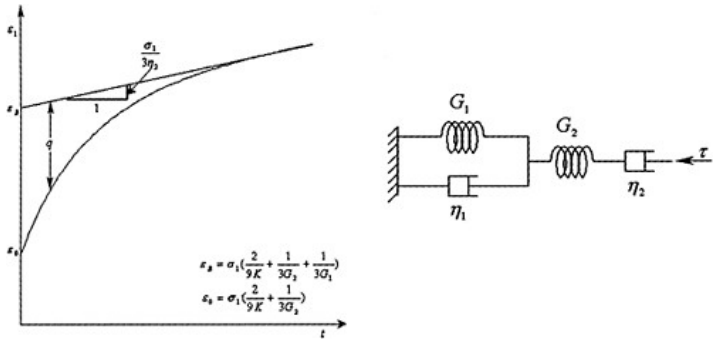

Figure 1. Burgers visco-elastic model and governing equations.

1.2 *Linear visco-elastic behaviour*

Coupling together two or more basic linear elements, a wide variety of properties can be approximated. One of the useful complex models is the Maxwell unit in series with the Kelvin unit as shown in Figure 1. This is generally known as Burgers model. Using Burgers formula, if at t=0, a constant stress σ_1 is suddenly applied, then the resulting strain is given by:

$$\varepsilon_1(t) = \sigma_1\left(\frac{2}{9K} + \frac{1}{3G_2} + \frac{1}{3G_1}\right) - \frac{\sigma_1}{3G_1}e^{-(G_1 t/\eta_1)} + \frac{\sigma_1}{3\eta_2}t \qquad (1)$$

in which K=E/3(1−2ν) and G=E/2(1+ν) are the bulk modulus and the shear modulus, respectively. The η is the dynamic viscosity which expresses the proportionality between shear stress τ and shear strain rate γ as τ=ηγ. The E and ν are the modulus of elasticity and Poisson's ratio, respectively [8]. The simplest method for determining visco-elastic constants η and G is through the unconfined compression of cylindrical specimens over prolonged periods under a constant axial stress of a and monitoring of the axial and lateral strains with time [9].

2 CHARACTERISTICS OF THE DAM AND PLASTIC CONCRETE

The Arasbaran dam is an embankment dam with a central clay core and a plastic concrete cut-off wall that is being constructed in the north of Azerbaijan province of Iran. The embankment is 36m high from the riverbed, and the cut-off wall is 0.7m wide and about 26m deep and penetrates at least 1.0m into the sandstone bedrock. The dam is being constructed over a fine alluvial deposit that is about 26m in thickness overlying bedrock. The cross section of the dam and cut-off wall position is shown in Figure 2.

Referring to the previous experiments and also geotechnical properties of the foundation ground, a plastic concrete containing 200 kg/m^3 of bentonite and cement (B+C), with variable bentonite cement ratios (B/C), as shown in Table 1, was proposed, and appropriate laboratory tests were carried out for determination of mechanical properties. The appropriate proportions of saturated surface dry (SSD) aggregate, Portland cement, bentonite gel and tap water, were mixed for six minutes and then were molded over a standard vibrating table. Type 2 Portland cement and a processed bentonite powder were employed. The bentonite liquid and plastic limits were 140 and

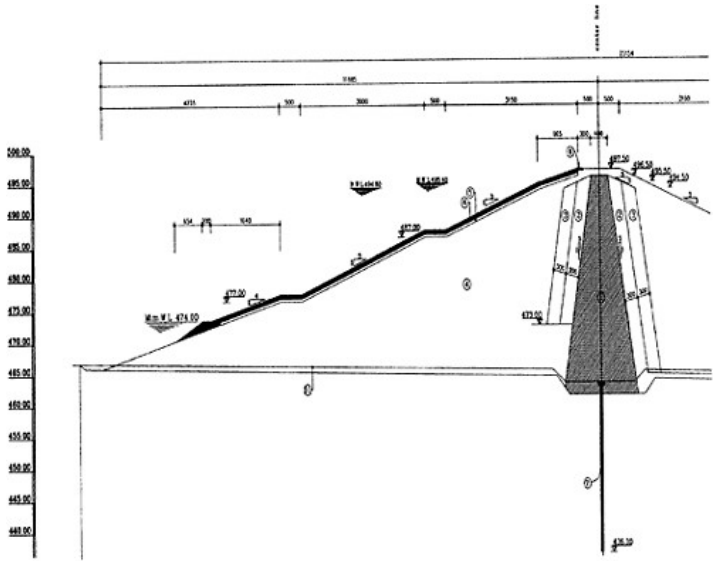

Figure 2. Typical cross section of the dam.

Table 1. Compositions and wet densities of specimens.

B+C kg/m^3	B/C	Aggregate kg/m^3	Water kg/m^3	Bentonite kg/m^3	Cement kg/m^3	Density kg/m^3
	0.25	1789	250	40	160	2239
	0.5	1737	273	66.7	133	2210
200	1.0	1573	339	100	100	2112
	2.0	1449	375	133	66.7	2024
	4.0	1322	439	160	40	1961

32 percent, respectively. The aggregate used was a well-graded riverbed gravelly sand of 0.076 to 19mm grain size. In order to evaluate the mechanical behaviour the plastic concrete, creep and uniaxial compression tests were carried out on specimens cured for 28 days. For creep tests, cylindrical specimens of 101mm in diameter and 206mm in height were prepared. However, to comply with practice, the uniaxial compression tests were carried out on 150mm side cubic specimens. The results are shown in Table 2, and q_u, σ, SL and ν represent unconfined compressive strength, normal stress, stress level, and Poisson ratio, respectively. Each result is the average of three tests.

In order to model and analyse the embedded plastic concrete and surrounding ground the ANS YS (1997) software was used [10]. The geometry of the substructure cross section comprises four separated surfaces connected using contact elements. The cut-off wall and the surrounding ground were defined using eight node elements PLANE-82 with plane strain behaviour. In this way, it was possible to introduce the non-linear behaviour of materials and it is possible to employ nonlinear contact elements for interaction analysis. In addition, the presence of shape functions of higher order with this element, in comparison with a four nodes element, results in achievements that are more precise.

In order to model the plastic concrete-surrounding soil interaction, the contact element CONTACT-48 was used. This element is suitable for defining a deformable medium. For modeling of the plastic concrete-bedrock and foundation soil-bedrock interactions contact elements TARGET-169 and TARGET-171 were employed, respectively. These elements are applied as deformable-rigid media contact elements. The foundation ground surrounding the plastic concrete wall consists of gravely sand sediments; and accordingly is assumed to be an elastic medium. Following on from the site and laboratory tests and investigations, the modulus of elasticity and Poisson's ratio of the foundation ground surrounding the cut-off wall were set as 20MPa and 0.3, respectively

In order to establish the initial loading scheme, it was assumed that after the cut-off trench was excavated and filled with fresh plastic concrete, the fresh concrete applies a hydrostatic lateral pressure. After the concrete final setting has been terminated, the lateral stress coefficient changes to $k_a=\tan^2(\pi/4+\varphi/2)$, in which $\varphi=32$ degrees is the effective friction angle of the surrounding soil. Accordingly, in order to establish the initial loading pattern it is necessary to consider the submerged density of the plastic concrete.

For the embankment, the consultant proposed two construction time schedules. The schedules that are for 365 and 730 days periods are depicted in Figure 3. The foundation surface loading due to the embankment construction was considered in time steps according to the proposed loading scheme. The average unit weight of the compacted materials was 20kN/m^3, and the final loading at each stage was considered to be product of the material unit weight and height of the embankment.

Table 2. Creep test data, and visco-elastic constants obtained (B+C=200kg/m^3).

B/C	q_u MPa	σ MPa	SL%	ν $\varepsilon_3/\varepsilon_0$	E MPa× 10^2	K MPa× 10^2	G_1 MPa× 10^2	G_2 MPa× 10^2	η_1 MPa.sec.× 10^3	η_2 MPa.sec.× 10^3
0.25	2.18	1.97	90	0.16	8.63	4.19	3.59	5.31	433.2	501.0
		1.62	74	0.18	10.16	5.19	5.62	6.00	1081.6	4052.7
		1.12	51	0.22	13.77	8.17	14.90	7.34	1177.3	≈ ∞
0.50	1.28	1.12	87	0.21	3.87	2.15	3.98	2.07	148.3	914.0
		0.93	72	0.21	3.65	2.14	4.20	1.96	878.4	4718.0
		0.71	55	0.20	4.59	2.54	6.93	2.56	928.5	86421.0

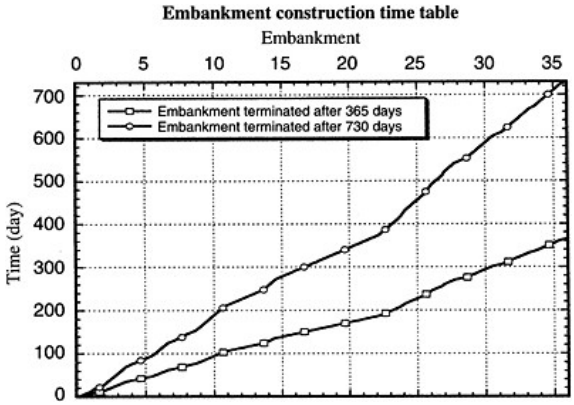

Figure 3. Proposed construction trends for the embankment height.

3 RESULTS AND DISCUSSION

Results of elastic and visco-elastic analyses of variations with time of the maximum vertical compressive stress in the cut-off wall adjacent to the bedrock are shown in Figure 4. It is seen that, considering visco-elastic behaviour of the plastic concrete, some significant stress relaxation with time occurs in the cut-off as the foundation surface loading proceeds due to the embankment construction.

In the same way, considering the plastic concrete as a simple elastic material, stress is accumulated as the loading proceeds and there is no relaxation. Comparing the two graphs, it is observed that the stress relaxation at the end of construction is of the order of 18 percent and grows up to around 57 percent in 540 days after the embankment construction has been completed.

It should be noted that, in order to conduct these analyses the, visco-elastic constants associated with B/C=0.25 and a stress level of $0.74q_u$ were adapted from Table 2. In addition, the internal friction angle along the cured plastic concrete and the surrounding ground interface was assumed to be 10 degrees. Finally, for the loading scheme the one-year construction period, from Figure 3, was considered.

In Figure 5a the trends of creep deformations of the cut-off wall, for two types of plastic concrete, are shown. As may be expected, the cut-off wall deformation due to the embankment construction increases as the B/C ratio is increased. In order to achieve these results the visco-elastic parameters relating to B/C ratios of 0.25 and 0.50, and corresponding stress levels of $0.74q_u$ and $0.72q_u$ have been employed from Table 2, respectively The internal friction angle on the soil-concrete interface was assumed to be 10 degrees and the one-year embankment construction period was employed fromFigure 3.

In order to evaluate the effect of the plastic concrete-surrounding soil friction angle on stress distribution, variations of the maximum normal stress with depth, for φ=0, 5 and 10 degrees, were analysed. The analysis was conducted for the visco-elastic properties relating to B/C=0.5 and a stress level of $0.72q_u$. The results are depicted in Figure 5b. It is observed that, the stress development due to the embankment construction increases in response to the friction angle increase. This analysis, was carried out for 540 days after the embankment completion date. It is seen that the friction angle plays a crucial role in the stress distribution in the cut-off wall and may cause the stress level to increase by a factor of two or even more, when it increases from 0 to 10 degrees.

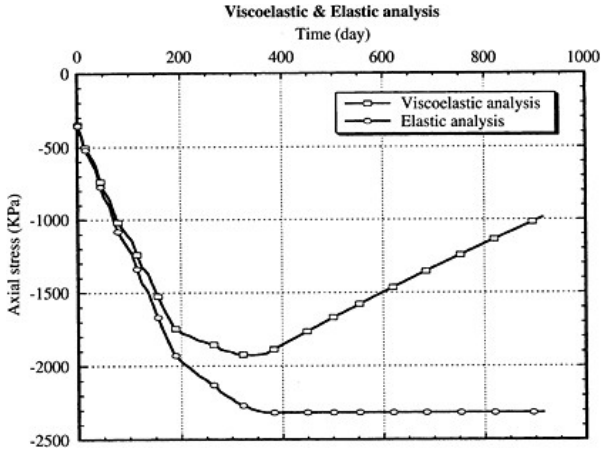

Figure 4. Maximum vertical compressive stress with time in cut-off wall at bedrock level.

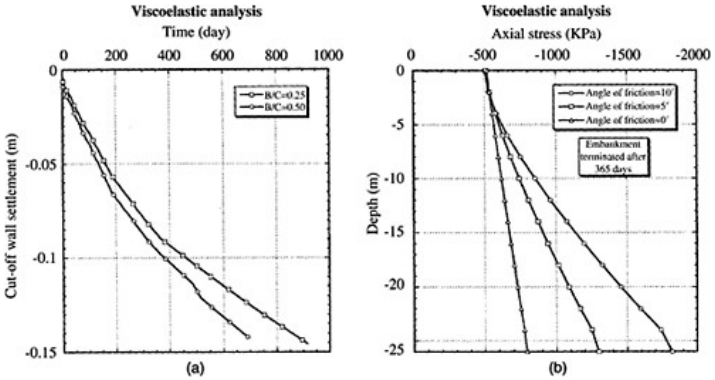

Figure 5. Time dependent settlement of cut-off wall (a), Internal friction angle effects on stress distribution in cut-off wall (b).

4 CONCLUSIONS

The visco-elastic behaviour of plastic concrete plays an important role in stress distribution and deformation development in the cut-off wall. While the normal stress due to the embankment construction increases in the cut-off wall, it also relaxes at the same time due to the creep of the plastic concrete. Although the rate and magnitude of stress relaxation depends on the plastic concrete mix design, in the case of the common plastic concrete, say B+C=200kg/m^2 and B/C=0.25~0.50, the relaxation may be considerable and may decrease to less than 50% of that obtained from the elastic analysis. The internal friction angle at the plastic concrete-surrounding ground interface is a dominating factor that affects the stress development in the cut-off. In the current case, as the friction angle was increased from 0 to 10 degrees the normal stress in the cut-off increased by a factor of two.

This work is an attempt to highlight the necessity of considering plastic concrete as a viscoelastic body rather than as a simple linear elastic body as is common in current engineering design and practice.

REFERENCES

[1] Chen, W.F. and Han, D.J. (1998) Plasticity for structural engineers. 1st ed., Springer Verlag.
[2] Sadrekarimi, J. (2002) “Plastic concrete mechanical behavior”. Journal of the Institution of Engineers (India), Vol. 82, pp 201–207.
[3] ICOLD, (1985) International commission on Large Dams, Filling materials for watertight cut-off walls, Bulletin 51.
[4] Alvarez, L. et al. (1982) “Characteristics of the plastic concrete of the diaphragm wall of Convento Viejo dam”. International Commission on Large Dams (ICOLD), Rio de Janeiro, pp 371–389.
[5] Visvanathan, N. (1999) “Foundation treatment for Dhaulinga dam”. International Commission on Large Dams (ICOLD), pp 299–317, Antalya.
[6] Xanthakos, P.P. (1979) Slurry walls, McGraw-Hill.
[7] Sadrekarimi, J. (1997) “Plastic concrete cut-off walls and an investigation into the mechanical behavior”, Proceedings of the 3rd International Geotechnical Engineering Conference, Cairo University, Egypt, 1997,364–368.
[8] Flugge, W. (1977) Viscoelasticity, 2nd ed., Springer, Berlin.
[9] Goodman, R.E. (1984) Introduction to rock mechanics. 2nd ed., John Wiley & Sons.
[10] ANSYS, (1997) Help, General element features, Swonson system co.

New Developments in Dam Engineering—Wieland, Ren & Tan (eds),

The basic design and a state-of-the-art construction work control standard for asphalt facing

T.Sasada & Y.Tashiro
Kyushu Electric Power Co., Inc., Japan

Y.Mitani & T.Esaki
Kyushu University, Japan

ABSTRACT: In Japan, technical standard for asphalt facing-typed dam or reservoir is not established. So, a unique method of stability evaluation for a reservoir fully surfaced with asphalt mixture has been proposed for upper reservoir of Omarugawa pumped-storage power plant in Japan. The asphalt facing work is now under execution, and it is aimed to complete in February 2006. A construction work control standard for asphalt facing of this site has been established on the assumption of a-year-round construction in consideration of the results of laboratory tests and trial construction.

Besides, some brand-new control methods have been established at this site including standardization of temperature of the last compaction work and execution of indirect leveling for the purpose of verifying the result of general layer thickness control method based on measurement of total weight of paved asphalt mixture.

In this paper, the basic concept on the design of a reservoir fully surfaced with asphalt concrete is interpreted first. Secondary, a state-of-the-art construction work control standard for the asphalt facing established for this site is described.

1 INTRODUCTION

Omarugawa Power Plant, under construction by Kyushu Electric Power Co., Ltd. at Kijo-cho, Koyu-gun, Miyazaki prefecture, is a pumped storage type power station with the maximum output 1200 MW. And it is planned to start commercial operation in July 2007 for the first phase.

In Japan, however, technical standard for asphalt facing-typed dam or reservoir is not established. Therefore, a unique method of stability evaluation for asphalt facing-typed reservoir has been proposed in consideration of following characteristics of this site; paving foundation consists of cut or fill, existence of four banks higher than 40m, and existence of connection areas between asphalt facing and concrete structures such as intake or spillway. The asphalt facing work is now under execution, and it is aimed to complete in February 2006. The construction work control standard for the asphalt facing was newly established on the assumption of year-round construction in consideration of the results of laboratory tests and trial construction.

In this paper, the basic concept on the design of a reservoir fully surfaced with asphalt concrete is interpreted first. Secondary, a state-of-the-art construction work control standard for the asphalt facing established for this site is described.

2 OUTLINE OF THE UPPER RESERVOIR

The upper reservoir of the plant is at the upper-most stream of Oseuchitanigawa, a tributary of the Omarugawa. The location is on the upper slope of a large mountain rising between two rivers running

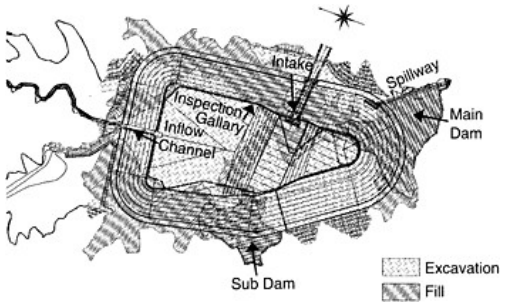

Figure 1. Distribution of excavation and fill of upper reservoir.

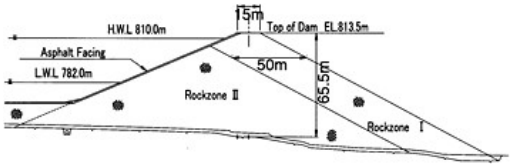

Figure 2. Cross section of the main dam of upper reservoir.

down in the same direction, the Omarugawa main stream and the Iwaitanigawa of the Hitotsusegawa system to the west of the Omarugawa. This is the first fully asphalt faced reservoir for Kyushu Electric Power Co., Inc.

The shape of the upper reservoir was determined to have four curves after comprehensively taking the following into consideration:

(i) Natural ground will be cut or filled to prepare the foundation
(ii) Right and left bank crests will be given increased thickness
(iii) Reductionof pavement area
(iv) Elimination of convexities on the paving foundation

Figure 1 shows the plan of the upper reservoir, and distribution of excavation and fill of the reservoir. Figure 2 shows the cross section of the main dam of the reservoir.

The gradient pitch is determined to be 1:2.5 for the upstream side of the dam (reservoir side) in consideration of workability for asphalt facing, and 1:2.0 for the downstream side in consideration of stability against sliding. The total excavation amount is roughly 6.7 million cubic meters, of which 4.5 million cubic meters is used for the main and subsidiary dam and other fillings.

3 BASIC DESIGN OF ASPHALT FACING

3.1 *Selection of the impervious work*

In the original design, the upper reservoir was planned with two rock-fill dams (main dam and sub dam) with vertical clay core, and the foundation grouting was also planned. As the progress of the geological survey, the following problems were found:

(i) Relatively high permeability zones spread around the right or the left side ridge surrounding the reservoir. In the right side, Lugeon value larger than 20 was observed in the depth of 50 or

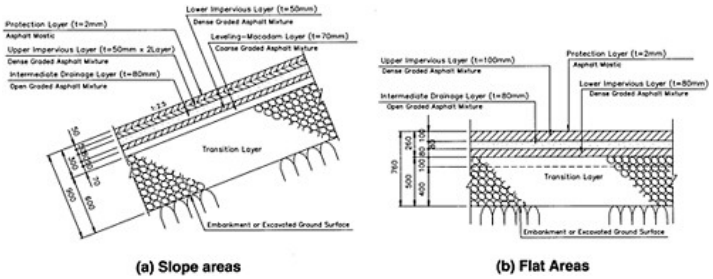

Figure 3. Composition of asphalt facing.

80m. In the left side, high permeability zones with Lugeon value larger than 20 scatter around in relatively deep areas of the bedrock.
(ii) Ground water exists relatively low elevation, and no ground water with the base elevation as high as the planned high water level was observed.

Considering above, the impervious work for the reservoir was determined as wholly asphalt facing type. Besides, among the impervious materials for the facing such as asphalt, concrete and rubber-sheet, asphalt was selected in consideration of reliability, workability and construction cost.

3.2 *Concept of the basic design*

In Japan, technical standard for asphalt facing-typed dam or reservoir is not established. Therefore, a unique and rational method of stability evaluation for asphalt facing-typed reservoir was developed in consideration of following features of this site; (a) existence of multiple boundaries between excavated bedrock and embankment at paving foundation, (b) existence of four banks higher than 40m, (c) existence of connection areas between asphalt facing and concrete structures such as the intake or the spillway.

In the planning of the basic design for this project, some important issues were picked up to be examined thoroughly as follows:

(i) Reduction of settlement
(ii) Evaluation of seismic resistance
(iii) Consideration of water leakage
(iv) Quality control of fill materials
(v) Quality control of asphalt concrete
(vi) Consideration of back pressure by ground water
(vii) Arrangement of monitoring equipment

And the basic design was conducted considering those issues.

3.3 *Stability evaluation of asphalt facing*

In consideration of the results of other sites, major features of this site, recent progress of the execution technology, laboratory material tests, and trial tests, the structures of the asphalt facing were determined as 5-layer structure with the thickness of 300mm for the slope areas, 3-layer structure with the thickness of 260mm for the flat areas. The structures of the asphalt facing are depicted in Figure 3.

The points to be considered in evaluation of mechanical stability of the upper reservoir are the following:
Under normal condition

(i) Deformation of asphalt facing due to settlement (water filling, creep, inundation)
(ii) Deformation of asphalt facing caused by differential settlement at the boundaries of fill and excavated bedrock or concrete structures

Under earthquake condition

(i) Stability against fill sliding of the main, subsidiary and other dam bodies
(ii) Seismic deformation of the dam bodies and asphalt facing
(iii) Deformation of asphalt facing due to seismic surface waves

For an asphalt facing-typed reservoir, it is important to prevent the asphalt facing from having fissures due to external forces to maintain its imperviousness.
Stability study flow for the asphalt facing is illustrated in Figure 4.
For an asphalt faced reservoir, it is essential to understand the behavior of asphalt facing during earthquakes because (1) the asphalt facing are thin, and have different natures and physical properties from fillings; (2) the reservoir is asymmetrically shaped with three corners; and (3) asphalt tends to rupture more easily as the strain rate increases.
Stability of the asphalt facing must be evaluated not by stresses but by strains because the peak strength of asphalt concrete varies widely depending on temperature and strain rate.

3.3.1 *A nalytical studies*

As for analytical studies, static analyses and dynamic ones were conducted as shown in Figure 4. Because maximum allowable strain of asphalt mixture varies depending on temperature and strain rate, it is essential to evaluate maximum strain that generates in asphalt facing in both static and dynamic condition. The 2-D static FEM analyses were executed aiming to evaluate maximum strain generated in the asphalt facing under long-term loading condition such as embankment of fill materials, water filling in the reservoir, creep deformation of the embankment, and settlement of embankment due to water seepage. As for the dynamic studies, 3-D and 2-D dynamic FEM

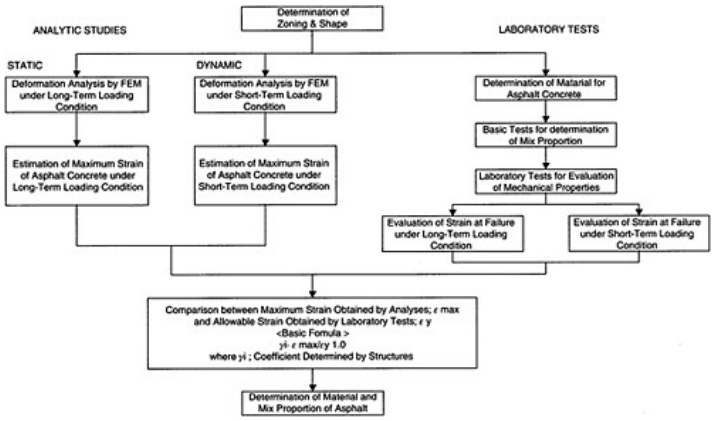

Figure 4. Flow chart for design of asphalt facing.

analyses were conducted in order to evaluate maximum strain generated in the asphalt facing during earthquake.

As for more details of 3-D and 2-D dynamic studies, please refer to the paper [1].

3.3.2 *Material tests of asphalt mixture*

Since the allowable maximum strain of asphalt mixture varies depending on temperature and strain rate, material tests of asphalt mixture should be executed regarding the appropriate testing condition for temperature and strain rate. In corresponding to the analytical studies, testing condition for temperature and strain rate was determined for both static and dynamic loading condition.

Figure 5 illustrates flow chart for material tests of asphalt mixture. Firstly, applicability of each material such as asphalt or aggregates was examined through laboratory tests and investigation of results of other sites. Next, preliminary mix proportion of asphalt mixture such as asphalt content was determined referring to the Marshall stability test results. Then, mechanical properties of asphalt mixture were examined by laboratory tests in order to determine standard mix proportion. Finally, full-scaled field trials simulating real execution of asphalt facing work were conducted in order to confirm validity of in-situ mix proportion regarding to quality and workability of the asphalt mixture.

Major functions of asphalt facing are considered as having low permeability, flexural deformability, and resistance against flowing on slopes. And practically, flexural deformability against tensile deformation of the asphalt facing is the most important function for stability evaluation of asphalt facing. Thus, a number of bending tests were conducted in order to evaluate allowable tensile strain of dense graded asphalt mixture used for the impervious layers. Table 1 shows test conditions for asphalt mixture. Figure 6 shows an example of bending test results. Allowable strain is

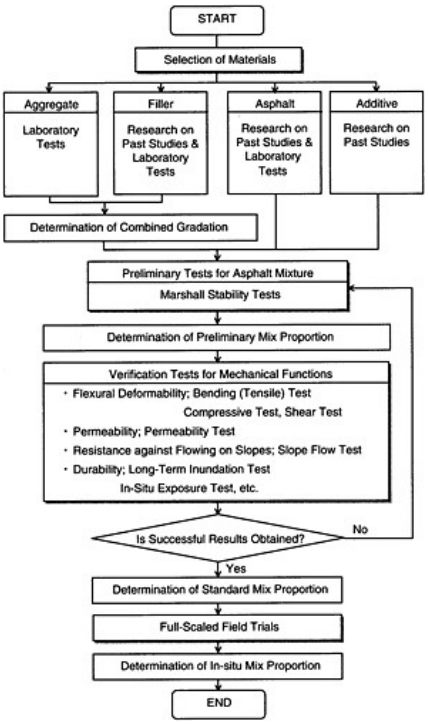

Figure 5. Flow chart for material tests of asphalt mixture.

Table 1. Test conditions for asphalt mixture.

Item	Test temperature (°C)	Strainrate(1/s) Tension (bending)	Compression	Shear
Seismic loading	−10(*1)	1×10^{-2}(*3)	1×10^{-2}(*3)	2×10^{-2}(*3)
Normal loading	5(*2)	4×10^{-5} (*3)	7×10^{-5} (*4)	2×10^{-4}(*4)

(*1) Set by the average value of the lowest temperatures observed in-situ in 6 years.
(*2) Set based on the expected lowest water temperature at the reservoir and the result of Yashiro dam.
(*3) Set based on the results of dynamic analyses.
(*4) Set by considering the effectiveness of the test because the strain rate is about 10−7 based on the change of water level in the reservoir.

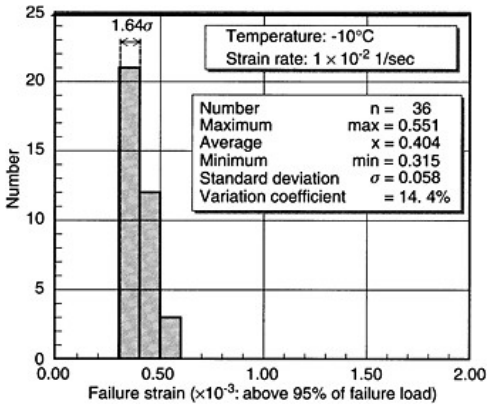

Figure 6. Bending test results of asphalt mixture in seismic loading condition.

determined in consideration of scattering of test results by subtraction of 1.64 a from averaged failure strain.

3.3.3 *Stability evaluation*

As shown in Figure 4, ratios of the computed maximum strain to the allowable strain obtained by material tests, i.e.$\gamma_i\varepsilon_{max}/\varepsilon_y$, were estimated for static and dynamic conditions. The calculated ratios are below 1.0 and satisfied the safety criteria in both conditions. The result indicated that the design of the structures and materials for asphalt facing could keep the safety of the asphalt facing.

4 CONSTRUCTION WORK CONTROL STANDARD FOR ASPHALT FACING

The asphalt facing work is now under execution, and it is aimed to complete in February 2006.The construction work control standard for the asphalt facing was newly established on the assumption of a-year-round construction in consideration of the results of laboratory tests and trial construction executed by our company. Because climate of the site of Omarugawa project is relatively warm all around a year, a-year-round construction of asphalt facing work is planed for the first time in Japan.

Besides, there was no rational standard established for site management of asphalt facing in Japan.

Therefore, a unique standard for execution of work has been established for this site based on results of laboratory test, and full-scaled field trials conducted mid-summer and mid-winter.

In this section, the standard for execution of work is outlined.

Table 2. Quality control and execution work control.

Classification	Location	Objective	Item
Quality control	Plant	Quality of material	Asphalt;
			– Penetration, softning point, mass variation & residual penetration after TFOT
			Aggregate;
			– Density, water absorption, etc.
			Filler;
			– Gradation, moisture content, etc.
		Quality of asphalt mixture	Asphalt content, additive content
			Combined gradation
	Pavement area	Quality of basement	Permeative depth of
		Quality of asphalt facing	Vaccumed ratio
Work control	Plant	Quality of material	Temperature of asphalt
			Temperature of filler
	Pavement area	Quality of asphalt facing	Method of compaction
			Finished thickness

4.1 *Quality control*

Major functions of asphalt facing are such as water-tightness and flexural deformability. However, it is impossible to take out specimen from asphalt facing after construction, so there is no way to confirm those functions of constructed asphalt facing. In addition, effective non-destructive test method to confirm those functions has not been established.

Therefore, laboratory tests and full-scaled field trials were conducted preceding real construction, and standard for execution of work was established based on the results of those tests and field trials. In the standard, detailed standardization on quality control of materials on method of execution is achieved aiming to secure satisfactory quality of asphalt facing. In addition, rationalized method of execution management is established in aiming to minimize standardization of temperature of asphalt mixture during execution in order to satisfy required quality.

Table 2 shows the details of standard on quality control and execution control of this site. Figure 7 shows basic procedure of asphalt facing work.

4.1.1 *Material*

The materials of asphalt mixture are classified into two groups. Coarse aggregate is produced at the construction site by crushing excavated rock materials. Other materials such as asphalt, fine aggregate and filler are purchased and delivered from outside of the construction site.

For those materials except for coarse aggregate, rigorous quality control based on Japanese Industrial Standard (JIS) are executed. In addition, the owner (Kyushu Electric Power Co., Inc.) demands for more detailed values to the producers aiming to conduct quality control strictly.

4.1.2 *Mix proportion of asphalt mixture*

Table 3 shows standard mix proportions of asphalt mixture.

Mix proportions of each asphalt mixtures are determined based on the results of laboratory tests and field trials. As for the mix proportion, flexible variation is enabled in consideration of conditions of construction area, meteorological condition, and characteristics of materials.

4.1.2.1 Asphalt content

As depicted in Table 3, asphalt content is varied depending on workability or atmospheric temperature. Thus, asphalt content is increased in cold winter in order to avoid generation of coarse

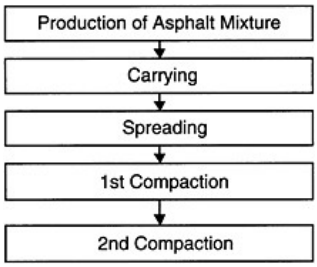

Figure 7. Basic procedure of asphalt facing work.

Table 3. Standard for mix proportion of asphalt mixture.

Layer	Asphalt mixture	Maximum size of aggregate (mm)	Asphalt content (%)	Aggregate content (%)	Filler content (%)	Additive content (%)
Slope area impervious layer	Dense graded TYPE 1	13	7.5±0.2	85.4	6.9	0.2(0.15)
Flat area upper impervious	Dense graded TYPE 2	20	7.2±0.2	86.9	5.7	0.2(0.15)
Flat area lower impervious	Dense graded TYPE 3	20	6.7±0.2	87.4	5.7	0.2(0.15)
Intermediate drainage layer	Open graded	20	4.0±0.2	93.9	1.9	0.2(0.3)
Leveling macadam layer	Coarse graded	20	4.8±0.2	93	2.2	–

during spreading work. Or asphalt content is decreased in hot summer in order to avoid generation of waving of asphalt mixture during spreading work.

4.1.2.2 Additive Content

Originally, cellulose fiber is utilized as additive in order to prevent asphalt mixture from flowing. However, additive content of impervious layers is decreased in order to improve workability depending on atmospheric temperature in winter. Besides, as for intermediate drainage layer, it is enabled to increase additive content in order to reduce rutting deformation in hot summer due to passing of construction machines during pavement of upper impervious layer.

4.1.2.3 Combined gradation of aggregate

Because combined gradation of aggregate affects on quality of asphalt mixture, standardization is targeted at control of combined gradation of aggregate as mixture of coarse aggregate, fine aggregate and filler. In addition, there is no classification of aggregate of coarse one or fine one.

4.2 *Execution work control*

In execution of asphalt facing work, temperature control of asphalt mixture is considered to be the most important to secure satisfactory quality of asphalt facing. Since a-year-round construction is

Table 4. Standard for temperature control during execution.

		Target temperature		Standardization on temperature	
				1st compaction	2nd compaction
Layer		Loading on dump trucks	Spreading work	At start	Atend
Slope area	Leveling	160°C	130°C	Higher than	Higher than 70°C
	Macadam layer			100°C	
	Lower impervious	180°C	160°C	*	Higher than 80°C
	Intermediate	160°C	130°C	Higher than	Higher than 70°C
	Drainage layer			100°C	
	Upper impervious	180°C	160°C	*	Higher than 80°C
Flat area	Lower impervious	180°C	160°C	*	Higher than 80°C
	Intermediate	160°C	130°C	Higher than	Higher than 70°C
	Drainage layer			100°C	
	Upper impervious	180°C	160°C	*	Higher than 80°C

Note: *Standard temperature is not standardized but temperature at end of 2nd compaction should be strictly followed.

planned for Omarugawa site, temperature of asphalt mixture is greatly affected by variation of atmospheric temperature. Therefore, standardization on temperature of asphalt mixture during execution of work is conducted considering the effect of temperature of asphalt mixture on quality of asphalt facing after completion of construction.

As for control on thickness of layer, averaged finished thickness is calculated based on total amount of asphalt mixture paved for the object area.

4.2.1 *Temperature control of asphalt mixture*

Table 4 shows standard for temperature of asphalt mixture during execution of work. Temperature of asphalt mixture during 1st compaction and 2nd compaction are considered to have great influence on quality of asphalt facing. And temperature of asphalt mixture at the end of 2nd compaction is standardized as the most important factor. Temperature of asphalt mixture at departure from asphalt plant is allowed to have certain variation as long as to follow standard on temperature at the end of 2nd compaction. This is same as temperature of asphalt mixture at spreading work.

Besides, in order to improve uniformity between neighboring lanes or layers, newly established quality control are conducted such as measurement of temperature on the surface of underlying layer or heating of the lane joint of neighboring lane.

4.2.2 *Thickness control of layers*

Because specimen sampling from completed asphalt facing is unallowable, direct measurement of finished thickness of a layer of a real structure is impossible.

So, at full-scaled field trial, verification of thickness control method is conducted by comparing directly measured thickness of cubically cut specimen and averaged estimated thickness derived from total weight of asphalt mixture used for the object area.

Figure 8 shows comparison of finished thickness between measured results and estimated results.

As the result, the latter method is revealed to have satisfactory accuracy for the thickness control.

In addition, indirect leveling survey is conducted at every 10m×10m grid as a complimentary of thickness control by above mentioned method.

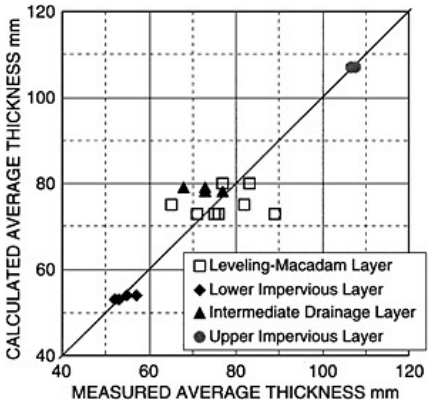

Figure 8. Comparison of finished thickness between measured value and estimated value.

5 CONCLUSIONS

In Japan, technical standard for asphalt-facing typed dam or reservoir is not established.

So, a unique design method of stability evaluation for asphalt facing-typed reservoir was established in consideration of features of the Omarugawa project site. These approaches are expected to contribute to give useful information for rational design of other reservoirs of the same type.

Besides, a state-of-the-art construction work control standard for the asphalt facing established for this site on the assumption of a-year-round construction in consideration of the results of laboratory tests and full-scaled field trials. As the result, rationalized quality control of asphalt facing work was achieved including standardization of temperature of the last compaction work and execution of indirect leveling for the purpose of verifying the result of general layer thickness control method based on measurement of total weight of paved asphalt mixture

Asphalt facing work started in December 2003, and its construction management has been successfully conducted under supervising by the owner's employee.

From now on, rigorous quality control is continued until completion of construction scheduled in February 2006.

ACKNOWLEDGEMENTS

The authors would like to express their profound gratitude to Mr. Teruo Sugawara, Professor Emeritus of Hokkaido University for providing appropriate guidance and advices to conduct design of asphalt facing, determination of mix proportion of asphalt facing including laboratory tests, full-scaled field trials and determination of construction work control standard for asphalt facing work.

REFERENCES

[1] Y.Tashiro, M.Oouchi, Y.Awazu, and T.Matsuda, "Seismic Evaluations of Reservoir Covered Wholly with Asphalt-Concrete", Journal of Japan Society of Dam Engineers, Vol. 11, No. 1, 2001, pp. 15–25 (In Japanese)

[2] Y.Awazu, H.Ookubo, H.Ikagawa, and T.Sasada, "Design of Asphalt facing for the Upper Reservoir of the Omarugawa Pumped-Storage Power Plant", Electric Power Civil Engineering (Denryoku Doboku) No. 291, 2001, pp. 36–40. (In Japanese)

New Developments in Dam Engineering—Wieland, Ren & Tan (eds),
© 2004 Taylor & Francis Group, London, ISBN 04 1536 240 7

Observed stresses and pore pressures in rock-fill dams

Nobuteru Sato
Head of Geological Engineering Research Division, Research and Training Institute, Japan WaterAgency, Japan

Hideki Soda
Senior Researcher, Experimental and Analytic Division, Research and Training Institute, Japan WaterAgency, Japan

Hideki Ohta
Dr. Eng, Professor, Department of International Development Engineering, Tokyo Institute of Technology, Japan

Koji Nakagawa
Dr. Eng, Professor, Department of Civil and Environmental Engineering, Faculty of Engineering, Yamaguchi University, Japan

ABSTRACT: On embankment construction of center-core type rock-fill dams, stress of filter zone is concentrated and stress of core zone decreases. Pore pressure occurs at core zone during embankment construction and eventually decreases during construction and after its completion. This paper shows analysis on observed data of stresses and pore pressures during embankment construction and after ponding at four dams owned Japan Water Agency. Based on the observed data, we examined actual conditions of stress concentration at filter zone and decreasing stress at core zone as well as decreasing tendency of pore pressure at core zone. We also analyzed decreasing tendency of pore pressure and factors to cause dam top settlement at core zone. This paper reports on remarkable mechanical behaviors related to stress and pore pressure of rock-fill dams and possible factors for those.

1 INTRODUCTION

Four center-core type rock-fill dams owned Japan Water Agency were designated for this study. Summary of each dam are listed in Table 1, and standard cross-sections are shown in Fig. 1. Height of these dams ranges from 60m to 158m. Fourteen years have been passed since the start of first filling at Naramata Dam and Agigawa Dam. Embedded monitoring equipment has been measuring valuable data such as earth pressure and pore pressure occurred at each dam.

2 STRESS CONDITIONS AT FILTER ZONE AND CORE ZONE DURING EMBANKMENT CONSTRUCTION

Fig. 2 shows changes with time in vertical stress at filter zone and core zone during embankment construction of Agigawa Dam. Vertical stresses shown in Fig. 2 are taken from measured data of

Research andTraining Institute, Japan Water Agency, 936 Jinde, Sakura-ku, Saitama City, Saitama Pref, 338–0812, JAPAN, E-mail: nobuteru_sato@water.go.jp

Table 1. Specificationof dams.

Dam		Naramata Dam	Agigawa Dam	Misogawa Dam	Yamaguchi Regulating Reservoir
Location		Gumma Prefecture	Gifu Prefecture	Nagano Prefecture	Fukuoka Prefecture
River system		Tonegawa river	Kisogawa river	Kisogawa river	
River		Naramata river	Agigawa river	Kisogawa river	
Dam height	m	158	101.5	140	60
Crest length	m	520	362	447	326
Dam volume	m^3	13,100,000	4,900,000	8,900,000	1,060,000
Dam top elevation	EL.m	896.0	417.5	1130.0	122.0
Normal water level	EL.m	888.0	412.0	1122.5	118.0
Limited water level	EL.m	881.0	400.5	1113.0	
Lowest water level	EL.m	800.0	363.0	1052.0	96.0
Dam foundation elevation	EL.m	738.0	316.0	990.0	62.0
Core base width		70.8	54.5	61.0	34.0
Core base width/Dam height		0.45	0.54	0.44	0.57
Beginning of embankment construction		1983/10/15	1986/3/16	1986/8/7	1994/12/22
Completion of embankment construction		1988/6/6	1988/2/15	1993/6/3	1996/4/27
Startoffirstfilling		1988/10/4	1989/10/2	1993/12/10	1997/11/6
Construction	Day	1696	701	2492	492
Total number of days from completion of embankment to start of first filling	Day	120	595	190	558
Total number of days from completion of embankment to present	Day	4196	4648	2755	1718
Total number of days from start of first filling to present	Day	4076	4053	2565	1160

earth pressure gages install at the elevation of 316m shown in Fig. 3. Fig. 2 also shows changes with time in weight of earth column calculated from embankment thickness above earth pressure gages. Multiplying the embankment thickness above earth pressure gage by the average unit volume weight gives the weight of earth column. Vertical stress at filter zone kept being larger than weight of earth column from early stage of embankment construction, while that of core zone kept being smaller and eventually difference became larger.

Fig. 4 shows the ratio of vertical stress to weight of earth column at the completion of embankment construction at each dam. A proportion of the ratio of filter zone to that of core zone is approximately 2:1 at each dam. It is reported that results observed at many other dams showed nearly the same proportion[1)]. The property of filter and core materials were exchanged for its of core materials, and stress-strain was analyzed using FEM. It showed that stress at core zone decreased by 10 to 20% as a result of concentration of stress to filter zone[2)]. It is assumed that vertical stress at filter zone was increasing at an early stage of embankment construction due to the weight of rock zone, which is exterior part of filter zone. It is considered that vertical stress at core zone became smaller than weight of earth column in the latter half of the embankment construction because the load to dam body, which is in triangle shape, was smaller than that of horizontal soil stratum.

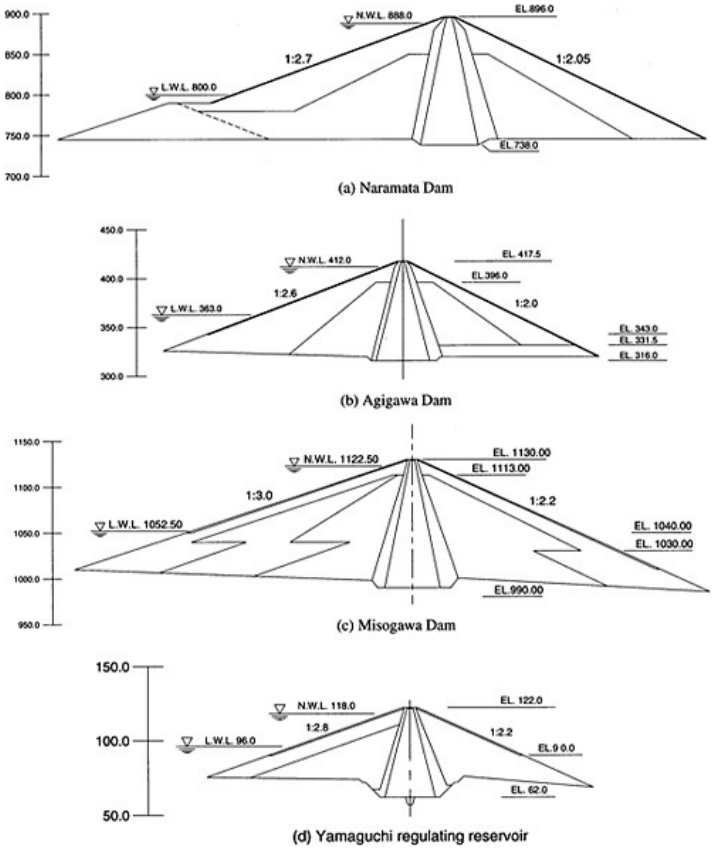

Figure 1. Standard cross section of designated dams.

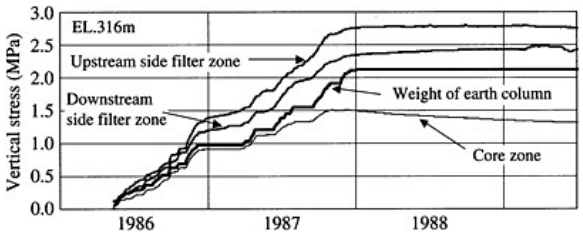

Figure 2. Vertical stress during embankment construction (Agigawa Dam).

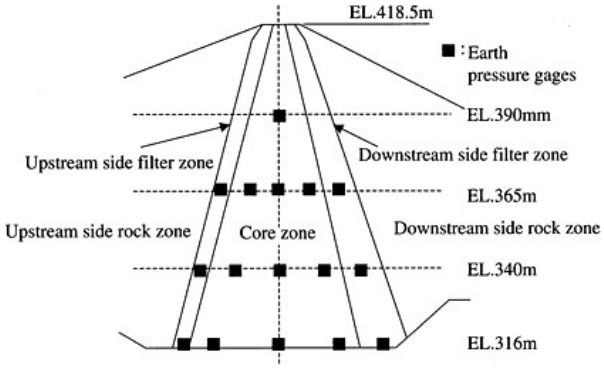

Figure 3. Location of earth pressure gages placed in dam body (Agigawa Dam).

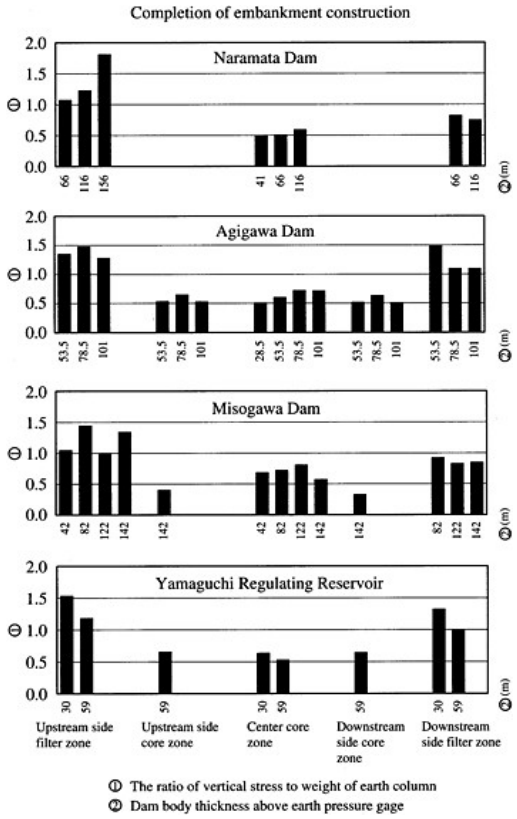

Figure 4. Comparison of the ratio of vertical stress to weight of earth column at completion of construction.

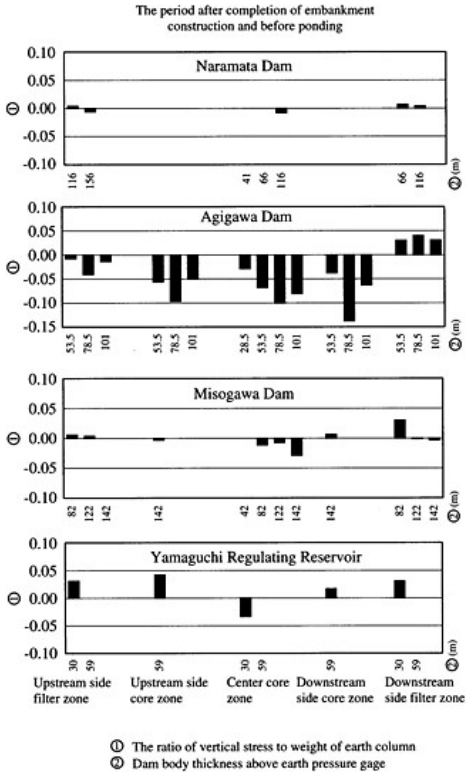

Figure 5. Comparison of the ratio of vertical stress to weight of earth column at the period after completion of construction and before ponding.

3 STRESS CONDITIONS IN DAM BODY DURING THE PERIOD AFT ERITS COMPLETION AND BEFORE PONDING

During the period after completion of dam body and before ponding, stress conditions in dam body basically stay constant. Fig. 5 shows stress changes during the period after completion of dam body and before ponding, with the ratio of vertical stress to weight of earth column on the vertical axis, setting its numeric value at completion of dam body to be zero. Fig. 6 shows measurement of dam top settlement of each dam during the period. Stress at core zone of Agigawa Dam and Yamaguchi Regulating Reservoir decreased largely. Measurements of dam top settlement of these two dams were also large. Generally, consolidation settlement occurs at core zone while it does not occur at filter zone. As a result, it is considered that vertical stress at core zone decreased, shifting load to filter zone.

4 STRESS CONDITIONS IN DAM BODY AFTER PONDING

Fig. 7 shows changes with time in vertical stress at filter zone and core zone after ponding at Naramata Dam. Reservoir water pressure at the elevation where earth pressure gages are

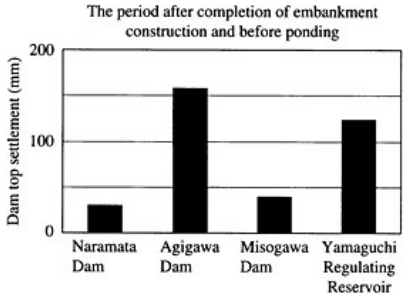

Figure 6. Dam top settlements measured at the period after completion construction and before ponding.

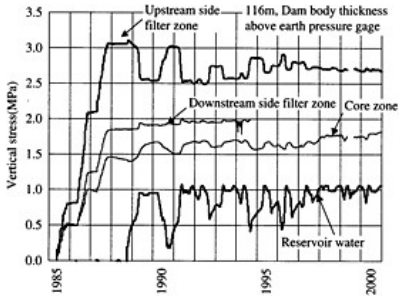

Figure 7. Vertical stresses and reservoir water pressure after ponding at Naramata Dam.

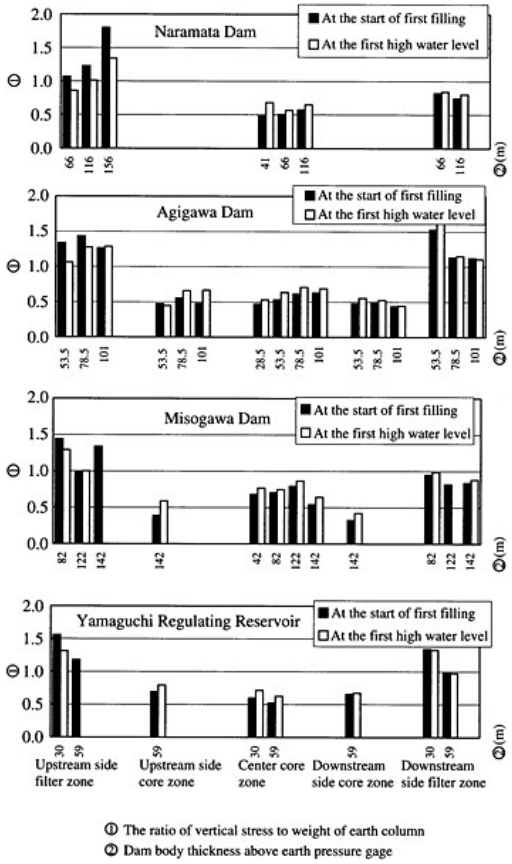

Figure 8. The ratio of vertical stress to weight of earth column at the start of first filling and first high water level.

placed is also shown. As reservoir water level increased, vertical stress (total stress) at upstream side filter zone decreased, and as reservoir water level decreased, vertical stress (total stress) at upstream side filter zone increased. Fig. 8 shows the ratio of vertical stress to weight of earth column in comparison between at the time of start of first filling and of the first high water level. Vertical stress at upstream side filter zone decreased as reservoir water level increased. When reservoir water level increases, it gives buoyancy to upstream side rock zone and effective stress decreases. Therefore, it is considered that when effective stress at upstream side of the dam decreases, the load of the rock zone which was weighing on the filter zone decreases, and it causes to decrease vertical stress (total stress) at upstream side filter zone.

5 PORE PRESSURE AND STRESS DURING CONSTRUCTION AND AFTER PONDING

Fig. 9 shows changes with time in pore pressure and vertical stress at four dams. Locations of embedded monitoring equipment that measured the changes are at lower elevation part (EL340 m) of core zone shown in Fig. 3, and that is the same for other three dams. Zero at horizontal axis indicates the start of first filling. Reservoir water levels were converted into reservoir water pressures to express their changes. At Naramata Dam, Misogawa Dam and Yamaguchi Regulating Reservoir, pore pressure at core zone increased as reservoir water level increased but they kept lower than reservoir water pressure. Vertical stress changed closely with reservoir water pressure as well.

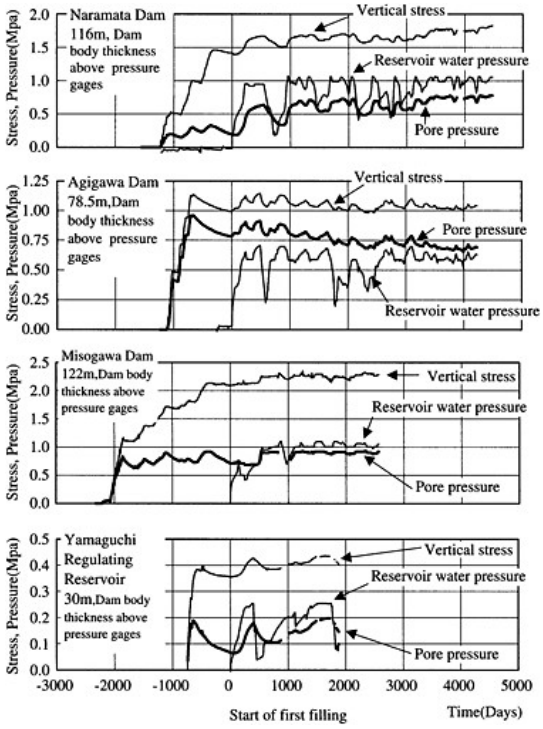

Figure 9. Vertical stress, pore pressure and reservoir water pressure at 4 dams.

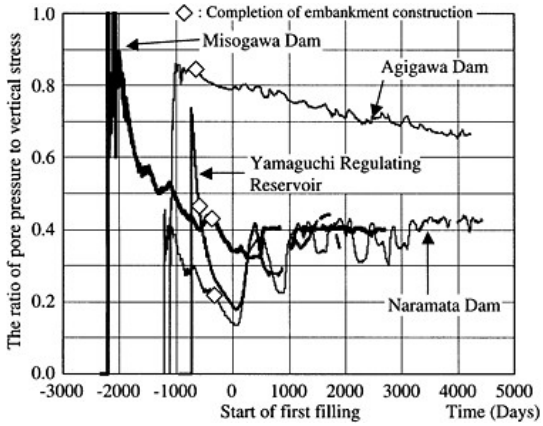

Figure 10. The ratio of pore pressure to vertical stress at 4 dams.

However, pore pressure was higher than reservoir water pressure at Agigawa Dam even before ponding, and pore pressure and vertical stress became higher as reservoir water level increased.

Fig. 10 shows the ratio of pore pressure to vertical stress to express the relationship between them as shown in Fig. 9. The ratio of pore pressure to vertical stress was more or less 0.4 after ponding at three dams except Agigawa Dam. The ratio changed closely with reservoir water level at Naramata Dam and Yamaguchi Regulating Reservoir. At Agigawa Dam, the ratio was about 0.8 when embankment construction was completed, then it decreased to about 0.65 at the present moment. The ratio did not change largely compare to reservoir water pressure at Agigawa Dam. No unusual behavior at dam body of Agigawa Dam was observed at the completion of construction, at the first high water level, and at the present moment. Effective stress has been gradually increasing since the start of first filling, and the dam body is considered to be in stable condition.

6 BEHAVIOR OF DAM BODIES AT WHICH PORE PRESSURES DECREASES SLOWLY

We compared Agigawa Dam with Naramata Dam in order to study behaviors of dam bodies at which pore pressure decreased slowly and quickly. Fig. 11 shows changes with time in reservoir water pressure, pore pressure and vertical stress during the period of five to eight years after ponding. Measuring equipment was used as same ones shown in Fig. 9. Pore pressure at Naramata Dam largely increased and decreased in conjunction with reservoir water pressure. Pore pressure at Agigawa Dam also increased and decreased in conjunction with reservoir water pressure, but its change was smaller than that of Naramata Dam and pore pressure always kept higher than reservoir water pressure.

Fig. 12 shows changes in pore pressure isobar at low and high water level. At Naramata Dam, they changed in conjunction with the change of reservoir water level at upstream side and central part of core zone. At Agigawa Dam, they hardly changed at central part of core zone, and it showed that high pore pressure remained at overall core zone.

Fig. 13 shows the relationship between pore pressure and reservoir water pressure during the period between 1994 and 1997, same period as shown in Fig. 11. At Naramata Dam, its movement was different when reservoir water level was increasing and decreasing. ③ shows the movement when reservoir water

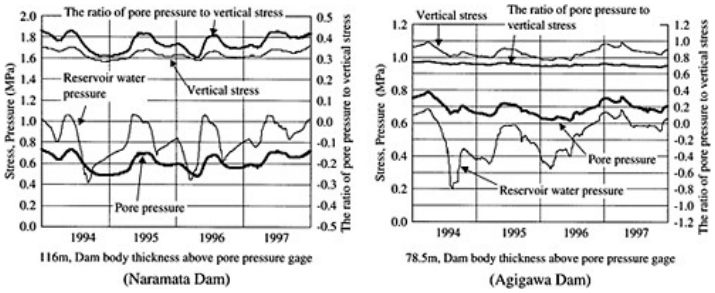

Figure 11. Vertical stress, pore pressure, reservoir water pressure and the ratio of pore pressure to vertical stress.

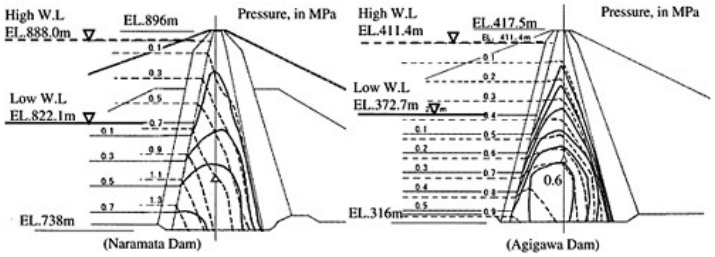

Figure 12. Distribution of pore pressure at high water level and low water level.

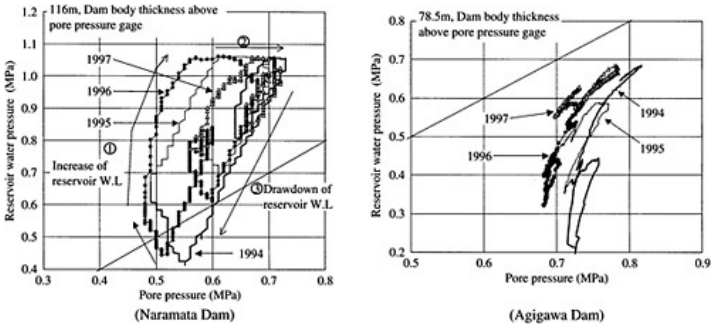

Figure 13. Relationship between pore pressure and reservoir water pressure.

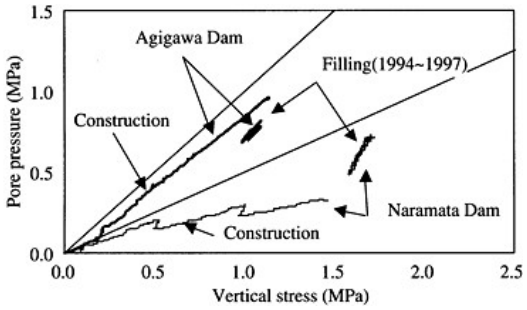

Figure 14. Relationship between vertical stress and pore pressure.

Table 2. Comparison of dam body behavior of pore pressure at Naramata Dam and Agigawa Dam.

	Naramata Dam	Agigawa Dam
Occurrence of excess pore water pressure	Decreased at the start of first filling.	Pore pressure kept higher than reservoir water pressure.
Relationship between reservoir water pressure and pore pressure	As reservoir water pressure changed, pore pressure changed with time lag. The relation was shown in loop shape.	Pore pressure changed in conjunction with reservoir water pressure. The relation was shown in arch shape.
Increase-decrease relationship between pore pressure and vertical stress	$u/\sigma_v=2$	$u/\sigma_v=1$
Changes in isobars of pore pressure	Pore pressure isobar in which upstream half of core zone largely changed up and down in conjunction with reservoir water level.	Pore pressure isobar in core zone hardly changed.

level was decreasing, and it indicates that there was time lag when pore pressure at core zone decreased. At Naramata Dam, the movement was in loop shape due to the time lag of pore pressure. At Agigawa Dam, the movement was in arch shape, moving up and down on the same line by year, with pore pressure always kept higher than reservoir water pressure. On a year-to-year basis, it shows that decrease of pore pressure was very little. The arch shape shifted to left as years went by, and it shows that pore pressure was gradually decreasing.

Fig. 14 shows the relationship between pore pressure and vertical stress during the period between 1994 and 1997, same period as shown in Fig. 13. The data during embankment construction are also shown for comparison. At Naramata Dam, the ratio of pore pressure to vertical stress after ponding was about 2, while it was about 1 at Agigawa Dam.

Table 2 shows behavior of dam bodies related to pore pressure at Naramata Dam and Agigawa Dam, summarizing stated above. Impervious materials used at Agigawa Dam were materials whose permeability was quite small. Therefore, it is considered that influence of ponding acted as stress but not hydraulic head. Fig. 15 shows a conceptual image of influence of reservoir water pressure at Agigawa Dam. As reservoir water level increased, core zone was sandwiched and pressed between water and downstream side rock zone, and pore pressure at core zone increased

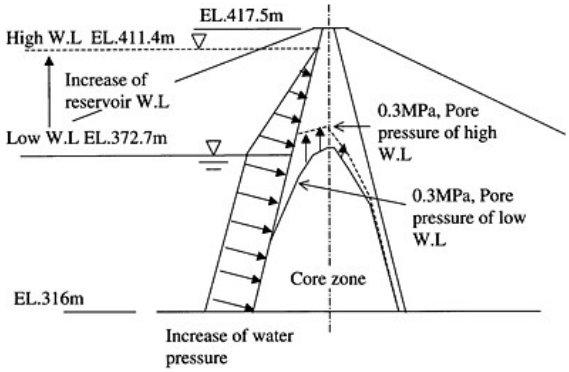

Figure 15. Concept image of acts of pore pressure and reservoir water pressure at Agigawa Dam.

more. As reservoir water pressure increased, pore pressure also increased without time lag, pore pressure and vertical stress increased at same rate.

7 BEHAVIOR OF PORE PRESSURES AND SETTLEMENTS ON DAM BODIES

Fig. 16 shows decrease of pore pressure at core zone and changes with time in settlement rate of dam bodies at each designated dam. Measuring equipment was used as same ones shown in Fig. 10. Reservoir water pressure can be calculated from reservoir water level and elevations where pore pressure gages are placed. Zero at horizontal axis indicates the completion of embankment construction. Excess pore pressures had been decreased when embankment constructions were completed at Naramata Dam and Misogawa Dam while it was still decreasing slowly at Yamaguchi Regulating Reservoir. At the Start of first filling, pore pressures were small enough at Naramata Dam, Misogawa Dam and Yamaguchi Regulating Reservoir. When compare dam top settlement rate, those at Naramata Dam and Misogawa Dam were not so large while that at Yamaguchi Regulating Reservoir was fairly large, but increasing rate was as small as those at Naramata Dam and Misogawa Dam. At these three dams, pore pressures increased as reservoir water level increased due to ponding, and it is considered that primary consolidation was almost completed when ponding began. Pore pressure at Agigawa Dam was still high at the completion of embankment construction and at the start of first filling, and it gradually decreased. Dam top settlement rate of Agigawa Dam at the start of first filling was smaller than that at Yamaguchi Regulating Reservoir but higher than those at Naramata Dam and Misogawa Dam. Although decreasing rate of pore pressure at Agigawa Dam was small, its settlement was quite large, which is unusual behavior. There seem to be other factors causing its settlement behavior during the period between after completion of embankment construction and before ponding other than primary and secondary consolidation.

Fig. 17 shows changes with time in long-term settlement of dam body after ponding. During the low water level at the first filling, settlement occurred at dam top and upstream side rock zone at each dam. Reservoir water level kept decreasing largely at Naramada Dam and Agigawa Dam. When reservoir water level was low, settlement at dam top and upstream side rock zone increased. It is presumed that core zone at Agigawa Dam had high degree of saturation and it was in undrained state since pore pressure was quite high and it decreased slowly. Primary consolidation cannot be good reasons that settlement of impervious material in undrained state increased when water level was low. Settlement of upstream side rock zone also increased at the second time of

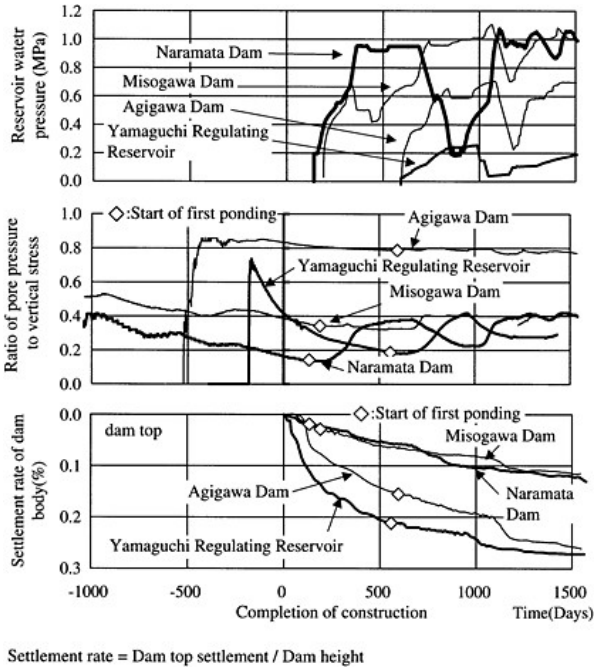

Figure 16. Reservoir water pressure, the ratio of pore pressure to vertical stress, and settlement rate of dam body at 4 dams.

low water level. It is considered that decrease of resisting forces between rock material grains at rock zone caused its settlement[3]. The resisting forces between rock material grains were presumed to be decreasing slowly within a few years after ponding. Effective stress at rock zone increased as reservoir water level decreased, and decrease of resisting forces between rock material grains caused slight shift of rock materials then settlement occurred. It is pointed out that large settlement occurs at high elevation part of core zone after ponding[4]. There is also a case example reported relationship that increase of vertical deformation is large at high elevation part of core zone during embankment construction, and that lateral displacement is large at high elevation part of rock zone[5] This case example shows that lateral displacement of rock zone tends to be larger and settlement of core zone tends to be larger at high elevation part. Fig. 18 shows the relationship between dam top settlement at core zone and lateral displacement of rock zone when reservoir water level is low. On the basis of the above statement, possible factors of settlement are as follows. Secular distortion after ponding causes decrease of resisting forces between rock material grains at rock zone, and rock zone becomes susceptible to lateral displacement of core zone. In addition, it is considered that pressure effect for lateral displacement is less since width in the upstream-downstream direction of rock zone is narrow at high elevation part of dam body. Under such circumstances, settlement of core zone occurs as reservoir water level decreases and buoyancy gets less. Core zone is in undrained state so that force of settlement acts as lateral displacement. Since resisting forces between rock rnaterial grains have been decreased, core zone gives lateral displacement to rock zone. As a result, it is considered that settlement at core zone occurs at high elevation of dam body, where rock zone tends to make lateral displacement. The reason why dam top settlement at core zone continues to occur even at the second time of low water level and after that, is an effect of lateral displacement due to the shape of dam body. At Agigawa Dam,

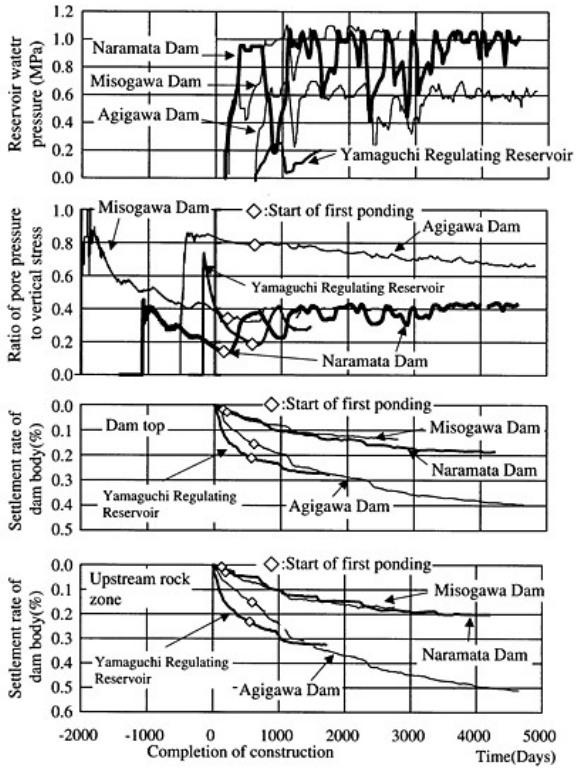

Settlement rate = Dam body settlement / Dam body thickness

Figure 17. Reservoir water pressure, the ratio of pore pressure to vertical stress, and settlement rate of dam body at 4 dams.

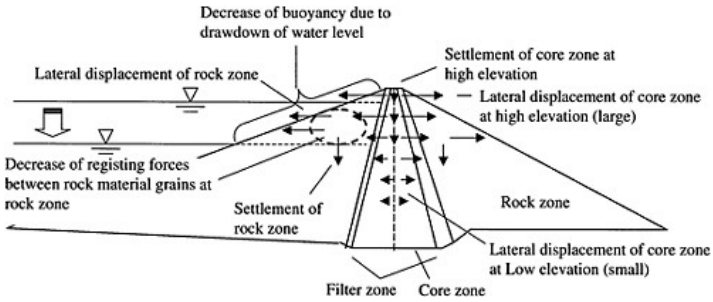

Figure 18. Conceptual image of dam top settlement and lateral displacement when reservoir water level decreases.

lateral displacement at rock zone has not been measured after ponding, and it is an important research subject for us in the future.

8 CONCLUSION

We conducted the comparative review of dam body behavior at four designated dams owned Japan Water Agency. The result shows stress concentration at filter zone and stress decrease at core zone during embankment construction, before and after ponding. In terms of the dam body behavior where pore pressure decreases slowly, it was studied that reservoir water pressure acted as stress to core zone. And the possibility was found that the triangle shape of dam body could cause settlement at core zone where pore pressure decreases slowly.

REFERENCES

1) Tadahiko Sakamoto, Seizo Takebayashi, Akira Nakamura, Nario Yasuda and Mitsuhiro Kojima: Safety assessment based on the observed behavior of zoned rockfill dams, Dai-Dam, No. 150, pp. 51–61, 1994.
2) Nobuteru Sato, Fumio Yonezaki, Katsumi Ooyabu, Hideki Ohta and Koji Nakagawa: Study on the Observed Stress and Strain of Rockfill Dams (in Japanese), Structural Engineering Journal, JSCE, 2004.
3) Norio Yagi, Ryuichi Yatabe and Meiketsu Enoki: Study on a few characteristics of compression and shear of compacted soil, Proceedings of the Symposium on present state of engineering property of unsaturated soil, pp. 29–34, 1987.
4) Hiroshi Yoshikoshi, Motoyuki Inoue, Masatoshi Tsuda, Yoshihisa Uchida, Tetsuo Fujiyama and Hideki Ohta: On the Behavior of Long-term Settlement of Impervious Zone in Rock-fill Dam (in Japanese), Structural Engineering Journal, JSCE, No. 582/III-41, pp. 197–205, 1997.12.
5) Nobuteru Sato, Fumio Yonezaki, Katsumi Ooyabu, Hideki Ohta and Koji Nakagawa: Study on the Observed Deformation of Rockfill Dams (in Japanese), Structural Engineering Journal, JSCE, No. 736/ III-63, pp. 179–192, 2003.6.

New Developments in Dam Engineering—Wieland, Ren & Tan (eds),
© 2004 Taylor & Francis Group, London, ISBN 04 1536 240 7

Composite clays: a suitable material for dam construction?

A.Shafiee, M.K.Jafari & N.Jalali
IIEES, Iran

R.Noroozipour
IAU, Iran

ABSTRACT: Composite clay is a mixture of clay, as the main body and aggregates which are floating within the clayey matrix. Compacted composite clays are widely used as the core material of embankment dams. An extensive test program was conducted on kaolin-gravel and kaolin-sand mixtures to investigate various effects of aggregate on the physical and mechanical properties of the mixtures. Compaction characteristics, Permeability, monotonic and cyclic behavior of mixtures were the main issues which were studied. Test results showed that permeability and dry density of the mixtures increase, when aggregate content is raised, meanwhile the dry density of the clayey matrix decreases. Monotonic test results revealed that shear strength increases with increasing aggregate content. Meanwhile when aggregate content is raised pore pressure rises for cyclic loading. The results of this experimental research program are presented and discussed in this paper.

1 INTRODUCTION

A review of past studies reveals the majority of research has been concentrated on pure sands or clays and research on gravely or sandy clays, for instance, has been sparse. However composite soils with properties between cohesive and granular materials are often found in nature. Moraine, which consists of unsorted materials of glacial origin, is a good example for this type of composite soils. Moraine has been used extensively in North America and northern countries, as fill material for impervious cores in zoned embankment dams or for the main body of homogeneous dikes [1]. It has also served as relatively good quality foundation for water retaining structures. Composite clays are other types of composite materials, which are usually broadly graded and encompass clay, sand, gravel, cobble and even boulder, while the clayey matrix govern the mechanical behavior. It is also a current practice to employ such soils as the core of embankment dams, usually constructed from pure clays. Furthermore in the case of lack of appropriate clayey materials e.g., due to high plasticity or gravelly clays deposit, the core material can be obtained through mixing available high plastic clay with adequate percentage of granular material to reduce post construction settlement and pronounced arching effect in the core. It is generally assumed that the coarser fraction of such soils imparts relatively higher shear strength, high compacted density and low compressibility, while the permeability of the soil is governed by the proportion and nature of the finer fraction. This generally results in a relatively serviceable and trouble free fill [2].

The lack of comprehensive studies on the behavior of aggregate-clay mixtures stems mainly from the fact that tests cannot be carried out on samples which are large enough to be truly representative of the soil mass. Another factor is that these soils are heterogeneous and are hence difficult to characterize. Therefore, a comprehensive laboratory testing program on this type of soils with different cohesive non-cohesive ratios and two different aggregate sizes were defined. The investigation described in this paper entails a study on the effects of aggregate on the physical and mechanical properties of compacted composite clays including dry density, permeability and monotonic and cyclic shear strength under triaxial conditions.

2 TESTED MATERIALS AND PROCEDURE

Seven types of clay-gravel and clay-sand mixtures were used in this study. In order to reduce the risk of plasticity variation in natural clay, commercial kaolin clay was selected as the cohesive part. The kaolin had a specific gravity of 2.74 and its liquid limit and plasticity index were 69% and 38% respectively. Both the used sand and gravel were retrieved from a riverbed and composed of subrounded aggregates with a specific gravity of 2.66. The soil passing sieve No. 10 and remaining on sieve No. 12 with a mean grain size of 1.84mm was selected as sandy materials and the soil passing sieve No. 1/4 and remaining on sieve No. 4 with a mean grain size of 5.55mm as gravelly materials. The gap graded gradation for aggregates was chosen to investigate, as precisely as possible, the effect of aggregate size on behavior, based on its average diameter. Kaolin was mixed with respective amounts of sand and gravel to obtain various mixtures. The seven samples of kaolin-aggregate were mixed in volumetric proportion and named as *K100, K80S, K80G, K60S, K60G, K40S* and *K40G*. The first letter is an abbreviation of Kaolin, the second number is the volumetric clay percent in the mixture, and the third letter indicates the type of aggregate in the mixture (S for Sand and G for Gravel). A minimum of 40% clay content was considered for two reasons: first, the results of this study should also be applicable to materials used as the core of embankment dams, and second, to avoid effects of interaction between large particles on the behavior. Several observations made by the authors revealed that for 40% clay content, some of the grains were in contact, while these in-contact grains were not sufficient to form a granular skeleton [3].

Specimens which used for permeability and triaxial tests were 50mm in diameter and 100mm in height. The specimens were compacted in 6 layers, with a dry density of 95% of maximum dry density obtained from standard compaction test method and water content of 2% wet of optimum. Soil layers were prepared separately and mixed with water at least 24 hours before use and sealed. Each layer was scored after it was compacted for better bonding with the next layer. This type of specimen preparation may result in higher density of bottom layers, but the authors attained layers of the same density by setting the number of hammer drops [3]. The specimens were saturated with a Skempton B-value in excess of 95%. Then specimens were isotropically consolidated under three different effective confining stresses of 100, 300 and 500 kPa. Following consolidation, permeability (under triaxial conditions) or undrained monotonic and cyclic triaxial tests were carried out. The significance of aggregate content on the physical and mechanical properties of kaolinaggregate mixtures is discussed below.

3 COMPACTION CHARACTERISTICS

Achieving a desired dry density under a reasonable compactive effort which can meet criteria of low permeability and high shear strength, is an important issue for the geotechnical engineers who design core of embankment dams. Several researchers have investigated the influence of aggregate on the compaction of clayey soils. Within the range of aggregate content normally of interest, the greater the aggregate content, the higher will be the dry density of the soil for a given compactive effort and compaction water content. This is mainly due to the specific gravity of the aggregate particles which is usually higher than the bulk specific gravity of the soil and aggregates.

Houston et al. [4] showed that for the compacted specimens of soils containing large aggregate, and for a given compactive effort and water content, the dry density increases with increasing aggregate content, up to 60%. Shakoor and Cook [5] concluded that the maximum dry density of soilaggregate mixtures increases with increasing aggregate content and peaks at 60–70% aggregates. Garga and Madureira [2] also found that the maximum dry density was achieved at about 70% aggregate content. Figure 1 shows the maximum dry density versus aggregate content for different

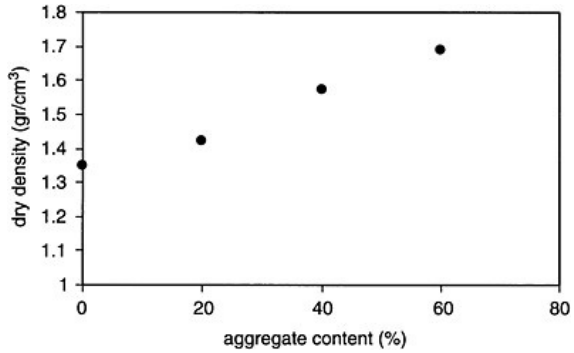

Figure 1. Maximum dry density versus aggregate content.

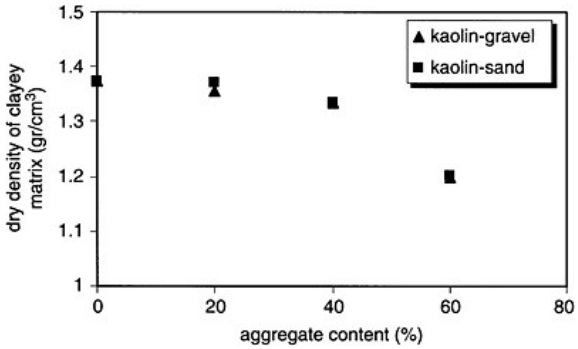

Figure 2. Effect of aggregates on after consolidation dry density of clayey matrix.

mixtures obtained in this study. It should be noted that compaction tests resulted in nearly the same values for dry density and optimum water content of the respective samples of kaolin-gravel and kaolin-sand mixtures. As seen in Figure 1, maximum dry density increases with increasing aggregate content. These results are in agreement with the previously mentioned investigations. In order to have a better understanding of the compaction characteristics of composite clays, it is prudent to observe the effects of aggregate on the dry density of the clayey matrix. Figure 2 shows variation of the after consolidation dry density of the clayey matrix in terms of aggregate content for a typical initial confining stress of 100kPa. As seen dry density of the clayey matrix decreases with increasing aggregate content. The decrease of the clayey matrix dry density may lead to the increase in permeabilty and decrease in shear strength as well. Thus, although adding aggregate into a clayey matrix may have some advantages, such as increase in the dry density, decrease in post construction settlement and decrease in the required time of in situ compaction and cost, but it may lead to higher permeability and lower shear strength. The significance of the aggregate content on the permeability and shear strength mixtures is discussed in the next sections.

4 PERMEABILITY

An important issue in accepting a soil material as the core of embankment dams, is its permeability characteristics. Erosion resistance and the potential for low permeability make a properly compacted

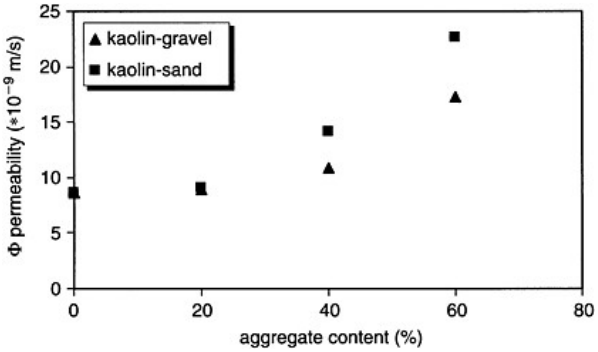

Figure 3. Permeability as a function of aggregate content.

clayey gravel soils an attractive candidate for use as core material for a dam. Actually, the prediction of the effect of the aggregate on permeability is complicated by the fact that solid, less permeable stones are being added to the clay, while the dry density of clayey matrix decreases when aggregate content is raised. The combined effect of these two may increase or decrease permeability when aggregate content increases. Dunn and Mehuys [6] conducted permeability tests on mixtures of cohesive soils and aggregate. They found that the permeability of soil-aggregate mixtures decreases as the volume concentration ratio of the aggregate in the mixture decreases. The studies by Shakoor and Cook [5] and Shelly and Daniel [7] also revealed that up to 50% to 60% aggregate content, permeability does not change appreciably

In order to investigate effect of aggregate on the coefficient of permeability, authors were conducted permeability tests on different samples consolidated at an initial confining stress of 100 kPa using triaxial cell with two back pressure systems [8]. Figure 3 shows variation of permeability coefficient in terms of aggregate content for kaolin-gravel and kaolin-sand mixtures. As seen for both type of mixtures, increasing aggregate content, does not change permeability remarkably up to 60% aggregate content, but for 60% aggregate content, the increase in permeability is significant. It should be noted that for 60% aggregate content, some grains were in contact with each other [3]. It seems that plasticity characteristics and fabric of the clayey matrix (e.g. compacted at dry or wet of optimum) affect permeability as well. Figure 3 also shows that coefficient of permeability for the respective samples of kaolin-gravel and kaolin-sand mixtures is approximately the same.

5 MONOTONIC BEHAVIOR OF COMPOSITE CLAYS

Holtz and Willard [9] may be the first who investigated the shear strength of clayey soils with gravel content varying from 0–65%. They concluded that the angle of shearing resistance increased and apparent cohesion decreased when gravel content was raised. For gravel content more than 50%, the effect of granular part was readily apparent. Patwardhan et al. [10] carried out series of direct shear tests on cobble-clay mixtures. The cobble content varied between 0 and 100%. The tests were performed without normal stress being applied. The results showed a gradual increase in the shear strength of mixture with increase in cobble content up to about 40%, followed by sharper increase beyond this value. Vallejo and Zhou [11] reported direct shear test results on simulated soil-rock mixtures which were developed by mixing kaolinite clay with sand. They indicated that when the sand content was less than 50%, the shear strength of the mixture was governed by the strength of the clayey matrix. When the concentration of sand varied between 50–80%, the shear strength of the mixture provided in part by the shear strength of the kaolin and in part by frictional resistance between sand grains.

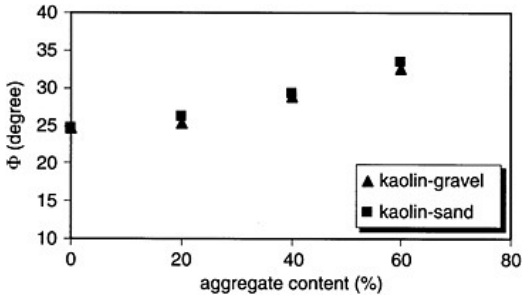

Figure 4. Mobilized angle of shearing resistance at critical state versus aggregate content.

In order to see effect of aggregate on monotonic behavior of compacted composite clays, static strain-controlled triaxial tests were performed under undrained conditions. On the basis of test results, the values of mobilized angle of shearing resistance at critical state, φ for different types of composite clays was computed. Figure 4 shows variation of φ with respect to aggregate content for kaolin-gravel and kaolin-sand mixtures. It is evident that for both kaolin-gravel and kaolinsand mixtures, shear strength increases gradually when aggregate content is raised. Interestingly, presence of 60% aggregate (either sandy and gravelly) only causes about 8–9° increase in φ. These results confirm well with the most of the previously mentioned investigations.

6
CYCLIC BEHAVIOR OF COMPOSITE CLAYS6

Although expensive methods such as full scale and physical model tests can be conducted for evaluating behavior of composite clays with oversized particles, in many cases laboratory triaxial tests are accomplished on materials of modified gradation. This modification in engineering projects can even be reduced to conduct tests only on pure clay by extracting the oversized particles. It is generally assumed that this results in conservative estimation of the mechanical soil properties. The monotonic test results presented above also confirm this hypothesis. However, Jafari and Shafiee [12] showed that in the case of cyclic undrained loading on compacted composite clays, the assumption that adding aggregate to pure clay improves its mechanical properties is questionable. They showed that composite clays containing 50% sandy gravel and 50% high plastic clay, failed in a lower number of loading cycles and consequently exhibited less cyclic strength (defined as the ratio of deviatoric stress to initial confining stress causing 5% axial strain) than pure clays. This was the triggering point for planning an extensive research program on cyclic behavior of compacted composite clays. In this respect, cyclic strain-controlled triaxial tests were performed on composite clay specimens under three different shear strain amplitudes of 0.15%, 0.75% and 1.5%. For all specimens tested in this study, a reduction in deviatoric stress would occur when loading proceeded, while the normalized residual pore pressure u_r^*, is the pore pressure normalized on the initial confining stress and computed where shear strain is zero) increased.

Figures 5 and 6 show variation of u_r^* in terms of number of loading cycles, N in kaolin-gravel and kaolin-sand mixtures for shear strain amplitudes, γ_c of 1.5% at initial confining stress of 100kPa. γ_c is computed as 1.5 times of axial strain. Figures 5 and 6 show that higher pore pressure is generated for the soils with higher aggregate content. Thus u_r^* is highest for *K40G* and *K40S* specimens and lowest for *K100* specimens. The reason behind this behavior can simply be explained: since the compressibility of the clayey matrix is greater than individual grains, all of the specimen deformations take place in the clay. Hence, during strain-controlled loading, the clayey matrix of the specimens containing more aggregate experiences more deformation for the same strain level, which directly leads to more pore pressure generation. It can be shown that the heterogeneous matrix developed in

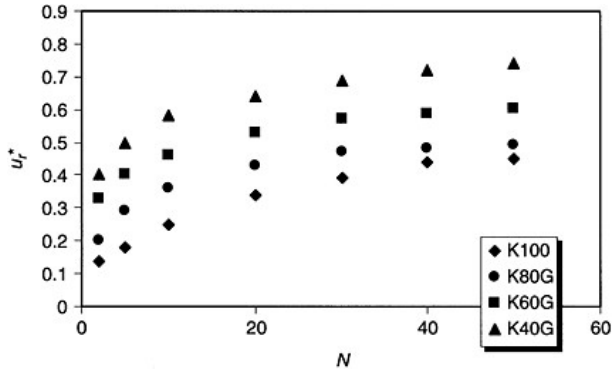

Figure 5. Variations of u_r^* in kaolin-gravel mixtures at initial confining stress of 100kPa and γ_c=1.5%.

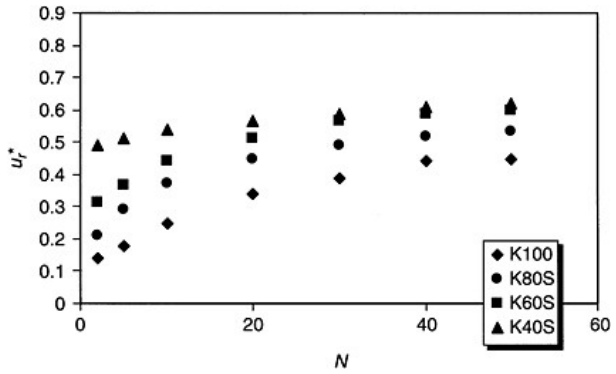

Figure 6. Variations of u_r^* in kaolin-sand mixtures at initial confining stress of 100kPa and γ_c=1.5%.

the clayey part of composite clays, leads to greater pore pressure generation in composite clays containing more volume of aggregates [13]. Greater pore pressure generation in composite clays containing more aggregates may cause some problems for embankment dams as will be discussed in the next section.

7. COMPOSITE CLAYS: A SUITABLE MATERIAL FOR DAM CONSTRUCTION?

The previous findings regarding more pronounced effect of aggregate content on pore pressure generation in cyclic loading deserves more attention. To discuss this matter in more detail, the stress path of pure clay, *K100* is compared with that of *K40G* for a shear strain amplitude of 1.5% and a confining stress of 300kPa, as shown in Figures 7 and 8 (note that q is deviatoric stress and p′ is mean effective stress). In these figures, the critical state lines are drawn based on φ values shown in Figure 4. As seen, although the slope of the critical state line of *K40G* is greater than that for *K100* (referring to Figure 4), while stress path of *K60G* moves more rapidly toward the critical state line than pure clay. This behavior leads to a very important conclusion: although adding aggregate to pure clays increases the angle of shearing resistance, the cyclic strength is smaller (as pointed out by Jafari and Shafiee [12]).

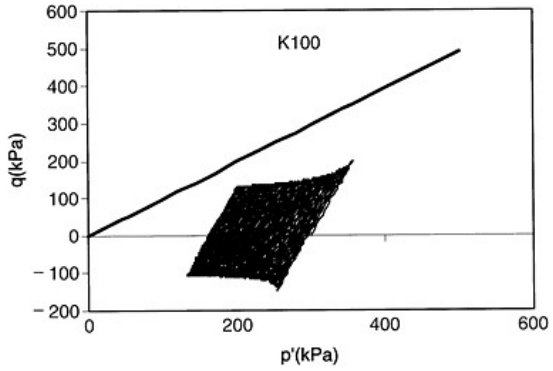

Figure 7. Stress path of sample *K100* during cyclic loading (γ_c=1.5% and confining stress=300kPa).

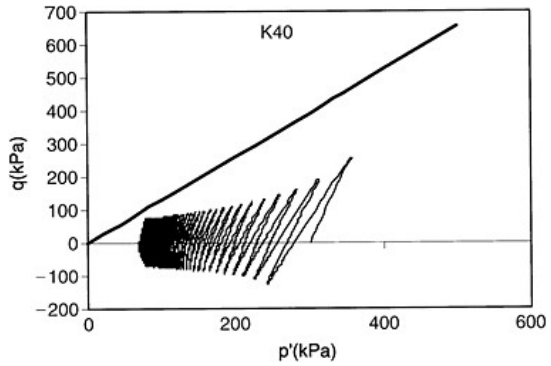

Figure 8. Stress path of sample *K40G* during cyclic loading (γ_c=1.5% and confining stress=300kPa).

The above-presented behavior of composite clays can have an immediate implication on design and construction of embankment dams. It was shown that composite clays exhibit higher pore pressures than that of pure clays. This may cause some problems for the cases in which composite clays should be used as the core of embankment dams, instead of pure clays. Hence, during the construction phase higher pore pressures can be generated inside the core leading to a possible increase of construction time. The eventual extra time needed for the construction phase should be determined based on the maximum allowable pore pressure generation inside the core, the predicted rate of pore pressure generation, and consideration of the rate of pore pressure dissipation in composite clays which is a function of permeability. Even though this problem can technically be resolved by considering a longer time schedule for the construction phase, the saturated core behavior under earthquake loading may threaten the dam safety especially at upper parts of the dam height (in the core) in which the current state of stress is near the critical state line. Furthermore dissipation of generated pore pressure may cause the free board of dam to be decreased significantly.

Thus, although composite clays may have some advantages over pure clays, such as decrease in required time and cost for compaction, higher static shear strength and low permeability, while they have serious problem during dynamic loading. In this case, using pure clays instead of composite clays at the upper parts of the dam height (in the core) or increasing the clay content with the height of the core are some of the solutions to overcome the deficiency of composite clays during dynamic loadings.

8 CONCLUSIONS

An experimental study was performed on the compacted mixtures of kaolin-sand and kaolingravel to investigate effects of aggregate on the compaction characteristics, permeability and monotonic and cyclic behavior of the mixtures. The following conclusions may be drawn based on this experimental study:

1. Compaction test results show that, maximum dry density increases with increasing aggregate content, while after consolidation dry density of the clayey matrix decreases with increasing aggregate content;
2. Permeability tests show that for both type of mixtures, increasing aggregate content, does not change permeability remarkably up to 60% aggregate content, but for 60% aggregate content, the increase in permeability is significant;
3. On the basis of the monotonic test results, the shear strength expressed in terms of the angle of shearing resistance at critical state, increases with increasing aggregate content;
4. Based on cyclic triaxial tests, increasing aggregate content causes more deformation of the clayey matrix for the same strain level, leading to more pore pressure generation during undrained loading. Thus, care should be taken in the cases in which composite clays are substituted for pure clays in the core of embankment dams.

REFERENCES

[1] International Commission on Large Dams (ICOLD). *Moraine as embankment and foundation material.* Bulletin 69, Paris, France, 1989.
[2] Garga, V.K. and Madureira, C.J. Compaction characteristics of river terrace gravel. *Journal of Geotechnical Engineering,* 1985. 111:pp. 987–1007.
[3] Shafiee, A. *Monotonic and cyclic behavior of composite clays with special view to pore pressure generation.* Ph.D.Thesis, Geotechnical Research Center, International Institute of Earthquake Engineering and Seismology (IIEES), Tehran, Iran. 2002.
[4] Houston, W.N., Houston, S.L. and Walsh, K.D. Compacted high gravel-content subgrade materials. *Journal of Transportation Engineering,* 1994. 104:pp. 193–205.
[5] Shakoor, A. and Cook, B.D. The effect of stone content, size and shape on the engineering properties of a compacted silty clay. *Association of Engineering Geologists Bulletin,* 1990. 27:pp. 245–253.
[6] Dunn, A. and Mehuys, G. Relationship between gravel content of soils and saturated hydraulic conductivity in laboratory tests. Proceeding of Symposium on erosion and productivity of soils containing rock fragments, Special Publication (Soil science society of America), 1984. 13:pp. 55–63.
[7] Shelly, T.L. and Daniel, D.E. Effect of gravel on hydraulic conductivity of compacted soil liners. *Journal of Geotechnical Engineering,* 1993. 119:pp. 54–67.
[8] Head, K.H. *Manual of soil laboratory testing,* John Wiley & Sons, West Sussex, England, Vol. 3, 1992.
[9] Holtz, W.G. and Willard, M. Triaxial shear characteristics of clayey gravel soils. *Journal of Soil Mechanics and Foundation Engineering,* 1956. 82:pp. 143–149.
[10] Patwardhan, A.S., Rao, J.S. and Gaidhane, R.B. Interlocking effects and shearing resistance of boulders and large size particles in a matrix of fines on the basis of large scale direct shear tests. In *Proceedings of the 2nd SoutheastAsian Conference on Soil Mechanics*. Singapore, 1970. pp. 265–273.
[11] Vallejo, L.E. and Zhou, Y. The mechanical properties of simulated soil-rock mixtures. *13th International Conference on Soil Mechanics and Foundation Engineering,* 1994. 1:pp. 365–368.
[12] Jafari, M.K. and Shafiee, A. Dynamic behavior of mixed materials used for core of Karkheh dam. *In Abstract Volume of Proceedings of the 11th European Conference on Earthquake. Engineering*. Paris, France, 1998. p. 179.
[13] Jafari, M.K. and Shafiee, A. Mechanical behavior of compacted composite clays. *Accepted paper to be published in Canadian Geotechnical journal.*

New Developments in Dam Engineering—Wieland, Ren & Tan (eds),
© 2004 Taylor & Francis Group, London, ISBN 04 1536 240 7

Application of GSQ24 shell element to nonlinear crack analysis of Arch dam

Guojian Shao & Jingbo Su
College of Civil Engineering, University of Hohai, P.R. China

ABSTRACT: An efficient versatile GSQ24 shell element is proposed, which is composed of the Mindlin plate element and the membrane element with drilling degrees of freedom. GSQ24 shell element has six degrees of freedom per node, and can avoid the problem of ill conditioning matrix when elements are co-plane. Thus, modeling of complex joint of shell surface sections and compatibility with other elements with rotation degrees of freedom can be easily made. The element herein passes the patch test, and has no spurious zero energy modes and no shear and membrane locking. Based on smeared crack model, a simple and efficient layered model is introduced and the midpoint rule integration scheme is adopted for each layer. The layered model can simulate the expanding of plastic and craze zone through the thickness of element. On the joint boundary of arch dam and foundation, direct introduction method has been used. The concrete as a low tensile material, four-parameter failure criterion is used. The fractured concrete is considered as anisotropic material. The corresponding FEM formulae have been given. Nonlinear crack analysis of an arch dam has been performed. Compared with the results from three-dimensional displacement element, the numerical results show the feasibility of the present method. A new method for nonlinear crack analysis of arch dam is provided.

1 INTRODUCTION

Nonlinear crack problem of arch dam is one of the hotspots in the analysis of hydraulic structure. As an attempt, the GSQ24 shell element which is introduced in conferences [1] and is adapt to thick and thin plate and shell structure is applied to nonlinear crack analysis of arch dam. The main feature of concrete is the lower tensile property, and that results in the occurrence of crack in lower tensile stress. There are two primary models for crack in FEM: discrete crack model; smeared crack model.

Discrete crack model shows that each crack is discontinuously disposed in finite element meshes. That the cracks must be along the boundaries of elements is the obvious shortcoming. So the cracks are very sensitive to meshes, and the formation of cracks depends on the change of meshes. Although new elements are imported and this makes the element boundaries are along the crack plane and reduced the dependence on meshes, but meshes need to be formed again, and these difficulties make the application of the model to be confined in general structure.

Smeared crack model does not consider factual discontinuity in finite element meshes, on the contrary, the crack concrete is supposed to keep continuity, but material properties consider the amendment to damage duo to crack. The model considers if certain element stress (in fact: certain sample point stress) goes beyond crack stress, the element (or certain region around the point) will crack and countless parallel cracks (not flaw) appear vertically to the direction of crack tensile stress. That is to say, the cracks are distributed in interior of the element, and they are slim and coequal each other. In the beginning “continuous” concrete is consider as isotropic material, but soon becomes anisotropic material duo to crack. After crack, the direction of material principal axis without crack becomes orthotropic. The material properties depend on the stress-strain state. The Young’s module reduces at the direction vertical to crack plane, the Passion’s ratio is neglected, and the cut module reduced along cut plane too. In numerical computations, smeared crack model has outstanding virtues, dominatingly because the mesh structure keeps changeless in total analysis and only the stress-strain relations are amended when the crack appears. So the model is applied for crack analysis in this paper.

2 GSQ24 SHELL ELEMENT AND LAYERED MODEL

GSQ24 shell element is a 4-node quadrilateral shell element. The element is obtained by combining the Mindlin plate bending element and membrane element with in-plane drilling degrees of freedom. The element has six degrees of freedom per node: three degrees of freedom are node linear displacements; the others are node angular displacements. In plate bending element, based on potential energy functional of Mindlin plate theory and the shear locking mechanism, the hierarchical displacement interpolation functions are used for lateral displacement and the bilinear interpolation functions are used for rotation. Besides, bilinear interpolation functions are essential for shear strains. In membrane element in-plane, based on variational principle employing modified Reissner functional, into which independent rotation field has been introduced, rotation field is interpolated by true rotation at each node and the nonconforming displacement functions being suitable for arbitrary quadrilateral element are denoted for the membrane displacement. In forming element stiffness matrix, by using static elimination method, the four corner node displacement functions are denoted by inner degree-of-freedom displacement. Finally, the 24×24 stiffness matrix of GSQ24 shell element is obtained by the combination of stiffness matrix of plate bending element and membrane element with in plane. The superiorities of GSQ24 shell element are: it can avoid the problem of ill conditioning matrix when elements are co-plane. Moreover, order matching of displacement interpolation functions between bending element and membrane element can be solved properly. Thus, modeling of complex joint of shell element surface sections and compatibility with order elements with rotation degrees of freedom can be easily made. And the shell element in connection is expediently disposed by direct introduction method when it is coupled with three-dimension solid displacement-type element.

The shell elements are divided into some layers along the thickness by layered model. The model considers that a material layer comes into yield (or crack) condition when the stress in middle plane of the layer arrives at yield (or crack) stress. The total stress condition in one layer is delegated by the stress condition in middle plane of the layer. The spread of plastics (or crack) zone along element thickness is described at full steam by layered model. Every layer may come into plastics (or crack) alone. So the crack condition on top of dam foundation is reasonable described by layered model in crack analysis of arch dam [2].

3 FAILURE MODES OF CONCRETE

3.1 *Four-parameter elastic-plastic crack model of concrete*

According to the concrete progressive failure experimentation under the complicated loading condition, the hypothesis of initial yield surface and failure surface having the same shape in stress space is brought forward by Hsieh S S *et al.* [3]. The hypothesis considers that the stress condition is elastic before the occurrence of yield; the stress condition is plastic between yield surface and failure surface; the concrete becomes anisotropic or rigidless broken mass beyond failure surface. And yield criterion and failure criterion are introduced with four parameters, as follows:

$$F_o = A\left(J_2 / f_c\right) + B\sqrt{J_2} + C\sigma_1 + DI_1 - f_c = 0 \tag{1}$$

$$F = A\left(J_2 / f_c^{*}\right) + B\sqrt{J_2} + C\sigma_1 + DI_1 - f_c^{*} = 0 \tag{2}$$

where f_c is uniaxial compression ultimate strength; *A, B, C, D* are defined by four failure tests respectively: uniaxial tension test, uniaxial compression test, biaxial compression test, triaxial compression test.

If the material properties of hardening and softening are considered, the loading function of concrete is taken as:

$$F = AJ_2 / H(\theta_p) + B\sqrt{J_2} + C\sigma_1 + DI_1 - H(\theta_p) = 0 \tag{3}$$

where $H(\theta_p)$ reflects hardening and softening strength of material, θ_p is plastic volumetric strain.

3.2 *Failure forms of concrete*

The lower tensile elastic crack model is adopted for concrete. It is a combined model, i.e. the material is destroyed by plastic yield, or maybe tensile crack. The necessary conditions of brittle failure or plastic failure are uniformly described by aforementioned material failure criterion. The failure modes of material are divided into three types:

(1) Crack. Differentiation criterion is F=0, I σ_1>0;

(2) Crushed. Differentiation criterion is F=0, **I** ε_1<0;

(3) Combined failure. Differentiation criterion is F=0, I $\sigma_1 \le 0$, I $\varepsilon_1 \ge 0$.

If purely crack type happens under imposed stress condition, σ_1>0 is supposed in this time. By using stress invariants, it is showed as

$$J_2 \cos\theta + I_1 /(2\sqrt{3}) > 0 \ , \quad |\theta| \le \pi/3 \tag{4}$$

where: $\theta = (1/3)\cos^{-1}[3\sqrt{3}J_3/(2J_2^{3/2})]$.

If purely destroyed type happens under imposed stress condition, all the strains are supposed as compressive strains in this time. That is to say, the maximum principal strain is non-positive, i.e. ε_1<0. By using approximatively the relations of Hook's law, principal stress and invariants, the following formula is gained:

$$J_2 \cos\theta + \frac{1-2\mu}{2\sqrt{3}(1+\mu)} I_1 = 0 \ , \quad |\theta| \le \pi/3 \tag{5}$$

The crunch coefficient α is introduced in references [3] as:

$$\alpha = -I_1 /(2\sqrt{3J_2}\cos\theta) \ , \quad |\theta| \le \pi/3 \tag{6}$$

Thus, the three failure conditions are distinguished by α as:

(1) crack type α<1, σ_1>0 is obtained by formula (4). It implied the material is ripped and becomes anisotropic body.

(2) crushed type: α>(1+μ)/(1−2μ), ε_1<0 is obtained by formula (5) approximately. It implied the material is crushed and lost rigid.

(3) combined type: 1≤α≤(1+μ)/(1−2μ). It implied the material is ripped partly and crushed partly. The crack direction is along the direction ε_1 and the rigid reduces by α(1+μ)/(1−2μ) at other directions.

3.3 *Constitutive equations of material*

The constitutive equations are in relative to work stage and failure type. They are divided into the following conditions:

(1) Elastic stage: When the material lies in initial elastic stage, elastic unloading stage in plastic zone and neutral changed load, the stress change accords with Hook's law, i.e.

$$\{d\sigma\}=\mathbf{D}\{d\varepsilon\} \tag{7}$$

(2) Elastic-plastic stage: At this stage, the loading and unloading conditions must be distinguished. According to Ilyshin's formula, the loading criterion is decided by l:

$$l=\{\partial f/\partial\{\sigma\}\}^T\mathbf{D}\{d\varepsilon\} \tag{8}$$

Plastic loading is gained when $l>0$; elastic unloading is gained when $l<0$. For shell and plate structures, by adopting Mindlin plate theory, then

$$\partial f/\partial\{\sigma\}=[\partial f/\partial\sigma_x\ \partial f/\partial\sigma_y\ \partial f/\partial\tau_{xy}\ \partial f/\partial\tau_{yz}\ \partial f/\partial\tau_{zx}]^T$$

At the plastic loading stage, the loading function is taken as formula (3). Supposed concrete is linear strengthening material, then in formula (3):

$$H(\theta_p)=f_c^{'}+E_p\theta_p \tag{9}$$

where f_c' is uniaxial compression yield strength.; E_p is the slope of strengthening curve.

The total forces properties of concrete are well described by aforementioned bilinear model. After the loading function (formula 3) is decided, the constitutive relations of concrete are established by general method in elastic-plastic mechanics.

(3) Destroyed stage: At destroyed stage, the constitutive relations of material are in relative to destroyed forms. For crack type, if the maximum tensile stress goes beyond the ultimate stress, the crack forms in the plane of vertical to tensile stress. So the concrete is not isotropic material, but orthotropic material. The direction of partial material principal axis is in accordance to the direction of principal stress and the normal rigidness along crack plane is zero. At every sample point, the orthogonality of crack direction is supposed. When the force is loaded farther, the secondary cracks come into being at the same point along former crack direction. After the production of initial crack, supposed the material principal axial keeps unchanged relative to the direction of principal stress, and the possible rotation of the direction principal stress is not considered, i.e. the direction of crack keeps fixed, the method is named as fixed crack method [3]. For destroyed type, the residual rigidness is not calculated and the rigidness of every direction is considered as zero. For combined type, the rigidness of the direction of maximum tensile strain is ordered as zero, and the rigidness of the other direction is reduced according to the degree of crush. Thus, the material gained is also anisotropic.

4 STRESS-STRAIN RELATION MATRIX OF ELEMENT AFTER CRACK FOR CONCRETE

4.1 *Stress-strain relation matrix of element after crack for concrete*

Before the crack of concrete shell structure, the stress-strain relation matrix is expressed as

$$\mathbf{D}_e=\begin{bmatrix} d_{11} & d_{12} & 0 & 0 & 0 \\ & d_{22} & 0 & 0 & 0 \\ & & d_{44} & 0 & 0 \\ & sym & & d_{55} & 0 \\ & & & & d_{66} \end{bmatrix} \tag{10}$$

If the material is isotropic, the elements of matrix in formula (10) are expressed as

$$\left.\begin{aligned} d_{11} &= d_{22} = E_c/(1-\mu^2) \\ d_{12} &= d_{21} = E_c\mu/(1-\mu^2) \\ d_{44} &= d_{55} = d_{66} = E_c/[2(1+\mu)] \end{aligned}\right\} \tag{11}$$

where E_c is instantaneous elastic modules. If total form is takes, E_c is secant modules; if incremental form is takes, E_c is tangent modules. If the concrete is anisotropic material, formula (10) has different form.

If the maximum principal stress goes beyond tensile strength at one sample point of element, the appearance of crack is considered and the direction of crack being vertical to the direction of maximum tensile stress σ_1 is supposed. After crack, the maximum principal stress σ_1 of concrete will be released and the redistributive stress appears. At the same time, the rigidness coefficient will be zero on this direction in stress-strain relation matrix. The o–x coordinate direction is taken as the direction vertical to crack, thus, the stress-strain relation matrix is amended according to reference [5] as

$$\mathbf{D}'_{cf} = \begin{bmatrix} 0 & 0 & 0 & 0 & 0 \\ & d_{22} - d_{12}^2/d_{11} & 0 & 0 & 0 \\ & & \eta d_{44} & 0 & 0 \\ & sym & & d_{55} & 0 \\ & & & & d_{66} \end{bmatrix} \tag{12}$$

where formula (12) is diagonal matrix and the elastic coefficients (vertical to crack) are zero. Of course, to avoid the instability of computation, the elastic coefficient is taken as appropriately lesser number. η is shear transfer coefficient.

If η=1, then the shear capacity is not affected by crack, it is the same to the condition of no crack; if η=0, then the shear capacity loses entirely. Apparently, though having crack after crazing, concrete can still keep partly shear capacity due to the action of aggregate interlock. So in factual condition there has $0 \le \eta \le 1$. There has no uniform conclusion for η owing to lots of factors. Generally, η is taken from 0.1 to 0.5, and 0.5 is taken for computation in this paper.

In the analysis of shell structure, because the layered extrusion along the direction of element thickness is neglected, the transverse shear stresses are ulteriorly ignored according to reference [5] when analyzing the crack. Substantially, the crack along the thickness is supposed by this disposal. In fact, the maximum tensile stress σ_1 for judging crack standard is the maximum tensile stres in layer plane of element. The stress-strain relation matrix in formula (12) is formed according to the coordinate system based on the direction of principal stress. When solving the element rigidness matrix, the coordinate system must be transferred to the total coordinate system. The directional cosines of principal stress in total coordinate system are l_i, m_i, n_i, (i=1, 2, 3). Thus, the stressstrain relation matrix in total coordinate system is defined by coordinate transformative matrix as

$$\mathbf{D}_{cf} = \mathbf{R}^T \mathbf{D}'_{cf} \mathbf{R} \tag{13}$$

where **R** is coordinate transformative matrix,

$$\mathbf{R} = \begin{bmatrix} l_1^2 & m_1^2 & l_1m_1 & m_1n_1 & n_1l_1 \\ l_2^2 & m_2^2 & l_2m_2 & m_2n_2 & n_2l_2 \\ 2l_1l_2 & 2m_1m_2 & l_1m_2 + l_2m_1 & m_1n_2 + m_2n_1 & n_1l_2 + n_2l_1 \\ 2l_2l_3 & 2m_2m_3 & l_2m_3 + l_3m_2 & m_2n_3 + m_3n_2 & n_2l_3 + n_3l_2 \\ 2l_3l_1 & 2m_3m_1 & l_3m_1 + l_1m_3 & m_3n_1 + m_1n_3 & n_3l_1 + n_1l_3 \end{bmatrix} \tag{14}$$

4.2 *Computation of stress relaxation after concrete crack*

When the maximum principal stress in elements goes beyond resistance to tensile stress, iterative process may be in progress for next step by the amendment for stress-strain relation matrix according to stress state (or strain state). When the maximum tensile stress goes beyond tensile strength, the effect of crack for stress-strain relation is still considered, for example, aforementioned $\mathbf{D}_c f$. On the other hand, the non-linear relation is different from that of compression. After crack in concrete, the stresses are not taken on at the direction vertical to the direction of crack, and so these stresses will be released.

For first crack, not only the incremental stresses of this grade are released, but also the cumulative stresses brought by former all-grade load are released.

If the crack already happened, all the incremental stresses will be released at the direction vertical to the direction of crack in subsequent iterative process.

If the compression stresses happen under any grade load at the direction vertical to the direction of crack, the crack may close.

4.3 *Computation process of FEM formulation in crack analysis of layered model*

(1) According to instantaneous material parameters, the element rigidness matrix **K** of shell structure has been calculated under a certain grade load $\{F_{i-1}\}$.

(2) To impose incremental load $\{\Delta P_i\}$, and to solve nodal incremental displacement $\{\Delta\delta_i\}=\mathbf{K}^{-1}\{\Delta P_i\}$.

(3) To solve incremental strain $\{\Delta\varepsilon_i\}=\mathbf{B}\{\Delta\delta_i\}$.

(4) To solve incremental stress $\{\Delta\sigma_i\}=\mathrm{D}\{\Delta\varepsilon_i\}$ and total stress $\{\sigma_i\}=\{\sigma_i-1\}+\{\Delta\sigma_i\}$. Where **D** is elastic matrix or elastic-plastic matrix or constitutive matrix after crack. It is decided by factual stress conditions.

(5) The crack matrix is taken if $\sigma_i>f_l$ (where f_l is the tensile strength of material) is satisfied at any Gaussian point of a layer of element.

If $F(\{\sigma\}, \theta_p)<0$, the elastic matrix is taken; If $F(\{\sigma\}, \theta_p)>0$, the elastic-plastic matrix is taken.

(6) To solve lopsided load. The lopsided load $\{\Delta p_i-1\}=\{F_i\}-\{P_i\}$ is gained by $\{P_i\}=\int_\Omega \mathbf{DT}\{\sigma_i\}d\Omega$. Turn to next grade load If $\|\{\Delta P_i-1\}-\{\Delta P_i\}\|$ is enough little.

Otherwise, to amend the material parameters by present stress state and to solve instantaneous rigidness matrix, then turn to step 2 to step 6 until the convergence is satisfied.

5 SAMPLE CASE ON THE NONLINEAR CRACK ANALYSIS OF ARCH DAM

Figure 1 shows a flat-roofed symmetrical arch dam with equal radius and equal curvature and no flooding. Its height is 40 meters; its width at the top of dam is 3 meters; at the bottom of dam is 6 meters. The applied loads are gravity and hydrostatic pressure up to the top. Supposed the mechanical parameters of foundations are identical with those of dam, we have: Young's modulus $E=2.0\times10^4$ Mpa, Poisson's ratio $\mu=0.2$, the unit weight $r=24.5\mathrm{kN/m}^3$, the uniaxial ultimate pressure strength is 20.7Mpa, yield strength resistance to compression is 12.4Mpa, the ultimate pressure strength in the interface is 20.7Mpa, the strength standards resistance to tensile are 1/10 of those in compression, the parameters of *A, B, C, D* in formula (3) are taken equal to 2.0108, 0.9714, 9.1412 and 0.2312 respectively, in hardening stage $E_p=5.0\times10^3$ Mpa. Half of the dam is analyzed duo to the symmetry. The dam is divided into 55 GSQ24 shell elements, and the foundation of dam is divided into 96 solid elements with eight nodes.

5.1 *Elastic analysis*

Under the loads of gravity and hydrostatic pressure up to the top, according to elastic analysis, the change law of radial displacement of the midline of arch coronal section along the height of dam is showed in Figure 2 by real line. The maximum radial displacement of vault is 7.548mm, and the

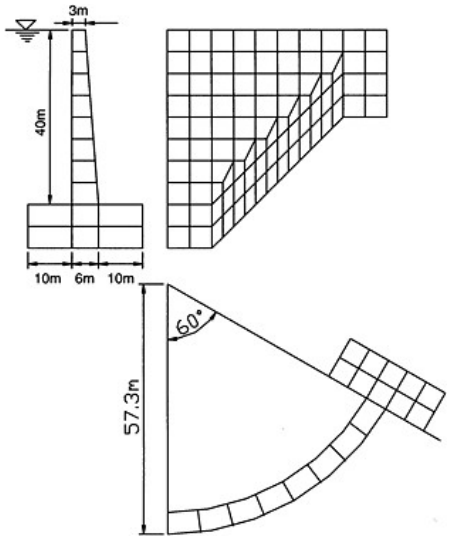

Figure 1. Flat-roofed symmetrical arch dam.

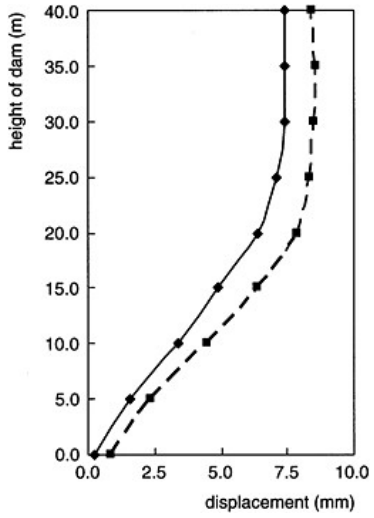

Figure 2. Radial displacement of the midline of arch coronal section.

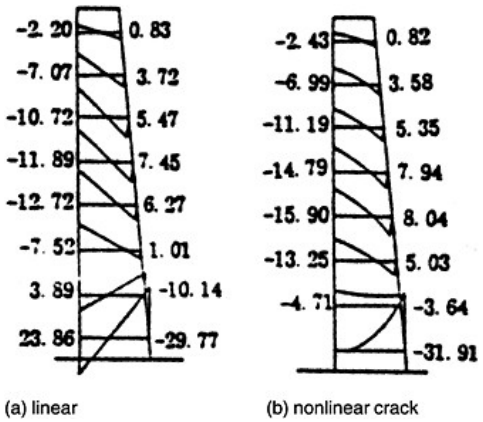

Figure 3. Cantilever stress components of arch coronal section.

high tensile stresses of arch dam appear mostly at the face of foundations of dam. The vertical tel sile stress in first layered elements at upriver heel of arch coronal section arrives at 2.386 Mpa, and this goes beyond tensile strength of concrete. The distributions of cantilever components and arch components of arch coronal section stresses are showed in Figure 3(a) and Figure 4(a).

The dam is divided into some hexahedral solid elements with three nodes along arch direction and twelve nodes along radial and vertical direction in reference [7]. By elastic analysis, the maximum radial displacement of vault is 7.3mm and the maximum tensile stress in at upriver heel of arch is 2.3 Mpa. The outcomes are similar to those by GSQ24 shell element.

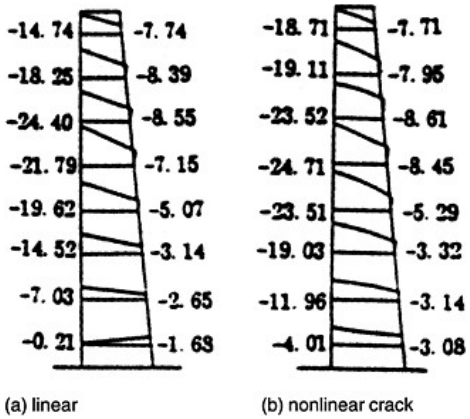

Figure 4. Arch stress components of arch coronal section.

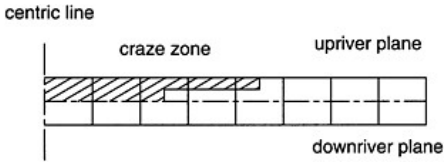

Figure 5. Distribution of crack zone at dam foundation plane.

5.2 *Nonlinear crack analysis*

The same meshes are adopted in nonlinear crack analysis. The stress conditions along thickness are simulated by layered model and GSQ24 shell elements along the thickness direction is divided into eight layers. According to nonlinear crack analysis, the change law of radial displacement of the midline of arch coronal section along the height of dam is showed in Figure 2 by broken line. The maximum radial displacement of vault is 8.576mm and increases by 13.62% by comparing with elastic outcome. However, according to nonlinear analysis using solid element, the maximum radial displacement of vault is 8.29mm and that is similar to the outcome by textual method.

The distributions of cantilever components and arch components of arch coronal section stresses are showed in Figure 3(b) and Figure 4(b). The distribution of crack zone along thickness at dam foundation plane is showed in Figure 5.

Considering the nonlinear crack of dam foundation plane, from the displacement law in Figure 2 and the stress law in Figure 3 and Figure 4, the displacement law has little change, but the stresses of dam have biggest change. After crack, the high tensile stresses near the upriver heel of dam disappear basically, and the maximum compression stress near the downriver heel of dam increases a little. Due to the crack near the dam foundation plane, the cantilever component of rigidness is cut down, so the burden of horizontal arch is added and the horizontal arch stresses near the dam foundation plane increase evidently showed in Figure 4.

6 CONCLUSION

On studying crack analysis of structure of concrete, the crack criterion must be decided firstly. Due to the complexity of computation methods and tests in fracture mechanics, the crack is still judged by routine strength parameters. Based on smeared crack model, GSQ24 shell element is developed to study nonlinear crack of concrete arch dam in this paper. The displacement and stress laws by sample case of arch dam are in according with those gained by solid elements, which is showed to be feasible by applying GSQ24 shell element to the nonlinear crack analysis of arch dam. Due to lots of uncertain factors in crack problems and analysis of arch dam, it is an attempt to apply GSQ24 shell element to the crack analysis of arch dam.

REFERENCES

[1] Shao G J, Zhuo J S. A simple and efficient finite element for analysis of thick and thin plates/shells. *Journal of Hohai University,* 1997, 25(1): 81~89 (in Chinese)
[2] Hsieh S S, Ting E C, Chen W C. A plastic-fracture model for concrete. *J Solid and Structure,* 1982, 18(3): 181~197
[3] Hinton E. *Numerical Methods Software.* Swansea UK: Prineridge Press, 1988
[4] Shen J M, Wang C Z, Jiang J J. *Reinforced Concrete Finite Element And Plates/Shell ultimate analysis.* Beijing: Tsinghua University Press, 1993 (in Chinese)
[5] Hinton E, Owen D R J. *Finite element software for plates shells.* Swansea UK: Prineridge Press Limited, 1984
[6] Fu Z X, Zhen X.. Nonlinear analysis of arch dam. *Design of Hydroelectric Power Station,* 1992, (2):1~6 (in Chinese)

This page intentionally left blank.

New Developments in Dam Engineering—Wieland, Ren & Tan (eds),

Cross-canyon vibration of earth dams

Zhen-zhong Shen & Zhi-ying Xu
Hohai University, China

ABSTRACT: Based upon the shear wedge analysis, a linear elastic model is developed for evaluating the dynamic characteristics, namely natural frequencies of the first, second and third vibration modes of longitudinal vibration of inhomogeneous earth dams in trapezoid canyons, where the inhomogeneity of the dam materials is taken into account by assuming a specific variation of the stiffness properties along the depth. By the use of the method of separation of variables and Bubnov-Galerkin approach, the approximate eigenvalue solutions are obtained for the first, second and third natural frequencies of longitudinal vibration of the earth dams. Then the dynamic behavior of earth dams is obtained by the Duhamal integral, such as dynamic displacement, velocity, acceleration, stress etc, and some calculation formulae for longitudinal earthquake response of the earth dams are proposed too, such as the maximum dynamic displacement, velocity, acceleration, stress, and so on.

1 INTRODUCTION1

Significant progress has been made in recent years towards understanding the dynamic behavior of earth dams subjected to earthquake shaking. However, the developed analytical methods for evaluating the seismic stability and potential deformations of earth dams consider only horizontal ground excitation, either in the upstream-downstream direction or in the longitudinal direction. It is widely believed that the lateral and longitudinal vibrations are solely responsible for the most frequently observed types of serious damage in embankment dams, namely longitudinal cracking near the crest center, sliding of soil masses from the upstream or downstream slopes, transverse cracking near the crest edges and large permanent displacements or bearing capacity failures due to liquefaction of saturated cohesionless soils in the dam. By now some analytical solutions have been obtained only in the simple rectangular canyons[1–4], semi-cylindrical canyons[5] and semielliptical canyons[6]. For other canyons, the analytical solutions have not be obtained yet because of the complex boundary. Xu[7,8] firstly obtained the approximate solutions of longitudinal and transversal vibration of homogeneous earth dams in triangular by the method of separation of variables and Bubnov-Galerkin approach. Then the authors have obtained the approximate analytical solutions for transversal, longitudinal and vertical vibration of both homogeneous and inhomogeneous earth dams in triangular canyons[9–13]. This paper proposes an approximate analytical method for evaluating the longitudinal earthquake responses of 3-D inhomogeneous earth dams in trapezoid canyons, which can be used in the more general rigid canyons.

2 DIFFERENTIAL EQUATION OF LONGITUDINAL VIBRATION

Because the earth dams are large three dimensional structures constructed from inelastic and inhomogeneous materials, the determination of their dynamic characteristics such as the natural frequencies and modes of vibration is extremely difficult. As a result, the following simplifying assumptions are adopted in order to derive the governing equation of earthquake motion.

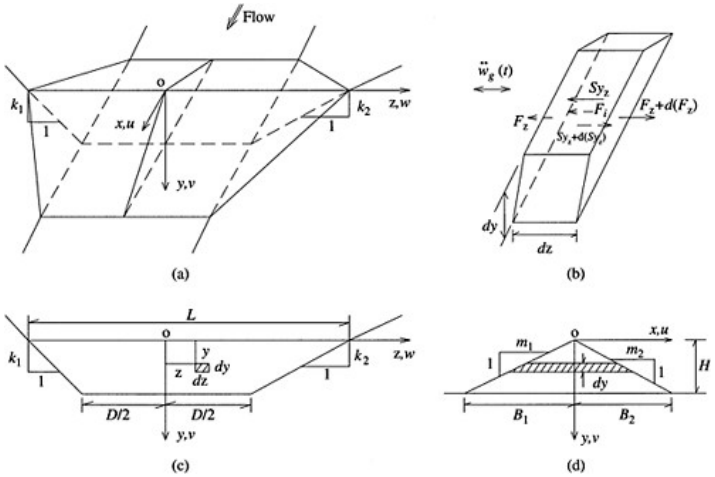

Figure 1. Analytical model of earth dam in trapezoid canyon for shear wedge analysis.

(1) The canyon is perfectly rigid, and the dam is represented by an elastic wedge, shown as in Figure 1. (2) The dam is modeled by a non-uniform elastic material that has uniform mass density and variable stiffness along the depth. The continuous variation of soil stiffness may be represented by a simplified function relationship, which the shear modulus increases as a general *(l/m)*th power of the depth[1]. (3) The dam material is linearly elastic. (4) The direction of the ground motion is along the dam axis. (5) The interaction between the dam and the water in the reservoir is negligible.

On the basis of the shear wedge analysis and the equilibrium of an element in dam, the governing differential equation of longitudinal motion is obtained for free vibration of the dam in rigid trapezoid canyon

$$\frac{\partial^2 w}{\partial t^2}=\frac{v_{s0}^2}{H^{\frac{l}{m}}}\left(1+\frac{l}{m}\right)y^{\frac{l}{m}-1}\frac{\partial w}{\partial y}+\frac{v_{s0}^2}{H^{\frac{l}{m}}}y^{\frac{l}{m}}\frac{\partial^2 w}{\partial y^2}+\xi\frac{v_{s0}^2}{H^{\frac{l}{m}}}y^{\frac{l}{m}}\frac{\partial^2 w}{\partial z^2} \tag{1}$$

where $w=w(y, z; t)$ is the vibration displacement at depth y in z-direction; t is time; H is the maximum height of dam; $v_{s0}=\sqrt{G_0/\rho}$ is the shear wave velocity of the dam material at the base, G_0 is the shear modulus of dam material at the base, ρ is the density of the dam material; l/m is called inhomogeneous coefficient, here l/m=0, 1/3, 2/5, 1/2 or 1; $\xi=2(1+\mu)$, μ is the Poisson's ratio of the dam material. The corresponding boundary conditions are

$$\begin{cases}\dfrac{\partial w}{\partial y}=0 & \text{at} \quad y=0\\ w=0 & \text{at} \quad y=H+k_1\left(z+\dfrac{D}{2}\right),\ y=H-k_2\left(z-\dfrac{D}{2}\right)\end{cases} \tag{2}$$

where k_1 and k_2 are the slope of canyon bank; D is the width at bottom of canyon, shown as in Figure 1.

3 SOLUTION FOR NATURAL FREQUENCY

By the method of separation of variables, *i.e.* $w(y, z; t)=\boldsymbol{\Phi}(y, z)T(t)$, the following equations are obtained for the time and space variables

$$T''+\omega^2 T=0$$

$$(1+\frac{l}{m})y^{\frac{l}{m}-1}\frac{\partial\Phi}{\partial y}+y^{\frac{l}{m}}\frac{\partial^2\Phi}{\partial y^2}+\xi y^{\frac{l}{m}}\frac{\partial^2\Phi}{\partial z^2}+\frac{\omega^2 H^{\frac{l}{m}}}{v_{s0}^2}\Phi=0 \tag{4}$$

where ω is the natural frequency. The solution of equation (3) is

$$T(t)=A_i\cos\omega t+A_2\sin\omega t \tag{5}$$

in which A_1 and A_2 are arbitrary constants. Since the boundary conditions given by equation (2) must be satisfied at all time, the following boundary conditions can be imposed on the function $\boldsymbol{\Phi}(y, z)$

$$\begin{cases}\dfrac{\partial\Phi}{\partial y}=0 & \text{at} \quad y=0\\ \Phi=0 & \text{at} \quad y=H+k_1(z+\dfrac{D}{2}),\ y=H-k_2(z-\dfrac{D}{2})\end{cases} \tag{6}$$

The closed form solution of equation (4) and the boundary conditions equation (6) is difficult to be obtained. However, an approximate eigenvalue solution can easily be obtained, which is a rather accurate value for the natural frequency of vibration of the dam system.

According to the Bubnov-Galerkin method[14], if a function satisfying the boundary conditions given by equation (6) can be found, the following integral

$$\int_0^H\int_{-\frac{1}{k_1}(H+k_1\frac{D}{2}-y)}^{\frac{1}{k_2}(H+k_2\frac{D}{2}-y)}P(y,z)\Phi(y,z)dydz=0 \tag{7}$$

yields an algebraic equation from which the frequency of the system can be determined, where the function $P(y, z)$ is defined as

$$P(y,z)=(1+\frac{l}{m})y^{\frac{l}{m}-1}\frac{\partial\Phi}{\partial y}+y^{\frac{l}{m}}\frac{\partial^2\Phi}{\partial y^2}+\xi y^{\frac{l}{m}}\frac{\partial^2\Phi}{\partial z^2}+\frac{\omega^2 H^{\frac{l}{m}}}{v_{s0}^2}\Phi \tag{8}$$

It can easily be proved that the following function can satisfy the boundary conditions equation (6)

$$\Phi(y,z)=\left(y^2-H^2\right)\left[y^2-\left(H+k_1\frac{D}{2}+k_1z\right)^2\right]\left[y^2-\left(H+k_2\frac{D}{2}-k_2z\right)^2\right]\Big/\left[H^2\left(H+k_1\frac{D}{2}\right)^2\left(H+k_2\frac{D}{2}\right)^2\right] \tag{9}$$

In addition, because of the characteristics of polynomial, the polynomial function like $r\boldsymbol{\Phi}^n(y, z)$ can satisfy the boundary conditions equation (6) too when $\boldsymbol{\Phi}(y, z)$ satisfies equation (6), in which r is a rational number and n is a positive integer. Then we form three following functions to obtain the mode shape functions

Table 1. Parameters for calculating first three natural frequencies of longitudinal vibration of earth dams in trapezoid canyons.

j	*l/m*	ω_{ij}	C_{ij}	P_{ij}	Q_{ij}
1	0	ω_1	0.01338	3.7849	0.8200
		ω_2	0.02210	4.7718	1.3379
		ω_3	0.02964	5.6211	1.7844
2	1/3	ω_1	0.00621	12.299	2.3945
		ω_2	0.01026	13.956	3.5007
		ω_3	0.01376	15.878	4.5249
3	2/5	ω_1	0.00533	15.712	2.9976
		ω_2	0.00880	17.483	4.2955
		ω_3	0.01180	19.799	5.5278
4	1/2	ω_1	0.00423	22.789	4.2202
		ω_2	0.00699	24.648	5.8753
		ω_3	0.00937	27.758	7.5191
5	1	ω_1	0.00134	155.77	25.091
		ω_2	0.00221	148.97	30.848
		ω_3	0.00296	166.80	39.047

$$\mathbf{\Phi}_1(y,z)=-\mathbf{\Phi}(y,z) \tag{10}$$

$$\Phi_2(y,z)=\frac{25}{16}\left[\Phi(y,z)+1.64\Phi^2(y,z)\right] \tag{11}$$

$$\Phi_3(y,z)=\frac{-125}{53}\left[\Phi(y,z)+4\Phi^2(y,z)+3.424\Phi^3(y,z)\right] \tag{12}$$

Substituting equations (10), (11) and (12) into equation (7) and performing the integrations, three algebraic formulae can be obtained for the first, second and third natural frequencies. Solving the equations, the natural frequencies of longitudinal vibration of earth dams in trapezoid canyons are obtained, *i.e.* ω_1, ω_2 and ω_3. Thus the aforesaid functions given in equations (10), (11) and (12) are corresponded to the first mode shape, second mode shape and third mode shape respectively. Because of the complexity of formulae for natural frequencies, we provide some simplified results in symmetric rigid canyons.

For example, when H=100m, D=150m, $k_1=k_2$=1.2, the natural frequencies ω_1, ω_2 and ω_3 can be written as the following formula, in which the parameters are shown as in Table 1.

$$\omega_{ij}=C_{ij}v_{s0}\sqrt{P_{ij}+Q_{ij}\xi} \quad i=1,2,3 \tag{13}$$

4 LONGITUDINAL EARTHQUAKE RESPONSE

It is easily proved that the governing equation of longitudinal vibration of the earth dams with damping under earthquake motion can be written as

$$\frac{\partial^2 w}{\partial t^2}+\frac{c}{\rho}\frac{\partial w}{\partial t}-\frac{G_0}{\rho H^{\frac{l}{m}}}\left[(1+\frac{l}{m})y^{\frac{l}{m}-1}\frac{\partial w}{\partial y}+y^{\frac{l}{m}}\frac{\partial^2 w}{\partial y^2}+\xi y^{\frac{l}{m}}\frac{\partial^2 w}{\partial z^2}\right]=-\ddot{w}_g(t) \tag{14}$$

where $\ddot{w}_g(t)$ is the acceleration of the rigid canyon in z-direction and c is the coefficient of damping.

Here the method of separation of variables is used again. Substituting $w(y,z;t)=\sum_{j=1}^{\infty}\Phi_j(y,z)T_j(t)$ into equation (14) and multiplying the two sides by $\boldsymbol{\Phi}_i(y,z)\rho ydydz$, the equation representing a mode shape $\boldsymbol{\Phi}_i(y,z)$ can be obtained based on the theory of orthogonality of mode shape. For the first three mode shapes, there are

$$T_i'' + 2\lambda_i\omega_i T_i' + \omega_i^2 T_i = -\eta_i \ddot{w}_g(t) \quad i=1,2,3 \tag{15}$$

$$(1+\frac{l}{m})y^{\frac{l}{m}-1}\frac{\partial\Phi_i}{\partial y} + y^{\frac{l}{m}}\frac{\partial^2\Phi_i}{\partial y^2} + \xi y^{\frac{l}{m}}\frac{\partial^2\Phi_i}{\partial z^2} + \frac{\omega_i^2 H^{\frac{l}{m}}}{v_{s0}^2}\Phi_i = 0 \quad i=1,2,3 \tag{16}$$

where ω_i is the i order natural frequency given by equation (13), λ_i, is the damping ratio of the i order mode shape, $\lambda_i=c/2p\omega_i$, and η_i is the mode participation coefficient of the i order mode shape, which is defined as following

$$\eta_i = \int_0^H \int_{-\frac{1}{k_1}(H+k_1\frac{D}{2}-y)}^{\frac{1}{k_2}(H+k_2\frac{D}{2}-y)} \Phi_i y dydz \Big/ \int_0^H \int_{-\frac{1}{k_1}(H+k_1\frac{D}{2}-y)}^{\frac{1}{k_2}(H+k_2\frac{D}{2}-y)} \Phi_i^2 y dydz \tag{17}$$

After substituting the function Φi given by equation (10)~(12) into equation (17) and performing the integration, the mode participation coefficients of the first three mode shapes are obtained, which are η_1=1.999, η_2=−1.826, η_3=1.775. Thus, the solution of equation (15) is obtained

$$T_i(t) = -\frac{\eta_i}{\omega_i'}\int_0^t \ddot{w}_g(\tau)e^{-\lambda_i\omega_i(t-\tau)}\sin[\omega_i'(t-\tau)]d\tau \tag{18}$$

where $\omega_i' = \omega_i\sqrt{1-\lambda_i^2}$, and the Duhamal integral in equation (18) may be calculated by numerical integration method.

Because the higher modes have little effect on earthquake responses of the earth dam, only a few lower modes (3~5 orders) are considered for practical requirement. So the longitudinal earthquake responses of the earth dams in rigid trapezoid canyons can be approximately written as following

$$w\approx\sum_{i=1}^{3}\Phi_i T_i,\quad \dot{w}\approx\sum_{i=1}^{3}\Phi_i\dot{T}_i,\quad \ddot{w}\approx\sum_{i=1}^{3}\Phi_i\ddot{T}_i,\quad \sigma_z\approx\sum_{i=1}^{3}E\Phi_{iz}'T_i,\quad \tau_{yz}\approx\sum_{i=1}^{3}G\Phi_{iy}'T_i \tag{19}$$

where $\boldsymbol{\Phi}_i$, $\ddot{T}i$ can be obtained by equation (18) and its derivatives. By use of the numerical integral the curves of earthquake responses of longitudinal vibration of earth dams can be obtained during the whole earthquake period. In engineering, it is most interesting in the maximum responses of the dam, so the following formulae of maximum responses are useful for earthquake-resistant design of the earth dams, in which the earthquake spectrum is used to instead of the Duhamal integral

$$w_{\max}\approx\sqrt{\sum_{i=1}^{3}(|\eta_i\Phi_i|S_{d,i})^2},\quad \dot{w}_{\max}\approx\sqrt{\sum_{i=1}^{3}(|\eta_i\Phi_i|S_{v,i})^2},\quad \ddot{w}_{\max}\approx\sqrt{\sum_{i=1}^{3}(|\eta_i\Phi_i|S_{a,i})^2} \tag{20}$$

$$\sigma_{z,\max}\approx\sqrt{\sum_{i=1}^{3}(\xi G|\eta_i\Phi_{iz}'|S_{d,i})^2},\quad \tau_{yz,\max}\approx\sqrt{\sum_{i=1}^{3}(G|\eta_i\Phi_{iy}'|S_{d,i})^2} \tag{21}$$

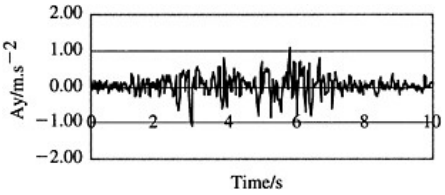

Figure 2. The earthquake acceleration record at Tangshan, China, Aug. 31, 1976.

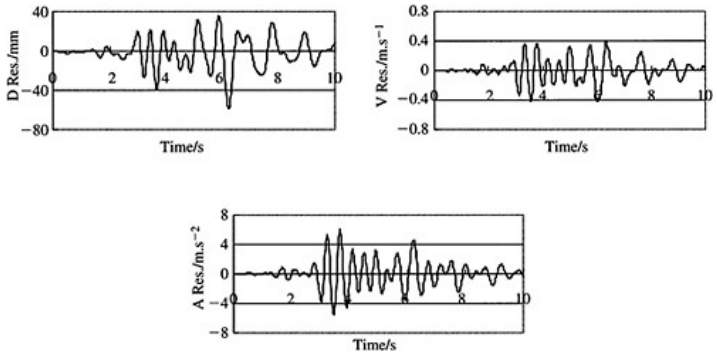

Figure 3. The displacement, velocity and acceleration response at point (0, 0).

where $S_{d,i}$, $S_{v,i}$ and $S_{a,i}$ are the displacement response spectrum, velocity response spectrum and acceleration response spectrum of the i order mode shape respectively.

5 EXAMPLE

Suppose a symmetrical earth dam in a symmetrical trapezoid canyon is subjected a longitudinal earthquake motion (Tangshan, China, Aug. 31,1976), shown as in Figure 2. The length of the dam crest is L=390m, and the length of dam bottom is D=150m. The maximum height of the dam is H=100m. And the slope of the canyon bank is k_1=k_2=1.2. The property of the dam material are ρ=2200kg/m^3, G_0=120MPa, μ=0.3 and λ_1=0.05, λ_2=0.03, λ_3=0.02.

Letting l/m=1/2, substituting the aforesaid known parameters into equation (13), the first three natural frequencies are obtained, *i.e.* ω_1=5.74, ω_2=10.31 and ω_3=15.05. By use of the Duhamal integral, the earthquake responses during the seismic period are obtained. Figure 3 shows the displacement, velocity and acceleration responses at point (0, 0) of dam, and Figure 4 shows the stress response at point (65,104) of dam. Figure 5 shows the maximum stress response of dam during earthquake period. The maximum displacement response is 58mm, maximum velocity response is 0.43m/s and maximum acceleration response is 6.03m/s^2. In addition, the maximum normal stress response is 223kPa and the maximum shear stress response is 44kPa.

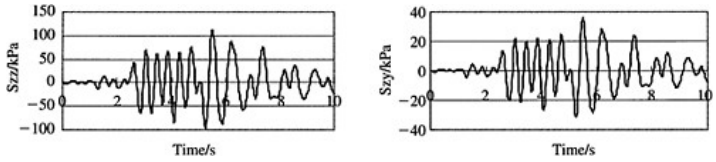

Figure 4. The normal and shear stress response at point (65,104).

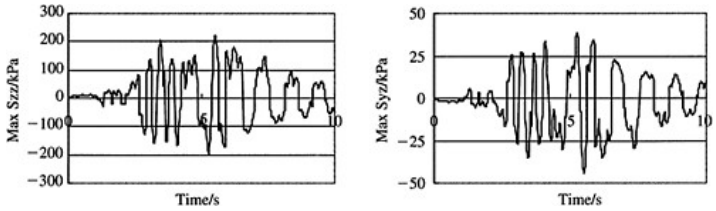

Figure 5. The maximum normal and shear stress response of dam during earthquake period.

6 CONCLUSION

The approximate analytical formulae developed in this paper are simple and they can be used for the analysis of the longitudinal vibration of inhomogeneous earth dams in trapezoid canyons under earthquake motion by the use of corresponding simplified method, like response spectrum technique. A detailed example has shown that the analytical model developed here can provide information of practical as well as academic significance.

REFERENCES

[1] Abdel-Ghaffar, A.M. & A.S.Koh. 1981. Longitudinal vibration of nonhomogeneous earth dams. *Int. J. of Earthq. Eng. and Structure Dyn.,* 9(4):279–305.
[2] Gazetas, G. 1981. Longitudinal vibrations of embankment dams. *Jour. Geotech. Eng. Div. ASCE,* 107(GT1):21–40.
[3] Gazetas, G. Vertical oscillation of earth and rockfill dams: analysis and field observation. *Soils and Foundations,* 1981, 21(4):56–68.
[4] Oner, M. Shear vibration of inhomogeneous earth dams in rectangular canyons. *Soils Dyn. and Earthq. Eng.,* 1984, 3(1):19–26.
[5] Dakoulas, P. & G.Gazetas. Seismic shear vibration of embankment dams in semi-cylindrical valleys. *Earthq. Eng. and Struc. dyn.,* 1986, 14(1):19–40.
[6] Dakoulas, P. & C.Hsu. Lateral response of dams in semi-elliptical rigid canyons. *Soils Dyn. and Earthq.* Eng., 1993, 12:497–507.
[7] Xu, Z.Y. Analysis of longitudinal vibration of earth dams in triangular canyons. *Proc. of 10th World Conf. on Earthq. Eng.,* Spain, 1992:4719–4722.
[8] Xu, Z.Y. Approximate analysis of transversal vibration of rock-fill dam in 3-D. *Proc. of Int. Symposium on Application of Computer Methods in Rock Mechanics and Engineering,* Xian, China, 1993.
[9] Shen, Z.Z & Z.Y.Xu. Shear vibration of 3-D inhomogeneous earth dams in triangular canyons. *Proc. of the 11th World Conf. on Earthquake Engineering by James Miline (Editor).* Acapulco, Mexico. Rotterdam: A.A.Balkema Press. 1996.

[10] Shen, Z.Z. & Z.Y.Xu. Vertical vibration of inhomogeneous earth dams in triangular canyons. *Proc. of the 9th Inter. Conf. of the Association for Computer Methods and Advances in Geomechanics by Jianxin Yuan (Editor).* Rotterdam: A.A.Balkema Press, Wuhan, China, 1997:1783–1787.
[11] Shen, Z.Z. & Z.Y.Xu. Simplified theoretical analysis of longitudinal earthquake response for earth-rock dams in triangular canyons. *Inter. Journal of Hydroelectric Energy,* 1999, 17(4):9–12.
[12] Shen, Z.Z. & Z.Y.Xu. Simplified analysis of transverse vibration for inhomogeneous earth-rock dams in triangular canyons. *Journal of Hydraulic Engineering,* 2002, (3):74–79.
[13] Shen, Z.Z. & Z.Y.Xu. Approximate solution to vertical vibration of earth-rock dams in triangular canyons. *Jour. of Hohai University, Natural Sciences Ed.* 2002, 30(2):84–89.
[14] Zienkiewicz, O.C. & R.L.Taylar. *The finite element method.* 5th ed. Oxford: Butterworth and Heineman, 2000, 39–86.

New Developments in Dam Engineering—Wieland, Ren & Tan (eds),
© 2004 Taylor & Francis Group, London, ISBN 04 1536 240 7

Durability of grout curtain strengthened with chemical materials*—an example from a hydropower station in southern China

Song Han-zhou
Faculty of Civil Engineering, Hohai University, Nanjing, P.R. CHINA

ABSTRACT: Assessment of anti-seepage performance of grout curtain under a dam foundation and its durability is usually of uncertainty because there are lots of factors involved. In this paper, the durability of the grout curtain strengthened with LW dissolved polyurethane in a case is analyzed from the macro-micro regime of groundwater and elutes in the domain. The hydropower station as a case study is located in the southern part of China. The following four aspects could be identified, as a result. (1) The uplift pressure value at Up6 behind the grout curtain had the tendency of increase with time, and the relation with the reservoir water level tended to be closed. (2) The flow-rate from G6–4 was relatively large, and the relation with the upstream water level also tended to be closed. (3) The local groundwater quality behind the grout curtain was abnormal. (4) The local groundwater solution behind the grout curtain was unsaturated, from which the local active flow behavior could be deduced in a sense. As a conclusion, it could be drawn that its anti-seepage performance tended to weaken locally, which may be useful for steps to be taken more effectively.

1 INTRODUCTION

LW dissolved polyurethane is a new kind of chemical material that has been used to improve the anti-seepage performance of the grout curtain for several hydropower projects in China. During the initial period, the ideal anti-seepage effect was received because of its specific characteristics[1]. However, its durability of anti-seepage performance should be concerned with after years.

In this paper, a case study as an example was carried out, which is located in the southern part of China. The macro-micro regime of the groundwater within the area is studied through in-situ measurement, sampling and data analysis and others. The durability of the anti-seepage performance of the grout curtain strengthened with this kind of chemical material is assessed from these aspects. The purpose for this is for better understanding the behavior of the anti-seepage performance of this kind of grout curtain with time.

2 GEOLOGY AND FORMATION OF GROUT CURTAIN STRENGTHENED

2.1 *Geology*

The studied area is located in a narrow valley. Within the area, the bedrock is rhyolite with a spot texture, in which silica and feldspar are major rock-forming minerals. The geological structure is mainly composed of various fissures which could be classified as the following three types: (1) N20~40°W/NE (or SW)∠70~90°; and (3) with dip angle smaller than 20°. Among the above, the strike of the first type is parallel to the surface water flow direction,

* The project is supported by Natural Science Foundation of China (No. 50139030)

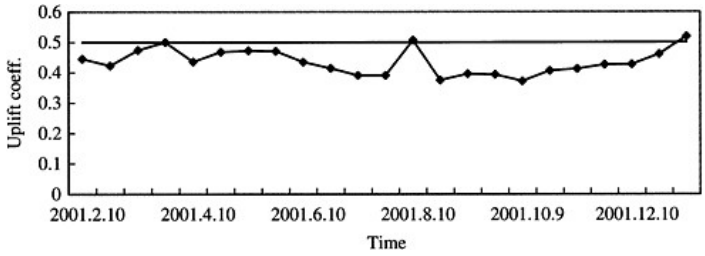

Figure 1. Regime of uplift pressure coefficient at Up6 in 2001.

while that of the second type is normal to it, and parallel to the dam axis. Therefore, the bedrock within the area is of fissured media. According to reconnaissance stage, there were confined water bodies at different depths in 10 boreholes around the dam site. The piezometric water level in elevation ranged from 211.52~231.62m, i.e. with 0.34~20.63m higher than the ground surface. The flow rate measured was between 0.0025~1.178L/min. From these, it could be drawn that within the area, the groundwater distributed largely in zones or veins.

2.2 *Formation of grout curtain strengthened*

The project has been operated for over 20 years. Although almost everything is smooth, some problems still exist. One is that the measured value of a local lift pressure behind the grout curtain in dam section 6 is beyond the designed one. For instance, the coefficient of uplift pressure measured at Up6 on 4 July in 1983 was up to 0.60, higher than the designed one (0.50). In order to decline it and meet the demands for safe operation, two engineering steps were taken. One is that the local grout curtain adjacent to Up6 was strengthened with LW dissolved polyurethane through 16 special boreholes. Another is that 1 borehole nearby Up6 was penetrated for drainage.

As to LW dissolved polyurethane, it has the following properties. Viscosity is 450cp and the time for coagulation is from seconds to minutes. Compressibility strength is affected by pH, i.e. if pH<7.0, the compressibility strength tending to decrease. Additionally, the permeability is low, i.e. $k=10^{-9}$cm/sec, and as a result, it has the better anti-extruding performance. However, it should be mentioned that this behavior be affected by the alteration of the width of the fissure concerned, which was resultant from the variation of the temperature. It means that if the width of the fissure tends to increase even slightly, the above anti-extruding ability weakens obviously.

From observation data, it could be seen that during the initial period, the anti-seepage performance of the grout curtain strengthened with LW dissolved polyurethane was improved significantly. For instance, during the period of June to July in 1989, the uplift pressure coefficient at up6 was only 0.14, when the surface water level was 276m or so. However, the above parameter has had the tendency of increasing in recent years, as shown in Fig. 1. Therefore, it is questioned that how the durability of the anti-seepage performance of the grout curtain strengthened with above chemical material will be.

3 ASSESSMENT OF ANTI-SEEPAGE PERFORMANCE AS TO GROUT CURTAIN

3.1 *Macro-micro regime of groundwater behind grout curtain*

The variation of flow rate from boreholes under the dam foundation and its relation with the reservoir water level can reflect the anti-seepage performance of the grout curtain and its time-variant, to a varying degree. There exist 5 boreholes (from G6–2~G6–5 and G6–7) for drainage in dam section 6, of which only 1, i.e. G6–4, is working. In another words, the groundwater level in other 4

Figure 2. Relation between flow rate from G6–4 and water level (a)—in 1998; (b)—in 1999; (c)—in 2000; (d)—in 2001.

boreholes was lower than the surface. The relationship between the flow rate from G6–4 and the water level in the reservoir in different years is shown in Figure 2. It can be seen from the figure that the relation between these two is time-variant. During the period from 1999 to 2000, the relative abrupt change of the relation took place, i.e. from the weak correlation in 1999 to the relative close correlation in 2000. From this, it may be drawn to a degree that the anti-seepage performance of the grout curtain strengthened in the domain weakened.

As another factor of groundwater regime in the domain, the uplift pressure can also be used to analyze the anti-seepage performance of the grout curtain strengthened. The relationship between the uplift pressure at up6 and water level in the reservoir in different years is shown in Figure 3. From the figure and with reference to Table 1, it can be seen that the correlation between these two is also time-variant. Before 1999, the relation is not "remarkable", but since 2000, the relation was altered to "remarkable". It seems that the variation of the uplift pressure behind the grout curtain is in consistence with that of the flow rate in the domain. Obviously, the period from 1999 to 2000 is that of the abrupt variation of the groundwater regime in the domain. Therefore, it could be drawn again that the anti-seepage performance of the grout curtain strengthened has the tendency of being weakened at least locally.

3.2 *Micro-regime of groundwater*

Figure 4 is a profile about the variation of some water quality components ($HCO_3^- + CO_3^{2-}$) at G6–2, G6–4 and G-7 in dam section 6 was higher than that at other points, while the content of Ca^{2+} of the groundwater under the dam foundation increased obviously, compared with the reservoir water. As to the formation of these components, it is believed that they were major resultant from the interaction

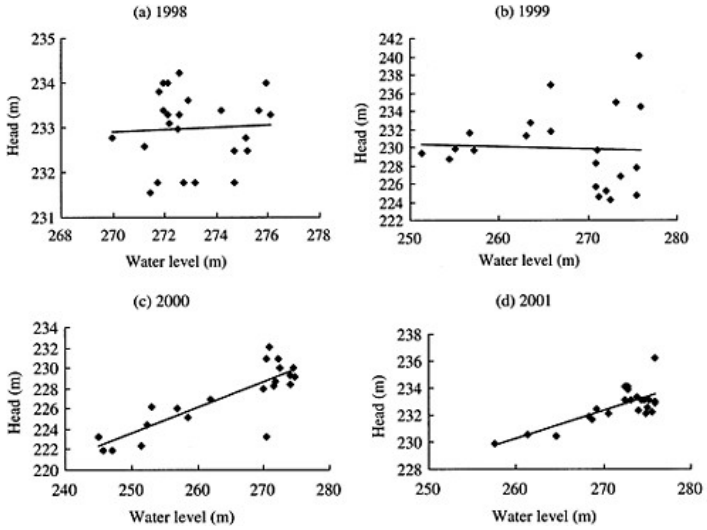

Figure 3. Relation between uplift pressure at Up6 and water level in different years (a)—in 1998; (b)—in 1999; (c)—in 2000; (d)—in 2001.

Table 1. Correlation between uplift pressure at Up6 and water level in years.

Year	Regression equation	R	F	$F^{\alpha}(n_1, n_2)$ (α=0.05)	R′	Notice
1998	H=0.0258H′+225.92	0.053	0.059	4.30	0.374	Not "re"
1999	H=−0.0297H′+237.84	0.056	0.069	4.38	0.401	Not "re"
2000	H=0.25 16H′+160.67	0.842	46.822	4.32	0.383	Highly "re"
2001	H=0.2079H′+176.23	0.737	22.040	4.30	0.374	"re"

In the table, H is the uplift pressure in head; H′, water level in the reservoir; R, correlation coefficient; R′, critical correlation coefficient; "re", remarkable.

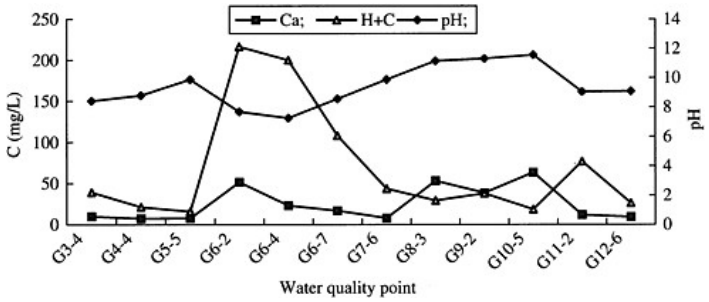

Figure 4. Profile as to some groundwater quality index along dam-axis.

between liquid and solid phases. The latter is composed of carbonate substances, such as calcite veins occurred in some discontinuities and some hydrated products such as $Ca(OH)_2$ from the grout curtain. The related reactions may be described as:

$$CaCO_3+H_2CO_3 \rightarrow Ca(HCO_3)_2 \quad (1)$$

$$Ca(OH)_2+Ca(HCO_3)_2 \rightarrow 2CaCO_3+2H_2O \quad (2)$$

$$CaCO_3 + H_2O \rightarrow Ca^{2+} + HCO_3^- + OH^- \quad (3)$$

When HCO_3^- will have the following:

$$HCO_3^- \rightarrow H^+ + CO_3^{2-} \quad (4)$$

From Eq. (3), it is known that if 1 mol $CaCO_3$ is dissolved, there will be 1 mol Ca^{2+}, $HCO_3^- = 1.773$. All are expressed in mol/L. From the mentioned above, it may be deduced that there was some other source that made the contribution to increase of HCO content in the domain. It is from the oxidation of some organic substance in solid media. The relation is as follows:

$$CH_2O + O_2 \rightarrow H^+ + HCO_3^- \quad (5)$$

Due to Eq. (5), HCO_3^- content of the water solution in dam section 6 tended to increase and on the other hand, pH value in the domain was lower than in other dam sections, even than the reservoir water as its source. It is thought that the organic substance was major from the chemical materials such as LW dissolved polyurethane contained in the grout curtain strengthened.

In addition to above, the state of interaction between water solution and some soluble substance, which can be described as saturation index (SI) could also reflect the anti-seepage performance of the grout curtain concerned. SI can be expressed by

$$SI = \lg \frac{IAP}{K} \quad (6)$$

In which, IAP is the activity of ions involved and K equilibrium constant as to thermodynamics. According to Eq. (6), the following could be identified:

(1) If SI=0, the solution is up to the critical state of dissolution-deposition;
(2) If SI<0, the solution is unsaturated, meaning that the reaction will continue to take place towards the dissolution of the mineral concerned;
(3) If SI>0, the solution is over-saturated, meaning that the reaction will take place towards the deposition of the mineral.

Under the similar conditions, the difference in state as to interaction between liquid and solid phases will be resultant largely from the different dynamic conditions within the region.

Considered some complex compounds in the solution, the state of interaction between water and carbonate components was analyzed quantitatively, as shown in Figure 5. It could be seen from the figure that SI is smaller in dam section 6 than in other dam sections, reflecting that the seepage behavior in dam section 6 is relatively active, compared with other dam sections. As to dam section 6 itself, SI at different boreholes is different. For example, at G6–4, SI<0; whereas at

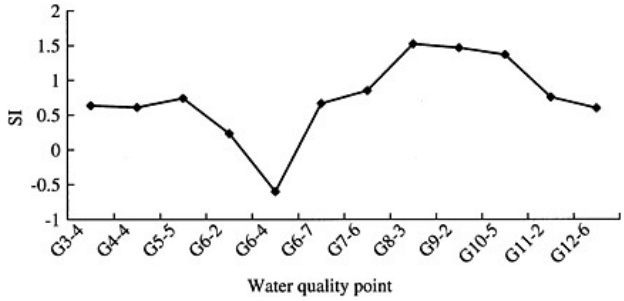

Figure 5. Profile of SI at different boreholes along dam-axis.

other 2 boreholes, SI>0. It means that that the seepage behavior at different boreholes is different within the domain. Obviously, the dynamic state at G-4 is more active. Therefore, it may be concluded that the anti-seepage performance of the grout curtain strengthened in dam section 6 weakened locally at least.

3.3 *Sludge of groundwater behind grout curtain*

It is known that after the completion of the grout curtain strengthened in dam section 6, sludge with different colors (red, black and intergrading between them) occurred around the boreholes behind it just one year later. The recent investigation carried has also found that the above sludge still occur within the domain. It is noted that there are no such as sludge in other dam sections. Some samples were taken and measurements were made not only for inorganic but also for organic substance. As to the later, it was analyzed by infrared spectrum measuring. The result shows that some organic substance was contained in all 4 samples from dam section 6 and comparatively, the content of the sample from G6–4 was higher than other 3. According to particular spectra, it could be identified as follows. Wave numbers at 3400cm^{-1} were produced by N-H vibration from RCONH^{-}, at 2925cm^{-1} by C-H vibration of CH_2, at 1020cm^{-1} by vibration of C=0, and others. It is believed that all bases above were mainly resultant from LW dissolved polyurethane in the grout curtain. Therefore, it may be concluded that the anti-seepage performance of the grout curtain strengthened in dam section 6 has weakened to a degree.

4 CONCLUSION

Assessment of the anti-seepage performance of the grout curtain is one of important aspects as to monitoring for dam safety. In this paper, the durability of the anti-seepage performance of the grout curtain strengthened with LW dissolved polyurethane was appreciated from in-situ measurement, sampling, data analyzing and others, taking a case study as an example. It is recommended that a synthetic analysis method be used because of the complexity of the geologic and hydrogeologic condition involved. By doing this, some uncertainties might be reduced greatly.

From the case study, it is known that the anti-seepage effect of the grout curtain in dam section 6 is ideal by using LW dissolved polyurethane for strengthening, but its durability is not ideal. The related evidences may be summarized as following: (1) The relation of the uplift pressure at Up6 behind the grout curtain with the reservoir water level has tended to more closely in recent years. (2) The variation of the flow rate from G6–4 has had the similar tendency with that of the uplift pressure in the domain. (3) The local groundwater quality behind the grout curtain was abnormal, i.e. lower pH value and higher content of HCO_3^- which resulted from the oxidation of organic substances in LW dissolved polyurethane, and furthermore, some organic substance was checked out in sludge. (4) The local groundwater solution behind the grout curtain was unsaturated, i.e. SI<0, from which the local active flow behavior could be deuced. As to next stage working, it is recommended that the more attention be paid to borehole G6–4 and its surrounding area for monitoring. To do this, more data will be available and steps could be taken if necessary.

REFERENCES

[1] BaoYin-hong. Application of LW dissolved polyurethane into grout curtain strengthened (J), Water Resources and Hydropower Engineering (in Chinese), 1985(10): 12–20

[2] Song Han-zhou, Zhou Zuo-quan. Locating anti-leakage deficiency of grout curtain with hydrogeochemistry method (J), Dam Observation and Geotechnical Tests (in Chinese), 2001(2): 13–16

[3] Zhou Zuo-quan, Song Han-zhou. Calculation of saturation index and its sensitivity analysis (J), Journal of Hohai University (in Chinese), 2001(6):90–93

This page intentionally left blank.

New Developments in Dam Engineering—Wieland, Ren & Tan (eds),
© 2004 Taylor & Francis Group, London, ISBN 04 1536 240 7

Investigation of factors causing problems in dam behaviour and dam safety using rough sets theory

Su Huaizhi, Wu Zhongru & Gu Chongshi
College of Water Conservancy and Hydropower Engineering, Hohai University, Nanjing, China
Wen Zhiping
Dept. of Computer Engineering, Nanjing Institute of Technology, Nanjing, China

ABSTRACT: The effects such as stress, deformation, crack, seepage are produced when dams are loaded by water pressure, temperature, earthquake and uplift. The relation between load set and effect set is main factor determining character of dam structure. In fact, the diagnosis of dam safety is a process of finding the factors causing problems in dam behaviour and dam safety. The information of dam safety, viz. data, rules, knowledge, need be analyzed through the integration of qualitative methods and quantitative methods. From the viewpoint of systems engineering, a diagnosis model was proposed to analyze dam behaviour. Rough sets theory was used to discover adaptively the influence factors of dam safety. A decision system was built to describe the qualitative or quantitative information on dam safety It was composed of problems in dam behaviour and influence factors determined by experiential knowledge and other projects. Rough sets theory was used to eliminate the redundant factors. The actual factors were found according to the dependency between effects and loads. The example of cracks diagnosis shows that the proposed method is feasible and effective, the analysis results are reasonable. The method can handle imprecise, uncertain or incomplete descriptions, and adapt variational environment. It can also offer a beneficial reference to diagnose the health of other structural engineering.

1 INTRODUCTION

Dam construction has developed very fast in China since 1950. There are now 17,526 dams 15–30m high and 4,578 dams exceeding 30m. These projects bring huge benefits in flood control, irrigation, power generation. However, hidden troubles exist in some dams due to hydrology, geology, design, construction and aging[1]. In addition, many more major projects are being constructed or will start in the 21st Century, including Three Gorges Project (height 175 m) on the Yangtse River, Xiluodu arch dam (height 273m) and Xiangjiaba gravity dam (161m) on the Jinshajiang River, Jinping 1st cascade (300m) on the Yalongjiang River, Hongjiadu concrete faced rockfill dam (178m) on the Wujiang River; Xiaowan arch dam (292m) on the Lancangjiang River, Longtan RCC gravity dam (216m) on the Hongshuihe River, Laxiwa arch dam (250m) on the Yellow River, etc. These projects will symbolize the further greater progress of dam construction in China. At the same time, it becomes more and more important to guarantee dam safety.

It is necessary and important to implement real-time analysis and reasonable diagnosis for dam safety, accordingly fulfill the effective control for dam life process of construction, run, aging and end of its useful life[2]. Based on prototype observations, the mathematical and mechanical methods are conventionally used to solve above problems. For example, the methods of time serial and multiple regression are adopted to build monitoring models, FEM is used to implement the structural calculation [3][4]. However, these methods lay usually no strong emphasis on the learning of experiences of other projects and expert knowledge[5][6].

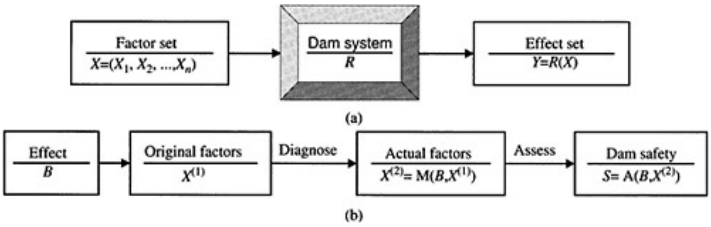

Figure 1. System model diagnosing dam safety.

As a new mathematical tool, rough sets theory can handle imprecise, uncertain or incomplete descriptions[7]. It can be used as the basis for performing formal reasoning with uncertain information, machine learning and knowledge discovery. In less than two decades, it has rapidly established itself in many real-life applications such as medical diagnosis, control algorithm acquisition and process control, information retrieval and structural engineering[8]~[10].

In practice, we can obtain the information such as observations, analysis results on structure character, experiences. The diagnosis of dam safety, in fact, is the process that knowledge on logic relation between dam behaviour and influence factors is obtained from above incomplete information. So systems engineering methods and rough sets theory can be used to solve above problems.

This paper is organized as follows. Section 2 presents the diagnosis model based on systems engineering. A decision system is built in Section 3. Section 4 proposes the algorithm finding the real factors causing problems in dam behaviour and dam safety. The factors on cracks of one concrete dam are found with the presented method in Section 5. Section 6 summaries the main conclusions reached in this work.

2 SYSTEM MODEL DIAGNOSING DAM SAFETY

A dam has the complicated structure. It runs under the abominable condition with the influence of many factors. The correlation between factors is very intricate and often alterable. So dam structural behavior shows strong non-linear and dynamic characteristics. From the viewpoint of systems engineer, dam can be regarded as an open and gigantic system. The inputs, main body, outputs of system are loads, dam and effects, respectively. The effects include stress, deformation, crack, seepage. Loads, namely factors causing above effects, have water pressure, temperature, time effect, earthquake, rainfall, uplift, construction, surroundings and so on. The relation between factor set and effect set determines the characteristics of dam safety. The process is described in Fig. 1a. To analyze and diagnose dam safety, the actual factors need to be found. This is a back question. In mathematics, back question has many results, which is resolved difficultly with usual analysis methods. HoWever, based on prototype observations, the same flowchart to analyze and diagnose dam safety is as follows (see Fig. 1b): firstly, according to dam behavior, routine factors are determined. Next, one method is used to mine the real factors based on the information of dam safety, viz. data, rules, knowledge. Lastly, dam safety is assessed.

3 DECISION SYSTEM OF FACTORS ANALYSIS

3.1 *Decision table*

To discover the rules hiding in information on dam safety, a decision system *(S)* need be built to describe the objects in the universe of discourse. As an example, this paper implement the factors

Table 1. Decision table of factors analysis.

Objects (U)	Attributes (C)				Decisions *(d)*
	c_1	c_2	…	c_m	
x_1	1	0	…	1	0
x_2	1	1	…	0	1
⋮	⋮	⋮	…	⋮	⋮
x_n	0	2	…	0	0

analysis for cracks. Knowledge on cracks is expressed by attributes and their values. A decision system of factors analysis with 4-tuple can be represented as follows.

$$S = (U, R, V, f) = (U, C \cup D, V, f) \tag{1}$$

where U is the universe which consists of a finite set of objects, $U=\{x_1, x_2, \ldots, x_n\}$, $v \in V_a$ is called a descriptor in S.

Table 1 shows a typical decision system used for rough sets analysis. x_i(i=1, 2,…, n) represent the objects of the set U to be classified; c_i(i=1, 2, …, m) denote the condition attributes; d represents the decision attribute. As a result, c_i and d form the set of attribute, R. For cracks, x_i denotes one record of cracks; c_i is one possible factor causing cracks; d represents the actual status of cracks.

The table is called decision table of factors analysis. It is a data table that represents descriptive knowledge. In the decision table, some condition attributes are not logical related with decision attribute, or some condition attributes have same effect to decision attribute. Hence, redundant attributes in condition attribute set need be eliminated.

There are two types of attribute values in the decision table. One is continuous attribute such as deformation and temperature, which describes factor to be observed. Its value is in one continuous universe. Other is represented by language or some discriminative value such as crack, casting method and maintenance effort of concrete. The attribute value needs to be described by discriminative data in rough sets theory. The continuous value needs to be discriminated.

3.2 *Discrimination of attributes*

For object x_i and its continuous attribute c, the attribute values $c(x_i)$ can be regarded as a group of data collected stochastically. According to one similarity degree, the group of data can be implemented the clustering analysis, and one partition for U can be obtained. Under the precondition assuring consistency of decision table, the partition need be found to make the highest efficiency of reduction.

Assume that α_i is the inconsistency degree of continuous attribute c_i. It can be defined as follows

$$\alpha_i = \frac{card(\widetilde{C}_i)}{card(U)} \tag{2}$$

where $\widetilde{C}_i$ is the inconsistent object for continuous attribute c_i, $card(E)$ denotes the radix of set E. The attributes are statistical independent when they are inconsistent. Assume that GL_S is the inconsistency degree of decision table. It can be expressed as follows

$$\alpha_S = \prod_{i=1}^{m} \alpha_i \tag{3}$$

If α_i are equal approximatively and are marked α, α_S is

$$\alpha_S = \alpha^m \tag{4}$$

According to Equation (4), α can be estimated as

$$\hat{\alpha} = \sqrt[m]{\alpha_S} \tag{5}$$

In theory, the decision table of factors analysis must be consistent when it is discriminated, namely α_S=0. In practice, α_s need only be the little adequately value. For the inconsistency degree (α_i) of every attribute, the following equation need to be satisfied

$$|\alpha_i - \hat{\alpha}| \le \beta \tag{6}$$

where β is the allowable error.

The flow of algorithm discriminating attribute values can be described as follows

(1) Determine the initial values of α_s, β and ε.

(2) Compute the inconsistency degree $\hat{\alpha}$ of decision table according to Equation (5).

(3) For i=1, 2,…, m, carry out repeatedly the following steps.

(a) For continuous attribute c_i and initial threshold ε, obtain one partition of c_i on U with clustering analysis method.

(b) Compute the inconsistency degree (α_i) of continuous attribute c_i according to Equation (2).

(c) If, let $i \Leftarrow i + 1$ and go back to (a). Otherwise, go to (d).

(d) If $\varepsilon \Leftarrow (1+\Delta)\varepsilon$ and go back to (a).

(4) The discriminated values of attributes are coded with 0, 1, 2,….

4 ALGORITHM OF FACTORS ANALYSIS

4.1 *Indiscernibility*

Given two finite, non-empty sets U and A, where U is the universe, and A, a set of attributes, for every attribute $a \in A$, it is possible to associate with it a set of values known as the domain of a. Any subset P of A that defines a binary relation $I(P)$ on A which is an indiscernibility relation, can be expressed as follows:

$$x I(P) y \text{ if and only if } a(x) = a(y) \text{ for every } a \in A \tag{7}$$

where $a(x)$ and $a(y)$ denote the values of attribute a for elements x and y, respectively.

4.2 *Upper and lower approximation of rough set*

Assume that U and A are non-empty finite set, U represents the universe of discourse, A is attribute set, B denotes any subset of A.

Lower approximation of set X for B can be defined as follows

$$B_*(X) = \{x \in U : B(x) \subseteq X\} \tag{8}$$

It is a set composed of these objects which are determined to belong certainly to X by existent knowledge.

Upper approximation of set X for B can be expressed as follows

$$B^*(X) = \{x \in U : B(x) \cap X \neq 0\} \tag{9}$$

It is a set composed of these objects which are determined to belong possibly to X by existent knowledge.

4.3 *Dependency of attributes*

Dependency between condition attributes and decision attributes is an important concept in rough sets theory. Assume that D and C are the subsets of attribute set A. Dependency between D and C can be defined as follows

$$k = \frac{|POS_C(D)|}{|U|} \tag{10}$$

where

$$POS_C(D) = \bigcup_{x \in U/I(D)} C_*(X) \tag{11}$$

|*| denote the cardinality of set *, for finite set, it is the number of elements in finite set, $POS_C(D)$ is named "C positive region of D", and it is a set of objects of U, which can be properly classified to the classes of D by employing the knowledge expressed by the classification C, $I(x)$ is a set of indiscernibility objects of x.

If $I(C) \subseteq I(D)$ then D depend fully on C. Because every group of data of condition attributes and decision attributes can be regarded as one rule, dependency k between D and C can be obtained based on the number of inconsistent rules divided by total number of rules.

For a decision table of factors analysis of cracks, rough sets theory is used to calculate the dependency between crack and one influence factor. In fact, the dependency shows the contribution of one influence factor to the crack. So according to the dependency, one or more factors of least contribution can be eliminated gradually.

5 APPLICATION

One hydroelectric project consists of major dam (concrete gravity-arch dam), gravity-mounts, gravity auxiliary dam, outlet structure, water diversion structure and hydropower station workshop. Maximum height of dam is 76.3m. Elevation of dam top is 126.3m. Design flood level of reservoir is 122.2m. Check flood level of reservoir is 124.6m.

To obtain the information on dam safety, large numbers of sensors are installed in dam body and foundation. According to observation objects of sensors, there are deformation sensors, seepage sensors, stress and strain sensors, temperature sensors, water level sensors, rainfall sensors and so on. The deformation sensors have mainly plumb-line equipment, static level instrument, extensometer, multipoint displacement transducter, joint gauge. The seepage sensors have mainly consolidation apparatus, seepage discharge gauge, water level gauge. The stress, strain and temperature sensors include stress metre, strain metre, non-stress metre, reinforcement metre, pore pressure metre, earth pressure metre, thermometer.

There were 35 cracks on downstream face since the reservoir began water storage. 9 cracks were monitored. As a example, this paper analyzes the crack (J12–60–15) on el.105m.

Table 2. Observations for diagnosing the crack.

Data	Water level (m)	Temperature (°C)	Rainfall (mm)	Uplift (m)	Cracks (mm)	
	19820128	102.27	−7.1	0	57.31	3.2
	19820216	102.06	2.6	0	57.2	3.05
	19820608	108.58	24.4	0	56.82	1.57
	19830127	104.87	0	2.5	57.63	3.07
	19830325	106.14	13.6	116.1	57.61	2.09
	19830826	112.31	29	19.7	58.55	1.57
	19840720	107.24	24.5	11.4	58.12	1.51
	19840515	111.97	21.6	0	58.28	1.37
	19840818	111.2	29.5	0	59.04	1.59
	19850302	101.64	5	0	58.71	3.01
	19860130	102.53	0.4	0	58.75	3.03
	19860827	109.39	28	0	59.58	1.55
	19870828	112.01	23.6	0	59.22	1.55
	19880510	113.04	18.1	0	59.07	2.73
	19880726	114.84	25.4	0.8	59.46	2.65
…	…					

Table 3. Decision table diagnosing the crack.

Samples	c_1	c_2	c_3	c_4	d
1	3	3	3	3	1
2	3	3	3	3	1
3	2	2	3	3	2
4	3	3	3	3	1
5	2	2	1	3	2
6	2	1	3	3	2
7	2	2	3	3	2
8	2	2	3	3	2
9	2	1	3	2	2
10	3	3	3	3	1
…	…	…	…	…	…

5.1 *Collect and handle data*

Table 2 shows the partial observations of crack, water level, temperature, rainfall and uplift.

5.2 *Establish the decision table*

Water level, temperature, rainfall and uplift are regarded as condition attributes, and are represented as c_1~c_4. Crack is as decision attribute, and is denoted as d.

The values of condition attributes and decision attribute come from observed data, and are continuous variable. So they need to be discriminated with the proposed algorithm. The results are shown in Table 3.

The set of condition attributes can be expressed as

$$C=\{c_1, c_2, c_3, c_4\}$$

where c_1~c_4 represents water level, temperature, rainfall, uplift, respectively. Their value domain is {1, 2, 3}. 1, 2, 3 denotes respectively high, medium, low observations of water level, temperature, rainfall, uplift.

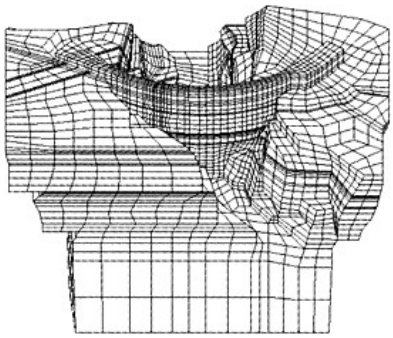

Figure 2. 3-dimensional model of finite element.

Decision attribute can expressed as

$D=\{d\}$

Its value domain is {1, 2, 3}. 1, 2, 3 denotes respectively high, medium, low observations of crack.

5.3 *Analyze factors causing crack*

With above method, condition attributes are reduced. The reduced attribution set of condition attribute set C on decision attribute d is obtained. It is

$C''=\{c_1, c_2\}$

where c_1, c_2 represents water level, temperature, respectively. It is known that the appearance and development of crack are mainly influenced by water level and temperature.

To determine the influence degree of water level and temperature for crack, FEM is used to calculate the stress of downstream face of dam. The model of finite element is shown in Fig. 2. The conclusions are as follows.

(1) When transverse joint isn't split, under water pressure and temperature, the maximal arch tensile stress is 0.8 MPa, the maximal beam tensile stress is 0.5MPa. When transverse joint is split to 1.88m~6.74m, under water pressure and temperature, the maximal arch tensile stress is 0.3MPa, the maximal beam tensile stress is 0.4MPa.
(2) The distribution of arch stress is differential remarkably in downstream face, considered transverse joint or not. When transverse joint isn't split, the arch stress presents continuous distribution. When transverse joint is split, the arch stress presents incontinuous distribution, the arch stress of split transverse joint is approximate 0.0MPa, the maximal arch stress appears in the middle of dam section and the value of arch stress becomes little.
(3) The distribution of beam stress isn't influenced remarkably, considered transverse joint or not. When transverse joint is split, the value of beam stress becomes little.
(4) The vertical-cracks on downstream face are mostly brought by arch tensile stress. The horizontalcracks are caused by beam stress.

6 CONCLUSIONS

Rough sets theory is introduced in the field of diagnosing dam safety. From the viewpoint of discovering knowledge, knowledge reduction method is used to find the actual factors causing problems in dam behaviour and dam safety. It is helpful for implementing the diagnosis of dam safety only by computers.

The applications of rough sets theory belong to the fields such as knowledge discovering, data mining. To improve the precision of diagnosing dam safety, the emphasis is on collecting and handling data on dam safety in future. After the actual factors causing problems are found, the influence degree for dam safety still need to be analyzed by mechanical methods. The integration of rough sets theory and mechanical methods should be studied.

ACKNOWLEDGEMENTS

This research has been partially funded by the projects from the National Natural Science Foundation of China (Grant No. 50139030), 973 Foundation of China for basic research on safety of major engineering project under the geo-hazard environment (Grant No. 2002CB412707) and the Science and Technology Innovation Foundation of Hohai University (Grant No. 2003411443).

REFERENCES

[1] Xing, L.S. & Tan, XJ. Dam safety and repair of hydropower stations in China. Dam and Safety. 2001, (5):4–8.
[2] Zhongru Wu & Huaizhi Su. Diagnosis and evaluation of dam health. First International Conference on Structural Health Monitoring and Intelligent Infrastructure. 2003, Japan: 79–86.
[3] Chuhan Zhang. Numerical modeling of concrete dam-foundation-reservoir system. Beijing: Tsinghua University Press, 2001.
[4] Humberto & Marengo. Considerations on dam safety and the history of overtopping events. Dam Engineering. 2000, XI(1):29–59.
[5] Oliver & Crepon. An analytical approach to monitoring. International Water Power & Dam Construction. 1999, (6):52–54.
[6] Zhongru Wu. Safety monitoring theories & applications of hydraulic structure. Beijing: Higher Education Press, 2003.
[7] Churn-jung Lian. An overview of rough set semantics for modal and quantifier logics. International Journal of Uncertainly, Fuzziness and Knowledge-Base System. 2000, 8(1):93–118.
[8] Wang G.Y. & Fisher P.S. Rule Generation Based on Rough Set Theory. In: Dasarathy B.V, ed. Data Mining and Knowledge Discovery: Theory, Tools, and Technology II, Proceedings of SPIE Vol. 4057, 2000, 181–189.
[9] Swiniarski R.W. & Hargis L. Rough sets as a front end of neural-networks texture classifiers. Eurocomputing. 2001, (36):85–102.
[10] Jianxu Luo & Huihe Shao. A neurofuzzy system based on rough set theory. Journal of Shanhai Jiaotong University. 2003, 37(11):1702–1705.

New Developments in Dam Engineering—Wieland, Ren & Tan (eds),
© 2004 Taylor& Francis Group, London, ISBN 04 1536 240 7

Dynamical evaluation of dam safety

Su Huaizhi & Wu Zhongru
College of Water Conservancy and Hydropower Engineering, Hohai University, Nanjing, China

Wen Zhiping
Dept. of Computer Engineering, Nanjing Institute of Technology, Nanjing, China

ABSTRACT: Dam runs under the abominable condition with the influence of many factors. The correlation between factors is very intricate and often alterable. So dam safety was conventionally assessed by the experiential knowledge of experts. The qualitative analysis can only be implemented. A method was proposed to evaluate dynamically dam safety. Firstly, the multi-index system of safety evaluation was built. It was a hierarchical structure. Secondly, a model was proposed to assess comprehensively dam safety with extension theory. The weights of index can be obtained by calculating the relational degree between evaluation index and grades. The numerical example shows that the proposed method is feasible and effective, and the evaluation results are reasonable. The health status can be described in qualitative and quantitative manner. By analyzing the development trend with time, dam behavior can be predicted. This method can also be used to assess slope stability, rock quality and dam aging.

1 INTRODUCTION

Dam structural behavior shows strong non-linear and dynamic characteristics. The information on dam safety includes geological data, results of numerical analysis, measurement data, experiential knowledge, and so on.

Based on prototype observation data, establishing the single mathematical model is one conventional method to analyze and forecast dam structural characteristics. The model is used to describe the relation between effects and loads of dam structure system, and approximate and predict the dynamic property and internal mechanism of dam operation. As a result, it is expected to monitor rapidly dam safety by comparing actual observation data and computed values with the mathematical model. However, any single mathematical model represents only the local property of non-linear, dynamic dam system [1]~[5].

To solve above problems, all information on dam safety need be analyzed compositively [6] [7]. In fact, dam safety evaluation does not only depend on the evaluation for actual observed characteristics of single item and single observation point, but also whole safety state reflected comprehensively by all items and different parts. On the other hand, the correlation between indexes influencing dam safety is very intricate and often alterable. So the weight of index need to be determined in real time.

This paper designs a system of evaluation index in Section 2. Section 3 introduces the basic process of safety assessment. A model is proposed to evaluate dam safety in Section 4. Section 5 presents a method calculating the objective weights. As a example, the proposed technology is used to assess one concrete dam in Section 6.

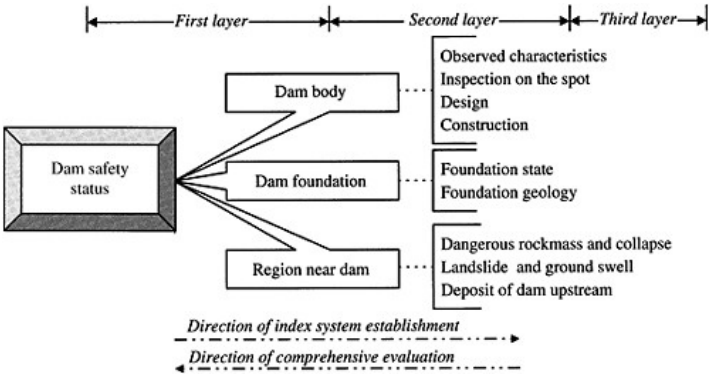

Figure 1. Index system of dam safety evaluation.

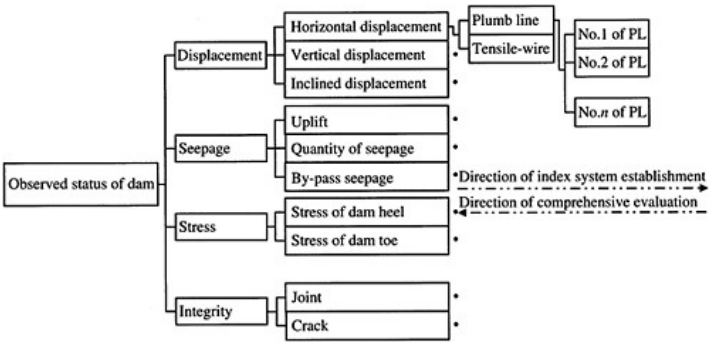

Figure 2. Index system of observed characteristics evaluation.

2 INDEX SYSTEM OF DAM SAFETY EVALUATION

Dam safety status is influenced by many factors. They include reconnaissance, design, construction and run management in the aspect of building program. From dam structural constitution, dam foundation, dam body, reservoir region near dam have relation to dam safety. In addition, they need to be considered such as the quality of dam built in whole construction period, observed characteristics, inspection on the spot, which are the foundation of dam safety evaluation. Figure 1 denotes an index system of dam safety evaluation, which is composed of large numbers of indexes, and is decomposed into many layers.

The indexes in Figure 1 can be decomposed continuously into some subsystems. For example, the observed characteristics can be reduced to deformation, seepage, strain and dam integrity. Displacement can be assessed by the lower layer of evaluation indexes (e.g. horizontal, vertical, and inclined displacement). The index system of observed characteristics evaluation is shown in Figure 2.

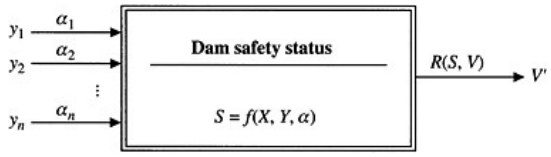

Figure 3. Sketch map of evaluation for dam safety.

3 BASIC PROCESS OF EVALUATION FOR DAM SAFETY

Assuming that X refers to the evaluation object, $Y=(y_1, y_2,\ldots, y_n)$ represents the evaluation index set corresponding X, $\alpha=(\alpha_1, \alpha_2,\ldots, \alpha_n)$ expresses the weight set of evaluation indexes, $V=(v_1, v_2,\ldots, v_n)$ is the evaluation grade set, namely collected set. Firstly, with one recursive algorithm ($f(\bullet)$), the characteristic value *(S)* of safety grade of evaluation object is calculated based on corresponding the characteristic values of all indexes. Next, according to one identification rule ($R(\bullet)$) and collected set *(V),* the grade *(V')* denoting the actual safety status of evaluation object is obtained. This assessment process can be described as Figure 3, which is the same with every layer of the evaluation index system.

The common flowchart of dam safety evaluation can expressed as follows:

Step 1. Built the muliti-index and multilayer of evaluation system for dam safety.

Step 2. Normalize the initial data of indexes in bottom layer.

Step 3. With one engineering method, compute the grades and grade characteristic values for the objects in one layer.

Step 4. By recursive algorithm, calculate grade and its characteristic value for whole dam safety.

Step 5. Repeat Step 2 to Step 4, compute the grades and grade characteristic values for whole dam safety in different run periods.

Step 6. Analyze the grades and grade characteristic values for whole dam safety in various run periods, find their changing trend, and evaluate dynamically the actual status of objects.

4 MODEL EVALUATING DAM SAFETY

Under abominable working environment, the safety status of dam changes dynamically, which emerges in the quantitative and qualitative change manners. Therefore, quantitative and qualitative changes need be considered comprehensively in the process of dam safety evaluation. In extension evaluation method, the professional knowledge in dam field is combined with extension theory [8]~[11]. The quantitative change and qualitative change of dam safety status are integrated into a matter-element. Based on the extensibility of matter-element of dam safety elevation, the contradictory problem for dam safety elevation can be solved with the extension evaluation method. The core of this method is to determine extension field, and the means is matter-element transformation of elements in extension domain.

4.1 *Matter-element of dam safety evaluation*

The research object in index system is defined as the matter *(S),* index set is expressed as the characteristics *(C),* normalized value set of index is denoted as the measure *(V)* of characteristics.

The matter-element *(R)* can be described as follows

$$R=(S,C,V)=\begin{bmatrix} S,C_1,v_1 \\ C_2,v_2 \\ \cdots,\cdots \\ C_n,v_n \end{bmatrix} \tag{1}$$
$$=\begin{bmatrix} \text{Object, Index } I_1\text{, Normalized value of } I_1 \\ \text{Index } I_2\text{, Normalized value of } I_2 \\ \cdots \quad\quad \cdots \\ \text{Index } I_n\text{, Normalized value of } I_n \end{bmatrix}$$

4.2 *Matter-element of classical domain*

According to the grade criterion of dam safety evaluation, matter-element of classical domain of research object in index system can be defined as follows

$$R_{0j}=(N_{0j},C_i,V_{0ij})=\begin{bmatrix} N_{0j},C_1,V_{01j} \\ C_2,V_{02j} \\ \cdots,\cdots \\ C_n,V_{0nj} \end{bmatrix} \tag{2}$$
$$=\begin{bmatrix} N_{0j},C_1,\langle a_{01j},b_{01j}\rangle \\ C_2,\langle a_{02j},b_{02j}\rangle \\ \cdots \quad \cdots \\ C_n,\langle a_{0nj},b_{0nj}\rangle \end{bmatrix}$$

where N_{0j}=grade of research object (e.g. observed characteristics of dam), j=1, 2,…, m; m=grade number, which is 5 in this paper; C_i=evaluation index of research object, i=1, 2,…, n; n=evaluation index number of research object; V_{0ij}=value domain of evaluation index C_i corresponding N_{0j}, which is called classical domain of grade of dam health for evaluation index of research object, $V_{0ij}=<a_{0ij}, b_{0ij}>$.

4.3 *Matter-element of whole domain*

Matter-element of whole domain of research object in index system can be denoted as follows

$$R_P=(P,C_i,V_{Pi})=\begin{bmatrix} P,C_1,V_{P1} \\ C_2,V_{P2} \\ \cdots,\cdots \\ C_n,V_{Pn} \end{bmatrix} \tag{3}$$
$$=\begin{bmatrix} P,C_1,\langle a_{P1},b_{P1}\rangle \\ C_2,\langle a_{P2},b_{P2}\rangle \\ \cdots \quad \cdots \\ C_n,\langle a_{Pn},b_{Pn}\rangle \end{bmatrix}$$

where P=family of grade of research object; V_{Pi}=value domain of evaluation index C_i for P of research object, which is called whole domain of evaluation index of research object, $V_{pi}=<a_{pi}, b_{pi}>$.

4.4 *Evaluated matter-element*

Evaluated matter-element of evaluated object *(N)* in sometime *(t)* can be expressed as follows

$$R_i = (N, C_i, v_i(t)) = \begin{bmatrix} N, C_1, v_1(t) \\ C_2, v_2(t) \\ \cdots, \cdots \\ C_n, v_n(t) \end{bmatrix} \tag{4}$$

where N=evaluated object in the index system of dam safety assessment; $v_i(t)$=normalized value of evaluation index C_i in sometime *(t)*.

4.5 *Dependent degree of single-index*

Dependent degree of the ith index of evaluated object *(N)* about safety grade *(j)* can be denoted

$$K_j(v_i(t)) = \begin{cases} \dfrac{\rho(v_i(t), V_{0ij})}{l_{ij}} & l_{ij} \neq 0 \\ -\rho(v_i(t), V_{0ij}) - 1 & l_{ij} = 0 \end{cases} \tag{5}$$

where

$$l_{ij} = \rho(v_i(t), V_{pi}) - \rho(v_i(t), V_{0ij}) \tag{6}$$

$$\rho(v_i(t), V_{0ij}) = \left| v_i(t) - \frac{a_{0ij} + b_{0ij}}{2} \right| - \frac{b_{0ij} - a_{0ij}}{2} \tag{7}$$

$$\rho(v_i(t), V_{Pi}) = \left| v_i(t) - \frac{a_{Pi} + b_{Pi}}{2} \right| - \frac{b_{Pi} - a_{Pi}}{2} \tag{8}$$

4.6 *Comprehensive dependent degree of multi-index*

Dependent degree of evaluated object *(N)* about safety grade *(j)* can be defined

$$V_j(N) = \sum_{i=1}^{n} \alpha_i K_j(v_i) \tag{9}$$

where α_i=weight of the ith index of evaluation object *(N)*, which satisfies as follows

$$\sum_{i=1}^{n} \alpha_i = 1 \tag{10}$$

4.7 *Determine the grade of dam safety*

If

$$K_{j0}(N) = \max_{j \in \{1,2,\cdots,m\}} (K_j(N)) \tag{11}$$

then the grade of actual status of evaluated object safety is j_0. Let

$$\bar{K}_j(N)=\frac{K_j(N)-\min\limits_{j\in\{1,2,\cdots,m\}}\left(K_j(N)\right)}{\max\limits_{j\in\{1,2,\cdots,m\}}\left(K_j(N)\right)-\min\limits_{j\in\{1,2,\cdots,m\}}\left(K_j(N)\right)} \tag{12}$$

$$CV(j_0)=\frac{\sum\limits_{j=1}^{m}j\cdot\bar{K}_j(N)}{\sum\limits_{j=1}^{m}\bar{K}_j(N)} \tag{13}$$

where $CV(j_0)$=characteristic value of actual status of evaluated object safety, more bigger denotes more worse for evaluated object safety.

4.8 *Evaluate the whole dam safety*

According to the index system of dam safety evaluation, all objects in the index system are evaluated one by one from the bottom up with above same steps. Lastly, the whole dam safety is evaluated.

4.9 *Evaluate dynamically dam safety*

With above approach, the dam safety status in different periods *(k)* is analyzed and assessed, the grades and characteristic values of dam safety in various periods *(k)* are calculated, which are expressed respectively as $j_{ok}(t)$, $CV_k(t)$ (k=1, 2, …, K). The variational trend of grades and characteristic values of dam safety need to be analyzed. If $j_{ok}(t)$ is very big, then dam safety status is very bad and dam need to be reinforced in time. It shows that dam safety status becomes bad, and observation frequency of dam need to be increased if $j_{ok}(t)$ is bigger and $CV_k(t)$ becomes gradually larger. If $CV_k(t)$ is almost invariable or decrescent, then dam safety status is steady or develops toward good direction. It shows that dam safety status is well if $j_{0k}(t)$ is lower and $CV_k(t)$ does not become gradually larger.

5 METHOD COMPUTING THE WEIGHT OF EVALUATION INDEX

Assume $V\in V_{Pi}$, the simple dependent degree of evaluation index about safety grade can be denoted

$$K_{ij}\left(v_i,V_{0ij}\right)=\begin{cases}\dfrac{2\left(v_i-a_{0ij}\right)}{b_{0ij}-a_{0ij}} & v_i\le\dfrac{a_{0ij}+b_{0ij}}{2}\\[2ex] \dfrac{2\left(b_{0ij}-v_i\right)}{b_{0ij}-a_{0ij}} & v_i\ge\dfrac{a_{0ij}+b_{0ij}}{2}\end{cases}\begin{pmatrix}i=1,2,\cdots,n\\ j=1,2,\cdots,m\end{pmatrix} \tag{14}$$

With Equation (15), the maximal dependent degree of evaluation index and corresponding safety grade can be determined.

$$K_{ij_{\max}}\left(v_i,V_{0ij_{\max}}\right)=\max_{j\in\{1,2,\cdots,m\}}\left(K_{ij}\left(v_i,V_{0ij}\right)\right)\quad(i=1,2,\cdots,n) \tag{15}$$

If the grade of evaluation index i is more larger, its weight should be more larger, then the weight of evaluation index i can be denoted

$$\alpha_i = \begin{cases} j_{\max} \times \left(1 + K_{ij_{\max}}\left(v_i, V_{0ij_{\max}}\right)\right) & K_{ij_{\max}}\left(v_i, V_{0ij_{\max}}\right) \geq -0.5 \\ j_{\max} \times 0.5 & K_{ij_{\max}}\left(v_i, V_{0ij_{\max}}\right) < -0.5 \end{cases} \tag{16}$$

Otherwise, if the grade of evaluation index *i* is more larger, its weight should be more less, then the weight of evaluation index *i* can be denoted

$$\alpha_i = \begin{cases} (m - j_{\max} + 1) \times \left(1 + K_{ij_{\max}}\left(v_i, V_{0ij_{\max}}\right)\right) & K_{ij_{\max}}\left(v_i, V_{0ij_{\max}}\right) \geq -0.5 \\ (m - j_{\max} + 1) \times 0.5 & K_{ij_{\max}}\left(v_i, V_{0ij_{\max}}\right) < -0.5 \end{cases} \tag{17}$$

For dam safety, if the grade of evaluation index *i* is more larger, the index is more disadvantageous to dam safety. So the weight of evaluation index of dam safety need be calculated according to Equation (16).

6 APPLICATION

One hydroelectric project is a huge hydropower project having many functions such as power generation, hump modulation, navigation and so on. Its installed capacity is 1,400MW. Key projects consist of concrete gravity dam, power station at dam toe, ship lock, vertical ship lift. Maximum height of dam is 101m, length of dam crest is 783m, and elevation of dam crest is 74m. It is composed of 42 monoliths, and No. 8–21 are water-diverting monoliths, No. 23–35 are overflow monoliths, No. 37 and No. 38 are monoliths of ship lock and ship lift, others are water-retaining monoliths.

6.1 *Evaluate observed characteristics of dam safety*

The dam safety status is decomposed into 5 grades, corresponding to 5 remarks as follows: normal, normal basically, little abnormal, abnormal, dangerous, which can be described as

$$V=\{V_1,V_2,V_3,V_4,V_5\}=\{\text{Normal, Normal basically, Little abnormal, Abnormal, Dangerous}\} \tag{18}$$

Above evaluation grade set is the same with all indexes in index system.

According to the grade criterion as Table 1, the characteristics values of lower layer of index in 1998 are shown in Table 1.

As an example, seepage behavior is assessed. Table 2 shows the dependent degree of single-index on grades calculated according to Equation(5).

According to Equation (9), comprehensive dependent degree of multi-index is obtained as Table 3. According to Equation (11)~Equation (13), grades and their characteristics values are computed as Table 3.

According to above steps, observed characteristics of dam safety from 1998 to 2002 is evaluated. The results are shown in Table 4.

It is known from Table 4 that the grades of dam observed characteristics are lower and characteristic values of grades are steady from 1998 to 2002. As a result, the conclusion can be drawn that dam observed characteristics is normal.

Table 1. Characteristics values of lower layer of index in Figure 2 in 1998.

		Grade criterion					
Assessed objects	Index	Normal	Normal basically	Little abnormal	Abnormal	Dangerous	Characteristics values
Deformation	Horizontal deformation	0.0~0.2	0.2~0.4	0.4~0.6	0.6~0.8	0.8~1.0	0.08
	Vertical deformation	0.0~0.2	0.2~0.4	0.4~0.6	0.6~0.8	0.8~1.0	0.12
Seepage	Uplift	0.0~0.2	0.2~0.4	0.4~0.6	0.6~0.8	0.8~1.0	0.09
	Quantity of seepage	0.0~0.2	0.2~0.4	0.4~0.6	0.6~0.8	0.8~1.0	0.29
	By-pass seepage	0.0~0.2	0.2~0.4	0.4~0.6	0.6~0.8	0.8~1.0	0.22
Stress	Stress of dam heel	0.0~0.2	0.2~0.4	0.4~0.6	0.6~0.8	0.8~1.0	0.19
	Stress of dam toe	0.0~0.2	0.2~0.4	0.4~0.6	0.6~0.8	0.8~1.0	0.06
Dam integrity	Joint	0.0~0.2	0.2~0.4	0.4~0.6	0.6~0.8	0.8~1.0	0.25
	Crack	0.0~0.2	0.2~0.4	0.4~0.6	0.6~0.8	0.8~1.0	0.26

Table 2. Dependent degree of single-index of seepage behavior in 1998.

	Uplift (v_1)	Quantity of seepage (v_2)	By-pass seepage (v_3)
$K_1(v_i)$	−0.9100	−0.2368	−0.0833
$K_2(v_i)$	−0.5500	0.4500	0.1000
$K_3(V_i)$	−0.7750	−0.2750	−0.4500
$K_4(v_i)$	−0.8500	−0.5167	−0.6333
$K_5(v_i)$	−0.8875	−0.6375	−0.7250

Table 3. Assessment results of lower layer of objects in Figure 2 in 1998.

Objects	Comprehensive dependent degree					Grade j_0		Characterisics values of grade
	K_1	K_2	K_3	K_4	K_5	Max.		
Deformation	1.1240	−0.4600	−0.7300	−0.8200	−0.8650	1.1240	1	1.3147
Seepage	−0.2427	0.2100	−0.3950	−0.5967	−0.6975	0.2100	2	2.0280
Stress	0.0456	−0.0565	−0.5282	−0.6855	−0.7641	0.0456	1	1.7725
Dam integrity	−0.1792	0.2800	−0.3600	−0.5733	−0.6800	0.2800	2	2.0172

6.2 *Evaluate safety of whole dam*

Figure 1 shows the index system assessing safety of whole dam. Table 5 shows the assessment results of whole dam from 1998 to 2002 with the proposed method. It is noticeable that the dam safety status is normal by analysis for variational trend of grades and characteristics values of the whole dam safety.

Table 4. Assessment results of observed characteristics of dam safety from 1998 to 2002.

Results	Year				
	1998	1999	2000	2001	2002
Comprehensive dependent degree					
K_1	−0.0298	0.0070	0.1830	−0.0282	0.0397
K_2	−0.0760	−0.1150	−0.1410	−0.0620	−0.1349
K_3	−0.5380	−0.5575	−0.5705	−0.5310	−0.5674
K_4	−0.6920	−0.7050	−0.7137	−0.6873	−0.7116
K_5	−0.7690	−0.7788	−0.7853	−0.7655	−0.7837
Grade	1	1	1	1	1
Characteristics values of grades	1.7964	1.7610	1.6786	1.8024	1.7370

Table 5. Assessment results of safety of whole dam in Figure 1 from 1998 to 2002.

Results	Year				
	1998	1999	2000	2001	2002
Comprehensive dependent degree					
K_1	0.1818	0.1929	0.1992	0.2059	0.2020
K_2	−0.1000	−0.1120	−0.0990	−0.1190	−0.1189
K_3	−0.5500	−0.5560	−0.5495	−0.5595	−0.5594
K_4	−0.7000	−0.7040	−0.6997	−0.7063	−0.7063
K_5	−0.7750	−0.7780	−0.7748	−0.7798	−0.7797
Grade	1	1	1	1	1
Characteristics values of grades	1.6988	1.6891	1.6931	1.6812	1.6826

ACKNOWLEDGEMENTS

This research has been partially funded by the projects from the National Natural Science Foundation of China (Grant No. 50139030), 973 Foundation of China for basic research on safety of major engineering project under the geo-hazard environment (Grant No. 2002CB412707) and the Science and Technology Innovation Foundation of Hohai University (Grant No. 2003411443).

REFERENCES

[1] Chuhan Zhang. Numerical modeling of concrete dam-foundation-reservoir system. Beijing: Tsinghua University Press, 2001.
[2] Luc, E.C. Statistical analysis in real time of monitoring data for idukki arch dam. 2nd international conference on dam safety evaluation, 1996, 381–385.
[3] Xing, L.S. & Tan, X.J. Dam safety and repair of hydropower stations in China. Dam and Safety. 2001 (5):4–8.
[4] Humberto & Marengo. Considerations on dam safety and the history of overtopping events. Dam Engineering, 2000, XI(1):29–59.
[5] Oliver & Crepon. An analytical approach to monitoring. International Water Power & Dam Construction, 1999(6):52–54.
[6] Zhongru Wu & Huaizhi Su. Diagnosis and evaluation of dam health. First International Conference on Structural Health Monitoring and Intelligent Infrastructure, 2003, Japan:79–86.
[7] Zhongru Wu. Safety monitoring theories & applications of hydraulic structure. Beijing: Higher Education Press, 2003.
[8] Cai, W. Extension engineering method. Beijing: Science Publishing House, 2000.

[9] Feng Xiating, Zhang Zhiqiang & Shen Qian. Identifying rock mass mechanical parameters of Three Gorges Prqject permanent shiplock using intelligent displacement back analysis method. Int. J. Rock Mech. Min. Sci., 2000(37):1039–1054.
[10] Habibagahi G. & Meidani M. Reliability of slope stability analysis evaluated using fuzzy set approach. Proc of 5th Int Conf on Civil Eng. Ferdowsi University, 2000:29–36.
[11] Dodagoudar G.R. & Venkatachalam G. Reliability analysis of slopes using fuzzy sets theory. Computer and Geotechnics, 2000(27):101–115.

New Developments in Dam Engineering—Wieland, Ren & Tan (eds),
© 2004 Taylor & Francis Group, London, ISBN 04 1536 240 7

Study on stress and bearing capability of Longtan Roller Compacted Concrete gravity dam

Sun Gongyao, Guo Xuyuan
Mid-South Design & Research Institute for Hydroelectric Projects, Changsha, Hunan, P.R. China

ABSTRACT: Longtan Roller Compacted Concrete (RCC) Gravity Dam is the highest gravity dam under construction in China to date. According to the features of RCC dam construction and the softening plastic property of the material, we studied the stress state of dam body by the elastic-plastic finite element method on the basis of the elastic-plastic increment theory formulated in strain space. Meanwhile, the stability theory and two different material strength reserve modes were adopted for the study of the bearing capability of gravity dam. This method can reflect the physical mechanism of instability of the gravity dam system resulting from the blemish and softening of concrete and rock material, and it makes the analysis be established on a rigorous mechanics basis.

1 INTRODUCTION TO LONGTAN HYDROPOWER PROJECT

Longtan Hydropower Project is of a normal storage level 400m, a RCC gravity dam as the water retaining structure with a crest elevation of 406.50m, a maximum dam height of 216.50m and a crest length of 836.50m, totaling 35 dam blocks and 6.8 million m^3 concrete for the dam body.

Longtan RCC gravity dam is the highest gravity dam under construction in China to date. A process of thin-layer spreading and vibratory compaction by rolling was adopted for the RCC dam construction. Sometimes, the interlayer weak plane may be included in the RCC of dam body. Through practices and studies, the basic factors that influence on the interlayer bonding have been defined but not fully be quantified. Furthermore, the elastic modulus vertical to the lift joint is reduced due to the existence of the interlayer weak plane; but all directions parallel to the lift joint, i.e. modulus direction, are of same elasticity, that makes the RCC be of transverse isotropic character. Through a great number of in-situ tests and studies, such parameters are defined as the initial elastic modulus of material, linear model of the softening section, peak stress strength, ultimate strain, breaking energy, ratio of tensile strength and compressive strength and ratio of dynamic and static strength, and the vertical to lift joint E_y (vertical elastic modulus) is induced to be 0.8 times of the elastic modulus parallel to lift joint E_x (transverse elastic modulus). It shows that the RCC material is of rather slight transverse isotropic character.

The statistics and linear regression analysis on friction factor f′ and cohesion c′ of shear parameter were conducted according to the obtained shear test results of lift joint. The actual dam construction is of great work quantity, long duration of concrete work and a great number of factors that influence on the quality of compaction by rolling of lift joint, so the discreteness of the shear strength parameter is big; however, the in-situ roller compaction test is of a short duration and a little factors that influence the quality of compaction by rolling of lift joint, so the discreteness of the shear strength parameter is small. Therefore, the value of coefficient of variation C_v of the shear strength parameter that was given by statistics and analysis on one (1) in-situ test could not

directly be used for Longtan Hydropower Project. After the analysis and study on the results of large-scale shear tests on the concrete dam foundations of 40 large and medium-sized projects be completed in China, the coefficient of variation C_v of friction factor f′ and of cohesion c′ were selected as 0.21 and 0.36 respectively and the probability rate was 80%, which were used for the suggested values of shear parameters f′ and c′ of the selected lift joint. For different locations and different dam body elevations, the corresponding shear parameter to the material zoning was selected.

2 METHOD FOR DISTINGUISHING THE CRITICAL STATE OF BEARING CAPABILITY OF LONGTAN RCC GRAVITY DAM

Analysis on stress and stability against sliding by the finite element method is usually required to study on the stress control standard and instability distinguishing rule for bearing capability of the gravity dam. According to the research results of the self-stressing function answer and corner eigenfunction that express the influence on dam body stress by dam foundation deformation, the control standard of dam body stress may be defined by the method of limiting the relative width of tensile stress area from the vertical positive stress on dam foundation plane; for bearing capability of stability against sliding of gravity dam, the research by stability theory and two different material strength reserve modes are carried out after studied on the traditional analysis method.

Study on stability against sliding of gravity dam is usually needed to suppose some possible sliding surfaces at first, such as dam foundation plane or weak lift joint of RCC for defining the safety factor through calculation and comparison of the sliding force and anti-sliding force on these surfaces. In the elastic-plastic finite element stress analyzed by the material strength reserve method, the safety factor F is defined that if the shear strength index of medium on dam body and dam foundation plane is reduced as c′/F & f′/F, the dam body reaches to the ultimate equilibrium state. The analysis method of strength failure of gravity dam (referred to as the strength analysis method) was educed from the conditions that the state of the yield failure zone in dam body be about to run through the upstream and downstream dam faces is regarded as an ultimate equilibrium state. Now, we adopted a new approach to treat the stability of gravity dam, i.e. setting up a criterion for judging the gravity dam stability in accordance with the structural stability theory.

The aim of the structural stability analysis is to find out the unstable equilibrium state between external load and inner resistance of structure, i.e. the state of deformation rapidly increasing. The instability of structure has two basic types, i.e. one is that the branch point is unstable for the perfect system, the other is that the ultimate value point is unstable for the non-perfect system with initial geometrical defect or load deviation. Small deformation theory is still used to solve its critical load of gravity dam stability. The judgment of instability of gravity dam is depended on the comparison between the configuration of gravity dam and dam foundation system deviating the equilibrium state and that of the equilibrium state, and the comparison is suitable for the energy principle. The of energy principle is formulated as, the positive definite second-order variation of general potential energy $\mathbf{\Pi}$ of structure system is the essential and sufficient conditions for guaranteeing the stable static equilibrium state. In the calculation of elastic-plastic stress finite element method of RCC gravity dam, the equilibrium state of each load increment step should be judged to identify it is stable or not, if it is a unstable one, it reaches the maximum load. This method for analyzing the gravity dam bearing capability is called as a stability analysis method.

Now to suppose an equilibrium state, the displacement $\mathbf{u}$, strain ε and stress $\boldsymbol{\sigma}$ of the dam body have been given out, a virtual displacement $\delta\mathbf{u}$ that is arbitrary, small and not violated geometric condition is supposed to add on this state, so a new state is achieved. If the virtual work made by the external load not exceeds the increase of the internal energy (elastic deformation energy and plastic dissipative energy of the medium material of dam body), the equilibrium of the gravity dam system will be stable. If a group of virtual displacement that makes the virtual work act by load

exceed the increase of the internal energy could be found, the gravity dam system will be in an unstable state. Then, the instability criterion may be expressed as follows:

$$\delta^2\Pi = \int_{V_e}\delta\varepsilon^T\delta\sigma dV + \int_{V_s}\delta\varepsilon^T\delta\sigma dV \le 0 \tag{1}$$

where, V_e denotes the elastic zone of RCC material of dam body, V_s denotes the strain softening failure zone after the material achieved strength standard, and $V=V_e+V_s$. For elastic zone V_e, known elastic matrix $[D_e]$, then the virtual variation of stress is $\{\delta\sigma\}=[D_e]\{\delta\varepsilon\}$; for strain softening failure zone V_S, known elastic-plastic matrix $[D_{ep}]$, then the virtual variation of stress is $\{\delta\sigma\}=[D_{ep}]\{\delta\varepsilon\}$.

In accordance with the expression of strain matrix and rigidity matrix for the calculation of finite element stress, the instability criterion expression (1) may be rewritten as

$$\delta^2\Pi=\{\delta U\}^T[K_T]\{\delta U\}\le 0 \tag{2}$$

where, $[K_T]$ denotes the tangent line rigidity matrix of the finite element analysis for dam body. Thus, that the structural equilibrium state is stable or not finally is depended on the character of tangent line rigidity matrix $[K_T]$: when $[K_T]$ is positive definite, the equilibrium is stable; when $[K_T]$ is negative definite, the equilibrium is unstable; and when $[K_T]$ is singular (i.e. det $[K_T]=0$), the structure is in critical state. Due to $[K_T]$ is a real symmetric matrix, its eigenvalues are all real numbers. To suppose λ_1 is its minimum eigenvalue, the condition

$$\lambda_1\le 0 \tag{3}$$

may replace the instability criterion expression (2) for distinguishing gravity dam. As under the condition that there is at least one negative eigenvalue, one disturbance $\delta\mu$ is always able to find out to make expression (2) come into existence, i.e. the gravity dam system is in unstable equilibrium state. And expression (3) is called as an instability criterion formulated by eigenvalue.

From the energy criterion expression (1) for distinguishing the stability of gravity dam system, it can be seen that the strain softening characteristic and occurrence of strain softening zone of the RCC medium are the essential conditions of the gravity dam's equilibrium in an unstable state. If the RCC medium is not a softening material, the condition of $\delta^2\Pi>0$ is constant because D_e is positive definite and D_{ep} is half-positive definite, which makes the state stable. Moreover, after the partial strain softening zone is appeared, only the second term in expression (1) is a negative one and its absolute value is so enough big that it is more than that of the former elastic zone, then the condition of $\delta^2\Pi<0$ could be satisfied. Therefore, the unstable equilibrium state may not occur until the plastic deformation and strain softening zone develop to a certain degree. Thus, it can be seen that the strain softening character of the concrete and rock mass is the essential condition of the instability of the gravity dam system.

3 ANALYSIS ON STRESS AND STABILITY OF DAM BODY

In order to analyze the influence on the dam body stress by transverse isotropic character of RCC material, six (6) conditions, i.e. vertical elastic modulus E_y is respectively 0.5, 0.6, 0.7, 0.8, 0.9 & 1.0 times (isotropy) of transverse elastic modulus E_x of RCC of dam body are taken into account and four (4) elevation planes are selected for studying the stress variation law. Now several typical results are listed for explaining its influence law. Under the action of water pressure and dead load, when E_y is varied from $1.0E_x$ to $0.5E_x$, the stress distributing law (including σ_x, σ_y, τ_{xy}) on each plane is not varied too much but basically same. Table 1 has listed out the stress value comparison in $E_y=0.5E_x$ and $E_y=E_x$ at dam heel and dam toe when the dam foundation plane elevation is under the action of water pressure and dead load respectively. A certain variation of stress values

Table 1. Stress value comparison at RCC dam heel and dam toe as E_y is varied.

		Stress of dam heel (MPa)			Stress of dam toe (MPa)		
		σ_x	σ_y	τ_{xy}	σ_x	σ_y	τ_{xy}
Dead load	$E_y=E_x$	−3.665	−7.974	−3.877	−1.274	−1.321	1.085
	$E_y=0.5E_x$	−7.225	−8.618	−4.405	−2.241	−1.694	1.364
	Variation	(−)Increase	(−)Increase	Increase	(−)Increase	(−)Increase	Increase
	range	97.1%	8.1%	13.6%	75.9%	28.3%	25.7%
Water pressure	$E_y=E_x$	5.419	8.309	6.297	−4.790	−3.855	3.642
	$E_y=0.5E_x$	9.068	9.298	6.284	−6.737	−4.616	3.867
	Variation	(+)Increase	(+)Increase	Decrease	(−)Increase	(−)Increase	Increase
	range	67.3%	11.9%	0.21%	40.6%	19.7%	6.2%
Dead load & water pressure	$E_y=E_x$	1.753	0.335	2.420	−6.064	−5.176	4.727
	$E_y=0.5E_x$	1.585	0.345	1.719	−9.000	−6.336	5.244
	Variation	(+)Decrease	(+)Increase	Decrease	(−)Increase	(−)Increase	Increase
	range	9.7%	3.0%	29.0%	48.4%	22.4%	10.9%

has shown in Table 1. For Longtan gravity dam, under the action of dead load, the maximum variation of horizontal positive stress has already reached up to 97% and the vertical positive stress at dam heel and dam toe are all increased. Under the joint action of water pressure and dead load, this zone is in the state of opposite stress centralization; under the actions of water pressure and dead load respectively, although the influence extent to the stress value is big, the combined stress value is reduced as the vertical elastic modulus of RCC as a result of counteraction of tensile stress and compressive stress, that induced a small variation of the relative value. Table 1 has listed out the comparison of stress value variation under joint action of water pressure and dead load, variation at dam heel σ_x and dam toe σ_y are 9.7% and 3.0% respectively, and variation of τ_{xy} is 29.0%. According to calculations, when E_y is varied from $1.0E_x$ to $0.5E_x$, vertical positive stress at dam heel is increased from 0.335MPa to 0.345MPa, approximately increased 3.01%, but the vertical positive stress at dam toe is increased from −5.176MPa to −6.336MPa, increased 22.41%. This phenomenon is similar to the influence of dam foundation deformation to dam body stress distribution under the condition of homogeneous isotropic medium, and the two results are basically same. For the homogeneous isotropic medium, the influence by dam foundation deformation to dam body stress distribution is expressed as the increase of vertical tensile stress of dam heel after the dam body elastic modulus reduced; and for transverse isotropic medium, the reducing of E_y is still expressed as the increase of vertical tensile stress of dam heel when the dam body E_x is kept without change. The results of stress distribution under these two conditions are same.

In order to take into account the plastic softening character of material during the analysis of elastic-plastic stress of gravity dam by definite element method, a constitutive theory and a loading-unloading criterion that are universally suitable for the strengthening, softening and idealized plastic materials were established on the elastic-plastic increment theory formulated in strain space. For the weak planes, such as dam body lift joint and dam foundation plane, shear failure usually occurs along weak plane and tension failure on the vertical weak plane, so the isoclinic strengthening-softening stratified material model was adopted; for dam body concrete and bed rock medium, the isoclinic strengthening-softening corrected Drucker-Prager model was adopted and it is internally tangent by the hexagon of Mohr-Coulomb yield failure criterion.

In the analysis and study of elastic-plastic stress and bearing capability of Longtan RCC gravity dam, the current design criterion of gravity dam was adopted for analyzing and studying the dam body stress state and stability safety factor against sliding. From Figure 1, the analysis results of elastic-plastic stress, it can be seen that under the normal load action, except for the plastic yield appears in partial stress concentration zone at dam heel and dam toe, the dam body is in an elastic state. Here, normally the vertical positive stress of dam body is compressive stress, the tensile

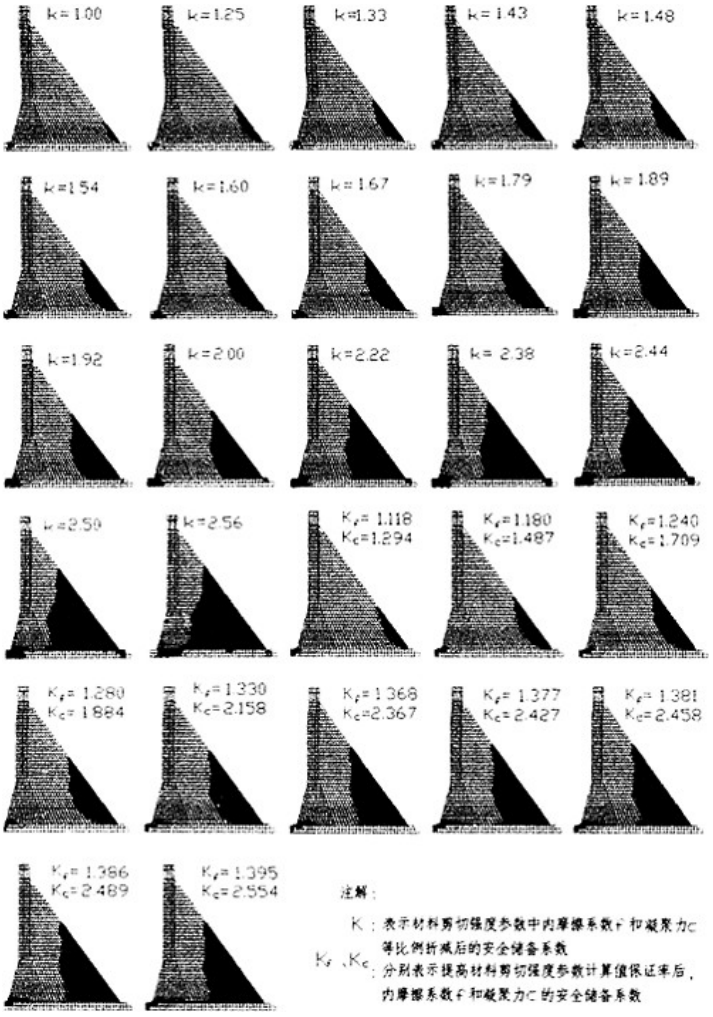

Figure 1. Correspondence relation of gradual failure process and emergency capacity factor of Longtan RCC gravity dam.

Notes of Fig. 1:

K: is factor of emergency capacity of friction factor f and cohesion c of material shear strength parameter after reduction in same proportion; and

K_f, K_c: respectively denotes factor of emergency capacity of friction factor f and cohesion c after increasing the calculation value probability rate material shear strength parameter.

stress only appears in a very small part of dam toe, and the stress distribution state is meeting with requirements of design criterion of gravity dam. For the peak shear strength parameters f′ & c′ and residual shear strength parameters f_r & c_r on the given dam foundation plane and dam body lift joint, the contrast of anti-sliding force and sliding force is used to solve the stability safety factor

Table 2. Peak and residual stability safety factor against sliding of Longtan RCC gravity dam.

Strength value	Calculation position		
	Dam foundation plane K_{dp} & K_{dr}	RCC1 lift joint K_{rsp} & K_{rsr}	RCC1 body K_{rbp} & K_{rbr}
Standard value of peak shear strength parameter f′ & c′	3.048	3.301	3.897
Standard value of residual shear strength parameter f_r & c_r	2.094	2.108	2.296

against sliding on dam foundation plane and its relevant RCC and lift joint, for short, peak stability safety factor against sliding and residual stability safety factor against sliding as shown in Table 2. From the results in Table 2, it can be seen that dam foundation plane and RCC lift joint are of enough stability safety factor against sliding, and the dam foundation plane is the control cross section of dam body stability against sliding. It shows that the sectional design of gravity dam is reasonable and safety factor accord with the requirements of the current criterion.

In the process of analysis and study of dam body bearing capability, two different methods for selecting the value of shear strength parameter were taken. The first method is, on the basis of standard values of peak shear strength parameter f′ & c′ and of residual shear strength parameter f_r & c_r, the values are calculated by the method of reducing the aforesaid standard values in the same proportion. Then, the study of the dam body bearing capability is carried out by elastic-plastic finite element method in light of the loading method of load increment. According to the instability criterion educed from stability theory, the factor of emergency capacity of dam body in instability critical state K_c=1.92 is given out. When the instability critical state occurs, the expanding speed of yield zone of strength analysis has obviously increased but still not goes rapidly. The corresponding yield failure zone range is about 40% of dam body width, which is shown in Figure 1. After the dam body stability reaches to a critical state, the yield failure zone is expanded rapidly. The yield failure state that is about to run through the upstream and downstream dam faces presented by strength analysis method will be regarded as the final ultimate state of dam body. Thus, the maximum emergency capacity factor K_1 of Longtan RCC gravity dam is given as 2.50. It can be known that this moment the ultimate state has permanently been changed from the original equilibrium configuration by the stability analysis. The gradual destructive course from the normal state to the final ultimate state of the dam body is shown in Figure 1. The second method for selecting the shear strength parameter is, on the premise of selecting the probability rate as 80% of the known initial calculation value (or standard calculation value) of shear strength parameter and the characteristic of small coefficient of variation V_{sf} of friction factor f′ & f_r and big coefficient of variation V_{sc} of cohesion c′ & c_r, the probability rate of calculation value is gradually increased and this moment the calculation values of friction factor and cohesion are reduced in different proportions for studying the bearing capability of Longtan RCC gravity dam. That is to say, comparing to the standard, the cohesion c′ & c_r from calculation analysis is of more reduction and that of friction factor f & f_r is less. Similarly, according to the instability criterion educed from stability theory, emergency capacity factors K_{cf} & K_{cc} of friction factor and cohesion in critical state are 1.33 and 2.16 respectively. In the contrast studies of strength analysis of instability critical state, it can be seen that the corresponding dam body yield failure zone on dam foundation plane is about 50% of dam body width, which is shown in Fig. 1.

After the dam body stability reaches to a critical state, the expanding speed of the yield failure zone along dam foundation plane and RCC lift joint is expanded rapidly. This phenomenon shows that after the values c′& c_r are reduced in a great extent, the shear strength on dam foundation plane and lift joint is obviously decreased. As the cohesion is related to tensile strength, the tensile strength of lift joint also decreases correspondingly. Therefore, the distribution type of the yield

Table 3. Emergency capacity factor of bearing capability of Longtan RCC gravity dam.

Value selection method of calculation parameter and probability rate	Dam body state			
	Critical state		Ultimate state	
Method of reducing standard value of shear strength parameter in same proportion	Factor of emergency capacity K_c 1.92		Factor of emergency capacity K_j 2.50	
Method of raising the probability rate of calculation value of shear strength parameter	Emergency capacity factor of friction factor K_{ef} 1.330	Emergency capacity factor of cohesion K_{cc} 2.158	Emergency capacity factor of friction factor K_{lf} 1.391	Emergency capacity factor of cohesion K_{lc} 2.522
	Probability rate of calculation value of shear strength parameter P 97.0%		Probability rate of calculation value of shear strength parameter P 97.8%	

failure zone in ultimate state is already very different from the research result got by the first parameter value selection method, and the difference could be seen in Fig. 1. The yield failure zone along dam foundation plane and RCC lift joint in ultimate state is increased by the second parameter value selection method and the yield range on other parts of dam body is decreased correspondingly. This moment the danger of yield failure on final ultimate state increases. So, the final ultimate bearing capability comparing to that of the first parameter value selection method is decreased. Finally, the emergency capacity factor of friction factor on ultimate state K_{lf} is given as 1.39 and emergency capacity factor of cohesion on ultimate state K_{lc} is 2.52. The emergency capacity factor of Longtan RCC gravity dam is gathered in Table 3.

In the study of bearing capability, on the one hand, it was conducted by the instability criterion educed from stability theory, on the other hand, the comparative analysis and demonstration was carried out in the strength analysis by distinguishing method of instability critical state and the comparative study was done by the method of the current criterion. For the first value selection method of shear strength parameter, the emergency capacity factor of dam body bearing capability on critical state K_c is 1.92, and this value is lower than the residual stability safety factor against sliding K_{dr}=2.09. The emergency capacity factor of dam body bearing capability in ultimate state K_1 is 2.50, it is between the peak and residual stability safety factor against sliding K_{dp}=3.05 and K_{dr}=2.09. For the second value selection method of shear strength parameter, factors of emergency capacity of dam body bearing capability in critical state and ultimate state are all lower than those of the first method of value selection of shear strength parameter and the yield failure type and range of the gravity dam are changed due to the shear strength and tensile strength of the dam foundation plane and lift joint decrease obviously. So, for the study of gravity dam bearing capability, the result made by the first method of value selection of shear strength parameter is of quite comparability; and the second value selection method of shear strength parameter and its study result are needed more attention since the danger of occurring critical state and ultimate yield failure state may be increased. Seen from the study results of gravity dam bearing capability, although the gravity dam designed by the current criterion is of the character that the emergency capacity factor on instability critical state is lower than the residual stability safety factor against sliding by traditional analysis method, the dam body still has a certain emergency capacity. The emergency capacity factor on ultimate state is higher than the residual stability safety factor against sliding, but it belongs to the unstable equilibrium state comparing to the original configuration due to the too more deformation of dam body.

4 CONCLUSION

For the analysis and study on non-linear stress and bearing capability of Longtan RCC gravity dam, the elastic-plastic theory of constitutive relation formulated in strain space was adopted for the finite element analysis of the dam body elastic-plastic stress, linear elastic stress and stability under the load action of normal high water level. This analysis had considered the strain softening plastic characteristic of RCC and rock medium material, and it based on the standard values of physics and mechanics strength parameter of the damming material. This analysis method could reflect the physical mechanism of instability of gravity dam system resulting from the blemish and softening of concrete and rock material, and it made the analysis be established on a rigorous mechanics basis. The research result shown that the stress distribution state and stability safety factor against sliding satisfy the regulations of design criterion and the sectional design of gravity dam was reasonable.

The study on the influence of transverse isotropic character of the RCC deformation to the dam body stress was carried out on the basis of material performance test and the possible variation range of elastic constant. Supposing the E_y/E_x of RCC varies in the range of 0.5~1.0, the analysis result of dam body stress shown that the influence of transverse isotropic character on the dam body stress was very small, and the stress distributing law was basically of no change but of a certain influence on the stress values at dam heel and dam toe. This influence state was same as the study result answered by self-stress function that expresses the influence of dam foundation rigidity to dam body stress after the homogeneous isotropic elastic modulus of dam body decreased.

The study of bearing capability of Longtan RCC gravity dam was carried out by the stability analysis and strength analysis method on the basis of the shear strength parameter value selection by emergency capacity method and loading principle of dam body load increment. The study stressed on the comparison of the internal relation of the analysis results that made by the aforesaid two methods so as to verify each other. The study of instability critical state of gravity dam was carried out on the basis of the stability analysis theory, and the analysis was conducted comparing to such phenomena of the strength analysis as the extending range, spreading speed and cuspidal point appears in the course of deformation development (or called as equilibrium path) of plastic yield failure zone of dam body. For the study of ultimate bearing state of gravity dam, the strength analysis method was adopted under the condition of making the yield failure state be about to run through the upstream and downstream dam faces as the ultimate state of dam body. Known from the stability analysis results, here the dam body was in an unstable equilibrium state comparing to the original equilibrium configuration. Two methods were used for value selection of shear strength parameter for bearing capability research. The study result that made by the first method of standard value reduction in same proportion was of quite comparability; and that made by the second method of increasing the calculation value probability rate was of the raising danger of ultimate yield failure, which was needed more attention.

REFERENCES

[1] Tolke F.Talsperren, Staudämme und Staumauern, Handbibliothek für Bauingenieure [M]. Berlin, 1938.
[2] Pan Jiazheng, “Design of Gravity Dam [M]” Water Conservancy and Hydroelectric Publishing Company, Beijing, China; 1987.
[3] Yin Youquan, “Introduction to Non-Linear Infinite Element of Solid Mechanics [M]”, Beijing University Publishing Company, Beijing, China; 1987.
[4] Yin Youquan and Fan Jianli, “Rigidity Element Method and Stability Analysis of Massive Rock [J]”, Mechanics Journal; 1990(5).
[5] Sun Gongyao, Yin Youquan and Qian Zhiguang, “Analysis and Study on Bearing Capability of Concrete Gravity Dam [A]”, Water Conservancy Journal; 2001(4).

New Developments in Dam Engineering—Wieland, Ren & Tan (eds),
© 2004 Taylor & Francis Group, London, ISBN 04 1536 240 7

Linear complementary model for nonlinear analysis of jointed arch dams

Lin-song Sun
College of Hydmulic & Civil Engineering, Yangzhou Univ., PR China

De-xin Wang & Xing-wen Guo
College of Civil Engineering, Hohai Univ., PR China

ABSTRACT: Arch dams are constructed as cantilever monoliths separated by vertical contraction joints. To simulate the discontinuous behavior of contraction joints, an incremental constitutive model is established by means of penalty coefficient. The contact conditions are expressed by the same form as the flow rule in a non-associated plastic flow problem, and a complementary virtual work equation is deduced. Based on the FEM, a linear complementary model for joints is proposed. Some numerical examples are given to show good performance of this model, and the influence of penalty coefficient value is discussed also. Then, the model is applied to analysis the influence of initial joints gap to Xiaowan arch dam. The calculation result indicates that the joint has little influence if there is no initial gap after grouting, but the influence will be remarkable if initial gaps exist. The maximum stress and displacement will increase with the increase of initial gaps.

1 INTRODUCTION

Arch dams are generally constructed as cantilever monoliths by contraction joints. Many methods have been proposed to model the joints in arch dams. Dowling (1989) adopted a special discrete springs element to treat the discontinuity of joints. However, such generalized nonlinear springs only consider then normal opening/closing of joints, do not include all the properties of contraction joints, e.g., shear keys properties, initial tensile stress, initial gap, etc. Many researchers have treated the joint/interface by using a quasi-continuum finite element. A curved surface interface element has been developed by O'Connor [1985] and is applied to the studies of arch dam joints. Fenves [1993] developed a nonlinear joint element modeling the contraction joints with a three-dimension eight-node isoparametric element consisting of two faces. In their studies, only nonlinear behavior of joints related to the joint normal displacement is considered. They assumed fully elastic behavior for joint response to tangential forces. Ahmadi [2001] presented a nonlinear joint element model with a coupled shear-tensile behavior. The model is useful to analysis jointed arch dams considering shear key behavior, joint damages etc. But it does not consider the initial gap may be exists in joints. Zhu [2001] proposed a joint element with small thickness, which deals with nonlinearity both in normal and tangential direction, including shear key behavior and initial joint gaps. Other workers treat the joint as a contact problem. Li [1992] introduced a substructure method under mixed coordinate system to the analysis of arch dam and obtained some reasonable results. The numerical process deal with the non-linearity of joint in these works is iteration method.

In this paper, a linear complementary method for contraction joint is proposed, which does not need iteration. The joint is modeled as no tensile in normal with/without initial gap and tangential failure as Mohr-Coulomb's law. With the use of penalty coefficients, the contact conditions are expressed as the same form of non-associated plastic flow problem. A linear complementary model based on FEM is introduced, and the non-linear problem of contact is transferred to a linear complementary problem.

2 CONSTITUTIVE MODEL FOR JOINT WITH INITIAL GAP

It is a contact problem essentially for the analysis of contraction joints. Let $\Omega^{(1)}$ and $\Omega^{(2)}$ are two adjacency monolith as shown in Figure 1. In the local coordinate system o$\tau_1\tau_2 n$ at contact point, the contact stress are p_n, $u_n^{(2)}$, $u_{\tau_1}^{(2)}$, $u_{\tau_1}^{(2)}$). The relative displacements is defined as

$$\left.\begin{aligned} \varepsilon_n &= u_n^{(1)} - u_n^{(2)} + \delta_n \\ \varepsilon_{\tau_i} &= u_{\tau_i}^{(1)} - u_{\tau_i}^{(2)} \quad (i = 1,2) \end{aligned}\right\} \tag{1}$$

Where subscript n represents normal direction, $\tau_i (i=1, 2)$ represent two tangential directions, and δ_n is the initial normal gap.

2.1 *Relations of contact stress and relative displacement*

The tensile strength of joints is very weak, and may be supposed zero. So, at normal direction, contact stress p_n and relative displacement ε_n should satisfy

$$p_n \leq 0 \tag{2a}$$

$$\varepsilon_n \geq 0 \tag{2b}$$

and $$\varepsilon_n p_n = 0 \tag{2c}$$

which is similarly to 1-D constitutive relations of perfect rigid-plastic body with yield function

$$f_1 = p_n \tag{3}$$

Be analogous to the method in plastic mechanics, a perfect elastoplastic body is adopted approximately, and ε_n is divided into elastic component $\varepsilon_{n^*}^p$. The relation of normal contact stress and relative displacement is

$$p_n = E_n(\varepsilon_n - \varepsilon_n^p) = E_n\varepsilon_n - E_n\frac{\partial g_1}{\partial p_n}\lambda_1 \tag{4}$$

Where E_n is penalty coefficient in normal direction, $g_1 = p_n$ corresponds to plastic potential in plastic mechanics, and $\lambda_1 \geq 0$ is analogous to flow parameter which is complementally to yield function, i.e. $f_1\lambda_1 = 0$.

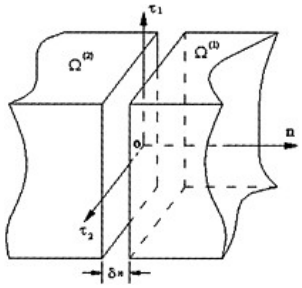

Figure 1. Local coordinate system at joint.

At tangential directions, Coulomb's law of friction is used, i.e.

$$\|\boldsymbol{p}_\tau\| + \mu p_n - c_0 \le 0 \tag{5}$$

In which, $\|p_\tau\| = (p_{\tau_1}^2 + p_{\tau_2}^2)^{1/2}$, μ is factor of friction, and c_0 is cohesion in contact surface.

The yield function of analogical perfect rigid-plastic body is

$$f_2 = \|\boldsymbol{p}_\tau\| + \mu p_n - c_0 \tag{6}$$

Similar to the treatment of normal component, the tangential stress and relative displacement satisfy

$$p_{\tau_i} = E_{\tau_i}(\varepsilon_{\tau_i} - \varepsilon_{\tau_i}^p) = E_{\tau_i}\varepsilon_{\tau_i} - E_{\tau_i}\frac{\partial g_2}{\partial p_{\tau_i}}\lambda_2 \tag{7}$$

where $g_2 = \sqrt{p_{\tau_1}^2 + p_{\tau_2}^2}$ is slip potential, and $\lambda_2 \ge 0$ is slip parameter with relation of $f_2\lambda_2 = 0$ to yield function f_2.

2.2 *Incremental constitutive model and complementary virtual work equation*

Let $\mathrm{d}\boldsymbol{u}_c^{(\alpha)} = (\mathrm{d}u_{\tau_1}^{(\alpha)}\ \mathrm{d}u_{\tau_2}^{(\alpha)}\ \mathrm{d}u_n^{(\alpha)})^{\mathrm{T}}$ be incremental displacements of contact body α(α=1, 2), the incremental relative diplacements are definite as

$$d\varepsilon_{ci} = d\Delta u_{ci} + \delta_{ci}\ (i=1, 2, 3) \tag{8}$$

in which, $\mathrm{d}p_c = (dp_{\tau_1}\ dp_{\tau_2}\ \mathrm{d}p_n)^{\mathrm{T}}$ can be expressed as

$$\mathrm{d}p_{ci} = D_{cij}(\mathrm{d}\varepsilon_{cj} - \mathrm{d}\varepsilon_{cj}^p) = D_{cij}\mathrm{d}\varepsilon_{cj} - D_{cij}\frac{\partial g_k}{\partial p_{cj}}\mathrm{d}\lambda_k \tag{9}$$

where D_{cij} are elastic constants, which expressed in matrix form is $\boldsymbol{D}_c = \mathrm{diag}(E_{\tau_1}\ E_{\tau_2}\ E_n)^{\mathrm{T}} \cdot \mathrm{d}\lambda_k$ complement with yield functions f_k(k=1, 2). With the introduce of relax variable v_k, the complementary conditions on joint surface are

$$\left.\begin{aligned} f_k + v_k &= 0 \\ v_k \mathrm{d}\lambda_k &= 0,\ \ v_k, \mathrm{d}\lambda_k \ge 0 \end{aligned}\right\} \tag{10}$$

Eqs. (9) and (10) consist the incremental constitutive model of joint.

Considering equilibrium equations, Eqs. (6) and other boundary conditions, a virtual work equation is deduced using the principle of virtual displacement,

$$\begin{aligned} &\int_\Omega \delta\mathrm{d}\varepsilon_{ij} D_{ijkl}\mathrm{d}\varepsilon_{kl}\mathrm{d}\Omega + \int_{S_c}\delta\mathrm{d}\Delta u_{ci} D_{cij}\mathrm{d}\Delta u_{cj}\mathrm{d}S \\ &= \int_\Omega \delta\mathrm{d}u_i \mathrm{d}b_i\mathrm{d}\Omega + \int_{S_p}\delta\mathrm{d}u_i\mathrm{d}\overline{p}_i\mathrm{d}S + \int_{S_c}\delta\mathrm{d}\Delta u_{ci} D_{cij}\frac{\partial g_k}{\partial p_{cj}}\mathrm{d}\lambda_k\mathrm{d}S - \int_{S_c}\delta\mathrm{d}\Delta u_{ci} D_{cij}\delta_{cj}\mathrm{d}S \end{aligned} \tag{11}$$

In which, $d\lambda_k$ is determinate by complementary conditions on joint surface. So, Eq. (11) is restricted by Eq. (10), and they consist the complementary virtual work equations of jointed structure.

3 FINITE ELEMENT DISCRETIZATION AND LINEAR COMPLEMENTARY MODEL

It is assumed that dam is divided into N_{ED} 8-nodes isoparametric element, and the nodes at adjacency dam segments appear in pairs. Joint element with 4-pairs nodes in Figure 2 is adopted, and

N_{EC} is used to denote the numbers of joint element. In joint element, increment relative displacement and initial gap are interpolated with the shape function

$$N_i = \frac{1}{4}(1+\xi_i\xi)(1+\eta_i\eta) \quad (i=1,2,3,4)$$

In matrix form, that is

$$\mathrm{d}\Delta\boldsymbol{u} = \begin{bmatrix} -N_{u1} & \cdots & -N_{u4} & N_{u1} & \cdots & N_{u4} \end{bmatrix} \begin{Bmatrix} \mathrm{d}u_1 \\ \mathrm{d}u_2 \\ \vdots \\ \mathrm{d}u_8 \end{Bmatrix} = N_c \mathrm{d}u^e,$$

$$\boldsymbol{\delta}_c = \begin{bmatrix} N_{\delta 1} & N_{\delta 2} & \cdots & N_{\delta 4} \end{bmatrix} \begin{Bmatrix} \delta_{c1} \\ \delta_{c2} \\ \vdots \\ \delta_{c4} \end{Bmatrix} = N_\delta \delta_c^e.$$

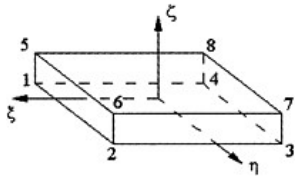

Figure 2. Joint element.

Where $\boldsymbol{N}_{ui}=\boldsymbol{N}_{\delta i}=\mathrm{diag}(N_i, N_i, N_i)$, $du_i=[du_x, du_y, du_z]^{\mathrm{T}}$, $\boldsymbol{\delta}_{ci} = [\delta_{\tau 1}\ \delta_{\tau 2}\ \delta n]^{\mathrm{T}} = [0\ 0\ \delta_n^0]^{\mathrm{T}}$.

Since virtual increment displacement is arbitrary, it can be obtained from virtual work equation Eq. (11) that

$$\boldsymbol{K}\mathrm{d}\boldsymbol{u}=\boldsymbol{H}\mathrm{d}\lambda+\boldsymbol{dP} \tag{12}$$

In which,

$$\boldsymbol{K} = \sum_{e=1}^{N_{EC}} \boldsymbol{C}_u^{e\mathrm{T}} k^e \boldsymbol{C}_u^e + \sum_{e=1}^{N_{EC}} \boldsymbol{C}_u^{e\mathrm{T}} k_c^e \boldsymbol{C}_u^e, \quad \boldsymbol{K}^e = \int_{\Omega^e} \boldsymbol{B}^{\mathrm{T}} \boldsymbol{D}\boldsymbol{B}\mathrm{d}\Omega, \quad \boldsymbol{K}_c^e = \int_{S_c^e} \boldsymbol{N}_c^{\mathrm{T}} \boldsymbol{T}^{\mathrm{T}} \boldsymbol{D}_c \boldsymbol{T} \boldsymbol{N}_c \mathrm{d}S,$$

$$\mathrm{d}\boldsymbol{P} = \sum_{e=1}^{N_{EC}} \boldsymbol{C}_u^{e\mathrm{T}} \mathrm{d}\boldsymbol{P}_0^e - \sum_{e=1}^{N_{EC}} \boldsymbol{C}_u^{e\mathrm{T}} \mathrm{d}\boldsymbol{P}_\delta^e, \quad \mathrm{d}\boldsymbol{P}_0^e = \int_{\Omega^e} \boldsymbol{N}^{\mathrm{T}} \mathrm{d}b \mathrm{d}\Omega + \int_{S_\sigma^e} \boldsymbol{N}^{\mathrm{T}} \mathrm{d}\bar{\boldsymbol{P}} \mathrm{d}S, \quad \mathrm{d}\boldsymbol{P}_\delta^e = \int_{S_c^e} \boldsymbol{N}_c^{\mathrm{T}} \boldsymbol{T}^{\mathrm{T}} \boldsymbol{D}_c \boldsymbol{N}_\delta \delta_c^e \mathrm{d}S,$$

$$\boldsymbol{H} = \sum_{e=1}^{N_{EC}} \boldsymbol{C}_u^{e\mathrm{T}} \left(\int_{S_c^e} \boldsymbol{N}_c^{\mathrm{T}} \boldsymbol{T}^{\mathrm{T}} \boldsymbol{D}_c \frac{\partial g}{\partial p_c} \mathrm{d}S \right) \boldsymbol{C}_\lambda^e.$$

where $\boldsymbol{C}_\lambda^e$ are element selection matrix of freedoms of degree and flow parameters respectively, $\boldsymbol{T}$ is transfer matrix from global coordinate to local coordinate.

The yield functions f_m(m=1, 2) can be approximated by the linear term of Taylor's series as

$$f_m(p_{ci}) = f_m^0 + \frac{\partial f_m}{\partial p_{ci}} \mathrm{d}p_{ci} \tag{13}$$

Substituting Eqs. (9) and (8) into Eq. (13), it can be get that

$$f_m(\mathrm{d}\Delta u_k, \lambda_k) = f_m^0 + \frac{\partial f_m}{\partial p_{ci}} D_{cij} T_{jk} \mathrm{d}\Delta u_k + \frac{\partial f_m}{\partial p_{ci}} D_{cij} \delta_{cj} - \frac{\partial f_m}{\partial p_{ci}} D_{cij} \frac{\partial g_k}{\partial p_{ci}} \mathrm{d}\lambda_k \tag{14}$$

where $d\Delta u_k$ is incremental relative displacement in global coordinate system, T_{jk} is transfer tensor from global coordinate system to local coordinate system, and f_m^0 is the value of yield function just before load increment is acting.

After finite element discretization, substitution of Eq. (14) into Eqs. (10) yields

$$\left.\begin{aligned} &\boldsymbol{W}\mathrm{d}\boldsymbol{u}-\boldsymbol{M}\mathrm{d}\boldsymbol{\lambda}+\boldsymbol{d}+\boldsymbol{v}=0\\ &\boldsymbol{v}^{\mathrm{T}}\mathrm{d}\boldsymbol{\lambda}=0 \quad \boldsymbol{v},\ \mathrm{d}\boldsymbol{\lambda}\geq 0 \end{aligned}\right\} \tag{15}$$

In which,

$$\boldsymbol{W}=\sum_{e=1}^{N_{EC}}\boldsymbol{C}_{\lambda}^{e\mathrm{T}}\left(\int_{S_c^e}\left(\frac{\partial f}{\partial p_c}\right)^{\mathrm{T}}\boldsymbol{D}_c\boldsymbol{T}\boldsymbol{N}_c\mathrm{d}S\right)\boldsymbol{C}_u^e,$$

$$\boldsymbol{M}=\sum_{e=1}^{N_{EC}}\boldsymbol{C}_{\lambda}^{e\mathrm{T}}\left(\int_{S_c^e}\left(\frac{\partial f}{\partial p_c}\right)^{\mathrm{T}}\boldsymbol{D}_c\frac{\partial g}{\partial p_c}\mathrm{d}S\right)\boldsymbol{C}_{\lambda}^e,$$

$$\boldsymbol{d}=\sum_{e=1}^{N_{EC}}\boldsymbol{C}_{\lambda}^{e\mathrm{T}}\int_{S_c^e}\left(\boldsymbol{f}^{0e}-\left(\frac{\partial f}{\partial p_c}\right)^{\mathrm{T}}\boldsymbol{D}_c\boldsymbol{N}_{\delta}\boldsymbol{\delta}_c^e\right)\mathrm{d}S$$

Substituting d$\boldsymbol{u}$ solved from Eqs. (12) into Eqs. (15), we obtain the complementary equation

$$\left.\begin{aligned} &\boldsymbol{v}-\boldsymbol{\Phi}\mathrm{d}\boldsymbol{\lambda}=\mathrm{d}\boldsymbol{q}\\ &\boldsymbol{v}^{\mathrm{T}}\mathrm{d}\boldsymbol{\lambda}=0 \quad \boldsymbol{v},\ \mathrm{d}\boldsymbol{\lambda}\geq 0 \end{aligned}\right\} \tag{16}$$

where $\boldsymbol{\Phi}=\boldsymbol{M}-\boldsymbol{W}\boldsymbol{K}^{-1}\boldsymbol{H}$ and $\mathrm{d}\boldsymbol{q}=-\boldsymbol{d}-\mathbf{W}\mathbf{K}^{-1}\,\mathrm{d}\boldsymbol{P}$ are related to state before load increment acts. So, Eq. (16) is a standard linear complementary problem (LCP), which can be solved with Lemke algorithm.

4 EXAMPLES AND DISCUSSIONS

The proposed model translates the contact non-linearity in jointed dams into a linear complementary problem. The complicated iteration process in "trial-error" method is avoided, and the scale of LCP Eqs. (16) is $2\times N_{EC}$, which is much less than that of governing equations in "trial-error" method. So, the model presented in this work is efficiently. In this section, a simple example is given to demonstrate the precision of the proposed method, and examine the sensitivity of results to penalty coefficients. Then, the model is used to analysis the influence of contraction joints on behavior of arch dams.

4.1 *A flat punch on elastic foundation*

A flat punch pressed on an elastic foundation. The thickness is 1mm, and other dimensions are shown in Figure 3. The Young's modulus of punch and foundation are E_1 and E_2 respectively, and Poisson's ratios are supposed to be zero. Considering the symmetric, only half structure is taken to analysis, and Figure 4 gives the FE mesh. In frictionless case, the normal contact stress distribution is shown in Figure 5. The results while E_1/E_2=100 are in good agreement with Hertz solution of rigid flat punch on elastic foundation.

To discuss the influence of penalty coefficients, it is assumed that $E_1=E_2=E=2\times10^5$MPa, μ=0.0, p=60MPa and $E_n=E_{\tau_1}=E_{\tau_2}=10^kE$. The normal contact stresses at x=1.25mm with different k are shown in Table 1. The numerical result is convergent while k=3, and even if k=0, the relative error is only 4.36%.

4.2 *Influence of contraction joints on behavior of arch dams*

In this section, the model proposed in the present paper is used to analysis the influence of contraction joints on behavior of arch dams. The results and discussions are for Xiaowan arch dam

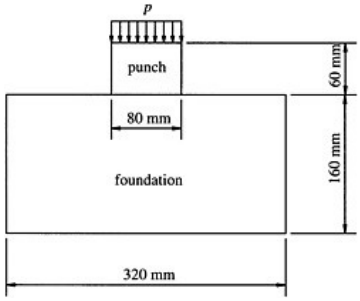

Figure 3. A flat punch on elastic foundation.

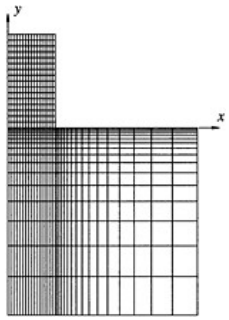

Figure 4. FE Mesh.

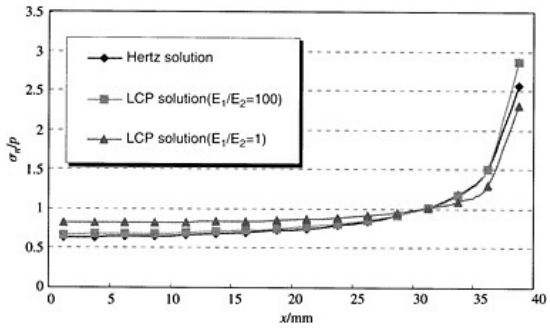

Figure 5. Normal contact stress distribution.

Table 1. Normal contact stress with different k.

k	0	1	2	3	4	
σ_n (MPa)		51.26	49.87	49.22	49.12	49.12
Relative error (%)		4.36	1.53	0.20	0.00	0.00

located on Lancangjiang river in Yunnan province, PR China. The dam is a 292m high double curvature parabolic type arch dam with 43 contraction joints. It is the highest arch dam in the world.

In FE model, all joints are simulated, and the dam and foundation are divided into 20424 elements with 25087 nodes, in which the number of joint element is 3108. Figure 6 shows the FE mesh for Xiaowan arch dam.

Table 2 gives six calculation schemes. In scheme 0, the dam is treated as an integral structure, i.e., there is no joint in dam after grouting. In scheme 1 to 5, joints are assumed to have different gaps after grouting. The loads are applied step by step. First, dam deadweight is considered, then joints are grouted and hydraulic pressure takes into action, and temperature fall loaded at last. Dam and foundation are assumed to be elastic, and material constants are shown in Table 3. Contraction joints are supposed no tensile with Coulomb's factor μ=1.0 and cohesion c_0=0.8MPa. The penalty coefficients $E_n = E_{\tau_1} = E_{\tau_2} = 10^3$, where E is Young's modulus of dam.

Most results are listed in Table 4, and the contours of first principal stress on upstream surface are shown in Figure 7. The contours are almost symmetric in every scheme, and the distributing law of dam stress is affected little by contraction joints. In scheme no. 0 and scheme no. 1, the

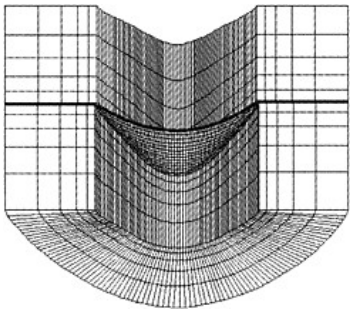

Figure 6. FE Mesh for Xiaowan arch dam.

Table 2. Initial gap considered in each calculation scheme.

Scheme	0	1	2	3	4	5
Initial gap/mm	No joint	0.0	0.5	1.0	1.5	2.0

Table 3. Material constants of dam concrete and foundation rock.

	Young's modulus E (GPa)	Poisson's ratio v	Unit weight pg (kN/m^3)	Thermal expansion coefficient α (1/°C)
Dam concrete	21	0.167	24	0.86×10^{-5}
Foundation rock	22	0.18	/	/

Table 4. Results of each calculation scheme.

Scheme	Stress on upstream surface/MPa				Stress on downstream surface/MPa			Maximum displacement along river/cm
	σ_{1max}	σ_{ymax}	σ_{ymin}	σ_{3min}	σ_{xmin}	σ_{ymin}	σ_{3min}	
0	9.38	6.11	−2.75	−7.49	−6.55	−13.92	−21.42	17.6
1	9.38	6.11	−2.75	−7.49	−6.55	−13.92	−21.42	17.6
2	10.54	7.21	−2.69	−7.57	−6.40	−14.35	−22.03	19.2
3	11.72	8.31	−2.64	−7.66	−6.25	−14.78	−22.64	20.7
4	12.90	9.41	−2.58	−7.76	−6.11	−15.20	−23.25	22.2
5	14.13	10.51	−2.53	−7.86	−5.96	−15.63	−23.86	23.7

maximum stresses are in very good agreement, i.e., if there are no initial gaps, contraction joints has little influence to dam stress. It is because temperature load is on the small side of loads borne by Xiaowan arch dam, and hydraulic pressure is the main load. The dam is pressed mostly in ring direction, only abutment of top arch, which is far away from where maximum stress occurred, has some tensile stress, and the re-distribution of these stress is in local after contraction joints opened. But, it should be noticed that if initial gaps exist, contraction joints would affect the maximum displacement and stress significantly. With the initial gaps increasing from 0.0 to 2.0mm, the maximum displacement along river increases from 17.6cm to 23.7cm, the maximum tensile principal stress increases from 9.38MPa to 14.13MPa, and the maximm pressure principal stress increases from −21.42MPa to −23.86MPa. The main reason is that initial gaps of joints destroyed the integrity of arch dam; the hydraulic pressure is endured by cantilever beam first, and the arch partakes of the load only after the deformation of beam encloses joints. So, the larger the

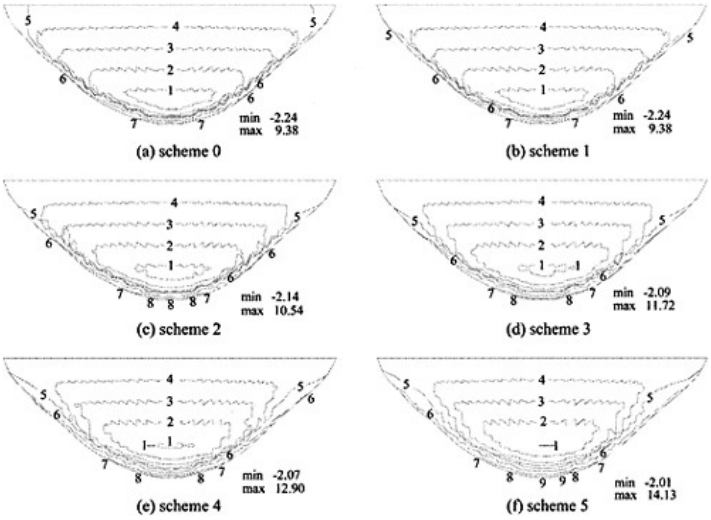

Figure 7. The first principal stresses on upstream surface (MPa)

1=−2.0; 2=−1.5; 3=−1.0; 4=−0.5; 5=0.0; 6=−2.0; 7=−6.0; 8=10.0; 9=14.0.

initial gaps are, the larger the deformation of cantilever beam occurred before arch takes into action is, and it causes the enlarging of beam stress.

5 CONCLUSIONS

In the present paper, an incremental constitutive model of joints is established with the use of penalty coefficient, and a complementary virtual work equation is deduced. Based on the finite element method, a linear complementary model for joint is proposed. The model avoids iteration, reduces the scale of problem and improves computing efficiency. Numerical example shows the model is insensitive to penalty coefficient. The application of the model to Xiaowan arch dam indicates that the initial gaps of contractive joints affect dam's behavior significantly, and if there is no initial gap, the joints have little affect to the stress and displacement of Xiaowan arch dam.

REFERENCES

Dowling MJ, Hall JF. Nonlinear seismic analysis of arch dams. J Engng Mech ASCE, 1989,115(4):768−789.

O'Connor JPF. The modeling of cracks, potential crack surfaces and construction joints in arch dams by curved surface interface element. In: Proc of 15th ICOLD, Lausanne, Switzerland, 1985. 389−406.

Fenves GL, Mojtahedi S. Earthquake response of an arch dam with construction joint opening. Dam Engineering, 1993, 4(2):63~89.

Ahmadi MT, Izadinia M, Bachmann H. A discrete crack joint model for nonlinear dynamic analysis of concrete arch dam. Comput & Struct, 2001, 79:403~420.

Zhu Bo-fang. Joint element with keys and the influence of joint on stresses in concrete dam. J Hydrau Engng. 2001(2):1~7.

Li Tongchun, Xia Songyou. Substructure method under mixed coordinate system for contact-friction problems with applications to arch dams. In: Practice and theory of arch dams—Proc of the int symp on arch dams, Nanjin, China, 1992, 257~264.

New Developments in Dam Engineering—Wieland, Ren & Tan (eds),

Dynamic analysis of El Infiernillo rockfill dam

S.Suppiah
Department of Civil Engineering, Periyar Maniammai College of Technology for Women, Vallam, Thanjavur, Tamil Nadu, India

ABSTRACT: The frequent occurrences of destructive earthquakes in the recent past years at various places, such as, Uttarkashi (India, 1991), Latur (India, 1993), Bhuj (India, 2001) and other places all over the world causing irreparable damage or total collapse to earth and rockfill dams have demonstrated the importance of protection of these structures against future earthquakes. Many rockfill dams of height of the order of more than 250m have been constructed at different locations (Nurek dam Russia; Tehri dam India), which lie in the regions of moderate to strong seismicity. These high dams warrant the simulation of nonlinear stress-strain characteristics of different materials as precisely as possible to the actual conditions during earthquakes.

In the present study, an earth and rockfill dam of height 146m (from the base) has been investigated for its dynamic behaviour. Interestingly, this dam has experienced an earthquake with a peak ground acceleration value of 0.25g (g: acceleration due to gravity) during its lifetime. The dam section has been idealized into 8-noded isoparametric elements. The nonlinear stress-strain characteristics of various materials constituting the dam section have been simulated using the Ramberg-Osgood (R-O) model. The dynamic response obtained using the R-O model has been compared with the results obtained through the very widely used Seed-Idriss (S-I) method of analysis. In all the cases, the seismogram recorded during the Taft earthquake (1952), and normalized to a peak ground acceleration of 0.25g has been adopted as the input motion.

1 INTRODUCTION

The frequent occurrences of destructive earthquakes in recent years, at various places, for instance, Bhuj (India, 2001); Latur (India, 1993); Uttarkashi (India, 1991), and other places all over the world causing irreparable damage or total collapse to rockfill dams have demonstrated the importance of protecting these structures against earthquakes. Many rockfill dams of height more than 250m have been constructed at different locations (Nurek dam, height=330m, Russia; Tehri dam, height=265m, India) lying in the regions of moderate to very strong seismicity.

In the present investigation, El Infiernillo rockfill dam of 146m, height from the base [1] has been evaluated for its dynamic response using a special purpose computer coding, FEADYNS. The dam section has been idealized using 8-noded isoparametric elements. The seismogram corresponding to the Kern County earthquake recorded at Taft (in 1952) with a peak ground acceleration of 0.25 g has been adopted as the input motion. Newmark ‘β’ method of time integration has been used to evaluate the dynamic response. The strain-dependent shear moduli and damping characteristics of the different materials constituting the dam have been simulated using the Ramberg-Osgood (R-O) model [2] and the widely used Seed-Idriss (S-I) method [3]. Prior to the dynamic analysis, the static stresses of the dam under saturated conditions have been evaluated using a computer coding FEADAM8 which incorporates the hyperbolic model as described by Duncan et al. [4]. The static stresses have been used as the initial condition for the subsequent dynamic response evaluation.

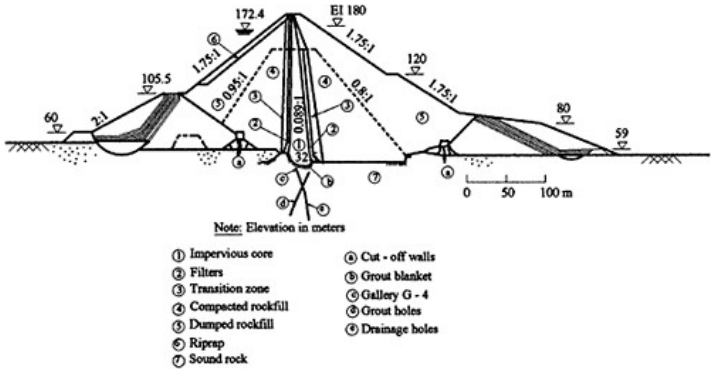

Figure 1. Maximum section of El Infiernillo dam [6].

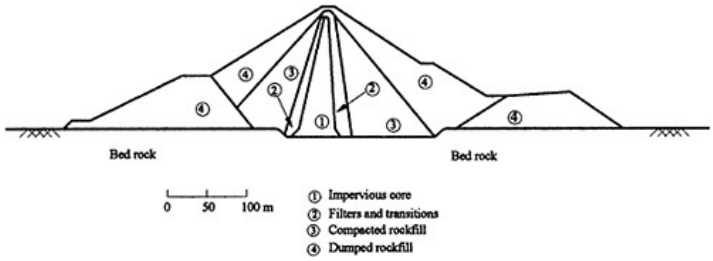

Figure 2. Idealized maximum section of El Infiernillo dam [5].

Interestingly, the El Infiernillo dam had experienced the ground motion on March 14, 1979, during the Mexico earthquake with a peak ground acceleration of 0.25g [5]. The recorded values of acceleration and displacement during this earthquake have been compared with the dynamic response values computed using the S-I method and the R-O model. In the static and dynamic study cases, only two-dimensional analyses have been considered.

2 DESCRIPTION OF THE ROCKFILL DAM

The El Infiernillo dam is located on the Balsas River (in Mexico) and has a maximum height of 146m above the foundation rock. The dam is a slender embankment with an average slope of 1.8:1 in the upstream and the downstream, and a symmetrical thin core with 0.089:1 slope. The width of the core corresponds to only 22 percent of the hydraulic head [6]. The maximum and the idealized sections of this dam are shown in Figs. 1 and 2 respectively.

3 MATERIAL PROPERTIES

The different material properties used in the static analysis are shown in Table 1. These properties have been adopted from ref. [5].

Table 1. Material properties used in the static analysis [5].

Material		Unit weight (kN/m^3)			
No. (1)	Identification (2)	Dry (3)	Saturated (4)	Cohesion (kN/m^2) (6)	ϕ (deg) (6)
1	Clay core	15.8	20.0	30	0
2	Filter	18.7	21.9	0	35
3	Compacted rockfill	18.5	21.6	0	45
4	Dumped rockfill	17.6	21.0	0	45

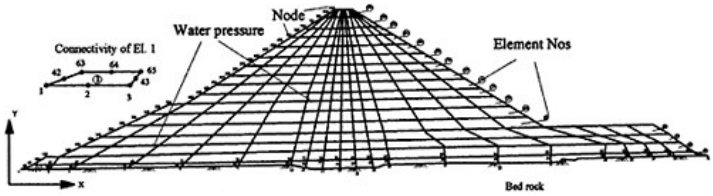

Figure 3. Finite element idealization of El Infiernillo dam.

4 FINITE ELEMENT DISCRETIZATION

The maximum section of the rockfill dam has been discretized into 17 layers, resulting in a total of 263 eight-noded isoparameteric elements and 864 nodes. The effective number of degrees of freedom was 1646 in the plane strain ($\epsilon_z = 0$) case of analysis. The finite element discretization is shown in Fig. 3.

5 STATIC ANALYSIS

The static (or pre-earthquake) stresses induced in the dam have been evaluated based on the hyperbolic model as adopted by Duncan et al. [4]. The nonlinear behaviour of the different soils has been simulated, considering the volume change characteristics and accounting for sequential construction. The shell and filter materials below the full reservoir level have been considered as submerged and the clay core below the phreatic line to be saturated. The materials lying above the maximum water level have been considered as moist. The downstream materials have been taken to be dry. The water pressure has been applied vertically along the top surface of the bedrock and normal to the upstream face of the core (Fig. 3). The static stresses computed for this case have been applied as the initial condition for the subsequent dynamic analysis.

6 DYNAMIC ANALYSIS

6.1 *Seed-Idriss method*

The mesh discretization generated for the static analysis that is shown in Fig. 3 has been adopted for the dynamic analysis as well. In the dynamic case the numbering of the nodes has been started from the crest and completed at the base of the dam. However, in the static case, the numbering was done beginning from the base and completed at the crest of the dam. The dynamic properties of various materials constituting the dam are shown in Table 2 and have been adopted from ref. [6]. These values have been used for estimating the low-amplitude shear modulus and the corresponding

Table 2. Material properties used in the dynamic analysis [6].

Material No. (1)	Identification (2)	Poisson's Ratio 'μ' (3)	S_u(kN/m^2) (4)	K_2(at $\gamma=10^{-6}$%) (5)	G/S_u (6)
1	Clay core	0.49	55.0–90.0	–	2150–2640
2	Filter	0.33	–	150	–
3	Compacted rockfill	0.33	–	150	–
4	Dumped rockfill	0.33	–	150	–

Note: S_u–undrained strength; K_2–a constant; G/S_u–normalized value of shear modulus.

Table 3. Modulus reduction factors for dynamic properties [3].

Effective shear strain Y_{eff}(%) (1)		Shear modulus reduction factor		Fraction of critical damping (%)	
	Log(Y_{eff}) (2)	Clay (3)	Sand (4)	Clay (5)	Sand (6)
≤1.00×10^{-4}	−4.0	1.000	1.000	2.50	0.50
3.16×10^{-4}	−3.5	0.913	0.984	2.50	0.80
1.00×10^{-3}	−3.0	0.761	0.934	2.50	1.70
3.16×10^{-3}	−2.5	0.565	0.826	3.50	3.20
1.00×10^{-2}	−2.0	0.400	0.656	4.75	5.60
3.16×10^{-2}	−1.5	0.261	0.443	6.50	10.00
1.00×10^{-1}	−1.0	0.152	0.256	9.25	15.50
0.316	−0.5	0.076	0.115	13.80	21.00
1.00	0.0	0.037	0.049	20.00	24.60
3.16	0.5	0.013	0.049	26.00	24.60
≥1.00×10	1.0	0.004	0.049	29.00	24.60

damping values, as suggested by Seed and Idriss [3]. The digitized values of modulus reduction factors and damping values used in the Seed-Idriss method of analysis are shown in Table 3.

6.2 *Ramberg-Osgood model*

The different dynamic properties given in Table 2 have been used for estimating the low-amplitude shear moduli and damping at shear strain (Y)≤10^{-4} percent only. At other values of shear strain (Y>10^{-4} percent) the shear moduli are estimated as given by streeter et al. [7] and expressed by Eq. 1.

$$\frac{G}{G_{max}} = \frac{1}{1+\alpha\left|\frac{G\ \gamma}{C_1\ G_{max}\ \gamma_r}\right|^{R-1}} \tag{1}$$

where

G/G_{max} the modulus reduction factor (the unknown quantity)

C_1 a factor relating the maximum shear stress and yield shear stress and taken as unity (=1.0)

α and R Ramberg-Osgood model constants

Table 4. R-O model constants for different types of materials [10].

Sl. no. (1)	Material in the dam section (2)	R-O model constants	
		α (3)	R (4)
1	Impervious core	249	2.50
2	Filter	288	3.10
3	Rockfill	105	2.10

Y shear strain (the known quantity)

Y_r reference strain and given by:

$$Y_r=\tau_m/G_{max} \quad (2)$$

in which

G_{max} low-amplitude shear moduli

τ_m maximum shear strength and given by Hara et al. [8]:

$$\tau_m = \frac{1 + K_0}{2\,\sigma'_v \sin\phi + C\cos\phi} \quad (3)$$

where

K_0 coefficient of earth pressure at rest

σ'_v effective overburden pressure

ϕ angle of internal friction

C cohesion

The coefficient of earth pressure at rest is given by:

$$K_0=\mu/(1-\mu) \quad (4)$$

in which

μ is the Poisson's ratio (from Table 2).

6.2.1 *Evaluation of Ramberg-Osgood model constants*

The dimensionless parameters in the Ramberg-Osgood model namely, α and R have been evaluated using a first order least-squares curve fitting algorithm as proposed by Jennings [9]. The different values of shear modulus and the corresponding shear strain are the input data to this algorithm. The values of a and R evaluated for different material constituting the dam are presented in Table 4 [10]. In the dynamic analysis these constants have been used as input data to evaluate the strain-dependent shear moduli in a functional form.

6.2.2 *Damping values*

In the R-O model, the damping values for materials as a function of strain have been computed using the following expression [11].

$$D=(2/\pi)\times\{(R-1)/(R+1)\}\times(1-G/G_{max}) \quad (5)$$

where

D damping; and other parameters remain as defined earlier.

Eq. 5 has been used to compute the various values of damping in a functional form, at different levels of shear strain for the different soils constituting the dam. The subsequent dynamic analysis was identical to the procedure followed in the Seed-Idriss method of evaluation.

Table 5. Computed values of acceleration at a few nodes using S-I method and R-O model.

Node (1)	Coordinate (m)		Computed acceleration in 'g'		Location/Remarks (6)
	X (2)	Y (3)	S-I method (4)	R-O model (5)	
1	283.0	146.0	0.52	0.29	Along the crest at upstream
15	290.0	146.0	0.51	0.29	Crest (along the axis)
29	297.0	146.0	0.55	0.30	Along the crest at downstream
37	291.5	142.8	0.58	0.35	Axis, below the crest *(maximum value)*
206	224.0	109.8	0.19	0.13	0.75 H from the base at upstream
213	288.9	109.8	0.24	0.15	0.75 H from the base along the axis
220	352.8	109.8	0.20	0.13	0.75 H from the base at downstream
382	171.7	75.8	0.27	0.18	0.50 H from the base at upstream
389	287.9	75.8	0.22	0.14	0.50 H from the base along the axis
396	402.4	75.8	0.27	0.18	0.50H from the base at downstream
566	82.7	38.0	0.32	0.24	0.25 H from the base at upstream
574	286.9	38.0	0.19	0.15	0.25 H from the base along the axis
581	461.8	38.0	0.30	0.21	0.25 H from the base at downstream
803	6.3	4.0	0.25	0.25	Toe at upstream
812	285.6	4.0	0.15	0.15	Axis at the bottom
823	613.8	4.0	0.25	0.25	Toe at downstream

Note: H is the height of the dam from the base.

6.3 *Input motion*

The Taft earthquake record, digitized at 0.02 seconds with a peak ground acceleration 0.25g (g is the acceleration due to gravity) has been used as the input motion for evaluating the dynamic response of the dam. The Newmark's time integration technique [12] has been adopted as the solver.

7 RESULTS AND DISCUSSION

7.1 *Acceleration*

The acceleration values computed using the S-I method and R-O model at a few pre-determined locations (nodes) are displayed in Table 5.

From Table 5, it can be noticed that deamplification has occurred in both the methods of analysis and it is to a greater extent in the R-O model. The computed values of acceleration at the crest of the dam are little more than twice the peak ground acceleration (=0.25g) value at the base of the dam using the S-I method. The R-O model does not predict such higher value of acceleration. However, both the methods yield the maximum value of computed acceleration at the same location lying just below the crest. This type of deamplification phenomenon has been reported in the analysis of Port Peck Dam elsewhere [13].

7.2 *Displacement*

The displacement values computed at a few locations, based on the S-I method and the R-O model are shown in Fig. 4. The deformed shape of the dam is also displayed in the same figure.

From the displacement values computed at a few locations, the values yielded by S-I method are lower than that the values obtained using R-O model. However, the maximum value of displacement computed by both the methods is noticed at the crest of the dam. This value is 11.12 cm using the S-I method and 13.13 cm by R-O model.

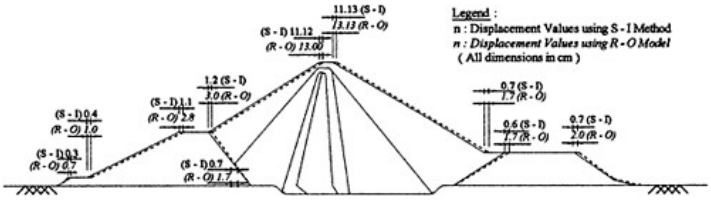

Figure 4. Displacement values computed using S-I method and R-O model.

Table 6. Computed values of shear strain at a few elements using S-I method and R-O model.

			Shear strain (%)				
	Coordinate* (m)			Dynamic		Total	
Element (1)	X (2)	Y (3)	Static (4)	S-I method (5)	R-O model (6)	(7)=(4)+(5)	(8)=(4)+(6)
12	322.1	4.0	2.376	0.041	0.055	2.417	2.431
13	354.0	4.0	1.277	0.016	0.050	1.293	1.327
84	257.8	38.0	1.346	0.044	0.065	1.390	1.411
93	444.6	38.0	1.264	0.020	0.046	1.284	1.310
142	266.6	75.7	2.144	0.052	0.072	2.196	2.216
151	391.4	75.7	0.873	0.065	0.120	0.938	0.993
201	291.1	109.7	0.306	1.138	1.680	1.444	1.986
207	346.8	109.7	0.485	0.082	0.153	0.567	0.638
241	286.4	135.7	0.844	1.699	2.223	2.543	3.067
242	288.5	135.7	0.677	2.170	2.435	2.847	3.112
243	290.7	135.7	1.328	1.378	2.406	2.706	3.734
244	292.9	135.7	0.520	1.658	2.180	2.178	2.700
257	290.6	142.2	0.176	1.548	1.070	1.724	1.246

* Coordinates correspond to the centre of the element.

7.3 *Shear strain*

The maximum values of shear strain computed at a few elements (at the centre of each element), using the S-I method and the R-O model are presented in Table 6. In the same table the shear strain values obtained in the static analysis and the total strain values (static+dynamic) are also presented.

From Table 6 it can be seen that the maximum values of dynamic shear strain is of the order of 2.17 percent by S-I method and 2.43 percent using the R-O model. Interestingly, these maxima are achieved at the same location, namely the centre of Element 242. Adopting a 5 percent shear strain as the failure criterion, the El Infiernillo dam is safe against the input motion with a peak ground acceleration of 0.25g.

7.4 *Comparison with the recorded values of acceleration and displacement*

An earthquake struck the El Infiernillo dam on March 14, 1979 [6]. The recorded values of acceleration and displacement during this earthquake are compared with that of the values computed in the present analysis using the S-I method and R-O model. These are shown in Table 7, in which that the values obtained using the R-O model are in very close agreement with that of the recorded values. The maximum value of acceleration yielded by S-I method is very high and the displacement computed is closer to the recorded value. The possible reason could be that the S-I method uses

Table 7. Comparison of computed and recorded values.

Sl. no. (1)	Parameter (2)	Method of analysis		Recorded values (5)	Reference (6)
		S-I method (3)	R-O model (4)		
1	Acceleration (g)	0.58	0.35	0.36	Moreno [6]
2	Displacement (cm)	11.12	13.13	13.00	Moreno [6]

the strain-dependent dynamic properties in a non-functional form whereas, in the R-O model, the dynamic properties are available in a functional form.

8 CONCLUSION

Based on the dynamic analysis performed on the well instrumented El Infiernillo dam the following conclusions are arrived at:

1. The S-I method yields excessively high values of acceleration and lower values of displacement in comparison with the recorded values during the March 14, 1979, Mexican earthquake.
2. The R-O model yields response values that are very close to the recorded values of acceleration and displacement.
3. More dynamic response evaluation should be performed using the R-O model.

REFERENCES

[1] Marsal, R.J. and Ramirez L.A., "Performance of El Infiernillo Dam: 1963–1966" *Journal, Soil Mechanics andFoundations Division,* ASCE, 1967, Vol. 93, No. SM4, pp. 265–298.

[2] Ramberg, W. and Osgood, W.T, "Description of Stress-Strain Curves by Three Parameters", *Technical Note 902,* National Advisory Committee on Aeronautics, Washington, D.C., 1943.

[3] Seed, H.B. and Idriss, I.M., "Soil Moduli and Damping Factors for Dynamic Response Analysis", *Report No. EERC: 70–10,* Earthquake Engineering Research Centre, University of California, Berkeley, USA, 1970.

[4] Duncan, J.M, Byrne, P., Wong, K.S. and Mabry, P, "Strength, Stress-Strain and Bulk Modulus Parameters for Finite Element Analysis of Stresses and Movements in Soil Masses", *Geotechnical Engineering Research Report No. UCB/GT/80-OL,* College of Engineering, Office of Research Services, University of California, Berkeley, 1980.

[5] Romo, M.P, Ayala, G., Resendiz, D. and Diaz, C.R., "Response Analysis of El Infiernillo and La Villita Dams", *Centro Editorial de la Commission Federal de Electricidad,* Rodano, Mexico, 1980, pp. 87–108.

[6] Moreno, E., "Description of El Infiernillo and La Villita Dams", *Centro Editorial de la Commission Federal de Electricidad,* Rodano, Mexico, 1980, pp. 1–15.

[7] Streeter, V.L., Wylie, E.B. and Richart, F.E., Jr., "Soil Motion Computations by Characteristic Method", *Journal, Geotechnical Engineering Division,* ASCE, 1974, Vol. 100, GT3, pp. 247–263.

[8] Hara, A., Ohta, T., Niwa, M., Tanaka, S. and Banno, T, "Shear Modulus and Shear Strength of Cohesive Soils", *Soils and Foundations,* Japanese Society of Soil Mechanics and Foundation Engineering, 1974, Vol. 14, No. 3, pp. 1–12.

[9] Jennings, P.C., "Periodic Response of a General Yielding Structure", *Journal of the Engineering Mechanics Division,* ASCE, 1964, Vol. 90, No. EM2, Proc. Paper 3871, pp. 131–166.

[10] Suppiah, S., "Static and Dynamic Analysis of Earth and Rockfill Dams", *Doctoral Dissertation, submitted to* University of Roorkee, Roorkee, Uttaranchal, India, 1990, 474p.

[11] Ishihara, K., "Evaluation of Soil Properties for Use in Earthquake Response Analysis", *lecture Notes,* distributed at the University of Tokyo, Japan, 1982, pp. 1–56.

[12] Newmark, N.M, "A Method of Computation for Structural Dynamics", *Proceedings, Journal Engineering Mechanics Division,* ASCE, 1959, Vol. 85, pp. 67–94.

[13] Marcuson, W.F, III and Krinitzsky, E.L., "Dynamic Analysis of Fort Peck Dam", *A Report submitted to Waterways Experiment Station,* Vicksburg, 1976, USA.

New Developments in Dam Engineering—Wieland, Ren & Tan (eds),
© 2004 Taylor & Francis Group, London, ISBN 04 1536 240 7

Stability analysis for hydraulic hoist cylinder of shiplock miter gate

Yishou Tao
Changjiang River Scientiflc Research Institute, China

Wenwei Wei
Changjiang Investigation, Planning and Design Research Institute, China

ABSTRACT: The hydraulic hoist cylinders of shiplock miter gate are usually slender and of large scale, and are placed horizontally. Their deflection calculation and stability analysis is important in engineering design. In this paper based on a stepped bar buckling model, an analytic method for calculating the deflection and buckling load of the cylinder has been obtained by establishing and solving the buckling equations. Comparison between calculation and check test result shows that this method has reached a high level in calculating accuracy. Unfavoured influence of deflection on stability of the cylinder is analysed, and "limit pressure" is suggested as a stability criteria for the cylinder with relatively large initial deflection. In addition, measures for reducing the initial deflection to enhance stability of the cylinder are discussed. It is proposed that in accordance with "deflection minimization" principle, structural and parameteric optimization would be made in design process to improve the operation reliability of the cylinder.

1 INTRODUCTION

Hydraulic cylinders are widely applied to various hoists of gates and valves in hydro-projects. The hydraulic hoist cylinders of shiplock miter gate are usually slender and of large scale, and placed horizontally. Because of their large slenderness ratio and horizontal location layout cylinders' large deflection may occur under the combined action of self weight and axial loads, resulting in further weakening of their stability. Therefore, close attention has been increasingly paid to the problem. For example, the hoist cylinder of miter gate at the Three Gorges Project's permanent navigation lock is extra-large scale and slender one, with its length of about 18m. Its operating reliability has direct influence on safe operation of the navigation lock, and its integrated stability is one of technical key questions of designers' interest.

At present, stability of a cylinder is usually measured by its buckling load. Buckling load is always calculated by using Eulerian formula for simplified prismatic buckling bar or some empirical formulas. However, calculations with the former gets lower accurate results, while the latter can not be used for some kinds of cylinder, especially those large ones, because of its limitation in selection of parameter value. Futhermore, the above-mentioned method can be used for deflection calculation which is a key point to be considered in design of stability for horizontal slender cylinder. In order to meet the needs of design and calculation of hydraulic hoist cylinder on miter gate of the TGP's navigation lock as well as other large hydraulic cylinder, this paper introduces an analytic method for calculating deflection and buckling load of a cylinder by setting up and solving the buckling differential equations. The method is developed on the basis of the stepped bar buckling model. The accuracy of the solution has been checked by model test results. After the influence of cylinder's deflection on its stability is analysed, relevent design principles are proposed, which are referable for cylinder design.

2 CALCULATION OF DEFLECTION AND BUCKLING LOAD FOR A CYLINDER

2.1 *Mechanical model*

The hydraulic cylinder is a composite construction, and its stressing state is similar to that of buckling bar. It has the poorest stability when extended fully. In the paper, the hydraulic cylinder is supposed to be a compressed stepped-bar corresponding to the barrel and the piston rod in fully extended length, and subjected to common action of self weight and axial pressure. See Figure 1 for its stressing and deflection mechanical model, axial pressures act on the two hing.

The mechanical model is set up on the basis of a hydraulic cylinder's common erection type with partial barrel projecting from the support. Thus, the calculation method developed on it can be used for analysing the stability of cylinder of all erection types. Isolation method can be used for stressing analysis on the projecting part of the cylinder and the part between two hinged supports. The projecting part can be analysed as cantilever beam, and the part between two hinged supports as a simply supported buckling stepped bar. Deflection of the cylinder is composed of the clearance deflection and the buckling deflection. The clearance deflection is caused by the clearance between the piston and the inside wall of barrel. Clearance deflection deviates the center line of the cylinder from the axial load acting lines, resulting in the bending moment caused by axial load and consequently buckling deflection.

2.2 *Buckling equation and its solution*

For the part between two hinged supports of the hydraulic cylinder, with assumed conditions of slight deformation and linear elasticity, the buckling deflection caused by the initial deformation, self weight and axial load can be described by the following differential equation:

$$\begin{cases} EI_1 \dfrac{d^2 y_{10}}{dx_1^2} + py_{10} = -\dfrac{1}{2} q_1 x_1^2 + R_1 x_1 - P\delta_1 - m \\ EI_2 \dfrac{d^2 y_{20}}{dx_2^2} + py_{20} = -\dfrac{1}{2} q_2 x_2^2 + R_2 x_2 - P\delta_2 \end{cases} \tag{1}$$

the general solution of equation (1) are:

$$\begin{cases} y_{10} = a_{11}\cos(k_1 x_1) + a_{12}\sin(k_1 x_1) + Y_1 \\ y_{20} = a_{21}\cos(k_2 x_2) + a_{22}\sin(k_2 x_2) + Y_2 \end{cases} \tag{2}$$

where:

$$k_1 = \sqrt{\frac{P}{EI_1}} \quad k_2 = \sqrt{\frac{P}{EI_2}}$$

y_1, y_2 are the spesial solution.

a_{11}, a_{12}, a_{21}, a_{22} are undetermined coefficients, they can be defined by substituting the boundary conditions into equation (2).

By substituting the boundary conditions into equation (2), we have

$$\mathbf{\Delta A = B} \tag{3}$$

where

$$\Delta = \begin{bmatrix} 1 & 0 & 0 & 0 \\ 0 & 0 & 1 & 0 \\ \cos(k_1 L_1) & \sin(k_1 L_1) & -\cos(k_2 L_2) & -\sin(k_2 L_2) \\ -k_1 \sin(k_1 L_1) & k_1 \cos(k_1 L_1) & -k_2 \sin(k_2 L_2) & k_2 \cos(k_2 L_2) \end{bmatrix}$$

$A = \{a_{11}, a_{12}, a_{21}, a_{22}\}^T$ $\quad B$ — constants

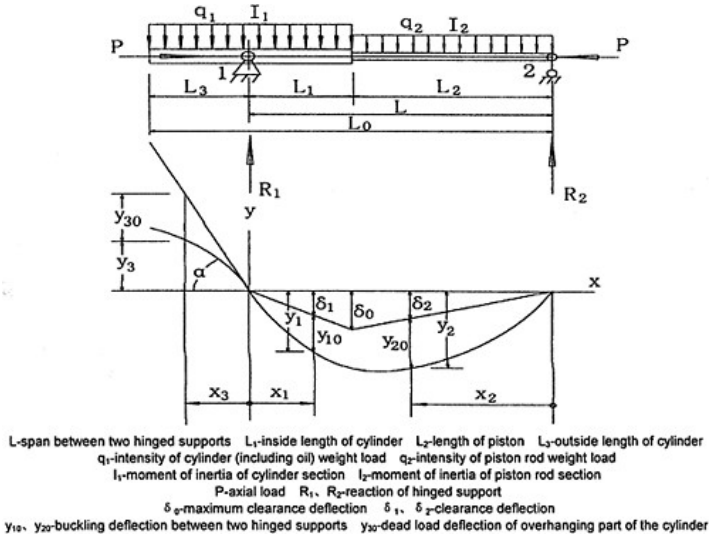

L-span between two hinged supports L_1-inside length of cylinder L_2-length of piston L_3-outside length of cylinder
q_1-intensity of cylinder (including oil) weight load q_2-intensity of piston rod weight load
I_1-moment of inertia of cylinder section I_2-moment of inertia of piston rod section
P-axial load R_1、R_2-reaction of hinged support
δ_0-maximum clearance deflection δ_1、δ_2-clearance deflection
y_{10}、y_{20}-buckling deflection between two hinged supports y_{30}-dead load deflection of overhanging part of the cylinder

Figure 1. Stressing and deflection of the cylinder.

Equations (3) are simultaneously solved, and then, substituting the resulting solutions back into equation (2), we can obtain the formulas for calculating the buckling deflection of the hydraulic cylinder.

2.3 *Total deflection calculation*

Expression (4) is the formulas for calculating total deflection of the cylinder. The formulas are expressed respectively by local coordinate systems showing in Figure 1. The deflection of the part between two hinged supports of the cylinder is composed of the clearance deflection and the buckling deflection; deflection of the overhanging of the cylinder is composed of the deflection caused by angle displacement at the hinged support 1 and the deflection caused by loads acting on the overhanging part.

$$\begin{cases} y_1 = y_{10} + \delta_1 \\ y_2 = y_{20} + \delta_2 \\ y_3 = y_{30} + \alpha x_3 \end{cases} \tag{4}$$

2.4 *Buckling load calculation*

From equation (3), we have the characteristic equation of the cylinder $|\Delta|=0$. By expanding $|\Delta|$, we have

$$k_1 \cos(k_1 L_1) \sin(k_2 L_2) + k_2 \cos(k_2 L_2) \sin(k_1 L_1) = 0 \tag{5}$$

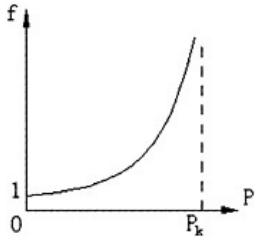

Figure 2. f-P curve.

Equation (5) is a transcendental equation in terms of axial load P. With known data E, I_1, I_2, L_1, L_2, from this equation, the buckling load P_k can be got.

2.5 *Discussion*

In equation (4), let $I_1=I_2=I$, $q_1=q_2=q$, $L_3=0$, $\delta_0=0$, x=L/2, the formula for calculating deflection could be simplified as the following:

$$y = -\frac{5qL^4}{384EI} \bullet \frac{12}{5u^4}\left(2\sec u - u^2 - 2\right) = y_0 \bullet f \qquad (6)$$

$$u = kL/2 = \frac{L}{2}\sqrt{\frac{P}{EI}}$$

Deflection y of the cylinder in equation (6) is composed of two factors the freebeam deflection (initial deflection) y_0 caused by evenly distributed gravity and coefficient f in relation to P. Figure 2 shows the f-P curve. In Figure 2, when P=0, f=1, $y=y_0$, only including freebeam deflection; when $P=P_k$, f→∞, y→∞ indicating the cylinder out of stability.

When the initial deflection of the cylinder $y_0=0$, no matter what the value of f is, deflection y will be zero all along. Only when P equals to the buckling load P_k, the cylinder will be out of stability. This is called the "1st type of failure by buckling".

As for the cylinder with initial deflection, coefficient f will take effect, and its value, consequently y, augments with the increase of P, after P exceeds certain value, y will augment rapidly in imitation of f-P curve. Finally, the cylinder will be out of stability when the axial load has not reached the buckling load level because of the extremely large deflection (elasto-plastic deformation caused by extremely large local bending stress). This is called the "2nd type of failure by buckling" or "extreme-value-points failure by buckling", and corresponding axial load is called P_u. Magnitude of P_u is in relation to the initial deflection of the cylinder. The greater the initial deflection, the smaller is P_u, and the poorer is the stability of the cylinder.

2.6 *Computer program*

Based on the above mentioned calculation method, the computer program CFD has be developed, see Figure 3 for its interface. Performing the program with Windows, and inputting basic parameters, one can immediately get the buckling load value, bending curve, location of the largest deflection as well as deflection and the maximum stress values therein. Since parameters can be changed arbitraril, and interactive computing can be made, the program is very convenient for scheme comparison and parameter optimization.

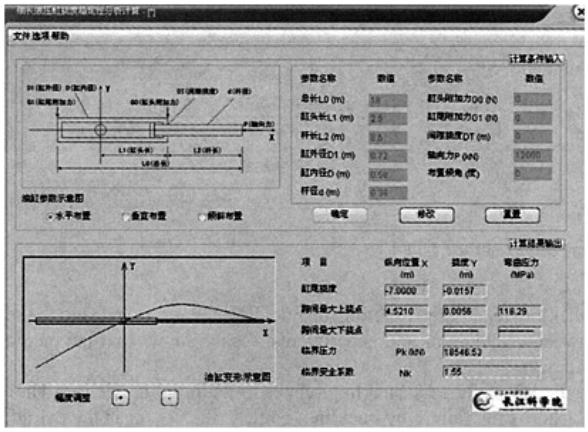

Figure 3. Interface of program.

Table 1. Main parameters of the cylinder.

Total cylinder length (m)	Span between two hinged support (m)	Outer barrel diameter (mm)	Inside barrel diameter (mm)	Piston rod diameter (mm)	Working load (kN)	Clearance between piston and barrel wall (mm)	Clearance between piston rod and guid housing (mm)
17.854	11.271	700	560	320	1280	0.32	0.20

Table 2. Calculation and test results.

	Initial deflection (mm)	Deflection increment (mm)	Buckling load (kN)
Calculated values	8.30	1.07	8,821
Test values	8.30	1.17	8,785

3 CALCULATION AND CHECK TEST

An actual calculation of the preliminary design schemes on the hydraulic hoist cylinder on miter gate of the TGP's permanent navigation lock is carried out by using the proposed analysis method. The corresponding check tests are also conducted. The comparsson between the calculations the model test results is made.

Table 1 shows the parameters of the cylinder. Calculation and test results showed in Table 2. Better agreement between calculations and test results proves the feasibility of deflection and stability analysis on the hydraulic cylinder by means of stepped-bar buckling model. The method has reached a high level in calculating accuracy.

4 CONCLUSION

In the paper, the horizontal slender hydraulic cylinder is considered as a stepped-bar with initial deflection bearing the axial load for its stability analysis. The formula for calculating the cylinder's

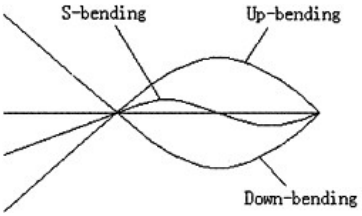

Figure 4. Bending patterns of the cylinder.

deflection and buckling load is get by setting up buckling equations and find the solutions of them. Comparison between calculations and experimental results shows that the method has reached a high level in accuracy.

The type of cylinder's failure by buckling relates to its initial deflection. The larger the initial deflection, the earlier is the failure by buckling, namely, the poorer is the cylinder's stability. On the contrary, reduction of initial deflection can cause the ultimate load P_u to increase and approach to the buckling load P_k, thus improve the stability of the cylinder. Large safety factors of stability (4~6) are often adopted in engineering practice. The buckling load P_k can be applied directly to the cylinder design, generally, without trouble, when the initial deflection is slight. However, if the initial deflection is rather large, especially for horizontal slender cylinder, initial deflection must be checked and controlled in the stability design.

The arrangement of hydraulic hoist cylinder on miter gate of navigation lock is usually of barrelend overhanging type. The cylinder's bending patterns are different because of the different structural parameters and overhanging situations. For the part between two hinged supports, the bending lines can be divided into three patterns: up-bending, down-bending and s-bending (Figure 4).

For the s-bending pattern, there is the smallest initial deflection, and the deflection increment is also very small, when subjected to axial load. Thus, such a cylinder has the best stability. Therefore, it is suggested that in cylinder design, according to "deflection minimization" principle, structure and parameters of the cylinder are optimized, achieving a s-bending to let the cylinder's stability approach that of an ideal centrally-compressed bar.

The proposed analytic method for calculating deflection and buckling load of the cylinder and the corresponding computer program are used in the TGP technical design and has achieved rather good effect.

REFERENCES

Guo Yinglong, Tao Yishou. Study on stability of hydraulic hoist cylinder on miter gate of TGP shiplock. China Mechanical Engineering, 1996. No. 7.
G.Schmausser, K.J.Pittner. Calculations involving Slender Cylinders. Mannesmann Rexroth, 1991. 12.
Wei Wenwei, Shi Bing, Fang Yang. Design of hydraulic hoist for TGP permanent shiplock's miter gates Yangtze River, 1998 Vol. 29 Supplementary issue.
Design specification of shiplocks (trial edition). Ministry of Communications, P.R. China, 1991.

New Developments in Dam Engineering—Wieland, Ren & Tan (eds),
© 2004 Taylor & Francis Group, London, ISBN 04 1536 240 7

The effect of crushing-type side wall on stress and deformation of concrete face rockfill dam

Tong Fuguo, Tian Bin & Chen Xiutong
College of Civil & Hydropower Engineering, Three Gorges Univ, Yichang, China

ABSTRACT: The concrete crushing-type side wall technology is a new method for constructing the upstream side-slope of concrete face rockfill dam. It helps to accelerate construction schedule and improve construction quality. Combining with the Shuibuya Project practice, this paper researches the effect of crushing-type side wall on stress and deformation of concrete face rockfill dam through three-dimensional nonlinear finite element calculation. Research proves that crushing-type side wall helps to improve stress and deformation of face slab, but it has a little effect on the stress and deformation of rockfill.

1 PREFACE

The concrete crushing-type side wall technology uses concrete haul formwork constructing technology in highway engineering for reference. Before each layer cushion material filled, make a semi-permeable continuous small concrete wall along design section by crushing-type side wall mechanism. After concrete solidification, fill dam cushion material inside according to design requirement, and then roll cushion material by vibratory roller. Repeat the above process, after this layer cushion material is rolled well. This technology overcomes such disadvantages in traditional construction method as the difficulty in assuring the compactness of cushion material on the slope, the complexity of the constructing process upstream slope face, cushion material filled overfull, the erosion of the slope face when unprotected for long time, and so on. Combining with the Shuibuya concrete face rockfill dam Project practice, this paper researches the effect of crushing-type side wall on mechanical properties of concrete face rockfill dam through three-dimensional nonlinear finite element simulation calculation on dam.

Shuibuya concrete face rockfill dam is located in middle reaches of Qingjiang river in Badong county of Hubei province. The dam crest level is 409.9m. Dam crest width is 12m. Dam upstream gradient is 1:1.4. Dam downstream integrated gradient is 1:1.4. Dam height maximun is 233m. Shuibuya concrete face rockfill dam was divided into seven main fill areas in addition to concrete face slab and crushing-type side wall. They are clay blanket area, weighting area, cushion material area, transition area, main rockfill area, hypo-rockfill area, downstream rockfill area, respectively. The dam typical section and divided material area are shown in fig. 1.

2 CALCULATION METHOD AND CALCULATION PARAMETER

The calculation of stress and deformation of Shuibuya concrete face rockfill dam based on concrete crushing-type side wall technology adopts three-dimensional nonlinear finite element method. Among them, the relation between stress and deformation of dam rockfill adopts E-B nonlinear model, which is used commonly. Face slab and toe wall concrete adopt linear elasticity

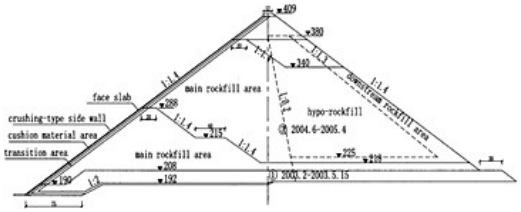

Figure 1. Shuibuya concrete face rockfill dam typical section.

model. The contact plane of face and crushing-type inclined wall adopts Goodman nonthickness contact plane element model. Face slab upright fissure and perimetrical fissure adopt joint element model. In order to analyze the effect of material physical properties of crushing-type side wall on stress and deformation of face rockfill dam, this paper researches concrete crushing-type side wall by linear elasticity model and E-**B** nonlinear model respectively.

2.1 *Rockfill element model and parameter*

In the three-dimensional analysis of this paper, consider the effect of intermediate principal stress on nonlinear tangential deformation modulus and tangential bulk modulus. In three-dimensional calculation, replace σ_3 and $\sigma_1-\sigma_3$ of plane with ball stress **P** and broad sense shear stress q, therefore, tangential deformation modulus of E-**B** model is given by:

$$E_t = KP_a\left(\frac{P}{P}\right)^n\left(1-R_f\frac{\left(\sqrt{3}\cos\theta_\sigma+\sin\theta_\sigma\sin\varphi\right)q}{3c\cos\varphi+3P\sin\varphi}\right)^2 \tag{1}$$

$$\text{where: } \theta_\sigma = tg^{-1}\left(-\frac{\mu_\sigma}{\sqrt{3}}\right);\quad \mu_\sigma = 1-2\frac{\sigma_2-\sigma_3}{\sigma_1-\sigma_3}。$$

The angle of internal friction of rockfill is:

$$\varphi = \varphi_0 - \Delta\varphi\lg\left(\frac{P}{P_a}\right) \tag{2}$$

The tangential bulk modulus of rockfill is:

$$B_t = K_bP_a\left(\frac{P}{P_a}\right)^m \tag{3}$$

when rockfill is unloading or loading again, elasticity modulus should be used.

$$E_{ur} = K_{ur}P_a\left(\frac{P}{P_a}\right)^{n_{ur}} \tag{4}$$

Detailed calculation parameter is shown in table 1.

Table 1. The physical mechanical parameter of material.

Material	γ(G/cm^3)	φ_0(degree)	$\Delta\varphi$(degree)	K	n	R_f	K_b	m
Main rockfill	2.15	52	8.5	1100	0.35	0.82	600	0.1
Hypo-rockfill	2.15	50	8.4	850	0.25	0.80	400	0.05
Downstream rockfill	2.15	52	8.5	1100	0.35	0.82	600	0.10
Transition material	2.18	54	8.6	1000	0.40	0.85	450	0.15
Cushion material	2.20	56	10.5	1200	0.45	0.78	750	0.20

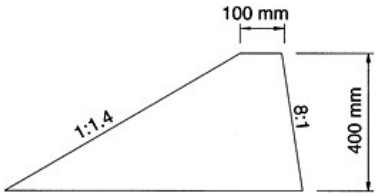

Figure 2. Crushing-type side wall section.

Table 2. The physical mechanical parameter of crushing-type side wall.

Material	γ (G/cm^3)	ϕ_0(degree)	$\Delta\phi$(degree)	K	n	R_f	K_b	m
Crushing-type side wall	2.00	58.2	15.4	2195.8	0.410	0.742	939.0	0.137

2.2 *Contact element model and parameter*

Presuming that local coordinate y of contact element is element normal, then the tangential strength of element is:

$$K_s = K_1\gamma_w\left(\frac{\sigma_y}{P_a}\right)^n\left(1-\frac{R_f\tau}{c+\sigma_y\tan\delta}\right) \tag{5}$$

where: δ−the angle of outside friction of material on the contact plane; σ_y−normal stress on the contact plane; γ_w−the unit weight of water. In this equation, K_1=4800; n=0.56; R_f=0.74; δ=36°.

2.3 *Crushing-type side wall element model and parameter*

The size of crushing-type side wall is shown in fig. 2.

Crushing-type side wall is calculated according to E-B model, and the parameter is shown in table 2.

2.4 *Concrete element model and parameter*

Concrete element adopts linear elasticity model, in this case, γ=24.0KN/m^3; E=20000MP; v=0.17.

3 THE ANALYSIS OF CALCULATION RESULT

Before storage, the stress and deformation of face slab and rockfill is relative small, and calculation also indicates that the effect of crushing-type side wall on rockfill is small. So this paper mainly analyze the stress and deformation of face slab after storage.

3.1 *Noncrushing-type side wall*

3.1.1 *Stress*

Vertical face slab normal stress maximum is 8.06Mpa, located in middle-lower part of main river bed section. There are certain tension stress around the contact of the lower face slab and circumferential foundation. Along dam axes, face slab normal stress maximum is 11.4Mpa, located in middle-lower part of main river bed section. Along slope direction, face slab normal stress maximum is 13.3Mpa, located in right-lower river channel. It is tension stress (figs. 3 to 4).

The σ_1 maximum of rockfill is 3.56Mpa, located in around the bottom of dam axes; σ_3 maximum is 0.84Mpa, located in around the bottom of upstream dam axes (figs. 5 to 6).

3.1.2 *Deformation*

Vertical face slab direction, the displacement maximum is 674mm; Along face slab direction, the displacement maximum is 60.6mm; Along dam axes direction, the displacement maximum is 55.1mm (figs. 7 to 9).

The displacement distribution of rockfill in main river bed section is shown in figs. 10 to 12. The displacement maximum along the river is 330mm, located in upstream of middle-upper part of dam; Vertical displacement maximum is 1440mm, located in the middle of dam; The displacement maximum along dam axes is 80mm, located in upstream of upper dam.

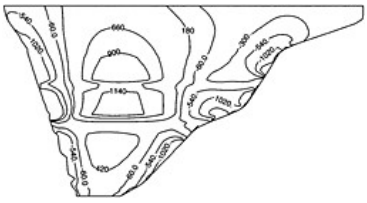

Figure 3. Normal stress distribution along dam axes (10^{-2}MPa).

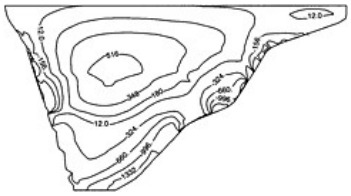

Figure 4. Normal stress distribution along dam slope direction (10^{-2}MPa).

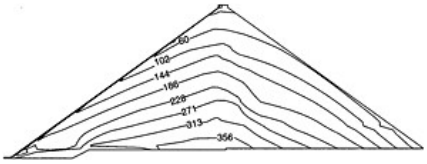

Figure 5. Major principal stress distribution in main river channel ($\times10^{-2}$MPa).

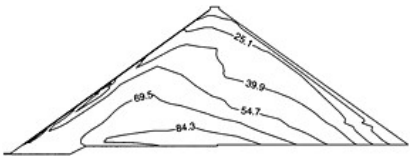

Figure 6. Minor principal stress distribution in main river channel ($\times10^{-2}$MPa).

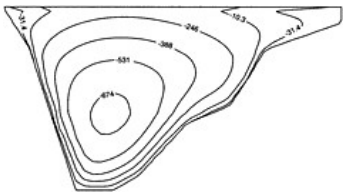

Figure 7. Face slab normal displacement distribution (mm).

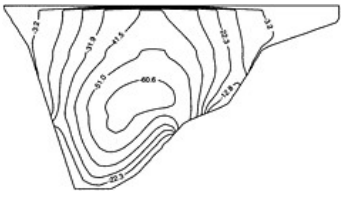

Figure 8. Displacement distribution along face slab direction (mm).

3.2 *Crushing-type side wall*

3.2.1 *The effect of crushing-type side wall on dam stress*

After crushing-type side wall technology adopted, the increment of face slab normal stress is 0.14~0.3MPa. The normal tension stress of circumferential face slab decreases, but the normal tension stress of middle face slab increases a little; The increment of normal stress along face slab slope is 0.01~0.08MPa. The tension stress of right river channel decreases somewhat and the pressure stress increases somewhat in middle face slab (figs. 13 to 14).

Besides, after crushing-type side wall technology is adopted, the stress change of rockfill is very small. So seeing from the angle of plane change, the stress change of crushing-type side wall is smaller than non crushing-type side wall, and it is advantageous to improve face slab circumferential stress, especially to reduce tension stress.

3.2.2 *The effect of crushing-type side wall on dam deformation*

After crushing-type side wall technology is adopted, the increment of face slab normal displacement is 0.0~0.6mm. Except local area, the normal displacement of face slab reduces somewhat. The displacement increment of face slab along slope direction is 0.0~0.2mm. The displacement reduces somewhat. The displacement increment along dam axes is 0.0~—0.6mm, The displacement reduces somewhat (figs. 15 to 16).

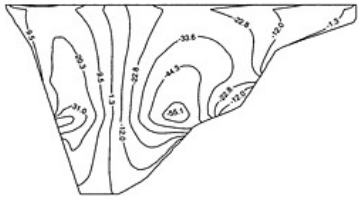

Figure 9. Displacement distribution along dam axes direction (mm).

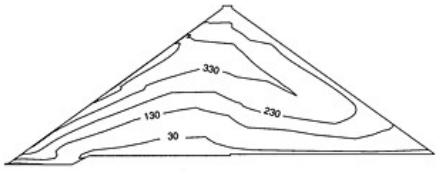

Figure 10. Displacement distribution along river direction in main river channel (mm).

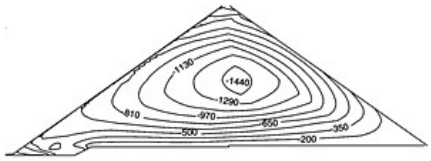

Figure 11. Verticaldisplacementdistributioninmain river channel (mm).

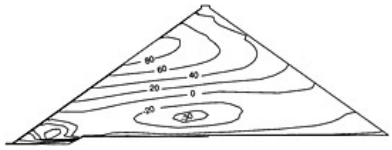

Figure 12. Displacement distribution along dam axes in main river channel (mm).

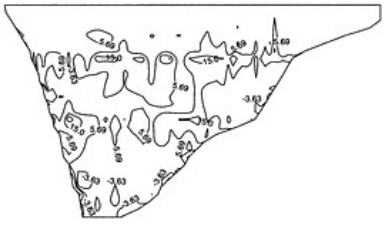

Figure 13. Normal stress increment distribution ($\times 10^{-2}$ MPa).

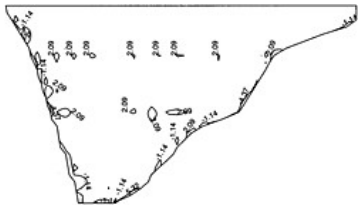

Figure 14. Normal stress increment distribution along slope direction ($\times 10^{-2}$MPa).

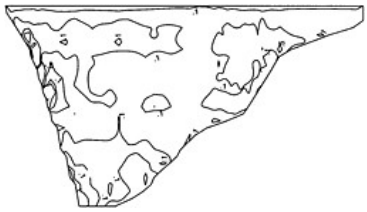

Figure 16. Displacement increment distribution along slope direction (mm).

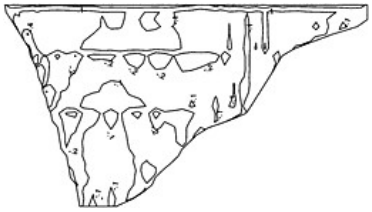

Figure 15. Normal displacement increment distribution (mm).

Besides, after crushing-type side wall technology is adopted, the displacement change of rockfill is very small. All is less than 1mm. So seeing from the angle of displacement change, the displacement change of crushing-type side wall is smaller than non crushing-type side wall, what's more, the displacement increment becomes smaller and it is advantageous to the dam.

4 IN CONCLUSION

According to the calculation and analysis above, it indicates that crushing-type side wall has following influence on the mechanical properties of concrete face rockfill dam:

1) Reduce circumferential tension stress of face slab, and increase somewhat pressure stress in the middle area of face slab. It is advantageous to improve the load conditions of face slab.
2) Reduce the deformation in deformation concentration area and increase somewhat deformation in unconcentration deformation area. It is advantageous to improve the deformation of face slab.
3) Reduce fissure deformation.
4) The effect on rockfill stress mainly concentrated on local area of cushion material area and transition area. It is mainly the change of minor principal stress and the increment is small. Major principal stress has no change basically.
5) The effect on rockfill strain is mainly upstream side of dam. Because the increment is small, the influence is also small.

The effect of crushing-type side wall on the mechanical properties of concrete face rockfill dam is small. Moreover, the effect is basically advantageous. Compared with traditional method, crushingtype side wall technology is obviously advanced in construction. It can improve project quality, quick up the schedule, and increase the safety of diversion and passing through flood season. It can also simplify construction process, reduce construction cost. So it is feasible, advanced, and economical to extend crushing-type side wall technology in the construction of upstream sideslope of concrete face rockfill dam.

REFERENCES

[1] Miao Shuying, Bai Zhao-peng. Application of sidewall extrusion method to concrete face slab dam construetion. Journal of shanxi water power, Xian, Vol. 17, No. 4 Dec. 2001.
[2] Sun Yujun, Dong Di. Application of the concrete crushing type sidewall technology in Gongboxia Concrete Face Rockfill Dam. Journal of water power, Beijing, No. 8 2002.
[3] Huang Qiuli, Lin Xinping. The test of the concrete crushing type sidewall in Gongboxia Concrete Face Rockfill Dam. Yellow river, Zhenzhou, Vol. 25, No. 12 Dec. 2003.
[4] Dai Yongzhi, Gu Ganchen. Three-dimensional nonlinear analysis for Gong Boxia concrete-face rockfill dam on thethe Yellow River. Red river, Nanning, Vol. 20, No. 4 2001.

New Developments in Dam Engineering—Wieland, Ren & Tan (eds),

Rehabilitation of old earth dams failed during heavy floods in 2002

Ivan Vanicek
Geotechnical Department Czech Technical University, Prague, Czech Republic

Jiri Vanicek
Geosyntetika Ltd, Prague, Czech Republic

ABSTRACT: Roughly between 300 up to 600 years ago many small earth dams were constructed in the south part of the Czech Republic. They were used mostly for fish production and flood protection. To our days roughly one third survived, it means close to the number 25000. Dam crest height is between 3 and 15m and these earth-fill dams were constructed as nearly homogeneous dams from the local soils. During catastrophic floods in 2002 many of them had some problems but less than 0.3% failed. Biggest concentration of failures is connected with small river Lomnice (situated roughly 100km south of the capital Prague), where 5 dams failed and 2 others were damaged, mostly by so called domino effect. Therefore in the paper the manners and reasons for dam failure are discussed together with new approach for the overall stability. Also some practical results from the phase of reconstruction are added.

1 INTRODUCTION

Heavy rainfalls during 7 and 9th August 2002 did not cause any problems; pond reservoirs were nearly full and fulfilled theirs flood protection role. The situation was improved during Saturday and Sunday (10–11 August) and with the help of directed outlets a certain reservoir volume was prepared, for example in 3 cases water level was 0.3–0.6m under normal level.

New heavy rainfalls started on Monday the result of which had very quick response due to the full saturation of surrounding land. On Monday evening the flow volume reached 100 years flow rate. But still all dams were able to catch all these volumes.

The critical situation started at around 4.am of the next day morning when—due to overflowing—the first dam (Melin) on this river-basin failed. Additional wave reached the crest of the next dam "Metelsky" in few minutes and very quickly also this dam failed in 2 places. Relatively large volume from this reservoir (about 1 mil. m^3) with the estimated (and recalculated) outlet more than $500m^3/s$ (which was much higher than 100 years flow rate—ca $20m^3/s$) affected the villages Metly and Predmir, where some houses failed and one man died. The embankment of the next pond "Vesky" withstand due to the very wide crest with asphalt pavement but was strongly eroded on the downstream side. The same situation was observed on the next pond "Zamecky" the rest of which is also protected by asphalt pavement—European road E 49 is passing through it. The embankment of the fifth pond (Podhajsky) resisted for few minutes even when the water went over the crest (the calculated 100 years capacity of spillway was not sufficient) but finally also failed in the place where the reconstruction was realized roughly 13 years ago.

Flood wave after that reached the railway track—bridge withstand but the consequential embankment on both sides of the bridge was eroded, leaving railway track in the air. Last two dams also failed, when the leading one (Horejsi) strongly affected the village "Tchorovice". After the failure of the last one (Dolejsi) the flood wave was getting flatter in much wider and flatter valley so that the impact on the town Blatna was a little bit eliminated. But even there the damages were very high.

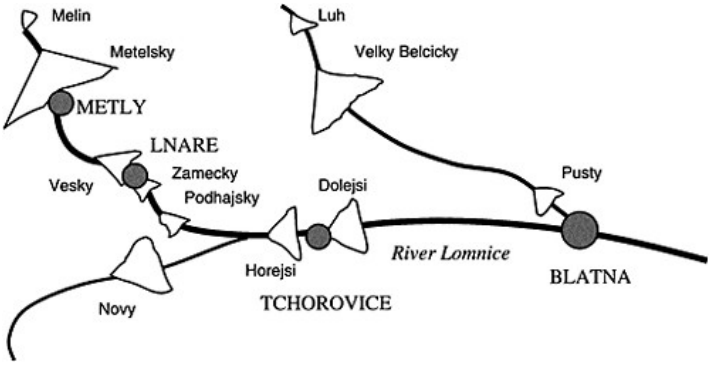

Figure 1. Little river Lomnice—situation.

Figure 2. Town Blatna—13.8.2002 morning.

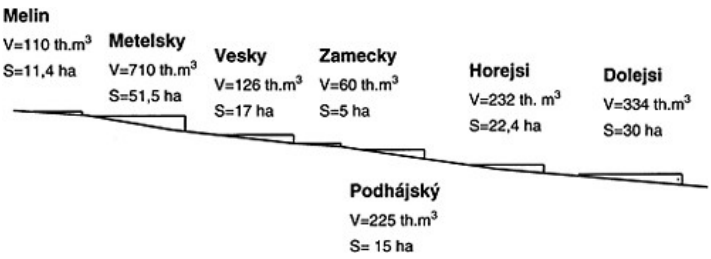

Figure 3. Scheme of dams on the litle river Lomnice.

2LIMIT STATES OF FAILURE

Usually the limit state of stability is getting the priority during the cross section design. Such sort of the failure was not observed in any case. That is in the agreement with a general opinion, that

the most of the earth and rock fill dams have problems with other limit states as is the limit state of deformation (leading to the development of cracks—see e.g. (1), (2)) and limit states of surface and internal erosion.

In all observed cases the surface erosion played the most important role, but in the two cases the internal erosion also probably participated in the final collapse. For example in one place of failure—gash—of the embankment of the pond Metly the part of the old wooden outlet was found. From the historical records this old outlet was left there roughly in 17th century, because from these days a new place for new outlet was selected. Roughly in this profile on the downstream side the place with higher humectation (moisture content) was observed for last decades, probably as the result of higher permeability in this profile. Due to higher hydraulic gradient, the clogging of this old outlet failed and internal erosion started in this place. It is interesting to note that the erosion started with a short delay when the water level in the reservoir went down due to the first failure. The second case, where probably the internal erosion also played the significant role was the pond Podhajsky the embankment of which was reconstructed 13 years ago and sealing wall performed by jet injection was applied in one part of the embankment. All downstream side was eroded; nevertheless the total failure occurred in the same place as sealing wall was installed. Probably the internal erosion started along the periphery of this sealing wall as the result of higher hydraulic gradients there and as the uncertainty of the connection of this wall with the rest of the embankment and also with the dam bedrock where large granite boulders were disclosed.

3 PRINCIPLES OF THE RECONSTRUCTION DESIGN

The reconstruction started very quickly after the failure. 2 dams, which did not fail completely and the crest of which is used as main roadway, were reconstructed during 3 months, in the autumn of 2002, with financial support of Roadway directory. All others were reconstructed during 2 years with the financial support from the state budget covering flood damages via Ministry of agriculture. For 2 of them situated just above villages the first step was provisional cofferdam to catch increased outlets. Detailed attention was directed to the following items (3):

– verification of hydrological conditions, recalculation of spillway capacity for 100 years outlets and supplemented increase of this capacity,
– selection and recommendation for most appropriate type of soil used for reconstruction,
– unification of the crest vertical alignment in the all length, because some differences up to 0.3m were observed.

3.1 *Hydrological data and new design of water diversion systems*

After the floods the Czech Hydro meteorological Institute recalculated data but the 100 years outlet was very close to the previous ones. It was proved that the capacity of water diversion systems for all ponds were goOd enough even for new data. Nevertheless the new proposal recommended to increase this capacity with the following points (4):

– where two defrayable spillways existed for the first one the spillway frontal crest was decreased about 0.2m,
– capacity of both spillways were increased by pulling down the intermediate column for the increase of flow profile and for the decrease of the possibility of the blockage by timber species, small trees etc.
– new arrangement of the lifting facilities allowing to rise of flood gates above the flow profile,
– construction of an additional unprotected spillway with the crest roughly 0.2–0.4m below the crest of the embankment—so that floods higher than 100 years flood will go firstly by this profile.

Photo 1. Dam Metelsky—gash with old wooden outlet.

Photo 2. Dam Metelsky—second gash.

3.2 *Geotechnical aspects—selection of fill material*

The preliminary estimation of the volume fill material for the reconstruction of all 3 dams was roughly 63000m^3. Firstly we have started with the tests on the existing dams. From the exposed profile of the gash, which was practically vertical, the tests proved that the material is composed from granite eluvium, soils which are typical for this region. Although the vertical walls stayed stable for nearly 2 years, grain size distribution curve had typical sandy character. The main reason for some cohesion and relatively lower permeability, than should be judged from this grain size distribution curve, is probably high content of mica. The surface of such compacted soil is very glossy, similar to the clayey soil. Some results on the material from the existing dams:

– percentage of fine particles (lower than 0.06mm)—between 10–35%,
– liquid limit W_L relatively high—30–37%,
– plasticity limit w_p 23–28% (but in some cases not detectable due to high sandy content)
– optimum moisture content according to the Proctor standard test—w_{opt}=12.5–17.0%
– coefficient of permeability after the compaction—k=10^{-8}–10^{-10}m/s.

Photo 3. Dam Zamecky in village Lnare—road E 49.

Photo 4. Dam Podhajsky—total gash with eroded downstream side.

Borrow pit was selected at the edge of field—after the removal and storage of humus layer the samples were tested from the different depth. Degree of weathering was in very different stages, but usually material closer to the surface had higher plasticity. Finally it was decided to construct the dams as zoned ones; more plastic material was situated on the upstream side, sandier one on the downstream side. Little bit higher moisture content was recommended than the optimum one to decrease the coefficient of permeability. During the summer time it was necessary to increase

the moisture content by sprinkling, storing the material in stockpile before using in the dam body. Heavy sheep foot roller was used and good experience was obtained, due to high disintegration of weathered material—also in the winter time, works continued up to −4°C in the night time if daily temperature was slightly above zero.

Great attention was devoted not only to the compaction control—samples were taken each 500m^3—but also to the connection of new part of the fill to the old one. Eroded slopes were arranged to the slope inclination at the least 1:7 to get good connection between old and new parts and to avoid cracks development. In longitudinal direction in the central part of the cross section the contact was done with the help of cut-off, in the bottom as well. The depth of this vertical sealing wall was selected according to the permeability of the excavated material. For the embankment of the pond Podhajsky, a special arrangement was recommended and applied in the part where in

Photo 5. Dam Podhajsky—old clay-cement jet injection sealing wall.

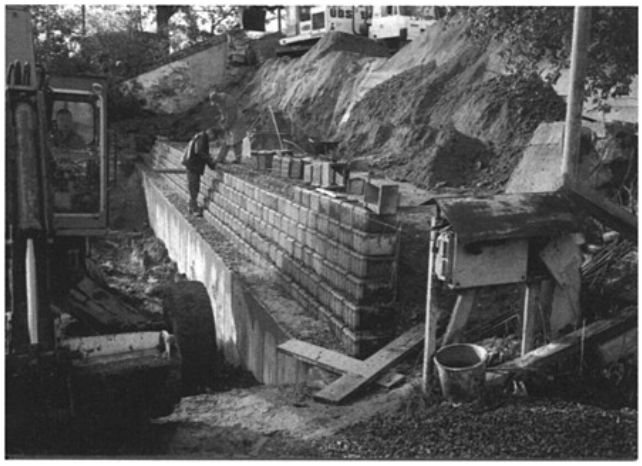

Photo 6. Dam Horejsi—retaining wall from the reinforced soils.

slope and in the bottom of the gash great granite boulders were disclosed—these boulders were coated with bentonite slurry and most plastic material was compacted there in small layers by smaller compaction tamp.

3.3 *Application of geosynthetics materials*

In spite of tendency to restore the dams as close to the old standard some new materials were also applied—for example the geosynthetics materials. Not only as the separation layer on the contact of the fills with upstream side protection layer composed from gravel and boulders, but also for slope reinforcement. Downstream slope on the pond Horejsi was composed from the concrete gravity retaining wall on part where fish-pond for nursery fish was very close to the embankment. After the failure of this retaining wall a new one from the reinforced soil was constructed there. Small prefabricated blocks were anchored to the slope with the help of reinforcing geogrid from polyester. Not only price but also aesthetically incorporation was better in this case than the old solution.

4 SOME RECOMMENDATION OBTAINED FROM THE RECONSTRUCTION

To minimize the negative impact of the heavy floods in the future the greater attention should be devoted to the following points.

4.1 *Domino effect*

Our engineering practise is not taking this effect into account, even as would be shown that this effect is playing the very important role. Our codes of practise are rather unambiguous—to ensure safe diversion of 100 years flood. With this the following notes can be added—possible demand for safe transfer of the higher flood can have following impacts:

–disproportionate increase in price, which from the long term look can significantly exceed pertinent price for the reconstruction and loss—this approach deserve a separate attention—definition of acceptable risk,
–securing the safe transfer of the higher flood can cause worsening of the situation below the dam—especially when this area is highly populated,

Photo 7. Dam Dolejsi—blocked protected old spillway (8 pcs).

Photo 8. Dam Dolejsi—new spillway (4 pcs)—without middle pillar.

Photo 9. Dam Dolejsi—new additional unprotected spillway.

–therefore we recommend the greater attention to devote to the increase of the storage capacity - first of all with the help of mud clearing in places where the fluvial deposit step down reservoir area above the level of dead storage.

However even increased capacity of spillways cannot be sufficient in the case which happened on the river Lomnice. In our case the second pond on this river-basin—pond Metelsk′ which failed—had higher storage capacity than the rest of following ponds below it. Therefore the flood wave from this pond had such a great negative impact on the safeness of the ponds below it. Practically all failures started with time delay when this wave reached individual pond. Generally we have “classical case” when the reservoir volume is increasing along river-basin. Therefore we recommend for the pond system in the Czech Republic to define this untypical cases and preferably for the most important pond with critical reservoir volume to define more strict conditions from the stability point of view.

4.2 *Interaction of the dam with road on its surface*

Positive effect of the road pavement (and usually with wider crest) was clearly observed for ponds Vesky and Zamecky, where flood wave only destroyed part of the downstream side. But in some other cases the negative impact of roads was observed. For the historical dams, the width of crest was relatively a small one. During last decades the asphalt pavement was applied with two negative impacts. The first one is connected with increasing transport especially with heavy tracks which causes additional settlement, very often a differential one—because the compaction in history was not so efficient. Very often there is additional dynamic effect (often caused by trailer), which not only influences the settlement but also the connection between old (very often wooden) outlet and fill or between this old wooden outlet and the new concrete feed-pipe—these contacts can be a preferential path for seepage water, which can be reason for an initiation of the internal erosion.

The second negative impact is connected with the effort to widen the crest width, when very often the asphalt pavement spills over original profile and when the longitudinal cracks are the result of heavy loading at this part. Potential risk of accident is therefore very high. The discussion between pond and road owners is therefore significant step which have to start.

4.3 *Utilization of local soils—granite eluvium*

These soils were used in spite of the fact that their properties, especially from the point of view of grain size distribution and plasticity are on the boundary of materials which are generally accepted for earth-fill dams. This approach was applied due to the negative experience with application of additional sealing element (jet injection sealing wall) along which perimeter the internal erosion probably started due to the high hydraulic gradient along this perimeter. According to our opinion the more coarse materials can be used when is able to fulfil sealing function and the total seepage is small enough. Because for all historical dams no special problems in this field were observed and the permeability tests proved this fact the local material was used which also guaranteed the same cross section as for the original dam. High content of the mica in granite eluvium is with high probability the reason for low permeability.

5 CONCLUSIONS

Limit states of surface and internal erosion were critical ones during small historical earth-fill dam failures during heavy floods in 2002. High concentration of failures in little river Lomnice are probably caused by domino effect, due to the fact that the dam with highest reservoir volume is at the beginning of river-basin. Reconstruction approach was directed to the main aim to decrease the probability of failure in the future. From the geotechnical engineering point of view the utilization of the original local soils even when they are on the boundary of soils generally accepted for earthfill dams were discussed. From the hydro engineering point of view the reconstruction of outlet and spillways are discussed, always capable to transfer 100 years flood and with special attention to increase this capacity by unprotected spillways constructed only few decimetres below dam crest on places where the surface erosion is expected to play a minimum role. The interaction of the transport along dam crest is also discussed.

ACKNOWLEDGMENTS

This paper was prepared with the help of grant project of the Ministry of Education and Youth CR No. 211100005—Environmental aspects in civil engineering.

REFERENCES

(1) Vanicek, I.: *Simple non-standard laboratory tests before and during construction of Dalesice dam.* In: Proc. 14th ICOLD, Vol.1, Rio de Janeiro, 1982, pp. 605–609.
(2) Vanicek, I.: *Development and behaviour of cracks in earth and rockfill dams.* (in Czech), SNTL, Praha 1988.
(3) Vanicek, L: *Lessons learned from the failures of ponds on river-basin Lomnice.* (in Czech). In: Proc. Dam days. Czech Committee of ICOLD, Ceske Budejovice, 2004.
(4) Vanicek, I: *Principles of the reconstruction design for 3 dams on the river-basin Lomnice.* (In Czech). In: Proc. Dam days. Czech Committee of ICOLD, Ceske Budejovice, 2004.

New Developments in Dam Engineering—Wieland, Ren & Tan (eds),
© 2004 Taylor & Francis Group, London, ISBN 04 1536 240 7

History of dam engineering

A.Vogel
Department for International Researches, Risk Assessment International (RAI), Austria

ABSTRACT: Old cultures and civilizations always have fascinated humans of modern times. Of course the science of archaeology is engaged in questions about the evolution and the extermination of cultures but often neglects infrastructural facilities which guaranteed the survival of humans. The science of techno-archaeology which started 150 years ago often changed the points of view about historical events. Investigations showed that exterminations of cultures caused by war or disease often traced back to the lack of drinkable water, the mean elixir of life.

Impressed by antique palatial buildings and our knowledge of political and cultural correlations as a result from the decoding of old scripts, we forget in most times the fundamental parameter, which were necessary, to found old communities and permit their long-time survival.

Even at the beginning of cultures, collectors, hunters and herdsmen were bound to places, where the amount of water was equivalent to their consumption. Although the point of transitional stage between the prehistoric human and the homo erectus is set by antropologes at the moment of his erect standing and by politologes at the moment of first founding of settlements, it is my opinion, that it was at that time, when humans recognized the necessity of a stable water economy to built up permanent settlements.

Starting with this eldest dam in the world, the history of dam engineering will be traced. Old Egypt, Mesopotamia, Persia, The Romans, Turkey, The Nabateans and Modern Europe will be lightened from the sight of old dam constructions.

1 INTRODUCTION

Dams are impressive constructions in our world and it is a fascinating chapter of our history to investigate the tribes to their origins. The history shows, that these constructions are not innovations of nowadays, because first predecessors have existed even 6000 years before our modern times.

2 THE WORLD'S OLDEST DAMS

The world's most ancient, well researched and documented dams are located approx. 100km northeast of the Jordan capital Amman. They were part of an elaborate water supply system for the town of Jawa, around 3000 BC. The selected site of Jawa was most favourable because on this site natural pools were existing. From these pools the Jawaites satisfied their water needs during the construction of the city and they dammed them for the first stage of their water supply system immediately to form artificial reservoirs. A diversion weir 3km northwest of Jawa diverted floods into 5 reservoirs, the largest of them was built by a 4, 5m high and 80m long dam (Figure 1). The internal construction of this dam consisted of two dry masonry walls, which enclosed an earth core with a thickness of 2m. Additionally an impervious blanket was provided in front of the upstream heel. The stability of the structure was assured by a downstream embankment. A heightening of the dam by 1m followed essentially the same principles and the width of the earth core was also

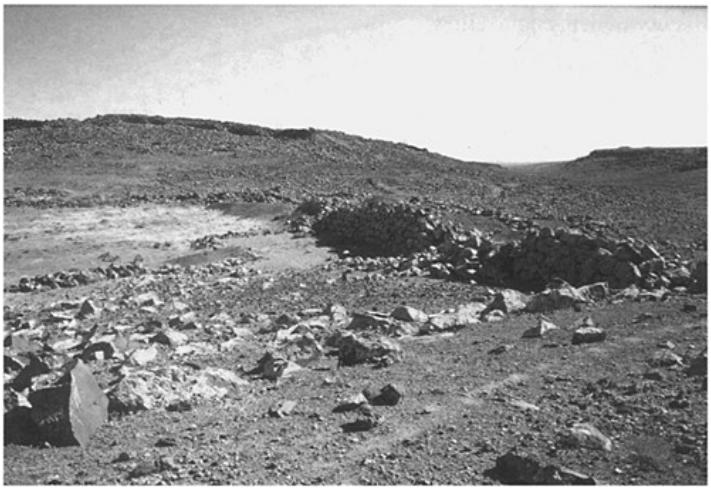

Figure 1. Ruins of the main dam of Jawa's old water supply, the oldest dam in the world.

increased to 28m. A pervious stonefill was provided behind the upstream wall for easy drainage during emptying the reservoir. Thus the wall was protected against the dangers of water-backpressure. This construction detail was very important and this fact had impacts to other civilizations.

3 EGYPT

Old Egypt was one of the most important civilizations of the past. The geographical situation on the one hand and the waters of the life line, the Nile river where causes of the long-time existence of this ancient culture. Egypt was protected by the natural boarders of the Mediterranean Sea in the north, the Arabic dessert and the Red Sea in the east, the Libyan dessert in the West and the Nile cataracts in the south. Egypt's history starts at 3000 BC with the union of Upper and Lower Egypt and ends at 332 BC the time of the arrival of Alexander the Great. Caused by the annual floods of the Nile river, it seems understandable, that only canals, dikes and low dams were necessary for an adequate irrigation of the area. Therefore no construction of a huge dam is delivered by hyroglyphs. But the real cause of this fact was a catastrophe in the pharaonic Egypt, which happened 2700 BC and which hit the first large dam construction in the world. The impacts of this event seemed to be so traumatic at the time of the birth stage of this culture, that for more than 1000 years no further dams were constructed.

The ruins of the Sadd el Kafara dam were discovered over one hundred years ago in the ravine Garawi, 30km south of the Egypt capital Cairo. With a height of 14m, a crest length of 113m and a storage capacity of 500,000m^3 it is the first large dam in the world (Figure 2).

The grossly over designed cross section of the dam was probably due to lacking experience. This is particularly true for the central impervious core of silty and gravel between the two shells of rockfill. The total volume of fill reached 87,000m^3, whereas the construction period took some eight to ten years. Also the fabrication and the careful placement of the 17,000 revetment blocks on both outer faces of the each dam weighing 300kg, must have been particularly time consuming. The

Figure 2. Ruins of Sadd el Kafara dam, the first large dam in the world.

construction shows no tunnel or channel to divert the river across or around the site during its long construction period. The dam therefore was most probably breached before its completion, because the left wing was never paved with revetment blocks.

4 THE HETHITS AND URARTU

At the beginning of the 2nd mill. BC spreading from Turkey to south and east an important kingdom was started to exist, which should reach in some times northern Syria and the boarders of the Egyptian empire. It was the empire of the Hethiths, who signed 1270 BC a peace treaty under the reign of their king Hattusili III (1275–1250) with the Egyptian pharao Ramses II, although they had conquered his troops at the battle of Kadesh at 1285 BC. Similar to the Egyptian hyroglyphs the Hethiths used cuneiform scripts and since the 17th century BC their capital was Hattusa, which was situated in central Anatolia.

Tribes of Hethithic water constructions can be found all over the Turkey. Near Eflatun Pinar, 100km west of Konya, there are still existing spring waters, which are stored by an U-shaped dam, the overflow section of it was built in form of a piece made of sand stone including three notches, where water was able to escape.

Much better known is the dam of Karakuyu in central Anatolia, which was built 1200 BC. Also built in U-shaped form, the 440m long dam had a maximal height of 8m. Its sluice gate was situated at the point of the maximal height and was covered with non mortared stone pavements, one piece of it includes a non finished cuneiform inscription. The dam obviously failed at this point and caused by the fact, that now siltage is existing, the piping along the outlet must have been happened shortly after its completion.

The legendary kingdom of Urartu, which was situated between the lakes Van, Sevan and Urmia in the boarder areas of Turkey, Persia and Russia was mentioned for the first time by Assyrian inscriptions at 1250 BC. The first Urartean king Arame reigned 850 BC, from whom the

Figure 3. Ruins of the southern Kesis Gölü dam, the oldest gravity dam in the world (Photo G.Garbrecht).

Armenians, the successors of the Urarteans have had their name. The first capital Tuspa, which was on the territory of the actual city of Van was found by the Urartean king Sardur I.

But the waters of the lake Van are not usable for drinking water resources till today, because of too high concentrations of natrium carbon, that under the reign of king Menua (805–785) a 60km long canal was necessary to be constructed, which enabled to transmit from a well 40 hm^3 of drinkable water in a year to the city. This aqueduct is still in use. The Urarteans were marvellous artists in water engineering and their neighbours, the Assyreans recognized this fact and started several times warlike expeditions to their territories to participate and copy their newest developments of water engineering. As 714 BC the Assyrian emperor Sargon II (721–705) was executing such an expedition the Urartean king Rusa I (730–714) changed the capital from Van Kale to the better armed Toprak Kale and for the water supply, 2500m above the sea level, the Kesis Golii lake was stored by two gravity dams to an artificial lake with a content of 100hm^3.

The northern dam was destroyed by a flood in 1891, was then restored in the years 1894/95 and finally heightened in the year 1952 to a height of 15m.

But the southern dam, 6m high, remained as an original ruin from the time of its construction. The construction consisted of two masonry walls and had an overall thickness of 27m and a crest length of 62m (Figure 3).

Downstream in the Doni valley two further dams were existing, one of them is still in operation. Also of high interest is the Faruk Bandi Dam downstream of the northern Kesis Golii dam, which probable was constructed in Roman times. Caused by the thickness of the alluvials in the river bed the construction was founded on a wooden grillage.

5 THE KINGDOM OF SABA

In the old testament in the 3rd book of the kings, chapter 10 and in the 2nd chronicle, chapter 9 there is reported about a visit of the legendary Queen of Saba with Salomon, which shall have

taken place approx. 950 BC. Here gifts and presents inferred on a high standard of life in their kingdom at the time, which was only possible caused by a well organized water supply. The well operating economy in the capital Marib and in the surrounding areas had its base in a number of large dams which stored the rivers of the mountains, prevented high floods and ground erosion and made an irrigation possible. The largest of these dams was the earth dam of Marib. The initial construction dates back to the 6th century BC and after some heightens it reached 14m of height and a crest length of 700m. On both ends of the dam on the rocky river beds there were situated outlet structures, built of excellent ashlar mortar. At the northern one there was a 50m long overflow spillway with an overflow capacity of 1500m^3/s. Up to it the storage capacity was about 30hm^3 or barely 15% of the annual river discharge, so that the reservoir silted up rapidly. Between the spillway sill and the 4m higher dam crest there was an additional storage capacity of 30hm^3, which was only enough to handle relatively frequent floods. Consequently the dam breached quite often by extreme floods. Five such failures are attested in old scripts and the last one happened in the 7th century AD after an operation time of 1300 years was reported in the 34th sura of the Koran. A further report of the Arabian historian Mas'udi reports as follows: "It happened under the reign of the King Amr B Amir, whose wife had dreams and visions which reported the forthcoming accident. "Goes to the bank", she said to her husband who believed her prophecies, "and if you see a rat digging holes into the embankment and moving large stones with her hind paws, then it is sure, it will come over us a great accident." The king went to the dam, and he watched in secret and truthful he saw a rat which moved such a large boulder that otherwise 50 men would have been necessary to move it. The waters broke through the dam, inundated the country and brought devastation near and far. The high floods went back and the country returned to culture and wealth, only the capital Marib remained destroyed and the Sabaeans vanished for ever from the history of mankind".

Not far away from the ruins of Marib, there are situated further old dams. In the Wadi Adr'a, which lies in the catchment area of the Marib dam, the ruin of an other dam is existing, from which only the southern wing of the once 20m high construction has remained. Each of its two outer walls was stepped back five times to obtain an average inclination of about 30%. In the centre of the rubble fill there was a 2.3m thick, vertical sand drain over almost the entire height, which was enclosed by dry masonry. Its purpose was to keep the downstream half of the dam dry and free of uplift forces in case of leakage through the plaster on the upstream face. A separate outlet tower was also situated at the upstream side.

6 THE NABATEANS

In the second century BC the Nabateans, people of still uncertain origin erected a kingdom in the Negev and the rose red city of Petra became their capital. Like the Jawaites before they were able to settle in the sparsely populated desert area in the south of Israel and Jordan, the only source of water in this area came from occasional showers and therefore dams played an important part in the daily fight of survival.

Dams were built across the beds of wadis in order to divert the sudden rush of water which followed a rainstorm, because the soil in this area has little capacity to absorb water. For the storage of water the Nabateans preferred underground cisterns, probably because they kept the water cool and minimized losses due to evaporation. Only rarely did the Nabateans resort to storage dams. The most impressive is one of a cascade of three dams on a ravine near the city of Kurnub, 85km south of Jerusalem, which has a height of 11m, a crest length of 24m and crest wideness of 7, 8m (Figure 4).

A second impressive construction was a huge diversion dam at the entrance to the ravine, where the city of Petra is situated. A 14m high and 43m long rockfill dam diverted flash floods through a 400m long tunnel safely into a secondary valley. At an unknown date the dam was destroyed and it stayed as a ruin until 1963 as a flash flood drowned 24 tourists, who were in the ravine on the way to the old city of Petra. The catastrophe showed the necessity of this dam and it was reconstructed in 1963. On the other way the Nabateans built dams to create fertile patches of ground

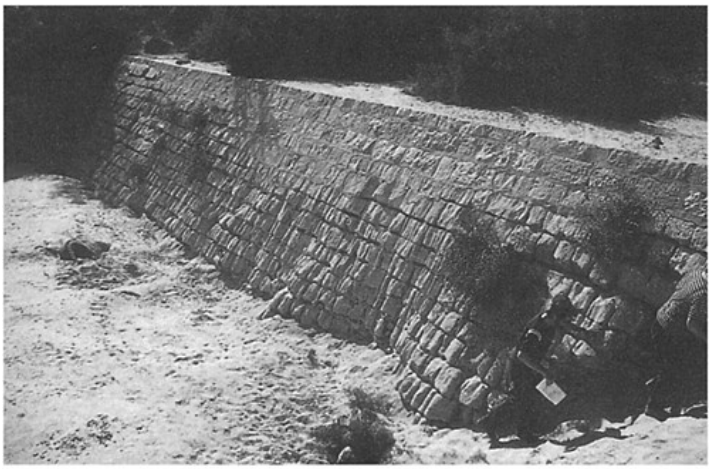

Figure 4. The large Nabatean dam near Kurnub in Israel (Photo T.Tsuk).

within these reservoirs. They were masters in water and soil conservation and were able to increase arable land up to fifteen fold. Most of their dams survived in full size up to our times, either with complete siltage or caused by a drainage stonefill behind the upstream walls, like that of the dams of the Jawaites.

In the first half of the century BC their kingdom attained its greatest extension, but 106 AD the Romans annexed the area and the emperor Traian proclaimed the province Arabia.

7 THE ROMANS

Within the centuries before Christ also the Romans have started to influence the history and gratitude of detailed historiography, we know very much about their culture, habits and politics.

In Anatolia, that was already confessed by the Urarteans as a country with excellent dam constructions, the Romans constructed three magnificent dams in the 2nd century. The largest of these dams is situated near the village of Örükaya, approx. 190km northeast from Ankara and had a height of 16m, a crest thickness of 5m and a crest length of 40m. The dam consisted of a double wall formed of limestone which contained a pulped earth's core. Once it stored a lake with a storage capacity of 400,000m^3 which is completely silted up today.

The second dam is located 210km south of Istanbul near the village of Cavdarhisar. It had got the same crosscut like the Örükaya Dam, but with 6m crest thickness it was considerably thicker, however it had a height of only 10m and a crown length of 80m. It contains a 6m wide and 2.5m high bottom outlet, which today only more than 1.5m highly juts out of the deposits in front of the dam. For lack of flood facilities, possible high floods may have passed either over the dam crest or only through the bottom outlet. Of course the high floods were levelled off considerably, why it seems reasonable that here a first primitive flood retention dam was set up through which the impressive thickness of the dam construction also became necessary (Figure 5).

Figure 5. Ruins of Cavdarhisar dam.

The third dam dating from Roman time is situated 120km to the northwest of Adana and is called Böget Dam. It also consisted of a double wall built from gabbro and tuff stones which was bedded in earth wedges on both sides, respectively. It had a height of 4m and a crown length of 300m. Once the reservoir was used as a reservoir for drinking water for the nearby city of Misli, which was a well known city at the Roman time. Today the edges made of earth have disappeared and the wall has partly collapsed and the storage dried out completely.

It was the Romans, who used for the first time the principle of arch in dam constructing in the 2nd century AD. For the Roman city of Glanum south of today's St.Remy de Provence in France they built a drinking reservoir which was accumulated by the first arch dam of the world. The last remains of the once 12m high and 18m long dam were covered almost completely by a new dam construction in 1891, but fortunately a rather precise plan of the Roman foundation excavations from the 18th century still exists and however the site of the foundations of the abutments of the dam are still recognizable at times of low water level. Typically for the Romans the 3.9m thick dam body consisted of two masonry walls, 1.3m wide on the upstream and 1.0m on the downstream side, with an intermediate earth core of 1.6m in width.

The ruins of the famous Roman dam of Harbaqa from the 2nd century AD lie in the Syrian desert approx. 70km to the southwest of the famous city of Palmyra. The 18m thick dam body has a core which consists of Roman concrete and which was covered carefully with masonry stones. Once the storage was used for irrigation purposes but today it is silted up and caused by wind and weather the siltage looks partly eroded again. But nevertheless the dam body of this enormous, 18m high and 365m long gravity dam has remained unchanged to this day (Figure 6).

After the incorporation of Spain to the Roman empire and after its colonialising famous towns were founded, like Merida or Toletum, the later Toledo. The Roman Emperor Trajan (98–117 AD) was born in the southwest of Spain and he promoted therefore this area in a special measure. Probably under his rule, a 38km long aqueduct for Toledo was constructed, whose starting point was a reservoir which was formed by the earth dam of Alcantarilla. It had a height of 14m, a crest length of 550m and a storage capacity of 3.5 million m^3. According to its crosscut, the dam is

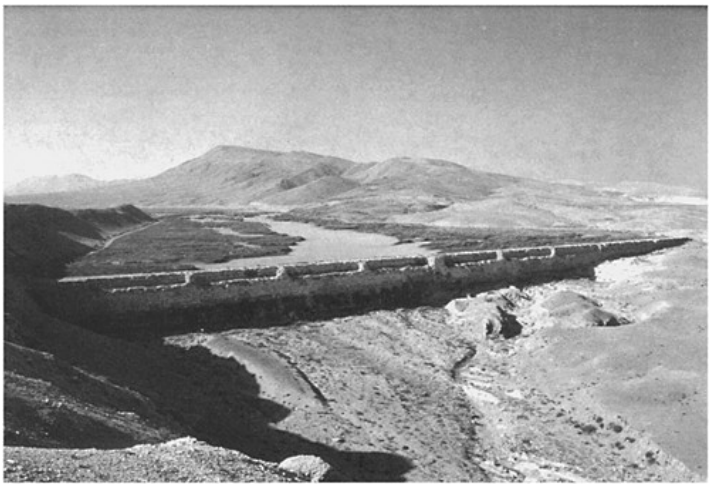

Figure 6. Ruins of Harbaqa dam in the Syrian desert near the city of Palmyra.

based on those dams of the already mentioned Nabateans, who once settled in today's Jordan and their territory was incorporated to the Roman empire under the reign of Traian. Caused by the fact, that these people were equipped with a high hydraulic engineering technical knowledge, the Nabateans might have come notwithstanding through the Roman annexation and the Romans took over much of their knowledge.

Alcatarilla Dam was the first dam, which was built by the Romans after the pattern of Nabatean dams. Obviously the Nabateans knew the danger, that a upstream situated dam wall could be pressed in by the supporting downstream earth body at times of low water and they ordered therefore a drainage between the dam wall and the supporting earth body. But the Romans overlooked this small structurally necessity and therefore the dam of Alcantarilla was pressed in by the supporting earth body in the time of the first low water and was destroyed in a very strange way, when the lake was empty.

For the water supply of the southwest Spanish city of Merida the dams of Proserpina in 110 AD and Cornalvo in 115 AD were constructed, both of these are in operation up in our days.

The successor dam to the dam of Alcantarilla is the 12m high and 427m long dam of Proserpina. Strikingly is the fact which absolutely seems understandable after the catastrophe of Alcantarilla, that the dam wall was improved and supported by small upstream pillars.

The earth dam of Cornalvo already appears rather modern with 19m of height and 194m of length. Its reservoir capacity amounted to some 10 million m^3. The most remarkable aspect at Cornalvo however is the precautions taken against upstream sliding by tilting the water retaining wall downstream, a measure which necessitated its support by a system of transversal and longitudinal masonry walls. The cells thus formed were filled with stone and clay and were then covered with concrete and an ashlar revetment.

Near Merida there is existing an other dam, whose downstream earth body was replaced by pillars made of masonry and mortar. The 5m high and 312m long Esparragalejo dam, which was restored in 1959 is regarded as the first precursor of today's buttress dams.

8 THE SASSANIANS AND THE PERSIANS

An historical and for further dam engineering important event lead over from Romans to the Persians art of dam engineering. At 260 AD at the battle of Urfa the Sassanian king Shapur I (241–272 AD) defeated the Roman emperor Valerian (253–260 AD) and captured him together with his army of 70,000 soldiers. Unlike to that time usual habits the prisoners were not killed but put for the construction of dams. Therefore with the Romans, who were very experienced in water engineering and bridge-building the age of bridge weirs was started in Persia. One of the most impressive and beautiful bridge weirs was constructed at 270 AD on the Karum river nearby the Persian city of Shushtar. The ground plan course was adapted to the optimal foundation conditions in the river bed. The approx. 2m high and approx. 6m thick weir piers are formed hydraulic optimally and stand on a continuous foundation. An old painting gives an impression of that once 516m long weir construction.

The remains of another bridge weir this might have been built also at 270 AD are situated at Dezful about 500km southeast of Teheran.

At the end of the era of bridge weirs, which were constructed over a period of about 700 years stands the Bend-e Emir dam, which is the master piece of these kinds of constructions and which was built at 980 AD. The 9m of high and 103m long dam construction, is situated northwestern of Schiras at the river Kor and is regarded as the first multi purpose plant of the world. The crest width is 7.5m where a bridge formed from 13 arches from brick masonry is put on it through which the total height of the building achieves 13.5m. The dam was used for the first time as a storage construction, on the second hand it served as a traffic route and on the third hand at the left dam wing there were found several inlets to altogether 30 water mills, which means that water power was also used for the first time at this site.

To make the continual technology export from Persia to Spain transparently, which was done by the mentioned Moors, the progress in dam construction practice should be indicated, which took place in Persia after the 10th century. After the era of the bridge weirs dams were constructed, which have to be counted to masterpieces in water engineering, caused by their design, their elegance and last but not least by their courageous dimensions. The Saveh gravity dam constructed at 1280 at the Gharatschai river, about 160km south of Teheran. The crest length was 65m, the crown thickness 18m and the height 25m (Figure 7).

The dam body consisted of blocks of masonry which were immediately broken on the spot, through which the dam body seems hardly recognizable in the surrounding area. Saveh dam was provided with a shaft near the upstream face, which contained seven inlets, their openings could be locked with wooden gates. The river deposits on which it was founded washed out probably upon the first impoundment and rendered the dam useless. After having bridged the river flowing beneath it for more than 700 years, it was demolished recently to spend a site for a modern dam.

At that time the Roman principle of arch dams experienced a new renaissance in a broader spectrum and it was the Persians who for the first time used this principle also for high dams. The oldest one, the Kebar arch dam constructed at 1300 has a height of 30m and a crest length of 55m. The mean arch is 21m long, has a radius of 28m and a center angle of approx. 50 degrees. The storage today is completely silted up.

More impressively is the arch dam Kurit, which is also located near Tabas and which has a modest crown length of only 28m, but however, a height of 64m. Built at 1350 with this height it was for five centuries the highest dam of the world and was surpassed only in 1904 by the 72m high Cheeseman Dam in the United States.

Nearby the north-east Persian city of Maschad in 1450 a group of gravity dams was constructed which stand by the most part into operation up to this day. The reservoir of Torogh dam with a height of 20m and a crest length of 51m is still used for irrigation. The shaft on the upstream side with inlet openings as a typical feature of this generation of dams needs no longer to be mentioned.

Although most part of the storage of Golestan dam is silted up today, the rest reservoir is still used for the water supply of Maschad. The dam body which consists of rubblework which was carefully covered with sandstones on both the upstream and downstream side is 16m high and

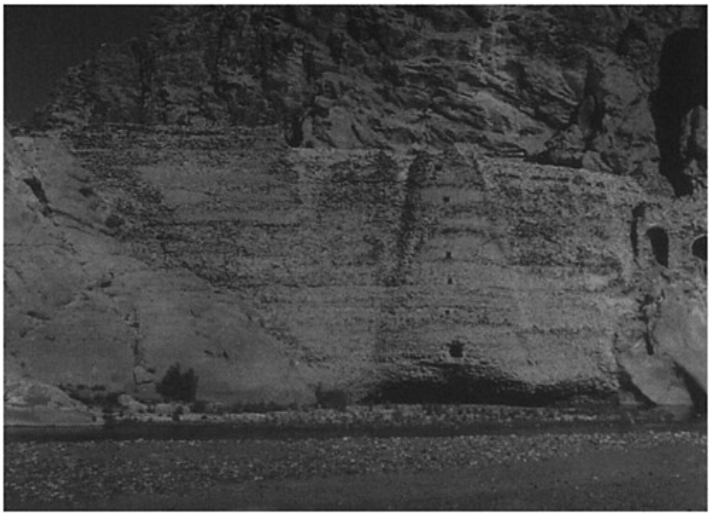

Figure 7. Ruins of Saveh dam, which was demolished in the meantime.

108m long. The Fariman dam situated also near Maschad was constructed at 1600 under the reign of shah Abbas II. The architectural history of this dam is extremely interesting because it was heightened for three times. The thick original rectangular dam body was used as a broad foundation for the first setup wall whose forces were supported via upstream arches onto the original dam crest. After a second rise the dam reached a height of 21m and a crest length of 90m and a surplus pyramid of brick was built on the downstream side. During the reign of shah Reza I the construction was heightened again by 1.5m and last but not least the dam finally gets its strange appearance of today.

At the end of Persia's history two further important dams, 90km southeast of Maschad should be presented, which are still in operation. The Akhlamad dam with 14m of height and 231m of length once had a storage capacity of approximately 4 millions m^3. The 20m thick dam body was strengthened on the upstream side by nine pillars by which four as inlet towers are improved.

9 SPAIN

Spain appeared already under the reign of the Romans as a country of active dam engineering and in 711, when it was occupied by the Moors for the most part, an intermixing of the Roman and the Persian knowledge of water engineering was noticed on their area. From these two historically and water economically epoch-making movements, the Spanish water civil engineers developed later a water architecture of their own with the consequence, that Spain became the world power in dam engineering for several centuries. This is the reason why today Spain is called the mother country of the modern dam constructing. In 1384 at Almansa a reservoir was constructed, which originally was formed by a 14.6m high arch dam. 200 years later this dam was heightened by a 6m high gravity dam, and since 1586 this strange construction is still in operation. It stores a lake with a capacity of 1.2 million m^3 and is regarded as the oldest arch dam in Europe, which is still in operation.

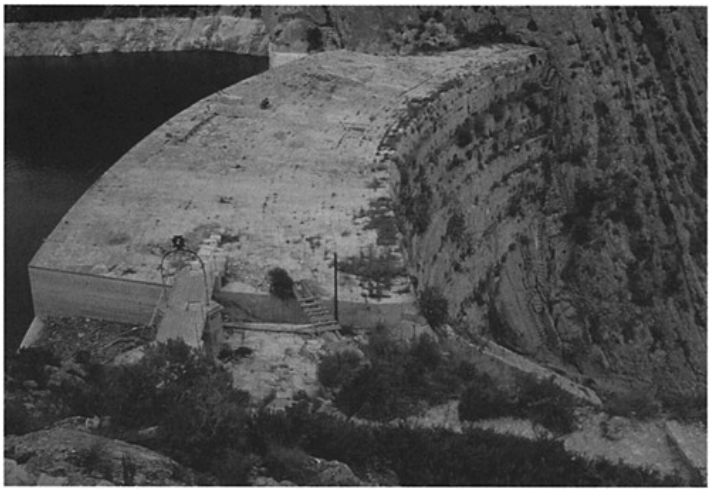

Figure 8. Tibi dam in Spain, which was never completely finished.

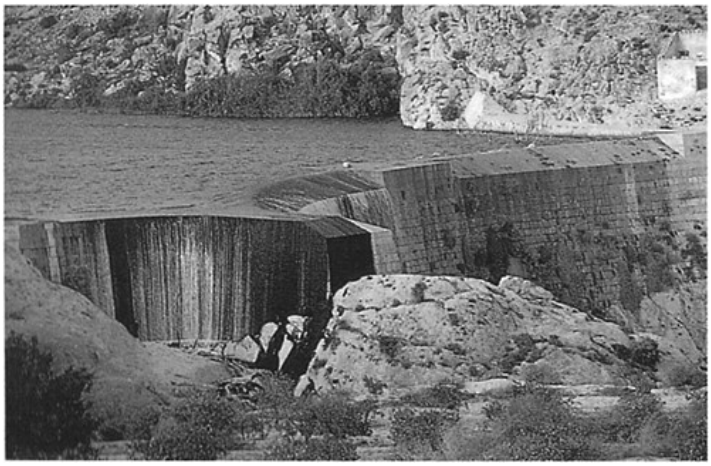

Figure 9. Elche dam in Spain, the first double arch dam in the world.

Also interesting for this construction was the fact, that the original project of 1384 included a spill canal to prevent siltage of the reservoir.

It was also the Spaniards who combined for the first time in Europe a dam construction with a water-mill power station, which come true at the Castellar dam in 1500. The Persians knew this principle of the first primitive water-power use already six centuries earlier, as we have seen at the Bend-e Emir dam. The gravity dam Castellar has a height of 19m and a crest length of 100m. At the foot of the dam there are three premises built with mortar for three water-mills.

The following example of the arch dam Tibi shows that it came also in historical time to occurrences which today would be described as “construction scandals”. The dam, which is situated 25km away from Alicante was constructed within the years 1580 to 1594 and stores till today a reservoir of 5.4 million m^3. It was projected as a 50m high construction but at a height of 42m only the necessary money went out and the contractor stopped the works and therefore today this dam is actually only a torso (Figure 8).

In 1632 the construction of the Elche dam was started. Caused by an unfavourable topography at the dam site a mixture of two different dam types was used. A small rock spur which was in the middle of the ravine was used as an artificial abutment. Left and right of this abutment there are situated two arches, built with mortar and with an ongoing small lateral gravity section the valley was finally locked. The main arch of the 23m high arch dam has a length of 70m, the complete crest length of the dam is 120m (Figure 9).

10 CONCLUSION

Historical dams are unique, irretrievable constructions of the technical mankind. Today’s water engineers often don’t find enough time to have a look at the history of the dam construction. Under the impression of newly temporal constructions their predecessors seem primitive and in the age of the computer also little noteworthy. But nevertheless we should have deep respect for the builders of dams in the antiquity. Their knowledge and last but not least their courage should have our admiration and in consideration of their wonderful buildings everybody, who is involved in dam engineering should be proud to be one representative in the long way of their evolution.

New Developments in Dam Engineering—Wieland, Ren & Tan (eds),
© 2004 Taylor & Francis Group, London, ISBN 04 1536 240 7

Dam made of cables and concrete plate elements (cable-plate dam)

Wang Chuansong, Liu Defu, Peng Hui, Cai Yizhou & Ye Jianjun
Three Gorges University, China

ABSTRACT: A new kind of "slim and thin" dam named cable-plate dam is put forward in this paper. This type of dam consists of cables and plates. The cables are made of high strength materials and anchored into both sides of riverside hill slope. And the plates are made of fiber reinforced materials and fixed on cables. As the whole body of dam is flexible and its stability relies on both sides of river valley cables anchored on. There are only tensile stresses exiting in dam body when dam is taken into use. When floods happens the dam can discharge water through it's body or over its top. The average thickness of dam is about several centimeters and as a result the needed local materials and excavation are fewer than common dams. Therefore, this kind of dam will hardly damage the natural environment of dam region. And it is feasible in technology and in economy.

1 INTRODUCTION

Constructing dams can bring lots of benefits, but at the same time it unavoidably creates different kinds of environmental damages. For example, after dam construction large area of land inundation will happen, lots of excavation are needed during dam constructing as well. In order to relieve this contradiction, people have to reduce the scale of each project for the sake of limiting the water level of reservoir and reducing the loss of inundation. However, so far, the environmental damage accompanying with dam construction has not been well solved. To solve this problem, in this paper, a new type of dam called cable-plate dam is put forward, which needs fewer construction materials and simpler construction technique than traditional dam. This new type of dam will not severely damage the environment of dam region.

2 NECESSITY

The environment damages caused by traditional dam construction include two sides at least. One is inundation loss, the other is the environmental damage in dam region caused by dam construction. The later includes:

(1) The excavation of construction materials. Materials are the foundation of dam construction. Different kind of dams is made of different kinds of materials. In order to meet the requirement of stress and stability of dam, gentle slope of dam surface is usually needed. As a result, large amount of materials is needed. For example, soil-fill dam, rock-fill dam and gravity dam all consume lots of materials, some other types of dams deriving from gravity dam such as wide-slot gravity dam, hollow-body gravity dam, buttress dam as well. Generally, most of dam construction materials comes from dam region, such as soil, rock, etc. As a result, serious environmental damage happens in dam region.
(2) The construction of temporary and attaching buildings. It includes building of working and living facility, transportation system construction in dam region, the construction and

demolishing of water-block and water discharge buildings. Although the type and scale of temporary buildings differ from different construction materials, it is indispensable to most traditional dams. For instance, in the place where lacks sand and pebble the artificial sand and gravel is needed to produce concrete. Therefore, a large concrete producing system is needed as well as a large scale of cooling system and quarry system. At the same time, mechanical repair plant, the plants for metal structure producing, steel bar treatment and moulds making are needed. Meantime, because the building materials transportation for a dam is intensive and distance between materials supply and dam is usually very long, and the starting point and terminal point of transportation system usually changes as the dam top rising, it needs cutting mountain for roads, which lead to occupying a large tract of land. And, if the dam locates in the area where the river valley is very narrow and both sides of the hill slope is steep, the transportation system usually appears sinuous. Hence, large pieces of land occupation will happen.

(3) Other excavation. It is the spandrel and foundation excavations and so on. These excavations not only damages the plants of slope, but also leaves large area of nude steep rock slope. Furthermore, if not taking proper measure to control soil erosion or landslide, lots of spoils will slides down or is carried by water into river and block the river. Some spoils will contaminate reservoir and ruin the arable lands.

The type of environment damages of dam region varies with the shape of dam and scale of the project. Although some damages can be rehabilitated to certain degree, most damages can't be avoided at all. When dam construction leads severe damages to local areas, it is difficult to restore in a short term. It is true that Arch dam as a kind of very thin dam which consumes less materials compared with gravity dam, it still needs rock, sand and other materials and causes damage to dam region environment. Therefore, it is urgent to find a new type of dam which brings much less sideeffect to environment.

3 THE APPROACH OF PROBLEM SOLVING

The seriousness of damage caused by dam construction is mostly decided by the type of construction materials. The reason is that the shape of dam and the dam surface gradient mainly depends on materials, which decides quarrying, processing, transportation system, etc., and the number of workers, the type of attaching buildings. The reason why traditional dam construction will bring severe environment damages is that the construction materials' strength are not high. If we use high strength materials to build dams, large scale of excavation will be avoided and the volume of dams can be reduced and the consumption of materials will be reduced a lot as well. Therefore, the application of high strength materials not only makes the dams slim and thin, but also reduces local materials consumption and avoids large scale of soil and rock excavation.

4 CABLE-PLATE DAM AND ITS SIGNIFICANCE ON ENVIRONMENT PROTECTION

Cable-plate dam is a new concept dam and consists of cables and water-block plates. The cables can be made of high strength steel wire or fibers bundles. The two ends of each cable are anchored into rock slopes in both sides of river valley. The plates are made of fiber reinforced composite materials and fixed on cables to form a whole face. The beneath and side edges of the face is imbedded in riverbed and slope of river valley respectively After reservoir comes into being, plates become water-block equipment, bearing water pressure and transmitting most pressure to cables. And cables deliver water pressure to mountains through anchorage. The mountains of both sides of river valley support the stability of dam. In fact, cable-plate dam can be looked as a big piece of sail or suspending bridge being rotated 90 degrees.

Cable-plate dam is a real thin and light dam and its construction will hardly damage the environment.

(1) Less materials consumption. Cable-plate draw advantages from rubber dam and its body consists of high strength materials. Generally, the tensile strength of cables and plates will at least reach l,800Mpa[1−2]. Which is much higher than that of traditional ones. At the same time, cable-plate dam absorbs lots of advantage from arch dam, that is its stability depends on the slopes of river valley which is quite different from gravity dam. As a result, the consumption of materials can be reduced to the least degree. Generally, cable-plate dam constructed on the river with narrow valley and steep slopes only needs several centimeter thick plates if the height of dam is not very high.
(2) Using industrious materials. Cable-plate dam construction mainly uses high tensile strength industrious materials, and needs very little local building materials. So nearly no materials excavation, no transportation and no processing are needed and therefore no damages will happen.
(3) Simple construction method. The cables and plates are industrious products and their construction focuses on cables anchorage, plates imbedding into riverbed and plates fixing on cables. It is easy to know from the framework of cable-plate dam that the total construction process is not very complicated. Generally, about a hundred workers is enough because most work focuses within a limited area—near dam foundation and spandrel. And, the transportation system and living establishment only occupy small piece of land. In addition, the process of cable-plate dam construction absolutely differs from the order of tradition dam construction. Its construction may begins from the top of dam and is hardly influenced by water-flow, and the work on diversion or flood-discharge structure is much more simpler.
(4) Permitting water-flow through dam body or over its top. It needs no other special waterdischarge buildings and no further environment damages will take place.
(5) Reliable and safe. Firstly, its slim and soft body can improve the anti-seismic capability of dam. Secondly, high strength steel wires have good extension character and its average extension rate is at least 3%[3]. The rupture deformation of plates is very high[4] and can be surveyed very easily by optical-fiber supervision system. Thirdly, even if one or several lengths of cables are broken under tensile force, some plates will be damaged and water maybe can pass through the dam body, the whole dam will not collapse. Fourthly, if the displacement of anchorage section of cables is not too tremendous, the stability of dam will be reliable. So, cable-plate dam is much better than traditional dam in reliability because the whole system collapse wouldn't happen in cable-plate dam but often happens in traditional dams.

5 FEASIBILITY

The feasibility of cable-plate dam construction involves technical and economical problems, mainly including cable anchorage and the cost of dam construction.

5.1 *Cables anchorage*

Undoubtedly, cables anchorage is the key to cable-plate dam construction. The fastness of cables anchorage and stabilization of the river valley cables anchored on is the determining factors of the dam's orderly operation. The following analysis indicates that cables anchorage is reliable.

(1) Compared with other kind of dams, the load of cable-plate dam is simpler. First, the dam body is very thin and light, and its weight can be burdened by cables drawn towards downstream, or can be counterpoised by the upward water pressure by making the dam body lean towards upstream slightly. So that the whole dam body would nearly only bear the level force. Second, the cables and plates of the dam are made of flexible materials, which have higher deformation capacity compared with the brittle materials such as concrete, And the dam is arc-shaped.

Therefore, cable-plate dam can survive all kinds threats, such as earthquake, uneven sink of the river valley, deformation of dam foundation, libration caused by dam top overflowing and temperature variety. Thirdly, windthrowing is the nonnegligible load, especially when the reservoir water is not full and the wind blows upstream, windthrowing probably causes dam body swinging or plate detaching. However, this problem can be resolved by arranging the construction period reasonably and regulating reservoir operation scientifically, such as avoiding constructing in windy seasons and lowing down reservoir water lever too much, or by fixing up ropes downstream to draw dam cables and strengthen the fastness of plates on cables.

(2) As for the low or medium dam in narrow and steep river valley, the needed cables are slim and can be anchored in the holes drilled in the river valley slope, which is feasible and be verified by many practices, such as the cables anchorage in suspension bridge building.

(3) The anchorage of cables is more reliable in cable-plate dam than in suspension bridge. The reason is that the latter's stability relies on the mass of the anchoring pier and of the soil covered on it, and the former on the anchorage length and the height of riverside. It is obvious that as long as the cables anchorage length and the height of the rock covered on the anchorage area is enough, the cables anchorage is reliable. And, it is easy to choose appropriate anchorage orientation and to decide enough anchorage length.

(4) The water pressure and the normal component of the cables tensile force acting on the riverside around the dam are opposite in direction. So, water pressure is contributive to the stability of the riverside slope at the dam as well as to cables anchorage.

(5) The cable anchorage area in rock of the riverside slope can be reinforced by using high strength anchorage cables. And the displacement or deformation of the anchor head and the anchorage area can be surveyed by using strain gauge resistor and light-guide fiber intelligent system and so on, which secure far more the riverside slope.

It must be pointed out that due to the dam's supporting framework is made of lengths of cables intertwined with lengths of steel wires, the breaking of a length of wire will only lead to stress redistributing in other wires in the same cable, not cause the whole cable breaking. Also, the breaking of a length of cable will only cause part of plate failure, not cause the whole system's collapse. In other words, Except for the failure of slope for anchoring cables, the cable-plate dam's failure only happens partially, thus the damage is limit and it is easy to repair.

5.2 *Construction cost*

Only taking the construction cost into account, cable-plate dam may be more expensive than arch dam. But, if considered comprehensively, the former probably is more economical. Because:

(1) Cable-plate dam can be built from top to bottom. Thus its building avoids largely the flow's disturbance. And because the diversion structure of the dam is very simple, the cost on diversion structure construction and its remove is very low.

(2) The dam construction can be carried out all the year, and needs no artificial temperature control. Except for the cable anchorage and plate insetting in the riverbed and riverside, the other construction work is simple, so the construction duration is short. Thus the project can be put into use early.

(3) As the cable-plate dam's construction needs little local building materials, and occupies small piece of land, it needs little soil and rock excavation and spoil discharging. Therefore, the cost for land occupation and vegetation damage is little.

(4) Water can overflow cable-plate dam or through its body, needless to build diversion way.

(5) Workers, equipments, temporary and attaching projects needed are few, and the cost on them is little.

(6) Little soil and rock excavation and spoil discharging leads little work of slope treatment and of environment rehabilitation, and the cost on them is little.

6 CONCLUSION

(1) Cable-plate dam owns the feature of rubber dam and is built with high strength materials, absorbing the advantage of arch dam in its stabilization relying on the riverside hill slope. It is very slim and its construction needs little local building materials. Meanwhile, the dam's construction needs little construction site, few workers, equipments, temporary and attaching projects. Therefore, its construction needs little excavation and spoil discharging, and nearly causes no environmental damage. Compared with traditional dam construction, which will leave large pieces of high nude steep rock slopes with the trouble of landslide, cable-plate dam is super.
(2) Cable-plate dam is feasible in technology and in economy

REFERENCES

[1], [3] National standard of PRC.GB/T5224–1995, *Prestressed Stranded Wire for Concrete*.
[2], [4] Chen Huahui, Deng Haijing, Li Ming, Lin Xiaosong, *Modern Composite Material*. China Material Press, 1998.

This page intentionally left blank.

New Developments in Dam Engineering—Wieland, Ren & Tan (eds),
© 2004 Taylor & Francis Group, London, ISBN 04 1536 240 7

Design study on impermeability and drainage structure of Longtan RCC gravity dam

Wang Hongbin, Ou Hongguang & Di Yuanfu
Mid-South Design & Research Institute for Hydroelectric Projects, Changsha, Hunan, China

ABSTRACT: This paper presents the seepage features of RCC and grout-enriched vibratable concrete (abbreviated as GEVR) and raises design illustrations regarding the dam impermeable structure placed jointly by GEVR and II-graded RCC.

1 PREFACE

The Longtan Hydroelectric Project lies on the upper reaches of the Hongshui River in Tian'e County of Guangxi Zhuang Autonomous Region, with a total installed capacity of 5,400 MW. The Project complex is comprised of the dam, discharge facilities and headrace power intake system and navigation works. The dam is a gravity type in design mainly consisting of retaining section, overflow section, bottom outlet section, power intake section and navigation section, with a dam crest elevation of 406.5m and the maximum dam height of 216.50m. Except the power intake section and navigation section to be placed by the conventional concrete, the rest are placed by rich mixture RCC in full lifts (the maximum cementitious contents in III-graded RCC of 200 Kg/m^3 and cementitious contents in II-graded RCC of 240 Kg/m^3). The spacing of transverse joints is determined at 20.00m for the overflow section and normally 22.00m for retaining section.

Since the RCC dam will be built up by means of continuous thin layer placement without longitudinal joints, there will be a lot of lift joints in a full dam width. Under the effects of aggregate segregation, placement intervals of subsequent layer, ambient temperature and rainfall during construction, construction quality and so on, these lift joints will be the planes of weakness of dam impermeability subject to poor lift joint bond strength or air voids on the high side and seepage paths. Excess lift joint seepage contributes to uplift pressure in lift joints increased with dam safety against sliding decreased, in addition, seepage solution application and high hydraulic gradient application will change the structure of voids inside concrete and thereby short the dam durability. Hence, as one of critical technique elements in need of answer all along in the design of impermeability and drainage structure of Longtan RCC dam, a lot of tests and studies have been done.

2 SEEPAGE FEATURES OF RCC AND GEVR

2.1 *Seepage features of RCC*

For the studies on the design of impermeability structure of Longtan RCC dam, the data relative to the material seepage feature tests for China and aboard RCC dams from the early to the present have been collected, besides that, plenty of tests have been done for Longtan Project itself, the understandings to the seepage features of RCC materials have been improved in depth step by step, to sum up them as follows:

- Distribution pattern of RCC seepage coefficient in conformity with logarithmic normal distribution.

- Parent RCC is good in impermeability and homogeneity. The increased cementitious contents are beneficial to improving the RCC impermeability. The impermeability of RCC with mediate cementitious contents or rich cementitious contents is significantly increased compared to that of lean mixture earlier. The impermeability of parent RCC with cementitious contents higher than 150 Kg/m^3 is basically equal to that of conventional concrete. With consideration to this, the seepage of parent RCC placed by rich mixture RCC would not be the main element in the dam design.
- The seepage coefficient of RCC in line with the lift joints is normally 10~100 times compared to that of RCC vertical to the lift joints due to the effect of lift joints on the RCC impermeability. After the increase in cementitious contents, the anisotropy (in normal and tangential directions) of RCC impermeability has a reducing tendency, the laboratory core testing indicates a seepage coefficient difference not more than 10 times, but this kind of difference may be more indicated by the hydraulic pressure test results.
- Proper contents of un-reactive materials (such as stone powder) is helpful to improving the workability of concrete mixtures and strengthening the ability against segregation and increasing impermeability, compactness and homogeneity as well as decreasing hydration heat.
- RCC layer placement intervals and lift joints treatment both have a great effect on the lift joint impermeability. The subsequent layer placed prior to initial set can achieve good impermeability due to short interval. The timely treatment in terms of bedding materials provided to initially set layer could significantly increase the lift joint impermeability. For the RCC to be the impervious structure, it is essential to provide the lift joint treatment to continuously placed layers to increase impermeability and homogeneity of lift joints. The impermeability of cold lift joints after long interval is not better than continuously placed lift joints in spite of the provision of lift joint treatment, in this case, the study on lift joint treatment has to be further strengthened.
- Construction workmanship has a direct effect on the RCC impermeability. Under the same climate condition, sloped layer method is helpful to increasing the RCC impermeability due to its short placement time. During RCC construction, lift joint bond strength is subject to concrete placement method, for example, truck transportation would pollute the placement surface. The RCD method would not be a perfect one for increasing impermeability.
- The coefficient of variation obtained from in situ hydraulic pressure test larger than that obtained from laboratory core seepage testing indicates that RCC construction is quite subject to the various factors such as environment, the corresponding seepage behavior is a larger discretion of seepage coefficient of lift surface or inter lifts. In spite of the quite homogeneity of integrated impermeability already achieved in some RCC dams, the discretion of impermeability in great majority of dams is still higher. Therefore, adequate space shall be considered in the design of drainage to ensure drainage pipe going though big strong seepage planes.
- Unless the occurrence of bigger cracks or the withstand of so higher hydraulic gradient subject to concrete voids structure broken, the RCC impermeability is stable and improved more over (that is self healing effect) with continuous secondary hydration under the effect of seepage water. Hence, impermeability structure shall consider necessary temperature control and limitation on hydraulic gradient.
- With the contribution of reducing the maximum particle size of aggregate and stronger ability against segregation increased thereby as well as increased cenmentitious contents, the integrated impermeability of II-graded RCC is significantly super compared to III-graded RCC. The results of hydraulic pressure test indicate that the difference between both kinds of RCC impermeability is three times approximately smaller than the 5~10 times of difference obtained from the laboratory core seepage test, in addition, the seepage rate of II-graded RCC can reach less 1 Lu when its guaranteed efficiency reaching 90%, say that the integrated impermeability of II-graded RCC approximately approaches to that of the conventional concrete impermeability. Hence, the design shall consider the full role of the impermeability of parent II-graded RCC.
- Being the weak planes for the stability and seepage of RCC dam, the lift joints has been paid high attention in the design and construction. With the improvement in construction workmanship and promotion of lift joint treatment, lift joint bond strength is increased significantly, seepage paths would probable occur in parent RCC or around the vicinity of coarse aggregates.

- A concern shall be given to such normal issue that initial seepage pressure is lower in the RCC core specimens, so the hydraulic gradient control in this kind of RCC which will act as impermeable structure shall be particularly considered.

2.2 *Seepage feature of GEVR*

In light of the analysis on the results of GEVR core seepage test for one project, we can get following GEVR seepage features. Based on these understandings, we think that it has great possibilities to apply GEVR to impermeability structural components of RCC dam. It deserves to mention that whole GEVR samples are obtained by coring effective depth of the dam and processed into specimens for test use. It can be regarded that laboratory core test for the GEVR basically indicates the integrated seepage feature of GEVR.

- The GEVR impermeability has reach conventional concrete level and can completely meet the seepage requirements by the RCC dam with a height class of 200m.
- The degree of homogeneity of in situ cement pastes for GEVR has high effect on characters of GEVR. The homogeneity of cement pasted GEVR after homogenously forced vibration approximately approaches to that of conventional concrete, far better than that of II-graded RCC, its anisotropy (in normal and tangential directions) of RCC impermeability is not obvious.
- The effect of layer is removed after vibration. The relatively weak planes resulting in GEVR seepage may probably occur at joint surface. The studies shall therefore be more given to construction joints treatment.
- The other mechanical indices of GEVR can meet the requirements of dam impermeable struc ture to be made of by GEVR.

3 DESIGN AND ILLUSTRATION OF IMPERMEABILITY AND DRAINAGE STRUCTURE

In light of the knowledge and in-depth understanding step by step of seepage features of RCC and GEVR, with comparison among alternatives of impermeable structure for Longtan Project in terms of thick conventional concrete, pre-cast slab pasted with PVC film internally, GEVR together with II-graded RCC, post-placed reinforced concrete face slab, asphalt mixtures, it is recommended to use the alternative of GEVR together with II-graded RCC for Longtan Project. This alternative has following critical design elements:

- Make full role of impermeability of parent II-graded RCC and take the II-graded RCC as the main component of impermeability structure.
- In spite of no exclusion to possible occurrence of seepage weak planes in GEVR, but due to so lower probability of such occurrence at the same part simultaneously, the GEVR is applied to the upstream of II-graded RCC to seal the RCC lift surface to prevent partial strong seepage planes in II-graded RCC from connecting with the reservoir, meanwhile, the super impermeability and homogeneity of GEVR compared to II-graded RCC forms a gradually increasing impermeable structure from upstream to downstream, say “block in the front and drainage at the behind”.
- The thickness of II-graded RCC is designed to be 1m ahead of approaching to the upstream side wall of upstream drainage gallery to ensure drainage holes placed within the III-graded RCC with good permeability to be beneficial to making their role of draining and pressure reduction. Spraying the mortar composed of cement and fly ash on each continuously placed II-graded RCC layer to further improve the inter-lifts impermeability within impermeable area.
- The thickness of GEVR varies upon the elevation. The thickness of 1.5m is used with the elevation below 270m. The thickness of 1m is used with the elevation between 270m and 342m. No less than 0.5m is required with the elevation above 342m. The thickness of GEVR mainly depends on the hydraulic gradient control in two kinds of impermeable materials. In addition, a layer of reinforcement for the purpose of constraining cracks shall be applied to the GEVR

surface to prevent harmful cracks occurrence from temperature difFerence between inside and outside.

- The spacing of drainage holes curtain in the dam mass is determined at 2.0m with the elevation below 270m, and 3.0m with the elevation above 270m. With consideration to the discretion of lift surface seepage, drainage holes shall be provided upwards from the inside of dam foundation pumping and drainage gallery to form a pumping and drainage system inside the dam mass to further control the uplift pressure in the lower lifts of the dam mass. This kind of drainage holes curtain has a top elevation of 230m and a spacing of hole of 4m.
- In light of the bad maintenance condition of upstream face of the Longtan Project, in order to prevent the dam impermeability system from the long-period effect of the possible harmful cracks occurring during project operation, an auxiliary impermeable measure in terms of provision of a coat of permeable crystal material shall be applied to the upstream GEVR surface with the elevation below 270m to make up the damage from the cracks.

Under the condition without considering the crystal material coat applied to the upstream, illustration works have been conducted with respects to seepage analysis, temperature artificial calculation and structure durability evaluation regarding the seepage control and structure dependability of the alternative in terms of composite impermeable structure composed of GEVR and II-graded RCC.

The parameters used in seepage calculations are established based on the results of laboratory core test and in situ hydraulic pressure test for the Longtan Project and other recently built-up projects. The calculations consider such various possible statuses as impermeable and drainage structure under normal running, occurrence of local vertical or horizontal cracks defects, seepage coefficient increased, decreased difference of seepage coefficients among GEVR, II- and III-graded RCC, spacing of drainage holes enlarged, local failure of drainage holes. Calculations indicate that since multiple impermeability and drainage systems considered in the design play granted roles generally under aforesaid statuses, safety and dependability of impermeability and drainage structure could be achieved. In spite of the larger difference of seepage flow under various statuses, the uplift pressure exerted in the lift joints all are controlled within the range permitted by the design even though the effect on the uplift pressure from the dam face cracking is also limited locally. Hence, it can be regarded that the impermeability alternative in terms of composite impermeable structure composed of GEVR and II-graded RCC can meet the need of RCC dam with a height class of 200m.

The temperature creeping stress calculations indicate that the dam face would have a high tensile safety coefficient when the dam section of 20m wide. With consideration to the dam structure layout, the spacing of transverse joints determined at 22m in the design can meet the crack resistance of the dam face. The temperature stresses at the same position within a thickness ranging from 0.5m to 1.5m have a slight but vague difference, say that the temperature stress shall not give an effect on the GEVR thickness selection within this thickness range.

Based on the study on RCC solution, an evaluation under the requirement of 100-year durability against solution is given to the RCC life when regarding the solvable CaO 10% and SiO_2 5% as the permitted values, theoretical calculation indicates that solvable contents of II- and III-graded RCC of the Longtan Project are only 12.81% and 26.96% of the permitted values respectively.

4 TECHNIQUE STUDIES FOR COMPLETION OF GEVR IMPERMEABILITY

There are still such issues as optimization of mix proportion and construction workmanship when employment of GEVR for the purpose of impermeability. Both issues directly decide the impermeable effect and quality of GEVR. During the design of impermeability structure alternative, we carried out a special topic study on both issues and basically solved the elements with respects to spreading theory of GEVR cement paste, cement pasting method, optimized cement pasting contents, synchronous with initial setting time of RCC. Special machine tools have been developed particularly used for mechanized construction of GEVR to control and ensure the homogeneity of cement pastes as well as production efficiency increased.

5 CONCLUSIONS

Since many years of studies and design works, the alternative of impermeability and drainage structure of the Longtan Project has experienced a sort of analysis on and comparisons among various alternatives. With the RCC technique development as well as gradually in-depth understanding of RCC impermeability, recently established alternative in terms of composite impermeable structure composed of GEVR and II-graded RCC can meet the need of RCC dam with a height class of 200m and adequately adapt to the need of quick construction workmanship. But the successful application of this alternative still has to depend on strict construction quality control and upon the check by actual operation.

This page intentionally left blank.

New Developments in Dam Engineering—Wieland, Ren & Tan (eds),
© 2004 Taylor & Francis Group, London, ISBN 04 1536 240 7

Influence of MgO on cracks on upstream face of gravity dam

Wang Jian
Department of Water Conservancy and Hydroelectric Engineering, Hohai University, China

ABSTRACT: By means of qualitative analysis and numerical calculation according to experimental data, the influence of MgO to the cracks on upstream dam face of one gravity dam is appraised. The result shows that because of the material differences between designed condition and construction condition, the actual autogeneous volume change of concrete in upstream dam face is smaller than that inside dam body, which additionally produces about 0.2~0.4MPa tensile stresses in the concrete of upstream dam face, unfavorable for crack-prevention. Therefore, more experiments on autogeneous volume change of concrete must be done to verify the conclusion of this paper, and proportions of MgO in cement must be optimized in the coming project construction to exert the crack-prevention effect of MgO.

1 INTRODUCTION

The Dam discussed in this paper (called X dam hereinafter) is a traditional concrete gravity dam. Dam concrete was placed section by section along axis, block by block from upstream to downstream, layers by layers with 1.5m~2.0m thickness of each. During the construction of the dam, scientific methods of quality control and project management have been used strictly As a result, the project is of high quality on the whole.

X dam is a structure of massive concrete which is easy to produce temperature cracks. In order to prevent or reduce the concrete temperature cracks, much attention has been paid to temperature control at design time and during construction, such as carefully designed system of joints and blocks adopted in the structure, optimized concrete mix proportions, integrated temperature control techniques with both pre-cooling of the concrete aggregates and post-cooling of the placed concrete in construction. In addition, the cement with 3.5 to 5 percent of MgO in proportion had been used purposely since April 1998, so as to take advantage of the delayed tiny expansion of MgO concrete to compensate the shrinkage while concrete temperature falls. Despite all this, in the second construction stage, a few cracks had been occurred on the dam. Analysis result indicated that these cracks were surface cracks, mainly caused by temperature stress, and would do no harm to dam safety as long as they were properly treated with.

This paper will not study temperature crack of X dam, but take non-flow section on the left bank as example to evaluate the influence of MgO to the cracks on upstream dam face.

2 GENERAL DESCRIPTION OF THE NON-FLOW SECTIONS

Non-flow sections on the left bank of X dam comprise 18 sections. Figure 1 shows the representative profile of non-flow section. Table 1 shows the grade and primary index of each type of concrete. Among all these non-flow sections, section10# is the one with most cracks on upstream dam face, its cracks distribution is sketched as figure 2. It could be found that cracks were most occurred between elevation 135m and elevation 173m in concrete numbered III.

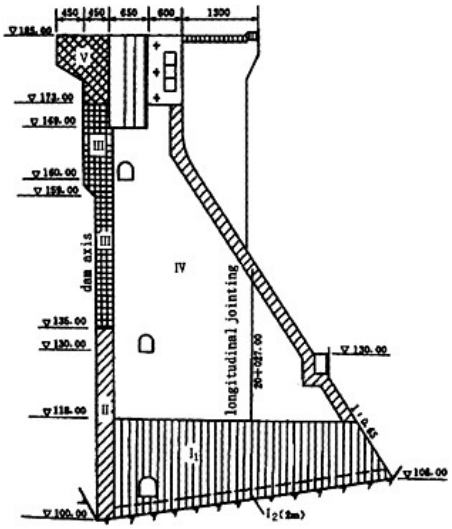

Figure 1. Representative profile of non-flow sections.

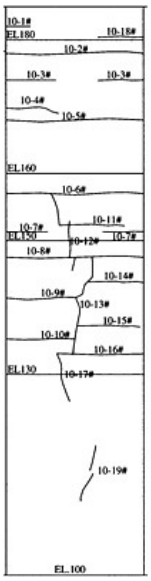

Figure 2. Sketch of cracks distribution of nonflow section 10#.

Table 1. Concrete grade and primary index of non-flow sections on the left bank.

No.	Position		Legend	Concrete grade	Age (d)	Ultimate tension ($\times 10^{-4}$)		Gradation
						28d	90d	
I_1	Bottom of foundation constrained concrete			#200	90	≥0.8	≥0.85	3
I_2	Foundation constrained concrete			#200	90	≥0.8	≥0.85	4
II	Exterior concrete	Always above or below water level		#200	90	≥0.8	≥0.85	3, 4
III	Among water level variational			#250	90	≥0.8	≥0.85	3, 4
IV	Inner concrete			#150	90	≥0.7	≥0.75	4
V	Structural concrete (1)			#300	90	≥0.8	≥0.85	2, 3
VI	Structural concrete (2)			#250	90	≥0.8	≥0.85	2, 3

In order to increase anti-crack ability of concrete, cement with 3.5 to 5 percent of MgO in proportion had been used purposely since April 1998 in second construction stage of the project. Figure 3 shows the relation of autogeneous volume change and age of concrete with MgO of designed condition and actual construction[1][2]. Here, figure 3(b) is mean value of different concretes.

3 INFLUENCE ANALYSIS OF MgO TO CRACKS

It could be discovered from figure 3 that actual autogeneous volume change of inner concrete is greater than that of exterior concrete (including concrete always above or below water level, and

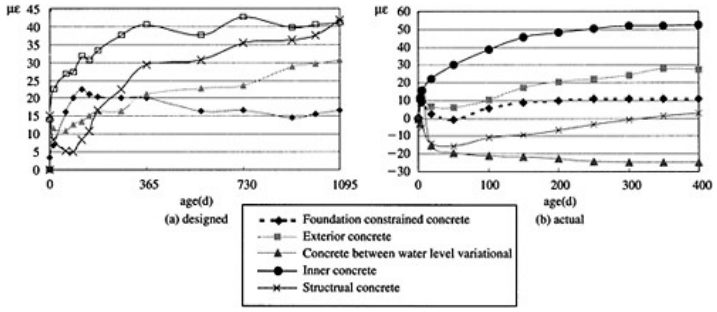

Figure 3. Autogeneous volume change of concrete of designed condition and actual construction.

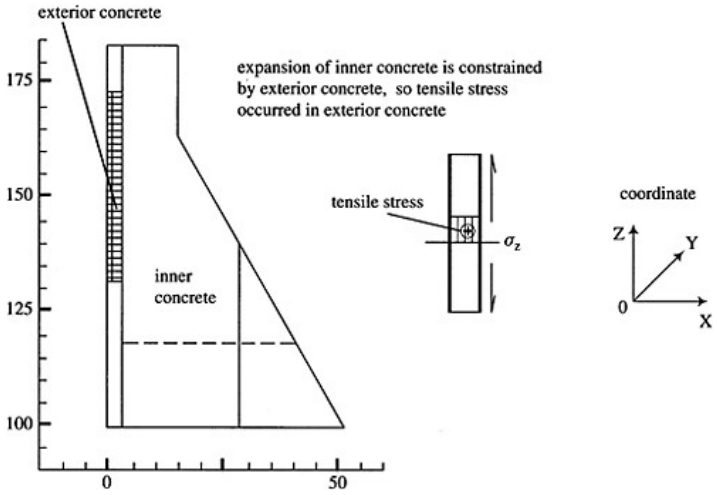

Figure 4. Tensile stresses occurred in exterior concrete in actual construction.

concrete among the field where water level is variational), which is contrary to designed condition, therefore, the expansion of inner concrete is constrained by exterior concrete, then tensile stress occurred in exterior concrete, as demonstrated in figure 4.

The previous qualitative analysis indicates that the material difference between designed condition and construction condition makes MgO concrete unfavorable for crack prevention. In order to quantify this qualitative result, numerical calculation has been executed with FEM. The main results of stresses produced by autogeneous volume change in non-flow section 10# are expressed as figure 5 and figure 6, of which σ_z represents vertical stress, σ_y represents horizontal stress along dam axis, and positive value represents tensile stress.

It could be known through figure 1 that elevation 135m and elevation 173m are the interfaces of concrete III & II and concrete III & V in the upstream dam face, this may be why there are stress jumps at these positions on figure 4 and figure 5.

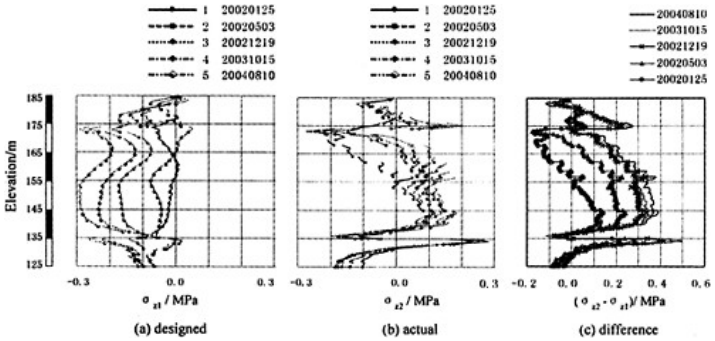

Figure 5. Vertical stresses under designed condition & actual construction and their differences.

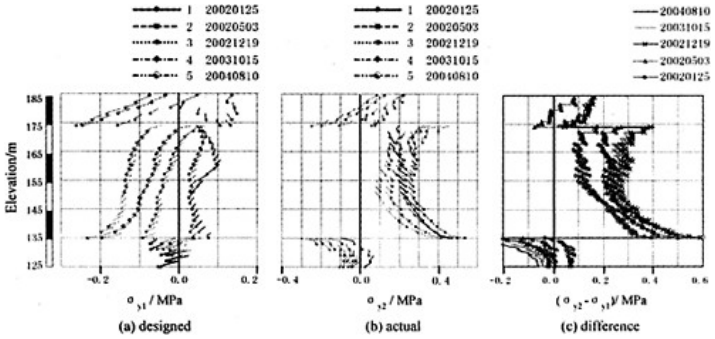

Figure 6. Horizontal stresses along dam axis under designed condition & actual construction and their differences.

Through figure 2, it could be found that cracks were most occurred between elevation 135m and elevation 173m. The stress distribution between these positions has been shown in figure 5 and figure 6. The stress distribution is consistent with crack distribution. It could be dig out through figure 5(b) that from elevation 135m to 173m, actual max vertical tensile stresses produced by autogeneous volume change is mainly between 0.1 to 0.2MPa, which is 0.2 to 0.4MPa greater than designed condition, sees figure 5(c). From elevation 135m to 173m, actual max horizontal tensile stress along dam axis is mainly between 0.25 to 0.35MPa, which is 0.3 to 0.4MPa greater than designed condition, sees figure 6(b) and figure 6(c).

Compare figure 5(b) and figure 6(b) or figure 5(c) and figure 6(c), it could be discovered that max vertical stress it smaller than max horizontal stress along dam axis at same elevation. This is because that concrete was placed layer by layer in elevation and there exists time interval between two layers.

4 CONCLUSIONS

Qualitative and quantitive analysis indicate that because of the material difference between designed condition and actual construction, actual max tensile stress is 0.2 to 0.4MPa greater than designed in exterior concrete of upstream dam face, which is unfavorable for crack prevention. It would be better that more experiments on autogeneous volume change of concrete be done to verify the conclusion of this paper, and proportions of MgO in cement be optimized in the coming project construction.

ACKNOWLEDGEMENTS

This work was granted financial support from China Postdoctoral Science Foundation.

REFERENCES

[1] YANG Fu-liang, “Temperature control measure of the X project concrete”, *Concrete,* No. 9, 2001, pp 36–40.
[2] Experiment Center, “Concrete performance experiments on crack-prevention”, 2002.

This page intentionally left blank.

New Developments in Dam Engineering—Wieland, Ren & Tan (eds),
© 2004 Taylor & Francis Group, London, ISBN 04 1536 240 7

Analysis of durability for sea dam foundation

Jingchun Wang, Weihong Hou & Xizhao Wang
Shijiazhuang Railway Institute, China

Riqing Xu
Zhejiang University, China

ABSTRACT: Durability analysis of sea dam foundation is an important problem which distressed people all the time, especially in eastern Linhai area, where with continuous alternation of salty and fresh water, high humidity, long time of high temperature, and adverse circumstances. In present paper Linhai sea dam foundation is studied from three sides as a typical case, which is the designed water-cement ratio, carbonation depth of concrete, thickness of protective course for concrete. The anti-corrosion measures and some suggestion are set forth. In addition the effect of inundation on the stability of sea dam is studied. The studied result may be used as a basic for the engineering design of sea dam in the future.

1 INTRODUCTION

In China the flood hazard is one of natural calamities that bring about the most serious economy lose. In recent years, as an important part of flood engineering system, although the sea dam has stood the flood test, at the same time also exposed a lot of problems. Zhejiang province is in the southeast coastal area, usually suffered by the raid of typhoon or spring tide because of the geographical position. Once the flood dam collapsed, which would bring the serious hazards for the people life, property and the development of social economy in coastal area. All the time the durability of flood dam is an important problem that distresses people[1] In this paper the sea dam in Linhai, Zhejiang province being an engineering example, combined the field investigations and laboratory experiments, the durability of concrete for sea dam foundation under the action of sea water and the stability of dam under the submerged condition have been studied in order to give a theoretical basis and a practical reference for the similar engineering in the future.

2 ENGINEERING OUTLINE

Linhai is in the central of Zhejiang province, close to the East Sea and a national historic city. In order to quicken the progress of urbanization and improve the capacity of flood prevention of city area, the first-stage flood protection works was decided to construct. The four types of dam were applied as follows: flood dam of reinforced concrete frame, strengthening engineering for seepage control by the standard of flood frequency 1/50 in the section of ancient rampart, earth fill dam of slope, and dam with earth slope in inner side and C20 concrete blocks as protection slope in outer side. The dam is on the alluvial-maritime deposit plain and the ground elevation is 2.7~6.0m.

The stratums in the area from top to bottom were showed in Table 1.

Table 1. Descriptions of stratum in dam area.

Strata code	Soil strata	Descriptions of soil strata	Level of strata top/m	Thickness of strata/m
I	Miscellaneous fill	The principal component were crushed stone and garbage, distributed along the dam.		0~2.3
II_1	Silty clay	Lark~gray, saturation, plastic-soft, medium compactibility	3.3~4.4	0~2.1
II_2	Interbedding of silty clay and silts	Lark~gray, saturation, medium compactibility; the silty clay was the state of soft-plasticity~flow-plasticity, and silts was slight dense	2.3~5.0	0~3.4
III_2	Interbedding of slime clay and silts	Caesious, saturation, the slime clay was the state of soft-plasticity~flow-plasticity, and silts, with high compactibility, was slight dense.	0.9~2	0~6.5
III_3	Slime with sandwich of sand and gravel	Caesious and saturation, the slime was the state of flow-plasticity and high compactibility. The distribution of sand and gravel was uneven, the diameter of gravel was 2~8cm.	−4.7~2.3	0~7.6
III_4	Slime	Caesious, saturation, high compactibility, flow-plasticity	−9.4~−4.4	0.7~9.4
V	Grave-sand cobble	Lark~gray, slight~medium dense, medium~lower compactibility, distributed along the dam and lowered gradually from upriver to down for the top level of strata	−16~−11	0~7.65

3 INVESTIGATIONS AND ANALYSIS OF DURABILITY FOR DAM FOUNDATION

3.1 *Investigations of durability for dam foundation*

Because Linhai is in the eastern coastal area, where with continuous alternation of salty and fresh water, high humidity, long time of high temperature, and adverse circumstances in recent years, the durability of structure is the concern of people all the while. By the end of 1999 there had been a lot of engineering works being similar to the sea dam in the area, whose age was between 5 years and 15 years. In order to guarantee the durability of sea dam to be constructed, based on the specification requests, the past structure had been investigated by these means such as eye-estimation, measurement, hammering and photography. The damage degree of foundation concrete had been statisticed and analyzed. On the basis of general investigation, for the foundation concrete eroded seriously sample by drilling, measure its content of chlorine ion, carbonation depth of concrete and thickness of protective course for reinforcement.

3.2 *Analysis of investigation result*

3.2.1 *Effect of concrete cover of reinforcement*

The investigation result showed, in the position of corrosion and crack of foundation, the thickness of concrete cover of reinforcement was not widely come up to the design request, whereas for the part without corrosion and crack that was mostly close to or exceed the designed thickness. In the past design the three thickness of concrete cover of reinforcement was used, which was 5cm, 6cm and 7cm. Among the measure points of 150, for the thickness of concrete cover of reinforcement

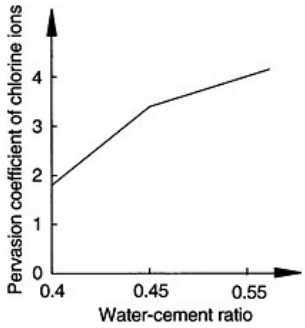

Figure 1. Relation between water-cement ratio and pervasion of chlorineions.

over 6cm there was no corrosion on the whole, and for that of foundation less than 4cm and the age of use over 10 years there corrosion and crack in a great measure.

3.2.2 *Effect of water-cement ratio*

The investigation result indicated to control strictly the water-cement ratio was one of important measures to ensure the durability of foundation for sea dam. Three kinds of foundation was studied, the first was raft foundation with C25 grade of concrete and 0.55 of water-cement ratio; the second cast-in-site bored piles with C30 grade of concrete and 0.4 of water-cement ratio; the last was precast concrete tube pile with C50 grade of concrete and 0.35 of water-cement ratio. It was thoroughly obviously the foundation durability of the first was far lower than the others.

The durability of foundation concrete for sea dam was mainly influenced by the erosion of reinforcement in concrete[2]. The ion of chlorine in seawater and air made the passivation film covering reinforcement damage, and with the congregation of chlorine ions on the reinforcement surface, when they amounted to a certain degree the rusting began. The volume swell of erosive production made the concrete crack, and the microcrack made also oxygen and water be supplemented, which accelerated farther the erosion, caused the volume of erosive production to increase continually and resulted in the longitudinal crack along the reinforcement in protective course of concrete. At this time a lot of chlorine ions penetrated and seawater directly contacted the reinforcement in concrete, the rate of erosion was speeded and the cross section of foundation decreased continuously until the failure. For the foundation concrete with different water-cement ratio and the ages of 5~10 years, the pervasion of chlorine ions was illustrated in Fig. 1.

Compared the raft foundation with the age of 13 years with the cast-in-site bored piles whose age was 15 years, the content of chlorine ions for the former was 3 times as much as that of the latter in the depth of 4~5cm for concrete. Although for the latter the discrete of thickness of concrete cover of reinforcement was larger while being constructed and the minimum was only 2cm, there was no destructive erosion besides the construction joint with few of longitudinal microcracks. In addition, compared the raft foundation whose water-cement ratio was 0.45 and age was 8 years with that of being respectively 0.4 and 10 years, the content of chlorine ions for the former was 2 times as much as the latter in the depth of 5~6cm for concrete. This was because, in the construction, the concrete workability of latter was poorer and the joltingly ramming was strengthened so as to ensure quality, which made the concrete compactness be improved, and the durability farther enhanced also.

3.2.3 *Carbonation depth of concrete*

From the present investigation we knew the carbonation depth of foundation concrete for sea dam was very small. The carbonation depth of concrete with the age of 5 years was almost equal to that with the age of 12 years, which were respectively 2.2mm and 2.5mm, and moreover that was 4.9mm in the air. The carbonation of concrete was not the main mode of failure for these foundations.

3.3 *Suggest*

According to the investigation and survey data in site, for guaranteeing the durability of dam structure the strict measures for the design and construction must be worked out. The grade of concrete should be greater than C30; the water-cement ratio of 0.4 or 0.5 applied according to the regulations; the thickness of concrete cover of reinforcement for the side adjoining water should be greater than 7cm and for the other 5cm; the frame of reinforced concrete should be placed in site as possible as, the quality of vibrating and curing insured, avoided being twisted if while being hung; 16Mn reinforcement used; the content of cement per cubic meter should not be lower than 350kg and the grain size of coarse aggregate controlled according to the density of placed reinforcement.

4 EFFECT OF INUNDATION ON STABILITY OF SEA DAM

In the course of flood the soil of sea dam above the normal water level would be submerged, and in theory the soil above the limit height of capillary rise would be allowed to keep saturation in little time, but in practice they were in the submerged condition for a long time and the saturation area would expanded continuously under the high water level, which made the strength and deformation of the soil change. If at this time the stability of sea dam had been analyzed by using the original index of strength, the calculation result would not accord with the practice and the dam was inclined to the state of insecurity. The effect of inundation on the stability of sea dam must be considered.

4.1 *Effect of inundation on property of soil*

In order to understand well the variety of soil properties under submerged condition the laboratory test had been carried out. Aiming at the practice of shallow soil in the area of sea dam, the representative soil samplings were chosen and the test conformed to test method and standard for soil (GB/T50123-1999). Considering the duration of flood and tide while the sampling be prepared, the submerged time were respectively 0 hours, 12 hours, 24 hours, 72 hours (3 days), and 120 hours (5 days). The test results were illustrated in Table 2.

4.1.1 *Variety of soil strength*

As showed in Table 2, the coherence of soil had been decreased clearly due to the submerged action. In the early of inundation the soil strengthen reduced rapidly, and with the development of submerged time the coherence of soil decreased farther and the extent of decreasing was lowered relatively. After a long time of submerging the soil coherence was almost equal to 0 because it mainly came from the cementing among soil grains and the inundation made the cementation be

Table 2. Soil parameters under submerged condition.

Strata code	Submerged time/h	Direct shear strength		Compression parameters	
		/kPa	ϕ/°	*Es*/Mpa	a_v/MPa^{-2}
II	0	25	33.8	6.04	0.34
	12	21	33.0	5.36	0.35
	24	17	33.2	3.39	0.56
	72	8	32.8	2.49	0.74
	120	3	37.7	2.23	0.83
II_2	0	17	27.7	3.65	0.58
	12	15	27.1	3.57	0.59
	24	10	30.3	3.29	0.63
	72	8	28.2	3.37	0.64
	120	6	31.2	3.06	0.71

destroyed. The degree of cementation was lowered continuously, which made the cementing force be quite weak and the coherence decrease to a great extent[3].

As showed in Table 2, the internal friction angle of soil had been changed on the whole, which is because it is depended on the component constituting soil grains. Although the degree of cementation among soil grains was deceased, the component of soil had not been changed.

4.1.2 *Variety of soil compactness*

Because the cementing force among soil grains was come down in full or part, the soil compactness was increased to a certain extent for the inundation and the settlement of dam was added also. With the increase of submerged time, the compression modulus of soil was lowered by a certain extent and the corresponding compression coefficient was increased. Taking one with another the extent of decreasing for compression modulus, based on the compression test, was between 17% and 63%.

4.2 *Effect of inundation on stability of sea dam*

In order to study the effect of inundation on the stability of sea dam, the representative cross was chosen to analyze (see Fig.2). The computed parameters was illustrated in Table 3, that of the $\square_1$ and $\square_2$ layers was taken as a reference for the miscellaneous fill (*I* layer) and shallow fill because the latter had not been sampled and the submersion test not be done. The layer of III_2 and III_3 was under the water lever and their properties were not affected by the submerged action. The computation principle was the simplified Bishop method[4]. The computed result was showed in Table 4.

From the above we concluded the safety coefficient of stability for sea dam had been decreased due to the inundation and, with the increase of submersion time, the degree of insecurity was enlarged. The effect of inundation on the stability for sea dam was relevant to not only the submerged time and the submerged range, which would endanger the stability and safety of sea dam.

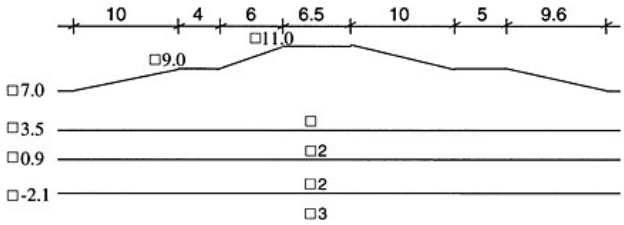

Figure 2. Representative cross section of dam.

Table 3. Computed parameters for stability of dam.

Submerged time of soil/h	Internal friction angle/°	Coherence/kPa
$0(II_2)$	27.7	17
$12(II_2)$	27.1	15
$24(II_2)$	30.3	10
$72(II_2)$	28.2	8
$120(II_2)$	31.2	6
III_2	20.0	7
III_3	31.0	10

Table 4. Safety coefficient of dam under submerged condition.

Submerged time of soil/h	Safety coefficient	Decrease of safety coefficient/%
0	2.497	0
12	2.459	1.6
24	2.442	2.2
72	2.373	5.0
120	20354	5.8

5 CONCLUSIONS

(1) The durability of foundation concrete for dam is influenced by the submersion of sea water, the thickness of concrete cover of reinforcement, water-cement ratio and the good construction, which affected the stability of the flood dam.

(2) The inundation will make the soil strength decrease and the compressibility enlarge, which could lower the safety coefficient of stability for the flood sea dam. The research showed the decrease was by the extent of 1.6%~5.8%, and the lower was that, the longer was the submersion time and the larger was the submersion range.

REFERENCES

[1] Li Tian, Liu Xila. *Analysis and Design of Durability for Concrete Structure.* Beijing: *Science Press.* 1999:1~30.

[2] Almusallam A A, Al-Gahtani A S, Rasheeduizzafar., *Effect of Reinforcement Corrosion on Bond Strength. Construction andBuildingMaterials,* 1996, Vol. 10 (2):123~129.

[3] Wei Rulong, Zhang Ling. *Strength Indexes for Stability Analysis. Chinese Journal of Geotechnical Engineering,* 1993, Vol. 15(2):24~30.

[4] Bishop A W. *The Use of the Slip Circle in the Stability Analysis of Slopes, Geotechnique,* 1955, Vol.5(1): 7~17.

New Developments in Dam Engineering—Wieland, Ren & Tan (eds),
© 2004 Taylor & Francis Group, London, ISBN 04 1536 240 7

Study on temperature crack of concrete dam using nonlinear methods

Wang Runying
College of Water Conservancy and Hydropower Engineering, Hohai University. Nanjing, China

ABSTRACT: On the basis of the analysis of self-organization behavior of temperature cracks of concrete dams, application of nonlinear methods such as fractal theory, synergetic theory, chaos dynamics, catastrophe theory and artificial neural networks are introduced in this paper. (1) Based on geometric characteristics of temperature cracks, the fractal dimension of fracture surfaces of the temperature crack and the fractal dimension of the surface distribution of the temperature crack are calculated with KOLOMOGROV Method. (2) Effect of temperature on the crack is analyzed, and with the consideration of advantages of several kinds of nonlinear methods, a new crack-forecast model is proposed. (3) Using Catastrophe Theory, the method of safety evaluation of the dam with temperature cracks is discussed.

The crack in concrete dams caused by free thermal deformation being restricted is called thermal crack. The crack would lead to the reduction of effective sections, strength and stiffness of structures, ability of resisting freeze-thaw action, fatigue and seepage, the increase of carbonization of concrete and the rust of steel bars in reinforced concrete, so it is very important to study the cause of formation, the propagation and the degree of damage of thermal cracks in dams. At present the majority of methods studying cracks are deterministic methods based on linear theory, which has made many assumption. But they have many forced analogies because the formation and propagation of thermal cracks in some degree are stochastic and non-linear due to the randomness of properties of concrete and load. In this paper we try to use non-linear method to study thermal cracks in concrete dams.

1 NON-LINEAR CHARACTERISTICS OF THERMAL CRACK

1.1 *Influencing factors of thermal crack and cracking criteria*

Many factors would cause thermal crack. In view of different stages of dam, different selections of cement, aggregate, water-cement ratio and foreign matter in design stage all would influence the lasting period and the velocity of hydration heat release, adoption of unsuitable temperature control method in construction stage and long-term adverse load condition in operation stage both would cause thermal crack. Characteristics of material and temperature fields must be considered in studying the formation of thermal crack. Here characteristics of material include thermodynamic characteristics, mechanical properties and geometric distribution of aggregates and micro cracks. Temperature fields include the temperature field of structure itself and that of environment. Formation and propagation of thermal crack are actually the result of coupling of factors above-mentioned and so, they have obvious non-linear characteristics.

1.2 *Description of crack*

Description of crack deals with planar distribution, shape of section plane, depth, length of crack and number or area (density) of crack in unit area. Observing dam face, we can find that single crack is zigzag with continuity and non-differential and distribution of the whole group of crack is approximately stochastic distribution. Observing crack section, we can find that the crack section is composed of many small planes and curved surfaces and many zigzags between them.

1.3 *Propagation of crack*

Propagation of crack is the process of out of stability, propagation and penetration of micro cracks. There are many micro cracks at a crack tip. Along which micro crack does the crack propagate on earth is obviously a non-linear process which can't be explained with linear theory.

Actually, the opening value of thermal crack shows obvious non-linear characteristics under temperature load. For example, the crack tends to close when temperature rises, but the opening value of the crack is approximately invariable with the change of temperature when the crack is closed (that is to say, the opening of the crack is about −0.04mm). In view of microcosmic, propagation of crack shows both gradational property of gradation and catastrophe phenomenon.

1.4 *Effect of crack on dam*

Generally speaking, surface crack would not affect the safety of dam, but in view of systematology and chaos, tiny change of original condition would result in much different sequent. A small crack may grow to important factor influencing dam safety while a larger crack may grow stable due to stress redistribution and stress relaxation and thus it would not threat dam safety badly.

2 ENERGY DISSIPATIVE AND SELF-ORGANIZATION DURING PROPAGATION OF THERMAL CRACK

Combined basic characteristics of dissipative structure with formation and propagation of thermal cracks of concrete, we can obtain following analyses[1][2]:

(1) Concrete structure is related to cement, aggregate of different grain size and all sorts of substances created by hydration reaction of cement and it is also related to base rock and concrete restricting it.

(2) A concrete dam is subject to not only water pressure but also radiation of the sun. Heat will radiate from concrete because of hydration reaction of cement and chemical reaction and heat convection with water and base rock would happen, so dam structure can be regarded as an opening system exchanging substance and energy with the environment all the while.

(3) Hydration heat and impact of cold wave and heat wave will keep the temperature field of structure away from equilibrium state. Stress will come into being in inner restricted region when temperature strain is restricted and the stress will keep the stress field of structure away from equilibrium state. Due to the forced exoteric constraint, if exoteric factors make the system develop away from the equilibrium state, finally the system will transit to another orderly state—cracking state. During this process, many process of energy transform will happen and the imbalance will dissipate with the propagation of cracks.

(4) There exists a critical state of cracking of concrete. For example, only when temperature stress developed to a certain degree, the temperature crack would come into being. There are many micro cracks and the actual development of cracks is always related to the fluctuation of vibration or cold wave. In view of microcosmic, there are more than one cracking direction at the crack tip, perhaps the actual cracking direction is not the direction with maximum stress or maximum cracking coefficient, and tiny fluctuation may exert huge influence to determine the cracking direction of a crack.

As a conclusion of above analyses, the concrete structure possesses four characteristics of dissipative system and can be regarded as the dissipative structure, so we can study it with related theories and methods[1][2].

3 NON-LINEAR METHODS STUDYING THERMAL CRACK

3.1 *Fractal theory*[3]

3.1.1 *Description of crack and related fields*

Studies show that distribution of cracks on dam surface and cracking surfaces both possesses fractal properties. Three-dimensional figures of acoustic measurement and rebound method which can reflect aging degree of concrete also show obvious fractal properties[4]. It is necessary to study thermal cracks of a dam with temperature fields. Isothermal curve and isothermal surface are often used to describe temperature fields of dam. The denser of the isothermal curve or isothermal surface is, the larger of the thermal gradient. The larger of curvature of the isothermal curve or isothermal surface is, the larger of the thermal gradient. So fractal dimension can well describe the thermal gradient and establish a foundation for analyzing cause of formation and propagation of thermal cracks. It has been proved by calculation that isoline and isosurface used to describe temperature fields and characteristic fields of material possess fractal characteristics. Therefore fractal theory can be used to analyze temperature cracks.

There are many kinds of definition of dimension describing fractal structure. Box dimension derived from KOLOMOGROV capacity dimension is more widely applied. KOLOMOGROV capacity dimension is defined as following.

We use (X, d) to denote a distance space, A is a set, $A \subset H(X)$. To each ε > 0, we use N(A, ε) to denote the minimum closed sphere to cover A with the radius of ε, if equation (1) exists, we call D_f as KOLOMOGROV capacity dimension of A.

$$D_f = \lim_{\varepsilon \to 0} \frac{\ln N(A, \varepsilon)}{\ln \frac{1}{\varepsilon}} \tag{1}$$

If the minimum closed sphere in above definition is replaced with cubes, and when covering the cubes are not intersecting with each other, then we can obtain the definition of box dimension as following.

Assume the set $A \subset R_n$ and use the box with the edge length of $1/K_n$ to cover A under Euclidian distance, use $N_n(A)$ to denote the minimum number of boxes to cover A, if equation (2) exists, we call D as box dimension of A.

$$D = \lim_{n \to \infty} \frac{\ln N_n(A)}{\ln K_n} \tag{2}$$

To calculate box dimension of cracks on the dam surface, first increase the value of K_n and calculate corresponding $N_n(A)$ and can obtain a data pair $(\ln K_n, \ln N_n(A))$, then calculate the slope of $\ln N_n(A)$ to $\ln K_n$ with the method of least mean square error, the slope obtained is the box dimension. The box dimension of thermal cracks on surface of Li-shi-men Dam, 1.035~1.318, is obtained by this method.

The method to estimate fractal dimension of joints or fracture surface is explained in detail in reference[5]. Calculation shows that there is obvious correlation between the fractal dimension of fracture surface and the size and the grade of aggregates. The distribution of aggregates in concrete is fractal so roughness and fractal dimension of section can be obtained based on studying the stochastic distribution function of aggregates. Detailed method and process are introduced in reference[6].

3.1.2 *Cause of formation and propagation of crack*

Principal factors affecting the cracking of concrete, such as thermal expansion coefficient, tensile strength, modulus of elasticity, creep properties, thermal diffusivity and hydration heat, are all

related to the sorts and distribution of aggregates of concrete. Many literatures show that fractal theory has been successfully used in studying adsorptive characteristics of sand and distribution of soil particles. Using the methods in those literatures, we can also use fractal method to study above-mentioned characteristics of concrete, especially the relation of fractal dimension of aggregate distribution and parameters above-mentioned.

In reference[7], the definition and expression of fractal damage variable are introduced, the rule of damage and the fractal relation of damage constitutive relation of material are derived. These lay a foundation for studying propagation and stability of cracks using damage mechanics and fracture mechanics achievements for reference.

Sequence of observed data is time sequence. The relation of Hurst index and fractal dimension as shown in equation (3) can be used.

$$D=2-H \tag{3}$$

In which D is Hausdorff dimension, H is Hurst index. Because it is comparatively easy to calculate H using observed data, it is easy to get D using equation (3). The correlation of the time sequence can be known by studying the value of H and the degree of obviousness of non-linear properties of the time sequence can be known by studying the value of D, so we can analyze observed data[8].

3.2 *Chaos theory*

Whether chaos characteristics exist or not lies on two basic characteristics. One is whether the attractor of phase space has fractal geometry of self-similar structure or not, the other is whether the system is sensitive to the original state or not. If the attractor possesses above two characteristics, the time sequence possesses chaos characteristics and it can be forecast with chaos theory.

Correlation dimension based on reconstructing technique of phase space proposed by Packard and Lyapunov index can be used to analyse the characteristics of dynamic system of time sequence. Sequence of observed data of thermal cracks in concrete dam possesses some chaos characteristics, which has been proved by the author, so chaos theory can be used to analyze it.

3.3 *Wavelet Neural Network method*

Wavelet Neural Network is more appropriate for describing crack because it is orthogonal, it has more wide selection and it can subtly describe catastrophe function step by step. Two methods can be used to combine Wavelet Neural Network with ANN model. One is the loose method, that is to say, Wavelet Neural Network is used as a pre-treating tool to get input characteristic vectors for ANN. The other is the close method, that is to say, wavelet function is directly used as the activation function of Neuron. The close method can be used for modelling of crack. Equation (4) and Figure 1 show its expression and structure respectively[9].

$$F(x) \approx f(x) = \sum_{m,k} C_{mk} \Phi_{mk}(x) \tag{4}$$

In Equation (4), F(x) is the observed opening of crack, $f(x)$ is the calculated opening by network.

In Figure 1, input vectors include 18 factors influencing opening of crack such as temperature, water pressure and time effect, the output is the width of crack, Mexican Hat function is used as the wavelet function, BFG method is used as the calculating method, the determination of size parameters and number of nodes of hidden layers is introduced in reference[10]. By comparing many aspects, such as simulating capacity, forecast precision, amount of work of calculating and modeling, especially non-linear simulation of reduction of crack width under the condition of temperature fall, we can find that Wavelet Neural Network occupy a dominant position compared to conventional ANN model.

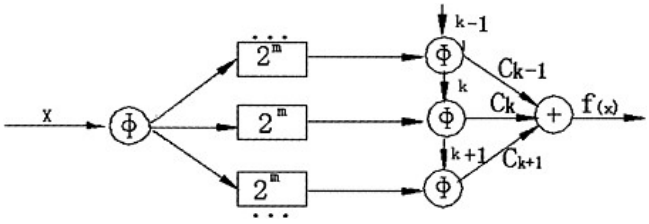

Figure 1. Structure of Wavelet Neural Network.

3.4 *Catastrophe theory*

Cusp catastrophe model[11] has been proposed for analysing propagation of cracks. Cusp catastrophe model has three corresponding states, among which one is unstable and the other two are stable, and two stable states can transform mutually under certain condition, so it is especially applicable to study stability of elastic compression member. From the point of view that propagation of crack is obviously an irreversible process, fold catastrophe model is more appropriate for study of stability of crack[12]. In fact, even if work of load and ductile failure and brittle failure of material are considered, fold catastrophe model can express the actual propagation of crack too. As to cracks, cold wave, sudden high temperature, sudden change of water level and other sudden load would be more likely to cause catastrophe damage. Slow change of material characteristics is less possible to cause catastrophe damage. The result of analyzing the catastrophe model based on observed data of Li-shi-men Dam is consistent to that of observed data.

4 SAFETY EVALUATION OF DAM WITH CRACK

Based on catastrophe theory[13], dam safety evaluation method includes two steps. The first is to build a potential function of crack as follows:

$$V=x^3+ux \tag{5}$$

In this function, x is the status variable which may be length (width) of crack or function of length(width), u is the control variable which may be temperature or function of temperature. According to the discriminant you can know statue development of crack. In the same way, you can get potential function of dam safety with the same expression as equation (5) in which x is the status variable which is safety degree of dam or its function, u is the control variable which may be fractal dimension of crack after catastrophe.

5 CONCLUSION

The non-linear method to study thermal cracks in concrete dams has made some progress. In order to obtain better results, non-linear methods mentioned above are often combined with non-linear numerical analysis, experiment and prototype observation.

Some problems must be resolved in using non-linear method, such as mutil-fractal and selfaffine fractal characteristics of surface crack, catastrophe model selection including fold catastrophe, cusp catastrophe, swallowtail catastrophe, butterfly catastrophe, wavelet function selection etc.

REFERENCES

[1] Shen Xiaofeng, Hu Gang, Jiang Lu. Dissipative Structure, Shanghai People Press, Shanghai, 1987.
[2] G.Nicolis, I.Prigogine. Self-organization in non-equilibrium system, from dissipative structures to order through fluctuations. New York: Wiley, 1977.

[3] Mandelbrot B B. The fractal geometry of nature. Freeman W.H., San Francisco, 1983.
[4] Yuan Qun, Zhao Guo-fan. Fractal characteristics of aged reinforced concrete structure, Journal of Hydraulic Engineering, 2000(12):18–24.
[5] Xie Heping, Parisean W G. Fractal Evaluation of JRC. China Science (B Edition), 1994, 38(5):524–530.
[6] Wang Xie-kang, Fang Duo, Yiao Ling-kan. The fractal characteristics of riverbed roughness with nonuniform sediment. Journal of Hydraulic Engineering, 1999(7):26–31.
[7] Xie He-ping, Ju Yang. A Study of Damage Mechanics Theory in Fractional Dimensional Space. ACTA MECHANICA SINICA, 1999, 35(3):10–18.
[8] Hurst H E. Long Term Storage in Reserviors: An Experimental study. Trans. Am. Soc. Civ. Eng., 1951.
[9] Gao Ping, Xue Gui-yu. Deformation monitoring model for dam based on wave-net and its application in forecasting. Journal of Hydraulic Engineering, 2003(7):107–110.
[10] Zhang J, Walter G G, Miao Y B, et al. Wavelet Neural Networks for Function. IEEE Trans on Signal Processing, 1995, 43(6):1485–1497.
[11] Li Xue-hong, Gu Chong-shi, Zhao Bin. The Mutation Model of Crack in Dam. International Journal HYDROELECTRIC ENERGY. 2000, 18(4):16–18.
[12] Pan yue. Fold Catastrophe Model of Damaging Process in Rock. Chinese Journal of Geotechnical Engineer, 1999, 21(3):299–303.
[13] Poston T, Stevant I. Catastrophe theory and its application. London: Pitman 1978.

New Developments in Dam Engineering—Wieland, Ren & Tan (eds),
© 2004 Taylor & Francis Group, London, ISBN 04 1536 240 7

Study on structural health monitoring design for defective dams

Wang Shijun & Dong Fuchang
Nanjing University, Nanjing Hydraulic Research Institute, Dam Safety Management Center of Ministry of Water Resources, Nanjing, China

Ge Congbing
Nanjing Hydraulic Research Institute, Dam Safety Management Center of Ministry of Water Resources, Nanjing, China

ABSTRACT: More than one third of the total over 84,000 dams in China are defective dams. Both the Central Government and local governments have greatly increased investment in the reinforcement of defective dams. Structural health monitoring is the key to inspection of the reinforcement effects, dam safety assessment and regulation operation for defective dams.

It is surveyed that most of defective dams are in shortage of structural health monitoring which is in need of being established urgently. Presented in the paper are existing situation of defective dams, contents of dam safety assessment, classification of dam safety, principles and contents of structural health monitoring design for defective dams.

1 INTRODUCTION

There are more than 84,000 dams in China, which rank the first in the world. More than 400 dams are large in size (each with a capacity of over 100 million cubic meters), more than 2700 are medium-sized (each with a capacity of 10–100 million cubic meters), and over 80,000 small-sized (each with a capacity of 0.1–10 million cubic meters).

Because of lack of scientific design and construction quality, limited investment and techniques, deterioration with growth of dam age and lack of proper maintenance, many serious safety problems have been resulted in. According to incomplete statistics, 42% of the larger-sized dams, 41% of the medium-sized dams and 36% of the small-sized dams are defective.

Dam safety plays an important role in the national economic construction, social development and stability in China. Both the Central Government and local governments have greatly increased investment in the reinforcement of defective dams. More than ten billion RMB have been invested in the reinforcement of defective dams in recent years and more budget will be made for the next few years.

Dam structural health monitoring is the key to dam behavior and tendency analysis, dam safety assessment, revealing of the potential problems and check of dam reinforcement effect. The International Commission on Large Dam (ICOLD) pays more attention to this subject. The dam safety monitoring committee was set up in the 71st annual meeting of ICOLD on large dam in Montreal, Canada in 2003.

The existing problems of defective dam structural health monitoring include incomplete monitoring items, ageing and low accuracy of instrumentation, obsoleteness of observation method and data analysis, and lack of automation system. Structural health monitoring is essential to the defective dams. A brief introduction of structural health monitoring framework of defective dams is presented in this paper.

2 DAM SAFETY ASSESSMENT AND CLASSIFICATION

2.1 *Dam safety assessment regulation*

"Methods for Dam Safety Appraisal" was enacted to improve appraisal practices for dam safety in 2003. "Guidelines for Dam Safety Evaluation" (SL 258–2000) was issued in 2000 to guide appraisal practices.

2.2 *Contents of dam safety assessment*

The guideline mentioned in chapter 2.1 has defined the appraisal activities in detail (including assessment of engineering quality, review of reservoir operation, check of flood control standards, assessment of seepage safety, assessment of structure safety, check of seismic design, evaluation of metal structures and comprehensive evaluation of dam safety appraisal reports), methods and standards.

2.3 *Classification of dam safety*

The method mentioned in chapter 2.1 has defined the three-grade classification. Dams with the classification of Grade I can safely operate as design standard without abnormal structural behavior and quality defection, and the flood control capacity can reach the design standard. Dams of Grade II can safely operate in the prerequisite of limited standard because the structural behavior is abnormal or flood control capacity only reaches the minimum standard made recently. Dams of grade III can not safely operate as design standard because the structural behavior is seriously abnormal or flood control capacity can not reach the minimum standard made recently.

3 DESIGN FRAMEWORK

3.1 *Principles*

Unlike dams under construction, the defects of existing defective dams have been recognized. Design should be emphasized in defects and abnormal behavior of the dams.

The existing monitoring apparatus should be checked and appraised in accordance with apparatus modification for the integrated monitoring layout.

Dam safety monitoring design should be simultaneous with reinforcement design and be applied to check the effect of reinforcement.

Instrumentation should be reliable, practical, effective and advanced. The manual monitoring should be incorporated with the automatic one. The automation degree is related to engineering grade, budget, personnel and requirements.

3.2 *Dam operation performance, structural defects and engineering reinforcement measures*

Dam operation performance is audio-visual appearance in the long-term operation period under the different conditions such as maximum reservoir water level, minimum reservoir water level, sudden variation of water level, and etc. It directly reflects the dam safety behavior.

The structural problems are most serious in defective dams. It is statistically estimated that the structural problems and seepage problems exist in 60% of the dams of Grade III. Several problems such as structural, seismic and seepage problems may happen in one dam. The defective dams should be reinforced. Dam structure, such as dam slope and impervious barrier, will vary after reinforcement. Dam safety monitoring design must be in accordance with reinforcement design and can check the reinforcement effect.

3.3 *Appraisal of existing monitoring apparatus and analysis of monitoring data*

Ageing, variation, loss of effectiveness and damage of monitoring apparatus decrease the accuracy and reliability. The appraisal and metrological test of existing monitoring apparatus is applied to determine their abolition, modification or utilization.

The reasonability and effectiveness of installed data of existing monitoring apparatus are checked to determine whether apparatus can be used.

The monitoring data is analyzed to know dam operation behavior, mechanism and tendency, find out potential defects, and provide parameters for mathematic model and dam safety criterion.

3.4 *Monitoring items and layout*

3.4.1 *Relevant technical specification*

"Technical Criteria on Earth-Rock Dam Safety Monitoring" (SL 60–94) was issued in 1994, "Technical Specification for Concrete Dam Safety Monitoring" (DL/T 5178–2003) was issued in 2003. The above two criteria provide guidelines for monitoring items and layout.

3.4.2 *Monitoring scope*

Monitoring spatial scope includes dam body, dam foundation, dam abutment, reservoir slope near the dam body which seriously affects dam safety, and other constructions which directly and seriously affect dam safety.

3.4.3 *Monitoring items*

Deformation, seepage and other items related to environments are considered.

3.4.3.1 Embankment dams

Seepage monitoring is the most important item for embankment dams. Piezometer water level in dam body, foundation, abutment and seepage flow should be included. Observing line and leveling are applied in surface deformation monitoring. Displacement meters are applied in deformation and fissures monitoring.

3.4.3.2 Concrete dams

Deformation monitoring is the most important item for concrete dams. Plumb line coordinator, wire alignment and vacuum tube laser collimating line are applied in horizontal displacement monitoring. Precise leveling and static hydraulic leveling are applied in vertical displacement monitoring. Uplift pressure and seepage flow also should be observed.

3.4.3.3 Other items

Other items include water temperature, atmospheric temperature, atmospheric pressure, rainfall, reservoir water level, and tag water level. Data of rainfall and reservoir water level can be obtained from the database of hydrological data acquisition system.

3.4.3.4 Layout

Layout is determined by topographical conditions, geological conditions, dam body filling quality, dam operation performance, reinforcement measures, and existing monitoring apparatus. Monitoring layout should be related with data analysis and controlling criteria determination. All points for different items are taken into general consideration.

3.4.3.5 Perambulation monitoring

Perambulation monitoring is very important. Instrumentation layout mentioned in chapter 3.4 is restricted in one point. Dam is heterogeneous. It is impossible to have monitoring points everywhere. Site inspection is necessary.

3.5 *Instrumentation*

Instrumentation includes sensors, monitoring controlling unit (MCU) and central controlling unit (CCU). They should meet the criteria of "Fundamental Specification of Equipment of Automation System for Dam Safety Monitoring" issued by the Ministry of Water Resources of P.R. China in 2001.

General functions and technical indexes of a sensor should reach the national criteria. The sensors which have no national criteria should reach the ministerial criteria or enterprises' criteria. Zero drift in one year can not exceed 40% of accuracy.

Monitoring controlling unit has the functions of measuring, controlling, communication, storage, automatic check, protection against lighting and interference, and power supply. Circuit design should be standardized and modularized. Manual measuring interface should be provided.

Central controlling unit should have the functions of automatic control, manual control, selfcheck and alarm for monitoring data, self-check of system and display of trouble, management of monitoring data, manual input and power supply.

3.6 *Network communication*

Communication between MCU and CCU and that between CCU and CCU should be considered.

All MCUs are connected with computers through a bus to transmit controlling command and measuring data. Transmission media may use electric cable, optic fibre, ultra-short wave and PSTN, etc. Communication among computers usually compose local area network. Remote computers receive monitoring data through PSTN and DDN.

3.7 *Dam safety management information system*

Dam safety monitoring really achieves its purpose by the application of dam safety management information system. Dam safety management information system includes data acquisition software, data compilation software, data analysis software and information software. Contents of analysis can meet the requirements of "Guidelines for Dam Safety Evaluation" (SL 258–2000) and "Regulations of Data Compilation for Earth-Rock Dam Safety Monitoring".

Information system may have the functions of management, inquiry and browse in INTERNET/ INTRANET. Related software is developed in VB, VC++, C# and etc.

4 CONCLUSION

Dam structural health monitoring is the key to appraise defective dam safety and check the effects of dam reinforcement. Design of dam structural health monitoring should be simultaneously made with dam reinforcement design. Dam operation performance, structural defects, engineering reinforcement measures, appraisal of existing monitoring apparatus and analysis of monitoring data should be considered in determination of monitoring layout.

Automation of dam structural health monitoring system is related to engineering grade, budget, personnel and requirements. Instrumentations should be reliable and practicable and their technical indexes and functions should reach relevant criteria. Dam safety management information system is a essential and eventual means of dam structural health monitoring.

REFERENCES

[1] Zhang Jiyao, "Speech in the National Conference on Defective Dam Reinforcement", 2001.
[2] *Guidelines for Dam Safety Evaluation* (SL 258–2000) issued by the Ministry of Water Resources of P.R. China in 2000.
[3] *Methods for Dam Safety Appraisal* issued by the Ministry of Water Resources of P.R. China in 2003.
[4] *Technical Specification for Concrete Dam Safety Monitoring* (DL/T5178–2003) issued by the National Economy and Trade Committee of P.R. China in 2003.
[5] *Technical Criteria on Concrete Dam Safety Monitoring* issued by the Ministry of Water Resources of P.R. Chinain 1994.
[6] *Fundamental Specification of Equipment of Automation System for Dam Safety Monitoring* issued by the Ministry of Water Resources of P.R. China in 2001.
[7] *Regulations of Data Compilation for Earth-Rock Dam Safety Monitoring* (SL 169–96) issued by the Ministry of Water Resources of P.R. China in 1996.

New Developments in Dam Engineering—Wieland, Ren & Tan (eds),
© 2004 Taylor & Francis Group, London, ISBN 04 1536 240 7

Analysis of monitoring data of landslide in Geheyan Reservoir using data mining algorithm

Zhi-wang Wang
China University of Geosciences, China; Changjiang River Scientiflc Research Institute, China
Man Zhang, Shui-shan Ma, Duan-you Li & Di Li
Changjiang River Scientiflc Research Institute, China

ABSTRACT: Safety monitoring is a very useful method for evaluating the stability of landslide and forecasting its developing trendency. Data mining has been widely applied to commercial fields such as bank, telecommunication, insurance, transportation and retail business. It has successfully helped to obtain lots of uncovered knowledge and solved many problems in such fields, as compared to other traditional statistics. But up to now, data mining was seldom applied in scientific research areas, particularly in analysis of monitoring data of landslide. This paper apply with association rule, one commonly used the technology of data mining, for analyzing the monitoring data of Maoping Landslide in Geheyan Reservoir of Qingjiang catchment, Hubei Province, China. Based on data mining method, we could obtain some rules and knowledge to help analyze effectively the deformation mechanism of the landslide. The results indicate that data mining is feasible and effective to deal with some problems that couldn't be solved though other common methods.

1 INTRODUCTION

Safety monitoring is a very useful method to evaluate the stability of landslide and to forecast its developing trendency. The monitoring data contains a lot of useful information of the landslide, however, no effective methodology was applied to interpret the monitoring data. Thus, it is necessary to seek for some more effective methods to delineate the monitoring data to successfully analyze the deformation mechanism and evaluate the stability of landslide.

Data mining is a kind of technology to obtain potential and useful information from lots of incomplete, noisy, fuzzy and random data. It is the core part of knowledge discovery in database (KDD) and the algorithm of data mining affects directly the result of discovering knowledge.

Data mining has been widely applied to commercial fields such as bank, telecommunication, insurance, transportation and retail. It has successfully helped to obtain lots of uncovered knowledge and solved many problems in such fields, as compared to other traditional statistics. But up to now, data mining was seldom applied to the scientific research areas, particularly in analysis of monitoring data of landslide because it is mainly designed to deal with the data of Boolean type.

A number of data mining algorithms have been introduced to the community that perform statistic description of the data, classification of data with respect to a target attribute, deviation detection, and other forms of data characterization and interpretation. One popular summarization and pattern extraction algorithm is the association rule algorithm, which identifies correlations between items in transactional databases. This paper tries to apply association rule mining technology to analysis of the monitoring data for landslide.

2 ASSOCIATION RULE MINING

A number of data mining algorithms have been recently developed that greatly facilitate the processing and interpreting of large stores of data. One example is the association rule mining algorithm, which delineates correlations between items in transactional databases.

2.1 *Description of association rule mining*

An association rule is something like an implication: $X \Rightarrow Y$ means that if itemset X occurs in a transaction, than itemset Y also occurs with high probability. This probability is given by the *confidence* of the rule. It is like an approximation of p(Y/X), it is the number of transactions that contain both X and Y divided by the number of transaction that contains *X,* thus

$$conf(X \Rightarrow Y) = \frac{\sup p(X \cup Y)}{\sup p(X)}.$$

The *relative support* of the association rule $X \Rightarrow Y$ is the support of itemset  . The lift of $X \Rightarrow Y$ tries to capture the independence of the antecedent and the consequent of the rule:

$$lift(X \Rightarrow Y) = \frac{\sup p(X \cup Y)}{\sup p(X) \sup p(Y)}.$$

An association rule is *valid* if its confidence, support and lift are greater than or equal to the corresponding threshold values.

In the association rule of mining problem, a transaction database and a relative support threshold (traditionally denoted by *min_supp*) a confidence threshold (traditionally denoted by *min_conf*), and a lift threshold are given and then all relative valid association rules are presented.

2.2 *The Apriori algorithm of association rule mining*

The Apriori algorithm is an example of association rule mining algorithm. An association rule discovery algorithm searches the space of all possible rule patterns that meet the user-specified support and confidence thresholds. One example of an association rule algorithm is the Apriori algorithm designed by Srikant and Agrawal[1]. Using this algorithm, candidate patterns, which receive sufficient support (often occurring sufficiently) from the database, are considered for transformation into a rule. This type of algorithm works well for complete data with discrete values. The process of discovering association rules can be divided into two steps:

(1) Find all itemsets (sets of items appearing together in a transaction) whose supports are greater than the specified thresholds. Itemsets with minimum support are called frequent itemsets.
(2) Generate association rules from the frequent itemsets. To do this, consider all partitionings of the itemset into rule of both left-hand and right-hand sides.

Confidence of a candidate rule $X \Rightarrow Y$ is calculated. All rules that meet the confidence thresholds are reported as discoveries of the algorithm.

L1:={frequent 1-itemsets};
k:=2; // k represents the pass number
While ($L_{k-1} \neq \varnothing$)
C_k=New candidates of size k generated from L_{k-1}
For all transactions $t \in D$
Increment count of all candidates in Ck that are contained in t
L_k=All candidates in C_k with minimum support
k=k+1
Report $U_k L_k$ as the discovered frequent itemsets

The first pass of the algorithm calculates single item frequencies to determine the frequent 1-itemsets. Each subsequent pass k discovers frequent itemsets of size k. To do this, the frequent itemsets L_{k-1} found in the previous iteration are joined to generate the candidate itemsets C_k. Next, the support for candidates in C_k is calculated through one sweep of the transaction list. From L_{k-1} the set of all frequent (k−1) itemsets, the set of candidate k-itemsets is created. The intuition behind this Apriori candidate generation procedure is that if an itemset X has minimum support, so do all the subsets of X. Thus new itemsets are created from (k−1) itemsets p and q by listing p.item1, p.item2, p.item(k−1), q.item(k−1). Items p and q are selected if items 1 through k−2 (ordered lexicographically) are equivalent for p and q, and item k−1 is not equivalent. Once candidates are generated, itemsets are removed from consideration if any (k−1) subset of the candidate is not in L_{k-1}.

3 AN EXAMPLE

The case study of the association rule mining aims at the monitoring data of Maoping Landslide in Geheyan Reservoir of Qingjiang catchment, Hubei Province, China. Based on data mining method, we could obtain some rules and knowledge to help analyze effectively the deformation mechanism of the landslide.

The Maoping Landslide firstly showed obvious deformation in 1993 and the displacement has been increasing rapidly from then on. Several inclinometers and underwater boreholes were installed to monitor the stability of the landslide in 1993. The selected data involves the accumulative displacement at orifice of the inclinometer No.l# located in the forehead of the landslide, the accumulative displacement at orifice of the inclinometer No.4# located in the heel of the landslide. The underground water level, rainfall, and the surface water level of Qingjiang River were observed through 1993–1995. The obtained monitoring data are characterized as typical numerical value type. The association rule used to deal with the data of Boolean type, thus the data of numerical type must be transformed into Boolean type to meet the requirements by the technology of association rule mining. This is also the reason why data mining is seldom applied in natural scientific researches. In this paper, the monitoring data are divided into several sections according to the values and then the data of numerical type is transformed into Boolean type (showed as Table 1).

By means of association rule technology, we could obtain some useful rules and knowledge about the landslide as followed:

Rule 1: w1-2=yes, rain-2=yes, waterleve-1=yes, $\mathbf{d4\text{-}2 = yes \Rightarrow d1\text{-}2 = yes}$, support: 1, confidence: 1

Rule 2: w1-2=yes, rain-2=yes, waterleve-1=yes, $\mathbf{d4\text{-}2 = yes \Rightarrow d1\text{-}2 = yes}$, support: 1, confidence: 1

Rule 3: rain-1=no, $\mathbf{waterleve\text{-}1 = yes \Rightarrow d1\text{-}1 = no}$, d1-2=no, d4-2=yes, support: 1, confidence: 1

Rule 4: w1-2=yes, rain-2=yes, waterleve-1=yes, $\mathbf{d1\text{-}2 = yes \Rightarrow d4\text{-}2 = yes}$, support: 1, confidence: 1

Rule 5: w1-1=no, rain-1=no, waterleve-2=no, $\mathbf{d4\text{-}2 = yes \Rightarrow d1\text{-}2 = yes}$, support: 1, confidence: 1

Rule 6: w1-2=yes, rain-1=no, waterleve-1=yes, $\mathbf{d1\text{-}2 = yes \Rightarrow d4\text{-}2 = yes}$, support: 1, confidence: 1

Rule 7: w1-2=yes, rain-1=no, $\mathbf{waterleve\text{-}1 = yes \Rightarrow d1\text{-}1 = no}$, d4–2=yes, support: 1, confidence: 1

Rule 8: rain-1=no, waterleve-1=yes, $\mathbf{d4\text{-}2 = yes \Rightarrow d1\text{-}2 = yes}$, support: 1, confidence: 1

Rule 9: w1-1=no, rain-1=no, $\mathbf{waterleve\text{-}2 = no \Rightarrow d1\text{-}2 = yes}$, d4–2=yes, support: 1, confidence: 1

Rule 10: w1-2=yes, rain-1=no, waterleve-1=yes, $\mathbf{d1\text{-}2 = yes \Rightarrow d4\text{-}2 = yes}$, support: 1, confidence: 1

Table 1. The calculated monitoring data of Boolean type transformed from the data of numerical type.

Monitoring No.	Low water table (w1-1)	High water table (w1-2)	Weak rainfall (rain-1)	Strong rainfall (rain-2)	Low water level of river (waterleve-1)	High water level of river (waterleve-2)	Deformation (1#, small) (d1-1)	Deformation (1#, large) (d1-2)	Deformation (4#, small) (d4-1)	Deformation (4#, large) (d4-2)
1	no	yes	yes	no	no	yes	yes	no	yes	no
2	yes	no	yes	no	no	yes	yes	no	yes	no
3	yes	no	yes	no	no	yes	yes	no	yes	no
4	no	yes	yes	no	no	yes	yes	no	yes	no
5	no	yes	yes	no	no	yes	yes	no	yes	no
6	yes	no	yes	no	no	yes	yes	no	yes	no
7	no	yes	no	yes	no	yes	no	yes	no	yes
8	no	yes	no	yes	yes	no	no	yes	no	yes
9	yes	no	no	yes	no	yes	no	yes	no	yes
10	yes	no	no	yes	no	yes	no	yes	no	yes
11	yes	no	no	yes	no	yes	no	yes	no	yes
12	yes	no	no	yes	no	yes	no	yes	no	yes
13	yes	no	no	yes	no	yes	no	yes	no	yes
14	yes	no	no	yes	no	yes	no	yes	no	yes
15	no	yes	no	yes	yes	no	no	yes	no	yes
16	no	yes	yes	no	yes	no	no	yes	no	yes
17	no	yes	yes	no	yes	no	no	yes	no	yes
18	no	yes	no	yes	yes	no	no	yes	no	yes
19	no	yes	no	yes	yes	no	no	yes	no	yes
20	no	yes	no	yes	yes	no	no	yes	no	yes
21	yes	no	no	yes	no	yes	no	yes	no	yes
22	yes	no	no	yes	no	yes	no	yes	no	yes
23	yes	no	no	yes	no	yes	no	yes	no	yes
24	yes	no	no	yes	no	yes	no	yes	no	yes
25	yes	no	yes	no	no	yes	no	yes	no	yes
26	yes	no	no	yes	no	yes	no	yes	no	yes
27	no	yes	yes	no	yes	no	no	yes	no	yes
28	no	yes	yes	no	yes	no	no	yes	no	yes
29	no	yes	yes	no	yes	no	no	yes	no	yes
30	no	yes	no	yes	yes	no	no	yes	no	yes
31	no	yes	no	yes	yes	no	no	yes	no	yes
32	no	yes	no	yes	yes	no	no	yes	no	yes

Rule 11: w1-2=yes, rain-1=no, waterleve-1=yes, $d1\text{-}2 = yes \Rightarrow d4\text{-}2 = yes$, support: 1, confidence: 1

Rule 12: wl-2=yes, rain-1=no, $waterleve\text{-}1 = yes \Rightarrow d1\text{-}1 = no$, d4-2=yes, support: 1, confidence: 1

Rule 13: rain-1=yes, waterleve-2=yes, $d1\text{-}2 = yes \Rightarrow d4\text{-}2 = yes$, support: 1, confidence: 1

On the basis of the association rules and knowledge, we could get some important results about the deformation regulation of the landslide as followed:

(1) Strong rainfall and high underground water level could cause rapid displacement in the heel of the landslide, which could also cause rapid displacement in the forehead of the landslide even though the water level of the river was not very high at the time.
(2) Under the strong rainfall, the whole landslide could show rapid deformation even though the water level of Qingjiang River was not very high at the time.
(3) Strong rainfall could cause high underground water level in the landslide, which could cause rapid displacement in the forehead of the landslide and then could also cause rapid displacement in the heel of the landslide even though the water level of Qingjiang River was not very high at the time.
(4) Under the condition of high water level of Qingjiang River and weak rainfall, the landslide could show rapid deformation in the forehead of the landslide, which could also cause rapid displacement in the heel of the landslide.

The above results show that the association rule is powerful to analyze the deformation mechanism of the landslide, to forecast the developing tendency, and to guide some similar projects to prevent potential and continual landslide deformation. The results also indicate that data mining is feasible and effective to deal with some problems that couldn't be solved though the common methods.

4 CONCLUSIONS

Data mining shows superiority over the traditional statistics to predict the deformation and development of landslide. The case study by applying with data mining targets the monitoring data from the Maoping Landslide in Geheyan Reservoir of Qingjiang catchment, Hubei Province, China. The monitoring data are divided into several sections according to the values and then the data of numerical type is transformed into Boolean type. The results show that the association rule is powerful to analyze the deformation mechanism of the landslide, to forecast the tendency and to guide some similar projects to prevent continual deformation. The results also indicate that data mining is feasible and effective to deal with some problems that couldn't be solved though the common methods.

ACKNOWLEDGEMENT

The research has been supported by a research program of Chinese Ministry of Science and Technology (2002DIB10044).

REFERENCES

[1] Srikant, R. and Agrawal, R. 1997. Mining Generalized Association Rules. Future Generation Computer Systems, 13(2–3).

This page intentionally left blank.

New Developments in Dam Engineering—Wieland, Ren & Tan (eds),
© 2004 Taylor & Francis Group, London, ISBN 04 1536 240 7

Dynamic experimental study of bond-slip between bars and the concrete in Xiaowan arch dam

Wu Shengxing
Hohai University, China

Chen Houqun
Institute of Water Resources & Hydropower Research of China, China

Qu Zhuojie & Chen Yuquan
Hohai University, China

ABSTRACT: The experimental study on the behavior of bond-slip between earthquake-resisting bars and concrete in Xiaowan arch dam is conducted. Tests are conducted on four groups of specimens. The position dependent constitutive relationship of bond-slip between the concrete and bars is obtained. The method can provide sufficient data for plotting the distribution of steel stress, bond stress, and slip. Finally, several practical conclusions are drawn.

1 INTRODUCTION

Contraction joints are going to open when arch dams are subjected to strong earthquake. The large opening width will result in cracking of the water-prove band, leaking and even failure of dams. In regular arch dam design, earthquake-resisting bars placed across the joints are used to restrict the opening width of the contraction joints. When earthquake-resisting bars are subjected to dynamic load, slip will appear between earthquake-resisting bars spanning contraction joints and the concrete. Several problems, such as the minimal safe anchorage length of the bars and the effect of its unbonded free sector cross over the contraction joint, have been studied on.

It has long been recognized that adequate bond strength is the key problem for the joint operation of bars and concrete. Many researches have been carried out on the real distribution of bond stress along a reinforcing bar embedded in concrete (Nilson 1972; Mirza et al. 1979; Eligehausen et al. 1983; Abrishami et al. 1996; Kankam 1997; Pecee et al. 2001; Harajli et al. 2002). However there is still no constitutive bond stress-slip relationship that can be fit for any case.

Four groups of specimens are designed in this research to study on the following objectives: (1) to find rational solution to aseismic measurement for arch dams (2) to deduce "position-dependent" constitutive bond stress-slip relationship.

2 EXPERIMENTAL DETAILS

2.1 *Specimens*

The section dimensions of specimens are all 600mm×600mm. The sketch of typical specimen is shown in Fig. 1. To fix the specimen, a sub-base is added to its bottom. A plastic tube is fixed to the loaded end of the bar to simulate the unbonded "free sector" to separate bar and the surrounded concrete.

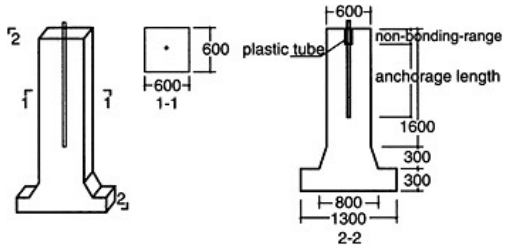

Figure 1. Shape and dimensions of specimens.

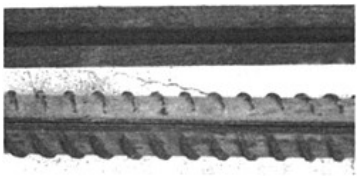

Figure 2(a). Bar fitted with strain gauges.

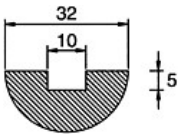

Figure 2(b). Instrumentation of bar.

Table 1. The mechanical parameters of concrete.

Test	1st group	2nd group	3rd group	4th group
Tensile strength (MPa)	2.99	2.77	2.61	1.31
Compressive strength (MPa)	47	42	38.4	13.64
Young's modulus (MPa)	–	25519	24537	25568

2.2 *Reinforcement*

Two kinds of bars with diameter of 32mm are used. In the first group of specimens, bars without distinct yield strength are used. The specified yield strength of the bar is about 1062MPa/mm^2. In the subsequent specimens, bars with distinct yield strength are used. The yield strength of the bar is about 472MPa/mm^2.

2.3 *Instrumentation*

The instrumentation of bars is prepared as shown in Fig. 2(a). A 32mm diameter steel bar is longitudinally sawn into two pieces. The half bar is milled to provide a channel 10-mm wide and 5-mm deep to stick strain gauges [Fig. 2(b)].

2.4 *Concrete*

The materials used in the preparation of the concrete are ordinary Portland cement, sand and graded gravel of 50-mm maximum size. The mechanical parameters are shown in Table 1.

2.5 *Test equipment*

The loading is implemented with dynamic hydraulic servo-actuator with 1000kN capacity, and the process of loading and real time collection of test data are controlled automatically with high precision. The upper part of the actuator is connected with the main beam of a rigid frame for loading,

Figure 3. Test equipment.

Table 2. Loading frequency.

Test	1st group	2nd group	3rd group	4th group
Loading frequency (Hz)	1	1	3	3

and the lower part with primary bar in the specimen. The lower end of the reinforced concrete specimens with the shape of upside-down T is connected with the counter force channel [Fig. 3].

2.6 *Test procedure*

All the specimens are tested under load control. The load is applied incrementally. Every load is composed of eight sine waves. Specimens are divided into four groups. The loading frequency for each group of specimens is shown in Table 2. Each load increment is followed by measurement of the strain in the embedded bar at different positions.

3 TEST RESULTS

The first test with only one specimen is preparatory test. Bars without distinct yield strength are used. When tension in the bars reaches about 700kN, the bottom of the specimen is pulled open, and on the concrete outside surface appears cracks, some of which are breakthrough. The pedestal failure of specimen is resulted from the weak shear strength. For that reason, the bottom dimensions of the specimens of the subsequent groups are increased. Due to uncontrollable ultimate load with bars without distinct yield strength, bars with distinct yield strength should be adopted in the subsequent specimens. In addition, the length of unbanded free sector of bars in the top part of the column (that is the length of plastic tube) is 500mm, consequently when subjected to compression the bar tends to be unstable; while when subjected to tension at the beginning the bar extends so much that the measurement of the slip will be affected. Hence, the length of free sector in the 2nd group of specimens is changed to 200mm from 500mm.

3.1 *The second group of specimens*

The second group includes four specimens, which are numbered as: II-1, II-2, II-3, II-4. The shape of the specimen pedestal is changed from cone to trapezoid in order to facilitate the construction without aifecting the test results. DifFerent from the bars used in the first group, primary

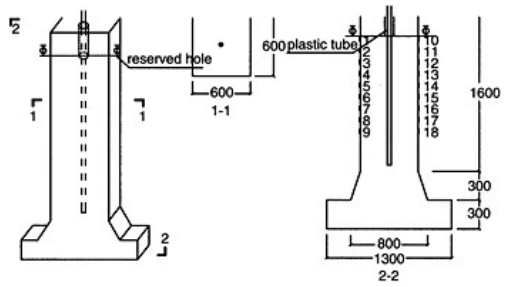

Figure 4. Position of strain gauges on the surface of the specimens.

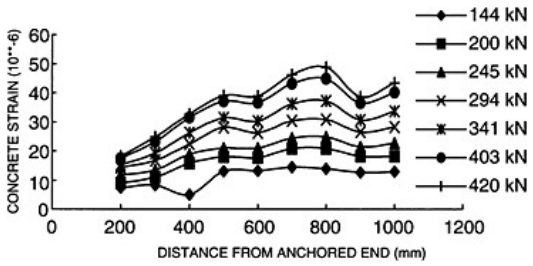

Figure 5. Strain distribution on the concrete surface of specimen II-3.

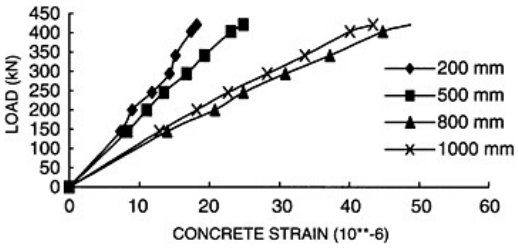

Figure 6. Development of strain on the concrete surface at different anchorage depth for specimen II-3.

bars with distinct yield strength are adopted, the diameter of which is still 32mm. Under the limitation of the rigid frame for loading, sine wave with 1Hz is adopted in this test. In order to prevent bars from buckling, a shift of zero position is given to the sine wave to get the bars under tension during the whole test. Every step of loading consists of 8 full waveform signals.

Eighteen strain gauges are disposed on the surface of the specimens to measure the change of the strain on the concrete surface [Fig. 4]. The strain increases gradually along the anchorage depth. The maximum value of the strain is at anchorage depth of 500mm to 600mm. At the end of the strain curve, the strain tends to descend [Fig. 5]. It is because that the concrete section is not tensioned uniformly. The tension is transferred by bond between bars and the concrete from the center of the section to the outward. And the bond is mainly concentrated in the anchorage depth

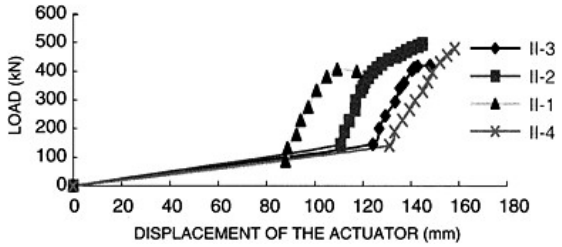

Figure 7. Curve of load and displacement of the actuator of II-4.

of 0mm to 600mm. During the loading history, the concrete strain on the surface of specimens varies linearly. The maximum tension strains are below 50×10−6, less than the ultimate tension strain of the concrete (2.77/25519=108×10−6) [Fig. 6]. Cracks are not observed in the corresponding places.

Figure 7 shows the curve of load and displacement of the actuator of II-4. The curve is divided into three parts. The slope of the first part is relatively small. Besides the bond slip between the concrete and the bar, the displacement of the first part mainly includes displacement of the actuator and the elongation of the bar that are caused by the interstice of the connections and the initial inflection of the bar respectively. The slope of the second part approaches infinity. It means the increment of displacement of the actuator is tiny with the load increasing rapidly. This part of displacement is composed of the elongation of the bar and the bond slip between the bar and the concrete. When the load reaches 360kN, the slope of the curve falls with obvious turning point. It means that displacement of the actuator still increases to a large degree. The third part of displacement is caused mainly by yield of the bar. The above is in good agreement with the fact that the yield strength of the bar is approximately 380kN in the material test.

The failure of the second group of specimens all occurs at the pedestal. The failure loads are 408kN, 480kN, 410kN, 479kN respectively, which all exceed the yield strength of bars. Owing to the 200mm unbonded free sector, no cracks occur on the top of the specimens and no cracks are observed above the pedestal until it falls. The bars are not pulled out, as the anchorage is deep enough. Also, there is no crack in the concrete.

3.2 *The third group of specimens*

The strain distribution of the bar along the anchorage length is measured with the strain gauges placed into the bar [Fig. 2(a), (b)], and the bar stress and the bond stress distribution are obtained indirectly. This group includes four specimens, the shape and dimensions of which are basically the same as those of the second group specimens. The differences of the specimens of this group from that of the second group are as follows: (1) the anchorage depth increases from 1000mm to 1500mm; (2) there is no plastic tube in the loaded end, that means the bar has no unbonded free sector; (3) there is no additional constructive bars; (4) the parameters of the four specimens are same for easy comparing; (5) the loading rigid frame is strengthened to increase its stiffness and the frequency of loading is changed from 1Hz to 3Hz. The measurements of the test mainly includes: (1) the longitudinal strain on the concrete surface; (2) the strain of bars; (3) the circumferential strain of the top of concrete; (4) the displacements of the both ends of the anchorage; (5) the displacement of the actuator. Due to the large displacement of the loaded end of bars the dial gauge is used to measure the displacement of bars. Strain on only one side of the concrete surface is measured.

Due to the fact that the yielding part of the bar is in the loaded end, it is believed that the bar in the concrete keeps elastic during the test, and so the stress of the bar is obtained through equation (1).

$$\sigma = E\varepsilon \tag{1}$$

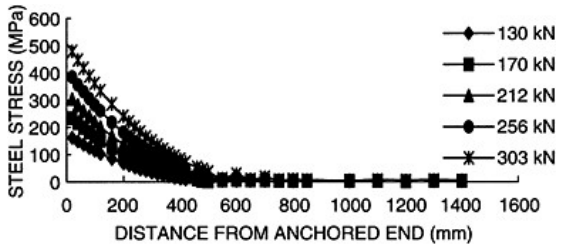

Figure 8. Distribution of the axial stress of bars for specimen III-1.

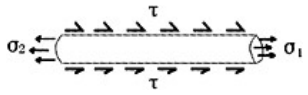

Figure 9. Segment of the Bar.

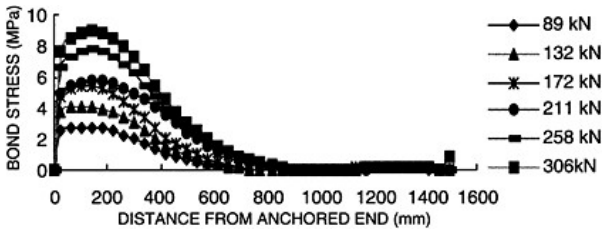

Figure 10. Bond stress distribution of specimen III-2.

Figure 8 shows the distributions of the axial stress of bars under different loads. As the curves show, the axial stress of bars at anchorage depth of 600mm to 1000mm is very small. It means that the load has been transferred to the concrete.

With the axial stress of bars known, the bond stress between bars and the concrete can be worked out by equilibrium equation. Equation can be founded by equilibrium condition of a segment of the bar as follows [Fig. 9]:

$$\tau\pi dl=(\sigma_1-\sigma_2)\pi d^2/4=\Delta\sigma\pi d^2/4 \tag{2}$$

With the aid of (1), we obtain

$$\tau=(d/4)(\Delta\varepsilon/l)E \tag{3}$$

Where d is the diameter of the bar, $\Delta\varepsilon$ is the strain margin of two ends of the segment, l is the length of the segment, E stands for the elastic modulus of the segment.

Figure 10 shows bond stress distribution along anchorage length for specimen III-2. Bond slip between the bar and the concrete is the difference between the displacement of the bar and the displacement of the concrete. The displacement of the bar can be obtained indirectly by the strain of the bar, while it is hard to measure the displacement of the concrete. Because strain gauges must be fitted onto the interface of the bar and the concrete, and the bonding condition will be affected

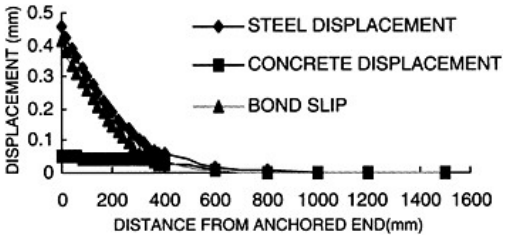

Figure 11. Slip distribution along the anchorage depth for specimen III-1.

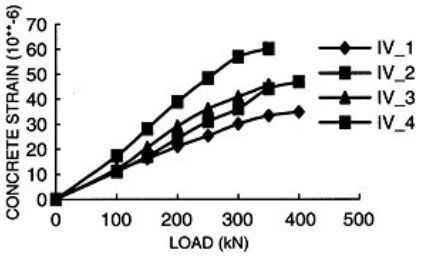

Figure 12. Strain history on the concrete surface at the anchorage depth of 650mm for four specimens.

by strain gauges. Consequently, nonlinear finite element method is applied to calculate the displacement of the concrete on the interface. It is fulfilled by applying the bond force onto the interface of the bar and the concrete in the finite element method. The strain on the surface of concrete measured in the test can be used as a reference to verify the calculated displacement of the concrete. The calculated displacement of the concrete on the interface is so small compared with the displacement of the bar that its error has little influence on the calculation of the bond slip. The slip between the concrete and the bar can be obtained by subtracting the displacement of the concrete from the displacement of the bar. Figure 11 shows the slip distribution along the anchorage length depth under load of 250kN. The curve shows that the distribution of the bond slip along the anchorage length has the similar tendency with the steel displacement.

In order to observe the failure configuration of specimen III-1, loading is continued after the yielding of the bar. When the load is up to 320kN, the bar yields for grooving weakens the section. Then the load is applied statically. When the load reaches about 370kN, breakthrough cracks appear obviously on the outside concrete surface on the anchorage depth of 400mm. The bond strength between bars and unsplit concrete continues to transfer bond force downward. When the load reaches 420kN, column is pulled open along the reserved hole (shown in Fig. 4). As for other specimens, loading is stopped when bars yield. Circumferential cracks can be observed obviously around the bar on the top of the specimens.

3.3 *The fourth group of specimens*

The length of unbounded free sector is set to 400mm. In order to investigate the case for low-strength concrete, the concrete grade of the fourth group of specimens is decreased, as shown in Table 1. Figure 12 shows the strain history on the concrete surface at the anchorage depth of 650mm. The concrete surface strain is relatively small near the loaded end and large near the free end compared with the above groups of specimens. It is because that the bond strength between

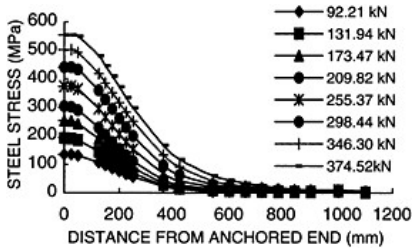

Figure 13. Stress distribution of the bar along the anchorage depth for specimen IV-1.

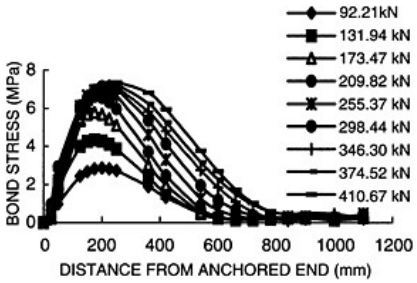

Figure 14. Bond stress distribution along the anchorage depth for specimen IV-1.

the concrete and the bar decreases with the adjustment of the concrete strength. The bond force near the loaded end is small compared with the above groups of specimens, accordingly the concrete surface strain is small relatively at the low anchorage length. On the other hand, for the decrease of the tension strength of the concrete, the concrete around the bar cracked prematurely and the damaged region expands outward. As a result, the concrete surface strain is large relatively at the deep anchorage length. The stress distribution along the anchorage depth for the bar of specimen IV-1 is showed in Figure 13. The stress of the bar at the anchorage depth of about 600mm vanishes to a large extent and the load has been transferred to the concrete by the bond force. Figure 14 shows the bond stress distribution along the anchorage depth for specimen IV-1. The peak value of the bond stress is less than that of the above groups of specimens and the bond stress curve appears to be plumper. The reason is that with the decrease of the concrete strength, the bond strength also decreases accordingly and the concrete at the deep anchorage depth also takes on comparatively large bond force.

The failure form is quite similar of the four specimens in this group. The failure is caused by the formation of a penetrated crack at the free end (the anchor end), which causes the concrete pulled apart along the full section. There are no obvious cracks observed on the top of the concrete before the failure occurs. Bar extends for yielding, the measured displacement of the bar at the column top with the dial gage is about 4mm, and about 1mm at anchor starting point. Those data can be adopted as the criteria for verifying the validity of the results of the Finite Element Method. The failure loads of the four specimens are quite close, which are between 410kN and 440kN.

3.4 *Constitutive bond stress-slip relationship*

The bond stress distribution and the slip distribution under various load steps can be obtained in the same way as those of the third group of specimens. The full cubic polynomial is used to fit the curve of the bond stres and slip relationship as follows:

$$\tau=a_0+a_1x+a_2s+a_3x^2+a_4xs+a_5x^2+a_6x^3+a_7x^2s+a_8xs^2+a_9x^3 \tag{4}$$

where $a_1,\ldots, a_9$=unknown coefficients.

Dealing with test data by the least square method and the optimal approach method, the unknown coefficients can be worked out, and then the "position-dependent" constitutive bond stress-slip relationship can be obtained, namely

$$\begin{aligned}\tau = {} & 1.63-0.002x-8.9s-1.475\times10^{-6}x^2+0.292xs+9.52s^2 \\ & +2.0\times10^{-9}x^3-3.5\times10^{-4}x^2s-0.279xs^2-2.353s^3\end{aligned} \tag{5}$$

It is necessary to satisfy two additional conditions: anchorage position $x<0$; slip $s=0$, $\tau=0$; $s>0.05$mm, τ is computed according to equation (5); $0<s<0.05$mm, τ is computed through linear interpolation between $\tau(0)$ and $\tau(0.05)$.

4 CONCLUSIONS

With the above tests, fundamental conclusions can be deduced as follows:

1. The earthquake-resistant bar should be made of steel with the distinct yield. With the usage of steel without the distinct yield, the ultimate load is uncontrollable, which will lead to the occurrence of penetrated cracks. With the application of steel with distinct yield strength, strain increases while stress remains unchanged after yielding of the bar, which will not bring about concrete cracks by tension.
2. The unbonded free sector is necessary to fit the opening of contraction joint. However, from test results of the 3rd group specimens, we can conclude that to specimens without unbonded free sector on their top, the inner damage in the concrete in the initial bonding range between the concrete and the bar has developed to a great degree. The crack depth along radial direction increases quickly to 150mm, and in the corresponding area the bonding behavior between the concrete and bars deteriorates; while to specimens with unbonded free sector the damage range is no more than 70mm around radial direction.
3. The tensile concrete strength should be no less than 1.5Mpa~2.0Mpa based on the test results that the concrete strength has a comparatively effect on the bond-slip behavior of reinforced concrete. When the concrete strength reduces (shown in 4th group), the peak bond stress on the stress distribution curve along the anchor depth moves deeper, the maximum value decreases and the bond stress distribution curve becomes plumper, with the length within the range of 1000mm before the yield of the bar. The failure load reduces with the concrete strength decreases. In order to assure that the concrete tensile failure does not occurs before the yield of the bar, the concrete tensile strength should not be less than the value of 1.5Mpa (dynamic strength no less than 1.9Mpa).
4. The anchorage depth of earthquake-resisting bars should be no less than 1500mm. When the anchorage depth is more than 1000mm, before the yield of the bar the bond stress is concentrated in the front of the bonding range.
5. "Position-dependent" constitutive bond stress-slip relationship has been deduced for the ribbed bars as shown in equation (5).

REFERENCES

Nilson, A.H. (1972). "Internal measurement of bond slip." ACI J., 69(7), 439–441.
Mirza, S.M., and Houde, J. (1979). "Study of bond stress-slip relationship in reinforced concrete." ACI J., 76(1), 19–46.
Eligehausen, R., Popov, E.P., and Bertero, V.V. (1983). "Local bond stress-slip relationships of deformed bars under generalized excitations." Rep. No. Ucb/eerc 83–23, Earthquake Engrg. Res. Ctr., Univ. of California, Berkeley, Calif.
Abrishami, Homayoun H., Mitchell, Denis. (1996). "Analysis of bond stress distributions in pullout specimens." Journal of Structural Engineering, V 122, 255–261.
Kankam, Charles K. (1997). "Relationship of bond stress, steel stress, and slip in reinforced concrete." Journal of Structural Engineering, V 123, 79–85.
Pecce, M., Manfredi, G., and Realfonzo, R. (2001) "Experimental and analytical evaluation of bond properties of GFRP bars." Journal of Material in Civil Engineering, V 13(4), 282–290.

This page intentionally left blank.

New Developments in Dam Engineering—Wieland, Ren & Tan (eds),
© 2004 Taylor & Francis Group, London, ISBN 04 1536 240 7

Flexural-tensile testing of fully-graded concrete in static and dynamic states for high arch dam

Wu Shengxing, Zhou Jikai & Shen Dejian
Hohai University, China

Chen Houqun
Institute of Water Resources & Hydropower Research of China, China

ABSTRACT: The static and dynamic flexural-tensile properties of fully-graded concrete are important for the seismic safety design of high arch dams. In this paper, the static and dynamic flexural-tensile properties of fully-graded concrete of high arch dam were studied through tests. The fully-graded concrete was loaded by electro-hydraulic servo device. In the static test, the loading rate was 250N/s. In the dynamic test, earthquake was simulated by repeating loading of triangle wave with fluctuating amplitude and 1Hz frequency. Some results were achieved from these tests. Compared with the static test, the flexural strength, initial Young's modulus and cracking strain were increased in dynamic test. The phenomena in the tests showed that the concrete wasn't destroyed immediately after it was cracked. The measured crack load was about 90% of the failure load. Besides, the fracture of large-size aggregates on fracture surface of specimens were also observed obviously. These results from the tests provide effective references for the seismic safety evaluation of structures such as high arch dam.

1 INTRODUCTION

A series of 300-metre high arch dams, such as Xiaowan, Xiluodu and Jinping etc, will be constructed during the western China development. Their seismic fortification intensities reach VIII or IX degree, and the seismic case becomes is the control condition in dam design. During intensive earthquake, the dynamic response and failure process of concrete dams are very complicated. The safety and rationality of seismic design of dams depend not only on the dynamic seismic analysis, but also rely to the dynamic characteristics of concrete used for dam.

Presently, with the recent development of mechanics and calculational methods, the dynamic seismic analysis of dam structure has had great progress. The development of test equipment and techniques makes it possible to relatively rationally simulate various influencing factors in dynamic model experiment of dams, which can better reflect the actual situation. In contrast, research on the dynamic characteristics of concrete in dams as one of the key factors affecting seismic safety, are relatively lagged behind. There are still many basic problems needed to be further studied, which is regarded commonly as the "bottleneck" problem of the seismic safety evaluation of dams.

The fully-graded concrete, normally with three-graded or four-graded aggregate, is always used for dam construction. However, most of the dynamic tests of massive concrete are carried out using small specimens after wet sieving for aggregates. In the small specimens aggregate bigger than 40mm was screened out. Thus, the content of coarse aggregate in the small specimens

Table 1. The mixing proportion of fully-graded concrete.

Strength grade	Gradation	Water cement ratio	Water kg/m^3	Cement kg/m^3	Fly ash kg/m^3	Water reducing agent ZB-1A%	Air entraining agent AEA‰	Slump cm	Air content %	Sand percentage %	Unit Weight kg/m^3
C35	3	0.42	104	173.3	74.3	0.70	1.4	6.4	4.49	30	2450

will decrease by half to two thirds, while the content of gel material will increase one to two times. The changes of mix proportion will inevitably affect the performance index of concrete used in actual dams. Besides, the stress and strain curve obtained from the measured data from a small quantity of normal concrete tests cannot reflect the actual nonlinear effects of fully-graded concrete under the action of dynamic loading, which affects the reasonable and correct assessment of the seismic safety of structures. It is recommended to perform dynamic tests of fully-graded concrete for dam construction, in order to provide scientific basis for safety evaluation of seismic intensity of high arch dam.

In the dynamic analysis for concrete dam under intensive seismic load, the tensile stress is normally the key factor. Concrete arch dam can be regarded as in the eccentric compression structure. So, for arch dams, the dynamic flexural-tensile strength of fully-graded concrete is an important index. In this research all the raw materials and its design mix proportion were related to Xiaowan arch dam. The fully-graded concrete beams were loaded according to tri-point loading method of simply supported beam using electro-hydraulic servo device, to determine the dynamic parameters of fully-graded concrete.

2 MATERIALS

2.1 *Raw material of concrete*

The 42.5 grade medium heat Portland concrete from Red Tower Dianxi cement Company, the I grade fly ash from Xuanwei Power Plant, and the granite man-made aggregates used in the Xiaowan arch dam were selected as the raw materials in the tests. The aggregate consists of biotite gneissic granite and hornblende plagioclase gneissic granite with the ratio of 7.5:2.5. The size grading of the aggregate is: large size stone (80–40mm): mid size stone (40–20mm): small size stone (20–5mm)=4:3:3. The mix proportion of concrete is shown in Table 1.

2.2 *The moulding and curing of concrete specimen*

Fully-graded concrete was mixed for 3 minutes using free falling mixer (250L). The specimen was vibrated to be dense and solid using high frequency resistance vibrator. The mould was removed two days after the moulding of the specimen. Then the specimens were covered with plastic membrane immediately. After curing with watering for one week, they were sealed and kept indoors till test. The specimens used in this test were prepared on Nov.15, 2003. Since the test was carried out on Jan.16, 2004, the age of the specimen is 61 days. The curing temperature was 10 to 20°C.

Six fully-graded concrete specimen (300×300×1100mm), three fully-graded concrete cube specimen (300×300×300mm) and three wet sieving concrete cube specimen (150×150× 150mm) were prepared.

3 TEST PROGRAM

The static and dynamic flexural-tensile test on fully-graded concrete specimen were carried out by using tri-point loading method for simply supported beam. The specimens were loaded using

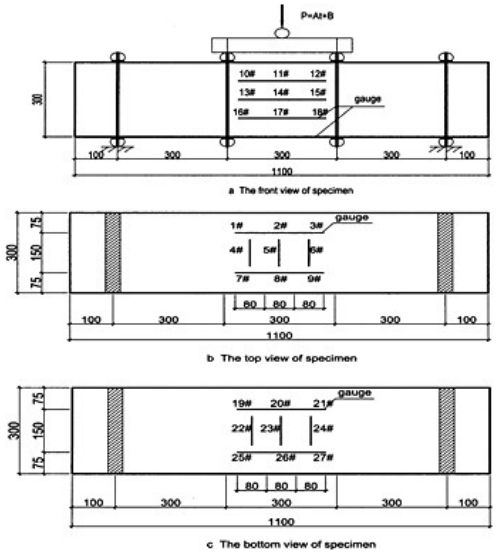

Figure 1. The loading method and the location of gauge.

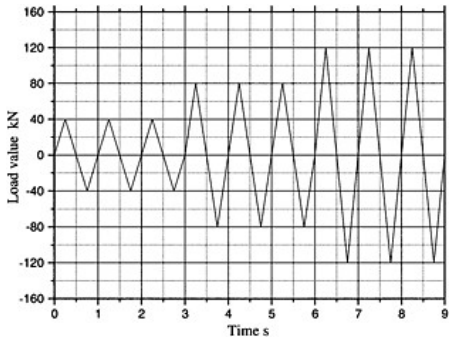

Figure 2. Changes of dynamic loading amplitude.

electro-hydraulic servo device. Data were collected with a sampling frequency of 400 point/s in dynamic test and 40 point/s in static test. The loading method and the location of gauge are shown in Fig. 1. The static loading rate was 250N/s. In dynamic test, specimens were loaded repeatedly using triangle wave with a frequency of 1Hz, which consistent with the fundamental frequency of the Xiaowan arch dam with full reservoir. Changes of loading amplitude are shown in Fig. 2.

4 RESULTS AND DISCUSSION

The six fully-graded concrete specimen were divided into two groups. Both static and dynamic tests were performed for each group. The flexural strength, Young's modulus, cracking strain and measured maximal nominal strain were obtained from these tests. The results are as follows.

Figure 3. The failure photograph of the specimen.

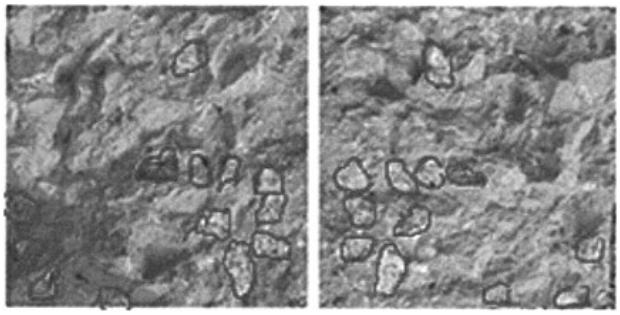

Figure 4. The fracture section photograph of the specimen.

4.1 *The failure phenomenon of specimen*

In the static flexural test, the fully-graded concrete specimens are loaded upwards and the flexural-tensile failure surface is its top surface concrete. In the dynamic test, the specimens are loaded reciprocally (see Fig. 2). Every specimen is failed at the first peak with the loading amplitude of 120KN. and the failure surface is also its top surface. The fracture section of all the six specimen is at the pure bending zone. The photograph of the failure specimen is shown in Fig. 3.

From the observation of the fracture section shown in Fig. 4, both in the static and the dynamic tests, the following fact deserves to be mentioned. In general, the interface strength of aggregate and mortar is considered to be weaker than the strength of the aggregate. However, for high-strength concrete, the coarse aggregate may also be fractured, especially, for the dam concrete with the large man-made aggregate.

4.2 *Static and dynamic flexural strength*

The flexural strength of fully-graded concrete specimen is calculated using the measured failure load, assuming the specimen to be elastic. The calculated results are listed in Table 2. The Values in the table have been deducted the effect of self-weight.

The mean strain rate in the static and dynamic tests is around 1.0×10^{-6} and 1.2×10^{-4} to 1.0×10^{-3}, respectively. The results show that the flexural strength of the fully-graded specimen in the dynamic tests is increased by 30.3% compared with that of the static.

Table 2. The flexural strength of fully-graded concrete specimen.

Specimen number	Loading mode	Flexural strength N/mm^2	Mean value N/mm^2	Rate of increment %
1115316	Static state	2.878	2.941	
1115416		2.970		
1115516		2.974		30.3
1115616	Dynamic state	3.980	3.833	
1115116		3.742		
1115216		3.803		

The static situation is the reference of the rate of increment.

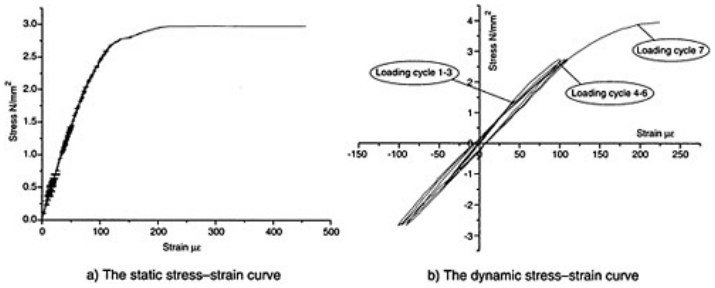

Figure 5. The static and dynamic stress-strain curve.

4.3 *The static and dynamic stress-strain relationship*

In the static and dynamic tests, the stress-strain curve is plotted according to the measured strain of the top surface and the calculated stress considering the specimen as elastic body. The static and dynamic stress-strain curves have its own rule correspondingly as shown in Fig. 5.

Figure 5a is the static flexural-tensile stress-strain curve of fully-graded concrete, and the specimens are in the elastic state in a relatively wide range. Then they are failed shortly after yielding. Figure 5b is the dynamic flexural-tensile stress-strain curve of fully-graded concrete. The specimens are in the elastic state in low stress region, and the hysteresis loop is small. In higher stress region, there is damage in concrete, and the hysteresis loop is bigger and bigger with the increase of stress, then yielding and failure happen. Because the stiffness of test equipment is not sufficient, the sloping portion is not detectable, but a relatively long horizontal portion is detected. This result only reflects that the specimens are distorted instantly, and doesn't indicate that the concrete has good ductility.

4.4 *Static and dynamic Young's modulus*

Young's modulus is one of the most important dynamic parameters of concrete. In the static and dynamic loading tests, according to measured relationship between stress and strain at tension and compression faces, the initial elastic modulus at each loading cycle is taken as the Young's modulus. The elastic modulus in the first dynamic loading process is compared with that in static loading process. The results are shown in Table 3.

It is indicated that the elastic modulus at flexural-tensile state and flexural-compressive state are nearly the same. At flexural-tensile state, the dynamic elastic modulus is 27.8% more than the static elastic modulus, while at flexural-compressive state, the increment amount is 24.9%.

4.5 *Variation of dynamic elastic modulus during loading process*

Normally, impact test is used in the dynamic experimental research on concrete. The concrete is failed after loading one time. Since earthquake action is reciprocal, the dynamic characteristics revealed from this loading method are not suitable for seismic safety design. For the short time reciprocal action, their fatigue effects on concrete can be neglected, while the damage is certainly

Table 3. Static and dynamic Young's modulus of fully-graded concrete specimen.

Specimen number	Loading mode	Young's modulus (N/mm^2) Flexural-tensile state	Mean value (N/mm^2)	Young's modulus (N/mm^2) Flexural-compressive state	Mean value (N/mm^2)
1115316	Static	27930	26520	25350	26587
1115416	state	25200		26200	
1115516		26430		28210	
1115616	Dynamic	35920	33880	36800	33210
1115116	state	32280		30940	
1115216		33440		31890	
Rate of increment %			27.8		24.9

The static situation is the reference of the rate of increment.

Table 4. Variation of dynamic elastic modulus during loading process of fully-graded concrete specimen.

			Loading cycle						
Specimen number		Item	1	2	3	4	5	6	7
1115616	Elastic modulus N/mm^2	Flexural-tensile state	35920	35850	36080	35460	32310	30700	33700
		Flexural-compressive state	36800	36360	37130	35410	32300	30670	
1115116		Flexural-tensile state	32280	32830	31580	31950	29370	25360	25770
		Flexural-compressive state	30940	31080	30760	27530	25410	24480	
1115216		Flexural-tensile state	33440	30750	30570	30540	29660	29530	28340
		Flexural-compressive state	31890	31030	30970	29020	27960	29320	

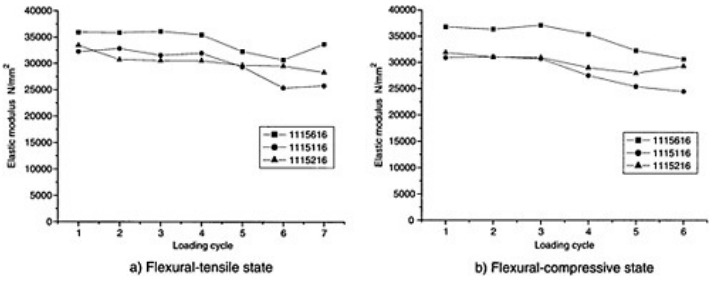

Figure 6. Variation of dynamic elastic modulus during loading process.

present under the effects of strong earthquake. In this test, the specimens are failed at the seventh cycle of loading. The elastic modulus at both flexural-tensile state and flexural-compressive state under the reciprocal loading action during loading period are calculated respectively. The initial elastic modulus at each loading cycle is taken as Young's modulus. The results are shown in Table 4 and Fig. 6.

The elastic modulus decreases with the progress of loading process, indicating that damage of concrete is developed. When the amplitude of loading cycle reaches 40kN, the damage is light. The damage becomes serious and the elastic modulus decreases relatively rapidly during the 80kN cycle.

4.6 *Static and dynamic cracking strain*

It is generally agreed that concrete is failed once it is cracked. In this test, data are collected with high rate, so the moment when concrete is cracked can be detected. Through the analysis of the measured data, it is discovered that when cracks appear, concrete doesn't lose its bearing capacity immediately. Therefore, it is very valuable to test the static and dynamic cracking strain of concrete. In order to detect the crack, the concurrent strain gauges along the top and bottom faces are patched in staggered way. When the strain of one of the three connected strain gauges increases suddenly, but those of the rest two decreases, the mean value of the three strain values at this moment is just the cracking strain. The results are shown in Table 5.

It is obtained from the test that the flexural-tensile cracking strain of fully-graded concrete is 113×10^{-6} during static loading process, and the corresponding flexural-tensile stress is 2.58N/mm^2, which is about 87.7% of the static flexural-tensile strength. During dynamic loading process, the flexural-tensile cracking strain is 154×10^{-6}, and the corresponding flexural-tensile stress is 3.45N/mm^2, which is about 90% of the dynamic flexural-tensile strength. The results show that the dynamic flexural-tensile cracking strain is 26.6% larger than the static one, and the increment of corresponding flexural-tensile stress is 33.7%.

4.7 *Static and dynamic measured maximal nominal flexural-tensile strain*

From the measured flexural-tensile stress corresponding to flexural-tensile cracking strain, it is indicated that concrete isn't failed immediately when it is cracked. From the crack to failure, the strain gauge can still detect the strain of crack deformation. The maximal nominal flexural-tensile strain can be measured by averaging the values of strain gauges at that point. The measured results are shown in Table 6.

Table 5. Static and dynamic cracking strain of fully-graded concrete specimen.

Specimen number	Loading mode	Flexural-tensile crack strain 10^{-6}	Corresponding flexural-tensile stress N/mm^2
1113416	Staticstate	110	2.36
1115416		109	2.67
1115516		121	2.72
Mean value		113	2.58
1115616	Dynamic state	110	2.83
1115116		188	3.71
1115216		164	3.80
Mean value		154	3.45
Rate of increment %		26.6	33.7

The static situation is the reference of the rate of increment.

Table 6. Static and dynamic measured maximal nominal flexural-tensile strain of fully-graded concrete specimen.

Specimen number	Loading mode	Maximal nominal flexural-tensile crack strain 10^{-6}	Corresponding flexural-tensile stress N/mm^2
1115316	Static state	352	2.86
1115416			
1115516		490	2.95
Mean value		421	2.91
1115616	Dynamic state	207	3.43
1115116		224	3.90
1115216		278	3.80
Mean value		236	3.71
Rate of increment %		−44	27.5

The static situation is the reference of the rate of increment.

The measured static maximal nominal flexural-tensile strain is 421×10^{-6}, and the corresponding flexural-tensile stress is 2.91N/mm^2, which is about 97.8% of static flexural-tensile strength. The measured dynamic maximal nominal flexural-tensile strain is 236×10^{-6}, and the corresponding flexural-tensile stress is 3.71N/mm^2, which is about 97.6% of dynamic flexural-tensile strength. The results show that the measured dynamic maximal nominal flexural-tensile strain is 44% less than the static one, and the corresponding flexural-tensile stress increases by 27.5%.

5 CONCLUSIONS

This paper is one of a series of studies. The number of test specimens used in this study is limited. As trial test, the obtained results should be validated by more tests. The dynamic characteristics of concrete are affected by various factors, such as static strength of concrete, water cement ratio, aggregate type, curing conditions, age, geometry of specimen (size and shape), dry-wet environment, initial static load, loading system and rate of loading etc. When high arch dam is constructed at high seismic intensity area, seismic safety is the most important technical problem required to be solved. From now on, a series of researches will be carried out on the main factors affecting the dynamic characteristics of fully-graded concrete discussed above. Reliable conclusions will be drawn, which can provide effective references for the seismic safety assessment of structures such as high arch dam.

ACKNOWLEDGEMENTS

The authors would like to thank Hohai University, and Institute of Water Resources & Hydropower Research of China, for their support of this project.

REFERENCES

Hou Shunzai, Li Jinyu, Cao Jianguo, Wang Ji, Guo Yonggang, Dynamic Tests and Study on the Fully Graded Concrete for High Arch Dam, *Water power,* 2002. 1, 51–68.
W.F.Chen, A.F.Saleeb, *Constitutive Equations for Engineering Materials,* 1994.
Xiao Shiyun, Lin Gao,Wang Zhe, Lu Lüzhou, Effects of strain rate on dynamic behavior of concrete in tension, *Journal of Dalian University of Technology,* 2001. 11, 721–725.
Test Code for Hydraulic Concrete (DL/T 5150–2001), Beijing, China, 2003. 1.

New Developments in Dam Engineering—Wieland, Ren & Tan (eds),
© 2004 Taylor & Francis Group, London, ISBN 04 1536 240 7

Seepage analysis of Tongjiahu dike in Yangtze river

Xu Qing
Hohai University, China; WaterPower Press, China

Chen Min-lin
Wuhan University, China

Wang De-guan
Hohai University, China

Chen Sheng-hong
Wuhan University, China; Hohai University, China

ABSTRACT: The study is conducted for the seepage analysis of Tongjiahu dike in Yangtze river, which is located in the east-west lake district near Wuhan, China. Firstly finite element method of three-dimensional free seepage flow is illustrated in the paper. Then the applications of this method to the dike are presented in detail. The results are valuable to the reinforcement and rehabilitation works of the dike.

1 INTRODUCTION

Seepage flow is an important factor to the safety and economy of embankment dam, and seepage analysis is the precondition to calibrate the deformation and stability of embankment dam, too. Through seepage calculation, the free surface, seepage gradient, quantities of the seepage etc. can be made certain.

Ever since 1970's, finite element method gradually becomes a main method in seepage analysis. Many scholars devote their energy into the research on numerical analysis of the seepage problem. Today, for complicated boundary conditions, homogeneous or heterogeneous materials, isotropic or anisotropic materials, saturated or unsaturated phenomena, the satisfied results can be obtained easily by FEM [1,2].

In this paper, finite element method is used to study seepage characteristics of Tongjiahu dike in Yangtze River. As comparison, limit analysis method is also used to study the stability of the dike. The results provide scientific foundation to the reinforcement and rehabilitation works.

2 THEORY OF FINITE ELEMENT ANALYSIS ON SEEPAGE FLOW PROBLEM

Denote $H=z+p/\gamma$ as hydraulic potential function, Ω as calculation domain. The governing equation is

$$LH=f \tag{1}$$

where $L=\{S\}^T[k]\{S\}$ is differential operator.

The boundary condition of the definite potential is

$$H|\Gamma_1=H_0 \tag{2}$$

The boundary condition of the definite flow rate is

$$\{n\}^T[k](\{S\}H)|\Gamma_2=-q \tag{3}$$

where $\{n\}$ is unit normal vector, $\{S\}$ is differential operator, $[k]$ is permeability matrix. They can be expressed as

$$\{S\} = [\frac{\partial}{\partial x} \quad \frac{\partial}{\partial y} \quad \frac{\partial}{\partial z}]$$

$$[k] = \begin{bmatrix} k_x & k_{xy} & k_{xz} \\ k_{yx} & k_y & k_{yz} \\ k_{zx} & k_{zy} & k_z \end{bmatrix}$$

The surface of the free seepage is a special boundary. Two conditions are satisfied at the same time as follows:

$$\left.\begin{aligned} H &= z \\ \{n\}^T[k](\{S\}H) &= 0 \end{aligned}\right\} \tag{4}$$

The variation equation corresponding to the differential equation (1) and the boundary conditions (2) and (3) is

$$I[H(x, y, z)] = \iiint_\Omega \frac{1}{2}[(\{S\}H)^T[k](\{S\}H) + fH]d\Omega + \iint_{\Gamma_2} qHd\Gamma = \min \tag{5}$$

After the discrete of the calculation domain into finite element mesh, hydraulic potential function is interpolated by

$$H = [N]\{\bar{H}\} \tag{6}$$

in which $[N]$ is the element shape function, $\{\bar{H}\}$ is the nodes' potential value. The variation equation (5) will lead to

$$[K]\left\{\begin{matrix}\cdot\\ H\end{matrix}\right\} = \{F\} \tag{7}$$

in which $[K]$ is conductivity matrix, $\{F\}$ is the vector corresponding to the inner and boundary flow rate.

$$[K] = \iiint_\Omega (\{S\}[N])^T[k](\{S\}[N])d\Omega \tag{8}$$

$$[F] = \iiint_\Omega f[N]d\Omega + \iint_{\Gamma_2} q[N]d\Gamma \tag{9}$$

By the Darcy theorem, the seepage velocity and the seepage gradient can be calculated respectively as follows:

$$\{v\}=-[k]\{S\}H \tag{10}$$

$$J=||\{S\}H|| \tag{11}$$

3 ENGINEERING APPLICATION

3.1 *Calculation condition*

Tongjiahu dike in Yangtze River is located in the east-west lake district near Wuhan, China. In the flood period of 1998, the dike underwent critical state. To guide the reinforcement and rehabilitation design works, it is necessary to judge which one is the control factor: seepage stability or stability against sliding. Therefore the following researches are carried out:

(1) The characteristics of the seepage flow within the dike.
(2) Under the situation of design water level, the seepage gradient distribution in the dike downstream outflow area.
(3) Under the situation of design water level, the slope stability of the dike.

Table 1 shows the physical and mechanical parameters of the dike body and foundation.

3.2 *Calculation results*

3.2.1 *Seepage analysis*

Figure 1 shows the seepage pressure contours of the dike. Figure 2 shows the seepage gradient distribution of the downstream surface under the situation of the design water level.

3.2.2 *Stability analysis against sliding*

Sweden circle method and Bishop method[3,4] are applied to analyze the stability of the dike. Table 2 shows the calculation results. Figures 3 and 4 show the most dangerous position of the upstream slope and the downstream slope respectively.

Table 1. Physical and mechanical parameters of the dike body and foundation.

Material	Permeability coefficient k_x (cm/s)	Permeability coefficient k_y (cm/s)	Cohesion (kPa)	Internal friction angle (°)	Unit weight (kN/m^3)
New earth-fill	2.36×10^{-7}	1.11×10^{-8}	34.2	14.3	18.8
Plain earth-fill	2.36×10^{-7}	1.11×10^{-8}	34.2	14.3	19.1
Clay	3.02×10^{-6}	3.66×10^{-7}	38.9	13.2	19.1
Silty clay	2.71×10^{-6}	1.75×10^{-7}	24.0	13.1	19.2
Sandy loam	26.23×1^{-7}	1.02×10^{-7}	66.0	25.6	20.2

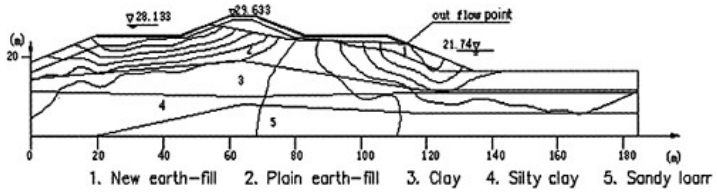

Figure 1. Seepage pressure contour of the dike.

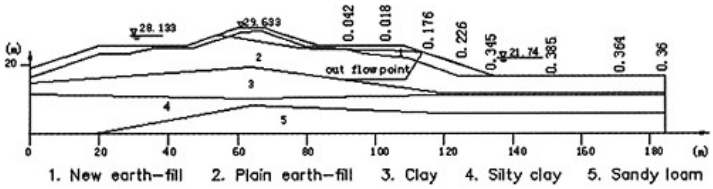

Figure 2. Seepage gradient distribution of the downstream surface.

Table 2. Calculation results of the slope stability.

	Sweden circle method		Bishop method		
Position	Radius (m)	Safety factor against sliding	Radius (m)	Safety factor against sliding	Remarks
Upstream	117.092	5.127	117.092	5.155	After the filling of soil
Downstream	92.185	2.986	92.185	3.022	After the filling of soil

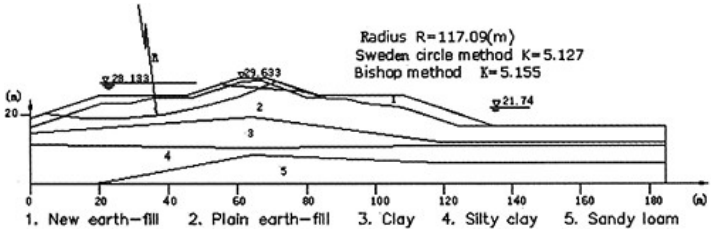

Figure 3. Most dangerous position of upstream slope.

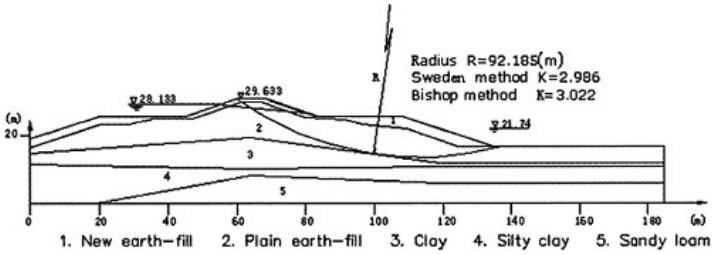

Figure 4. Most dangerous position of downstream slope.

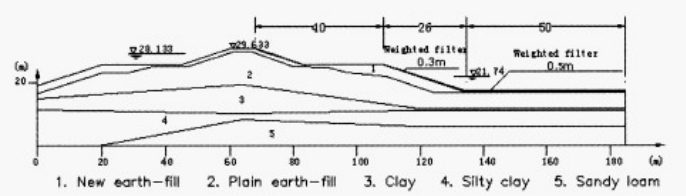

Figure 5. Design of the weighted filter.

3.3 *Results analysis and suggestions*

3.3.1 *Stability against sliding of the dike slope*

The results show that under the situation of design water level, stability against sliding of the dike slope is satisfied according to the design code. Therefore, sliding failure is not the main control factor in the reinforcement and rehabilitation works.

3.3.2 *Seepage stability*3.3.2

Generally, seepage stability of the outflow position can be judged according to the seepage force in the soil as follows:

(1) Seepage force upwards: $\gamma_w J$;

(2) Submerged unit weight of the soil: $\gamma'=\gamma_w(1-n)(\gamma_s/\gamma_w-1)$;

(3) The frictional force between the soil grain: $J_c=\frac{\gamma}{\gamma_w}(1+\frac{1}{2}\xi\ \ tg\phi)+\frac{c}{\gamma_w}$ is the internal friction angle of the soil;

(4) The cohesion of the unit soil: c.

Using the equilibrium condition of above four kinds of forces, critical outflow gradient can be obtained:

$$J_c=\frac{\gamma}{\gamma_w}(1+\frac{1}{2}\xi\ \ tg\phi)+\frac{c}{\gamma_w} \tag{12}$$

Based on the physical and mechanical properties of the soil in the dike downstream outflow area, when the value K of safety coefficient for the seepage stability is equal to 3 (K=3), the value $[J]$ of the permissible seepage gradient is approximately equal to 0.3 ($[J]$=0.3). Accordingly, the judgment can be made that the seepage gradient of the outflow area of Tongjiahu dike in Yangtze river is too large and seepage stability is not satisfied.

According to the above results, we can believe that seepage stability is the crucial problem in Tongjiahu dike in Yangtze river. Therefore, the suggestion is to lay high permeable material with large unit weight in the dike downstream outflow area, in order to drain and protect downstream surface soil layer from seepage deformation failure. Based on the control criterion of the seepage gradient ($J\leq 0.3$) under the situation of design water level, the weighted filter is adopted. The position, the length and the thickness of the weighted filter are showed in Figure 5.

The reinforcement and rehabilitation works have been completed and the dike is operating well so far.

4 CONCLUSIONS

Nowadays finite element method for seepage problem is a sophisticated tool in structural engineering, and a lot of achievements have been obtained. However, in the engineering practice the method is restricted sometimes, and the practicability and the reliability of the results are not so convincing. The research of Tongjiahu dike in Yangtze river shows that when the boundary conditions and the parameters of the material are rather reliable, finite element method can be used as main tool for seepage control design. Of course, the experiences of the engineers are very important, too.

REFERENCES

[1] Desai C.S. Finite element residual schemes for unconfined flow. *Int. J. Num. Meth. Eng.,* 1976, 10(6): 1415–1418.
[2] Chen S.H.,Wang W.M., She C.X. and Xu M.Y. Unconfined seepage analysis of discontinuous rock slope. *J. of Hydrodynamics,* 2000, 12(3):75–86.
[3] Bishop A.W. The use of the slip circle in the stability analysis of slopes. *Geotechnique,* 1955, 1(1):7–17.
[4] Wright S.G., Kulhawwy F.H. and Duncan J.M. Accuracy of equilibrium slope stability analysis. *J. Soil Mech.,* 1973, 99(10):783–791.

New Developments in Dam Engineering—Wieland, Ren & Tan (eds),
© 2004 Taylor & Francis Group, London, ISBN 04 1536 240 7

Environmental protection measures for hydroelectric projects construction in China

Xue Lianfang
Mid-South Design and Research Institute for Hydroelectric Projects, Changsha, Hunan, P.R. China

ABSTRACT: This paper, on the basis of the practices in ecological and environmental protection for construction of hydropower projects in China in the last ten years or more, introduces the environmental management system for construction of hydroelectric projects in China, as well as the scientific studies and detail measures for environmental protection in construction of hydroelectric projects, mainly involving protection of rare animals, protection of rare plants, protection measures for hydrobios and fish resources etc. It also raises recommendations on countermeasures for the problems existing in the operation of the reservoirs.

PREFACE: China is rich in hydropower resources. In the last 50 years or more, construction of hydropower projects devotes a lot to the society and the economy. It also obtains distinct environmental benefits as follows: (1) optimizing the structure of the power sources, minimize pollution of the power generation to the environment; (2) flood control and disaster mitigation, mitigating the damage of the flood on the ecology and environment of the downstream riverbank areas, as well as people's dread to floods; (3) affecting the local climate, improving the ecology and environment of the reservoir area; (4) improving the downstream water environment and saving the money for sewage treatment; (5) promoting the economic development and improving the regional environmental quality; (6) adding the tourism resources and promoting the tourism industry. Nevertheless, activities such as the reservoir inundation, dam's blocking the river, project construction and resettlement etc. will impact on the ecology and environment. In order to coordinate the contradiction between the hydroelectric project construction and the ecological and environmental protection, promote the sustainable development in economy, society and environment, the Government of China and the concerned authorities has paid high attention on it, and worked out a series of laws and regulations on the basis of the domestic conditions in China and organized to carry out a lot of studies. Since the beginning of 80s, the Environmental Impact Assessment System has been implemented in China. In late 80s, it is gradually required that "three simultaneousness" must be implemented for the construction projects. Therefore, with regard to environmental impacts of the hydroelectric construction, environmental protection design and comprehensive supervision on environmental protection are carried out. The implementation of such measures plays an important role in mitigating the impacts of hydroelectric construction on the ecology and environment and promoting the sustainable hydroelectric development.

1 FULL PROCESS ENVIRONMENTAL MANAGEMENT FOR HYDROPOWER DEVELOPMENT

Hydroelectric developments have characteristics as large scale, extensive involvement, complicated technology and long developing cycle. They normally include a implementation cycle including stages as planning and site selection, feasibility study, engineering and design, construction,

completion acceptance and taking over and being put into service. In accordance with the national laws and regulations on environmental protection, corresponding environmental protection shall be done in each stage, and shall follow the principles as “taking the prevention as the major measure, combining prevention with improvement, and comprehensive improvement”, “whoever pollutes shall improve and whoever ruins shall recover”, and “three simultaneousness” system, namely, that the environmental protection works shall be designed, constructed and put into service simultaneously with the main works, shall be implemented.

Environmental Impact Assessment (EIA) is an important part for the feasibility study for a hydropower development. EIA shall, on the basis of the survey and analysis on the regional environment status to be impacted by the project, in accordance with the scale and features of the project, in the light of the relevant laws and regulations and standards, identify, forecast and objectively evaluate the impacts of construction and operation of the project on the ecology and environment, propose practical and economic counter measures against unfavorable impacts, give requirements and recommendations on environmental protection aiming at the potential unfavorable requirements, so as to give full play of the favorable impacts of the project on the ecology and environment and minimize the unfavorable impacts. In a viewpoint of protection of ecology, the feasibility of the construction of the project is justified. At the beginning of 80s, China began to implement EIA, at present the EIA report is a must document for project identification of hydropower development. The practices prove that EIA has played an important role in effectively mitigating the unfavorable impacts of hydropower development on ecology and environment and giving full play of the environmental benefits of hydropower plants. For example, the EIA report of Dongjiang HPP proposed counter measures aiming at mitigating the unfavorable impacts of the reservoir construction on the ecology and environment, reasonably developing and utilizing the resources in the reservoir area and protecting the ecology and environment. Those proposed measures attracted the high attention of the local government and related authorities and were gradually implemented. Construction in several years has made Dongjiang reservoir area become a resort for tourism and recreation with pleasant climate, green hills and clear water, good environment and beautiful landscape. The reservoir water quality is generally good and the water is clear. The reservoir surrounding area has high rate of vegetation coverage. The water and soil loss being aggravated at the beginning stage of the production development for resettlement gradually disappeared. The coordinate development of society, economy and environment in the reservoir area has been primarily realized. Gezhouba hydroelectric project blocked up the migration passageway of the migration fishes, especially brought out great impacts on the rare fishes such as Chinese sturgeon. For the purpose of protecting Chinese sturgeon, a lot of survey and studies were done before the project development and protection measures as artificial propagation and release and establishment of natural reserves were proposed. The Chinese Sturgeon Artificial Propagation Institute releases 5000 sprags of Chinese sturgeon to the Yangtze River every year from 1984. At present, the Chinese sturgeons retained in the river section downstream the dam can fertilize naturally in the newly-formed hatchery that plays an important role in protecting the Chinese sturgeons.

The environmental protection design carries out, on the basis of the conclusions in the EIA report, the detail design of the countermeasures to mitigate the unfavorable impacts. Although currently due to the reasons of technology and management, there still exist some problems, the role and necessity of environment protection has gradually been recognized along with commencement and construction of a number of large scale hydropower projects. For example, design, construction and service of the waste water treatment system for the aggregate processing plant in the construction area of Longtan HPP, the landfill for treatment of domestic rubbish resulted from the construction area of the Three Gorges HPP, design and implementation of fish rescue program in Dayuandu project on the Xiang River, play an important role respectively in environment improvement of construction areas of Longtan andThree Goreges HPPs and protection of fishes resources in the Xiang river.

The construction period is the critical time for implementing the “three simultaneousness” of environment protection. The practices in Xiaolangdi, Three Gorges, Wanjiazai, Longtan indicate that: enhancement of environment management in construction period can effectively control the environmental pollution and ecological damage resulted from construction of a project. For the purpose of doing well the environment management in construction period, the fist point is establishment of an environment management institution and identification of responsibilities of environment management. For hydropower projects of small scale, an environment management system shall be set up, and for hydropower projects of large scale, a capable and effective environment management institution shall be set up. The second point is well preparation of the implementation program for environment protection in construction period and preparation of environment protection provisions in bidding documents and construction contracts. The main contents of the implementation program for environment protection shall include the engineering measures and managerial measures for environment protection to be implemented and the corresponding investment, schedule and assurance measures etc. The third point is conscientious implementation of the environment supervision system, launching environment monitoring and strengthening the monographic acceptance of environment protection.

2 PROTECTION OF RARE ANIMALS

First, the resources, distribution and quantities of rare animals living below the inundation line and within the resettlement area must be ascertained. For the rare animals above the inundation level of the reservoir, the critical point for protection is protection of the existing natural vegetation. Only when the forest is protected, can the rare animals resource in the reservoir area be effectively and fundamentally protected. For protection of the rare animals below the inundation level of the reservoir, migration measures shall be taken before impounding. Thus, as of a rare animal to be relocated, the habitual nature and surviving conditions shall be studied, the food structures and habitats etc. shall be ascertained, so as to select a new habitat (in the non-inundated area close to the reservoir area) similar to its original one and plan a passageway for migration. And small migration experiment shall be done. A proposed large scale reservoir in Guangxi will inundate some area of the Buliuhe reserve and the Chuandonghe reserve and affect 95 groups of rhesus monkeys. In the project design, on the basis of survey and study, the protection measures for artificial migration is determined and the migration route for the rhesus monkeys is worked out.

In order to prevent the rare animals and their habitats from damage by the construction persons and resettlers, fence protection shall be used if necessary. In Datian National Mountain Deer Reserve surrounding the completed Daguangba HPP in Hainan, the project design proposed to resettle more than 7000 people surrounding the Reserve, and activities of human beings aggravated after migration of the resettlers and affected the Reserve. Therefore, it was decided to use fence protection.

3 PROTECTION OF RARE PLANTS

First, the survey on the rare plants, their distribution and quantities shall be well done, especially the species and the protection classification of the rare plants in the reservoir inundation area and the resettlement area shall be ascertained. In order to effectively protect the terrestrial plants and rare species in the reservoir region, it is necessary to work out a terrestrial plant protection program. It is planned in the reservoir surrounding area of the Three Gorges Project under construction to establish a forest park (Tianbaoshan Forest Park in Yichang City), a natural reserve (Longmenhe Reserve for Broad-leaved Evergreen forests in Xinshan), a landscape reserve (Little Three Gorges Reserve for Landscape and Ecology among Wu Mountains), reserve spots for the three rare species (adiantum reniforme L. var. sinense Y.X.Ling, myricaria laxifflora (French) PY.Zhang et YJ.Zhang and Chuanminshen viloaceum Sheh et Shan) and single tree protection for aged and large trees of rare species. The impacts of inundation of a large scale reservoir in Guangxi involves five natural reserves such as Buliuhe, Chuandonghe, Shuangjiang, Duyi and Luoyang, bringing out impacts of different degrees on the protected objects in the reserve areas such as the water supply conservation forests, monsoon forests and rare plants as heartleaved buerretiodendron hsienmu. For the purposes of strengthening construction of the natural reserves, minimizing loss resulted from inundation and protecting the rare plants resources, protection plan and implementation measures have been worked out in the project design and it is planned to build water supply conservation forests equivalent to the inundated ones above the inundation line in the Buliuhe and Chuandonghe Reserves. In Shuangjiang, Duyi and Luoyang Reserves, management and protection on the existing monsoon forest is to be strengthened, forest flora similar to that of a primitive monsoon forest is to be built with an area equivalent to that to be inundated. For rare plants as heartleaved buerretiodendron hsienmu, cycas revolute etc., artificial forest will be built by means of seed introduction and reproduction, different place protection will be carried out and experiments and study on difference place protection will be done.

4 PROTECTION OF RARE AQUATIC ANIMAL AND FISHES

4.1 *Establishment of natural reserve*

The practices prove that establishment of natural reserves is an effective way to protect the rare hydrobios. The main tasks of the natural reserves are: (1) to provide superior natural surviving conditions for the protected objects, avoid artificial interference as far as possible, and protect the propagation of the species; (2) to regularly observe and record the regular activity patterns and change in population of rare hydrobios in the reserves; (3) to provide proving ground for studying the rare species. There are six species of rare aquatic animals (White-flag dolphine, Chinese paddlefish, Chinese sturgeon, acipenser dabryanus, Neomeris phocaenoides, neomeris phocaenoides), which are listed under the Class A and Class B protection by the national government, in the Sanxia Project Affected area. Hence it was proposed to establish 5 natural reserves for rare aquatic animals, of which four have been established up to date. The Hejiang river section of the upper Yangtze is the hatchery distribution range for rare fishes such as Chinese paddlefish, Chinese sturgeon (before construction of Gezhouba Dam), acipenser dabryanus, myxiocyprinus asiaticus etc. and the major cash fishes such as Coreius heterodon and Leiocassis longirostris ect. In 2000 this river section was set up as the national reserve for rare fishes. After construction of Gezhouba Dam, the river section between the Hejiang Reserve and Zhijiang river section becomes the hatchery for rare fishes as the Chinese sturgeon and myxiocyprinus asiaticus. There also distributes hatchery for the four Chinese carps. In 1996 a provincial reserve for rare fishes was set up in this river section. In 1992 two national reserves for white-flag dolphine were set up respectively in the river section between Luoshan to Xintankou and at the Tian'ezhou Gudao some 20km downstream of Shishou. A a sprag reserve for Chinese sturgeon and Chinese paddlefish is planned to be set up in the intertidal waters of the Yangtze River estuary, some 30km east to the Congming island.

4.2 *Artificial propagation and release*

Distinct benefits have been achieved in multiplying fishes in the United Kingdom of Great Britain and the United States by means of artificial propagation and release. China also succeeds in artificial propagation and release of Chinese sturgeon in construction of Gezhouba Project. The measures were proposed to protect the rare fishes for the Three Gorges HPP as follows: (1) artificial propagation and release stations for myxiocyprinus asiaticus and Chinese paddlefish in the upper reaches of the Yangtze River; (2) artificial propagation and release stations for acipenser dabryanus in the upper reaches of the Yangtze River; (3) artificial propagation and release stations for rare fishes in the middle reaches of the Yangtze River (being expanded on the basis of Gehzouba Artificial Propagation Institute for Chinese sturgeon). At present, the reproduction technology for Chinese sturgeon, acipenser dabryanus, myxiocyprinus asiaticus has achieved success in experiments, and sprags of Chinese sturgeon have been reproduced and raised over years and released downstream of Gezhouba, further work has to be done in solving the problems as food supply, disease control and control of sex gland development through nutrition of the parent sturgeons for raising sprags and little sturgeons etc. The artificial propagation of Chinese paddlefish has not been successful. The main reason is that the mature parent surgeon is not easy to obtain and the raising of parent surgeon has low survival rate. At present the critical technology for continuation of sex gland development and mature of sex gland under artificial raising is under study.

4.3 *Fish fecundation centers*

The impoundment of the reservoir, in one hand, plays a good role in fish production due to increase of hydrobios, and in the other hand also ruins propagation of some cash fishes. From the viewpoint of developing fishery resources and as a compensation measure, it is very necessary to set up fish fecundation centers. Generally speaking, the propagation technology for the cash fishes is simple and mainly consists of establishing the artificial hatchery, setting up hatching and sprag nursery, cultivation water are and feed production farm, periodically putting fish fries in the preset spots of the reservoirs. Construction of Dayuandu Project on the Xiangjiang River in Hunan cut off the passageway for migration of the four Chinese carps (black carp, grass carp, silver carp, variegated carp). As the special ecological environment such as depth, flow and temperature necessary for a hatchery is changed, it gives considerable impacts on the resources of the four Chinese carps. Justification on multi-alternatives was carried out before construction of the project and it was decided to multiply the resources by means of artificial fecundation and release. By implementation of this scheme, in may of 1995, the first batch of fries of Chinese Carps by artificial fecundation was release into the Dayuandu reservoir area in Hengyang City, and thereafter fries released year by year that effectively protect the migration fish resources in the Xiang River.

5 CONSTRUCTION OF ECOLOGICAL ENVIRONMENT DURING RESERVOIR OPERATION

Construction of a reservoir inundates a lot of forest, villages and towns and fertile farmland, making the reservoir area lose some resources. However, the broad water area of the reservoir is favorable for aquatic cultivation and the reservoir also creates conditions for tourism development. The effects of the water body on the local climate improve the growing conditions of the crops in the reservoir surrounding area. Therefore new resources form. In the past, due to lack of recognition and short of unified planning and management, the resources were lack of effective protection and hence resource wasting occurs. With regard to this problem, a unified institution shall be set up to strengthen the macro-management in the reservoir area, work out the regulations on development and environmental protection in the reservoir area. Protected reserves may be set up if necessary. For the development of the resources in the reservoir area, first is to ascertain the changes in the resource structure and environment resulted from construction of the reservoir, survey the quantities, distribution and developable situation of the water resource, the land resource, the forest resource, the climatic resources and the tourism resource in the reservoir area and the surrounding area. On the basis of a strategy of sustainable development, the resource development plan shall be worked out. The development shall be done with reasonable utilization and moderate development and on the premise of protection, following a guideline of protecting in development, realizing unification of social, economic and environmental benefits, creating virtuous cycles of living, production and ecology, and promoting the sustainable and steady development of the economy of the reservoir area.

The reservoir and the catchment area are integrity inseparable. The protection on the reservoir ecology and the environment cannot go away from the catchment area and is only limited to the reservoir or the reservoir surrounding area. It shall be done with a strategic viewpoint of the catchment area, considering the reservoir and the catchment area as integrity. For example, the Yuan River catchment area has famous Xiang-Qian (Hunan-Guizhou) mercury ore deposit zone, and also is very rich in phosphorus resources. Improper mining and processing of these mineral resources would bring about unfavorable impacts on the water quality of the cascade reservoirs on

the Yuan River. The discharge of poisonous and phosphate waste water, from the chemical plants and phosphorus mines located at the reservoir end and by the main stream and tributaries of Wuqiangxi reservoir, worsens the water quality of the bends of Wuqiangxi reservoir suitable for aquaculture and make it not utilizable, while fishes caught the in some reservoir sections are not edible due to their high content of heavy metals or poisons in the fish body, and the water quality cannot meet the sanitary requirements for potable water. Similar situation occurs in other reservoirs as Wujiangdu, Xin'anjiang etc. To solve the problem, catchment area environment plan shall be done, identifying the function zoning of waters and protection classification, calculating the environmental capacity. On the basis of survey on resources and environment in the catchment, the industrial plan shall be done and the industrial structure shall be adjusted in accordance with the requirements on environment protection and with a consideration of the local resource situation. EIA shall be done before construction of a new project and "three simultaneousness" shall be implemented in construction. The existing pollution sources shall, in accordance with the national industrial policies and in combination with technical improvement, be improved within limited time period following a principle as "whoever pollutes shall improve". Meanwhile, construction of ecology and environment in the catchment shall be vigorously launched, minimizing water and soil loss.

New Developments in Dam Engineering—Wieland, Ren & Tan (eds),
© 2004 Taylor & Francis Group, London, ISBN 04 1536 240 7

Quality assurance for second stage construction of Three Gorges Project

Xue Lisheng & Ding Qihua
Department of Project Construction, China, Three Gorges Project Corporation

ABSTRACT: The Three Gorges Project (TGP) is a main project to improve and develop Changjiang River, the quality and safety of the project are most important to national policy and people's livelihood. The TGP dam construction in the second stage has some characteristics, such as enormous amount of work, complex structure, strict technical demand, time limit of construction and high construction intensity, and so on. In order to guarantee the construction quality of the project, every construction unit, taking part in building must have highly responsible master-attitude to set up and perfect quality assurance system, to take various effective measures and strengthen construction quality management, guaranteed construction to achieve stage aim on schedule.

Dam construction quality of every part-engineering in the second stage had been tested; it met national criterion and quality standard of the TGP, and met designing demand. After water storage, result of dam security monitoring showed: every index was in the permitted range of design. Since dam had been employed, every construction could normally run. So construction quality of the second stage of the Three Gorges Dam achieved excellent level in total.

1 INTRODUCTION

The Three Gorges dam is a concrete gravity dam, the length of dam crest adds up to 2,309.5m, the elevation of dam crest is 185.0m, the concrete gravity dam has been divided into seven separate parts: Spillway dam section, Left and Right Bank non-over flow dam sections, Left and Right Intake dam sections, Temporary Navigation Lock and Ship Lift dam sections. Spillway dam section lies in the middle of riverbed, Intake dam sections and non-over flow symmetrically stand two sides of Spillway dam section on the whole, the total volume of the whole dam's concrete adds up to 15,860,000m^3, dam's metal include various sluice gates, headstock gear, penstock and trash-rack, their total weight adds up to 144,000t.

The engineering of the Three Gorges Dam in the second stage include: Left Bank non-over flow dam sections, Ship Lift dam section, Temporary Navigation Lock dam section, Left Power Intake dam sections, Left Guide Wall section and Left Guide Wall, Spillway sections, Right Cofferdam dam section and so on, the crest length of these dam sections adds up to 1,644.5m, dam's concrete total volume adds up to 11,551,000m^3, the total weight of metal structures and generators adds up to about 104,000t.

The engineering of the Three Gorges Dam in the second stage has some characters, such as enormous work amount, complex structure, urgent time limit of construction, high difficulty and high construction intensity, and so on. The quantity of concrete in the second stage can compete with the total quantity of Itaipu Hydropower Station—the biggest hydropower station at present in the world. Spillway dam section has three layers of hole structure with big sizes, resulting complex structure, highly technical demand, high difficulty. Annual peak of dam concrete construction intensity in the second stage is up to 4,000,000m^3, the highest monthly intensity reaches 450,000m^3, mensal intensity of 400,000m^3 lasts 9~10 months, which is the first in the world.

In order to guarantee engineering construction quality, every unit of taking part in building was in line with master-attitude spirit of "matter of fundamental importance in millennium masters national future", with the realistic attitude of "treading on thin ice, feeling like standing upon the edge of an abyss", according to the management objectives of "zero quality accident, zero incident", took the effective measure, seriously organized construction, had guaranteed engineering quality and achieved construction goal on schedule.

On October 2002, the elevation of dam crest in the second stage reached 185.0m very completely, the three main aims about "conservation storage, open up to navigation, generated electricity" of the TGP were realized on scheduled in 2003, the second stage of the project constructed and finished, the project entered the third stage construction.

2 SYSTEM AND MEASURES OF QUALITY ASSURANCE DURING THE SECOND STAGE CONSTRUCTION

2.1 *System of construction quality assurance*

The TGP construction had pursued regarding "quality" as prerequisite, "3 control" (quality, schedule, investment) as the goal, management mode of taking managing in contract as foundation. Center on the management mode and quality demand of first-class project, the TGP Head Office had put forward the management objectives of "zero quality accident, zero security incident". Every unit of taking part in building had set up quality management organization, and the TGP Head Office had taken the lead in organizing every unit of taking part in building to establish the TGP quality management committee. Since the beginning of project to go into operation, examination system by oneself had set up by every unit of taking part in building, supervision unit held the pass on the whole, every project department coordinated and supervised the quality management system; In the course of engineering construction, the TGP Head Office engaged the domestic and international senior consultant expert to serve as a professional quality director, to reinforce supervision and technological guidance to the key specialty; The Three Gorges Multi-purpose Project Quality Examination Expert Panel of the State Council had been established by the TGP Construction Committee of the State Council, carried on the authority inspection and estimation to the construction quality of the TGP; The TGP had come into being quality guarantee and management systems of "4+1" increasingly.

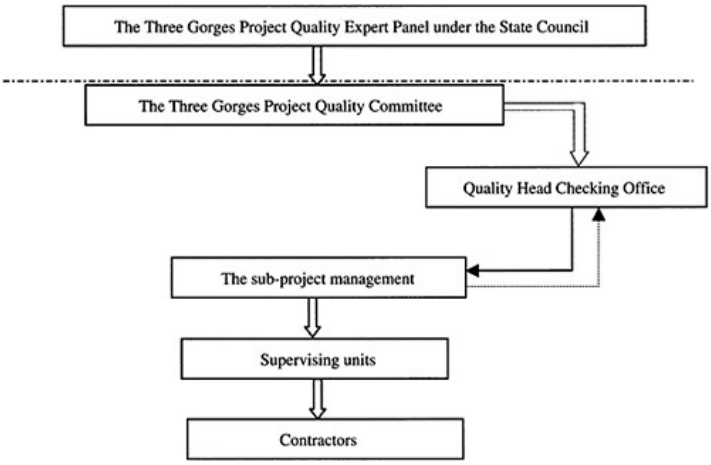

2.2 *Quality assurance measures*

2.2.1 *Through competitive bidding to select the high-qualifled contractors*

The second stage of dam and hydropower station building are divided into three packages to invite public bidding, such as Spillway dam section, Left Bank Intake dam section and Left Bank dam section, left bank hydropower station building. According to the principle of "open, fair, and just", the capable contractors are selected, which had guaranteed effectively the engineering construction.

2.2.2 *Through specialize research and selection in a long time, selecting the construction scheme relying mainly on tower crane*

Dam construction in the second stage had enormous engineering amount, urgent time limit, high construction intensity, the design considered that the bottom of the dam adopted roller compacted concrete to solve the difficult problem of high construction intensity, and recommended the construction scheme relying mainly on portal and tower cranes. After the project went into operation formally, the Three Gorges Head Office organized technical staff and designer jointly to survey and study professionally on the basis of argumentation in the past, the Head Office recommended adopting and relying mainly on tower-belt crane finally, complementing it with construction scheme of employing portal crane and tower crane, and submitted to the TGP Construction Committee of the State Council to authorize. The implementation of the scheme, that had solved the difficult problem of the high dam construction intensity in the second stage, actual construction annual production capacity was up to more than 4,000,000m^3, created new world record in every field of hydroelectric construction.

2.2.3 *Setting up and perfecting the scientific construction quality management system, carrying out responsibility system*

There had come into being the quality management system of "4 +1" increasingly in the TGP, managed by different levels, every level bore the corresponding duty, which made the engineering construction in the state of being controlled to guarantee the engineering construction quality.

Construction unit must fulfill the stipulated duty that the contract as B-party of the contract, and finish the stipulated task of the contract on schedule. Every construction unit has set up 2 or 3 grades management quality organization, and allocated full-time quality technician, to be responsible for the visa of quality management and quality examination specially, every unit has his own testing laboratories and survey team, according to criterions and relative standards, they undertake the test of raw materials and concrete performance and survey at the scene, to grasp the on-the-spot construction quality trend and instruct the on-the-spot construction. The quality test organization of construction unit is the first level of construction quality management at the scene.

Supervision unit stands for owner to manage construction, is the first responsibility-person of management at the scene. In order to attain unified and standardized management aim, every supervision unit sets up correlative departments corresponding to the owner's management departments to develop correlative work. Every supervision unit sets up laboratories to test the random samples of the raw materials and concrete mix, and also sets up survey team to re-check engineering construction and important control observation points. Supervision unit is the second level of construction quality management at the scene.

The Department of Project Construction under ChinaThree Gorges Corporation serves as owner's deputy at the scene, adopts separate item management at the basis of contract. The Sub-project Department, Left Bank Power Plant and Dam Department is responsible for coordinating management at the dam construction scene in the second stage. Five centers were set up to serve as technical guarantee and quality monitoring, such as measuring, testing, safe monitoring, check-up of metal structures, water regime and meteorology and so on.

The laboratory center tests the random samples of the raw materials and concrete mix, and studies correlative experiments, to offer decision-making service for project management; The safety monitoring center is responsible for the unified management of safety monitoring, supervising and managing the implementation of the project, and through analyzing monitoring data, feed-backing

to the relative unit in time, to offer reference for designing and construction; The metal structure monitoring center supervises and tests the random samples of electromechanical equipment making and quality in the course of installing, offers the decision-making basis for project management; The surveying center is responsible for re-surveying and maintaining the survey control grid in the whole work area, offering achievement of survey control grid to units of taking part in building, and re-surveying important laying-out points, to guarantee the accuracy of construction laying-out; The water regime and meteorology center is responsible for announcing the information of water regime and meteorology, announcing the warning of climatic calamity in time, to organize construction and take some effectively precautionary measures at the scene. The staff of project management and on-the-spot supervisors cooperate closely, coordinate the contradiction among every bid section in time, is the third level of on-the-spot construction quality management.

The TGP Quality Management Committee is a supreme organization of on-the-spot quality management of the TGP; its member includes the first responsibility-person and main quality administrative staff of every unit of taking part in building. Its on-the-spot representative organization is the director's office of quality, according to the need of on-the-spot construction, the Three Gorges Head Office has also engaged the domestic professional and known experts to serve as professional quality director, the professional quality director does not substitute the function of supervisor, but carry out high-qualification, authoritative supervision and instruction on behalf of the Head Office, to potential problems in constructing, give warning and suggestion in time, to the question taking place, give correcting and treating measure, and propose the opinion and suggestion about engineering quality management, construction technology and craft at the same time, carry on the professional technical training to the quality administrative staff of unit of taking part in building according to the need, this is the fourth level of quality management.

The TGP Quality Expert Panel under the State Council is the supreme authoritative organization of the TGP quality management, and supervises and inspects the construction quality of the TGP on behalf of State and government. Through inspecting whether every unit of taking part in building has healthy quality guarantee system, perfect quality system and strictly perform relative rule and criterion, the Quality Expert Panel inspects and evaluates yearly the construction quality, and submits quality inspection report of the TGP to the TGP Construction Committee of the State Council annually, so that the superior leader can grasp the construction quality and trend of the TGP, and effectively help every unit of taking part in building of the TGP to improve quality consciousness and construction quality.

2.2.4 *Making strict quality criterion and various construction technical demands*

"China TGP quality criterion" is on the basis of the current national criterion and standard, combining with the concrete conditions of the TGP and being based upon contract to workout, its content includes different specialties, such as the foundation excavating and dealing engineering, the seepage control engineering, the support engineering, raw material test, concrete engineering, making and installing of metal structure and electromechanical equipment. The quality criterion of the TGP comes from national standard and criterion, but part standard is stricter than the national standard, is concrete embodiment and importantly reflection of the first-class engineering quality goal, to offer the important basis to engineering quality management.

In order to improve the construction technical qualification, the construction technical designing system of cell engineering has been carried out in all fields of the TGP, such as technical designing of concrete pouring silo, grouting technical instruction, installing technical instruction of mental structure and so on, use it to standardize the construction operational technology and guarantee construction quality; In order to further perform the quality criterion of the Three Gorges Project, a series of technical demands have been made out and announced, such as "concrete construction technical demand about sealing method of the Three Gorges Project (temporarily)", "formwork construction technical demand of overflowing area and forever revealing area of the Three Gorges Project's construction (temporarily)", "treating technical demand about concrete external defect of the Three Gorges Project's main constructions in the first and second stage (temporarily)", "executing detail measure about concrete curing blanket of the Three Gorges Project (temporarily)", "evaluation criterion about boring to examine the concrete compatibility of the Three Gorges Project's main constructions in the first and second stage (temporarily)" and so on, implement of these technical demands effectively improved construction technology a qualification and accelerated to improve construction quality.

2.2.5 *Selecting superior concrete raw material and strictly managing the quality of raw material*

The owner directly supplies main raw materials of the TGP concrete, such as Aggregates, cement, fly ash and so on. The coarse aggregate of the TGP in the second stage has been supplied by pro cessing system of artificial aggregate at Gushuling, fine aggregate has been supplied by processing system of manufactured sand at Xiaanxi, cement and fly ash have been stocked by the TGP Head Office. In order to improve the concrete endurance of dam, technical criteria of cement and fly ash are stricter and superior than criterion of similar engineering at home and abroad, management criterion of cement alkali content: less than 0.6% in moderate heat cement, control index of MgO content is 3.5%~5.0%; class I high quality fly ash had been adopted in all field of the TGP, water demand ratio is less than 0.95%. External material mixture has been tested and recommended manufacturer and variety by the laboratory center, construction unit stocks him. The TGP Head Office extends the quality management system and examining system of raw materials to the whole course about producing, transiting, storage and supplying of settled supplier's product. Each correlative unit has been committed to test the cement, according to the batch of materials, construction unit, supervision unit and laboratory center must test the random samples of raw materials entering the scene, if test result isn't qualified, the materials will not permit to be used for the TGP.

2.2.6 *Optimizing concrete mix proportion*[1]

The design test of concrete mix proportion in the second stage had carried out since 1995, China Institute of Water Resources and Hydropower Research and Changjiang Scientific Research Institute were both committed to independently test, they submitted the test result to the TGP Head Office early or late in 1997. Because the two results had many differences each other, laboratory center of the TGP Head Office performed verification test, further optimized concrete mix proportion and recommended it to construction unit. In the course of construction, construction unit just did fine adjustment according to the test result of raw materials and condition of construction at the scene, ensured the concrete every performance index to meet the demand of designing and criterion.

2.2.7 *Making and strictly fulfilling temperature control measures for concrete placement of Three Gorges dam*

At the basis of selecting first quality raw materials and optimizing concrete mix proportion to improve concrete crack-resistance ability, in the course of dam construction in the second stage, through adopting the methods and measures of pre-cooling concrete, thermal insulation in the transportation process, strictly controlling the placing and cast temperature, fit seam height and interval, fitly disposing construction procedure and progress, cooling concrete in initial stage by circulating chilled water in pipe system embedded, watering on the concrete surface for curing, covering concrete with heat-insulating material, reinforcing coordination management, these methods and measures can control the most temperature of concrete and effectively prevent the crack in the concrete surface.

The volumetric capacity of concrete refrigeration plant of the Three Gorges dam in the second stage added up to 76,177kw, concrete mix outlet temperature was 7° C in summer, in order to guarantee the concrete mix outlet temperature, the technology of secondary air-cooling aggregate second-cool aggregate had been first used to the TGP after testing and studying again and again. The innovation of second air-cooling aggregate lay in not adopting usual water-cooling aggregate but air-cooling aggregate on the ground, that used preparative regulating bin after aggregate had been secondly sized grading to cooling bin, with highly effective cold air machine and its corresponding air supply system to form the cold air closed cycle system that it had been used to continuously cool aggregate. Through adopting the second air-cooling technology, which guaranteed low temperature

concrete yielding capacity of mixing system, created condition for strong intensity concrete construction of dam, and provided important guarantee for engineering quality.

In order to further reinforce coordinating management, the TGP Head Office had taken the lead in and the main quality administrative staff of every unit of taking part in building taken part in organizing the temperature control lead group, they orderly held regular meeting, analyzed the existent problem and brought forward the improving measure, ensured every temperature control measure to put into effect.

2.2.8 *Unifying the defect-treat criterion, completely and timely treating various defects*

In order to guarantee that engineering defect could be treated in time, to guarantee the defect patching quality, special defect-treat criterion had been made out, the demand of technology and operation had been fine converted, which guaranteed quality defect being treated in time, the result past allied examination and inspection.

In order to carry out the demand of quality expert panel about "Not leaving engineering hidden defect is up-most principle of the TGP construction", every bid stage set up four-side leading group of quality inspection and defect treatment, established the system of meeting every day and regular meeting every week, to study and solve the existent problem, to coordinating deal with work development, to guarantee quality inspection and defect treatment being successfully developed and accomplished on schedule.

2.2.9 *Adopting computer message management, back feeding quality message in time*

The TGP Head Office associated with Canadian AGRA Monenco engineering firm to develop TGP Message System (TGPMS), the system had been begun to use since 1998, in the same time the Head Office set up Office Automation System (OAS) working on the platform of Lotus Notes.

TGPMS includes quality management message subsystem; every supervision unit inputs intra-day correlative data and message of testing concrete raw materials, operational sequence process control, assessment and acceptance subgroup engineering quality, engineering quality problem and so on to the subsystem, correlative personnel can look up relative message in network at working time of second day.

You can back feed timely correlative message at Daily Notes system of Lotus Notes, also back feed timely relative quality message to correlative personnel and leader of Head Office through notice and e-mail.

Through using these back-feeding message methods, which accelerates speed of back-feeding message, so decision level can easily grasp on-the-spot quality trend and make relative decision.

2.2.10 *Reinforcing relative personnel's training, promoting quality consciousness and working ability*

The Quality Head Checking Office had taken the lead to timely organize units of taking part in building, to carry out and study a series of important indication of the State Council made according to construction quality problems of the TGP and suggestion of the TGP Quality Expert Panel under the State Council, successfully improved quality consciousness of every unit of taking part in building, in the same time, through specialty lectures and training, to train quality-inspectors and improve their working ability and qualification. Every unit of taking part in building also held similar training and lecture, to train a gleam of constructor for correlative technique and improve improvement of construction technology and qualification.

3 CONSTRUCTION QUALITY OF THE SECOND STAGE OF DAM

3.1 *Foundational excavation and treatment engineering*

3.1.1 *Foundational excavation engineering*

There had been comprehensively utilized bench blasting, slope pre-split blasting and protective covering smooth surface blasting in blasting excavation. Excavation control measure was very

suitable, excessive and lacking excavation had been controlled in the range of −20m~+5m, engineering integer designing had been preferably controlled. The lengthways sound wave speed in basic plane of dam was more than 5000m/s.

In the connection of fault, fault cross zone, low-angle dip face and slope top with platform margin, the part of it had been excavated and grouted, to improve integrity of foundation rock and meet designing demand of dam foundation.

3.1.2 *Consolidation grouting engineering*

Consolidation grouting included grouting of I and II arrays bores in the second stage of dam foundation, average unit pouring capacity was 4~5kg/m. With the distance between bore arrays being shortened, the unit pouring capacity evidently reduced, that met usual rule.

After grouting, result of sonic scan showed that sonic wave speed had been improved and hydraulic conductivity of foundation rock met designing demand.

3.2 *Influent control engineering*

3.2.1 *Curtain grouting engineering*

Curtain grouting engineering included: upstream main curtain and downstream closed curtain, divided into I, II and III arrays bores to boring and grouting, and added some shallow chemical curtain grouting in the dam section where grout consumption of main grouting was needed lesser.

Analytical and statistical result of curtain cement and chemical grouting showed, before the I, II and III arrays bores had been grouted, trend of hydraulic conductivity and unit pouring capacity was degressive, that met normal rule of grouting.

After grouting, result of boring inspection showed well-cemented rock, and Vp of sonic wave had improved to some extent, hydraulic conductivity met designing demand.

3.2.2 *Foundation drain hole engineering*

Construction quality of foundation drain hole met designing demand.

3.3 *Concrete engineering*

3.3.1 *Quality detection of concrete raw materials*

Manufactory gave leaving factory quality card of Raw materials of cement, fly ash and external material and so on, when raw materials entered into the scene, accepting and using units carried out sampling inspection. Producing and providing unit of coarse and fine aggregate gave quality detection result and leaving factory quality card of every batch of product, when the product entered into the scene, using units detected the sample of it. Supervision unit and the laboratory center of Three Gorges Head Office monitored and carried out sampling inspection to raw materials being used.

Passing sampling inspection of every supervision unit and the laboratory center of Three Gorges Head Office, every quality inspection index of raw materials being used to the project all met contact demand and quality criterion of the TGP, such as cement, fly ash, external material, coarse and fine aggregate, reinforcing steel and steel seal and so on.

3.3.2 *Quality inspection of concrete mix*

Construction unit, supervision unit and the laboratory center of Three Gorges Head Office carried out sampling inspection of air content, slump and temperature of concrete mix at outlet, result of sampling inspection showed, the index of concrete mix met designing demand and quality criterion of the TGP, and the quality achieved excellent level of national criterion demand.

3.3.3 *The compressive strength checking for concrete*

According to the criterion and the quality standard of the Three Gorges construction, the concrete strength from mixing equipment is checked by the construction unit, the supervising engineering unit and the test center of China CHANGJIANG TGP Development Corporation. The different

Table 1. The result analytical table of overall performance checking for concrete.

Position	Frost resistant			Anti-seepage			Ultimate tension		
	Spot check group	Eligible group	Acceptance rate of testing (%)	Spot check group	Eligible group	Acceptance rate of testing (%)	Spot check group	Eligible group	Acceptance rate of testing (%)
Left non-flow dam blocks	34	30	88.2	19	18	94.7	22	10	45.5
Left hydroelectric plant	142	139	97.9	124	123	99.2	179	170	95.0
Floodway	50	46	92.0	48	48	100	60	59	98.3

grade concrete exceeds its strength on a certain extent. The acceptance rate of testing for concrete strength is above 96%. The coefficient of variation value is between 0.093 and 0.194. It contents the national criterion and the quality standard of the Three Gorges construction.

3.3.4 *The overall performance checking for concrete*

The frost resistant, anti-seepage of the Second-stage of Dam concrete and the ultimate tension value of concrete arrive at the demand of design but ultimate tension value of concrete is on the small side at the left bank dam blocks through spot check by the construction unit, the supervising engineering unit and the test center of China TGP Development Corporation. The result is shown in Table 1.

3.3.5 *Temperature control for concrete*

The heat of hydration in cement is decreased because the amount of cement is reduced by selecting the good raw and processed material of the concrete and optimizing mix proportion. The measures of the fall layers discontinuous raising, the pre-cooled concrete using, the artificial cooling through embedded cooling water pipes, the entered barn of tower belt high strength, the spraying in bin's surface in Summer, the covering heat preservation quilt etc. are adopted. The temperature of the dam contents the highest temperature of the criterion and design.

3.3.6 *The checking of the concrete density*

On the basis of checking through boring by the construction unit, China CHANGJIANG TGP Development Corporation entrusts third party with the checking qualification of boring and taking core, the design and supervising engineering unit arrange the location of the bore according to the continuity totality, randomicity, pertinence principle. The concrete density is examined and the concrete quality is assessed generally through the core aspect, the core arrangement, the pressure water checking, the pump water checking, the TV in the bore, the sonic wave detection, the testing research of mechanics properties etc.

The core aspect is slick, compact and the aggregates distribute equably. The proportion of gaining core is 97%~100%. The acceptance rate of testing is above 97.1% by TV in the bore. The acceptance rate of testing is above 98.15% by the sonic wave detection. The acceptance rate of testing of the compressive strength and density is 100%. The acceptance rate of testing is 93.5% by the pressure water checking. For the unqualified bore in the pressure water test, new bores are added and grouted. After grouting, the pressure water checking is eligible. In a ward, the concrete densities of the Second-stage of Dam are better.

3.3.7 *The joint grouting structure of the dam*

There are 203 irrigation areas at the left non-flow dam blocks. The grout areas are 40.3 thousands square meter. There are 806 irrigation areas at the left hydroelectric plant dam blocks. The grout areas are 178.5 thousands square meter. There are 1271 irrigation areas at the spillway sections.

Table 2. The measuring result analytical table of the main structural bodily forms.

Position	Calculating amount	Warp value 0~7mm Proportion (%)	Warp value≤20mm Proportion (%)
Water inlet of 1~10# turbine-generators and silt discharging tunnel of 1~3#	629		93.6
Water inlet of 11~14# turbine-generators	784	52.7	95.1
Bottom diversion outlets	12679	50.3	92.6
Deep outlets	11453	65.7	99.0
Crest spillway sluices	2601	56.4	98.5
Float drains outlets of left guide wall	873	77.1	97.6

The grout areas are 194.9 thousands square meter. The fill is close in cracks and the cementation is good with the cement. The construction quality arrives at the design demand at the joint grouting.

3.3.8 *The inspection ways and handling ways of the dam sealing and drainage system*

According to the demand of design, the draining troughs of the dam transverse slot and the draining pipes of the dam body are all checked through pressure water. The draining troughs of the dam transverse slot and the draining pipes of the dam body are disposed according to the result of checking. Some draining troughs and pipes by jammed are dredged. Some draining troughs without means to dredge; they are disposed by grouting the trough slot in up stream face. Some draining pipes without ways to dredge, they are disposed by boring new holes again. For existing hidden leakage default and seeped out in up stream face, the transverse slots between draining troughs and up stream face are grouted. For existing hidden leakage default and without seeped out, the parts must be grouted when the seepage quantities exceeds 1L/min. The system of the dam sealing and drainage fulfils the demand of design.

3.3.9 *The bodily form measuring of the main structure*

After finishing the Second-stage of Dam, the main structural bodily forms were general measured before the reservoir storage and checking. All structural bodily forms arrive at the demand of the criterion and design. The result is shown in Table 2.

3.4 *The making and fixing engineering of the metal structure and the electromechanical system*

The metal structure and the electromechanical system of the Second-stage of Dam Constructs are made by monitor in the factory. They are carried to the Three Gorges site after finishing make and checking qualification. The fixing of the equipment must strict to carry out the checking by the construction unit, the checking again by the supervising engineering unit and the sampling inspection by the checking center of the Three Gorges. The questions are found and dealt with on time during the fixing. The fixing qualities of the equipment all arrive at the demand of the criterion and design. The operation situations are good.

4 THE SITUATION OF THE DAM SAFETY MONITORING

4.1 *The deformation of the dam body and foundation*

The horizontal displacements of the dam foundation are very small. They are between −1mm and 1mm. The deformations are towards the downstream by the hydraulic pressure and the temperature load in the period of water storage. The deformations of the dam body take on the periodic deformable rule. When the water level arrives at 135 meter, the displacements of the dam crest are 3.18mm towards downstream (June 11, 2003). When the water level arrives at 139 meter, the displacements of the dam crest are 4.86mm towards downstream (Nov 5, 2003). The deformations are 8.75 meter towards downstream and less than the value of design on Mar 12, 2004.

4.2 *Seepage flow through the dam foundation*

The seepage quantities of the dam foundation are reducing in the mass. The Maximum seepage quantity is 1036L/min. It is 861.56L/min by the middle ten days of 10. At present, the seepage quantities of the dam foundation are 797.98L/min. It decreases 265.02L/min comparing with the max and less than the allowable value of the design. The reduction coefficients of the drainage curtain uplift of the base culvert on upper are less than 0.15 except for few testing pore in left hydroelectric plant. They are less than 0.25 of the design value.

4.3 *Stress at dam heel*

There is all compression at dam heel. When the water level arrives at 135 meter, the practical stress measure results are between −3.04Mpa and −5.5Mpa. At present, the practical stress measure results are between −2.83 Mpa and −5.43 Mpa.

5 CONCLUSION

The Second-stage of Dam Constructs has passed the storage water acceptance check of the Second-stage acceptance committee under the council on May 21, 2003.The conclusion is that the quality of design, construction, manufacture and erection accord with the correlative technical offense of nation and trade at the foundation engineering, the hydroelectric building, the metal structure, the electromechanical system and the safety monitoring. The project quality can satisfy the demand of design by disposing the disfigurement and accident of quality arising during construction and erection.

The Three Gorges reservoir began to storage water on June 1, 2003. The water level arrived at 135 meters on June 10. The results of the safety monitoring indicated after storage-water that all buildings could normally operate and the deformation of the dam, the reduction coefficient of the foundation uplift, the seepage flow of dam foundation etc were less than the allowable value of the design. It indicated the quality of the Second-stage of Dam construction is good.

REFERENCE

[1] Luyoumei, *The Concrete construction on Three Gorges Dam,* China electric power publishing firm, April, 2003.

New Developments in Dam Engineering—Wieland, Ren & Tan (eds),
© 2004 Taylor & Francis Group, London, ISBN 04 1536 240 7

Water quality characteristics and seepage of rock dam foundation

Yang Guangzhong, Zhai Liquen & Peng Hanxing
Hohai New Technology Development Corporation, Hohai University, Nanjing, China

ABSTRACT: During the process of its seepage towards dam foundation, as a solution, reservoir water not only presents physics nature such as water pressure, water quantity etc., but also produces physicochemistry reaction with dam foundation rock, grout curtain, concrete and forms new water quality characteristics. A seepage field of rock dam foundation consists of water physical field together with water chemical field. Water quality of dam foundation has various characteristics such as complexity of ingredients, variety of water chemistry types and larger change of pH values etc. These characteristics can reflect the runoff condition, supply sources of groundwater in the dam foundation and the geochemistry environment that the groundwater belongs to. The seepage field can be divided into runoff expedite zone and runoff tardy zone. Runoff expedite zone can also be divided into major and minor seepage channel.

1 INTRODUCTION

During the process of its seepage towards the dam foundation, as a solution, reservoir water produces interactions with dam foundation rock, grout curtain, concrete. The formation of water quality characteristics in dam foundation is the results of these interactions. The condition of groundwater runoff in the dam foundation restrict velocities and extent of these interactions, and, contrariwise, water quality characteristics of the groundwater in dam foundation can reflect the condition of groundwater runoff in the dam foundation. More exactly, water chemical field in the dam foundation is an important component of a seepage field; i.e. a seepage field of dam foundation consists of water physical field (water pressure, water flow and water temperature etc.) together with water chemical field.

2 BASIC CHARACTERS OF WATER QUALITY OF DAM FOUNDATION

2.1 *Component complexity of water quality*

Generally the range of dam foundation in a narrow canyon is limited, but the components of water in dam foundation are complex. Apart from the main ion components there are components of molecules, gases, colloids and organic matter.

For the gases the common components are H_2S, CH_4 and CO_2. A kind of rotten egg odor can be smelled evidently when H_2S emits from drain boreholes of dam foundation. The maximum content of H_2S is high to 3.5mg/l in the drain boreholes of foundation of Xinanjiang Dam. Gas having rotted egg odor as well as flammable gases emits from observation boreholes of uplift pressure, in No. 5 and No. 6 of section 21 of Danjiangkou Dam. According to quantitative analysis saturated hydrocarbon (methane CH_4, ethane C_2H_6, etc.) in these gases accounts for 11.38~23.4%. The others are hydrogen sulfide, nitrogen, etc.

The water in part of drain boreholes of dam foundation contains abundant colloid. Varieties of colored colloidal educts, such as red, black, white and sometimes yellow, brown as transitional

color, often formed around the mouth of drain boreholes. According to X-ray diffraction analysis of the educts no diffraction peaks were created. It indicates that they are non-crystal colloids. From the point of view of chemical analysis there are positive colloids such as $Fe(OH)_3$, $Al(OH)_3$, $CaCO_3$ etc., as well as negative colloids such as SiO_2, MnO_2, etc. Most of the colloids consist of elements of iron, manganese, calcium etc., and much less silicon and aluminum[1].

It is difficult to measure the content of organic matter in water. The chemical oxygen demand (COD) of water is a suitable index for evaluating the organic matter content. In Xinanjiang reservoir the COD value in surface layer water is lower but higher in bottom layer water, which is 10 times as much as that in surface layer water and reaches 15mg/l. It shows that the organic matter content is abundant in bottom layer water. The water in most dam foundations contains no or less COD but in a few of drain boreholes contain abundant organic matter which can reach 11~20mg/l.

2.2 *A variety of water chemistry types*

Generally the water chemistry type of reservoir water is simple. Water in lower layer belongs to type HCO_3–Ca or type HCO_3–Ca·Mg and in most instances it belongs the former. As the groundwater in the dam foundation is in the drainage area of reservoir water, the groundwater possesses a variety of water chemistry types. As to the components of anions, apart from type HCO_3 and type $HCO_3{\cdot}SO_4$, because of abundance of CO_3^{2-}, OH^- in the water, type OH, type CO_3 and type $CO_3{\cdot}OH$ appear too. This phenomenon is rare in groundwater of mountain area. As to the components of ions, type Ca, type K+Na or both of them are the majority.

The variety of water chemistry types reflects that during the transfer progress of reservoir water to dam foundation the strength and condition of water chemistry action are different.

2.3 *Large variation of water pH value*

The variation of water pH value in dam foundation is very much. For example, in Xinanjiang dam the variation range of water pH value in dam foundation is between 5.15 (drain borehole No. 2–C_3) and 12.6 (drain borehole No. 24–1). According to their pH value the chemistry characters of water in dam foundation can be divided from weak acid to basic, till strong basic.

In the gallery of dam section 9 of Danjiangkou Dam the pH values of water in borehole No. 1 and No. 2 are above 10.25, in borehole No. 3~7 are only 8.01~8.32, while in No. 8 is high to 11.34 again. It is evident that along this dam section the pH values are higher on the both ends and lower in the middle. Only in a distance of 2~3 meters there are a difference of water pH values reaching to 2.24~3.02 and the chemistry character of water changes from weak basic to strong basic. It makes the water have notable differences in chemical components and types. The water having low pH value belongs to type HCO_3, while high, type $CO_3{\cdot}OH$.

3 CAUSE OF FORMATION OF WATER QUALITY AND RUNOFF CONDITION IN DAM FOUNDATION

The formation of water quality is closely relative to condition of groundwater runoff in dam foundation. So the components of water quality in dam foundation offers important basis to analyze and determine condition of groundwater runoff.

Water pH value is an important index that reflects the components of water quality. Under the condition of dam foundation water pH value is closely related with the seepage state.

The drain boreholes in dam grouting gallery are located behind the grout curtain. So the pH values of water in drain boreholes are related with the strength of interaction between water in dam foundation and cement stone. The reaction is:

$$3\ CaO{\cdot}SiO_2+Z\ H_2O=Ca(OH)_2+xCaO{\cdot}ySiO_2{\cdot}aq\ \ Ca(OH)_2+Ca(HCO_3)_2=2CaCO_3+2H_2O$$

Calcium carbonate is hydrolyzed:

$$CaCO_3 + H_2O = Ca^{2+} + OH^- + HCO_3^-$$

Along with the proceeding of hydrolysis of calcium carbonate the content of OH^- increases and the basicity of water in drain boreholes is larger and larger. In the basic environment CO_3^{2-} enrichment in the water. But calcium carbonate is a kind of mineral which is soluble difficulty in water. Its hydrolysis is going very slowly Only under the condition that the velocity of underground runoff is very low, the water with basicity or strong basicity, that has larger pH value, can be formed. So when this kind of water appeared behind the grout curtain of dam foundation it shows that the velocity of underground runoff is very low. The larger the basicity is the slower the runoff flows.

Similarly when the water, that mainly belongs to the chemistry type of CO_3^{2-} or OH^-, is found in dam foundation it can be a sign that underground runoff flows very low. This phenomenon appears along with the formation of basic or strong basic water.

The water pH value is 11.59 averaged in 5 years in drain borehole No. 1 at dam section 24 and 9.8 at dam section 23 of Xinanjiang Dam. The chemistry type of water belongs to type OH or CO_3. During several years the water levels in the boreholes change little. Especially the level in drain borehole No. 24–1 is considered as "dead water". It shows that the runoff in dam foundation flows very slow. So when this kind of water appeared behind the grout curtain of dam foundation it can be treated as a sign that the function of anti-seepage grout curtain is perfect. On the contrary if the water pH values in drain boreholes behind the grout curtain of dam foundation are similar to those in low layer of reservoir, it shows that the runoff flow under the dam foundation is unobstructed. Here the pH value is about 7 and the water presents weak acidity or weak basicity.

The water presents weak basicity (pH value is 7.75) in low layer of reservoir in front of Danjiangkou Dam. The water pH values of drain boreholes are similar to that in the reservoir when the flow rates of the drain boreholes in the dam gallery are larger (larger than 0.51/min). The water type belongs to weak basicity in about 78% of boreholes. In the other 22% the water presents basicity, but the pH values are smaller, near 8.5[2] The largest drainage flow presents in dam section 28. Its measure data on site (table 1) show that the water in borehole No. 28–4 presents strong basicity. Its drainage flow is only 0.00511/min and presents stable state. The water pH values and chemical components of other drain boreholes are similar to those in low layer of the reservoir and they belong to the drain boreholes that have larger flow rate. It is evident that drain borehole No. 28–4 is located in an isolated stagnant water. The other boreholes in dam section 28 are located in strong runoff strip. On the contrary the most water pH values of drainage flow of dam section 29 are above 8.50 and the largest, 10.10. The drainage flow rate of the whole dam section is less than 11/min, 6 times less than dam section 28. So the foundation of dam section 29 is in sluggish runoff strip.

There are data of water pH values of drain boreholes measured systematically on site for dam section 9 and 10 and analyses of their water chemical components. They show that although the drainage flow rates of drain borehole No. 3, 4, 5, 7 are much smaller, only dropping, the pH values are 8.01 to 8.31 and the water chemistry type is similar to the reservoir water. It indicates that the runoff condition is good and the location of these boreholes can be considered in strong runoff

Table 1. Flow rate list of drain boreholes in dam section 28 in Danjiangkou Dam (1997.9.15).

Number of boreholes	pH	Flow rate (1/min)	Number of boreholes	pH	Flow rate (1/min)
28–1	8.19	0.69	28–6	8.08	0.52
28–2	8.17	1.09	28–7	8.09	0.41
28–3	8.17	0.95	28–8	8.13	0.2
28–4	12.28	0.005	28–9	8.03	0.55
28–5	8.17	0.35	28–10	8.07	0.51

strip too. The drain boreholes on both sides are located in sluggish runoff strip. Their drainage flow rates are small because the mouths of these boreholes have higher elevation.

According to the above examples it is indicated that the water quality characteristics can obviously reflect the runoff state of dam foundation. Based on this principle the dam foundation can be divided into strong runoff strip, sluggish runoff strip and isolated stagnant water.

The components of groundwater in dam foundation can reflect the supply source and dynamic condition of groundwater. In right bank of Xinanjiang Dam foundation the water pH values in most drain boreholes are less than that of the reservoir water obviously. Its lowest value is only 5.15. The water here is rich in erosive CO_2 and its water quality characteristics is similar to the groundwater of dam foundation under the right bank slope. The latter is weak acid too and rich in erosive CO_2. The cause of formation of this water quality is that there are multiple layers of thin carbonized shale in the bedrock made of quartz-sandstone and the organic matter in the shale is decomposed into weak acid water. So the groundwater under dam foundation of the right bank is supplied by the water of the bank slope instead of the reservoir water. Under the action of high water pressure (under the dam foundation of bank slopes the hydraulic grade of groundwater is high up to 1.13) it is advantage to water infiltration and decomposition of the organic matter. So the water formed has lower pH value and is rich in erosive CO_2. Here the water quality reflects not only the supply source of water under the dam foundation but also the water dynamic condition.

The emission of H_2S from the drain boreholes is a sign that indicates the water is in an environment of deoxidization or weak deoxidization and the groundwater runoff in this strip flows slowly. When the water environment changes (from deoxidization or weak deoxidization to oxidization) there is deposition of colloidal educt around the mouths of drain boreholes. This is relative with chemical suffosion of dam foundation instead of mechanical piping erosion made by water dynamic action.

4 CONCLUSION

(1) The seepage field of dam foundation consists of both water physical field and chemical field. The water quality components are the products of interaction made by water-bedrock, water-grout curtain and water-concrete. It can reflect the flow directions and conditions of runoff during the course of reservoir water running towards dam foundation.

There are a lot of drain boreholes with small spaces in the drainage gallery of a dam, which provides us an advantageous condition to study water chemical field in dam foundation. It is necessary to conduct a periodic, systematic and all-around tests of pH values on site, and water quality analyses of samples taken at chosen points. The information got from the tests and analyses not only provide detailed and important basis to evaluate the character of seepage prevention of the grout curtain, but also has a great significance to know well the complex character of seepage field of dam bedrock. It is worthy to pay more attention.

(2) In despite of a relatively stable water head in a reservoir the distribution of groundwater in the dam foundation becomes complex because the geological condition is complex, the fissure distribution of bedrock is uneven and multiple engineering measures are applied. For the complex seepage field of dam foundation it is necessary firstly to divide the field into different hydrogeological units on the basis of comprehensive analysis, i.e. strong runoff strip, sluggish runoff strip and isolated waters (stagnant, fluent) and so on. Then to choose different parameters and conduct numeral calculation. In this way some analysis results can be found which match well to the fact.

(3) The gas emission from drain boreholes of dam foundation and jelly deposition around the mouths of these drain boreholes not only reflect the condition of runoff in dam foundation but also are signs of earth chemical environment and its change in which the dam foundation located. They are significant to evaluate the change of characteristics and seepage stability of dam bedrock (especially weak rock) that is in soak condition for long period. On this subject there are a lot of works to do in the future.

REFERENCES

[1] Peng Hanxing: Subjects on Valley Engineering Geology, Nanjing China, Hohai University Press, 1993.
[2] Yang Guangzhong, et al.: Evaluation of Water Quality Characteristics and Grout curtain Feature of Dam Foundation of Danjiangkou, Journal of Hydroelectric Engineering, 2000. 4, pp. 33–39.
[3] Zeng Kaihua et al.: Some Questions in Analysis of Educts from Dam Foundation. J. Dam Observation and Geotechnical Tests, 2000. 3, pp. 10–12.

This page intentionally left blank.

New Developments in Dam Engineering—Wieland, Ren & Tan (eds),
© 2004 Taylor & Francis Group, London, ISBN 04 1536 240 7

Deformation characteristics of key dam block of Geheyan project under operational stage

Jian Yang
Changjiang River Scientiflc Research Institute, China

Jun-xiang Cheng & Fa-jie Jiao
Three Gorges Exploration Survey Research Institute, CWRCY, China

ABSTRACT: Geheyan project has the power capacity of 120×10^4kw, with the crest elevation is 206m, the maximum dam height is 151m which has a corresponding crest length of 653.5m. The dam is an arch gravity dam with gravity dam at the superstructure and arch dam at the infrastructure. The elevation of arch spring line is 150m in the left bank, 180m in the riverbed, 160m in the right bank. The arch crown and arch abutment are the key dam block. The project was put into use after checked and accepted by the administration in 1997. In 1998, the river experienced the especial hundred-year frequency flood. In order to adjust the peak flood of Yangtze river, the project underwent the especial flood with the reservoir water level at El. 206m, which was 1.96m higher than the designed reservoir water level. There were obvious deformation in arch crown and arch abutment under high water, but the deformation was in the designed ranges. The monitoring results from plumb line and inverted pendulum in the past several years indicated that the deformation in some important position was influenced by the environmental factors. But the deformation has the common regular pattern as others, so the dam's behaviour is in order now.

1 INTRODUCTION

Geheyan project lies on an anisomerous valley of Qingjiang river of Hubei province. The topography above the elevation of 130m on the left bank becomes less steeper than the topography on the right bank. The foundation of gravity frusta is designed on the elevation between 130m and 150m to make up with the shortage of terrain. The dam is designed as gravity dam above the elevation of 150m. So the dam is an special arch gravity dam with gravity dam at the superstructure and arch dam at the infrastructure. The design waterlevel is El. 200m and the check flood water-level El. 202m. The dam is made up of 30 block showed as figure 1.

The foundation rock is mainly made of limestone of cambrian system. The strike of the terraine is orthographical with the river. The tendency is to upper reaches of the river with obliquity of 25~30°. The total thickness is up to 142~175m. There are three interlayers and ten faults. The rock on abutment of dam is limestone and the rock of foundation is interbedded limestone and shale. There are several faults and soft interlayers, which destroys the holism of the rock foundation and is harmful to the stability of rock foundation.

2 MONITORING SYSTEM

The monitoring system is made mainly up of some plumb lines and inverted pendulums from the foundation to the crest in several dam blocks. According to the geologic condition of the foundation

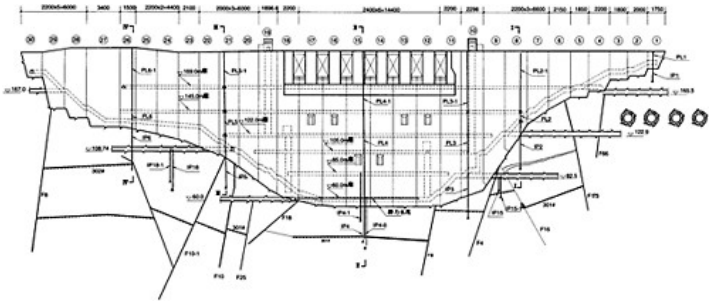

Figure 1. The sketch layout of deformation monitoring on Geheyan dam.

Table 1. Plumb lines and inverted pendulums in dam blocks of arch crown and skewback*.

El. (m)	▽203.5							
Archcrown 15#	IP151	IP1521	PL15301	PL15401	PL15501	PL15601	–	IP15801
Left skewback 21#	–	–	IP21301	PL21401	PL21501	PL21601	PL21701	PL21801
Right skewback 10#	–	IP1011	PL10301	PL10401	PL10501	PL10601	PL10701	PL10801

*: IP-inverted pendulum; PL-plumb line.

and the characteristic of dam structure, people pay more attention to the stability of the dam and foundation, especially in such dam blocks nearby 1/4 arch ring of skewback as No. 10# dam block on the right bank and No. 21# dam block on the left bank. So those dam blocks in the arch crown and skewback are key monitoring dam block to be monitored for long-term. The main deformation monitoring system is showed as figure 1 and table 1.

3 MONITORING RESULTS

The plumb lines and inverted pendulums are designed to monitor the horizontal deformation in the radial and tangential direction of the dam. The radial deformation is regulated as "+""when the deformation is tended to backward position. And the tangential deformation is regulated as "+" when the deformation is tended to left bank.

3.1 *The radial deformation of the dam*

The design water level is El. 200m and the check flood water level El. 202m. The scanty water level is E1.163m. The water level of the reservoir is normally between El. 163~190m. The frequent change of the reservoir water level influences the stability of the dam.

(1)Archcrown

The monitoring results of horizontal deformation in dam blocks of arch crown are showed as table 2 and figure 2(a).

The radial deformation is influenced mainly by the water level of the reservoir and shows the increscent tendency in the direction of downriver while the water level increases. In 1998, the river experienced the especial hundred-year frequency flood. In order to adjust the peak flood of Yangtze river, the project underwent the especial flood with the reservoir water level over the

Table 2. The eigenvalue of deformation (radial/tangential) in No. 15# dam block (unit: mm).

Instrument	IP15101	IP15201	PL15301	PL15401	PL15501	PL15601	PL15801
1998–08–17	9.23/−1.33	4.48/−1.31	12.42/− 1.42	15.07/−2.2	9.23/−0.74	10.53/−1.71	12.58/−1.7
2000–03–06	6.41/−0.98	7.8/−0.05	7.4/−0.03	8.5S/−3.29	0.64/−0.24	0.71/−1.64	0.97/−0.13
2001–09–05	6.43/0.69	7.72/−0.16	6.79/−0.82	6.15/0.15	−2.83/0.3	−6.36/−1.38	−11.93/−1.0
2002–05–21	8.04/−0.96	10.95/−0.09	12.84/−0.07	15.74/−1.24	10.08/0.58	5.48/0.16	8.85/−0.22
2002–12–24	6.97/−1.12	7.81/−0.31	9.25/−0.66	10.79/−2.09	2.33/0.36	1.267–1.09	1.12/−0.45
Max.	9.23/0.69	10.95/−0.05	12.84/−0.03	15.74	10.08	10.53	12.58
Min.	6.41/−1.33	4.48/−1.31	7.4/−1.42	−3.29	−2.85	−6.36	−11.95
Amplitude	2.82/2.02	6.47/1.26	5.44	19.03	12.93	16.89	24.53

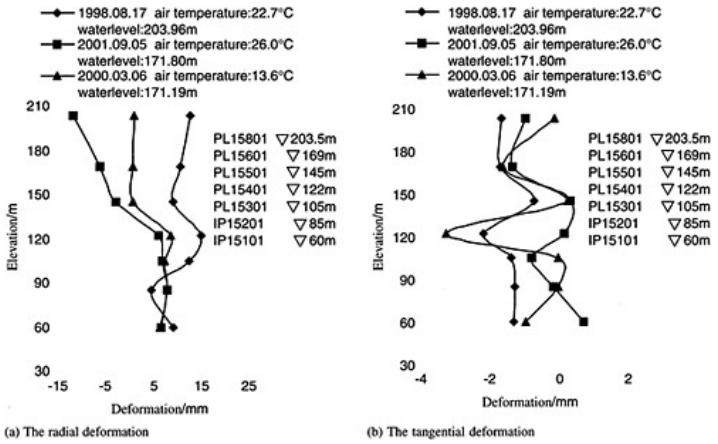

Figure 2. Curves indicating the relation between deformation and elevation in No. 15# dam block.

designed water level. The reservoir water level is El. 203.96m on 17th of August, which is 1.96m higher than the check flood water level and is the maximal in the history. The radial deformation of IP15101 and IP15201 is 9.23mm and 4.48mm. The radial deformation of PL15301, PL15401, PL15501,PL15601 and PL15801 is 12.42mm, 15.07mm, 9.23mm, 10.53mm and 12.58mm.The deformation shows positive corelation with the change of the water level of the reservoir. The radial deformation minishes in the direction of downriver while the water level decreases. For example, the water level is El. 171.80m on fifth of September in 2001. The radial deformation of IP15101 and IP15201 is 6.43mm and 7.72mm. The radial deformation of PL15301, PL15401, PL15501, PL15601 and PL15801 is 6.97mm, 6.15mm, −2.83mm, −6.36mm and −11.93mm.

(2) Skewback

The deformation regularity of dam blocks of skewback is the same as that of arch crown. The radial deformation shows the increscent tendency in the direction of downriver while the water level increases. And the deformation on the top is bigger than that of undersurface as showed in table 3 and figure 3(a) and figure 4(a).

Table 3. The deformation (radial/tangential) in No. 10# dam block of skewback (unit: mm).

Instrument	IP10101	PL10301	PL10401	PL10501	PL10601	PL10701	PL10801
1998–08–17	4.1/−1.08	9.55/−2.69	10.93/−2.72	12.26/−2.44	11. 33/−4.48	11.9/−1.3	12.1/−3.3
2000–01–03	3.48/−1.04	7.87/−3.1	S.53/−3.43	8.08/−1.77	6 19/−3.19	5.45/0.43	5.83/−2.15
2001–09–05	3.6/−0.85	7.78/−1.76	8.09/−1.43	7.72/−0.16	2.01/−2.42	−0.61/0.95	0.83/−0.25
2002–5–21	5.12/−1.05	10.88/−2.17	12.55/−2.81	14.1/−1.84	13.4/−3.77	14.96/−0.79	15.9/−3.05
2002–12–24	3.94/−0.74	8.17/−1.07	6.19/−1.88	8.95/−0.84	6.73/−2.25	7.35/1.34	6.16/−1.11
Max.	5.2/−0.74	10.8/−1.07	12.5/−1.88	14.1/−0.84	13.4/−2.25	14.9/1.02	15.9/−1.11
Min	3.48/−1.1	7.87/−2.69	6.19/−3.43	8.08/−2.44	6.19/−4.48	5.45/−1.3	5.S3/−3.3
Amplitude	1.72/0.36	2.39/1.62	6.31/1.55	6.02/1.60	7.21/2.23	9.45/2.05	10.13/2.19

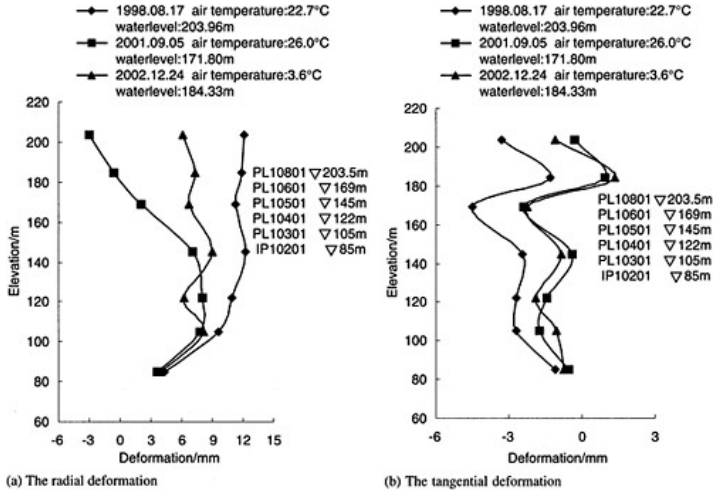

Figure 3. Curves indicating the relation between deformation and elevation in No. 10# dam block.

3.2 *The tangential deformation of the dam*

(1) Archcrown

The tangential deformation is pointing to right bank while the water level is very high. The tangential deformation in No. 15# dam block of arch crown is −1.31mm, −1.42mm, −2.2mm, −0.74mm, −1.71mm and −1.70mm as showed in figure 2(b). The tangential deformation in dam blocks of arch crown is influenced by water level more sightly.

(2) Skewback

The tangential deformation in dam blocks of left skewback is pointing to left bank and the tangential deformation in dam blocks of right skewback is pointing to right bank while the water level is very high. But the tangential deformation in dam blocks of left skewback is pointing to right bank and the tangential deformation in dam blocks of right skewback is pointing to left bank while the water level is very low show as figure 3(b) and figure 4(b).

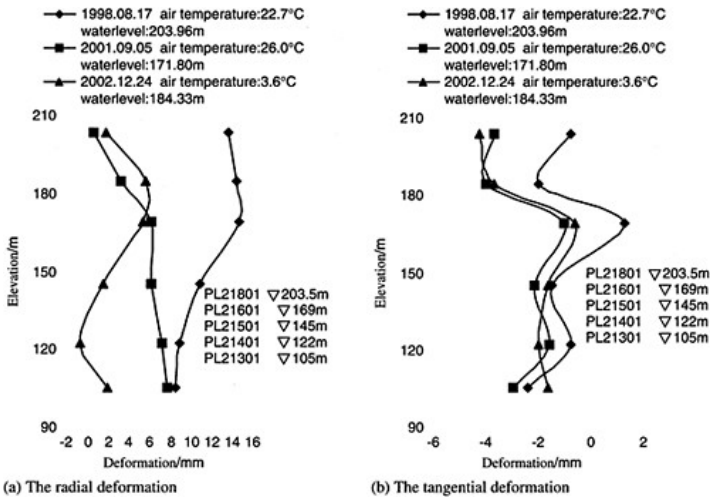

Figure 4. Curves indicating the relation between deformation and elevation in No. 21# dam block.

Table 4. The deformation (radial/tangential) in No. 21# dam block of skewback (unit:mm).

Instrument	IP21301	PL21401	PL21501	PL21601	PL21701	PL21801
1998–08–17	8.44/−2.43	8.86/−0.79	10.82/−1.52	14.64/1.31	14.47/−2.01	13.67/−0.81
2000–01–11	7.58/−2.64	7.43/−1.02	7.95/−2.3	8.08/−1.29	8.08/−4.28	8.22/−3.78
2001–09–05	7.67/−2.99	7.15/−1.60	6.02/−2.19	6.04/−1.03	3.15/−4.04	0.45/−3.74
2002–4–21	8.24/−2.5	8.75/−0.68	10.75/−2.08	13.99/0.34	14.75/−3.05	15.07/−1.74
2002–12–24	1.81/−1.68	*−0.8/−2.04	1.42/−1.68	5.22/−0.64	5.5/−3.73	1.77/−4.29
Max.	8.44/−1.68	8.86/−0.43	10.75/−0.49	14.64/1.66	14.75/−1.23	15.07/−0.26
Min.	1.81/−2.64	−0.8/−2.04	1.42/−2.3	5.22/−1.29	5.5/−4.28	1.77/−4.09
Amplitude	6.63/0.96	9.66/1.71	9.33/1.81	9.42/2.95	9.25/3.05	13.3/3.83

3.3 *The influence of air temperature*

The influence of air temperature on the deformation could be indicated by means of contrast on the deformation under the condition of similar water level and distinct air temperature in different seasons. The monitoring result (showed as table 2 and figure 2(b)) indicates that the radial deformation on the top of the dam is influenced greatly by the air temperature and that the deformation shows decreasing tendency from the top to the foundation.

4 CONCLUSIONS

The aboved analysis on the monitoring results indicates that the radial deformation regularity is: (1) The radial deformation is influenced mainly by the water level of the reservoir and shows the increscent tendency in the direction of downriver while the water level increases. The radial deformation minishes in the direction of downriver while the water level decreases. The deformation

shows positive corelation with the change of the water level of the reservoir. (2) The radial deformation on the top of the dam is influenced greatly by the air temperature and that the deformation shows decreasing tendency from the top to the foundation. The deformation shows negative corelation with the change of air temperature.

The tangential deformation regularity is: (1) The tangential deformation in dam blocks of left skewback is pointing to left bank and the tangential deformation in dam blocks of right skewback is pointing to right bank while the water level is very high. (2) The tangential deformation in dam blocks of left skewback is pointing to right bank and the tangential deformation in dam blocks of right skewback is pointing to left bank while the water level is very low. (3) The tangential deformation in dam blocks of left skewback is pointing to right bank and the tangential deformation in dam blocks of right skewback is pointing to left bank while the air temperature increases. (4) The tangential deformation in dam blocks of left skewback is pointing to left bank and the tangential deformation in dam blocks of right skewback is pointing to right bank while the air temperature decreases.

New Developments in Dam Engineering—Wieland, Ren & Tan (eds),
© 2004 Taylor & Francis Group, London, ISBN 04 1536 240 7

Qingjiang Shuibuya concrete face rockfill dam under construction

Yang Qigui & Xiong Zebin
Changjiang Institute of Survey, Planning, Design & Research, CWRC, China

ABSTRACT: The Qingjiang Shuibuya concrete face rockfill dam, 233m high, is the highest of its kind completed or under progress in the world. The design of the dam and the new technologies and workmanship applied during construction are presented in the article. The pattern of "A+X" suggested by J.Barry Cooke is adopted for the plinth of the dam, strong tamping is used for riverbed foundation treatment, and crushed curb is applied to the upstream slope of the dam. The use of these techniques exerts positive influence to the smooth implementation of the project as scheduled.

1 GENERAL OF THE PROJECT

The Qingjiang Shuibuya Project, located in Badong County, Hubei Province, 117km from Enshi City upstream and 92km from Geheyan Hydropower Project downstream, is the pioneer project in the cascade development on the Qingjiang River. Originating from Longdong gully on the Qiyue Mountain in western Hubei Province and flowing into the Yangtze River at Zhicheng City, the Qingjiang is the first large tributary of the Yangtze river after flowing out of the Three Gorges. The Qingjiang river, 423km long with a total fall of 1430m, has a catchment area of about 17000km^2. The Shuibuya dam, in the middle stream of the Qingjiang river, has a controlled area of 10860km^2, with an average annual flow of 299m^3/s and a yearly runoff of 9.44 billion m^3 accordingly at the dam site.

The normal water level of the reservoir is at El. 400m and the dead water level at El. 350m, with a reservoir capacity of 4.312 billion m^3 and a regulation capacity of 2.383 billion m^3 respectively. It is a yearly regulation reservoir. The power station has a total installed capacity of 1600MW with a guaranteed output of 310MW and an average annual power generation of 3.92 billion kW.h accordingly. It is categorized as a large-scale water conservancy and hydropower project with functions mainly for power generation and flood control as well as for other purposes.

The dam is located at the waist of S-type section of the Qingjiang river. The waist is some 800m long in straight line, flowing at NE30°, where the banks are high and steep on both sides with a height difference of more than 230m. The valley is generally in an asymmetric V-shape with an average slope of 52° on the left bank and 35° on the right bank. The overburden is generally 12.0~14.42m thick on the river bed where the alluvial deposit consists mainly of sand, pebble and gravel, containing erratic boulder and block layer as well as silt and silty clay lens with sand and gravel. The strata at dam site are mainly the Maokou formation(P_{lm}) and Xixia formation (P_{1q}) of the lower Permian, with distribution of Longtan formation(P_{2l}) of the upper Permian in the left abutment above El. 395~400m. The Maokou formation consists of thick to extremely thick lime-stone, hard and intact, while the Xixia formation consists of interbedded strata of medium thick limestone and carbonaceous bio-clastic limestone, with multi-bedding and multi-shear zones in between. Faults and fissures develop in the river section at dam site. The Maokou limestone belongs to strong karst stratum, while the Xixia formation belongs to the stratum of strong and weak karst alternately. Karst develops on the surface and underground on both banks. The basic

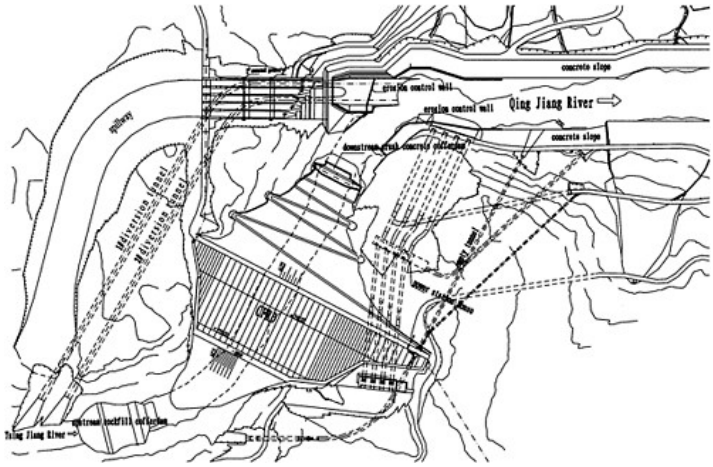

Figure 1. Plan layout of the project.

seismic intensity is VI at dam site, however, the major structures are designed against a seismic fortification intensity of VII. The dam area is short of impervious clay materials but abundant of rock materials.

The Project consists of the dam, spillway, powerhouse and emptying tunnel, see Fig. 1 for the general layout of the project.

The dam is a concrete face rockfill dam, located at the waist of the S-type section of the Qingjiang river. The dam crest is at El. 409.0m with a maximum height of 233.0m. It is 12.0m wide at crest and 660.0m long in axis direction. The river-bank type spillway is on the left bank, provided with 5 upper bays sized at 14.0m (width)×21.8m (height), with a total discharging capacity of 18320m^3/s. The diversion-type underground power station is located on the right bank, installed with 4 turbine-generating units, 400MW each, 1600MW in total. The emptying tunnel, acting as diversion tunnel in the middle and later stages of construction, is located at the right side of the power station, with a max discharge capacity of 1600m^3/s.

The duration of the project construction is scheduled as 8.5 years. Preparatory work started before 2000; construction preparation was from 2001 to 2002, where the river closure was achieved in late October 2002; the construction for the main works of the project was planned from 2003 to 2007, with power generation of the first set of generating unit in July 2007; from July 2007 to June 2009 will be the completion period of the project.

2 DESIGN OF THE DAM

The dam is mainly composed of the plinth (standard and anti-seepage), slab and its joint waterstop system, filled dam body, and dam crest breakwater wall. Cover is provided in the upstream of the dam and measuring weir provided at the downstream dam toe for seepage observation. The volume

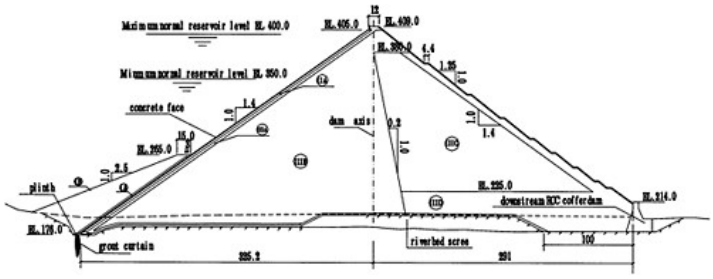

Figure 2. Dam section (m).

of the rockfill dam body is 14.64 million m^3 and that of the upstream cover is 620,000m^3, totally 15.26 million m^3. The concrete slab has an area of 137,000m^2 and the joint is 12500m in total.

A 5.4m high L type breakwater wall is provided on the top of the dam, with the bottom at El. 405.0m and crest at El. 410.4m. The dam is at a slope of 1:1.4 upstream, while in the downstream, a 4.5m wide Z type berme is provided with a slope of 1:1.25 locally and 1:1.4 synthetically. The downstream cofferdam is combined with the dam body.

2.1 *Zoning and material design*

The section and zoning of the dam is shown in Fig. 2.

The design control and compaction parameters of the fills in various zones are shown in Table 1.

2.2 *Foundation treatment*

Most foundation of the plinth lies on the weak unloading zone of the Xixia formation with partial foundation on the strong unloading zone of Xixia formation.

The overburden of the riverbed within a range of 150m downstream of the plinth is mostly removed by excavation, with partial remained which is treated by strong tamping to improve its density.

It is required for the dam foundation on both banks that the overburden and loose rock mass upstream of the dam axis should be removed where the reverse slope is formed by scaling or proper concrete backfill with a slope not higher than 1:0.3, while the overburden and loose rock masses downstream of the axis should be cleared away.

Fissures develop in the river section where the dam is located, especially in the upstream riverbed and around the left bank plinth where faults are densely distributed and it is strongly eroded. Unloading fissures also develop on both banks. In addition, the inter-bedding shearing develops in the rock mass of the Xixia formation where strong and weak strata exist alternately. As a consequence, the rock mass is discontinuous and non-homogeneous. Therefore, to prevent the dam foundation from non-uniform deformation and seepage failure, some portions are cleared and backfilled with concrete.

Spacing arrangement and grouting depth for the consolidation grouting of foundation: the consolidation grouting is arranged in a stagger shape. The hole spacing is 2m and row distance 1.5~2.0m at the location of plinth. A row of 17.0m deep holes is arranged respectively on the upstream and downstream of the impervious curtain as supplementary curtains, while other holes are 7.0m deep. On the location of the cutoff slab, the row distance is 2.5m×2.5m, with the holes 5m deep.

Table 1. Design compaction parameters of the dam fills.

Zoning	Name	Source of Fill Materials	Dary density (g/cm^3)	Porosity (%)	Grade requirements			Compaction			
					d_{max} (mm)	<5mm (%)	<0.1mm (%)	Lift thickness (cm)	Number of passes	Watering amount (%)	Weight of roller (t)
IAA	Mini-zone	Artificially crushed Maokou limestone in borrow site									
IIA	Cushion	Artificially crushed Maokou limestone in borrow site	2.25	17.0	80	35~50	4~7	40	8	Proper amount	18
IIIA	Transit	Blasted Maokou limestone in borrow site and tunnel excavated Xixia hard rock	2.20	18.8	300		<5	40	8	15	18
IIIB	Main fill	Maokou limestone at borrow site and excavated materials	2.18	19.6	800		<5	80	8	15	25
IIIC	Secondary fill	Excavated materials and Xixia limestone	2.15	20.7	800		≤5	80	8	10	25
IIIC	Downstream fill	Excavated materials and Xixia hard limestone	2.15	20.7	1200		<5	120	8		25

Design standard for impervious curtain: q≤3 lu for the dam foundation and the section near the bank and q≤5 lu for the section far from the bank. The depth of the curtain is 0.4 times of the dam height in the riverbed location and the curtain at the left abutment is the deepest, with the max depth of 260m.

2.3 *Plinth*

Plane plinth is arranged, with its line controlled by the intersecting line (Y) of the bottom face of the slab and the downstream face of the plinth.

The plinth is 8m wide below El. 348m. To meet the hydraulic gradient, an additional cutoff slab is provided (50cm thick) downstream. It is 6m wide above El. 348m. The thickness of the plinth ranges from 1.2 to 0.6m at different elevations.

The plinth line is 1100m long in total without permanent joints. A 2m wide slot is provided every 12~16m, where concrete is poured 90 days after the concrete placement on both sides, with reinforced bars passing through the wide slot. C25 concrete is used for the plinth, with the anti-seepage class as W12 and anti-freezing class as F200. Slightly expansive concrete is used for the cutoff slab and the backfill of the slot, and it is required that self volume deformation be $\geq 100\times10^{-6}$.

Single layer double direction reinforcement is provided on the surface of the plinth, with a reinforcement rate of 0.35% of the design thickness of the plinth. Single layer double direction reinforcement is provided also on the upper part of the cutoff slab, with a reinforcement rate of 0.35%.

Anchor bars are provided in the plinth, which enter into the rock by 5.0m, with a spacing of 1.5m×1.5m. Hooks are provided on the top to connect the reinforcement layer of the plinth.

2.4 *Facing slab*

The slab is 0.3m thick on the top and 1.1m on the riverbed. The thickness varies in the between, on a straight-line basis by the formula of t=0.3+0.0035H, where t is the thickness (m) of the slab and H is the vertical distance (m) between the calculated section and El. 405m.

The spacing of the vertical joints of the slab is 8m in the strain zone of the slab on the left bank abutment and in the Miaobao sliding body zone on the right bank and 16m on other locations. 11 and 26 tension joints are provided respectively on the left bank and the right bank. The vertical joints are within 1.0m from the normal direction of the peripheral joint on both banks and are arranged vertical to the peripheral joint. The slab is poured by 3 phases, provided with 2 horizontal construction joints. The phase I slab is at El. 276m on the top, the phase II at El. 342m on the top and the phase III to the crest. The reinforcement of the slab passes through the joint face.

C25 concrete is used above El. 346m and C30 concrete below El. 346m for the slab. The anti-seepage class of the concrete is W12 and anti-freezing class is F200, with the ultimate tensile strength not less than 100×10^{-6} and the slump of 4~7cm. Efficient and multi-functional composite additives are used and 15~25% class I fly-ash is mixed.

Single layer double direction reinforcement is arranged in the slab, with a reinforcement rate of 0.4% in the slope direction and 0.35% in the dam axis direction. Reinforced bars are arranged on the bottom of the slab within a 20m range near the peripheral joint and double layer reinforcement is arranged within a 10m range both above and below the phased construction joints along the slab, the upper reinforcement protection layer is 15cm thick and the lower protection layer is 10cm thick.

2.5 *Joints and water stops*

The dam is provided with the peripheral joint, the vertical joints of the slab, the horizontal joints between the slab and the plinth, the settlement joints of the breakwater wall, and the constructionjoints.

(1) Peripheral joint

3 rows of water stops are provided below El. 350.0m, see Fig. 3. On the bottom and in the middle are the copper water stops, while on the top is the flexible caulking protected by corrugated

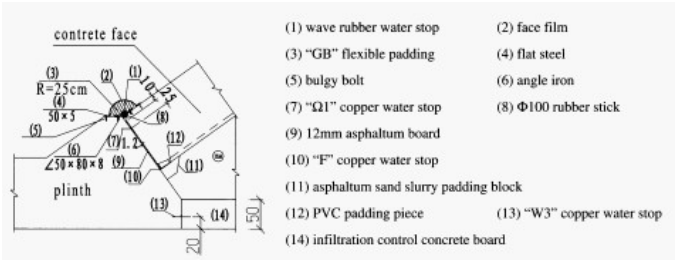

Figure 3. Water stop section (cm).

rubber water stop. Only two rows of water stops are used above El. 350.0m, on the top and on the bottom without the middle water stop.

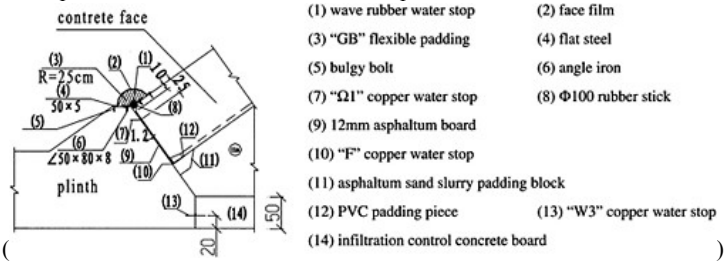

Water stop on the top: A rubber rod ( ) is arranged at the joint and corrugated rubber water stop arranged on the rod, with flexible materials filled in between. Flexible materials are laid on the corrugated water stop, with the surface sealed with reinforced rubber strip. Functions of the waterstop are as follows: (a) the rubber rod at the joint acts as support to the water stops above to ensure the water stop on the top would not sink into the joint under the water pressure; (b) the corrugated water stop can adapt to the large deformation of the peripheral joint and function separately as water stop, and meanwhile, to seal the flexible fill above; and (c) the flexible padding above and the reinforced rubber strip on the surface function both as separate seepage prevention of the upper water stop and as seepage prevention by flowing into the joint like conventional flexible filler in case of seepage or failure of the water stop on the top.

The water stop in the middle is the Ω-shaped copper strip, which is arranged in the center (a little bit to the surface) of the peripheral joint, while that on the bottom is the F-shaped copper strip.

(2) Vertical joint of the slab

As the tension and stress of the vertical joint of the slab can not be accurately predicted, to ensure the integrity of the waterstops, the sealing structure of the vertical joint of the slab in design is treated as tension joint, with all vertical joints in the same sealing structure, copper strip on the bottom and flexible padding on the top. Water stop is provided accordingly in the middle of the vertical joint within the range of 5.0m from the peripheral joint below El. 275.0m to ensure the tightness of the water stop in the middle of the peripheral joint.

W_1 copper water stop is used on the bottom. While on the top, flexible padding is used with a radius of 20cm. A rubber rod (ϕ 40 mm) is provided on the bottom of the padding and reinforced rubber strip on the surface. Galvanized angle iron is used to fix and seal on both sides.

(3) Other joints

The horizontal joint between the breakwater wall and the slab is provided with two water stops, flexible padding on the top and W_2 copper strip on the bottom, with the structure same as the vertical joint.

In the joint of the cutoff slab and the standard slab is provided with a copper water stop.

A settlement joint is provided every 16.0m in the breakwater wall, in which a PVC water stop is provided which is connected with the copper strip on the bottom of the breakwater wall.

2.6 *Observation design*

The dam observation includes three monitoring items, i.e., deformation, seepage, and slab stress and temperature. There are 3 major monitoring sections and 1 normal section.

(1) Arrangement of deformation monitoring facilities

The surface deformation monitoring system consists of the horizontal and vertical displacement monitoring of the slab and the rockfill body, which is mainly performed by the dam deformation automatic measurement system (SMDAMS). 15 bedrock deformation meters are provided in the dam foundation of the 3 major monitoring locations (sections) for the overburden, faults and interbedding shear zones to monitor the relative settlement of the dam foundation face.

Horizontal and vertical displacement meters are used to monitor the internal deformation of the rockfill body.

Fixed inclinometer is used to monitor the deflection of the slab. The deflection monitoring points are arranged on the slab of the two major monitoring sections (0+108m and 0+188m). Measurement points are arranged at spacing of 5~8m on the horizontal construction joints of the slab and near the 1/3 dam height, while for other locations, the measurement points are arranged at spacing of 10~15m in general based on the principle of sparse distribution in the upper and dense distribution in the lower.

The spacing between the slab and the cushion is observed by double direction jointmeasurement meters, with measurement points located at the construction joints on the top of the phase I and phase II slab.

The peripheral joint is monitored by triple direction joint-measurement meters, the joint between the slab and the breakwater wall by double direction joint-measurement meters, and the joint between slabs by single direction joint-measurement meters.

(2) Arrangement of seepage monitoring facilities

The seepage monitoring includes the seepage pressure of the dam foundation, the seepage discharge of the dam body, the location of seepage, and the seepage flow around the dam.

6 osmometers are provided respectively in the dam foundation of the 3 major monitoring sections to monitor the seepage pressure of the dam foundation. In addition, to monitor the seepage pressure in the base rock before and after the curtain of the plinth, osmometers are installed before and after the curtain of the dam foundation of the 3 major monitoring sections.

A measuring weir is provided at the dam toe downstream to monitor the total seepage volume of the dam body and the foundation.

A set of distributed optical fiber seepage measurement system is arranged on the bottom of the slab along the downstream location of the peripheral joint, which can find out the potential lowtemperature seepage zones by the distributed temperature measurement of high accuracy.

(3) Arrangement of stress and temperature monitoring facilities of the slab

The stress monitoring of the slab includes the stress of the concrete and the reinforcement. The concrete stress is monitored by chord strain meter, non-stress meter and optical fiber strain meter, while the reinforcement stress is monitored by chord reinforcement meter. The chord strain meter and reinforcement meters for slab stress are also used to measure the concrete temperature.

3 CONSTRUCTION DIVERSION

The diversion during construction is implemented by closing the river bed with cofferdam, using tunnel to discharge. In the initial stage, the cofferdam is used to retain flow and the diversion tunnel to discharge in dry season and the cofferdam is overflowed and diversion tunnel used to jointly discharge the flood during flood season. In the middle stage, the dam, when rising to a certain level having the condition to retain flow, is used to retain flow and the diversion tunnel and the emptying tunnel to jointly discharge the flow. In the final stage, the emptying tunnel is used to discharge flow in the first dry season when the diversion tunnel is closed and the spillway and the power house take over thereafter. The upstream earth and rock overflowing cofferdam can retain a maximum instantaneous flow of 3960m^3/s at 5% frequency during November to April, with two tunnels to discharge, then the upstream water level is at El. 221.93m correspondingly, therefore, the crest of the overflowing earth and rock cofferdam is determined at El. 223m and the cofferdam

Table 2. Sources of materials for dam fill (10^4m^3).

Item	Qty	Location and quantity							
		Spillway	Diversion tunnel	Powerhouse system	Mayan slope	Other structures	Gongshanbao	Qiaogou	Total
IIA	38.13						38.13		
IIIA	67.55			3.43			30.17	33.95	67.55
IIIB	699.22	436.6					115.5	147.12	699.22
IIIC	470.58	221.2	30	97.2	48.18	70			470.58
IIID	172.66	43.87		18	94.29			16.5	172.66
Sub-total	1448.14	701.67	30	118.63	142.47	70	183.8	197.57	1448.14

Note: IA and IB materials and downstream rock revetment are not included in the table.

28m high. The temporary flood standards of the dam during construction are determined as follows based on the dam pattern and the reservoir capacity before the dam and in combination with the characteristics of the Shuibuya concrete face rockfill dam during construction:

(1) The overflowing protection standard of the dam in 2003 flood season is a max instantaneous discharge of 11600m^3/s at 3.3% frequency in the whole year;
(2) The flood retaining standard of the dam in 2004 flood season is a max instantaneous discharge of 14900m^3/s at 0.5% frequency in the whole year;
(3) The flood retaining standard of the dam in 2005 flood season is a max instantaneous discharge of 15500m^3/s at 0.33% frequency in the whole year;
(4) The flood retaining standard of the dam in 2006 flood season is raised to a max instantaneous discharge of 15500m^3/s at 0.33% frequency in the whole year;
(5) In the dry season between 2006 and 2007 when the phase III slab of the dam is constructed, the diversion standard will be a max instantaneous discharge of 6030m^3/s at 5% frequency in May;
(6) The flood retaining standard of the dam in 2007 flood season is a max instantaneous discharge of 16500m^3/s at 0.2% frequency in the whole year;
(7) Normal impoundment will be achieved in the 2008 flood season.

4 MATERIAL SOURCE PLAN

The fill for the dam is mainly to use the excavated materials of structures, to be supplemented by exploitation from borrow sites. The excavated materials of structures to be used for the dam fill mainly are the excavated Maokou limestone and Xixia limestone from the left bank spillway, diversion tunnels, right bank Mayan slope treatment, and the underground powerhouse system. The Maokou limestone and Xixia limestone excavated from the dam, the emptying tunnel and the seepage control works, although not very much, but can also be used for dam fill. There are two borrow sites, Gongshanbao on the left bank and Qiaogou on the right bank, with a reserve of 9 million m^3 and 10 million m^3 respectively. The sources of materials for the dam fill are shown in Table 2.

5 CHARACTERISTICS OF THE PROJECT

5.1 *Plinth arrangement and concrete placement*

The suggestion of J.Barry Cooke [1] is adopted for the design of plinth for the Shuibuya Project, which is divided into two parts: one is to use a standard width to meet the need of grout oozing control, the other is to use concrete to extend to the dam body downstream to meet the hydraulic

Table 3. Test values of dry shrinkage of concrete of different ages.

Class	Water-gel ratio	Dry shrinkage of concrete ($\times 10^{-6}$)						
		3d	7d	14d	28d	60d	90d	180d
C30	0.40	58	84	149	253	310	347	395
C30	0.43	101	143	202	314	401	457	507

gradient. 8m is adopted as the standard width of the plinth, while the width downstream is supplemented by an allowable 1/15 hydraulic gradient. Because of the narrow river valley and high and steep relief at the Shuibuya dam site, the adoption of J.Barry Cooke's suggestion for the layout pattern of the plinth can reduce the excavation by nearly 200,000m^3 comparing with the alternative all plinth provided in the upstream.

Conventionally, the plinth of the concrete face rockfill dam is generally provided with a expansion joint every 15~20m along the axis of the plinth, which has a disadvantage of complicated connection of the sealing structure of the expansion joint with the three water stops of the peripheral joint and of easily causing artificial defects. The concrete face rockfill dams recently built generally have no expansion joints, which leads to the serious concrete fissuring. To avoid such problems, the plinth of Shuibuya dam take the measure of reserve wide slots in advance, that is, a 2m wide slot is reserved every 12~16m along the axis of the plinth, with reinforcement bars passing through the slot without providing any water stops but treated as construction joints. Conventional concrete is used for both sides of the slot, which is backfilled with concrete 90 day after the concrete on both sides of the slot is poured. The time of backfill is determined based on the tests and the experience. Table 3 shows the test values of dry shrinkage of two groups of concrete. It is indicated that if the values of 180-day dry shrinkage are taken as the reference, over 87% of the dry shrinkage of concrete can be achieved in 90 days. Slightly expansive concrete is used for the wide slot to prevent from crack due to self shrinkage. The concrete placement has been completed for the plinth below El. 300m by May 2004 without any crack in the plinth concrete basically.

5.2 *Sand and gravel overburden treatment on riverbed*

The riverbed overburden at Shuibuya is 12.0~14.42m thick. The alluvial deposit consists mainly of sand, pebble and gravel, containing erratic boulder and block layer as well as silt and silty clay lens with sand and gravel. To meet the stability and safety requirements, the overburden within the range of 150m upstream and 100m downstream of the dam foundation is removed by excavation. To reduce the intensity of foundation excavation and the construction of the first dry season after river closure, the riverbed overburden near the dam axis is remained, for which FEM analysis has been conducted. It is estimated that the max deformation of the overburden is 21.46cm when the dam is filled up to El. 250m and 60.44cm when the Project is completed. To reduce the deformation of the overburden, it is decided to treat the overburden by strong tamping. Productive tests are conducted prior to implementation of strong tamping. 251 crawler crane is used during the trial tamping, with the hammer off hook automatically when it is lifted to the rated height to tamp the foundation by gravity with a fall of 13m. The hammer is round, 20.81, with a diameter of 2.2m and a bottom area of 3.8m^2. Trial tamping is performed in three areas, with a spacing of tamping points of 3.5m×3.5m (180m^2, 17 points), 5m×5m (250m^2, 15 points) and 6m×6m (162m^2, 8 points). 12 passes of tamping are applied except in the area of 3.5m×3.5m where 8 passes are applied. The settlement by single-point tamping is 0.29~0.83m in the area of 3.5m×3.5m, averaging at 0.6m; 0.53~1.01m in the area of 5m×5m, averaging at 0.78m; and 0.59~0.88m in the area of 6m×6m, averaging at 0.814m. The average settlement at the site is 0.3~0.4m as calculated according to the topography at site before and after tamping.

Inspection tests are conducted on the following items during strong tamping tests: (a) dry density by pit detecting method (water injection); (b) permeability coefficient by double ring method; (c) grain analysis by screening method; extra heavy dynamic cone penetration by side pressure tests; and (d) surface wave prospecting tests. The test results indicate:

(1) The dry density is 1.98~2.11g/cm^3, averaging at 2.07g/cm^3 before tamping, and 2.10~2.28g/cm^3, averaging at 2.18g/cm^3 after tamping, which has a increase of over 5%. The permeability decreases to a certain extent, generally within the range of i×10^{-2}cm/s. The fine grains change insignificantly after tamping.
(2) The extra heavy dynamic cone penetration indicates that the loading capacity of the sand and pebble layer is close to 300kPa before treatment by strong tamping and increased to over 600kPa (in 5m depth) after treatment.
(3) The side pressure test results indicate that the side pressure modulus of the sand and pebble layer is 7~9MPa under natural state without distinct trend of change with the depth. After being tamped, the side pressure modulus is doubly increased in the area of 3.5m×3.5m and in the 3m depth in the area of 5m×5m, while there is no distinct change below 5m.
(4) The comparison tests of surface wave before and after tamping indicate that the influence of strong tamping is to the depth of about 4m and the amplitude of wave velocity increases slightly, about 100m/s.

Based on the test results of strong tamping, the construction parameters of strong tamping are determined as: tamping energy not less than 300tm, spacing of tamping points 3.5~4m, average number of passes 9. The construction is performed alternately by 3 sequences: in the first sequence, jumper bit in about 1.5m diameter is used with 10 passes of compaction to increase the tamping pressure and the consolidated depth; in the second sequence, flat hammer in some 2m diameter is used with 8 passes of compaction; full tamping is applied in the third sequence.

To monitor the foundation deformation of the overburden, totally 9 base rock deformation meters are embedded. By March 28, 2004, the max deformation of the overburden is 3cm when the dam is filled to El. 250m, far lower than the design estimation, indicating conspicuous effect of the strong tamping.

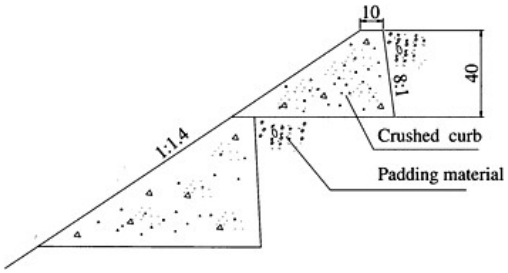

Figure 4. Crushed curb detail.

Table 4. Material composition per m^3 of the crushed curb.

Material	IIAA	32.5 cement	Water	Water reduction agent (NF-21)	Quick setting agent (8604)
Consumption (kg)	2144	70	91	0.56	2.8

5.3 *Upstream slope protection of the dam*

Based on the experience of ITA Dam [2] in Brazil and the Gongboxia Dam [3] in China, to simplify the flood protection upstream, crushed curb is used for slope consolidation upstream of Shuibuya concrete face rockfill dam. The IIAA material for dam fill is used, mixed with a small amount of cement, which is crushed on site by self-made crusher for the crushed curb. The cross-section of the curb is shown in Fig. 4 and the materials for the curb is determined after tests, see Table 4.

Placement of padding materials begins 2 hours after the crushed curb is crushed into shape and roller compaction can start 5 hours later.

6 CONCLUSIONS

Through a large number of tests and studies, the 233m high Shuibuya Concrete Face Rockfill Dam is in general designed based on conventional concept, with more emphasis to detail design and treatment. The adopted design of the plinth, the treatment of the riverbed sand and pebble layer, and the slope consolidation by crushed curb for the upstream of the dam have provided good foundation for the smooth implementation of the project. The practice and experience thereof will function the role of reference for other projects to a certain extent.

REFERENCES

[1] J.Barry Cooke, Plinth of Concrete face rockfill Dam, *CFRD'2000, Proceedings of International Seminar on Concrete Face Rockflll Dams, Beijing, China, Sept.18, 2000,* pp 18–24.

[2] Bayardo Materon and Rui Mori, Concrete Face Rockfill Dams construction features, *J. Barry Cooke volume concrete rockfill dams* Beijing China, 2000, pp177–219.

[3] Miao Shuyin and Bai Zhaopeng, Studies on the Slope Consolidation Techniques by Crushed Concrete Curb Cushion for Concrete Face Rockfill Dams, *Questions and Experiences about Earth and Rockfill Dam Construction,* Shaanxi People's Publish House, September, 2002, pp457–463.

This page intentionally left blank.

New Developments in Dam Engineering—Wieland, Ren & Tan (eds),

FEM analysis for layered rock slope

Tian-tang Yu & Qing-wen Ren
College of Civil Engineering, University of Hohai, P.R. China

ABSTRACT: The layered rock is of obvious anisotropic mechanical behavior. A failure criterion for layered rocks is presented. The discontinuity (e.g. joint, fault, or weakness plane) is used with the directional Mohr-Coulomb criterion. The rock matrix is used with the continuous anisotropic failure criterion (Pariseau criterion). The character of low tensile strength is considered in the two criteria. A relative 3-D elasto-plastic FEM code is developed. Taking an underground opening as example, the numerical analyses are carried out for two cases of transversely isotropic rock and isotropic rock, respectively, some valuable conclusions are obtained.

1 INTRODUCTION

Layered rock is often met in rock engineering. Due to the preferred fabric orientation or the existence of non-random discontinuity, the elastic constants and strengths are different in the directions parallel and normal to the bedding plane, thus layered rocks exhibit strong inherent anisotropy.

In mechanics, layered rock is usually treated as transversely isotropy. The relationship of stress and strain is expressed with five elastic coefficients[1]. The failure modes of layered rocks are complex, strongly depending on the loading orientation and confining pressure. Various failure criteria for layered rocks have been proposed. However, according to the assumptions and techniques used in each one, it appears possible to classify these criteria in to four kinds as follows. The first kind are that extending the yielding theories of isotropic body by introducing one parameter describing the anisotropy of material, e.g. Criteria of Hill, Hoffiman and Smith[2–3]. The criteria of the second kind are named empirical continuous models. The strength anisotropy is simply described by the determination of variation laws as a function of the loading orientation for some material parameters use in an isotropic criterion[4] [5]. The third kind is to extend the form of traditional criterion by introducing one tensor made up of shear strength or tension strength in the principal direction of the material, searching the possible failure planes under some stress condition, e.g. Nova criterion. An expression in which the shear strength parameters c, ϕ of layered rock varying with the direction of a plane with respect to the inclination of cleavage is suggested, the inclination of shear failure plane of layered rock is obtained[6]. The forth kind is that the inherent anisotropy is described by introducing one microstructure tensor into the yielding criterion[7,8].

An anisotropic failure criterion for continuous and discontinuous layered rocks is presented in the paper. The rock matrix is used with the continuous anisotropic failure criterion (Pariseau criterion). The discontinuity (e.g. joint, fault, or weakness plane) is used with the discontinuous failure criterion (directional Mohr-Coulomb criterion). The character of low tensile strength is considered in the two criteria. A relative 3-D elasto-plastic FEM code is developed. Taking an underground opening as example, the numerical analyses are carried out for two cases of transversely isotropic rockmass and isotropic rockmass, respectively, some valuable conclusions are obtained.

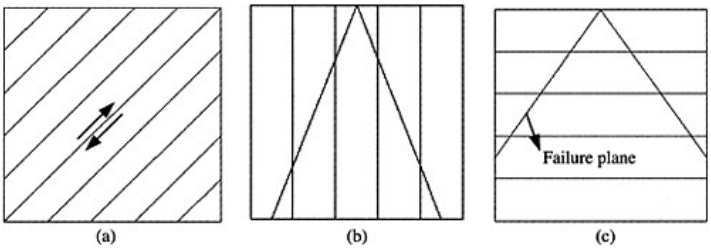

Figure 1. Three typical failure modes for layered rocks.

2 FAILURE MODES OF LAYERED ROCK

A large laboratory investigation project has been achieved on layered rocks. These experiments have shown complex failure modes of the layered rocks, strongly depending on the loading orientation and confining pressure (Figure 1). Main failure mechanisms of the layered rocks can be summarized as follows:

(a) For the loading orientations between 30° and 60°, the failure is clearly dominated by sliding of bedding planes.
(b) For the loading orientation is 0°, the failure mode depends on confining pressure. The failure takes place by bursting of bedding planes under low confining pressures, while a mixed mode of bursting of bedding planes and shearing of rock matrix is obtained when the confining pressure is higher.
(c) For the loading orientation is 90°, the failure occurs by strain localization in the rock matrix. For all other loading orientation, the failure can occur in a very complex way.

3 CONSTITUTIVE MODEL FOR LAYERED ROCK

Figure 2 shows the definition of a coordinate system for layered rocks. The elastic matrix in the local coordinate system $(x'y'z')$ is

$$[D'] = \frac{E_2}{(1+\mu_1)p}\begin{bmatrix} n(1-\mu_2^2 n) & n(\mu_1+\mu_2^2 n) & n\mu_2(1+\mu_1) & 0 & 0 & 0 \\ n(\mu_1+\mu_2^2 n) & n(1-n\mu_2^2) & n\mu_2(1+\mu_1) & 0 & 0 & 0 \\ n\mu_2(1+\mu_1) & n\mu_2(1+\mu_1) & 1-\mu_1^2 & 0 & 0 & 0 \\ 0 & 0 & 0 & \frac{np}{2} & 0 & 0 \\ 0 & 0 & 0 & 0 & m(1+\mu_1)p & 0 \\ 0 & 0 & 0 & 0 & 0 & m(1+\mu_1)p \end{bmatrix} \quad (1)$$

where $n = E_1/E_2, m = G_2/E_2, p = 1 - \mu_1 - 2n\mu_2^2$, E_1 is the modulus of elasticity in the bedding plane, μ_1 the Poisson's ratio in the bedding plane, E_2 the modulus of elasticity in the direction normal to the bedding plane, μ_2 the Poisson's ratio in the direction normal to the bedding plane and G_2 the shear modulus in the direction normal to the bedding plane.

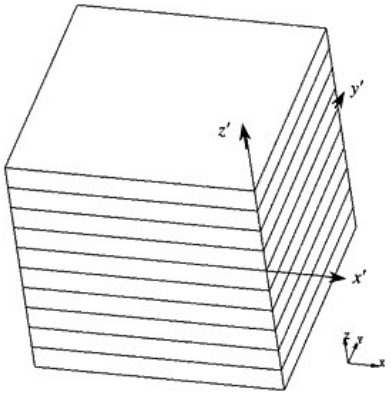

Figure 2. Local and global coordinate systems.

The constitutive equations in the global coordinate system is

$$\{\sigma\}=[D]\{\varepsilon\} \tag{2}$$

where $[D]$ is the elastic matrix in the global coordinate system.

$$[D]=[L][D'][L]^T \tag{3}$$

$$[L]=\begin{bmatrix} l_1^2 & l_2^2 & l_3^2 & 2l_1l_2 & 2l_2l_3 & 2l_3l_1 \\ m_1^2 & m_2^2 & m_3^2 & 2m_1m_2 & 2m_2m_3 & 2m_3m_1 \\ n_1^2 & n_2^2 & n_3^2 & 2n_1n_2 & 2n_2n_3 & 2n_3n_1 \\ l_1m_1 & l_2m_2 & l_3m_3 & l_1m_2+l_2m_1 & l_2m_3+l_3m_2 & l_3m_1+l_1m_3 \\ m_1n_1 & m_2n_2 & m_3n_3 & m_1n_2+m_2n_1 & m_2n_3+m_3n_2 & m_3n_1+m_1n_3 \\ n_1l_1 & n_2l_2 & n_3l_3 & n_1l_2+n_2l_1 & n_2l_3+n_3l_2 & n_3l_1+n_1l_3 \end{bmatrix} \tag{4}$$

where l_i, m_i, and n_i (i=1, 2, 3) are the direction cosines between the local coordinate axes and the global coordinate axes.

4 FAILURE CRITERION FOR LAYERED ROCK

4.1 *Failure criterion for rock matrix*

4.1.1 *Yielding failure*

Criterion of Pariseau is adopted here, and n=1[9].

$$\begin{aligned}\{F(\sigma_x-\sigma_y)^2+G[(\sigma_y-\sigma_z)^2+(\sigma_z-\sigma_x)^2]+(2G+4F)\sigma_{xy}^2+M(\sigma_{yz}^2+\sigma_{zx}^2)\}^{1/2} \\ -[U\sigma_z+V(\sigma_x+\sigma_y)]-1=0\end{aligned} \tag{5}$$

$$V=\frac{1}{2}\left(\frac{1}{T_{//}}-\frac{1}{C_{//}}\right) \qquad U=\frac{1}{2}\left(\frac{1}{T_{\perp}}-\frac{1}{C_{\perp}}\right) \qquad G=\frac{1}{4}\left(\frac{1}{T_{\perp}}+\frac{1}{C_{\perp}}\right)^2$$
$$F=\frac{1}{4}\left(\frac{1}{T_{//}}+\frac{1}{C_{//}}\right)^2-G \qquad M=\left(\frac{2}{C_{45}}+U+V\right)^2-(F+G) \tag{6}$$

where $T_{//}, T_{\perp}, C_{//}, C_{\perp}$ are the uniaxial tension and compression strengths in the directions parallel and normal to the bedding planes. C_{45} the uniaxial compression strengths in the loading orientation of 45°

4.1.2 *Low tension failure*

It is very complex of low-tension failure for rock matrix. For simplicity, the low-tension failure in the directions parallel and normal to the bedding planes are considered.

The crack in the direction normal to the bedding plane occurs when $\sigma_{//}^1 > T_{//}$ ($\sigma_{//}^1$ is the first principal stress in the direction parallel to the bedding plane).

4.2 *Failure criterion for rock joints*

In order to describe the discontinuity, thin layer elements are used for weakness planes. The low-tension Mohr-Coulomb criterion is used for the materials.

The crack in the direction normal to the bedding plane occurs when $c-\sigma_{\perp}\tan\varphi<\sqrt{\tau_{z'x}^2+\tau_{z'y'}^2}$ (c is the cohesion and φ is the friction angle in the bedding plane).

5 NUMERICAL EXAMPLE

As an example, the excavation of a tunnel is considered. It is assumed that the tunnel is located at a depth of 300m. The inclination angle and the direction angle of layer planes are 45°. The section

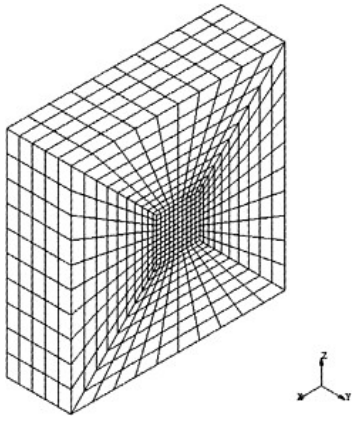

Figure 3. FEM mesh.

of excavation is rectangular 20×20m. Two cases of transversely isotropic rock and isotropic rock are considered, respectively. The FEM mesh is shown (see Figure 3). In this study, the following values are used; μ1=0.25, μ2=0.35, E_1=20GPa, E_2=10GPa, γ=25Kn•m^{-3},$C_{\perp} = 116$ MPa, $C_{45} = 85$MPa for transversely isotropic case; averaging the values of anisotropic parameter for isotropic case. The displacements of keys points on opening periphery are shown in Table 1.

From the above results, it is obtained that the symmetry of displacements and yield region around the opening is not in existence for transversely isotropic case.

Table 1. Displacements of key points on opening periphery (unit: cm).

	Vertical displacements		Horizontal displacements	
Type of rock	Point 1	Point 2	Point 3	Point 4
Isotropic rock	−4.3	2.1	1.4	−1.4
Layered rock	−6.6	3.2	3.4	−3.6

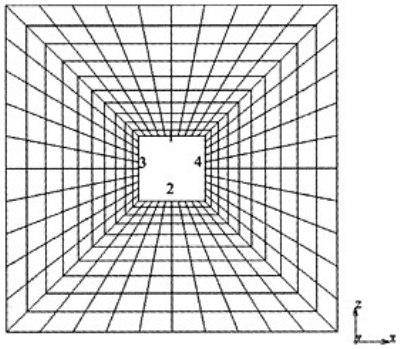

Figure 4. Key points diagram.

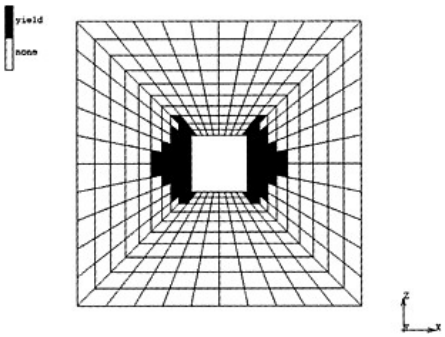

Figure 5. Yield region of isotropic rock.

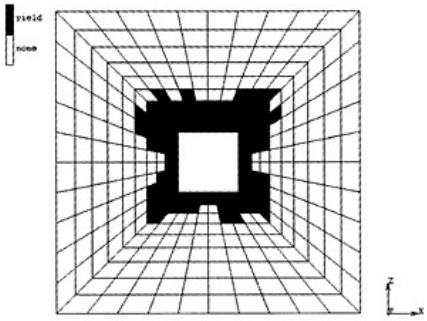

Figure 6. Yield region of layered rock.

6 CONCLUSIONS

- A failure criterion for layered rocks is presented. The discontinuity (e.g. joint, fault, or softer layer surface) is used with directional Mohr-Coulomb criterion. The rock matrix is used with the continuous anisotropic failure criterion (Pariseau criterion). The character of low tensile strength is considered in the two criteria.
- The basic rules of displacements and stresses for the isotropic and anisotropy are completely different.
- The anisotropy must be considered in the simulation computation when the mechanics parameters are apparently anisotropic.

REFERENCES

[1] Luo Zhudao, Li Sijian. Anisotropic Material mechanics [M]. Shanghai: Publishing company of shanghai jiaotong university, 1994, 11–15
[2] Zhao Qusen. Composition Material [M]. Beijing: Publishing company of state denfence, 1979, 137–151
[3] Smith B., Cheatham JR B. Anisotropic compacting yield condition applied to porous limestone [J]. Int. J. Rock Mech. Min. Sci., 1980, 17(3):159–165
[4] Nova R. The failure of transversely isoptropic rocks in triaxial compression [J]. Int. J. Rock Mech. Min. Sci., 1980, 17(6):325–332
[5] Nova R. An investigation into the tensile behaviour of a schistose stone [J]. Int. J. Rock Mech. Min. Sci., 1998, 35(3):301–324
[6] Zhang Yujun, Liu Yiping. Anisotropy of shear strength of layered rocks and determination of shear failure plane [J]. Rock and soil mechanics, 2001, 22(3):254–257
[7] Pietruszczak S., Mroz Z. Formulation of anisotropic failure criteria incorporating a microstructure tensor. Comp. & Geotechnics. 2000, 26:105–112
[8] Yu Tiantang, LuYingfa, Shao J.F., Pietruszczak S. An Anisotropic Model of Sedimentary Rocks [J]. Rock and soil mechanics, 2002, 23(1):47–50
[9] Duveau G., Shao J.F., Henry J.P. Assessment of some failure criteria for strongly anisotropic geomaterials [J]. Mechanics of Cohesive-frictional Materials, 1998, 3:1–26

New Developments in Dam Engineering—Wieland, Ren & Tan (eds),

Prediction and prevention of inconsonant deformation between face and body of concrete-faced rock-fill dam

Yuan Junping & Lu Tinghao
Hohai University, China

ABSTRACT: During the construction of concrete-faced rock-fill dam (CFRFD) as Tianshenqiao hydraulic power station, a space occurred between the face and body of the dam, which threatened the safety of the dam. Researches are leaded to find out the reason of the phenomenon, as well as prediction and prevention methods. In this study, three-dimensional nonlinear FEM simulation is conducted for a concrete-faced rock-fill dam with 139m in height, considering material distribution, construction sequence and loading process etc. The deformation and stress of the dam are analyzed, especially focused on the inconsonant deformation between face and body of the dam. Numerical simulation results show that the deformation of concrete face cannot keep up with that of body, which results in a space occurring between face and under-layer. Further analysis show that the space between face and body is influenced by the material distribution, construction sequence and loading process of the dam. The phenomenon of inconsonant deformation between face and body may occur when the face construction process is divided into several parts. Finally, prediction and prevention methods are put forward based on the analysis. Several measures to prevent and cure the phenomenon are proposed.

1 PREFACE

In hydraulic engineering construction, concrete-faced rock-fill dam (CFRFD) is one of dominating types because of its advantages such as safety, economic, convenient to construction, and good flexibility to geological conditions. As development of construction techniques, improvement of design theories and accumulation of experiences, higher CFRFD over 200m is designed and constructed [1], of which the stress and deformation states are paid more attention to. CFRFD is a complicated spatial structure, in which many regions have deferent materials such as rock fill, concrete-face, vertical slots in face, surrounding slots, interface etc. Therefore, by conventional method, it is very difficult to know the stress and deformation of CFRFD, which are influenced by many factors. To insure the safety of CFRFD, three-dimensional non-linear, elastic-plastic, or visco-elastic-plastic FEM models are generally selected in the numerical simulations.

During the construction of CFRFD as Tianshenqiao hydraulic power station, a space occurred between the face and body of the dam, which threatened the safety of the dam. In order to find out the reason why this phenomenon occurs as well as the methods to predict and prevent, attentions are paid on the mechanism. In former numerical analyses for CFRFD, no attentions are paid on the inconsonant deformation between face and body of CFRFD and data related are not analyzed. In this research, three-dimensional nonlinear FEM simulation is conducted for a CFRFD with 139m in height, considering material distribution, construction sequence and loading process etc. The deformation and stress of the dam are analyzed, especially focused on the inconsonant deformation between face and body of the dam.

2 INTRODUCTION OF THE SIMULATION

The CFRFD is 139m in height. The construction of the face is divided into two stages. In the first stage, after the body is filled up to 85m, the face is constructed up to the same height. The second stage of face construction begins after the body is filled to the designed height. In the simulation, considered are material distribution, construction sequence and loading process etc.

In the three-dimensional non-linear FEM numerical simulation for the CFRFD, following models used widely are adopted: E-B non-linear model for rock fill, linear elastic model for face and concrete toe wall, Goodman zero-thickness-contact-element model for the surface of contact between face the underlay, joint element model for the vertical slots in face and surrounding slots [1,2]. Comparative analyses are conducted between different material parameters for rock fill (Scheme A—saturated state, Scheme B—unsaturated state).

The stress and deformation of the whole CFRFD are obtained from the numerical simulation. While, focus is only on the inconsonant deformation between face and body in this paper.

3 PREDICTION OF INCONSONANT DEFORMATION BETWEEN FACE AND BODY

During the design and construction of Tianshengqiao hydraulic power station, the inconsonant deformation between face and body is not paid attention to, without special analysis for the phenomenon in the FEM simulation. Now the construction of the CFRFD has been completed and the project has worked for several decades. Later investigation and tests show that the space occurred between the face and body in the construction stage. Obviously, too large space will do harm to the safety of the CFRFD. Therefore, it is necessary to find out an effective method to predict the deformation and suitable countermeasures to avoid the phenomenon before construction. Special focuses are on the reason why the inconsonant deformation occurs and prediction methods by three-dimensional FEM analyses.

Results show that it is able to predict the inconsonant deformation between the face and body of CFRFD by FEM simulation. The method is to analysis the comparative deformations of interface elements between face and underlay, which reflect the deformation difference between underneath of the face and outside of the underlay. Minus deformations indicate that the interface elements are in tensile states, viz. spaces occurs between face and body. By this method, the inconsonant deformation between face and body can be figured out, and then to predict the space development.

Results also show that according to designed construction sequence, the space mainly takes place near the joint place between faces constructed in first stage and constructed in second stage. The position located at about 25m lower than the joint slot of the face, which height is about 1/4~1/3 height of the dam (Fig. 1, Fig. 2). Maximum space between face and body calculated is 20.5mm. Of course, further researches are needed to determine the limits of harmful and unallowed space.

4 ANALYSIS AND PREVENTION MEASURES TO INCONSONANT DEFORMATION BETWEEN FACE AND BODY

Theoretically, calculated space between face and body relates on the model and parameters of interface elements, rock filling, joint elements, as well as on construction sequence. Although the calculated values of spacing are not consistent with the practice, the simulation results can qualitatively indicate the space occurring between face and underlay. The main reasons to explain why this phenomenon occurs are as following: After the construction of face for first stage, the rock filling constructed before deforms during the succedent construction of rock filling. Consequently, the outside of the underlay constructed in first stage does not maintain the original state when the construction of rock filling for second stage does not start yet. With continuous construction of rock filling for second stage, the deformation of the dam grows. Positive Poisson

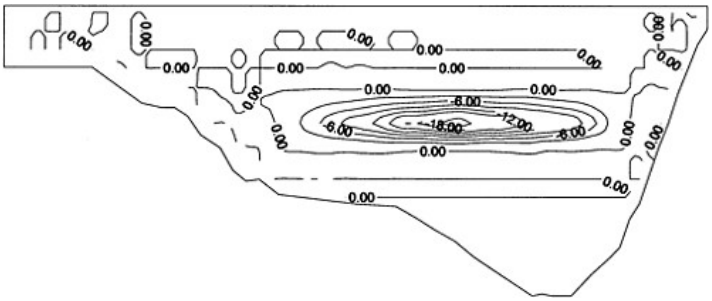

Figure 1. Scheme A space between face and underlay at upside of the face constructed in first stage (mm) ("-" indicates interface in tensile states, viz. spacing between face and body).

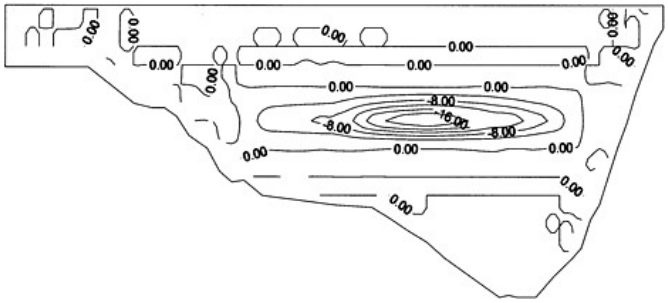

Figure 2. Scheme B space between face and underlay at upside of the face constructed in first stage (mm) ("-" indicates interface in tensile states, viz. spacing between face and body).

rate of materials lead to lateral deformation. The face is pushed by the protruding deformation of the outside of underlay at lower part of the dam. While the module of concrete outclasses that of rock filling, the concrete face cannot harmoniously deform along with the rock filling without outside force's function. Bulgy deformation of the body in flow direction makes the underneath of the face constructed in first stage departs away from the outside of the underlay. Hence, space occurs between the face and body constructed in first stage. Obviously, if some loads are brought up to the rock filling after the construction of face for second stage is finished, new lateral deformation of the dam will lead the space grows at the upper part of the face constructed in second stage.

Out of question, the influenced factors to this phenomenon conclude the model and parameters of interface elements, rock filling, joint elements [3,4], as well as on construction sequence. It is complicated to avoid this phenomenon. As far as the understanding goes, some suggestions are put forward as following:

1) The materials of underlay, transition and sub-dam with smaller compression coefficient (greater modules of deformation), smaller Poisson rate are good to smaller horizontal displacement along river, less extrapolate to the face, hence reduce the inconsonant displacement.
2) Based on the numerical results, the height of face lower than 1/4 to 1/3 of the height moraine constructed, if the construction contains several stages.
3) If the dam is not too high, the face can finished construction without interruption after construction of the moraine finished. Of course, this comes down to time limit for the project, investment as well as advanced generating electricity, lucubrating is needed.

4) If the construction is divided into several stages and the measures mentioned above cannot prevent space occurring between face and body absolutely, remediation measures by grouting must be adopted. If some pipes for grouting are constructed on the underlay during construction, the remediation measures will be very convenient and successful.

In addition, because more or less the materials for rock-filling have the characteristics of flow, the spacing phenomenon may occur near top of the dam if the deformation of the face cannot keep up with the deformation of the moraine induced by flowing. Because difficult to get satisfied precise numerical result, it is hard to predict the inconsonant displacement induced by flowing.

5 CONCLUSION

Through FEM numerical simulation, the inconsonant deformation can be predicted by the results. The method to judge whether spacing phenomenon occurs is to analysis the displacements of interface elements between face and underlay, which indicate the deformation difference between lower surface of the face and outer surface of the underlay.

The numerical analysis above has already show the feasibility of prediction and approximate rules of inconsonant deformation between face and underlay. Based on the analysis, some suggestions to reduce the inconsonant deformation are put forward as following: (1) Materials with smaller compression coefficient (greater modules of deformation) and smaller Poisson rate are good to reduce horizontal displacement along river and extrapolate to the face. (2) The face is constructed lower than 1/4 to 1/3 of the height moraine constructed in the same stage, when the construction contains several stages. (3) To the dam not too high, the face can finished construction without interruption after construction of the moraine finished. (4) If the construction is divided into several stages and the measures mentioned above cannot prevent space occurring between face and body absolutely, remediation measures by grouting must be adopted. If some pipes for grouting are constructed on the underlay during construction, the remediation measures will be very convenient and successful.

REFERENCES

[1] Fu Zhian, Feng Jiayi, Concrete Faced Rockfill Dams, Huazhong University of Science & Technology Press, 1993
[2] Lu Tinghao, Shao Songgui, 3-D Nonlinear FEM Analysis for TSQ-I Hydroelectric Project Concrete Face Rock fill Dam, HongShui River, Vol. 15, No. 4, 1996
[3] Lu Tinghao, Bao Fubo, A Coupled Constitutive Model for Interface Thin Layer Element, Journal of Hydraulic Engineering, No. 2, 2000
[4] Lu Tinghao, Bao Fubo, Interface Model Study and Applied in CFRD, Hongshui River, No. 4, 2000

New Developments in Dam Engineering—Wieland, Ren & Tan (eds),

Slope stability study and section optimization of Nuozhadu's earth core rockfill dam

Yuan Youren & Zhang Zhonglan
Kunming Investigation, Design and Research Institute, P.R. China

ABSTRACT: Nuozhadu's earth core rockfill dam has a maximum height of 261.5m, which occupies the first in China and fourth in the world in similar dams. This article generalizes the achievements on the studies of dam slope stability analysis and dam cross section optimizing.

1 PROJECT INTRODUCTION

The Nuozhadu Project is the fifth grade of the cascade plan of mid-downstream Lancang River. The river catchment above the damsite is $14.47\times10^4 km^2$, river way is 1886km long.

This project is primarily for power generation and is also for flood prevention and navigation. The normal water storage level of water reservoir is 812m, reservoir capacity below water storage level is $217.49\times10^8 m^3$, its regulating capacity is $113.35\times10^8 m^3$. Total installed capacity is 5850MW, firm output is 2406MW.

The project complex is made up by gravel earth core embankment dam, spillway on left bank, flood discharge tunnel and underground water diversion structure.

The earth core embankment dam is 261.5m high which ranks the highest in China and the fourth in the world. It's width at top is 18m, and gradient of upstream slope is 1:1.9 with downstream is 1:1.8.

2 STABILITY ANALYSIS BY TRADITIONAL METHOD

The existing design code for embankment type dam still uses traditional dam slope stability analysis method, namely dam materials parameter are determined by test from smaller values and then calculating safety factor of dam. The safety factor should be bigger than allowed safety factor in relation to scale of dam and calculated condition.

This study takes only linear and non-linear stability of dam slope to the maximum dam section of vertical and inclined core rockfill dam by the Bishop method. In the calculation, completion period and reservoir water level drop are calculated by total stress method and operation period is calculated by effective stress method. Calculation results are seen in Tables 1 and 2. As seen from Table 1, in either vertical or inclined core rockfill dam, the calculated minimal safety factors are bigger than allowed safety factor, showing that the dam is stable and safe. As seen from Table 2, the safety factors from non-linear analysis under various working condition are bigger than that of linear analysis except for downstream dam slope under normal working condition because non-linear strength is too low at dam materials, particularly at rockfill material at zone II.

Table 1. Linear stability analysis result at maximum dam slope.

Working condition	Condition for calculation		Vertical core rockfill dam	Inclined core rockfill dam	Allowed safety factor
	No.	Condition notes			
Normal	1	Downstream slope at stable seepage flow, upstream and downstream normal water level	1.682	1.682	1.50
	2	Upstream slope at stable seepage flow (minimum reservoir level at El.760.00m and downstream normal level)	1.730	1.729	
Abnormal-I	3	Upstream slope at completion period, no water action both on upstream and downstream sides	1.775	1.775	1.30
	4	Downstream slope at completion period, no water action both on upstream and downstream sides	1.682	1.682	
	5	Upstream slope when reservoir drops abruptly from normal level to dead level	1.690	1.550	
Abnormal-II	6	Condition 1 subject to earthquake density VIII	1.308	1.308	1.20
	7	Condition 2 subject to earthquake density VIII (most unfavorable reservoir level at El.812.00m)	1.210	1.209	

Table 2. Linear stability analysis result at maximum dam slope.

Working condition	Condition for calculation		Vertical core rockfill dam	Inclined core rockfill dam
	No.	Condition notes		
Normal	1	Downstream slope at stable seepage flow, upstream and downstream normal water level	1.675	1.699
	2	Upstream slope at stable seepage flow (minimum reservoir level at El.760.00m and downstream normal level)	1.997	1.884
Abnormal-I	3	Upstream slope at completion period, no water action both on upstream and downstream sides	2.073	1.970
	4	Downstream slope at completion period, no water action both on upstream and downstream sides	1.869	1.859
	5	Upstream slope when reservoir drops abruptly from normal level to dead level	1.800	1.691
Abnormal-II	6	Condition 1 subject to earthquake density VIII	1.423	1.456
	7	Condition 2 subject to earthquake density VIII (most unfavorable reservoir level at El.812.00m)	1.589	1.512

3 STABILITY ANALYSIS BY RELIABILITY METHOD

Traditional method of analyzing dam slope reflects the impact of all influential factor on dam slope stability only by a safety factor K. Sometimes it is on the conservative side and sometimes it is on the risky side.

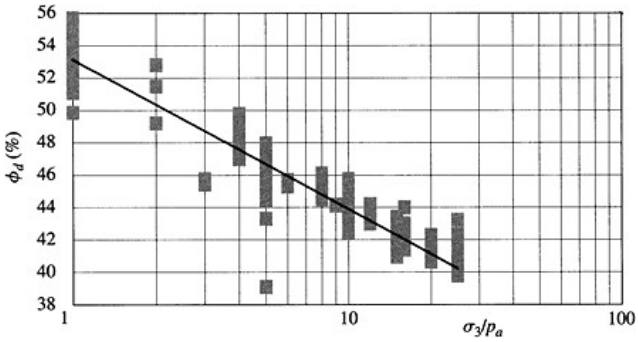

Figure 1. Test data statistics at rockfill zone I (137 samples of 26 groups).

Table 3. Non-linear data statistic of rockfill test zone I.

	$\Delta\phi$				
	μ	σ	μ	σ	ρ
Matrix	53.716	2.084	9.412	1.469	−0.697
Linear method	52.505	2.455	8.592	1.312	−0.993

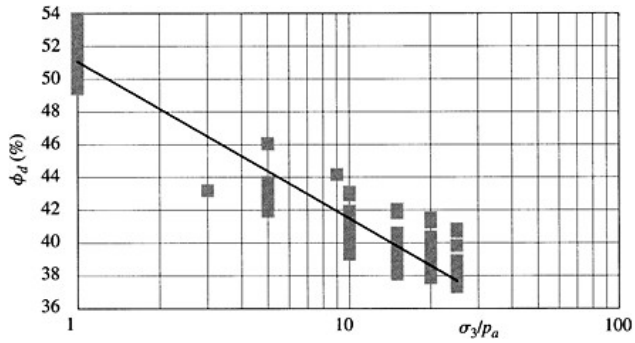

Figure 2. Test data statistics at rockfill zone II (137 samples of 26 groups).

Reliability analysis method not only takes consideration of all influential factors on dam slope stability, but also assesses the safety of dam slope stability by reliability index.

3.1 *Statistical analysis of dam material test data and dam material parameter*

We have made many tests and studies and got rich fundamental data for statistics and analysis. Statistical analysis results are seen in Figure 1 and Table 3 for 137 samples of 26 groups in rockfill zone I, and in Figure 2 and Table 4 for those of 126 samples of 22 groups in rockfill zone II.

Table 4. Non-linear data statistic of rockfill test zone II.

	$\Delta\phi$				
	μ	σ	μ	σ	ρ
Matrix	51.252	1.338	9.305	0.857	−0.800
Linear method	50.591	1.912	9.078	0.621	−0.940

Table 5. Allowed β value of sustained structures.

Safety class	Grade I	Grade II	Grade III
Destruction A	3.7	3.2	2.7
Destruction B	**4.2**	3.7	3.2

Table 6. Reliability analysis result of typical alternative.

		Minimum reliability index	
	Alternative	β	Typical slide plane
1	Upstream slope of vertical wall	5.462	(d)
2	Downstream slope of vertical wall	4.791	(b)
3	Upstream slope of inclined wall	5.495	(a)
4	Downstream slope of inclined wall	5.022	(c)

3.2 *Allowed reliability index*

In our country, water resources and hydropower engineering structure reliability design adopts unified standards and codes. The allowed β value of sustained structures is indicated in Table 5. Destruction class A stands for un-abrupt destruction, evidently foreseen before occurring and slow in the process. Destruction class B refers to abrupt destruction, not evidently foreseen before occurring and difficult to repair once occurring.

Nuozhadu dam is of grade A. According to Table 5, destruction B such as dam slope instability should adopt 4.2 for value β.

3.3 *Dam slope stability reliability analysis*

The result calculation for normal storage level condition is shown in Table 6. As can be seen, allowed reliability design indexes are all greater than 4.2.

4 STABILITY ANALYSIS BY FEM

The above analysis method is rigidity limit balance method. The method comprises some assumption under the static balance condition and slide plane. As there is no deformation coordination condition, no information about slope deformation is given. The FEM fully satisfies static allowance, strain and stress. Likewise, as the value analysis method is used, no irregularities of side slope and unevenness limit of materials used take effect. The method, therefore, is an ideal way to analyze the slope stress, deformation and stability status.

However in the previous practice, the use of FEM still has problems of how to connect the calculation result with traditional safety factor. It is inappropriate to directly take it as a judgement

Table 7. Calculation of dam slope stability by FEM in strength depreciation.

Dam type	Safety factor F	$E\delta_{max}/\gamma H^2$	Times
Vertical earth core	1.3	0.133	25
	1.4	0.1424	35
	1.5	0.1493	36
	1.7	0.168	37
	1.8	0.1830	42
	1.85	0.205	60
	1.88	0.23	120
Inclined earth core	1.3	0.175	75
	1.4	0.1815	85
	1.5	0.19	87
	1.7	0.21	88
	1.8	0.2273	101
	1.84	0.2388	103
	1.845	0.2408	115

Table 8. Statistical data of rockfill dam higher than 240m abroad.

No.	Dam	Country	Dam type	Height (m)	Seismic intensity (degree)	Upstream gradient (V:H)	Downstream gradient (V:H)
1	Rogun	Tadzhikistan	Inclined core	335	9	1:2.4	1:2.0
2	Nurek	Tadzhikistan	Vertical core	300	9	1:2.25	1:2.2
3	Boruca	Costa Rica	Vertical core	267	Unknown	Unknown	Unknown
4	Chicoasen	Mexico	Vertical core	261	9	1:2.1	1:2.0
5	Tehri	India	Inclined core	260	8	1:2.5	1:2.0
6	Guavio	Columbia	Inclined core	247	?	1:2.2	1:1.8
7	Mica	Canada	Inclined core	242	7~8	1:2.25	1:2.0

basis for slope design. This study uses, on the basis of study result by Griffith, non-linear finite element method for dam slope stability analysis and has achieved good effects. This method takes non-linear plastic finite element calculation as the judgement of structural failure. The results fully coincide to traditional limit balance method in both safety factor and destruction plane aspect.

This method is used to calculate the normal storage water level for the Nuozhadu earth core rockfill dam with the calculation process shown in Table 7. As can be seen from the Table, the safety factor for vertical core rockfill dam is 1.88, inclined core rockfill dam is 1.845, with corresponding plastic deformation zone shown in Figs. 8 and 9.

5 OPTIMIZATION STUDY OF DAM CROSS SECTION

Table 8 shows statistical data of rockfill dam higher than 240m abroad. Dam slope is all gentler than 1:2.0.

The Nuozhadu earth core rockfill dam has the maximum height of 261.5m, standing in the 4th of its kind in the world and the 1st in China. In the initial stage of design, the Nuozhadu dam slope is proposed at 1:2.2 for upstream side and 1:2.0 for downstream side with reference to the experience of similar projects.

The upstream dam slope can be change to 1:1.8 and downstream slope to 1:1.8 after repeated and try-and-error method with consideration of optimization of dam material zoning study. The above changed dam slopes proves feasible as confirmed by seepage calculation and analysis, FEM stress and strain calculation as well as FEM dynamic response analysis.

With the aim of having some proper space, upstream dam slope finally slowed down to 1:1.9. Downstream dam slope remained at 1:1.8. This result is accepted in feasibility study report of Nuozhadu hydropower project and it is examined and approved by department concerned.

New Developments in Dam Engineering—Wieland, Ren & Tan (eds),

Preliminary research on flood discharge dissipation of Xiangjiaba Hydropower Project

Zeng Xionghui, Cheng Hao & Li Yannong
Mid-South Design and Research Institute for Hydroelectric Projects, Changsha, Hunan, P.R. China

ABSTRACT: Due to the environment and navigation conditions, underflow energy dissipation is advisable to be employed in the design of Xiangjiaba Hydroelectric Project. However, it is rare in China and yet in the world to use such an underflow energy dissipater for such a high water head and a large flow discharge. With a great number of laboratory tests and studies, the high- and low-sill alternative has been proposed, with which the hydraulic indices are to be controlled within the acceptable range and that can well solve the issue of flood discharging and energy dissipation in the Xiangjiaba Hydroelectric Project.

1 BACKGROUND

Xiangjiaba Hydropower Project (HPP), located 15km upstream of Shuifu county seat and 1km away from the Yunnan Provincial Natural Gas Chemical Plant, is the last cascade HPP on the Jingsha River in its main stream plan. It consists of non-spillway dam sections, a spillway, a powerhouse behind the dam, an underground powerhouse, a one-stage vertical shiplift and irrigation water intakes on the banks. It has an installed capacity of 6000MW, a mean annual flow at the damsite of m^3/s, a total storage capacity of $5.16\times10^9m^3$ and a maximum discharging flow of $48600m^3/s$.

As Xiangjiaba HPP is located on a navigation river section and close to Shuifu county seat and the Yunnan Provincial Natural Chemical Plant, in order to prevent the navigation, urban environment and the Chemical Plant from impacts of flood discharging, it is advisable to use an underflow dissipater for discharging dissipation in Xiangjiaba HPP.

Underflow dissipater is a classic type for dissipation. It is frequently used due to its steady flow ff into the stilling basin, high dissipation efficiency, small riverbed re-building, low tailrace water fluctuation and small impacts of atomization of the discharging flood. However, the studies and practices of this type of dissipater have been limited in the discharge dissipation of medium and low water head and small unit discharge with medium and low Froude Number. There are a number of worldwide operation failure cases of underflow dissipaters for spillways with high water head and large discharge.

Xiangjiaba HPP has a maximum dam height of 161m, a maximum discharge of about $48600m^3/s$, a maximum discharging power over 40000MW, a maximum unit discharge in the stilling basin of 225m3/(s•m) and a flow velocity into the basin of about 35m/s. All the indices of the dissipater for the Project far exceed the level of the completed projects in China. In comparison with the similar projects worldwide, the high frequency of flood discharging, large discharge ow and large unit discharge flow of Xiangjiaba HPP are exceptional. Therefore, the issue of flood discharge energy dissipation in Xiangjiaba HPP is extremely striking.

2 WORLDWIDE STUDY LEVEL OF UNDERFLOW DISSIPATERS

In 70s, with regard to hydropower projects such as the Gezhouba Project on the Yangtze River, China carried out systematic studies on dissipaters with low water head, large flow and low Froude number. The key study is on the provision of auxiliary dissipation elements in the stilling basin to enhance the energy dissipation efficiency and protection of downstream riverbed. In 80s, with regard to Wuqiangxi and Ankang HPPs, studies on underflow dissipaters with medium water head and large unit discharge were further done and the flaring pier scheme was raised that changes the flow pattern into the stilling basin, forms three elements of water jump to raise the dissipation efficiency and hence solves the engineering problem properly. However, due to various reasons, damages of the bottom slab of the stilling basins in different degrees have occurred in the early operation time of the stilling basins of Ankang and Wuqiangxi HPPs. Thereafter, the focus of studies in China is on the flood discharge energy dissipation for high arch dams, and less studies are carried out on the underflow dissipation.

With regard to utilization of underflow dissipater in worldwide hydropower projects, Sayano-Shushensk Project in the former Soviet Union is the most representative. The project has a maximum dam height of 245m and employs a plane contracting stilling basin. The stilling basin had been damaged for several times when operating in construction period and was finally remedied to achieve good operation.

The key point for study in the past on high dam dissipater was the dissipation results. Less attention was paid to the stability and safety of the stilling basin itself. As the damage in various degrees of the stilling basins of the worldwide high dams, at present the hydropower circles pay extremely high attention to the safety of stilling basins with high dam and large unit discharge.

3 CONCEPTION OF FLOOD DISCHARGE ENERGY DISSIPATION FOR XIANGJIABA HPP

3.1 *Putting dissipater's safety at the first place*

Xiangjiaba HPP has a dam foundation of Triassic system sandstone of fluvial and paludal deposit. The spillway dam section is located in Limeiwan geniculated flexture zone, where the rock foundation is of quality poorer than other locations of the dam foundation because the beddings dip downstream at a dip angle of some 15° and the rock has relatively poor integrity. Therefore, the dam safety is likely to be affected in case of damage of the stilling basin. To ensure the safety of the project, the check level for the stilling basin is raised to that for the dam check, namely, the stilling basin is designed with a 100-year return flood and checked with a 5000-year return flood.

3.2 *Study on new dissipater*

As stated above, in 80s a flaring pier alternative was proposed in China with regard to dissipaters with medium water head and large flow. The function of the flaring piers is to contract the water flow transversely and extend the water flow longitudinally, while the water flow diffuses in the transversal direction after flowing into the stilling basin, increasing the turbulence intensity of the water flow. Besides this, all the water flows in different direction collide with each other, a pattern of three-element dissipation can be realized that can resolve the dissipation in the kind of projects such as Ankang and Wuqiangxi HPPs. The dissipater of Xiangjiaba HPP is related to high water head and large discharge. If a conventional stilling basin is used, the basin inflow velocity will be up to 35m/s, and the Jingsha River is rich in sediment, hence the pulsation pressure of the stilling basin will be very large, the issue of stability and erosion of the bottom slab of the stilling basin will be relatively outstanding. If a flaring pier dissipater is employed, there is a worry about dissipation atomization. Thus, a new dissipater shall be studied.

The new dissipater not only shall dissipate most of the energy of the discharging flow without producing large atomization but also shall not produce a large pulsating pressure to the bottom slab and a large bottom flow velocity for the purpose of not affecting the steady of and avoiding erosion to the bottom slab, and shall not produce a surface flow for the purpose of avoiding large fluctuation of the downstream water flow and hence preventing the navigation from being affected and the downstream river banks from scouring. The solution to these contradictions is that the energy of the discharging flow shall be eliminated mainly within the water body itself. That requires the stilling basin to keep a certain volume of water within it. No matter how large the flow discharged from the upstream is, the main discharging flow can flow, diffuse and dissipate in the water body of the stilling basin. In one hand, if the main flow underflows, it will increase the pulsation pressure to the bottom slab and the bottom flow velocity and in the other hand, if the main flow floats up, it will form a surface flow. Neither way can realize the purpose. The start point and the fundamental point for study of the new type of dissipater is that no matter how the upstream and downstream water levels and the discharge flow vary, the main discharging flow can be ensured to flow and dissipate in the middle part of the water body of the stilling basin. This kind of dissipater is like a cushion pool with horizontal flip bucket dissipation. The only difference is that the water flow from the flip buckets tamps into the water body in the cushion pool passing through air but the water flow of this new type of dissipater jets into the water body of the stilling basin passing through the end of the spillway surface.

4 PRELIMINARY STUDY ON FLOOD DISCHARGING DISSIPATION FOR XIANGJIABA HPP

A number of hydraulic model tests have been carried out for Xiangjiaba HPP during its feasibility study. There are mainly three alternatives, namely, the classic stilling basin alternative, the continuous sill basin alternative and the high- and low-sill alternative. The main study findings are introduced as follows.

4. *Alternative of classic stilling basin*

The middle and surface bays of the classic stilling basin are shown in the following figure. This alternative has a steady flow pattern but has a disadvantage of large bottom flow velocity, that the maximum measured bottom flow velocity is up to 26.02m/s, and this alternative has a large range of large-bottom-flow-velocity zone, that the range of a bottom flow velocity larger than 20m/s is about 80m long.

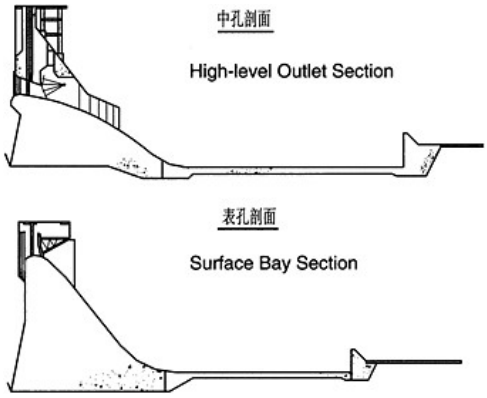

4.2 *Continuous sill stilling basin alternative*

The cross section of the continuous sill stilling basin alternative is shown in the following figure. The so-called continuous sill means that the sill, which is for the water flow when it discharges

into the stilling basin from the spillway, for the medium and surface bays has the same height so that it is seen as continuous in the direction of the dam axis.

The bottom flow velocity and the pulsating pressure of the continuous sill alternative are closely related to the parameters such as the sill height. The general law is that with the increase of the sill height, the bottom flow velocity and the pulsating pressure decrease but the steadiness of the flow pattern gets worse. Let's take an example of a sill height of 12m, the dissipation scheme has a small bottom flow velocity, a recorded bottom flow velocity of some 11.5m/s, a very small root-mean-square of only about 1.0×9.8kPa. It has a disadvantage as relatively poor steadiness of flow pattern. The flow pattern is related to the initial status such as the downstream water depth at the time of opening the gate etc. This alternative also has a disadvantage that eddies with horizontal axis are easy to form below the sill.

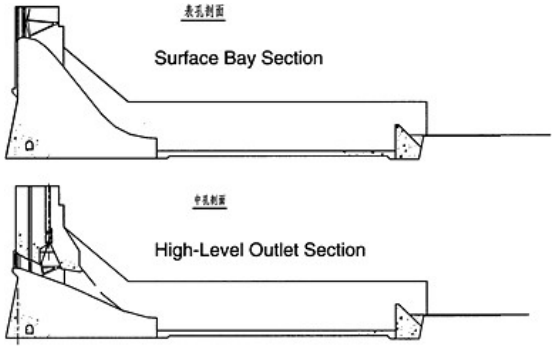

4.3 *High- and low-sill alternative*

The cross section of the high- and low-sill alternative is shown in the following figure. In this alternative, the sills for the middle and surface bays have different heights and are separated by training wall between each other. This alternative has steady downstream flow pattern with a recorded maximum bottom flow velocity of 11.32m/s and a root-mean-square of pulsating pressure of 3.82×9.8kPa. It has a disadvantage that vertical eddies are easy to form downstream of the sill when only the high-level outlets open as there is a surface bay between each two high-level outlets, and also other disadvantages as that horizontal eddies exist and that this kind of dissipater has a more complicated structure.

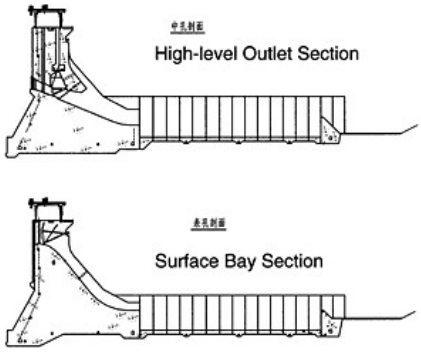

4.4 *Comparison of alternatives*

The classic stilling basin alternative has unequivocal characteristics, of which the bottom flow velocity is too large so that the safety of the stilling basin cannot be ensured. It is not advisable to be employed in Xiangjiaba HPP.

Both the continuous sill alternative and the high- and low-sill alternative can reduce the bottom flow velocity and root-mean-square of the pulsating pressure of the stilling basin. In the continuous sill alternative, as the water flow diffuses on the sill, it is thin before it enters the stilling basin, especially, in the case that only the high-level outlets are open, the water flow is even thinner. After jetting into the stilling basin, the water flow is largely affected by the downstream water depth. In case that the downstream water is relatively shallow, the water flow floats in the upper part of the water body in the stilling basin and forms a surface flow. While the downstream water increases to a certain depth, the water flow underflows in the lower part of the stilling basin and forms a returning bottom flow. The steadiness of the flow pattern is relatively poor. Certainly, adjustment of parameters such as the sill height, the sill surface slope and the stilling basin end sill height etc. can form relatively steady jetting underflow. However, to meet the requirements from the large variation of the downstream water level of Xiangjiaba HPP (where the maximum variation is 27m), the continuous sill alternative is hard to realize. As of the high- and low-sill alternative, as the discharging flows have separate ways and do not diffuse before they flow into the stilling basin, they have thicker water depth into the stilling basin, especially in case that both the middle and surface bays are open, as the sills for the middle and surface bays have different heights and have relatively large height difference, when the water flows jet into the water body in the stilling basin, the water flow generally keeps flowing in the middle part of the water body, forming a steady underflowing jet.

For the vertical eddies formed in the high- and low-sill alternative, as the sill for the high-level outlets has a height of 15m, which is equivalent to that there is a water cushion of 15m thick underneath the vertical eddies, further study on whether the vertical eddies can extend to the bottom of the stilling basin needs to be done. With regard to the horizontal eddies, the continuous sill alternative can form steady horizontal eddies under the dam, while the high- and low-sill alternative can hardly form steady horizontal eddies as it only form zigzag horizontal eddies due to difference of sill heights, and it also have interference from the upper vertical eddies. With regard to the dissipation efficiency, the continuous sill alternative basically has a plane dissipation pattern, while the high- and low-sill alternative have water flows, from the middle and surface bays, staggered in elevation and thus has a pattern of space dissipation. It separates the water body into several flows jetting into the stilling basin and produces more strong shearing flowing planes with high flow velocity gradient than those by the continuous sill alternative. On the basis of the experiments, the high- and low-sill alternative has smaller water surface fluctuation that indicates the dissipation efficiency of the high- and low-sill alternative is higher.

5 CONCLUSIONS

The Feasibility Study Report recommends the high-and low-sill alternative as the dissipater for Xiangjiaba HPP. This alternative basically realizes the purposes as minimizing the atomization's impacts on the environment, reducing the bottom flow velocity and pulsating pressure of the stilling basin, protecting the safety of the dissipater and minimizing the impacts of the downstream water flow fluctuation on navigation. However, this alternative still have problems as vertical and horizontal eddies which need to be further studied.

This page intentionally left blank.

New Developments in Dam Engineering—Wieland, Ren & Tan (eds),
© 2004 Taylor & Francis Group, London, ISBN 04 1536 240 7

Study and application of simulation to Sanbanxi CFRD construction

Zhang Jing[1,2], Jiang Xinqiang[1], Hu Chengshun[2] & Zhong Denghua[2]
[1] *Mid-South Design & Research Institute for Hydroelectric Projects, SP, Changsha, Hunan, China*
[2] *School of Civil Engineering, Tianjin University, Tianjin, China*

ABSTRACT: Due to the complexity and randomicity in high rockfill dam construction, it is hard to obtain accurately some important parameters for construction planning by conventional method. On the basis of the existing Cyclic Operations Network (CYCLONE) technology and GIS-based three-dimensional visualization technology, this paper presents a computer aided design method for construction programming of rockfill dams through integral whole-process simulation, which combines organically the embankment material transport subsystem and the dam fill subsystem. By that means reasonable parameters and a visual expression of the complicated logic space-time relations in the construction process are obtained. Based on the above ideas, simulation software for rockfill dam construction is developed and has been applied in the high rockfill dam construction of Sanbanxi.

1 INTRODUCTION

Located in Jinping County of South-east Guizhou Autonomous Prefecture, Guizhou Province, Sanbanxi Hydropower Project is on the middle reaches of the Qingshui River and was commenced officially on July 1, 2002.

The project consists of a concrete-faced rockfill dam (CFRD), a headrace power system, spillways, flood release tunnels, and other main structures. The project will have an installed capacity of 1000MW. The CFRD, laid on the riverbed, has a maximum height of 185.50m, a width-height ratio of 2.28, and a total volume of 8,670,700m^3. It is classified as a high CFRD on narrow riverbed. The spillways are arranged on the left bank and to their left are the flood release tunnels. The headrace power system on the right bank is composed of three main systems, i.e., diversion system, powerhouse system, and tailrace system. The powerhouse is of 147.20m×22.70m×60.01m (L×W×H).

The dam site is at the outlet of an asymmetric "V"-shaped transversal valley with steep cliffs on either side. A diversion scheme of once river closure is adopted.

The rockfill dam construction of the Sanbanxi Project has following features: (1) Compact and complicated structure layout; (2) Giant dam body with a maximum height of 185.50m; (3) Difficult access arrangement owing to the narrow valley whose width-height ratio is of 2.28; (4) A number of possible material sources for dam filling, for instance, quarries, borrow areas, excavated materials of structures, and transit packing areas; (5) Different demands of sections to be filled on the quality of embankment materials (mainly refers to the gradation) and the time of supply; (6) Rolled superhard rock dam, the maximum saturated compressive strength of mother rock being 300MPa; (7) High flood protection requirements; (8) Tight construction schedule and high filling intensity during a long period with an average monthly filling rate over 400,000m^3.

In previous studies on the rockfill dam construction, the embankment material transportation rate is derived from the proposed construction schedule. Then proper mechanical equipment is selected, and mean vehicle flow, mechanical equipment availability, and other relevant indexes are

calculated. Actually, the construction process is a very complicated one: accidental factors and random events of various kinds may occur at any time; the cyclic running time of different vehicles in the transportation system, loading time of the loaders, unloading time and loading capacity of the dump trucks, and quantity of unloading spots are uncertain; and the vehicles may be waiting in line at the crossings of roads, loading spots, and unloading spots. It is difficult to consider all these uncertain factors by conventional methods.

On the basis of the GIS-based 3D visualization and CYCLONE technologies, the paper proposes a visual computer-aided design method for rockfill dam construction programming. The method provides not only a way of simulation modeling for rockfill dam construction process, but also a vivid description on the complicated logic space-time relations in the construction process through a visualization platform in simulation. Consequently, it offers a scientific and rational decision-making basis in respects of preparing practical dam construction program, predicting project progress, and real time control and management on the site.

2 SIMULATION OF ROCKFILL DAM CONSTRUCTION PROCESS

2.1 *General description of rockfill dam construction process*

The construction process of rockfill dams is shown in Fig. 1. It consists of two subsystems: embankment material transport subsystem and dam fill subsystem. The embankment material transport subsystem includes the excavation and transport of earth-rock materials, i.e., excavation, transportation, loading, and unloading. The dam fill subsystem refers to the spreading and filling of earth-rock materials, normally including spreading, leveling and water spraying, compaction, quality check and scarifying. Some of these processes can be combined depending on the size of the working area. For systems characterized by cyclic construction, cyclic network simulation technology is workable.

Cyclic network simulation technology [4,5] is a network technology that brings queuing theory and computer simulation technology in network planning technology. Through the simulation on cyclic process and random time of engineering objects by computer, the progress and cost of cyclic construction processes under different resources levels and construction programs can be obtained and relevant congestion points be found. In addition, a scheme optimal in mechanical equipment combination, construction duration and cost can be obtained through sensitivity analysis.

Embankment material transport subsystem and dam fill subsystem are relatively independent but interact on each other. They are linked by the volume transported to the dam for dam filling. As shown in Fig. 1, the end of the unloading process in the embankment material transport subsystem is the start of the spreading process in the dam fill subsystem. If the earth-rock materials

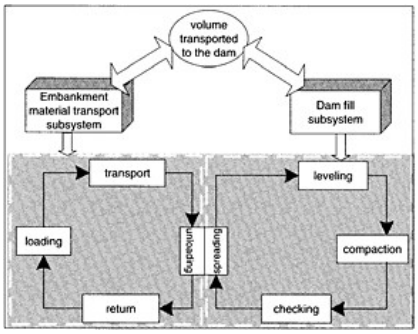

Figure 1. Rockfill dam construction process.

transport rate does not satisfy the demands of dam filling, dam filling will be delayed. Whereas, if the dam filling rate does not meet the demands of material transport rate, that will require the reduction of transport rate. Therefore, to ensure the coherence of the two subsystems is essential in the simulation of rockfill dam construction process.

2.2 *Simulation program design for rockfill dam construction*

In the study, minimum event step method is adopted to simulate both subsystems simultaneously. Two substances are set in the program to operate the simulated timer, one is vehicle, and the other is lift of dam zones. Vehicle serves as the leading substance controlling the simulated timer, and the lift as the sub-leading substance controlling the raise of dam body. During the simulation, the leading substance delivers the right to control to the sub-leading substance only during the dam filling. The right to control is transferred alternatively between the two substances until the end of the simulation.

At the beginning of the program, number the vehicles by loop according to the quantity in each loop and set them to be waiting in front of the loaders, at this time $t(i)=0$ ($t(i)$ is the sub-timer value of vehicle No. i, i=1, 2L L M; M is the total number of vehicles). When the vehicle No. i is loaded, the sub-timer value $t(i)=t(i)+\Delta_t$ (Δ_t is the loading time for vehicle No. i). Next, change its status and rescan the system in order to find vehicle No. i that has minimum sub-timer value and loop j it belongs to. After that, determine the next activity of vehicle i according to its existing status, calculate the time duration for that activity, and renew the sub-timer value of vehicle i. Then the leading substance can start next activity and its status is changed accordingly. When the vehicle arrives at the unloading spot on the dam, the right to control will be delivered to the sub-leading substance, and the sub-leading substance will control the dam filling.

When the lift gets the right to control, check the restrictions for its raise. If they are satisfied, check whether the placement of the lift is finished according to the actual earth-rock volume transported to the dam and renew the system; Otherwise, the dam fill subsystem will hold off the embankment material transport subsystem and a delay mark will be set until the restrictions are satisfied. In this system, a switching variable is set for the lift of each zone. With an initial value of "0", it is changed to "1" when the placement of a lift is finished. Hereafter, the time searching for lifts to be filled can be reduced in the light of this variable.

Afterwards, the sub-leading substance delivers the right to control to the vehicle again and the system is rescanned. The cycle is repeated until all the loops reach the preset status.

3 SIMULATION RESULTS FOR SANBANXI ROCKFILL DAM

3.1 *Dam volume*

The staged plan of the dam body is shown in Fig. 2. The dam will be placed in five stages. It is planned to be filled up to El. 390m on the upstream side at Stage 1, to El. 400m at Stage 2, to El. 405m on the downstream side at Stage 3, to El. 438m at Stage 4, and to the dam crest at Stage 5. Three-dimensional physical models of the dam body for the five stages were established respectively.

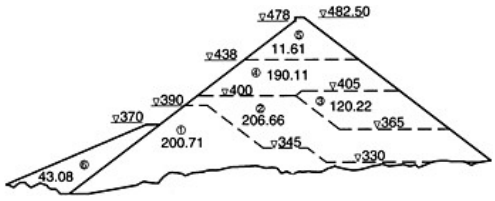

Figure 2. Staged plan of dam body ($10^4 m^3$).

Table 1. Dam volume statistics by stage.

Description	Stage 1	Stage 2	Stage 3	Stage 4	Stage 5	Total
Elevation section	293.9~390.0	326.8~400.0	365.0~405.0	400.0~438.0	438.0~482.5	293.9~482.5
Volume	205.2104	194.3167	122.8483	188.0853	112.8017	823.2624

Note: Upstream blankets Zone IA and Zone IB and concrete face slab are not included in the table.

The three-dimensional physical model for each stage of dam zones was dissected by a certain step such as 1m to obtain the volume of each elevation section. Then the volume of a step was treated with linear interpolation at a 0.01m interval to converse the dam volume into a reference value with an increment step of 0.01m. Thus the volume of any elevation at any stage can be calculated. The detailed statistics by stage are presented in Table 1 (all volumes in the table are in 10^4m^3).

3.2 *Simulation results for dam construction*

3.2.1 *Simulation models and other parameters*

For Sanbanxi Project, monthly effective working time is set as 25 days with three shifts per day and 7 working hours per shift, i.e., the monthly effective working time is 525 hours. Lift thickness is 0.8m, and 0.4m for the intermediate layer and the cushion layer. The height difference of adjacent zones is 2m. Eight combinations of transport equipment have been considered. As for the project, except that $4m^3$~20t equipment configuration is employed for the cushion layer and the intermediate layer, $6m^3$~32t configuration is adopted for all the other loops. The running velocity of trucks is set as 20km/h when loaded and 25km/h at empty return. Two types of rolling equipment have been considered, i.e., 15t self-propelled vibratory roller and 18t towed vibratory roller. The rolling belt is 2m wide, roller-running velocity 2m/s, and lap length of rolling belts 0.3m. The purpose of simulation is to select a proper number of the machine combination for each loop so as to find a transport scheme reasonable both in economy and in intensity.

Sanbanxi CFRD is planned to be filled up by five stages. Stage 1, which has relatively high filling intensity, is divided into two conditions for simulation at El. 345m where the working area is reduced. The simulation model of Stage 1 is shown in Fig. 3, where different symbols represent various types of nodes (please refer to the References). Symbol ① represents the loop number, the value in the shadow oval means the transported volume of the loop, and the value on the upper left of the node for material transportation or empty return means the distance of transportation in meter.

3.2.2 *Dam fill duration*

According to the summary results of simulation presented in Table 2, the time for dam fill totals 21.5 months from December 1, 2003 to September 17, 2005 with a maximum mean monthly intensity $427,500m^3$. Because of the narrow site, difficult access arrangement, long transport distance from the quarries, and limited heading face for excavation, effective measures such as preparing materials in advance must be taken to reach such a high construction intensity. Meanwhile, it is impossible to fulfill the target unless the construction company has good organization and reasonable deployment.

The quantity and availability of dump trucks, loaders and other main construction machines are listed in Table 3. In addition, the quantity of rolling equipment has been determined based on the transport intensity of embankment materials.

3.2.3 *Embankment material transport intensity*

The volume of earth-rock materials transported to dam at any time is recorded in the whole-process simulation. Then the daily volume transported to dam is obtained through statistics. Thereby, the max., min., and mean embankment material transport intensity can be derived. The simulated construction process is quite authentic and thus that provides a reference to the construction planning.

Figure 3. Simulation model of stage 1.

Table 2. Summary simulation results of five stages.

		Stage 1	Stage 2	Stage 3	Stage 4	Stage 5
Volume of filling (10^3m^3)		2052.1	1943	1228.5	1880	1128
Working time (d)		120	125	74	126	86
Duration		Dec 1, 2003~May 1, 2004	May 2, 2004~Oct 3, 2004	Oct 3, 2004~Jan 3, 2005	Jan 3, 2005~June 3, 2005	June 3, 2005~Sept 7, 2005
One-way vehicle density	Per hour	59	44	43	35	38
	Position	Entrance to dam on right bank	Entrance to dam on right bank	Entrance to dam on left bank	Entrance to dam on right bank	Entrance to dam on left bank
Max. monthly filling rate (m^3/month)		471, 300	407, 500	460, 200	479, 600	390, 600
Mean filling rate (m^3/month)		427,500	388,600	415,000	373,000	327,500
Daily volume transported to dam (m^3)			Max.: 20,800m^3,	Min.: 5,800m^3,		Mean: 15,000m^3

Table 3. Summary of simulation results for Stage 1.

		Truck		Loader						
Loop no.	Vol.	Qty	Availability	Qty	Availability	Description of roller	Time	Intensity	Intensity of stage	Time (d)
①	6.0	8	92.06	2	58.96		19	7.89	42.95	72
②	25.12	6	86.81	2	90.58	Model: 15t	37	16.97		
③	40.0	10	94.38	2	63.74	Qty: 1	72	13.89		
④	11.0	8	99.85	2	99.96	Model: 18t	15	18.33		
⑤	41.57	10	99.45	2	69.11	Qty: 3~4	72	15.63		

Daily volumes transported to the dam were plotted for all the five stages. Fig. 4 illustrates the curve of Stage 1, where the columnar strips mean the daily volumes transported to dam, the longitudinal coordinates represents the accumulative of volumes transported to dam, which is shown by the curve. Known from the simulation results, the max daily volume transported to dam is 208,000m^3, the min. 5800m^3, and the mean value 15,000m^3. It must be noted that of each stage the daily volumes transported to dam are quite uneven due to the large quantity of loops to the dam and differences in time and volume of transportation for each loop. Therefrom it can be concluded that the max., min., and mean intensities obtained are an objective reflection to the real system.

3.2.4 *Vehicle density*

The vehicle density of different stages has been counted at the crossings to the dam in the whole-process simulation. Bayanghe quarry, which is situated on the right bank, is the main source of excavated materials for the dam. If the materials are transported to the dam only from the right bank, the one-way vehicle density at the entrance to dam on the right bank will be as large as 90 times/hour. Therefore it is planned to transport the materials from that quarry from both banks. In the left bank route, the materials are transported to the dam via Qingshuijiang Bridge downstream the dam and the highway on the left bank. Fig. 5 is a vehicle density diagram for the most intensive 130 hours during the construction process considering transport to the dam through both banks, on which the max. vehicle density is 59 times/hour, occurring at the entrance to the dam on the right bank. It can be concluded that the vehicle density is reduced to a large extent when transportation to the dam is from both banks. Because of the high rate of filling at that period, a unified direction and rational deployment are required at the site to ensure the expedite access.

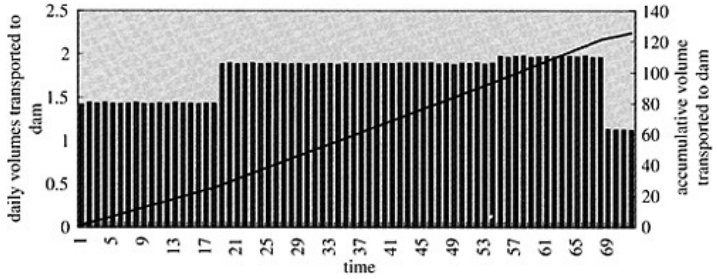

Figure 4. Daily filling rate of Stage 1 and cumulative curve (10^4m^3).

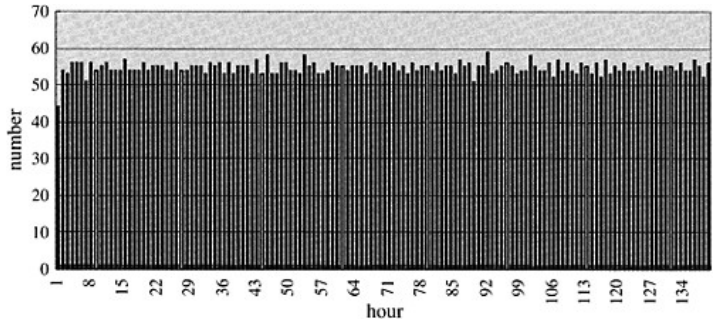

Figure 5. Vehicle density diagram of Stage 1.

3.2.5 *Dynamic 3D demonstration for dam body construction*

By introducing the calendar time parameters for each lift of stages obtained from simulation calculation to GIS and appending topographical information of the dam body, dynamic 3D demonstration of the dam filling process can be created through program design.

4 CONCLUSIONS

Taking the Sanbanxi CFRD as an example, the paper presents an integral simulation study on the whole process of rockfill dam construction by employing the system simulation and cyclic network technologies. Easy to use, the method is a saving of time and labor, and its detailed simulation results can provide a basis for making correct and reliable decision in construction planning and site construction.

REFERENCES

[1] Wang Renchao, "Computer Simulation in Embankment Dam Construction Process", *Hydro & Power Technology,* 1990(6):38–42
[2] Halpin, D.W., *CYCLONE-A method for modeling job site processes.* J. Constr. Div., ASCE, 1977, 103(3): 489–499
[3] Ioannou, P.G., *UM_CYCLONE user's guide.* Dept. of Civil Engrg., University of Michigan, Ann arbor, Mich. 1989
[4] Sun Xiheng, Zhong Denghua, *Cyclic Operations Network Technology,* Systems Engineering Group, Construction Commission, Chinese Hydraulic Engineering Society, 1988(6):7–12
[5] Zhong Denghua, Sun Xiheng, "Cyclic Operations Network Simulation Technology", *Theory and Practice of Systems Engineering,* 1994(2):7–12
[6] Sun Xiheng, Qidonghai, *Computer Simulation and Program Design for Water Conservancy and Hydroelectric Projects* [M], Hydraulic and Hydroelectric Press of China, 1997

This page intentionally left blank.

New Developments in Dam Engineering—Wieland, Ren & Tan (eds),

Calculation and analysis of the three-dimensional seepage flow of Yellow River XiaoLangDi key water control project

Zhang Junxia, Li Haixiao & Li Li
Yellow River Institute of Hydraulic Research, YRCC, China

ABSTRACT: The Yellow River XiaoLangDi Key Water Control Project has the features of complex geology, many structures, large-scale and the high stone & soil dam on the thick covering layer, therefore the seepage flow is rather serious. On the basis of the correct confirmation of the research area, model scope, boundary conditions, stratigraphic dispersal and fault analog, as well as the correct selection of the seepage factor, the calculation & analysis is made on the seepage flow site, the study is carried out on the seepage control measures and the seepage control design proposal is tested & verified. The seepage control effects on the various project items are calculated and analyzed, especially on the seepage-proof concrete wall, which is inserted into the dam, the effectiveness of the depth of the concrete seepage-proof wall into the both banks, the effectiveness of the crevices on the seepage-proof wall the functions of the natural coverage, the seepage control structure of the mountain bodies on both sides, the function of the heavy curtain and water drainage, as well as the effectiveness of the treatment of F1 fault. The calculation & analysis reflected the seepage state of the key water control Project after the storage of water calculated the seepage trend of the key water control project as a whole.

The XiaoLangDi Key Water Control Project is situated on the mainstream of the Yellow River, 40km north of Luoyang City, Henan Province. The Key Water Control Project is composed of the big dam across the river, structures of flood-and-sand-discharge, buildings of generation, etc. The big dam is stone dam with inner soil layer oblique wall. The level of the dam summit is 281m; the level of normally-stored water is 275m. The maximum dam height is 154m and the length of the dam top is 1317m. According to the topographic and geologic conditions of the XiaoLangDi dam site, the tunnels (15 tunnels for flood-and-sand discharge and water introduction for generation) are all centrally arranged on the left bank. A normal spillway and an abnormal spillway are also arranged on the left bank. A sinking pond is set up in the lower stream with central sinking form. The hydro power station adopted the underground building.

1 HYDROLOGICAL AND GEOLOGICAL CONDITION

The foundation stone strata in the key water control project are mainly composed of Permian and Triassic systems and the sediments of the fourth system are mainly scattered in the benches and the valleys. The foundation stone strata can be divided into five groups of P_2^1, P_2^2, P_2^3, P_2^4 and T. In the key water control project area, there are five main faults which take the seepage control function or greater impact on the project, i.e. F_1, F_{28}, F_{236}~F_{238}, F_{461} and F_{230}. Besides F_{28} the others are distributed as per east-west direction. F_{230} is softly permeable and the others are water interceptive on the horizontal directions.

The relation of the underground water supply and drainage in the key water control project area shows the water discharge from both banks into the Yellow River. The normal annual water lever in the Yellow River is about 135m. As per the geological structure and hydrologic characters in this area and in light of the arrangement of the buildings as well as the key seepage flow control

Table 1. Seepage factors of various strata and construction materials.

No.	Stratum	Area	k(m/d)	No.	Stratum	Area	k(m/d)
1	P_2^4		0.010	21	P_2^{3-4}		0.2260
2	T_1^{1+2}		0.030	22	P_2^{3-5}		0.0935
3	T_1^{3-1}		0.100	23	P_2^{3-6}	Right	0.3400
4	T_1^{3-2}	Left	0.010	24	P_2^4	bank	0.2100
5	T_1^4	bank	0.300	25	South of F_{230}		0.0200
6	T_1^5		0.053	26	F_{230} fault		0.0030
7	T_1^6		0.010	27	Stone dam shell	Dam	86.400
8	F_{28} impacted belt		1.000	28	Covering layer	River bed	36.400
9	P_2^{3-6}	River	0.2296	29	Inner inclining clay wall	Dam	8.64×10^{-5}
10	P_2^4	bed	0.1400	30	Concrete seepage-proof wall	River bed	8.64×10^{-6}
11	T_1^1		0.2275	31	Box dam seepage-proof wall	River bed	8.64×10^{-4}
12	T_1^2	River bed	0.3000	32	Inner paved cover	IB 区	8.64×10^{-5}
13	T_1^{3-2}		0.1800	33	Inner paved cover	5 区	8.64×10^{-4}
14	P_2^1		0.0030	34	Natural paved cover		8.64×10^{-3}
15	P_2^{2-1}		0.1748	35	Grouted curtain	$k \geqslant 0.3$ 时	0.03
16	P_2^{2-2}		0.0148	36	Grouted curtain	k=0.3~0.03	0.01
17	P_2^{2-3}	Right	0.0714	37	F_1 fault	河床	0.00
18	P_2^{3-1}	bank	0.0128	38	F_1 fragment belt	Over EL 30m	10.0
19	P_2^{3-2}		0.1113	39	F_1 fragment belt	Under EL 30m	0.01
20	P_2^{3-3}		0.0215	40			

points, the key water control project area is basically divided into six district: on the left bank from the north of F_{236}~F_{238} to F_{461} is District I; the south of F_{236} to the shoulder of the dam is District II; the river bed (the side of left bank to the north of F1) is District III; F1 is District IV; the north of F_1 to F_{230} is District V; the south of F_{230} to the Temple Slope is District VI. The geological prospecting data show there is no seepage in the horizontal direction of F_{236}~F_{238}, therefore, District I and II are basically considered to have no relation of waterpower. Because of the level and seepage difference of various strata, it is impossible to take the whole key water control project area as the boundary of the lower impermeable strata of the seepage area and they are also impossible within the same layer. According to the stratum water permeability and seepage effect, District I & II on the left bank take P_2^4 as the impermeable stratum; the river bed (including District III & IV) takes P_2^{3-5} as the impermeable stratum; the right bank (District V & VI) takes P_2^1 as the impermeable stratum. See the seepage factors of various strata of the above districts in Table 1.

2 SEEPAGE CONTROL MEASURES

The seepage-proof concrete wall is adopted for the dam foundation in the riverbed and the grout heavy curtain with drainage measures are adopted on both banks to control the seepage. The length of the seepage-proof concrete wall in the riverbed is 440m and thickness 1.2m. The upper concrete wall body inserted into the inner soil wall for 12m and both ends into the soil wall for 20m. The grout heavy curtain is set up for the lower rock foundation. Foundation rock P_2^4 is take as relative impermeable stratum with its intactness and weak seepage and there is no grout curtain for this section. Anti-seepage treatment is carried out for F_1 and grout curtain is set up in the influenced belt to ensure the seepage control of left bank as whole and the stability of the Thin Ridge. A grout heavy curtain and a main drainage curtain are set up across the Thin Ridge from south to north. The main drainage curtain is set up along the back of the grout heavy curtain with a distance of 30

to 80m. The interval of the drainage holes is 3.0m and the aperture of the drainage hole is 130mm. A seepage-proof and drainage system is set up around the underground generation building with the interval of 3.0m and aperture of 76.0mm of the drainage holes. A seepage-proof and drainage system is also set up for the sinking pond in the lower stream, the main purpose of which is to reduce the free surface and uplift pressure near the sinking pond. On the right bank, besides the grout heavy curtain a drainage curtain of "L" form is set up. The drainage curtain is set up along he back of the grout heavy curtain with a distance of 50 to 100m starting from the north of F_1, extending to the north of F_{230}, then turning east and extending along F_{230} to form an "L".

3 SIMULATION OF SEEPAGE FLOW FIELD

3.1 *Calculation of the model plan and confirmation of the boundary situations*

It is known from above mentioned that the geological conditions, building arrangement and seepage control measures of the XiaoLangDi Key Water Control Project are rather complex, which brings some difficulties for the calculation of the three-dimensional seepage flow in the key water control project area. According to the geological structure, permeability of the strata and distribution of the main buildings, and also in light of the impermeable feature along the horizontal direction of F_{236}~F_{238}, the seepage flow field of the key water control project is considered as two components: one is on the left bank the north of F_{236}~F_{238} to F_{461} (i.e. District I); the other is the north of F_{236}~F_{238}, including the dam in the river bed, up to the Temple Slope in the north of F_{230} (i.e. District II to VI). Since the impermeability of F_{461} in the northern side on the left bank, it is considered as the northern border of the whole seepage flow field of the key water control area; the nearby Xigou Reservoir is deemed as the inletting seepage boundary; to the west on the left bank, the horizontal impermeable F_{28} is as the border; the Qiaogou River in the lower stream on the left bank is as the border. For the river bed section and right bank, in light of the natural coverage in the upper stream, the seepage border is selected at a distance of 1100m to the foot of the dam and in the lower stream the border is selected at the same distance of the mouth of the Qiaogou River and on the right bank (south of the seepage flow field) the proper distance near the Temple Slope in the south of F_{230} is taken as the border. As the geological conditions are not same in the various district, the bottom impermeable border of the seepage flow field is selected as per the above mentioned "Hydrological and geological condition". The water lever in the upper stream reservoir is taken as 275.0m and that in the lower stream as 141.5m. After water storage of the reservoir, under the level of 275m of the dam and the slopes on both banks facing the water are all inlet seepage area of the seepage flow field and the upper water head is controlled as 275m. The water level of the Xigou Reservoir on the left bank is controlled as 217.5m. Under the level of 141.5m in the lower stream of the dam and of the both banks is seepage discharge area; the upper water head is controlled as 141.5m. The seepage flow field of the key water control project are proposed to have 66 sections each section with 260~400 nodes, totaling 23600 nodes.

3.2 *Simulation of the project part in F_1 fault*

(1) As the F_1 fault is situated at the key part of the dam, the thickness of the fault body is considered as 4m and impermeable; fragment belt of 10m is set up in each the two sides of the fault; the seepage factor is taken as 10m/d and the seepage factor for the grout curtain in the fault belt is taken as 0.03m/d.

(2) Besides the calculation of the fine quality of the wall body ($k=10^{-8}$cm/s) in the simulation of the concrete seepage-proof wall, calculation is also carried out on the problems of the working quality which is not up to the requirement in some part of the concrete seepage-proof wall or fork left in the work performance.

(3) The top level of the natural cover is considered as 200m; the length is considered as 1000m from the dam foot in the upper stream and the seepage factor is taken as 0.00864m/d.

(4) For the calculation methods of the water drainage hole curtain and simulation of the fork in the seepage-proof wall and the analog of the water discharge curtain in the seepage flow field ditches' method instead of juxtaposition are taken. See the details of the methods in the document[1]. See the concrete calculation of the fork in the concrete seepage-proof wall in the document[2].

4 ANALYSIS OF THE EFFECTS OF THE SEEPAGE-PROOF MEASURES FOR THE DAM

4.1 *Analysis of the seepage-proof effects of the concrete seepage-proof wall*[3][4]

For the seepage-proof effect of the concrete seepage-proof wall, calculation & analysis are carried out on the impact of the seepage-proof effect from the inserting depth of the concrete seepageproof wall, the length of both ends of the seepage-proof wall into the core wall and poor quality of part of the concrete seepage-proof wall. The calculation results of the seepage flow field and seepage gradient shows that it is proper for the upper concrete wall body to insert into the inner soil wall for 12m and both ends into the soil wall for 20m. It is realistic that in the normal conditions, the safety factor of the seepage gradient in the contact area is not less than 10. If the maximum contact seepage gradient of the seepage-proof wall inserting into the core wall is in the outlet area of the seepage flow on the back of the seepage-proof wall, counter filter shall be set up to protect it.

For the part poor quality of the concrete seepage-proof wall, if mainly seepage factor is not up to the design standard and merely the seepage factor in some individual part is enlarged, the seepage-proof wall can also keep the anti-seepage strength. The calculation results of this analog (See Table 2) shows that the seepage gradient borne by the seepage-proof wall is a little lowered and there is no big change of the seepage gradient in the contact areas of the covering layer and seepage-proof wall. Therefore it is deemed that there is no threat of the seepage stability of the dam foundation in this kind of conditions. If some fork appears in the seepage-proof wall, the problem shall be complicated. The key point is that the seepage factor in the fork area shall be great, which shall form central seepage flow, enlarge the seepage gradient of the contact area on the covering layer and seepage-proof wall. Thus contact seepage flush and seepage deforms of the recovering layer can rise to threat the safety of the dam.

4.2 *Seepage-proof function of the natural recovers*

As per the concrete conditions of XiaoLangDi, with the function of the concrete seepage-proof wall, the natural cover shall also take some role of the seepage-proof. According to the calculation, the natural cover can normally lower 11.0% of the water head and thus the maximum seepage gradient borne by the seepage-proof wall can be lowered from 100 to about 87 (See Table 2). Table 2 shows that if the quality of the seepage-proof wall is good, the coverage layer of the strong seepage flow shall be thoroughly cut and the function of the natural cover shall be lowered. On the contrary, the function of the natural cover shall be enlarged and the seepage stability of the dam foundation, especially that of the seepage-proof wall, appears very important. Therefore, according to the conditions of XiaoLangDi, a prudent policy shall be adopted to use the natural cover to take precautions against the poor quality of the seepage-proof wall. The quality standard of the concrete seepage-proof wall shall never be lowered. The analysis results shows that with the function of the natural cover the seepage gradient is 3~4 and without the function of the natural cover the seepage gradient is 1~1.5.

4.3 *Seepage-proof treatment for F_1 fault*

For F_1 fault, the measures to strengthen grout curtain, extend the seepage runoff and set up counter filter protection can effectively reduce the water head and minimize the seepage gradient in the outlet area of the lower stream. The heavy curtain can approximately reduce 40% of the water head

Table 2. Results of the different quality of the seepage-proof wall with or without natural cover.

Quality of seepage-proof wall	Natural cover	Water head in the upper stream of the seepage-proof wall	Water head reduction	Slope reduction borne by the seepage-proof wall	Water head rising behind the wall(m)	Remarks
Good	Without	93%	7%	96.34~99.79		Slope reduction
	With	About 82%	About 11%	84.11~87.55	0.00	borne by seepage-proof wall: from 100 to 87
Poor	With	About 80%	About 12%	81.77~83.66	0.35~1.42	Q enlarge 1192.36m^3/d
With fork	With	Width of fork: 15cm, k=36.4m/d		81.77(average in the fork J)	1.42	

Table 3. Calculation results of different combination of Fj fault and natural cover.

F_1 fault	Natural cover	Water head reduction of the grout curtain	Max. slope reduction borne by the curtain	Water head behind the curtain	Lower stream outlet area at the bottom of the inclined core wall J_{max}	Through F_1 fault Q(m^3/d)
Thickness of fault: 4m impermeable,	With	40.3%~47.0%	12.55	14.8%~16.7%	0.534	4714.55
fault with grout curtain	Without	46.6%~54.5%	14.55	16.3%~18.5%	0.599	5117.8

and make the maximum seepage gradient in the outlet area of the lower stream at 0.5~0.6. Table 3 shows the calculation results of different combinations of F_1 fault and natural cover.

From Table 3 it is known that natural cover plays the function to extend the seepage runoff of the dam foundation, minimize the seepage gradient in the lower stream outlet and control the seepage volume of the dam foundation but the extent is small and its function is limited. Though the seepage gradient in the outlet area of the lower stream of F_1 fault is not big, it is still necessary to set up good counter filter protection in the outlet area of the lower stream considering the scale of F_1 fault is big, uneven seepage would appear and F_1 fault is in the key position of the dam.

5 ANALYSIS OF THE SEEPAGE ON BOTH BANKS AND CONTROL EFFECTS

The main function of the grout curtain across the Thin Ridge on the left bank and the main water curtain control the seepage on the left bank as a whole and lower the free water surface to a certain limit. For some buildings such as the underground power building and sinking pond in the lower stream, special system of seepage drainage shall be set up to further lower the seepage pressure. It is known from the analysis of the calculation results that the results of the drainage and pressure reduction in the seepage drainage system of the underground power building are realistic. It can lower the level of the free surface in the underground power building under 140m, which reached the expected results (Figure 1); because the extension of the drainage curtain, the level of the free surface in the area of the tailrace channel is lowered to about 140m. The harmful impact on the area of the tailrace channel from the Xigou Reservoir is basically eliminated. Since the drainage curtain is set up in the T_1^{3-2} stratum with weak permeableness takes the function of isolating layer to prevent the re-rising of the water head behind the drainage curtain.

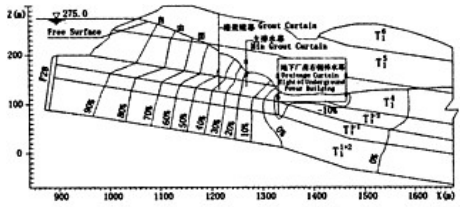

Figure 1. Right section of equipotential line of drainage.

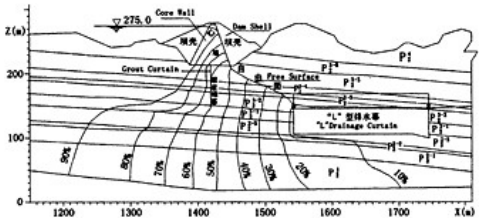

Figure 2. South section of equipotential line of drainage.

Curtain for the Underground Power Building on left bank Curtain of the L Form on the Right Bank, The hydrologic and geological condition on the right bank has got two features, i.e. pressure water and impact of F_1 and F_{230} faults. The trends of F_1 and F_{230} faults are generally paralleled with the river trend and across the right bank from east to west. Their common characters are to prevent the seepage on the right bank from draining into the river valley. Since their positions are not same, their impact on the free surface are different. The seepage prevention of F_{230} fault shall lower the free surface on the right bank while the seepage prevention of F_1 fault shall raise the free surface on the right bank, which is unfavorable to the stability of the rock slope on the right bank. The L form drainage curtain between F_1 and F_{230} faults has remarkable effectiveness on the pressure reduction (Figure 2). It can greatly reduce the free surface of the vast area north of F_{230} fault and the level is generally to about 150m. It does not only effectively reduce the free surface of this area but also provide advantages to keep stability of the rock slope on the right bank.

6 CONCLUSION

The calculation results of the seepage flow field of the key water control project show that after water storage of the reservoir, under the action of the design water level of 275.0m, the area of the key water control project shall form a whole seepage flow field and the source of the seepage shall be the seepage from the reservoir. The main discharge area shall be the river bed of the lower stream of the dam and the seepage drainage system along the both banks. The underground water shall mainly seep through the dam body and foundation. The potential energy shall centrally reduce in the dam seepage-proof body and the water heads in the inclined core wall and concrete seepage-proof wall. It reaches about 80%~90% and the remained water head behind the seepage-proof wall shall be about several meters, which shows the seepage-proof effect of the dam seepage-proof body is remarkable. The effect of the seepage-proof measures for the F_1 fault is also good without obvious rising of the water head behind the dam. Therefore, taking the seepage-proof area of the key water control project as a whole, the dam seepage-proof body played its proper role and showed the advantages of the vertical waterproof when the dam is constructed on the thick covering layer.

The underground water on the two banks shall round the dam ends and then drain into the river valley. Since there is drainage system, the most potential energy of the underground seepage shall reduce in the drainage system to lower the free surfaces in the two banks. The control of the seepage flow on the two banks is generally the function of seepage drainage system to drain and reduce the pressure of the seepage flow. Since the seepage drainage system reduces the water head, the seepage flow shall pass through drainage curtain to greatly lower the free surface of the area behind the main drainage curtain. It is advantageous to the stability of the rock slope on the two banks and minimization of the action of the seepage flow on the buildings.

The calculation results of the seepage flow show that the seepage volume flowing through the section of the riverbed is the biggest one covering 55.7%, with 39.67% on left bank and 4.63% on the right bank. Since the covering layer in the section of the riverbed is rather thick, the seepage runoff through the seepage-proof body is short, the lower rock foundation is permeable and the influence of F_1 fault happens, the volume of the seepage flow covers over half of the total. The big seepage flow is because of the long Thin Ridge and the great reduction of the drainage aperture of the underground power building.

The whole calculation results show that because of the necessary measures taken, the free surface and seepage flow pressure of the XiaoLangDi area are greatly reduced, the seepage flow volume is reasonably controlled, which created advantages for the building operation. Taking it as a whole, the measures of seepage control are reasonable, the effects are relatively realistic and the expected purpose is basically obtained.

REFERENCES

[1] Li Bin and Zhang Junxia, Attached Unit Method of Ditches instead of Juxtaposition in Numerical Value Calculation [J] Water Conservancy Study, 1996, (3):51~56.
[2] Du Yanling and Xu Guoan, Finite-element and Electric-net Methods of Seepage Flow Analysis [M] Water Conservancy and Power Publishing House, 1992.
[3] Liu Jie and Miu Liangjuan, Contact Seepage Control Test and Research of the Seepage-proof Wall and Core wall in the Dam of XiaoLangDi Reservoir [J]. Yellow River 1993, (5):19~22.
[4] Xu Guoan, Yang Kaihong and Wu Guisheng, Impact of the Crevices in the Seepage-proof Wall of the Dam of the XiaoLangDi Reservoir on the Seepage Flow Control [J]. Yellow River 1993, (9):28~31.

This page intentionally left blank.

New Developments in Dam Engineering—Wieland, Ren & Tan (eds),

Analysis of sediment outflow of turbidity current in Naodehai Reservoir

Qin Zhang & Yan Lei
Research Institute of Water Resources and Hydropower, Shenyang China

Chengjun Wang
Liaoning Investigation andDesign Research Institute of Water Resources and Hydropower, Shenyang China

ABSTRACT: Naodehai Reservoir in Liaoning Province is a large hydraulic project located at the upstream of the sandy Liu River. The reservoir was built in 1942 with a total storage of $1.93\times10^8 m^3$. The primary dam is the concrete gravity dam with a maximum height of 41.5m. In the dam, there are 2 middle holes with intake bottom elevation of 163.5m and 5 bottom holes with intake bottom elevation of 151.5m. The original aim is the flood prevention and detention without benefit use. From the spring of 1970, the run mode was set to reserve in winter and discharge in spring, and exhaust flood during summer. From 1995, in order to improve the benefits of the reservoir, experiments were made which included extending the water reserving time, maintaining clearness and getting rid of turbid under the low water stage. In practice, three turbidity currents happened on June 23rd of 1995, June 21st of 1996 and June 11th of 1998 respectively. The main purpose of the paper is to introduce some turbidity current observations and statistical analysis results, and suggest to adopt the proper sediment outflow mode in the practical applications according to different situations: if the mean daily discharge over $100 m^3/s$, or the sediment concentration over $100 kg/m^3$ in June or September, exhausting flood mode should be taken to make the erosion and deposition balance. With regard to other flood occurring in June or September, turbidity current should be utilized to reduce the siltation in reservoir area.

1 INTRODUCTION

Naodehai Reservoir is located at Naodehai village, Mantanghong town, Zhangwu county, LiaoNing Province and located at Liu River, a left-bank branch of Liao River. The drainage area of Naodehai Reservoir is $4051 km^2$. Three branches, such as Kou River, Wugengao River and Yangxumu River, are located at the upstream of Naodehai Reservoir. Shimenzi, Baimiaozi and Sanjiazi hydrological stations are at three rivers, respectively. Figure 1 shows the position of Naodehai Reservoir. The reservoir was planed originally to use as the flood prevention and sediment outflow when it was completed in 1942. However, the run mode was set to reserve in winter and discharge in spring after the reservoir was modified in 1970. The sluices are shut off to reserve water and irrigate for the backward position from October to next May, while the reservoir is exhausted to prevent flood from June to September annually. From 1995 the water pool level is controlled below 174m in June and September to supply water to Fuxin city and the reservoir is emptied to deal with the flood in July and August. Flood and siltation are remarkable problems in June and September after water reserve mode being changed.

Liu River is a high sand concentrated branch of Liao River. The drainage area upstream Naodehai Reservoir is half-drought regions, annual mean precipitation is about 460mm. There are abundant rainstorm and floodwater in summer, but drought in winter. Landform of the drainage region of Yangxumu River is characteristic of rolling and swampy, and runoff still exists in non-flood

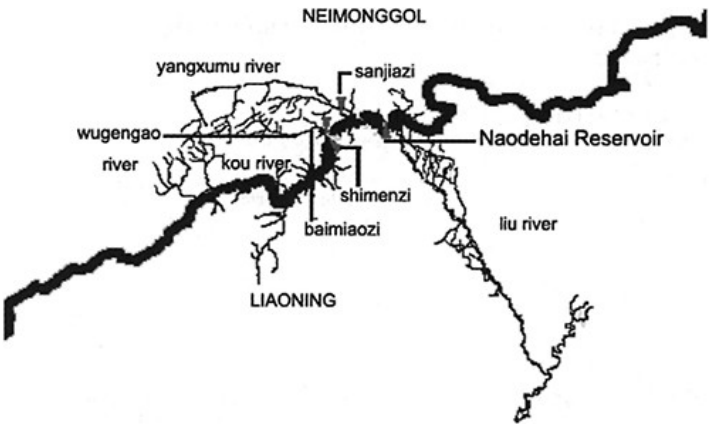

Figure 1. The position of Naodehai Reservoir.

Table 1. Statistical results of water and sediment amount in June and September.

Periods	Terms	The first ten days in June	The middle ten days in June	The last ten-days in June	The first ten days in Sept	The middle ten days in Sept	The last ten-days in Sept
80~89	Water volume	310	422	479	1043	407	287
	Sediment weight	3.1	8.6	155	123.1	6.8	2.3
90~96	Water volume	430	679	978	570	502	419
	Sediment weight	5.5	19.0	30.3	8.4	16.5	5.4
80~96	Water volume	364	536	701	833	449	346
	Sediment weight	4.2	13.2	22.1	72.1	11.1	3.7

Note: The unit of water volume is $10^4 m^3$ and that of sediment mass is $10^4 t$.

season because of abundant groundwater which comes from infiltrative rainwater during flood season. Frequent flow interruptions occur in Kou River and Wugengao River during non-flood season. Averagely, the maximum reserving water of the reservoir is $4673\times10^4 m^3$ in July, and the minimum is $367\times10^4 m^3$ in February, and the former is 12.7 times as much as the latter. The distributions of transported sand are different in a year. The average maximum of transported sand is $324\times10^4 t$ in July, and the minimum is $0.66\times10^4 t$ in February. 515 times relation is found between them. Water and sediment influx reach the maximum in the last ten-day of June, and especially the latter shows such behavior, and it accounts for 60% of the total sediment content in the whole month. In September, sediment influx occurs mostly in the first ten days of the month, accounting for 80% of the total. Table 1 shows the statistical results of water and sediment influx in June and September for many years.

Table 2. Feature parameters of sediment composition in hydrological stations.

Station	d<0.025 (%)	0.025~0.05 (%)	d>0.05 (%)	Average grains size (mm)	D_{max} (mm)
Shimenzi	44	24	32	0.043~0.074	0.40
Baimiaozi	26.2	19.9	53.9	0.006~0.092	1.30
Sanjiazi	16	27	57	0.047~0.189	1.00

The drainage region upwards Shimenzi is low hilly brokenterrain and loess donga terrain. While the drainage region upwards Baimiaozi is uniform loess donga terrain and the type of the eroded soil is uniform. The compositions of sediment are different because the type of eroded soil is various in different drainage regions. Sediment is coarse in Yangxumu River but it is fine in Kou River, and modest in Wugengao River. Table 2 shows the parameter features of sediment composition from the branches.

It is necessary that small flood is operated to discharge in order to ensure water level not over 174.0m in June and September after the run mode being altered. Three turbidity currents happened in June of 1995, 1996, 1998, respectively. The turbidity current often can be observed in the rivers and sea, and sometimes can bring damages [1,2]. However, the turbidity current can play a favorable role in the sediment outflow if it is utilized reasonably. In this paper the role of the turbidity current in the sediment transportation in Naodehai Reservior is investigated. And the formation process of the turbidity current is also discussed.

2 TURBIDITY CURRENT OBSERVATION

2.1 *Basic situation of the turbidity current*

On June 22nd of 1995 medium and heavy rain happened throughout the areas upstream Liu River with daily rainfall of 18.8mm and the maximum rainfall of 57mm. At 1 o'clock of 23rd the water level was 172.10m and the influx into the reservoir was 107m^3/s. Muddy water was drained out of the bottom holes by the sluice regulation at 5 o'clock. At 14 o'clock, the results showed that the sediment concentration, turbidity and d50 grain size was 6.26kg/m^3, 10000 and 0.036mm, respectively. The measured sample from the position at the elevation of 155.0m and distance of 100m away from the dam, but the sediment concentration was 0.057kg/m^3 and the turbidity was 50 for the position of the elevation of 165.0m. Calculation based on the above data shows that the sediment influx was 16.58×10^4t and sediment outflow by turbidity current was 3.49×10^4t, and the corresponding sediment outflow ratio was 21%. The 3rd rain for June hit Liu River drainage region on June 20th, 1996. The field data showed the water level was 174.50m, and the daily precipitation 21.9mm with the maximum value of 53.0mm, and the maximum influx of 287m^3/s. The sluice regulations were executed at 15, 21:30 and 6 next day. The turbidity current reached the dam and Was discharged through the bottom holes on 22nd morning. At 11 o'clock the samples got at a distance of 100m upstream from the dam showed the sediment concentration to be 30.4kg/m^3, turbidity to be 66000NTU and d50 to be 0.029mm at the elevation of 152m, but sediment concentration is 0.18kg/m^3, turbidity 250NTU at the elevation of 165m. The sediment influx was 49.89×10^4t and sediment outflow by turbidity current was 31.96×10^4t, and the corresponding sediment outflow ratio was 64%. The observations on June 11th, 1998 are neglected due to the data insufficiency.

2.2 *Channel fluvial form*

The turbidity current drives the high sediment current to the dam along the bed. The turbidity current rise and muddy reservoir were avoided by regulating the sluice in time, which ensured the water supply to the Fuxin City. And the excess siltation was avoided because much sediment was outlet from the bottom holes. But most sediment was left in the reservoir due to the small sediment outflow ratio (21%~64%). The low water level operated and the reserve backwater end decreased from the Cl 1 section to the C7. And the backwater below 174m remained in the main channel and the sediment distributed along the main channel nonuniformly due to the narrow surface (100~500m). In 1995 and 1996 observations showed turbidity current imported around W4 section, which formed obvious delta siltation. The measured map of vertical section showed obvious protuberance before the main flood. When the mode of emptying reservoir or exhausting flood during flood was carried out, retrogressive erosion and streamwise erosion occurred. The subdelta disappeared almost after the flood because the subdelta was located in the main channel.

3 ANALYSIS OF THE TURBIDITY CURRENT

3.1 *Formation of turbidity current in Naodehai Reservoir*

Two conditions should be satisfied to form the turbidity current. One is the hydraulic condition, Froude number Fr=0.6. Another is sediment condition which means the fine sand (d<0.01mm) covers mass percentage. When these factors are satisfied with, the turbidity current occurs to move down to the bottom. When the flood time lasts longer than the turbidity current time, and the water amount of the flood more than the turbidity current or the water amount of the turbidity current plus the lost amount over the influx, the turbidity current can reach the dam. Opening the floodgate in time will discharge the turbidity current. Thus flood and muddy reservoir will not take place.

Naodehai Reservoir is located at Liu River, where the flow is high-concentrated. Flood of Wugengao River, the upstream branch of Liu River, often contains large amount of fine sand in the flow. During the water storing in June and September, the water level is controlled below 174.0m, i.e. operation at low level. The backwater affects a short distance from the dam and the water influx centralizes at the main channel, thus the slope is large. The narrow valley also facilitates the formation of turbidity current. The high sediment concentration influx will go down to the reservoir region to form the turbidity current when certain condition is satisfied.

The regulating capacity is low when the reservoir operates at low water level: $950\times10^4m^3$ below 174.0m, and $650\times10^4m^3$ in the range of 174.0~169.0m. And the floodpost storage already starts in September. So it is necessary to open the floodgate often in June. Once the flood happens the discharge must be enlarged to get the desired level, which facilitates the turbidity current movement and discharge. The inspection is necessary although the reservoir can self-regulate. The turbidity and excess sediment can be prevented by opening the floodgate to exhaust the siltation in time.

In summary, the total sediment influx was 66.47×10^4t and sediment outflow was 35.45×10^4t, and the sediment outflow ratio was 53.33% during the turbidity current happening in 1995 and 1996.

3.2 *Effect of sediment outflow by turbidity current on fluvial balance in Naodehai Reservoir region*

The run mode of Naodehai Reservoir is flood and sediment detention or exhausting flood for several years. The fluvial balance in reservoir region depended mainly on the flush of flood season, especially on medium-long-time flood. Although favorable effect has been obtained for sediment outflow by turbidity current, more siltation still exists compared to emptying reservoir. The balance of flush and sediment deposition has been kept for fifty years. Serious siltation did not occur for a long time. From the calculation of the flood occurred before, sediment content entering the reservoir is 1139×10^4t, and sediment outflow by turbidity current is $884\times^4t$, and sediment left is 407×10^4t in reservoir region and sediment outflow ratio is 77.6%. The measured sediment discharge is 806×10^4t by exhausting flood, indicating sediment outflow delivered by turbidity current is more than $1213\times^4t$. Therefore, the storage in June and September can be regulated

according to forecasting, inspection and transportation. Although the sediment outflow delivered by turbidity current can work, it will have negative effect on the sediment balance in the reservoir. In addition the delta will form at the imported spot. The field observation of the turbidity current for two years shows that the retrogressive erosion will clear away the delta by exhausting flood during the flood season. But the data are insufficient. Analysis shows when the daily flux is over $100m^3/s$ or the sediment content over $100kg/m^3$, the fluvial balance can be ensured by exhausting flood, otherwise turbidity current or other methods should be considered to reduce the siltation in the reservoir region in June and September.

4 CONCLUSION

Research of turbidity current is an important issue in sediment study Our result shows that the turbidity current formation at low level will not make Naodehai Reservoir muddy if the sediment is discharged in time by opening the floodgate in the storage months of June and September. In comparison with emptying reservoir, the residual sediment in the reservoir has obvious effects on the fluvial balance. So different mode should be taken corresponding to different situation, and the water supply and the fluvial balance can both be ensured.

REFERENCES

[1] Wynn, Russell B.Stow, Dorrik A.V, "Classification and characterisation of deep-water sediment waves", *Marin geology,* Vol. 192, 2002, 7–22.
[2] Mccave, I.N., Carter, L., "Recent sedimentation beneath the Deep Western Boundary Current off northern New Zealand", *Deep Sea Research Part I: Oceanographic Research Papers,* Vol. 44, 1997, 1203–1237.

This page intentionally left blank.

New Developments in Dam Engineering—Wieland, Ren & Tan (eds),

Research on abutment stability of high arch dam

Qing Zhang, Guojian Shao & Jiashou Zhou
Hohai University, P.R. China

ABSTRACT: On the basis of evaluation on the analysis methods of high arch dam abutment stability, this paper points out their deficiency, presents the formula of stability safe factor for the possible sliding body based on the non-linear FEM analysis. With the application of the formula and the disturbing energy method, the stability evaluation is made on six possible slide bodies of the highest double-cured arch dam would-be in the world with the height of 305m.

1 INTRODUCTION

About 70% waterpower resources centralize in the southwest and the northwest in China. The mountains and canyons provide the good terrain and geologic conditions for building high arch dams. Since the working mechanism of arch dam is passing load to the dam abutment rock on two banks by the action of arch, the stability of dam abutment rock becomes one of the important factors to secure the arch dam's global degree of safety.

Presently, the analysis of the stability of the dam abutment rock mainly employs limit equilibrium method, FEM and model experiment method. As to the rigid body limit equilibrium method, its engineering physical concept is clear, the calculation is brief and convenient, and most of all, the method has been used in engineering for a long time and has accumulated much practical experience. Besides, there is a set of judging standard for the analysis of the stability of the dam abutment rock accordingly. However, this method has its deficiency, because it can't consider the rock stress-strain relation, and it can't reflect the destructive mechanism of the dam abutment rock and the interaction of arch dam and the rock. Moreover, as to the high arch dams at the lever of 300m, the height of dam already exceeds the limitation the specifications cover. The model experiment method is direct and practical, but its expense is rather high, and it has limitation to some degree. As for the non-linear FEM, it comprehensively reflects the mechanical properties of complex rock and the interaction effect of arch dam and rock, and presents the strain and stress fields accordingly, and also it can help us get the damage field distributing character of the dam abutment rock, which is in favor of the analysis of destroy mechanism for dam-abutment rock system. If the possible sliding body is given by geologic engineers, we can get the anti-sliding force and sliding force on the considered body surface by synthesizing the results obtained by the nonlinear FEM, and get the stability safety factor of the possible sliding body by projection.

However, among the formulas in existence to calculate the stability safety factor, especially for the three-dimensional problems, the projective mode is rather jumbled, leading to the great difference of the calculating results. Moreover, if we can't find the possible sliding surface in advance, we cannot answer the question that if the dam abutment rock is stable. There are some papers judging stability by point safety factor in the analysis of FEM. Since the yielding point must be within the material yielding surface, the point safety factor will not be smaller than 1 in principle, this factor reflects the Mohr-coulomb strength criterion virtually. Besides, the slide direction corresponding to each point safety factor is different, the contour of point safety factor mainly reflects the state of the rock material strength instead of the destruction channels.

Facing the background above and beginning with the friction principle and vector geometry, the paper educes the calculating formula of the stability safety factor for the three-dimensional possible sliding body based on the non-linear FEM analysis. By employing the mechanical mechanism of engineering stabilization problems, the paper establishes the disturbing energy method of the stability judgment to ascertain the possible sliding body, dangerous sliding direction of dam abutment rock and the stability safety factor accordingly, which provides an efficient method for the stability analysis of the dam abutment rock.

2 THE FORMULA OF STABILITY SAFETY FACTOR FOR THREE-DIMENSIONAL POSSIBLE SLIDING BODY

Generally, the stability safety factor k is defined by the ratio value of anti-sliding force to sliding force on the sliding surfaces. The precondition is that the sliding surfaces of the considered body are given beforehand, besides, there are other two problems must be solved.

1. The determination of the most dangerous sliding direction. As the space sliding body slides along the sliding surfaces, the displacement value and the sliding direction of any point on the surfaces are different with each other, but those can be composed into the general sliding vector, and we call its direction the general resultant sliding direction. The value of k calculated along different sliding direction is also different, of which the one that can make k minimal must be the most dangerous sliding direction, and then we need to find the way to solve it.
2. The correct definition of sliding force, anti-sliding force and stability safety factor

- Generally speaking, the sliding force can be solved by the sum of the product of each segment's shearing stress multiplying the area accordingly, while on the space sliding surface, the shearing stress value and direction of each point is not the same, but after all, it can be composed into general resultant sliding force vector (includes value and direction).
- The anti-sliding force is composed by the friction and the cohesion of each point on the sliding surface. As to its direction, some literatures hold it is contradictory with the resultant shearing stress of the point accordingly, which we do not think proper. Because according to the friction principle, the direction of each point's anti-sliding force is opposite with the one of relative displacement of this point on the sliding surfaces. As each point's direction of the relative displacement is different, each point's direction of the anti-sliding force is also different, but it can be composed into the general resultant anti-sliding force vector (includes value and direction).
- The stability safety factor is a scalar quantity, so when we calculate the ratio of the anti-sliding force to the sliding force, which is expressed by K_S, we must adopt the one that they are in the same direction. Since the ratio on different direction is also different, and what we are interested in is the minimum value of K_S, we must solve K_S by adopting the most dangerous resultant sliding direction as defined above to obtain the minimum stability safety factor.

With the knowledge of the above two problems as well as the friction principle and the conception of vector geometry, we educe the calculating formula of the stability safety factor and the most dangerous resultant sliding direction for the three-dimensional possible sliding body based on the non-linear FEM analysis as follows

$$K_s(\bar{r}) = \frac{\sum_{i=1}^{N_e} (c - f\sigma_{z'}) A_i \sqrt{l_i'^2 + m_i'^2}}{\sum_{i=1}^{N_e} [l_i' \tau_{z'x'} + m_i' \tau_{z'y'}]} \tag{1}$$

where, z' is the normal direction of one element on the sliding surface, x' and y' are the two local coordinates of the shearing direction of the element on the sliding surface. n_i' are the

direction cosine of the angle of the considered body's general sliding direction expressed by $\bar{r}$ and the local coordinate x', y', z' respectively, A_i is the sliding surface area of i element, $(c-f\sigma_z)_i$ is the anti-sliding stress of the i element, c and f are the cohesive coefficient and the frictional coefficient, respectively, $\sigma z'$, $T_{z\acute{x}}$, and $T_{z\acute{y}}$, are the normal stress and two shearing stress of the element on the sliding surface, respectively. N_e is the sum of the element on the slide surfaces.

In Eq. (1), the numerator denotes the component of the resultant anti-sliding force vector on the direction of $\bar{r}$, and the denominator expresses the one of the resultant sliding force.

We can also educe the condition that ascertains the most dangerous resultant sliding direction by using Eq. (1). Assume l, m, n are the cosines of the angles between $\bar{r}$ and the local coordinate axes x, y, z, respectively, and use the relations as follows

$$\frac{\partial K_s(l,m)}{\partial l}=0 \qquad \frac{\partial K_s(l,m)}{\partial m}=0 \tag{2}$$

And by inserting it into Eq.(1), we get $\bar{r}_0$, and by the condition

$$\Delta\Pi_p=\Pi_p\left(u_i^0+\delta u_i\right)-\Pi_p\left(u_i^0\right)=\delta\Pi_p+\frac{1}{2}\delta^2\Pi_p+\cdots\cdots \tag{3}$$

to solve the minimum k_s. Then we can solve the most dangerous sliding direction $\Pi_p(u_i^0)$ which makes k_s achieve minimum.

3 THE DISTURBING ENERGY METHOD OF THE HIGH ARCH DAM ABUTMENT STABILITY

3.1 *The energy criterion and the disturbing energy expression of the system stability*

The equilibrium of a considered body is possibly stable, instable or critical state, respectively. Now, we give an object which is in one kind of equilibrium state an arbitrary little disturbance, and after we remove the disturbance, if it can return to the original equilibrium state, we call this kind of equilibrium steady equilibrium, if it can not and even depart further and further, this one is not steady, if it can keep equilibrium under the new position, this one is critical equilibrium. It is easy to see that if we want to prove one kind of equilibrium state is steady, we must review all possible disturbances, only if the considered body can return to the original state after removing all these possible disturbances can we get the result that this equilibrium is steady. And we can confirm the equilibrium is unsteady or critical only if we find one kind of disturbance under which the considered body cannot return to the original state or keep equilibrium under new position.

Considering that the potential energy Π_p on the equilibrium state has its extremum, if Π_p is minimum, the equilibrium is steady; if Π_p is maximum, it is unsteady; if Π_p keeps fixedness, it is critical. Mathematically, we can adopt the second order variation $\delta^2\Pi_p$ of Π_p as the criterion, that is to say, $\delta^2\Pi_p>0$, $\delta^2\Pi_p<0$ and $\delta^2\Pi_p=0$ is corresponding to the steady, unsteady and critical equilibrium state, respectively.

As to one equilibrium system, the potential energy increment after suffering disturbance is

$$\Delta\Pi_p=\Pi_p\left(u_i^0+\delta u_i\right)-\Pi_p\left(u_i^0\right)=\delta\Pi_p+\frac{1}{2}\delta^2\Pi_p+\cdots\cdots \tag{4}$$

$$l_i'=l\cos(x,x')+m\cos(y,x')+n\cos(z,x')$$
$$m_i'=l\cos(x,y')+m\cos(y,y')+n\cos(z,y')$$

where, $l^2+m^2+n^2=1$ is the one after the body is disturbed, δu_i is the disturbing displacement,

$\Delta\Pi_p$ is the disturbing energy value corresponding to the disturbing displacement. Since the total potential energy before being disturbed has stationary, i.e. $\delta\Pi_p$=0, we have

$$\Delta\Pi_p = \frac{1}{2}\delta^2\Pi_p \tag{5}$$

Obviously, the value of $\Delta\Pi_p$ can be used to judge the body's steady state as well as the value of $\delta^2\Pi_p$, while the value of $\Delta\Pi_p$ can be solved by numerical calculation.

Considering the geometrical nonlinear effect, and by systemic deduction and calculation, we get the nonlinear expression of the disturbing energy as follows

$$\Delta\Pi_p = \sum_e^{Ne}\left[\int_{\Omega_e}\left(\Delta\mathbf{e}^T\boldsymbol{\sigma}^0 + \frac{1}{2}\Delta\boldsymbol{\varepsilon}^T\Delta\boldsymbol{\sigma}\right)d\Omega - \left(\Delta\boldsymbol{\delta}^e\right)^T\mathbf{R}_e^0\right] = \Delta U - \Delta W \tag{6}$$

where, $\mathbf{R}_e^0$ denote the element stress and equivalent node load array of the considered object under the original equilibrium state, respectively. $\Delta\boldsymbol{\delta}^e$, $\Delta\mathbf{e}$, $\Delta\boldsymbol{\varepsilon}$ and $\Delta\boldsymbol{\sigma}$ indicate displacement increment, strain increment, strain increment corresponding to small deformational state and stress increment of element induced by small disturbance.

3.2 *The most unfavorable disturbing displacement*

Since different disturbing displacement can correspond to different disturbing energy, and what can be used as the stability criterion is the disturbing displacement corresponding to the minimum disturbing energy, which is called the most unfavorable disturbing displacement for short. Such displacement should make the disturbing energy i.e. $\Delta\Pi_p$ appear minimum value at first; secondly, it should be small and accord with the condition that the displacement is harmonious. On the basis of this, we can select the combinative equation of vibration mode functions as the test function of the disturbing displacement, as shown in the following equation

$$\Delta\boldsymbol{\delta}^e = \left(\mathbf{u}^0\right)^e + \alpha_1\boldsymbol{\delta}_1^e + \alpha_2\boldsymbol{\delta}_2^e + \cdots + \alpha_n\boldsymbol{\delta}_n^e \tag{7}$$

where, $(\mathbf{u}^0)^e$ is the initial term of the disturbing displacement of the element node and should satisfy the displacement compatibility condition; $\boldsymbol{\delta}_i^e$ is the amplitude of the element node displacement corresponding to *ith* vibration mode; α_i is the constant to be solved corresponding to the *ith* vibration mode.

The most unfavorable disturbing displacement must need the disturbing energy value to get its minimum, so we have

$$\frac{\partial\Delta\Pi_p}{\partial\alpha_i} = 0 \qquad (i=1,2,\ldots,n) \tag{8}$$

We can get a set of linear equation group from the above equation. After we solve α_i, and insert it to Eq. (7), we can obtain the most unfavorable disturbing displacement.

3.3 *The stability safety factor*

As mentioned above, ΔU is of benefit to the stability of considered body, while ΔU is opposite. In order to reflect the degree of stability safety under some loading state or computational case, we give the definition of safety factor of stability according to mechanical concept, i.e.

$$K_G = \frac{\Delta U}{\Delta W} \tag{9}$$

Obviously, the value of K_G can reflect the degree of safety of structure stability under the considered loading state. K_G>1 indicates that the structure is stable, K_G<1 indicates unstable, while K_G=1 indicates critical state.

Since the disturbing energy is scalar quantity which has no direction, we can also obtain the degree of stable safety of each element or interested local part according to Eq. (9).

3.4 *The possible sliding mass and the most dangerous sliding direction*

Disturbing energy method can provide theoretical fundamentals for finding the potential sliding mass and sliding surface of the considered body. After having obtained the value of disturbing energy and stability safety factor of each element, we can draw the contour surfaces (lines) of disturbing energy and safety factor in the considered body, respectively. In theory, sliding mass must posses the air face and its disturbing energy is negative (the slide must occur) or the smallest compared with the other parts (the slide is potential or possible). If the range of the sliding mass is determined, the corresponding sliding surface can be found, while the most dangerous sliding direction is the general resultant direction composed by the most unfavorable disturbing displacement vector of each point on the corresponding sliding surfaces.

4 THE COMPREHENSIVE CRITERION OF HIGH ARCH DAM ABUTMENT STABILITY

(1) Ascertain the location of the possible sliding surface according to the minimum of the isograms of disturbing energy. If necessary, we can amend it on the basis of geologic structures and man-made experiences.
(2) Ascertain the most dangerous sliding direction according to the resultant vector direction composed by each point's most unfavorable disturbing displacement on the possible sliding surfaces. If necessary, we can choose other sliding directions as supplement or check according to the engineering need.
(3) Based on the possible sliding surfaces and the most dangerous sliding direction ascertained as above, solve K_s applying Eq. (1) which calculates stability safety factor, and solve K_G of the sliding body upon the possible sliding surfaces according to Eq. (9).
(4) When the two factors K_s and K_G are all larger than 1, the considered body can be thought to be in the stable equilibrium state. When one of them is littler than 1, then we think it is non-steady or requires more evidence.

5 NUMERICAL EXAMPLE

The highest double-cured arch dam in the world, which locates in the south-west of China, will be built on the base lever of 1580m, with its peak altitude of 1885m and the height of 305m. The river valley is of an typical deep 'V' shape with a slope angle of 45°~80° on the left bank and

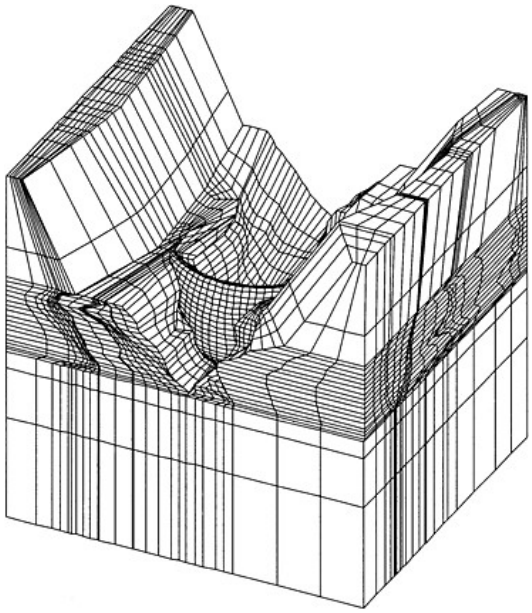

Figure 1. The three-dimensional finite idealization of the arch dam.

Table 1. The stability safety factors of six considered sliding bodies by limit equilibrium method.

No. of six considered sliding bodies	Computational case		
	Before the building of the dam	Natural foundation after the building of the dam	Reinforced foundation after the building of the dam
(1)	2.190 (1.342)	1.960 (1.246)	3.193 (1.977)
(2)	1.937 (1.293)	1.924 (1.284)	4.459 (2.094)
(3)	2.303 (1.461)	2.299 (1.464)	3.093 (1.754)
(4)	2.801 (1.553)	2.793 (1.575)	2.806 (1.578)
(5)	3.778 (2.959)	3.902 (3.062)	3.906 (3.064)
(6)	2.676 (2.053)	2.748 (2.113)	2.749 (2.113)

40°~90° on the right bank. The maintain body is strong and thick, which has good conditions for building high arch dam.

But the geologic structure of the dam site is very complicated. The river bed and dam abutment are cutted by many fault zones, and the rock properties on the two banks are quite different. Those will introduce some unfavorable effects on the safety of the high arch dam. The dam abutment stability is one the key problems for the design of the dam.

In the analysis of non-linear FEM, the computing range includes the global arch dam and enough large size of the rock foundation. Figure 1 shows the three-dimensional finite idealization of the arch dam.

The six possible sliding bodies have been taken for analyzing the dam abutment stability according to the geologic case, the first four possible sliding bodies on the left bank of river and the others on the right bank. On the basis of computational results of non-linear FEM, we solve the

Table 2. The stability safety factors by the disturbing energy method.

No. of six considered sliding bodies	(1)	(2)	(3)	(4)	(5)	(6)
The stability safety factor	1.721	1.867	1.795	1.816	1.639	1.821

stability safety factors of six considered sliding bodies by limit equilibrium method. Table 1 shows the results, in which the value refers to stability safety factor considering the friction and the cohesion of rock, while the value in brackets refers to stability safety factor considering only the cohesion of rock. Besides, we also conduct the stability analysis by the disturbing energy method for natural foundation after the building of the dam, the results are shown in table 2.

From these results, we know that the dam abutment stability is ensured because the K_s and K_G of all the six possible sliding bodies are larger than 1. As the first three possible sliding bodies on the left bank are located in the reinforced region, their stability safety factors have much increased after the foundation has been reinforced.

6 CONCLUSIONS

The analysis of the dam abutment stability is one of the key problems during the design of the high arch dam. Besides checking it with the limit equilibrium method, we should also conduct the stabilization analysis of the possible sliding body by using the results of the non-linear FEM. Because theoretically, the method advised by this paper not only considers the interaction of the dam and the abutment rock, but also satisfies the equilibrium law, construction law and the compatibility law. So it is more close to reality than the limit equilibrium method. However, since there is no corresponding judge criterion, it is of important practical meaning to further develop the study within this field.

The disturbing energy method follows the basic theory of mechanics strictly and gives the stability safety factor of the system or local part in the view of energy. Since the energy is a scalar, the disturbing energy method avoids the disunion of the formula which are used to calculate the stability safety factor resulting from the different projection method. However, the safety factor got by the disturbing energy method has different mechanical mechanism with that of traditional safety factor to some degree. The inner relation between the two methods also lacks comprehensive study, and there is not stability judge criterion responding to the new method in engineering. Despite these disadvantages, the disturbing energy method can be used as a complementary and reference, especially used to ascertain the potential sliding body and the dangerous sliding direction, and also to make synthesis judgment of the stability of the dam abutment rock by combing with the limit equilibrium method.

REFERENCES

[1] Pan Jiazheng, *The analysis of sliding stability of constructions,* water conservancy and hydroelectricity press, Beijing, 1980.
[2] Wang Liutai. *The stability analysis of the dam abutment rock in the arch dam,* Guizhou people press, Guiyang, 1982.
[3] Zhuo Jiashou. *The generalized variation theory in the elastic-plastic mechanics,* water conservancy and hydroelectricity press, Beijing, 1989.
[4] Zhuo Jiashou, Shao Guojian. The disturbing energy method to ascertain the sliding surface, the sliding direction and the safety degree in the engineering stability problems, *shuilixuebao,* No. 8, 1997, 80–84.

This page intentionally left blank.

New Developments in Dam Engineering—Wieland, Ren & Tan (eds),
© 2004 Taylor& Francis Group, London, ISBN 04 1536 240 7

Earthquake analysis of the Longtan dam including dam-water-foundation rock interaction

Qing Zhang & Xuanmao Peng
Hohai University, P.R. China

ABSTRACT: A model of dam-water-foundation rock dynamic interaction of the Longtan dam is established and seismic computation is performed base on the 3-D FEM for bottom hole monolith. Hydrodynamic pressure as well as characteristics of free vibration of bottom hole monolith is obtained, and mode-decomposed response spectrum method defined in the *specifications for seismic design of hydraulic structures of China* is also used in dynamic analysis. Evaluations have been made on the seismic safety effect of the dam, which points out some weak regions.

1 INTRODUCTION

Longtan hydroelectric station, the leading power station among the Hongshui River step exploration, is located in Tian'e county, Guangxi Zhuang Autonomous Region in the southwest of China. As the Med-Himalayas seismic belt, which is the largest in the Asia-Europe continent, passes through this area, the seismic risk is great. According to the analysis of the seismic risk, Longtan dam is a I grade building, whose designed earthquake intensity is 8, and the designed earthquake acceleration is 0.2g. So in order to make sure the security of the dam coming across earthquake, it has important practical meaning to conduct the seismic analysis and evaluations on the seismic safety effect of the dam scientifically.

The paper founds the model of the dam-water-foundation rock dynamic interaction, and conducts the seismic analysis of the bottom hole section based on the three-dimensional dynamical FEM. In the case of establishing mode, we simulate the dam body complex geometry shape, bottom hole steel liner and all types rocks, especially pay much attention to the body hole, brake frusta, dam heel, dam toe, typical interface and other important parts. In the analysis, we get the dynamic water pressure based on the FEM, solve the problem of free vibration using the filter frequency method. According to the mode-decomposed response spectrum method defined in the *specifications for seismic design of hydraulic structures* of *China,* we conduct the dynamical analysis of the dam, and evaluate the seismic safety effect of the dam.

2 CALCULATION MODEL AND ANALYSIS METHOD

2.1 *The movement equation of water domain and dam body*

Under the seismic loads, the motions of the reservoir water and the dam body are affecting each other. The water will induce hydrodynamic pressure due to the movement of the dam body, while the pressure will act on the dam in return, and will consequently affect the movement of the dam body. So we must consider the dam-water dynamic interaction when conducting the seismic analysis of dam.

Assuming water to be linearly compressible and neglecting its internal viscosity, the small amplitude irrotational motion of water is governed by the three-dimensional wave equation[1]

$$\nabla^2 p = \frac{1}{c^2}\frac{\partial^2 p}{\partial t^2} \tag{1}$$

in which p(x, y, z, t) is the hydrodynamic pressure (in excess of the hydrostatic pressure) and the velocity of sound in water $C = \sqrt{gK/\rho_w}$ where K and ρ_w are the bulk modulus and unit weight of water, respectively, and g=acceleration of gravity.

The boundary conditions are:

p=0 on the water surface (2)

$$\frac{\partial p}{\partial n} + \rho_w \frac{\partial^2 u_n}{\partial t^2} = 0 \qquad \text{on the interface of the water and dam} \tag{3}$$

where, u_n is the normal displacement of the interface.

In addition, the hydrodynamic pressure in the upstream infinite boundary of water domain drives to zero. In the surfaces of reservoir bottom or bank, the boundary conditions should have the similar form as equation (3).

Under the earthquake loads, the dam movement equation can be expressed in matrix form as follows

$$[K]\{u\} + [C]\{\dot{u}\} + [M]\{\ddot{u}\} = -[M]\{\ddot{u}_g\} + \{F_t\} \tag{4}$$

where, the first term in the right of equation (4) is the equivalent seismic force, the second term is the equivalent load of the hydrodynamic pressure acting on the dam, $\{\ddot{u}_g\}$ is the ground acceleration matrix, *[K], [C], [M]* is the stiffness matrix, damping matrix and mass matrix, respectively, and they can be assembled by element ones.

Now, the basic form of reservoir water movement equation and the boundary conditions are keeping fixed, except that in equation (4). But, the normal absolute acceleration of dam surface should conclude the effects of the dam elastic deformation, and it can be expressed by the combination of the seismic acceleration and the dam relative acceleration.

Since the basic unknown functions in the dam movement equation are displacement components, and those in the water movement equation are hydrodynamic pressure, they contact each other by the conditions of the interface of dam and water. Generally, the two types of equations cannot be solved separately, so we call it the coupling problem.

2.2 *The application of FEM*

Applying FEM, we assume the inner hydrodynamic pressure of the water element distributes as follows

$$p = [\overline{N}]\{p\}^e \tag{5}$$

From equations (1), (3) and (5), we can induce the water movement equation[2] after being discreted using FEM

$$[H]\{p\} + [G]\{\ddot{p}\} + \rho_w [S]\left(\{\ddot{u}_g\} + \{\ddot{u}\}\right) = 0 \tag{6}$$

where, *[H], [G]* and *[S]* are assembled by the sub-matrices of water element accordingly, their meanings and the specific expressions are shown in paper [3].

It can be proved that the relation between the equivalent loads of hydrodynamic pressure $\{F_s\}$ and the hydrodynamic pressure *{p}* is[3]

$$\{F_s\}=[S]^T\{P\} \tag{7}$$

Introducing this relation into equation (4) and combining it with equation (6), we can obtain the basic equation group to solve the water-dam dynamic coupling problem by FEM

$$\begin{bmatrix} K & -S^T \\ 0 & H \end{bmatrix}\begin{Bmatrix} u \\ p \end{Bmatrix}+\begin{bmatrix} c & 0 \\ 0 & 0 \end{bmatrix}\begin{Bmatrix} \dot{u} \\ \dot{p} \end{Bmatrix}+\begin{bmatrix} M & 0 \\ \rho S & G \end{bmatrix}\begin{Bmatrix} \ddot{u} \\ \ddot{p} \end{Bmatrix}=\begin{Bmatrix} f_1 \\ f_2 \end{Bmatrix} \tag{8}$$

in which $\{f_1\}=-[M]\{\ddot{u}_g\}$, $\{f_2\}=-\rho[S]\{\ddot{u}_g\}$.

Since the coefficient matrices of equation (8) are not symmetrical, the workload of calculation is rather large, so generally we always try to find decoupling technology to predigest the calculation.

One of the relatively practical method is induced based on the assumption that the water cannot be compressed. With this assumption, the velocity of sound in water C→∞, and accordingly *[G]*=0. Then we can obtain directly from equation (6)

$$\{p\}=-[H]^{-1}\rho[S]\left(\{\ddot{u}_g\}+\{\ddot{u}\}\right)$$

Using the above equation to eliminate *{P}* from equation (4), we get

$$[K]\{u\}+[c]\{\dot{u}\}+[M^{**}]\{\ddot{u}\}=-[M^{**}]\{\ddot{u}_g\} \tag{9}$$

where $[M^{**}]=[M]+[M_p]$, $[M_p]=\rho[S]^T[H]^{-1}[S]$.

This equation is similar with the one of the structure movement equations when there is no water. The additional mass matrix $[M_p]$ concerned with hydrodynamic pressure has nothing to do with the disturbing frequency. Once $[M_p]$ is formed and joins the structure mass matrix to get $[M^{**}]$, it will be the same as the structure analysis method without water. So, this practical method assuming the water uncompressed is widely adopted in the engineering seismic analysis.

2.3 *The solution of free vibration characteristic and dynamical response*

When the structure is under free vibration, the generalized character equation is:

$$([K]-\omega^2[M^{**}])\{\delta_0\}=0 \tag{10}$$

Generally, as to the hydraulic structure, we only need to solve several lower frequencies and the relevant vibration modes. The direct frequency-filtering method can be employed based on the iterative method [4].

We can adopt mode-decomposed response spectrum method to solve the structure dynamic response, with which we can use the standard design response spectrum directly, and avoid the difficulty to choose the recording of the seismic acceleration.

When we calculate the seismic response with the response spectrum method, we should first solve several lower modes and periods. With the periods and the design response spectrum diagram, we can get the response spectrum value β_i corresponding to each mode. Consequently, we can get the largest acceleration vector, the largest dynamic load vector, the largest displacement vector and the largest stress vector of each mode.

3 THE SEISMIC ANALYSIS OF LONGTAN DAM

The three-dimensional finite idealization of the bottom hole monolith of Longtan dam is shown in Figure 1. Water in the reservoir is up to EL.400.0m, and the dam top altitude is 406.5m. In the calculation, considering the dam site as type I field, we decide its character period is 0.20s and the dam concrete damp ratio is 8%. When conducting the dynamic analysis, we consider the effects of the horizontal earthquake that is vertical with the dam axial and the vertical earthquake. The earthquake responses can be obtained by the mode-composed method of SRSS, while the total response can be obtained through the root of the sum of squares of the horizontal response and the vertical one.

3.1 *The analysis of dam auto vibration characteristic*

Figure 2 shows the first five mode diagrams of the right brim of the bottom hole monolith, while table 1 shows the free vibration period (s), frequency (s^{-1}) and the modal participation factor of each mode.

From the results we can see that under the seismic loads, the lower modes of the bottom hole monolith are mainly oscillated horizontally and the higher ones are mainly vertical. The dam free vibration characters agree with the general law of the gravity dam.

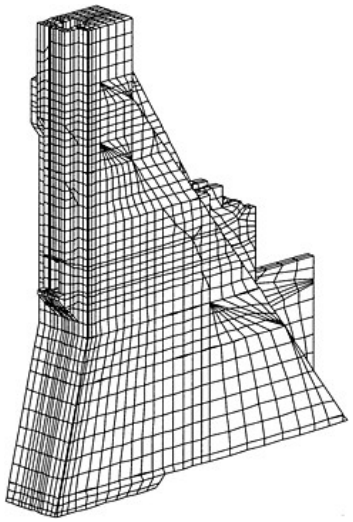

Figure 1. The three-dimensional finite idealization of the bottom hole monolith of Longtan dam.

Figure 2. The first five mode diagrams of dam.

3.2 *Dam displacement*

According to the free vibration periods, by using the response spectrum value β_i of each mode obtained by the design spectrum diagrams, and by adopting the mode-decomposed response spectrum method, we can get the largest displacement vector of each mode, and then combine them to get the dynamic displacement of dam.

Table 1 shows the dynamic displacement of dam peak, dam heel and dam toe of six different sections of the bottom hole monolith. We can see that the values of displacement of each section have little discrepancy, the deformations of dam agree with the law and the largest values all occur in dam peak.

3.3 *Dam stress*

The distribution of normal stress σ_x along the horizontal direction and the normal stress σ_z along the vertical direction in the section of bottom hole center are shown in figure 3 and figure 4. From the results we can see that under the seismic load, there is the stress centralization at the dam heel and dam toe, especially at the dam heel, where the largest vertical dynamic stress comes to 3.00 Mpa and has already exceeded the tensile strength of the concrete. However, since the seismic action is instantaneous, once the stress on the dam heel exceeds the tensile strength and

Table 1. Dynamic displacement of dam peak, dam heel and dam toe of six different sections (cm).

Section		Right brim	Right brake Frusta center	Bottom hole center	Left brake Frusta center	Introduction wall center	Left brim
Dam peak	u	3.70	3.69	3.69	3.69	3.69	2.89
	w	1.21	1.43	1.43	1.43	1.43	1.29
Dam heel	u	0.35	0.35	0.35	0.35	0.35	0.35
	w	0.42	0.44	0.44	0.44	0.44	0.42
Dam toe	u	0.35	0.35	0.35	0.35	0.35	0.35
	w	0.35	0.36	0.36	0.36	0.38	0.38

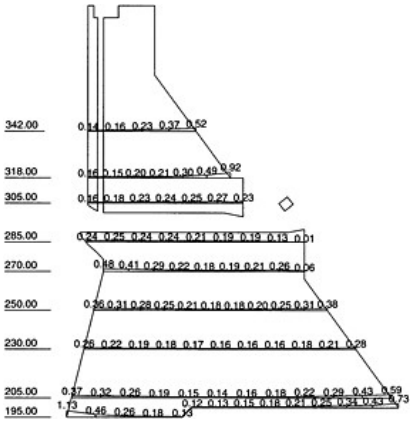

Figure 3. Distributing diagram of σ_x of the bottom hole center section (MPa).

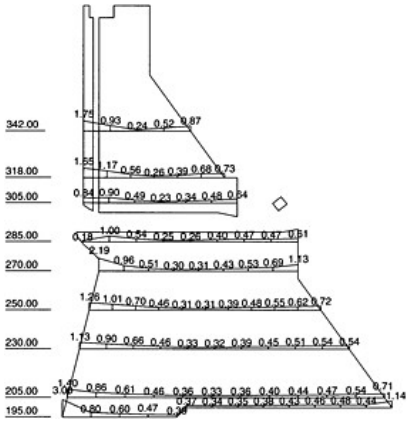

Figure 4. Distributing diagram of σ_z of the bottom hole center section (MPa).

appears little crack, the seismic load and the dynamic stress on the dam heel will decrease obviously, so it will not threaten the general safety of the dam.

4 CONCLUSIONS
CONCLUSIONS

The calculating results of the seismic analysis of bottom hole monolith of Longtan dam shows that the value of the dam dynamic displacement under the design seismic load is not large and has rather good law, and the dam stress basically satisfies the design demand except dam heel and the other locations. But it is important to note that under the seismic loads there is dynamic stress centralization to some degree at the parts where the geometry figure chops. Besides, in the fields near the upper course of the upside of the dam, the dynamic tensile strength of the rolling concrete is about 1.3 MPa, according to the design standard, while the calculating dynamic stress in these regions has exceeded this value, especially for the interface materials of rolling concrete whose tensile strength is lower in these fields. This requires adequate attention.

REFERENCES

[1] Zhang Qing, The semi-analysis of dam-water-foundation interaction, *shuilixuebao,* No. 10, 1991, 67–74.
[2] Jiang Hongdao, Chen Hequn, *The programmer design of FEM,* Hydraulic and Power Press, Beijing, 1986.
[3] Fu Zuoxin, *The analysis and the calculation of the mechanics problems in hydraulic structure,* Hohai University Press, Nanjing, 1993.
[4] East China college of water resources, *The FEM of the elastic mechanics problems,* Hydraulic press, Beijing, 1982.
[5] Wang liangshen, *The seismic dynamic analysis of concrete dam,* Earthquake Press, Beijing, 1981.

New Developments in Dam Engineering—Wieland, Ren & Tan (eds),
© 2004 Taylor & Francis Group, London, ISBN 04 1536 240 7

Analysis of monitoring results of foundation of Left-Bank Powerhouse of Three Gorges Project

Zhang ShuGuang, Yu SanDa, Zhu QuanPing
China Yangtze Three Gorges Project Development Corporation, China

ABSTRACT: It briefly analyses the basic information on foundation seepage flow and pressure and rock mass sedimentation deformation & horizontal deformation of founation rock mass, on which Left-Bank Powerhouse dam section No. 1 to No. 5 are based, during the construction of superstructure. The preliminary analysis shows that deformation of rock mass is reasonable and foundation anti-leakage and drainage facilities have achieved the anticipated effect. Principally the rock body behind the main drainage wall of the foundation is basically in dry condition. The seepage pressure of the dam foundation and the joint face of deep rock mass are far smaller than the designed value. The dam foundation seepage pressure is safe, and the structure runs normally.

1 GENERAL INTRODUCTION

Left-Bank Powerhouse Dam Section No. 1 to No. 5 are located at Left-Bank slope of Yangtze River in Sandouping of Yichang, Hubei Province, its left side is Left-Bank Non-overflow Dam Section, and right side is Left-Bank Powerhouse Dam Section No. 6 to No. 14. The floor elevation of the dam foundation gallery is EL.95m (EL.90m for the upstream foundation grouting gallery). Under the dam foundation two sets of drainage tunnel are set respectively vertical and horizontal to the mountain. The elevation of the floor space for the dam construction is EL.90m (EL.85m for dam heel key trench). The lowest elevation of the floor space for downstream Powerhouse construction is EL.22.2m. This shapes a rear-dam slope of approximately 54°, 67.8m in temporary height and 39.0m in permanent height. Especially, cracks of the gradual oblique angle are well developed elatively where Left-Bank Powerhouse dam section No. 3 is located, which makes the deep stability of the dam against sliding along the gradual oblique angle structure plane be an important technical issues, so the location becomes a key point. The property of the structure and the stability of high slope of foundation bing considered, monitoring facilities on deformation, seepage pressure and stress strain etc. have been installed.

2 STABILITY ANALYSIS

2.1 *Dam foundation sedimentation analysis*

63 pcs of precision benchmarks are set inside the foundation gallery (including upstream and downstream grouting gallery) and Drainage Tunnel 1 and 2 of the dam foundation. The earliest monitoring on parts of the benchmarks began in Oct. of 1998 and was continued till 2000 when fiducial value of all benchmarks was obtained. Those monitoring data demonstrated following sedimentation deformation and its distribution (see Figure 1).

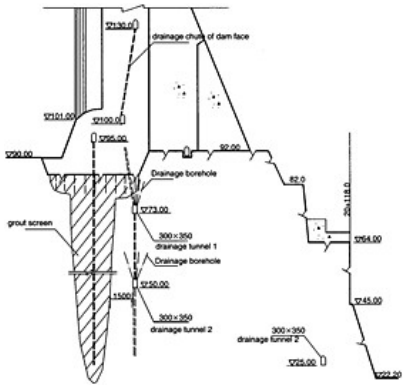

Figure 1. The sketch of the Left-Bank Powerhouse dam section 3 foundation cross section.

2.1.1 *Analysis of sedimentation displacement rule*

(1) Along with dam concrete placement and reservoir filling (raise), it makes the load on the foundation increased and the whole deformation of dam foundation trend to sink gradually. Up to Dec. of 2003, the monitored real maximum accumulated sedimentation deformation is 18.50mm, the specific numbers are as followed:

Items	Accumulated sedimentation displacement
Up-stream foundation gallery (EL.94m)	14.31mm to 18.50mm
Down-stream foundation gallery (EL.94m)	15.43mm to 17.33mm
Upstream grouting gallery (EL.90m)	13.33mm to 14.64mm
Foundation EL.74 (Drainage Tunnel 1)	12.43mm to 17.81mm
Foundation EL.50 (upstream tunnel of Drainage Tunnel 2)	9.64mm to 13.01mm
Foundation EL.25 (downstream tunnel of Drainage Tunnel 2)	8.28mm to 9.72mm

(2) The weight of the dam itself is one of the main effects, making the foundation sedimentate gradually and continuously. The largest quantity of concrete was poured in 2001, which made sedimentation increment of upstream and downstream foundation gallery (EL.94m) reach to 4.51mm to 5.05mm and 4.29mm to 5.26mm respectively, and the annual deformation increment became biggest too. Along with completion of massive dam concrete placement, the deformation rate was decreased obviously (see Figure 2).

(3) The reservoir impounding has great impacts on foundation sedimentation. Along with the reservoir load increasing rapidly when water level reached to 135m from May to June of 2003, the dam foundation sedimentation deformation rate increased obviously (see following chart). After reservoir impounding, the rate of sedimentation deformation for dam foundation decreased. During reservoir impounding to water level 135m, the foundation sedimentation deformation increment are as followed:

Items	Sedimentation deformation increment
Up-stream and down-stream foundation gallery (EL.94m)	5.40mm to 6.29mm
Upstream grouting gallery (EL.90m)	4.63mm to 4.86mm
Foundation EL.74 (Drainage Tunnel 1)	4.80mm to 5.37mm
Foundation EL.50 (upstream tunnel of Drainage Tunnel 2)	4.02mm to 4.67mm

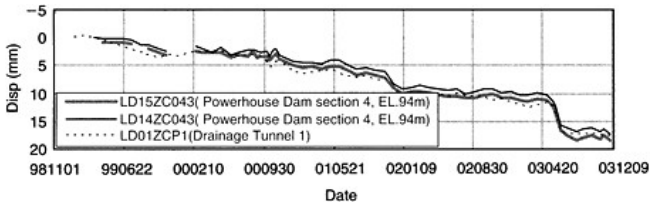

Figure 2. Procedure line of settlement displacement for part of precision benchmarks on dam foundation.

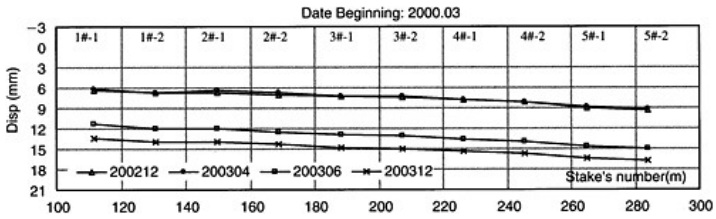

Figure 3. The distribution graph of vertical displacement for downstream foundation gallery EL.94m on dam section 1 to 5.

(4) Reservoir impounding has few impacts on Foundation at EL.25 (downstream tunnel of Drainage Tunnel No. 2), for it is low and relatively far from dam axis, sedimentation there changed from only 0.53mm to 1.14mm.

2.1.2 *Sedimentation deformation distribution rule analysis*

(1) It has the distribution rule along the dam axis from left to right, that the sedimentation at the same elevation during the same period changed from small value to big value (see figure 3), which is related to the whole section of construction floor space lying at a variable slope landform, different concrete pouring depth and load distribution.
(2) During concrete placement, along the same cross section at different elevation, it basically trends to sink down synchronously. During the period of latter reservoir impounding and reservoir operation, the sedimentation deformation at the upper is a litter bigger than that at the lower (see 2.1.1).
(3) There is no uneven (unequal) settlement deformation for adjacent dam sections. Followed table gives the accumulated settlement displacements difference for different elevations. It can be seen that only one difference reaches to 1.3mm, larger than 1mm.

Items	Accumulated settlement difference
Up-stream and down-stream foundation gallery (EL.94m)	0.04mm to 0.84mm
Upstream grouting gallery (EL.90m)	−0.61mm to 0.34mm
Foundation EL.74 (Drainage Tunnel 1)	0.26mm to 1.30mm
Foundation EL.50 (upstream tunnel of Drainage Tunnel 2)	0.31mm to 0.55mm
Foundation EL.25 (downstream tunnel of Drainage Tunnel 2)	0.25mm to 0.63mm

2.2 *Dam foundation horizontal deformation analysis*

2.2.1 *Pendulum wire monitoring results analysis*

Two sets of direct inverted pendulum are respectively set in the first dam block of the second part of powerhouse dam section No. 1 and section No. 5. Two sets of inverted pendulum are respectively

set in the second dam block of the second part of powerhouse dam section No. 1 and section No. 5. Taken the elevation 34m or so as the relative base level for calculating displacement, the horizontal deformation of dam foundation is monitored as follows mainly:

(1) As the whole, the deformation on both banks is slender and the tendency law of deformation is not obvious. For the moment, the deformation along the U/S-D/S direction changes from −0.85mm to 0.57mm and the deformation horizontal to axis of dam changes from −0.77mm to 0.29mm. These deformation values are lower than 1.0mm.
(2) The deformation along U/S-D/S direction tends to air face because the inverted pendulum of the elevation 94m in the second dam block of powerhouse dam section 1 and 5. Moreover, range of deformation of section 5 is higher than that of section 1, but both are less than 1mm. The law of deformation for the first dam block with section 5 are the same as section 1 before Dec. 2002 and after reservoir filling in June 2003. Section 5 was deformed towards D/S with the max. horizontal displacement up to 1.08mm while section 1 deformed was deformed towards U/S with the max. horizontal deformation up to −1.16mm from Dec 2002 to June 2003 (see figure 4).
(3) After reservoir was impounded to EL.135m, the dam foundation had a short time tendency to move upstream. It's around 0.5mm.
(4) Along the dam axis, the deformation in different places mainly trended to right side. It is probably because the dam base lies at the bank with a variable slope.

2.2.2 *Stretched wire monitoring results analysis*

Two sets of stretched wires are set individually at chainage 20+016m of drainage tunnel No. 1 at elevation of 74m and at chainage 20+034 of the downstream foundation gallery at EL.95m. Monitoring data on all stretched wire began in April of 2003 and most of the deformation value are less than 0.5mm. The property of deformation is as follows:

(1) Foundation gallery at elevation 94m (ch20+034) close to rear-dam slope: The deformation value of each dam section is plus ("+"), meaning moving towards upstream. At present the deformation is within 0.01mm and 0.55mm.
(2) Drainage gallery No. 1 at elevation 74m (ch20+016) located dam heel area: The deformation value of each dam section is minus ("−"), meaning moving towards downstream. The horizontal deformation is within −0.46mm and −0.23mm.

2.3 *Analysis for surface layer rock deformation on the rear-dam slope*

Along with the consrtuction of dam & the powerhouse and the slope concrete pouring, the line of sight for observation was obstructed. Except that vertical displacement observation for points No. 2, No. 4 and No. 5 on platform EL.92m has been continued, most monitoring points on the slope were dismantled or observation was interrupted. Recently it came back to take horizontal

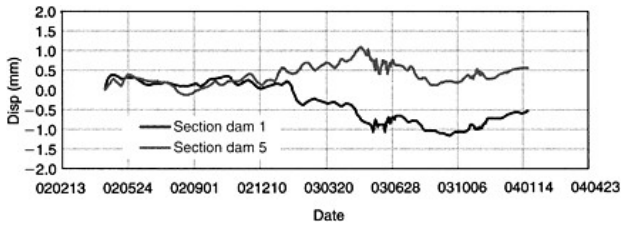

Figure 4. Deformation vertical to dam axis on Left-Bank Powerhouse dam section 1 to 5.

displacement observation for those 3 points mentioned above. The main characteristics of the deformation are as follows:

(1) Effected by excavatation for unit pits of the Powerhouse and dam concreting etc. during the period of construction, the horizontal displacement has priority to move to the free face downstream. Before observation being halted in Nov. 2000, the max. accumulated displacement to downstream is monitored to be 15.08mm, and deformation to downstream free space for points No. 2, No. 4 and No. 5 on platform EL.92m are 2.87mm, 1.65mm and 2.16mm respectively. Up to Feb. 2004 after observation was recovered in Jan. 2004, the deformations for those 3 points increased to 4.95mm, 5.79mm and 8.37mm respectively.

(2) Due to load release when excavating bedrocks, rock mass relaxation and ground stress release, it was shown that the vertical displacement during excavation period was mainly springback. The max. springback is around 6mm. For dam concreting was started in 1998, the up-load on foundation rock mass added and the monitored points began to sink. From Aug. 2000 to Aug. 2001, the rock mass averagely sank 4.5mm and the deformation came to 6mm when reservoir impounded to EL.135m. At present, the accumulated sedimentation for the above 3 points is 16.02mm, 17.40mm and 19.77mm respectively. The general deformation laws, deformation quantity for all monitored points are consistent with those points on the same cross section of the dam base.

2.4 *Analysis for deformation of borehole inclinometers*

The deformation of deep layer rock mass for side slope of dam foundation is continuous and no obvious mistach has been found there during the construction period of the Left-Bank Powerhouses dam section No. 1 to No. 5. The measured relative deformation of inclination survey hole moving toward to free face is less than 1.0mm generally and the max. value is not greater than 1.8mm. The max. accumulated displacement of borehole exbort moving toward to free face is 11.4mm. These deformation took place during early period of construction. Now the deformation is stable basically (see figure 5 and chart 1).

Following with the data of the borehole inclinometer, the deformation increment of dislocation moving toward to free face for inclinometers is less than 0.2mm generally during reservoir impounded to elevation 135m. This shows that the deformation of the side slope is not obvious and the side slope is stable.

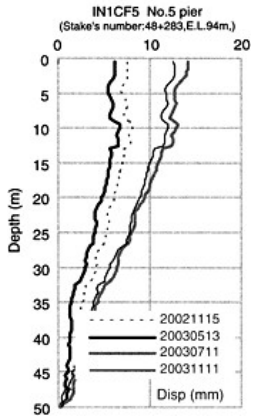

Figure 5. Distribution curve of displacement at IN1CF5.

Chart 1. The result table of borehole inclinometer.

Number of borehole inclinometer	IN1CF2#	IN1CF5	IN1CF3#
Position	Pier 2	Pier 5	Monitoring tunnel 1
Deformation of "AA" (mm)/depth (m)	0.92/16.5	0.89/12.5	0.89/42.0
The deformation moving toward to fair face	Without obvious mistach, the dislocation deformation is less than 1.0mm and the accumulated deformation of borehole export is 2.12mm.	The dislocation deformation is less than 1.0mm and the accumulated deformation of borehole export is 11.4mm.	Without obvious mistach, the max dislocation deformation is less than 0.89mm and the accumulated deformation of borehole export is 6.81m.

Notes: The direction "A" means the max. displacement of dislocation moving toward to free face.

2.5 *Analysis on monitoring materials of dam foundation seeping*

2.5.1 *Dam foundation seepage flow and pressure*

The construction floor space for Left-Bank Powerhouse Dam Section No. 1 to No. 5 is around 80m to 90m. It is arranged with main seepage proof curtain and main drainage curtain on the upperstream dam foundation and arranged with closing cut-off and drainage curtain on the downstream dam foundation. At both ends, horizontal secondary drainage gallery and hole-curtain are arranged respectively at Left-Bank Powerhouse dam section 7 and Left-Bank non-overflow dam section 17, forming closing drainage-area. Two layers of drainage tunnels are arranged parall to the dam axis in the dam foundation rock mass. In these tunnels drainage curtain are set to drain fully the seepage flow of dam foundation.

(1) Seepage pressure at the foundation base of dam

It mainly uses piezometer pipe to observe the seepage pressure of the dam foundation of Left-Bank Powerhouse Dam Section 1 to 5. The U/S side of seepage proof curtain axis, inside main drainage curtain, on the upperstream and downstream dam foundation gallery of dam section 1 to section 5 is fixed a piezometer pipe respectively, 20 pcs in total.

Before reservoir impounding in May 2003, the water level in front of the dam was below the construction floor space, 4 piezometer pipes were dry, water level in the others were under the level of the gallery floor. After reservoir impounding, piezometer pipes at main drainage curtain of Left Bank Powerhouse Dam section 3 were still dry, water level of the other piezometer pipes at the upperstream of seepage proof curtain raised a little. Up to Dec. 2003, 6 of the 10 piezometer pipes at the up-stream and down-stream foundation gallery were dry. The other 4 have water inside, but all water level were under the floor of the gallery, the same or a little bit slow down than that before reservoir impounding. This showed that these piezometer pipes may not be penetrated, the water inside was dead, which didn't present the dam foundation seepage water level.

After reservoir impounding, the monitoring results showed that:

(a) The water level of the piezometer pipes at the main drainage curtain in Left-Bank Powerhouse Dam Section 1 and 4 were very low, and basically no change (see figure 6).
(b) The water level of the pipe H02CF02 in Left-Bank PowerStation Dam Section 2 was raising all the while until coming to EL.100.96m in Dec. 2003. It raised around 16m.
(c) The water level of the pipe H02CF05 in Left-Bank PowerStation Dam Section 5 raised rapidly and came to EL.111.4m in Aug. 2003. It raised around 30m. After taking television inspection inside the hole, no concentrated penetration was found. But there were many cracks on the rock mass. Another drainage hole was made in Aug. 2003 30cm right of the hole H02CF05 and got a drain quantity about 0.061/min, which made the water level in pipe H02CF05 slowed down about 21m and basically not changed latter (see figure 6).

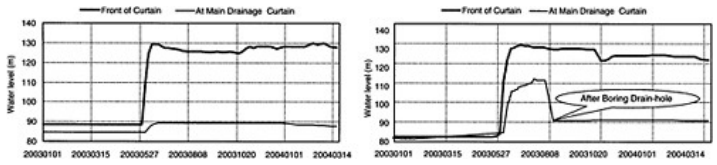

Figure 6. Water level proceeder line of piezometers pipe at section 4 and 5.

(d) Up to the end of 2003, the coefficient of reduction for seepage uplift on the dam base basically kept under 0.25.

(2) The water level of the piezometer pipes in the drainage tunnel

The piezometer pipes in Drainage Tunnel 1, setting inside the main drainage curtain, were 10m deep. The pipes in Drainage Tunnel 2 were all 5m deep. All the piezometer pipes in Drainage Tunnels were set vertically. The real groundwater monitoring showed:

(a) In Drainage Tunnel 1 the water level in piezometer pipes mainly reflected the range of the groundwater level at the drain wall. After reservoir impounding, except the water lever at Dam Section 4 H06CF was about 1.5m higher out of the edge, all water level in the other pipes were under the bottom of the tunnel.
(b) In Drainage Tunnel 2, except few of the piezometer pipes, water level in all the others raised no more than 6m after reservoir impounding.

2.5.2 *Seepage quantity of the dam foundation*

Closing drainage method was taken for the foundation of Left Bank Power Station dam section. Main drain hole was set inside the foundation grouting gallery. The drain holes in drainage tunnels were not only vertically downward, but also some ones in Drainage Tunnel 2 were vertically upward. The real monitoring showed there were no seepage spillage from the main drain holes inside the foundation grouting gallery, only the some seeping in drain holes in Drainage Tunnel 1 and Drainage Tunnel 2. After reservoir impounding, the leakage flow in Drainage Tunnel 1 was only 1.691/min, and only 11 of the 129 drain holes were seeping. This showed the foundation above EL.75m was basically in dry situation. Drainage Tunnel 2 was at a lower elevation, there were about 395 of the 440 drain holes seeping, and the leakage flow was only 9.21/min after reservoir impounding, a little increasing than before.

On all accounts, integrating the monitoring results of foundation seeping pressure and leakage after reservoir impounding, it could say:

(a) The facilities for dam foundation anti-leakage and drainage reached the anticipated effect. The rock mass behind the main drain wall was basically in dry situation. The water level in piezometer pipes of the main drain wall at Dam Section 2 and Dam Section 5 were relatively high. But this is local phenomenal, and mainly due to seepage from local fractures. Most of the piezometer pipes in foundation gallery behind main drain wall were dry holes, which showed generally no seeping pressure for this part of foundation.
(b) Principally the seeping pressure at the dam foundation and the deep rock mass structure was far smaller than the designed one. The foundation seepage was safety.

2.6 *Stress monitoring of anchor rod*

Two anchor rod stress meters were set on rear dam slope at Non-penstock section 2 and Non-penstock section 5 respectively. The characteristics of anchor rod stress ranging are as follow:

(1) For the moment, the anchor rod stress meters are basically in compressing condition. The max. compressed stress measured at RC1CF2 EL.88.5m in pier 2 is −70.28 Mpa and reasonable.

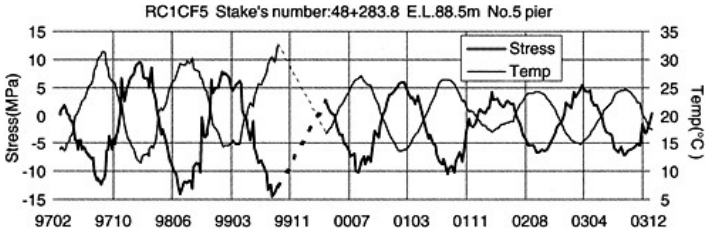

Figure 7. Stress and temperature-time procedure line of RC1CF5.

(2) The dam heel slope didn't bear large load. The air temperature had great impact on anchor rod stress change. The max. range in 2003 reached 12.94Mpa.

The typical stress process of anchor rod stress meters in the PowerStation and Dam section might be divided into 3 types. The first type is stress inverse to temperature, which had the property when the rock mass temperature is higher, the stress of anchor rod bocomes smaller (see figure 7). Secondly is stress-temperature direct ratio, the anchor rod had the property when the rock mass temperature is higher the anchor rod stress becomes higher, vice versa. The third is anchor cable installation impact type. When the anchor cable is restrained, the stress of anchor rod decreased rapidly. The reason is the anchor cable compress the rock mass which lead the anchor rod compressed. Latter due to the impact of temperature, the stress ranges periodically.

3 CONCLUSION

Analysed monitored results of the high slope of Left-Bank Powerhouse Dam Section No. 1 to No. 5, it demonstrates that:

(1) During construction period, the deformation of deep rock mass in the foundation slope changes continuously and no obvious mistaching has been found. The deformation was formed mainly at the beginning of the construction. Reservoir impounding to 135m had no obvious impact to the deformation of deep rock mass. The deformation basically trends to be stable at the moment.
(2) The slope anchor cable stress trend to be stable. The anchor rod stress meters are basically in compressed condition. The tensile stress is small. The anchor rod has no big load at moment. Anchor rod stress ranges periodically with the impact of the air temperature.
(3) The facilities for dam foundation seepage prevention and drainage have reached the anticipated effect. The rock mass behind the main drain wall is basically in dry situation. The water level in piezometer pipes of the main drain wall at Dam Section 2 and Dam Section 5 are relatively high. But this is local phenomenal, mainly due to seepage from local fractures. Principally the seeping pressure at the dam foundation and the deep rock mass structure is far smaller than the designed one. The foundation seeping is safe.
(4) Due to the impact of concrete placement, the deformation of dam foundation trends to settle gradually, and the deformation rate is related to the concrete placement intensity. During the reservoir impounding to EL.135m, the settlement increased markedly, the max. exceeds 6mm. There is no uneven sedimentation happen. The uneven sedimentation in adjacent dam section is basically smaller than 1mm. The deformation ratio be obviously intend to slow at moment.
(5) Foundation horizontal displacement is not abnormal, the accumulated displacement were all less than 1mm, and the tendency is not clear. Under the present operation condition, the foundation is stable.
(6) The foundation geological structure is complicated and the operation condition will change frequently, therefore it is necessary to take continuous monitoring and make a further analysis.

New Developments in Dam Engineering—Wieland, Ren & Tan (eds),
© 2004 Taylor & Francis Group, London, ISBN 04 1536 240 7

Design and practices of Tianshengqiao-1 concrete faced rockfill dam

Zhan Zhonglan, Feng Yelin & Wang Yuanliang
Kunming Investigation, Design and Research Institute, State Power Corp. of China,
Kunming, Yunnan, China

ABSTRACT: Tianshengqiao-1 concrete faced rockfill dam was completed in 2000 and has been operated normally for 4 years. Instrument data show that the dam is safe. This article generalizes the design, construction, and operating experiences and probes into the design experiences of high concrete faced rockfill dam, these experiences modify, supplement and improve the traditional design concept.

1 NATURAL CONDITIONS

The Tianshengqiao-1 hydropower station is located on the mainstream of Nanpan River upstream the Hongshui River, it is the first stage of Hongshui River. Anlong county of Guizhou and Longlin county of Guangxi locate at the left and right bank of the dam site respectively.

At the dam site, river valley is wide and water flows moderately slowly, the river valley appears to be an unsymmetrical and longitudinal valley.

Dam foundation at right bank is of limestone and sandstone interbed, with weak interlayer of thin mudstone and extremely thin mudstone. Rock formation goes almost parallel with the river flow and inclines to the left bank.

Dam foundation at the left bank is of mudstone and sandstone interbed, the rock formation inclines to the mountain, the inclination angle is 35~45°.

Total reservoir capacity is 10.26Gm^3, installed capacity is 4×300MW. The project is mainly for power generation. The dam is designed for a flood in 1000 years (p=0.1%), and checked by possible maximum flood (P.M.F).

The reservoir design flood level (p=0.1%) is 782.87m; check flood level (P.M.F) is 789.86m; normal water level is 780.00m; dead water level is 731.00m.

2 DESIGN

2.1 *Layout of main structures*

Main structures comprise of concrete faced rockfill dam, spillway, emptying tunnel, power generation tunnel and powerhouse. The dam is 178m in height with crest length of 1104m, "Z" shaped dam access is located on downstream dam slope. Spillway is located on saddle-back of right bank and emptying tunnel is located at the right bank. The power generation structures are located at the left bank with four tunnels and four turbines, the installed capacity is 4×300MW.

2.2 *Design of dam section*

According to experiences from the already built projects, the dam width is proposed to be 12m, upstream dam slope ratio is 1(V):1.4(H), the downstream general slope ratio is 1(V):1.4(H), dam slope angle between road is 1(V):1.4(H).

2.3 *Division of dam body and design of dam materials*

The total rockfill quantity for dam of Tianshengqiao-1 is $18\times10^6m^3$, the excavation materials can be used for rockfill is about $14\times10^6m^3$, which is about 87% of the total quantity. Inside which soft rock of $4.8\times10^6m^3$ (1/4 of the total rockfill quantity) will be used. The rockfill area of the dam is divided into different areas: cushion area, transitional area, main rockfill area, secondary rockfill area and soft rock area.

Horizontal width of cushion area (IIA) is designed to be 3m, during the rockfilling, that above El. 768m is changed to be 2m, and 0.3 H (H is water head) is extended downstream at the cushion area of the dam foundation. Horizontal width of the transitional area is 5m and increases to 6m at above El. 768m. Main rock stock area (IIIB) is at the upstream of dam axis; secondary rock stock area (IIIC) is of sand-mud stone at above El. 660m, its upstream border overlaps with the dam axis; secondary rock stock area (IIID) is of limestone, all is IIID downstream of dam axis except IIIC area.

Cushion materials: the cushion materials employ fresh limestone which has been crushed twice. As required by cushion materials' function and mechanical construction, its horizontal width is designed to be 3m, maximum gravel diameter is 8 cm, that <5mm is 35% ~55%, that <0.1mm is 4%~8%, gradation is continuous; seepage parameter is $(2\sim9)\times10^{-3}$ cm/s, void content is 19%, design dry density is 2.2 t/m^3, filling coverage layer is 40 cm thick.

Transitional materials: transitional materials are from blasting operation of stockyard. Its width is designed to be 5m, maximum gravel diameter is 30 cm, that with a gravel diameter less than 0.1mm will not be over 5%, seepage parameter is $(2\sim9)\times10^{-1}$ cm/s, void content is 21%, design dry density is 2.15 t/m^3, filling coverage layer is 40 cm thick.

Main rock stock materials: main rock stock materials employ limestone from excavation of spillway, maximum gravel diameter is 80 cm, that <5mm is less than 20%, that <0.1mm is less than 5%, and that <25mm is less than 40%, seepage parameter is (3~10)×10°cm/s, void content is 23%, design dry density is 2.1 t/m^3, filling coverage layer is 80 cm thick.

Secondary rock stock materials: secondary rock stock materials employ big blocks of lime-stone from excavation of structures, maximum gravel diameter is 160 cm, gradation is not specified, void content is 24%, design dry density is 2.05 t/m^3, filling coverage layer is 160 cm thick.

Soft rock: soft rock employs sandstone and mudstone mixtures from excavation of each structure, maximum gravel diameter is 80 cm, that <0.1mm is not over 8%, seepage parameter is not less than 10^{-2} cm/s, void content is 22%, design dry density is 2.15 t/m^3, filling coverage layer is 80 cm thick.

2.4 *Faced slab*

According to the undertaken water head, formula of the faced slab thickness is T=0.3+ 0.0035H (H is the vertical height from section to top of faced slab), space between vertical joints of faced slab is 16m, there are altogether 69 pieces. The faced slab shall be placed in 3 different stages, elevation at different stages is 680m and 746m.

Grade of faced slab concrete strength is C_{25}, anti-seepage grade is S_{12}, anti-freezing grade is D_{100}, water cement ratio is not greater than 0.5, slump is 4~8 cm, reinforcement bar shall be laid in a single layer and in two directions, the bar content is 0.3~0.4%. Reinforcement bar shall be laid in a single layer and in two directions, the bar content is about 0.3%.

2.5 *Toe slab*

Foundation of toe slab is mostly located 2m under the weakly weathered top line. Width of toe slab is decided according to the allowed seepage gradient ratio (J=15). Width of toe slab is 10m, 8m and 6m respectively, thickness is 1.0m 0.8m, 0.6m respectively.

2.6 *Joint and water stop*

Three water stop are laid in the peripheral joint, which are the bottom water stop copper sheet, middle water stop below El. 680m is sheet copper and above El. 680m is PVC strip, fly ash and powder fine sand shall be filled into the top joints.

Vertical joint of faced slab at the right and left dam abutment is tension joint and at other places is compression joint. A sheet of copper water stop is laid at each bottom of the two joints. Fly ash is added to the top of tension joint.

3 AREA DIVISION AND PERIODS OF CONSTRUCTION

See Table 3.1 and Figure 3.1.

Table 3.1 Filling process of dam body in different stages.

Stage	Construction period	Filling process	Work quantity (10^6m^3)	Average speed (10^6m^3/month)
1	Jan. 15, 1996~May 20, 1996	El. 635m~642m of river bed left bank El. 662.5m and right bank El. 660m	1.33	0.312
2	May 21, 1996~Nov. 10, 1996	Left bank El. 673m and right bank El. 725m	2.90	0.62
3	Nov. 11, 1996~June 20, 1996	725m section passing flood	4.10	0.54
4	June 21, 1997~June 20, 1998	768m section passing flood	5.55	0.40
5	June 21, 1998~Jan. 31, 1999	All section to 787.3m	2.60	0.36

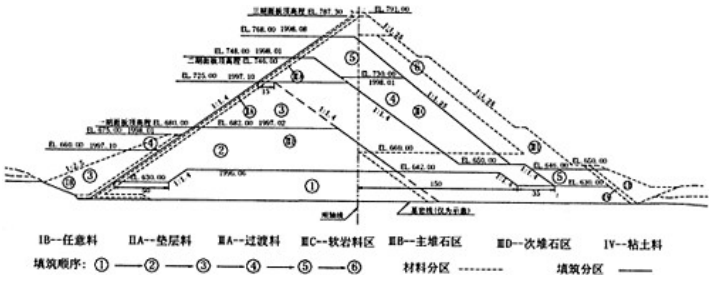

Figure 3.1 Embankment zoning of face slab rockfill dam for Tianshengqiao-1 hydropower station.

4 OPERATIONAL STATE

Dam seepage had two peak values respectively reaching 165 L/s on October 3, 2000 (rainfall on dam area is 56.1mm on October 2) and 183 L/s on October 8, 2003 (rainfall on dam area is 95mm on October 7). In case reservoir level is about 770m, observed seepage in most time is approximately 80 L/s.

In general, dam deformation of Tianshengqiao is normal compared to other completed projects. Seepage is smaller and dam is operated satisfactorily.

4.1 *Cracks on slope surface of cushion materials*

Cracks appear on slope surface of cushion materials. Due to deformation of embankment, prior to placement of faced slab, deficit slope appears on slope face of cushion materials, which originally reached designed line of slope with corresponding protection. Quantity of deficit slope for placement of stage-2 face slab is within 30~50 cm, for stage-3 face slab is 49~68 cm and on local place is over 100 cm.

37 cracks were found on slope face of cushion materials in December of 1998. Cracks occurred on left bank at the Chainage of 0+954 m~0+478m and within the height of 748m~768m. Strike of cracks is divided into two types, namely, inclined crack having a maximum length of 40m and maximum width of 27mm and horizontal crack having a maximum length of 400m and maximum width of 150mm, both of them are almost vertical. Cracks are mainly caused by large deformation of rockfill.

Reasons for large deformation of rockfill are: in order to pass flood season, sectional filling is carried out for dam in dry season according to requests for passing flood season and two banks are filled in flood season. It causes transverse and longitudinal high filling differences along dam and results in large differential settlement; filling strength is not steady during construction and it is higher in a short period of time. For instance, monthly filling strength had reached 1.17 million m^3 and daily strength had been over 40000m^3. This caused concentrated deformation. Because filling strength in peak time is higher than average strength (50,0000m^3~55,0000m^3/month). And, there is not sufficient rolling equipment or dozer, so rolling is not conducted according to specified rolling parameters. Soft rock materials are mudstone excavated from structures, but slightly weathered or fresh rock is required in design. And, materials are not carefully selected. This causes large variety of the physical mechanics, especially the compressibility. Additionally, actual filling quantity of soft rock materials is increased compared with originally designed quantity, so settlement volume is increased accordingly.

4.2 *Crack of faced slab*

Investigation before January of 2001 suggested there are 1300 cracks in total, in which 355 cracks are more than 0.3mm wide and maximum width is 4mm. In two faced slab investigated, the crack is respectively 34 cm and 10 cm deep. The thickness of corresponding faced slab is 45 cm. In April~July of 2002, faced slab above the elevation of 748.6m was investigated again and 4537 cracks were found (including branch cracks), in which 61% of total are newly developed cracks. Total length of cracks is about 22000m; length of single crack is below 10m. 80 cracks are more than or equal to 0.3mm wide. Maximum depth is 41.7 cm, which has penetrated the thickness of faced slab. Crack group has general descending direction from both sides of bank to the riverbed.

In addition to initial temperature stress, main reason why cracks caused on faced slab is deformation of cushion materials and rockfill. As abovementioned, large deficit slope of cushion materials occurred in time of filling, and materials additionally filled were too thick while compaction on slope was unfavorable. Interface between old and new face was not closely bonded, which formed a weak layer on slope surface. After cracks were found on faced slab, observed dry density is 2.08 g/cm^3 (design value is 2.2 g/cm^3), the corresponding porosity is increased from 19% to 26%. It shows cushion materials on bottom of faced slab where crack occurred are loose, compressibility modulus is low and deformation is large. As above described, one of a reason is deformation of rockfill. Besides, because concrete pouring of faced slab is conducted immediately after filling of dam, this does not keep away from peak hours of deformation of rockfill. This is one of the reason causing cracks on face slab.

4.3 *Empty between faced slab and cushion materials*

Investigation suggested the top of most slabs on each stage is emptied from cushion materials. The numbers of emptied faced slab account for 85%, 85% and 52% of faced slab on various stages. Maximum emptying height is 15 cm and detectable depth is 10m. In June of 2002, geophysical prospecting detection was carried out on face slab above elevation of 760m at Chainage 0+446m~1+038m. An area of 27805m^2 was prospected. The results show there is 64 emptying area among 34 faced slabs, total emptying area is 8314m^2 and maximum area of single slab is 400m^2. Emptying height is 1cm~5cm, in which 8 emptying area has 4cm~5cm height.

The reason is that deformation of concrete and rockfill is not compatible while there is large deformation of cushion materials and rockfill.

4.4 *Local damage of concrete on vertical joint of faced slab*

On July 18, 2003, damage was found on joints L3 and L4 of faced slab of dam. The damage extends downward to water face from bottom of wave wall on slab L4 (EL. 757.18m) with exposed reinforcement on local place of slab. Damage part has an average width of 1m and maximum width of 1.58m. Further investigation was carried out in July 25. It was found concrete damage at the elevation of 781.5m and 786.14m is serious, copper seal is damaged in local places and separated from concrete in local place. Underwater investigation showed damage face extends below water surface to EL. 752.92m. This was temporarily repaired in time of impounding and passing flood season in August of 2003. During repairing, further investigation on underwater conditions suggested damage extended to EL. 748m, in which damage on EL. 754m~748m is wide with maximum width of 3.5m while a crushed zone as wide as 0.5m~0.9m was found. Thickness of concrete in crushed zone is 5 cm.

Main reason is deformation of dam. The slab moves to riverbed along with rockfill of dam to press slab on middle of riverbed, but vertical joints on the middle part are only painted with thin layer of asphalt emulsion in joints and this joints belong to hard joints. This saved a large amount of potential strain energy. Finally, the energy cracked and released causing damage of concrete in local places. Impounding operation in 2003 showed there is no clear difference on seepage in time of damage of faced slab and after repairing works on damage. So, damage of faced slab causes no impacts on safety operation of dam.

5 SUMMARY OF EXPERIENCES

Due to difference on properties of anti-seepage faced slab and rockfill, two materials deforms inconsistently. In order to ensure rockfill's effective support on faced slab, deformation of rockfill (especially the uneven deformation) shall be seriously under control. Uneven deformation is mainly caused by property difference of filling materials and uneven loads. To control deformation in a reasonable scope, further studies shall be conducted in the following aspects:

(1) Requests on zoning and materials of high dam: properties of filling materials, zoning, filling standard and constructional partition shall be comprehensively considered according to stress deformation characteristics of dam. In use of dam materials, humidification, creepage and variation in storage and conveyance shall be fully considered while zoning of dam materials and filling zoning shall be jointly considered to reduce uneven deformation of dam on various stages.

(2) In addition to conventional testing, studies shall be conducted for gradation of cushion materials on grain contents of fine materials (<5mm) and extra fine materials (0.1mm) combined to permeability coefficient. Studies show only when grain contents (<5mm) >35%, permeability coefficient can reach 10^{-3} cm/s, but when grain content is increased from 0 to 10%, a grade of permeability coefficient is reduced. It shows the more the fine grain size is, the smaller the permeability is. But compressibility is increased. The most important requirement on cushion materials is reduce compressibility to prevent deformation of faced slab. So, the value of fine grain content shall be determined taking account of requests on compressibility and permeability

(3) Cracks of face slab include temperature cracks and structural cracks. Structural cracks are caused by bending or pulling of faced slab due to uneven deformation of dam while stress exceeded tensile stress of concrete. Temperature cracks can be avoided or reduced by improving concrete's properties, restricting conditions and strengthening curing of concrete. And, measures such as optimizing selection of placing time of faced slab or water-spraying curing of concrete can prevent temperature cracks. Preventative measures for structural cracks mainly include control of dam's deformation and improvement of faced slab's stress. Either temperature crack or structural crack cannot be avoided. But structural cracks have more harm than temperature cracks. So, crack resistance shall be improved via properties of materials and structure. According to observed value by re-bar stress meter embedded in dam, it shows stress is undertaken by reinforcement. Arrangement of reinforcement for Tianshengqiao has two types i.e. ② double layer reinforcement, the upper and lower protective layer is respectively in 10 cm and 5 cm. But cracks occurred on faced slab with such arrangement of reinforcement. And cracks on location protected by double layers of reinforcement are within 10 cm; it suggested the reinforcement restricted the cracks. Crack depth of other parts are not observed because they are submerged into water. So, further studies shall be conducted on location and numbers of reinforcement establishment.

(4) The standard of passing flood season matching the high dam is relatively higher, so embankment quantities of each stage are large. Requests on passing flood season shall be properly coordinated with embankment procedure of dam in stages to avoid transverse or longitudinal uneven settlement. Meantime, time for placement of rockfill and concrete of faced slab shall be properly arranged to prevent large deformation of dam. Construction organization shall be optimized to fill dam in balance. Construction shall be carried out strictly according to filling parameters while rolling standard of rockfill for high dam shall be increased.

(5) Cohesionless material is used on seal top of peripheral joint and tensile joint. The materials are matched to fine cushion layer II AA on bottom of joint, which has self-curing function. The operation of dam and 1:1 simulated model test suggest it is a preferable way for water seal.

New Developments in Dam Engineering—Wieland, Ren & Tan (eds),
© 2004 Taylor & Francis Group, London, ISBN 04 1536 240 7

Dynamic design for high slope treatment for left bank underground power house intake of Longtan hydroelectric project

Zhao Hongmin, Dai Qianxun, Deng Xiangyang, Zhou Haihui & Feng Weiqing
Mid-South Design & Research Institute for Hydroelectric Projects, Changsha, P.R. China

ABSTRACT: The high slope treatment for left bank underground powerhouse intake of Longtan hydroelectric project is one of the important technical issues for the project construction. The excavation and strengthening scheme was determined after pre-exploration, lots of scientific experiments and stability study having been carried out. Furthermore, emphasis was placed on strengthening dynamic design and control for the project in the period of the construction. This paper gives a brief introduction for the slope geological conditions, outline of the design general situation, dynamic design concept and procedures and the dynamic design and control for the project in the construction practice.

1 INTRODUCTION

The arrangement area of the left bank underground power house intake of Longtan hydroelectric project is located nearly to the natural slope in which a bending and titling deformation occurred with a vertical depth of 30~76m and a volume of 12,880,000m^3 of titling deformation. The left bank titling and creeping rock mass has linked together with the water intake high slope, which is a typical antithetic lamellar structure rock high slope with a height of excavated slope of 435m and a slope area of 270,000m^2; nine (9) diversion tunnels with a diameter of 12~13.35m have already been excavated at the toe of the slope. The water intake dam section is located closely to the rock slope, and the stability of the dam is depended upon the slope rock mass, in addition, the deformation of the rock mass will directly bring effects on the normal operation of the intake structures, therefore the slope has particularities of high operation requirements and different operation conditions from other slopes. The design criteria, excavation, strengthening and supporting scheme are determined after many years' study and tackle key problems in science and technology. The excavation and strengthening construction of the project was started in July 2001. A dynamic design concept has been kept in the period of construction and the strengthening measures and construction procedures are timely adjusted in accordance with the exposed geological conditions and the monitoring data gained. By the end of October 2003, the treatment works was basically completed. The prototype observation indicates that the slope is under stable situation, and this ensured the implementation of the closure of Longtan hydroelectric project as scheduled and the concrete placement of the intake dam section in April 2004.

2 GEOLOGICAL CONDITIONS AND OUTLINE OF DESIGN

2.1 *Topographic and geological conditions*

(1) Creep rock mass area A

The natural topography is approximately slope with an angle of 28°~37° distributing along the river for 750m at EL. 230~640m. Creep area A and area B are zoned in accordance with the influence extent to the project by the creep rock and the rock creep position.

The area A is located near the water intake of the underground powerhouse with a volume of 3,560,000m^3. The normal strata attitude is 345°~355°/NE ∠60° and the strike of it nearly parallels to the flow direction of the river. The slope rock is composed of Banana Group rock strata (T_{2b}) of Triassic system with sandstone alternating with mud-slate rock strata but mainly consist of sandstone. The soft strata are alternating with the hard strata, the bedding fault is developing, and there is fracture F_{98} plane along the slope. From the surface to the deep of the mountain slope, there is no obvious transition interface among the titling loosen zone, bending disjunction, transition zone and normal rock zone, in addition there is no continuous bending breakdown plane in the rock mass.

Area A is divided into three small areas, namely, area A_1, area A_2 and area A_3 according to the formation and the extent of creep. Area A is located in the intersection of the F_{69}, F_{119} and F_{63} with a volume of 1,760,000m^3. The upper wall rock mass of F_{98} with a volume of about 1,200,000m^3 is a potential unstable one. Area A_2 is located at the toe of the slope and mainly consists of collapse accumulation with a thickness of 20–30m. Area A_3 is located in the contact transient zone of the creep rock mass and the normal rock with the rock mass crept lightly.

(2) Water intake arrangement area

The water intake arrangement area is located downstream of the creep rock mass, closely the lower part of the creep area A_1 with a natural slope angle of 35°~43° and a residual slope eluvium thickness of 1~5m.

The regional outcropping strata belongs to Banana Group T_{2b}^{10-38}, with a orientation of rock formation **345°~355°/NE ∠55°~62°**. All other rock strata mainly consist of sandstone or rock strata of sandstone alternating with mud slate except rock strata T_{2b}^{18} mainly consists of mudslate rock.

The east-north fault and interlayer fault develop in this region and the representative faults are F_{63}, F_{69}, F_{119}, F_1 and F_5, F_8, F_{28}, F_{32} etc. For the fissure development of predominant joint, the steep dip is the main fissure development, and the joint of the gentle dip develop compactly around fault F_1 and relatively undeveloped in other area.

Generally speaking, the depth of the weathered rock is: 10~30 for the strongly weathered rock, 30~50m for the weakly weathered rock and 70~100m for the lightly weathered rock.

The subsurface water belongs to underground water of bedrock crack, which is mainly coming from atmospherically precipitation, and it is discharged away to the riverbed direction along the crack of the strata plane, the fault and the fissure of the joint. The depth to the water table in the dry season generally is 60~80m, the mean hydraulic gradient slope is 0.5~0.6, and the water level vary with seasons with a stage variation of 20~40m.

As a result of abrasion effect of the topography, the maximum principal stress is 6~9Mpa, the direction of σ_1 principle stress is N20°~50°E, the horizontal stress is the principal stress, and the factor of the lateral pressure is 1.3~1.6.

2.2 *General design situation*

The treatment for the left bank creep rock mass and water intake high slope for Longtan hydroelectric project is one of the key technical issues in the pre-exploration, the study and design. After having carried out overall scientific experiment and stability analysis on the slope problems, a basic slope treating scheme was put forward, namely, after the completion of excavation for the potential unstable one of the upper wall rock of F_{98} fault, then the slope excavation is carried out based on the criteria of meeting water intake structures arrangement requirements and keeping the slope in self-stability. A basic treatment scheme of completing drain holes and anchoring prior to employing water cutoff, watertight, water drainage and anchoring strengthening measures for the slope treatment. Strict requirements are put forwarded for the construction procedures of the excavation and strengthening, the strengthening and support for the single-stage slope plane (See Fig. 1 and Fig. 2).

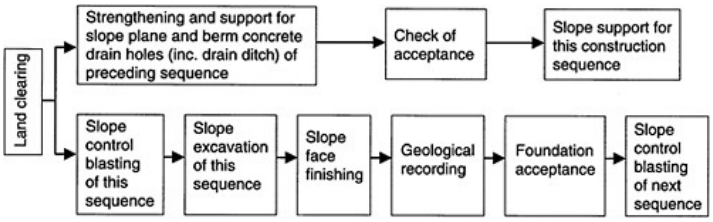

Figure 1. Critical procedures for slope excavation and strengthening.

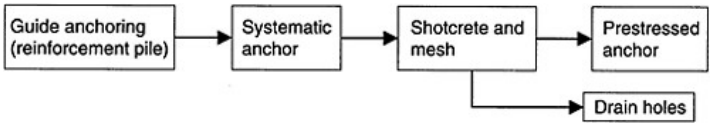

Figure 2. Critical procedure for slope face strengthening and supporting.

3 DYNAMIC DESIGN CONCEPTS AND PROCEDURES

3.1 *Dynamic design concepts*

(1) Pay a great attention to the analysis and judgment for the geological conditions exposed by excavation and the monitoring data gained.

As the design for the high slope involve many special fields of study and many branches of learning such as exploration, geology, experiment, structure and monitoring, furthermore, there are many kinds of influencing factors for the stability of the slope and every influencing factor has undefinition thus the mathematical model can not provide correct description on the high slope design. The macro correct judgment cannot be given out until quick stability analysis calculation work was added on the basis of the geological conditions exposed in excavation, the prototype monitoring data gained. As it is impossible for all problems were exposed in the pre-exploration, experiments and stability analysis, and many unexpected geological problems will occur during the excavation construction.

In the light of complexity and the un-definition of the influencing factors for the slope stability, there is much discrepancy even no consistence with the situations in construction practice of slope strengthening and supporting work based on the normal or pre-calculation. Therefore the feedback analysis and prototype monitoring data analysis based on the prototype monitoring and the data gained from the exposed geological conditions are very important.

In order to reach a goal of safety and economy, a dynamic design concept and method for the high slope design must be followed in the period of the overall high slope design and construction, namely the design scheme should be timely adjusted, optimized and perfected in accordance with the prototype monitoring data and the geological feedback data from the construction.

(2) Pay a great attention to the conceptual design for high slope treatment.

At present, the design for the high slope is still in the empiric stage or is closing to the semi-empirical stage or tending to semi theoretical stage, and therefore the engineering experience, similar engineering experience and expert experience will become the important basis for high slope design. As the high slope design has characteristics of non-structure, non-parameterization and non-standardization, the conceptual design based on the engineering experience and theoretic basis occupies important position in the design for high slope.

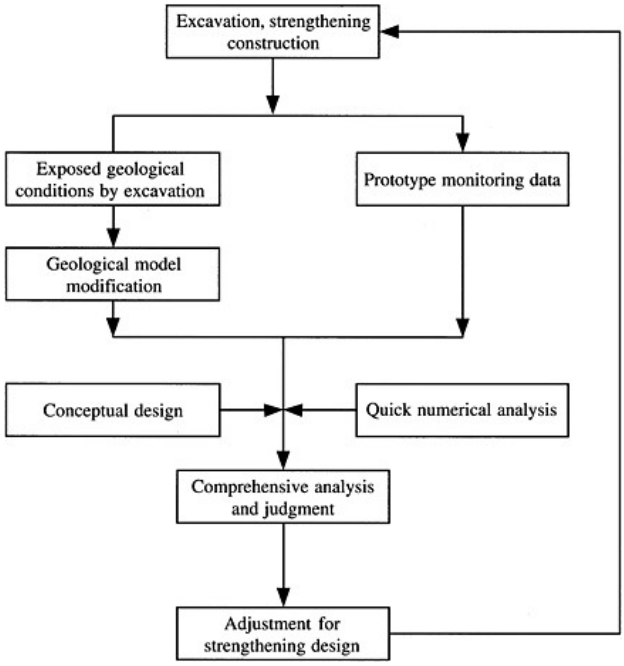

Figure 3. Dynamic design procedures.

(3) Pay a great attention to the strengthening for the predominant breach (which control the stability of the slope) and guide anchoring.

The process of the rock failure and deformation starts from the breach and then gradually develop, therefore giving priority to strengthening the breach and sensitive deformation location is very important in the strengthening supporting design. The location of the outer boundary line of the berm, the fracture structural zone, the soft stratum zone and the tunnel inlet all belong to predominant deformation breaches. Guide strengthening must be provided for the predominant deformation location and predominant structural plane.

In addition, construction factors and site information should be fully considered during the dynamic design and a quick and timely dynamic design information feedback should be provided to the construction.

3.2 *Dynamic design procedures*

Following dynamic design procedures should be followed in the period of construction practice based on the features and problems of the left bank water intake high slope of the Longtan hydroelectric project, the exposed geological conditions by the pre-exploration and the conclusions of pre-stability analysis (See Fig. 3).

4 DYNAMIC DESIGN PROCESS AND CONTROL

4.1 *Treatments for fissures and deformation above EL. 580m*

On November 6, 2001, in the period of excavation at EL. 500~480m, cracking occurs in the slope face and inside berm above EL. 580m with a maximum crack width of 7mm and a cracking speed

about 1~2mm/d. The site visiting and observation show that the crack has following features: The crack develop along the intersection plane of the creep rock mass after excavation and the normal rock mass; the slope face inclined crack extend basically along the attitude of the rock stratum; the berm crack location basically is lower inside the berm and higher outside the berm, it means the rock mass located outside of the crack has a tendency of moving toward the air face; the crack mainly develop in the slope face and berm above EL. 580m, only partial and light crack developed in the slope face (the contact plane of the shotcrete and berm in-situ concrete).

In the light of the above features and the comprehensive analysis and judgment made combining with the exposed geological conditions, the situations (no deformation) inside the drain holes (El. 560m), the monitoring data gained, the main causes of crack producing are known as: the slope structure and formation of the soft and hard bedded antidip structure rock mass; after unloading, the structure strength difference between the loosen creep rock mass and the normal rock mass cause un-affined deformation, with down cutting excavation, the un-affined deformation become more aggravated, then final crack occur in the boundary of the creep rock mass and the normal rock mass; and the quick down cutting excavation (the monthly mean decreasing of excavation elevation 27.5m), the blasting and the precipitation have quickened the rock mass deformation. But this kind of cracks only belongs to surface rock deformation and they will not cause rock sliding.

On the basis of analysis and judgment above, following engineering measures are employed: strengthening monitoring work and paying a great attention to the deformation in the boundary of the creep rock mass and normal rock mass; providing more drain blind holes and drain curtain holes so as to drain away the seepage in the boundary of the creep rock mass and normal rock mass; strictly control the blasting and improve the blasting quality; providing more anchor cable to control the development of the crack; timely seal the crack. After the implementation of the engineering measures above, till today no more crack extension was found and the monitoring data shows that the slope is stable.

4.2 *Optimization and adjustment for the systematic anchor which are provided downstream side of F_{63} at EL. 480~382m*

This slope section is located on upper steep slope of the downstream slope (EL. 382~295m), the construction details show that the ø32 systematic anchors are arranged at intervals with a length of 10m or 8m. On the basis of the situations for the drain holes at EL. 480, 480, 460, 425, 382m, the exposed geological conditions at EL. 480~460m, and the monitoring results gained from the operating monitoring facilities, a feedback analysis for this slope section had been carried out, finally the ø25 anchor cable with a length of 5m is adopted instead of ø32 anchor with a length of 10m, therefore, the project cost is saved. After the implementation of optimization and adjustment measures mentioned above, the monitoring data indicate that the slope is stable and the deformation magnitude and the stress of the anchorage cable in this location are within the range of control.

4.3 *Parameter optimization and adjustment for the prestressed anchorage cable located on dam abutment slope at EL. 382~301m*

In order to ensure the integrity the upper and lower wall rock of F_{119} and control the deformation of the residual creep rock, 2000kN grade prestressed anchorage cable is arranged at intervals basically with an interval of 4×5m. As the excavation exposed that the boundary of the creep rock mass and the normal rock mass move upwards, after analysis, the planned 2000kN grade anchorage cable is adjusted to be 1000kN grade one and at the same time the length of the anchorage cable is also adjusted according to the depth of the residual creep rock mass exposed by the excavation of the drain holes, thus the work qualities for anchorage cable is reduced.

4.4 *Treatment for unstable rock mass at power tunnel inlet for Unit ①*

The scarfing unstable rock mass in the tunnel intake slope at EL. 280~382m dissected by faults $F_{138,}$ $F_{58,}$ F_{26} and F_7 and it has a maximum volume of 74,000m^3, a width of 65m and a thickness

of 35m. In order to ensure the stability, pre-stressed anchorage cable is mainly adopted to strengthen the unstable rock mass as the construction main backbone road has already been built up and there is no space condition for excavation work. After excavation of the drain hole in this location, the attitude and behavior of the main slip plane of F_{138} are further defined, in addition, some scattered small crack-type fault with a medium dip angle are also found. In consideration of safety and in order to avoid the local small rock mass collapse on slope bringing unstable factors to the slope monolithic stability, many rows of vertical reinforcement pile have been provided on the slope platform of berms located in different elevations, in addition, the platform is required to be finished prior to next bench excavation. The implementation of this kind of advance anchoring measures reduced the next bench blasting influence to surface rock mass, and controlled the loosening and deformation of the crack type fault. The application of the pressure grouting technology with the consolidation pile itself being provided with pressure grouting pipe provide a consolidation for cracks, kept and strengthened the shear strength of structural plane; ensured the integrity of surface rock mass and the stability of the local small rock mass; and created favorable conditions and raced against time for the treatment of the large rock mass.

4.5 *Other adjustment and optimization*

During the construction, besides the large adjustment and optimization mentioned above, some other optimization for anchorage cable structure also were made for the convenience of construction as the hole drilling in the soft and hard bedded rock mass is difficult and there is appearance of anchorage cable getting stuck in anchorage cable installation. To improve the early strength of the anchorage grouting and quicken the construction schedule in consideration of characteristics of pressed project duration and easily overturning and deformation for the soft and hard bedded antithetic structure slope. As there is cross construction for Slope Contract Section and Power Conduit Intake Contract Section, Some modification have been made for the construction procedure in accordance with the actual construction progress and construction situations, namely, the original construction procedure is to excavate the power intake tunnel from the slope inside to the slope face, and now the modified construction procedure is to start excavation from the slope face to the depth of mountain after the slope was finished. In addition, a great attention was paid to the applying of the random anchor rod, anchorage cable, and stylolitic anchor rod for upper and lower wall fault and advance anchor rod. And priority was given to the strengthening for the dominant deformation and breaking location.

The dynamic design and timely control mention above ensure the safety and stability of the construction duration and create conditions for the closure of the Longtan hydroelectric project.

5 CONCLUSIONS

5.1 Till Oct. 2003, the main work quantities of the excavation and the strengthening supporting for the water intake high slope of the left bank underground power house of Longtan hydroelectric project have basically been completed since it started in July 2001. Thanks to the implementation of dynamic design concept and timely adjustment for strengthening supporting measures in the period of the construction, a safe and smooth construction was ensured.

5.2 The pre-exploration, study and the understanding about the slope are the bases of the dynamic design for the slope treatment in construction duration, especially for the macro judgment on slope stability and deformation.

5.3 The excavation of the drain tunnel on the rock high slope will be completed ahead (comparing with the slope face excavation), beside the function of drainage, the drain tunnel has functions of providing supplementary exploration, monitoring, anchoring and possibly reducing disturbing influence to the excavated slope face. In addition, it will be of importance in guiding the dynamic design for slope.

5.4 In the period of the excavation and the dynamic design for the slope, giving priority to the strengthening of the dominant deformation location and dominant structural plane through

providing guide consolidating for these location is very important for controlling the slope deformation and ensuring the stability of the slope. The conceptual design based on the engineering experience, similar engineering experience, expert experience and theoretic analysis is the important basis of the dynamic design, as the numerical analysis can not be able to mirror the features of the rock mass and the construction situations. A great attention should be paid to the prototype monitoring and the feedback for the construction information combining with the rock mass structure exposed by excavation.

5.5 Though the excavation for the high slope of the left bank water intake of the Longtan hydroelectric project was completed, and it has withstood the rainy season of 2003, with the slope complexity, further analysis for the deformation tendency will be made in the next construction stage, and the deformation law should be grasped so as to ensure the construction and operation safety of structures of the water intake dam section.

AUTHORS

Zhaohongmin, born in Henan, China, is a senior engineer. He has many years of experience in design of dam general layout and slope design for hydroelectric project.

Dai Qiangxun, born in Hunan, China is a design chief and senior engineer.

Deng Xianyang, born in Hunan, China is an engineer.

Zhou Haihui, born in Hunan, China is a senior engineer.

Feng Weiqing, born in Hunan, China is an engineer.

This page intentionally left blank.

New Developments in Dam Engineering—Wieland, Ren & Tan (eds),
© 2004 Taylor & Francis Group, London, ISBN 04 1536 240 7

The improved convert permeability coefficient method and variable permeability coefficient method used for seepage calculation in karst regions

Jian Zhao & Zhen Zhong Shen
Hohai University, China

Miao Lai
Shanghai Flood Risk Information Center, China

ABSTRACT: Based on summarizing various kinds of methods used to calculate karst groundwater seepage, aimed at the seepage characteristics in karst regions, two methods that can simultaneously consider Darcy and non-Darcy flows are put forward, i.e. Improved Convert Permeability Coefficient Method and Variable Permeability Coefficient Method. Considering the drawbacks of present convert permeability coefficient method, the formulas to calculate tensor of karst conduit in general coordinates system are deduced. According to the basic differential equation for karst seepage, the finite element method (FEM) equations applied for calculating karst seepage are deduced on the basis of Galerkin FEM. Verification of examples indicate that two methods raised in this paper are feasible and reasonable.

1 INTRODUCTION

In karst regions the extremely inhomogeneous developed rocks diversify the water bearing media, which include matrix pores, cracks and karst conduits etc. Karst conduits are very permeable, and in which the groundwater is very often in the state of non-Darcy flow, therefore, Darcy and non-Darcy flows simultaneously exist in the groundwater. Early karst groundwater seepage studies mainly adopt systematical analysis and such mathematical methods as porous medium model[1] double media model[2] on the basis of Darcy Law. Later, the confluence calculation method[3][4], coupling media model[5] and triple media model[6] are put forward. Among which, the triple media model based on convert permeability coefficient method can better solve the problem of groundwater movement in water bearing system of highly developed karst regions and has broad application prospects. Study shows that this method needs to be further improved and perfected for such problems as: ③ when solving the finite element equation, the seepage (hydraulic conductivity) matrix is not reformed for iteration of each time step. Aimed at above problems, an improved convert permeability coefficient method is put forward in this paper; at the same time, the finite element method to study seepage field of non-Darcy flow in the rockfill coarse grain is extended to the convert permeability coefficients method, which is suitable for solving the seepage field in karst regions.

2 IMPROVEMENT OF CONVERT PERMEABILITY COEFFICIENT METHOD AND VARIABLE PERMEABILITY COEFFICIENT METHOD

2.1 *Convert permeability coefficient method and its improvement*

In order to unify the expressions of Darcy and non-Darcy flows for the water bearing media in karst regions, so as to establish the control equation, the concept of convert permeability coefficient K_L can be introduced[6]. That is, various flow regimes will satisfy:

$$V=K_L J \tag{2-1}$$

where: V—seepage velocity (LT^{-1}); K_L—convert permeability coefficient (LT^{-1}); J—hydraulic gradient (dimensionless).

When groundwater is in the state of Darcy flow, K_L is nothing to do with Reynolds number R_e, and $K_L=K$ (K is the permeability coefficient of Darcy flow); when groundwater is non-Darcy flow, K_L varies with R_e, $K_L=K_L(R_e)$. Therefore, the control equation for Darcy and non-Darcy flows can be established by adopting the form similar to that of groundwater control equation of Darcy flow:

$$\nabla\cdot(K_L(R_e)\cdot\nabla H)+\varepsilon=\mu_S\frac{\partial H}{\partial t} \tag{2-2}$$

where: H—water head *(L)*; K_L—convert permeability coefficient (LT^{-1}); ε—intensity of source and sink (LT^{-1}); μ_s—unit storage coefficient LT^{-1}); t—time *(T)*.

Groundwater in matrix cracks is generally Darcy flow, $K_L=K$; while groundwater in karst conduits is normally non-Darcy flow, $K_L=K_L(R_e)$. When the form of karst conduits is more regular, the flow regime is close to pipe flow, the formula of convert permeability coefficient K_L can be deduced from the equation of Darcy-Weisbach (see equation (2-3)).

$$h_f=\lambda\frac{l}{d}\frac{u^2}{2g} \tag{2-3}$$

where: h_f—head loss *(L)*; λ—streamwise head loss coefficient (dimensionless); l—length of pipe *(L)*; d—diameter of pipe *(L)*; u—mean velocity within pipe (LT^{-1}); g—gravity (LT^{-2}).

Considering the porosity of the pipe n=1, the seepage velocity $V=nu=u$, substitute V and $J=h_f/l$ into equation (2-3), obtains:

$$Jl=\lambda\frac{l}{d}\frac{V\cdot V}{2g} \tag{2-4}$$

$$V=\frac{2gd}{\lambda V}J \tag{2-5}$$

Define convert permeability coefficient as:

$$K_L=\frac{2gd}{\lambda V} \tag{2-6}$$

equation (2-1) can be obtained.

When solving for K_L, the key is able to calculate corresponding λ in terms of the flow regime of seepage, and the value of λ depends on R_e as well as relative roughness. According to the experimental curve of Nikurades, when R_e<2300, flow is in laminar zone:

$$\lambda=64/R_e \tag{2-7}$$

When 2300<R_e<10000, turbulent smooth zone:

$$\lambda = 0.236 / R_e^{0.25} \tag{2-8}$$

When R_e>10000, turbulent roughness zone, and λ has nothing to do with R_e, but only depends on the roughness of the inner pipe wall.

Equation (2-3)-equation (2-8) are the processes for solving convert permeability coefficient K_L in the literature [6]. It can be seen that before the improvement of the convert permeability coefficient the turbulence transition zone is not considered in the calculation of streamwise head loss coefficient in karst conduits, and the formula of turbulence roughness zone λ is not given. Before the improvement of convert permeability coefficient method, it is not proper for using Reynolds number R_e to distinguish the turbulence zones. According literatures [7] and [8], roughness Reynolds number $u_*\Delta/v$ should be adopted as the criteria to distinguish turbulent zones (u_* is frictional velocity $u_* = u\sqrt{\lambda/8}$, u, u means velocity, Δ means roughness of pipe, v means kinematical viscosity coefficient). However, $u_*\Delta/v$ is associated with u_*, while u_* depends on λ, therefore, it is hard to use roughness Reynolds number to distinguish the three zones of turbulence in finite element analysis. For this, the simplified formula of λ is deduced from Colebrook, C.F. formula[8] (it is simplified as Col equation hereinafter) in this paper. Which is:

$$\frac{1}{\sqrt{\lambda}} = 1.74 - 2\lg\left(\frac{2\Delta}{d} + \frac{18.7}{R_e\sqrt{\lambda}}\right) \tag{2-9}$$

where: Δ—pipe roughness, d—pipe diameter.

The Col equation is the formula to solve for the λ of turbulence transition zone, After carefully checking this equation, it is easily found that when Δ/d is very small, the first term in the brackets can be neglected, and λ only depends on Reynolds number R_e, which accords with the motion law of turbulence smooth zone, Col equation is reduced to the computational equation of λ in turbulence smooth zone:

$$\frac{1}{\sqrt{\lambda}} = 1.74 - 2\lg\frac{18.7}{R_e\sqrt{\lambda}} \tag{2-10}$$

When R_e is very large, the second term in the brackets of equation (2–9) can be neglected, λ only depends on relative roughness Δ/d, which conforms to the motion law of turbulence roughness zone, the Col equation is reduced to the computational equation of λ in turbulence roughness zone:

$$\frac{1}{\sqrt{\lambda}} = 1.74 - 2\lg\frac{2\Delta}{d} \tag{2-11}$$

It can be seen that Col equation is suitable to calculate the sreamwise head loss coefficient λ for three different turbulence zones. It must be noticed that λ to be solved by Col equation is an implicit function and has to be transformed into following explicit equation for easily solving:

$$\frac{1}{\sqrt{\lambda}} = 1.14 - 2\lg\left(\frac{\Delta}{d} + \frac{21.25}{R_e^{0.9}}\right) \tag{2-12}$$

As the water motion principle in critical zone, which is between turbulence and laminar flow, is unknown so far, to simplify calculation, it is merged into turbulence smooth zone. Accordingly, the computational formula of streamwise head loss coefficient λ in karst conduits can be obtained in terms of the λ of laminar zone and equation (2-12):

laminar flow (R_e<2320) $$\lambda = \frac{64}{R_e} \tag{2-13}$$

turbulence ($R_e \geqslant 2320$) $$\lambda = [1.14 - 2\lg(\frac{\Delta}{d} + \frac{21.25}{R_e^{0.9}})]^{-2} \quad (2\text{-}14)$$

In practical use, according to different seepage flow regimes, corresponding formula can be selected to calculate K_L. For karst conduits, if seepage is laminar flow, equation (2-13) can be used to calculate water head loss coefficient λ, if turbulence, equation (2-14) is selected, then equation (2-6) is used to calculate convert permeability coefficient K_L.

Because equation (2-14) is a formula suitable for solving the streamwise head loss coefficient λ of three turbulence zones, it can be used along with equation (2-13) to calculate the λ of seepages in four zones (laminar zone, turbulence smooth zone, turbulence transition zone and turbulence roughness zone), therefore, λ is more accurately calculated in comparison with the method in literature [6].

Improved convert permeability coefficient unifies the flow regimes of four seepage zones in karst conduits into one, so as to integrate flows in karst conduits with pose as well as cracks.

2.2 *Variable permeability coefficient method*

Variable permeability coefficient method expresses the permeability coefficient of karst conduits as the function of water head to be solved and exponent of flow regime, so as to integrate the non-Darcy flow in karst conduits with the Darcy flow in other media. This method is extended from the research results of seepage in rockfill and other coarse media seepage fields[9].

According to literature [10] and [11], seepage law of the mixed flow (Darcy flow as well as non-Darcy flow) can be expressed as follows:

$$V = K_C J^{\frac{1}{m}} \quad (2\text{-}15)$$

where: K_C—permeability coefficient of porous media in mixed flow condition; m—flow regime index ($1<m\leq 2$).

After deduction from equation (2-15)[9], the permeability coefficient K_x, K_y and K_z in coarse media can be expressed as:

$$K_x = K_y = K_y = K_C(h_x^2 + h_y^2 + h_z^2)^{\frac{1-m}{2m}} \quad (2\text{-}16)$$

where: h—water head to be solved.

It can be seen from equation (2-16) that K_x, K_y and K_z are not fixed values, which not only depend on the features of media and flows, but also are functions of water head h to be solved. In literature [9], K_x, K_y and K_z are directly used to solve for the seepage of whole computational region, it is reasonable for solving the seepage field in such coarse grain media as rockfill, because seepage in this kind of media is generally non-Darcy flow. However, because of the diversity of seepage flow regimes in karst regions, the method for solving K_x, K_y and K_z in equation (2-16) can only be applied to the permeability coefficient of non-Darcy flow in karst conduits, for other media, the permeability coefficient of Darcy flow must be used. Moreover, seepage movement in karst conduits possesses strong anisotropy, K_x, K_y and K_z obtained from equation (2-16) can only be used after tensor transformation.

The permeability of karst conduits is mainly shown in axial direction for karst conduits media, so that three-dimensional problem is turned into one-dimensional problem. After setting up a regional coordinate system $OX'Y'Z'$, and making its positive direction of OX' axis parallel to the axis of karst conduits, we have $K_{y'}=0$, $K_{z'}=0$. Define the variable permeability coefficient of such media K_v as follows:

$$K_V = K_{x'} = K_C(h_{x'}^2 + h_{y'}^2 + h_{z'}^2)^{\frac{1-m}{2m}} \quad (2\text{-}17)$$

There is $K_v=K$ (K is the permeability coefficient in Darcy flow) for the pores and cracks in water bearing media of karst, therefore, seepage principle in karst media can be unified as:

$$V=K_V J \tag{2–18}$$

3 CALCULATION OF SEEPAGE TENSORIN KARST CONDUITS UNDER GENERAL COORDINATES SYSTEM

The convert permeability coefficient K_L obtained is directly substituted into equation (2–2) to solve for pressure head in literature [6]. It is obviously that an important feature of karst water bearing media is overlooked in this treatment, i.e. karst conduit is the main conductive medium in karst water bearing media, in which flow movements are anisotropy. Therefore, the value of K_L calculated from the convert permeability coefficient method under regional coordinates system must be transformed into the form of tensor under general coordinates system (the geodetic coordinates system) of computational region, it can be substituted into equations to carry out calculation. The value of K_V resulted from variable permeability coefficient method must be treated in the similarly way.

4 FINITE ELEMENT METHOD OF KARST SEEPAGE CALCULATION

If the effects of capillary zone, unsaturated zone, infiltration from rainfall and evaporation above the free surface (or lateral) are not taken into consideration, the basic differential equation for unsteady seepage of karst may be expressed as:

$$\frac{\partial}{\partial x_i}\left(k_{ij}\frac{\partial h}{\partial x_j}\right)=S_s\frac{\partial h}{\partial t} \tag{4–1}$$

where: h—water head; S_s—storage coefficient; k_{ij}—seepage tensor; t—time.

It can be seen from equation (4–1) that there is no practical difference between the differential equations of karst seepage and non-karst saturated seepage. In fact, however, the seepage tensor k_{ij} in equation (4–1) has multiple meanings: For matrix pores and cracks, k_{ij} is the seepage tensor in Darcy flow; for the media of karst conduits, when the method of convert permeability coefficient is adopted, k_{ij} is the tensor of convert permeability coefficient under general coordinates system, while when the method of variable permeability coefficient is used, k_{ij} is the tensor of variable permeability coefficient under general coordinates system and is not a constant.

Based on equation (4–1) and using Galerkin finite element method, the finite element equation[12] for karst seepage can be derived from $h=p/\gamma+z$, which is expressed as:

$$[K]\{P\}+([S]+[G])\left\{\frac{\partial P}{\partial t}\right\}=\{F\} \tag{4–2}$$

where: *[K]*—seepage matrix; *{P}*—pressure head column matrix of nodes; *[S]*—storage matrix; *[G]*—drainage matrix; *{F}*—unbalanced force column matrix.

5 CASE STUDY

Figure 1 is a schematic diagram for the core wall of a dam, which is 21.0m in length (Y direction), and a karst conduit runs through the upstream and downstream river bed (Y=10.5m), which is 1.0m in diameter. The permeability coefficients K of the dam shell, core wall and river bed materials are

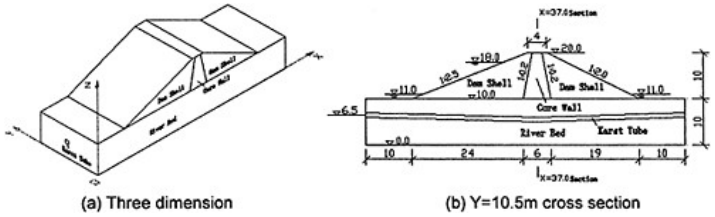

Figure 1. Schematic diagram of core wall dam.

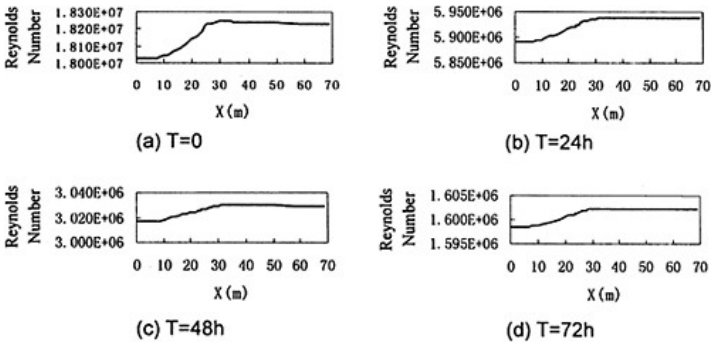

Figure 2. Reynolds number of karst conduit.

respectively 2.11×10^{-5}m/s, 3.12×1^{-7}m/s and2.34×10^{-5}m/s; The specific yields μ of the three materials are 0.050, 0.022 and 0.051, respectively; the storage coefficients S_s of the three materials are all equal to 0. Kinematical viscosity of water v equals 1.141×10^{-6}m^2/s. The upstream and downstream beginning water levels of the dam are 18.0m and 11.0m, respectively. When upstream water level suddenly drops to 11.0m, the unsteady seepage conditions of dam at T=0, 24h, 48h and 72h are respectively calculated in terms of convert permeability coefficient method as well as variable permeability coefficient method. During the calculation, river bed surface (Z=0m) as well as four lateral surfaces (X=0m, X=69.0m, Y=0m and Y=21.0m) are treated as impervious boundaries.

When conduit roughness Δ=0.02m, the results calculated by convert permeability coefficient method are shown in Fig. 2 as well as Fig. 3 (a) and (c). It can be seen from Fig. 2 that Reynolds number R_e of karst conduits during the period of 0–72 h possesses following characteristics: (a) R_e has the tendency of decreasing; (b) when 0<X<30m, R_e is increasing, and X>30m, R_e does not vary much; (c) all R_e is greater than 10^6, i.e. the seepage in karst conduits is in turbulent roughness zone.

Because the seepages of karst conduits are all in turbulent roughness zone during the period of 0–72 h, when the convert permeability coefficient method is used for the calculation, 2 is taken as the flow index m and an estimated value of 1.0m/s is taken for Kc. Results from variable permeability coefficient method are shown in Fig. 3 (b) and (d).

It can be seen from Fig. 3 that results are basically the same for two methods. The decline speed of saturation curves is quite fast within 0 to 24 h, and is getting slow after 24 h; while during the

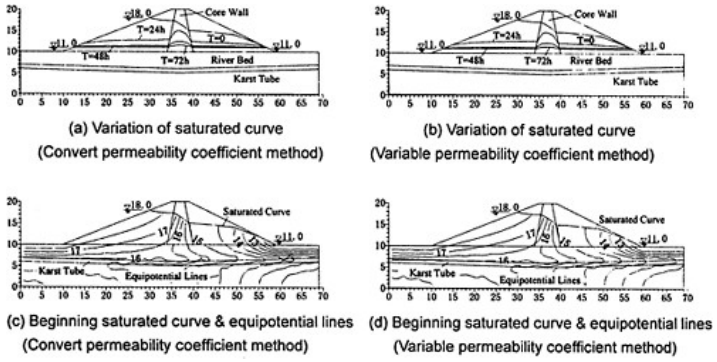

Figure 3. Calculation result (Section Y=10.5m).

period of 0–72 h, the saturation curves inside core wall always lay behind in variation than those inside dam sell because of its low permeability. It can be seen from Fig. 3 (c) and (d) that the permeability coefficients (convert permeability coefficient and variable permeability coefficient) of karst conduits calculated from the methods of convert permeability coefficient and variable permeability coefficient are very big and result in very small head losses of the seepage in karst conduits, and the equipotential lines adjacent to karst conduits obviously shift downstream. From the fact that the shifting amount from the result of convert permeability coefficient method is greater than that from variable permeability coefficient method, it also shows that the permeability coefficient obtained from convert permeability coefficient method is greater than that obtained from variable permeability coefficient method. The analysis of discharge is carried out for the cross section at X=37.0m. Discharges obtained from the convert permeability coefficient method at T=0, 24 h, 48 h, and 72 h are respectively 3780.90 cm^3/s, 232.76 cm^3/s, 45.34 cm^3/s and 8.90 cm^3/s; corresponding discharges obtained from variable permeability coefficient method are 3670.15 cm^3/s, 229.98 cm^3/s, 45.12 cm^3/s and 8.89 cm^3/s, respectively. Discharges resulted from convert permeability coefficient method are greater than those resulted from variable permeability coefficient method.

Because covert permeability coefficient method is based on the formula of pipe flow, the geometric and hydraulic parameters of the karst conduits must be in details during the computation. Though the form of karst conduits is unnecessarily needed in details when variable permeability coefficient method is used, the difficulties are to determine parameters K_C and m. Therefore, for karst conduit seepage, when the geometrical and hydraulic parameters are sufficient, and the water flows satisfy (or approximately satisfy) pipe flow principle, convert permeability coefficient method can be adopted for calculation; of course, when the flow regime in the karst conduit is well known, variable permeability coefficient method can also be used. When m and K_C are properly selected, the calculation results of convert permeability coefficient method are close to those of variable permeability coefficient method, which has been confirmed by above case studies. When the form of karst conduit is very irregular, in which the flow is not conform to pipe flow principle, variable permeability coefficient method can be used after m and K_C are determined by relevant model experiments.

6 CONCLUSION

Seepage calculation methods for karst regions are soundly studied in this paper. Aimed at the drawbacks of exiting convert permeability coefficient methods, the improved convert permeability coefficient method used in karst conduit media is put forward. After extending the finite element mathematical model for solving non-Darcy seepage in rockfill gravel materials, the variable permeability coefficient method for solving seepage fields in karst regions is raised. Case studies show that it is feasible and reasonable for using both methods to calculate karst seepages.

REFERENCES

[1] Song Hanzhou & Wang Jieping, Study on Karst Leakage Problem In Bianken Reservior [J]. Carsologica Sinica. 1992, 11(1), 15~19
[2] Xue Yuqun & Zhang Youkuang et al. "Application of Dual Media Flow Model and its Ritz Finite Element Solution in Forecast of Mine Groundwater Discharge". Hydrogeology and Engineering Geology. 1984, (2), 33~39
[3] Ding Shiqun & Fu Ruijin, Analysison Karst Development and Seepage Auxiliary Dam Area of The Upper Reservior of Lang Yashang Pumped Storage Hydroplant, Karst in China [J]. 1997, 16(1), 75~81
[4] Zhou Hongwen & Zou Chengjie, Reserch on Karst Leakage of Mapatang Reservior [J]. Gui Zhou Geology, 1996, 13(2), 190~195
[5] Xia Riyuan & Guo Chunqing, Study on The Method of Unit-Network Mathematic Simulation (UNMS) of Karst Groudwater System. Karst China, 1992, 11(4), 267~276
[6] Cheng Zhongxi, Groudwater Flow Modle and Simulation Method in Triple Media of Karst Tube-Fisurepore [J]. Earth Science, 1995, 20(4), 361~366
[7] Yu Bu. Hydraulics[M], South China University of Technology Press. 2001
[8] Li Wei & Xu Xiaoping. Hydraulics[M], Wuhan University of Hydraulic and Electric Engineering Press. 2000
[9] Ding Liuqian & Xu Guoan. Finite Element Analysis of Three Dimentional Non-Darcy' Seepage Flow [J], Journal of Hydraulic Engineering 1990, (10), 49~54
[10] Gu Weici.eepage Calculation theory and its application[M]. Chinese Building Material Industry Press. 2000
[11] Li Junting & Wang Yuji. Groundwater Dynamics[M], Geological Publishing House, 1987
[12] Lai Miao, "Study on Seepage Characteristics and Calculation Methods in Karst Region", Dissertation for Master Degree of Science of Hohai University, 2003

New Developments in Dam Engineering—Wieland, Ren & Tan (eds),

Study on reinforcement of stability of abutments and foundation of arch dam

Zhao Yin, Shen Qiangxi, Ren Qingwen & Yu Tiantang
Hohai University, China

ABSTRACT: The stability and reinforcements of arch dam abutments and foundation are problems which people have paid close attention to at all times. So far a great deal of research achievements have been made in reinforce measures. But there are a lot of problems still waiting solved. This paper will research working mechanism and mathematics-simulating methods about reinforce measures of arch dam foundation, not only considering the rigidity effect brought about the methods, but also taking into account the change of parameters of rock material. It presents that the strain energy principle can be used to measure the reinforcing effect with ease and to find the better reinforcing scheme. Taking as an example the practical project of Xiao Wan high arch dam, the paper optimizes the reinforcing ranges in dam abutments and the scheme based on the analysis result of 3-D non-linearity FEM. It can provide important basis for reinforcing design of Xiao Wan arch dam abutments and foundation.

1 INTRODUCTION

How to improve the safety degree of arch dam abutments and foundation is a problem to which people have paid close attention all the time. There are typical reinforcing measures such as dam foundation excavation, consolidation grouting, impervious drapery, dam foundation drainage, prestressed anchorage for arch dam abutments and foundation and side slope [1]. So far a great deal of research achievements have been made in reinforcing measures, but there are a lot of problems still waiting to be solved. This paper will research how to measure reinforcing effects? how to determine physical and mechanical parameters of rock material, to which the reinforcing mechanics, mathematics-simulating about reinforcing measures and optimization of reinforcing programs are all related.

2 MEASUREMENT OF REINFORCING EFFECTS

Besides economy, reinforcing effect is the most important index to decide which kind of reinforcing method and programs should be used. Previous measurements to reinforcing effect are mainly based on numerical analysis results, the comparison of the maximum displacement and stress, range of plastic zone, and integral safety coefficient generated fore-and-after reinforce. But, displacement and stress are local variables. Perhaps the same maximum numbers will occur in different regions. It is difficult to compare the range of plastic zone for it also has the same regional problem. Moreover, it is indicated from actual analysis that above variables, including integral safety coefficients, aren't sensitive to reinforcing programs. That is to say, these variables change little for different reinforcing measures and programs. Therefore, this paper accepts deformation energy to measure reinforcing effects.

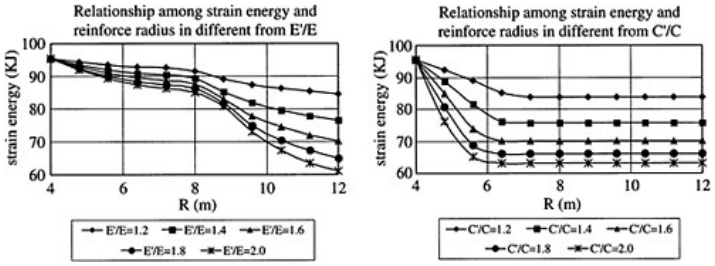

Figure 1. Relationship among deformation energy with radius of caulking ring, and material parameters of immerged circle tunnels.

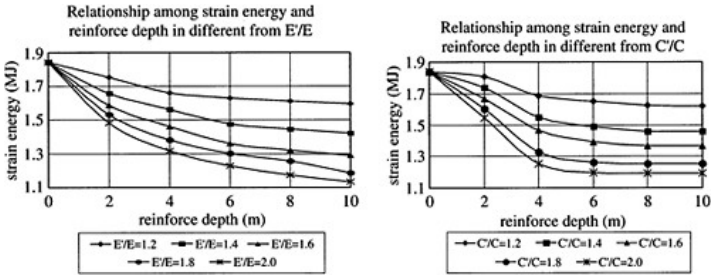

Figure 2. Relationship among deformation energy with range of reinforce, and material parameters of semi-infinity space.

During these years, many scholars have researched structural topology optimization through deformation energy and information entropy, regarding minimum energy of deformation or maximum entropy as their objective functions. They consider structures that have the best topology shape have the minimum deformation energy [2]. It can be proved similarly that the firm the system is, the less energy of deformation will be. Therefore, minimum deformation energy can be used for objective functions of system reinforce. And it produces the best program.

Figure 1 illustrates relationship among deformation energy under uniform internal pressure, radius of caulking ring, and material parameters of immerged circle tunnels. Figure 2 illustrates relationship among deformation energy under concentrated load, range of reinforce, and material parameters of semi-infinity space. E and E′ is material elastic modular fore-and-after reinforce respectively, C and C′ is cohesions respectively, R is radius of caulking ring. It can be seen that the larger the range of caulking ring is, the better the material property will be, and also the less the deformation energy will be.

3 SIMULATING ABOUT REINFORCE MEASURES

3.1 *Non-prestressed bolt*

Its contribution to rigidity being considered, an anchor bar, as for a pole element, can't reflect real condition. Its contribution to rock strength should be taken into account. Friction coefficient and

cohesions are denoted by f_r, C_r, shear strength by τ_s, sectional area by A_s, distance between anchor bars by $a \times b$. Shear strength in rational section areas should be the sum of resisting forces of rock and anchor bars:

$$T = \sigma_n f_r \frac{ab - A_s}{\sin\alpha} + C_r \frac{ab - A_s}{\sin\alpha} + \tau_s \frac{A_s}{\sin\alpha} \tag{1}$$

α is the included angle of section and anchor bars. If uniform anchor bars, then

$$T = \sigma_n f \frac{ab}{\sin\alpha} + C \frac{ab}{\sin\alpha} \tag{2}$$

f, C are uniformed equivalent friction coefficient and cohesions. Let $f=f_r$, because $A_s \ll ab$, compare (1) and (2), then equivalent cohesions can be obtained:

$$C = C_r(1 - \frac{A_s}{ab}) + \tau_s \frac{A_s}{ab} \tag{3}$$

3.2 *Grouting*

Grouted rock masses not only can improve deformation modulus, but also can reinforce its shear strength. This paragraph determines changes of shear strength by changes of deformation modulus of rock masses fore-and-after grouting. Rock masses with height H and area A have gap area A_c, void ratio is $n=A_c/A$. Elastic modulus of grouted paste is E_c, deformation modulus of rock masses is E_r, gap is filled by cement paste after grouting, so its equivalent synthesis modulus is E, according to deformation compatibility condition:

$$\frac{EA\Delta}{h} = \frac{E_r(A - A_c)\Delta}{h} + \frac{E_c A_c \Delta}{h}$$

Δ is deformation value in height. So

$$E=E_r(1-n)+E_c n \tag{4}$$

Before grouting, $E_c=0$, synthesis modulus is $E_1=E_r(1-n)$, according to (4)

After grouting, $E_c \neq 0$, synthesis modulus is $E_2=E_r(1-n)+E_c n$, according to (4)

If E_c is known, then E_r and n can be obtained. If $E_c=E_r$, then $E_2=E_r$. So

$$E_1=E_2(1-n)$$

Then

$$n=1-E_1/E_2 \tag{5}$$

Void ratio of rock masses then can be obtained from equation (5) and synthesis modulus.

It is assumed that friction coefficient and cohesions of rock masses are denoted by f_r, C_r, friction coefficient and cohesions of grouted paste are denoted by f_c, C_c. Existence of gap being considered, equivalent synthesis value of friction coefficient and cohesions can be denoted by f, C, then resistance force T in section wise can be analyzed according to synthesis value (Eqn. 6) or rock masses and gap, respectively (Eqn. 7):

$$T = \sigma_n f \frac{A}{\sin\alpha} + C \frac{A}{\sin\alpha} \tag{6}$$

$$T = \sigma_n f_r \frac{A - A_c}{\sin\alpha} + C_r \frac{A - A_c}{\sin\alpha} + \sigma_n f_c \frac{A_c}{\sin\alpha} + C_c \frac{A_c}{\sin\alpha} \tag{7}$$

Assuming $f_c = f_r$, then (7) changes to:

$$T = \sigma_n f_r \frac{A}{\sin\alpha} + C_r \frac{A - A_c}{\sin\alpha} + C_c \frac{A_c}{\sin\alpha} \tag{8}$$

Because (6) equals to (8), then:

$$C = C_r(1-n) + C_c n \tag{9}$$

Before grouting $C_c = 0$, so $C_1 = C_r(1-n)$

Cohesions after grouting is $C_2 = C_r(1-n) + C_c n = C_1 + C_c n$

Substituted into (5), then synthesis cohesions of rock masses after grouting is:

$$C_2 = C_1 + C_c(1 - E_1/E_2) \tag{10}$$

We can see that cohesions after grouting can be obtained by (10), according to modulus value fore-and-after grouting.

3.3 *Concrete substitution*

There are two cases about concrete substitution to faults and erosion alteration zones, they are:

a) Entirely substitution. In this case, material parameters of substitution elements are only changed into concrete's.
b) Partly substitution. Considering substituted part is not surely a complete element, a uniform method can be used.

There are two kinds of damage forms for faults and erosion alteration zones: one is compression or tension along vertical layers; the other is the shear along layers. It is assumed that substituted total area in layers is A, concrete area is A_c, elastic modulus is E_c, cohesions is C_c, compression strength and tension strength is $[\sigma_{cc}]$ and $[\sigma_{ct}]$ respectively. Changing modulus, E_c cohesions is C_c, compression strength and tension strength of rock masses are $[\sigma_{rc}]$ 和 $[\sigma_{rt}]$ respectively. $n = A_c/A$, then according to the principal of deformation energy equation, we can obtain:

Synthesis modulus $E = E_c n + E_r(1-n)$ (11)

Synthesis compression strength $[\sigma_c] = [\sigma_{cc}]n + [\sigma_{rc}](1-n)$ (12)

Synthesis tension strength $[\sigma_t] = [\sigma_{ct}]n + [\sigma_{rt}](1-n)$ (13)

Synthesis cohesions $C = C_c n + C_r(1-n)$ (14)

4 A CASE STUDY

Xiaowan hydropower station lies in the middle and down reach of Lancang River. This concrete dam mass is a parabolic double-curved arch dam. River valley appears as "V", banks of which are steep on both sides, local area being even upright. Shear and unload tension fracture develop on bank sides, and the tension is parallel to both sides. There is fault F_{11} and seven minor faults grade IV in the range of dam foundation. There are also erosion alteration zones there, such as E_8 (f_{20}), E_1, E_4, E_5 and so on,

mostly of which concentrated on right bank of dam abutments. Physical and mathematical parameters of all kinds of materials such as dam body, rock mass, structural surface are given in chart 1.

The following research is made on design and treatment programs on consolidation grouting, faults and alteration zones, prestressed anchorage and injection anchor support is based on treatment programs and reinforce range of Xiaowan arch dam abutments, foundation, bank slope, which are supplied by Kunming Exploration and Design institute.

4.1 *Reinforcement simulating*

4.1.1 *Consolidation grouting*

In this design, consolidation grouting was proceeded along entire dam base lever, and extended 5~10m to upper reach of dam heel and to down reach of dam toe. Consolidation grouting pores in the range of upstream can also be used as subsidiary drapery, and the depth of pores is 20m. In the down stream of dam toe, the depth of pores which lies in region of high stress is 15~20m. The depth of general pores lies in the confluence of faults and erosion sidebands in 20m, and part of the pores were deepened to 30~40m. Because dam foundation were excavated to micro-effloresced belt and fresh rock, the property of rock is good, as can be seen in formula (5), (10). Let material parameter after grouting be same as original I, II, which can be seen in chart 2.

Chart 1. Physical and mathematical parameters of all kinds of materials.

Types of materials	Modulus E (Gpa)	Poisson's ratio μ	Cohesions c′ (Mpa)	Friction coefficient f′
Concrete I in dam body	21	0.167	2.5	1.0
Concrete II in dam body	21	0.167	2.5	1.0
Rock mass type I, II	22	0.24	2.0	1.45
Rock mass type III, IV, V	8	0.31	0.8	1.0
F_7	1.0	0.35	0.03	0.3
F_{11}	1.8	0.35	0.04	0.4
F_{10}	1.2	0.35	0.04	0.4
F_5	1.1	0.35	0.04	0.4
F_{27}	1.7	0.35	0.04	0.4
F_{19}	1.7	0.35	0.04	0.4
F_{22}	1.7	0.35	0.04	0.4
F_{23}	1.7	0.35	0.04	0.4
F_{20}	1.7	0.35	0.04	0.4
El	2.4	0.30	0.45	0.9
E4, E5	2.4	0.30	0.45	0.9
E8	0.7	0.30	0.04	0.4
Base surface ▽953	18	0.25	1.3	1.3
Left base surface ▽963, ▽975	19	0.25	1.3	1.3
Left base surface ▽990, ▽1010	26	0.21	1.3	1.3
Left base surface ▽1030~▽1070	22	0.24	1.23	1.26
Left base surface ▽1090, ▽1110	25	0.22	1.3	1.3
Left base surface ▽1130~▽1170				
Right base surface ▽990, ▽1010	23	0.23	1.3	1.3
Left base surface ▽1190~▽1210				
Right base surface ▽1070~▽1190	17	0.26	1.23	1.26
Left base surface ▽1230	5.5	0.3	1.0	1.13
Left base surface ▽1245	8.0	0.29	1.0	1.13
Right base surface ▽963, ▽975	21	0.25	1.3	1.3
Right base surface ▽1030, ▽1050	20	0.25	1.28	1.29
Right base surface ▽1210, ▽1245	17	0.26	1.0	1.13
Right base surface ▽1230	3.0	0.35	1.0	1.13

Chart 2. Physical and mathematical parameters of rock body after support.

Types of materials	Modulus E (Gpa)	Poisson's ratio μ	Cohesions c′ (Mpa)	Friction coefficient f′
Consolidation grouting	22.0	0.24	2.0	1.45
Concrete plug substitution of F_{11} in the left dam abutment	4.843	0.328	0.368	0.567
Concrete plug substitution of E_8 in the left dam abutment	11.016	0.257	1.088	0.935
Concrete plug substitution of F_{11} in the right dam abutment lies in ▽1010m~▽1110m	8.57	0.302	0.769	0.709
Concrete plug substitution of F_{11} in the right dam abutment lies in ▽1110m~▽1130m	9.304	0.297	0.848	0.754
Concrete plug substitution of F_{11} in the right dam abutment lies in ▽1130m~▽1270m	20.0	0.22	2.0	1.4
Concrete plug substitution of E_1 in the right dam abutment	13.136	0.251	1.396	1.205
Concrete plug substitution of E_4+E_5 in the right dam abutment	9.165	0.269	1.046	1.192
Injection anchor support	8.0	0.31	0.865	1.0

4.1.2 *Treatment to faults and weak crush belts*

Based on the reinforce design of Kunming institute, waffle concrete plugs were substituted located in the range of ▽1085~▽1145m, 3 layers of concrete level plugs were set numbered E_1, the clear distance between them was 15m, the height of the plug was 8m. The synthetic parameters of concrete level plugs, concrete-substituted rock mass were derived from formulas 11~14, which can be seen in the chart 2.

4.1.3 *Prestressed anchor lines*

Unload rock mass has developed deep on both banks of Xiao Wan dam. Schist interlayer in the unload layers were mostly softened, part of which were argil lied, and the property of the rock mass around the fault in the unload layer became worse. In order to improve the integral stressed performance of rock mass located in down stream, prestressed anchor lines were laid out on both sides of the bank. On the left side, prestressed anchor lines level 3000 KN were adopted, the length of which ranges in 42m~60m, the level interval is 5m, and the difference of elevation ranges in 5m~8m. These cables were laid out trapezoidally in ▽990m~▽1430m, the width along river of which is in the range of 500m. On the right side, prestressed anchor lines level 1000 KN~6000 KN were adopted, the length of which ranges in 40m~76m. the level interval is 4m~5m, and the difference of elevation ranges in 4m~8m. These cables were laid out trapezoidally in

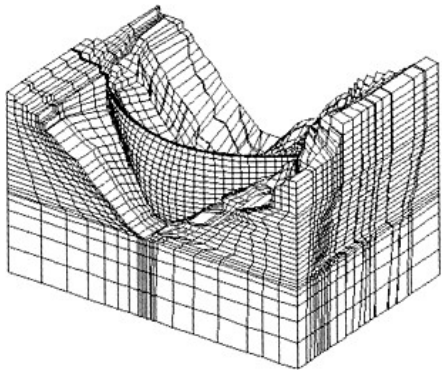

Figure 3. Entirely 3-D FEM mesh of Xiao Wan arch dams.

▽990m～▽1315m the width along river of which is in the range of 700 m. A pair of variable forces were adopted to simulate the function of anchor lines.

4.1.4 *Injection bolt support*

Bolt is a kinds of "surface" protection method. Directed towards that dam body always discharge flood, the scope of water vapor is large, and the excavation of water apron disturbed the base of slope, such measures were adopted as cleaning part of unstable rock bodies in slope wash deposit, and high-effloresced, high-unloaded rock layers, laying out injection anchor supports, injection anchor supports with nets on the slopes. Shear strength of bolt is taken as τ_s=300 Mpa, then the synthetic parameters of rock body after support can be calculated from formula (3), as can be seen in chart 2.

4.2 *Analysis on the effect of reinforcement*

Here 3-D non-linearity FEM is adopted to analyze the stability of Xiao Wan arch dam and foundation system. There are 13352 elements, 15892 notes in the entire mesh, in which the basic simulation is made on the structure feature, situation of base surface, terrain and physiognomy, rock constitution, including major faults such as F_5, F_7, F_{10}, F_{11}, F_{19}, F_{20}, F_{22}, F_{23}, F_{27} and erosion alteration zones such as E_1, E_4, E_5, E_8 Dam body and foundation were mostly adopted in hexahedron and 8 notes iso-parametric elements, minor of which was adopted in pentahedron and 6 notes elements. Faults and base surfaces were 8 notes film interfacial elements. All of the 3-D mesh can be seen in Figure 3. In the reinforcing plan on rock body in the dam foundation, abutments and slope, the safety degree is K=1, result can be calculated under the case of designing loads.

4.2.1 *Safety degree*

Seen from the changing situation of the displacement process line of several characterization positions, range of plastic zones and whole safety degree fore-and-after reinforcement, all these val ues are not sensitive to the reinforcement programs, that is to say, their values do not change obviously.

4.2.2 *Deformation energy*

When the whole safety degree K=1, the strain energy before reinforcement is 1.835×10^{10} J, and decreases to 1.628×10^{10} J after reinforcement. These values change obviously.

4.3 *Optimization of reinforce programs*

The results can tell us that an arch dam has no failure zones under designing load before being reinforced. Except for F_7, faults and erosion alteration zones have only minor destructions areas

appear in the coming out the bank slope or the inner side, while the rock itself has no destruction areas. The entire stability is good, and the safety degree is larger than 3.0. So, we optimize reinforcement programs according to the results that the strength reserve is 3.0.

a) Consolidation grouting

The original designed consolidation-grouting program eliminated the destructive areas before grouting basically. But there is also superficial layers in the right dam foundation lying in $\nabla 953\,\mathrm{m}\sim\nabla 954\,\mathrm{m}$ So it is recommended that the range of grouting should be extended to dam axis. After doing that, that destruction areas disappeared.

b) Treatment to faults and weak crash zones

It is calculated that when the faults and erosion alteration zones have not been processed, F_{11} broke down in the left bank located in $\nabla 1170\,\mathrm{m}\sim\nabla 1190\,\mathrm{m}$. The results indicated that after optimization, there are no fault zones in the above regions.

c) Anchorage treatment

The reinforcing effect of anchor lines can hardly be reflected in the calculation. Considering there are partial destruction areas on the right abutment, and there are power station under ground, and though the destruction areas are small on the left abutment, there is a fault F_{20} along river, the layout of prestressed anchor lines is necessary. And the distance between the cables on the bank slope can be increased a little, while the range is reduced properly. Thus the entirety of the abutment and the stability of the bank slope can be improved and the project cost can be reduced as well.

d) Injecting bolts to support

The supporting measures, such as injecting bolts, are essential to the excavation of the side slope. The results also show that when safety reserve K=3.0, the strain energy is 11.202×10^{10} J before reinforcement. Supposing the strain energy is 11.016×10^{10} J under the design program, and then it changes to 11.042×10^{10} J after optimization. And the effect is obvious. And the effect is even more apparent when the calculation range of the strain energy is limited to the reinforced area.

5 CONCLUSION

This paper puts forward that strain energy criterion can measure the reinforcement effect greatly and it yields a better program through the reach to the all kinds of working mechanics and simulation methods to the arch dam foundation, considering not only the effects on the rigidity, but also on the rock material parameters after reinforcement. The research method is simulating and analyzing the effect of the design programs and the range of reinforcement to the deformation and stability of the Xiaowan arch dam abutment and foundation. Based on this, the optimal scope of the dam abutment and foundation is determined and the economical and safe reinforcement program is chosen. The research denotes that this method not only has important theoretical meaning, but also has high application value, which can supply basis to the reinforcement design of the Xiaowan high arch dam abutment and foundation.

REFERENCES

[1] 混凝土拱坝设计规范．中华人民共和国水利部, SL282–2003, 32–37.
[2] 段宝岩，陈建军．基于极大熵思想的杆系结构拓扑优化设计研究．固体力学学报, 1997(4):229–335.

New Developments in Dam Engineering—Wieland, Ren & Tan (eds),

Interface behaviour of Roller Compacted Concrete Dams

Zheng Dongjian & Zhong Lin
Hohai University, China

ABSTRACT: As the particular construction technology and the existential horizontal conjoint interface, the structure behaviors of Roller Compacted Concrete Dams (RCCD) are evidently different between the horizontal direction and the vertical direction. The construction joint between RCC layers is the key of RCCD safety. In order to evaluate the behavior of RCCD conjoint interface, the series model of composite material structure was applied to simulate the effect of the conjoint interface to the modulus of elasticity of the whole dam body and a method of inversing the effect thickness of RCCD interface and its physical mechanics parameter based on observation data was presented. And the field similar index of deformation is applied to optimize the parameter. A sample was given.

1 INTRODUCTION

RCCD is made of thin concrete lift and roller compaction layer by layer. As the particular construction technology and the existential horizontal conjoint interface, the structure behaviors of RCCD are evidently different between the horizontal direction and the vertical direction. The badly cementation of the horizontal conjoint layers easily become relatively weak planes and turn into the vulnerable components of dam's seepage, strength and stability. So, to simulate the effect of conjoint layers objectively is key to accurately analyze the structure and seepage behavior of RCCD. Meanwhile, with the passage of dam's run time, the erosion of influent, the aging of material and the influence of environment, the conjoint interface behavior also can change. Besides, how to evaluate the behavior of RCCD conjoint interface is the difficult point to evaluate the RCCD safety. For the sake of these, this paper presents a method of inversing the effect thickness of RCCD construction conjoint interface and its physical mechanics parameter based on observation data. And the field similar index of deformation is applied to optimize the parameter.

2 RCCD INTERFACE PARAMETER ANALYSIS

For RCCD, its effect thickness of conjoint interface (b_a) and its modulus of elasticity (E_a) are rather difficult to be simulated accurately through some experiment. But, the modulus of elasticity of the RCC layers could be set easily with corresponding experiment. Now, we will discuss the feedback method of two parameters (b_a) and (E_a), which based on observation data.

2.1 *The RCCD modulus of elasticity considering the conjoint layers' effect*

The RCCD modulus of elasticity are different between the direction which is vertical to the conjoint layer (E_1) and the direction which is parallel (E_2). For analysis convenience, we make some hypotheses as follows: the RCC body and the conjoint layer are isotropy, and they also have their own modulus of elasticity—(E_C) and (E_a), b_c is the body's thickness, b_a is the effect thickness of conjoint layer (the subscripts c and a each mean 'body' and 'conjoint layer'). Generally, bodies

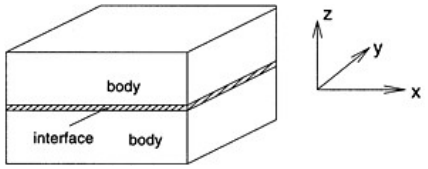

Figure 1. Sketch of RCC body and conjoint layer.

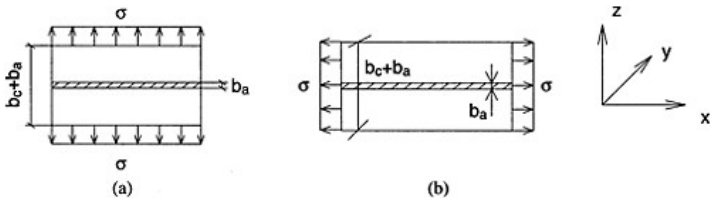

Figure 2. The series model of defining RCC Young's modulus.

separate every conjoint layer and the conjoint layer to the whole dam body is comparatively small. According to the structure theory of composite material, we can apply the series model of composite material structure to simulate the conjoint layers' effect to the modulus of elasticity of the whole dam body. Figure 1 shows the diagram of RCC body and conjoint layer; Fig. 2 shows the volume unit of the series model.

When the volume unit is under the action of the stress as Fig. 2, the deformation that is vertical to the conjoint layer is as follows

$$\Delta b=\varepsilon_1(b_c+b_a)=\varepsilon_c b_c+b_a\varepsilon_a \tag{1}$$

$$\varepsilon_1=\varepsilon_c v_c+v_a\varepsilon_a=\varepsilon_c(1-v_a)+\varepsilon_a v_a \tag{2}$$

In formula (1) and (2), v_c and v_a are the volume contents of body and layer, $v_c+v_a=1$, considering $\varepsilon=\sigma/E$, modulus of elasticity E_1 which is vertical to the layer of RCC is:

$$\frac{1}{E_1}=\frac{1}{E_c}(1-v_a)+\frac{1}{E_a}v_a \tag{3}$$

Similarly, when the mean stress of Fig. 2 (b) acts on the volume unit, rely on the plane hypothesis of material mechanics, the deformation ε_2 paralleled the layer of RCC is:

$$\varepsilon_2=\varepsilon_a=\varepsilon_c \tag{4}$$

and $\sigma(b_c+b_a)=\sigma_c b_c+\sigma_a b_a$, $\varepsilon=\sigma/E$, then

$$E_2=E_a v_a+E_c(1-v_a) \tag{5}$$

Usually the body modulus E_c is determined by tests, if the modulus of elasticity E_1 and E_2 can be feedback analyzed, E_a and v_a can be gotten from the formulas (3) and (5). At the same time, the geometric dimension of special dam is a constant, the average influential thickness ba of RCC conjoin layer can be gotten from v_a.

2.2 *The feedback analysis of two-way anisotropy of RCCD*

(1) Objective function

The similar divergence factor index can image the similarity of model and number, so it can be used as objective function to optimize parameters. Suggest that i and j have the same element distributions under standardization, the elements of them are X_{ik} (k=1, 2, Λ n) and X_{jk} (k=1, 2, Λ n), n is the number of elements. The similar divergence factor indexes of i and j are:

$$C_{ij}=\frac{1}{2}(S_{ij}+D_{ij})$$

n the formula $S_{ij}=\frac{1}{n}\sum_{k=1}^{n}\left|X_{ijk}-E_{ij}\right|$, $D_{ij}=\frac{1}{n}\sum_{k=1}^{n}\left|X_{ijk}\right|$, and $X_{ijk}=X_{ik}-X_{jk}$,

$$E_{ij}=\frac{1}{n}\sum_{k=1}^{n}X_{ijk}.$$

(2) Feedback method

Referent document (2), the statistical model of deformation of dam is:

$$\delta=\delta_H+\delta_T+\delta_\theta \tag{6}$$

in formula (6): δ_H—component of water press δ_T, δ_θ—component of temperature change, component of prescription period.

The statistical models are these:

$$\delta_H=\sum_{i=0}^{m}a_i(H^i-H_0^i) \tag{7}$$

$$\delta_T=\sum_{i=1}^{m_1}[b_{1i}(\sin\frac{2\pi it}{365}-\sin\frac{2\pi it_0}{365})+b_{2i}(\cos\frac{2\pi it}{365}-\cos\frac{2\pi it_0}{365})] \tag{8}$$

$$\delta_\theta=c_1(\theta-\theta_0)+c_2(\ln\theta-\ln\theta_0) \tag{9}$$

in these formulas, a_i (i=3~4) is regressive coefficient of water pressure weight; H is water depth of observation day; H_0 is water depth of the first observation day; b_{1i}, b_{2i} are regressive coefficient of thermal factor; m_1=1~2 is a year or half a year cycle; c_1, c_2 are regressive coefficient of time effect factor; t is accumulative time in days from the first observation day to observation days; t_0 is time in days from the first observation day to the initial day of calculating period; θ is observation time in days starting from the first observation day to initial day of calculating period multiply 0.01.

So, we could obtain the weight of water pressure according to equation (6),

$$\begin{aligned}\delta_H&=\delta-\delta_T-\delta_\theta\\&=\delta-a_0-\sum_{i=1}^{m_1}[b_{1i}(\sin\frac{2\pi it}{365}-\sin\frac{2\pi it_0}{365})+b_{2i}(\cos\frac{2\pi it}{365}-\cos\frac{2\pi it_0}{365})]-c_1(\theta-\theta_0)-c_2(\ln\theta-\ln\theta_0)\end{aligned} \tag{10}$$

After work out the weight of water pressure in the light of equation (10), the general inversing computing is that to apply finite elements computing to a certain deformation point of dam acting on different water loads, then to apply multinomial to mimic the correlation between water depth and the weight of water pressure of deformation, and consider regulating coefficient X as the influence discrepancy between computing parameters employed and actual parameters, which is

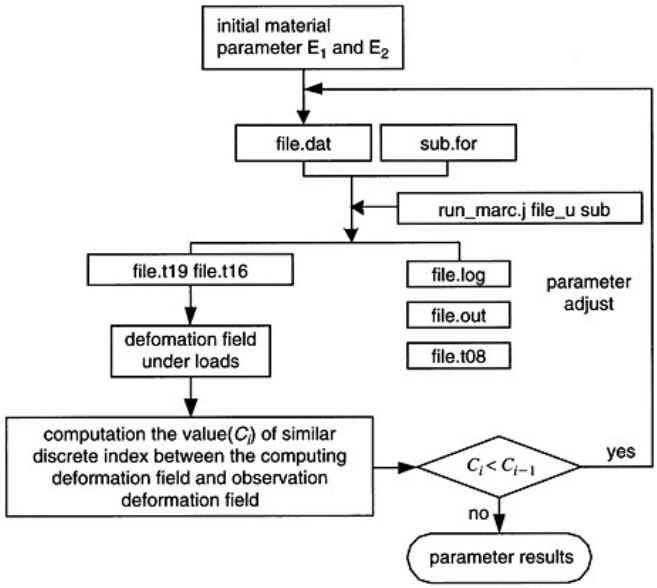

Figure 3. Flow chart of computing process.

expressed by $\delta_H = X\sum_{i=0}^{m} a_i H^i$, but as far as RCC characteristic of two-direction imparity of elastic modulus be concerned, it is difficulty for us to regulate this discrepancy, by the way of employing a coefficient X alone. For as much this point, in the available range of elastic modulus E1 and E2, which is perpendicular or parallel to the direction of conjoint layer respectively, we can obtain the E1 and E2, with minimum value of similar discrete index in the computing deformation field and observation deformation field by means of trying out computation repeatedly. Thus we can work out the values of Ea and va by equation (3) and (5), at the same time, we also could obtain the average effect thickness of dam construction layer ba.

2.3 *Computing flow chart*

According to the principle mentioned above, the RCCD interface effect thickness and mechanic parameters concerned could be obtained by inversing computation employed the computing program of three dimension finite elements, Marc, the computing flow chart in Fig. 3.

3 A EXAMPLE

Certain Hydropower Station's dam is monolithic roller compacted concrete dam, dam axis lays out as mansard for the purpose of riverside's conjoin. The length of dam is 196.62m. On the rest and has a maximum height of 63m, its crest elevation is 145m. The spillway dam section is placed in the center of riverbed, while the non-overflow dam sections are plated on its both bands. The total reservoir capacity is 0.106 billion m^3. The normal water level is 143m, dead water level is 137m, and check flood level is 144.17m. The dam site is located in the middle of gorge with a length about 200 m. The dam foundation mainly consists of granite, partly of tuff sandstone and rhyolite, which locate in central and lower rock in weakly or slightly weathered rock mass. There are mainly three faults F_1, f_1, F_4 and fissure in dam foundation. Deformation observation system is embedded

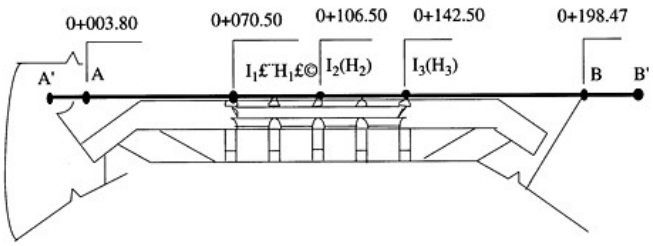

Figure 4. Arrangement of observation.

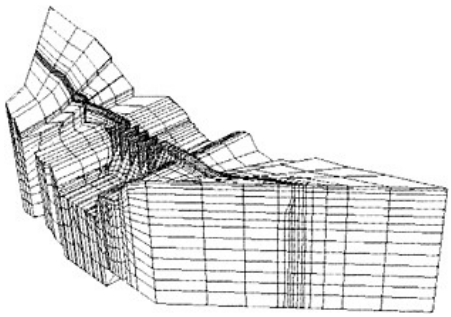

Figure 5. Finite elements model of dam.

in the dam, collimation lined are provided I the upstream crest (behind the dam 0–001m) for the monitoring of horizontal displacement with its total length 198.47m each band places work base point A and B and check base point A′ and B′ separately. In the middle of collimation lines there are three observation podium, that is 11 (0+070.50), 12(0+106.50), 13(0+142.50). The arrangement of observation point is shown in Fig. 4.

3.1 *Establishment of finite elements model*

According to the feature of the dam and geological condition of dam foundation and the arrangement of the observation point, the area of the finite element model is from upstream 200m (about 3 times as much as max height of dam) to downstream 150m (about 2.5 times as much as max height of dam). Considering the mansard axis of dam makes it have some characteristic of arch dam, it is 150m withdrawn from both left and right abutment separately. The element division is according to the RCC placement, and nodal point should be placed by the position of displacement as possible. In order to correspond to the actual situation, the element division in dam foundation should base on the strike fault, weak band's distribution and the variety of geological condition. The element configuration adopts hexahedron-eight modals or pentahedron-six modals are parametric unit. Three dimensions finite net model graph with total 7104 is parametric units and 9099 nodal points shown in Fig. 5.

3.2 *Calculative parameter and the selecting of load condition*

(1) RCC elastic modulus (E_1) in vertical layer and (E_2) in paralleled layer should take 100 thousand to 35.0 thousand MPa at the beginning calculating. Base rock's modulus of deformation *(E_j)*

Table 1. Statistical table of deformation modulus in dam foundation and both river banks (MPa).

Altitude	Left bank	Right bank
Above 132m	2.0×10^4	2.0×10^4
105m~132m	2.5×10^4	2.2×10^4
Below 105m	2.9×10^4	2.9×10^4

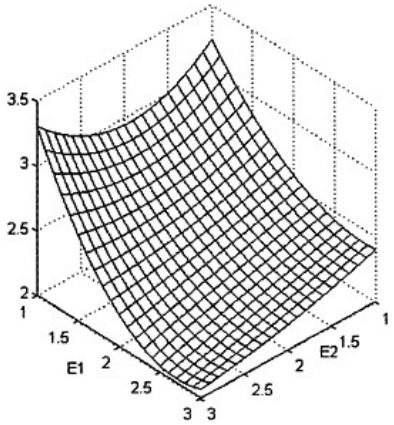

Figure 6. the change of the I2 point horizontal displacement towards downstream under the typical water level with the $E_1\times10^4$ and $E_2\times10^4$.

mainly refers to experimental data and analogous projects. The corresponding value is shown in table 1. The modulus of deformation of fault F4 takes 2.5 billion MPa.

(2) Firstly, establish statistical model for measuring pointing, separate hydraulic pressure ponderance of horizontal displacement of dam crest. Then those close to or exceed the normal water level in the work status are chosen to inverting the modulus. At last, take the average values of typical load conditions as the final value.

3.3 *Analysis of achievement*

(1) According to the calculating above, we find the elastic modulus (E_1) of the vertical direction is 2.5812×10^4Mpa and the elastic modulus (E_2) of the parallel direction is 2.7144×10^4MPa. So (E_2) is 1.3 times as much as (E_1), this phenomenon is similar with the achievement of some experiments that have been written in some books. Figure 6 shows the change of the 12 measure point's parallel displacement towards downstream, which is under the action of typical water level. It indicates that (E_2) takes a more important part in effecting the parallel displacement.

(2) After obtaining (E_1) and (E_2), we get (E_c) equals 2.023×10^4 MPa~3.6751×10^4 MPa by doing on-the-spot experiment and command that (E_c) equals 2.8435×10^4 MPa. Then we can work out (E_a) equals 1.2704×10^4 MPa and v_a equals 8.201% by using equation (3) and (5). We also can obtain the average effect thickness of RCCD construction layers is about 16mm~30mm.

4 CONCLUSION

(1) Using the modified equivalent layer we can simulate the affect of RCCD interface. The method presented in this paper is feasible to inverse the effect thickness of RCCD and its physical mechanics parameter based on observation data, theory of compound material, 3-D finite element method and field similar ides of deformation.
(2) The construction of RCC conjoint layer is the key of RCCD safety. With inversing the effect thickness of RCCD interface and its physical mechanics parameter based on observation date, a new factor was afforded to evaluate the safety of RCCD.
(3) Field similar index of deformation is applied to optimize the parameter, and its result can reflect the structure characters of the dam. It benefits us in evaluating the behavior of the dam. At the same time, the sample indicates that the computational results tally with the reality.

ACKNOWLEDGEMENT

Financial support for this paper was provided by National Natural Science Fund of China (50139030) and 973 Project Fund of China (2002CB412707).

REFERENCES

[1] Wang Yao Xian, The structure Design of Compound Material, Chemistry Industrial Press, Beijing, 2001.
[2] Wu Zhong Ru, Monitoring Technology of Dam Safety and the Practice, Higher Education Press, Beijing, 2003.
[3] Bakanovichus S., As, Bertorv M., Sudakov V.B., Vasilevsky V.V. (Soviet Union), Character of RCCD's Strength, Deformation and Trim, Int. symp. on RCCD, Beijing, 1991.

This page intentionally left blank.

New Developments in Dam Engineering—Wieland, Ren & Tan (eds),
© 2004 Taylor & Francis Group, London, ISBN 04 1536 240 7

Risk analysis of dams based on observational data[1]

Zheng Dongjian[1], Hong Yun[1,2], Xu Shiyuan[3], Liu Chengdong[1] & Zhou Hong[1]
[1]Hohai University, Nanjing, China;
[2]Fujian Company of Huadian Group, Fuzhou.;
[3]Gutian Water Power Station, Gutian.

ABSTRACT: The practical risk factors of dam and their quantization methods are hard to dam risk evaluation. Dam observation data is a complex reflection on the current dam safety. Therefore based on dam observation data and risk analysis theory, this paper conducts a risk analysis method of the current dam safety. The dam risk, such as the risk of deformation, seepage and stress-strain, could be analyzed by monitoring index of dam safety obtained by probability or structure emulation program. The whole dam safety risk index was discussed synthetically by weight function of dam safety decided by fuzzy mathematics or expert. The dam safety risk analysis computer system based on observation data was developed.

1 INTRODUCTION

The action of dam operation and management risks engineering safety and economy. It must consider the benefit of flood control, generation, irrigation etc., as well as the safety bearing capacity of dam body. Risk analysis and evaluation, as a new method of making dam safety decision, involves every aspects of the complicated concepts of dam safety decision and society risk. During the nineties of the 20th century, dam safety risk had been paid much more attention to, and a lot of views and comments about its quantitative analysis emerged in China and abroad. Presently, some other countries, such as U.S.A, England, Portugal etc., appraise the risk by means of a set of influence information of dam to mankind, to property and to our environment. And they grade dams in order to optimize dam safety management[1][2]. For instance, risk analysis and evaluation, as a part of dam safety management, is regarded as a way to improve the management by USBR (United States Bureau of Reclamation). They established the dam safety management program and applied the site rating to measure dam risk. Then, they could determine dams whose risk is inadmissible, and take engineering or non-engineering measures to lower or eliminate the risk. For a safe dam, USBR thinks that its risk should be acceptable to the public firstly, and the accomplishment of predetermined functions of the dam is following. Meanwhile, dam risk evaluation, as one decision means, could direct that the capital be invested in the project with maximum risk. In China, the analysis theory has had a development to some extent. The practical risk factors of dam and their quantization methods are hard to dam risk evaluation. Dam observation data including deformation, seepage and stress-strain is a complex reflection on the current dam safety. Therefore a risk analysis method of the current dam safety based on dam observation data and risk analysis theory was presented.

[1] Financial support for this paper was provided by Natural Science Fund of China (50139030) and 973 Project Fund of China (2002CB412707).

2 INDEXES OF RISK EVALUATION

2.1 *Dam safety risk rate*

Suppose the symbol of risk rate is RI. There are n mutual independent random variables that constitute dam-generalized resistance R, and m variables like that which constitute dam-generalized load S. The joint density function of S and R is $f_{rs}(r,s)$. So the RI's representation formula is as follows[3][4].

$$RI = P_f = \int_0^R \int_0^S f_{RS}(r,s)drds \tag{1}$$

Where: r: single factor resistance; s: effect of single load; P_f: the probability that R is less than S.

Under present technical conditions, to obtain the analytic formula of $f_{rs}(r,s)$ is rather difficult. Therefore, to get the RI's value, we have to depend on the approximate probabilistic method and the structural method in structural reliability theory. For the sake of making the risk appraisal to dam in certain area coverage, the quantization of factors must establish a more unified standard. And the dam risk factors usually include structure, seepage, engineering age, construction quality, storage capacity, water head, hidden danger, flood, seism and so on. At the same time, risk indexes should reflect the effects of environment and time. Factors affecting dam safety mainly consist of deformation, seepage, stability, strength and so forth. While the observation data of deformation, seepage and stress-strain are these safety factors' corresponding concentrated expression. And the data also reflect the characteristics of dam safety risk's variation with environment and time. So, the risk indexes of dam operation's deformation, seepage and stress-strain could be presented based on their own observation data.

2.1.1 *Deformation*

According to dam safety norm:

$$F-F_c \geq 0 \tag{2}$$

Where: F: dam or dam foundation resistance; F_c: gross effect of critical loads association.

If F is an allowable resistance or within the range of variation allowed based on dam operation principle, every monitoring effect amount caused by the loads association which accords with the inequality (2) is a warning value. If F is a limit value, it is the extreme. The capacity resisting possible loads can be evaluated and predicted according to the capacity of dam & dam foundation resistance to happened loads. On this basis, the monitoring effect warning value and the extreme could be assigned.

The safety index or risk of dam deformation could be reflected by the approximation degree between the observation deformation amount and the monitoring index of dam deformation safety. And the deformation safety monitoring index could be obtained by three methods: the confidence interval method, the canonical little probability method and the limit load method[5]. Namely, based on the practical condition of every dam, under the same structure system, we can put forward the monitoring and control warning value or deformation monitoring and control index E_m. Within some evaluating time interval, while the extreme of practical monitoring effect amount to every observation item is E_i. When the situation is $E_i > E_m$, we think that the dam is abnormal or will have an accident. Then, the safety risk rate of deformation E_i for dam point is as follows.

$$(RI)_{11} = (E_i/E_m) \times 100\% \tag{3}$$

And the risk rate for dam deformation destruction:

$$(RI)_1 = \sum_{i=1}^{n1} \alpha_{1i}(RI)_{1i} \tag{4}$$

Where: $(RI)_{1i}$: risk rate of deformation amount E_i for dam point i at time t; α_{1i}: importance index for dam point i.

2.1.2 *Seepage flow*

The seepage monitoring includes three parts: uplift pressure, seepage amount and ground water level. The seepage condition reliability can be reflected by the observation value's ratio to the seepage index. And the uplift pressure safety condition can be reflected by the observation value's proportion in the design allowable value or by the proportion of the gross observation uplift pressure in the design gross uplift pressure. The seepage amount-monitoring index can be computed based on the observation data by the probability statistics method or by the seepage simulation computation. The monitoring and control for ground water level is usually obtained through the stability computation of a slope or dam shoulders, or through the probability statistics for observation data. On this basis, the destruction risk rate for seepage flow is as follows.

$$(RI)_2 = \sum_{i=1}^{n2} \alpha_{2i}(RI)_{2i} \tag{5}$$

Where: $(RI)_{2i}$: dam seepage safety risk rate for point i, time t; α_{2i}: importance index for point i.

2.1.3 *Stress*

The strength monitoring and control can be generally determined based on the strength of materials and the corresponding safety coefficients. Suppose the allowable strength of extension is σ_1, the allowable compression strength is σ_2. Besides, the observation stress value is σ (positive for tension; negative for pressure). The stress reliability is as follows.

$$(RI)_{3i} = [2\sigma^2 / (\sigma_1^2 + \sigma_2^2) - 2(\sigma_1 + \sigma_2)\sigma / (\sigma_1^2 + \sigma_2^2) + (\sigma_1 + \sigma_2)^2 / (\sigma_1^2 + \sigma_2^2)] \times 100\%$$

$$(RI)_3 = \sum_{i=1}^{n3} \alpha_{3i}(RI)_{3i} \tag{6}$$

Where: $(RI)_{3i}$: stress safety risk for point i, time t; α_{3i}: importance index for point i.

2.1.4 *Routine inspection*

Inspection towards dam and dam's foundation regularly or irregularly in some coverage of dam area is an important way to ensure dam safe. The inspection includes two parts: deformation and seepage. Of course, the inspection information is shown through the qualitative method rather than the precise value or function. We can apply fuzzy mathematics to quantitate and analyse this kind of qualitative and fuzzy monitoring data. And the subordination degree computation for evaluation indexes usually includes three methods: the expert score method, the interval score method and the method of binary order contrast.

$$(RI)_4 = \sum_{i=1}^{n4} \alpha_{4i}(RI)_{4i} \tag{7}$$

Where: $(RI)_4$: safety risk embodied by the inspection information for point i, time t;
α_{4i}: importance index of inspection information for point i.

2.1.5 *Dam safety risk rate*

In approximation probability method, the failure probability only aims at the failure of specific destruction form for dam's some cross-section. Therefore, to obtain the solution of RI, we need the further analysis. Now, for dam's structural component, its probability of specific destruction form is P_{fj}, and its corresponding dam safety single risk rate is RI[4].

$$L = \sum_{i=1}^{3} l_i \tag{8}$$

As everyone knows, dam every segment's operation mode is the series mode. Once a certain segment has an accident under any kind of destruction, the whole dam also has an accident. So, the dam safety gross risk rate is as follows.

$$RI = P(RI_1 \cup RI_2 \cup \cdots \cup RI_i) \tag{9}$$

2.2 *Consequences of dam accident*

The consequences are the effects of its accident with mutual independence, a certain of form and specific degree, after making a division to the accident The consequences usually consist of three parts: life loss, economy loss and environment deterioration. So, the consequences' representation formula is:

$$L = \sum_{i=1}^{3} l_i \tag{10}$$

Where: l_1, l_2, l_3: corresponding expected values to the three kinds of losses.

2.3 *Dam safety risk evaluation*

The failure probability for dam body is taken account of in the evaluation, the consequences and effects of dam accident as well.

$$RD=RI\times L \tag{11}$$

Where: RI: failure probability for dam body; L: consequences of dam accident.

3 A EXAMPLE FOR DAM SAFETY RISK ANALYSIS

This example is about some cascade development dams with 4 steps. For the step-1, its control valley area is 1295km^2, accounting for 73 percent of the gross valley. It is a concrete sotted gravity dam, with a buried power plant. The gross installed capacity is 66MW, and annual energy output is 3.71GkWh. The dam is 71.0m in maximum height, the overall length of dam crest is 412.0m, and has 21 segments. For the step-2 hydropower station, it is a mixed power station, taking generation as the dominant factor. The dam with steel reinforced concrete facing is 37.0m in maximum height. Its installed capacity is 130MW. For the daily regulation reservoir, its storage capacity is about 1.54×10^7m^3. For the step-3 dam, it is a deck dam with steel reinforced concrete, with 27 deck buttresses whose span are 7.5m. Its crest altitude is 137.70m,the maximum height is about 43m, the crest overall length is 225.0m, and its installed capacity is 33 MW. For the step-4 hydropower station, it is a gravity dam, with 13 segments. The maximum height is 43.0m, and the crest length is 234.1m. Its installed capacity is 34MW, and its pluri-ennial average output is 1.342×10^4kWh.

3.1 *Determination of dam risk degree*

Based on the observation data and formula (2)—formula (8), we can compute the risk indexes and determinate the risk degree or the safety margin. The table-1 puts forward three safety margins for three working conditions—normal high water level, design high water level and high water level for maximum flood.

3.2 *Dam risk evaluation*

Lack of the data of dam's influence to the environment, four indexes—safety margin, capitalized cost, economic benefit and accident consequence—are adopted. To simplify the calculation, the

Table 1. Safety margins under the circumstances of typical level.

Safety margins	Step-1	Step-2	Step-3	Step-4
Normal level	0.55	0.103	0.42	0.45
Design level	0.54	0.12	0.05	0.10
Check level	0.79	0.42	0.20	0.272

Table 2. Risk evaluation results for the step-dams based on observation data.

Working condition	Step-1	Step-2	Step-3	Step-4
Normal level	1.93	2.36	1.79	1.50
Design level	1.92	2.44	2.31	2.00
Check level	1.73	2.45	2.46	2.24

last three indexes are separately evaluated by three parameters—the height of dam, the installed capacity and the storage capacity & water head. The table-2 is the evaluation results.

According to the principle that the less the risk is, the better the dam is. We can make a good and bad order for step-dams for three working condition.

Normal level: Step-4>Step-3>Step-1>Step-2
Design level: Step-1>Step-4>Step-3>Step-2
Check level: Step-1>Step-4>Step-2>Step-3

The symbol ">" indicates that the former dam's whole operation is better than the latter. Now, step-2 and step-3 dams are being reinforced.

4 CONCLUSIONS

(1) The safety observation data is a complex reflection on the dam safety. Based on the above analysis of theories and the example, it indicates that we could apply the observation data to work out the dam complication risk rate and realize the dam safety risk analysis.
(2) The risk analysis contributes to overall evaluating the operations of dam safety and its benefit. We could achieve the safety management and the optimization of technology reform, and ensure that the limited capital is applied to the project with maximum risk.
(3) The dam failure probability and the accident consequences and effects are taken into consideration in the safety risk evaluation. The quantization of society economy index, especially ecological environment index, is the key to risk evaluation.

REFERENCES

[1] Doug Johnson, Washington, D.C. in U.S.A. Ten years' successful experience of dam safety analysis method based on risk. Dam and Safety. The first issue, 2001.
[2] Alton P.Davis, Jerrold W.Gotzmer. The grade guide—criterion to determinate dam's potential danger. Dam and Safety. The first issue, 2001.
[3] Sa ermeng, Dam Safety Risk Analysis, Express Water Resources and Hydropower Information. The fifteenth issue, 1993.
[4] Kajjper H.Vtijling J. Probabilistic approach and risk analysis [A], Netherlands: A.A. Balkema, Rotterdam, 1998.
[5] Wu zhongru, Safety Monitoring and Control Theory and Its Application for Hydraulic Structure. Higher Education Press, Beijing, 2003.

This page intentionally left blank.

New Developments in Dam Engineering—Wieland, Ren & Tan (eds),

Construction process simulation for the RCC cofferdam in Three Gorges Project

Zheng Ying
Three Gorges University, Yichang, Hubei, China

ABSTRACT: The third stage Roller Compacted Concrete (RCC) cofferdam of the Three Gorges Project (TGP) is a dam with the biggest construction rate in the world. According to the TGP's general schedule, 1.2 million m^3 concrete has to be placed within less then five months which is from February to June in 2003, and the maximum daily pouring intensity 19,200 cubic meters, far exceeds the world's record. In order to select the suitable construction method, the construction process simulation method is used during planning. For the construction process of RCC dam has dynamic, stochastic and cyclic properties, Dynamic Random Cyclic Operation Network (DRCYCLONE) technology is used to build the simulation model, which can show those properties fairly well such as random time parameters, some certain working activities cycle over and over and resource disposition changes continually and so on. This paper introduces how the simulation of DR-CYCLONE is used for the RCC cofferdam. The result of the simulating calculation demonstrates that simulation model advanced in this paper is practical utility, and draws a conclusion that this project cannot be built on schedule unless adopt the scheme of *full-face spreading and thinlayer continuous pouring* during the construction process.

1 INTRODUCTION

The construction of TGP, the largest hydropower project in the world, would last 17 years. In order to ensure the navigation in permanent shiplock and generate power revenues at initial stage of project construction, a temporary cofferdam would be built to retain reservoir water. The RCC cofferdam, 90m in height and 1.2 million m^3 in volume, would be built in one dry season. The RCC cofferdam, together with dam sections formed at the 2nd phase construction of TGP, would retain reservoir water and, at the same time, joining the downstream earth-and-rock cofferdam and a concrete longitudinal cofferdam to form the 3rd phase construction pit of TGP, within which the right-bank dam sections and powerhouse would be built. Because of the features of tight schedule and high construction intensity and so on, the maximum daily pouring intensity 19,200 cubic meters far exceeds the world's record, it is necessary to simulate the whole RCC construction process by the method of DR-CYCLONE according to the construction condition and preselected construction scheme, in order to evaluate the scheme and the schedule, and to provide a propositional scheme of the construction method and main machines.

2 DR-CYCLONE SIMULATION METHOD

The Cyclic Operation Network is the first method used for the simulation of the RCC construction system. This method is a network planning technology started in seventies of last century, which applies random queuing theory and computer simulation technology to network planning technology so as to fully reflect the cyclic characteristics of the construction process and the stochastic character of some activity duration. By simulation, the construction cost, corresponding to different resources level and construction arrangement, can be calculated to find the block point. And the optimum scheme with the reasonable machine selection and schedule and cost can be found by the sensitive analysis.

2.1 *Constitute of DR-CYCLONE model*

Cyclic Operation Network Model is composed of Flow Units, Arrows and Nodes. Flow Unit is the state continuous changing and flow resource entity in the system, such as man power, machine and material.

Arrow shows the flow direction of Flow Unit and the logic relationship between Nodes or activities.

Node is the assembled place of Flow Unit, and shows the finished process of some one activity. There are Normal, Compound, Queuing, Statistic and Control node in the model.

Normal shows the free work and the active state. When Flow Unit reaches to the input position of the Node, it will freely entry to Node to be under the state of working for a certain of time.

Compound shows the restricted activity. After the conditions of all of resources entities ready to entry into the activity have been met, all of Flow Units can entry into the Node at the same time to be under the state of working for a certain of time.

Queuing node describes the Flow Unit under the positive state, and is used for storing idle and queuing Flow Unit, and has the function of times production and statistic and so on.

Statistic node calculates the times of passing the node, and has the function of combining several same types of Flow Units to one.

Control node is also named calculator with controlling and calculating function. It controls the running and the end of the simulation process by statistical value.

Besides above nodes, the DR-CYCLONE model has been added function to describe the variety of the quantity of Flow Units entities, service desk, time parameters and control variants in the simulation process.

2.2 *Building and simulating calculation of DR-CYCLONE model*

DR-CYCLONE is a network drawing consisted of a series of orderly arranging nodes and arrows by some certain of rules. When building model, firstly it must make sure the construction activities, the logic relationship between the activities and the necessary resources, then put these concrete scenario corresponding to abstract conception and figure of DR-CYCLONE simulation method to build the construction process simulation model. After building the simulation model, it is not only to add some active parameters of Flow Units into the model, named as construction parameters, such as resources quantity, machine quantity, activity duration and working quantity and so on, but also some functions corresponding to these parameters should be defined to describe their dynamic characteristics in construction process. So a completed DR-CYCLONE model has been formed.

After the model having been build and the simulation parameters having been added, the event-step-length method can be adopted to do simulating calculation. While doing simulating calculation, construct a event table to store the event doing at some one time and done beforetime, and the event should be arranged by the order from big to small.

3 RCC DAM CONSTRUCTION SIMULATION MODEL

RCC dam construction system includes the transporting system and placing system.

3.1 *RCC dam transporting system simulation model*

RCC transporting system includes two parts of concrete mixing and concrete transporting, which corollary equipment quantity should meet the requirement of the two parts. Firstly, the mixing

plant must have adequate volume to meet concrete design production rate, and the transporting equipment from mixing plant to pouring place must meet the transporting capacity required by concrete pouring intensity. Secondly, it should make corollary equipment and road using rate as economic and reasonable as possible to reduce equipment idle and queuing time and to keep road standard middle.

Considering the actual situation of the TGP, two transporting types of simulation model have been built.

3.1.1 *Belt transporting mode*

Belt transporting system is composed of four parts such as accepting device, conveying belt, unloading device and distributing device. The task of the accepting device is to transform the materials from the mixing plant or dumping truck to the conveying belt in order to make the discontinuous production of the mixing plant to the continuous transportation of the belt. The unloading device is to meet the requirement of the continuous supplying materials with the dam upward. The distributing device is to resolve the conflict between the continuous supplying of the belt and the discontinuous job of the transferring machine in the dam surface.

So the actual running system of the belt transportation is shown as following.

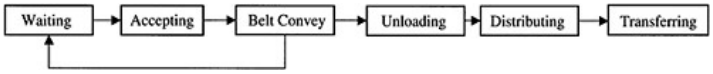

The belt itself is mainly considered in the simulation analysis, but accepting, unloading and distributing materials are supposed to meet the requirement of the belt production rate.

3.1.2 *Mode of directly transporting to the pour by dumping truck*

In the RCC construction process, the continuous forcing or self-dropping type of mixing plant is usually used. If not considering the fault of the mixing plant, the acceptance service of dumper at the mixing plant is only loading, namely there is not the activity of dumper waiting for mixing. Dumpers queuing before the mixing plant need certain of time because of loading.

The actual system of the mode of directly transporting to the pour by dumper is shown as following.

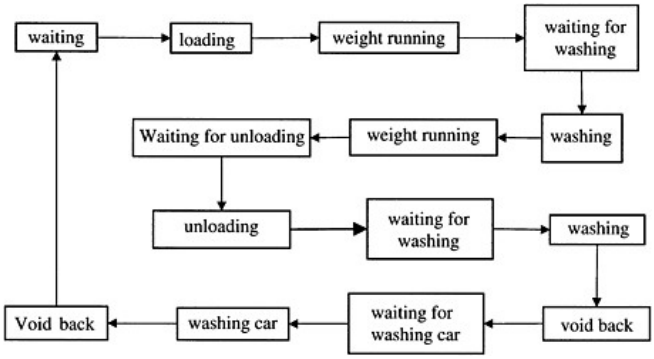

In the system, may supposed that the loading and washing durations subordinate to Normal distribution, the unloading duration subordinates to negative-Exponent distribution, the loaded running duration and void back duration of dumping truck on road can adopt corresponding value according to the transporting distance and the running speed of the dumping truck.

3.2 *RCC placing system model*

The RCC placing process is composed of a series cyclic activity of spreading, leveling, rolling, making joint, interval between two layers, rushing and placing mortar. RCC method generally adopts thin-layer rolling, that is rolling one layer after just spreading one layer. The interval between two layers is required not more than the initial setting time to complete one lift's pouring, and then pausing for about 4 days, the horizontal joint would be treated and the mortar would be spread to begin next lift cyclic construction. The construction network model of the actual RCC placing system is shown as following.

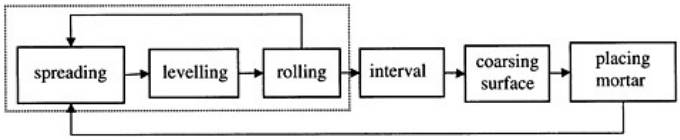

4 SIMULATION ANALYSIS OF THE RCC COFFERDAM CONSTRUCTION OF TGP

4.1 *Basic conditions*

The 3rd stage RCC cofferdam of TGP is a gravity dam with the crest of 140m and the width of 8m. Its axis is upstream 114m of that of TGP dam, and the length is 572m and the total concrete volume is 1.68 million cubic meters. 4m from the upstream face is an impervious layer. The concrete volume of 0.473 million m^3 has been finished in the first stage of the TGP construction. The axis length corresponding to the remained part is 380m with the highest height of 90m and the concrete volume of 1.207 million m^3. It would be planed to be completed in 4 to 5 months with the monthly peak pouring intensity of 0.398 million m^3 and the monthly biggest lifting height of 22.5m.

The belt feeding lines and tower-belt cranes, altogether with 20t dumping trucks, would be initially selected as RCC construction scheme. The method of full face spreading and thin-layer compaction is used with the compacted thickness of 30 centimeters.

4.2 *Simulation calculation and results analysis*

Based on the construction conditions and the technical performances of equipments, the following basic data are used in the simulation:

2 mixing plants of $4\times3m^3$	The loading duration to dumping truck is a Normal distribution with average value of 2.6 minutes and variance of 1.5, and the production rate of each plant is $180m^3/h$
2 mixing plants of $4\times4.5m^3$	The loading duration to dumping truck is a Normal distribution with average value of 2 minutes and variance of 1.5, and the production rate of each plant is $240m^3/h$;
Dumping truck	20 tons, $8m^3$ per dumper; loaded average speed on road 20km/h, void average speed 30km/h; running speed on the dam surface 3 km/h; unloading duration 2 minutes per dumper; washing duration 2 minutes per dumper
Working time of each shift	Continuous working 7 hours
Vibrating roller	Average rolling speed 1.75 km/h with variable of 0.25; Width of rolling strip 5 m; 8 passes

By the construction process simulation analysis of the 3rd stage cofferdam of TGP, the scheme of the *full-face spreading and thin-layer continuous pouring* is suggested with each lift as much as

possible, otherwise it could not be built on time. The quantity of dumping trucks and rollers is in the changeable state, with 40 transporting dumpers and 10 rollers using below El 90m, 30 transporting dumpers and 8 rollers using between El 90m and El 115m, and 15 transporting dumpers and 4 rollers using above El 115m.

The construction started on Dec. 16, 2002 and the cofferdam reached its crest level on Apr. 16, 2003. The total construction duration was 4 months. The practice testified that the simulation method applying to TGP gave powerful support for the selection of the last construction scheme, and was successful.

This page intentionally left blank.

New Developments in Dam Engineering—Wieland, Ren & Tan (eds),
© 2004 Taylor & Francis Group, London, ISBN 04 1536 240 7

Visual analysis of rock mass classification in high arch dam foundation and its application

Denghua Zhong & Mingchao Li
School of Civil Engineering, Tianjin University, Tianjin, China

Gang Wang
Chengdu Hydroelectric Investigation & Design Institute, Chengdu, China

ABSTRACT: Rock mass quality classification is an important means of evaluating engineering geologic conditions, and plays a very significant part in treatment of dam foundation for hydropower engineering. However, the represents of most classified results are now limited to static 2D manner and have been hard to satisfy analytical demands. Therefore, it is necessary for meeting higher expectations of classification results expression to study the visualization of rock mass classification.

This paper studied the visual treatment of the dam foundation in Jinping first-level hydropower station as an engineering example, in which the design height of the arch dam is 305m. Firstly with a new data structure, 3D structural model of classification results was constructed by NURBS tool. Then, according to the disposal scheme of dam foundation, a series of analyses were operated by relevant algorithms, including the visualization of classification in the treatment region and the contrast between pre and post treatment. It can offer engineers corresponding information more directly and effectively, and has achieved well practical effects.

1 INTRODUCTION

With the development and construction of many water conservancy and hydroelectric projects in the world, abundant problems on engineering geology make people realize the importance of rock mass quality classification in the engineering region. During the feasibility and preliminary design stages of a project, when very little detailed information on the rock mass and its stress and hydrologic characteristics is available, the application of a good rock mass classification scheme can be of considerable benefit[1,2]. A dam is the most critical part of a hydro project, and its foundation have to be treated correctly.

Dam foundation requirements are based on the type of dam proposed and are largely dependent on the strength, deformations, and permeability characteristics of site rocks[3]. To a large extent, the recognition and analysis to rock mass in the dam foundation area is a decisive factor for a successful dam construction. Therefore, rock mass classification plays a very significant part in geological criterion quantification, optimization design of dam and reasonable foundation plane for treatment of the dam foundation in hydropower engineering.

At present, evaluating methods of rock mass quality classification are studied further[2,4,5,6]. However, the represent of most classified results is limited to static 2D manner, and they are marked roughly by some simple data tables or plane graphs[7] These traditional ways have been hard to satisfy the demands of spatial analysis and cannot express the relevant results or data of rock mass assessment visually and fully. Therefore, it is necessary for meeting higher expectations of classification results expression to realize 3D visualization of rock mass quality classification.

This paper studies rock mass quality classification of the dam foundation in Jinping first-level hydropower station as an engineering example, in which the design height of the arch dam is 305m. Firstly the classification scheme are determined by geologic conditions and proposed method. Then, 3D structural model of classification results is constructed using Non-Uniform Rational B-Spline (NURBS) tool. Next, according to the disposal scheme of arch dam foundation, a series of analyses are operated by relevant algorithms, including the visual results of classification in treatment region and the contrast between pre and post treatment. It can help engineers understand rock mass classification in 3D space and deal with the dam foundation more effectively. Finally, conclusions are provided.

2 ROCK MASS CLASSIFICATION IN DAM FOUNDATION AREA

According to different kinds of engineering structures such as dams, tunnels and slopes, there are various methods to study the rock mass classification system, which has been developing for over 50 years since Terzaghi[8] applied it to tunnel design in deed firstly. So rock mass classification systems of underground engineering are abundant and perfect. Relatively, the systems of dam foundation are still in process of exploration because of complex factors and short research time. Even so, since seventies of 20th century, more than ten multi-parameter classification schemes have been applied to evaluate rock mass quality in dam foundation area successfully and acquire some good achievements[1].

Summarizing previous classification schemes, we present some principles and an integrated method to assess rock mass quality of high arch dam foundation. Based on physical circumstances of engineering rock mass, from analyzing single factor to appraising multiple factors synthetically, a complete classification system can be established through the thought of system engineering.

Firstly, the basic classification principles are as follows:

- The requisitions for foundation rock mass of high concrete arch dam in the region of dam site have to be considered.
- To ensure that assessment results are objective and reliable, primary geologic factors which control physical mechanics characters of rock mass are taken as basic parameters to evaluate rock mass. These factors include qualitative and quantitative data coherently.
- The classification standard adopts multiple mechanics parameters according to different combinations of engineering geologic factors. This will be in favor of contrasting with prevailing rock mass classification systems.

Based on above principles, the integrated method consists of the following steps:

(1) Preliminary rock mass classification. On the basis of stratigraphic horizons and rock association characters of rock mass, we divide basic geologic elements and classify rock mass quality initially, considering the effect of structural features and stress release of rock mass.
(2) Modification of rock mass classification. Correlation analysis of the initial classification and test results of rock mechanics proceeds to study the coherence and regularity between main geologic factors and mechanics parameters further. Thus the initial classification may be summarized and modified.
(3) Final rock mass classification. Referring to the specification of rock mass quality classification in dam foundation, the classification results can be determined finally.

Then, the next sections illustrate rock mass quality classification in the dam foundation area of Jinping first-level hydropower project on Yalongjiang River of Sichuan, China, and construct corresponding visualization model and analyze the treatment of dam foundation.

3 CONTEXT OF ENGINEERING ROCK MASS IN THE DAM AREA

3.1 *Basic geologic conditions*

The planned Jinping first-level hydropower facility is located at the west side of Jinping great river gulf, and the middle reaches of the Yalongjiang River. The geologic structure of this area is very

complex due to the great variability in terms of lithology and lithofacies, intensive tectonic deformations and drapes, abundant fractures, and widespread metamorphic terranes.

The design height of the arc dam is 305m, and it will be the highest arc dam in the world. The dam site locates in the reach of 1.5 km between Pusiluo gulley and Shoupa gulley. The region of interest stretches towards northeast along the Yalongjiang River, 700 meters long and 1200 meters wide. The bedrock of riverbed and two side banks in dam area is mainly composed of metamorphic rocks of Zagu'nao formation (T_{2-3z}), earlier Triassic series, and a few intrusive lamprophyre veins later. It can be divided into greenschist $T_2^3 - 3z$ by petrographic formation character. The terrains dip to left riverbank, and occurrence is N15~65°E, NW <15~45. Lamprophyre veins have cropped out in each bank, taking on straight and outstretched nervation and have clear borderlines with wall rocks. Tectonic movement later contributes to develop many faults, interlayer squeezing belts with dip offset, and joint fissures. There are about 13 large faults relevant to the engineering. The joint fissures in dam area are classified to two types by their different origins. One is the original texture which includes mainly bedding planes in sand-slate and marble, another type is the structural fissure, which are mostly of steep dip angle.

3.2 *Rock mass quality classification scheme*

From above description we generalize some important geological characters of rock mass in the dam area: (1) many litho horizons and complex rock association; (2) developmental faults and joint fissures; (3) high environmental ground stress; (4) intense relief effect, especially deep fissures at left bank. These features make up of basic geologic factors affecting rock mass quality.

Rock mass quality in dam foundation area depends on coupling contribution. The integrated method is used to evaluate the rock mass quality. Firstly, we analyze in depth the influence of each single factor, such as horizons and lithologic association, rock mass structure, compactness of rock mass and developmental conditions of deep fissures. And preliminary rock mass classification can be carried through respectively. Then, integrating with test results, the initial scheme is adjusted through the synthetic multi-parameter assessment way. Finally, the rock mass in the dam area are classified as four major types or seven sub-class types, which are listed in Table 1. Moreover, Fig. 1 gives a typical section about rock mass classification along the arch dam axis.

4 3D STRUCTURAL MODEL OF ROCK MASS CLASSIFICATION

4.1 *Modeling method and principle*

3D structural model of rock classification is actually the extension of 3D geological model, which is an important challenging topic in engineering geology, and has attracted more attention[9]. However, many modeling methods have some limitations at present, such as simple structural analysis, small processing data quantity, too large storage and slow analysis speed. So, for complex and special hydropower engineering geology, we have proposed a new approach to overcome these limitations and built some applied models of practical projects[10].

In a general way, this method interprets the actual discrete data to create a series of 2D CAD sections first, in which rock mass classes are marked. Then, through interpolating these sections and trend surface analysis, a variety of structural planes are constructed using triangulated irregular network (TIN) and NURBS technique. Further, the 3D rock mass class model can be created.

Here we import NURBS tools and put forward a mixed data structuring model integrating with TIN. NURBS technique is the exclusive expression way of free-form curves and surfaces in the STEP of ISO[11]. To irregular and complex geologic bodies, NURBS tool is computationally efficient, which means lower computational memory requirements and faster data processing. It supports space uniqueness and geometry inalterability for representing geological structures. There is very high applied cost for 3D geological expression[12]

Table 1. Rock mass quality classification in the dam area.

Rock class	Subclass	Horizons	RQD (%)	Distributing location	Assessment of rock mass
II	II	$T_{2-3Z}^{23)\sim(5),(7),(8)}$, $T_{2-3Z}^{3(2),(4),(6)}$ $T_{2-3Z}^{2(2),(6)}$	>85	Under weak relief belt at riverbed and right bank	Relatively intact, belonging to well foundation
III	III_1	$T_{2-3Z}^{2(7),(8)}$, $T_{2-3Z}^{3(2),(4),(6)}$ $T_{2-3Z}^{3(1),(3),(5)}$ $T_{2-3Z}^{2(3)}$	65–85 (part 40–50)	Weak relief belt at two side banks	Relatively intact, but some flabby parts must be treated technically
				Intact rock mass between deep tension fractures at left bank	
				Weak relief belt at left bank superficial part at riverbed	
	III_2	T_{2-3Z}^{1}, $T_{2-3Z}^{2(1),(2)}$ $T_{2-3Z}^{2(3)}$	45–65	Superficial part at riverbed and right bank	Relatively poor integrity, lower strength, not suitable for high dam foundation
		$T_{2-3Z}^{3(1)\sim(6)}$, T_{2-3Z}^{2}		Surface layer of bedrock at riverbed	
				Weak relief belt at two side banks	
		DikeX		X below 1680m at left bank	
IV	IV_1	$T_{2-3Z}^{3(1)\sim(6)}$, T_{2-3Z}^{2}	25–45 (part 45–70)	Intense relief belt at two side banks	Poor integrity, low strength, must be excavated out
	IV_2	T_{2-3Z}^{2}, T_{2-3Z}^{3}		Flabby belt at left bank	Poor integrity, low strength, must be fastened technically
		DikeX		X over 1680m at left bank	
V	V_1	Faults	—	f_{13}, f_{14}, f_2, and f_5, f_8 over 1680m	Broken rock mass, must be fastened specially or
	V_2	T_{2-3Z}^{2}, T_{2-3Z}^{3}			
				Intense flabby belt at left bank	

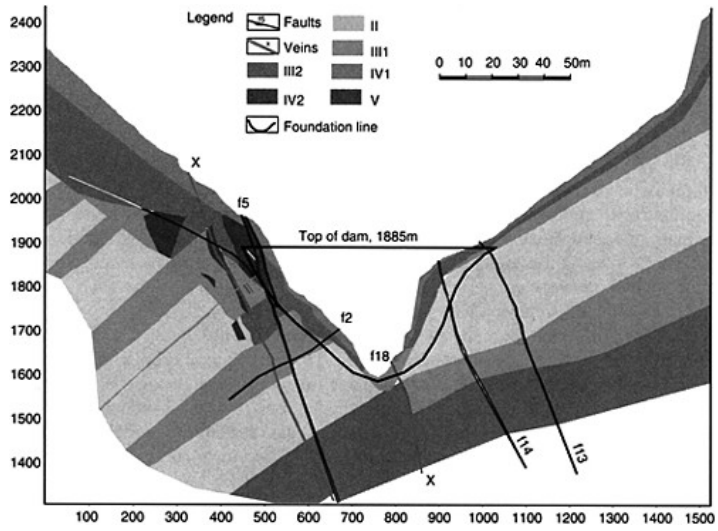

Figure 1. 2D section of rock mass classification along the arch dam axis.

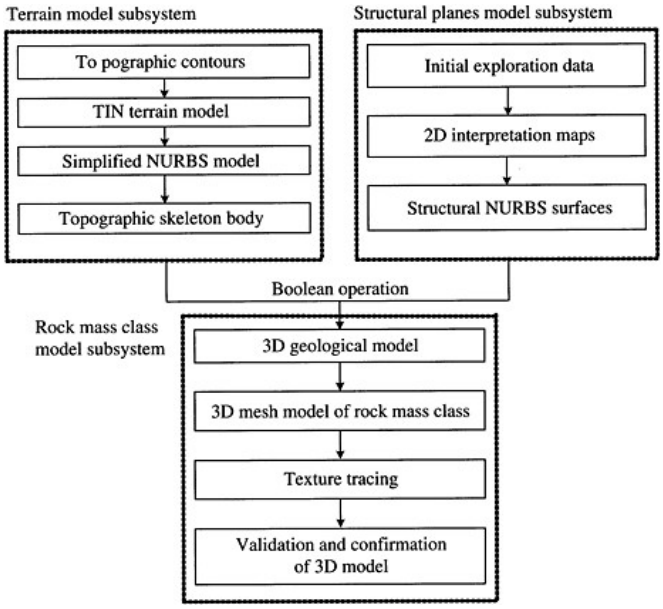

Figure 2. Flow chart of 3D structural model.

4.2 *Realization of 3D model*

The realization procedure of 3D structural model is shown as Fig. 2. It is composed of three subsystems, including terrain model, structural planes model and rock mass class model. Terrain subsystem is used to obtain the topographic skeleton body of dam area, which is the receptor of all operations during 3D model construction. Structural planes model system generates all structural surfaces by NURBS tools, such as horizons, faults, veins and deep fissures. The objective of rock mass class model subsystem is to build the reliable 3D structural model of rock mass classification after validation and confirmation.

According to the classification scheme, 3D structural model which consists of six types rock mass, class II, III, III2, IV1, IV2, V (V1 an V2), is constructed by the implemented method. Due to the rock masses of class III2, IV2 and V are of poor quality and have a bad effect on engineering construction, they are represented by striking textures or colors. Figure 3 gives the geometrical drawing of the final model, in which the dam foundation has been excavated.

5 VISUAL ANALYSIS OF ROCK MASS IN TREATMENT OF THE DAM FOUNDATION

The main rock mass in dam foundation area of Jinping first-level project is of II and III1 classes. However, there are still some geological defects, such as faults f5 and f8, lamprophyre veins, deep fissures and local rock mass of IV2 class in left bank, and faults f13 and f14 in right bank. These defects must be well analyzed and treated through multiple ways, for example, concrete pillow, consolidation grouting, and substitutive concrete.

To observe the treatment effect and adjust some irrational disposal measures visually, a series of visual analyses of rock mass in treatment of dam foundation are designed and managed, based on the established 3D rock mass classification. Figures 4 and 5 represent some typical 3D exhibitions

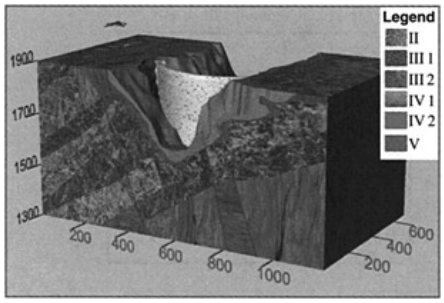

Figure 3. 3D structural model of rock mass classification.

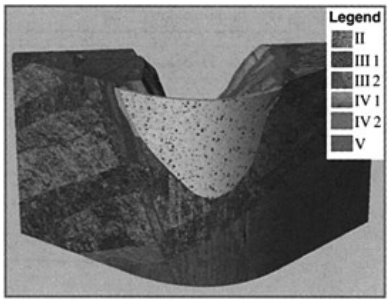

Figure 4. 3D view along the dam axis.

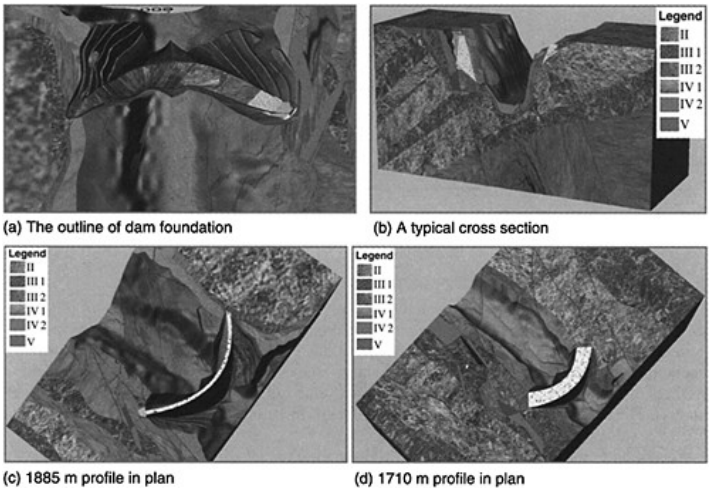

Figure 5. Visualization of rock mass analysis in the dam foundation area.

of rock mass treatment. The cyan parts in these figures are treated with consolidation grouting and substitutive concrete. And, the current disposal scheme is determined by modifying the initial scheme, in which the visual analyses have found some irrational treatments. Therefore, the visualization of dam foundation treatment offers engineers much impersonal and intuitive information to design several schemes easily.

6 CONCLUSIONS

With the increasing improvement of design requirement for hydraulic and hydroelectric projects, the visualization of engineering design is an inevitable trend. The presented visual analysis of rock mass quality classification in treatment of dam foundation is just an important content therein. For assessing rock mass quality of high arch dam foundation objectively, this paper advances an integrated classification method and some corresponding principles firstly. Then, the rock mass classification scheme in dam area of Jinping first-level hydropower project is determined as an example. And the 3D structural model is constructed quickly through our implemented modeling tool. Finally, based on 3D model, we analyze the treatment of dam foundation from various angles and modify some irrational designs. It shows that this study has acquired very good effects on the application.

REFERENCES

[1] Hu, X.W., Huang R.Q. A simple discussion on quality classification of the rock mass in a water conservancy and hydroelectric project. Journal of Chengdu Institute of Technology, 1996, 23(3), 64–68
[2] Hoek, E. Practical Rock Engineering. http://www.rocscience.com/hoek/pdf/Practical Rock Engineering. zip, 2000, 40–60
[3] Fraser, W.A. Engineering geology considerations for specifying dam foundation objectives. In: Ferriz, H. and Anderson, R., (eds.), Engineering Geology Practice in Northern California: Association of Engineering Geologists Special Publication 12 and California Division of Mines and Geology Bulletin 210, 2001,311–318
[4] Du, S.G., Wang, S.J. Review and trend of quantifying rock quality. Journal of Engineering Geology, 1998, 6(3), 230–237
[5] Stille, H., Palmström, A. Classification as a tool in rock engineering. Tunnelling and Underground Space Technology, 2003, 18, 331–345
[6] Sena, Z., Sadagahb, B.H. Modified rock mass classification system by continuous rating. Engineering Geology, 2003, 67(3–4), 269–280
[7] Jiang, H., Xu, W.Y., Xie, S.Y and Jiang, P. Automatic generation of 3D digital model for rock mass quality assessment. Journal of Engineering Geology, 2000, 8(1), 123–126
[8] Terzaghi, K. Rock defects and loads on tunnel supports. In: Proctor, R.V and White T.L., (eds.), Rock tunneling with steel supports 1. Youngstown: Commercial Shearing and Stamping Company, 1946,17–99
[9] Houlding, S.W. 3D Geoscience Modeling: ComputerTechniques for Geological characterization. New York: Springer-Verlag, 1994
[10] Li, M.C. Research on 3D Visual Analysis Theory and Application for Complex Engineering Geologic Information. Tianjin: [M.S. Dissertation] Tianjin University, 2003
[11] Piegl, L., Tiller, W. The NURBS Book, 2nd edn. New York: Springer, 1997
[12] Li, Q.Q., Li, D.R. Data structure in 3D geographic information systems. Journal of Wuhan Technical University of Survey in gand Mapping, 1996, 21(2): 128–133

This page intentionally left blank.

New Developments in Dam Engineering—Wieland, Ren & Tan (eds),
© 2004 Taylor & Francis Group, London, ISBN 04 1536 240 7

Study on rapid construction scheme for Longtan high RCC dam

Zhou Huifen, Shi Qingchun & Li Yonggang
Mid-South Design & Research Institute for Hydroelectric Projcects, Changsha, Hunan, P.R. China

ABSTRACT: Longtan Hydroelectric Project has a high RCC gravity dam over 200m, requiring a total concrete quantity of 5.8 million m^3, being the highest RCC dam under construction in the world. The dam construction is characterized by tight construction schedule, high placing intensity and continuous year-around construction. In order to ensure the quality and meet the construction schedule, advanced construction machinery and technology must be used. On the basis of technical and economic analysis of several feasible concrete placing schemes and sufficient justification, a continuous conveying and placing scheme with a major means of high-speed belt conveyors plus tower belt machines has been selected. Detailed construction layout design has been conducted on the basis of the selected scheme.

1 GENERAL

The Longtan RCC gravity dam is designed to have a crest elevation of 406.500m, and a maximum height of 216.5m. The project is proposed to construct in two stages. In the first stage, the dam will have a crest elevation of 382.00m, a maximum height of 192m, a maximum base width of 169m, and a crest axis length of 746m. It consists of 31 blocks, Block 5 serving as the navigation section, Blocks 12 and 19 as low-level outlet sections, Blocks 13 through 18 as the overflow section, Blocks 22 through 30 as the power intake section, and the rest as the non-overflow section. The dam will be built maily with RCC. However, conventional concrete will be placed at the navigation section and the power intake section above the intake inverts. GEVR will be placed at the downstream and upstream slope faces, around the bank slopes, waterstops, galleries, lift shaft and other orifices. The concrete to be used will total 5.80 million m^3, including 3.85 million m^3 of RCC (accounting for 66% of the total).

River closure was achieved with the construction of the upstream and downstream RCC cofferdams and the diversion tunnel. The master construction schedule is as follows: the power intake section commenced concrete placement in February 2004, and will reach the dam crest by the end of Year 2006; and the other dam sections will commence concrete placing in September 2004, and reach the power generation elevation by the end of May 2007, involving a concrete volume of 5.55 million m^3, a construction period of 33 months and a mean monthly placing intensity of 170,000 m^3. Year 2005 will be the peak placing year, with a concrete volume up to 2.32 million m^3. The peak placing periods will be from November 2004 to April 2005, and from October 2005 to April 2006, when the mean monthly placing intensity will be up to 316,000m^3 (255,000m^3 for Blocks 2 through 21).

The Longtan dam site is of the subtropical climate, with high temperature and heavy rains in the flood season. In order to avoid the flood scouring, the non-overflow sections on both banks and low-level outlet sections will be preferably raised first, and the overflow section, as the notch for passing flood, will be continuously raised with some heigh difference from the non-overflow sections.

Considering that Blocks 2 through 21 will be mainly built with RCC with considerable construction difficulty, and will be critical for controlling the construction progress and quality, this paper focuses on the study of the construction scheme for dam section of Blocks 2 through 21.

2 STUDY ON THE CONCRETE TRANSPORT AND PLACING SCHEME

2.1 *Basic design principles*

The concrete transport and placing scheme is characterized with high quality, high-efficiency and rapidness. The following requirements should be met: no aggregate separation or grout loss, short transport time, high placing intensity, continuous placing in large areas, simultaneous placing in different areas to meet the requirements of passing flood through notches, placing intensity of conventional concrete, and hoisting operation for reinforcement, forms, gates, etc.

2.2 *Selection of concrete transport and placing scheme*

In the light of the construction characteristics, placing intensity requirements and experiences from the RCC dams existing and under construction both at home and abroad, a construction scheme of belt conveyor, dump truck, suction chute plus cable conveyor was conscienciously studied.

High-speed belt conveyor is a continuous conveying machinery, with high productivity, a broadth of 650 to 900mm, a speed of 4m/s and a maximum angle up to 25°. It can be elevated along the mast, hence suiting to projects with a high dam and a large work quantity. Through economic and technological comparison, the scheme of adopting 2 sets of high-speed belt conveyors plus tower belt machines, 2 suction chutes and 2 sets of 20t cable conveyors was selected. This scheme is favorable for the construction quality and progress of the project as it has a relatively simple arrangement and efficient equipment, and is suitable for placing of both RCC and conventional concrete.

2.2.1 *Arrangement of tower belt machines and high-speed belt conveyors*

In order to fully use the tower belt machine, it is arranged to possibly cover the RCC placing area vertically and horizontally. In addition, notches will be remained in the overflow section for passing flood, hence the tower belt machine will be preferably of the stationary type, and will be arranged across the end of the overflow section. In view of the dam structure, the non-overflow section is favorable for the arrangement of the tower belt machine. Nevertheless, the productivity of the tower belt machine requires that the two tower belt machines be arranged at the left and right low-level outlet sections respectively, which can provide concrete for most of the non-overflow section and the overflow section, and are structurally reasonable. The mast will be embedded in the dam with the elevation of the dam body. The tower belt machine has a maximum placing radius of 100m, and with the help of crawler conveyor, has an actual maximum placing radius up to 120m. The tower belt machine can operate with a theoretical angle of ±20°, but actually ±10°, and locally ±15°.

Two high-speed belt conveyor compatible with the tower belt machines will be connected with the 2 sets of low-level (deck elevation 308.50m) 2×6m^3 forced batch plants, and their heads will be connected with the tower belt machines. One mobile and flexible belt conveyor will be arranged at the hopper of each batch plant so as to feed to any supply belt conveyor. In order to ensure that the belt conveyor is free from adverse impacts from outage of the batch plant, one belt conveyor from the high-level (deck elevation 360m) forced batch plant will be connected with the connecting belt converyor of Conveyance Systems 1 and 2. In this way, the three forced batch plants can provide concrete for each tower belt machine, and the continuous operation of the tower belt machine can be guaranteed.

The high-speed belt conveyors 1 and 2 (each 760m wide) will share the same posts along the conveyance line. The space between two adjacent posts will be no more than 75m and the maximum free height of posts 74m. The maximum angle out of the dam area will be controlled within ±10°, and that in the dam area within −15° ~+20°. The belt conveyors 1 and 2 will be 489.5m and 401.5m long respectively, and will be of one stage arrangement.

2.2.2 *Arrangement of suction chute and feeder line*

The suction chute will assist the tower belt machine 2 to place some of the RCC for the nonoverflow section on the right bank. The placing intensity analysis shows that three 600mmdiameter suction chutes will be required including one standby. As Block 5, the navigation section, will be placed with conventional concrete, the suction chute will be located at Block 6. Due to the gentle slope of the dam base on the right bank, approximately 30°, the suction chute will be arranged in one stage and provide concrete for El. 231.00 to 280.00 so as to meet the angle requirements of chute arrangement (preferably no less than 45°), and rationalize the support quantity.

High-speed belt conveyor No. 3 (760mm wide and 347m long) will be connected with the highlevel (deck elevation 360m) 2×6m^3 forced batch plant hopper. It can transport some concrete for the dam above El. 280.00m directly into the placing area, which will then be spread by trucks.

2.2.3 *Arrangement of cable conveyor and horizontal transport*

Based on the topographical condition and the placing area of the cable conveyor, 2 sets of 201 horizontal-movement moderate-speed cable conveyors will be arranged at the same deck, with the main cable controlled within 0–013.00~0+125.00m. In order to avoid interference with the tower belt machine and create condition for elevation of the dam body, the main tower will be located at the right deck El. 450.00m, and the auxiliary tower at the left deck 480.00 m. The main tower will be 45m high, with the crest elevation of 495m, and the auxiliary tower 10m high, with the crest elevation of 490m. The span between the main and auxiliary towers will be 915m or so, and the controlled elevation of the hook will range from 190.00~442.00m.

The 20t-capacity dump truck will be used for horizontal transport of concrete.

Layout for the dam concrete transport and placing is shown as below.

2.3 *Arrangement of the concrete mixing system*

The concrete processing system for the right dam sections will be arranged downstream, with 3 sets of 2×6m^3 forced batch plants (production capacity of 3×300m^3/h) and one set of 4×3m^3 gravity batch plant (production capacity of 1×240m^3/h). The concrete batching systems will be arranged on two decks with differecent elevations. The low-level system, consisting of two sets of 2×6m^3 forced batch plants, will be arranged at the navigation section El. 308.50m;

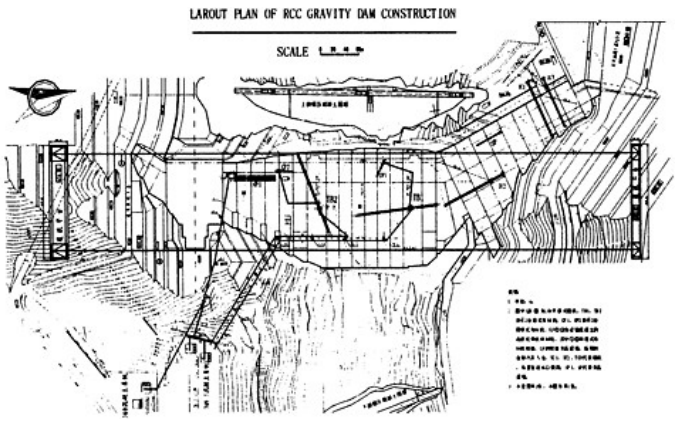

and the high-level system, consisting of one set of 2×6m^3 forced batch plant and one set of 4×3m^3 gravity batch plant, will be arranged at El. 360.00m. The batch plant will be located 300.00~320.00m away from the dam axis.

2.4 *Placing equipment*

In order to meet the RCC placing requirements of large placing area, high quality and high intensity, especially the high-speed belt conveyor plus tower belt machine (and plus crawler conveyor) which is characterized with continuous feed at a single point, and to bring the tower belt machine into full play, conscicious study was conducted on the placing equipment. The placing equipment mainly include bulldozer, vibratory roller, cutter, roughening machine (or brusher), grout spreader, GEVR grout machine, etc. The vibratory roller and bulldozer are critical to the raising speed of the dam body. The analysis shows that one tower belt machine will be provided with 2 sets of D65P-12 bulldozers and 4 sets of BW-202AD vibratory rollers. The strip width of the placing area is no less than 8 m. During the peak placing period when 3 high-speed belt conveyors are simultaneously in service (two to be connected with the tower belt machines, and one with the suction chute), 6 sets of bulldozers and 12 sets of 10t vibratory rollers will be required.

3 STUDY ON CONSTRUCTION TECHNOLOGY AND METHODS

3.1 *Construction technology*

In order to accelerate the construction progress and minimize the joint treatment, RCC construction technology has been adopted, i.e., spreading RCC in large placing area and thin layers, compacted layer thickness of 0.3m, and continuous raise of the dam body.

The RCC will be continuously placed for 5 to 10 layers (each layer 0.3m-thick) to form a lift; and in summer when horizontal placing method is used, the RCC will be continuously placed for 4 to 5 layers. The allowable time for placing the upper layer must be within the initial set time of the lower layer, in summer 2 to 4 hours (the smaller value for sloping method), and in other seasons within 6 hours (to be finalized by field test).

3.2 *Construction methods*

(1) Horizontal method: This method is practicable for the tower belt machine system which is characterized with high intensity and rapid transport. In normal seasons, the horizontal method will prevail. When the two tower belt machines are in service, the maximum placing area will be controlled within 10,000m^2. In hot season when one (or two) tower belt machine is in service and the placing area is less than 2,500m^2 (or 5,000m^2), the horizontal method will also be available, and the spread layer thickness will be within 34 cm.

The spreading direction will be parallel to the dam axis, and the unloading line normal to the dam axis. The two tower belt machines will provide concrete for the same placing area. In order to avoid operation disturbance, the placing area will be divided into two halves, one for each tower belt machine. The strip width will be 8m and the spreading operation will keep the aggregate free from separation and make the layer surface even with uniform thickness so as to obtain the optimum compaction effects.

(2) Sloping method: Due to the limit of allowable time for placing the upper layer in summer, the sloping method must be employed. Two sloping spreading directions may be adopted, one normal to the dam axis (i.e., the layer surface will dip towards upstream, and RCC placing will go from downstream to upstream), and the other parallel to the dam axis (i.e., the RCC placing will go from one bank to the other bank). Where the dam base is wide, the former is preferable, as it is favorable for the dam to resist both seepage and shear. Hence, the sloping method with the spreading direction normal to the dam axis will be used, with a slope of 1:15~1:20 and a lift of

1.5~3m (the smaller value for summer operation). In addition to taking measures to prevent aggregate from separation, the following provisions will also be made.

a. The first layers of concrete will be spread in the specified direction. The key point lies in that the layer should become thinner and thinner with the advance toward the upstream and the lower layer should be fully covered by the upper layer so as to form a sloping surface.
b. The slope toe is not allowed to extend into the two-graded impermeable zone, which must be built with the horizontal method.
c. As for concrete placing for the last layers of a lift, concrete surface of the previously placed lift will be subject to cleaning, flushing, mortar placing. Then the dog-leg path (inclined first, then horizontal) advance method will be employed, with a horizontal strip width of 8 to 12m.

4 CONCLUSIONS

Based on the characteristics of the Longtan RCC dam such as large size and high placing intensity, the concrete placing scheme of using tower belt machines, suction chute and cable conveyor was selected. The placing progress analysis and simulation analysis and justification show that the placing intensity and raising speed of the dam can all meet the master construction schedule. Nevertheless, the construction organization and management should be strengthened so as to ensure the quality and progress of the concrete placing.

In order to bring the tower belt machine system into full play, and suit to the RCC construction characteristics of large placing area and high intensity, sufficient placing equipment must be provided, especially advanced and efficient vibratory rollers and bulldozers. In addition, the placing areas and strips should be arranged in a reasonable way. Sufficient man power should also be arranged to timely assist the sloping operations.

This page intentionally left blank.

New Developments in Dam Engineering—Wieland, Ren & Tan (eds),
© 2004 Taylor & Francis Group, London, ISBN 04 1536 240 7

Design for restoration works of right stilling basin of Wuqiangxi Hydropower Station

Zhou Liben
Mid-South Design & Research Institutefor Hydroelectrical Projects, Changsha, Hunan, P.R. China

ABSTRACT: The right stilling basin of Wuqiangxi Hydropower Station was severely damaged by flood during July 1996, in which a large scouring hole about 50,000m^3 was made. The restoration design and construction for the damaged stilling basin was executed after this flood and no abnormal conditions have occurred to the repaired stilling basin after experiencing many times of large flood since 1998. The paper analyzes the causes of damage and introduced the restoration design and calculation analysis on three-dimensional finite element, as well as represents the repaired stilling basin can meet the requirements of safe operation of the hydropower station.

1 GENERAL

Wuqiangxi Hydropower Station, located on the Yuanshui River within Yuanling County, Hunan Province, is a multipurpose complex project with the main purpose of power generation and concurrently with the auxiliary benefits of flood control and navigation. The station has a normal storage level of 108.0m and installed capacity of 1200MW.

Wuqiangxi Hydropower Station is composed of a left overflow dam section, a right powerhouse at dam toe and a left three-stage lock. The flow discharge structure is designed with 9 surface bays, 1 high level outlet and 5 low level outlets. The 9 surface bays are divided to 3 bays on the right (orifices No. 1~3) and 6 bays on the left (bays No. 4~9) by the high level outlet. The low level outlet is 19m wide in net for each inlet with the crest at El. 87.80m. The high level outlet is 9m×13m (wide×high) with the inlet floor at El. 76.00m. The low level outlet is 3.5m×7.0m (wide×high) for each outlet with the inlet floor at El. 67.00m. Each low level outlet is arranged under each midpier of the 6 surface bays on the left dam section.

The energy dissipation structure of Wuqiangxi Hydropower Station is a combined energy dissipator with flaring pier for surface bay-ski-jump for low level outlet-stilling basin. According to the initial operation and relevant data obtained from the prototype observation, it is indicated the effect of comprehensive energy dissipation of the combined energy dissipator is very ideal.

The maximum flood with multi-peaks appeared in July 1996 on the Yuanshui River based on the hydrological recording ever since and at the same time 2 flood peaks over than 40,00m^3/s occurred at the damsite. In order to protect the safety of life and property at the downstream area, the reservoir had to store water close to 113.26m high water level, which was 5.26m higher than the normal storage level (NSL) and close to the water level for 5,000-year flood under the conditions of incompletion of the Project and strictly controlling the discharging flow not more than 26,400m^3/s. Since the Project was under construction at that time and the gate could not normally operate, the right stilling basin was severely damaged and subsequently produced a large scouring hole with a volume of 50,000m^3 and 40m deep. The nearest distance of upstream side of the scouring hole was only 3~4m away from the dam toe, which directly threaten the safety of the dam.

The analysis was carried out for the damage of the right stilling basin in December 1996 and then the restoration design thereof was also made. The restoration construction was basically completed in May 1997 and the right stilling basin was basically able to discharge flow. In the winter of 1997, the inspection of core boring was done, and it indicated the quality of underwater concrete of the stilling basin was poor. Therefore, the design and construction for strengthening treatment for underwater concrete were subsequently implemented and the second strengthening treatment thereof was executed in 1998. The final quality inspection is indicated the right stilling basin can meet the requirements of the operation of the Project.

2 DAMAGED CONDITIONS AND ANALYSIS OF DAMAGING CAUSES OF THE RIGHT STILLING BASIN

2.1 *Damaged conditions of the right stilling basin*

The right stilling basin is 72.00m wide and 131.185m long (including part of ogee section), with a 4m thick floor slab and the concrete was placed from the lower to the upper with 3 lifts together. Through the flood of 1996, the inspection was carried out for the right stilling basin after dewatered and the damaged conditions was as follows: a large scouring hole appeared along water flow inside the stilling basin, it was approximately 50m long, 25m wide (on upstream side)~16m wide (on downstream side); the upstream side of the hole was 13m away from the dam toe; the central line of the hole was almost on the extending line of the central line of the bay No.2 towards downstream; the deepest scouring point of the hole was at El. 0+122.00m of the dam; the bottom of the hole was at El. 2.5m approximately. The max. depth of the hole was about 40m. In addition, some of concrete slab round the scouring hole was torn off with a thickness of 1~2m and the torn range was 5~6m towards upstream, 15~20m towards two sides and 30~40m towards downstream. The rock mass round the scouring hole was severely undercut, which made the existing slabs overhung. The overhung part covered 15~16m on both sides, 8~10m on upstream side, 15~16m on downstream side. The area of the hole opening was about 1,200m^2 or 2,300m^2 including the area of the overhung part. The volume of the damaged hole was more than 50,000m^3. Especially the upstream side of the hole was only 3~4m far away from the dam toe, which severely threatened the safety of the dam.

2.2 *Analysis on damaging causes*

According to the analysis on the gate operations and the damaging causes of the right stilling basin during 96–97 flood, the main damaging causes are as follows:

(a) Wuqiangxi Hydropower Station suffered the maximum recorded flood and the inflow was close to 100-year flood. In order to protect the safety of downstream life and property, the discharge flow was strictly limited and the reservoir water level subsequently reached as high as that for 5000-year flood. Meanwhile, the downstream water level was 67.40m, which was a little higher than that of 20-year flood. The bay No. 2 had to open fully to form the poor operation conditions of discharging at extremely high water level and energy dissipation at extremely low water level, which resulted in long-distance hydraulic jump that was not allowed in the design.

(b) Due to various limitations, the gate hoisting could not operate in evenness, synchronism and symmetry as required by the design. The bay No. 2 had to fully open for a long time and the bay Nos. 1 and 3 had to partly open, which made water flow excessively concentrated, the distribution of water flow in the horizontal direction severely uneven and the flow regime extremely aimless. Especially the energy of the discharge flow from the bay No. 2 increased 95% compared with the normal operation conditions, it exceeded the withstanding capacity of the energy dissipator.

(c) During 96–97 flood period, the Project was not completed yet and the construction for the chute of the high level outlet was not executed either. So the high level outlet could not take part in flood discharge. The bay No. 6 could not work, because the hanger bearing for the radial gate of the bay No. 6 was broken. The bay Nos. 1, 3 and 4 could open in small opening only. 4 of 5 bottom outlets could not take part in flood discharge. The overflow surfaces of the bay Nos. 1, 2

and 3 below El. 57.50m were under construction so that a sharp bank connection was formed between the above-said overflow surfaces and the floor slab of the stilling basin, where the turbulent current occurred and cavitation erosion was easily produced. Because of the abovementioned causes, the gate operation was greatly restricted during this flood period.

(d) The inspection indicated most of the bedding combinations of the scoured concrete floor slab of the stilling basin at El. 41.00m were not good and under the effect of the pressure of flow water and uplift force in the floor slab, the surface concrete was easily lifted up, and gradually to form scouring hole.

Summing up the above-mentioned, the main causes of the damage to the right stilling basin were subjected to over standard flood and operation at non-design conditions. At that time, the Project was not completed yet and the gates could not rationally operate, which made the right stilling basin work under the extremely poor conditions as well as the poor combination of the concrete bedding of the floor slab. Hence, it resulted the damage to the floor slab of the stilling basin. Since the faults and joints within the bedrock under the stilling basin are well developed and the rock mass is not sound, the high speed water flow directly flushed the bedrock to form a large scouring hole.

3 DESIGN FOR RESTORATION OF THE RIGHT STILLING BASIN

3.1 *Review of safety and stability and strengthening measures during construction period*

After the scouring hole formed, the bedrock at downstream of dam sections 14 and 15 were exposed, which would threaten the safety of the dam. Meanwhile, the rock mass round the scouring hole was overhung, especially the rock mass of the left consequent slope would be out of stability. Therefore, the review of safety and stability of the dam and the slope of the scouring hole had to be carried out.

The calculation was carried out on the handicap dam section 15 based on the reservoir water level of 108.00m and the downstream water level dewatered to El. 30.00m for the construction period. The calculation indicated that, for dam section 15, the stability against sliding along the bedding plane and joint plane of the cutoff trench, the prism slip formed along soft interbedded layer and F_{200} of the bedrock and the slip along 3 different prism were all in basically stable conditions. But the careful monitoring should be carried out during the construction period.

Severe scouring occurred at the slope base of the slope rock of the scouring hole and especially the left rock mass is of a bedding slope, so the conditions were severe. According to the verified results, the safety factors K against sliding for various slip planes were much less than 1.0, which could not meet the requirements of stability. Therefore, the strengthening measures had been taken for the slope rock before dewatering.

Anchor piles were used for strengthening treatment for slope rock. 48 anchor piles were arranged in 3 rows, of which two rows were on the left and one row on the right with 28 piles for each row and spacing of 2m for each hole. The depth of the pile hole was 13.0~21.0m and the diameter was 130mm. $\phi 300$ supporting steel pipes were added under each overhung part and the pipes were grouted with C20 underwater concrete.

3.2 *Restoration scheme for the right stilling basin*

Besides the restoration design for the floor slab of the stilling basin was based on the original design, the key point of the restoration design was what kind of backfilling scheme would be adopted for the scouring hole to ensure the quality and construction period, i.e. the restoration construction was required to be completed before the flood season of May 1997. Through calculation, in order to ensure the safety of the dam and stability of slope round the scouring hole, the water in the stilling basin above El. 30.00m was required to pump out for the normal concrete backfilling and the underwater construction was executed for the location below El. 30.00m.

The underwater C20 concrete backfilling was carried out with concrete mixed with gelatinizer by tremie method for the location below El. 30.00m and the construction was required to lift up continuously and evenly. The spacing of the tremie pipe was 3~4m and the tremie pipe was required to be buried into underwater concrete. The mouth of the tremie pipe was not allowed to be out of concrete.

3.3 *Technical requirements for various locations construction*

3.3.1 *Technical requirements for underwater concrete construction*

The underwater concrete backfilling was adopted for the location of the scouring hole below El. 32.00m. The concrete was required to be with good liquidity, slump of 16~18 cm and the initial setting time not less than 24 h. The tremie method was adopted and the tremie pipe was gradually lifted up as the underwater concrete raised up. The diameter of tremie pipe was not less than 200mm to make the underwater concreting lift up evenly. The end of the tremie pipe was required to be buried in concrete and the mouth was required not to be out of concrete surface.

Due to the extremely large area of the scouring hole, the concreting was divided into three lifts. The tremie pipe was required to feed concrete evenly and the concrete could raise up evenly in each placement. The spacing of the tremie pipe was determined based on the radial of the liquidity of the concrete and usually it is 3~4m. After study, the max. spacing of the tremie pipe was enlarged to about 6m due to the extremely large area of the scouring hole. For the overhung part, holes were drilled on the floor slab to arrange the feeding pipes and the deep parts of each placement were placed with the overhung part together.

3.3.2 *Technical requirements for El. 32.00m~38.00m construction*

When the underwater concrete was placed to El. 32.00m, the waterlogging in the scouring hole could be dewatered. C20 normal concrete backfilling was required within this range and the main requirements were as follows:

(a) The loose rock mass on the wall of the scouring hole and on the top of the overhung part were required to clean, and then flush by high pressure water. The residue concrete on the top of the underwater concrete and unacceptable loose concrete were required to cut completely and then flush by high pressure water. The waterlogging was required to pump out.

(b) ϕ36@1500 steel bars were put from El. 32.00m, extended to El. 41.90m and then fastened with the surface reinforcing steel of the floor slab. For some locations of the overhung part that is not convenient for putting reinforcing steel, the anchor piles were installed by drilling hole from the floor slab of the stilling basin after concreting completion instead.

3.3.3 *Technical requirements for construction of the floor slab of the stilling basin*

The floor slab of the stilling basin from El. 38.00 m~42.00m had direct relationship with the safety of the Project, so that the strict requirements were required as follows:

The placing area at El. 38.00m was roughened by pneumatic pick and the waterlogging was dewatered.

The anchor bar (or lattice girder) in the deep part of the scouring hole extended to the top steel mesh and buckled with them. For concreting the surface layer of the damaged area, the ϕ25@ 1000 steel bars were put on the whole floor slab by drilling holes to strengthen the bedding combination at El. 41.00m.

The joints of the floor slab were arranged according to the original design and key grooves were designed on the structure joints. Two layers of copper water seal were installed on El. 41.10m and 41.50m respectively. BW-II expansive water seals were put in the non-structure joints and in the bedding layer of the new and old concrete.

C35 concrete was used for the damaged area with III-grade aggregate. Adequate vibration was required during construction to prevent cracking.

Backfill grouting was adopted through the holes of anchor piles for the overhung part. The packer grouting method was employed and the plug was put at El. 37.00m to avoid blockage of the drainage system at El. 38.00m. In order to strengthen the combination of the backfill concrete with the wall, a row of deep holes were arranged round the scouring hole with the hole's spacing of 3m. The holes went through the underwater concrete and then into bedrock with a depth of 2m. The descending stage drilling and grouting was employed.

The control-joint grouting was adopted for the placing surface at El. 41.00m. For the placing surface with wearing depth deeper than 10cm, C35 concrete with I-grade aggregate was placed after the surface treatment. For the placing surface with wearing depth less than 10cm, M45 ganister sand was use for mending, compacting and trowelling.

4 STRENGTHENING OF UNDERWATER CONCRETE FOR THE RIGHT STILLING BASIN

The quality of 33,000m^3 underwater concrete placed for the reparation of the right stilling basin directly affected the stress distribution and deformation of the floor slab of the right stilling basin, as well as the safety of the dam. The inspection holes were made for the underwater concrete in the end of 1997 and they indicated the underwater concrete was poor in integrity with a high absorption rate and a low wave velocity measured by geophysical prospecting. The cement grouting was adopted for completely strengthening the underwater concrete from December 1997 to April 1998. After that, the inspection indicated the underwater concrete was greatly improved in density, the absorption rate was obviously reduced and the wave velocity also accelerated measured by geophysical prospecting.

Large flood occurred continuously on the Yuanshui River and Wuqiangxi reservoir suffered 5 times of large flood with the flow exceeding 15,000m^3/s one after another from June to August 1998. The max. reservoir inflow was as much as 35,000m^3/s and the max. discharge flow was as much as 23,000m^3/s in July. At that time, all the 9 surface bays and 5 low level outlets took part in flood discharge, so that the right stilling basin faced a severe ordeal after restoration. After flood season, inspection was carried out after dewatering, no abnormal conditions were occurred for the right stilling basin.

From the point of view of safety of the Project, the design and construction for the second strengthening treatment for the underwater concrete were executed from the end of 1998 to the beginning of 1999. All together, the cement for grouting was 757.5t with 190 grouting holes. In addition, the mending and treatment were also carried out for the other existing defects.

According to the final data from 14 inspecting holes, the quality of the underwater concrete was greatly further improved after the second strengthening treatment and the results are as follows: the core recovery ratio of the underwater concrete increased to 61%; the absorption rates of the underwater concrete were all less than 20 Lu for 39 water pressure tests in the inspecting holes, of which, 31% were less than 5 Lu in absorption rate and 64% were less than 10 Lu in absorption rate; 14 water pressure tests were carried out for contacting part of the underwater concrete and the overhung part, the absorption rates were also less than 20 Lu, of which 79% were less than 5 Lu and 93% were less than 10 Lu; the physical mechanics test was carried out for the typical core in the inspection holes and it indicated the physical mechanics performance of the mediate grade underwater concrete basically met the design requirements; the ultrasonic testing and the elastic wave chromatography image formation were made and it indicated the most of wave velocity in the underwater concrete were faster than 3,300 m/s, the underwater concrete with wave velocity less than 3,300 m/s reduced to 10.4% and distributed in scatter without any connection. The color TV showed each wall of the inspection holes was integrated without any obvious hole collapse and activity of the underground water.

5 ANALYTICAL CALCULATION OF THREE-DIMENSIONAL FINITE ELEMENT

In order to gain the loading combination of the dam and the stilling basin after reparation treatment, the analytic and calculation of three-dimensional finite element were carried out for dam

sections 14 and 15 and the floor slab of the stilling basin, and the bedrock, as well as simulating backfilling conditions of the scouring hole. The calculations indicted after backfilling the scouring hole, the safety factors all were greater than 3.0 in various operation conditions with consideration of resisting force at dam toe. After reparation treatment of the right stilling basin, the stability against sliding of the dam was guaranteed. In addition, the results of the displacement and stress at dam toe indicated the max. horizontal displacement at dam toe was 1.77mm, in case the deformation modulus of the backfilling underwater concrete was calculated based on the modulus of elasticity of C7.5 concrete and the max. horizontal displacement at dam toe was 1.87mm, in case the deformation modulus of the underwater concrete reduced to 60%; the max. major compressive stress at dam toe was 0.55MPa and this stress was also equal to the stress transferring from dam toe to the floor slab of the right stilling basin; meanwhile, the max. major compressive stresses all were less than 0.24MPa at 0+070.000m, below El. 32.00m, that was the stress dam transferring to the underwater concrete through dam foundation. After two times of strengthening the underwater concrete, the quality of the underwater concrete can basically meet the design requirements and can completely withstand this grade of stress.

The original floor slab of the stilling basin was 4m thick. According to calculation, 6.3m deep anchor rod was required to be installed to meet the stable requirements for against floatation by means of anchoring the floor slab of the stilling basin and the bedrock as a whole. For backfilling the scouring hole of the right stilling basin, the location above El. 32.00m was placed with normal concrete. During construction period, the 60cm×60cm lattice girder (for construction platform) with a spacing of 4.0m extended from El. 32.00m to the surface steel bars and then welded with them. For the overhung part, many feeding pipes and supporting pipes were arranged, 10m deep normal backfilling concrete calculated from El. 32.00m was put into a whole. Therefore, after reparation treatment, the stability against floatation of the floor slab can completely meet the original design requirements.

According to the calculation of three-dimensional finite element, after reparation treatment to the stilling basin, the max. settlement displacement was 1.82mm for the floor slab at normal operation conditions and 2.69mm at operation conditions with check flood, and the max. relative differential settlement of the floor slab was 0.35mm. The values of the max. settlement displacement and the max. relative differential settlement were small. In addition, the calculation was carried out base on the deformation modulus for C7.5 underwater concrete with a discount of 40% (i.e. 8.7 Gpa). Comparing with the finial quality record and the results of physical mechanics testing for core boring of the underwater concrete, the settlement displacement has great margin. Therefore, the uneven settlement of the floor slab of the stilling basin is within the allowable range.

6 CONCLUSIONS

(a) After reparation and strengthening treatment for the right stilling basin, the quality inspection and analytic calculation of three-dimensional finite element indicate the right stilling basin can meet the requirements of dam's stability and stress transferring, the stability of the floor slab can be guaranteed and the uneven settlement of the floor slab is within the allowable range, which can meet the requirement for safe operation of the Project.

(b) After reparation treatment of the right stilling basin, the Project suffered many times of large flood in succession. The max. reservoir peak inflow was as much as 35,000 m^3/s, 37,000 m^3/s, 26,900 m^3/s and 26,900 m^3/s and the corresponding discharge was as much as 23,000m^3/s, 23,900m^3/s, 17,300m^3/s and 20,700m^3/s in 1998, 1999, 2002 and 2003 respectively. Many inspections after dewatering indicate no abnormal conditions occur for the stilling basin, so the reparation treatment is successful.

New Developments in Dam Engineering—Wieland, Ren & Tan (eds),
© 2004 Taylor & Francis Group, London, ISBN 04 1536 240 7

Inverse analysis of groundwater movement parameters in double fractured media

Zhou Zhifang
College of Civil Engineering, Hohai University, Nanjing, P.R. China

ABSTRACT: According to the geological and hydrogeological conditions exposed by TGP's 2nd-stage construction, the physical and mathematical model for the groundwater movement through the 3D double fractured media of rock mass during construction is set up in this thesis. Based on discontinuity-control inverse theory, some relative parameters (hydraulic conductivity coefficient tensor, specific storativity, transference coefficient, et al.) of double fractured media are inversed with flux being the known quantity and calibration of water table the objective function. Synchronously, the seepage field of the construction region is systematically analyzed and simulated, the results of which exhibit that the double fractured media model of fracture water can comprehensively and correctly describe the geological and hydrogeological conditions in the construction region. Conclusions of parameter and hydrogeological qualitative analysis are basic consistent.

1 INTRODUCTION

The concept of double porosity was originally proposed by Barenblatt et al.[1], in order to quantify flow in fractured rocks. Extensions of double porosity flow models have been used to describe flow regimes dominated by single fractures that transect a less porous matrix aquifer by Gringarten and Ramey[2]. However, Moench's studies showed double porosity model considering fracture flow require information about the number of fractures in the research area, their geometry and hydraulic aperture, as well as the nature of the fluid interchange between the fractures and the matrix[3]. Zhang Youkuan calculate dual media seepage problems of two-dimension fracture-karst aquifer based on finite element method[4].

Double porosity models are often favored by the ground water industry. McConnell made use of several case studies to aim at describing the merits of applying double porosity models[5]. Recently, three-dimensional discrete fracture network flow model to describe the dominant fracture networks, and porous medium seepage, tensor model to describe the minor fractures, and doublemedium model by combining the two models which can well describe the karst-fracture water flow and the water-bursting characteristics are developed by Pan Guoying and Wu Qiang[6]. Mathematical model of dual media confined fracture water is established and a most suitable solution (finite volume method) is proposed by Han Hua and Yang Tianxing[7].

However, literature on the study of groundwater movement problems, especially parameter inverse problems, of 3-D seepage in double fractured media is scare. In the past time, based upon singular fracture media, plenty of research on seepage field of TGP's dam site has already been made [8]. In this thesis, based on the basic flow equation of groundwater flow in double media of rock mass and with three dimensional finite element methods, after inversing the seepage tensor, the specific storativity and the transference coefficient, the character of seepage field in TGP's construction region is simulated.

2 ENVIRONMENTAL GEOLOGY

2.1 *Topography and physiognomy*

The spilling monoliths are located in the formal wadi of Yangtse River and in the right flood bed (including Sijin Beach, Zhongbao Island). The topography after excavation is basically similar to the desired figure. The small difference only exists in local monoliths due to optimization design and limited treatment. On the whole, the bearing surface altitude of each monolith depresses from Zhongbao Island to the principle riverbed. Spill $1^{\#}$ to Spill $4^{\#}$ are in the deep groove of the riverbed, the bearing surface altitude of which ascend from upstream (4–10m) to downstream (15–21m) with the ratio 1:6; the altitude of Spill $5^{\#}$ to Spill $8^{\#}$ increase gradually from 21m to 31m; that of Spill $9^{\#}$ to Spill $17^{\#}$ from 21m to 35m; and that of Spill $18^{\#}$ to Spill $23^{\#}$ from 38m to 50m.

2.2 *Lithology and tectonics*

The lithology of bearing rock mass is mainly off-white carbon black amphibole-mica-plagioclase granite (γNPt) of Pre-sinian, in which there invade off-white light red granite vein(γ), flesh-red pegmatite vein*(ρ),* and small quantity of amphibole inclusion.

Faults in the research area can be classified into the following 4 groups according to their strikes: Group NNE, Group NE-NEE, Group NWW and Group NNW. Of Group NNE, the strikes vary from 5° to 30°, the direction of dip is mainly NE, dip angles are between 55° and 75°, and mostly intersect the spill monolith obliquely. The number of this group found is 25 (37.3% of the total). Of Group NE-NEE, the strikes vary from 54° to 85°, the direction of dip is mainly NW, dip angles are between 65° and 85°, the number of which found is 12 (17.9% of the total). Of Group NWW, the strikes vary from 270° to 295°, the direction of dip is mainly NE, dip angles are between 58° and 83°, the number of which found is 12 (17.9% of the total). Of Group NNW, the strikes vary from NW330° to NW353°, the direction of dip is mainly SW, dip angles are between 58° and 80°, the number of which found is 11 (16.4% of the total). There are 18 fractures shorter than 18m, 23 ones between 30m and 50m, 15 ones between 50m and 100m, 8 ones between 100m and 200m, and 3 ones longer than 200m.

There are 5827 fractures observed in spilling monoliths, among which high-angle ones are 3773 (64.8% of the total), mid-angle ones are 1386 (23.8% of the total), and low-angle ones are 668(11.4%ofthetotal).

According to the statistic of unit absorption *(ω)* in the Lugeon water test for the consolidation grout and auxiliary curtain in each spilling monolith, the ω value of the rock mass under that for base is greater than 1.0 L/min.m.m, and there are 12 badly permeable monoliths. According to statistic, of the rock mass for base of spilling monolith, the weakly permeable or very weakly permeable (ω<0.05) ones take 92.1% of the total, the mid-permeable ones 3.8%, the seriously permeable ones 3.8%, and the very seriously permeable ones 0.3%.

3 DOUBLE MEDIA MODEL AND BASE THEORY OF FINITE ELEMENT METHOD

3.1 *Double media model*

Above mentioned, the amphibole-mica-plagioclase granite tectonic faults in TGP's dam site can be classified into the two kinds. Groundwater in rock mass is stored in ramification fracture, and flows through artery one, therefore, on the whole, the rock mass make up of the double media of "ramification-artery fracture". In order to set up the differential equation for the groundwater flow through the double media of ramification-artery fracture, it is assumed that the ramification-artery fracture is widely developed throughout the whole research area and forms two overlapped continuum system, the permeability of the rock mass depends on that of the artery fracture, and that the water head of each point in the field are made up of two parts: ramification fracture water head (H_r) and artery fracture water head (H_a). Initially, the ramification fracture water head is equal to

artery fracture water head, and then the exchange of water between the two is proportional to the difference of the water head. From the continuity theory of water flow, the 3D differential equation for groundwater flow through double media can be easily derived[9],

$$\mu_s^a \frac{\partial H_a}{\partial t} + \mu_s^r r \int_0^t e^{-r(t-\tau)} \frac{\partial H_a}{\partial \tau} d\tau = div(K^a grad H_a) \tag{1}$$

where, K^a is the seepage tensor of artery fracture; $r = c/\mu_s^r$ is transference coefficient, c is ratio constant and t is time.

Compared to the general differential equations for groundwater flow, the formula above has an additive second term in its right end, which is called retard term. The formula above can be neatly expressed with tensor form

$$\mu_s^a \frac{\partial H_a}{\partial t} + \mu_s^r r \int_0^t e^{-r(t-\tau)} \frac{\partial H_a}{\partial \tau} d\tau = \frac{\partial}{\partial x_i}(K_{ij}^a \frac{\partial H_a}{\partial x_j}) \tag{2}$$

Where i, j=1, 2, 3, in conformity with Einstein summation convention.

The corresponding definite condition is:

$H_a(x_i,t)|_{t=0}=\varphi_0(x_i)$, $(x_i) \in \Omega$, Initial condition;

$H_a(x_i,t)|_{\Gamma_1} = \varphi_1(x_i,t)$, $(x_i) \in \Gamma_1$, $t>0$, Boundary condition for the first type;

$K_{ij}^a \frac{\partial H_a}{\partial x_j}\cos(n,x_i)\Big|_{\Gamma_2} = q_0(x_i,t)$, $(x_i) \in \Gamma_2$, $t>0$, Boundary condition for the second type;

Where $\varphi_0(x_i)$, $\varphi_1(x_i, t)$, and q_0 are the known functions, and n is outer normal direction of the boundary $1'_2$.

3.2 *Theory of finite element method for seepage through double media*

In the right coordinate *oxyz,* by omitting the subscript and superscript a of H_a, K_{ij}^a respectively, the trial solution of the research area is defined with Garlerkin Method, with $N_L(x_i)$ as the weight function. According to the theory of definite integral, we have

$$\sum_e \iiint_e \left[(K_{ij} \frac{\partial \hat{H}^e}{\partial x_j}) \frac{\partial N_L}{\partial x_i} + \mu_s^a \frac{\partial \hat{H}^e}{\partial t} N_L(x_i) + (\mu_s^r r \int_0^t e^{-r(t-\tau)} \frac{\partial \hat{H}^e}{\partial \tau} d\tau) N_L(x_i) \right] d\Omega$$
$$= \iint_D (K_{ij} \frac{\partial \hat{H}}{\partial x_j}) \cos(n,x_i) N_L(x_i) ds \tag{3}$$

The integral term caused by the retard effect of ramification fracture in a certain element can be formulated as:

$$\iiint_e (\mu_s^r r \int_0^t e^{-r(t-\tau)} \frac{\partial \hat{H}^e}{\partial \tau} d\tau) N_L(x_i) d\Omega \tag{4}$$

By approximating the triplex integral with repeated summation and discretizing the time interval $[0, t]$ into n_t parts with the step Δt, we have

$$r_e \iiint_e \sum_{k=1}^{8} N_k N_L d\Omega \frac{dH_k}{dt} \tag{5}$$

Therefore, in a certain element *e,* we have

$$[G^e_{L,k}]\{H_k\}+[P^e_{L,k}]\left\{\frac{dH_k}{dt}\right\}+[R^e_{L,k}]\left\{\frac{dH_k}{dt}\right\}=F^e_L \tag{6}$$

Where

$$G^e_{L,k}=\iiint_e (K_{ij}\frac{\partial N_k}{\partial x_j})\frac{\partial N_L}{\partial x_i}d\Omega,\ P^e_{L,k}=\iiint_e \mu^a_s N_k N_L d\Omega \tag{7}$$

$$R^e_{L,k}=r_e\iiint_e N_k N_L d\Omega\ ,\ F^e_L=\iint_D qN_L ds \tag{8}$$

$$r_e=\mu^r_s r(\sum_{i=1}^{n_t} e^{-r(t-i\Delta t)}\Delta t)\quad (L=1,2,\Lambda\ ,8;\quad k=1,2,\Lambda\ ,8) \tag{9}$$

After accumulating each matrix element above, and approximating *dH/dt* with implicit-difference method, we can easily derive the algebra equations.

4 INVERSE CALCULATIONS FOR DOUBLE MEDIA

4.1 *Calibration of water table*

Presently, TGP's 2nd-stage constructions are being strenuously and orderly carried on. The exposures of excavated rock mass in the dam base clearly reflect the "ramification—artery fracture" double media feature of the rock mass for dam base. In the channel of the spilling monolith, borehole **1x-□-6** has recorded the yield and the borehole top water table versus time detailedly (figure 3). The pumping test was begun at 4:42pm, Nov. 22nd, 2000 and finished at 1:27, Nov. 25th, 2000. Of the borehole, the geography coordinate is known as (20012.8, 48723.3). The top altitude is 15.0m. The depth is 104.8m, and the corresponding bearing surface altitude is 10.0m. In order to acquire groundwater movement parameters, based on discontinuity-control inverse theory and hydrogeological conditions, groundwater movement parameters are inversed by taking 4 artery fractures as the discontinuity to govern water flow, flux as known, and the goodness of calibrating water table as objective function. The inversion area is between the upstream and downstream of the whole dam's 2nd-stage projects, and extends east north to the temporary lock and west south to the open conduit channel (figure 1). The research area is descretized into 11256 hexahedron elements and 13242 nodes (figure 2). During the corresponding period, the river water table (67.0m) around the research area, the pond water table (38.0m) in front of the dam and between Spill 1$^{\#}$ and 16$^{\#}$, the draining foundation trench water table (34.26m) in front of the dam, and the draining foundation trench water table (10.80m) at the back of the dam are treated as the boundary conditions for the first type.

In the 34 observe periods in all, water head at 6 interval time is chosen for calibration, after adjusting the parameters repeatedly, the comparison of calculated water head with observed one can be derived (listed in table 1). The test borehole was descritized into 6 nodes verticality. The maximum, minimum and weighted average water table of the 6 nodes versus time is illustrated in figure3, together with the 34 (in all) observed water table. From figure3, the calculated water table correctly reflects the observed water table versus time.

4.2 *Results of parameter inversion and some relative analysis*

Corresponding to calibration of water table, the groundwater movement parameters are inversed (see figure 2 and 3) with axis *y* parallel to the axes of the dam, axis *x* leading from upstream to downstream and axis *z* accordant to right-hand rule.

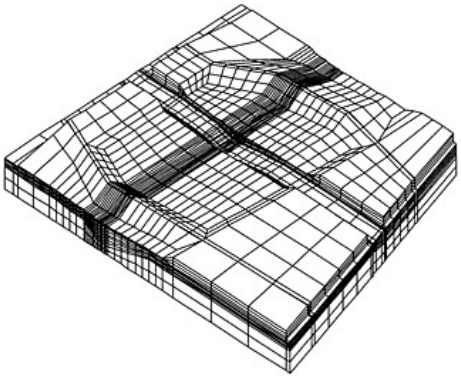

Figure 1. Area of double media model.

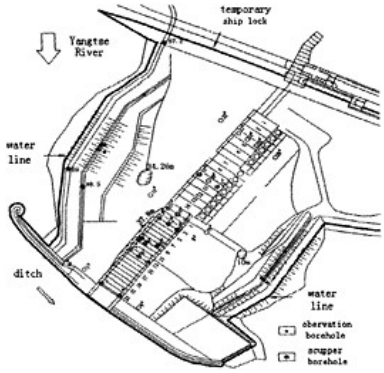

Figure 2. Discretization of research area.

Table 1. Calibrating water head during inverse calculation.

Period	Time (h)	Calculated water head (m)	Observed water head (m)	Absolute errors (m)	Remark
1	0.0833333	36.43			The mean yield of
2	0.5833333	31.71			observe well is
3	3.4633333	27.15	27.00	0.15	48.36 (m^3/d)
4	11.428924	25.11	25.00	0.11	
5	29.460520	24.27	24.00	0.27	
6	49.180920	23.72	23.00	0.72	
7	62.512920	23.14	23.20	0.06	
8	69.628920	22.58	22.00	0.58	

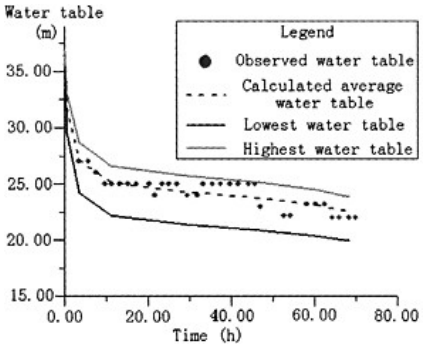

Figure 3. Calibration of water table versus time.

From table 2, the inversed tensors of hydraulic conductivity of artery fractures in the deep groove area of spill monolith are greater than that in other places for about one order of magnitude, which validates that the granite rock mass in the deep groove area of spilling monolith relatively is intensely weathered, broken, and permeable and which accord to the abnormal Lu value derived from Lugeon water test in this area.

Table 2. Inversed principle seepage value and principle seepage orientation of the anisotropic rock mass under dam base.

Position		In the deep groove area of spilling monolith			In other places		
Principle seepage value (m/d)		K_1 0.00726	K_2 0.02250	K_3 0.02976	K_1 0.00104	K_2 0.00321	K_3 0.00425
Principle seepage orientation	$\cos\alpha_1$	0.8688	0.4066	0.2820	0.8688	0.4066	0.2820
	$\cos\alpha_2$	−0.3867	0.9130	−0.1260	−0.3867	0.9130	−0.1260
	$\cos\alpha_3$	−0.2924	0.0351	0.9511	−0.2924	0.0351	0.9511

Table 3. Other relative parameters calculated with inverse methods.

Name of parameters	Specific storativity of artery fracture μ_s^a (1/m)	Specific storativity of ramification fracture μ_s^r (1/m)	Transference coefficient r(1/d)	Hydro conductivity* of cofferdam (m/d)	Hydro conductivity* of the grout in the dam (m/d)
Magnitude	0.000069	0.00048	0.417	0.20	0.0864

Note: The superscript * means that the parameters have been specified or defined.

Because the test boreholes are at the deep groove of the deep groove area of spilling monolith, the specific storativity inversed from table 3 mainly reflect the medium feature of the deep groove area in spilling monolith. From table 3, the specific storativity of the artery fracture μ_s^r inversed from table 3, coefficient of water exchange between ramification fracture and artery fracture can be calculated:

$$c = r\mu_s^r = 2.0 \times 10^{-4}(1/\text{m.d}).$$

Transference coefficient r reflects the connectivity between ramification fracture and artery fracture, the greater r, the more water transports from ramification fracture to artery fracture.

5 CONCLUSION

Based on discontinuity-control inverse theory and the observed groundwater data of long duration, the hydrogeology parameters of double media are inversed in this thesis. These parameters can more comprehensively and systematically reflect the fracture media feature of the research area than that of singular media.

The numerical simulation of the seepage field of double media in TGP's 2nd-stage construction region indicates that a stripe depression cone was formed due to the concentrative pumping in the front drain and the back drain. The occurrence of the stripe depression cone is basically accordant to the deep groove and direction of relatively high permeability in rock mass. The pumping of borehole 1×-I-6 only effect on its vicinity seepage field, and the whole seepage field in construction has not changed sharply. The residual water head of pumping borehole had something to do with that the borehole is situated at the deep groove and near the front pond of the dam and that the dam base has not been treated with grout curtain.

In conclusion, the 3D double media model for groundwater movement through the fractured rock mass in TGP's 2nd-stage construction region can systematically, comprehensively and correctly described the geological and hydrogeological conditions exposed by construction region.

REFERENCES

[1] Barenblatt, G.I., Yu.P.Zheltov and I.N.Kochina. Basic concepts in the theory of seepage of homogeneous fluids in fissured rocks[J]. Journal of Applied Mathematical Mechanics, 1990, 24(5): 1286–1303.
[2] Gringarten, A.C. and H.J.Ramey Jr. Unsteady state pressure distributions caused by a well with a single horizontal fracture, partial penetration or restricted entry[J]. Socie tv of Petroleum Engineers Journal, 1974, 5:413–426.
[3] Moench, A.R Double-porosity models for a fissured groundwater reservoir with fracture skin[J]. Water Resources Research, 1984, 20(7): 831–846.
[4] Zhang Youkuan. Double media seepage model and its FEM in fracture-karst aquifer[J]. Geotechnical Investigation & Surveying, 1984, 4:32–35.
[5] McConnell, C.L. Double porosity well testing in the fractured carbonate rocks of the Ozarks[J]. Ground Water, 1993, 31(3): 75–83.
[6] Pan Guoying and Wu Qiang. Characteristics and model researches of the seepage flow in double-medium karst fracture networks at jiao zuo coal mining area[J]. Carsologica sinica, 1998, 17(4): 363–369.
[7] Han Hua and Yang Tianxing. Finite volume method and its application of mathematical model for dual media confined fracture water[J]. Geotechnical Investigation & Surveying, 1999, 3:32–34.
[8] Jin Zhongqing and Zhou Zhifang. Inverse Problems in Engineering Hydraulics[M], Nanjing: Press of Hohai University. 1997, 59–138.
[9] Zhou Zhifang and Teng Jianren. Analysis on seepage control in dam foundation of the Three Gorges Project [J]. Chinese Journal of Rock Mechanics and Engineering, 2001, 20(5): 700–704.

This page intentionally left blank.

New Developments in Dam Engineering—Wieland, Ren & Tan (eds),
© 2004 Taylor & Francis Group, London, ISBN 04 1536 240 7

Influence of rain on stability of unsaturated rock slope

Zhou zhifang & Huang yong
College of Civil Engineering, Hohai University, Nanjing, P.R. China

ABSTRACT: Flood discharge will produce lots of rain in water resources and hydropower engineering. It may have important effect on dam and water conservancy buildings. In this paper, as an example of Jinping hydroplant, quick depressed reasons of unsaturated matrix suction for slope are analyzed on the action of rain. Rocks' stability of two banks slope is discussed considering rain of different intension. And effect on slope stability safety coefficients between rain and natural equivalent intension rain is compared. The calculation results show that stability of slope rocks is obviously different on the condition of two different rains.

1 GEOLOGICAL ENVIRONMENT IN DAM AREA

1.1 *Topographty and physiognomy*

The dam site of Jinping hydroelectric power station locates in 1.5km long stream segment between Pushinuo and Shoupa trench in Yalong River downstream. The flow direction of river is about between NE25° and NE27°. River valley is typical deep incision gorge, and its shape shows "V". Topographty of left bank is comparatively integrity and contradictorily direction slope. Height difference is between 1500m and 1700m. The altitude of 1900m is threshold of valleyside slope. It is gorge below it and slope degree is approximately from 60° to 80°. It is dale above it and slope degree is 45°. Right bank is incised by Pushinuo and Shoupa trench and shows slope direction is the same. Ranges of slope degrees are considerably big in different altitude.

1.2 *Lithology and constitution*

Stratum distributed and disclosed in dam area is mainly Zagunao group of middle Triassic. Lithology is divided into three segments from top to bottom. Lithology of the first segment ($T^3_{2\text{-}3z}$) are marble and sand slate individually. Furthermore, there is also lamprophyre vein in dam site. Its thickness is between 2m and 5m. It shows weathering from weakness to strength above the altitude of 1720m, and lithology is looseness. Below the altitude of 1720m, lithology is integrity

There are total 30 faults in dam area. There faults in the research area can be classified into the following 4 groups according to their strikes: Group NEE, Group NNE, Group NW and Group NE. Of Group NEE, the strikes vary from 50° to 80°, the direction of dip is mainly SE, dip angles are between 70° and 75°, and mostly intersect the spill monolith obliquely The number of this group found is 12 (40.0% of the total). Of Group NNE, the strikes vary from 35° to 45°, the direction of dip is mainly SE, dip angles are between 70° and 85°, the number of which found is 5 (16.7% of the total). Of Group NW, the strikes vary from 310° to 335°, the direction of dip is mainly NE, dip angles are between 50° and 85°, the number of which found is 6 (20.0% of the total). Of Group NE, the strikes vary from NE3°to NE58°, the direction of dip is mainly NW, dip angles are between 40° and 56°, the number of which found is 7 (23.3% of the total). Furthermore, there are 52 deep cracks, and which are classified into two groups according to preponderant directions. One varies from NE30° to NE50°. The direction of dip is mainly SE. Dip angles are between 50° and 60°. Other varies from NE70° to NE85°. The direction of dip is mainly SW. Dip angles are between 60° and 80°.

2 STABILITY CALCULATION THEORY OF SLOPE

In the stability analysis of slope, it is necessary to divide rocks above the sliding plane into several vertical blocks (Janbu Method). The forces of acting on a rock block are showed as Fig. 1. Furthermore, the forces are calculated as unit width, that is to say, it is considered as a unit in the direction of verticality between the force and sliding plane.[1,2]

The shear strength of unsaturated rocks is given by Fredlund (1978) applying to extended Mohr-Coulomb formula[3]

$$\tau = c' + (\sigma_f - u_a)\tan\phi' + (u_a - u_w)\tan\phi^b \tag{1}$$

Where, c'; Φ^b is dip angle of curve on account of increase of matrix suction resulting in the increase of shear strength. u_f–u_a is net normal stress of failure plane. u_a is pore air pressure of failure plane. u_a–u_w is matrix suction of failure plane. Shear force, S_m at the bottom of rock blocks is written as by formula (1)

$$S_m = \frac{\beta}{F}[c' + N\tan\phi' - u_w\tan\phi^b] \tag{2}$$

The force between rock blocks is given as function

$$E_R = E_L + [W - (X_R - X_L)]\tan\alpha - \frac{S_m}{\cos\alpha} \tag{3}$$

Assuming that there is relation to shearing force and normal stress, E between rock blocks[4]

$$X = \lambda f(x) E \tag{4}$$

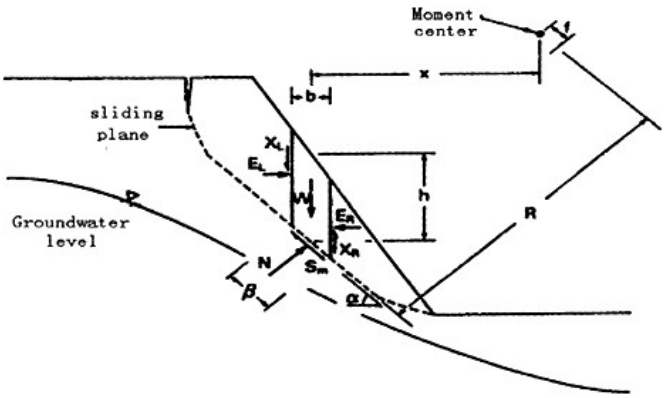

Figure 1. The forces of acting on a rock block on the sliding plane.

Normal stress, N at the bottom of rock blocks can be calculated as

$$W-(X_R-X_L)-S_m \sin\alpha-N\sin\alpha=0 \tag{5}$$

Substituting formula (2), (3) and (4) into (5), normal stress can be expressed as

$$N=\frac{W-AW\tan\alpha+(A/\cos\alpha-\sin\alpha)\frac{\beta}{F}(C'\sin\alpha-u_w\sin\alpha\tan\phi^b)}{\cos\alpha+\beta(\sin\alpha\tan\phi')/F-A\beta\tan\phi'/(F\cos\alpha)} \tag{6}$$

where, $A=\lambda f(x)/(1+\lambda f(x)\tan\alpha)$.

Safety coefficient of moment balance, F_m is given as

$$F_m=\frac{\sum[c'\beta R+(N-u_w\beta\frac{\tan\phi^b}{\tan\phi'})R\tan\phi']}{\sum Wx-\sum Nf} \tag{7}$$

Safety coefficient of force balance, F_f

$$F_f=\frac{\sum[c'\cos\alpha+[N-u_w\beta\frac{\tan\phi^b}{\tan\phi'}]\tan\phi'\cos\alpha]}{\sum N\sin\alpha} \tag{8}$$

Where, W is total weight of rock blocks, its width and length is b and h individually. N is total normal stress acting on the bottom of rock blocks. S_m is shear force at the bottom of rock blocks. E is horizontal normal stress between rock blocks. X is vertical shearing force between rock blocks. R is the radius of circle arc sliding plane or the force arm of moment at the random shape sliding plane. F is vertical distance from action line of normal stress to turning or moment center. x is horizontal distance from midline of rock blocks to turning or moment center. h is vertical distance from the midpoint at the bottom of rock blocks to that at the top of them. α is angle between tangent of midpoint at the bottom of rock blocks and horizontal plane. It is positive if direction of the angle corresponds to that of slope angle, or else negative. β is inclined length at the bottom of rock blocks. E_R, E_L are horizontal normal stress between rock blocks. Subscript L and R means left and right sides individually.

It is noted that $f(x)$ describes function relation of X/E along the range of sliding plane. Its value is generally 1, and λ is proportion coefficient. If right normal stress of the last rock blocks is 0, it is considered as balance conditions. When different λ values are given, F_m, F_fCan be calculated at the condition of balance. When λ is constant, if F_m is equal to F_f, stability coefficients of slope are $F=F_m=F_f$.

3 DETERMINATION OF PARAMETERS AND POSITION ON SLIDING PLANE

At first, position of sliding plane must be determined. According to calculation results of three dimensional seepage fields in dam area, we find that groundwater level in the slope is very low. It is considered that position of sliding plane is not below saturated level, that is, it locates in unsaturated area above saturated level. However, it is considerable difficult to locate in the extract position of sliding plane. In the paper, based on field investigate and research report of design on choosing dam, the position of sliding plane is assumed. Two positions are considered according to difficult lithology, discontinuity incise and fault growth.

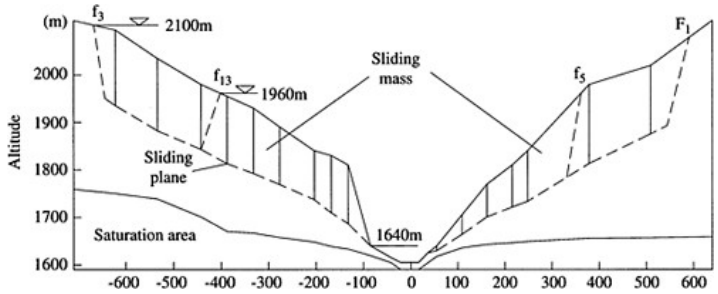

Figrue 2. Sketch map of sliding mass.

The first is assumed that extend line of fault F_1 is considered as incise plane behind sliding mass in the left bank. On account of deep crack disclosed between 1690m and 1820m, mean depth of sliding mass is considered as 130m. Altitude of overflow points in slope angle is 1640m. In the right bank, extend line of fault f_3 is considered as incise plane behind sliding mass. Mean depth of sliding mass is considered as 130m. Altitude of overflow points in slope angle is 1640m. The second is assumed that extend line of fault f_5 is considered as incise plane behind sliding mass in the left bank and f_{13} in the right bank. Other conditions are same as those of the first (see Fig. 2).

Secondly, parameters of sliding plane must be determined. According to the research report of design on choosing dam, c', ϕ' Coordinate of moment center is 0.45m and 2509m.

4 RESULT ANALYSIS

Stability safety coefficients of slope are calculated by GLE in rainfall and rain for high slope of Jinping power station. And these are compared with that without matrix suction. According to calculation results of unsaturated seepage, matrix suction of slope is considered as load. As a result, stability of slope is appraised. At the course of calculation, continuum equal strength rainfall and rain are involved. The biggest strength of rain is 1000mm/d. The slope of two banks is divided into many blocks. Different stability safety coefficients are calculated by computer program (See Table 1, Fig. 3 and Fig. 4). Figure (a) and Figure (b) correspond to sliding plane (i) and (ii) individually.

Table 1 shows that in the two assumption of sliding plane, stability safety coefficients are higher than 1.0. In natural condition, stability safety coefficients with matrix suction are higher than these without it. It makes clear that slope stability is fine with matrix suction. That is to say, matrix suction can increase slope stability.

On the condition of rainfall, matrix suction of slope will reduce quickly, and stability safety coefficient will also decline. But the extent of decline is not big. It has invisibly important effect on stability of slope. On the condition of rain, the declining extent of stability safety coefficient is large. Therefore, there is obviously different effect for the two types.

Stability safety coefficients of calculation applied to assumption of sliding face (i) are larger than those applied to assumption of sliding face (ii). Since from river valley to two bank slope, weathering and stress release action of rocks weak gradually. Integrity of rocks is fine inside mountain, and stability of it is also finer. Simultaneously, region of sliding mass applied to assumption of sliding face (ii) is almost inside rainfall region of rain. Rainfall strength of the

Table 1. Compare of safety coefficient with matrix suction and without it in natural condition.

Scheme	(□) Stability safety coefficient		(□) Stability safety coefficient	
Matrix suction (kPa)	−40	0	−40	0
Left bank	1.4467	1.4285	1.5806	1.5198
Right bank	1.2555	1.2207	1.6720	1.6254

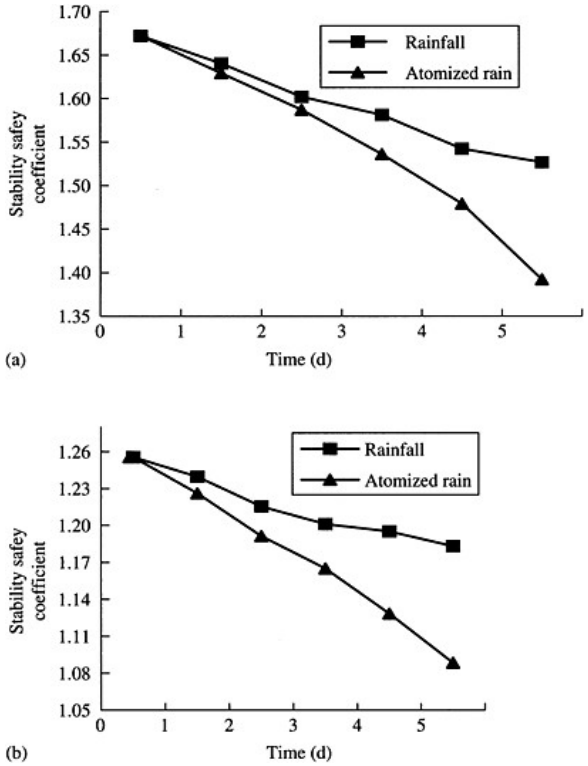

Figure 3. Relation between stability safety coefficient and rainfall time in right bank.

region is large, so stability safety coefficients are relatively low. Furthermore, stability of rocks is lower nearer river valley.

According to the assumption of sliding plane (i), stability safety coefficients of left bank are lower than those of right bank. The value is 0.15. It is impossibly related to strike direction and construction of rock formation. Strike direction of rock formation in dam region is an arrangement in right bank and contradiction in left bank. Furthermore, fissures of left bank are more considerable development than those of right bank. Therefore, it is receivability to occur to difference of stability safety coefficient between left and right bank. Figure (a) and Figure (b) show that based on different sliding plane, different stability safety coefficient can be gained.

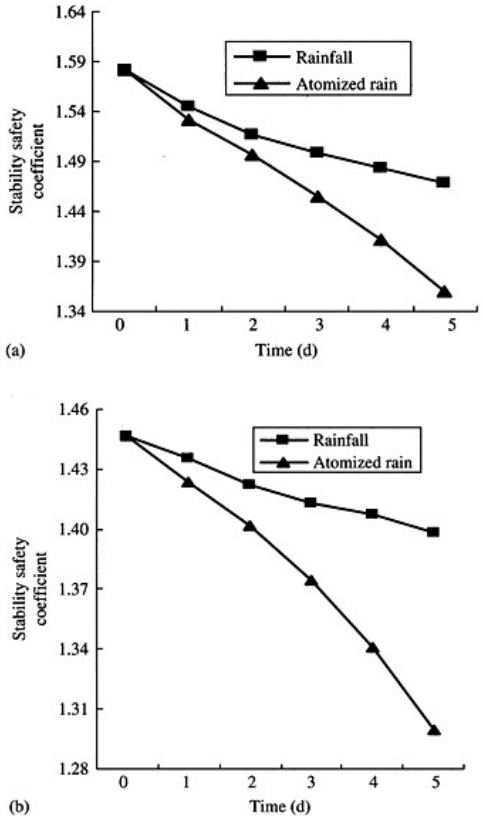

Figure 4. Relation between stability safety coefficient and rainfall time in right bank.

5 CONCLUSION

Loss or decrease of matrix suction in rocks resulted from rainfall influent seepage is main mechanism resulted in decrease of slope stability. On the condition of equal rainfall time, if strength of rainfall is very large, decreasing extent of slope safety coefficient is obvious. On the condition of equal strength, rain has obvious effect on stability of slope than rainfall.

REFERENCES

[1] Peters R R, Klavetter E A. A continumn model for water movement in an unsaturated fractured rock mass[J]. *Water Resour. Res.,* 1988, 24(3):416~430.
[2] Wu Hongwei, Chen Shouyi. Parametric study of effects of rain in filtrationon unsaturated slopes[J]. *Rock and Soil Mechanics.* 1999(3):1~13.
[3] Fredlund D G. (Cheng zhongyi, Zhang zaiming Trans.). Mechanics of Unsaturated Soil[M]. Beijing, *Chinese Construction Industry Press.* 1997, 8.
[4] Li Zhuofen, Chen Hong. Rain percolation and landslide hazard in HongKong[J]. *Hydrogeology and Engineering Geology.* 1997(4):34~38.

New Developments in Dam Engineering—Wieland, Ren & Tan (eds),
© 2004 Taylor & Francis Group, London, ISBN 04 1536 240 7

The allowable stress of large aggregate concrete in arch dam design*

Eryu Zhu
Beijing Jiaotong University, P.R. China

Huichao Dai
China Yangtze Three Gorges Projet Development Corp., P.R. China

Chunliang Li
Hebei institute of engineering, P.R. China

Xiaowei Zhu
Beijing Jiaotong University, P.R. China

ABSTRACT: In this paper, by considering the comprehensive effect coefficient of concrete size effect and aggregate size, the scale coefficient of concrete discontinuity strength, the stress state factor and the loading rate factor on concrete compressive or tensile strength, the large aggregate concrete allowable stress is studied. While concrete grade is fixed, the arch dam's allowable stress is computed. According to the compute results and the US bureau of reclamation provided, some limits are found in code[2] about the allowable stress selection.

1 INTRODUCTION

It's an important problem for selecting allowable stress and factor of safety in dam design, which has a bear on economy and safety. Generally speaking, it's a tendency that increases the allowable stress and decreases the factor of safety in world dam practice. The increase of allowable stress reflects the accumulated experience of dam construction and rising level of dam construction technology. This is why some high arch dams have been built in the earthquake areas.

The allowable stress selection in the past is defined by compressive strength or tensile strength obtained by the test of small concrete samples, and divided by an experience safety coefficient. But sometimes the allowable stress determined by this method is very large, and sometimes it is very small. Therefore, allowable stress selection should be studied on fully graded aggregate concrete.

2 THE ALLOWABLE STRESS FORMULA FOR LARGE AGGREGATE CONCRETE

According to the reference [1], considering specimen size effect and aggregate size effect, discontinuity and loading state, the allowable stress formula for large aggregate concrete can be expressed as following

$$[\sigma c] \leq f_c \cdot k_1 . k_2 . k_3 . k_4 \tag{1}$$

* This Project is Supported by the Natural Science Foundation of China through Grant No. 59379408 and the Youth Science Foundation of Beijing Jiaotong University.

$$[\sigma_t] \le f_t \cdot k_1' \cdot k_2' \cdot k_3' \cdot k_4' \tag{2}$$

where $[\sigma_c]$, $[\sigma_t]$ is the concrete allowable compressive strength and allowable tensile strength respectively.

f_c, f_t is the wet-screened aggregate concrete standard cube compressive strength and tensile strength respectively.

k_1, k_2' is the comprehensive effect coefficient considering concrete size effect and aggregate size on compressive strength and tensile strength respectively.

k_2, k_2' is the scale coefficient of concrete discontinuity strength divided by compressive or tensile strength respectively.

k_3, k_3' is the stress state factor on concrete compressive or tensile strength respectively.

k_4, k_4' is the loading rate factor on concrete compressive or tensile strength respectively.

2.1 *Determination of coefficient* k_1 *and* k_2'

According to reference [1], the size effect for concrete material varied in a limited range no matter how large or small the test pieces are. The strengths tend to be a constant value when test blacks' size reached a certain limit. Reference [6] indicates that the cylinder compressive strength is almost the same for diameter 457, 610 and 914mm, and their strength relative error is no more than 5%. Therefore, we may accept the fact that the strength properties of diameter 450mm cylinder, section 450×450 cube or prism fully graded concrete represent mainly the strength properties of large volume concrete.

A lot of fully graded concrete strength tests need many materials, and large capacity pressure machine. Therefore, for the dam concrete strength tests, wet-screened aggregate concrete small blocks are needed in engineering practice. When small concrete blocks of different size and shape are used to test large volume concrete strengths, a kind of conversion relation is given as following

$$\frac{f_{cu}}{f_{cu15}} = 1.317 - 0.1694\left(\frac{V}{b_{15}dh} + \frac{h}{d}\right) \tag{3}$$

in which V is the volume of test pieces, d is the cylinder diameter, h is the height. f_{cu} is the compressed strength. f_{cu}, b_{15} is the 15cm cube compressed strength and section size respectively. All the length unit is cm, the strength unit is MPa.

When small concrete blocks of different size and shape are used to convert the fully graded aggregate concrete tensile strength, splitting strength and flexural strength, a kind of transforming formula is used as following

$$f_i = \frac{f_{b15}}{-3.631\frac{A_{b15}}{A_i} + 1.279\frac{C_{fb15}}{C_{fi}} + 3.436\frac{D_{ab15}}{D_{ai}}} \tag{4}$$

in which f_i *(i=t, p, b)* indicates the concrete tensile strength, splitting strength and flexural strength while *i=t, p, b,* its unit is MPa. A_t is section area, its unit is cm^2. D_{ai} is the maximum aggregate size, its unit is cm. C_{fi} is the loading state factor, C_{fi} is 0.63, 0.77 and 1.00 while the loading state is tensile, splitting and flexural. f_{b15}, A_{b15}, C_{fb15}, D_{ab15} is 15cm cube's flexural strength, section area, loading state factor (C_{fb15}=1.0) and maximum aggregate size (D_{ai}=4cm).

The strength conversion coefficient is shown in Table 1, while the concrete blocks have different shapes such as cylinder, cube, prism, and different loading states such as compressive, tensile, splitting and flexural loading. Table 1 suits concrete strength grade about C20, test period about 90 days.

Table 1. The strength conversion coefficient.

Loadmg state	Size (cm)	Compressive blocks' shape and size (cm)					
		Cube		Cylinder		Prism	
		45×45×45	15×15×15	ϕ 45×90	ϕ 15×30	45×45×90	15×15×30
Tensile	45×4×120	0.068	0.052	0.096	0.065	0.115	0.065
	15×1×30	0.098	0.074	0.137	0.093	0.165	0.093
Splitting	45×45×45	0.085	0.064	0.120	0.081	0.144	0.081
	15×15×15	0.115	0.087	0.161	0.109	0.194	0.110
Flexural	45×45×165	0.096	0.072	0.134	0.091	0.161	0.091
	15×15×55	0.179	0.135	0.250	0.170	0.302	0.170

According to large aggregate concrete compressive strength test results, the comprehensive effect coefficient k_1 and k_1' considering concrete size effect and aggregate size on compressive strength are about 0.55~0.75, respectively.

2.2 *Determination of coefficient* k_2 *and* k_2'

In order to avoid concrete structure part destroy, discontinuity strength should be used in engineering design. We use ultimate strength as the strength of destroy criterion, and work stress or discontinuity strength as the strength of design criterion. The elasticity limit as the lower limit design criterion of discontinuity is reasonable and convenient. Therefore, we can assume elastic limit as allowable stress to design concrete structure. Whether compressive and tensile test or biaxial compression-tension, their stress-strain relation is linear under 0.4~0.5 ultimate strength. For this reason, the scale coefficient of concrete discontinuity k_2 and k_2' are 0.4~0.5 respectively.

2.3 *Determination of coefficient* k_3 *and* k_3'

Great part areas of the arch dam are in complicate stress states such as biaxial compression-compression, biaxial compression-tension, triaxial compression-compression-compression. When concrete is in compression area, which including biaxial compression-compression, triaxial compression-compression-compression, its combined strength is greater than axial compression strength, that is to say the stress state factor k_3>1. While concrete is in tension area, its combined strength is less than axial tension strength, that is to say the stress state factor k_3' 1. Therefore, when choosing concrete strength, we should consider the stress state factor.

The coefficient k_3 under triaxial compression-compression-compression is in 1.05~2.00, it can be selected as following

$$k_3 = 1 + K\sigma_3 / R_c, K = 7.902\sigma_3^{-0.31} \tag{5}$$

The coefficient k_3' under biaxial compression-tension, according to the experimental results, can be selected as following

$$k_3' = \sigma_1 / f_t = 1 - \sigma_2 / f_c \tag{6}$$

in which σ_1 and σ_2 is the tensile and compressive strength under biaxial compression-tension, f_t and f_c is the tensile and compressive strength under uniaxial stress state. The coefficient k_3 is in 0.97~0.50 basing on Eq. (6).

The coefficient k_3' under biaxial tension-tension, according to the experimental results, is close to uniaxial tensile strength. Therefore, k_3'=1.

The coefficient k_3' under triaxial compression-compression-tension, can be determined by octahedron stress

$$\frac{\tau_{oct}}{f_c} = -0.079 - 0.583\frac{\sigma_{oct}}{f_c} \tag{7}$$

in which, σ_{oct} is octahedral normal stress, and τ_{oct} is octahedral shear stress.

2.4 *Determination of coefficient* k4 *and* k_4'

The loading time for every action in arch dam employing is not the same. According to experimental results of calculating the arch dam concrete strength, the loading rate effect should be considered. On the basis of test data, concrete strength in fast loading is greater than that in slow loading obviously. The compressive strength will be increased by a factor of 30% under earthquake load. Meanwhile, the tensile strength will be increased by a factor of more than 30%. The compressive strength under long term loading will decrease to 70%, comparing to the situation under short term loading. The tensile strength will decrease to 90% at the same situation.

3 ALLOWABLE STRESS CHECKING RESULTS AND CONCLUSION

The concrete strength grade which is often used in arch dam construction is C35 and more, sometime achieves C50. Comparing to the recent code [2], the concrete strength grade may be assumed C35–C40.

Example 1

(1) *Comprehensive effect coefficient* k_1

Based on Eq. (3), we can ascertain 45×90cm cylinder's compressive strength.

$$f_{cu} = f_{cu15}\left[1.317 - 0.1694\left(\frac{V}{b_{15}dh} + \frac{h}{d}\right)\right]. \text{ This shows}$$

$$\begin{aligned} k_1 &= \left[1.317 - 0.1694\left(\frac{V}{b_{15}dh} + \frac{h}{d}\right)\right] \\ &= \left[1.317 - 0.1694 \times \left(\frac{\pi \times 22.5^2 \times 90}{15 \times 45 \times 90} + \frac{90}{45}\right)\right] \\ &= 0.579 \end{aligned}$$

(2) *The scale coefficient* k_2

The concrete discontinuity scale coefficient k_2 can be obtained by its average value, that is k_2=0.45.

(3) *The stress state factor* k_3

The concrete strengths relating to their work stress states under the other condition are unchangeable. According to above analysis, the concrete strength under triaxial compressive stress state is greater than that under biaxial compressive stress state. Therefore, whether it is upstream dam shell or downstream dam shell, principal stresses that perpendicular arch dam surface may not be considered. We can only consider the strength influence of other two direction stress combination. This simplify is safe under compressive areas, and it does not control the dam concrete required strength in tensile area. Therefore, the triaxial stress state can be simplified to biaxial stress state, as the reference[4]. Under biaxial compression-compression, while a=1, A:$_3$ is approximate 1.3.

(4) *Loading rate factor* k_4

k_4=0.7 under long-team loading, and k_4=1.3 under earthquake loading. Then, large aggregate concrete allowable stress under long-term loading is

$$[\sigma_c]=f_c \cdot k_1 \cdot k_2 \cdot k_3 \cdot k_4=0.579\times0.45\times1.30\times0.7\times f_c=0.24f_c$$

While concrete strength grade is C35~C40, the allowable compressive stress is 8.4~9.6MPa. The allowable stress under earthquake loading is

$$[\sigma_c]=f_c \cdot k_1 \cdot k_2 \cdot k_2 \cdot k_3 \cdot k_4=0.579\times0.45\times1.30\times1.3\times f_c=0.44f_c$$

While concrete strength grade is C35~C40, the allowable compressive stress is 15.4~17.6 MPa. In code[2], the allowable compressive stress safety factor is 4.0 under main load combination, and 3.5 under particular load combination. According to this code, while concrete grade is C35~C40, the allowable compressive stress is 8.75~10MPa under main load combination, and 10~11.4 MPa under particular load combination. Thus it can be seen that the allowable compressive stress is close to the code's[2] under main load combination, and greater than the code's[2] under particular load combination. The allowable compressive stress proposed by the US Bureau of Reclamation[3] is 10.6MPa under main load combination, and 15.7MPa under particular load combination, which match the results in this paper. Therefore, we can conclude that the safety factor should reduce under particular load combination in the code's[2].

Example 2

Similar to Example 1, we can get the large aggregate concrete allowable tensile strength. While concrete grade is C35~C40, the allowable tensile stress is 0.70~0.80 MPa for axle tensile large aggregate concrete under long-term loading, and 0.98~1.11 MPa for flexural large aggregate concrete under long-term loading. Under earthquake, the allowable tensile stress is 1.02~1.16MPa for axle tensile large aggregate concrete, and 1.41~1.61 MPa for flexural large aggregate concrete.

According to the above results, the allowable stress is not the same at different loading states. The allowable stress for flexural test is greater than the stress for tensile test. The tensile stress control criterion is not the same for different loading states[5]. Flexural strength represents the collapsing strength of the cantilever beam and arch bending in load calculation of arch dam, and the tensile strength represents the part tensile strength at dam body cracking tip. Therefore, the tensile strength should select flexural test results in assess arch dam structure, in which bending is the leading action.

The allowable stress in the code[2] is less than 1.2MPa under main load combination, and is less than 1.5MPa under particular load combination. According to above results, the flexural large aggregate concrete allowable stress under long-term loading is less than the code[2], and is greater than 1.06MPa[3], which is the value provided by the US Bureau of Reclamation. The allowable stress test result under earthquake loading is close to that of the code[2] and 1.58Mpa provided by the US Bureau of Reclamation.

REFERENCES

[1] Eryu Zhu. Experimental Studies on Fully Graded Aggregate Concrete Multiaxial Strength Theory and Stress-Strain Relationships in Mass Concrete under Multiaxial Stresses. Doctoral Dissertation, Dalian University of Technology, November 1996.

[2] Concrete Arch Dam Design Code (SDL45–85). Water Conservancy and Electric Power Ministry, P.R. China, April 1990.

[3] Pan Jiajing, Li Maizhan. Water Conservancy Project Building Design Collection—Arch Dam. China Water Conservancy and Power Press, October 1982.

[4] Japan Dam Committee. Dam Design Code (In Chinese), 1981.

[5] R.Dungar H.Kreuzer. Apparent Tensile Strength for Arch Dam Design: A Review of Rate, Size and Strength Dependency. Dam Engineering, Vol. III, Issue 3.

[6] U.S. Department of the Interior Water and Power Resource Service. Concrete Manual. Eighth Edition, Revised Reprint 1981.

This page intentionally left blank.

New Developments in Dam Engineering—Wieland, Ren & Tan (eds),
© 2004 Taylor & Francis Group, London, ISBN 04 1536 240 7

Investigation to arch action and hydraulic fracturing of core rockfill dam

Jun-Gao Zhu & Jun-Jie Wang
Institute of Geotechnial Engineering, Hohai University, China

ABSTRACT: In design of rockfill dams, the arch action and hydraulic fracturing of the core are two important and unsolved problems. This paper analyzes the stress-deformation behavior of a high rockfill dam with a vertical core in clay using three-dimensional Finite Element Method (3D FEM). Special attention is placed on the arching action and hydraulic fracturing of the core. Two types of factors influencing on the arch action, i.e., the properties of the materials filling dam and the structure of the dam, are investigated. It is found that increasing of Young's modulus or Poisson's ratio of the material of the core results in reduction to the arch action in core. On the other hand, both decreasing of the slope of the core or dam and increasing of the core thickness are helpful to reduce the arch action. The likelihood of hydraulic fracturing is dependent on how strong the arch action is.

1 INTRODUCTION

A great number of high earth dams are going to be constructed in Western China where water resources are very abundant. Among those earth dams, most of them are core rockfill dams. It is well known that cracks frequently occur in cores of rockfill dams. The cracks are believed to result from arching action and/or hydraulic fracturing. Care must be taken to prevent such cracking and the Engineer must decide whether the cracks are likely to extend and become serious or whether they are stable and can be backfilled. The cause of arch action is the large different deformations between the dam shell and the core. The arch action is often concerned to increase the likelihood of the hydraulic fracturing of the core. It is thus significant to investigate the hydraulic fracturing, as well as the arch action.

Nobari et al (1973)[1] analyzed the influence of dam structure and material on major principal stress in upstream side of the core using plane strain finite element method (2D FEM). Kulhawy and Gurtowski (1976)[2] also studied the main influencing factors on major principal stress in upstream side of the core using 2D FEM. They indicated that the height of embankment, embankment side slopes, and thickness of transition zones have relatively little significance. Of greater importance are the thickness, position, and slopes of the core, and the most significant factor in assessing the likelihood of hydraulic fracturing is the placement water content of the core. Schober et al (1989)[3] studied the arch action induced by the restriction of bank rock-bed to the settlement of the core using model testing and 2D FEM. Zeng (2000) [4] analyzed the influence of the Young's modulus and Poisson's ratio of dam shell and core, and the slope of the core on the minor principal stress in the upstream side of the core. Zeng indicates that increasing Poisson's ratio of the shell and dam, decreasing the difference of the Young's modulus between the shell and core, and reducing the slope of the core, increase the minor principal stress in the upstream side of the core.

The findings mentioned above are all obtained under the plane strain condition, i.e., 2D-FEM is used in the investigations. It is well known that a dam behaves in three-dimensional stress-strain

states, and it is therefore better to analyze the arch action using 3D FEM, and investigate the relationship between the hydraulic fracturing and arch action.

The objective of this paper is to study the arch action and hydraulic fracturing of a core rockfill dam using 3D FEM. As an example, a high earth rockfill dam in design is analyzed. This dam is located in Western Ghina, and will be the highest core rockfill dam ever designed in China so far.

2 BEHAVIOR OF STRESS-DEFORMATION OF A HIGH EARTH DAM

2.1 *Brief introduction to the dam*

The earth dam has a vertical clay core of which the top and bottom thickness is 10.0m and 111.8m, and the slope is 1:0.2. The maximum height of the dam is 261.5m, top length is 608.16m, and top width is 18.0m and the maximum bottom width is 960.78m. The slopes of the upstream and downstream sides of the dam are 1:1.9 and 1:1.8, respectively. The slope of banks almost symmetrically is 1:1.16. The deepest transverse section of the dam is shown in Fig. 1.

2.2 *Finite element model and material parameters*

A hexahedron isoparametric element with 8 nodes is employed in the FE model. In order to simulate the potential slippage between core and inverted filter, and between concrete cushion and clay, Goodman interface elements are used. The 3D mesh of the dam, which contains 9039 nodes and 8631 elements, is shown in Fig. 2.

The bed-rock and concrete are taken as linear elastic material. Duncan-Chang E-B nonlinear elastic model is used to simulate the stress-strain relationship of rockfill (shell) and soil in dam. The model parameters of rockfill and soil in dam are determined from large-size consolidated-undrained triaxial tests, and are shown in Table 1. For the materials in the core dam, nonlinear strength is followed, i.e., $\varphi=\varphi_0-\Delta\varphi\log(\sigma_3/p_\alpha)$, where p_a is the atmosphere pressure.

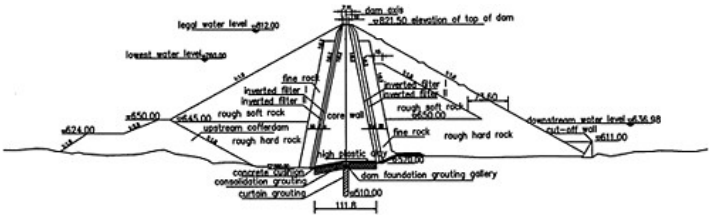

Figure 1. Deepest transverse section of the dam.

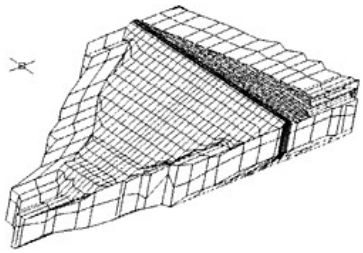

Figure 2. Mesh of 3D finite element.

2.3 *Behavior of stress-deformation*

According to the settlement contour-lines of the deepest transverse section of the dam at the completion of construction and of the reservoir filling (as shown in Fig. 3 (a) and Fig. 3(b)), the settlement at the middle part of the core is larger than other positions. The maximum settlements at the completion of construction and after the reservoir filling are 288.3cm and 305.0cm, which are 1.10% and 1.17% of the height of the dam respectively.

Figure 4 shows the major principal stress contour-lines in the deepest transverse section of the dam at the completion of construction and after water impounding. It indicates that the major principal stress in the core is smaller than that in inverted filter evidently, and this results from the arch action.

Figure 5 illustrates the vertical stress in the core. It is found easily that the reduction of vertical stress in the side zone of the core is more serious than that in the central of the core due to the arch

Table 1. Material parameters in E-B model.

Materials	Density (g/cm^3)	ϕ_0 (Degree)	$\Delta\phi$ (Degree)	K	n	K_b	m	R_f
Rough hard rockfill	2.00	54.37	10.47	1491	0.241	683	0.101	0.719
Rough soft rockfill	2.11	51.36	9.58	1400	0.175	474	0.145	0.706
Fine rockfill	2.04	53.04	8.01	1300	0.270	650	0.155	0.632
Inverted filter II	1.89	52.60	10.16	1100	0.235	340	0.170	0.761
Inverted filter I	1.94	51.35	8.70	1000	0.115	400	0.103	0.678
Core	1.99	39.47	9.72	388	0.311	206	0.257	0.755

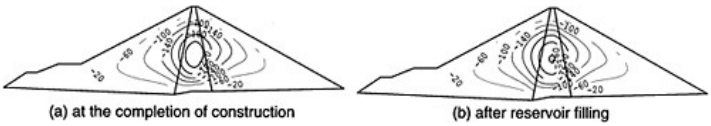

Figure 3. Settlement contour lines in deepest transverse section (cm).

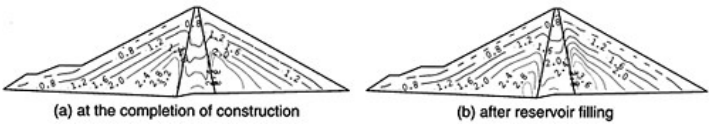

Figure 4. Major principal stress contour lines in deepest transverse section (MPa).

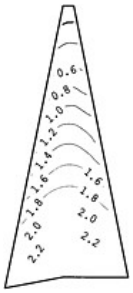

Figure 5. Vertical stress contour lines in deepest transverse section at the completion of construction (MPa).

action. This implies that at the side zone of the core, there is greater tendency to initiate the hydraulic fracturing. Furthermore, once fracturing takes place in certain zone, it may extend to the nearby zone. Therefore, it is very important to keep the upstream zone of the core in good quality of construction.

3 FACTORS INFLUENCING ON ARCH ACTION

After analyzing the mechanism of generation of the arch action, the factors to affect arch action may be divided into two types, namely materials filling the dam and structure of the dam. Both of them will be investigated in the following of this paper.

It is known that there are two causes inducing the reduction of stresses in the core. One is the restriction of the shell of the dam to the settlement of the core. The other is that the dam is in three-dimensional stress states, and the settlement of the core will be restricted by the bank rock-bed. The former may be investigated from the vertical stresses in the transverse section, and the latter may be studied from those in the longitudinal section (dam-axis section). The average of vertical stresses of the core elements at a certain altitude in the deepest transverse section or in the longitudinal section is examined, and used to study the arch action. In order to analyze the arch action conveniently, a parameter, the average load transfer ratio, R_L, is introduced as follows:

$$R_L = \bar{\sigma}_z / [\gamma(H - z)] \tag{1}$$

where, $\bar{\sigma}_z$ is the average of vertical stresses of the core elements at a given elevation in a given section; γ is unit weight of core material; H is the height of the dam; z is the distance from the bottom of the dam to the element investigated. The value of R_L is in the range of 0 to 1, and the lower value of R_L indicates the stronger arch action. In the following, each ratio of R_L is obtained from the elements at a given elevation of the deepest transverse at the completion of construction, except for that in Section 3.2.3.

3.1 *Influence of material properties*

Incompatible settlements between core and shell result from the great difference in the properties of core and shell materials, and induce the arch action. It is, therefore, reasonable to study the arch action by varying material parameters of core and shell. For convenience, two simplifications are made, i.e., (1) the dam is constructed with only two homogenous materials, core soil and shell rockfill, and (2) the constitutive relationship of the soil and rockfill can be simulated by the linear elastic model, and the two elastic parameters are Young's modulus, E, and Poisson's ratio, v.

Twenty-two different cases (Table 2) are employed to investigate the influence of materials on arch action.

If the dam is homogenous, i.e., is constructed using one type of material (Cases 1 to 5), the increase of Poisson's ratio results in the increase of the average load transfer ratio, R_L, as shown in Fig. 6(a), especially in the lower zones near the bottom of the core. This may be induced by only the arch action along the longitudinal section, because in the case of homogenous dam there should be no arch action in transverse section. This phenomenon can only be revealed by 3D FEM, and can not be found in the analysis of 2D FEM. The change of Young's modulus, on the other hand, has little effect to R_L (Fig. 6(b)).

If the dam comprises the materials of core and shell with different properties, both Young's modulus and Poisson's ratio of core and shell materials affect the arch action clearly. The influence of Young's modulus on arch action can be found from the results of Cases 6 to 14, and that of Poisson's ratio can be obtained from the results of Cases 10,17 to 22, as illustrated in Fig. 6(c) and Fig. 6(d).

Figure 6(c) shows that the decreasing ofYoung's modulus of shell material or the increasing of Young's modulus of core material, under the condition of keeping other elastic parameters constant,

Table 2. Cases used to analyze the influence of materials on arch action.

Case No.	Shell material		Core material	
	E_s (MPa)	v_s	E_c (MPa)	v_c
1	800	0.2	800	0.2
2	800	0.35	800	0.35
3	800	0.48	800	0.48
4	300	0.35	300	0.35
5	1200	0.35	1200	0.35
6	800	0.35	100	0.35
7	800	0.35	300	0.35
8	800	0.35	500	0.35
9	1200	0.35	100	0.35
10	1200	0.35	300	0.35
11	1200	0.35	500	0.35
12	1600	0.35	100	0.35
13	1600	0.35	300	0.35
14	1600	0.35	500	0.35
15	1200	0.2	300	0.2
16	1200	0.2	300	0.35
17	1200	0.2	300	0.48
18	1200	0.35	300	0.2
19	1200	0.35	300	0.48
20	1200	0.48	300	0.2
21	1200	0.48	300	0.35
22	1200	0.48	300	0.48

Note: The subscript "s" or "c" of E_s, E_c and v_s, v_c denotes the materials of shell or core.

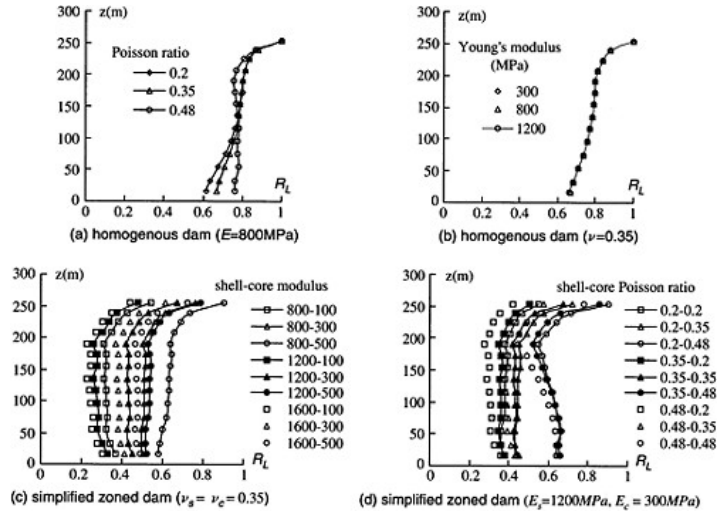

Figure 6. Influence of materials on arcing action.

Table 3. Cases used to analyze the influence of dam structure on arch action.

Case No.	Maximum dam height (m)	Top length (m)	Top width (m)	Bottom width (m)	Top thickness of core (m)	Bottom thickness of core (m)	Upstream dam slope	Core slope	Bank slope
A	261.5	608.16	18.0	960.78	10.0	111.8	1:1.9	1:0.2	1:1.16
B	174.33	405.44	12.0	640.52	6.67	74.53	1:1.9	1:0.2	1:1.16
C	87.17	202.72	6.0	320.26	3.33	37.27	1:1.9	1:0.2	1:1.16
D	174.33	608.16	18.0	960.78	10.0	111.8	1:2.85	1:0.3	1:1.16
E	87.17	608.16	18.0	960.78	10.0	111.8	1:5.7	1:0.6	1:1.16
F	261.5	608.16	28.0	970.78	20.0	121.8	1:1.9	1:0.2	1:1.16
G	261.5	608.16	38.0	980.78	30.0	131.8	1:1.9	1:0.2	1:1.16
H	261.5	486.53	18.0	960.78	10.0	111.8	1:1.9	1:0.2	1:0.93
I	261.5	364.90	18.0	960.78	10.0	111.8	1:1.9	1:0.2	1:0.70
J	261.5	243.26	18.0	960.78	10.0	111.8	1:1.9	1:0.2	1:0.46

leads to the increase in the value of the average load transfer ratio, and thus reduces the arch action. This is widely recognized. In these cases, compared with the core, the shell becomes softer, and closer to the case of homogenous dam.

Figure 6(d) indicates that decreasing the Poisson's ratio of shell material or increasing that of core material, and keeping other elastic parameters as a constant, can also increase the value of the average load transfer ratio and reduce the arch action.

From Fig. 6(c) and Fig. 6(d), it is found that the average value of ratio R_L in the core is the range of 0.2 to 0.6 in all cases examined. In Fig. 6(a) and Fig. 6(b), however, the average value of ratio R_L is about 0.75. This difference, 0.75–0.6=0.15, should result from the arch action. In all cases examined in Fig. 6(c), the ratio of R_L reaches a minimum value and strongest arch action, when Young's modulus of the core is equal to 100MPa and that of the shell is 1600MPa. And in Fig. 6(d), the case with the strongest arch action is that with Poisson's ratio of the core is equal to 0.2 and that of the shell is 0.48.

From Fig. 6(c) and Fig. 6(d), it is seen that either the variation of Young's modulus or that of Poisson's ratio can induce great changes of the average value of ratio R_L, i.e., result in quite dif ferent intensity of arch action.

3.2 *Influence of structure of dam*

The dam structure parameters influencing arch action include height of dam, thickness of core, slope of core and slope of bank. In this section there are 10 cases employed to investigate the influence of dam structure on arch action, as listed in Table 3. In all of the 10 cases, the material zones are unchanged as shown in Fig. 1, and the material parameters used are listed in Table 1.

3.2.1 *Influence of dam height*

We choose two different methods to change the maximum dam height from 261.5m to 174.33m and 87.17m. One is to change the length and width of dam at the same time of changing the height, and the structures of dams with different heights are similar (Cases *A–C*). The other is only to change the height of dam, and in these cases (Cases *A, D* and *E* in Table 3) the structures are not similar. The results from 3D FEM are presented in Fig. 7.

Figure 7(a) shows that the relationship between the average load transfer ratio and normalized height of dam changes little with the difference of the dam heights if the structures are similar, i.e., in Cases *A–C*. The similar conclusion has been drawn from 2D FEM by Kulhawy and Gurtowski (1976)[2]. From this figure, it is found that the average value of the ratio R_L is lower, and is less than 0.5. Figure 7(a) presents the results including Case *A,* which is the same as the design of the real dam. This implies that the arch action of the real dam is relatively strong.

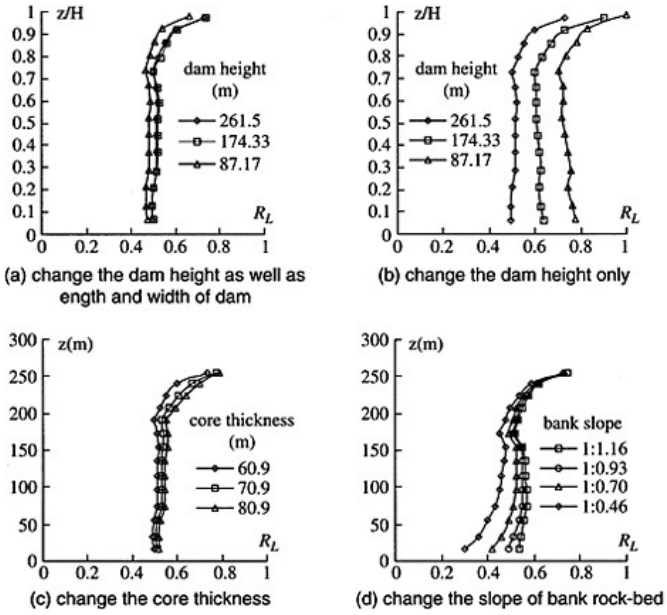

Figure 7. Influence of dam structure on arcing action.

If the structures are dissimilar, the average load transfer ratios from Cases *A, D* and *E* are different for different dams with various heights, as shown in Fig. 7(b). This principally results from the difference in slopes of cores, not from the difference in dam heights actually, because the slope of dam side has little effect on arch action according to Kulhawy and Gurtowski (1976). This implies that the steeper the core slope, the lower the average ratio R_L and the stronger the arch action.

3.2.2 *Influence of thickness of core*

Cases *A, F* and *G* in Table 3 have only different thickness of core, and the other parameters are the same as those of real dam, i.e., Case *A*. With widening of the core, the average load transfer ratio, especially in the upper zones of the core, increases, as illustrated in Fig. 7(c). From Fig. 7(c), we may conclude that with the limit variation of core thickness, the changes of the average ratio are in a small range. This implies that increasing the core thickness is not a good way to reduce the arch action.

3.2.3 *Influence of slope of bank*

Since arch action can also be induced by the restriction of bank rock-bed to the settlement of the core, the average load transfer ratio should also change with the bank slope. In this section, the results on dam-axis section are used to analyze the arch action.

For Cases *A, H, I* and *J* in Table 3 the only difference is in bank slopes, and the results from these cases are presented in Fig. 7(d). From this figure it is clearly seen that the average load transfer ratio, especially in lower part of the core, increases with the reducing of bank slope. The steeper the bank slope, the lower the average value of ratio R_L, and the stronger the arch action. For the steep bank slope, attention should be paid to the lower zones of the core, and measures may be needed to prevent the possibility of hydraulic fracturing.

4 HYDRAULIC FRACTURING

Hydraulic fracturing becomes one of the major problems in earth and rockfill dam engineering since it plays significant roll in the initiation and extension of cracks in dam foundation or in core material in a dam body. The cause of destruction of Teton dam in American at the first filling of water is generally believed to be hydraulic fracturing[5],[6]. This section will study the hydraulic fracturing in core, and attention is paid to the condition of hydraulic fracturing development and the relation between hydraulic fracturing and arch action.

4.1 *Condition of hydraulic fracturing*

According to the definition of hydraulic fracturing, it can occur under conditions both with and without cracks in the core. However, based on the "water wedging" action mechanism of the hydraulic fracturing, the authors believe that there are two indispensable conditions for the happening of hydraulic fracturing. One is that there must exist cracks or weakened zones in the core to initiate the hydraulic fracturing. The other is that the hydraulic fracturing occurs in the period of water impounding, instead of that of steady seepage.

In the early of quick impounding of water, the water pressure is applied on the upstream surface of the core. If no tension crack exists, no hydraulic fracturing can initiate and develop. If there is a crack or weakened zone near the upstream surface of the core, as shown in Fig. 8(a), the surface pressure on *BC* and *CD* may contribute to the extension of the crack, and hydraulic fracturing may initiate and develop further. This is the most dangerous case. Here, we think that the "water wedging" action due to the existence of crack contributes to the hydraulic fracturing.

If the steady seepage has formed, and no crack exists at this moment, there will be no crack to be developed, and thus no hydraulic fracturing to be initiated. The cause is that during the formation of steady seepage, the deformation of the core completes. Even if in the case that there is a crack or weakened zone in the core, as shown in Fig. 8(b), *ABC,* it is not critical. Take soil particles in either *DACE, BFGC* or *abcd* as a free body in Fig. 8(b), and there are flow force, buoyant force and forces from particles around the free body exerting on it. The effect of these forces on hydraulic fracturing will be investigated further as follows.

The flow force and buoyant force result from the void water, and if the hydraulic fracturing which is also induced by the void water is initiated, either the flow force or buoyant force or both must be the agent. The buoyant force is relatively small and is due to the static water pressure, and does not induce the hydraulic fracturing. Otherwise, is there any soil body in static water to fail due to hydraulic fracturing?

As for the flow force, it directs downstream, and it increases the horizontal stress in core, and thus increases the vertical stress. This will have effect to prevent the happening of hydraulic fracturing. Furthermore, during the formation of steady seepage, most displacement and deformation complete, and no further at least only small part of displacement and deformation may take place.

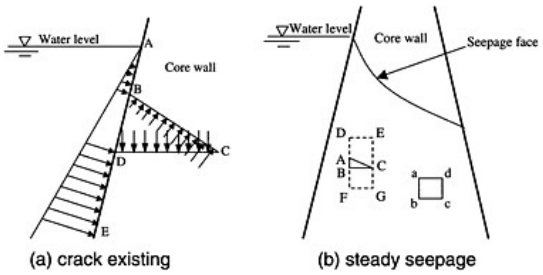

Figure 8. Condition of hydraulic fracturing.

That is no force imposing the body of *DACE* to move up, body of *BFGC* to move down, and body of *abcd* to split, therefore, the crack *ABC* will not extend. It is consequent that no hydraulic fracturing will be developed.

4.2 *Relation between hydraulic fracturing and arch action*

According to the definition of hydraulic fracturing, the development of hydraulic fracturing is due to the reduction of stresses in the core. The arch action, on the other hand, can reduce the stresses of the core. It is certainly that the hydraulic fracturing is related to the arch action.

Referring to the definition of load transfer ratio mentioned above, a new ratio, which is defined as water pressure divided by overburden pressure of the core, is used here. It is written as:

$$R_w=\gamma_w(H-z-b)/[\gamma(H-z)] \tag{2}$$

where γ_w is unit weight of water, and its value is 10kN/m^3; b is the distance from water level to the top of dam, and the meanings of other parameters are same as those in Eq.(1).

In order to conveniently analyze the relationship between hydraulic fracturing and arch action, some assumptions are made here. They are (1) the cracks or weakened zones exist in core; (2) water level reaches scheduled elevation suddenly, namely the seepage of water in the core is ignored. (3) the above discussed "water wedging" action mechanism actually accepts that hydraulic fracturing belongs to tension failure. As a consequence, we made the third assumption, i.e., the condition of hydraulic fracturing is that the average of vertical stress of core elements in a given elevation in the deepest transverse section less than water pressure at the given elevation, i.e., $\bar{\sigma}_z < \gamma_w (H - z - b)$. According to Eqs.(1)–(2), the condition can then be expressed as $R_w \geq R_L$.

For convenient comparison between R_w and R_L, Fig.9 gives the distribution of R_w of cases with different water level, and that of R_L of cases of real dam and with minimum and maximum R_L.

The curves of R_w~z from different cases, of which water levels are in lowest, legal and checked flood level, are shown in Fig. 9. The relationships of R_L~z of three different cases that are Case 2 (its R_L is maximal) and Case 12 (its R_L is minimal) in Table 2, and Case *A* in Table 3 (real dam) are also shown in Fig. 9. Figure 9 shows that for the case with minimal R_L, hydraulic fracturing may occur even under lowest water level, and for real dam, the likelihood of hydraulic fracturing is low under legal water level, but high under checked flood level. For the case with maximal R_L, hydraulic fracturing is unlikely to develop under any water level.

Furthermore, we found from the above figures that R_w is higher at the lower zones of the core, and on the contrary, R_L is lower at the lower zones of the core. According to the condition of $R_w >= R_L$, we may conclude that the lower zones of the core control the development of hydraulic fracturing.

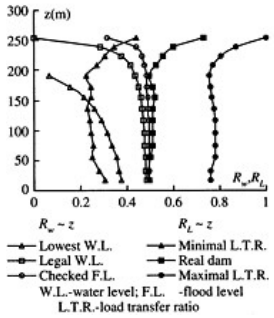

Figure 9. Relationship between R_w~z and R_L~z.

Assuming $R = \bar{\sigma}_z/[\gamma_w (H - z - b)]$, and combining this equation with Eq.(1), one may obtain.

$$R = \frac{R_L \gamma (H - z)}{\gamma_w (H - z - b)} \tag{3}$$

In Figure (6), (7) and (9), it is found that for zoned dam, the ratio of R_L at lower zones of core is almost constant, not change with z. If the dam is high and water level is high, we may assume $H-z \approx H-z-b$, and Eq.(3) is expressed as

$$R = \frac{R_L \gamma}{\gamma_w} \tag{4}$$

If the ratio of R_L is found, Eq.(4) may be simply used to decide the development of hydraulic fracturing. R>1, no hydraulic fracturing occurs, and R<=1, it is danger for hydraulic fracturing to take place. As for R_L, it is possible to find some values as experience to be referred to.

5 CONCLUSIONS

The principal factors influencing on arch action, as well as the condition of hydraulic fracturing, in core rockfill dam are investigated by using 3D FEM, and the following conclusions can be drawn:

(1) Increase of Young's modulus or Poisson's ratio of core material is helpful to reduce arch action.
(2) Decrease of slope of core or that of bank rock-bed, or increase of thickness of core results in the reduction of arch action.
(3) Likelihood of hydraulic fracturing is decided by the intensity of arch action, because arch action reduces vertical stresses in the core. To prevent the development of hydraulic fracturing it is, therefore, significant to reduce the arch action.
(4) A new parameter is presented, which can be simply used to decide the development of hydraulic fracturing.

REFERENCES

[1] Nobari, E.S., Lee, K.L. and Duncan, J.M. Hydraulic fracturing in zoned earth and rockfill dams, *Report to the Offlce, Chief of Engineers U.S.Army, Waterways Experiment Station.* University of California Berkeley, ReportNo.TE-73–1, 1973.
[2] Kulhawy, F.H. and Gurtowski, T.M. Load transfer and hydraulic fracturing in zoned dams. *Journal of the GeotechnicalEngineeringDivision, ASCE,* 102 (GT9), 1976,963–974.
[3] Schober, W., Hammer, H. and Hupfauf, B. Load transfer in embankment dams—Model testing. *Proceedings of the 12th International Conference on Soil Mechanics and Foundation Engineering,* Vol. 2, 1989, 973–976.
[4] Zeng, K.H. and Yin, Z.Z. Factors affecting hydraulic fracturing of high earth core dam. *Journal ofHohai University,* China, Vol. 28(3), 2000, 1–6.
[5] Independent Panel to Review Cause of Teton Dam Failure, (1976). *Report to U.S. department of the interior and the State of Idaho on failure of Teton dam.* U.S. Bureau of Reclamation, Denver, Colo.
[6] Seed, H.B. (1981). The Teton Dam failure, A retrospective review. *Proceedings of the 10th International Conference on Soil Mechanics and Foundation Engineering,* Vol. 4, 219–238.

New Developments in Dam Engineering—Wieland, Ren & Tan (eds),
© 2004 Taylor & Francis Group, London, ISBN 04 1536 240 7

Three Gorges Project: safety checking of Maopingxi asphalt-concrete core rockfill dam

Zhu-sheng
Hohai University, China

Guang-jing Cao
Three Gorges Project Corporation, China

ABSTRACT: Three Gorges Project is the key backbone one for rehabilitation and development of the Yangtze River. The main tasks of TGP are: controlling the floods of the Yangtze, developing the hydro-power resources and improving the navigation condition. Maopingxi defense project is one of TGP. At the first construction phase of Maopingxi rockfill dam completed and checked before accepted, it is doubted whether the dam behaves safely, especially whether impervious core produces hydraulic fracture because the asphalt concrete core material trixial experiment modulus value K is on the low side. In this thesis, the dam safety is checked by nonlinear visco-elasto FEM using locale monitoring data during construction, the actual mechanics parameters of asphalt concrete core material are given out by back-analyzing. It is also revealed that the complicated deformation and stress characteristic of high zoned rockfill dam whose impervious barrier is a core of asphalt concrete. The suggestions are brought forward being dead against the dam's zoned design and structure pattern of asphalt concrete impervious core according to analysis of Maopingxi rockfill dam.

1 INTRODUCTION

Maopingxi, a branch of Yangtze River, flows into Yangtze river about 1km upstream the axis of main dam of Three Gorges Project. The valley belongs to hilly ground, and covers the total cultivated area of 22.67km^2, the population of 3,1000. The area is about 113.24km^2 and plays the role as the main grain store of Zigui County where the immigration work is hard to perform. In order to prevent the farmland from being flooded, Maopingxi rockfill dam is built as a part of Three Gorges Project. The design proposal adopts rock fill dam with asphalt concrete core wall as water retaining structure, and the sectional view is shown as fig. 2. On the whole, the axis of dam is laid along the ridge.

The core wall, with height of 94m, crest elevation of 185m and bottom elevation 91m, connects with concrete impervious wall in the foundation of bank slope, concrete base and backer in the river bed. Those combine the grout curtain to form the dam's holistic impervious system. According to the standard SDJ1-88, designers select 0.6m as the crest width of core wall, and 1.2m as the bottom width of it. The grades of slopes of core wall are both 1:0.004. Table 1 shows the quality requirement of asphalt concrete core wall. Maopingxi rockfill dam is mainly filled with the excavated rock of the key project. The construction can be divided into two stages: stage I began since April, 1994, and completed in December, 2000, while the construction of asphalt concrete core wall began in December, 1997; The work of this stage included filling the embankment to the elevation 140m, control of abutments and bank slopes' seepage, and so on. The total construction quantity is 6 million cubic meters. According to the data from the spot quality inspection, it is found that all the indexes of rockfill material meet the requirements, except some parts

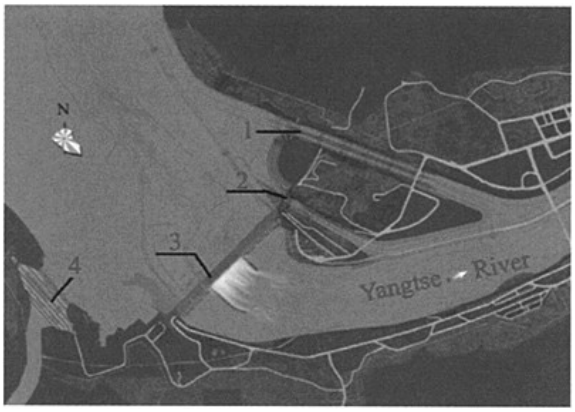

Figure 1. The Three Gorges Project layout: (1) navigation lock; (2) ship elevator; (3) concrete grave dam; (4) Maopingxi rockfill dam.

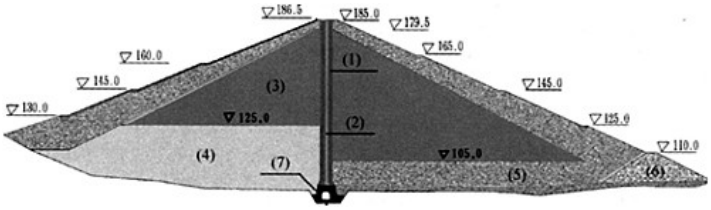

Figure 2. Dam's section structure: (1) transition zone; (2) asphalt-concrete; (3) ballast mixes; (4) decayed rock; (5) rock ballast; (6) displacement hull; (7) concrete basement.

Table 1.

Density (g/cm^3)	>2.40
Porosity (%)	<2.0
Permeablity coefficient (cm/s)	$<1.0\times10^{-7}$
Marshall stability (N)	>5000
Water stability factor (%)	>0.85
Modulus K	600~800*
Friction angle (°C)	26~35*
Cohesive (Mpa)	0.35~0.5*

* 16.4°C, indoor static pressure molding samples.

approaching water and two sides of core wall where the content of coarse granule in the rock and transition material are slightly below the design standards.

By now, Maopingxi rockfill dam, with asphalt concrete core wall, is the highest one among the same kind dams built on bedrock in China. So there are few available data and related information for reference. In order to monitor the status of dam during construction and operation, a large number of monitor-instruments are arranged in dam body respectively in both two sides of bank and the bed. The monitored work consists of the vertical stress and deformation of core wall and dam body, the strain and seepage and the temperature of core wall. Figure 4 is the general view of monitoring instruments' arrangement.

Figure 3. Dam's construction site.

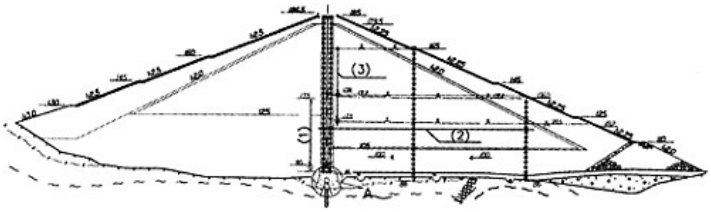

Figure 4. Dam's monitoring instrument system: (1) vertical strain measurement zone; (2) settlement gauge; (3) water-tube settlement instrument.

In process of acceptance check after work of the first construction phase was finished, experts found that, to drill hole sampling in field engineering, the modulus value K of asphalt concrete was low in trixial test, and the average value of K of asphalt concrete core was below 200. So, the anxiety arose if dam could behave safely, and if hydraulic fracture could occur in impervious core. Through utilizing spot monitoring data of yet-built dam below elevation 154.0m, this paper gives further safety check of dam.

2 ANALYSIS ON DAM SAFETY

2.1 *Material constitutive model*

The formula of Duncan-Zhang model is brief, and its parameters have explicit physical meanings. The results of trixial test indicate that Duncan-Zhang model can properly reflect the nonlinear relationship between stress and strain of soil. In this paper, E~μ model is selected as the constitutive model of rockfill material.

As is known, asphalt concrete is a heterogeneous dispersive system with spatial mesh structure composed of rock aggregate, cementing material and pore space. In most cases, considering the adhesive aggregation of asphalt, recent studies usually adopt colloid theory. When it comes to the mechanical property of asphalt concrete, the self-strength of rock aggregate is far stronger than the bond strength of asphalt, and the failure mechanism is similar with shear failure. It can be reasonable that asphalt concrete is a kind of dispersive granular material, so the constitutive model of soil can be used when studying the stress-strain relative of asphalt concrete core wall.

The results of trixial test indicate that the mechanical property of asphalt concrete is in accordance with temperature, content of asphalt, method of samples' molding, loading speed, and means of

mould unloading. Comparison with the results of trixial test of three kinds of samples, indoor static pressure mold, compacted mold, spot core, and conclusion is that the methods of test have much to do with the results of test. Modulus value K varies in several multiples and the results of test on different samples are divergent to a great extent. So, the result of indoor trixial test has some difficulty in reflecting spot practical situation. Only depending on the results of indoor trixial test, it is hard to come to the conclusion whether dam can behave safely or not. According to the spot monitoring data collected during construction, the model parameters of asphalt concrete are inversed in this paper, iteration method of initial stress increment is used to solve nonlinear problems. First, calculate the deformation or stress valve of measuring points under a certain load combination; then, fit the theoretical value and the observing value of n points' deformation or stress, and residual sum of squares will be got. It is the objective function in process of parameter inversion and optimization to seek the actual value approaching spot parameter properties of rockfill material. Considering that the operation of monitoring instruments were inevitably disturbed by some uncertain factors during construction, it need took a long time for asphalt concrete to reach its temperature stability. Hence, it is proper to divide the objective function into several time steps. The objective function can be expressed as follows:

$$F(X)=\sum_{i=1}^{m}\sum_{j=1}^{n}\omega_{ij}(u_{ij}^{c}/u_{ij}^{m}-1.0)^{2} \tag{1}$$

where m is the number of time steps in inversion; n is the number of selected measuring points; ω_{ij} is the weight of monitoring value of j point in time step i. u_{ij}^{m} is corresponding observation value.

Reference to the result of trixial test, the estimated range of parameter X of asphalt concrete can be determined, and it becomes the constraint condition of Equation (1). When solving the implicit nonlinear optimization problem with constraint condition, the convergence criterion can be defined as follows:

$$\left[\frac{1}{2n}\sum_{i=1}^{2n}\left(f(X^{(i)})-f(X^{(i)})\right)^{2}\right]^{\frac{1}{2}}<\varepsilon \tag{2}$$

where ε is a small positive number given previously.

Due to the adhesive aggregation of asphalt, asphalt concrete appears high adhesiveness and takes on creep property. This will cause a sharp creep deformation in dam body. With the development of creep, stress distribution in dam body will be adjusted automatically; the rheological property of asphalt concrete must be taken into account in calculation of finite element.

Figure 5(a) is the indoor trixial creep curve of asphalt concrete under three different groups of confining pressure, and fig. 5(b) is the logarithmic creep curve of fig. 5 (a). It can be seen from two figs that the creep of asphalt concrete follows a apparent nonlinear property, and the logarithmic curve between strain and time is almost a group of parallel lines. Considering that the creep of asphalt concrete has intensive lateral effect, the isochronal curve between stress and strain is expressed by hyperbola. The function between stress-stain-time is expressed as:

$$\varepsilon=\frac{(D_{\max})_0}{(E_i)_0}\frac{\overline{D}_0}{1-(R_f)_0\overline{D}_0}\left(\frac{t}{t_0}\right)^{\lambda} \tag{3}$$

where t_0 is unit interval; $D_{\max}$, E_i, R_f and are failure shearing stress, initial tangent modulus and failure ratio at t_0; $\overline{D}_0$ is stress level at $t_0\lambda$ is the rate of grade of curve In ε–ln t at a certain stress level.

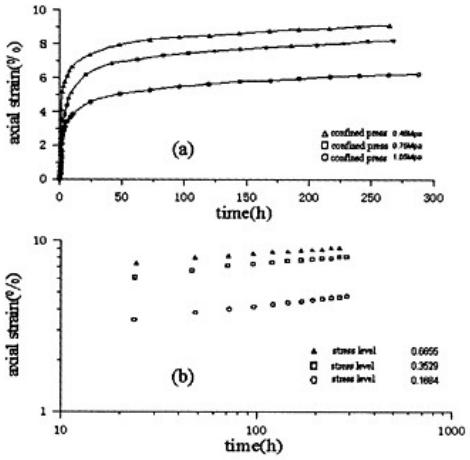

Figure 5. Curves of asphalt concrete trixial creep test.

For different load process, especially during construction, the initial time of each computing unit in calculating creep are not same; in order to avoid difficulty in calculation, equation (3) is changed as follows:

$$\varepsilon = \frac{(D_{\max})_0}{(E_i)_0} \frac{\overline{D}_0}{1-(R_f)_0 \overline{D}_0} \left(\frac{\dot{\varepsilon}_0}{\dot{\varepsilon}}\right)^c \tag{4}$$

Where $\dot{\varepsilon}_0$ is strain ratio at t_0; $c=\lambda/(1-\lambda)$. Equation (4) removes the explicit time, and creep value at each calculation step is determined only by the creep and stress value at former step.

2.2 *Numerical analysis*

Biggest dam section is selected as the calculation object. The drafted time of dam completion is June, 1st 2003, then dam has been built up to elevation 185m; from June 1st 2003 to June 15th 2003, the reservoir impounds water to elevation 135m, the initial power generation water level; by October 2013, the water level will arrive at elevation 175m, the normal impounded level. The embankment construction is divided into two periods; period I began from April, 1996, and ended in November, 2000. In this period, the dam was built up to elevation 140 m; period 2 is from June, 2001, to June, 2003.

2.2.1 *Calculation parameters*

According to the mechanical property research report of Maopingxi rockfill material, the calculation parameters of rockfill material are decided by the result of trixial test on samples taken from fixed dam section on the site.

Parameters of asphalt-concrete constitutive model can be inversed from the available monitoring data. The cut-off time of construction was February 2002 and dam reached elevation 154m. In inversion, complex method is adopted. t_0, parameter of asphalt concrete's creep properties, is the unit interval and its units is day; A is average value of slop coefficient of curve $\ln \varepsilon - \ln t$ under three different stress level, and equal to 0.00554; According to the result of indoor uniaxial tension test, the tensile strength of asphalt concrete is 0.106Mpa.

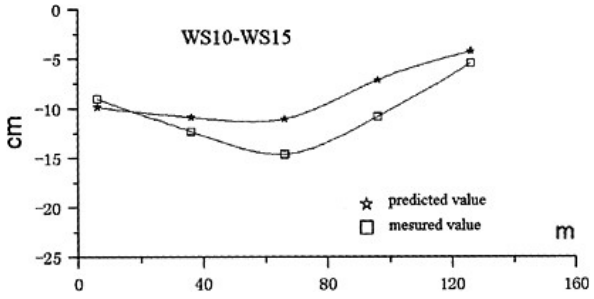

Figure 6. Increment value of measure and calculation in water-tube settlement Instrument at the el 119m.

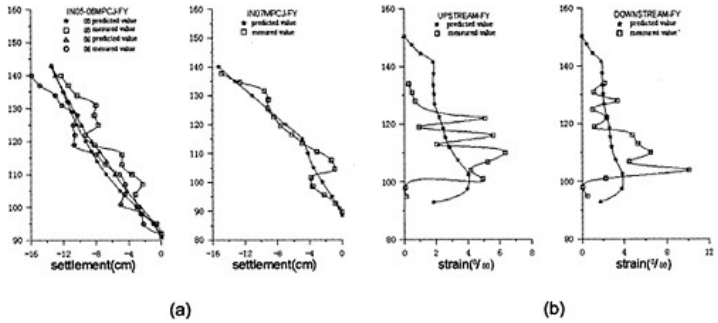

Figure 7. increment value of measure and calculation; (a) settlement in settlement gauge; (b) asphalt-concrete core wall vertical strain along the altitude.

2.2.2 *Parameters inversion of asphalt-concrete*

By back-analyses in search scope, the model parameters of asphalt concrete can be got: R_f=0.5628, K=342.0, n=0.249, G=0.3868, F=0.02825, D=29.09. Select No.5 settlement tube in upstream transition region, No.6 in downstream transition region and No.7 in down-stream rockfill region as subject, and fig. 6 is the distribution of measure and calculated settlement increment of tube settlement instruments at the elevation 119m, it can be seen that the measure value is close to the calculated value. Figure 7(a) shows the distribution of measure and calculated settlement increment along the altitude when dam was built up to the elevation 154m. Figure 7(b) shows the distribution of vertical strain increment of two sides of core wall along the altitude. The measure value is well consistent with the calculated value. It also must be pointed that the measure value of vertical strain increment is rather disperse. The reason is mainly that the high deformation property of asphalt concrete and the disequilibrium of construction quality.

2.3 *The simulation analysis of nonlinear visco-elasto method*

Using the parameters of asphalt concrete core wall got in inversion, the dam's simulation numerical analysis is pursued by the finite element method.

Figure 8 is the calculated result of dam section 0+700. Figure 8(a) shows the distribution of calculated horizontal deformation along the altitude, the maximum of core wall's deformation of is

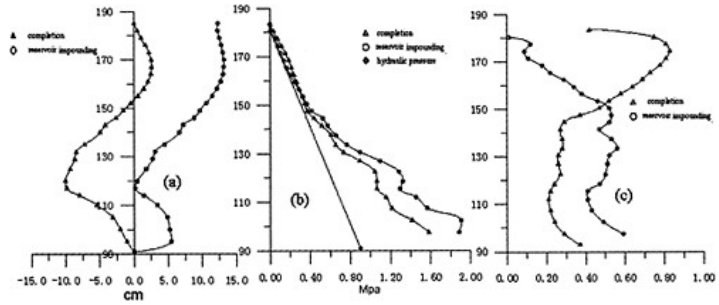

Figure 8. Calculation value of asphalt-concrete core at 0+700 section: (a) horizontal deformation; (b) vertical stress; (c) principle stress ratio.

13.3cm, occurred around elevation 170m, the ratio of deflection to span is 1.5%. The deformation of core wall and dam shell is basically harmonious, and there isn't any sharp break. It must be mentioned that Maopingxi rockfill dam is mainly filled with the deserted rock material of Three Gorges Project's excavation. Due to the requirement of progress of project, the early-excavated weathered rock had to be filled at the bottom of dam. Especially in May 1998, the sediment percentage (<0.074mm) of the weathered rock, which was the excavation material of the diversion channel on right bank and filled in the upstream side between the elevation 110m and 130m, was up to 12%. Those flexible zones of the weathered rock caused the core wall here deformation towards upstream, and, at the elevation of 117m, it almost reached 10cm. The axis of core wall had a rather obvious curving deformation during construction.

Figure 8(b) shows the distribution of vertical stress of the core wall along the altitude. It can be seen that: (1) the transition zones beside the core wall, which are filled with gravel material, have obvious arch-effect, and this effect reduces the vertical stress of the core wall. After completion, the extreme value of vertical stress is only 1.59Mpa. The elevation 152m is the place of inflection point of vertical stress's distribution variation between completion and impounding. When below this elevation, the vertical stress of core wall after impounding is bigger than that after completion, and the extreme value grows from 1.59Mpa to 1.94Mpa; while above this elevation, the water pressure causes the vertical stress reduced. It can come to the collusion that, to rockfill dam with asphalt concrete core wall, the place where most likely occur hydraulic fracture is not at the lower part but the middle-upper part of dam; (2) when fully impounded, generally, the vertical stress of core wall is bigger than water pressure. Only above the elevation 152m occurs that they are very close to each other. So, if taking the tension strength of asphalt concrete into account, there stands no chance of hydraulic fracture; (3) between elevation 110m and 130m, the gradient of vertical stress of core wall varies sharply. As is mentioned before, the weathered rock "interlayer" with lower parameters was filled in this zone downstream, and this can explain why the stress and strain status are complicated here.

Figure 8(c) shows the distribution of principle stress ratio of core wall axis. The maximum value of principle stress ratio is 0.83 after completion, and the values are all bigger than 0.7 between the elevation 176m and 180m. After impounding, the principle stress ratio has reduced appreciably, while the maximum value falls to 0.6. This is in accordance with the distribution of the vertical stress of core wall. The distribution regularity of the principle stress ratio after completion and impounding also changed at the elevation 152m. Comparing with completion, for the effect of water pressure, the larger principle stress of core wall below the elevation 152m increases obviously, while above the elevation 152m the value of lateral principle stress has an obvious increase.

3. CONCLUSIONS

According to the simulation of the dam construction process and using spot monitoring data, the mechanical parameters of asphalt-concrete core wall are inversed in this paper. It can be deduced from the calculation that the vertical stress of the bottom of core wall increases, and the hydraulic fracture can't happen in core wall after impounding and dam can behave safely. Studying the result of feedback analysis on the observing data of deformation and stress, there are still some problems worth researching for high rockfill dam with asphalt concrete core wall: (1) the thickness of asphalt-concrete core wall is smaller. When dividing the region of different filling materials, the designer should avoid the larger difference between the mechanical properties of filling materials in different regions upstream or downstream in the middle of dam. That should be avoided that there is any sharp deformation gradient in the axis of impervious core wall. At the same time, in order not to deteriorate the locale deformation and stress of impervious core wall, "weak interlayer" in dam should be avoid; (2) As the vertical impervious structure, the stress distribution of core wall is complicated under the effect of water pressure. Asphalt concrete has a strong lateral expansion effect, due to the effect of water pressure after impounding, in the lower part of core wall where is under the restriction of foundation the vertical stress and principle stress ratio all increase, while reduce in the upper part. After completion and during impounding, the distributions of calculated value of core wall's stress indexes have a obvious inflection point along the altitude, and the result is that hydraulic fracture is possible between 1/3~1/2 upper the core wall. It needs a further study on the structural style of asphalt concrete wall of high rockfill dam. (3) The transition zones on the two sides of core wall have obvious arch effect. This effect reduces the vertical stress of core wall, but it is advantageous to the deformation stability of the asphalt concrete core wall which has stronger lateral effect. Therefore, the transition zones of gritting material should be designed carefully. (4) For the mechanical properties of asphalt concrete are much close to the temperature, it must be deliberate to build high rockfill dam with asphalt concrete impervious structure in the temperate zone.

REFERENCES

[1] Qi Shijing. Rolling Asphalt-concrete Core Wall Construction Technology in Earth Dam [M]. Beijing. Dec, 2000.
[2] Zhu Sheng, Gu Gancheng. CFRD Built on the Alluvial Deposit[A]. Proceedings International Symposium High Earth Rockfill Dams[C], Beijing: Sponsored by ICOLD, 1993. 184–195.
[3] Wang Weibiao, K.Hoeg. Effects of compaction method on the properties of asphalt concrete for hydraulic structure[J]. Hydropower and Dams, Issue six, 2002, 63–71.
[4] K. Hoeg. An evaluation of asphaltic concrete cores for embankment dams[J]. Water power and Dam Construction, July, 1992, 32–34.
[5] W.Pircher, H.Schwab. Austria's Finstertal rockfill dam[J]. Water power and Dam Construction, June, 1980, 43–47.
[6] Zhu Sheng. Deformation and Stress calculation for a 200m High CFRD[J]. Journal of Hohai University (Natural Science), Dec, 2003, 631–634.

New Developments in Dam Engineering—Wieland, Ren & Tan (eds),

Review on embankment dam breach modeling

Yong-hui Zhu[1,2], P.J.Visser[2] & J.K.Vrijling[2]
[1]*College of Water Conservancy and Hydropower Engineering, Hohai University, China*
[2]*Faculty of Civil Engineering and Geosciences, Delft University of Technology, The Netherlands*

ABSTRACT: Huge losses in both human lives and economic properties can be resulted from an embankment dam failure. Therefore modeling of embankment dam breaching is of tremendous significance for dam failure damage assessment, risk analysis, disaster control and mitigation, etc. The embankment dam breach mathematical models developed in the last more than forty years are classified and summarized; their characteristics are analyzed, respectively. The physical model tests on embankment dam breaching performed in the recent several decades are also classified and summarized. A new erosion mechanism for embankment dam breaching, i.e. headcut erosion, is described; the models available so far for calculation of the headcut migration are summarized and analyzed. Finally, recommendations for future development of embankment dam breach modeling are proposed.

1 INTRODUCTION

In many countries in the world, embankment dams are of large benefit to people. However, devastating disasters will occur if an embankment dam suffers a failure. For instance, the breaching of South Fork Dam in 1889 in USA, the breaching of Nanaksagar Dam in 1967 in India and the breaching of Banqiao Reservoir in 1975 in China all caused enormous losses to both human lives and economic properties.

However, the magnitude and extent of the losses depend highly on the breaching rate of the embankment dams, which determines the dam breach flood discharge and its propagation velocity. Analysis results of historical cases of the U.S. Bureau of Reclamation indicates that loss-of-life varies from 0.02% of the population-at-risk with more than 90 minutes of warning time, to 50% of the population-at-risk when advance-warning time is less than 15 minutes[1]. Therefore it is absolutely necessary to develop a breach-simulation model to predict the breach parameters (e.g. breach width, depth, rate of development and outflow hydrograph).

Unfortunately, breaching process simulation and breach parameter prediction are considered to contain the largest uncertainty of all aspects of embankment dam breach flood forecast[2]. The breaching process of embankment dam is believed to depend upon various factors including the causes for the breach, the type of dam material, and the shape and dimensions of the dam, etc. These factors vary greatly from case to case.

Nevertheless, despite the many difficulties encountered in modeling of embankment dam breaching, considerable progress has already been achieved. A variety of mathematical models have been developed in the past more than forty years for simulation of embankment dam breaching; and many large or small scale physical model tests have been carried out in order to gain more insight into the mechanism of embankment dam breaching.

2 MATHEMATICAL MODELS

Generally, the mathematical models mentioned above can be classified as parametric based or physically based models[3]. Parametric based models use key parameters (e.g. final breach geometry,

breach formation duration) to represent the hydraulics and breach development in embankment dams, and the breach growth is then simulated as a simplified time-dependent process (e.g., linear increase of breach dimensions). Some parametric models contain various regression equations to compute the peak breach discharge and time of failure by use of parameters as the reservoir volume and the dam height etc. Among these models are the many equations proposed by various Chinese investigators and institutes, see Pan and Loukola (1993)[4] and Wang et al.[5]. The majority of these equations were developed on the basis of an instantaneous dam breaching assumption,

Table 1. Summary of main characteristics of embankment dam breach models.

Model and time developed	Flow	Sediment transport	Breach geometry	Input parameters
Cristofano (1965)	Broad-crested weir flow	Empirical formula	Trapezoidal	Cohesion, angle of repose, o
Harris and Wagner (HW) (1967)	Broad-crested weir flow	Modified Schoklitsch (1934) bed-load formula	Parabolic	Embankment geometry, typ filled material, etc.
BRDAM (1981)	Broad-crested weir flow	Schoklitsch (1934) bed-load formula	Parabolic	Soil properties, tailwater, oth
Ponce-Tsivoglou (PT) (1981)	Full hydrodynamic system	Meyer-Peter and Müller (1948) bed-load formula	Constant peak flow width	Initial breach geometry, soil properties, others
DAMBRK (1984)	Broad-crested weir flow, orifice flow	Linear predetermined erosion	Rectangular, triangular, trapezoidal	Final breach shape, failure ti others
BEED (1987)	Broad-crested weir flow	Einstein-Brown (1950) bed-load formula	Rectangular, trapezoidal	Soil properties, initial breach others
BREACH (1988)	Broad-crested weir flow, orifice flow	Meyer-Peter and Müller formula, DuBoys relation	Rectangular, trapezoidal	Soil properties, dam geometr others
SMPDBK (1991)	Broad-crested weir flow	N.A.	Rectangular, trapezoidal	Final breach shape, failure ti others
Bechteler and Broich (1991)	Broad-crested weir flow	Meyer-Peter and Müller formula, Smart (1984) and Cristofano (1965) formulae	Varies in time	Soil properties, others
Renard/Rupro (reported by Paquier et al., 1998)	Orifice flow	Meyer-Peter and Miiller formula	Circular ⇒ half circular (lower)+ rectangular (upper)/ rectangular	Soil properties, dam dimensi others
Loukola and Huokuna (LH) (1998)	Broad-crested weir flow, orifice flow (Fread 1988)	Meyer-Peter and Müller (1948) formula	Trapezoidal	Geometry of the dam, soil properties, hydrological data
BRES (1998)	Broad-crested weir flow	Bagnold-Visser (1989), Engelund-Hansen (1967) and Van Rijn (1984a, b)	Trapezoidal	Geometry of the embankme foundation, soil properties, e
Mohamed et al. (2002)	Broad-crested weir flow, orifice flow	Yang (1979),Visser (1989), and Chenand Anderson (1986)	Varies in time due to erosion	Soil properties, initial breach others

which certainly leans to the conservative and safe side. Sudden and instantaneous breaching is however generally the fashion of concrete dam failure; embankment dams constructed with soil (cohesive or non-cohesive) would breach gradually in a certain long period.

For other parametric based models readers are referred to the review made by Wahl (1998)[6]. Parametric based models are generally simple and are easy for utilization. However on the other hand, the foundation for their development is relatively unsolidified and their accuracy of prediction could be questionable.

Physically based embankment dam breach models use principles of for instance, hydraulics, sediment erosion, and soil mechanics to develop time-stepping solutions of the "actual" breach growth process and the breach outflow hydrograph, e.g. Ponce and Tsivoglou (1981)[7], Fread (1988)[8], Singh and Scarlatos (1988)[9], Bechteler and Broich (1991)[10], and Mohamed et al. (2002)[11]. Physically based models are more complicated in structure and possess the potential to model more detailed and more accurate embankment dam breaching process, although they are restricted by the understanding degree of the dam breaching mechanism.

Table 1 shows some of the physically based embankment dam breach models and their main characteristics[7]~[16]. Among the models, Cristofano, PT, SMPDAM, BEED and BRES deal with embankment dam breach due to overtopping; Renard and Rupro cares only piping failure of embankment dams; and HW, BRDAM, DAMBRK, BREACH, LH and Mohamed et al. take both overtopping and piping into account. The tailwater effect is considered in the models like BRDAM, DAMBRK, BREACH, BEED and BRES. The BREACH model, BEED model and Mohamed et al. contain also the breach side slope stability analysis.

Nevertheless, understanding so far of the mechanism of embankment dam breaching is still unsatisfactory, and the state-of-the-art of the breach modeling technology is far from advanced. For instance, almost all of the mathematical models available now are limited to the breach in homogeneous embankment dams due to overtopping and/or piping. The formation of the initial opening in the dam, the composite dam structure, and the effect of dam slope protective layers are all neglected in the models. Besides, most of the embankment dam breach mathematical models do not distinguish the flow erosion rate of dam-material and the flow sediment transport capacity, despite the significant difference in meaning of the two concepts.

During the literature review it is also found that the available data on the numerous historical embankment dam failures in the world is very limited and rough, and is mostly based on eyewitness report. Many dam breaching processes have not been recorded or have not been accurately and detailedly recorded. However, on the other hand, prototype data in good quality is of great importance for calibration and validation of the embankment dam breach models. It is a big surprise that most of the available models are discovered to use the same a few limited prototype dam failure cases (e.g. the breach of Teton Dam in USA) for their calibration and validation.

3 PHYSICAL MODEL TESTS

Breach formation and development in embankment dams is a very complicated process with still little understanding. Therefore physical model tests on embankment dam breaching are at least for the moment, very valuable and irreplaceable for gaining more insight into the process, and for the development, calibration and validation of the dam breach mathematical models.

It is found from literature that various embankment dam breach model tests have been performed during the last several decades, particularly since the end of 1980's. These tests include both field large-scale tests and laboratory small-scale tests. The latter include numerous flume and wave basin embankment breach tests, which can be found in, e.g. Pan and Loukola (1993)[4], Powledge and Dodge (1985)[17], Fujita and Tamura (1987)[18], Steetzel and Visser (1993)[19], Andrews et al. (1999)[20], Hahn et al. (2000)[21] and Mohamed (2002)[22]. Almost all of these laboratory-tested embankment dams have less than 1m height. However, height of embankment dam models is important because scale effects sometimes may interpret an unreal mechanism of breach erosion.

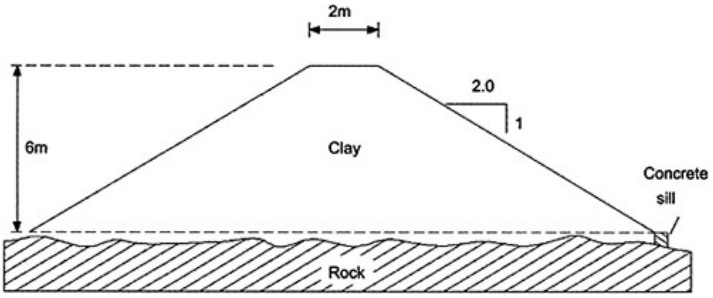

Figure 1. Cross-section of one of the field model tests in Norway[28].

Therefore, large-scale model tests in the field are preferable when condition permits. Relevant tests have been carried out in many countries such as China, The Netherlands, United States, United Kingdom, Norway and Germany. For details on these tests readers are referred to Pan and Loukola (1993)[4], Visser (1998)[16], Visser et al. (1991,1996)[23,24], Hanson et al. (2002)[25], Chen and Anderson (1987)[26], Meadowcroft, et al. (1996)[27], Hoeg et al. (2004)[28] and De Vroeg et al. (2002)[29].

Figure 1 shows the cross-section of one of the field embankment dam model tests performed recently in Norway.

4 HEADCUT EROSION DURING EMBANKMENT DAM BREACH

Wahl (1998, 1997)[6],[30] and Hanson et al. (1999)[31] stated that the primary weakness of the available embankment dam breach models is their use of tractive stress-based erosion models. Based on laboratory model tests and observations of real embankment dam failures, Ralston (1987)[32], Dodge (1988)[33], Wahl (1998)[6], Powledge et al. (1989)[34], and Hanson et al. (1999)[31] proposed that most embankment dam breaches are dominated by headcut erosion, i.e. flow shear erosion may still take place to a certain extent, however, erosion due to headcutting is often the dominant mechanism determining breaching. A headcut here means a vertical or near vertical drop or discontinuity on the flow-bed, and headcutting means the upstream movement of a headcut due to flow erosion.

Ralston (1987)[32] described the mechanics of embankment dam breach erosion. He put forward that for cohesive embankment dams, breaching takes place by headcutting rather than tractive stress erosion. In some cases a series of stair-step headcuts forms on the dam downstream face after the erosion is initiated. Seepage through the embankment dam exiting on the eroding face will increase the rate of erosion, this effect has also been noted by Powledge et al. (1989)[34].

Temple and Hanson (1994)[35] stated that formation and migration of headcut are also part of the erosion process in vegetated earth (soil and rock) auxiliary or emergency spillways. Mathewson, et al. (1998)[36] concluded from post-flow field inspections of eroded spillway channels that once erosion was initiated at some geometric anomaly, the primary erosion mechanism was either boundary shear or headcutting.

The Hydraulic Engineering Research Unit (HERU), USDA, USA, has recently performed some large-scale embankment dam (2.3m and 1.5m high) overtopping and breaching tests (see e.g. [21], [25] and [31]). Based on test observations and data recorded, process of embankment dam overtopping erosion was described (e.g. [21] and [31]). First rill and micro-rill erosion on the down-stream slopes of the embankment dam were initiated by the overland sheet flow (see Figure 2b).

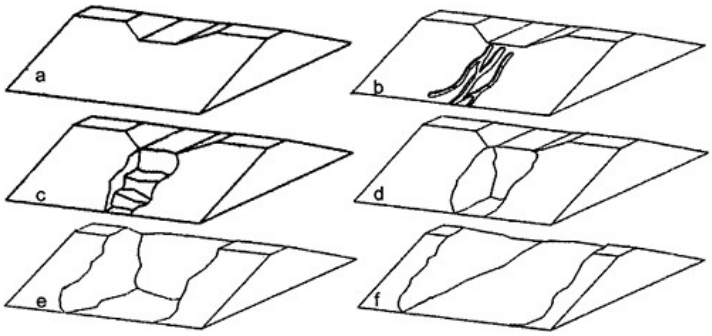

Figure 2. Observed breaching process during embankment dam model tests of USDA[21]

The erosion eventually developed a network of rills that gradually developed into a master rill(s) (i.e., gully). This dominant channel initially consisted of multiple cascading overfalls (see Figure 2c) that in time migrated upstream while simultaneously widened, until only a single large head-cutting channel remained (see Figure 2d). The headcut eventually migrate to the upstream end of the embankment dam crest, from then on any further upstream migration of the headcut resulted in a crest lowering (see Figure 2e) and increased discharge from the reservoir. This progression finally led to a full breach (see Figure 2f).

The gully widening and the headcut upstream migration were believed to be due to the turbulence and hydraulic stresses within the jet impingement area just downstream of the headcut[21]. The hydraulic stresses erode the base of the headcut, cause it to become unstable and ultimately produce mass failure. The mass failure induced the breach widening and headcut upstream migration.

The material used in USDA model tests varied from SM silty sand to CL lean clay. For embankment constructed with non-cohesive soil (e.g. sand), the breaching process was found in a field model test (see e.g. [24]) to be more or less similar to that in cohesive embankment dams, despite the considerable differences in their erosion mechanism.

Predicting headcut migration is a very intricate problem. The process of headcut migration may involve scour of jet impingement to the downstream bed, mass failure and/or shear erosion from the headcut surface, erosion along the approaching bed, and removal of the failed material from the scour hole. There is presently no generally accepted model for prediction of the headcut migration. However, recently there have been some simplified approaches to calculate the rate of head-cut migration (e.g. De Ploey (1989)[37], Temple (1992)[38], Temple and Moore (1994)[39], Hanson et al. (1999)[40], Robinson and Hanson (1994)[41], Wu et al. (1999)[42] and Zhu et al. (2004)[43]), among which, [37]~[39] are simple equations generally link the headcut migration rate with the energy at the overfall by a material dependent factor. [41]~[43] are relatively more complicated models with more factors taken into account. Table 2 lists the simple equations, and Table 3 summarizes the main characteristics of the latter three models.

During literature review, however, it is found that research on headcut erosion for embankment dam breach is only in a preliminary phase[43]. Little information exists on the variation of scour hole morphology and the headcut migration dynamics. Understanding of the headcut formation and migration is not complete and far from mature to be described mathematically. Although there are already some models trying to predict the migration rate of headcut, most of them are very empirical and simplified.

Table 2. Summary of the equations predicting headcut migration.

Model and time developed	Equation	Explanation
De Ploey (1989)	$R=Cq[g+u^2/(2h)]$	R=rate of headcut migration; C=a material dependent factor; q=unit discharge; g=gravity acceleration; u=flow velocity at headcut brink; h=headcut height;
Temple (1992)	$R=Cq^m h^n$	m and n=exponents;
Temple and Moore (1994)	$R=C[(q\gamma H)^a-E'^a]$	γ=unit weight of water; H=the change in elevation of the energy grade line through the headcut; a=an empirically determined exponent; E'=threshold energy required to generate headcut migration;
Hanson et al.(1999)	$\mathrm{R}=\frac{TE}{E_v}$	T=average retreat distance at each mass failure; E=soil detachment rate; and E_v=the amount of erosion required into the vertical wall to induce failure.

Table 3. Summary of the main characteristics of the latter three headcut migration models.

Model and time developed	Flow	Scour downstream of the headcut	Seepage	Headcut migration distance
Robinson and Hanson (1994)	Experimental data fitted equation for jet flow	An excess stress equation	Not considered	Assumed half of the headcut height
Wuetal. (1999)	The flow model of FAST3D.river code	The sediment transport model of FASTSD.river code	Not considered	The maximum of those induced by vertical surface shear erosion and toe scour
Zhu et al. (2004)	Theoretically calculated jet flow	The analytical development of Steinetal. (1993)[44]	Considered	Calculated through mechanical method

5 CONCLUSION

Modeling of embankment dam breaching is of enormous significance for the dam failure early warning system and emergency evacuation plan, consequently also for the disaster mitigation. Considerable progress has been achieved over the past more than forty years in the modeling of embankment dam breaching, in spite of the very complicated process involved. Many tools are now available for the embankment dam breaching simulation, and these models can be generally classified into two categories: parametric based and physically based.

Various embankment dam breach model tests, both field large-scale and laboratory small-scale, have been performed during the last several decades. Based on observation of model tests and actual embankment dam failures, headcut erosion is recently proposed by some investigators as the dominant erosion mechanism in most embankment dam breaches (e.g. [31]~[34]). And recently there have been some simplified models trying to predict the rate of headcut migration.

Nevertheless, understanding of the mechanism of embankment dam breaching so far is still unsatisfactory, and the state-of-the-art of the breach modeling technology is far from advanced.

For the headcut erosion, little information is existing and there is presently no generally accepted model for prediction of the headcut migration.

Besides, data on prototype embankment dam breaches, which are very important for calibration and validation of the embankment dam breach mathematical models, are found during literature review to be very limited with poor quality.

Therefore to better model the embankment dam breaching process, more research including desktop work as well as physical model tests should be conducted in the future. Physical model tests, especially full-scale and large-scale tests are vital for a better understanding of the erosion mechanism of embankment dam breaching and for calibration and verification of the mathematical models. Professional collection and preserving of data on real embankment dam failures should be seriously emphasized and carried out. It is expected that the recent advances in technology of soil erosion, hydraulics, headcut erosion, and vegetated surfaces erosion, etc. should be taken into account in the new embankment dam breach mathematical models for a better modeling.

REFERENCES

[1] Brown, C.O and Graham, W.J., 1988. Assessing the Threat to Life From Dam Failure. *Water Resources Bulletin,* Vol. 24, No. 6, 1303–1304.

[2] Wurbs, R.A., 1987. Dam-breach Flood Wave Models. *J. Hydraulic Eng.,* Vol. 113, No. 1, 29–16.

[3] Fread, D.L., 1998. Dam-Breach Modeling and Flood Routing: A Perspective on Present Capabilities and Future Directions. *Proc. Int. Dam Breach Processes Workshop,* Stillwater, USA.

[4] Pan Shuibo and Loukola, E., 1993. *Chinese-Finnish Cooperative Research Work on Dam Break Hydrodynamics.* National Board of Waters and the Environment, Helsinki, Finland.

[5] Wang Weidi, Zhu Yuansheng and Wang Ruichen, 1995. *Engineering Hydrology of Hydropower Station* (in Chinese). Hohai University Press, Nanjing, China.

[6] Wahl, T.L., 1998. *Prediction of Embankment Dam Breach Parameters—A Literature Review andNeeds Assessment.* DSO-98–004, Dam Safety Research Report, U.S. Bureau of Reclamation.

[7] Ponce, V.M. and Tsivoglou, A.J., 1981. Modeling Gradual Dam Breaches. *J. Hydraulic Div.,* Vol. 107, No. HY7, 829–838.

[8] Fread, D.L., 1988. *BREACH: An Erosion Model for Earthen Dam Failures.* National Weather Service (NWS) Report, NOAA, Silver Spring, USA.

[9] Singh, V.P. and Scarlatos, P.D., 1988. Analysis of Gradual Earth-Dam Failure. *J. Hydraulic Eng.,* Vol. 114, No. 1, 21–42.

[10] Bechteler, W. and Broich, K., 1991. Eifects in Dam-Break Modelling. *Proc. 24th Congress IAHR,* Madrid, Spain, A189–A200.

[11] Mohamed, M.A.A., Samuels, P.G. and Morris, M.W., 2002. Improving the Accuracy of Prediction of Breach Formation Through Embankment Dams and Flood Embankments. *Proc. Int. Conf. Fluvial Hydraulics,* Louvain-la-Neuve, Belgium, 663–673.

[12] Singh, V.P., 1996. *Dam Breach Modeling Technology.* Kluwer, Dordrecht, The Netherlands.

[13] Wetmore, J.N. and Fread, D.L., 1991. *The NWS Simplified Dam-Break Flood Forecasting Model.* National Weather Service Report, NOAA, Silver Spring, USA.

[14] Paquier, A., Nogues, P. and Herledan, R., 1998. Model of Piping in Order to Compute Dam-Break Wave. *Proc. CADAM Workshop on Dam-breach formation and Development,* Munich, Germany.

[15] Loukola, E. and Huokuna, M., 1998. A Numerical Erosion Model for Embankment Dams Failure and Its Use for Risk Assessment. *Proc. CADAM Workshop on Dam-breach formation and Development,* Munich, Germany.

[16] Visser, P.J., 1998. Breach Growth in Sand-Dikes, PhD thesis, Delft University of Technology, Delft, The Netherlands.

[17] Powledge, G.R. and Dodge, R.A., 1985. Overtopping of Small Dams—An Alterative for Dam Safety. *Proc. Specialty Conference,* ASCE, 1071–1076.

[18] Fujita, Y. and Tamura, T., 1987. Enlargement of Breaches in Flood Levees on Alluvial Plains. *J. Natural Disaster Science,* Vol. 9, No. 1, 37–60.

[19] Steetzel, H.J. and Visser, P.J., 1993. Profile Development of Dunes Due to Overflow. *Proc. 23rd Int. Conf. Coastal Eng.,* Venice, Italy, 2669–2679.

[20] Andrews, D.P., Coleman, S.E., Webby, M.G. and Melville, B.W., 1999. Noncohesive Embankment Failure Due to Overtopping Flow. *Proc. 28th Congress IAHR,* Graz, Austria.

[21] Hahn, W., Hanson, G.J. and Cook, K.R., 2000. Breach Morphology Observations of Embankment Overtopping Tests. *Proc. 2000 Joint Conf. Water Resources Engineering and Water Resources Planning and Management.* Minneapolis, USA. (CD-ROM)
[22] Mohamed, M.A.A., 2002. Lab and numerical modelling at HR Wallingford. *Presentation at the 1st IMPACT Project Workshop,* HR Wallingford, UK. (CD-ROM)
[23] Visser, P.J., Vrijling, J.K. and Verhagen, H.J., 1991. A Field Experiment on Breach Growth in Sand-Dikes. *Proc. 22nd Int. Conf Coastal Eng.,* Delft, The Netherlands, 2087–2100.
[24] Visser, P.J., Kraak, A.W., Bakker, W.T., Smit, M.J., Snip, D.W., Steetzel, H.J. and Van de Graaff, J., 1996. A Large-Scale Experiment on Breaching in Sand-Dikes. *Proc. Coastal Dynamics' 95,* Gdansk, Poland, 583–594.
[25] Hanson, G.J., Cook, K.R. and Temple, D., 2002. Research Results of Large-Scale Embankment Over-topping Breach Tests. *Proc. 2002 Annual Conf,* Association of State Dam Safety Officials, Tampa, USA.
[26] Chen, Y.H. and Anderson, B.A., 1987. *Development of a Methodology for Estimating Embankment Damage due to Flood Overtopping.* Report No. FHWA/RD-86/126, Federal Highway Administration, US Department of Transportation.
[27] Meadowcroft, I.C., Morris, M.W., Allsop, N.W.H. and McConnell, K., 1996. *Tollesbury Managed Set Back Experiment: Breach Design and Construction, and Embankment Failure Experiment.* HR Wallingford Report TR 5, HR Wallingford, UK.
[28] Hoeg, K., Lövoll, A. and Vaskinn, K.A., 2004. Stability and Breaching of Embankment Dams: Field Tests on 6m High Dams. *Int. J. Hydropower & Dams,* Vol. 11, Issue 1, 88–92.
[29] De Vroeg, J.H., Kruse, G.A.M. and Van Gent, M.R.A., 2002. *Erosion due to Overtopping and Overflow.* Project identification: DC030202/H3803, Delft Cluster, Delft, The Netherlands.
[30] Wahl, T.L., 1997. Predicting Embankment Dam Breach Parameters—A Needs Assessment. *XXVIth IAHR Congress,* San Francisco, USA.
[31] Hanson, G.J., Temple, D.M. and Cook, K.R., 1999. Dam Overtopping Resistance and Breach Processes Research. *Proc. 1999 Annual Conf.,* Association of Stade Dam Safety Officials, St. Louis, USA. (CD-ROM)
[32] Ralston, D.C., 1987. Mechanics of Embankment Erosion During Overflow. *Proc. 1987 ASCE National Conference on Hydraulic Engineering,* Williamsburg, USA, 733–738.
[33] Dodge, R.A., 1988. *Overtopping Flow on Low Embankment Dams—Summary Report of Model Tests.* REC-ERC-88–3, U.S. Bureau of Reclamation, Denver, Colorado.
[34] Powledge, G.R., Ralston, D.C., Miller, P., Chen, Y.H., Clopper, P.E. and Temple, D.M., 1989. Mechanics of Overflow Erosion on Embankments. II: Hydraulic and Design Considerations. *J. HydraulicEng.,* Vol. 115, No. 8, 1056–1075.
[35] Temple, D.M. and Hanson, G.J., 1994. Headcut Development in Vegetated Earth Spillways. *Applied Engineering in Agriculture,* Vol. 10, No. 5, 677–682.
[36] Mathewson, C.C., Cato, K.D. and May, J.H., 1998. *Geotechnical Aspects of Rock Erosion in Emergency Spillway Channels.* Technical Report REMR-GT-3, U.S. Army Corps of Engineers, Waterways Experiment Station, Vicksburg, MS.
[37] De Ploey, J., 1989. A Model for Headcut Retreat in Rills and Gullies. *CATENA,* Supplement 14, 81–86. Cremlingen, W. Germany.
[38] Temple, D.M., 1992. Estimating Flood Damage to Vegetated Deep Soil Spillways. *Applied Engineering in Agriculture,* 8(2):237–242.
[39] Temple, D.M. and Moore, J.S., 1994. Headcut Advance Prediction for Earth Spillways. *Presented at the 1994 ASAEM. Winter Meeting,* Atlanta, Georgia. PaperNo. 942540, ASAE.
[40] Hanson, G.J., Robinson, K.M. and Cook, K.R., 1999. Prediction of Headcut Migration Using a Deterministic Approatch. *Presented at the 1999 ASAE/CSAE-SCGR Annual Int. Meeting,* Paper No. 992160, ASAE.
[41] Robinson, K.M. and Hanson, G.J., 1994. A Deterministic Headcut Advance Model. *Transactions of the ASAE,* 37(5):1437–1443.
[42] Wu, W.M., Wang, S.S.Y., Jia, Y.F. and Robinson, K.M., 1999. Numerical Simulation of Two-Dimensional Headcut Migration. *Proc. ASCE Int. Water Resources Engineering Conf.,* Seattle, USA. (CD-ROM)
[43] Zhu, Y.H., Visser, P.J. and Vrijling, J.K., 2004. A Model for Prediction of Headcut Migration. *Accepted for publication and presentation at 9th ISRS,* Yichang, China.
[44] Stein, O.R., Julien, P.Y. and Alonso, C.V., 1993. Mechanics of jet scour downstream of a headcut. *J. Hydraulic Res.,* Vol. 31. No. 6, 723–737.

New Developments in Dam Engineering—Wieland, Ren & Tan (eds),
© 2004 Taylor & Francis Group, London, ISBN 04 1536 240 7

Study on mechanism and effectiveness of measures for control of seepage in foundation of concrete dams

Yue-ming Zhu[1], Feng Kuang[1], Stephan Semprich[2] & Erich Bauer[2]
[1]*Hohai University, Nanjing, China*
[2] *Graz University of Technology, Graz, Austria*

ABSTRACT: Regarding to the mechanism and effectiveness of seepage control with grout and drainage curtains, a comprehensive study on the seepage behavior and the seepage control characteristics for a concrete gravity dam via modern calculation theories and techniques are carried out. Many relevant impact factors are considered, such as the depths and permeability of grout curtains; the diameter, spacing, drain type and drainage altitude of relief holes; and the interaction between the impervious and drainage measures. It is found that the interaction of the grout and drainage curtains is of extreme important to the safeties of the dam and the foundation as well. It is believed in general that under the support of the drainage curtains the relative impervious degree of the grout curtains is easily reached and the coefficient of permeability of the grout curtain beneath a concrete dam is only 2~3 times less than that of the rock mass surrounding the grout curtain.

1 INTRODUCTION

The mechanism and effectiveness of the seepage control measures of grout and drainage curtains in the rock foundation of concrete dams are one of the most common problems concerned by the dam engineers. The answer to the problem seems to be very simple at the time being, but in reality one still don't understand it deeply and completely. The late famous Prof. Casagrande from Harvard University had carefully studied the problem in the 1950s and got some useful conclusions and also provided some practical examples, which are still useful for engineer [1]. But due to the complication and the research means and conditions, there are still some questions not to be explained at that time. On the basis of his work and today's modern study methods, the authors here restudied them comprehensively and got some new results related to the mechanism and the effectiveness. The results should be of especially valuable to the respective owners, designers, constructors and operators of concrete dams.

2 SOLUTION TO PROBLEMS OF SEEPAGE WITH FREE SURFACE OF SEEPAGE WITHOUT MESH ITERATION

There are a few of numerical methods for solution to unconfined seepage problems without mesh iteration in the relevant references and here the procedure of nodal virtual flux [3,4] is adopted. It is completed based on the reference [2] and the basic idea is that the total area is divided into the virtual area, Ω2, above the free surface of seepage and the real area, Ω1, below the free surface (Fig. 1). The elements located in Ω2 and Ω1 are referred to as virtual and real elements, respectively. The following Eq. 1 is the FEM iteration equations for the solution to the boundary nonlinear problem. About the details of the procedure, one could consult the references [3,4].

$$[k]\{h\}=\{Q\}-\{Q_2\}+\{\Delta Q\} \tag{1}$$

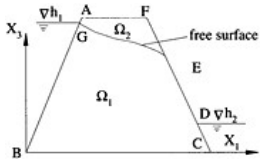

Figure 1. Seepage problem in embankment.

Figure 2. Elemental mesh for calculation.

3 MECHANISM AND EFFECTIVENESS OF MEASURES OF GROUTING AND DRAINAGE IN FOUNDATIONS

3.1 *Calculating model and mesh*

For the current study, a concrete dam with 103m high was selected. The basic descriptions about the character of seepage of the foundation and the design scheme of seepage control are as follows:

The main grout curtain beneath the dam is located 10m far behind the dam heel, 4m thick, 60m deep. The position of the drainage holes consisting of the upstream drainage curtain is 4.5m down-stream behind the grout curtain. In the area of the dam toe, there are a extra grout and drainage curtains and the grout curtain is about 30m deep and 3m thick. The spacing of the drainage holes at centers is 3m and the diameter of all the holes is 15cm. The depths of the two drainage curtains are about equal to the relevant half of the depths of the grout curtain. The depth of the upstream water is 100m and that of the tailwater is 10m. It is assumed that the rock is homogeneous and isotropic. The Darcy's coefficients of permeability of grout curtains and the rock are respectively equal to 1.0×10^{-5}cm/s and 1.0×10^{-4}cm/s. The domain for the seepage calculation and its relevant elemental mesh are shown in Figure 2. The thickness of the domain in the direction of the dam axis is 1.5m, which is just the half of the spacing of two adjacent drainage holes. The calculation variations/cases are listed in Table 1 for the study.

3.2 *Analysis of calculation results*

The variations from case 1 to case 3 are for sensitivity analysis of the curtains beneath the dam. In Figures 3 and 4 there are the calculated results of the hydraulic headlines on the cross section through the center of a drainage hole and the distribution of the uplift on the stand surface of the dam from the cases 3 and 4. Under the mutual functions of the grout and drainage curtains, the results practically almost don't have any changes to each other. The reason for this phenomenon is the permeability of the grout curtain is relative smaller enough than that of the surrounding rock mass and just behind the curtain there is the drainage curtain, which is totally not jammed, has a low elevation of the top-drainage exit and has practically drained up the water all round the drainage hole and behind the grout curtain. On the basis of the numerical tests, it is needed only that the coefficient of permeability of the grout curtain is smaller than that of the rock mass by about 3 to 5 times to fulfill the aim of a successful control of seepage if the permeability of the rock is not large and the relief holes keep open.

In the case 4, no grout curtain beneath the dam is adopted and in despite of the fact of non-curtain, except for the local area upstream of the drainage holes the whole behavior of seepage is almost the same as that mentioned above. The reason for the result is the strong effect of the drainage curtain and the small permeability of the rock. But in the current case, due to the absence of the upstream grout curtain the hydraulic gradients round the drainage curtain, especially in the area of the very holes' circumference, become much large and the danger of seepage deformation of the rock mass could appear relatively. If the quality of the foundation rock is very good and such a danger would never emerge, the costly grout curtain is not necessary.

Table 1. Computational cases.

Case no.	Description of the computational cases
1	The basic case described above, the coefficients of permeability of the grouting curtains are one order of magnitude less than that of the foundation rock around the curtains. There is no grouting curtain and drainage curtain on the downstream side of the dam.
2	The coefficients of permeability of the grouting curtains are half order of magnitude less than that of the foundation rock. Other things are the same as in case 1.
3	The coefficients of the grouting curtains are one thirds time of that of the rock mass.
4	There is no grouting curtain in the foundation of the dam; the others are same as in case 1.
5	No drainage hole in the foundation or all they are jammed; the others are same as in case 1.
6	The half of the total drainage holes is jammed or the spacing of the holes at centers is enlarged into 6m and the other things are the same as in case 1.
7	There are also a grouting curtain and a drainage curtain on the downstream side of the dam. The depths of the grouting and drainage curtains are 30m and 15m, respectively.
8	Extra 2 rows of drainage holes in middle of the dam foundation and in the longitudinal direction are embedded the rock foundation and they are 8m deep beneath the bottom surface of the dam. The others related to this case are the same in case 7.
9	Extra 2 rows of the drainage holes in the middle of dam foundation are assumed in the foundation and only 4m deep beneath the dam stand surface. The others are same as in case 7.
10	The depths of the drainage holes in upstream and downstream are 35m and 18m. The others are same as those in case 7.
11	The mean dip angle of one of the two assumed fractures' groups of the foundation rock is about 60° and the fractures incline to the downstream side.

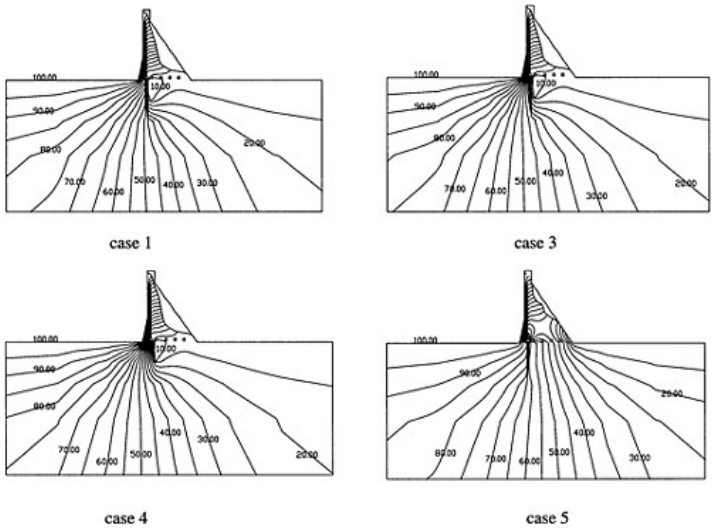

Figure 3. Distributions of hydraulic head of different computational cases (Unit: m).

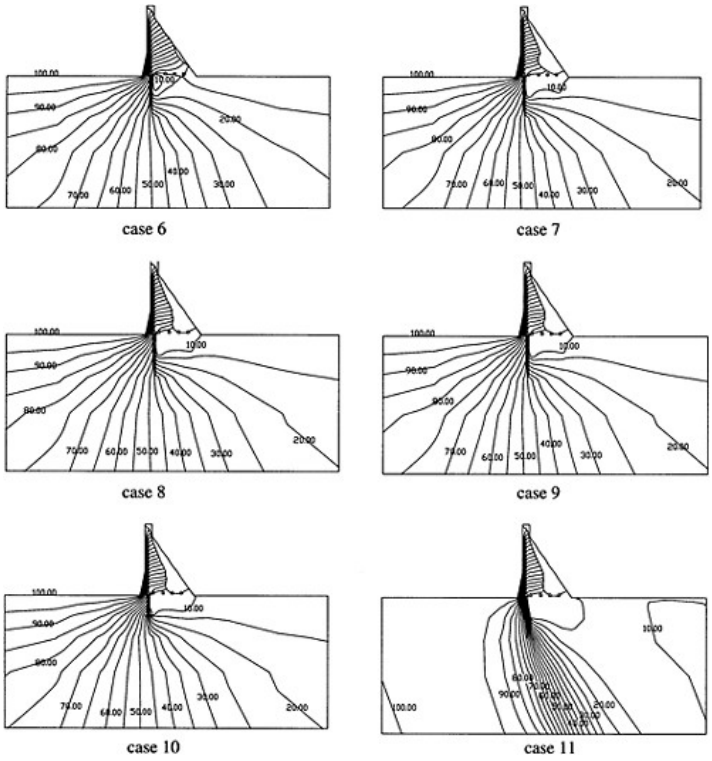

If the drainage curtain is not constructed beneath the dam (case 5), as shown in the Figures 3 and 4, the seepage behavior in the foundation has changed greatly. Although the coefficient of permeability of the curtain reaches one order magnitude less than that of the surrounding rock, the curtain almost totally does not have any effect on the seepage control. The uplift has a linear triangle distribution on the bottom surface and it should obviously exceed the allowable design value. In practice, with conventional cement suspension grout, it is not easy and sometimes difficult to make a decision of the determination of the coefficient of permeability of a grout curtain[5].

With comparison of the results from the cases 1, 4 and 5, it can be drawn that the 59.83m difference of the hydraulic heads between the upstream and downstream sides of the main curtain in case 1 couldn't prove the existence of a very good effect of the grout curtain and it is produced by the influence of the drainage curtain. If a practical non-difference of hydraulic heads on both sides of a grout curtain is measured with piezometers or osmometers, which are respectively located on the upstream and downstream sides of a grout curtain, this couldn't still prove that the grout curtain is certainly not integrated or already deteriorated when the drainage curtain losses its function. On the other hand, if a big difference of hydraulic heads is measured with piezometers or osmometers located on both of the sides of a grout curtain and this could only verify a good function of the drainage curtain, and don't give the exact information about the degree of the impermeability of the grouting curtain.

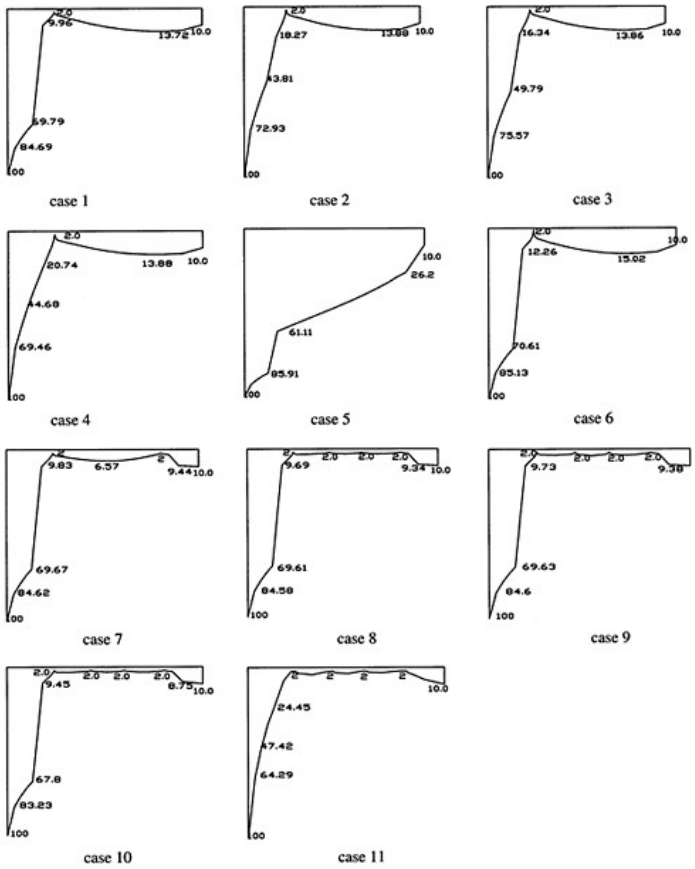

Figure 4. Distributions of uplifts on dam stand surface in different cases (unit: m).

If half of the drainage holes is jammed or the spacing of the adjacent drainage holes at centers reaches 6m (case 6), the both distributions of the hydraulic heads and the uplifts on the stand surface of the dam are practically not changed. Further more numerical tests show that the seepage behavior in the foundation could be still controlled well if the spacing reaches 8m and even 10m. Such, the authors of the current paper believe that the spacing of two adjacent drainage holes could be increased to 4–5m instead of the traditional 3m adopted in the practices of dam engineering. The more important thing to the safety of the concrete dams is non-block of drainage holes during any time of the operations.

In the case 8, extra grout and drainage curtains are also constructed in the area of the dam toe. It is shown that the functions of the prevention from the water infiltration from the downstream

riverbed into the foundation area directly beneath the bottom surface of the dam is well; see the figures about the case 7 in Figures 3 and 4. The maximal hydraulic head of the uplift is only 6.57m in the middle of the stand surface instead of 13.72m in the standard case 1. If the tailwater depth is large, such a grout and drainage curtains could be designed like in the practices of the Chinese dam engineering.

On the basis of the case 7, extra two 8m-deep shallow drainage curtains are arranged between the upstream and downstream grout and drainage curtains. The results from this case show that the maximal hydraulic head of the uplift decreases to about 2m, which is just the margin of the over-flowing altitude of the drainage holes in the foundation and the elevation of the stand/bottom surface of the dam. The total dynamic hydraulic head of the uplift is vanished and the hydraulic gradients in the area near the stand surface and behind the upstream grout curtain are about equal to zero.

With comparing to the case 1, only the depths of the grout and drainage curtains are halved in the case 10. As shown in Figures 3 and 4, almost the same seepage control effects are achieved. It means if there are no special geological conditions, one only needs short grout and drainage curtains instead of the conventional deep ones to control the seepage behavior in the dam foundation. It should be obviously economical and reasonable that a relevant numerical study is carried out before the final design scheme of seepage control for a concrete dam is determined.

In the case 11, the influence of the anisotropy of permeability of the rock mass is considered. It is assumed that there are two groups of mutually orthogonal fractures in the rock mass and the mean equivalent coefficients of permeability of the rock which are caused by the fractures are $k_{F1}=1\times10^{-4}$cm/s and $k_{F2}=1\times10^{-5}$cm/s, respectively. The dip angle of the fractures of one of the two groups is 60°, and it inclines to the downstream side and it runs parallel to the dam axis. The principal coefficient of permeability of the rock in the direction of the dam axis equals to 1×10^{-4}cm/s The coefficients' tensor of permeability of the rock can be calculated[2]. According to the Figures 3 and 4, except for the direct areas of the grout curtains, the tendencies of the hydraulic-head isolines are mainly parallel to the planes of the fractures. That means that the seepage resistance in the direction of the fractures' plane are relatively much smaller than that in the direction perpendicular to the fracture plans and it results in no loss of hydraulic head in the small-resistance direction. But as illustrated in the Figures, the uplift on the bottom surface of the dam essentially remains the same as shown in the case 1 under the strong influence of the drainage curtains.

4 CONCLUSIONS

With the help of the results from different numerical tests, the effectiveness of the seepage control with grout and drainage curtains in concrete dam foundation was studied in detail. It has been found there is a co-existence in the seepage control system, namely the effectiveness of the grout curtain is effectively guaranteed by the function of the drainage curtains and the drainage curtains do need the co-work of the grout curtains located before the drainage curtains to block the paths of seepage into the drainage holes and to avoid the danger of hydraulic deformations in the near areas of the holes. Under the support of the drainage holes, the main hydraulic heads of seepage would concentrate inside the grout curtain. If the depth of the tailwater is large, a grout curtain and a drainage curtain on the downstream side of the dam and two or three shallow longitudinal drainage curtains in the middle of the stand surface could be designed to further decrease the uplift on the bottom surface of the dam if the width of the bottom surface is special large.

The distributions of the hydraulic heads and uplifts beneath a concrete dam can be only controlled with drainage curtains and the grout curtain practically has no effect on the distributions of the hydraulic heads without the help of drainage curtains. Therefore, it is not easy to correctly evaluate the real function of a grouting curtain only according to the measurements of the hydraulic heads on both of the sides of the grout curtains with piezometers and/or osmometers. For the controlling of the uplifts on the dam stand surface, relative shallow grout and drainage curtains instead of those with large depth are enough in general.

REFERENCES

[1] Casagrande. Control of seepage through foundation and abutments of dams [J]. ASCE, Journal of Geotechnique, 1961, 3:161–182.
[2] W.Wittke. Rock mechanics theory and applications with case histories [M]. Berlin: Springer-Verlag, 1990.
[3] Zhu Y.M., Chen Z.L., Chen Q. et al. Solution to problems of complicated seepage in surrounding rock masses of underground power station with technique of improved drainage substructure [J]. Chinese Journal of Hydraulic Engineering, 1996.9. (in Chinese).
[4] Zhu Y.M., Zhang L.J. Technique of improved drainage substructure for solution to seepage problems [J]. Chinese J. of Geotechnic Engineering. 1997,Vol.l6, No2, pp69–76. (in Chinese).
[5] E-K. Ewert. Rock grouting with the emphasis on dam sites [M]. Berlin: Springer-Verlag, 1986.

This page intentionally left blank.

New Developments in Dam Engineering—Wieland, Ren & Tan (eds),
© 2004 Taylor & Francis Group, London, ISBN 04 1536 240 7

Analysis of pipe-cooling system in mass concrete*

Yue-ming Zhu, You-zhi Liu, Zhi-qiao Xiao, Jin-ren He, Zhi-xiang Lin & Yue-feng Ma
College of Water Conservancy & Hydropower Eng., Hohai Univ., Nanjing, China

ABSTRACT: Pipe cooling is a very useful measure for the engineer to control temperature and to prevent concrete from cracking. How to accurately calculate its effect on thermal and stress changes resulted from the system is a rather complex and even one of the most concerned problems of engineers. Based on some preceding research works, a numerical iterative procedure has been improved and perfected to exactly deal with the performance of the pipe-cooling system. With the improved iterative procedure, an application to an arch dam being under construction is presented. The results from a whole block of the dam are finally analyzed.

1 INTRODUCTION

In mass concrete dam engineering, the temperature rise occurs inside the concrete may reach more than 20°C due to the heat of cement hydration and the characteristic of the low thermal conductivity of concrete. It is a quite common phenomenon that the thermal stresses caused by the temperature change in concrete will result in cracking. For concrete dams, the temperature change might last a few of decade years or even more than hundred years until to reach the final quasi-steady temperature without artificial cooling measures.

To fulfill the requirements of applications in engineering, since the 30's years of the last century pipe-cooling system has been adopted to decrease and control the rises of the temperature and thermal stresses in mass concrete. Because the cooling water in pipes is moving and the distributions of the temperatures of the water along a pipe are forehead unknown, the solution to the problem about the actual performance of the system can't easily got. Therefore, a lot of research work for the solution has been devoted to the respective theories and computational procedures since the problem has appeared for long years.

In China, Zhu[1] has paid special attentions and efforts to this problem for a long time, and obtained some very useful achievements. He presented for first a finite element iterative procedure for the simulation of pipe cooling. In iterative procedure, in order to determine the water temperature of all the nodes on the pipe external surface, which is taken as a prescribed temperature boundary, a numerous solutions of two-dimensional thermal problems relating to the cross sections being perpendicular to the pipeline have to be required forehead in each iteration of solution to the three-dimensional problem. Although the iterative idea of the procedure is good for the solution in general, up to now it has not been widely applied in practices because of the numerous, inexact and strenuous solutions to the two dimensional problems. To improve the procedure and to decrease the request of the internal storage space of computer, Liu and Liu[2] attempted to solve the numerical problem of pipe cooling system with substructure technique. The highlight in the

* (The current work was financially supported by both of the academic development fund of Hohai University (HHYS0023) and the project of development of new technology granted by the ministry of water resources (SCXC2003–10).

reference[2] is the improvement of the iteration method mentioned above. But in fact, the substructure technique of finite element method is not suitable to deal with the problem of thermal fields with pipe cooling and there are disadvantages in the increasing of calculation efforts.

Based on the work[1], the authors[3] have also separately modified the above-mentioned numerical iterative procedure[1], and the modified method becomes more rigorously in theory and solution, considerably simplified and much stricter, and also much easier to be used to practical projects. Up to now, the improved method has been successfully applied to several real projects in hydraulic engineering including RCC dams and CC arch dams. Some results from the application to a practical arch dam block are presented and illustrated. Because the precision of the results can be remarkably improved and the numerical implementation of the method is also much easier, the method being presented here should be quickly popularized to using to practical projects.

2 THEORY ON SOLUTION TO TRANSIENT TEMPERATURE

According to the well-known variation principle, the equilibrium equation of heat transfer Eq. 1 can be

$$\text{trans-}\ \frac{\partial T}{\partial \tau}=a\left(\frac{\partial^2 T}{\partial x^2}+\frac{\partial^2 T}{\partial y^2}+\frac{\partial^2 T}{\partial z^2}\right)+\frac{\partial \theta}{\partial \tau} \tag{1}$$

formed into the following recursion matrix Eq. 2 by using the backward difference for time when all the prescribed and convection boundary conditions between concrete and atmosphere are satisfied.

$$\left[[H]+\frac{1}{\Delta t_n}[R]\right]\{T_{n+1}\}-\frac{1}{\Delta t_n}[R]\{T_n\}+\{F_{n+1}\}=0 \tag{2}$$

where θ means the adiabatic temperature rise of concrete, a stands for the coefficient of thermal conductivity, [H] is the matrix of thermal conductivity; [R] presents the matrix of special heat capacity, $\{T_n\}$ and $\{T_{n+1}\}$ indicate the vectors of the nodal temperature at the nth and $(n+1)$th time steps, respectively; $\{F_{n+1}\}$ is referred to as the vector of the nodal thermal loads at the $(n+1)$th time step; n stands for the number of time step; Δt is the time interval of iteration. After Eq. 2, the solution of the nodal temperature $\{T_{n+1}\}$ will be got on the basis of the previous solution of $\{T_n\}$.

3 FINITE ELEMENT PROCEDURE FOR SOLUTION TO THERMAL PROBLEM IN CONCRETE WITH PIPE COOLING

3.1 *Calculation of temperature rising of the water along cooling pipe*

Due to the water in pipe is moving and the water temperature is unknown forehead, the calculation of the water temperature along cooling pipes is rather complex. Supposing that Fig. 1 is an arbitrary element of a cooling pipe and according to the Fourier's law of thermal conductivity, the specific thermal flux from the concrete around the external surface of the pipe into the water is $q=-\lambda(\partial T)/(\partial n)$. In general, the pipe is so thin that its thermal change could be neglectful for the problems in engineering. In the following, the thermal convection between the cooling water and the adjacent concrete during any time interval, Δt is analyzed.

Figure 1. Sketch of thermal convection between pipe-cooling water and adjacent concrete.

1. The influx heat from the concrete into the cooling water through the external surface of the pipe, Γ^0, is

$$dQ_c = \iint_{\Gamma^0} q_i ds \cdot dt = -\lambda \iint_{\Gamma^0} \frac{\partial T}{\partial n} ds \cdot dt \tag{3}$$

2. The influx heat through the cross section, W_1 in Figure 1 is

$$dQ_{w1} = c_w \rho_w T_{w2} q_w dt \tag{4}$$

3. The outflow heat through the cross section, W_2, in Figure 1 is

$$dQ_{W2} = c_w \rho_{wTw2} q_w dt \tag{5}$$

where q_w, c_w, ρ_w, are the flux, specific heat and density of cooling water, respectively; T_{w1} and T_{w2} respectively means the temperatures of the influx and outflow water of the elemental pipe segment.

4. The increased or decreased heat between the sections W_1 and W_2 of the pipe segment is

$$dQ_w = \int_{l_1}^{l_{2l}} c_w \rho_w \left(\frac{\partial T_{wP}}{\partial t} dt \right) \cdot A_p dl \tag{6}$$

where T_{wP} is the water temperature in pipe, l indicates the coordinate along the pipe's axis, and A_p stands for the area of the pipe cross-section.

According to the following equilibrium condition of heat,

$$dQ_{w2} = dQ_{wl} + dQ_c - dQ_w \tag{7}$$

One could obtain the incremental water temperature in the pipe segment as follows [3]:

$$\Delta T_{wi} = \frac{-\lambda}{c_w \rho_w q_w} \iint_{\Gamma^0} \frac{\partial T}{\partial n} ds + \frac{A_p}{q_w} \int_{l_1}^{l_{2l}} \frac{\partial T_{wP}}{\partial t} dl \tag{8}$$

Because the volume of the water in the pipe segment is very small in comparison with the total flowing water flux, so it should be valid for practical problems to simplify Eqs. 8 as follows

$$\Delta T_{wi} = \frac{-\lambda}{c_w \rho_w q_w} \iint_{\Gamma^0} \frac{\partial T}{\partial n} ds \tag{9}$$

During the implementation of finite element method program, the integral $\int_{\Gamma^0} \int (\partial T/\partial n) ds$ on curve surface will be strictly obtained by a Gauss's integral on the concrete element surfaces contacting to the pipe external surfaces.

The influx water temperature is known and one can calculate the temperatures of all the nodes along the pipe in iteration[1–3]. It is assumed that a water pipe has divided into m elemental segments, the influx water temperature of the pipe is T_{w0}, and the increment of the water temperature of the ith segment is ΔT_{wi}, then the temperature of the nodes, T_{wi}, at the outflow cross section of the ith segment can be obtained with Eq. (10)[1].

$$T_{wi} = T_{w0} + \sum_{j=1}^{i} \Delta T_{wj}, \; i = 1,2,3, \cdots, \; m. \tag{10}$$

3.2 *Numerical iterative solution to the problem with pipe cooling system*

Because the water temperatures along a pipe are unknown forehead and the water temperature increments are related to $\partial T/\partial n$, which depends on unknown of temperature, after Eqs. 9 and 10, such the temperature with pipe cooling system is a nonlinear complicated thermal problem. The final solution to the unsteady problem can't be directly got by one step. To solve the problem, one has to adopt a numerical iterative procedure[1]. The authors have separately modified and perfected the numerical procedure[3]. Firstly, the temperatures of the water in the whole pipes are assumed the same as temperature of influx water and according to the Eq. (2) the solution in the first step of iteration is obtained. Then, in the second step the temperatures of water in pipes can be approximately calculated with Eqs. (8) or (9) and (10), and the new solution can be respectively got. Repeating the iterative process until the concrete temperature and the temperature of water reach a numerical convergence.

4 APPLICATION TO AN ARCH DAM BEING UNDER CONSTRUCTION

Figure 2 is the mesh of the 8th concrete block of Huaguangtan arch dam in Zhejiang province. The length and the height of the block is 18m and 103.85m, and the widths are from 18.88 to 5.8m along the height. In Figure 3 the relatively fine elements around cooling pipe are shown. The spacing at center between two adjacent pipes in horizontal direction is 2m and that one in vertical direction is 3m. The thickness of the lift layers of the concrete placement is 2 to 3m. The pipe cooling has two effects and the first one is to deal with the problems of the high rising of temperature of the dam concrete in early age and to cut off the peaks of temperature and to control the related thermal gradients in summer when the environmental temperature and the initial temperature of concrete are high. The second effect of the pipe cooling is to let the temperature of the dam body decrease inside the assigned temperatures to fulfill the requirement of the grouting of the construction joints in the dam body.

The initial temperatures of the cooling water for the two aims were 15°C and 10°C, respectively. The average discharge of the moving water in a pipe was equal to q_w=15L/min. The running time of every cooling pipe approximately lasted 18 days for the first effect mentioned above for each time and varied from 25 to 5 days with the construction rising of the dam body for the second effect. During the running of the pipe cooling, the direction of the water moving in every pipe was changed once a day to homogenize the temperature in the concrete.

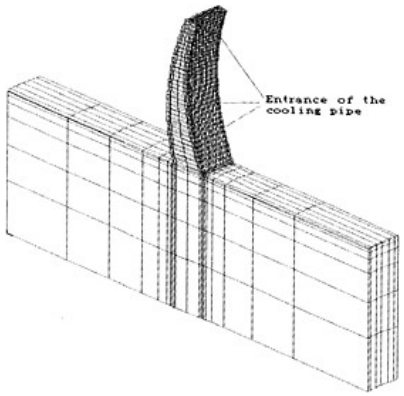

Figure 2. Finite elemental mesh of the dam block.

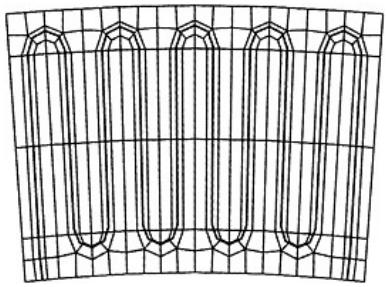

Figure 3. Elements refined around cooling pipe.

Figure 4 is the distribution of the temperature isolines in the center cross section, y=0m, after the running of the pipe cooling for the first effect when the block was placed from the elevations of 346m to 398m. In Figure 5, the results of the corresponding distribution of the temperature isolines at the same time are shown if the pipe cooling was not adopted in the construction. One can find the highest temperature occurring in the dam would be 38.62°C (in Fig. 4) and 8.90°C less than the maximal temperature 45.52°C in Figure 5. It means the pipe-cooling system in the dam body has played a very effective role in the time of the construction for controlling the temperature in the high temperature seasons. It should also be pointed that the thermal gradients around the pipes are relatively high and it ought to be noted. The lowest temperatures in the two Figures are almost the same and are 13.85°C and 13.82°C.

Figure 6 and Figure 7 are the distributions of the thermal isolines after the running of pipe cooling for the second effect when the construction heights of the dam block reach to the elevations of 420m

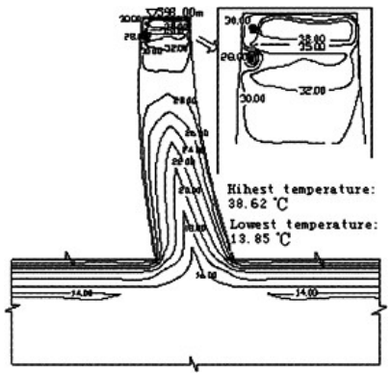

Figure 4. Distribution of thermal isolines with pipe cooling.

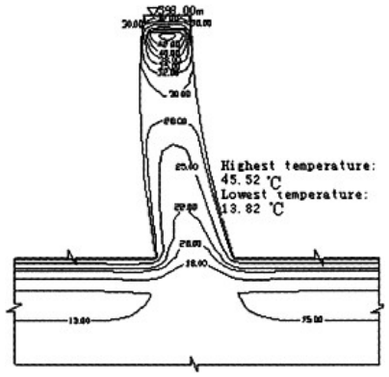

Figure 5. Thermal distribution without pipe cooling.

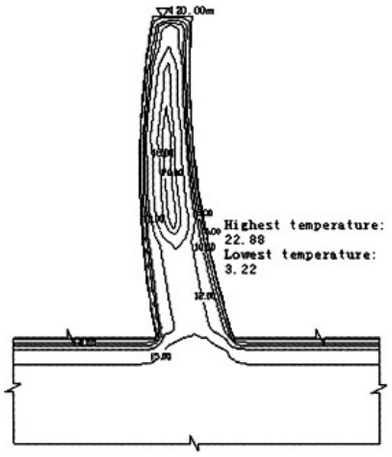

Figure 6. Distribution of thermal isolines before the first time of grouting of the joints (Unit: °C).

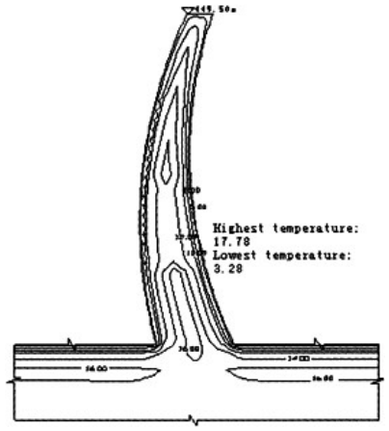

Figure 7. Distribution of thermal isolines before the second time of grouting of the joints (Unit: °C).

and 449.5m, respectively. According to the results, the thermal isolines show the relative uniformity distributions of the temperatures in the areas of the pipe cooling in both of the figures and the respective thermal gradients are much smaller than those in the areas without pipe cooling. Therefore, the pipe cooling can also play a nice effect on the temperature control before the grouting of the construction joints.

5 CONCLUSIONS AND SUGGESTIONS

Based on the theory on a numerical and strict iteration procedure for solution to transient thermal problems of mass concrete with pipe cooling and the results from the application of the procedure to a dam block of an arch dam, the following conclusions and suggestions are drawn:

1. The current paper presents a modified FEM procedure for calculating of temperature in mass concrete with pipe cooling system. The modified iterative method is strict in theory and has the character of good convergence.
2. Numerical example reveals that the cooling pipes embedded in the high-temperature regions in a concrete dam have significant effects on temperature control and cracking prevention. They can obviously improve the temperature and thermal gradient distributions in the concrete either for cut-off of peak temperature or decreasing the temperature inside a required level before the grouting of the construction joints.
3. As a low cost and highly flexible temperature controlling measure, the modified numerical procedure for solution to thermal problems in mass concrete with pipe cooling system should have a good prospect of the application in dam engineering in the future.
4. To improve the calculating precision, the mesh around the pipe should be refined and that will enlarge the size of the solving the problem and increase the relevant computational effort significantly if there are more cooling pipes, especially in a project of high arch dam. For the reason, one might have to use the technique of parallel algorithm[5].

REFERENCES

[1] Zhu B.F. and et al.: Finite element analysis of the effect of pipe cooling in concrete dams (in Chinese) [J]. Journal of Shuli Xuebao, 1985 (4):27–36.
[2] Liu N. and Liu G.T.: Sub-structural FEM for the thermal effect of cooling pipes in mass concrete structures (in Chinese) [J]. Journal of Shuli Xuebao, 1997 (12):43–49.
[3] Zhu Y.M., Xu Z.Q. and et al.: Computational method of pipe cooling in concrete (in Chinese) [J]. Journal of Yangtz Scientific Research Institute, 2003, 20 (2):18–22.
[4] Zhu Y.M., He J.R., Liu Y.J. and et al.: The temperature control and cracking prevention of Longtan high RCC gravity dam (in Chinese) [R]. College of Water Conservancy & Waterpower Eng., Hohai University, China, 2003.
[5] Zhu Y.M., Lin Z.X. and Xiao Z.Q.: Thermal stress analysis of high arch dams with pipe-cooling system using parallel algorithm. (Submitted to the Chinese J. of Computational Mechanics).

New Developments in Dam Engineering—Wieland, Ren & Tan (eds),
© 2004 Taylor & Francis Group, London, ISBN 04 1536 240 7

Author index